

(57)

TRACERS
IN THE SE~~ABER~~

WALLACE SMITH BROECKER
COLUMBIA UNIVERSITY

AND

TSUNG-HUNG PENG
OAK RIDGE NATIONAL LABORATORY

A PUBLICATION OF THE LAMONT-DOHERTY GEOLOGICAL OBSERVATORY,
COLUMBIA UNIVERSITY, PALISADES, NEW YORK 10964

GC 11b
B764
1982

1495724



Copyright © 1982 by Wallace S. Broecker and Tsung-Hung Peng

All rights reserved. No part of this book may be reproduced by any means without the written permission of the authors.

Printed in the United States of America

Tsung-Hung Peng's work at Oak Ridge was sponsored jointly by the National Science Foundation's Ecosystem Studies Program under Interagency Agreement No. DEB 8115316 and the Carbon Dioxide Research Division, Office of Energy Research, U.S. Department of Energy, under contract W-7405-eng-26 with Union Carbide Corporation.



Dedication

We dedicate this book to our long-time friend, Arnold Bainbridge. It was largely because of his efforts that the Geochemical Ocean Sections program was such a remarkable success. His mating of the best in geochemical instrumentation with state-of-the-art computer systems made possible the large number of precise shipboard chemical measurements necessary to the success of this program. His judgment in hiring and skill in management created the cadre of people required to build and operate his systems. There is little doubt that he was a person uniquely capable of discharging this great task. Although Arnold passed away in February 1979, the data he and his group generated will, through extensive and continued use, constitute a reminder of Arnold's great contribution to the science of marine geochemistry. It is thus appropriate that this book, which depends so heavily on the GEOSECS data set, be published in his honor.

Foreword

A decade has passed since Chemical Oceanography, the predecessor to this book, was written. During this time our knowledge of the chemistry of the oceans has mushroomed. The Geochemical Ocean Sections program (GEOSECS) fleshed out our sketchy picture of the distributions of chemical, isotopic and radiochemical tracers in the sea. The discovery of ridge crest hydrothermal systems has added a new dimension to ocean chemistry. The results of sediment trap deployments, of pore water measurements, and of in situ filtrations of particulate matter have expanded our knowledge of the cycle of particulate matter in the sea. Hence, rather than revising Chemical Oceanography, we decided to write a new book, Tracers in the Sea. While this new book follows the outline of its predecessor and contains material from its predecessor, about 75% of the material is new. Unlike Chemical Oceanography, which could be read from cover to cover in a few sittings, Tracers in the Sea has far more meat and cannot be so quickly digested.

The objective of this book is to demonstrate how the distribution of tracers in the sea and its sediments can be used to aid us in deciphering the operations plan and history of operation for the ocean as a chemical plant. To do this requires the integration of chemical information with information based on studies of ocean sediments, of organisms living in the sea, and of ocean currents. This integration leads to a description of how the ocean "works" from the point of view of a geochemist. Such integrations are not common to the field of oceanography because only in attempting to understand the chemistry of the sea is it necessary to consider the results from all the sister disciplines.

One dominant theme which recurs in the book is the operation of the earth's carbon cycle. Carbon is a key element in organisms and their shells. It is a constituent of the key greenhouse gas in our earth's atmosphere. It has two isotopes of great importance as tracers, namely, ^{14}C and ^{13}C . In the book we explore not only the present day distribution of this key element but also how this distribution may have differed during the last glacial period and how it will differ during the coming fossil fuel CO₂-induced superinterglacial period.

While aimed both at the professional and at the student, the book has the format of a text. As such it puts more emphasis on explanation than on documentation. To counter the somewhat thin referencing in the body of the text a rather elaborate reference list is given at the end of the book. This list contains over 700 entries and is organized by topic. Thus, a reader interested in finding all the papers which bear on, let's say, the distribu-

tion of ^3He or of lead in the sea has only to look up the sections on these properties in the reference list to find a fairly complete list of papers written on these subjects. As the papers on each topic are listed in order of publication date and as they are annotated with a sentence or two stating their contribution, the reader can get some sense of development of the data base and thinking in a given area by looking through this reference list. Hence, the reference numbers in the text and in the figure and table captions serve a dual purpose. They give the reader the source of specific information used in the book and they lead him to the section in the references which lists related papers not specifically mentioned in the text.

Every text book in science needs problems. They reinforce the concepts in the text and force the student to think carefully about the quantitative aspects of the subject. We include both the usual short problems and also what we call superproblems. The latter give the student a better in-depth view of key material and also good training in box modeling which plays such an important role in marine geochemistry. As the superproblems require 4-10 hours of work, the instructor should consider having students work in pairs on the problems and having each student work on only 1 or 2 of the problems during a semester. We have found that presentations of the solutions by the students doing the work to the rest of the class proves very effective. Solutions to both the problems and superproblems can be obtained by writing to the authors.

Much of this book was written during a sabbatical leave in Germany. I (WSB) would like to thank the Alexander Von Humboldt Foundation for providing fellowship support for a nine month visit to Heidelberg and to Karl Otto Munnich and Wolfgang Roether and their colleagues in the Umweltphysik group for their friendship and help during this time. The drafting for the book was done by Patty Catanzaro and the typing by Vicky Costello, Rae Pochapsky and Andrea Radigan. Ellen Coxe acted as liaison between these production efforts at Lamont and the writing and modeling activities by T.-H. Peng at Oak Ridge National Laboratory and by W.S. Broecker in Heidelberg. The sketch of Arnold Bainbridge and the cover design were done by Dee Breger, a member of the technical staff in geochemistry at Lamont-Doherty. The cover photo, a rosette cast from the Woods Hole Oceanographic Institution research vessel KNORR, was taken by David Chipman of the Lamont-Doherty Geochemistry group.

We thank Heinrich Holland for encouraging us to follow a rather unconventional plan for publication. The Lamont-Doherty Geological Observatory served as publisher. Author-ready copy was prepared using the geochemistry group word processor under the supervision of Patty Catanzaro. The printing was jobbed out to Edwards Brothers Incorporated, Ann Arbor, Michigan. The advertising and distribution were handled by Observatory staff. We thank C. Barry Raleigh, director of the Observatory, for his courageous backing of this dangerous experiment.

Table of Contents

CHAPTER 1 INTERNAL CYCLING AND THROUGHPUT

Pathways from River Mouth to Sea Floor

Introduction	1
Depth Profiles of Sea Salt Composition	2
Constituent Classification	6
The Chemical Composition of Marine Organic Matter	8
Composition of Particulate Matter Caught in Sediment Traps	13
A Simple Model for Biologically Utilized Constituents	15
The Distributions of Biointermediate Constituents	22
Estimation of Input Rates	25
Horizontal Segregation of Constituents in the Deep Sea	28
Summary	40

CHAPTER 2 THE SEDIMENTARY SINK

Factors Influencing the Distribution of Sedimentary Constituents	
Introduction	45
Sediment Types	45
Distribution of Opal Production	47
Opal Solution on the Sea Floor	49
Distribution of Calcite in Marine Sediments	58
Degree of Calcite Saturation	61
Variation in the Carbonate Ion Content of Sea Water	62
Spacial Variations in the CaCO_3 Saturation of Sea Water	71

Factors Controlling the Rate of Calcite Solution	84
Thickness and Shape of the Sublysocline Transition Zone	89
Variation of Sediment Type with Time	94
Manganese Nodules	98
Summary	106

CHAPTER 3 THE ATMOSPHERIC IMPRINT

The Cycles of Gases within the Sea

Introduction	110
Solubilities of Gases in Sea Water	111
The Rate of Gas Exchange	113
Stagnant Film Thickness Derived from Natural Radiocarbon	118
Stagnant Film Thicknesses Determined by the Radon Method	122
Oxygen Concentrations in Surface Ocean Water	127
Oxygen Deficiencies in the Deep Sea	131
The Marine N ₂ O Cycle	139
Excess Helium	147
The Carbon Dioxide Content of Surface Ocean Water	149
Origin of the Equatorial Pacific CO ₂ Anomaly	158
Summary	161

CHAPTER 4 REACTIVE METALS AND THE GREAT PARTICULATE SWEEP

The Cycle of Metals in the Sea

Introduction	166
Products of Uranium and Thorium Decay	168

Thorium Isotopes in the Sea	172
Protactinium-231 to Thorium-230 Activity Ratios	184
The Distribution of Lead-210	189
The Distribution of Polonium-210	198
The Distribution of Radium-226	200
Anthropogenic Plutonium in the Sea	203
Toward a Model of Metal Transport	205
Distributions of Stable Metals in the Sea	215
Stable Isotope Ratios in Reactive Metals	221
Transport of Iron and Manganese in the Sea	226
Lessons from Controlled Ecosystem Studies	230
Distribution Coefficients	230
Summary	230

CHAPTER 5 HOW FAST DOES THE MILL GRIND?

Rates of Vertical Mixing and Sediment Accumulation

Introduction	236
Rate of Vertical Mixing	236
Implication to the Distribution of Radium-226	243
Distribution of Radiocarbon in the Ocean	245
Rate of Continental Runoff	247
Sediment Accumulation Rates	253
Radiocarbon Dating	255
Uranium Series Dating	257
Beryllium Dating	264
Potassium-Argon Dating	264

Agreement Among Dating Methods	269
Comparison of Model and Observed Rates of CaCO_3 Solution	269
Summary	271

CHAPTER 6 WHAT KEEPS THE SYSTEM IN WHACK?

Control Mechanisms Operating in the Sea

Introduction	275
Phosphate Controls	275
Silicate Controls	280
Carbon Controls	280
Interactions between the Phosphate and Carbon Controls	281
Nitrate Controls	284
Dissolved Oxygen Controls	284
Major Anion Controls	287
Major Cation Controls	289
Possible Causes for Perturbations	300
Recorders of Paleocean Chemistry	301
The Marine Geochemistry of Carbon-13	306
The Uranium Content of Coral	311
Factors Influencing Nutrient Gradients in the Deep Sea	312
Summary	314

CHAPTER 7 FREIGHT TRAINS AND FICKIAN CONFUSION

The Movement of Water Through the Deep Sea

Introduction	317
Types of Motion	317

One Dimensional Advection - Diffusion Model	318
Tracers for Diapycnal and Isopycnal Mixing	324
Mixing Rates Based on Radon-222 and Radium-228	325
The Distribution of Helium-3 in the Deep Pacific	331
Sources of Deep Water	334
Northern Component Water	335
Conservative Properties of NCW	341
Initial Radiocarbon to Carbon Ratio in NCW	343
Feed for NCW Production	343
Southern Component Water	349
Ventilation of the Deep Atlantic Ocean	359
Ventilation of the Deep Pacific and Indian Oceans	365
The Grand Cycle of Radiocarbon in the Deep Ocean	368
Biological Short-Circuiting	372
Temporal Variations in Radiocarbon Production	374
Argon-39	377
Summary	379

CHAPTER 8 THE ANTHROPOGENIC INVASION

The Movement of Water Through the Oceanic Thermocline

Introduction	383
Input Functions	383
Hydrology of the Main Thermocline	388
Tritium Distribution within the Thermocline	399
Temporal Trends in Tritium	402
Tritium as a Guide to Deep Water Formation	406

Supplementary Information from Strontium-90	412
Bomb Carbon-14 Distribution within the Thermocline	412
Explanations for Low Equatorial Bomb Carbon-14 Inventories	422
Implications of Equatorial Upwelling to the Tritium Budget	425
An Upwelling Rate Based on the Equatorial CO ₂ Anomaly	427
Helium-3 Distribution in the Main Oceanic Thermocline	432
Purposeful Tracers	438
Summary	439

CHAPTER 9 ICE SHEETS AND OCEAN PHOSPHATE

Glacial to Interglacial Changes in Ocean Chemistry

Introduction	444
Temperature and Salinity Changes	446
Formation and Destruction of Organic Materials	451
Changes in CaCO ₃ Storage	456
Evidence for an Early Post-Glacial Lysocline Change	457
Changes in Phosphate Concentration	466
The Combined Evidence from Deep Sea Cores	472
Cause of the Oceanic Phosphate Change	479
An Alternate Scenario	480
Wrap Up of the CO ₂ Record	481
The Oxygen Record	484
Glacial to Interglacial Changes in Ocean Mixing Rate	485
Glacial to Interglacial Lysocline Changes	485
Changes in the Distribution of Nutrients in the Deep Sea	491
Summary	496

CHAPTER 10 CAN MAN OVERRIDE THE CONTROLS?

The Buildup of Fossil Fuel CO₂ in the Atmosphere and Oceans

Introduction	500
CO ₂ Production in the Past	500
CO ₂ Production in the Future	505
Capacity of the Sea for Fossil Fuel CO ₂ Uptake	511
Utilizable Capacity - Simplified Calculation	513
Utilizable Capacity - Rigorous Calculation	517
Kinetics of Fossil Fuel CO ₂ Uptake by the Sea	524
Numerical Model	526
Crosschecks on the Validity of the Numerical Model	534
Prediction of Future CO ₂ Levels	550
Solution of Sea Floor Calcite	552
Summary	564

REFERENCES, CONSTANTS, DEFINITIONS, ABBREVIATIONS AND INDEX

Introduction to the References	569
Subject Outline for the References	569
Annotated Reference List	574
Frequently Used Constants	680
Definitions of Isotope Notations	681
Abbreviations	682
Index	683
Foldout Caption	690

Chapter 1

INTERNAL CYCLING AND THROUGHPUT PATHWAYS FROM RIVER MOUTH TO SEA FLOOR

INTRODUCTION

The sea is a way station for the products of continental erosion. All substances received by the sea are ultimately passed along to the sediment and rock lining its floor. The great tectonic forces that continually modify the geography of the earth's surface eventually push the material buried in this way back above sea level where it becomes subject to erosion. Then another trip through the sea begins.

The greater proportion of the products of erosion enter the sea in particulate form. They are dropped by the winds to the sea surface or disgorged by rivers into coastal waters. These rock fragments and soil residues are chemically quite inert. They travel only as far as the currents can carry them before reaching the sea floor. They play a minor role in the story we have to tell.

Of great interest to us are those substances that dissolve during erosion and are carried to the sea in ionic form. They constitute the sea's salt. As long as they remain dissolved, gravity cannot influence them. Although the processes at work in the sea ultimately "reprecipitate" these ions, most constituents of sea salt wander through the sea long and far before becoming entombed in the sediment. The temporary entrapments in particulate matter experienced by these wandering ions will prove of particular interest to us.

The composition of sea salt reflects not only the relative abundance of the dissolved substances in river water but also the ease with which a given substance becomes entrapped in the sediments. Sodium, for example, is both abundant in the dissolved matter in rivers and sparingly reactive in the sea. This combination is reflected by its high concentration in sea salt. Calcium, although even more abundant in river water than sodium, is an important ingredient in the shells of marine organisms. Because of this special mode of entrapment, the abundance of calcium in sea water is far lower than that of sodium.

Many components of sea salt show little variation in concentration within the sea. Others show very large changes in concentration from place to place. As we shall see, these differences are largely the result of cycling by organisms. Plants live only in surface waters, from which they extract certain constituents

needed to construct their tissues. While much of this plant matter is consumed by animals living in the surface ocean, some insolubles and indigestibles (i.e., fecal matter) move into the deep sea under the influence of gravity - and so the life cycle leads to chemical segregation. Destruction of plant matter occurs, on the average, at greater depths than formation. The interaction of this life cycle with the large-scale water circulation pattern in the sea results in inhomogeneities in the distribution of these species, not only within the sea itself but also in the sediments deposited on the ocean floor.

One of the aims of this book is to point out the factors that influence the average concentrations of the various components of sea salt and the factors that produce chemical inhomogeneities within the sea and its sediments. The approach might be termed "inverse chemical engineering". The ocean is a great chemical plant that processes the dissolved matter added from rivers and dispenses it as sediment. Unlike most chemical plants, the sea has no advance operational blueprint. As chemical oceanographers, we wander through the plant measuring inputs, outputs, and internal compositions - trying to reconstruct the missing design. As in most chemical plants, the two critical features of the ocean are the manner in which the ingredients are mixed and the manner in which the ingredients react with one another. Oceanic mixing is accomplished by a complex system of currents and a host of turbulent eddies. Many of the chemical reactions are catalyzed by the enzymes in living organisms. Thus any study of the chemistry of sea water is heavily dependent on knowledge derived from physical oceanographic and marine biologic studies.

In this book, we will focus on the first-order processes operating within the sea. Until these are mastered, it is fruitless to proceed to the more complex "details". With this in mind, let us turn our attention to our first subject - the grand chemical balance existing in the sea.

DEPTH PROFILES OF SEA SALT COMPOSITION

The salt dissolved in sea water is remarkably uniform in its major constituents. This fact has greatly simplified the task of the physical oceanographer interested in mapping water density patterns within the sea. He needs only to measure the water temperature, the water pressure and one major property of sea salt (for example, the chloride ion content or the electrical conductivity) to make a very accurate estimate of the in situ density of a given sample of sea water. This task would be extremely complex if the composition of sea salt were more varied.

Yet it is fortunate, too, that the compositional constancy of the major components of sea salt does not extend to all the minor components. If this were not the case, the oceanographer would lose one of his most powerful tools, for the variations in the minor constituents of sea water bear important clues regarding mixing, biological, and sedimentary processes taking place within the sea. They are the tracers about which this book is written.

The major ion matrix of sea salt consists of the following constituents: Chlorine in the form of Cl⁻ ion; sulfur in the form

of $\text{SO}_4^{=}$ ion; and magnesium, potassium, calcium and sodium in the form of Mg^{++} , K^+ , Ca^{++} , and Na^+ ions, respectively. These six ions dominate sea salt; their ratios, one to another, are very nearly constant. In fact, only calcium has been shown to vary measurably from place to place in its ratio to the other five constituents. Although this constancy also extends to many of the lesser components of sea water (boron, bromine, fluorine, uranium, cesium, and others), it does not extend to all of them.

The best known of the variations in the composition of sea salt arise from the removal of constituents from surface sea water by plants and the subsequent destruction of plant-produced particles after downward movement. Deep water masses are richer in the constituents utilized by plants than surface water is. If the ocean were sterile, the chemical composition of sea salt would be almost perfectly uniform. The main differences in composition would be those resulting from the transfer of gases between the atmosphere and surface waters of differing temperature would exist.

Plants live only in surface water, where there is enough light to permit photosynthesis. By the time the components of their debris are returned to the ionic form as a result of tissue oxidation or hard part solution, downward movement under the influence of gravity or migrating animals has occurred. It is not surprising, then, that the primary chemical differences observed in the ocean are all of the type just mentioned: deep water is enriched relative to surface water. The only major exception is dissolved oxygen.

Figures 1-1 and 1-2 show the distribution with depth of potential temperature*, of salinity and of the concentrations of six biologically utilized sea salt constituents at a station in the North Pacific Ocean. In all cases, the most dramatic change occurs in the upper thousand meters of the water column. This so-called main thermocline constitutes the zone of transition between the warm surface waters and the cold deep waters. The nutrient species nitrate (NO_3^-), silicate (H_4SiO_4), and total dissolved inorganic carbon ($\Sigma\text{CO}_2 = \text{CO}_2 + \text{HCO}_3^- + \text{CO}_3^{=}$) show the deep water enrichment mentioned above. Alkalinity and barium show patterns similar (but not identical) to that of silicate. Dissolved oxygen gas, by contrast, shows a depletion. Unlike NO_3^- and ΣCO_2 , which are released during respiration, O_2 is consumed during respiration. Its pattern is also complicated by the fact that cold waters descending from the surface carry with them more dissolved gas than descending warm waters. The salinity minimum at about 600 meters depth is generated by the lateral intrusion of intermediate waters. Keep in mind that these fractional salinity differences are quite small compared to the fractional differences in

*Sea water is heated by compression (i.e., about $0.1^\circ\text{C}/\text{km}$) as it descends from the surface. Potential temperatures are corrected for this heating. Hence the potential temperature is the temperature a water sample would have were it returned to the sea surface.

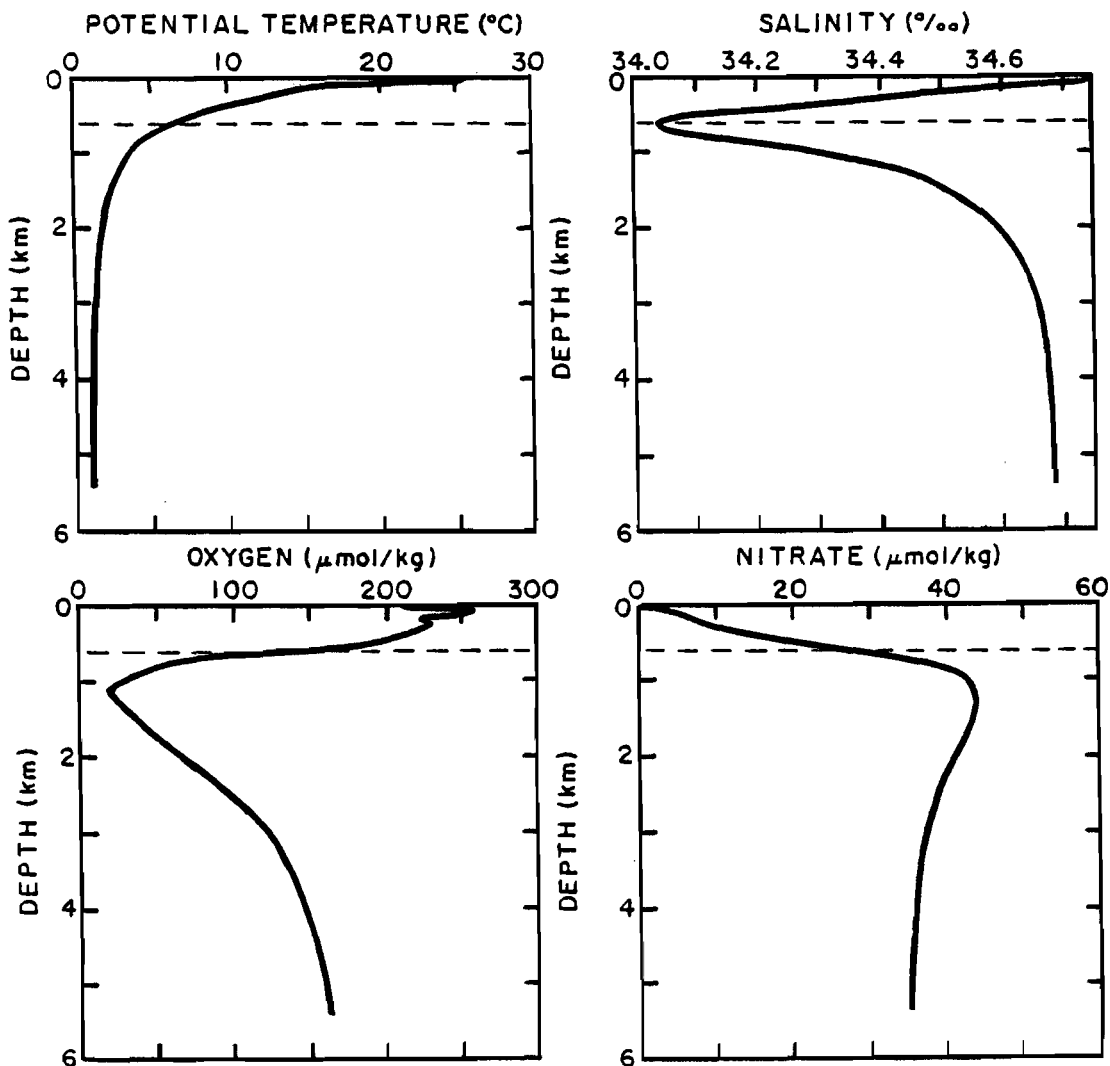


Figure 1-1. Plots of temperature, salinity, dissolved oxygen content and nitrate content as a function of water depth at GEOSECS station 214 in the North Pacific (32°N , 176°W). Potential temperature rather than the temperature measured *in situ* is given. The salinity profile in this region of the ocean shows a pronounced minimum at a depth just over 600 meters. This intermediate water (as it is called) forms in the northern Pacific and sinks and flows laterally beneath the waters of the warm temperate ocean. The level of this minimum is shown in the other diagrams by a dashed line. Dissolved oxygen is utilized by animals and bacteria living in the deep sea to "burn" the organic debris falling from the surface. Thus all deep waters are deficient in oxygen compared to the amount they received from the atmosphere before descent. As oxygen is consumed, nitrate is produced. Thus the shapes of the profiles of these two properties have an inverse relationship. These results were obtained as part of the GEOSECS program (425). The location of this station can be seen on the foldout map.

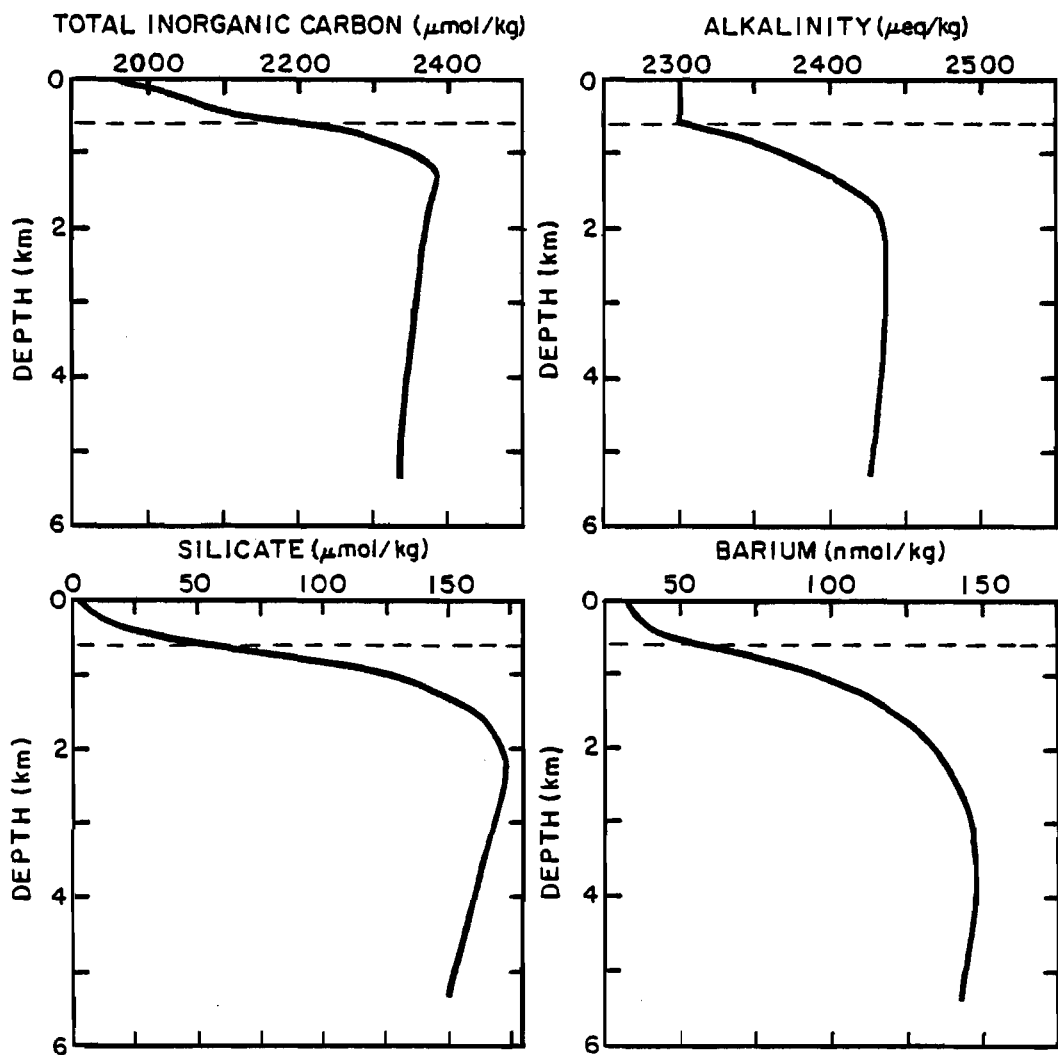


Figure 1-2. Plots of total dissolved inorganic carbon, alkalinity, dissolved silicate, and dissolved barium as a function of water depth at GEOSECS station 214 in the North Pacific (32°N , 176°W). As in figure 1-1 the dashed line represents the depth of the salinity minimum. The alkalinity of the sea changes mainly because Ca is extracted from surface waters by organisms to form CaCO_3 skeletal material. Much of this CaCO_3 dissolves after falling to the deep sea. The depth profiles of these constituents differ from one another and from that of nitrate because they are carried down in different forms; C and N in organic debris, C and Ca in CaCO_3 , Si in opaline silica, and Ba in some as yet unidentified form. The depth spectrum of the destruction of these various phases is not the same. The skeletal matter reaches, on the average, greater depths before dissolving than the organic debris reaches before consumption. This gives rise to deeper maxima for alkalinity, silicate and barium than for nitrate and carbon. These results were obtained as part of the GEOSECS program (425).

the concentrations of the nutrient species.*

CONSTITUENT CLASSIFICATION

Roughly one quarter of the 92 elements will be considered in this book. They are shown in table 1-1, grouped as they appear in the chemist's periodic table. The first column contains a group of elements known as the alkali metals; they have a valence of +1 (that is, in sea water each atom loses one electron and becomes an ion with a single positive charge). The alkaline earths occupy column two. These elements have a common valence of +2 (two electrons are given up upon solution in sea water). The noble gases are in column eight. They do not undergo chemical reactions in sea water, but remain in gaseous form. Column seven contains elements with the common property of accepting an extra electron (one of the electrons released by the alkali metal and the alkaline earth metal atoms). These elements are present in sea water with a charge of -1. The elements in columns three, four, five and six all combine with oxygen, and sometimes with hydrogen, to form multiaiton ions. In most cases, they form negatively charged ions; in a few cases, they form neutral groupings. Those dissolved units with negative charges are known as anions; those with positive charges, as cations. In addition to the elements listed in table 1-1 the marine chemistry of a number of the transition metals (iron, manganese, copper, zinc, nickel, and cadmium) and heavy metals (uranium, thorium, protactinium, polonium, lead and plutonium) will be considered.

The chemical constituents of sea salt can be divided into three major categories: the biolimiting constituents (those which are almost totally depleted in surface water); the biointermediate constituents (those which are partially depleted in surface water); and the biounlimited constituents (those which show no measurable depletion in surface water).

The six known biolimiting constituents are nitrate (NO_3^-), phosphate ($\text{HPO}_4^{=}$), silicate (H_4SiO_4), zinc (Zn^{++}), cadmium(Cd^{++}) and germanium (H_4GeO_4). Plant activity (and, in the case of silicate, animal activity as well) is efficient enough to extract these six constituents almost completely from surface water. The deep sea constitutes a large reservoir for these constituents. When deep water is returned to the surface, these constituents become available to photosynthetic organisms. They are fixed into particulate material and are then carried by gravity back to the deep sea, where they are largely returned to solution.

The question naturally arises as to how more than one chemical ingredient can limit plant growth. The answer lies in the fact that many types of plants live in the ocean. Different types have different chemical needs and abilities. For example, a group of plants called diatoms need H_4SiO_4 to manufacture the opaline

*A 0.6 per mil salinity change is equivalent to a two percent change in salt concentration. A per mil ($^{\circ}/\text{o}$) is a part per thousand; just as a percent ($^{\circ}/\text{o}$) is a part per hundred.

Table 1-1. Abbreviated periodic table showing the elements whose marine chemistry are discussed in this book. For each element the important ionic and molecular forms found in sea water are noted. For those elements whose distribution within the sea is sufficiently well understood, the designations biolimiting, biointermediate, and biounlimited are given. Not shown are the transition metals (Fe, Mn, Cd, Zn, Ni, and Cu) and heavy metals (U, Th, Pa, Po, Pb, and Pu) which are discussed in Chapter 4.

(1)

(8)

Hydrogen H_2O H^+ Unlimited	(2)	(3)	(4)	(5)	(6)	(7)	Helium He Unlimited
Lithium Li^+	Beryllium Be^{++}	Boron H_3BO_3 $H_4BO_4^-$ Unlimited	Carbon HCO_3^- $CO_3^=$ CO_2 Intermediate	Nitrogen N_2 Unlimited	Oxygen H_2O Unlimited	Fluorine F^- Unlimited	Neon Ne Unlimited
Sodium Na^+ Unlimited	Magnesium Mg^{++} Unlimited	Aluminum $Al(OH)_4^-$ $Al(OH)_3^o$	Silicon H_4SiO_4 Limiting	Phosphorus $HPO_4^=$ $H_2PO_4^-$ Limiting	Sulfur $SO_4^=$ Unlimited	Chlorine Cl^- Unlimited	Argon Ar Unlimited
Potassium K^+ Unlimited	Calcium Ca^{++} Intermed.		Selenium $SeO_3^=$, $SeO_4^=$ Intermediate			Bromine Br^- Unlimited	Krypton Kr Unlimited
Rubidium Rb^+ Unlimited	Strontium Sr^{++} Intermed.						Xenon Xe Unlimited
Cesium Cs^+ Unlimited	Barium Ba^{++} Intermed.						Radon Rn Unlimited
	Radium Ra^{++} Intermed.						

capsules within which they dwell. Thus, the dissolved silica in sea water limits the extent to which diatoms grow.* Another plant type, the blue-green algae, has the capability to produce forms of "fixed" nitrogen (i.e., NO_3^-) from dissolved nitrogen gas (i.e., N_2). Thus, the growth of these plants need not be limited by the availability of NO_3^- . All plants need the element phosphorus. Hence, phosphorus is the ultimate limiting nutrient for plant growth. The biological roles of Zn and Cd are unknown. Plants may inadvertently incorporate them in their quest for phosphorus.

A constituent is biounlimited if its ratio to total salt in both surface and deep sea water samples are equal within measurement error. The elements currently classified as biounlimited are sodium, potassium, rubidium, cesium, magnesium, boron, sulfur, fluorine, chlorine, bromine and uranium. If more accurate analyses could be made, one or more of these elements might be eliminated from the biounlimited category.

We are certain of eight biointermediate elements: calcium (Ca), strontium (Sr), nickel (Ni), copper (Cu), selenium (Se), carbon (C), barium (Ba), radium (Ra). The Ca content of surface water salt is about one-half percent less than that of salt in deep water. The C content of surface water salt is 15 percent less than that of deep water, and the Ba content of surface water salt is 70 percent less than that of deep water.

In order to fit into the classification adopted here a constituent must be recycled within the sea several times before removal to the sediments. Some elements are so reactive that they pass through surface water only once. They become firmly fixed onto particles which fall through the sea to the sediment. These constituents will be referred to as noncycling. Iron, thorium, protactinium and lead fall in this category.

THE CHEMICAL COMPOSITION OF MARINE ORGANIC MATTER

Three major types of particles fall from surface water into deep water: organic tissue, calcium carbonate (CaCO_3), and opaline silica (SiO_2). All plants and animals produce organic tissue. Plants extract the ingredients for this tissue from the dissolved salt in surface sea water. Animals reuse these ingredients by devouring plants and other animals. Roughly, 90% of the organic matter eaten by animals is consumed in the production of energy.

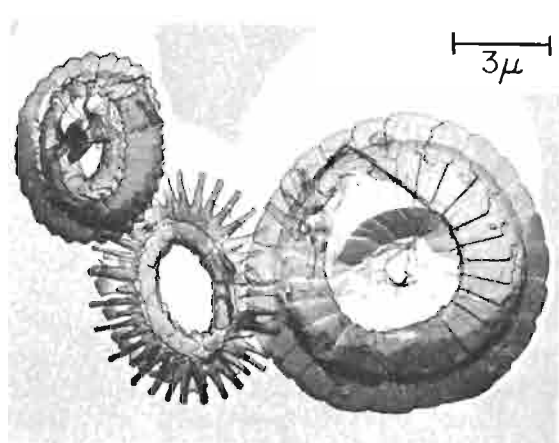
*At the time we were completing this book a paper by Froelich and Andrae of Florida State University was published showing an almost perfect covariance between the concentrations of the elements germanium and silicon for samples from various depths at a North Pacific GEOSECS station. While it is tempting to conclude from this that Ge and Si have identical marine chemistries (i.e., they act as a single element), Froelich has further unpublished data suggesting that the situation is not nearly so simple (378).

The products of this "combustion" are returned to the sea in ionic form. Thus only about 10% of the organic matter survives each step in the food chain. Of this some is rejected in fecal pellets which fall toward the sea floor. Many microscopic plants and animals also produce hard parts consisting of CaCO_3 or SiO_2 . Hard parts made of CaCO_3 are produced by coccolithophorida (plants), foraminifera (animals), and pteropods (animals). Hard parts made of SiO_2 are produced by diatoms (plants) and radiolarians (animals). Photographs of the hard parts produced by these organisms appear in figure 1-3.

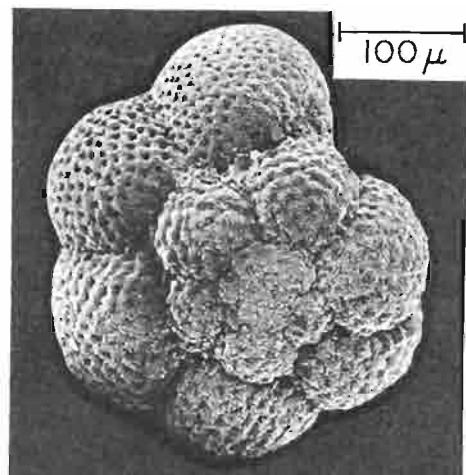
The chemical composition of the organic soft tissue formed by plants is thought to be relatively constant: for every atom of P in this tissue there are on the average about 15 atoms of N and on the average 105 atoms of C. The approximate ratios of these same elements dissolved in deep sea water are 15 atoms of N and 1000 atoms of C for every atom of P. When a batch of typical deep Pacific water returns to the surface, plants extract phosphate and nitrate until both of these constituents have been depleted. Neglecting for the moment the carbon lost to CaCO_3 , only 105 of the 1000 atoms of C will be used. Roughly 90 percent of the carbon will remain in dissolved form. In the absence of additional phosphate and nitrate, plants have no use for this remaining dissolved carbon. Animal tissue has roughly the same P/N/C ratio as plants. This makes one aspect of ocean chemistry quite simple. To the first approximation, parcels of sea water differ in their P, N, and C contents to the extent that living organisms have removed or added these elements in a reasonably fixed ratio.*

One of the mysteries of sea water chemistry concerns the P/N ratio. When deep water upwells to the surface, by the time all of its dissolved phosphate has been consumed, by chance or by design, so has its dissolved nitrate. Why N and P are present in sea water in the same ratio as in organisms is a little like the chicken and the egg problem. Do organisms use N and P in the 15/1 ratio because this is the ratio in which these elements occur in sea water, or do organisms maintain this 15/1 ratio in the sea? The answer is almost certainly that organisms drive the ratio of N/P in sea water toward the 15/1 biochemical ratio. The mechanism must be ecologic. If the amount of nitrate in the sea were to drop below the amount required to maintain this ratio, then species which are capable of fixing molecular nitrogen (i.e. con-

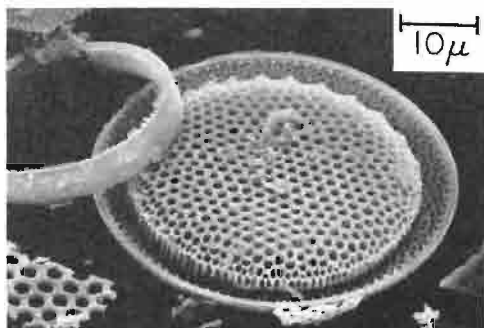
*This ratio is known as the Redfield ratio in honor of Alfred C. Redfield who demonstrated the relationship between organism composition and ocean chemistry. Although the C:N:P proportions of 105:15:1 are widely used the exact values are still quite uncertain. For example, analyses of material from surface water yields a range in C:P ratios of 50 to 200 (692). A similar range is observed in fresh waters. Thus, while representing a fair average composition of the micro-organisms in the oceans, sizable differences are to be expected from place to place in the sea.



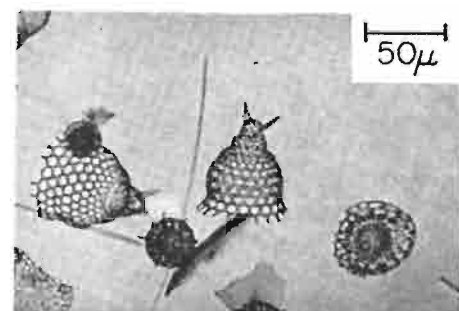
(a)



(b)



(c)



(d)

Figure 1-3. Photographs of hard parts produced by (a) cocolithophora, (b) foraminifera, (c) diatoms, and (d) radiolarians.

verting N_2 to NO_3^-) would gain an advantage and would begin to produce nitrate faster than it was being destroyed within the sea. On the other hand, if an excess of NO_3^- relative to the amount needed to match the biochemical ratio existed within the sea then those species that do not fix nitrogen might be expected to have an advantage. Presumably the ecology of the sea adjusts until a balance is achieved such that the rate of nitrification just matches the rate of denitrification. This balance is struck when the N/P ratio in sea water is quite close to that in the micro-organisms which dominate the life cycle in the sea. The plot in figure 1-4 of NO_3^- versus PO_4^{3-} for waters from throughout the Atlantic Ocean demonstrates the remarkable constancy in the ratio of these two constituents in the sea.

Carbon is also used by organisms to construct their calcium carbonate hard parts. In $CaCO_3$ there is one C atom for every Ca atom. In sea water there are 20 C atoms for every 100 Ca atoms. Thus, the generation of $CaCO_3$ depletes carbon about five times more rapidly than it does calcium.

On the average, for every four C atoms that fall from the surface sea in the form of organic tissue, one C atom falls in the form of $CaCO_3$. Thus for every P atom in the composite of the organic and $CaCO_3$ debris that fall toward the deep sea there are 131 C atoms, 105 of which are part of organic material and 26 are part of $CaCO_3$. Accompanying them, of course, would be 26 Ca atoms paired off with the carbon atoms in the $CaCO_3$ (see table 1-2). In deep sea water, on the average, for every atom of P there are 1000 atoms of C and 5000 atoms of Ca. Upon total depletion of N and P only 131 (13 percent) of the 1000 C atoms originally present in deep sea water are used to form organic tissue and $CaCO_3$. For every 5000 Ca atoms available, organisms consume only 26 (i.e., only 0.5 percent of the available Ca). This explains why calcium is almost but not quite constant in the sea salt of the world ocean.

For every atom of P in the deep ocean there are about 50 atoms of Si. Since surface-dwelling organisms use essentially all the available silica, we can add the appropriate amount of opal to the debris. Because the amount of opal containing 50 Si atoms has nearly the same weight as the amount of $CaCO_3$ containing 26 C atoms and as the amount of organic tissue containing 105 C atoms, the average batch of falling particulate matter consists of equal weights of its three major constituents. At any particular point in the ocean, their proportion may vary significantly from this average because of local ecologic differences in the overlying surface water and because the hard parts ($CaCO_3$ and SiO_2) fall to greater depths before destruction than does the organic tissue. As organic tissue sustains animal life it is a rapidly consumed commodity; hard parts, on the other hand, have no energy value and are left to undergo gradual inorganic solution.

Indirect evidence leads us to believe that barium is removed from sea water largely as barium sulfate ($BaSO_4$). In order to explain the observed depletion in surface water, only 1 atom of Ba need be removed for every 3000 atoms of C; thus the presence of $BaSO_4$ in the debris can easily go unnoticed.

Figure 1-4. Nitrate versus phosphate scatter diagram for waters from throughout the Atlantic Ocean as determined during the GEO-SECS program (685).

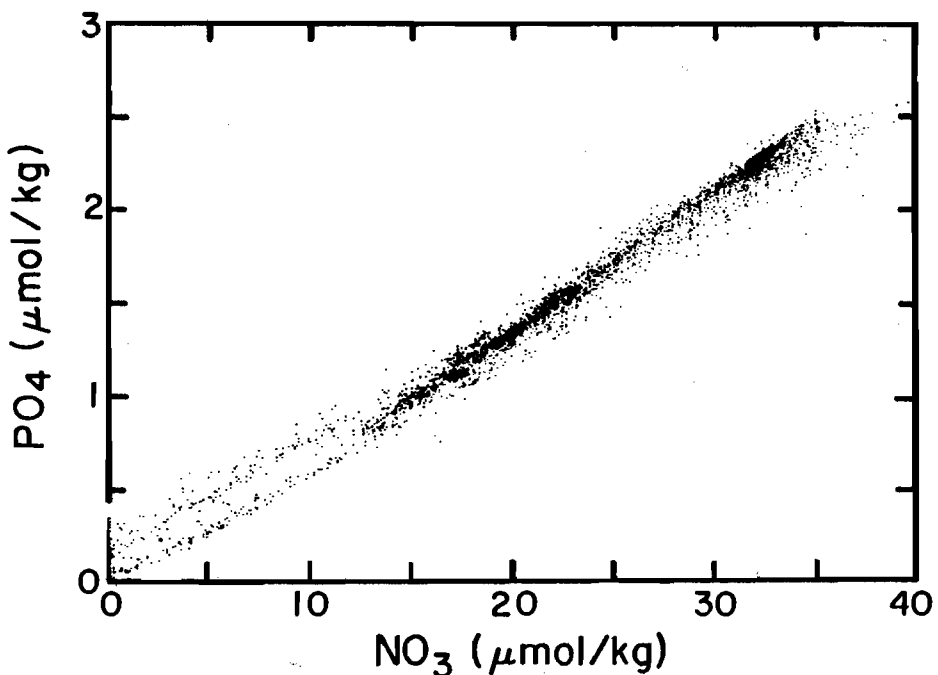


Table 1-2. "Redfield" ratios in particulate debris falling from the surface toward the deep sea compared with the elemental composition of average surface and deep water. These compositions are termed Redfield ratios in honor of Alfred Redfield who did the early work on this subject (346). For comparison actual P:N:C ratios measured in material sieved from surface waters are shown. These latter results were taken from a summary by Goldman (692).

		P: N: C : Ca:Si
Particulate Debris	Soft Tissue	1:15: 105: 0: 0
	Hard Parts	0: 0: 26: 26:50
	Composite	1:15: 131: 26:50
Sea Water	Deep	1:15:1000:5000:50
	Warm Surface	0: 0: 869:4974: 0

	P: N: C
Western North Atlantic (Jan. '62)	1: 5: 59
Western North Atlantic (Apr. '62)	1:13: 68
Equatorial Atlantic	1:21:163
North Pacific Gyre	1:29:410
Central North Pacific	1:18:152

The element radium has chemical affinities almost identical to those of barium, and the element strontium (Sr) has affinities quite similar to those of calcium. Thus the formation of BaSO₄ and CaCO₃ depletes radium and strontium as well as barium and calcium in surface water. However, because the Sr/Ca ratio in most marine CaCO₃ is only about one-fifth that in seawater, the expected depletion of Sr (about 0.1%) lies within the limits of measurement error. Strontium has been shown, however, to be deficient by about 1% in surface water. The likely explanation for this larger than expected deficiency is that the mineral celestite (SrSO₄) is produced by some organism living in surface waters. As sea water is highly undersaturated with respect to this mineral phase, it redissolves after only a few hundred meters of descent.

COMPOSITION OF PARTICULATE MATTER CAUGHT IN SEDIMENT TRAPS

The most direct way to study the composition of marine particulate debris is to deploy and recover traps designed to catch this material as it settles through the water column. This technique has been used effectively in the open ocean only during the last several years. Even now only a few of the results of such studies have appeared in the literature. The late bloom of this line of research parallels the development of large deep sea moorings by physical oceanographers. The big international programs initiated in the 1970's led to the design and testing of bottom moored open ocean devices on which it was possible to mount current meters arrays covering the entire water column. Such moorings can be called back after many months of service by means of sonic systems. The weight which carries the instrument string to the bottom and holds it in place there is released by a sound message sent from the recovery ship; the buoyant spheres attached to the arrays then float the whole system back to the surface where it can be hoisted onto the recovery ship.

Honjo, at Woods Hole, first mated this technology with modern sediment traps. His traps were large (cross section about 1 m²) as he wanted to trap enough material to permit the myriad of chemical, radiochemical, stable isotope, paleontologic and sedimentologic analyses demanded by such studies. To date Honjo has deployed his traps in the north temperate Atlantic, the north temperate Pacific, the equatorial Atlantic and in the equatorial Pacific close to Panama. His efforts have paid off handsomely! In this chapter we will mention some of the chemical and sedimentologic results. In chapter 4 we will discuss the radiochemical results obtained on these samples.

The results for the sediment traps deployed by Honjo in the open ocean are summarized in table 1-3. With increasing depth continental detritus constitutes an ever greater fraction of the material caught. While this change is in part the result of destruction of the biogenic components as they fall through the water column, it is also in part the result of increasing flux of detrital material with depth in the sea. This increase is the result of resuspension of detritus from the "bottom" and "sides" of the ocean. Silicate detritus dominates this resuspended material

Table 1-3. Sediment trap data from the Atlantic and Pacific Oceans. The depths at which the traps were deployed are given at the top of each column. These results were obtained by Honjo and his coworkers at the Woods Hole Oceanographic Institution (541).

ATLANTIC	2° S				30° N	
	0.4 km	1.0 km	3.8 km	5.1 km	1.0 km	4.0 km
Clay (%)	7	16	25	31	7	12
CaCO ₃ (%)	63	55	57	49	59	68
Opal (%)	10	12	9	9	7	9
Organic Matter (%)	20	17	10	11	27	11
Org C (moles/m ² yr)	0.21	0.12	0.05	0.05	0.074	0.027
CaCO ₃ (moles/m ² yr)	0.15	0.09	0.09	0.08	0.040	0.043
Opal (moles/m ² yr)	0.035	0.031	0.023	0.023	0.008	0.010
Clay (gm/cm ² 10 ³ yr)	0.2	0.3	0.4	0.5	0.005	0.08
CaCO ₃ (gm/cm ² 10 ³ yr)	1.5	0.9	0.9	0.8	0.40	0.43
Opal (gm/cm ² 10 ³ yr)	0.2	0.2	0.1	0.1	0.05	0.06
C:N (mole:mole)	7.6	8.5	10.9	8.4	5.1	9.3
N:P (mole:mole)	23.7	31.8	16.5	23.7	17.7	11.9
C:P (mole:mole)	180	270	180	199	90	111

PACIFIC	15° N				
	0.4 km	1.0 km	2.8 km	4.3 km	5.6 km
Clay (%)	2	3	2	3	4
Opal (%)	3	9	15	15	21
CaCO ₃ (%)	35	72	68	72	61
Organic Matter (%)	60	16	14	11	14
Org C (moles/m ² yr)	0.108	0.017	0.033	0.027	0.020
CaCO ₃ (moles/m ² yr)	0.014	0.019	0.041	0.042	0.024
Opal (moles/m ² yr)	0.003	0.016	0.016	0.015	0.014
Clay (gm/cm ² 10 ³ yr)	0.01	0.01	0.01	0.02	0.02
CaCO ₃ (gm/cm ² 10 ³ yr)	0.14	0.19	0.41	0.42	0.24
Opal (gm/cm ² 10 ³ yr)	0.01	0.02	0.09	0.09	0.08
C:N (mole:mole)	8.4	9.6	10.6	10.2	10.0
N:P (mole:mole)	-	-	29.1	26.1	-
C:P (mole:mole)	-	-	309	266	-

because the biologic components which reach the deep sea floor are largely destroyed by respiration and solution.

Also shown in this data set is evidence that organic tissue suffers greater destruction as it falls through the water column than do CaCO_3 and opal. Honjo has shown that the flux of calcite is almost constant with depth. The changes in the CaCO_3 flux that are seen are result of aragonite solution.

The C/P and N/P ratios in the sediment trap material are substantially higher than the Redfield ratios discussed above. Whether this is an artifact of microbial activity in the traps or analytical procedures or a true measure of the time flux ratios has yet to be demonstrated.

A SIMPLE MODEL FOR BIOLOGICALLY UTILIZED CONSTITUENTS

Now let us be a bit more quantitative about the operation of the ocean's internal cycles. Geochemists who study the sea find it convenient to treat this immense system as a series of well mixed reservoirs. For our rather elementary look at the ocean, we will divide it into just two such reservoirs - the warm waters and the cold waters. We do so because the main obstruction to mixing within the sea is the density difference between the thin skin of warm surface water which covers the equatorial and temperate regions of the ocean and the cold water found at the surface in the polar regions and throughout the deep sea. The zone separating these two major water types (referred to hereafter as the oceanic thermocline) lies between 70 meters (the average thickness of the wind-stirred surface mixed layer) and 1000 meters (the beginning of the deep water regime). As the poles are approached, the oceanic thermocline rises to the surface and provides a horizontal separation between polar and temperate surface waters. The bulk of the ocean's plant life lives in the upper, sunlit portion of the warm water mass. Although the cold reservoir is also lighted by the sun at its polar "outcrops", the area of this exposure is relatively small. This simplification of the ocean allows us to quantify its basic processes rather easily. Once we understand the two-box model shown in figure 1-5, we will have a first-order view of how the ocean operates.

We will make further simplifications. First, we will assume that the only way a constituent is added to the sea is by runoff from the continents. We will neglect other means of entry, such as hydrothermal activity on the ocean floor and ground waters seeping out along the continental margins. Second, we will assume that the only way biologically utilized constituents are removed from the ocean is by the fall of organism-produced particles to the sea floor. Since such particles are not entirely destroyed by predators, scavengers, bacteria, and corrosive waters, a small fraction of this debris is permanently buried in the sediment. Thus rivers add material to the sea and the particles formed in surface waters fall to the bottom, removing material from the sea. We know that the biologically used constituents are being replaced in the ocean with great regularity (at least geologically speaking). The sea gains from rivers (and loses to its sediments) its total content of most of the biologically important constituents

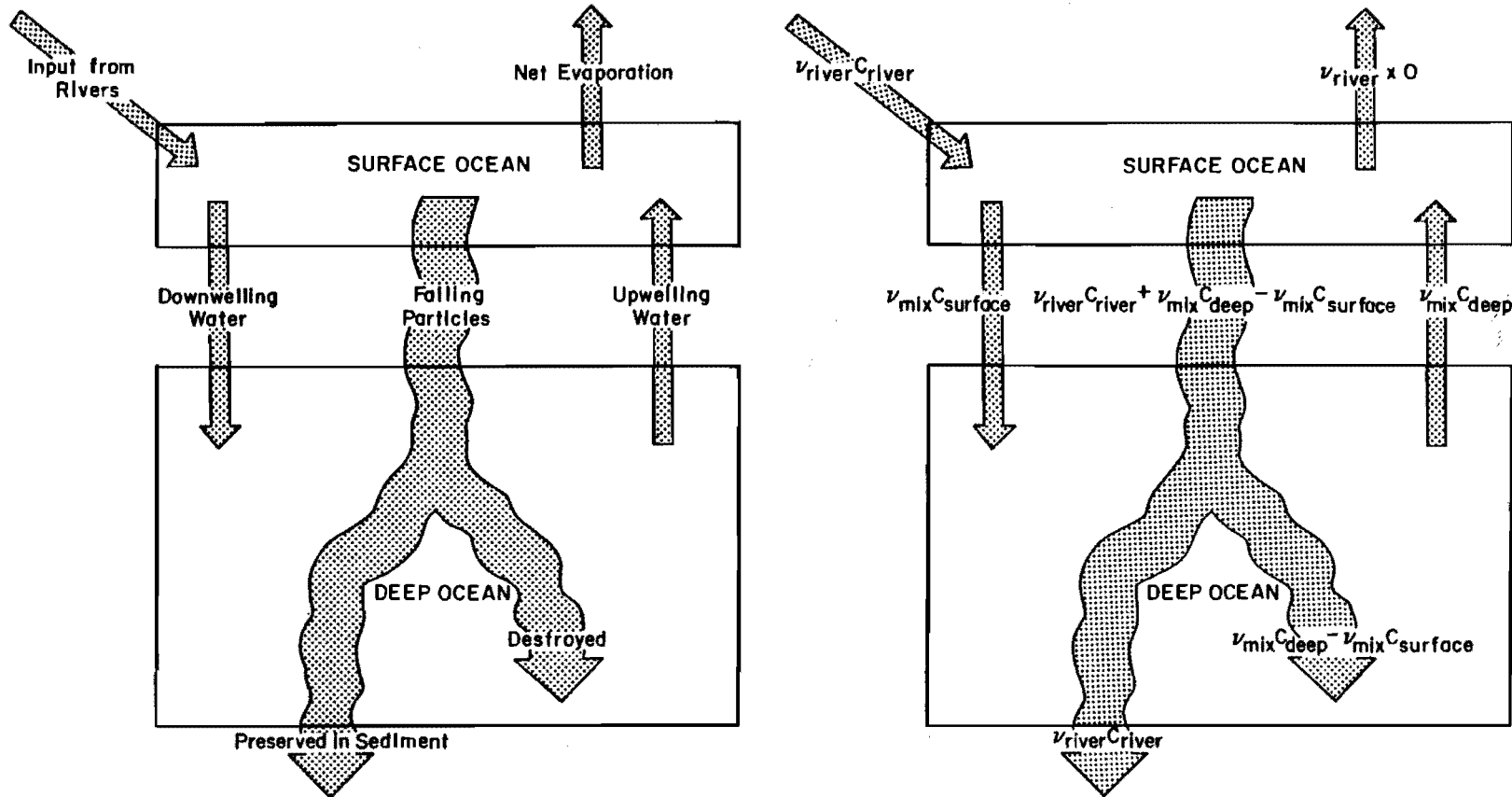


Figure 1-5. The diagram at the left is the two-box model showing the major fluxes of water and of biologically produced particles in the sea. Straight arrows indicate the fluxes of water; wavy arrows indicate the fluxes of particles. The diagram at the right shows the same model with the fluxes labeled in accord with the parameters defined in the text.

in time periods between 10,000 and 1,000,000 years.

Recent studies of the chemistry of the waters that are circulated between the deep sea and the hot basaltic rock which is continually being added to the expanding ridge crests suggest that the basalt-water interactions act as a sink for some constituents of sea salt (i.e., they are lost from the sea water as it percolates through the hot rock) and as a source for others (i.e., the heated water leaches material from the basalt and carries it to the sea). As these interactions do not appear to have an important impact on the budgets of the biologically important constituents we neglect the effects of this process in our first order model.

In our model, we will further assume that the operation of the ocean is at steady state. By this, we mean that the rates of input and output of any constituent from the ocean as a whole as well as from the warm or the cold reservoirs have remained constant for a sufficiently long time that the concentrations at any point in the sea are not changing with time. The system has stabilized so that gain just balances loss. The content of any constituent is being steadily renewed, but its amount is not changing. The situation is much like the flow of bottles through a Coca Cola bottling machine. Empty bottles are steadily added at one end of the conveyor system; full bottles emerge at the other. The number of bottles on the conveyor is always the same. Photographs taken at various times would look alike.

As biologically active constituents pass through the ocean, they participate in its internal cycles. Warm surface waters receive their supply of dissolved constituents from two sources: river water and water from the deep ocean which exchanges with surface water. If the concentration of a given constituent in the surface ocean is to remain constant, then loss with downwelling water and with settling particles must match these two inputs. If, as is the case for biologically active constituents, the concentration of a constituent in warm water is less than it is in cold water, then downwelling alone is not adequate. Since the water exported to the cold reservoir carries away less of each constituent than the upwelling water brings back, particulate loss must account for the difference.

We can rather simply estimate the amount of any element that drifts down as a constituent of particles. The fluxes to be considered in such a calculation are shown in figure 1-5. The volume of river water entering the ocean each year is v_{river} ; the volume of deep water rising to the surface each year is v_{mix} ; the concentration in moles per liter* of the element in average deep water is C_{deep} ; the concentration of the element in average surface water is C_{surface} ; and the concentration of the element in average river water is C_{river} . The amount of an element entering the surface ocean from river water must be $v_{\text{river}} C_{\text{river}}$ (the volume of water per year multiplied by its concentration of the constituent of interest) plus the upwelling contribution

*There are 6×10^{23} atoms in a mole. One mole of any element has a weight in grams equal to the atomic weight of the element. Thus a mole of C weighs 12 g; a mole of Si, 28g; and a mole of H, 1 g.

$v_{mix}C_{deep}$ (the volume of upwelled water multiplied by its concentration of the constituent of interest).

This input to the surface ocean must be balanced by the loss fluxes. The amount of an element leaving the surface via downwelling is $v_{mix}C_{surface}$. For every unit of water entering the ocean from rivers, one unit is lost by evaporation followed by continental rainfall. As this evaporated water does not carry significant amounts of the constituents of concern to us in this chapter, it does not participate in the removal process. The particle flux, P, can be calculated by summing the two inputs to the surface reservoir and subtracting from this total the amount being carried to the deep reservoir by downwelling water:

$$P = v_{river}C_{river} + v_{mix}C_{deep} - v_{mix}C_{surface} \quad 1-1$$

If we define "g" as the fraction of a given constituent reaching the surface reservoir removed in particulate form, then the balance between loss and gain for the surface reservoir can be reexpressed as follows:

$$\frac{g(v_{river}C_{river} + v_{mix}C_{deep})}{v_{river}C_{river} + v_{mix}C_{deep} - v_{mix}C_{surface}} = \quad 1-2$$

Solving for g,

$$g = \frac{v_{river}C_{river} + v_{mix}C_{deep} - v_{mix}C_{surface}}{v_{river}C_{river} + v_{mix}C_{deep}} \quad 1-3$$

or

$$g = 1 - \frac{\frac{v_{mix}}{v_{river}} \frac{C_{surface}}{C_{river}}}{1 + \frac{v_{mix}}{v_{river}} \frac{C_{deep}}{C_{river}}} \quad 1-4$$

As we shall see in chapter 5, in the present-day ocean the ratio of v_{mix} to v_{river} is about 30; that is, 30 times more water is added to the warm reservoir by upwelling than by river runoff. Thus:

$$g = 1 - \frac{30 \frac{C_{surface}}{C_{river}}}{1 + 30 \frac{C_{deep}}{C_{river}}} \quad 1-5$$

For the constituent phosphorus, C_{deep}/C_{river} is about 3 and $C_{surface}/C_{river}$ is 0.15 (on the average, river water carries three times less phosphate per liter than deep sea water, and seven times more than surface sea water). The corresponding value of g is 0.95 (95 percent of the phosphate reaching the surface ocean

is carried away by falling particles).

On the average, the amount of any given constituent leaving the sea, L, must be matched by that being added by rivers:

$$L = v_{\text{river}} C_{\text{river}} \quad 1-6$$

Thus, if the removal is accomplished by the burial in the sediments of particles which survive destruction, then the fraction, f, of a given constituent carried to the deep sea in particles that survive destruction, must be equal to the river input:

$$fP = v_{\text{river}} C_{\text{river}} \quad 1-7$$

or

$$f(v_{\text{river}} C_{\text{river}} + v_{\text{mix}} C_{\text{deep}} - v_{\text{mix}} C_{\text{surface}}) = v_{\text{river}} C_{\text{river}} \quad 1-8$$

or

$$f = \frac{1}{1 + \frac{v_{\text{mix}}}{v_{\text{river}}} \left[\frac{C_{\text{deep}}}{C_{\text{river}}} - \frac{C_{\text{surface}}}{C_{\text{river}}} \right]} \quad 1-9$$

And since $v_{\text{mix}}/v_{\text{river}} = 30$:

$$f = \frac{1}{1 + 30 \left[\frac{C_{\text{deep}}}{C_{\text{river}}} - \frac{C_{\text{surface}}}{C_{\text{river}}} \right]} \quad 1-10$$

For phosphate, f turns out to be about 0.01. Only 1 percent of the phosphorus carried to the deep sea by falling particles is not recycled.

Now if we multiply the parameter f by the parameter g, we obtain a rather interesting piece of information. Since g tells us the fraction of a constituent that reaches the surface and is removed in particulate form, and f tells us the fraction of those particles that survive destruction, the product f x g gives us the fraction of an element that is removed per oceanic mixing cycle (that is, per transfer from the cold to the warm reservoir).

$$f \times g = \frac{1}{1 + \frac{v_{\text{mix}}}{v_{\text{river}}} \frac{C_{\text{deep}}}{C_{\text{river}}}}$$
$$f \times g = \frac{1}{1 + 30 \frac{C_{\text{deep}}}{C_{\text{river}}}} \quad 1-11$$

For phosphate, the product of f x g would be 0.01 (for f) x 0.95 (for g), or about 0.01. Thus 1 percent of the phosphate in

the ocean is lost to the sediment during each mixing cycle. If we wait the length of time necessary for upwelling to recycle all the water in the ocean through the surface ocean layer and allow the plants to extract the phosphorus, a loss to the sediment of 1 percent of the phosphate in the ocean will ensue.

As we will see from the ^{14}C distribution in the ocean (to be discussed in chapter 5), the time required for one mixing cycle is about 1000 years. Every 1000 years, the entire amount of any given constituent in the ocean is sent through the surface water mill. To find the time, τ , required to remove an amount of a constituent equal to that stored in the sea, we divide the mixing time, T_{mix} , by the product of $f \times g$. In equation form:

$$\tau = \frac{T_{\text{mix}}}{fg} = \frac{1000}{fg} \text{ years}$$

1-12

Since phosphate is removed at the rate of 1 percent every mixing cycle ($f \times g = 0.01$), the average lifetime of a P atom in the ocean must be about 100,000 years. The results of these calculations for the phosphorus are summarized in table 1-4. In words, a typical P atom, upon release to solution from some sedimentary or metamorphic rock by erosion, is carried by rivers to the sea. It then goes through an average of 100 oceanic mixing cycles: 100 times surface dwelling organisms fix it into a particle that sinks and is destroyed in the deep sea. Each time, it waits in the dark abyss about 1000 years before being sent back to the surface. On the average, during the hundredth cycle, the particle bearing the P atom survives destruction and is trapped in the sediment. So our P atom makes 100 round trips of 1000 years each during its stay in the ocean. It then becomes part of the sediment, where it remains for about 100 million years until it is uplifted and exposed again to continental erosion. The life of a typical P atom is by human standards indeed bleak. It spends 99.9 percent of its time trapped in the sedimentary rocks of the earth. Out of every 100,000,000 years it has only one 100,000 year stint in the ocean. Since the volume of the surface water reservoir is small compared to that of the deep water reservoir, the P atom spends most of its ocean stints in the cold dark abyss. Out of every 1000 years spent in the sea only a few years are spent in warm surface water!*

*The volume of the warm reservoir (plus one half of the main thermocline) is only about one-tenth that of the cold reservoir (plus the other half of the thermocline). As water resides in the cold reservoir for 1000 years, it must reside in the warm reservoir about 100 years. Since the concentration of P in the warm reservoir is only 5 percent of that in the cold, the probability that P is removed by particulate matter must exceed the probability that P is removed by downwelling water by a factor of 20. The removal time of P from the warm reservoir must then be 20 times shorter than that of its companion water molecules. Thus the residence time of a P atom in the warm reservoir is only about 5 years.

Table 1-4. Example calculations for the constituents phosphorus, barium, and calcium.

Phosphorus	Barium	Calcium
$f = \frac{1}{1 + \frac{v_{mix}}{v_{river}} \left[\frac{C_{deep}}{C_{river}} - \frac{C_{surface}}{C_{river}} \right]}$		
$\frac{1}{1 + 30(3-0.15)} = 0.01$	$\frac{1}{1 + 30(0.3-0.1)} = 0.14$	$\frac{1}{1 + 30(25-24.8)} = 0.14$
$g = 1 - \frac{\frac{v_{mix}}{v_{river}} \frac{C_{surface}}{C_{river}}}{1 + \frac{v_{mix}}{v_{river}} \frac{C_{deep}}{C_{river}}}$		
$1 - \frac{30 \times 0.15}{1 + (30 \times 3)} = 0.95$	$1 - \frac{30 \times 0.1}{1 + (30 \times 0.3)} = 0.70$	$1 - \frac{30 \times 24.8}{1 + (30 \times 25)} = 0.01$
$f \times g = \frac{1}{1 + \frac{v_{mix}}{v_{river}} \frac{C_{deep}}{C_{river}}}$		
$\frac{1}{1 + (30 \times 3)} = 0.01$	$\frac{1}{1 + (30 \times 0.3)} = 0.10$	$\frac{1}{1 + 30 \times 25} = 0.0013$
$\tau = \frac{T_{mix}}{f \times g}$		
$\frac{1000}{0.01} = 1 \times 10^5$	$\frac{1000}{0.10} = 1 \times 10^4$	$\frac{1000}{0.0013} = 8 \times 10^5$

Table 1-5. Summary of model parameters for the elements P, Si, Ba and Ca

Category	Element	$C_{surface}$	C_{deep}	g	f	$f \times g$	τ yrs
		C_{river}	C_{river}				
Biolimiting	P	0.15	3.0	0.95	0.01	0.01	1×10^5
	Si	0.02	0.7	0.97	0.05	0.05	2×10^4
Biointermediate	Ba	0.1	0.3	0.70	0.14	0.10	1×10^4
	Ca	24.8	25	0.01	0.14	0.0013	8×10^5

If we are given the values for f and g for a particular constituent, we can determine the ratio of its concentration in surface water to that in river water, in deep water to that in river water, and in surface water to that in deep water. To do this, we must solve our equations for the concentration ratios in terms of f, g, v_{river} , and v_{mix} . The resulting equations are:

$$\frac{C_{\text{surface}}}{C_{\text{river}}} = \frac{1 - g}{fg} \quad \frac{v_{\text{river}}}{v_{\text{mix}}} \quad 1-13$$

$$\frac{C_{\text{deep}}}{C_{\text{river}}} = \frac{1 - fg}{fg} \quad \frac{v_{\text{river}}}{v_{\text{mix}}} \quad 1-14$$

$$\frac{C_{\text{surface}}}{C_{\text{deep}}} = \frac{1 - g}{1 - fg} \quad 1-15$$

Sample calculations for phosphorus, barium and calcium are shown in table 1-4 and a summary of the values of f and g obtained for these three constituents and for silicon are given in table 1-5.

THE DISTRIBUTION OF BIOINTERMEDIATE CONSTITUENTS

Biointermediate elements merit a bit more discussion. If the composition of marine organic material is nearly constant then the surface water residuals for these elements should be nearly the same from place to place in the warm surface ocean. As can be seen in figure 1-6 this is to a good approximation the case for carbon and for barium. The variability from one place to another in surface waters between the latitudes 40°N and 40°S is small compared to the difference between the concentrations of these constituents in mean warm surface and mean deep water. It thus appears that these constituents are taken up by plants in a constant proportion to phosphorus and when phosphorus has been depleted their concentrations cease to change.

One element, selenium, in the biointermediate category, has a geochemical complexity not shared by its brothers.

As shown in figure 1-7 Measures and his colleagues at MIT found that selenium is partially depleted in surface waters. Measures made separate determinations of total selenium and of selenium in the +4 state (the concentration of +6 selenium could then be determined by difference.) As shown in figure 1-7 the concentration of Se+4 in surface water drops nearly to zero, while that of Se+6 drops to 35% of its ambient deep water value. Measures points out that the shape of the depth profile of Se+4 resembles that of PO₄ and the shape of the Se+6 profile resembles that of H₄SiO₄ and infers that Se+4 is incorporated in organic tissue and Se+6 in opal.

Like many oxidation-reduction reactions those for selenium are kinetically impeded. Measures points out that neither the ratio of Se+4 to Se+6 in surface water nor that in deep water corresponds to the equilibrium thermodynamic ratio for the ambient O₂ contents of these waters. Hence he tentatively concludes that

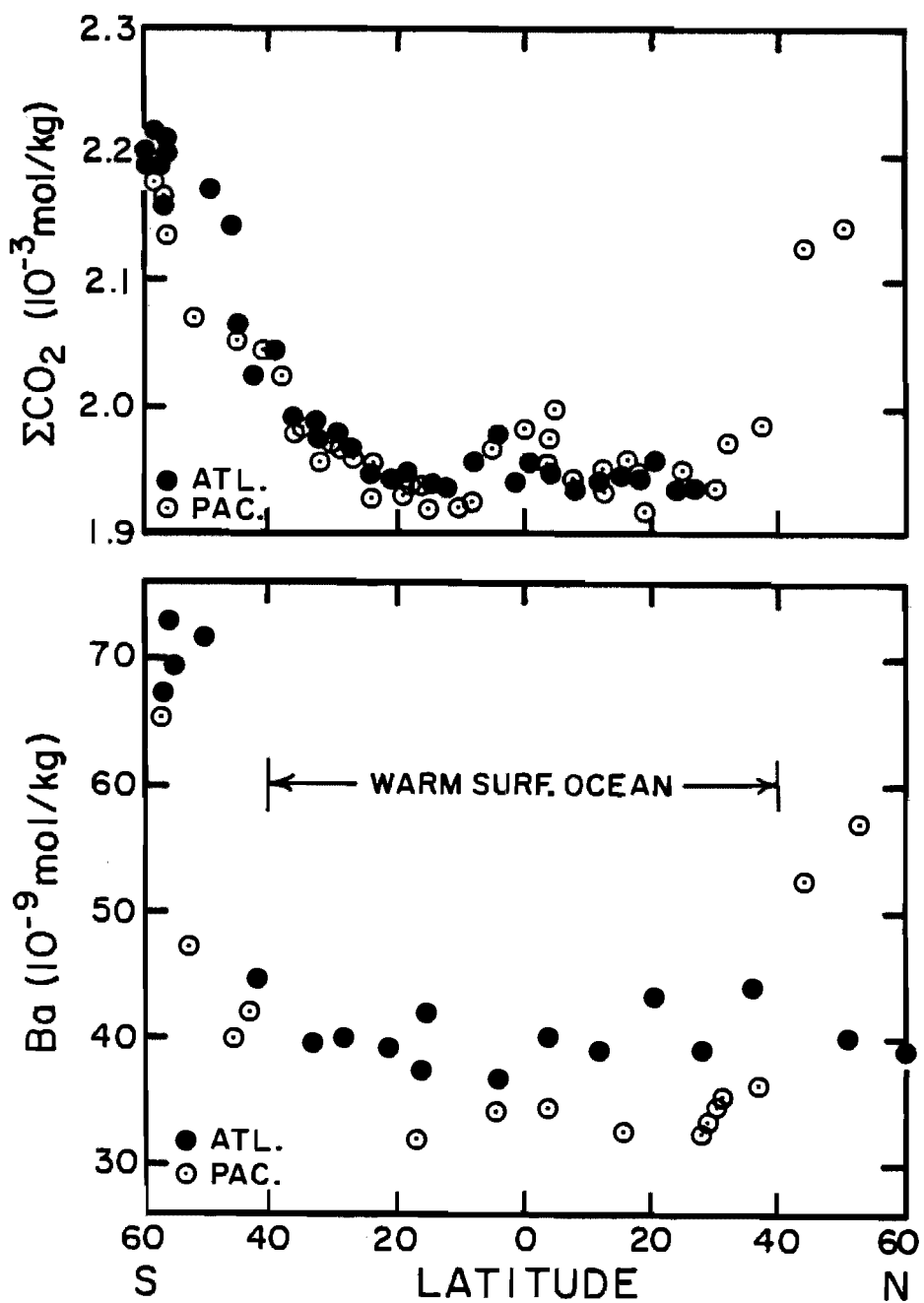


Figure 1-6. Plots of the barium and total dissolved inorganic carbon (normalized to constant salinity) in surface waters as a function of latitude. The values for warm surface water (40°N to 40°S) are remarkably constant. These results were obtained as part of the GEOSECS program. The barium measurements were made by John Edmond at M.I.T. and L.H. Chan at L.S.U. (375). The total dissolved inorganic carbon results were obtained by shipboard titration (406).

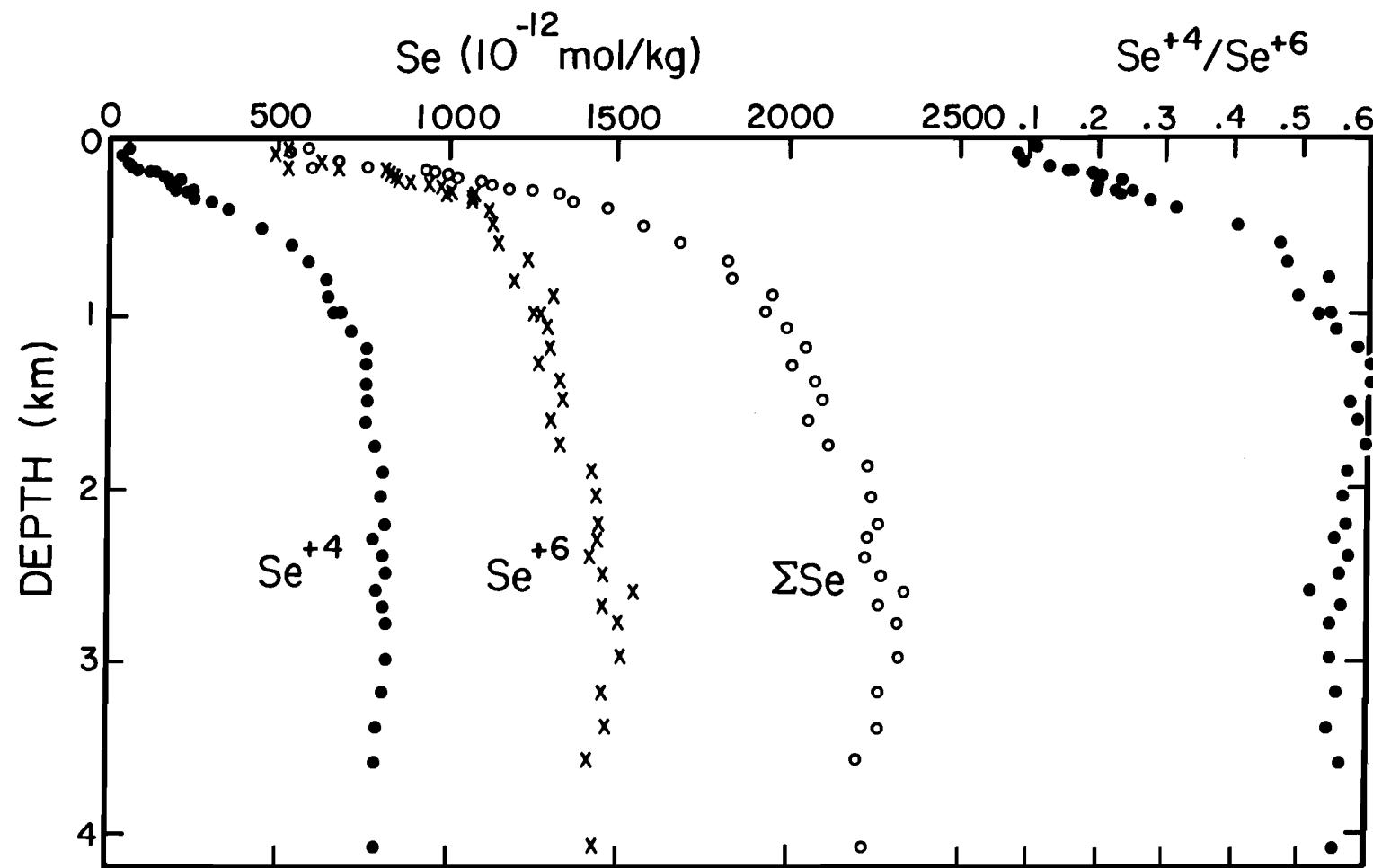


Figure 1-7. Plot of total selenium versus depth in the northeastern Pacific Ocean (29°N , 122°W). Also shown are the concentrations of selenium in the two oxidation states of this element (i.e. +4 and +6). These measurements were made by Measures and his coworkers at MIT (451).

some types of organisms must irreversibly transform Se+6 to Se+4 and others Se+4 to Se+6. Since about one third of the selenium in the ocean is in the Se+4 oxidation state and two thirds in the Se+6 oxidation state the ocean-wide reduction probability must be about one half the ocean-wide oxidation probability.

ESTIMATION OF INPUT RATES

Thus far we have not mentioned how the estimates of the concentration of elements in average river water is determined. As it turns out these estimates are not so easily obtained. There are several reasons for this.

- 1) The reliability of many of the analyses of at least the trace constituents in river waters is open to question.
- 2) Man's activities have changed the chemistry of many rivers.
- 3) The dissolved concentration of a constituent in river water may not be an adequate measure of the input of this constituent to the sea. Some constituents may be carried in organic tissues which will decompose in the ocean. Others will partially precipitate in the estuaries. Others will desorb from silicate detritus in estuaries.
- 4) Rivers differ from one another in their chemistry. A given river may have a different chemistry during flood stages than during low water periods. Thus averaging is not easy.

Despite these difficulties attempts have been made to assess the average input rate of a larger number of elements to the sea. These estimates are summarized in table 1-6. This table also gives estimates of the mean concentrations of these elements in sea water. For those elements where both pieces of information are available residence times (i.e., mean ocean concentration multiplied by ocean volume divided by mean river concentration multiplies by annual river flux) are also given. The entries in this table are taken from standard compilations and do not always agree exactly with the ones employed in this chapter. As none of the input rates are known to better than 20% these minor differences are not significant.

In our discussion and in table 1-6 the rate of input to the sea of the various constituents of seasalt is determined by measurements of their concentration in river water. This approach is not always reliable. Estimates can also be made from the rate of accumulation of the constituent on the sea floor. Phosphorus provides a good example. The historical data on phosphate in rivers is sketchy and often inaccurate. Present day rivers carry excess phosphate released from agricultural land and from sewage plants and some of the phosphorus carried by rivers is a constituent part of living organisms and their residues and hence is not included in analyses of soluble phosphate. Thus estimates of the steady state rate of phosphorus addition based on river data are very uncertain. An alternate estimate can be made by considering the rate at which phosphorus has been removed from the sea into marine sediments during the last several thousand years. This is done by measuring the accumulation rate and phosphorus content of various

Table 1-6. Element concentrations in average river water and in average ocean water. Also given are the corresponding mean oceanic residence times.

Atomic No.	Element	Conc. Mean River ¹ (10^{-6} moles/kg)	Conc. Mean Sea ² (10^{-6} moles/kg)	τ ³ (yrs)
1	H (as H ₂ O)	-	5.4×10^7	-
2	He	-	1.8×10^{-3}	-
3	Li	1.7	2.5×10^1	5.7×10^5
4	Be	-	(6.5×10^{-5})	-
5	B	1.7	4.2×10^2	9.6×10^6
6	C (inorganic) (organic)	-	2.3×10^3	-
7	N (dissolved N ₂) (NO ₃)	-	5.8×10^2	-
8	O (as H ₂ O) (dissolved O ₂)	-	3.0×10^1	-
9	F	*5.3	5.4×10^7	-
10	Ne	-	2.2×10^2	6.8×10^1
11	Na	-	7.5×10^{-3}	8.3×10^7
12	Mg	-	1.6×10^2	5.3×10^4
13	Al	-	(3×10^{-2})	1.3×10^2
14	Si	-	1.9×10^2	6.2×10^2
15	P	-	1.0×10^2	2.0×10^4
16	S	-	1.3	6.9×10^4
17	Cl	-	2.8×10^4	-
18	Ar	-	5.5×10^5	-
19	K	-	1.5×10^1	1.5×10^1
20	Ca	-	10.2×10^3	1.2×10^7
21	Sc	-	3.6×10^2	10.3×10^3
22	Tl	-	8.9×10^{-5}	(1.5×10^{-5})
23	V	-	2.1×10^{-1}	$(<2.0 \times 10^{-2})$
24	Cr	-	2.0×10^{-2}	2.3×10^{-2}
25	Mn	-	1.9×10^{-2}	4×10^{-3}
26	Fe	-	1.5×10^{-1}	10^{-3}
27	Co	-	7.2×10^{-1}	(1×10^{-3})
28	Ni	-	3.4×10^{-3}	(3×10^{-5})
29	Cu	-	3.8×10^{-2}	8×10^{-3}
30	Zn	-	1.6×10^{-1}	4×10^{-3}
31	Ga	-	4.6×10^{-1}	6×10^{-3}
32	Ge	-	1.3×10^{-3}	(3×10^{-4})
33	As	-	7×10^{-5}	-
34	Se	-	2.3×10^{-2}	2.3×10^{-2}
35	Br	-	2.3×10^{-3}	1.7×10^{-3}
36	Kr	-	2.5×10^{-1}	8.4×10^2
37	Rb	-	1.4	3.4×10^{-3}
38	Sr	-	1.8×10^{-2}	1.4
39	Y	-	6.9×10^{-1}	8.7×10^1
40	Zr	-	$*7.9 \times 10^{-3}$	(1.5×10^{-4})
41	Nb	-	-	(3×10^{-4})
42	Mo	-	5.2×10^{-3}	$(<5 \times 10^{-5})$
				-
				1.1×10^{-1}
				8.2×10^5

Table 1-6. (continued)

Atomic No.	Element	Conc. Mean River ¹ (10^{-6} moles/kg)	Conc. Mean Sea ² (10^{-6} moles/kg)	τ^3 (yrs)
43	Tc	-	-	-
44	Ru	-	-	-
45	Rh	-	-	-
46	Pd	-	-	-
47	Ag	2.8×10^{-3}	(2.5×10^{-5})	3.5×10^2
48	Cd	-	7×10^{-4}	-
49	In	-	(1×10^{-6})	-
50	Sn	-	(4×10^{-6})	-
51	Sb	8.2×10^{-3}	1.2×10^{-3}	5.7×10^3
52	Te	-	-	-
53	I	$*5 \times 10^{-2}$	4.4×10^{-1}	3.4×10^5
54	Xe	-	5.0×10^{-4}	-
55	Cs	2.6×10^{-4}	2.2×10^{-3}	3.3×10^5
56	Ba	4.4×10^{-1}	1.0×10^{-1}	8.8×10^3
57	La	3.6×10^{-4}	3×10^{-5}	3.2×10^3
58	Ce	5.7×10^{-4}	2×10^{-5}	1.4×10^3
59	Pr	5.0×10^{-5}	4×10^{-6}	3.1×10^3
60	Nd	2.8×10^{-4}	2×10^{-5}	2.8×10^3
61	Pm	-	-	-
62	Sm	5.3×10^{-5}	4×10^{-6}	2.9×10^3
63	Eu	6.6×10^{-6}	9×10^{-7}	5.3×10^3
64	Gd	5.1×10^{-5}	6×10^{-6}	4.6×10^3
65	Tb	6.3×10^{-6}	9×10^{-7}	5.6×10^3
66	Dy	$*3.0 \times 10^{-4}$	6×10^{-6}	7.8×10^2
67	Ho	6.1×10^{-6}	2×10^{-6}	1.3×10^4
68	Er	2.4×10^{-5}	5×10^{-6}	8.1×10^3
69	Tm	5.9×10^{-6}	8×10^{-7}	5.3×10^3
70	Yb	2.3×10^{-5}	5×10^{-6}	8.5×10^3
71	Lu	5.7×10^{-6}	9×10^{-7}	6.2×10^3
72	Hf	-	$(<4 \times 10^{-5})$	-
73	Ta	-	$(<1.4 \times 10^{-5})$	-
74	W	$*1.6 \times 10^{-4}$	6×10^{-4}	-
75	Re	-	(2×10^{-5})	-
76	Os	-	-	-
77	Ir	-	-	-
78	Pt	-	-	-
79	Au	1.0×10^{-5}	(2.5×10^{-5})	9.7×10^4
80	Hg	$*3.5 \times 10^{-4}$	(5×10^{-6})	5.6×10^2
81	Tl	-	6×10^{-5}	-
82	Pb	4.8×10^{-3}	1×10^{-5}	8.1×10^1
83	Bi	-	(1×10^{-4})	-
90	Th	-	$(<3 \times 10^{-6})$	-
92	U	$\sim 1 \times 10^{-3}$	1.3×10^{-2}	$\sim 5 \times 10^5$

¹Main source: A summary by Martin and Meybeck (631) with values for F, Se, Y, I, Dy, W, and Mg, values with * are taken from Turekian (628).

²Main source: A summary by Bruland (456). The values in parenthesis are highly uncertain.

³The residence time is obtained by dividing the total amount of the element dissolved in the sea by the amount delivered by rivers each year.

types of marine sediments (see table 1-7). If the input and output rates are equal, the mean phosphorus content of river water can then be estimated. Froelich, who has carried out the most detailed analysis of this sort, concludes that 3.5×10^{15} moles of phosphorus are dissolved in the sea and that its sedimentation rate is about 3.5×10^{10} moles of phosphorus per year. The residence time obtained in this way is 100,000 years (the value used in our discussion of phosphorus). It is of interest to note that while 80% of the phosphorus leaves the ocean with biologic remains (in keeping with our first order model) half of this phosphorus is bound in CaCO_3 rather than in organic tissue.

A similar problem exists with the river based estimates for carbon. Much of the bicarbonate ion dissolved in river water originates from atmospheric CO_2 which neutralizes the bases produced during rock weathering processes. This CO_2 is recycled ocean-atmosphere carbon rather than new carbon being added by weathering or volcanism. While means are available for correcting for the contribution of recycled carbon they are not entirely adequate. Again sediment accumulation rates of carbon can be used to provide an independent cross-check. Using this approach Froelich obtains a carbon residence time of 180,000 years (634).

HORIZONTAL SEGREGATION OF CONSTITUENTS IN THE DEEP SEA

The simple two box model of ocean chemistry has permitted us to describe in a quantitative manner the primary features of the marine chemistry for biologically utilized constituents. In the real world the concentration of a given constituent shows considerable geographic and depth variability in the cold ocean. As shown in figures 1-1 and 1-2 the concentrations of the biologically active constituents increase with depth in the North Pacific to a mid-depth maximum and then decrease somewhat toward the bottom. This type of profile characterizes the Pacific and Indian Oceans (to about 40°S). In the Antarctic Ocean the profiles show much less structure. In the Atlantic the concentrations of these constituents increase all the way to the bottom.

Figures 1-8, 1-9, 1-10 and 1-11 show the geographic patterns of the concentrations of H_4SiO_4 , Ba^{++} , NO_3^- and O_2 along the 4000 meter depth horizon. For several reasons these maps do not have a familiar look. First, were the oceans drained to a depth of 4000 meters, their geography would look quite different. The mid-ocean ridges would rise above the surface and would divide the Atlantic into two separate oceans, the Indian Ocean would be divided into a series of basins and the Pacific into a major and a minor basin. The continents would be larger and the oceans smaller. Hence the shapes of the margins of the 4000-meter horizon do not closely resemble the margins of the present ocean. Further, in order to make these maps page size, we have stretched the distance between latitude lines by a factor of two. Finally, we have not compensated for the poleward shortening of the distance around the globe on a given latitude. This makes the polar oceans look too large and the equatorial oceans too small.

As can be seen on these maps, the concentration of the nutrient constituents increase "down" the Atlantic and "up" the Pacific

Table 1-7. Summary of phosphorus burial rates in marine sediments as obtained by Froelich and his coworkers (634).

Form	Burial rate 10^{-9} moles cm 2 yr	Burial rate 10^9 moles yr
Organic matter	4	14
CaCO ₃	4	14
Hydrothermal	1	4
Phosphorite	<1	<4
Fish debris	<u><0.2</u>	<u><1</u>
TOTAL	~10	~35

Table 1-8. Horizontal segregation of biologically utilized constituents between the deep North Atlantic and the deep North Pacific. To permit meaningful calculations for the biointermediate elements, carbon and barium, only the deep water excess is considered. Note that the horizontal segregation is more pronounced for those elements incorporated into hard parts (silicon and barium) than for those incorporated into soft parts (nitrate and phosphate).

Constituent	$\frac{(C_{\text{deep}} - C_{\text{surface}})_{\text{Pacific}}}{(C_{\text{deep}} - C_{\text{surface}})_{\text{Atlantic}}}$
NO ₃	2
PO ₄	2
H ₄ SiO ₄	5
Ba	4

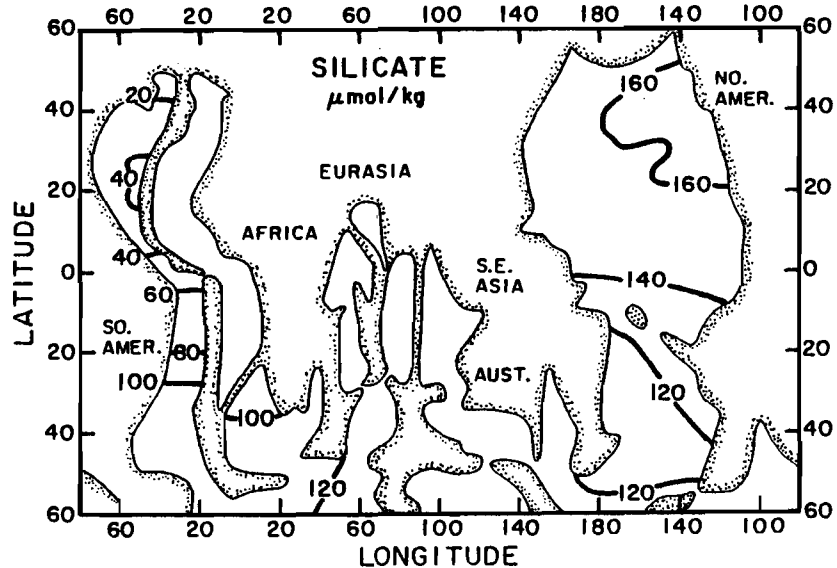


Figure 1-8. Distribution of dissolved silicate at 4000 meters depth in the world's major ocean basins. The boundaries of the ocean are those at which the 4000 meter horizon abuts the sediment. The Atlantic Ocean basins are on the left, the Indian Ocean basins in the center and the Pacific Ocean is on the right. Based on results obtained during the GEOSECS program (424, 425, 426).

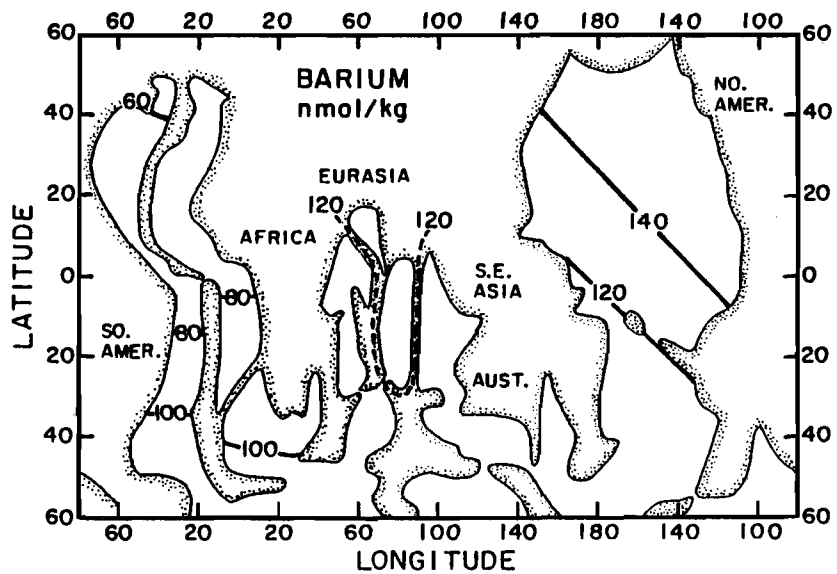


Figure 1-9. Distribution of dissolved barium at a depth of 4000 meters in the world's major ocean basins. Based on results obtained by John Edmond of M.I.T. and L.H. Chan of L.S.U. on GEOSECS samples (375).

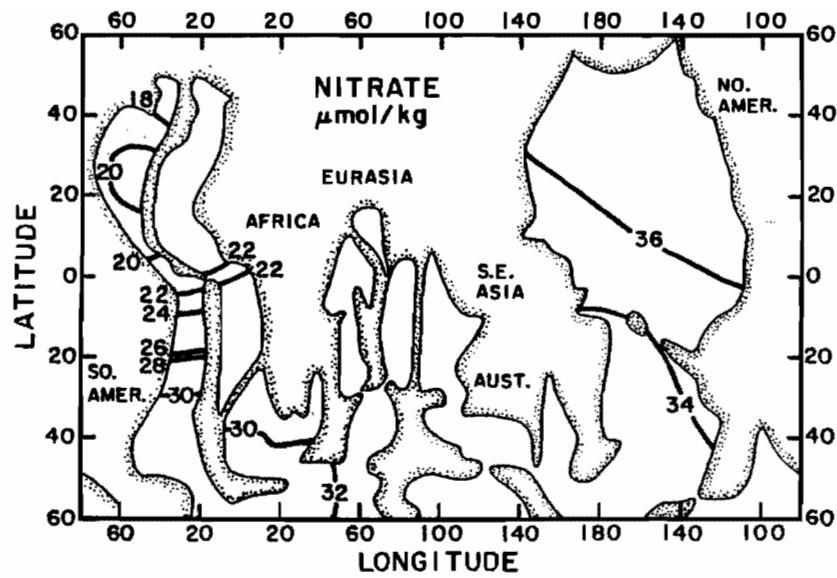


Figure 1-10. Distribution of dissolved nitrate at a depth of 4000 meters in the world's major ocean basins. Based on results obtained during the GEOSECS program (424, 425, 426).

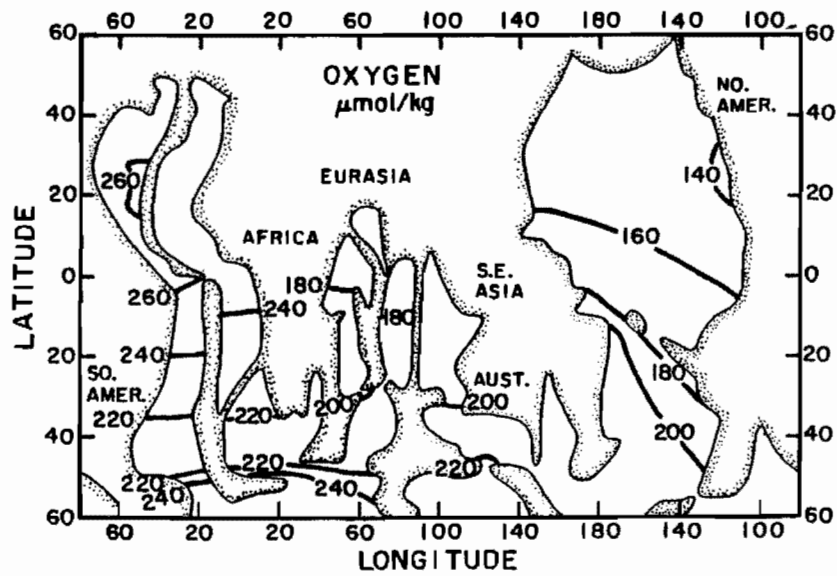


Figure 1-11. The distribution of dissolved oxygen of 4000 meters depth in the world's major ocean basins. Based on results obtained during the GEOSECS program (424, 425, 426).

and Indian Oceans. Dissolved oxygen has, as expected, the reverse sequence of concentrations. Like the vertical distributions, the horizontal distributions of these properties have similar major structures. However, the details differ from property to property. For example, oxygen shows a strong maximum along the margin of the Antarctic continent. Equivalent minima are not seen for nitrate or silicate. As shown in table 1-8, the Pacific to Atlantic enrichment of the biologically utilized constituents is different for the hard-part constituents than for the soft-part constituents.*

The difference between the enrichment of these biologically active constituents in the deep Pacific and in the deep Atlantic depends on the deep water circulation pattern in the world ocean. About half the water being fed into the deep ocean is generated at the northern end of the Atlantic Ocean. As shown in figure 1-12 this water flows down the western Atlantic. It enters the eastern Atlantic through a break in the Mid-Atlantic Ridge located close to the equator. It enters the Antarctic through the southern end of the western basin of the South Atlantic and joins the eastward flowing circumpolar current. Part of the water in this circumpolar current penetrates northward into the basins of the Pacific; part passes through the Drake passage and starts a second trip around the Antarctic continent.

There is one major complication: the circumpolar flow is joined by water which has been re-cooled at the surface of the Antarctic Ocean. This cold water sinks along the margin of the Antarctic adjacent to the South Atlantic. Thus it is a mixture of this re-cooled water and water emerging from the Atlantic that flows into the Indian Ocean and into the Pacific Ocean. As we shall see, the water formed in the Weddell Sea area of the Antarctic continental margin is virtually unmodified in its nutrient constituent concentration.

Oceanographers tell us that the production of new deep water is balanced by the upwelling of water to the surface throughout the world ocean. With this in mind, it is not difficult to see why there is a tendency for a biologically active element to be enriched in deep Pacific water relative to deep Atlantic water. Plant activity has partially depleted these nutrients in surface water sinking into the deep Atlantic. As this water passes through the Atlantic, particles bearing these biolimiting constituents fall into it from the surface. Its nutrient content is thereby increased. This enrichment process continues as the water moves into the Indian and Pacific deeps. As it proceeds along its path (see figure 1-13), the current is continually weakened by upwelling. The water lost in this way returns via surface currents to the deep water source region (the Norwegian Sea). The nutrients, however, are extracted by organisms and returned to the abyss in particulate form.

*These enrichment factors are calculated by subtracting the surface water concentration for a given constituent from its deep water concentration and dividing this difference for the North Pacific by that for the western North Atlantic.

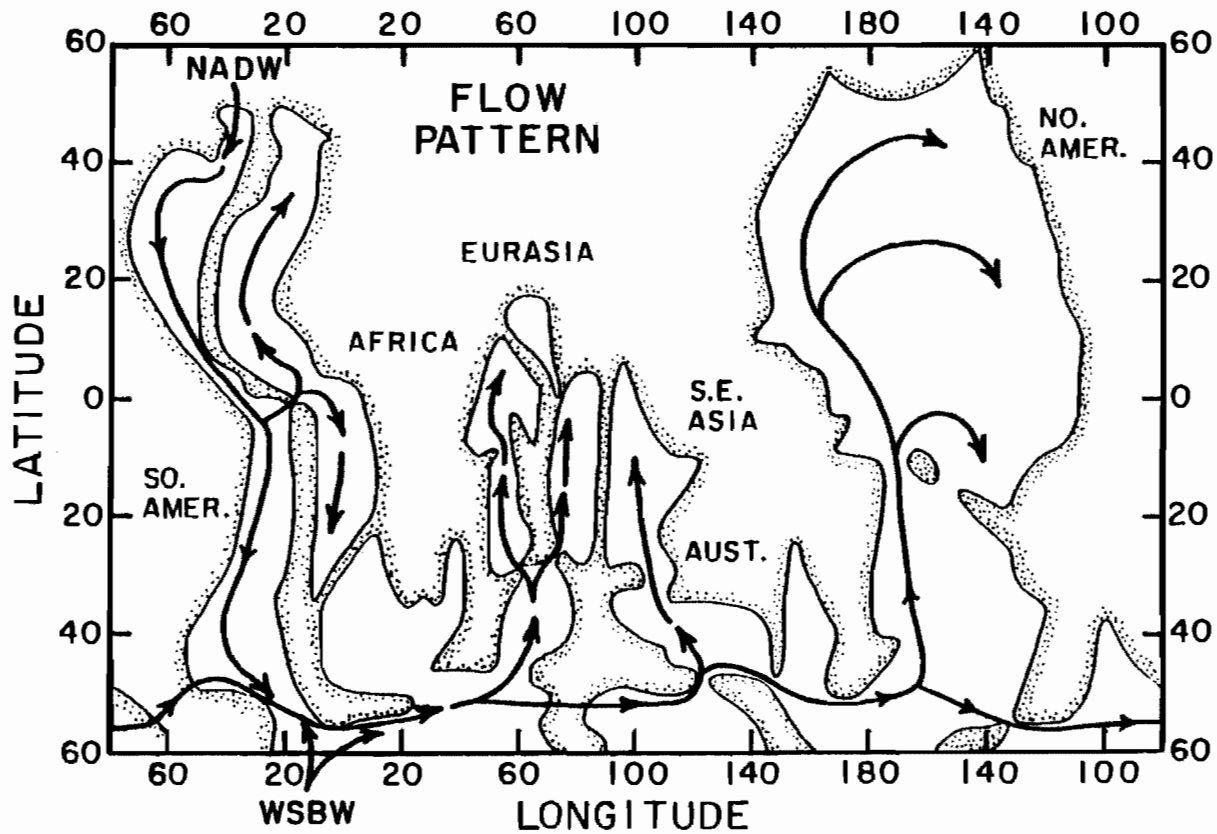


Figure 1-12. Flow pattern at a depth of 4000 meters. The major inputs to this horizon are North Atlantic Deep Water (NADW) which enters at the northern end of the western basin of the Atlantic and Weddell Sea Bottom Water (WSBW) which enters from the margin of the Antarctic continent adjacent to the South Atlantic.

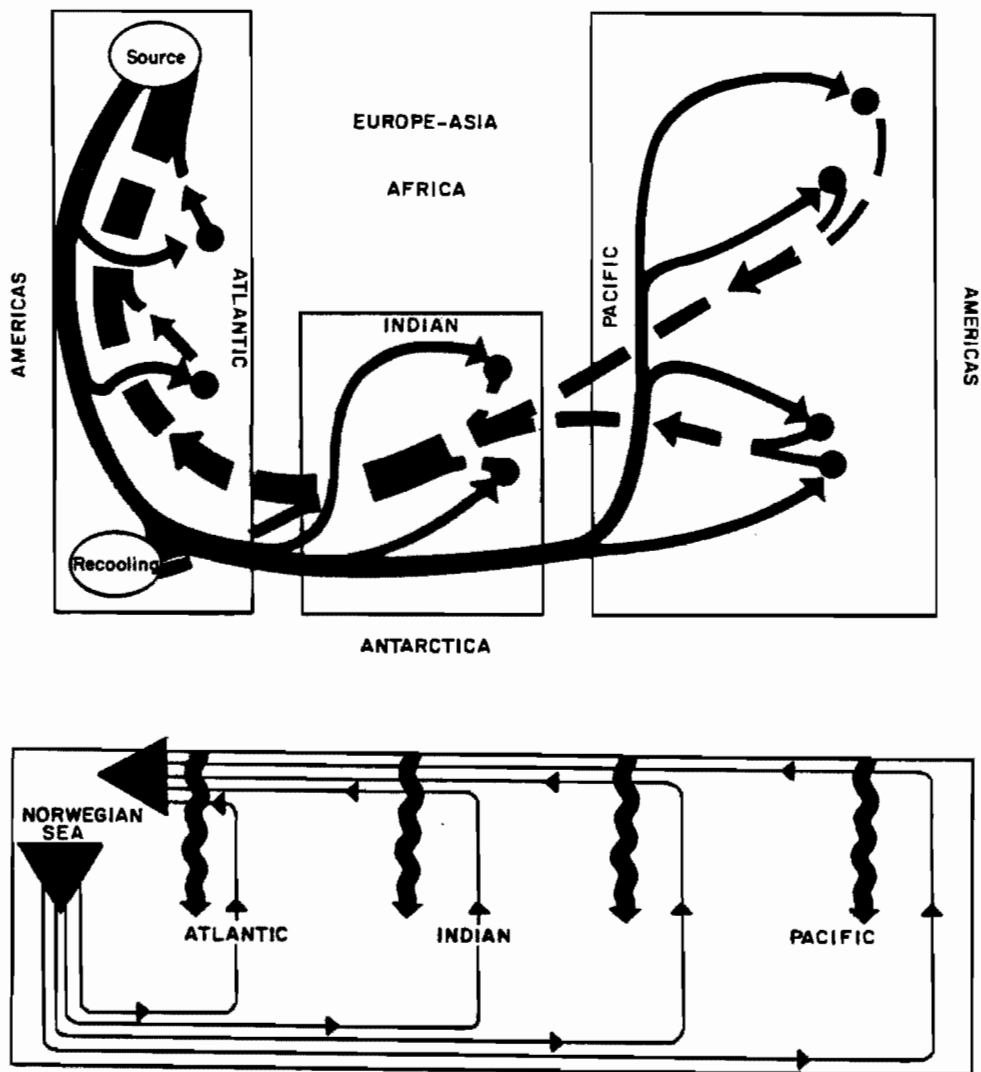


Figure 1-13. The upper diagram is an idealized map of the patterns of deep water flow (solid lines) and surface water flow (dashed lines). The large circles designate the sinking of NADW in the Norwegian Sea and the recooling of water along the perimeter of the Antarctic Continent; the shaded circles indicate the distributed upwelling which balances this deep water generation. The lower diagram is an idealized vertical section running from the North Atlantic to the North Pacific showing the major advective flow pattern (solid lines) and the rain of particles (wavy lines).

The net result is a steady push of nutrients toward the deep Pacific. They can ride the deep current away from the Atlantic but not the returning surface current. This creates an increase in nutrient content along the path of the deep current. The gradient has become sufficiently steep so that horizontal mixing at depth moves the nutrients back toward the Atlantic as fast as they can be exported by the deep current. Thus a dynamic balance is achieved which stabilizes the Pacific-ward concentration gradient. It is the interaction between oceanic circulation and biologic activity that generates the enrichment of these elements in the waters of the deep Pacific relative to those of the deep Atlantic.

An analogy will clarify the essentials of this cycle. The exhibits in a fun house are located on two levels. The upper floor has a large conveyor belt that moves from right to left; the lower floor, a belt that moves from left to right. Those who enter are free to observe the horrors in any order they wish. There are innumerable escalators from the lower to the upper level. However, there is only one escalator from the upper to the lower level, located at the end of the upper belt. Those who venture to the upper level are harassed by monsters lurking in dark alcoves. These monsters grab the unsuspecting visitors and, after a suitable frightening, drop them through holes to the lower level. The average fun-seeker has to ride to the upper level many times to view all its mysteries before leaving the fun house.

If, on a busy Sunday afternoon, we were to snap on the lights suddenly and photograph the distribution of people, we would find many more fun-seekers downstairs than up (the untiring monsters quickly track down those who step from the escalator tops and promptly throw them back down to the lower level, relatively close to their point of ascent). On the lower floor, more people would be at one end of the building than at the other (the steady movement of the lower-level belt would carry the wanderers toward the crowded end). As long as people remained in the fun house for a period covering several belt cycles, their distribution would not depend on where they entered or left. Rather it would depend on the speed of the belts and the efficiency of the monsters.

Obviously the fun-seeker is the limiting nutrient and the monster is the plant. The belts and escalators represent the organized flow of water, and the wandering of the people is the turbulent mixing superimposed on this organized flow. Although not perfect, this analogy does capture the important factors influencing the distribution of nutrients in the sea.

Now let us consider the more detailed features seen in the vertical profiles in figures 1-1 and 1-2 and in the horizontal distributions of properties at 4000 meters in figures 1-8, 1-9, 1-10, and 1-11. The mid-depth nutrient element maxima seen in the Pacific Ocean are generated by the general upwelling of bottom water combined with the progressive destruction of the particulate matter which falls from the surface into this rising column. This feature is absent in the Atlantic because of a strong along-bottom counterflow of water laden with nutrients from the Antarctic into the Atlantic. This along-bottom counterflow is possible because the deep water formed in the Weddell Sea is more dense than that formed at the northern end of the Atlantic. The fact that the

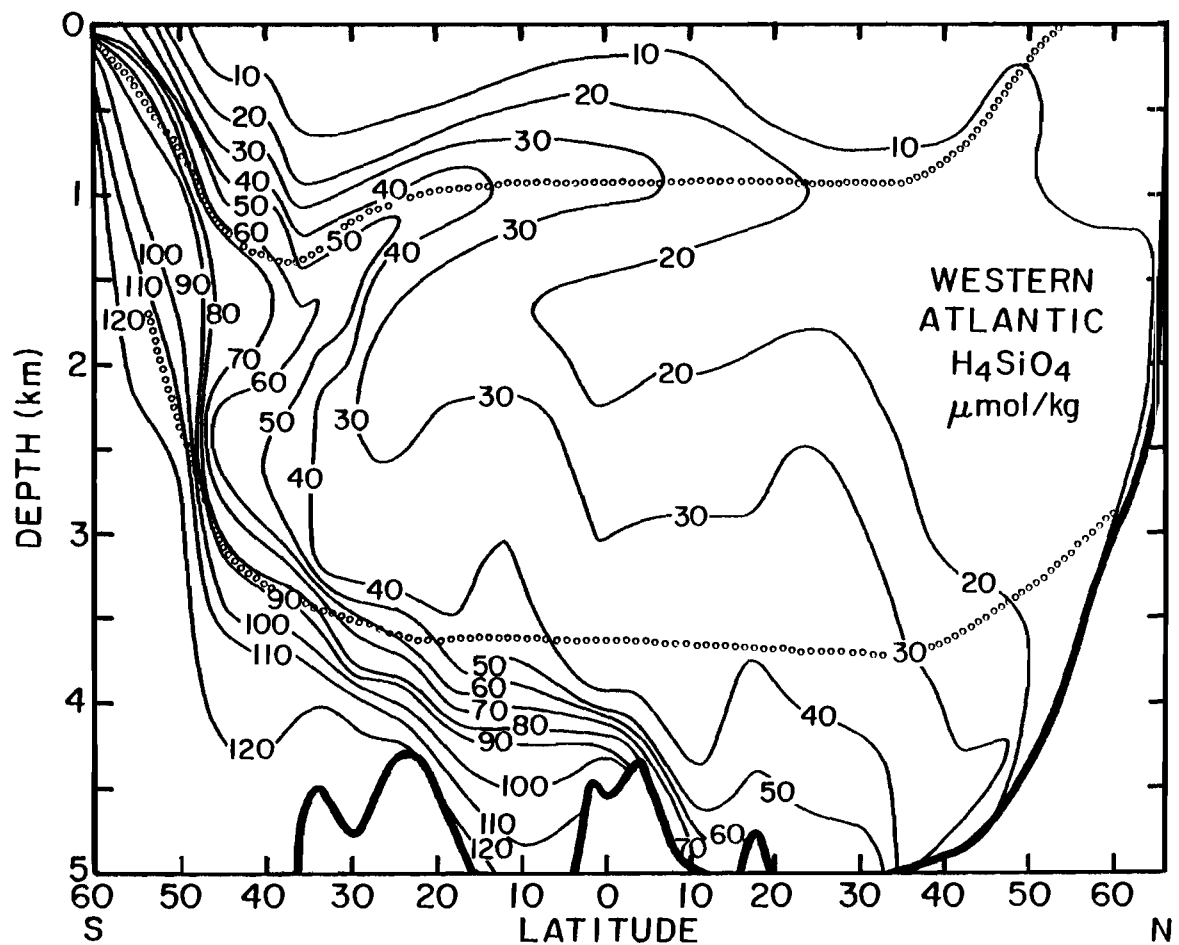


Figure 1-14. Vertical section along the western basin of the Atlantic Ocean showing the distribution of dissolved silicate. Contours are drawn at intervals of 10 micromoles per kilogram. The main features to be seen are the southward penetrating tongue of low silicate North Atlantic Deep Water, the northward penetrating wedge of high silicate Antarctic Bottom Water, the northward penetrating tongue of high silicate Circumpolar Intermediate Water, and the low silicate content of surface water everywhere except in the Antarctic. Two horizons of constant density are shown by the dotted lines (the upper is the $\sigma_0 = 27.0^{\circ}/\text{o}$ isopycnal and the lower the $\sigma_4 = 45.2^{\circ}/\text{o}$ isopycnal). In the Antarctic the concentration contours neatly parallel the density horizons. Based on results obtained during the GEOSECS program (424). The tracks along which this and subsequent sections are drawn can be seen on the foldout map.

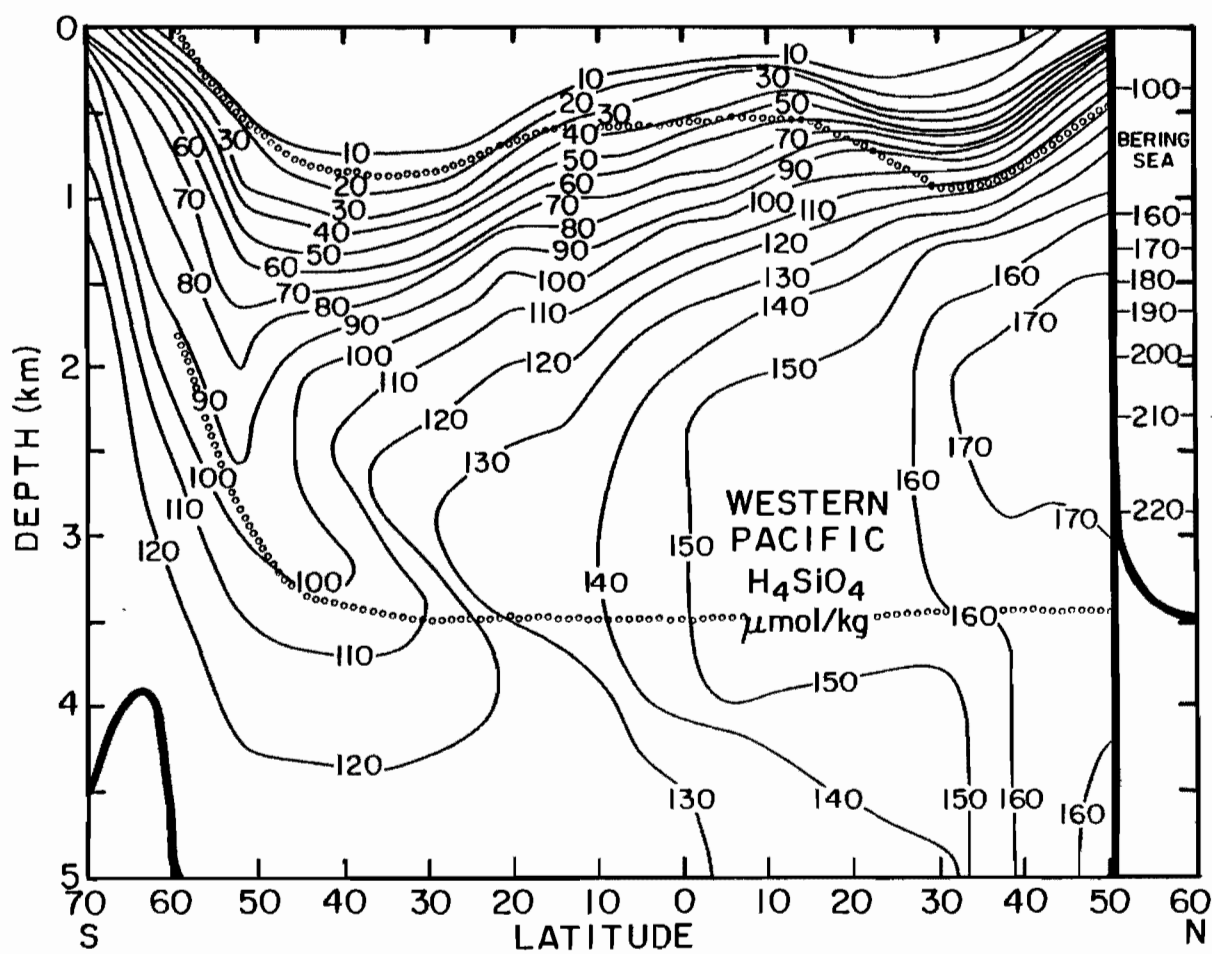


Figure 1-15. Vertical section along the western side of the Pacific Ocean showing the distribution of dissolved silicate. Contours are drawn at 10 micromoles per kilogram intervals. As for the Indian Ocean (see figure 1-17) the silicate content of deep water increases toward the north. Again a trough of low silicate water centered between 40 and 50°S is seen. Two horizons of constant potential density are shown by the dotted lines (the upper is the $\sigma_0 = 27.0^{\circ}/\text{oo}$ isopycnal and the lower is the $\sigma_4 = 45.2^{\circ}/\text{oo}$ isopycnal). Based on results obtained during the GEOSECS program (425).

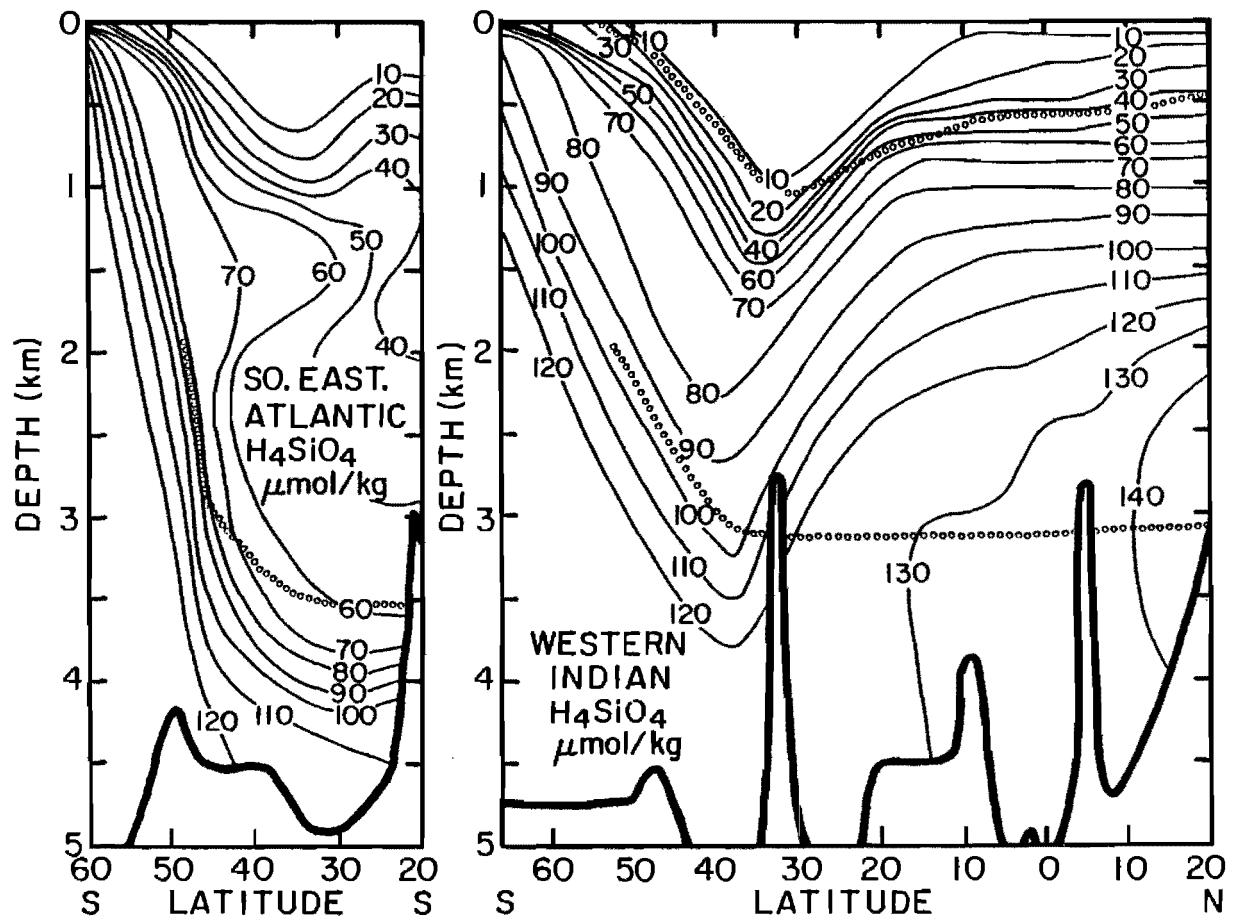


Figure 1-16. Vertical section of dissolved silicate concentration in the eastern Atlantic to the south of the Rio Grande Rise which isolates the deep eastern basin of the central Atlantic from the Antarctic Ocean. The low-silicate deep water on the right is the extension of the North Atlantic Deep Water tongue. It lies against the high-silicate circumpolar deep water which hugs the flank of the Antarctic continent. Again a horizon of constant potential density is shown by the dotted line (the $\sigma_4 = 45.2^{\circ}/oo$ isopycnal). Based on results obtained during the GEOSECS program (424).

Figure 1-17. Vertical section along the western basins of the Indian Ocean showing the distribution of dissolved silicate. Contours are drawn at 10 micromoles per kilogram intervals. By contrast to the sections for the Atlantic shown in figures 1-14 and 1-16 silicate concentrations in deep water increase northward of 40°S. A feature of interest is the trough of low silica content water between the latitudes of 30 and 50°S. It represents the continuation of the North Atlantic Deep Water tongue. Two horizons of constant potential density are shown by the dotted lines (the upper is the $\sigma_0 = 27.0^{\circ}/oo$ isopycnal and the lower is the $\sigma_4 = 45.2^{\circ}/oo$ isopycnal). Based on results obtained during the GEOSECS program (426).

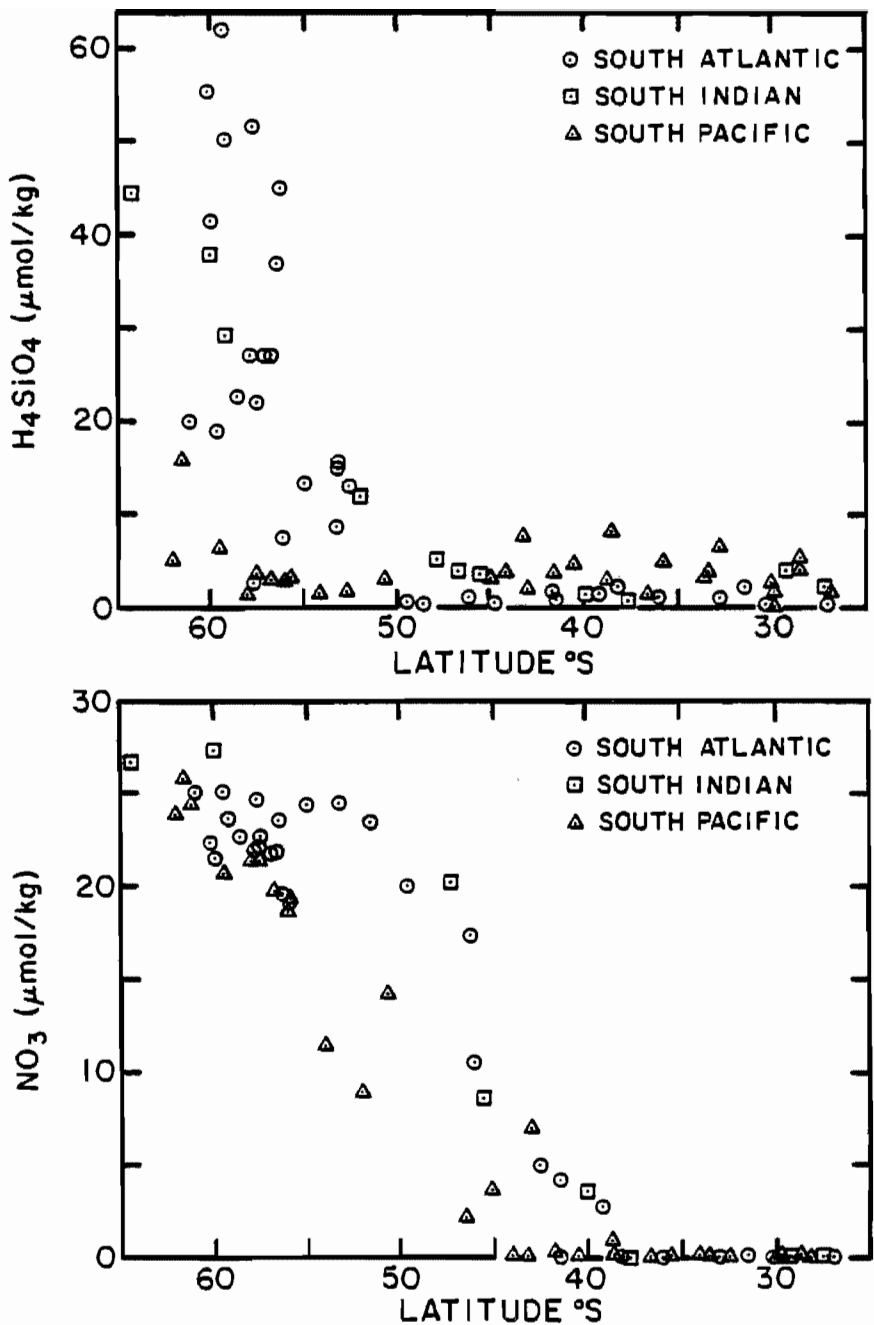


Figure 1-18. Dissolved silicate and nitrate content of surface water as a function of latitude in the southern oceans. Both constituents are found in low concentration in temperate surface waters and in high concentrations in Antarctic surface waters. The transition from the high to low values occurs at higher latitudes for silicate than for nitrate presumably reflecting the predominance of silicate utilizing plants (i.e., diatoms) in polar surface waters. Based on results obtained during the GEOSECS program (424, 425, 426).

mid-depth extrema are deeper for constituents carried in hard parts (i.e., H_4SiO_4 , alkalinity and barium) than in those carried in soft parts (i.e., NO_3 and PO_4) is the result of the fact that mineral solution occurs on the average at greater depths than respiration. This same factor accounts for the greater Pacific-ward enrichment of the products of hard part solution than for the products of respiration. The north-south sections of silica concentration for the three oceans shown in figures 1-14, 1-15, 1-16 and 1-17 nicely portray these features.

The high oxygen content of deep water found in the Antarctic adjacent to the Weddell Sea is a consequence of the input of new bottom water in this area. The absence of corresponding anomalies in NO_3 and H_4SiO_4 is, however, unexpected. The new deep water formed during the dark winter in the Weddell Sea is in contact with the atmosphere long enough to be cooled and long enough for dissolved oxygen to be replenished but does not lose a significant portion of its nutrient elements to plants.

Figure 1-18 (and also figure 1-6) clarify the distinction between cold and warm surface waters by showing that the nutrient content of high latitude surface water is more akin to that of deep water than to that of warm surface water. The nitrate values in surface water are all nearly zero until $40^{\circ}S$ is reached. Then, over the latitude range $40^{\circ}S$ to $55^{\circ}S$, they rise to the rather high values characteristic of polar waters. The silicate concentration is also low in temperate surface waters. These low silicate values of temperate surface waters extend to higher latitudes than do those for nitrate. This is consistent with the fact that diatoms dominate the plant communities found at high latitudes.

SUMMARY

In this chapter, two important aspects of marine chemistry have been discussed. First we have examined the factors controlling the distribution of the biologically utilized constituents within the sea. Because these species remain in the sea for times far longer than that required for the ocean to mix, their distributions do not reflect their points of entry to the sea or their points of removal from the sea. Rather their distribution reflects the interaction between the large-scale circulation pattern of the sea and the life cycle in the sea. The latter drives these constituents from surface to deep water. The former pushes them from the deep Atlantic around toward the deep northern Pacific. The differences in the vertical and horizontal distributions of these constituents are the result of differences in the depth to which the various particulate phases fall before being returned to solution. Some of these species are totally depleted in warm surface water; others are only partly depleted. The degree of depletion depends on the relationship between the biochemical demand and the ocean availability of the particular constituent.

Second we have examined the factors controlling the residence time of biologically important constituents in the ocean. We have shown that both the extent to which a constituent is depleted in warm surface water and the extent to which the phases so produced

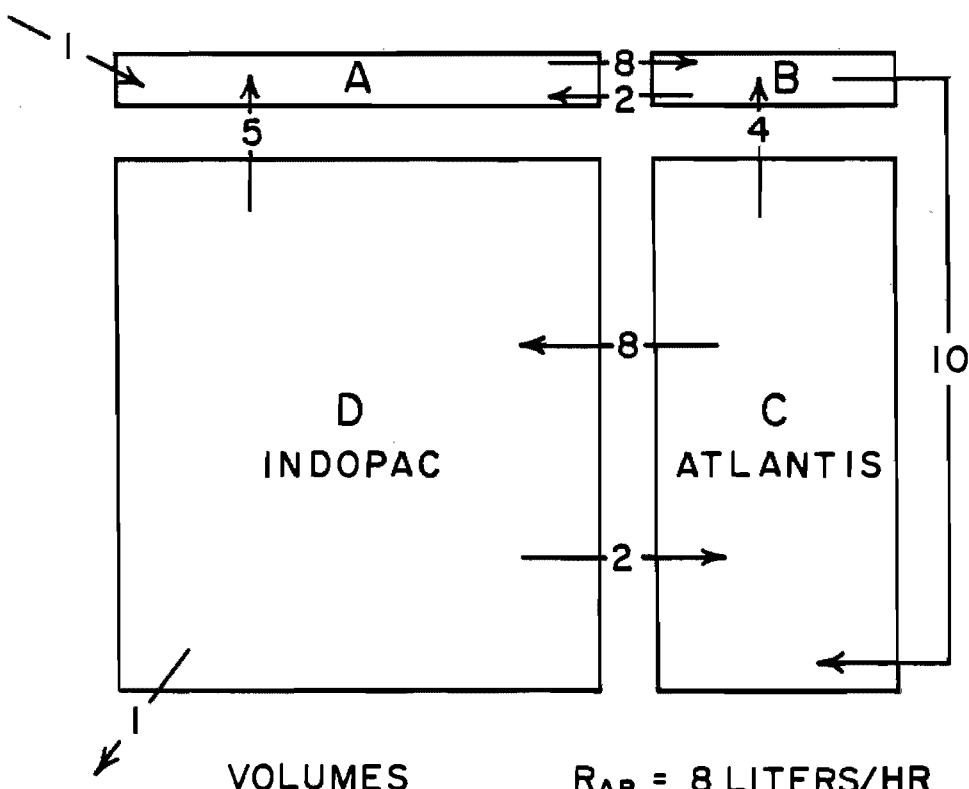
are able to survive destruction in the deep sea influence the elapsed time between entry into the sea and burial in the sediments.

PROBLEMS

- 1-1 Constituent x has an average concentration of 2 milligrams per liter (mg/l) in river water, 4 mg/l in surface water, and 16 mg/l in deep sea water. What are the values of g, f, and τ for this constituent?
- 1-2 For constituent y 20% of the material falling to the deep sea is preserved in the sediment (i.e., 80% is recycled). Fifty percent of this constituent reaching the warm ocean is fixed into particulate matter which falls back into the deep sea. Its concentration in average river water is 10 micrograms per liter ($\mu\text{g/l}$). What is its average concentration in deep sea water? In surface sea water? What is its average residence time in the sea?
- 1-3 Marine organisms use Sr as well as Ca to build their CaCO_3 shells. The ratio of Sr to Ca in shells is only one-fifth that in the water in which they dwell. If this is the only means by which Sr is removed from sea water, how would the Sr/Ca ratio in river water compare to that in average sea water? What would be the ratio of the residence times of Sr and of Ca?
- 1-4 If, at some time in the past, deep water formed at the north end of the Pacific rather than at the north end of the Atlantic, how would the chemistry of the sea differ from what it is today?
- 1-5 If organisms were to become less efficient than they now are in consuming the organic debris falling to the deep sea, how would the chemistry of the sea change? On what time scale would these changes occur?
- 1-6 Were life in the ocean suddenly to be destroyed, what changes would occur in the nutrient constituent chemistry of surface water on a time scale of a hundred of years? What changes would occur on the time scale of 100,000 years?

SUPERPROBLEM #1

A biologist named Johannes Theft constructs a special four-reservoir aquarium, designed to portray the distribution of nutrients in the world ocean (see figure 1-19). The upper two reservoirs are open to the air and illuminated by aritifical lights. The lower two are sealed from contact with the air and are dark. Stirring devices are installed so that the waters in each reservoir remain well mixed. Pumps are installed to transfer water between the reservoirs at fixed rates. Pumps are installed to add



VOLUMES

$$V_A = 600 \text{ LITERS}$$

$$V_B = 300 \text{ LITERS}$$

$$V_C = 3000 \text{ LITERS}$$

$$V_D = 6000 \text{ LITERS}$$

PUMPING RATES

$$IN_A = 1 \text{ LITER/HR}$$

$$OUT_D = 1 \text{ LITER/HR}$$

$$R_{AB} = 8 \text{ LITERS/HR}$$

$$R_{BA} = 2 \text{ LITERS/HR}$$

$$R_{BC} = 10 \text{ LITERS/HR}$$

$$R_{CB} = 4 \text{ LITERS/HR}$$

$$R_{CD} = 8 \text{ LITERS/HR}$$

$$R_{DC} = 2 \text{ LITERS/HR}$$

$$R_{DA} = 5 \text{ LITERS/HR}$$

$$R_{AD} = 0 \text{ LITERS/HR}$$

Figure 1-19. The design of Johannes Theft's four-reservoir aquarium of superproblem #1.

new sea water to reservoir A and remove an identical amount of water from reservoir D. Theft fills the system with sea water with an NO_3 concentration of 30×10^{-6} moles/liter and a PO_4 concentration of 2×10^{-6} moles/liter. The input water has the same concentration of these nutrients. Theft inoculates the surface water with algae and the deep water with bacteria. Theft adds a dozen or so snails to each deep reservoir. Finally, Theft installs a filtering system in each surface reservoir, so that the water can be purged of living plants and suspended particulates. These filters are transferred at frequent intervals to the underlying reservoirs and "back-flushed", dispersing their catch in the deep water.

Theft views his creation with some satisfaction and then puts it into action. The lights go on, the pumps go on, the filtering systems go on, and the mixers go on. He then begins a program monitoring the NO_3 and PO_4 content of the four reservoirs. As expected, the concentrations in the surface reservoirs quickly drop to near zero values. That in the smaller of the two deep reservoirs, which is appropriately named Atlantis, also begins to drop but levels out at a constant value. After some time, all the concentrations stabilize; steady state has been achieved. Theft notes with pride that no organic slime accumulates on the sides or the bottom of the deep reservoir. The bacteria and snails do their job and consume the material back flushed from the filters.

What are the steady state NO_3 and PO_4 concentrations in Atlantis? In Indopac? If the dissolved oxygen content of the water descending from the surface is 350×10^{-6} moles/liter and, if the C/N/P ratio in the material caught on the filters is 105/15/1, then what is the O_2 content of the waters in Atlantis and in Indopac? Roughly how long did Theft have to wait for steady state to be achieved?

After showing off to his colleagues and students the success of his creation, Theft becomes a bit bored and decides to change some things. First he halves the NO_3 and PO_4 content of the feed water. As he expects, after a suitable time the concentrations of nutrients drop to and remain at half their previous steady state values. The productivity of the plants also falls to half its previous value.

After restoring things to their original state, Theft cuts off three of the pumps and merely circulates water at the rate of 10 liters per day from tanks A to tank B to tank C to tank D and back to tank A. He is amazed by what happens to the nutrient concentration and snails in Atlantis. Calculate the new steady state nutrient concentrations in both Atlantis and Indopac. What fate befell the snails in Atlantis (but not those in Indopac)?

Once again Theft restores the tanks to their original mode of operation. While contemplating what experiment he might next try, a geochemical colleague named Spencer Crane drops in. After viewing the aquarium for some time he tells Theft that, while his system is a very clever one, which does indeed reproduce the major nutrient distribution in the ocean, it has one flaw.

"Your Indopac reservoir always seems to end up with a nutrient concentration equal to that in the feed water," says Crane. "That is hardly the situation in the ocean." As a means of recti-

fying this deficiency, Crane suggests that the outflow be switched from reservoir D to reservoir B, and that a second set of much smaller filters be run in parallel with the existing filters, and that their catch be discarded rather than back-flushed into the underlying reservoirs. Theft sees the point and makes the changes. He first drops the pumping rate D to B, C to D, and D to A by one liter per hour so that water balance is maintained for the new arrangement. He sets the relative catches of the primary filter and secondary filter (i.e., added throwaway) to be 100. In this case, what would be the steady state NO_3 and PO_4 concentrations in Atlantis? In Indopac? What would the O_2 concentrations be? If the area of the surface of reservoir A is 3 times that of reservoir B, what would be the ratio of the plant debris rain rates (per unit surface area) from these reservoirs?

NOTE: On page 570 are listed some constants that will prove handy for the problems in this and in subsequent chapters.

LAST MINUTE ADDITION (SEPTEMBER 1982)

As this book was being written and corrected exciting results were being obtained on the oceanic distributions of Pb, Be (722), and Ge (728), and the rare earths. The list of classifiable elements grows rapidly and the complexity of the oceanic distribution patterns become more complex. We shall have more to say about some of these findings in chapter 4.

Chapter 2

THE SEDIMENTARY SINK

FACTORS INFLUENCING THE DISTRIBUTION OF SEDIMENTARY CONSTITUENTS

INTRODUCTION

On the average the opal and calcite generated by the organisms living in the sea make up about 50% of the sediment accumulating on the sea floor. The geographic distributions of these phases are, however, far from uniform. Sediments consisting of nearly pure opal and of nearly pure calcite cover large reaches of the sea floor. So also do sediments nearly free of both of these phases. The abundance of these phases at any point on the sea floor reflects both their rate of production in the overlying water column and the extent to which they are subjected to solution on the sea floor. Since both the rate of production and the extent of solution of opal and calcite are related to distribution of nutrient constituents in the sea the abundance patterns of these phases in sediments offer valuable clues regarding the operation of the earth's largest chemical plant. Our major goal in this chapter will be to exploit this information.

SEDIMENT TYPES

Deep sea sediments consist of three major components. The most voluminous of these is detrital material derived from the mechanical and chemical fragmentation of the materials which make up the continents (see table 2-1). Most of this material is in the form of alumino-silicate minerals. It is dropped by winds onto the sea surface and is disgorged by rivers into coastal waters. As might be expected, this detritus accumulates most rapidly along continental margins and more slowly in areas of the sea floor more remote from land. Sediment cores taken more than a few hundred kilometers from land masses show detritus accumulation rates between 0.2 and 1.0 grams per square centimeter of ocean floor per 1000 years. Deep sea sediments rich in this component are called red clays.

So-called authigenic minerals in sediments are formed by spontaneous crystallization within the sediment or water column. They make up only a small fraction of the total sediment. The most important of these is the iron-manganese oxide material in sediments formed through reduction of these metals at depth in the sediment column coupled with upward migration and redeposition in the oxygenated upper layers of sediment. This material is also a by-product of hydrothermal activity near the ridge crests. Hot

Table 2-1. Mineralogy of alumino-silicate detritus transported from the continents into the sea via rivers and air.

Mineral	Chemical Composition
Quartz	SiO_2
Orthoclase	KAlSi_3O_8
Plagioclase	$x\text{NaAlSi}_3\text{O}_8 + (1-x)\text{CaAl}_2\text{Si}_2\text{O}_8$
Kaolinite	$\text{Al}_2\text{Si}_2\text{O}_5(\text{OH})_4$
Illite	$\text{KAl}_3\text{Si}_3\text{O}_{10}(\text{OH})_2$
Smectite	$\text{Al}_2\text{Si}_4\text{O}_{10}(\text{OH})_2 \cdot x\text{H}_2\text{O}$
Chlorite	$(\text{Mg},\text{Fe},\text{Al})_6(\text{Al},\text{Si})_4\text{O}_{10}(\text{OH})_8$
Vermiculite	$\text{Mg}_3\text{Si}_4\text{O}_{10}(\text{OH})_2 \cdot x\text{H}_2\text{O}$

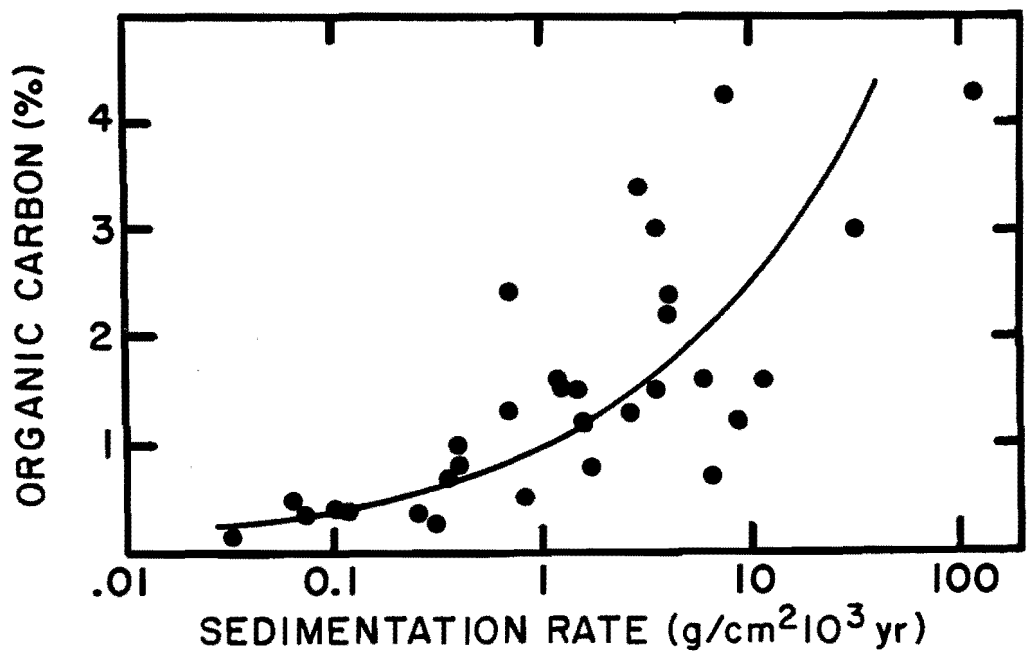


Figure 2-1. Organic carbon content of marine sediments as a function of bulk sediment accumulation rate. Results summarized by Ross Heath and his colleagues (531).

waters entering the sea in these regions carry with them sizeable amounts of reduced Mn and Fe. On venting, these metals encounter the dissolved oxygen in the deep sea water, become oxidized, flocculate, and settle to the sea floor. In some ridge crest sediments, these oxides of Fe and Mn make up several tens of percent of the sediment.

The biogenic component of sediment consists mainly of two substances that are produced as hard parts of organisms. These are calcite and opal precipitated by plankton living in the waters of the surface ocean. As mentioned in chapter 1, calcite is formed by coccoliths (plants) and by foraminifera (animals); opal is formed largely by diatoms (plants) and radiolarians (animals). The distribution of calcite and of opal in ocean sediments is not at all uniform. In some places on the floor of the Antarctic Ocean we find an enormous amount of opal mixed with the ever present detrital alumino-silicates. On the crests and upper flanks of mid-ocean ridges we find that the ever-present blanket of clay is diluted with a large amount of calcite. At great depths in the temperate ocean, we find neither opal nor calcite; alumino-silicate debris accumulates virtually alone.

Soft tissue residues rarely make an important contribution to deep sea sediments (a tribute to the efficiency of the animals and bacteria that feed on it). We do not have a good understanding of the details of the accumulation pattern for this material. The results in hand do, however, show a correlation between increasing sediment accumulation rate and increasing organic carbon content (see figure 2-1). Sediments that accumulate at rates less than one centimeter per thousand years have an organic carbon content of only a few tenths of a percent. By contrast, where sediments accumulate at rates greater than 10 centimeters per thousand years, organic carbon contents of several percent are found. Only in anaerobic basins such as the Black Sea and Carioca Trench are sediments containing more than 10 percent organic carbon found.

DISTRIBUTION OF OPAL PRODUCTION

The abundance pattern of opal in deep sea sediments is closely related to the pattern of productivity of diatoms and radiolarians in the overlying waters. As shown in figure 2-2, high opal contents are found around the perimeter of the Antarctic continent, along the equatorial belt in the Pacific, off the coast of Africa in the Atlantic, and in the northernmost Pacific. In all of these regions surface waters are all characterized by high nutrient content. These high concentrations are maintained by intense upwelling. One might ask why it is opal producing plants that dwell in these areas of intense upwelling and not, for example, calcite producing plants. The answer to this question, like most of those regarding ecologic interactions, is not known. It can only be said that based on observation, if sufficient dissolved silicate is present in surface water, it will be diatoms that flourish. Only when silica has been depleted from the water do other plant types come to the fore. In this connection we can point back to figure 1-18, which shows the distribution of NO_3^- and H_4SiO_4 in high-latitude surface waters. It is clear from these

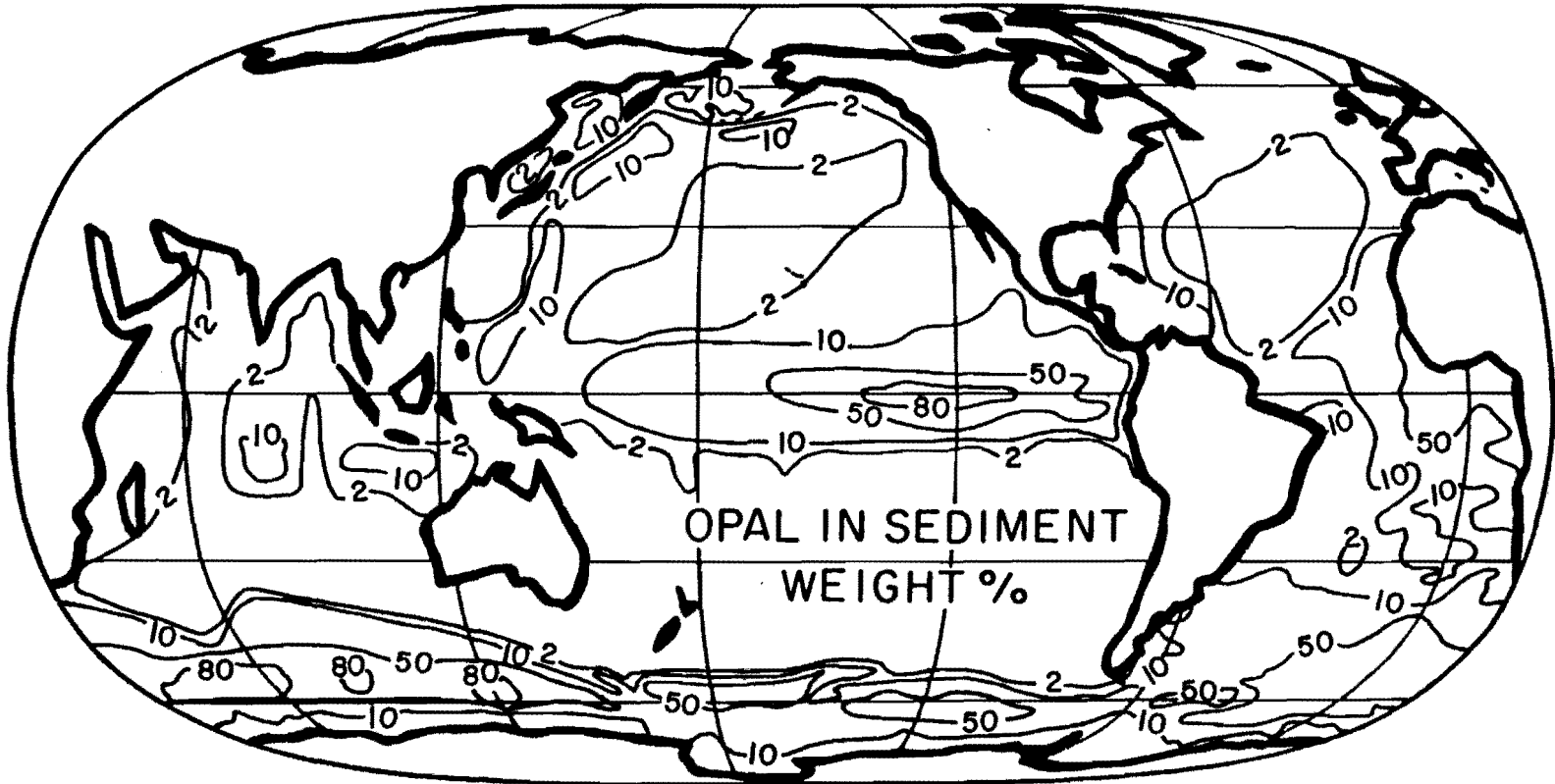


Figure 2-2. The distribution of opal in marine sediments. Prepared by Ross Heath of Oregon State University. It must be kept in mind that, since this map shows the proportion of opal in the sediment, the patterns depend on the rate of accumulation of the non-opal components of the sediment as well as that for opal.

distributions that silicate is depleted from the water before nitrate (i.e., high concentrations of nitrate extend much further equatorward in surface water than do those of silicate). This difference must be the chemical imprint of high diatom productivity!

OPAL SOLUTION ON THE SEA FLOOR

The ocean is everywhere undersaturated with respect to the mineral phase opal. Thus once formed the hard parts of diatoms are immediately subject to solution. As can be seen from the sediment trap data in table 1-3, there is no marked decrease in the amount of opal caught as a function of depth. Apparently the opaline material suffers relatively little solution as it falls through the water column. Rather, most of the opal solution occurs on the sea floor. In the paragraphs which follow we will see that this sea floor solution enhances the contrast between the opal content of sediments forming beneath areas of high and low opal production.

The extent to which the opal raining to the sea floor dissolves depends on three major factors. First, it is influenced by the thermodynamic driving force which is a function of the temperature, pressure and H_4SiO_4 content of the bottom water. The greater this difference the greater the tendency for the opal to dissolve. Second, it is influenced by the rate of rain of non-opaline material. This material dilutes the opal in bottom sediments and thereby cuts down the rate at which it dissolves. For a given thermodynamic driving force the rate of opal solution will be proportional to the fraction of opal in the sediment. Finally, it is influenced by the rain rate of opal itself. The higher the rain rate the greater the probability that a grain of opal will become buried before succumbing to solution.

An analogy will help to clarify this situation. A botanist receives a grant to study the process of "leaf detachment." He hires a research assistant and takes him off to a nearby experimental forest where he has marked off several study plots. The assistant is instructed to begin each day by raking one of the plots clean and then to spend the day picking up each oak leaf that falls to the ground within the plot. These leaves are to be put into a box for weighing at the end of each day. On the first day the assistant chooses a plot containing only oaks. The air is calm and he has little trouble picking up all the oak leaves which fall. He decides that he has landed an easy job. The next day he again picks a plot containing only oak trees. All goes well for the first half hour and then the wind picks up, bringing down a great deluge of leaves. Try as he may, he can not keep up with this onslaught, and by the end of the day he finds that he is scurrying about on a carpet of oak leaves. On the third morning the somewhat disillusioned assistant comes up with a clever idea. He chooses a patch within which oaks make up only a small fraction of the trees. Less work, he conjectures. Despite more moderate winds than on the previous day, he immediately runs into trouble. Not being an expert on leaf identification, he finds himself pondering each leaf so long that he cannot get to all the leaves which fall. By noon he notes that oak leaves, buried under leaves

of other kinds, have missed his immediate attention. At the day's end he trudges back to the laboratory carrying his sparse catch and wondering what new surprises his next day on the job would bring.

The assistant's first days were analogous to the situation in the Antarctic Ocean, where it is largely diatoms that rain to the sea floor. The factor which determined whether or not oak leaves accumulated was the rate at which these objects fell compared to the maximum rate at which he could retrieve them. His third day was analogous to the more usual situation in the deep sea, where far more non-opal than opal fragments fall. In this case his retrieval rate decreased greatly due to the competition by non-oak leaves for his attention. Furthermore, the more oak leaves he did retrieve, the more difficult it became to find the few that remained.

In order to quantify this situation we must define 6 quantities:

- 1) the rain rate of opal, R_{opal}
- 2) the accumulation rate of opal, A_{opal}
- 3) the accumulation rate of non-opaline material, A_{other}
- 4) the solution rate of opal, S_{opal}
- 5) the solution rate of a hypothetical sediment consisting of pure opal, S^*_{opal}
- 6) the fraction opal in the sediment, f .

These 6 variables are interrelated by 3 equations. First, the actual rate of opal solution is related to the hypothetical rate at which a sediment consisting of pure opal would dissolve by the fraction of opal in the sediment. This relationship can be stated as follows:

$$S_{\text{opal}} = f^n S^*_{\text{opal}}$$

2-1

The value of the exponent, n , depends on the nature of the solution process. Were only grains sitting on the top of the sediment column dissolving, then n would be one. However, as we shall see if solution occurs mainly in the pores of the sediment then the appropriate value of n is one half. Second, as sediments accumulate on any given region of the sea floor at nearly uniform rates over long periods of time, there must be a balance between the rain rate of biogenic silica, the accumulation rate of biogenic silica, and the solution rate of biogenic silica. This balance can be written as follows:

$$R_{\text{opal}} = A_{\text{opal}} + S_{\text{opal}}$$

2-2

The third relationship stems from the definition of f , i.e.:

$$f = \frac{A_{\text{opal}}}{A_{\text{opal}} + A_{\text{other}}}$$

2-3

The parameters f and S_{opal} can be eliminated by simultaneous solution of these three equations yielding the following expression for the ratio of the rate at which opal accumulates in the sediment to the rate at which biogenic silica rains onto the

sea floor (i.e., the fraction of opal preserved).

$$\frac{A_{\text{opal}}}{R_{\text{opal}}} = 1 - \frac{S^*_{\text{opal}}}{R_{\text{opal}}} \left[\frac{A_{\text{opal}}}{A_{\text{opal}} + A_{\text{other}}} \right]^n \quad 2-4$$

Although the solution to this equation is algebraically cumbersome, its main message can be understood by considering two limiting cases.

For sediments rich in biogenic silica we can simplify the equation using the following approximation:

$$\frac{A_{\text{opal}}}{A_{\text{opal}} + A_{\text{other}}} = 1 \quad 2-5$$

Thus regardless of the choice of n:

$$\frac{A_{\text{opal}}}{R_{\text{opal}}} = \frac{R_{\text{opal}} - S^*_{\text{opal}}}{R_{\text{opal}}} \quad 2-6$$

or

$$A_{\text{opal}} = R_{\text{opal}} - S^*_{\text{opal}} \quad 2-7$$

Such sediments can form only if R_{opal} is greater than S^*_{opal} . Although we don't have a firm knowledge of the value of S^*_{opal} , it must be on the order of $5 \text{ g/cm}^2 10^3 \text{ years}$ (i.e., much higher than ordinary opal rain rates). If so, then in order to achieve an opal accumulation of $20 \text{ g/cm}^2 10^3 \text{ years}$, as is observed in some parts of the Antarctic Ocean, rain rates of $25 \text{ g/cm}^2 1000 \text{ years}$ would be required.

As shown in figure 2-2 most deep sea sediments are very low in biogenic silica (less than a few percent by weight). For these sediments,

$$A_{\text{opal}} \ll A_{\text{other}}$$

With this approximation the equation becomes:

$$\frac{A_{\text{opal}}}{R_{\text{opal}}} = 1 - \frac{S^*_{\text{opal}}}{R_{\text{opal}}} \left[\frac{A_{\text{opal}}}{A_{\text{other}}} \right]^n \quad 2-8$$

If the exponent n is taken to be equal to unity, then the equation can be rewritten as follows:

$$\frac{A_{\text{opal}}}{R_{\text{opal}}} = \frac{1}{1 + \frac{S^*_{\text{opal}}}{A_{\text{other}}}} \quad 2-9$$

For deep-sea sediments with accumulation rates of less than 0.5

$\text{g/cm}^2 \text{yr}^3$ years, S^* is much greater than A_{other} . Hence:

$$\frac{A_{\text{opal}}}{R_{\text{opal}}} \approx \frac{A_{\text{other}}}{S^*_{\text{opal}}} \quad 2-10$$

For example, for a sediment with an accumulation rate of $0.5 \text{ g/cm}^2 \text{yr}^3$ and an S^* of $5 \text{ g/cm}^2 \text{yr}^3$, approximately ten percent of the silica reaching the sea floor would be preserved.

Thus we see that our intuition is confirmed. Sediments under areas of high opal production will lose only a small fraction of their opal to solution. By contrast sediments under areas of low opal production will experience large fractional losses. The solution process enhances the contrast between the opal content of sediments forming under areas of high and low opal production!

Now let us consider what is the appropriate value for the exponent, n . Measurements of the dissolved silica content of pore waters in sediments provide us with important clues. As seen in figure 2-3, these concentrations increase with depth in the sediment column and gradually approach a constant value.* This observation suggests two things. First, some of the solution must occur mainly within the sediment column (the products of the solution process are carried from the sediment by molecular diffusion through the pore spaces). Second, the rate limiting step for solution must be the time required for the pore waters to reach the steady state concentration. If so, then at any given depth in the sediment the following balance must be maintained:

$$D_s \frac{\partial^2 C_{\text{pore}}}{\partial z^2} = -k (C_{\text{sat}} - C_{\text{pore}}) \quad 2-11$$

where D_s is the whole sediment diffusion coefficient**, C_{sat} and C_{pore} are the concentrations of silica at "saturation" with opal and in the pore water at depth z in the sediment, k is the fraction of the residual pore water inequilibrium (i.e., the difference between C_{sat} and C_{pore}) removed each second. The solution to this differential equation is as follows:

$$(C_{\text{pore}} - C_{\text{bot}}) = (C_{\text{sat}} - C_{\text{bot}}) [1 - \exp(-z\sqrt{k/D_s})] \quad 2-12$$

where C_{bot} is the concentration of silica in the bottom water. This mathematical model predicts an exponential shape for the pore water silica content with an asymptotic approach to the steady state value. The observed profiles (see figure 2-3) have this

*This steady state pore water value is lower than the saturation value measured in the laboratory (see figure 2-4). It must reflect a kinetic balance between the solution of opal and the deposition of some crystalline phase of SiO_2 or the recrystallization of some clay mineral.

** $D_s = \phi D / \theta^2$ where D is the molecular diffusion coefficient, ϕ is the porosity and θ is the tortuosity factor.

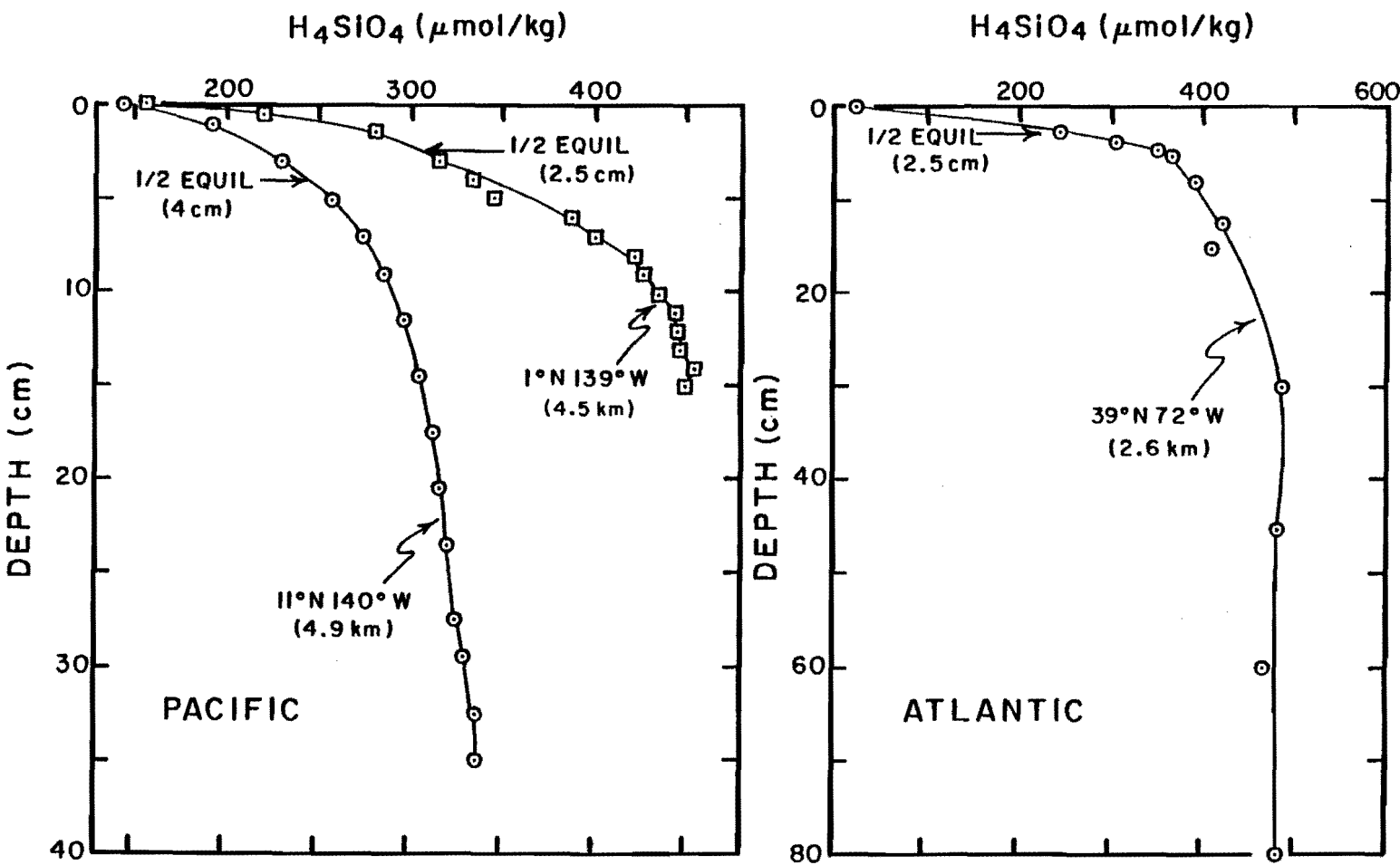


Figure 2-3. On the left are shown pore water profiles for two cores from the equatorial Pacific Ocean. The core from 11°N contains 18 percent opal and that from 1°N contains 13 percent opal. The results were obtained by Steve Emerson and David Heggie at the University of Washington, using conventional methods for shipboard pore water extraction. On the right is shown a pore water profile for a hemipelagic sediment from the continental margin of the North Atlantic. The results were obtained by Fred Sayles of Woods Hole Oceanographic Institution, using an in situ pore water extraction device (529a).

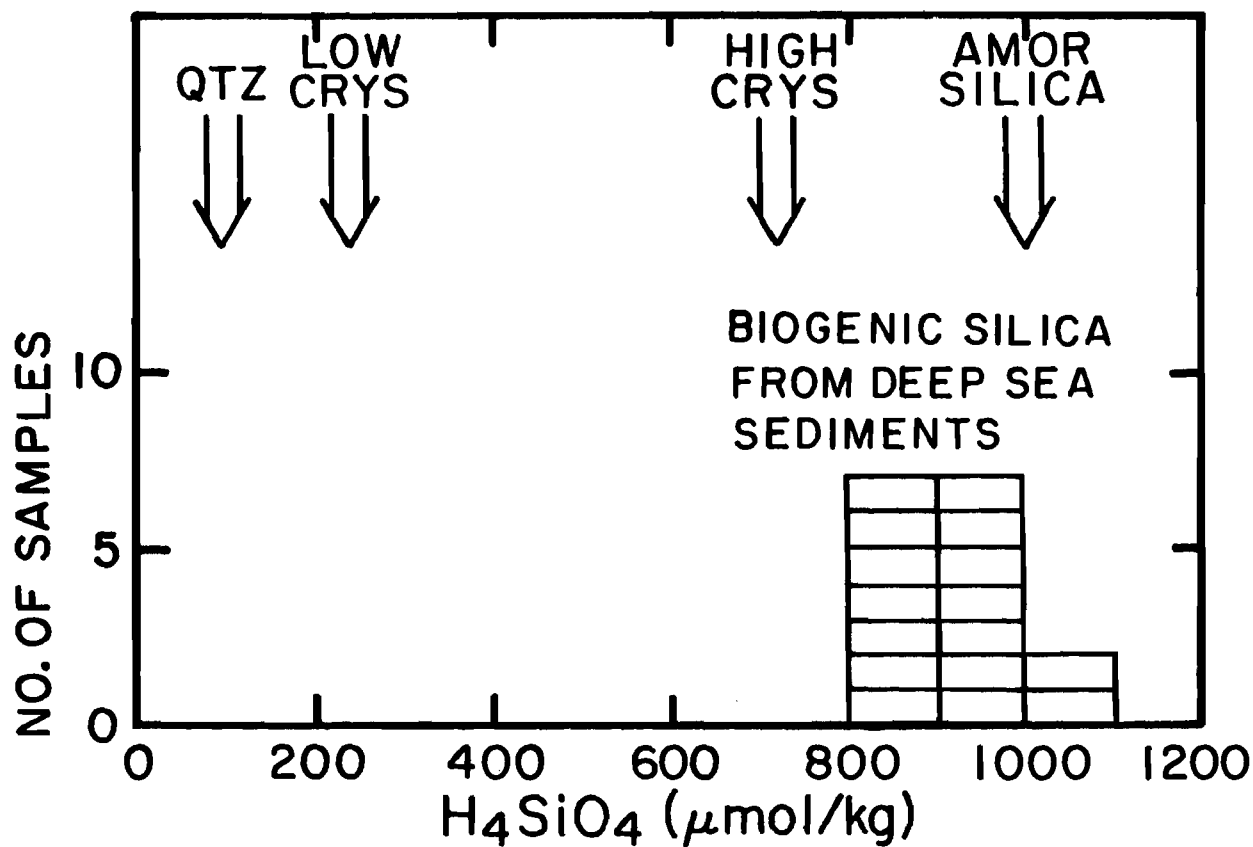


Figure 2-4. Measurements of the solubility (in seawater at 3°C) of acid-cleaned biogenic silica separated from deep sea cores collected in central equatorial Pacific. The measurements were made by Hurd and his colleagues at the University of Hawaii (522). Also shown are the solubilities of the minerals quartz, low crysotobalite and high crysotobalite and the solubility of amorphous silica glass.

basic shape. The e folding depth in the sediment z^* (i.e. the depth at which the opal saturation and the bottom water concentration difference decreases by a factor of $1/e$) is given by:

$$z^* = \sqrt{D_s/k} = \sqrt{D_s \tau} \quad 2-13$$

where τ , the resaturation time for the silicate content of pore waters, is the reciprocal of k .

Solving for τ we obtain:

$$\tau = \frac{(z^*)^2}{D_s} \quad 2-14$$

From the profiles for silica-rich sediments shown in figure 2-3, the value of z^* can be estimated to be about 4 cm. The whole sediment diffusion coefficient for silica in sea water (at 2°C) is about $2 \times 10^{-6} \text{ cm}^2/\text{sec}$. Hence:

$$\tau = \frac{4^2}{2 \times 10^{-6}} = 8 \times 10^6 \text{ sec}$$

or about 100 days. This implies that if we could by magic replace the pore water in these sediments with silicate-free sea water it would take about 100 days for enough opal to dissolve to bring the silicate concentration $1/e$ of the way to the saturation value.

The time required for the pore waters to resaturate with silica would depend on the fraction of opal contained by the sediment. The time required in a sediment containing 50% opal would logically be twice that for a core of pure opal. As the sediments on which the pore water studies were performed averaged only 10% opal, the pore water resaturation time for a sediment of pure opal should be only about 10 days. If we call the saturation time for a core with pure opal τ^* then:

$$\tau = \frac{\tau^*}{f} \quad 2-15$$

Our equation then becomes:

$$(C_{\text{pore}} - C_{\text{bot}}) = (C_{\text{sat}} - C_{\text{bot}}) [1 - \exp(-z\sqrt{f/D_s \tau^*})] \quad 2-16$$

The flux of dissolved silica through the sediment water interface is given by the relationship:

$$\text{Flux} = D_s \left. \frac{\partial C}{\partial z} \right|_{z=0} = (C_{\text{sat}} - C_{\text{bot}}) \sqrt{\frac{f}{\tau^*}} \quad 2-17$$

This yields:

$$\frac{S_{\text{opal}}}{S^*_{\text{opal}}} = f^{1/2} \quad 2-18$$

The upshot of all this is then that in the case of opal solution, the best choice for n is $1/2$. Let us apply this rule to our botanical assistant. If he could pick 64 leaves a minute when only oak leaves were present on the ground then his harvest would fall to 45 leaves per minute when half the leaves were from oak and to 32 leaves per minute when one quarter of the leaves were oak.

Solutions of equation 2-4 (using $n = 1/2$) are shown in figure 2-5, where the fraction of opal which accumulates (i.e., $A_{\text{opal}}/R_{\text{opal}}$) is plotted against opal rain rate (i.e., R_{opal}) for several values of the pure opal solution rate (i.e., S^*_{opal}). For any given value of S^*_{opal} the fraction of opal preserved increases with increasing opal rain rate.

What are the appropriate rates for the ocean? An estimate of the mean ocean opal rain rate can be obtained by dividing the total amount of silicate dissolved in the ocean (about 18×10^{16} moles) by the area of the ocean ($3.6 \times 10^{18} \text{ cm}^2$) and by the mean ventilation time of the deep sea (1000 years).^{*} This yields an average opal rain rate of 5×10^{-2} moles/cm² 10^3 yrs or about $3 \text{ g/cm}^2 10^3$ years.

This result can be compared with the average solution rate of opal as calculated from the pore water gradients of H_4SiO_4 . As shown above, these profiles can be approximated by the equation:

$$(C_{\text{pore}} - C_{\text{bot}}) = (C_{\text{sat}} - C_{\text{bot}}) [1 - \exp(-z/z^*)] \quad 2-19$$

The flux through the sediment water interface is given by:

$$D_s \left. \frac{\partial C}{\partial z} \right|_{z=0} = \frac{D_s (C_{\text{sat}} - C_{\text{bot}})}{z^*} \quad 2-20$$

If we take D_s to be $2 \times 10^{-6} \text{ cm}^2/\text{sec}$, z^* to be 4 cm, and $C_{\text{sat}} - C_{\text{bot}}$ to be 400×10^{-6} moles/kg (4×10^{-7} moles/cm³) the flux becomes 2×10^{-13} moles/cm² sec or 0.4 g per cm² 10^3 yrs. Although this estimate of the rate of silicate regeneration is almost a factor of ten lower than the rate of production, two factors must, however, be considered when making this comparison:

1) The cores for which the pore water measurements are shown come from areas of low opal production.

2) Some of the opal dissolves as it falls through the water column; some also dissolves on the sea floor before it is stirred into the sediments by burrowing organisms.

Taking the average rain rate of opal to be $3 \text{ g/cm}^2 10^3$ yrs and the average fraction of opal preserved in the sediment to be 0.05 we can see from figure 2-5 that the appropriate value of S^*_{opal}

*As we shall see in chapter 5 the distribution of radiocarbon suggest that the waters of the deep sea are flushed with water from the warm surface ocean (transported to the polar regions and cooled) about once each 1000 years. This in turn implies that all the water in the deep sea passes through the warm surface ocean layer about once each 1000 years. As it does so its dissolved silicate will be converted to opal and rained to the deep sea.

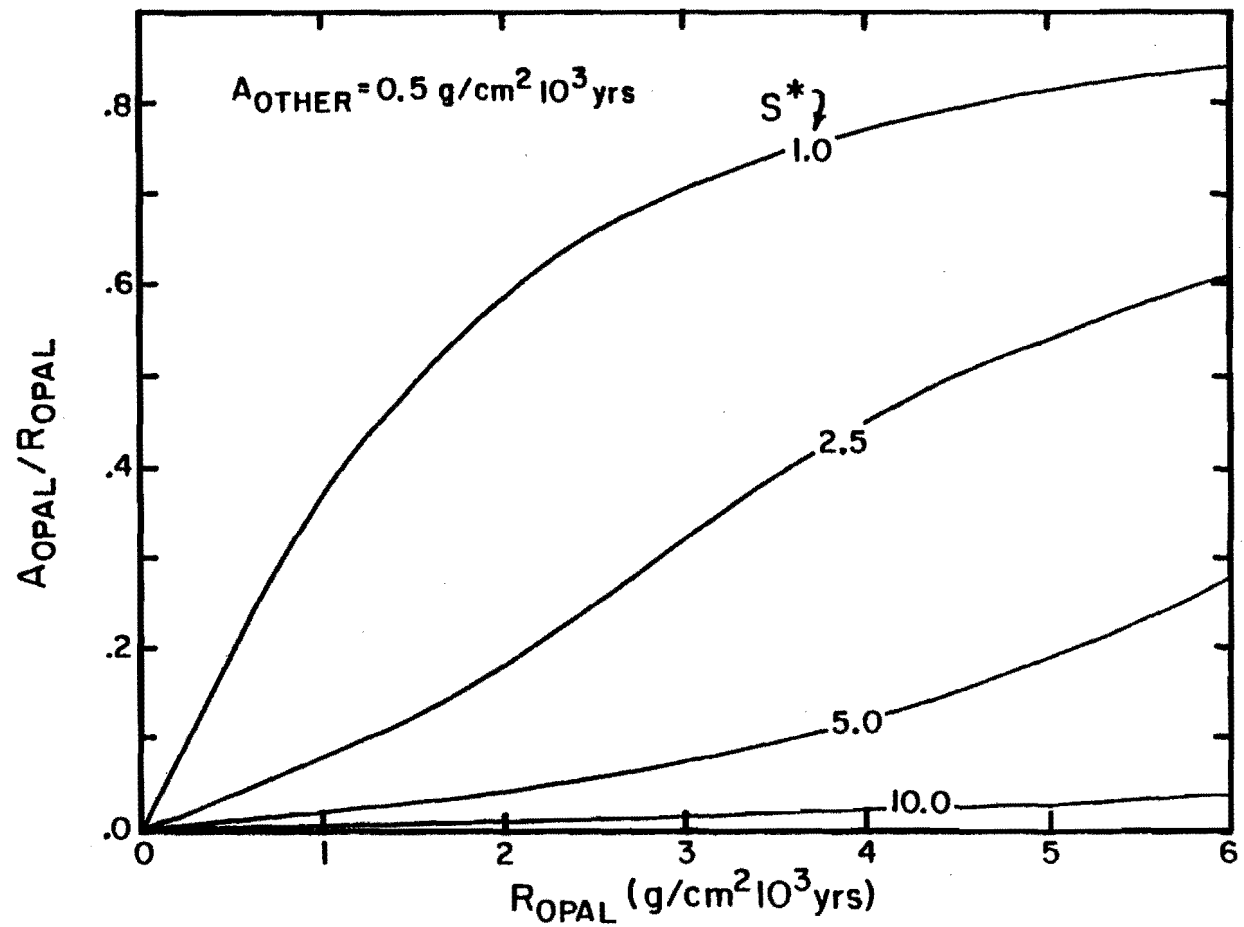


Figure 2-5. The relationship between the fraction of opal falling to the sea floor which accumulates in the sediment (i.e., $A_{\text{opal}}/R_{\text{opal}}$) and the rain rate of opal (R_{opal}) for various values of the solution rate for a deposit of pure opal (i.e., values of S^*). The accumulation rate of non-opaline components (A_{other}) is taken to be $0.5 \text{ g/cm}^2 10^3 \text{ yrs}$. The units for S^* are $\text{g/cm}^2 10^3 \text{ yrs}$.

would lie between 5 and 10 g/cm²10³ years. In making this calculation we must keep in mind that because of the wide range of opal rain rates in the sea the use of averages is not entirely appropriate. However, it does allow us to get an idea of the magnitude of S*_{opal}.

Thus we see that the accumulation of opal varies greatly from place to place on the sea floor for two major reasons. First, the production of opaline silica is concentrated in areas of upwelling. Second, the solution process enhances this primary contrast.

DISTRIBUTION OF CALCITE IN MARINE SEDIMENTS

The distribution of calcite in sediments differs greatly from that of opal (see figure 2-6). While the locations of opal rich sediments correspond closely to areas of upwelling, calcite rich sediments in the open ocean are found on ridge crests and other topographic highs. As the mountains of the continents are draped with snow, the mountains on the ocean floor are draped with sediment rich in calcite! One factor contributing to this difference in distribution is the geographical uniformity of the production of calcite by organisms in surface waters. The abundance of the organisms producing calcite is limited by the availability of nitrate and phosphate rather than by the availability of silicate. Unlike opal which falls into the deep sea before solution the organic tissue containing phosphate and nitrate is largely oxidized within the surface sea permitting these two constituents to travel much further from their point of upwelling than does silicate. It is the combination of the dominance of diatoms in upwelling areas and the recycling of the ingredients of soft tissue which gives rise to the great difference in the geographic patterns of opal and calcite production.

Unlike the situation for opal, not all parts of the sea floor are bathed in water undersaturated with respect to calcite. While the deepest waters in the ocean are corrosive toward calcite the waters which bathe the crests of the mid-ocean ridges are supersaturated with respect to calcite. The nature of the sediments in these areas reflect this difference. Sediments on ridge crests contain abundant calcite which shows little or no solution effects. By contrast sediments in the deepest parts of the ocean have lost almost all their calcite by solution. Thus while opal is subject to solution attack everywhere on the sea floor, calcite is attacked in some places and not in others.

Thus, unlike the distribution of opal in sediments which reflects mainly the great contrast in opal production from place to place at the sea surface, the distribution of calcite reflects contrasts in the extent of solution with depth in the sea.

The depth dependence of the calcite content of sediments from various regions of the ocean is shown in figure 2-7. As can be seen the boundary between sediments with well preserved calcite and sediments free of calcite is not sharp. A zone of gradation in the extent of calcite dissolution is found separating calcite ooze and red clay. We shall see that this transition zone owes its origin to the finite time required for pore waters to reach saturation with respect to the mineral calcite.

would lie between 5 and 10 g/cm²10³ years. In making this calculation we must keep in mind that because of the wide range of opal rain rates in the sea the use of averages is not entirely appropriate. However, it does allow us to get an idea of the magnitude of S*_{opal}.

Thus we see that the accumulation of opal varies greatly from place to place on the sea floor for two major reasons. First, the production of opaline silica is concentrated in areas of upwelling. Second, the solution process enhances this primary contrast.

DISTRIBUTION OF CALCITE IN MARINE SEDIMENTS

The distribution of calcite in sediments differs greatly from that of opal (see figure 2-6). While the locations of opal rich sediments correspond closely to areas of upwelling, calcite rich sediments in the open ocean are found on ridge crests and other topographic highs. As the mountains of the continents are draped with snow, the mountains on the ocean floor are draped with sediment rich in calcite! One factor contributing to this difference in distribution is the geographical uniformity of the production of calcite by organisms in surface waters. The abundance of the organisms producing calcite is limited by the availability of nitrate and phosphate rather than by the availability of silicate. Unlike opal which falls into the deep sea before solution the organic tissue containing phosphate and nitrate is largely oxidized within the surface sea permitting these two constituents to travel much further from their point of upwelling than does silicate. It is the combination of the dominance of diatoms in upwelling areas and the recycling of the ingredients of soft tissue which gives rise to the great difference in the geographic patterns of opal and calcite production.

Unlike the situation for opal, not all parts of the sea floor are bathed in water undersaturated with respect to calcite. While the deepest waters in the ocean are corrosive toward calcite the waters which bathe the crests of the mid-ocean ridges are supersaturated with respect to calcite. The nature of the sediments in these areas reflect this difference. Sediments on ridge crests contain abundant calcite which shows little or no solution effects. By contrast sediments in the deepest parts of the ocean have lost almost all their calcite by solution. Thus while opal is subject to solution attack everywhere on the sea floor, calcite is attacked in some places and not in others.

Thus, unlike the distribution of opal in sediments which reflects mainly the great contrast in opal production from place to place at the sea surface, the distribution of calcite reflects contrasts in the extent of solution with depth in the sea.

The depth dependence of the calcite content of sediments from various regions of the ocean is shown in figure 2-7. As can be seen the boundary between sediments with well preserved calcite and sediments free of calcite is not sharp. A zone of gradation in the extent of calcite dissolution is found separating calcite ooze and red clay. We shall see that this transition zone owes its origin to the finite time required for pore waters to reach saturation with respect to the mineral calcite.

Figure 2-6. Map showing the distribution of calcite-rich sediments on the sea floor. Sediments containing more than 75% CaCO_3 are shown by the cross-hatched area. This map is based on an Atlantic map published by Biscaye and his colleagues (489), a Pacific map published by Berger and his colleagues (491), and an Indian Ocean map published by Kolla and his colleagues (490).

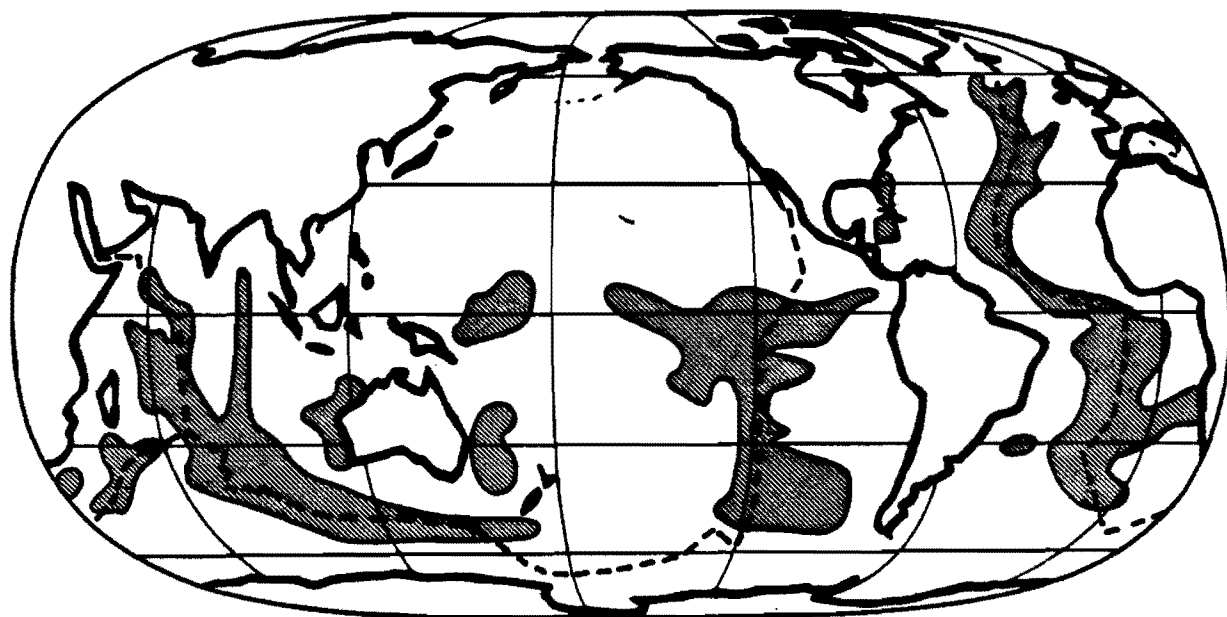


Table 2-2. Saturation carbonate ion content of sea water as a function of temperature and pressure for the minerals calcite (precipitated by coccolithophorida and foraminifera) and for the mineral aragonite (precipitated by pteropods).

Temperature, °C	Pressure, atm*	Saturation Carbonate Ion Content 10^{-6} moles/kg	
		Calcite	Aragonite
24	1	46	66
2	1	48	69
2	250	71	101
2	500	106	152

*A pressure of 100 atm is achieved at close to 1000 meters depth in the sea.

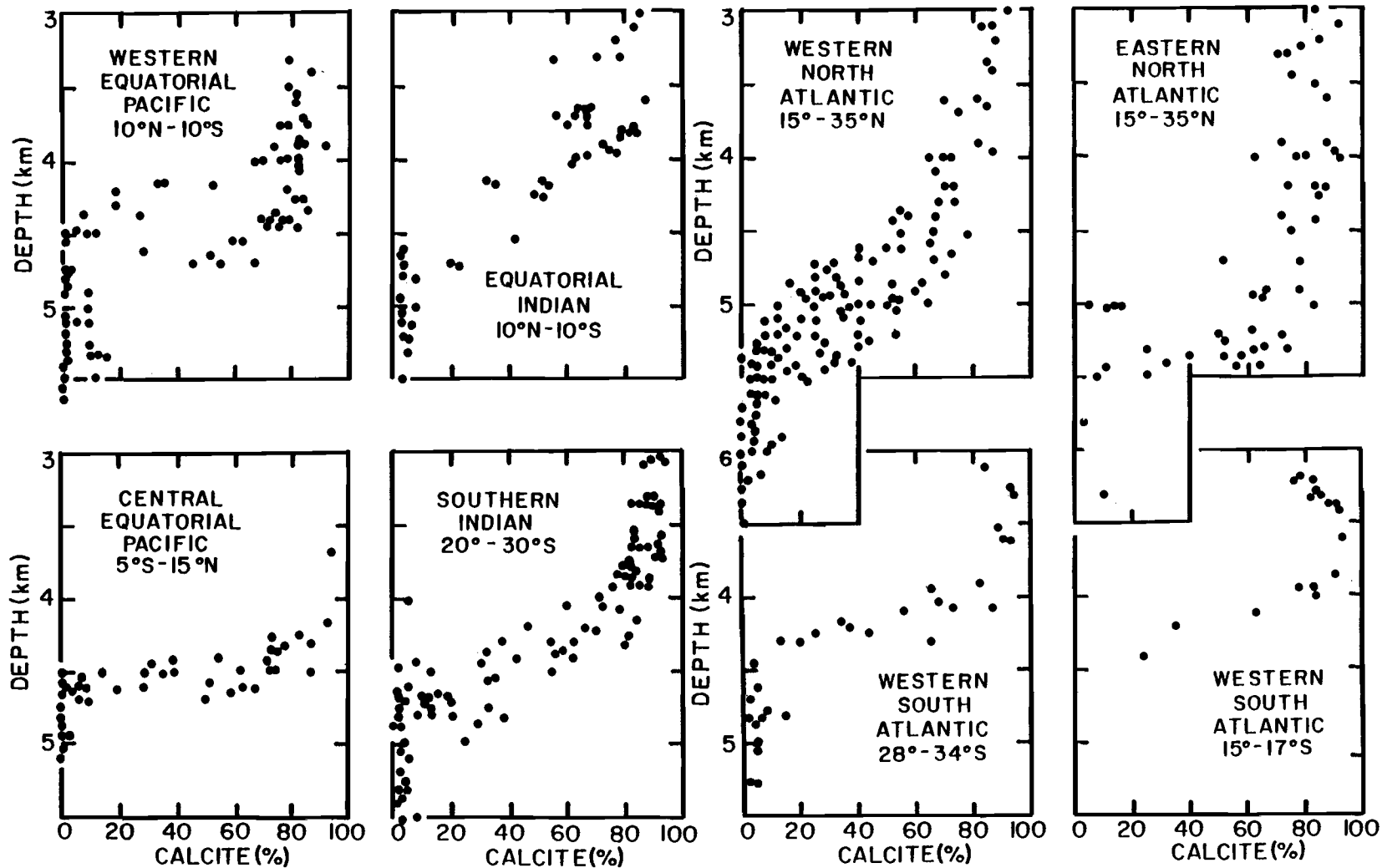


Figure 2-7. Plots of percent CaCO₃ for core top samples as a function of water depth for various regions of the ocean. Based on a data compilation provided by Pierre Biscaye of the Lamont-Doherty Geological Observatory.

Before we continue, it must be pointed out that not just the mineral calcite (the stable form of CaCO_3 , at any temperature and pressure found within the ocean) but also the mineral aragonite (a metastable form of CaCO_3 under oceanic conditions) is precipitated by marine organisms. Since all surface ocean water is supersaturated with respect to both calcite and aragonite, organisms generate whichever form of CaCO_3 they find easier to precipitate. Foraminifera and coccolithophorida choose to form calcite; pteropods choose to form aragonite. Although these two mineral phases show the same basic pattern of abundance in sediments, the boundary between aragonite-bearing and aragonite-free sediments occurs at much shallower depths than that for calcite.

DEGREE OF CALCITE SATURATION

To understand the relationship between the distribution of CaCO_3 in sediments and the distribution of biologically utilized constituents within the sea, we need to define the designations: saturation, undersaturation and supersaturation. For any mineral placed in contact with sea water, the product of the concentrations of the ions formed during its solution will reach a limit at which the solution has reached equilibrium with the given mineral. This limit depends on the temperature and pressure (the depth) of the sea water. In the solution of CaCO_3 , calcium ions and carbonate ions are formed. The degree of saturation D is written as:

$$D = \frac{([\text{Ca}^{++}][\text{CO}_3^=])_{\text{sea water}}}{([\text{Ca}^{++}][\text{CO}_3^=])_{\text{sea water saturated with calcite}}} \quad 2-21$$

where the brackets indicate the concentration of the enclosed ion.

Obviously, working with measurements on sea water samples alone will give us only the values in the numerator of this expression for D. It will not tell us the degree of saturation of CaCO_3 for the sample. To determine the value of the denominator, we must add crystals of calcite to a sea water solution maintained in the laboratory and wait long enough for the water and the solid to achieve equilibrium. The ratio of the oceanic ionic product to the ionic product obtained from these laboratory experiments gives D.

For studies in the open ocean, the equation can be simplified. The calcium content of sea water is nearly constant, it varies with respect to the salt matrix only by about 0.5 percent and as a result of salinity differences by only another percent or two.* Since the variations in $\text{CO}_3^=$ ion are by comparison far larger, we can assume that the Ca^{++} ion content is the same everywhere in the sea and in the sea water samples used in the laboratory. Thus our expression for D can be simplified to:

*The evaporation-precipitation cycle results in salinity differences from place to place in the sea. The salt is left behind when water evaporates, raising the salinity of the residual sea water.

$$D = \frac{[\text{CO}_3^=]_{\text{sea water}}}{[\text{CO}_3^=]_{\text{saturated sea water}}}$$

2-22

D is then simply the ratio of the carbonate ion content in the sea water sample to the carbonate ion content in the sea water solution saturated in the laboratory at the same temperature and pressure. The saturation carbonate ion content varies with temperature and pressure and of course is different for the mineral calcite than for the mineral aragonite. Aragonite is more soluble than calcite; thus the equilibrium carbonate ion content of aragonite is always higher at any given temperature and pressure than that of calcite (see table 2-2).

The temperature range in the ocean extends from about -1°C in deep and polar waters to about 30°C in tropical surface waters; the pressure range extends from 1 atmosphere (atm) at the surface to 550 atm at a depth of 5500 meters (the maximum bottom depth for much of the sea). Now CaCO_3 is an unusual salt: the colder the water, the more soluble it becomes! The difference in the saturation concentration of $\text{CO}_3^=$ ions in a surface water sample from the warm surface ocean, where the temperature averages 24°C , and a surface water sample from the polar regions, where the average temperature reaches 2°C , is about 5 percent (see table 2-2). The solubility of CaCO_3 also increases with pressure, and pressure increases with depth. All the water in the deep ocean is cold. Hence there is no point in considering what happens at a high pressure and a temperature of 24°C ; we only need to know what happens close to 2°C . Table 2-2 shows that both calcite and aragonite are slightly more than twice as soluble at 500 atm (2°C) as they are at 1 atm (2°C). In the deep sea the effect of pressure is clearly greater than that of temperature. Moreover, since the temperature below 1000 meters is nearly constant, variations in the solubility of CaCO_3 within the deep water mass are entirely due to the increase of pressure with depth.

Although much work has been done to pin down the exact solubilities of the mineral phases, calcite and aragonite as shown in tables 2-3 and 2-4 and in figure 2-8 uncertainties still remain.

VARIATIONS IN THE CARBONATE ION CONTENT OF SEA WATER

One important question remains. How does the carbonate ion concentration vary from place to place within the sea? With this information in hand, we could see how the degree of supersaturation of sea water with respect to the CaCO_3 minerals calcite and aragonite varies from place to place within the sea. To understand these variations, we must probe more deeply into some of the chemical reactions taking place in the ocean.

The $\text{CO}_3^=$ ion content of sea water must vary with the total amount of dissolved inorganic carbon. We have seen in chapter 1 that the total dissolved inorganic carbon content is about 20% higher in deep North Pacific water than in warm surface water. As we shall see, the range in carbonate ion content is far larger than this (a factor of 6) and in the opposite sense (high in warm surface water and low in deep North Pacific water).

The source of these variations is changes in the fraction

Table 2-3 Estimates of the solubilities of the minerals calcite and aragonite in surface sea water (35.0‰ salinity).

Investigators	Institution (year)	Ref.	Temp. °C	Solubility $10^{-7} \text{m}^2/\text{kg}^2$	Sat. $\text{CO}_3 =$ $10^{-6} \text{m}/\text{kg}$
CALCITE					
Ingle and Coworkers*	Oregon State (1973)	(459)	25 2	4.5 4.7	44 46
Broecker and Takahashi**	Lamont-Doherty (1978)	(463)	2	4.8	47
Plath and Coworkers*	Oregon State (1980)	(466)	25 5	4.7 4.8	46 47
Morse and Coworkers*	Miami (1980)	(465)	25	4.4	43
Sayles+	Woods Hole (1980)	(464)	2	4.4	43
Adopted for this book			2	4.8	47
ARAGONITE					
Berner*	Yale (1976)	(461)	25 5	8.8 11.4	86 111
Plath and Coworkers*	Oregon State (1980)	(467)	25	8.7	85
Morse and Coworkers*	Miami (1980)	(465)	25	6.6	64
1.43 times calcite sol.++			25 2	6.6 6.8	64 66
Adopted for this book			2	6.9	67

* Based on laboratory equilibrations.

** Based on lysocline depths and in situ saturometry.

+ Based on pore water measurements.

++ Solubility ratio based on thermodynamic arguments.

Table 2-4. Estimates of the pressure dependence of the solubility of calcite.

Investigators	Institution (year)	Ref.	Method	ΔV^* cm ³ /mole
Pytkowicz and Fowler	Oregon State (1967)	(457a)	Laboratory equilibration	-31
Hawley and Pytkowicz	Oregon State (1969)	(458)	Laboratory equilibration	-33
Ingle	Oregon State (1975)	(460)	Laboratory equilibration	-42
Millero and Berner	Yale (1969)	(458a)	Partial molar volumes	-39
Duedal	Oregon State (1972)	(458b)	Partial molar volumes	-43
Broecker and Takahashi	Lamont-Doherty (1978)	(463)	Lysocline depths and <u>in situ</u> saturometry	-37
Sayles	Woods Hole (1980)	(464)	Pore water measurements	-42
Adopted for this book				-37

$$*[CO_3^{=}]_{sat}^z = [CO_3^{=}]_{sat}^o e^{-\Delta V/RT}$$

where ΔV is the difference between the volume occupied by Ca⁺⁺ and CO₃⁼ in solution in sea water and in the lattice of the mineral calcite.

Table 2-5. Charge balance in sea water: the excess cation charge is balanced by the dissociation of carbonic acid (H₂CO₃) into bi-carbonate (HCO₃⁻) and carbonate (CO₃⁼) ions.

Positive			Negative		
Cation	Mass moles/kg	Charge eq/kg	Anion	Mass moles/kg	Charge eq/kg
Na ⁺	0.470	0.470	Cl ⁻	0.547	0.547
K ⁺	0.010	0.010	SO ₄ ⁼	0.028	0.056
Mg ⁺⁺	0.053	0.106	Br ⁻	0.001	0.001
Ca ⁺⁺	0.010	0.020	Σ	-	0.604
Σ	-	0.606	HCO ₃ ⁻ + CO ₃ ⁼	-	0.002
			Σ'	-	0.606

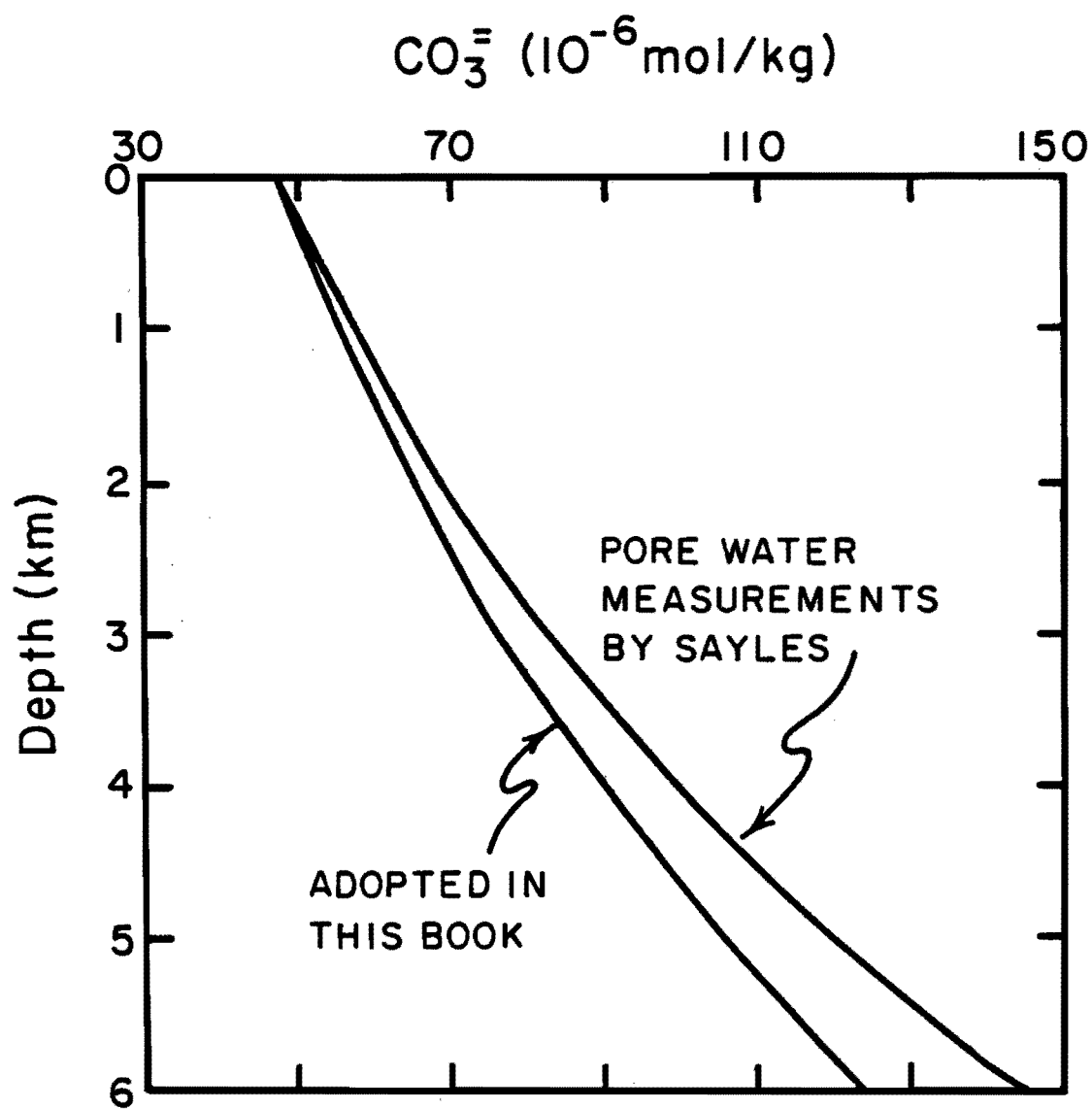


Figure 2-8. Plots of the saturation CO_3^{\pm} ion concentration versus depth in the sea based on the analysis by Broecker and Takahashi (463) of lysocline depth and saturometer data and measurements by Sayles (464) of the CO_3^{\pm} ion content in pore waters extracted in situ from deep sea sediments.

of the total dissolved carbon that is in the form of carbonate ion. Dissolved carbon is present in the ocean in three forms: dissolved carbon dioxide gas (CO_2), bicarbonate ion (HCO_3^-) and carbonate ion ($\text{CO}_3^{=}$). Carbon is one of the few elements in the ocean that can exist in ions having different charges: as HCO_3^- ion with a charge of -1; as $\text{CO}_3^=$ ion with a charge of -2. The amount of gaseous CO_2 in the ocean is very small and will for the sake of simplicity be neglected in the discussions which follow.

The ratio of $\text{CO}_3^=$ to HCO_3^- plays an important role in the sea's balance of electrical charge. The major contributors of positively charged ions (cations) in the sea are Na^+ , K^+ , Mg^{++} , and Ca^{++} (see table 2-5). To find the total number of units of positive charge per kilogram of seawater, we multiply the moles/kg of each cation by its charge and total the results. This yields 0.470 equivalents of charge from Na^+ , 0.010 equivalents from K^+ , 0.106 equivalents from Mg^{++} , and 0.020 equivalents from Ca^{++} . The total is 0.606 equivalents of positive charge per kilogram.* Since sea water can have no overall charge, the number of equivalents of negatively charged ions (anions) must add up to exactly the same value. If we take the three major anions (chloride (Cl^-), sulfate ($\text{SO}_4^{=}$), and bromide (Br^-)), we find that their charges add up to 0.604 equivalents of negative charge per kilogram, so we are short 0.002 equivalents of negative charge per kilogram of sea water. This difference between the sum of the negative charges is balanced mainly by the dissolved carbon ions HCO_3^- and $\text{CO}_3^=$. The ratio of these two anions to one another varies in such a way that charge is balanced. When more negative charge is needed to balance the cations present, HCO_3^- is converted to $\text{CO}_3^=$; when less is needed, $\text{CO}_3^=$ is converted to HCO_3^- . The amount of excess positive charge balanced by bicarbonate and carbonate ions is a small part of the total but, as we shall see, a very important residual that holds the key to the carbonate ion distribution within the sea.

In the discussion which follows we neglect the element boron. The presence of boron in sea water requires a small correction in all the calculations outlined here, for it also exists in two forms (B(OH)_3 and B(OH)_4^-). In this first look at carbonate chemistry we keep things more simple by considering a hypothetical boron free ocean.

To understand what determines the ratio of carbonate ions to bicarbonate ions in a given unit of sea water, we must recognize two restrictions. First, the total amount of dissolved carbon present in the water cannot be changed as a result of our manipulation of the charges. There is a fixed number of carbon atoms and these must exist in either bicarbonate or carbonate form. Second, the sum of all the bicarbonate and carbonate charges must just balance the excess cations so that the sea water maintains its electrical neutrality. Respectively, these two restrictions can be stated mathematically as:

*Chemists measure alkalinity in units of equivalents/kg. An equivalent is equal numerically to a mole. One mole of Na^+ ions carries one equivalent of positive charge; one mole of $\text{SO}_4^=$ ions carries two equivalents of negative charge.

$$[\Sigma\text{CO}_2] = [\text{HCO}_3^-] + [\text{CO}_3^{=}]$$

2-23

where ΣCO_2 stands for total dissolved inorganic carbon, and

$$[\text{Alk}] = [\text{HCO}_3^-] + 2[\text{CO}_3^{=}]$$

2-24

where Alk is the alkalinity of the water (that is, the excess positive charge to be balanced by $\text{CO}_3^{=}$ and HCO_3^- ions). The alkalinity is given by:

$$[\text{Alk}] = [\text{Na}^+] + [\text{K}^+] + 2[\text{Mg}^{++}] + 2[\text{Ca}^{++}] + \dots - [\text{Cl}^-] - 2[\text{SO}_4^{=}] - [\text{Br}^-] - \dots$$

If we subtract equation 2-23 from equation 2-24, we find that:

$$[\text{CO}_3^{=}] = [\text{Alk}] - [\Sigma\text{CO}_2]$$

2-26

Thus the carbonate ion content of any unit of sea water sample is equal to its alkalinity (excess positive charge) minus its total dissolved carbon content. Substituting this result in either of the original equations, we obtain:

$$[\text{HCO}_3^-] = 2[\Sigma\text{CO}_2] - [\text{Alk}]$$

2-27

Here we see that the bicarbonate ion content equals twice the total dissolved carbon content minus the alkalinity.

So to understand how the carbonate ion content of sea water varies from place to place, all we need to know is how the alkalinity of the water and how the total dissolved carbon content of the water vary.

As we have already seen, the total dissolved carbon content of sea water varies because plants extract carbon from surface sea water and because the remains of these plants (or of the animals they support) sink into deep parts of the oceans where they are largely destroyed. Two processes are at work: organic tissue formation and destruction and hard-part formation and destruction. The formation of organic tissue consumes carbon and hence changes the ΣCO_2 of the water. This carbon loss has no effect on the alkalinity of the water because none of the ionic concentrations appearing in the equation defining alkalinity change. However the incorporation and release of nitrogen by organic matter does make small changes in alkalinity. When organically bound nitrogen is released during respiration, the NO_3^- ion so produced adds to the anionic charge and reduces the alkalinity of the deep water. Correspondingly, the removal of the NO_3^- ion to form organic matter increases the alkalinity of surface water.

Removal of CaCO_3 from the water changes both concentration of the total dissolved carbon and the alkalinity. Organisms use carbon to form CaCO_3 and thus remove it from the water. The alkalinity of the water changes because when CaCO_3 is formed, Ca^{++} ion (one of the contributors to the net positive charge) is removed. Each mole of CaCO_3 formed results in the extraction of 2 moles of positive charge; thus the creation of CaCO_3 changes the alkalinity

of sea water by just twice the amount that it changes the carbon content. The formation of the third type of particulate material, opal, affects neither the alkalinity nor the total carbon content of the water.

In chapter 1, we estimated that for every four C atoms that are removed from surface water as organic tissue, one C atom is removed as CaCO_3 . Table 2-6 shows the total effect on sea water of adding or subtracting organic debris plus CaCO_3 . From the table, we see that for every five C atoms used (four in organic material and one in CaCO_3) one Ca atom is used. This uses up two positive charges and correspondingly reduces the alkalinity. For each 4 moles of carbon incorporated by plants about 0.6 moles of nitrogen are incorporated. This raises the alkalinity by 0.6 equivalents partly compensating for the reduction of alkalinity due to CaCO_3 formation. For the combined organic- CaCO_3 debris, the change in alkalinity is equal to 28% the change in total dissolved carbon. If the composition of the debris being formed and destroyed were constant everywhere, then the carbonate ion content of sea water would follow some very simple rules. Although this is not quite the case, it provides a good first approximation of the operation of the system.

To see how the $\text{CO}_3^{=}$ ion content varies, let us start with surface water that is phosphorus-free. Remember that this water contains the minimum amount of carbon. Such phosphorus-free sea water has an alkalinity of 2.20×10^{-3} equiv/kg and a total dissolved carbon content of 2.00×10^{-3} moles/kg. The carbonate ion content in this water must be equal to 2.20×10^{-3} equiv/kg minus 2.00×10^{-3} moles/kg, or 0.20×10^{-3} moles/kg.

Now let us assume that our sample of surface water is transferred to the deep sea. While in residence there, it receives the oxidation products of enough organic tissue and the solution products of enough CaCO_3 to raise its total dissolved carbon by 0.20×10^{-3} . So instead of having a ΣCO_2 content of 2.00×10^{-3} moles/kg, we have a ΣCO_2 content of 2.20×10^{-3} moles/kg. If the organic tissue and the CaCO_3 are destroyed in roughly the same proportions in which they are formed (so that for every increase of 5 moles in ΣCO_2 , there is an increase of 1 mole in Ca^{++} and an increase of 0.6 equiv in NO_3^-), then the alkalinity increase is 0.06×10^{-3} moles/kg.* Since surface water has an alkalinity of $2.20 \times$

*Actually the ratio of CaCO_3 dissolved to organic tissue respired increases with depth. This can be seen in figure 2-9 where alkalinity (normalized to a salinity of 35.0‰) is plotted against ΣCO_2 concentration (normalized to a salinity of 35.0‰). On this diagram points for temperate and Antarctic surface water and for various deep water types are shown. The expected slopes are calculated from the following equation:

$$\frac{\Delta\text{Alk}}{\Delta\Sigma\text{CO}_2} = 2 \frac{\Delta\text{C}_{\text{CaCO}_3}}{\Delta\text{C}_{\text{CaCO}_3} + \Delta\text{C}_{\text{org}}} - \frac{15}{105} \frac{\Delta\text{C}_{\text{org}}}{\Delta\text{C}_{\text{CaCO}_3} + \Delta\text{C}_{\text{org}}}$$

The second term in this equation is the correction for nitrate. As can be seen the deep waters of the Indian and Pacific oceans fall along a trend consistent with a ratio of one mole of CaCO_3 dissolved per one mole of organic residues respired. On the other hand, the line connecting warm surface water and mean deep water has a slope equivalent to one mole of CaCO_3 dissolved per four moles of organic residues respired.

Table 2-6. The impact of particulate matter formation on the chemical composition of sea water.

Constituent Change	Component Formed		
	Organic Tissue	Calcite	Aggregate
$\Delta[\Sigma\text{CO}_2]$	-4.0	-1.0	-5.0
$\Delta[\text{Ca}^{+2}]$	0.0	-1.0	-1.0
$\Delta[\text{NO}_3^-]$	-0.6	0.0	-0.6
$\Delta[\text{A}]$	+0.6	-2.0	-1.4

69

Table 2-7. Idealized carbonate chemistry of average surface and deep water.

Water Type	Gaseous CO_2 10^{-3} moles/kg	Bicarbonate Ion (HCO_3^-), 10^{-3} moles/kg	Carbonate Ion ($\text{CO}_3^{=}$) 10^{-3} moles/kg	Total Dissolved Inorganic Carbon (CO_2^+ $\text{HCO}_3^- + \text{CO}_3^{=}$), 10^{-3} moles/kg	Alkalinity ($\text{HCO}_3^- + 2\text{CO}_3^{=}$) 10^{-3} eq/kg
Surface	0.01	1.80	0.20	2.01	2.20
Deep	0.03	2.14	0.06	2.23	2.26

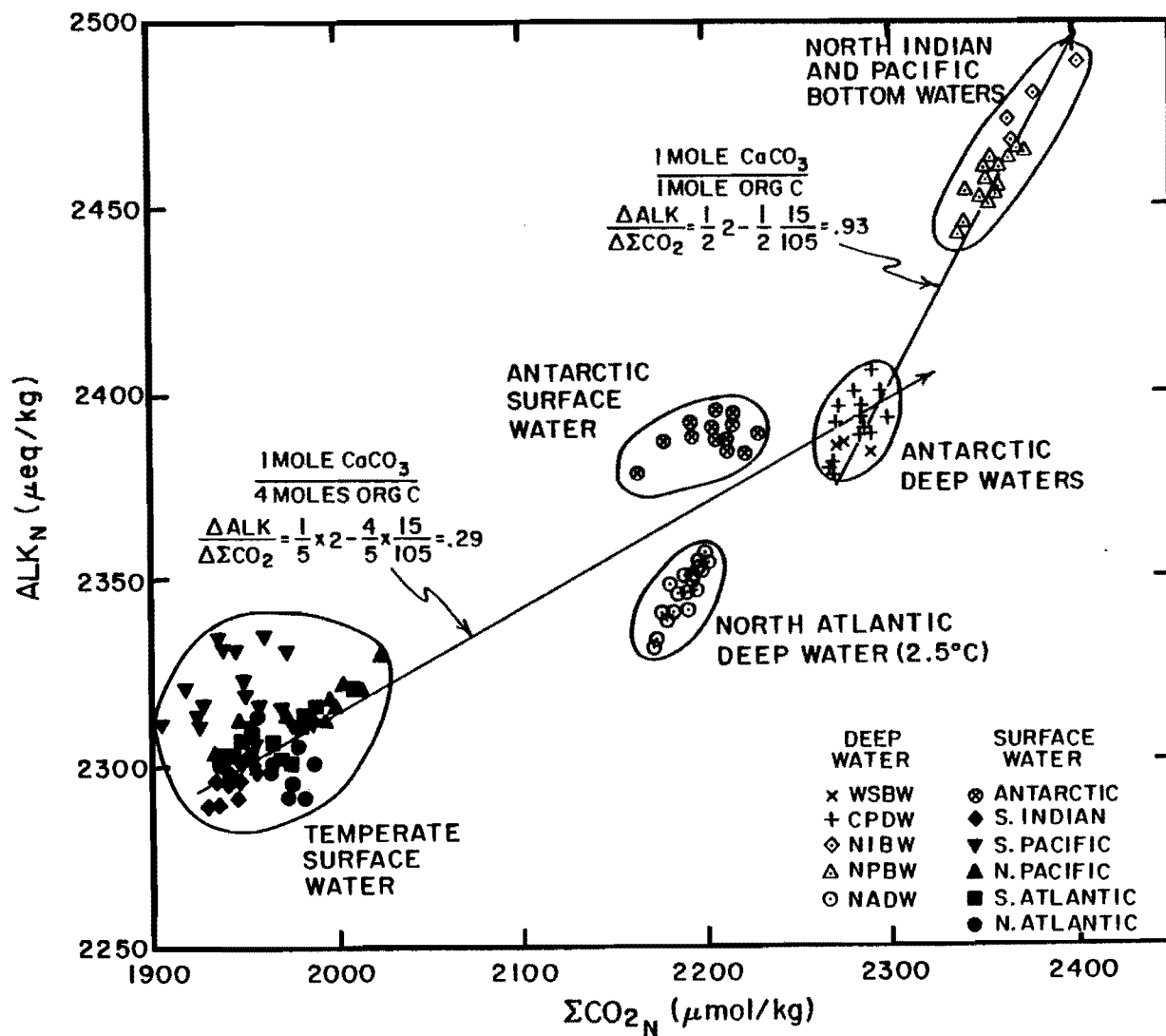


Figure 2-9. Plot of alkalinity against ΣCO_2 concentration (both normalized to a salinity of 35.00‰) for major surface and deep water types in the world ocean. The solid lines show the trends expected for CaCO_3 to organic C input ratios of 1:4 and 1:1. Based on results obtained as part of the GEOSECS program (406).

10^{-3} equiv/kg, our deep water must have an alkalinity of 2.26×10^{-3} equiv/kg. The difference between alkalinity and total dissolved carbon in our deep water sample is 0.06×10^{-3} moles/kg. Despite the fact that deep water has 10 percent more total dissolved carbon, it has only about one third the carbonate ion content of surface water. This is so because more CO_2 is released to deep water by the oxidation of organic tissue than $\text{CO}_3^{=}$ ion by the solution of CaCO_3 . The excess carbon dioxide combines with carbonate ion to form bicarbonate ($\text{CO}_2 + \text{CO}_3^{=} + \text{H}_2\text{O} \rightleftharpoons 2\text{HCO}_3^-$). The HCO_3^- ion content of the deep water is 2.14×10^{-3} moles/kg, which is, of course, higher than that in surface water. Table 2-7 summarizes these calculations. In this table the dissolved CO_2 (but not the borate contribution) is included.

The vertical distribution of carbonate ion content (calculated without any of the approximations used above) along north-south sections in the world ocean (calculated with all species included) is shown in figures 2-10 (the western central Atlantic Ocean), 2-11 (the western central Indian Ocean), and 2-12 (the eastern and western Pacific Ocean). A quick look at these figures shows that the large difference in carbonate ion concentration obtained in the simplified calculation is also found in the real ocean. Between 30°N and 30°S the concentration in surface water generally is above 200×10^{-6} moles/kg, reaching nearly as high as 300×10^{-6} moles/kg. By contrast, the values in deep water range from 65 to 115×10^{-6} moles/kg. A closer look at the deep water values reveals that they decrease from the Atlantic Ocean to the Indian and Pacific Oceans (a distribution consistent with that of dissolved oxygen and of nitrate). Further, the basal part of the main thermocline in all three oceans shows a carbonate ion content minimum. This minimum corresponds to the minimum in dissolved oxygen content (again consistent with expectation).

SPACIAL VARIATIONS IN THE CaCO_3 SATURATION OF SEA WATER

Having established the distribution of carbonate ion in the ocean we can now compare it with the saturation carbonate ion content for calcite and for aragonite. To illustrate this relationship, the carbonate ion concentration versus water depth curve for a station in the South Atlantic is compared in figure 2-13 with the saturation carbonate ion versus depth curves for calcite and aragonite. As can be seen, the carbonate ion saturation curve for aragonite crosses over the observed carbonate ion concentration curve at a depth of 3.4 kilometers. The calcite saturation curve crosses over the in situ curve at a depth of 4.3 kilometers. The waters above these cross-over depths are supersaturated with respect to this mineral phase. The waters beneath the cross-over depth are undersaturated with respect to calcite. The difference between the two values (i.e., $[\text{CO}_3^{=}]_{\text{in situ}} - [\text{CO}_3^{=}]_{\text{sat}}$) is a measure of the tendency for the calcite to dissolve. Positive values indicate supersaturation and negative values undersaturation; the greater the difference, the greater the extent of supersaturation or undersaturation.

To show how the depth of the saturation horizon for calcite varies within a given ocean and between oceans, vertical sections

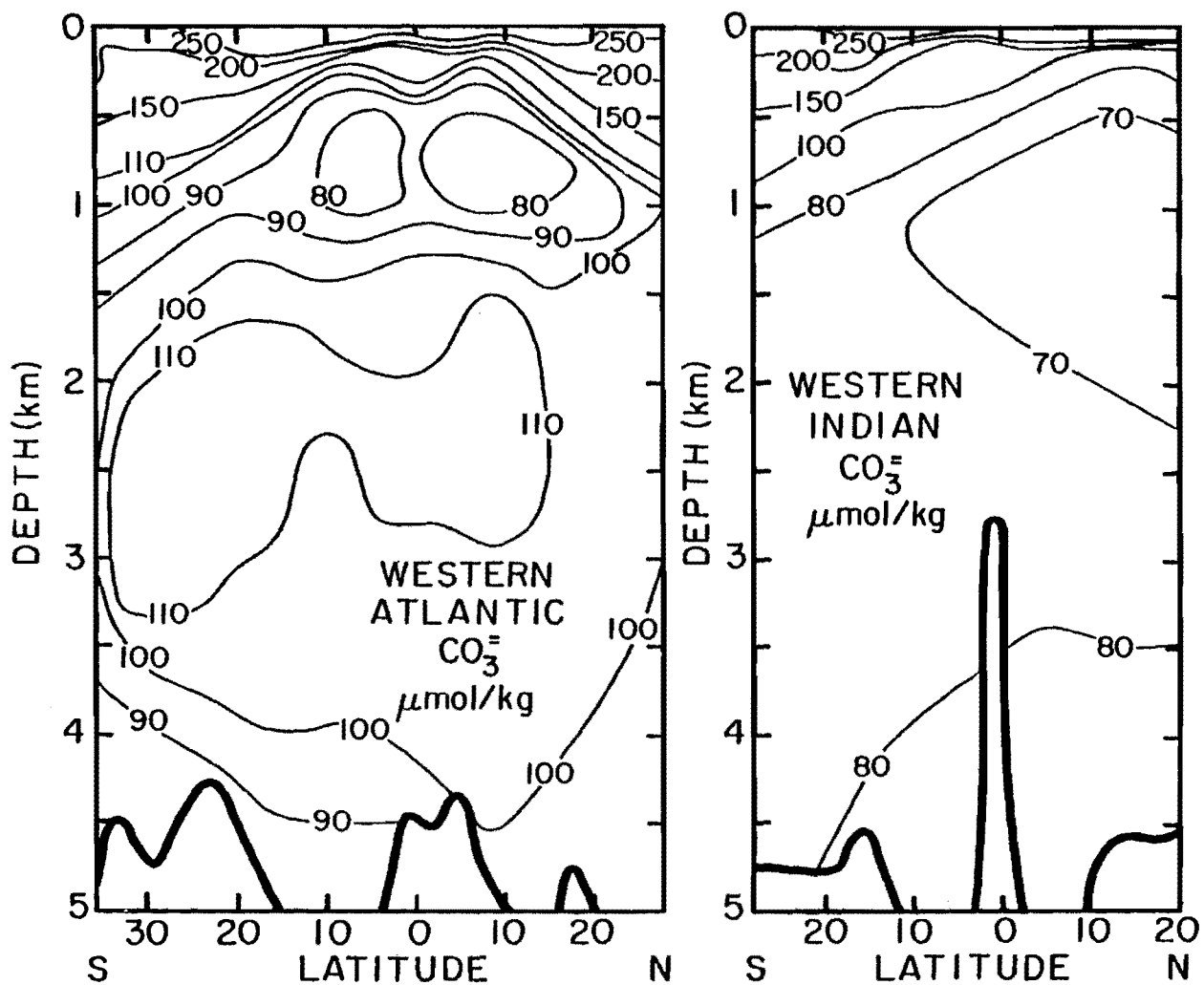


Figure 2-10. The left hand diagram shows the distribution of carbonate ion concentration with depth along a north-south section in the western basin of the Atlantic Ocean. The minima in carbonate ion content water at a depth of about 0.75 kilometers to the north and to the south of the equator are the result of higher productivity supported by upwelling in the equatorial zone. The wedge of low carbonate concentration water at the bottom of the South Atlantic is due to the invasion of Antarctic Bottom Water. Based on the results obtained as part of the GEOSECS program (406). The tracks along which this and the sections which follow were drawn can be found on the foldout map.

Figure 2-11. The right hand diagram shows the distribution of carbonate ion concentration with depth along a north-south section in the western Indian Ocean. Because this ocean has no northern source of deep water, respiration effects are large and the carbonate ion contents correspondingly low. Based on results obtained as part of the GEOSECS program (406).

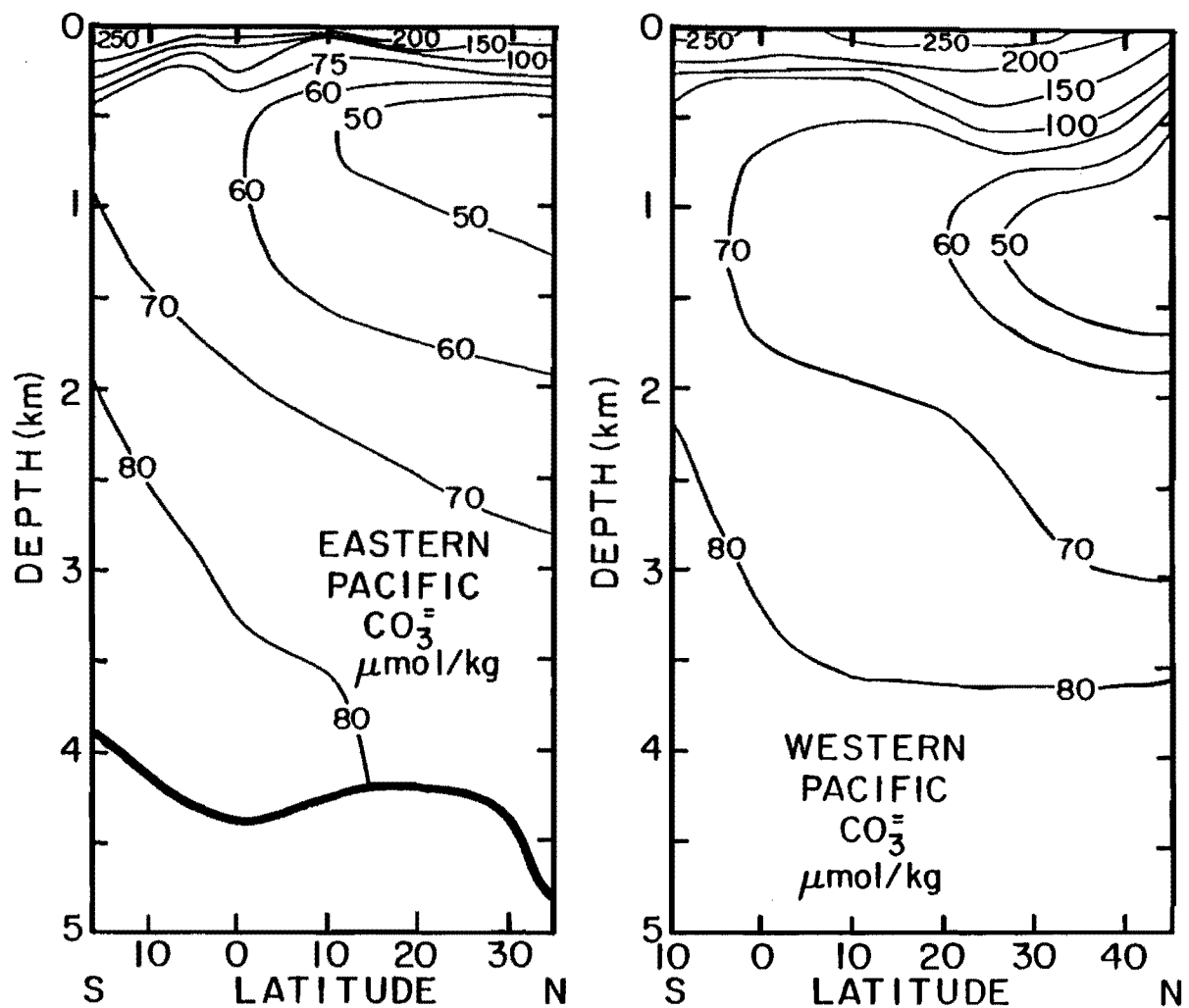


Figure 2-12. Sections of carbonate ion concentration with depth along north-south sections in the eastern (to the left) and western (to the right) Pacific Ocean. Again, because there is no deep water source in the North Pacific, the effects of respiration become stronger going from south to north, leading to a northward decrease in carbonate ion content in the deep waters. Based on results obtained as part of the GEOSECS program (406).

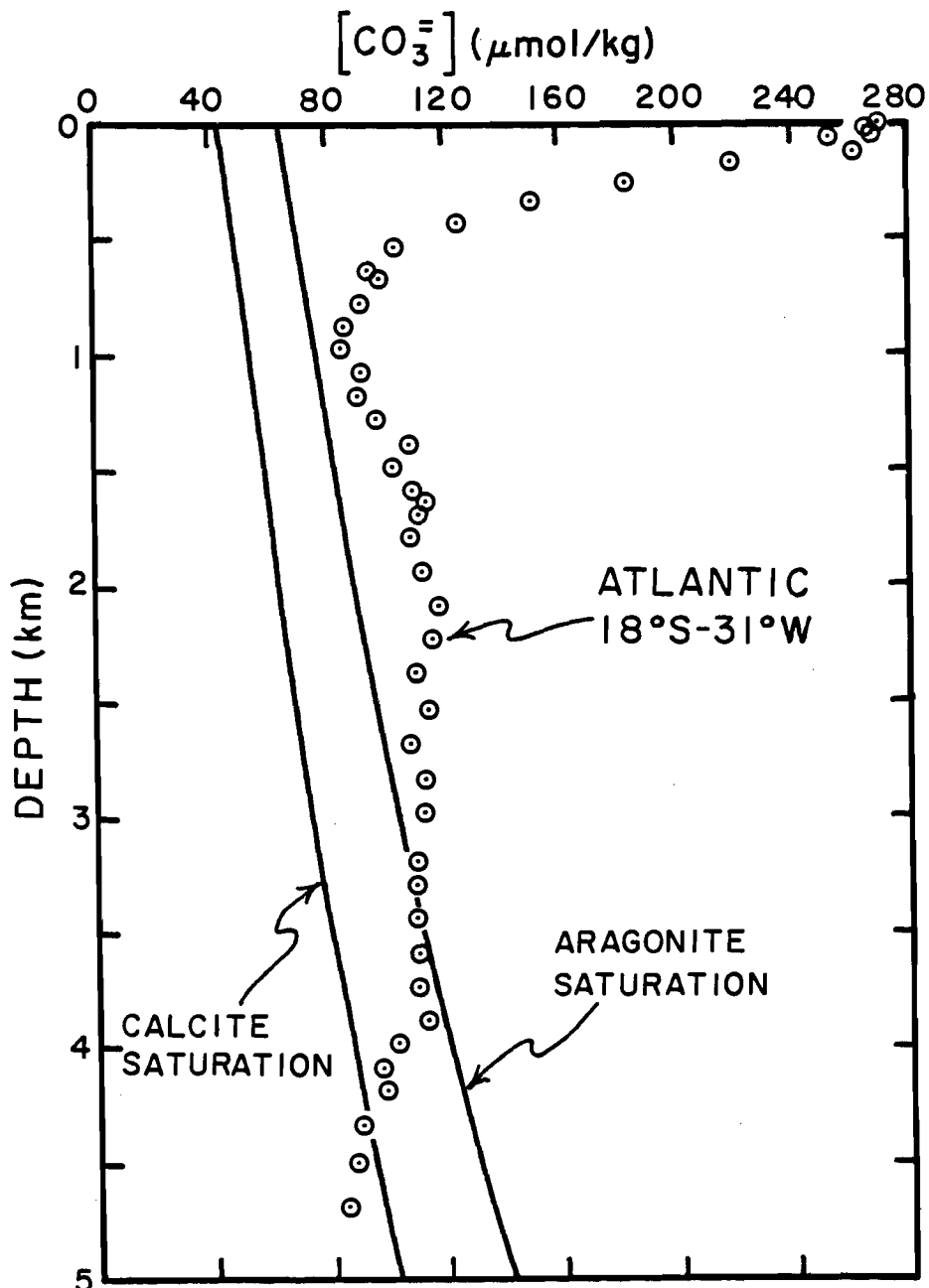


Figure 2-13. Plot of carbonate ion concentration versus water depth for a station in the western South Atlantic. Also shown are the saturation carbonate ion concentrations increase with depth mainly because of the pressure effect (calcium and carbonate ions occupy less volume when dissolved in sea water than when locked in $CaCO_3$). The concentration of carbonate ion remains fairly constant through the North Atlantic Deep Water mass. It is higher in this mass than in the underlying wedge of Antarctic Bottom Water and in the overlying tongue of Antarctic Intermediate Water. These results were obtained as part of the GEOSECS program (406).

running north to south through the three major oceans for the property ΔCO_3 (i.e., $[\text{CO}_3^=]_{\text{in situ}} - [\text{CO}_3^=]_{\text{sat}}$) have been prepared (see figures 2-14, 2-15 and 2-16). In these diagrams the zero contour represents the saturation horizon. The contours for negative values represent undersaturated water, and those for positive values supersaturated water. The saturation horizon is deepest in the western Atlantic Ocean (~ 4500 meters), intermediate in the western Indian Ocean (~ 3500 meters) and shallowest in the North Pacific (< 3000 meters).

Figure 2-17 shows a similar section constructed for aragonite in the western Atlantic.* Consistent with its metastability (and hence higher solubility), the depth of the saturation horizon for aragonite in the western Atlantic is about 1000 meters shallower than that for calcite. In the Pacific and Indian Oceans the saturation horizon for aragonite is located within the main thermocline.

The depth of the saturation horizon determined from sedimentary evidence is broadly consistent with that determined from carbonate ion measurements. As shown in figures 2-14, 2-15 and 2-16, the depth at which the effects of solution are first seen in the sediments (termed the lysocline) is about the same as the depth of the saturation horizon. As both depth estimates are subject to uncertainties of several hundred meters, the differences between the saturation horizon depth and the lysocline depth seen in these diagrams lies within our ability to measure them.

Below the lysocline, the percent calcite in sediments accumulating on the flanks of the mid-ocean ridges drops from the value of 90 percent characterizing sediments above the lysocline to just a few percent 300 to 1000 meters below the lysocline. Figure 2-18 shows the trend of the calcite content of sediments as a function of bottom depth for several regions of the sea floor. These diagrams also show the water depth interval over which the difference $[\text{CO}_3^=]_{\text{in situ}} - [\text{CO}_3^=]_{\text{sat}}$ changes from 0 to 10×10^{-6} moles/kg. It can be seen from these diagrams that an undersaturation of 10×10^{-6} moles/kg is enough to dissolve almost all the calcite falling to the sea floor.

In order to provide yet another independent estimate of the depths at which the minerals calcite and aragonite begin to dissolve, an oceanographer named Mel Peterson came up with a clever new approach (473). He hung calcite spheres at various depths on a mooring set by physical oceanographers interested in measuring the speed and direction of currents in the deep sea. By carefully weighing these spheres before and after deployment in the sea, he was able to gain a sense of this variation of the rate of calcite solution with depth in the sea. His results showed considerable scatter, but yielded the trend shown in the left panel of figure 2-19. Since Peterson's demonstration of the utility of this method, other investigators have done similar experiments. The most elaborate of these was carried out by Honjo (475). They deployed

*As the saturation horizons for aragonite in the central Indian and Pacific Ocean are shallower than 600 meters, there is no point in presenting corresponding diagrams.

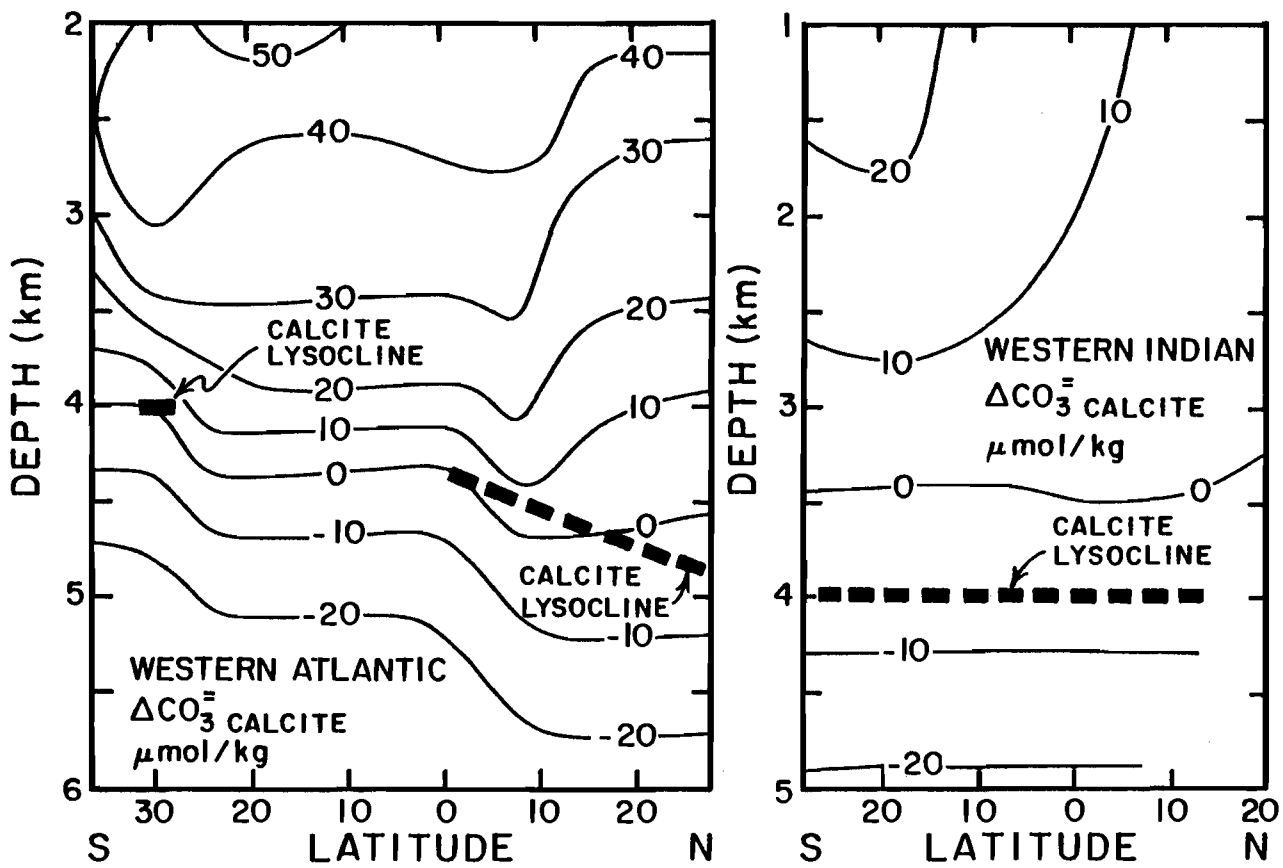


Figure 2-14. The left hand diagram shows a section in the western central Atlantic of the vertical distribution of the difference between the in situ carbonate ion concentration and the saturation carbonate ion concentration for the mineral phase calcite. Where this difference is zero, the waters are saturated with calcite. Where it is negative, calcite dissolves. The rate of solution is proportional to the magnitude of this difference. The rise in the saturation horizon to the south is related to the invasion of bottom water from the Antarctic carrying lower carbonate ion content than does the deep water formed at the northern end of the Atlantic. The depth of the lysocline for calcite as determined from sediment studies is also shown. These results were obtained as part of the GEOSECS program (406).

Figure 2-15. The right hand diagram shows a section in the western central Indian Ocean of the vertical distribution of the difference between in situ carbonate ion concentration and the saturation carbonate ion concentration for the mineral phase calcite. The depth of the lysocline for calcite as determined by studies of the deep sea sediments is shown for comparison. Based on data obtained as part of the GEOSECS program (406) and on the solubility of calcite and recommended by Broecker and Takahashi (463).

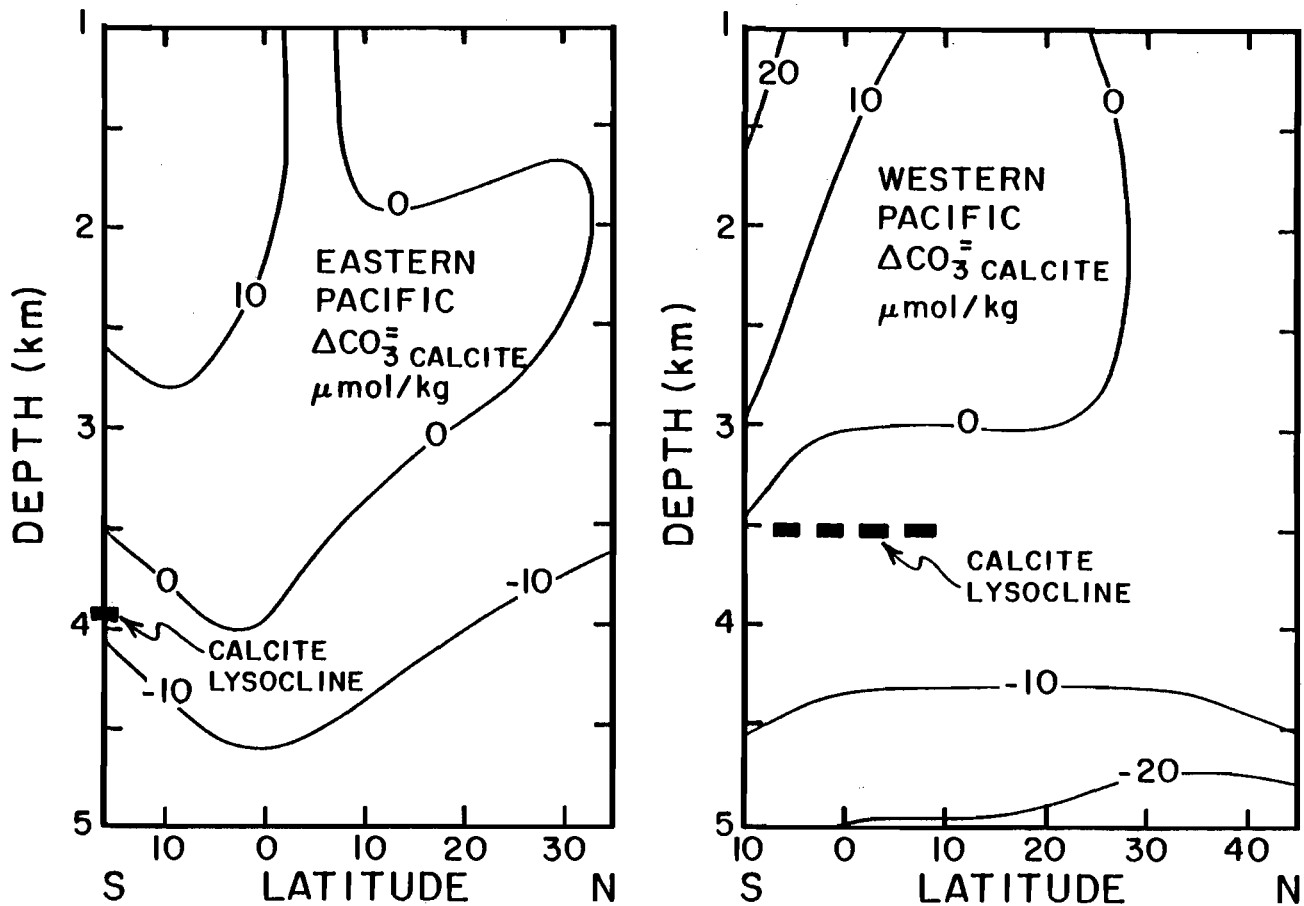


Figure 2-16. Section in the eastern (on the left) and western (on the right) Pacific showing the vertical distribution of the difference between the *in situ* carbonate ion concentration and the saturation carbonate ion concentration for the mineral phase calcite. It can be seen that the saturation horizon rises to depths less than 1000 meters in the north Pacific. The depth of the lysocline as determined from sediment studies is shown for comparison. Based on data obtained as part of the GEOSECS program (406) and on the solubility of calcite recommended by Broecker and Takahashi (463).

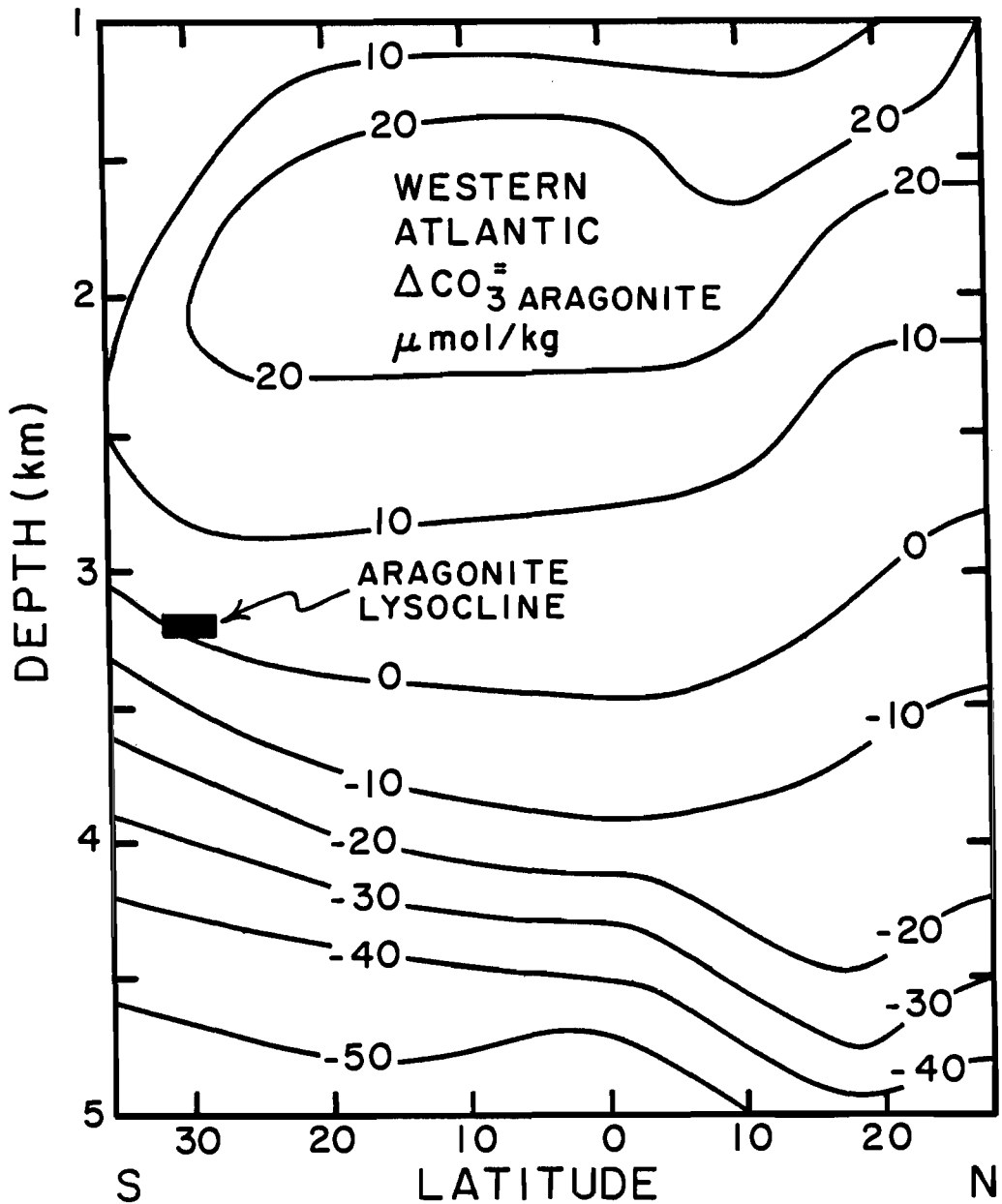


Figure 2-17. Section in the western central Atlantic showing the vertical distribution of the difference between the *in situ* carbonate ion concentration and the saturation carbonate ion concentration for the mineral phase aragonite. The saturation horizon is at a shallower depth than that for calcite (see figure 2-14). The depth of the lysocline for the aragonitic shells of pteropods based on sediment studies is shown for comparison. Based on data obtained as part of the GEOSECS program (406) and on the solubility of aragonite recommended by Broecker and Takahashi (463).

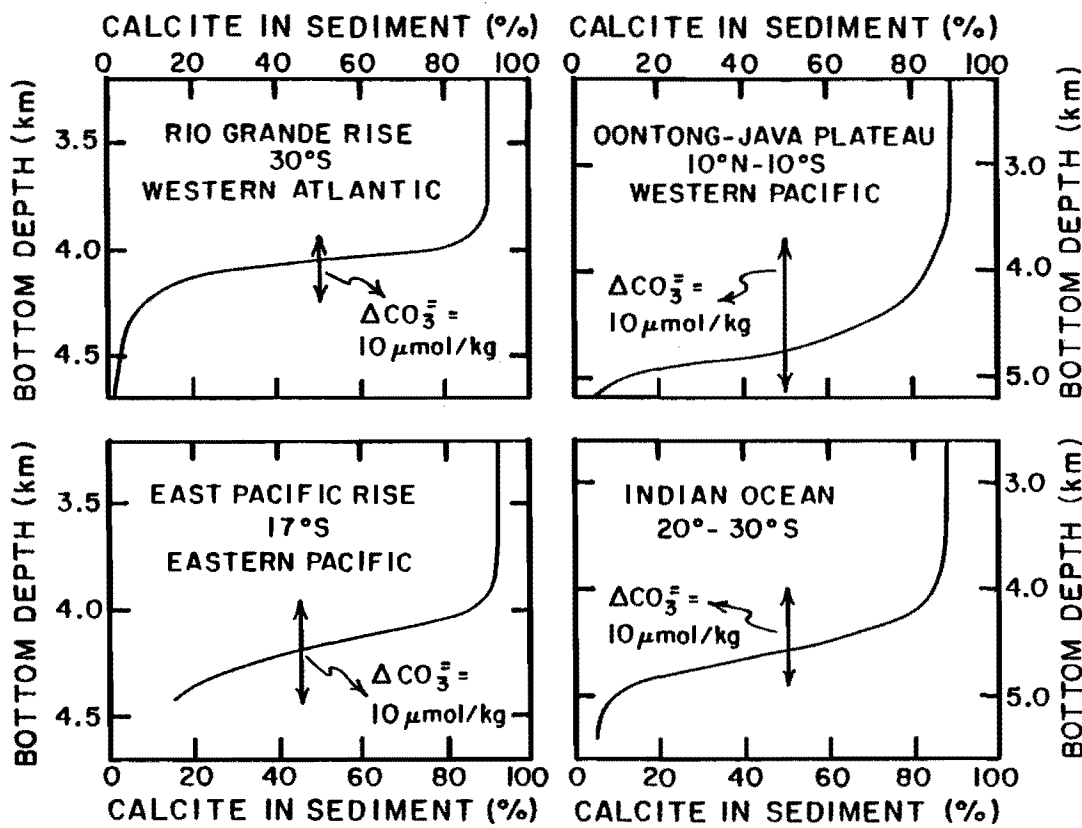


Figure 2-18. Generalized plots of the calcite content of material from sediment core tops versus water depth (on the flanks of mid-ocean ridges and plateaus). While individual data points show a fair amount of scatter, enough measurements have been made to permit the mean trends shown here to be defined. The depth at which the calcite content of the sediment begins to decline is designated as the lysocline. Below this depth, solution becomes progressively more intense until nearly all the calcite which rains to the sea floor dissolves. This progressive intensification of solution reflects the increase in the degree of undersaturation with water depth beneath the saturation horizon. The arrows show the water depth interval over which the difference between the in situ and saturation carbonate ion concentrations changes by 10×10^{-6} moles/kg. The top of each arrow is at the lysocline. The data on which these generalized diagrams are based are shown in figure 2-7.

small pumps at three depths on a mooring and pulled water over various types of calcite and aragonite. The pumps eliminated the effect of differing current flows. Each pump pushed water across the crystals at the same rate. Their results are also shown in the right panel of figure 2-19. While more detailed measurements of this type are needed, the results of those carried out to date are certainly consistent with the distribution of calcite and aragonite in sea floor sediments.

The results of a more recent deployment of Honjo's pumps in the Panama Basin are summarized in figure 2-20 (476). In this experiment both calcite and foraminifera shells were placed in the chambers. After exposure the calcite crystals were reweighed and the foraminifera shells viewed for breakage. As can be seen in the figure the chambers at water depths less than 3 kilometers showed some weight loss (3 to 8%) and some breakage of foraminifera shells (presumably from solution damage). The chambers located at 3.8 kilometers showed much greater calcite weight loss (24 to 33%) and far more foraminifera shell damage (15 to 23% of the shells were broken). These changes are nicely reflected by the calcite content of sediment samples taken at various depths in this area. Sediments from depths less than 3 kilometers are high in calcite (>80%). Below 3 kilometers a rapid drop in calcite content is seen. The deepest sample (at 3.5 km) had only 43% calcite. As can be seen from figure 2-16 in this region of the eastern Pacific, the waters between 2 and 3 kilometers depth are just slightly supersaturated (the Honjo data suggest that perhaps they are just slightly undersaturated) and that at about 3.4 kilometers they become undersaturated. The data in figure 2-16 also suggest that at depths in excess of 3.4 kilometers the degree of undersaturation increases with depth (Honjo's data suggest that this increase commences at about 3.0 kilometers depth). Thus the two sets of measurements agree to within a $\Delta\text{CO}_3^{\text{eq}}$ value of about 5×10^{-6} moles.

One other line of evidence must be discussed. Almost two decades ago Peter Weyl invented a technique for the direct measurement of the undersaturation and supersaturation of calcite (or aragonite) in sea water (469). His procedure was as follows. He filled a tube with crystals of calcite (or aragonite) and buried the tip of the glass electrode of a pH meter in these crystals. He then pumped sea water through the crystals at a high enough rate so that the pH in the water leaving the tube was exactly the same as that in the water entering the tube. He then stopped the flow of the water through the tube and in so doing isolated a batch of sea water within the crystal pores. He then observed the change in pH of this water with time (if the water was initially undersaturated, the pH rose and if the water was initially supersaturated, the pH fell). Examples of the responses found for undersaturated sea water are shown in figure 2-21. As shown, the pH approaches a constant value asymptotically. Assuming this value to be that for saturation with respect to the mineral phase present in the column, Weyl showed that the ratio of the initial to the final CO_3^{eq} ion concentration could be obtained from the pH results using the following relationships:

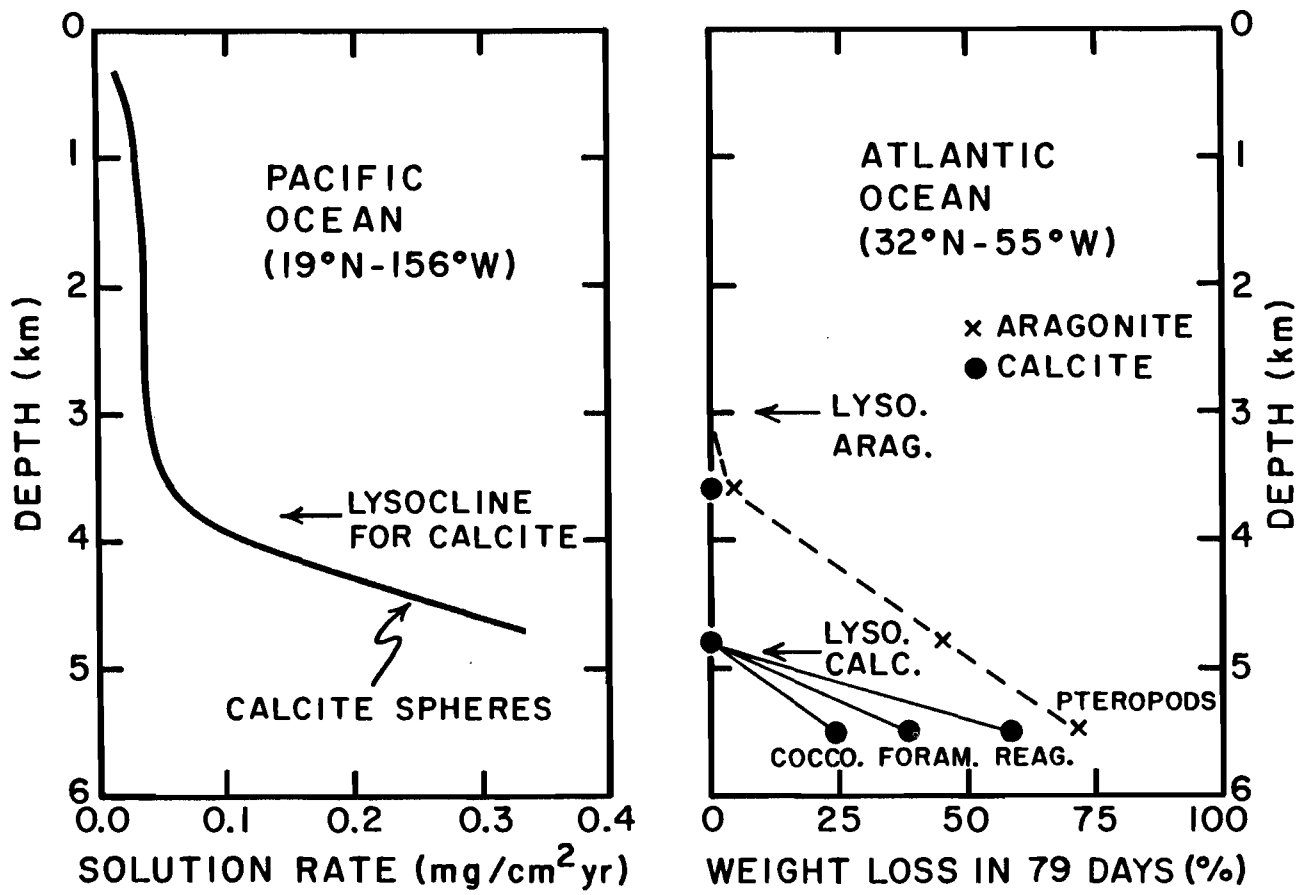


Figure 2-19. Results of mineral exposure experiments performed on deep sea moorings (473). The experiment depicted on the left was conducted by Peterson of the Scripps Institute of Oceanography in 1965 for a period of 250 days using calcite spheres hung directly in the sea. The experiment depicted on the right was conducted by Honjo and his coworkers at the Woods Hole Oceanographic Institution in 1976 for a period of 79 days (475). In this experiment, the materials (coccoliths, foram shells, reagent calcite, and pteropod shells) were held in chambers through which water was drawn by a pump. The depth of the lysocline for the respective mineral phases as established through studies of the sediments are shown for comparison.

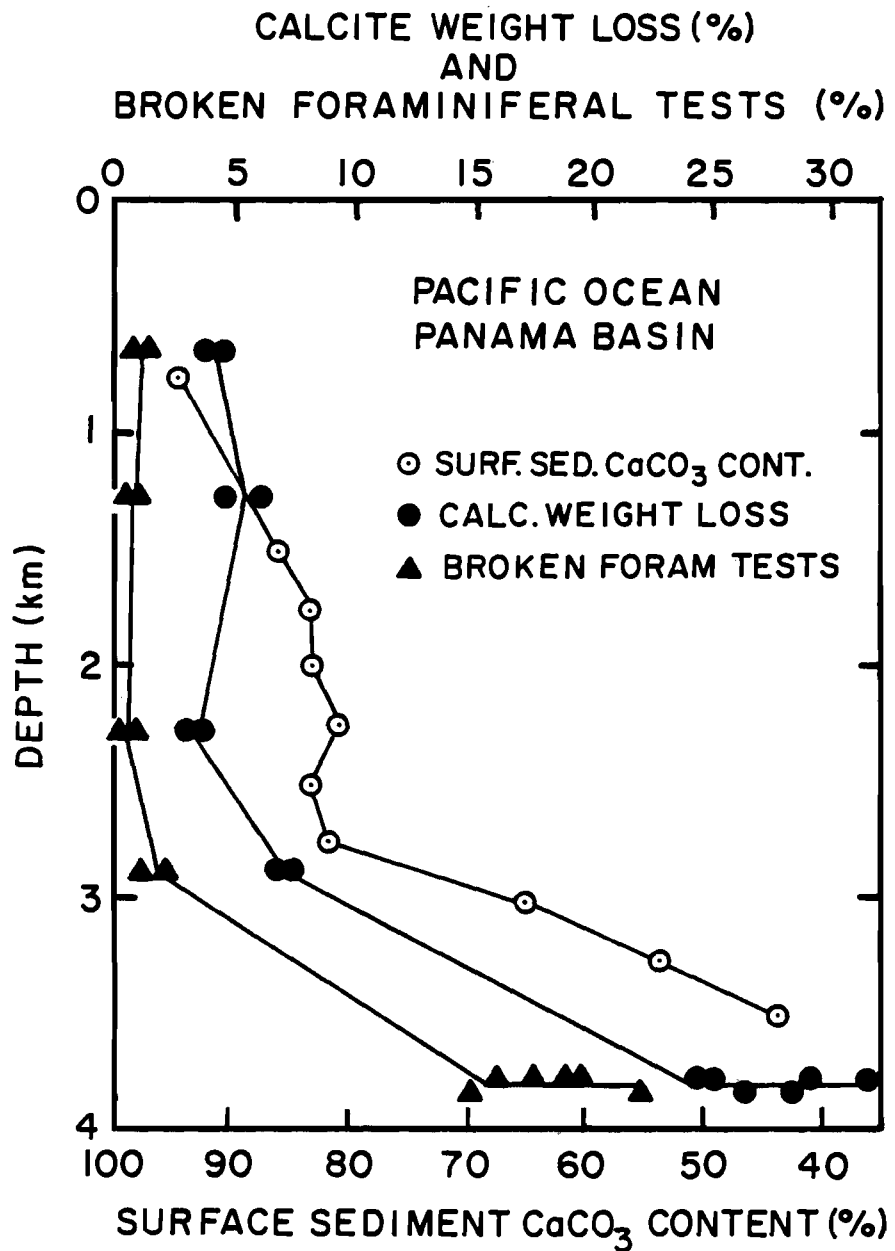


Figure 2-20. Comparison of weight loss (solid circles) and percentage of broken foraminiferal tests (solid triangles) for an *in situ* mineral and shell exposure conducted in the Panama Basin by Honjo and his coworkers at the Woods Hole Oceanographic Institution (476) with the percentage of calcium carbonate (open circles) for surface sediments taken at various depths in the same area.

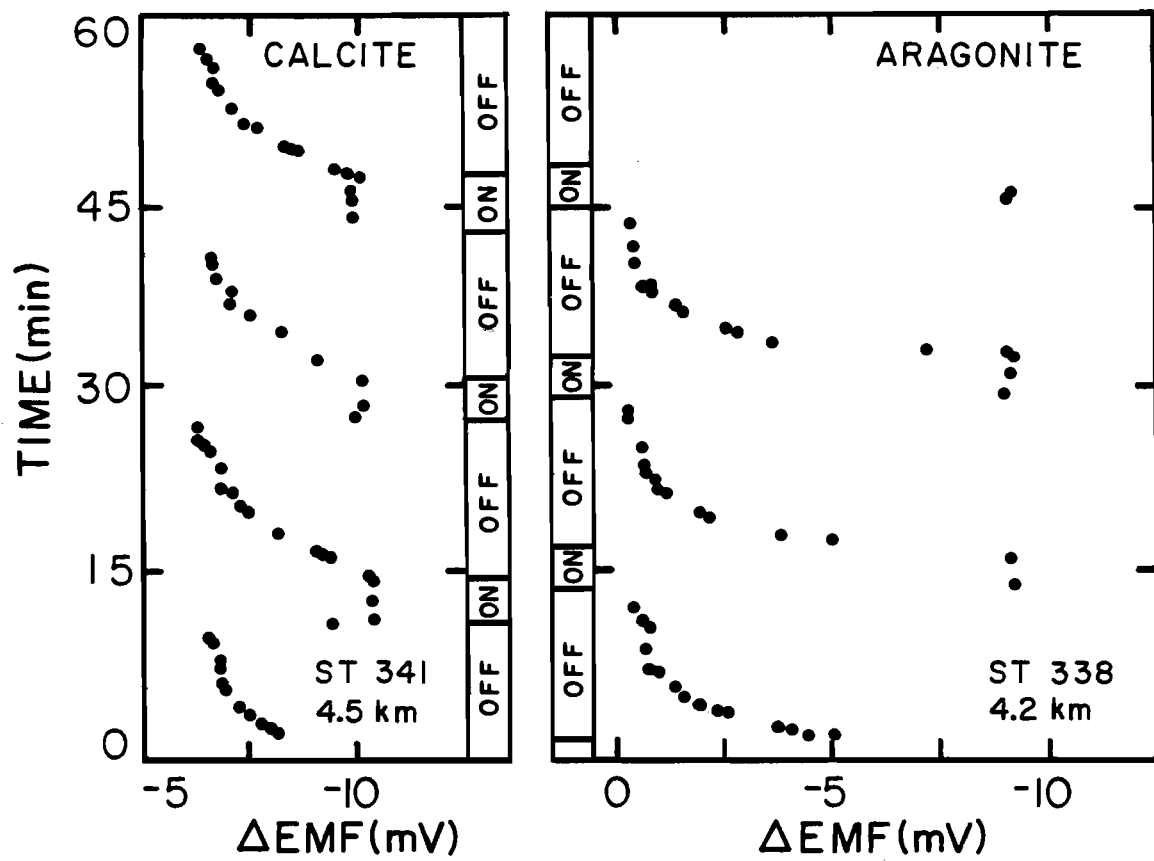


Figure 2-21. Electromotive force (i.e., potential) difference between the pH electrodes immersed in calcite (on the left) and in aragonite (on the right) against time using the Weyl-Ben Yaakov in situ saturometer. The sharp offsets occur when the pump flushes fresh seawater through the column. When the pump goes off, the pH drifts toward the saturation value. These results were obtained during the GEOSECS program.

$$\frac{[\text{CO}_3^=]_{\text{Final}}}{[\text{CO}_3^=]_{\text{Initial}}} = \frac{[\text{H}^+]_{\text{Initial}}}{[\text{H}^+]_{\text{Final}}} \quad 2-29$$

Further, if the $\text{CO}_3^=$ ion concentration in the input water were known, then the difference between the saturation and initial $\text{CO}_3^=$ ion concentrations could be obtained:

$$[\text{CO}_3^=]_{\text{sat}} - [\text{CO}_3^=]_{\text{I}} = \left[\frac{[\text{H}^+]_{\text{I}}}{[\text{H}^+]_{\text{F}}} - 1 \right] [\text{CO}_3^=]_{\text{I}} \quad 2-30$$

Some years after Weyl invented this clever technique, Sam Ben Yaakov adapted it to work within the sea (471). He built a unit which could be lowered from a ship into the deep sea. It had a pump which went on and off in a fixed time cycle and it had a tape recorder which kept track of the electrode potential difference and hence of the pH. The records shown in figure 2-21 were obtained by this unit.

These measurements of the depth of the saturation horizon are compared in figure 2-22 with those obtained by assuming that the sediment lysocline represents the saturation horizon. The agreement is quite good. One might ask why an ocean-going saturometer should be used to measure the solubility of calcite and aragonite when such measurements can be made in the laboratory. The answer is that the laboratory measurements prove to be very difficult. It is not easy to maintain sea water at low temperatures and high pressures without changing its alkalinity due to interactions with the container or its ΣCO_2 content due to biological activity or to CO_2 release from the container. Experiments in the deep sea circumvent the need to maintain all these properties.

FACTORS CONTROLLING THE RATE OF CALCITE SOLUTION

Can the same arguments made for the rate of opal solution be applied to calcite? While the answer to this question is yes, there are several major differences between the solution of these two phases. The first has to do with the driving force for solution. Since the saturation silicate content of sea water (with respect to opal) is so much larger than the ambient silicate content of deep sea water, the driving force for silica dissolution is nearly constant over the entire deep sea floor (i.e., S^* is nearly constant). We have seen that for calcite the driving force varies widely, it ranges from zero at the lysocline to as high as 30×10^{-6} moles/kg difference in $\text{CO}_3^=$ ion concentration in the deepest parts of the ocean. Thus the variability in S^* for calcite becomes a major factor in determining the distribution of calcite in sediments.

Another difference is that the pore water resaturation time for calcite appears to be about 4000 times smaller than that for opal! We know this from the response seen using the Weyl-Ben Yaakov "saturometer" (see figure 2-21). Rather than taking 10 days ($\sim 8 \times 10^5$ sec) as calculated from the silicate versus depth profiles in sediment pore waters, only a few minutes ($\sim 2 \times 10^2$

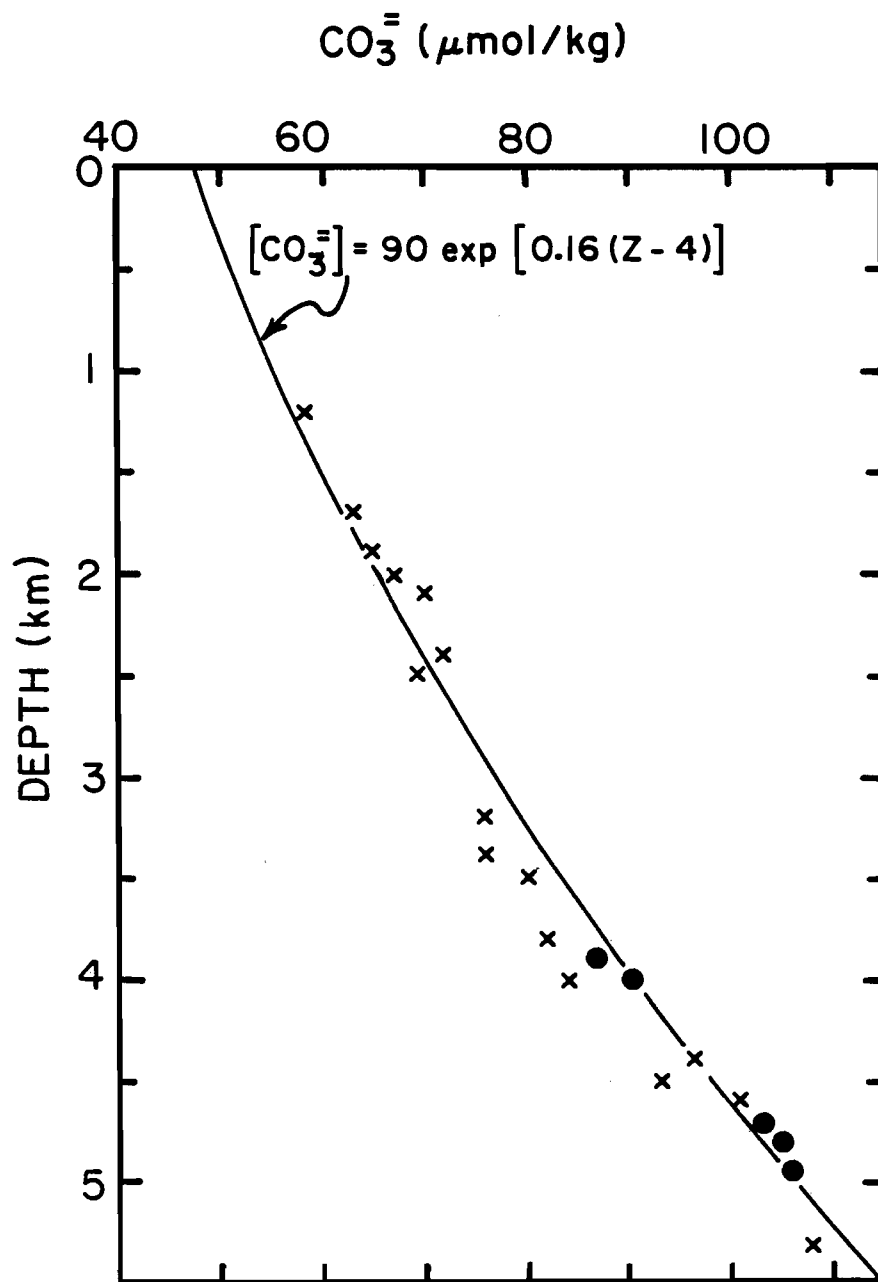


Figure 2-22 Plot of saturation CO_3^{\pm} ion concentrations obtained using the Weyl-Ben Yaakov in situ saturometer (crosses) and by assuming that the lysocline represents the saturation horizon (solid circles). The curve drawn through these points has the exponential shape demanded by thermodynamic theory. Z in the equation indicates water depth in kilometers. This summary was made by Broecker and Takahashi (463).

sec) are required for the pH to adjust in a calcite-filled column.

As shown in equation 2-13, the relationship between the characteristic resaturation depth and the characteristic resaturation time is:

$$z^* = \sqrt{D_s \tau} \quad 2-31$$

Hence,

$$\frac{z^*_{\text{calcite}}}{z^*_{\text{opal}}} = \sqrt{\frac{\tau_{\text{calcite}}}{\tau_{\text{opal}}}} \approx 0.016 \quad 2-32$$

The resaturation depth for pure opal is about 1 cm. Thus that for pure calcite must be on the order of 0.16 millimeters (160 microns).

This fast response time allows calcite to dissolve as fast as opal despite the fact that the difference between the steady pore water concentration and the bottom water concentration for opal ($\sim 300 \times 10^{-6}$ moles/kg) is 30 times larger than that for calcite (at the base of the transition zone between calcite rich and calcite free sediment the value of ΔCO_3 is about 10×10^{-6} moles/kg). As shown in equation 2-17, the flux is given by:

$$\text{Flux} = (C_{\text{sat}} - C_{\text{bot}}) \sqrt{\frac{D_s}{\tau}} \quad 2-33$$

Hence the 30 fold difference in concentration gradient is compensated by the 4000 fold difference in resaturation time!

There are two other factors which might influence the rate of solution of calcite. First, fluid dynamicists tell us that at the sediment water interface there is a barrier to molecular transport. We can approximate the resistance imposed by this boundary layer by thinking of it as a "stagnant film" through which ions pass only by molecular diffusion. The resistance of the film will be proportional to its thickness. Although it is not possible to determine the effective thickness of this film, the best guesses place it in the range 30 to 3000 microns. The point is that, if the thickness lies at the low end of this range, the resistance which it poses is small compared with that posed by the diffusion path within the sediment (averages about 100 microns in length). On the other hand, were it to lie at the high end of the range, then its influence would be greater than that posed by the diffusion path in the sediment. These situations are shown diagrammatically in figure 2-23. Since silicate has a characteristic diffusion path of several cm in the sediment, its solution rate would not be significantly altered by even a film of 3000 microns (i.e., 0.3 cm) in thickness.

Whether it is the "stagnant film" just above the sediment water interface or the diffusive pathway within the pore waters of the sediment which constitutes the limiting resistance for calcite solution has implications for the distribution of calcite on the sea floor. Were the stagnant film the limiting resistance, then

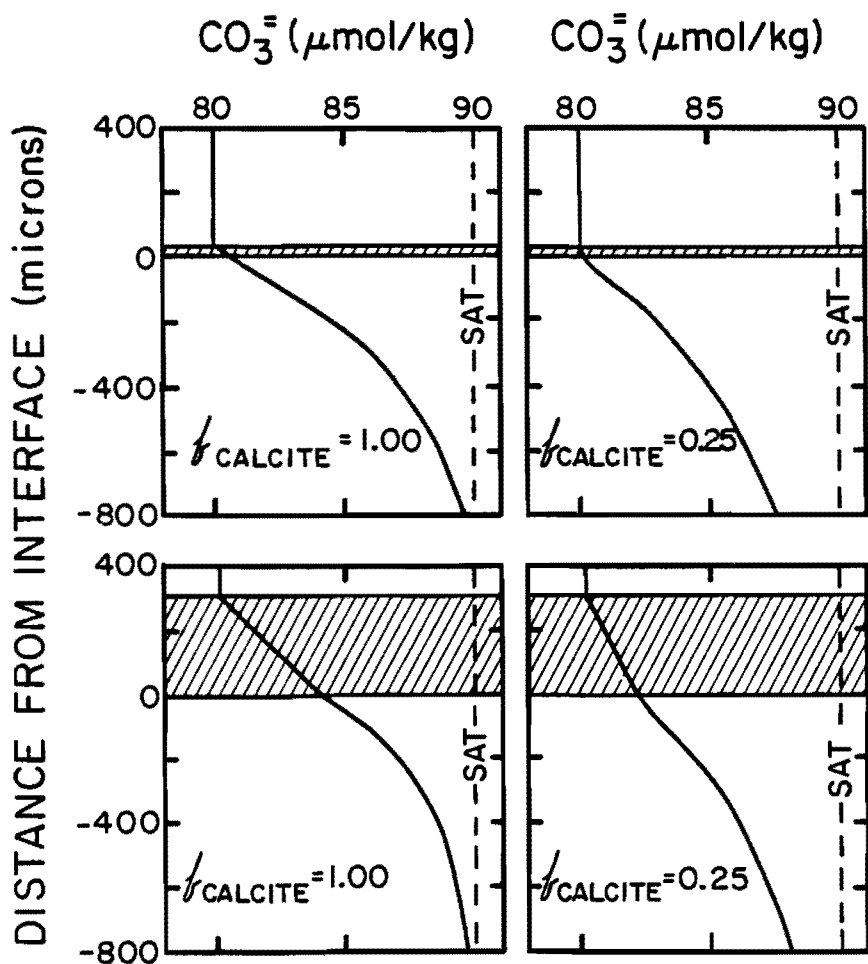


Figure 2-23. Hypothetical plots of $\text{CO}_3^=$ ion content versus distance away from the sediment water interface. In the upper two diagrams the boundary layer is assumed to exert a resistance to ionic transport equivalent to that of a stagnant film 15 microns in thickness, and in the lower two diagrams it is assumed to exert a resistance equivalent to that of a stagnant film 300 microns in thickness. The left hand diagrams are for sediments with 100% calcite and the right hand diagrams are for sediments with 25% calcite. If the pore water resaturation time is inversely proportional to the calcite content of the sediment, then the resaturation depth will be proportional to the square root of the fraction of calcite in the sediment. Thus a two times greater resaturation time would be found for the 25% calcite sediment than for the 100% calcite sediment (i.e., an e-folding depth of 600 microns rather than 300 microns). In each diagram the saturation $\text{CO}_3^=$ ion content is shown.

the rate of solution would depend on the factors controlling the thickness of this film (i.e., current velocity and turbulence in the abyssal waters). The rate of solution would not depend on the calcite content of the sediment. On the other hand, if the diffusive pathway within the sediment pore waters constitutes the limiting resistance then the solution rate would depend on the calcite content of the sediment but not on the water flow rate and turbulence in the abyssal waters. Thus it is important that we learn more about the magnitude of the resistance to molecular transport posed by the dynamic boundary layer just above the sea-sediment interface.

During the period this book was being written Santschi and his coworkers at the Lamont-Doherty Geological Observatory devised and tested a method to measure the resistance posed by so-called benthic boundary layer (696). Using Alvin, a research submersible, Santschi deployed and recovered flat plates of alabaster from the sea floor off Central America. Based on the weight loss during the period of four days residence on the sea floor he was able to show that the stagnant boundary film thickness over the alabaster was about 120 microns. As the bottom currents in the area of deployment were considerably higher than average this result is likely smaller than the ambient deep sea value. Once this method has received further testing and wide deployment it may be possible to determine whether it poses a significant resistance to calcite solution.

As proposed by Emerson of the University of Washington and Bender of the University of Rhode Island there is another way in which the solution process for calcite differs from that for opal. If organic material raining to the sea floor is stirred into the sediment column before being eaten by scavengers or bacteria, then the CO₂ generated from its destruction will be added to the pore waters. Before this CO₂ can diffuse out it will be neutralized by the solution of calcite. The products of this reaction would then diffuse through the pore spaces out into the overlying sea. This process would lead to calcite solution at all depths in the sea, even above the lysocline (519).

The ratio of organic residues to calcite entering the sediment column is critical for this process. If there were one or more moles of organic carbon per mole of CaCO₃ then it would have the potential to dissolve all the calcite. On the other hand, if the ratio is less than 0.1, then the destruction of organic matter would be secondary in importance. As we pointed out in chapter 1, sediment traps deployed near the sea floor generally collect particulates with an organic residue carbon to CaCO₃ carbon ratio close to unity. How much of this organic debris gets mixed into the sediment before being eaten? As organic matter accumulates in deep sea sediments at only 1% the rate at which it rains toward the sea floor, virtually all is eaten. The fragments of organic matter falling to the sea floor provide the sole source of food for bottom-dwelling organisms, thus one might expect these organisms to be adept at reaching and consuming newly fallen morsels before they are buried. It would therefore be surprising if a substantial fraction of the organic matter were inadvertently stirred into the sediment by the very organisms seeking it for

food! On the other hand, one might argue that the organisms which burrow through the sediment do so in search of food which they have purposely mixed down as a way of preventing it from being eaten by organisms which cannot burrow, or that some fraction of the organic material is inedible by bottom-dwelling animals and is eventually consumed by bacteria living within the sediment. Right now we simply do not know what fraction of the raining organic debris gets buried before it is eaten.

Another question that arises for calcite is whether its dissolution rate can be assumed to be proportional to the $\Delta\text{CO}_3^{\text{sat}}$ value. Indeed, evidence exists that this may not be the case. Measurements carried out by Keir in Berner's laboratory at Yale with calcite grains suspended in a rapidly stirred solution have shown that the solution rate is proportional to the fourth power of ΔCO_3 (479). If these results apply to the sea floor, then the rate of solution is 16 times higher for a ΔCO_3 of -20×10^{-6} moles/kg than for a ΔCO_3 of -10×10^{-6} moles/kg!

THICKNESS AND SHAPE OF THE SUBLYSOCLINE TRANSITION ZONE

If we put aside for the moment the possible resistance imposed by the boundary film at the sediment-water interface, the possibility that the relationship between the solution rate of pure calcite and the $\Delta\text{CO}_3^{\text{sat}}$ value is other than first order and the influence of the organic matter stirred into the sediment, then we can easily ascertain the factors controlling the width of the zone separating sediments experiencing little calcite solution from those for which nearly all the calcite has dissolved and the shape of the calcite content versus water depth curve across the zone. If the calcite content of the sediments within this zone is assumed to be at steady state (i.e., conditions in the ocean have remained constant for many thousands of years), then the calcite solution rate, S , can be equated to the difference between the rain rate, R , and accumulation rate, A . Hence:

$$S = R - A \quad 2-34$$

This equation can be rewritten:

$$S = R \left[1 - \frac{f}{f_L} \frac{(1-f_L)}{(1-f)} \right] \quad 2-35$$

where f_L is the fraction of calcite in the sediment above the lysocline and f is the fraction of calcite at some depth lying within the transition zone.

As shown above, if the rate of solution is limited by the time required for pore water saturation and if this reaction is first order, then:

$$S = (\text{CO}_3^{\text{sat}} - \text{CO}_3^{\text{bottom}}) \sqrt{\frac{D_s \cdot f}{\tau^*}} \quad 2-36$$

or

$$S = \Delta CO_3^{\bar{z}} \sqrt{\frac{D_S f}{\tau^*}}$$

2-37

Hence the shape of the calcite content versus depth curve is given by the equation:

$$\Delta CO_3^{\bar{z}} \sqrt{\frac{D_S f}{\tau^*}} = R \left[1 - \frac{f(1-f_L)}{f_L(1-f)} \right] \quad 2-38$$

Most places in the sea the value of $\Delta CO_3^{\bar{z}}$ increases at a constant rate with depth beneath the lysocline. Hence:

$$\Delta CO_3^{\bar{z}} = a(h-h_L) = a\Delta h \quad 2-39$$

where h_L is the lysocline depth and h the depth of interest within the transition zone. Our equation then becomes:

$$\Delta h = \frac{R}{a} \sqrt{\frac{\tau^*}{D_S f}} \left[1 - \frac{f(1-f_L)}{f_L(1-f)} \right] \quad 2-40$$

While this equation cannot be solved conveniently for f , graphs can be made showing how f varies with Δh for various values of a , R , and f_L . D_S and τ^* are assumed to have the same value everywhere on the sea floor (i.e., $\tau^* = 120$ sec and $D_S = 2 \times 10^{-6}$ cm²/sec). The curves in figure 2-24 show how the transition zone would look for several calcite rain rates for a value of $f_L = 0.9$ and a value for the constant a of 10×10^{-6} moles/kg km (both are typical for much of the deep sea). Under these conditions:

$$\Delta h = R \sqrt{\frac{1}{f}} \left[1 - \frac{0.1f}{0.9(1-f)} \right] 0.25 \text{ km} \quad 2-41$$

As can be seen, the entire range of thicknesses for the transition zones observed in various parts of the ocean (see figure 2-7) could simply be the result of a four fold range in the rain rate of calcite. Indeed the transition zone thickness differences from region to region do roughly parallel changes in rain rate!

A similar equation can be written down for the situation where a stagnant film limits the rate of accumulation. In this case:

$$\Delta h = \frac{R \Delta z}{a D} \left[1 - \frac{f(1-f_L)}{f_L(1-f)} \right] \quad 2-42$$

Taking the same values as above for f_L and for the constant a , a calcite rain rate of $1 \text{ g/cm}^2 10^3 \text{ yrs}^{-1}$, a value for the diffusivity of $CO_3^{\bar{z}}$ in bottom water as $1 \times 10^{-5} \text{ cm}^2/\text{sec}$ and a stagnant film

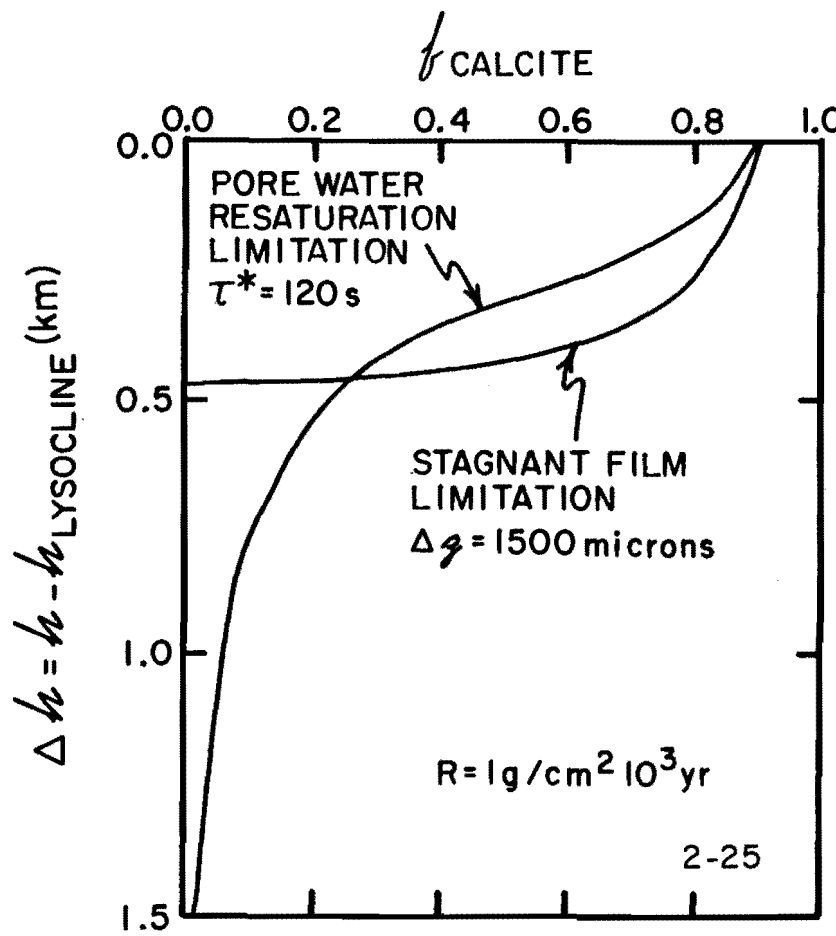
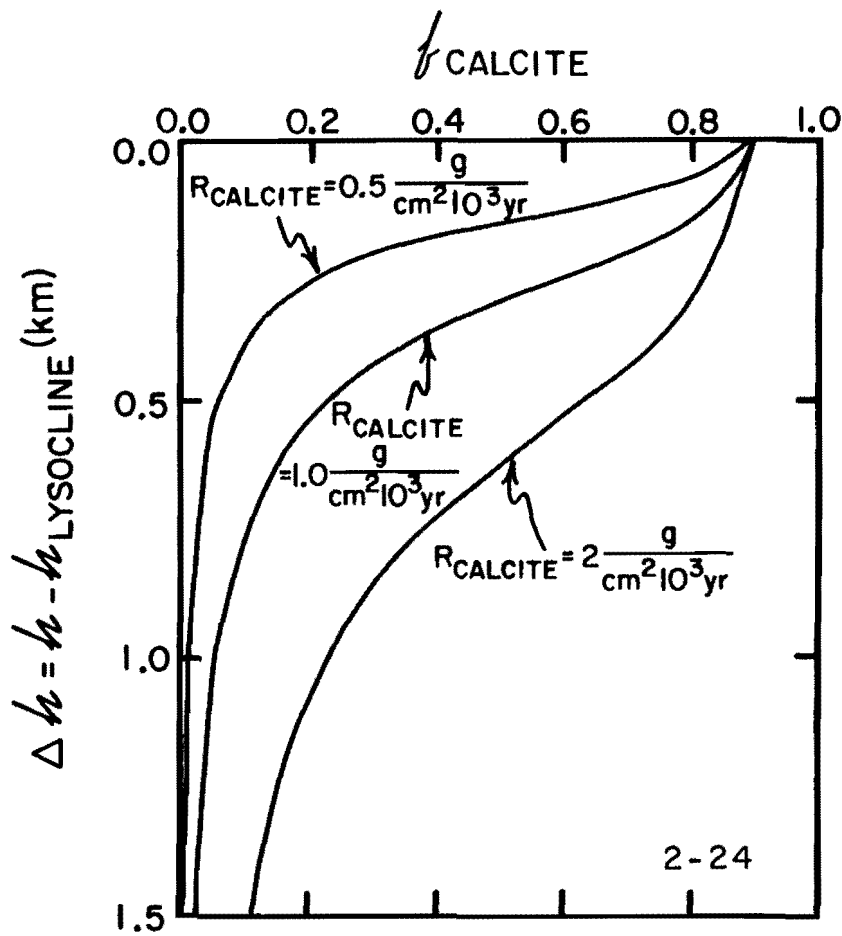


Figure 2-24. Plots of calcite content of sediments as a function of depth below the lysocline as calculated from the pore water saturation model. The diffusion rate of $\text{CO}_3^{=}$ ion in the sediments is assumed to be $2 \times 10^{-6} \text{ cm}^2/\text{sec}$, the difference between the saturation and bottom water carbonate is assumed to increase at the rate of 10×10^{-6} moles/kg per km and the pore water saturation time τ^* is assumed to be 120 seconds.

Figure 2-25. Plots of the calcite content of sediments as a function of depth beneath the lysocline for the stagnant film model compared with that for the pore water resaturation model.

thickness, Δz , of 1500 microns, the equation becomes:

$$\Delta h = \left[1 - \frac{0.1f}{0.9(1-f)} \right] 0.48 \text{ km}$$

A comparison between the calcite versus depth curve for this model and that for the pore water saturation case is given in figure 2-25. As can be seen, the shapes are very different. One model predicts a long tail of low calcite sediments, and the other a rather sharp base for the transition zone. The observations (see figure 2-7), while showing considerable scatter, appear to be more in tune with the shapes given by the porewater resaturation model than by the stagnant film model.

Before leaving this subject, one last point must be made. The relationship between the calcite content of a sediment and the extent of calcite solution that it has experienced is not what intuition might lead us to believe. The situation is depicted in figure 2-26. In this example, above the lysocline the accumulation rate of calcite and of other components of the sediment are in the 9 to 1 proportion in which they rain onto the sea floor. This sediment has 90% calcite. At a depth below the lysocline where $\Delta CO_3^=$ reaches a value of -3×10^{-6} moles/kg, 5/9 of the calcite dissolves, yet the calcite content of the sediment is still 80%! At a depth where $\Delta CO_3^=$ reaches a value of -6×10^{-6} moles/kg the S^* value for calcite is twice as high. However, as the calcite content of the sediment will be lower, the actual solution rate will not be twice as high. As shown in the diagram, the solution rate will rise from 5 to 8. This will lead to a solution of 89% of the calcite but will yield a sediment of 50% calcite content! At a depth where the $\Delta CO_3^=$ reaches -9×10^{-6} moles/kg the rate of solution cannot rise much above what it was at a $\Delta CO_3^=$ of -6×10^{-6} moles/kg (it can only go from 8 to 9 and then no calcite will be left to dissolve). Hence the rise must be balanced by a drop in the fraction of calcite in the sediment. In this situation the following relationship holds:

$$\frac{(\Delta CO_3^=)_{\text{depth 1}}}{(\Delta CO_3^=)_{\text{depth 2}}} = \left[\frac{f_{\text{depth 2}}}{f_{\text{depth 1}}} \right]^{1/2} \quad 2-43$$

Hence:

$$f_{\text{depth 2}} = \left[\frac{\Delta CO_3^=_{\text{depth 1}}}{\Delta CO_3^=_{\text{depth 2}}} \right]^2 f_{\text{depth 1}} \quad 2-44$$

In our example:

$$f_{\text{depth 2}} = (6/9)^2 0.50 = 0.23$$

As shown in figure 2-26, a sediment with 23% calcite would have experienced 97% calcite solution! So we see that the percent calcite in the sediment drops far more slowly with the extent of solution than one might guess.

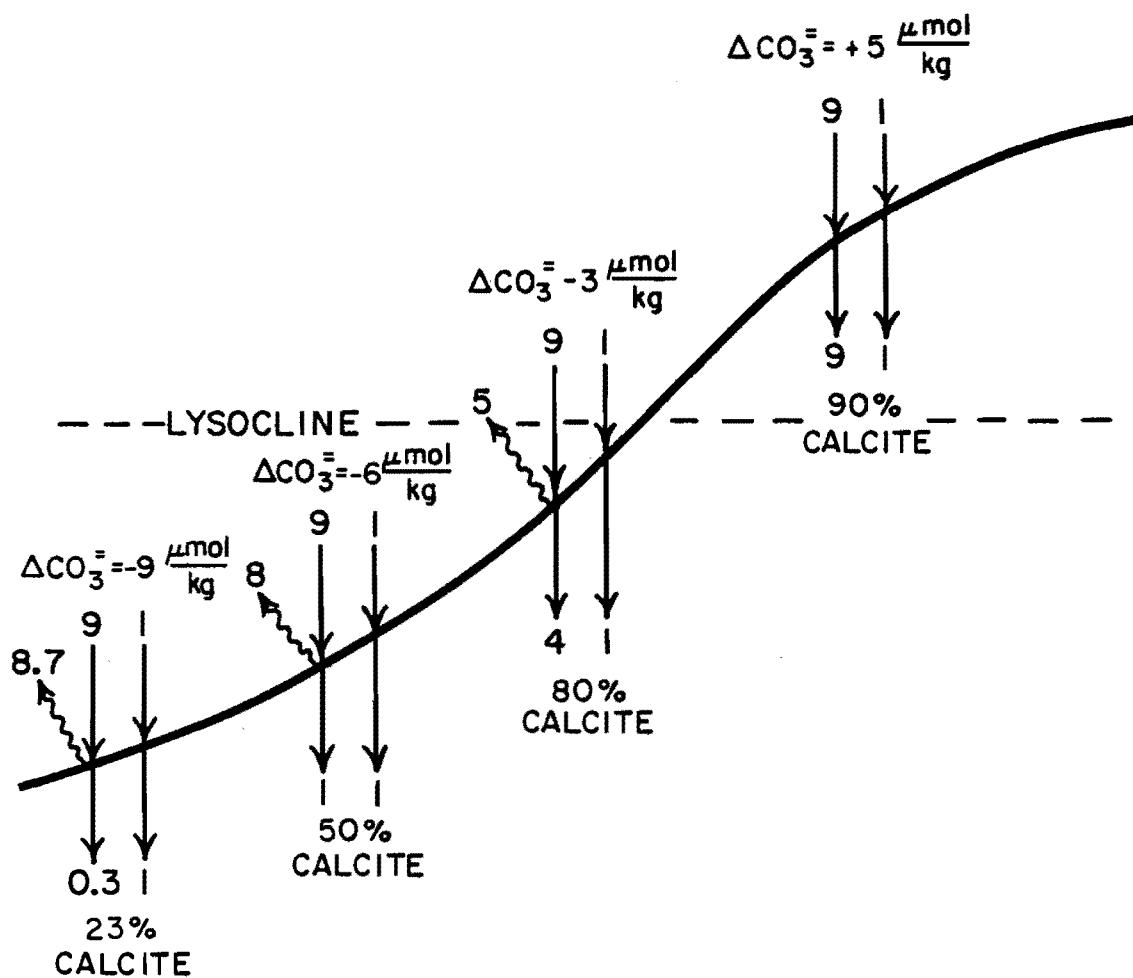


Figure 2-26. A diagrammatic view of changes in the driving force for calcite solution, the rate of solution and the percent calcite in the sediment with water depth. In each example the right hand arrows give the rain rate and accumulation rate of non CaCO₃ debris and the left hand arrows the rain rate and accumulation rate of calcite. The wavy arrows represent the solution rate of calcite. It can be seen that the fraction of calcite in the sediment gives a misleading view of the fraction of the raining calcite which dissolves.

VARIATION OF SEDIMENT TYPE WITH TIME

The interaction between the factors controlling the distribution of opal and calcite in the sediments forming on the sea floor and the great tectonic processes operating in the earth lead to a rather interesting sequence of sediment type with depth in the sedimentary column at any given point on the sea floor. Geophysicists have shown that the ocean crust is moving away from the crests of mid-ocean ridges at the rate of a few centimeters a year. New crust is constantly being generated to fill the void created by this movement (see figure 2-27). As the newly formed crust moves away from its point of origin on the ridge crest, it accumulates more and more sediment. Indeed, the thickest sediments are found furthest away from the mid-ocean ridges.

In addition to this lateral motion, there is a vertical motion.* The mid-ocean ridge crests have a more or less constant elevation, projecting to within about 2500 meters of the ocean surface. The ocean floor well away from the ridge crests lies about 6000 meters below the sea surface (actually, by this point, 500 meters of sediment have accumulated and the water depth is only about 5500 meters). As the ocean floor moves away from the ridge crests, it drops about 3000 meters in elevation. Thus at the time any particular portion of crust was first formed, it was bathed in CaCO_3 supersaturated water. However, as the crust moves away from the ridge crest, it eventually drops below the calcite saturation horizon. As it does so, CaCO_3 accumulation will slow and then cease. The CaCO_3 already accumulated will then be buried by a layer of red clay (figure 2-27). We would expect that if a boring were made through the sediments in any region of the sea floor which currently lies below the saturation horizon, the red clay encountered at the top of the core would eventually give way to carbonate-rich sediment. This sequence has indeed been found in numerous deep sea drillings.

The movement of the ocean floor will often carry a segment of the crust across the equator (see figure 2-28). Since opal deposition today is very rapid along the equator in the Pacific Ocean, we would expect to find a silica-rich horizon in the sedimentary record of any crustal segment which made such a crossing. Only during the period when the crust lay beneath the high productivity zone, would it accumulate opal-rich sediment. The expected pattern of sediments with depth is shown in figure 2-28. This pattern has been found by during the course of the deep-sea drilling program.

The composition of the sediments forming at a given point on the sea floor often show short-term cyclic changes as well as the long term changes associated with sea floor spreading. These short-term changes have been shown to be in tune with the waxing and waning of large ice masses which existed in what is now Canada and Scandinavia during glacial periods. An example of such changes is provided by the calcite content of sediment from the equatorial region of the Pacific Ocean. As shown in figure 2-29,

*The lithosphere near the ridge crests is quite hot. As it moves away, it cools; as it cools, it contracts. This contraction produced a drop in elevation of the sea floor with age.

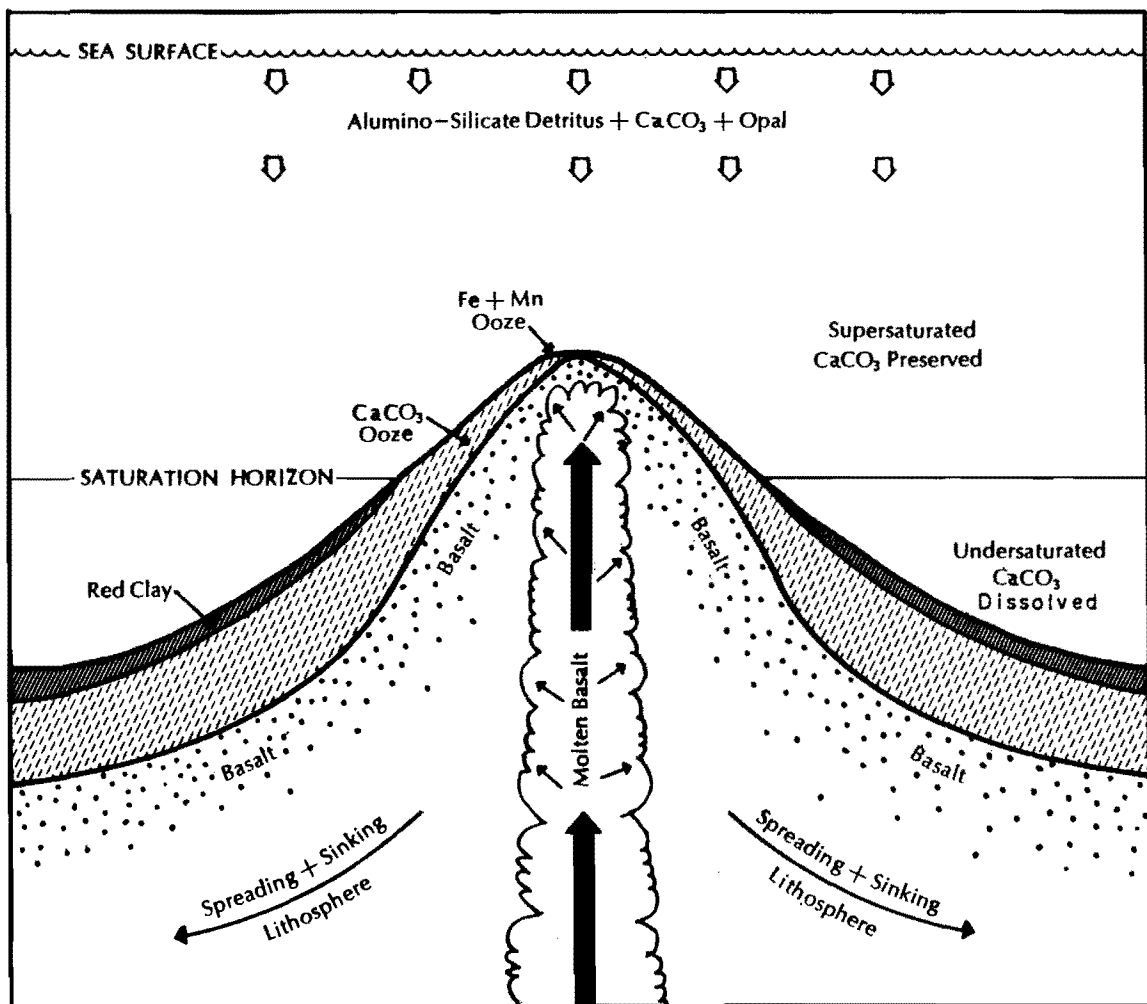


Figure 2-27. Sequence of sediment types accumulated by the great lithospheric plates as they move away from the crest of mid-ocean ridges. The first sediment to be deposited is rich in iron and manganese oxides, which are products of hydrothermal circulation. At a distance of more than a few kilometers from the spreading center, the sediment no longer receives hydrothermal material and is dominated by calcite falling from the surface. At a distance by about 1000 kilometers from the crest the plate subsides below the saturation horizon for calcite, and calcite no longer accumulates. Beyond this point, continental detritus dominates the sediment. Cores bored through sediment capped with red clay encounter buried calcite ooze and then a thin layer of iron- and manganese-rich sediment just before entering the underlying basalt.

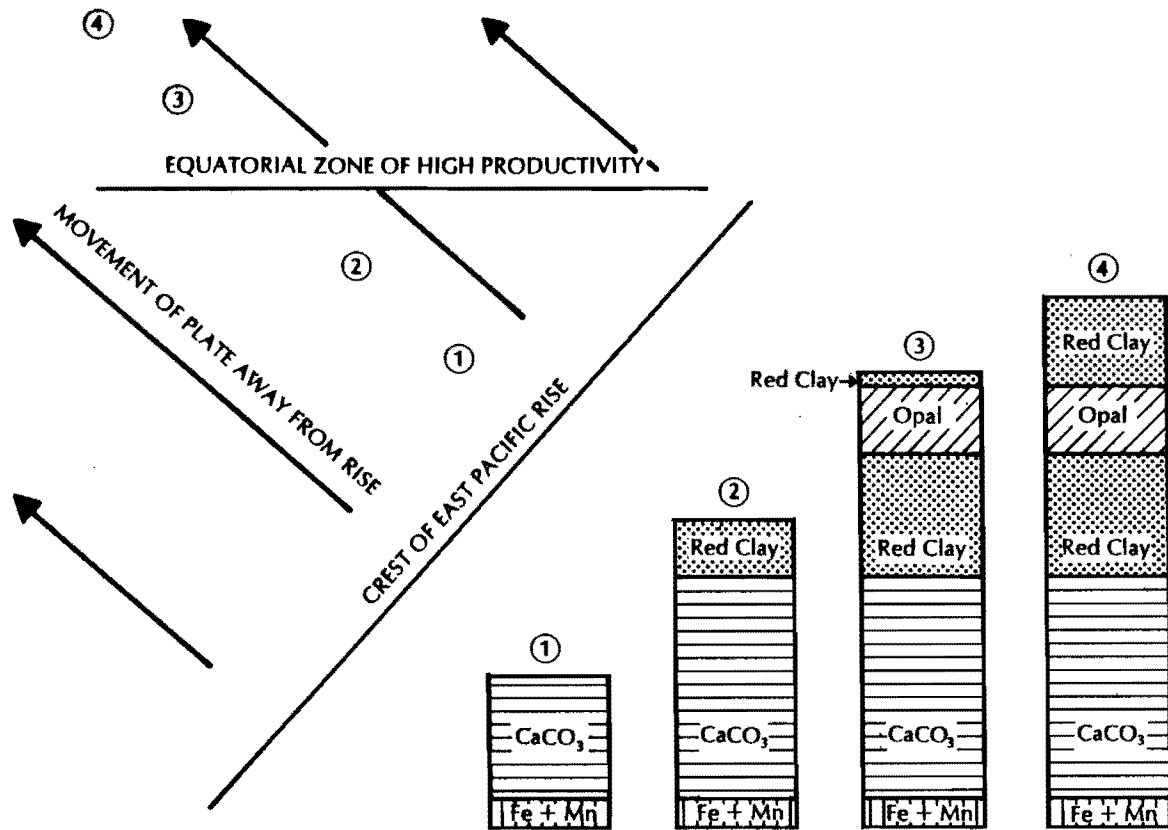


Figure 2-28. Sequence of sediments accumulating on a lithospheric plate which crosses the high productivity equatorial belt in its movement away from a ridge crest. The numbers relate the map locations to the corresponding sedimentary sequences found in borings made at these points.

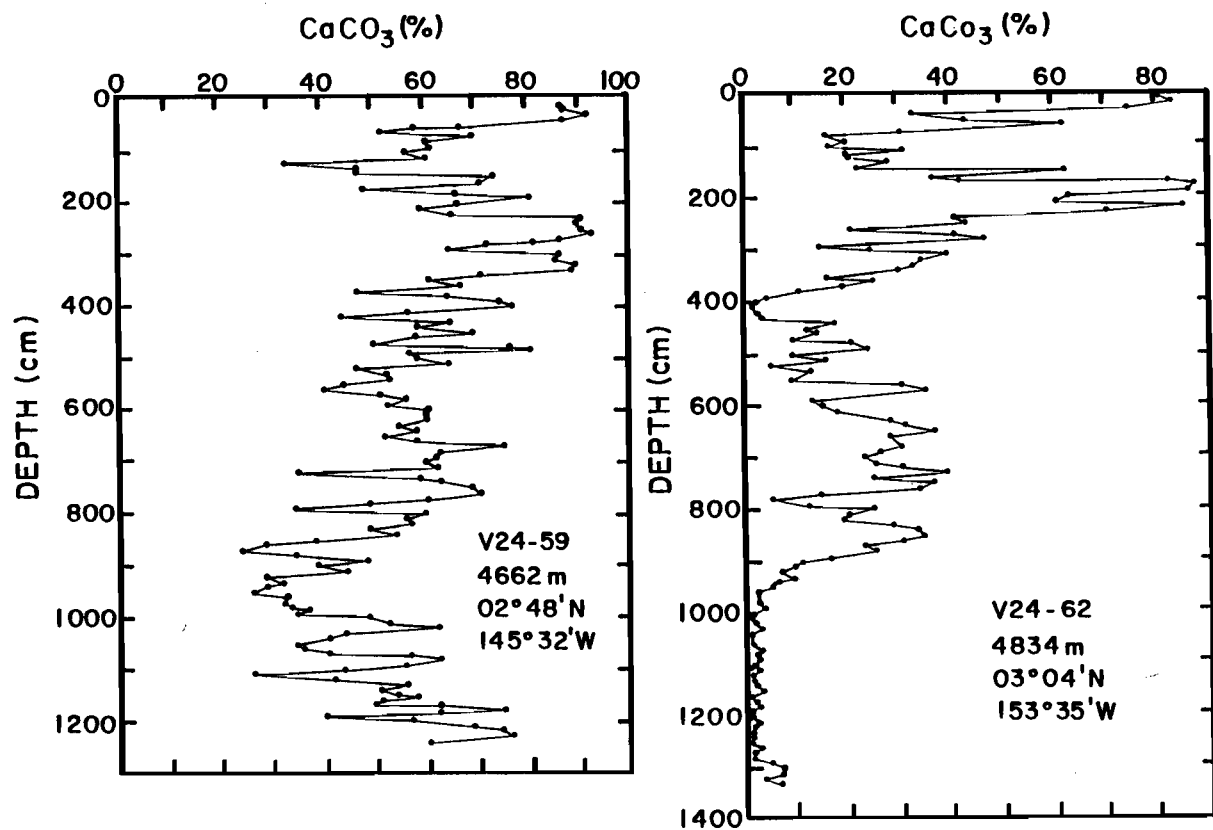


Figure 2-29. The content of CaCO₃ versus depth in two cores from the central equatorial Pacific. Both were obtained at depths below the lysocline and have experienced calcite solution. As we will show in chapter 9, fluctuations on the depth scale of 100 cm are related to glacial to interglacial climate cycles. The longer term change in core V24-62 reflects either a gradual deepening of the lysocline or a thickening in the calcite transition zone beneath the lysocline. These results were obtained by Hays and his coworkers at the Lamont-Doherty Geological Observatory (499).

the CaCO_3 content of cores in this region fluctuated with time. These variations could, of course, result from either changes in the relative rain rates of materials making up the sediment cores or from changes in the extent of solution of the calcite. Studies of these cores show that the latter is the dominant cause for the observed changes. These studies involved measurements of the ratio of the fragments of foraminifera tests to whole foraminifera shells and also of the ratio of the shells of benthonic foraminifera (organisms which live on the sea floor) to the shells of planktonic foraminifera (organisms which inhabit the upper water of the ocean). The utility of the first of these indices is obvious. As solution of the shells proceeds, the chambers which make up an individual test tend to become disconnected (just as they did in Honjo's chambers). Hence, the higher the ratio of fragments to whole foraminifera shells, the greater the extent of solution. The second method is useful because the shells of benthonic foraminifera are thicker and more rugged than the shells produced by their planktonic cousins. They are thus more resistant to the attack of waters undersaturated with respect to calcite. The ratio of whole shells of benthonic foraminifera to whole shells of planktonic foraminifera increases with the extent of dissolution. An example of the time variation in the latter ratio is shown in figure 2-30. These studies show that the lysocline was deeper in the Pacific Ocean during times of glaciation than during times of interglaciation such as we are experiencing today.

The oceanic lysocline also shows changes on the time scale of millions of years. Evidence for these changes is found in the long borings made at over 500 sites on the ocean floor. As mentioned above the transition from overlying red clay to underlying calcite-rich ooze was found in many of these borings. The age of this transition can be obtained from the fossil assemblage in the uppermost calcite bearing sediment. On the basis of this age and a knowledge of the rates of sea floor subsidence* the elevation of the sea floor at the time of transition can be determined. Each such point provides a paleolysocline elevation. The temporal history of the lysocline for the three major ocean basins obtained in this way is shown in figure 2-31.

MANGANESE NODULES

In addition to silicate detritus, calcite, opal, and a trace of organic matter, deep sea sediments contain concretions of iron and manganese oxide which the oceanographer calls manganese nodules. These objects litter the sediment surface in about 50% of the areas of the deep sea floor. Nodules are also frequently encountered at depth in deep sea cores. A photograph showing an area of dense nodule coverage is shown in figure 2-32. A cross-

*As mentioned above, the oceanic crust drops in elevation due to shrinkage caused by cooling. As the rate time dependence of heat loss (and hence of cooling and shrinking) can be calculated from basic principles, the elevation change during any time interval in the history of a given plate can be calculated.

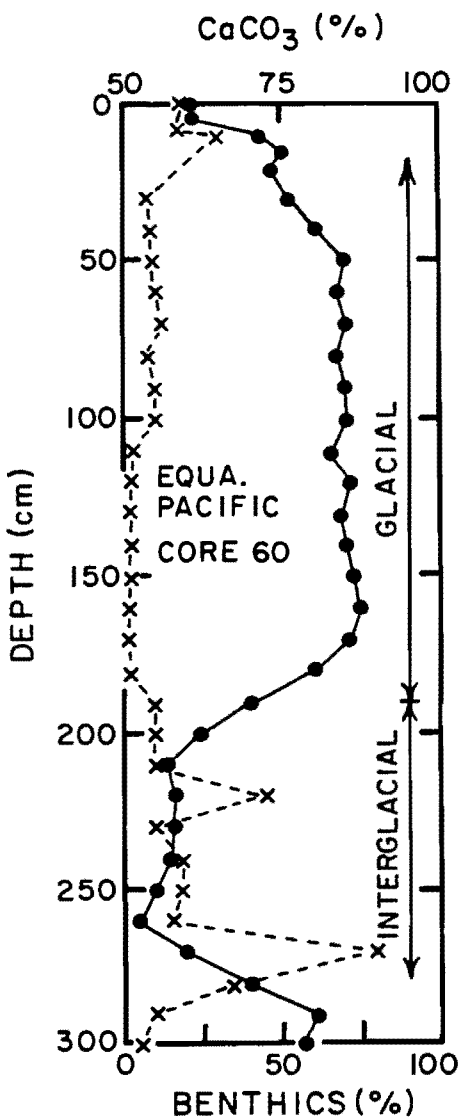


Figure 2-30. Plots of CaCO_3 content (solid circles) and percent benthic forams in total whole foram assemblage (crosses) as a function of depth in the sediment for a core from the equatorial Pacific Ocean. It can be seen that, the percentage of CaCO_3 was much lower during the last interglacial period than during the last glacial period and that the percentage of the shells of benthic forams in the coarse fraction sieved from the sediment was much higher. This combination is the fingerprint for changes brought about by the solution effects. Sediments which have suffered no solution effects have only a few percent benthic shells in the total foram fraction. During the last interglacial, one sample shows up to 75% benthics (i.e., 3 benthic shells to every one planktonic shell)! To achieve this proportion, more than 99% of the planktonic shells must have been reduced to fragments by solution. These data were obtained by Arrhenius and his colleagues on materials obtained during the Swedish deep-sea expedition (496).

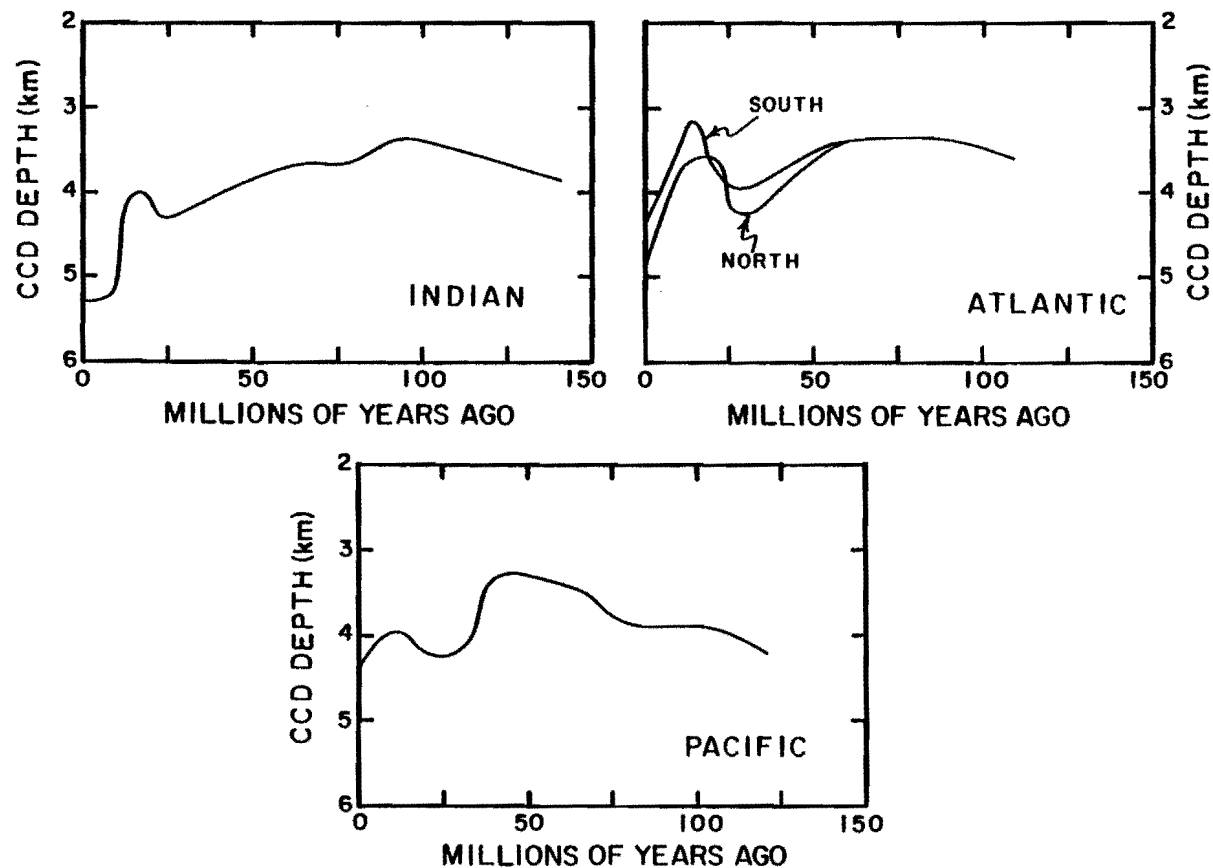


Figure 2-31. A reconstruction of the depth at which the CaCO_3 content of sediments reaches 20% (termed the calcite compensation depth, or CCD). The reconstruction is accomplished by finding the age (and depth) of the transition from CaCO_3 -rich to CaCO_3 -poor sediment in a large number of long borings made as part of the Deep Sea Drilling Program. The transitions are assumed to have occurred as the sea floor subsided beneath the CCD. A correction is then made for the extent of subsidence between the time of this crossing and today. These reconstructions were by Van Andel of Stanford University (508).

section through a nodule is shown in figure 2-33. Their mode of origin remains somewhat of a puzzle. The elements of this puzzle are as follows:

1) As iron and manganese are both extremely insoluble in sea water, it is not clear how these oxides become concentrated into concretions in areas of the sea floor remote from continental margins and ridge crests.

2) Various methods of radioactive dating give concordant growth rates for nodules averaging about 3mm per million years. As manganese nodules have radii of a centimeter or more, they must be several million years old! Where the sediments in nodule fields have been dated, sedimentation rates of several meters per million years are usually obtained. How then does a nodule remain atop the sediment during its long period of growth? During its lifetime a typical nodule must have worked its way up through ten meters or more of sediment.

The first of these difficulties can be overcome when one considers that both iron and manganese are very soluble in their reduced form. Most sediments around the margins of the continent become sufficiently reduced at depth of several centimeters permitting the mobilization of Mn and Fe. This mobility allows these metals to escape back to the sea. Thus even though very insoluble under the oxidizing conditions of most sea water, iron and manganese atoms could, in a series of water-to-sediment-to-water jumps, eventually work their way to the remote deep sea, where a stable home in a manganese nodule (or in oxidized sediment) can finally be found.

The second difficulty is not so easily overcome. As nodules are more dense than the sediments upon which they rest, gravity cannot be called upon to keep them "afloat" on the ever-thickening sediment column. One favorite hypothesis claims that worms which live in the sediment every so often nudge a nodule and lift it through the ever-encroaching sediment. As no one has ever observed this process in action, its credibility is marginal. Other explanations such as the action of tidal-wave-induced bottom currents are even less palatable.

The implausibility of the mechanisms proposed to keep the nodules afloat on the sediment-water interface has led some investigators to doubt the validity of the figures for the growth rate of nodules or those for the rate of sediment accumulation. Beyond the supporting arguments based on the concordancy of the various methods used to determine these rates, a quite impressive argument can be made in defense of the ratio of the rate of nodule growth to the rate of sediment accumulation. If the process of nodule formation has reached steady state (as it must), then for each new nodule which nucleates, an old one must become buried in the sediment. The nodules so buried could either accumulate as plums in the sediment pudding, or be dissolved away. As the nodules found buried in sediments show no evidence of "corrosion", it is likely that the fate of most old nodules is permanent burial. If so, then the ratio of nodule growth rate to sedimentation rate can be used to predict the density of nodules (i.e., the plums) in the sediment (i.e., the pudding). For example, in an area where the

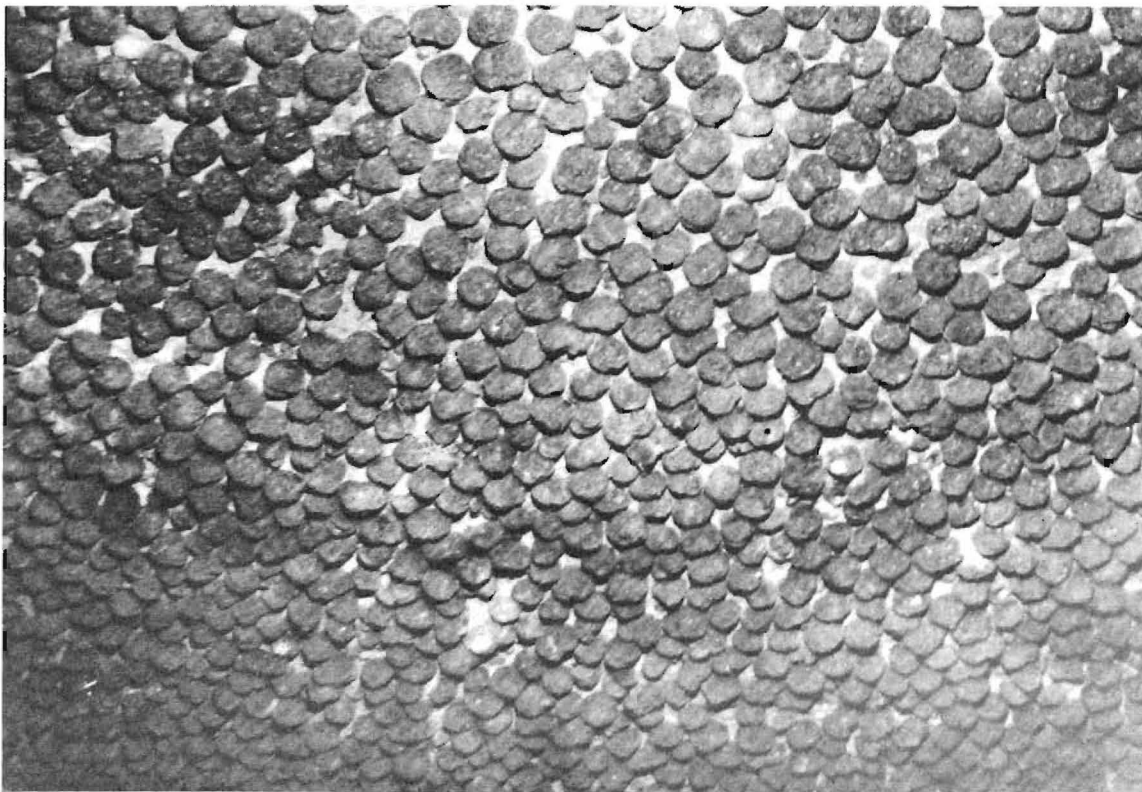


Figure 2-32. Photograph showing a field of unusually closely spaced manganese nodules on the bottom of the Antarctic Ocean. The mean nodule diameter is 6 centimeters. Photograph provided by Charles Hollister of the Woods Hole Oceanographic Institution.

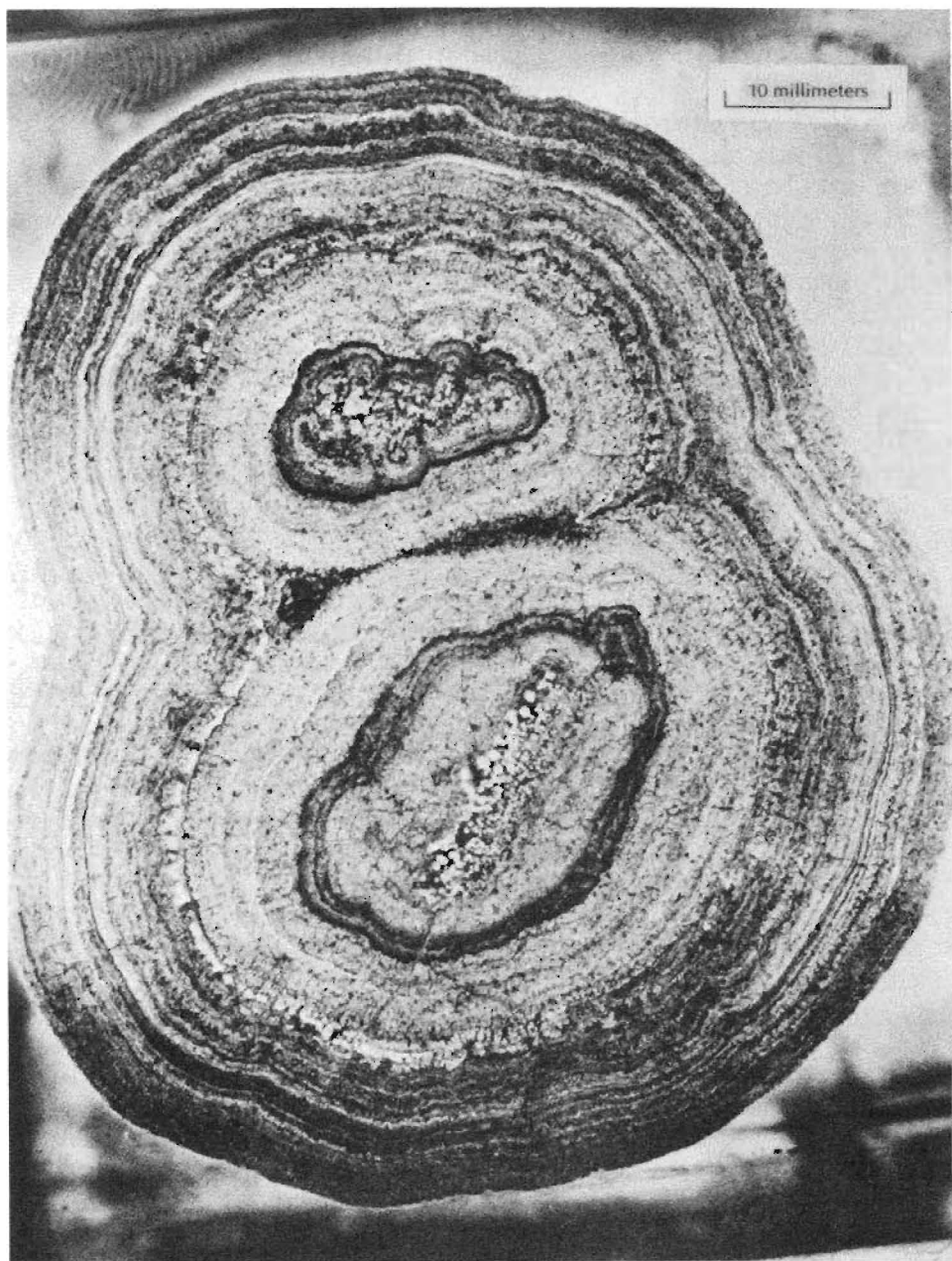


Figure 2-33. Photograph of a cross-section cut through a manganese nodule with two growth centers. The altered volcanic material at the center served to nucleate the nodule's growth. Crude growth rings representing temporal changes in texture and composition can be seen. This nodule has a radius of 2 centimeters. At a growth rate of $3 \text{ mm}/10^6 \text{ yrs}$, it must have been born about 7,000,000 years ago. Photograph provided by Sorem and Foster of Washington State University.

sediment accumulation rate is three meters per million years, and where the mean age of the nodules on the sediment surface (as measured by their radius and growth rate) is three million years, the number of nodules found in the upper 9 meters of the sediment column should equal the number found on the surface. In other words, the previous generation of nodules must lie buried in three million years' worth of sediment.

For an analogy to this situation, consider a group of space pioneers living on a large glacier covering the polar region of a distant planet. After realizing the futility of shoveling aside the ever-accumulating snow, these colonialists reconcile themselves to lifting their bodies and their belongings out of each new layer of snow. They also find that they need not bury their dead; the next snowfall will do the task for them. After 1000 years of continuous habitation with a steady population of 10,000, their resident archeologist, out of sheer boredom, digs a deep trench in an attempt to find relics of their arrival. Finally, when his trench has reached a depth of 300 meters, he succeeds. Having made note of the artifacts of his forefathers' arrival, he ponders the number of bodies he uncovered during his digging. He correctly calculates that, as his trench covers 0.1% of the area of the colony, 10 people should on an average be living within its bounds at any one time. The average lifetime of these colonists was 100 years. Thus over the 1000 years of occupation, about 100 people should have died and become buried in the snow on the site of his excavation. The first generation of pioneers lay in the lowest 30 meters of his excavation, the second in the overlying 30 meters, and so forth. The members of the eleventh generation currently dot the surface (working from birth to death to keep their heads above the ever-accumulating snow).

While marine geologists cannot dig trenches on the sea floor to see whether the appropriate number of "dead" nodules lie buried in each meter of sediment, they can punch out many, many deep sea cores. By comparing the number of nodules which by chance were encountered within these cores with the number encountered on the tops of these cores, an estimate of the ratio of "dead" nodules per cubic meter of sediment to "live" nodules per square meter of sediment surface can be made. The results of such a study (221) are consistent with the prediction made from the mean age of surface nodules and the mean accumulation rate of the sediment. The number of nodules in a sediment layer several meters thick is about the same as the number of nodules on the surface!

Thus, at this point, the worms appear to have the upper hand. If each year worm nudges were to lift a nodule 3 microns, then in a million years it would be raised by the required 3 meters! Unfortunately, we have no worm nudge tracers. So the puzzle remains an annoyance to those who study the sea floor.

One last question that might be raised about manganese nodules is how these objects manage to capture the small amounts of dissolved Fe and Mn which reach the deep sea floor. It turns out that the implication implicit in this question, namely, that nodules attract more than their share of manganese and iron, is simply not correct. As shown in table 2-8, the sediments adjacent to the nodules accumulate manganese at an even greater rate than the

Table 2-8. Comparison of Mn accumulation rates in nodules and in sediment. These rates are obtained by multiplying the accumulation rate of the sediment or growth rate of a nodule (normalized to the area of sea floor it covers) by their respective Mn contents (444).

Ocean	Nodules	Sediment
	g/cm ² 10 ⁶ yrs	g/cm ² 10 ⁶ yrs
Whole ocean	0.6(5)*	1.2 (30)*
North Atlantic	0.4(1)	1.5 (8)
South Atlantic	-	0.6 (1)
Indian	-	1.1 (7)
Antarctic	-	0.4 (4)
South Pacific	0.2(1)	1.4 (2)
North Pacific	0.8(3)	1.4 (8)

*Numbers in parentheses indicate number of nodules or cores upon which the average is based.

nodules themselves! Boudreau and Scott (695) have suggested that the Mn accumulating on nodules is supplied from the dissolved Mn in bottom water and that the rate limiting step for this accumulation is the stagnant boundary film discussed above. Santschi and his coworkers (696) show that at the site where their alabaster plates were deployed this may well be the case. The growth rate of $20 \text{ mm}/10^6 \text{ years}$ calculated from the Mn content of bottom water and the measured film thickness of 100 microns agrees with the growth rate of the nodules in this area.

SUMMARY

Ocean sediments are dominated by alumino silicate debris (red clay) from the continents and opal and calcite hard parts formed by marine organisms. The rain rate of clay debris decreases away from the continental margins. Opal accumulates most rapidly beneath areas of strong upwelling. As all ocean water is undersaturated with respect to opal, solution of this mineral occurs everywhere. By contrast, calcite is produced more uniformly over the ocean surface, but it falls into water which is in some places supersaturated and in others undersaturated. In any given ocean basin, calcite is absent in the deepest sediments but is present in great abundance on ridges and plateaus which project above the sea floor. These factors lead to strongly contrasting sediment types. The deep sea floor generally is lined with red clay (>90% alumino silicate debris). The flanks of the mid-ocean ridges are blanketed with sediments rich in calcite. Belts of opal-rich sediment are found in the Antarctic Ocean, along the equator in the Pacific Ocean and along some continental margins.

The extent of opal and calcite solution on the sea floor depends on the degree of undersaturation of the bottom water, the rain rate of these phases, and the rain rate of the diluting material. In both cases, solution occurs primarily in the pore spaces of the sediment from whence the products of solution diffuse into the overlying bottom water. CO_2 generated by organisms living within the sediment may contribute to the solution of calcite below the lysocline and even lead to partial solution above the lysocline. The benthic boundary at the base of the water column may impede calcite solution but not the rate of opal solution.

The movement of the lithosphere away from the mid-ocean ridge crests and to greater depths determines the long-term sequence of sediment types on any given portion of the sea floor. On a shorter time scale, the composition of ocean sediments is influenced by climatic changes. For example, during glacial times the calcite dissolution in the deep equatorial Pacific was less intense at any given depth than it is today.

Nodules of iron and manganese oxide dot the sediment-water interface in many parts of the ocean. Similar nodules are also found buried in marine sediments. These objects nucleate on sharks teeth, volcanic fragments and other hard fragments which by chance reach the sea floor and tend to grow for millions of years before succumbing to the incessant rain of sediment. The great mystery associated with these objects is the process that keeps them afloat so long atop the accumulating sediment blanket.

PROBLEMS

- 2-1 If a water sample from 4000 meters depth in the North Pacific is returned to the laboratory and placed under the following conditions, in each case write an expression based on the simplifying assumptions used in the text for the ratio of the new carbonate ion content and of the new hydrogen ion content to their in situ values:
- (a) at 2°C, 1 atm pressure?
 - (b) at 24°C, 1 atm pressure?
- Assume that there is no ΣCO_2 , alkalinity or salinity change during storage.
- 2-2 What is the alkalinity of each of the following solutions?
- (a) One mole of NaCl dissolved in 400 liters of CO_2 -free distilled water.
 - (b) One mole of Na_2CO_3 dissolved in 1000 liters of CO_2 -free distilled water.
 - (c) One mole of CaSO_4 dissolved in 5000 liters of CO_2 -free distilled water.
 - (d) One mole of CaSO_4 and 2 moles of $\text{Ca}(\text{HCO}_3)_2$ dissolved in 3000 liters of CO_2 -free distilled water.
- 2-3 Organic tissue containing 0.2 moles of carbon is added to a 1000-liter sample of deep water from the North Pacific bottom water. The bacteria in the sample respond and consume the organic matter drawing on the residual oxygen (100×10^{-6} moles/l). Which respiration ingredient will run out first - oxygen or tissue? At this ingredient's point of disappearance, by how much will the carbonate ion concentration have changed? Again use the simplifying assumptions adopted in the text.
- 2-4 If the rate of sea floor subsidence averages 30 meters per million years, what is the age of the sea floor when it passes through the calcite lysocline? (Assume the ridge crest elevation to be 2500 meters and the calcite lysocline to be at 4000 meters.) If the mean rate of accumulation of noncarbonate sediment is $0.5 \text{ cm}/10^3 \text{ yrs}$, how deep would one have to bore into the sea floor to reach CaCO_3 -bearing sediment at a water depth of 5000 meters? If the mean CaCO_3 accumulation rate at depths shallower than the lysocline is $1.5 \text{ cm}/10^3 \text{ yrs}$, how much further would you have to bore to reach the basalt at the base of the CaCO_3 -bearing sediment?
- 2-5 In a given area of the sea floor the rain rate of opal is $1.0 \text{ g/cm}^2 10^3 \text{ yrs}$, that of calcite is $1.0 \text{ g/cm}^2 10^3 \text{ yrs}$, and that of alumino silicates $0.2 \text{ g/cm}^2 10^3 \text{ yrs}$. The potential dissolution rate of opal is $1 \text{ g/cm}^2 10^3 \text{ yrs}$ and that of calcite is $2 \text{ g/cm}^2 10^3 \text{ yrs}$ for this geographic location and water depth. If the respective solution rates depend on the square root of the opal and calcite content of the sediment what will be the steady state opal and calcite content of the sediment?

- 2-6 A Mn nodule grows at a radial rate of $2 \text{ mm}/10^6 \text{ years}$ and is 20 percent manganese by weight. The underlying sediment is accumulating at the rate of $0.2 \text{ cm}/10^3 \text{ yrs}$ and contains 11,000 ppm of manganese. Per unit area (as viewed from above), which is "capturing" more Mn - the nodule or the adjacent sediment? What is the ratio of these accumulation rates? Assume the sediment to have 0.6 g of mineral matter per cm^3 and the nodule 2.5 g of Mn plus Fe oxides per cm^3 . The Mn to Fe ratio in the nodules is two.
- 2-7 Mn nodules are found at a frequency of $10/\text{m}^2$ on a given region of the sea floor. They average 8 centimeters in diameter, and each has a shark's tooth at its center. If these nodules grow at the rate of $4 \text{ mm}/10^6 \text{ yrs}$ and if all the teeth from all the sharks living in the overlying surface water end up in nodules, how many sharks would you expect to find living in each square kilometer of surface water? (The average lifetime of a shark is 20 years; each shark produces 200 teeth during its lifetime.)

SUPERPROBLEM #2

A sedimentologist named Taco Hashish, fascinated with the problem of what controls the proportions of opal, calcite, and alumino-silicates in deep sea sediments constructs a large tank in which to conduct solution experiments. His tank has a stirring device which not only keeps the water well mixed but also disperses any sediment grains that he adds so that they settle uniformly over the bottom. Hashish fits the bottom with a set of rotating "spits" designed to homogenize the sediment which accumulates. Finally, he installs a pump which injects new water into the tank. The amount of water in the tank is kept constant by an overflow. He then chooses three types of sediment grains. The first is a silicate known for its insolubility in water. The second is a sparsely soluble organic compound which he terms calcilite. The third is a moderately soluble organic compound which he terms opalite. Before starting his experiments Hashish measures the solubility of calcilite and opalite. He also devises a means of measuring the pore water resaturation time of calcilite and opalite. His results are as follows:

	solubility gm/liter	saturation time sec
calcilite	2.0×10^{-3}	1×10^2
opalite	1.0×10^{-1}	4×10^6

Hashish then starts his first experiment. He fills his tank with water free of dissolved opalite and calcilite and pumps in the same water at the rate of 1 liter/minute. (His tank has a volume of 1000 liters.) Hashish then starts to inject his three crystal types at the rate of $1 \times 10^{-3} \text{ g}/\text{minute}$ each. The grains become

dispersed in the water but settle to the bottom a few seconds after their injection (the area of the tank bottom is 1 square meter). He then lets the pump and the grain injector run until 6 cm of sediment has accumulated.* He then installs a device which removes sediment as fast as it accumulates (i.e., the thickness of the sediment remains the same). After running the system for some time he stops it and removes the water and performs a chemical analysis of the accumulated sediment to find the proportions of calcilite, opalite and silicate. He also analyzes a sample of the water for the amount of dissolved calcilite and the amount of dissolved opalite. Assuming that all the solution takes place in the pores, and that upon dissolving opalite and calcilite, produce a single neutral ion rather than a pair of oppositely-charged ions, predict the steady state water and sediment composition (the molecular diffusivity of each dissolved product in the sediment is $2 \times 10^{-6} \text{ cm}^2/\text{sec}$). What would the τ values for calcilite and opalite be? How would the pore water profile look? How thick a "stagnant film" would it take to void these calculations? In what proportions would Hashish have to add the grains if he wished to get proportions of 8 parts silicate, 1 part calcilite and 1 part opalite in the accumulated sediment?

*Fortunately Taco is a patient and long-lived man. If the density of these mineral phases is 2 g/cm^3 and the porosity of the sediment is 50%, this sediment would weigh 6×10^4 grams. Depending on the extent of solution the accumulation rate would be between 1 and 3×10^{-3} grams per minute. Hence about 4×10^7 minutes (i.e., 75 years) would be required for the sediment column to reach its steady state thickness of 6 cm.

LAST MINUTE ADDITION (SEPTEMBER 1982)

A new method for the study of the extent of CaCO_3 solution within the pore waters of sediments has been independently proposed by Curran and Sayles at Woods Hole Oceanographic and Quay and Emerson at the University of Washington. Both groups have measurements of the $\delta^{13}\text{C}$ and ΣCO_2 in sediment pore waters. These profiles provide proof that significant CaCO_3 solution is occurring.

Honjo and his coworkers at Woods Hole Oceanographic have used their in situ calcite exposure method to study opal (720). Their results show a dramatic temperature dependence of the solution rate. It appears to be about 100 times greater at 25°C than at 2°C !

Chapter 3

THE ATMOSPHERIC IMPRINT

THE CYCLES OF GAS WITHIN THE SEA

INTRODUCTION

Overlying and interacting with the ocean is the atmosphere. In our discussion in chapter 1 of the chemical inhomogeneities within the ocean, we did not treat the dissolved gases because their distribution is influenced not only by the formation and the destruction of particulate material but also by their interchange with the atmosphere. It is now time to discuss this interchange process and its influence on marine chemistry.

The elements listed in table 1-1 include a series of six that are chemically inert - helium (He), neon (Ne), argon (Ar), krypton (Kr), xenon (Xe), and radon (Rn). As we shall see, isotopes of four of these gases (^3He , ^{39}Ar , ^{85}Kr , and ^{222}Rn), have important applications as tracers in the sea. Nitrogen (N_2), although it is converted to and from nitrate ion (NO_3^-) by various organisms living in soils and in natural waters, is much like the six inert gases. It does not undergo any chemical reactions which measurably alter its abundance in sea water.

In addition to these inert gases, two other dissolved gases - oxygen and carbon dioxide - are of particular interest to us here. These two gases are, as we already have seen, heavily involved with the chemical processes taking place within the sea. Hence their distributions will occupy much of our attention in this chapter. Oceanographers have long known that oxygen gas is, as the result of consumption by animals and bacteria, deficient in most subsurface ocean water. The longer a water mass is isolated from the atmosphere, the lower its oxygen content becomes. This fact has led to the wide use of O_2 as a circulation tracer. Carbon dioxide (CO_2) has a characteristic not shared by the other gases. It reacts with $\text{CO}_3^=$ ion to produce two HCO_3^- ions. In surface water, on the average only about one carbon atom in 200 is in the form of CO_2 gas. Because of its large reservoir of HCO_3^- and $\text{CO}_3^=$ the ocean ultimately determines the atmosphere's CO_2 content, rather than vice versa.*

There is one other gas we shall consider. During respiration not all the nitrogen bound in organic debris is released as nitrate ion. A small fraction becomes nitrous oxide (i.e., N_2O).

*This is not true for the other gases. Since over 95 percent of the total of the inventory of these gases is found in the atmosphere, the atmosphere dictates the ocean's gas content.

The distribution of this gas in the sea provides some clues regarding the cycle of nitrogen in the sea.

The amount of all the dissolved gases in surface ocean water is controlled by their concentrations in the overlying atmosphere and by temperature.* The task of establishing these surface ocean concentrations is simplified by the fact that the atmosphere is almost perfectly mixed with regard to the gases we will examine here. Even for CO₂ (the most likely to vary), the difference in the atmospheric concentration from one place to another is only a few percent. The assumption that the air over every region of ocean has the same composition proves quite adequate for our purposes. The total pressure the atmosphere exerts on the sea surface is also very nearly the same from place to place. It varies only because of the highs and lows of the meteorologist.

All deep water was once at the sea surface. When this water lost contact with the atmosphere, it carried with it a near equilibrium amount of each atmospheric gas. So when we examine deep sea water, we would expect the content of its gases (except CO₂, O₂, He and, of course, Rn) to be determined by their atmospheric content and by the temperature of the water when it left the surface. This has been checked and, indeed, the amount of each of these gases in deep water proves to be within a few percent of the expected amount. The deep waters bear witness to the fact that they were once equilibrated with air.**

SOLUBILITIES OF GASES IN SEA WATER

Let us first consider how the solubilities of gases vary with molecular weight and with temperature. The data in table 3-1 portray a correlation between the solubilities of the noble gases and their molecular weights. Note that the higher the mass of the noble gas, the more soluble it is in sea water. Helium (mass = 4)

*Radon is an exception. As this gas is radioactive with a half-life of only four days, its partial pressure in sea and air never become equal. As we shall see, the concentration of this isotope in the surface ocean is of great importance to our understanding of the rate of flow of gases between the air and sea.

**In making this comparison, the potential temperature of the water rather than the in situ temperature must be used. The pressure on a parcel of water increases from 1 to about 500 atmospheres as it sinks from the surface of the ocean to a water depth of 5000 meters. This pressure increase results in a slight increase in the density of the water, which in turn leads to a rise in its temperature. For a 5000 meter descent, this warming averages about 0.4°C. Thus, thermometers sent to the abyss record temperatures higher than the temperature of the water when it began its descent! When comparing the properties of various waters within the deep sea, oceanographers use a temperature which has been corrected for the pressure-induced warming rather than the actual temperature measured using an in situ thermometer. This corrected temperature is called the potential temperature of the water.

Table 3-1. Solubilities of various gases in sea water per atmosphere pressure of that gas*.

Gas	Molecular Weight g/mole	Solubility cc/liter		Solubility** 10 ⁻³ moles/kg		Ratio of Solubility at 0°C to Solubility at 24°C	Volume Partition Coefficient (Air/Water) at 24°C	Ref.
		0°C	24°C	0°C	24°C			
He	4	7.8	7.4	0.34	0.32	1.1	135	(655)
Ne	20	10.1	8.6	0.44	0.37	1.2	116	(655)
N ₂	28	18.3	11.8	0.80	0.51	1.6	85	(653)
O ₂	32	38.7	23.7	1.69	1.03	1.6	42	(653)
Ar	40	42.1	26.0	1.83	1.13	1.6	39	(654)
Kr	84	85.6	46.2	3.8	2.1	1.8	22	(658)
Xe	131	192	99	8.4	4.3	1.9	10	(660)
Rn	222	406	186	17.8	8.1	2.2	5.4	(660)
CO ₂	44	1437	666	63	29	2.2	1.5	(656)
N ₂ O	44	1071	476	47	21	2.2	2.1	(659)
CCl ₃ F	137	-	677	-	29	-	1.5	(+)

*The solubilities of He, Ne, O₂, N₂, Ar and CO₂ in sea water are those recommended by Weiss of Scripps Institution of Oceanography. The solubilities of Xe and Rn are from the CRC Handbook of Chemistry and Physics with the salt effect extrapolated from other gases.

**Average density of sea water = 1.025 g/cm³

+Personal communication P.W. Balls and P.S. Liss, East Anglia Univ., Norwich, England.

is the least soluble; radon (mass = 222) is the most soluble of those listed. The situation for multiautom reactive gases is more complicated because of their chemical reactivity.

In the third and fourth columns of the table, the solubilities are given as the number of standard cc's of gas* which would dissolve at 0°C and at 24°C in 1 liter of sea water at 1 atmosphere pressure of that gas. For example, if we were to expose sea water at 0°C to pure helium gas at a pressure of 1 atm, 8 standard cc's of He would dissolve in each liter of water; for 1 atm of xenon, 192 standard cc's would dissolve per liter. In the fifth and sixth columns the solubilities are restated in units of moles/kg.

In the last column of table 3-1 the solubilities are expressed as volume partition coefficients. Think of the following experiment. One liter of sea water is placed in contact with 1 liter of air. Some xenon is injected into this system, and allowed to distribute between the water and gas phases at 24°C. It would turn out that for every atom of Xe that takes up residence in the water 10 atoms of Xe would take up residence in the air. The volume distribution coefficient of xenon is 10 (at 24°C). If we were to repeat this experiment with helium, for every He atom found in the water 135 would be found in the air. The volume distribution coefficient of helium is 135 (at 24°C).

All gases become more soluble in water as the temperature is decreased. Table 3-1 also lists the solubilities of a number of gases in sea water at 0°C and 24°C. Figure 3-1 presents this same information graphically. Note that the temperature dependence of He is small, changing by only 5 percent over the 24°C temperature range, whereas the temperature dependence of Xe is quite large, changing by a factor of 2 over the same temperature interval.

Table 3-2 gives the composition of water-vapor-saturated air and the corresponding amounts of each gas to be expected in surface sea water at 0°C and at 24°C (obtained by multiplying the fraction of each gas in air times its solubility at 1 atm pressure).

THE RATE OF GAS EXCHANGE

By making a rather simple model we can establish the magnitude of the exchange flux of gases between the ocean surface and the atmosphere. Our model assumes that the upper few meters of the ocean have a uniform concentration of the gas of interest. The same assumption is made for the column of air above the sea surface. These two well-mixed reservoirs are assumed to be separated from one another by a "stagnant" film of water. Gases cross this boundary layer only by molecular diffusion (the random motion of individual gas molecules). Although diffusive processes are nondirectional, if a concentration gradient exists, this chaotic motion will lead to a net transfer of material from the zone of high concentration to the zone of low concentration.

*One standard cc of a gas is the amount contained at 1 atm pressure and 0°C temperature in a volume of one cubic centimeter. The units cc and ml are interchangeable.

Table 3-2. Equilibrium concentrations of various gases in surface ocean water.*

Gas	Partial Pressure in Dry Air atm	Equilibrium Concentration in Surface Sea Water			
		cc/liter		moles/kg	
		0°C	24°C	0°C	24°C
He	5.2×10^{-6}	4.1×10^{-5}	3.8×10^{-5}	1.8×10^{-9}	1.7×10^{-9}
Ne	1.8×10^{-5}	1.8×10^{-4}	1.5×10^{-4}	7.9×10^{-9}	6.7×10^{-9}
N ₂	0.781	14.3	9.2	6.2×10^{-4}	4.0×10^{-4}
O ₂	0.209	8.1	5.0	3.5×10^{-4}	2.2×10^{-4}
Ar	9.3×10^{-3}	0.39	0.24	1.7×10^{-5}	1.1×10^{-5}
Kr	1.1×10^{-6}	9.4×10^{-5}	5.1×10^{-5}	4.2×10^{-9}	2.3×10^{-9}
Xe	8.6×10^{-8}	1.7×10^{-5}	8.5×10^{-6}	7.2×10^{-10}	3.7×10^{-10}
CO ₂	3.2×10^{-4}	0.46	0.21	2.0×10^{-5}	9.3×10^{-6}
N ₂ O	3.0×10^{-7}	3.2×10^{-4}	1.4×10^{-4}	1.4×10^{-8}	6.3×10^{-9}

*Salinity is assumed to be 35.00‰.

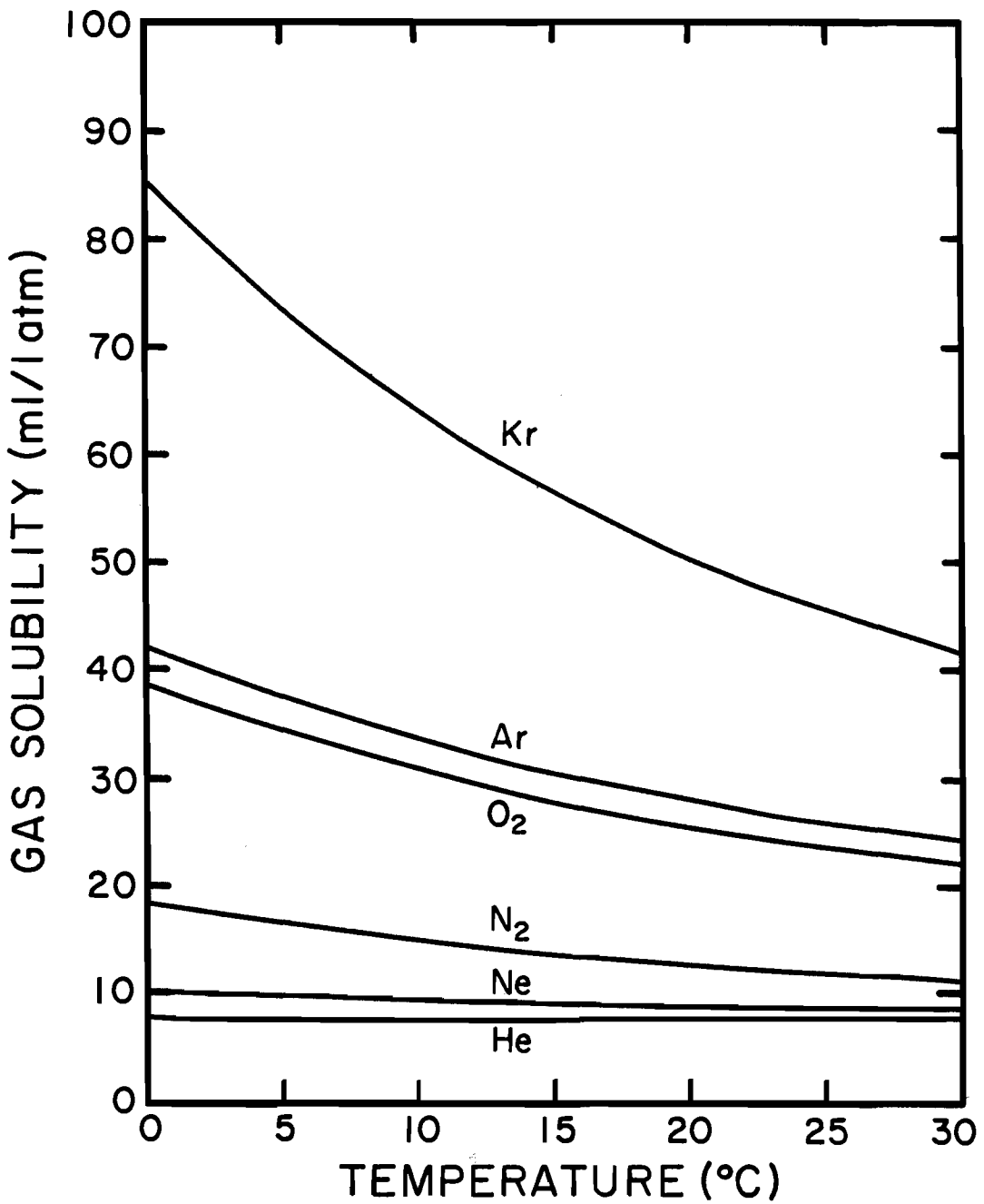


Figure 3-1. The solubilities of various gases in sea water as a function of temperature. The units are standard cubic centimeters of gas contained by a liter of water per atmosphere of pressure exerted by the gas.

Thus, if the concentration of gas in the water is not at equilibrium with the concentration of gas in the air, there will be a net flow of gas through the stagnant film. The rate at which the gas is transferred across the air-sea interface then depends upon:

1. the thickness of the film (the thicker the film, the longer the gas molecules will take to wander through it);
2. the rate at which the gas molecules diffuse through sea water (the warmer the water, the more rapid the molecular motion);
3. the magnitude of the disequilibrium between the gas content of the air and the gas content of the water (the greater the concentration gradient, the more rapid the diffusive transfer).

Figure 3-2 shows the concentration of the gas as a function of distance from the interface, as depicted by our model. Beneath the base of the stagnant film, the concentration is constant and equal to that in the surface sea water. At the very top of the stagnant film, the concentration is at equilibrium with the overlying air: the uppermost molecular layers of the film are assumed to be in rapid contact with the air and to have a gas content exactly equal to that dictated by the pressure of the gas in the air and by the air temperature. Between the top and the bottom of the boundary film, diffusion creates a linear gradation from the atmosphere-dictated value to the ocean-dictated value.

If the partial pressure of the gas in the air happened to yield a concentration of gas at the top of the film equal to the concentration below the film, then equilibrium would exist and there would be no net transfer of gas. As much gas would enter the sea as would leave it. If, on the other hand, the gas concentration at the top of the boundary layer was higher or lower than the gas concentration in the water, then a gradient would be established and molecules of gas would be transferred through the stagnant film. The rate of this transfer, or the flux of the gas, is stated as the amount of gas going into or out of a given unit of area of sea surface during a given unit of time. We will state gas fluxes in units of moles of gas transferred across one square meter in one year (moles/m²yr).

The flux of any diffusing substance is proportional to the concentration gradient. The proportionality constant is referred to as the coefficient of molecular diffusion. The concentration gradient is obtained by subtracting the concentration of the gas at the base of the boundary layer from the concentration of the gas at the top of the boundary layer and dividing by the thickness of the layer. Therefore:

$$F = D \frac{[gas]_{top} - [gas]_{bottom}}{z_{film}} \quad 3-1$$

where F is the gas flux, [gas]_{top} and [gas]_{bottom} are the gas concentrations at the top and the base of the stagnant boundary layer, z_{film} is the thickness of the boundary layer, and D is the coefficient of molecular diffusion. Ions in solution diffuse at room temperature at a rate of about 2×10^{-5} cm²/sec or ap-

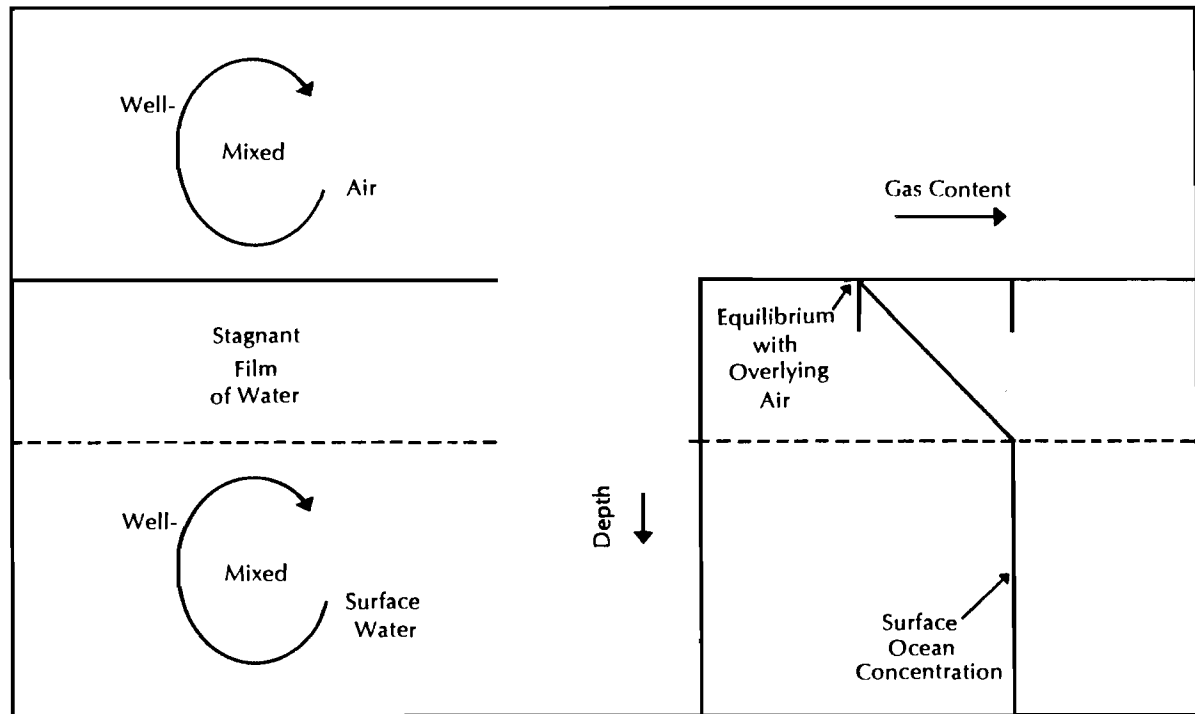


Figure 3-2. Gas exchange model. A thin film of "stagnant" water separates the well mixed overlying air from the well mixed underlying surface water. Gases are transferred between air and water only by molecular diffusion through this film. The concentration of gas within the film grades from that corresponding to equilibrium with the overlying air at the top to that found in the surface ocean at the base. The film thickness decreases as the degree of agitation of the interface increases. In the ocean, this film averages about 40 microns in thickness (a micron is one-millionth of a meter).

proximately $6 \times 10^{-2} \text{ m}^2/\text{yr}$. The actual diffusion rates depend on the temperature and on the gas: D increases with temperature and decreases with the mass of the diffusing molecule (see table 3-3). The thickness of the boundary film depends on the wind stress; the higher the wind velocity, the thinner the film. When concentration difference is placed across a thinner film, the resulting concentration gradient is larger. Therefore gas flows back and forth between the air and sea more rapidly during periods of high winds than during calm periods.

The stagnant film model is not the only one which has been used to characterize the transfer of gases across the air-water interface. The film replacement model provides another such characterization. In this model slabs of fluid are assumed to reach the interface and remain for a set time before being replaced by another slab. Each slab carries with it to the surface properties identical to those for the bulk fluid. When the slab reaches the surface its upper few molecular layers immediately reach equilibrium with the air (as we assumed for the top of the stagnant film). Molecular diffusion carries this surface anomaly into the body of the slab. The thickness of the slab is assumed to be large enough that the concentration at its base remains constant during its time of residence at the surface (i.e. the slab can be treated mathematically as a semi-infinite half space). When the film is pushed back into the interior of the fluid it carries with it the excess (or deficiency) of gas it received during its residence at the surface.

For this model the rate of transfer of gas between air and water depends on the frequency at which the film is replaced. The shorter the residence time of the film at the surface the more rapidly the gas is transferred. Thus τ , the replacement time, plays the role of z , the stagnant film thickness. The main difference between the models lies in the dependence of gas exchange rate on molecular diffusivity. In the case of the stagnant film model the rate of gas exchange is proportional to the first power of molecular diffusivity. In the case of the film replacement model the rate of gas exchange is proportional to the square root of the molecular diffusivity. Thus if we were to use radon data to calibrate one model or the other the exchange rates predicted for oxygen by the two models would differ by the square root of the ratio of the diffusivities of these two gases.

Both theoretical considerations and wind tunnel experiments involving the simultaneous measurement of heat and gas transport favor the film replacement model(194). Field studies involving the simultaneous measurement of gases differing in diffusivity support the stagnant film model(179). Fortunately the differences in diffusivity among the gases of interest are sufficiently small that the choice of models is not critical to any current ocean studies.

STAGNANT FILM THICKNESS DERIVED FROM NATURAL RADIOCARBON

The ^{14}C distribution between the atmosphere and the surface ocean can be used to estimate the average value of the stagnant boundary layer thickness for the global sea surface. As we will

Table 3-3. Rates of molecular diffusion of various gases in sea water. Also given are the products of the solubility of the gas, S, and its molecular diffusivity, D, relative to this product for oxygen. This index is useful in evaluating the relative importance of bubble entrainment for various gases.

Gas	Molecular Weight, g/mole	Diffusion Coefficient* $\times 10^{-5} \text{ cm}^2/\text{sec}$		$(SxD)_{\text{gas}}$ $(SxD)_{O_2}$	Ref.
		0°C	24°C		
He	4	2.0	4.0	0.54	(662,665)
Ne	20	1.4	2.8	0.44	(662,665)
N ₂	28	1.1	2.1	0.45	(662,665)
O ₂	32	1.2	2.3	1.00	(662,665)
Ar	40	0.8	1.5	0.72	(662,665)
Kr	84	0.7	1.4	1.2	(664,663a)
Xe	131	0.7	1.4	2.5	(664,663a)
Rn	222	0.7	1.4	4.8	(661,662 666)
CO ₂	44	1.0	1.9	23	(662,663)
N ₂ O	44	1.0	2.0	18	(662,663)

*A wide range of experimental results are given in the literature. Discussion of the possible causes for this variability is beyond the scope of this book. Measurements in sea water have yet to be carried out to confirm these results. The temperature effect is derived from reference 662. The values for Kr and Xe are calculated using diffusivity ratios given in reference 664.

discuss in more detail in chapter 5, ^{14}C atoms are born in the atmosphere, where they become $^{14}\text{CO}_2$ molecules. They are transferred into the ocean by gas exchange. By studying the exchange pattern of this radioactive breed of carbon dioxide, we can find the exchange rates of CO_2 and other gases.

Prior to anthropogenic alterations the ^{14}C cycle has been running for so long a time that it should have been at a steady state; in other words, the amount of ^{14}C at any point in the system should have been constant with time. If this is true, then the number of ^{14}C atoms that were added to the ocean each year by gas exchange with the atmosphere must have exactly balanced the number of ^{14}C atoms that disappeared within the ocean by radioactive decay. To determine how many ^{14}C atoms enter the ocean every year as a result of gas exchange, we multiply the concentration gradient of $^{14}\text{CO}_2$ across the stagnant boundary layer by the diffusion coefficient for $^{14}\text{CO}_2$. This can be stated in the form of an equation as:

$$\text{Input of } ^{14}\text{C} = D \left[\frac{[^{14}\text{CO}_2]_{\text{top}} - [^{14}\text{CO}_2]_{\text{bottom}}}{z_{\text{film}}} \right] A_{\text{ocean}} \quad 3-2$$

^{14}C is measured in ratio to normal carbon, or C^*/C . It is therefore appropriate to reexpress the $^{14}\text{CO}_2$ concentration as:

$$[^{14}\text{CO}_2]_{\text{bottom}} = \frac{\text{C}^*}{\text{C}} \left(\frac{\text{C}^*}{\text{C}} \right)_{\text{ocean}} [\text{CO}_2]_{\text{bottom}} \quad 3-3$$

and

$$[^{14}\text{CO}_2]_{\text{top}} = \frac{\text{C}^*}{\text{C}} \left(\frac{\text{C}^*}{\text{C}} \right)_{\text{atm}} \frac{\alpha^{14}\text{CO}_2}{\alpha\text{CO}_2} [\text{CO}_2]_{\text{top}} \quad 3-4$$

where $[\text{CO}_2]_{\text{bottom}}$ and $[\text{CO}_2]_{\text{top}}$ are the CO_2 gas concentrations at the base and the top of the stagnant boundary layer, and the ratio $\alpha^{14}\text{CO}_2/\alpha\text{CO}_2$ reflects the fact that because of their greater mass $^{14}\text{CO}_2$ molecules (molecular weight = 46) are 1.5 percent more soluble than ordinary CO_2 molecules (molecular weight = 44). Thus the $^{14}\text{C/C}$ ratio at the top of the boundary film is slightly greater (1.7 percent) than the $^{14}\text{C/C}$ ratio measured in atmospheric carbon.

At steady state there can be no net transfer of ordinary carbon between the ocean and atmosphere. Hence:

$$[\text{CO}_2]_{\text{top}} = [\text{CO}_2]_{\text{bottom}} = [\text{CO}_2]_{\text{surface}} \quad 3-5$$

If so, equation 3-2 for the input of ^{14}C atoms can be rewritten as:

$$\text{Input of } ^{14}\text{C} = \frac{D[\text{CO}_2]_{\text{surface}} A_{\text{ocean}}}{z_{\text{film}}} \left[\frac{\alpha^{14}\text{CO}_2}{\alpha\text{CO}_2} \frac{\text{C}^*}{\text{C}} \right]_{\text{atm}} - \frac{\text{C}^*}{\text{C}} \left[\frac{\text{C}^*}{\text{C}} \right]_{\text{surface}} \quad 3-6$$

The number of ^{14}C atoms being lost by radiodecay must match this gain. To find an expression for the loss rate per year, we begin with the number of ^{14}C atoms in the sea. To calculate this, we multiply the volume of the ocean (expressed as the area of the surface ocean, A_{ocean} , times the mean depth of the ocean, h) by the average total dissolved carbon content and then by the average ratio of $^{14}\text{C}/\text{C}$ in this oceanic carbon. We then multiply this number of ^{14}C atoms in the sea by the fraction undergoing radioactive decay per year (i.e., by λ). This yields:

$$\text{Loss of } ^{14}\text{C} = A_{\text{ocean}} h [\Sigma \text{CO}_2]_{\text{ocean}} \left(\frac{\text{C}^*}{\text{C}} \right)_{\text{ocean}} \lambda \quad 3-7$$

Setting the right hand sides of equations 3-6 and 3-7 equal to one another and solving for z_{film} , we obtain:

$$z_{\text{film}} = \frac{D}{\lambda h} \frac{[\text{CO}_2]_{\text{surface}}}{[\Sigma \text{CO}_2]_{\text{ocean}}} \left[\begin{array}{c} \frac{(C^*/C)_{\text{surface}}}{(C^*/C)_{\text{atm}}} \frac{\alpha \text{CO}_2}{\alpha^{14}\text{CO}_2} \\ \hline \frac{(C^*/C)_{\text{ocean}}}{(C^*/C)_{\text{atm}}} \frac{\alpha \text{CO}_2}{\alpha^{14}\text{CO}_2} \end{array} \right] \quad 3-8$$

The average value for the molecular diffusion coefficient, D , is $5 \times 10^{-2} \text{ m}^2/\text{yr}$ for CO_2 in surface sea water, the mean depth of the ocean, h , is 3800 meters, and the reciprocal of the decay constant of ^{14}C , $1/\lambda$, is 8200 years. The average concentration of CO_2 gas in the surface ocean is 0.012 moles/ m^3 , the average ΣCO_2 content of ocean water is 2.2 moles/ m^3 , and the $\alpha \text{CO}_2/\alpha^{14}\text{CO}_2$ ratio is 0.983. The $^{14}\text{C}/\text{C}$ ratio in average ocean carbon was, prior to nuclear testing, about 0.83 that in atmospheric CO_2 . The $^{14}\text{C}/\text{C}$ ratio in surface ocean carbon is, on the average, 4 percent lower than the $^{14}\text{C}/\text{C}$ ratio in atmospheric carbon dioxide. This last factor is the one that leads to the largest uncertainty in the determination of z_{film} . The difference is known to no better than one percent. A one percent error in the measurement of the average $^{14}\text{C}/\text{C}$ ratio in surface water carbon relative to that in atmospheric carbon would create a 15 percent error in the estimate of z_{film} !

When z_{film} is calculated from these figures we obtain 40×10^{-6} meters. For lengths this small, it is more convenient to use the unit micron (one-millionth of a meter). So z_{film} is 40 microns. Keep in mind that the boundary should be thinner than this average value in areas of high wind velocity and thicker in areas of low wind velocity; our calculation gives us only an oceanwide average.

Since the coefficients of molecular diffusion do not vary greatly from gas to gas, it proves convenient to think of the gas exchange process in terms of the ratio D/z . Because the dimensions of D and z_{film} are, respectively, m^2/yr and meters, the ratio D/z has the dimension of m/yr (hence those of velocity). We might think of this ratio as the velocity of two imaginary pistons: one moving up through the water pushing ahead

of it a column of gas with the concentration in surface water, and one moving down into the sea carrying a column of gas with the atmosphere equilibrium concentration found in the upper few molecular layers of the water column. On the average these pistons push CO_2 at the rate of $5 \times 10^{-2} \text{ m}^2/\text{yr}$ divided by 40×10^{-6} meters or 1200 m/yr . Thus each day a column of sea water about 3.3 meters thick exchanges its gas with the atmosphere! The piston concept clarifies the fact that even if the atmosphere and ocean are at equilibrium, the transfer of gas continues: the amount "pushed in" just matches the amount "pushed out."

From the piston velocity we can calculate another important geochemical time constant, i.e., the characteristic time required for ordinary gases in the ocean surface mixed layer to equilibrate with the atmosphere. Since the mixed layer ranges in thickness from 20 to 100 meters with a piston velocity of 3 meters a day the equilibration time lies in the range of one week to one month. Because of their differing diffusivities the flushing times for various gases will differ somewhat from one another. These differences are summarized in table 3-4. O_2 has a diffusivity (and hence a piston velocity) about 20% higher than that of CO_2 . For Rn the diffusivity (and hence piston velocity) is about 25% lower than that for CO_2 . As shown in this table for any given film thickness the piston velocity will also change with temperature (because the diffusivity changes). However, because of the change in solubility with temperature the absolute invasion rate changes more slowly with temperature than does the piston velocity.

STAGNANT FILM THICKNESSES AS DETERMINED BY THE RADON METHOD

Another tracer method exists which allows the rate of exchange in local areas at the ocean to be measured. It involves the escape of the radioactive gas ^{222}Rn from the sea to the overlying air. Radon is generated in sea water by the decay of its parent ^{226}Ra . Away from the interfaces with air and sediment the radioactivity of radon is identical to that of its parent. However, as we shall discuss in chapter 7, radon leaks into the sea from its sediments, giving bottom waters a higher radon activity than expected from the radium content of the water. Of interest in this chapter is the fact that the surface layer of the ocean has a deficiency of radon activity. This is because the air over the open ocean is nearly devoid of radon. Hence the flux of radon atoms from sea to air is not matched by a return flux. Some of the radon atoms generated in the surface layer of the sea escape to the atmosphere before undergoing radiodecay. The fraction which escapes provides a means for determining the piston velocity of gases as a function of wind velocity.

The task of finding the deficiency of radon atoms in the surface water column is greatly simplified by the fact that in most regions of the surface ocean there is a wind-mixed layer from 20- to 100-meters thick in which radon atoms are well mixed. This layer is underlain by the upper thermocline which mixes vertically at such a very slow rate that none of the radon atoms in this zone reach the overlying water during their average lifetime of 5.5 days. This being the case, the flux, F , of radon atoms from a

Table 3-4. Invasion rates and equilibration times of various gases assuming a stagnant film thickness of 40 microns and a mixed layer depth of 40 meters.*

Gas	0°C					24°C				
	D 10^{-5} cm^2 sec	v m day	τ days	S $\frac{\text{moles}}{\text{m}^3}$	I $\frac{\text{moles}}{\text{m}^2 \text{ yr}}$	D 10^{-5} cm^2 sec	v m day	τ days	S $\frac{\text{moles}}{\text{m}^3}$	I $\frac{\text{moles}}{\text{m}^2 \text{ yr}}$
He	2.0	4.3	9	1.8×10^{-6}	2.8×10^{-3}	4.0	8.6	5	1.7×10^{-9}	5.3×10^{-3}
N ₂	1.1	2.4	17	0.64	561	2.1	4.5	9	0.41	673
O ₂	1.2	2.6	15	0.36	342	2.3	5.0	8	0.23	417
Rn	0.7	1.5	27	-	-	1.4	3.0	13	-	-
CO ₂	1.0	2.2	18**	0.021	17	1.9	4.1	10**	9.5×10^{-3}	14
N ₂ O	1.0	2.2	18	1.4×10^{-5}	1.1×10^{-2}	2.0	4.3	9	6.5×10^{-6}	1.0×10^{-2}

*D stands for the molecular diffusivity, v for the piston velocity, τ for the mixed layer equilibration time, S for the equilibrium concentration in surface water and I for the invasion rate of the gas into the sea.

**Neglecting the chemical influence of HCO₃⁻ and CO₃⁼ (i.e., for a Coca Cola ocean).

square meter of sea surface to the atmosphere can be estimated as follows:

$$F = h (\lambda^{226}\text{Ra} [\text{Ra}] - \lambda^{222}\text{Rn} [\text{Rn}]) \quad 3-9$$

where h is the thickness of the wind-mixed layer at the ocean surface, $\lambda^{226}\text{Ra}$ and $\lambda^{222}\text{Rn}$, the respective decay constants for ^{226}Ra and ^{222}Rn , $[\text{Ra}]$ the concentration of radium in the surface-mixed layer and $[\text{Rn}]$ the concentration of radon in surface water. As the product decay constant times the concentration is the activity, A , of the respective isotopes, this equation can be rewritten:

$$F = h (A^{226}\text{Ra} - A^{222}\text{Rn}) \quad 3-10$$

Using the stagnant film model, the flux of radon atoms can also be written as:

$$F = \frac{D^{222}\text{Rn} [\text{Rn}]}{z} \quad 3-11$$

or

$$F = \frac{D^{222}\text{Rn} A^{222}\text{Rn}}{z \lambda^{222}\text{Rn}} \quad 3-12$$

Setting these two expressions for radon flux equal to one another (i.e., assuming that steady state exists for the radon concentration in surface water) and solving for z , we get:

$$z = \frac{D^{222}\text{Rn}}{\lambda^{222}\text{Rnh}} \frac{1}{\frac{A^{226}\text{Ra}}{A^{222}\text{Rn}} - 1} \quad 3-13$$

An example of the application of this method is given in figure 3-3. Beneath the mixed layer (as defined by the temperature profile) the radon activity is found to be within the measurement error of that of radium. By contrast, within the mixed layer the radium activity is about 1.6 times the radon activity. The mixed layer thickness in this example is 40 meters, the decay constant for radon is $2.1 \times 10^{-6} \text{ sec}^{-1}$, and the diffusion rate of radon $1.4 \times 10^{-9} \text{ m}^2/\text{sec}$. Hence:

$$\begin{aligned} z &= \frac{1.4 \times 10^{-9} \text{ m}^2/\text{sec}}{2.1 \times 10^{-6} \text{ sec}^{-1} \times 40 \text{ m}} \left[\frac{1}{1.6-1} \right] \\ &= 28 \times 10^{-6} \text{ meters} \\ &= 28 \text{ microns} \end{aligned}$$

A large number of such profiles have been determined in the sea. The stagnant film thicknesses derived from them are summarized in the histograms of figure 3-4. In the north and south

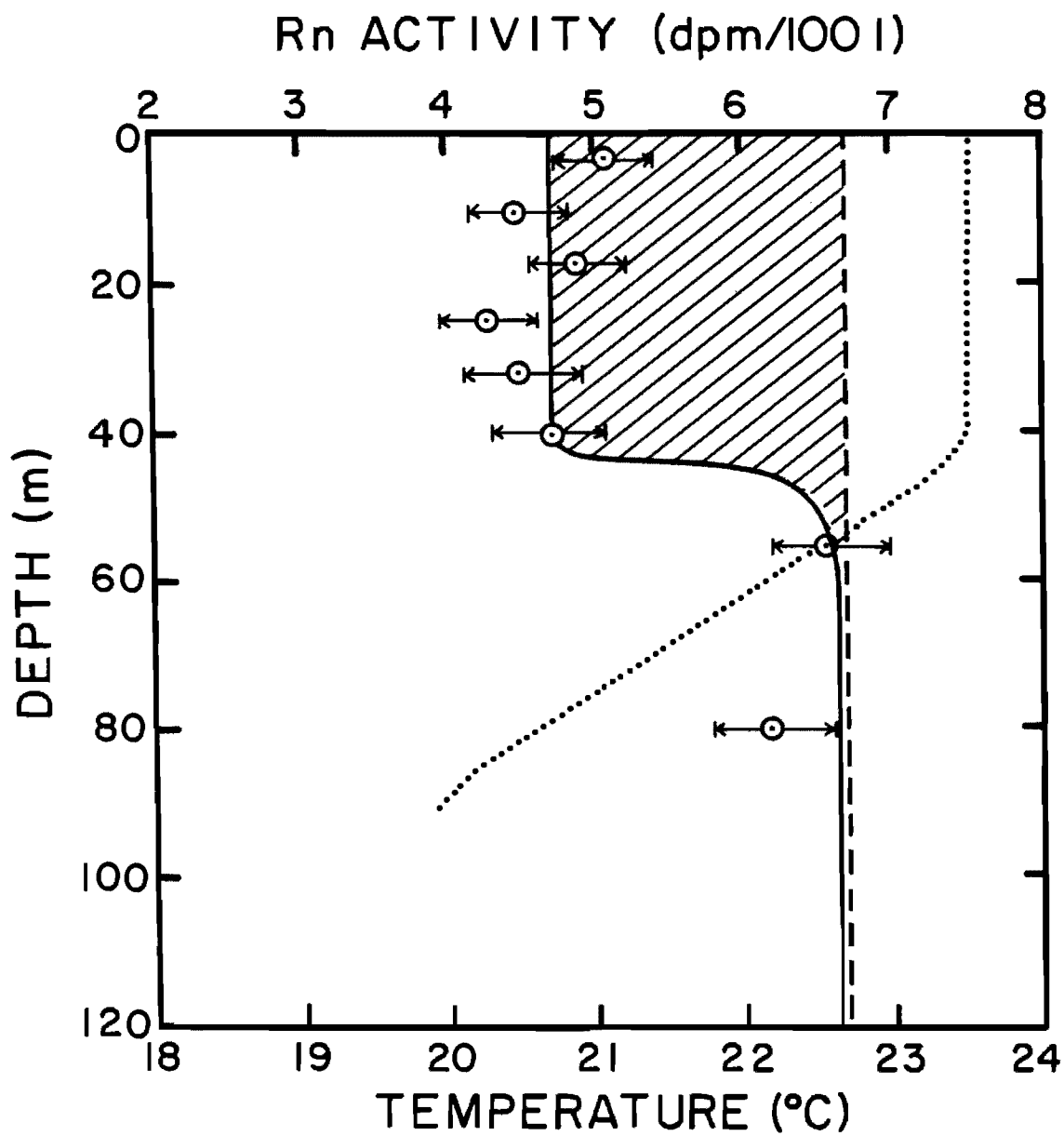


Figure 3-3. Concentration of radon gas as a function of depth at Atlantic GEOSECS station 57 (24°S 35°W). The concentration expected if no radon were escaping to the atmosphere is shown by the dashed line. The difference between this equilibrium value and the observed value is a measure of the amount of radon lost to the atmosphere. The shaded area is a measure of the total amount of radon lost to the air. From the amount of missing radon it is possible to determine the piston velocity for gas exchange. The dotted line is the temperature profile at this station defining the depth of the wind stirred layer. These results were obtained as part of the GEOSECS program (175).

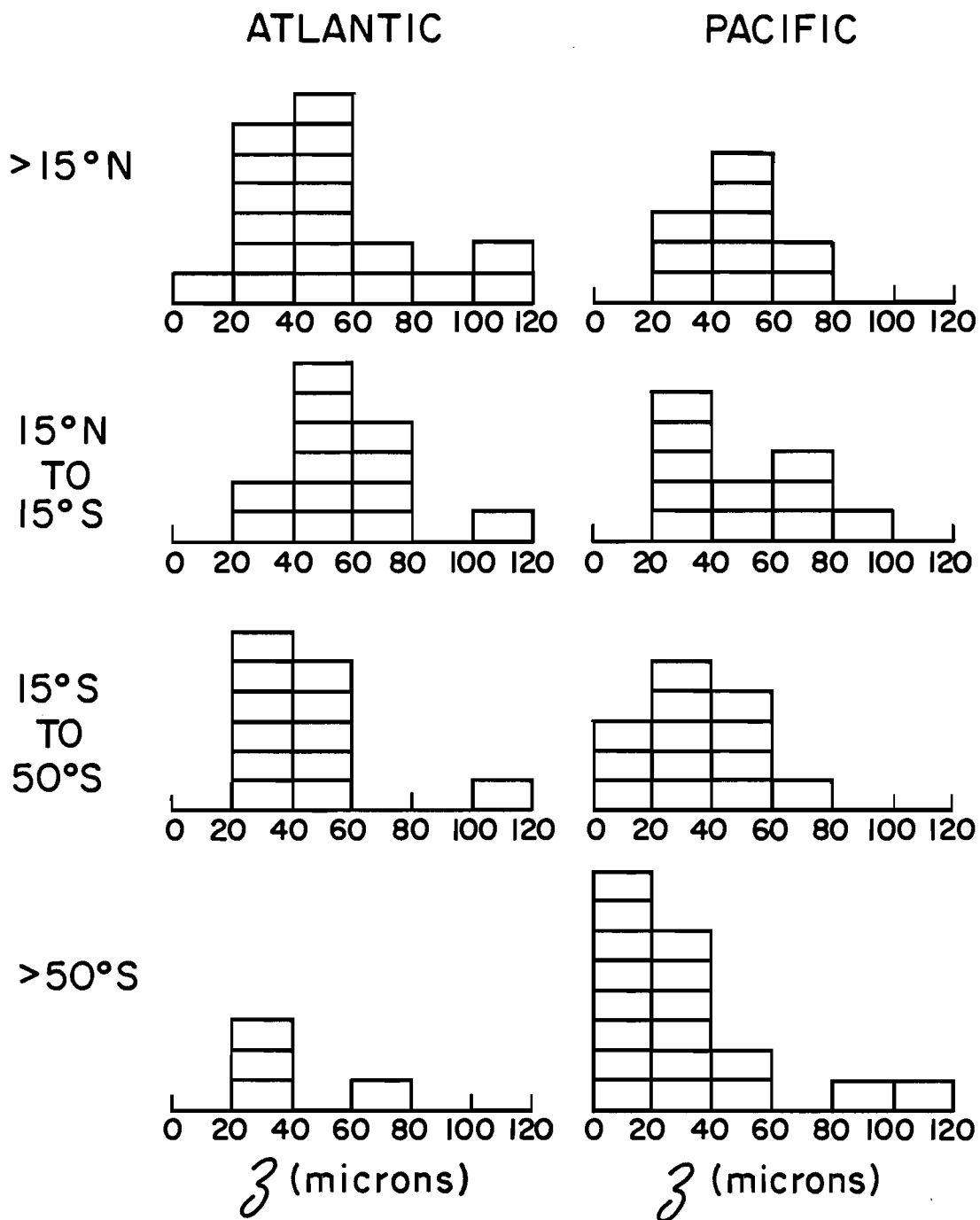


Figure 3-4. Histograms of stagnant film-thickness estimates based on radon measurements in the surface waters of the Atlantic and Pacific Oceans. The measurements are separated according to latitude belt. There is a suggestion that the exchange rate is somewhat lower than average in the equatorial zone (15°S to 15°N) and somewhat higher than average in the Antarctic zone ($>50^{\circ}\text{S}$). These measurements were made as part of the GEOSECS program (175, 176).

temperate zones the values fall largely in the range 20 to 60 microns; in the equatorial zone the values fall mainly in the range 20 to 80 microns; in the Antarctic they are mainly in the range 10 to 40 microns. This distribution is consistent with the fact that wind velocities are on the average somewhat higher over the Antarctic Ocean and somewhat lower over the equatorial ocean than over the temperate ocean. However, as none of the high latitude measurements were made in winter (i.e., the period of greatest storminess), the difference between the various zones may be even larger than suggested by these results.

A comparison between stagnant film thicknesses measured in a wind tunnel and those measured by the radon method at sea in areas with differing mean wind velocities are shown in figure 3-5. As can be seen, while the trends are similar the environmental film measurements are larger at any given wind velocity than those measured in wind tunnels. More field research will have to be carried out before a firm estimate of the wind velocity dependence of the gas exchange rate can be given.

OXYGEN CONCENTRATIONS IN SURFACE OCEAN WATER

When the dissolved oxygen contents of surface ocean waters are compared with those for saturation with the overlying air it is found that they are on the average supersaturated by several percent (see figure 3-6). Since subsurface waters are all highly undersaturated with dissolved oxygen, this excess is not the result of incomplete equilibration between upwelled water and the atmosphere. There are several possible explanations for departures from equilibrium.

1) Bubbles injected into the water lose part of their gas to the water during entrainment. As any excess introduced in this way must be balanced by diffusion through the stagnant film back to the atmosphere, bubble entrainment could maintain an overpressure of gases in surface water.

2) Plants living in surface water produce oxygen. The accumulation of this oxygen could lead to observed supersaturation.

3) The waters on which these measurements were made were undergoing seasonal warming, and hence had dissolved oxygen contents reflecting previous lower temperatures. As the GEOSECS measurements were made in the fall as well as in the spring and summer, and as in equatorial waters there is no seasonality, this explanation is not acceptable.

Our knowledge of the rate at which dissolved oxygen goes back and forth between the atmosphere and surface sea helps us to distinguish between possibilities 1) and 2). Let us first consider the possibility that photosynthesis produces the excess.

Warm surface water at equilibrium with the air contains about 0.24 moles/m³ of O₂. Thus a mixed layer 50 meters in thickness contains about 12 moles/m² of O₂. At a piston velocity of 3 m/day, about 0.7 moles of atmosphere O₂ will invade each square meter of interface each day. Under these circumstances the average O₂ molecule is replaced in the ocean-mixed layer once each 12/0.7 or 17 days. This is the time then that the average O₂ molecule produced by photosynthesis will reside in the ocean-

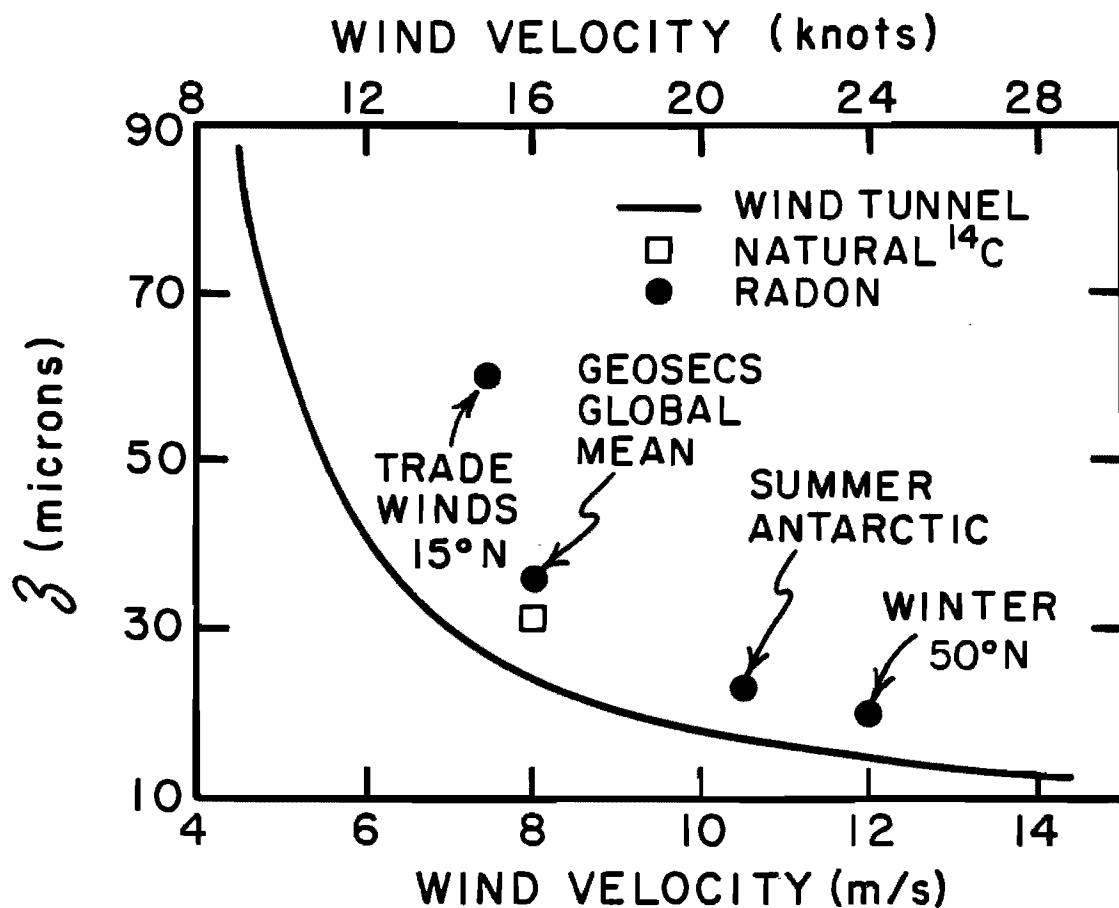


Figure 3-5. Plot of film thickness against wind velocity. The solid line represents measurements made in a wind tunnel. The solid circles are film thicknesses based on radon measurements in the ocean. The open square represents the global average film thickness based on the distribution of natural radiocarbon. While both the open ocean and wind tunnel data show increases in film thickness with decreasing wind velocity, the tunnel measurements give consistently lower film thicknesses than do the ocean measurements. This offset may reflect the following differences between the two situations. The large waves present in the sea are not present in the wind tunnel. Fresh water is used in the wind tunnel experiments. Also, the method used to adjust the tunnel wind velocities (measured a few tens of centimeters above the water surface) to the equivalent velocities over the sea (measured at a height of about 15 meters) may not be correct. The wind tunnel experiments were conducted by H.C. Broecker and his colleagues in Hamburg, W. Germany (188). The radon results were obtained by scientists at the Lamont-Doherty Geological Observatory (172,173, 175,176).

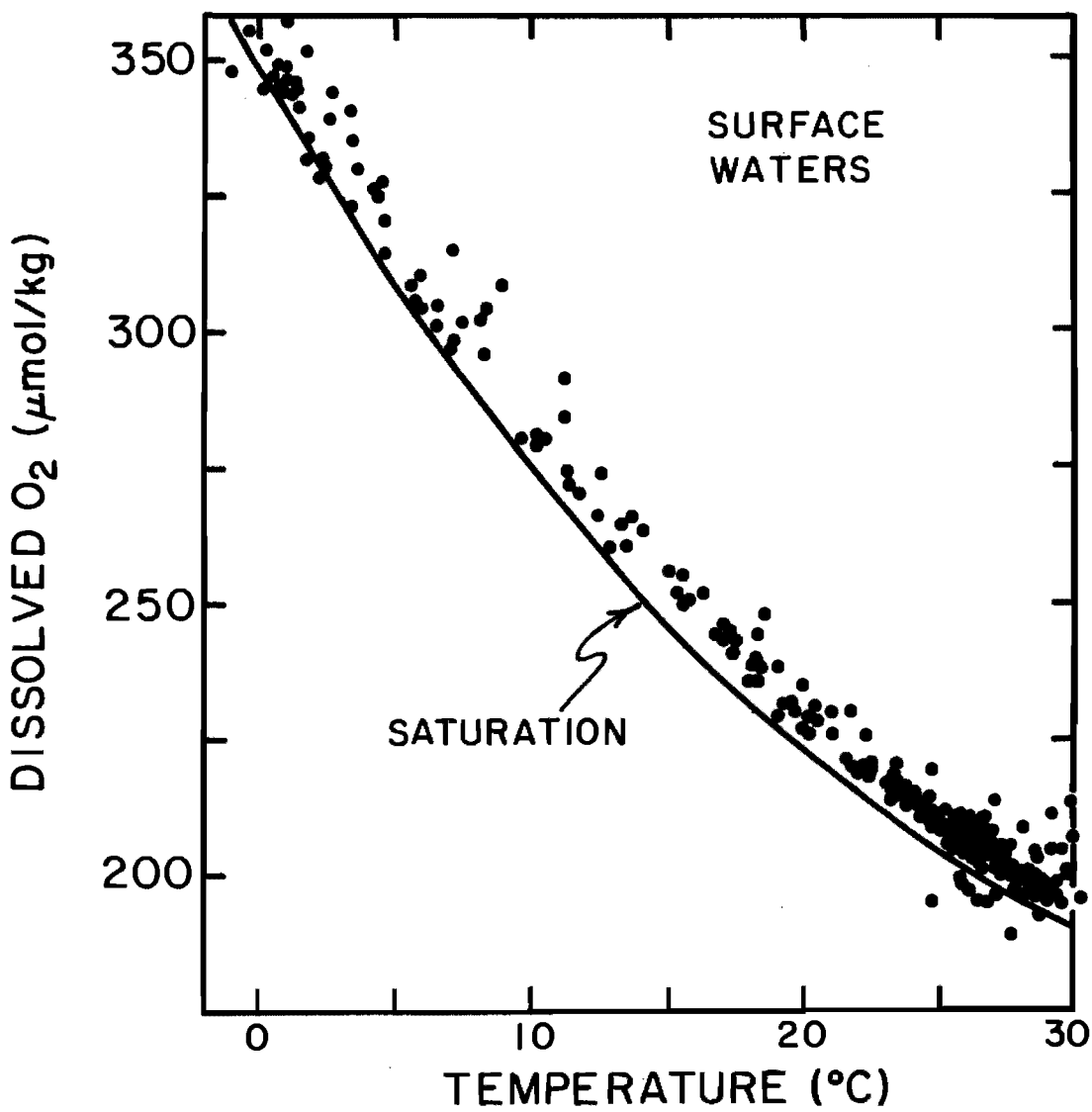


Figure 3-6. Plot of the dissolved oxygen content measurements on surface waters made as part of the GEOSECS program as a function of water temperature (424, 425, 426). The solid line represents the saturation value. Surface ocean waters are supersaturated by an average of 7 $\mu\text{mol}/\text{kg}$ (i.e., by about 3%).

mixed layer before escaping to the atmosphere. The rate of plant productivity in the ocean-mixed layer has been determined by marine biologists at many points on the sea surface and at many times during the year using a tracer ^{14}C method developed by an inventive Dane named Steeman-Nielsen. The mean for all of the measurements made in the open ocean is about 0.3 moles of carbon fixed per square meter of ocean surface per 17 days (i.e., about 6 moles/ m^2yr). As much of the plant matter produced in the sea is promptly eaten by animals and bacteria living in the mixed layer, the rain rate of organic material from the mixed layer is less than the production of organic matter within the mixed layer. On the average only about 15% of the matter formed in the mixed layer falls beneath the mixed layer before being consumed. Thus the net fixation rate of carbon in the mixed layer is only about 0.045 moles/ m^2 per 17 days. For each mole of carbon sinking beneath the mixed layer, 1.3 moles of O_2 are left behind dissolved in the mixed layer. Thus the net production of oxygen in the mixed layer is 0.06 moles/ m^2 per 17 days. This may be compared to the atmospheric equilibrium value of 12 moles O_2/m^2 . The overpressure needed to exhaust the biogenic oxygen is only 0.06/12 or about 0.5% of total.* Thus production of oxygen by plants does not appear to explain the observed mean overpressure of this gas. This could only be the case if the amount of organic material falling from the mixed layer were about five times that of 1 mole/ m^2yr estimated here.

There is no doubt that if enough bubbles are entrained and if these bubbles penetrate to a depth of several meters, the observed oxygen supersaturations could be generated. The pressure at a depth of two meters is 1.2 atmospheres, hence bubbles carried to this depth would continue to lose gas to the adjacent water until a 20% supersaturation was produced. So the potential is there. The difficulty with this hypothesis comes in attempting to quantify the flux of gas borne by bubbles into the sea. It depends in a complex way on the spectrum of winds and waves. So, while promising, this hypothesis remains unproven.

One means by which the bubble injection hypothesis could be checked would be to simultaneously measure the degree of supersaturation of a number of gases. If the oxygen supersaturation were produced by photosynthesis then none of the other gases would show excesses. If these gases are supersaturated the excesses should not be the same because the solubilities of gases differ. For example, were a bubble to be carried deep enough beneath the surface and remain long enough to dissolve completely, the gas it gave up would produce a much greater percentage of change in the helium content of the water than in the xenon content of the water. Even if the bubble didn't completely dissolve, the tendency would be the same, and the low-solubility gases would be enhanced in the sea more than the high-solubility gases. Working against this effect, however, would be the fact that the lower

*We have checked this result using the 1-D ocean model presented in chapter 10. The model, which yields a reasonable average vertical distribution of PO_4 in the sea, yields a mean O_2 supersaturation for surface water of 0.4%.

solubility gases could escape back through the air-sea interface faster due to their higher molecular diffusivities. As can be seen in table 3-3 the diffusivity changes almost as much from gas to gas as does the solubility, hence; the solubility effect will be partly compensated by the diffusivity effect. In any case, sufficiently accurate measurements for a variety of gases measured simultaneously in surface sea water are not yet available, so this check has yet to be made.

As shown in figure 3-7 a narrow belt of surface ocean along the equator in the Pacific Ocean shows deficiencies in dissolved oxygen. These deficiencies are maintained by events of upwelling of waters deficient in oxygen. Because of the intensity of this process, invasion of O_2 from the air does not have time to wipe out this deficiency.

OXYGEN DEFICIENCIES IN THE DEEP SEA

Even though the oxygen content of surface waters is observed to be slightly supersaturated, concentration of this gas in newly formed deep waters is the most predictable of all the biologically utilized constituents. As we have already pointed out, the biolimiting nutrient constituents (i.e., H_4SiO_4 , NO_3 and PO_4) are only partially utilized in cold surface water. Hence, it is difficult to predict how much of any one of these constituents found in deep water was produced by respiration within the deep sea and how much was carried down with newly formed deep water.* The same difficulty applies to ΣCO_2 and to radio-carbon. The fact that dissolved oxygen is carried to the sea's interior in nearly known amounts provides possible means for recreating the compositions of deep waters at their time of origin. For any given water in the deep sea, we can determine how much oxygen was utilized by subtracting the observed oxygen content from the saturation oxygen content. Oceanographers have termed this quantity the apparent oxygen utilization and refer to it as AOU. The adjective "apparent" is added to alert users of this property that it is not an exact measure of utilization. The waters leaving the surface likely carry more than the saturation amount of oxygen. Due to the nonlinearity in the solubility of oxygen with temperature, any mixing between waters of differing temperature will produce a slightly higher oxygen concentration than would be expected for the intermediate temperature. However, as these effects are small compared to actual utilization, AOU is quite close to TOU (true oxygen utilization).

Before examining the reliability of AOU in separating the preformed contribution to the observed deep water concentrations of the various nutrient constituents, let us look at the distribution of this property in the sea. Figure 3-8 shows how AOU changes along the 4000 meter horizon. As would be expected, AOU is lowest in the northwestern Atlantic and highest in the northern Pacific. The pattern is similar to that for dissolved silica (see figure 1-8). However when the vertical sections for AOU

*In the sections which follow we will refer to these concentrations in newly formed deep water as the preformed values.

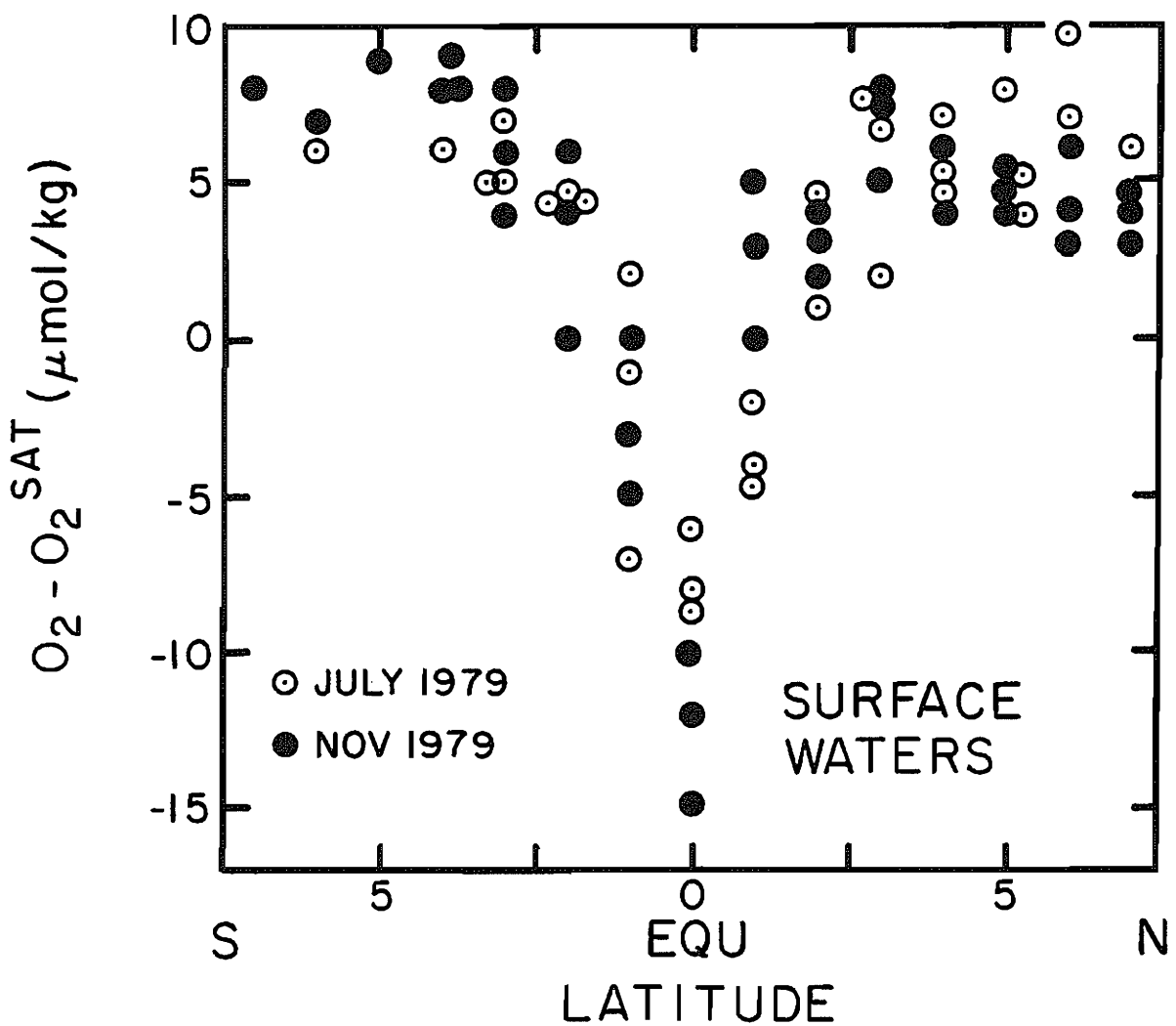


Figure 3-7. Difference between the observed and saturation O_2 contents for surface waters in the equatorial zone between Hawaii and Tahiti. Intense upwelling very close to the equator brings up water deficient in O_2 . These measurements were made by Bob Williams and his group at Scripps Institution of Oceanography as a part of a program organized by Wyrtki at the University of Hawaii (433).

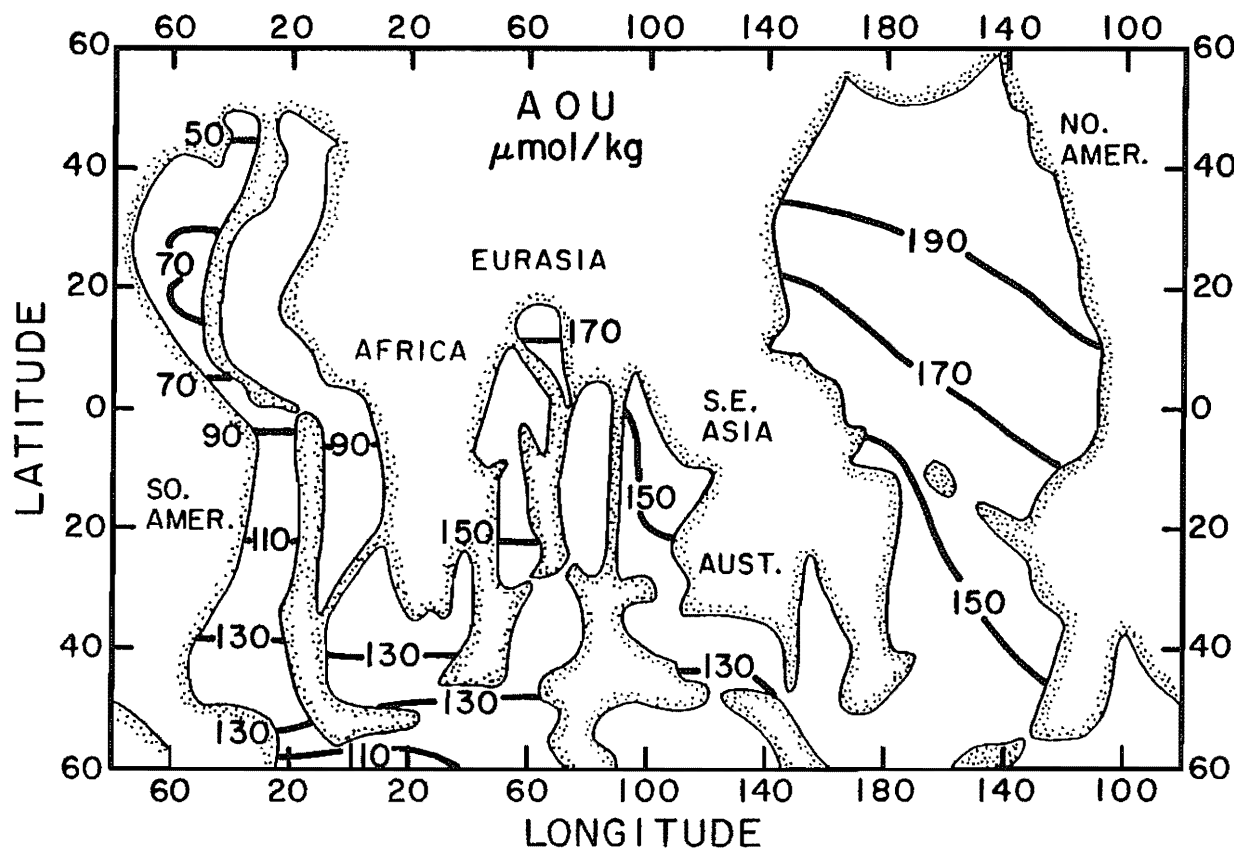
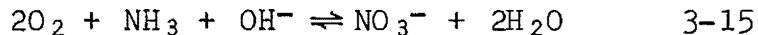
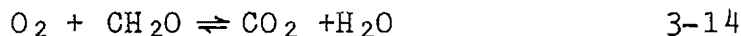


Figure 3-8. Distribution of AOU (saturation oxygen content minus measured oxygen content) at a depth of 4000 meters. Based on the results obtained during the GEOSECS program (424, 425, 426).

(figures 3-9, 3-10, 3-11 and 3-12) are compared with those for silica (figures 1-14, 1-15, 1-16 and 1-17), it can be seen that the distribution of AOU is not the same as that of silica. A prominent example of this difference can be seen in the western Atlantic where AOU reaches its highest value in the equatorial thermocline while silica reaches its highest value in bottom waters. While some of this difference is due to the high preformed silica of deep waters formed in the Antarctic, this is not the only cause. As mentioned earlier, the frustules of opaline silica formed by organisms reach, on the average, considerably greater depths before dissolving than do fragments of organic tissue before being eaten. Thus, while the distributions of both silica and AOU reflect the main circulation pattern of waters in the deep sea, they also have important differences generated by processes occurring at the sea surface (i.e., gas exchange and plant uptake) and within the body of the sea (respiration and silica solution). Thus, while AOU may help us understand the distributions of the constituents of soft tissue (C, N and P), it will be of no particular use in understanding that of hard part constituents (Si, Ba and Ca).

The ratio between carbon release and oxygen consumption during oxidation of organic material has been established in the laboratory. When the debris of marine plankton is oxidized, about 1.3 moles of oxygen gas are required to combust an amount of organic material containing one mole of carbon. In other words, in this experiment, for each mole of CO₂ that appears as a combustion product, 1.3 moles of O₂ gas disappear. In the reaction the combustion products are CO₂, NO₃⁻, and H₂O. The chemical reactions are:



where CH₂O and NH₃ are the chemical forms of carbon and nitrogen in organic tissue. About one O₂ molecule is required to "burn" each C atom present in the organic tissue, and about two O₂ molecules are required to "burn" each N atom present. The other constituents which undergo oxidation are so low in abundance relative to C and N that their O₂ requirements can be neglected. Since there are about 15 atoms of N for every 105 atoms of C in falling organic debris, 135 molecules of O₂ are required for each 105 atoms of C.

While these ratios apply to the average organic matter formed in surface water, they need not necessarily apply to the organic matter falling to the deep sea. The problem is that the respiration occurring in shallow water may oxidize one constituent more efficiently than another. If so, the residues falling as fecal pellets need not have the same composition as plants. Also, in some regions of the deep sea, organisms use NO₃⁻ ion as an oxidant (they convert NO₃⁻ to N₂). To check this, we show in figures 3-13 and 3-14 the changes in PO₄ versus that in NO₃, in NO₃ versus that in O₂, in O₂ versus that in ECO₂, and in alkalinity versus that in ECO₂ along constant density horizons in the major ocean basins. We choose constant density surfaces to avoid the problem that deep

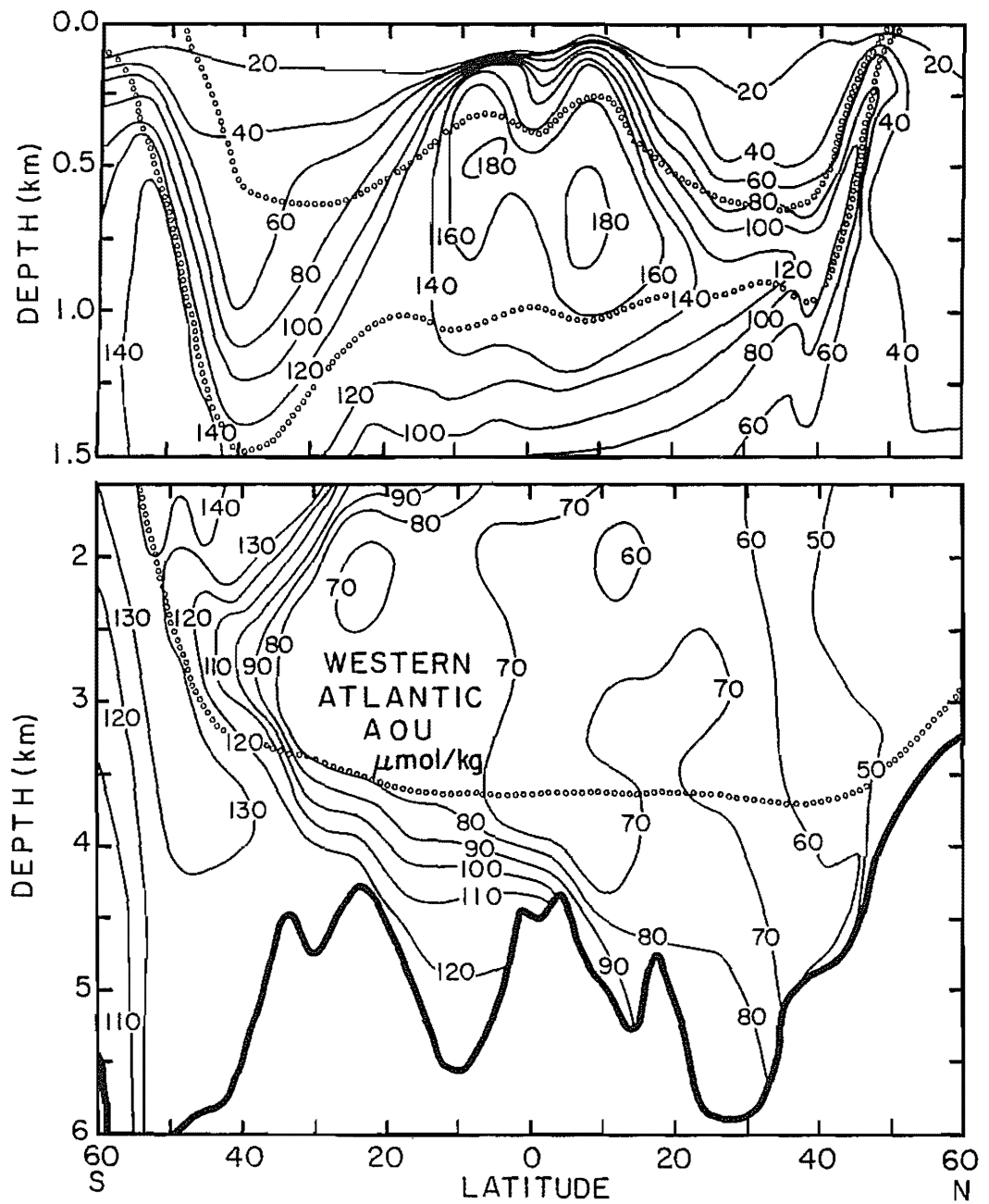


Figure 3-9. Vertical section of AOU (saturation oxygen content minus measured oxygen content) along the western basin of the Atlantic Ocean. The section is broken at 1500 meters. The vertical exaggeration for the upper ocean is twice that for the deep ocean. The contour interval for the upper ocean is 20 $\mu\text{mol/kg}$; that for the deep ocean is 10 $\mu\text{mol/kg}$. Also shown by dotted lines are the $\sigma_0 = 27.0^\circ/\text{o}$ isopycnal (upper), the $\sigma_0 = 27.5^\circ/\text{o}$ isopycnal (middle) and the $\sigma_4 = 45.2^\circ/\text{o}$ (lower) isopycnal horizons. Based on the results obtained by the GEOSECS program (424). The tracks along which this and the following sections were drawn can be found on the foldout map.

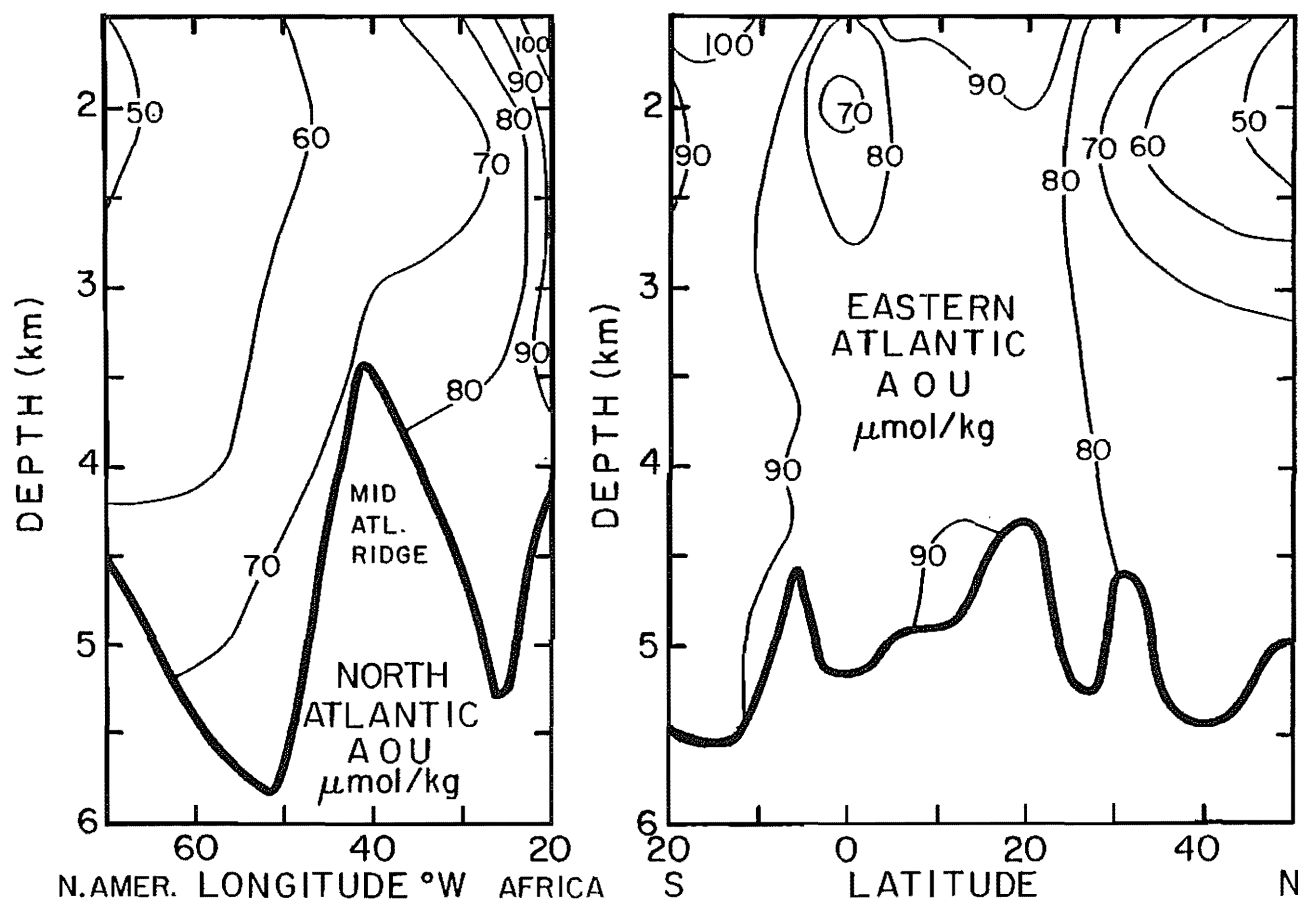


Figure 3-10. Vertical sections of AOU (saturation oxygen content minus measured oxygen content) for the waters below 1500 meters depth across the North Atlantic (at about 32°N) and in the eastern basin of the Atlantic Ocean. Based on the results obtained by the GEOSECS program (424).

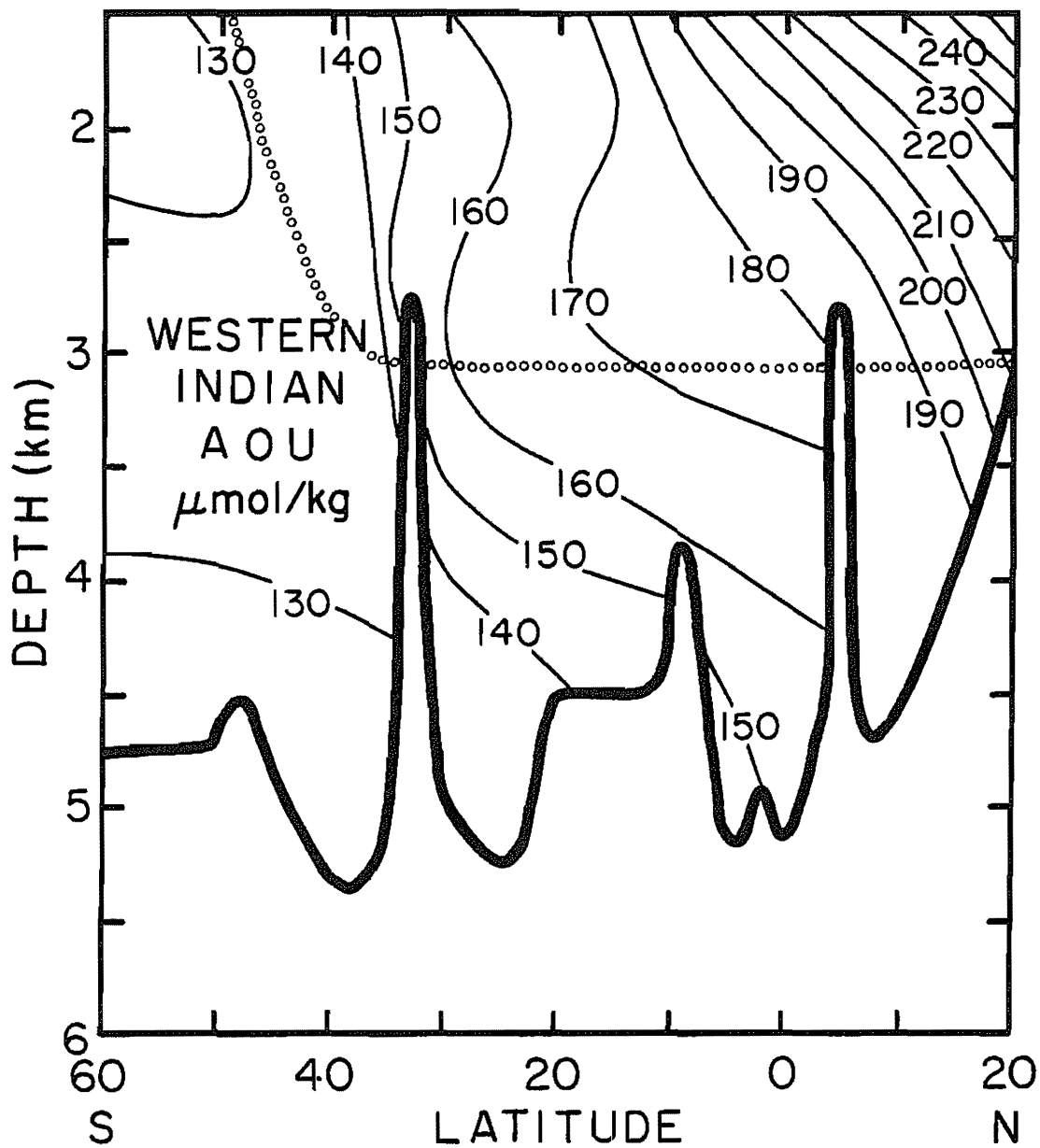


Figure 3-11. Vertical section of AOU (saturation oxygen content minus measured oxygen content) below 1500 meters along the basins of the western Indian Ocean. Also shown by the dotted line is the $\sigma_4 = 45.2^{\circ}/\text{o}$ isopycnal horizon. Based on results obtained by the GEOSECS program (426).

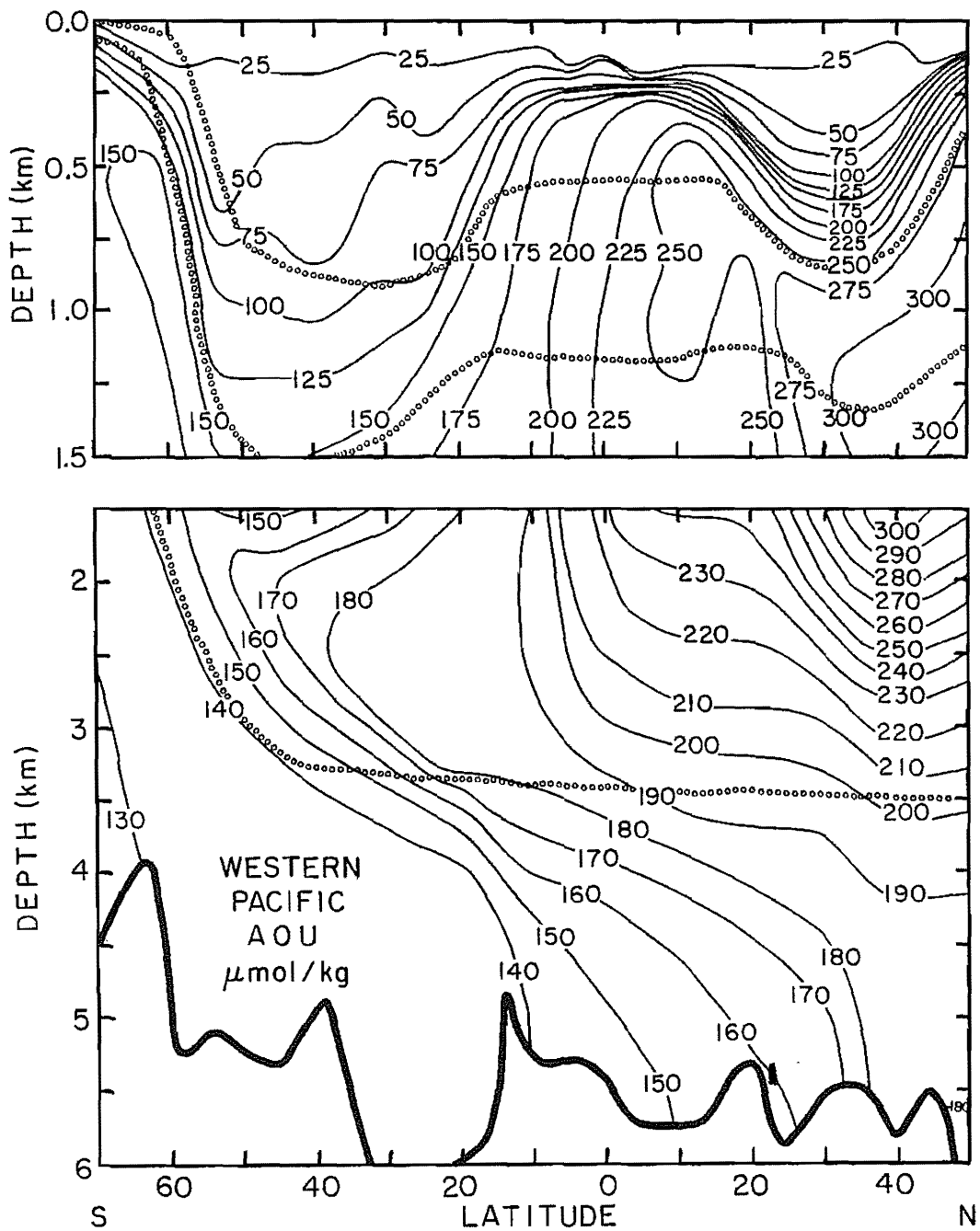


Figure 3-12. Vertical section of AOU (saturation oxygen concentration minus measured oxygen concentration) along the western Pacific Ocean. The section is broken at a depth of 1500 meters. The vertical exaggeration for the upper ocean is twice that for the deep sea. The contour interval for the upper ocean is 25 $\mu\text{mol}/\text{kg}$. That for the deep ocean is 10 $\mu\text{mol}/\text{kg}$. Also shown by dotted lines are the $\sigma_0 = 27.0^\circ/\text{o}$ isopycnal (upper), the $\sigma_0 = 27.5^\circ/\text{o}$ isopycnal (middle) and the $\sigma_4 = 45.2^\circ/\text{o}$ (lower) isopycnal horizons. Based on results obtained by the GEOSECS program (425).

waters of different origin carry different preformed concentrations of PO_4 , NO_3 , ΣCO_2 and alkalinity. Within a single ocean basin, waters on a given density surface have the same origin and hence the same preformed nutrient constituent concentrations. We include an alkalinity versus ΣCO_2 plot so that the contribution of CaCO_3 solution to the change in the ΣCO_2 concentration can be accounted for. The results of these comparisons are summarized in table 3-5. The first column in this table summarizes the ratios of the concentration changes expected if the composition of the material released during respiration were the same as the composition of average marine plant matter. As the ratio of CaCO_3 to organic tissue produced depends on ecology rather than biochemistry, no entries are made for those ratios involving ΣCO_2 or CaCO_3 . The upper four entries in the last three columns of this table are taken directly from the graphs in figures 3-13 and 3-14. The lower four entries are calculated from the upper four, using the following relationships:

$$\Delta\text{CaCO}_3 = 1/2 (\Delta\text{Alk} + \Delta\text{NO}_3) \quad 3-16$$

$$\Delta\text{ORG} = \Delta\text{CaCO}_3 - \Delta\Sigma\text{CO}_2 \quad 3-17$$

The first of these equations yields the contribution of ΣCO_2 derived from CaCO_3 solution. The second gives the change in ΣCO_2 from the oxidation of organic debris.

The entries in this table make it clear that while the proportions are roughly as expected, a substantial range is found. In particular the ratio of organic C to PO_4 and to NO_3 for the Atlantic is smaller than expected. The ratio of carbon added to deep water from the oxidation of organic residues to that added by the dissolution of CaCO_3 ranges from 2.6 in the Atlantic to 1.3 in the Indian Ocean. The reason these values are less than the value of four given in chapter 2 is that the oxidation of organic matter occurs, on the average, at shallower depths than the solution of CaCO_3 (i.e., the ratio $\Delta\text{ORG}/\Delta\text{CaCO}_3$ decreases with depth in the ocean).

Thus our strategy of using AOU as a means for reconstructing the initial composition of the deep waters in the sea meets with only limited success. It cannot be used for the constituents bound in hard parts (this eliminates C as well as Ca, Ba and Si). Since the composition of the debris falling into the deep sea varies from region to region in the ocean the use of a universal correction factor will lead to errors in the reconstructed initial PO_4 and NO_3 values.

THE MARINE N_2O CYCLE

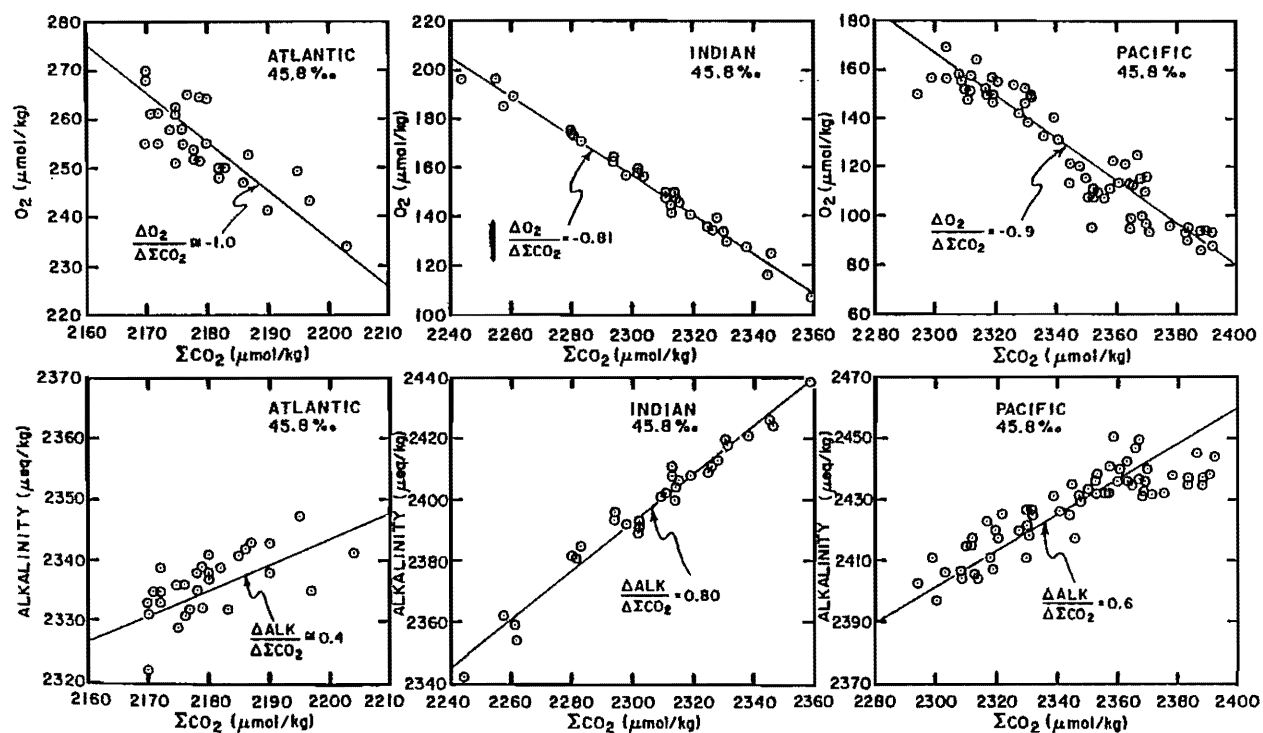
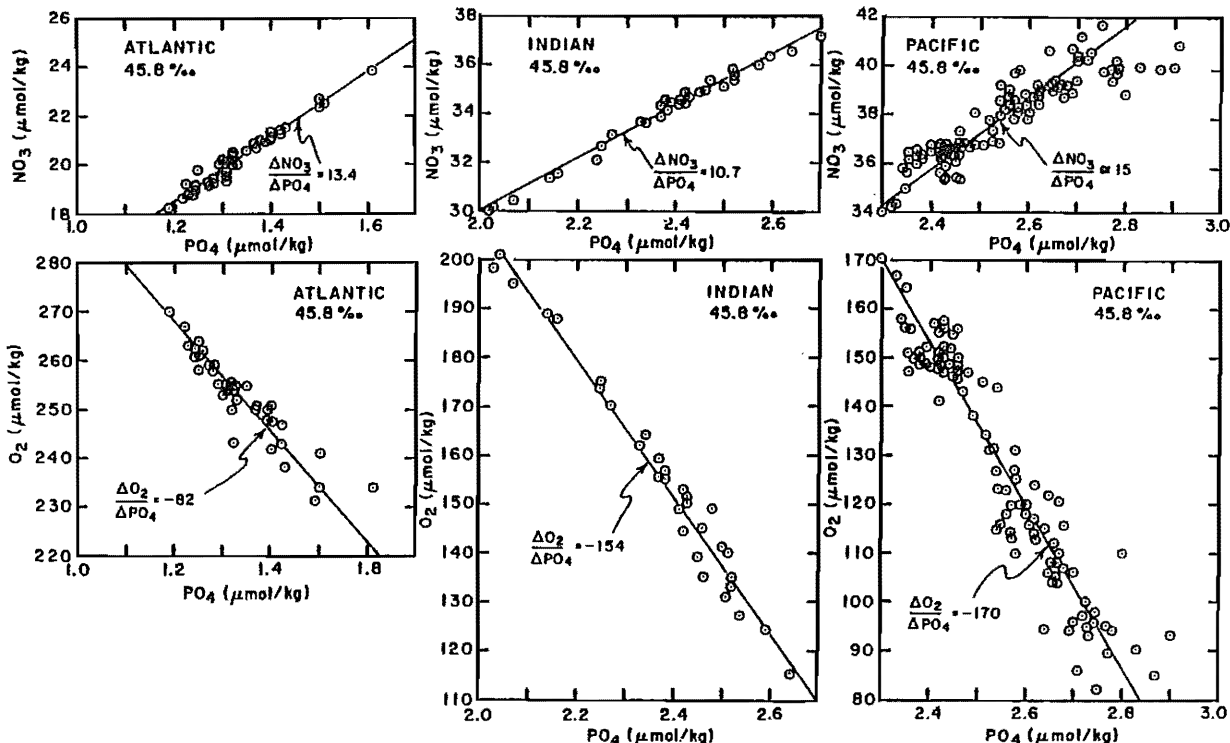
During the oxidation of organic material by organisms living in the sea some of the nitrogen is converted to nitrous oxide gas (N_2O) rather than back to nitrate ion. Dramatic evidence for this is shown in figure 3-15. The profile of dissolved nitrous oxide in the northwestern Atlantic has a shape which is the inverse of that for dissolved oxygen! As shown in the insert in this diagram, when the excess N_2O concentration (over that for equilibrium

Table 3-5. Property-Property trends along the $\sigma_4 = 45.8^{\circ}/oo$ isopycnal horizon in the deep sea (~2500 meters depth).

Property Ratio	Reference Value	Atlantic Ocean	Indian Ocean	Pacific Ocean
From Graphs in Figures 3-13 and 3-14				
$\Delta NO_3 / \Delta PO_4$	15	13	11	15
$\Delta O_2 / \Delta PO_4$	-136	-82	-154	-170
$\Delta O_2 / \Delta \Sigma CO_2$	-	-1.0	-0.8	-0.9
$\Delta Alk / \Delta \Sigma CO_2$	-	0.4	0.8	0.6
Calculated from the above using equations 3-16 and 3-17				
$\Delta O_2 / \Delta ORG\ C$	-1.3	-1.4	-1.4	-1.4
$\Delta ORG\ C / \Delta NO_3$	6.3	5	10	8
$\Delta ORG\ C / \Delta PO_4$	105	59	110	125
$\Delta ORG\ C / \Delta CaCO_3\ C$	-	2.6	1.3	1.9

Figure 3-13. The upper diagram on the facing page shows plots of nitrate versus phosphate concentration and of dissolved oxygen versus phosphate concentration along the $45.8^{\circ}/oo$ isopycnal surface (~ 2500 meter depth) in the Atlantic, Indian and Pacific Oceans. The slopes of these relationships give the proportions of these constituents for respiration taking place in the deep sea. Based on results obtained by the GEOSECS program (424, 425, 426). J.F. Minster correctly points out that the trends seen for the deep Atlantic are likely dominated by mixing with Antarctic waters. Hence they are not indicative of respiration occurring in the deep Atlantic.

Figure 3-14. The lower diagram on the facing page shows plots of dissolved oxygen versus total dissolved inorganic carbon content and of alkalinity versus total dissolved inorganic carbon content along the $45.8^{\circ}/oo$ isopycnal horizon in the Atlantic, Indian and Pacific Oceans. The slopes of these trends reflect the composite effects of respiration and calcium carbonate solution in the deep sea. Based on results obtained as part of the GEOSECS program (424, 425, 426).



with the atmosphere) is plotted against the deficiency of oxygen (i.e., AOU), a good correlation is found. For every 10,000 molecules of O_2 utilized, about one molecule of N_2O is produced. Since there is about one unit of NO_3^- produced for each 10 units of O_2 consumed, this means that on the order of 1 N atom in 1000 is converted to N_2O rather than to NO_3^- during respiration. This N_2O appears to be nearly inert in sea water and accumulates until the water contacts the atmosphere at which point the N_2O is lost. Once in the atmosphere the N_2O is gradually converted to N_2 . This mechanism alone would destroy all the NO_3^- in the sea in about 1,000,000 years (1000 mixing cycles at 1000 years per cycle).

Not all the N_2O produced in the sea escapes to the atmosphere. At a few places in the sea the oxygen content is drawn all the way to zero (see figure 3-17). In the northern part of the western Indian Ocean there is a layer almost one kilometer thick with near zero oxygen content. In this layer nitrate is used as an oxidizing agent. This can be shown from the very low NO_3^- to PO_4^{3-} ratios or by comparing the observed NO_3^- content with that predicted by multiplying the phosphate content by 15 (see figure 3-16). A similar situation is found in the eastern Pacific Ocean in the 10° to $20^\circ N$ latitude belt (see figure 3-16). In this region N_2O measurements have been made. As shown in figure 3-18 the N_2O concentration continues to rise with decreasing O_2 concentration until O_2 levels very close to zero are achieved. Then, along with the nitrate content, the N_2O content starts to drop. Waters have been found which are nearly free of N_2O as well as of oxygen.

In addition to learning about a sink for N_2O within the sea, we have also found evidence for the destruction of NO_3^- within the sea. Although a bit off topic for this chapter (i.e., gases in the sea), let us explore this evidence for nitrate consumption a bit further. It is not only in waters free of O_2 that we have evidence for NO_3^- consumption. The deep waters of the Bering Sea which are trapped behind the Aleutian arc also show evidence for such depletion. They are ventilated by deep Pacific waters which enter the basin through a deep gap in the arc near its western end. The chemistry of waters of the same salinity inside and outside the arc are compared in table 3-6. It can be seen that the Bering Sea waters are, as might be expected, lower in dissolved oxygen and higher in phosphate than their open Pacific counterparts. The ratio of O_2 deficiency to PO_4^{3-} excess is more or less as would be expected. Nitrate, however, is slightly lower in Bering Sea waters than in the open Pacific. Thus, denitrification must be occurring within the deep Bering Sea. This is not to be expected, as the oxygen contents are everywhere in the Bering Sea well above zero. One explanation for the NO_3^- depletion might be that the fecal pellets falling into the deep waters develop anaerobic cores and that these cores then become the sites of nitrate utilization. In any case, we can add another item to our growing list of sites in the ocean where NO_3^- is being destroyed.

Whatever process is operative in the Bering Sea may well be at work in parts of the open Pacific. In figure 3-13 it can be seen that the highest phosphate deep waters (i.e., those in the far northeast of the deep Pacific) show nitrate values falling

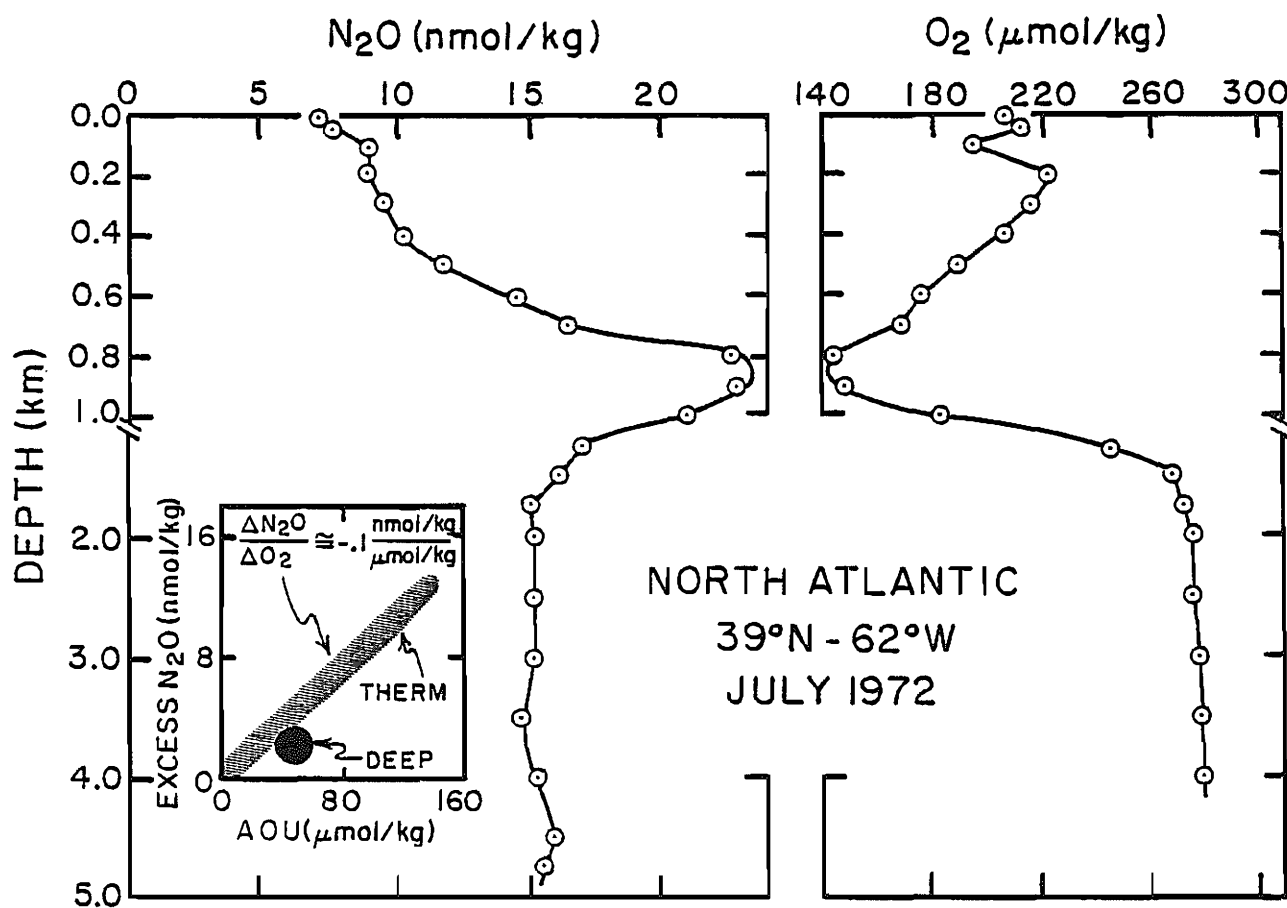


Figure 3-15. Plots of dissolved oxygen and nitrous oxide concentration as a function of depth in the northwestern Atlantic Ocean (note the change in the depth scale below 1000 meters). As shown by the insert, when the excess N_2O content of the samples (i.e., measured N_2O minus saturation N_2O content) is plotted against AOU (saturation oxygen content minus measured oxygen content), an excellent correlation is found. One molecule of N_2O is produced for every 10,000 molecules of O_2 utilized. While the ratio of N_2O production to O_2 utilization varies somewhat from place to place in the sea, except for regions where O_2 is totally depleted, N_2O builds up as O_2 is used. These results were obtained by Yoshinari at Dalhousie University in Halifax, Canada (419).

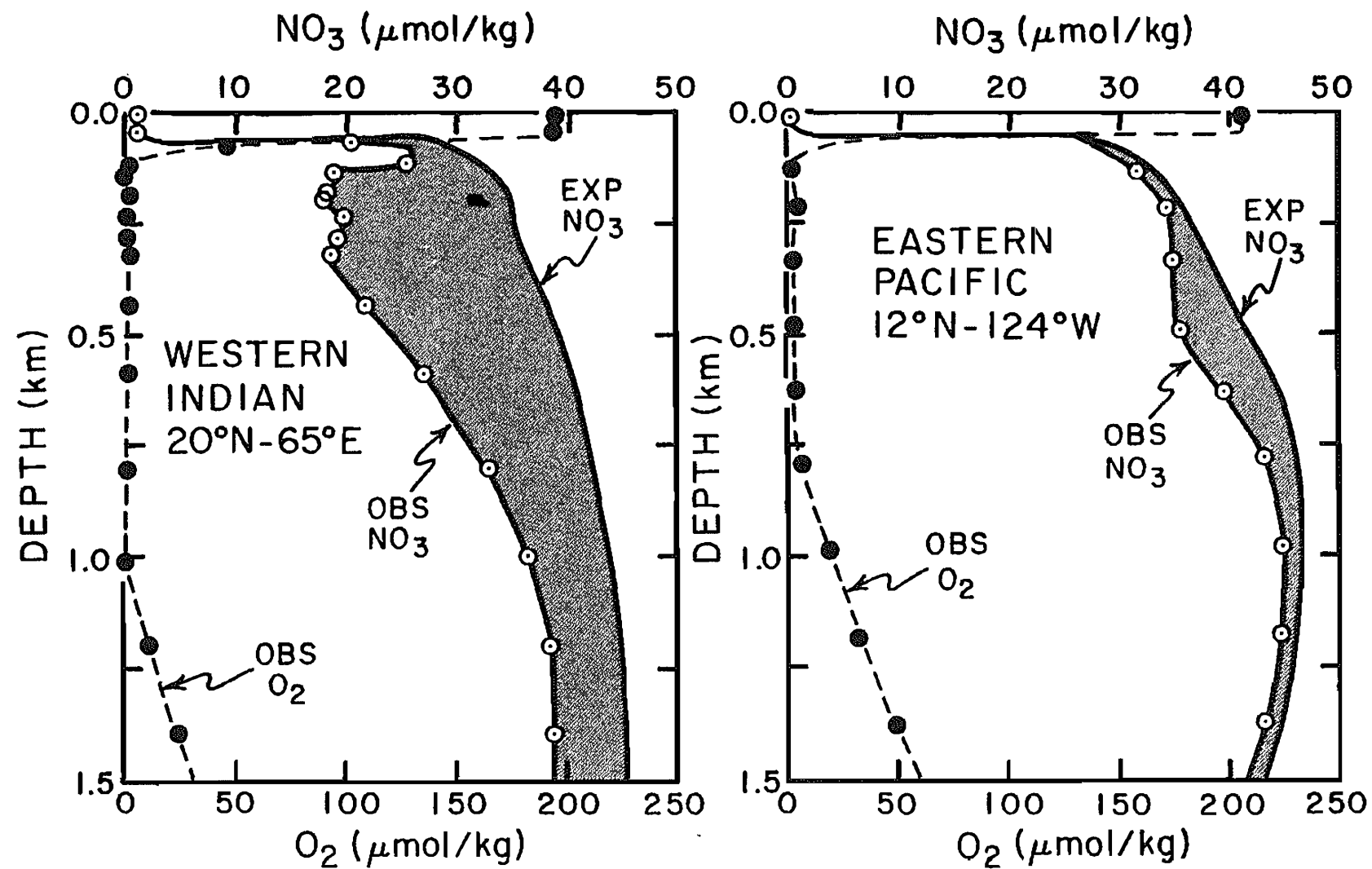


Figure 3-16. Plots of the dissolved oxygen and of the nitrate concentration versus depth in the northern part of the western Indian Ocean and in the eastern part of the equatorial Pacific. Both areas have thermoclines in which the dissolved oxygen content goes to zero. In these waters nitrate is utilized by bacteria as an oxidizing agent leading to nitrate deficiencies in the water column (see the shaded area between the measured and the expected nitrate concentration curves). The expected nitrate concentration is calculated by multiplying the measured PO₄ concentration by 15. These results were obtained as part of the GEOSECS program (425, 426).

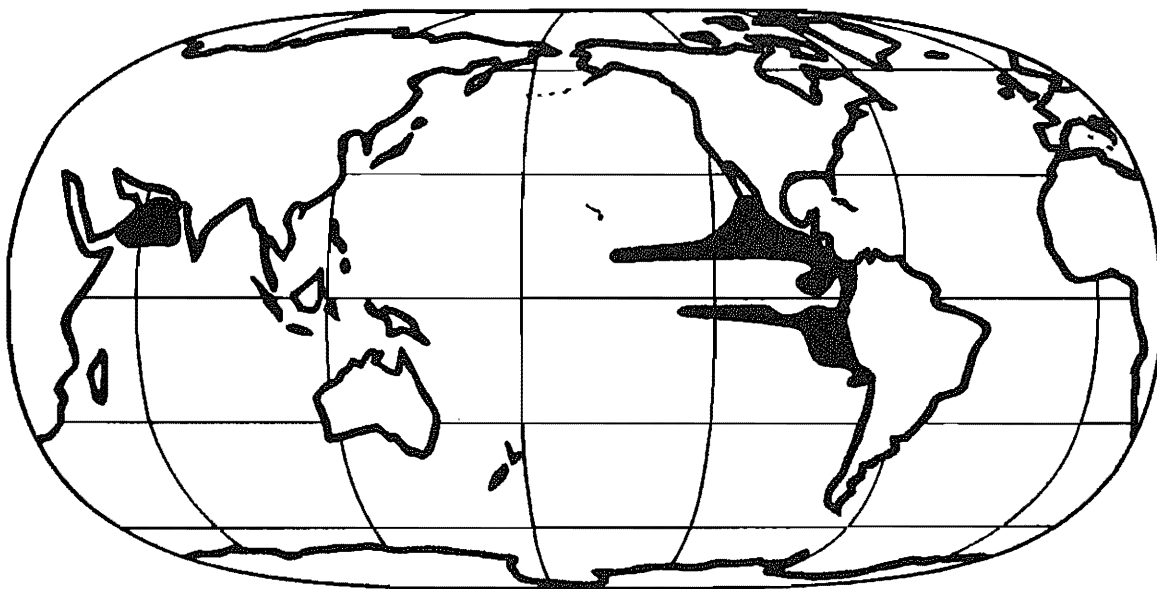


Figure 3-17. Map showing those regions of the ocean where dissolved oxygen goes to less than 20 $\mu\text{moles}/\text{kg}$ in the main thermocline. This diagram was constructed by Werner Deuser at the Woods Hole Oceanographic Institution.

Table 3-6. Evidence for nitrate utilization in the deep Bering Sea†

Salinity °/oo	OPEN PACIFIC			BERING SEA			BERING - PACIFIC		
	O_2 $\mu\text{m}/\text{kg}$	PO_4 $\mu\text{m}/\text{kg}$	NO_3 $\mu\text{m}/\text{kg}$	O_2 $\mu\text{m}/\text{kg}$	PO_4 $\mu\text{m}/\text{kg}$	NO_3 $\mu\text{m}/\text{kg}$	ΔO_2 $\mu\text{m}/\text{kg}$	ΔPO_4 $\mu\text{m}/\text{kg}$	ΔNO_3 $\mu\text{m}/\text{kg}$
34.625*	91	2.71	41.1	72	2.90	40.6	-19	0.19	-0.5
34.636	100	2.69	40.5	79	2.89	40.1	-21	0.20	-0.4
34.647	110	2.62	40.0	87	2.86	39.3	-23	0.24	-0.7
34.658	124	2.57	39.3	96	2.81	38.8	-28	0.24	-0.5
34.669**	133	2.53	38.7	109	2.75	38.5	-24	0.22	-0.2

†Based on the results obtained at GEOSECS Stn. 219 (425).

*Depth 2500 meters.

**Depth 3700 meters.

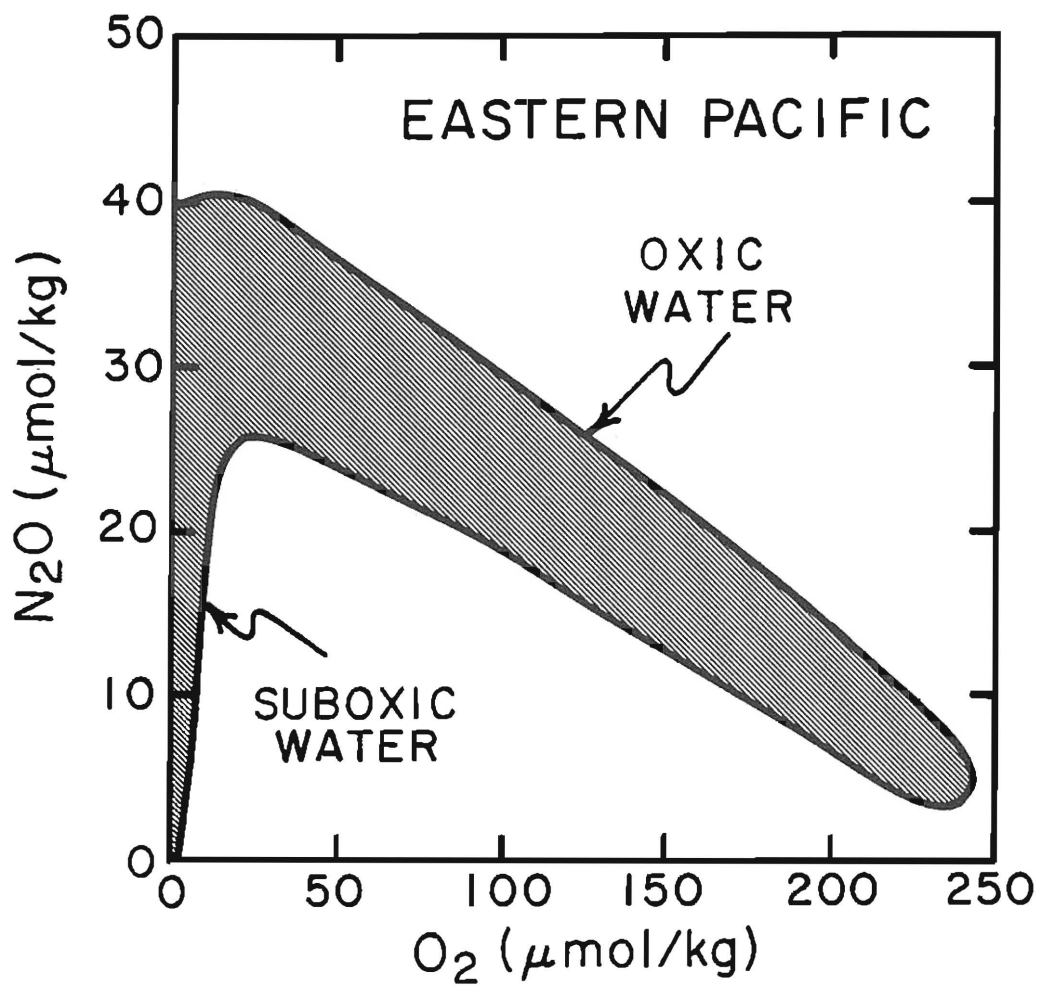


Figure 3-18. Generalized diagram showing the trend of nitrous oxide versus dissolved oxygen in waters from the eastern Pacific (same area as that discussed in figure 3-16). The usual trend of increasing N_2O concentration with decreasing oxygen content is broken in waters of very low oxygen content. Here the N_2O is consumed! These results were obtained by Cohen and Gordon of Oregon State University (420).

well off the trend found for waters with lower phosphate contents. Again NO_3^- reduction appears to be occurring!

Before leaving the subject of the gases of nitrogen in the sea, we should mention that, whereas the destruction of NO_3 within the sea should produce increases in the nitrogen gas content of sea water, it must be remembered that deep sea water contains about 600 micromoles of N_2 per kg. The greatest NO_3 deficiency so far measured in sea water is about 10 $\mu\text{mole/kg}$. The corresponding N_2 increase would be only two percent - well within the range of supersaturation effects.

EXCESS HELIUM

Two gases are being generated within the earth, ${}^{40}\text{Ar}$ from the radioactive decay of the long-lived isotope, ${}^{40}\text{K}$, and ${}^4\text{He}$ from the radioactive decay of the long-lived isotopes, ${}^{238}\text{U}$, ${}^{235}\text{U}$, ${}^{232}\text{Th}$ and their respective daughter products. From our knowledge of processes occurring in the upper atmosphere it is possible to show that the average ${}^4\text{He}$ atoms are able to "evaporate" from the atmosphere to outer space on a time scale of about one million years. By contrast the escape time for an ${}^{40}\text{Ar}$ atom greatly exceeds the age of the earth. Hence, while virtually all the ${}^{40}\text{Ar}$ atoms which have reached the atmosphere from the earth's interior are still there, only those He atoms which leaked from the interior during the last few million years are present. From our knowledge of the amount of ${}^{40}\text{Ar}$ in the air and of the amount of the element potassium in the earth, it is possible to show that a fair fraction (~50%) of the atoms of the radiogenic argon produced within the earth have managed to reach the earth's surface. Based on this observation, it seems likely that ${}^4\text{He}$ atoms are outgassing from the earth's interior at close to the rate at which they are being produced in the earth. Indeed, the calculated evaporation rate of ${}^4\text{He}$ atoms from the top of the atmosphere turns out to be similar to the rate at which ${}^4\text{He}$ is being produced within the earth. As 70% of the earth's surface is covered by ocean water, a fair fraction of these ${}^4\text{He}$ atoms must pass through this reservoir on their way to the atmosphere. Since the deep ocean waters are replaced on a 1000-year time scale, it was possible to show that this flux should produce a measurable excess (over saturation) of ${}^4\text{He}$ in the deep sea. Suess and Wänke (265) were the first to attempt to find these excesses. Their results placed only an upper limit of six percent. Subsequent measurements of the absolute helium concentration in deep sea water samples made by Bieri, Koide and Goldberg of Scripps Institution of Oceanography (266,267) suggested that considerable excesses of ${}^4\text{He}$ (5 to 20%) were to be found. Harmon Craig of Scripps Institution of Oceanography and Brian Clarke of McMaster University set out to check the validity of these measurements by determining the ${}^3\text{He}$ to ${}^4\text{He}$ ratio rather than the absolute concentration of helium in deep sea water samples. The logic was that unlike ${}^4\text{He}$, ${}^3\text{He}$ is not being produced in the earth's interior. Rather the trace amount of ${}^3\text{He}$ found in atmospheric helium was thought at that time to be produced by the spallation of the nuclei of atmospheric gases by cosmic rays. If excess ${}^4\text{He}$ of earth's interior origin was indeed to be found in

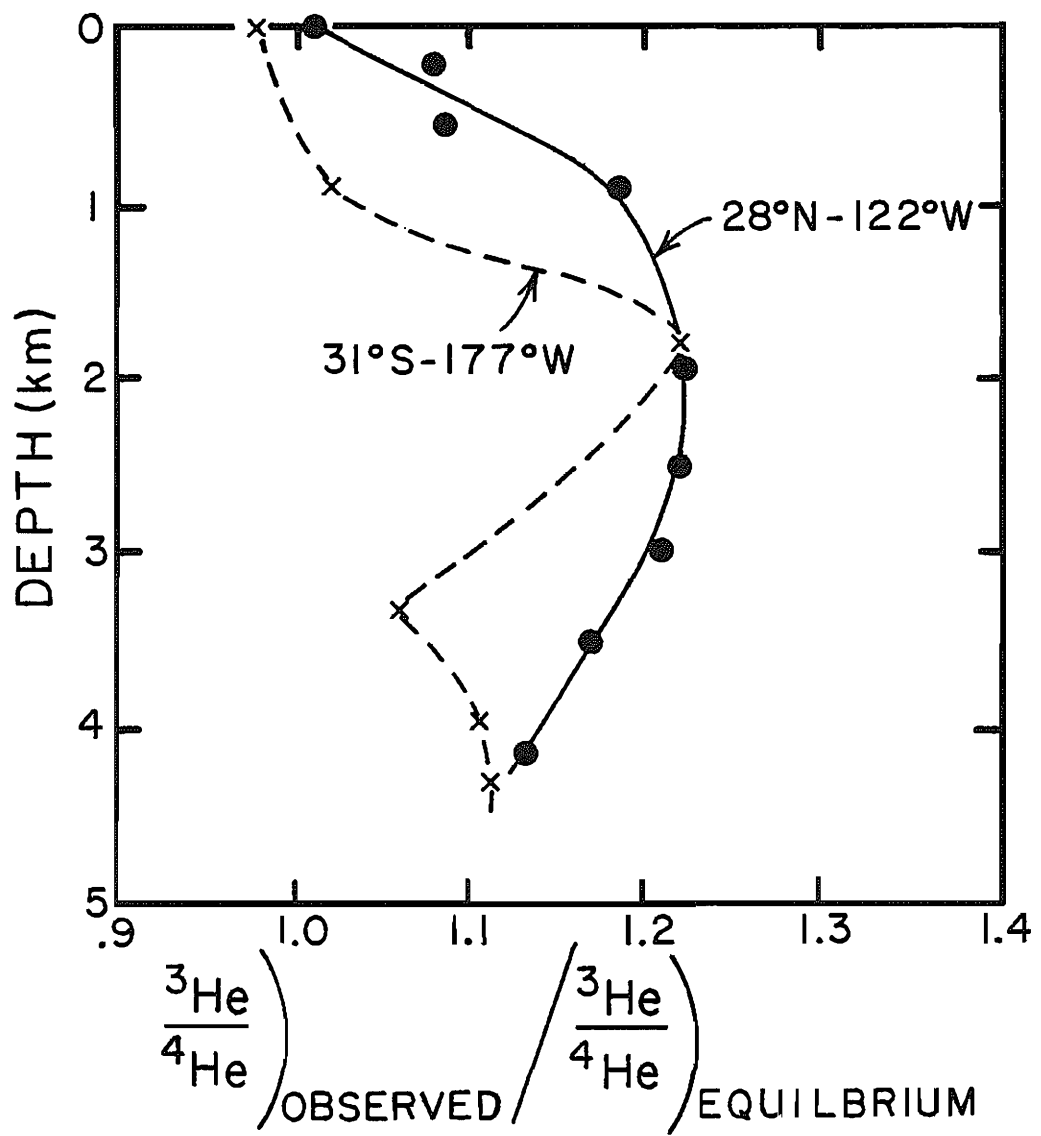


Figure 3-19. Deviations of the ${}^3\text{He}/{}^4\text{He}$ ratio from the value for equilibrium with the atmosphere versus water depth at two locations in the Pacific Ocean. These results were obtained by Brian Clarke at McMaster University, Hamilton, Canada on samples collected by Harmon Craig of the Scripps Institution of Oceanography (269,270).

the deep sea, then the $^3\text{He}/^4\text{He}$ ratio in deep sea water should be less than that in atmospheric samples. Craig collected new deep-water samples and Clarke and his associates analyzed them on a newly constructed mass spectrometer capable of highly sensitive and accurate helium-isotope ratio measurements(269). To their great surprise they found that rather than having lower $^3\text{He}/^4\text{He}$ ratios than atmospheric samples, these samples had higher ratios! To their glee, they immediately realized that they had made a major discovery. ^3He built into the planet at its beginnings was still seeping out into the atmosphere! As their measurements on samples from the deep Pacific showed up to 20% higher $^3\text{He}/^4\text{He}$ ratios than that for atmospheric helium and since their measurement errors were less than 1%, there was no question that they were right. Indeed, subsequent measurements have confirmed this finding.

The depth profiles of the ^3He anomalies found by Craig and Clarke in the Pacific Ocean revealed another bonanza. As shown in figure 3-19, they found that the maximum in this anomaly was not at the bottom of the ocean but rather at about 2 kilometers depth. This suggested that the excess ^3He was coming from the crests of the mid-ocean ridges! Measurements of helium in the recently discovered hydrothermal vents on these ridges reveal very large excesses of both ^4He and ^3He . The $^3\text{He}/^4\text{He}$ ratio in these hot waters is eight times higher than that in atmospheric helium. Since the maximum ^3He anomaly shown in figure 3-19 is about 25%, the maximum ^4He anomaly would be expected to be only 3%. As we shall see in chapter 7, the deep sea ^3He anomalies have great importance for studies of the mixing processes occurring in the deep sea.

Subsequent to the work on ^3He anomalies in the deep sea by Craig and Clarke, a graduate student named Jenkins working in Clarke's laboratory found another type of ^3He anomaly in the sea (271,274). ^3He has, over the last few decades, been produced in the upper ocean at significant rates by the decay of the tritium produced during nuclear weapons tests. This ^3He is largely confined to the upper kilometer of the ocean because the tritium produced by nuclear testing has not penetrated in significant amounts to depths greater than this. The distribution of this "anthropogenic" ^3He allows important constraints to be placed on the manner in which the main thermocline of the ocean is ventilated. We will have more to say about this in chapter 8.

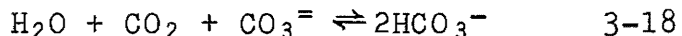
THE CARBON DIOXIDE CONTENT OF SURFACE OCEAN WATER

Prior to man's interference with the carbon cycle through deforestation and the burning of fossil fuels, the CO_2 content of the surface ocean and atmosphere was presumably at steady state (i.e., there was no net transfer of CO_2 gas between air and sea). We say "steady state" rather than "equilibrium" because sizable variations in the CO_2 partial pressure in surface ocean water exist from place to place and from season to season. By contrast the atmosphere has a more nearly uniform CO_2 content.

The variations of CO_2 partial pressure in the surface ocean stem from a complex interplay between the seasonal temperature cycles, mixing dynamics of the upper ocean, and the biological

cycles of the sea. CO_2 transfer between the air and sea tends to eliminate these differences, but, as the time constant for the achievement of equilibrium between air and surface sea is about 10 times longer for CO_2 than for O_2 (i.e., about 1 year rather than about 1 month), this process is not altogether effective. One might say that, although at any given locale the surface water tries to come to equilibrium with the air, it never quite catches up with the processes tending to disrupt this equilibrium.

In order to understand this chase, we must first learn what controls the CO_2 gas content of surface water. We have already seen that most of the carbon in sea water is in the form of HCO_3^- and $\text{CO}_3^{=}$ ions and that less than 1% is in the form of CO_2 gas. Throughout the ocean, the following chemical reaction is continually taking place:



One water molecule, one dissolved CO_2 gas molecule and one carbonate ion react to form two bicarbonate ions. This reaction proceeds rapidly in sea water and chemical equilibrium is maintained. Thus the concentrations of these ingredients obey the following rule:

$$K' = \frac{[\text{HCO}_3^-]^2}{[\text{H}_2\text{O}][\text{CO}_2][\text{CO}_3^=]} \quad 3-19$$

where K' is the equilibrium constant for the reaction.* Since the concentration of water itself does not change measurably as the result of its participation in the reaction,** the CO_2 content of any sea water sample is proportional to the square of the HCO_3^- ion concentration divided by the $\text{CO}_3^=$ ion concentration. We have already seen in chapter 2 that at any place in the ocean the HCO_3^- ion concentration and the $\text{CO}_3^=$ ion concentrations are fixed by the alkalinity, Alk, and the total dissolved carbon content ΣCO_2 of the water. Using the approximations adopted in chapter 2 we obtain:

$$[\text{CO}_2] = \frac{1}{K'} \frac{(2[\Sigma\text{CO}_2] - [\text{Alk}])^2}{[\text{Alk}] - [\Sigma\text{CO}_2]} \quad 3-20$$

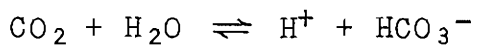
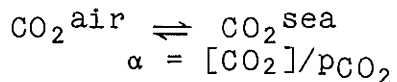
The pressure of CO_2 gas in air equilibrated with this water will be:

$$p_{\text{CO}_2} = \frac{[\text{CO}_2]}{\alpha} \quad 3-21$$

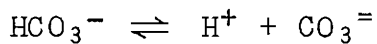
*As shown in table 3-7 and figure 3-20, this constant is related to the so called first and second dissociation constants for carbonic acid. These constants are functions of temperature, pressure and salinity. In table 3-7 $[\text{CO}_2]$ is given as the product of αp_{CO_2} .

**Sea water contains 54 moles/kg of H_2O molecules and only 2×10^{-3} moles/kg of the various carbon species.

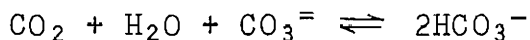
Table 3-7. Equilibrium constants for reactions involving the species CO_2 , HCO_3^- , $\text{CO}_3^=$ and H^+ . The reactions are as follows.^t



$$K_1' = \frac{a_{\text{H}^+} [\text{HCO}_3^-]}{[\text{CO}_2]}$$



$$K_2' = \frac{a_{\text{H}^+} [\text{CO}_3^=]}{[\text{HCO}_3^-]}$$



$$K' = \frac{\alpha K_1'}{K_2'} = \frac{[\text{HCO}_3^-]^2}{\text{pCO}_2 [\text{CO}_3^=]}$$

For sea water of salinity 35.0/oo at 1 atmosphere pressure the constants are as follows:

T °C	α^* moles/kg atm	$K_1'^{**}$	$K_2'^{**}$	$\alpha K_1'/K_2'$ moles/kg atm
0	6.29×10^{-2}	6.33×10^{-7}	3.53×10^{-10}	113
5	5.21×10^{-2}	7.17×10^{-7}	4.04×10^{-10}	92
10	4.39×10^{-2}	7.98×10^{-7}	4.72×10^{-10}	74
15	3.74×10^{-2}	8.73×10^{-7}	5.58×10^{-10}	59
20	3.24×10^{-2}	9.41×10^{-7}	6.59×10^{-10}	46
25	2.84×10^{-2}	10.00×10^{-7}	7.69×10^{-10}	37
30	2.52×10^{-2}	10.47×10^{-7}	8.77×10^{-10}	30

*Based on measurements by Ray Weiss of the Scripps Institution of Oceanography (403).

**Based on measurements by Merbach and his coworkers at Oregon State University (400).

^t a_{H^+} is the activity of hydrogen ion.

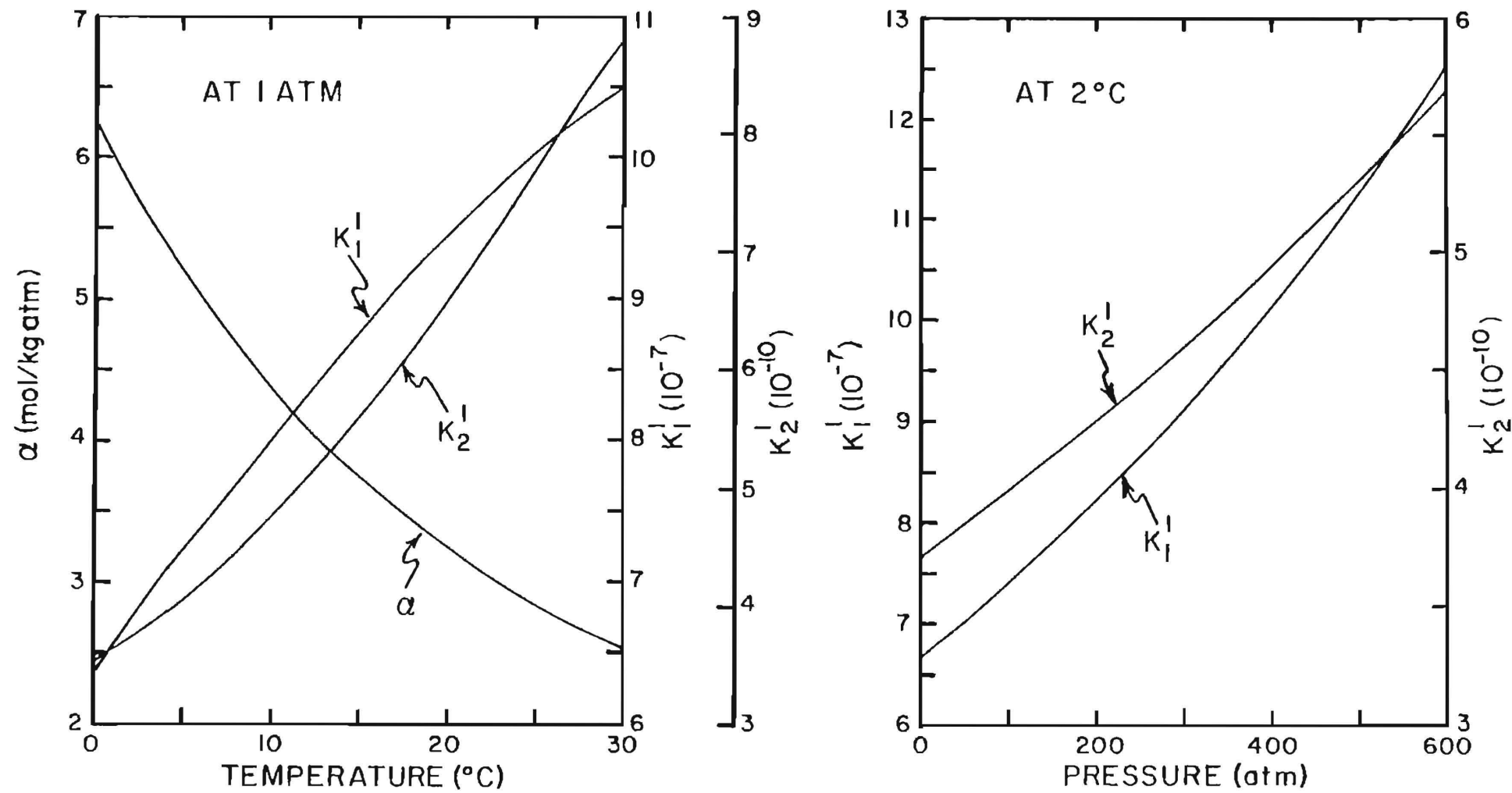


Figure 3-20. Equilibrium constants (at 35‰ salinity) for the carbonate system in sea water. The left hand panel shows the values of the constants for surface ocean water as a function of temperature. The right hand panel shows the pressure effect on the constants for cold sea water (i.e. at 2°C). The dissociation constants (K_1' and K_2') were determined by Merbach and his coworkers at Oregon State University (400). The solubility of CO₂ gas was determined by Weiss at Scripps Institution of Oceanography (403).

where α is the solubility of CO_2 in sea water at the temperature of interest (see table 3-7). Combining with the previous equation, we obtain:

$$p_{\text{CO}_2} = \frac{1}{\alpha K'} \left[\frac{(2[\Sigma\text{CO}_2] - [\text{Alk}])^2}{[\text{Alk}] - [\Sigma\text{CO}_2]} \right] \quad 3-22$$

Since both α and K' depend on temperature and salinity, so does the equilibrium CO_2 partial pressure.

The temperature dependence of the equilibrium constant product raises a problem. Were it true that all surface water had lost its phosphate and nitrate to plants and that this loss brought the alkalinity and total dissolved CO_2 content to uniform values, then the $[\text{HCO}_3^-]^2/[\text{CO}_3^-]$ ratio would be nearly constant throughout the surface ocean. However, even in this idealized ocean there would be a problem. Since $\alpha K'$ varies with temperature, the equilibrium CO_2 pressure for any given area of the ocean would depend on the temperature of the water. As the equilibrium CO_2 pressure rises 4 percent per degree-centigrade increase in temperature, the equilibrium CO_2 pressure for tropical water would be about 2.5 times as great for polar water! This would tend to create a poleward decrease in atmospheric CO_2 content. However, the atmosphere mixes so rapidly that no such gradient would be generated.

If, then, the CO_2 partial pressure for polar surface sea water is lower and the CO_2 partial pressure of tropical water is higher than the steady state CO_2 pressure for the well-mixed atmosphere, CO_2 must be flowing out of tropical surface water and into polar surface water. This flow would then disrupt the geographic uniformity of ΣCO_2 in our idealized surface ocean. We can thus consider two extreme cases, one where this transfer is ineffective and the CO_2 partial pressure in tropical surface waters is far higher than that in polar surface waters; and the other where the transfer goes to completion, alleviating the CO_2 partial pressure difference between these two regions of the ocean. For the latter case the ΣCO_2 concentration in surface would increase toward the poles in accord with the following equation (obtained by solving equation 3-22 for ΣCO_2):

$$[\Sigma\text{CO}_2] = \frac{1}{8} \left[4[A] - \alpha K' p_{\text{CO}_2} + \sqrt{(\alpha K' p_{\text{CO}_2})^2 - 4[A]^2 - 16[A](A - \alpha K' p_{\text{CO}_2})} \right] \quad 3-23$$

In this equation A denotes Alk. These two extreme scenarios are shown diagrammatically in figure 3-21.

Where in the range between these extremes would we expect the situation in the real ocean to lie? To venture this judgment we must know the response time for the adjustment of the ΣCO_2 content and CO_2 partial pressure in the surface ocean. We learned earlier in this chapter that the time required for an ordinary gas to achieve equilibrium between the atmosphere and the surface ocean mixed layer is a few weeks. If this time were also to apply to CO_2 , then gas exchange would be able to keep pace with the

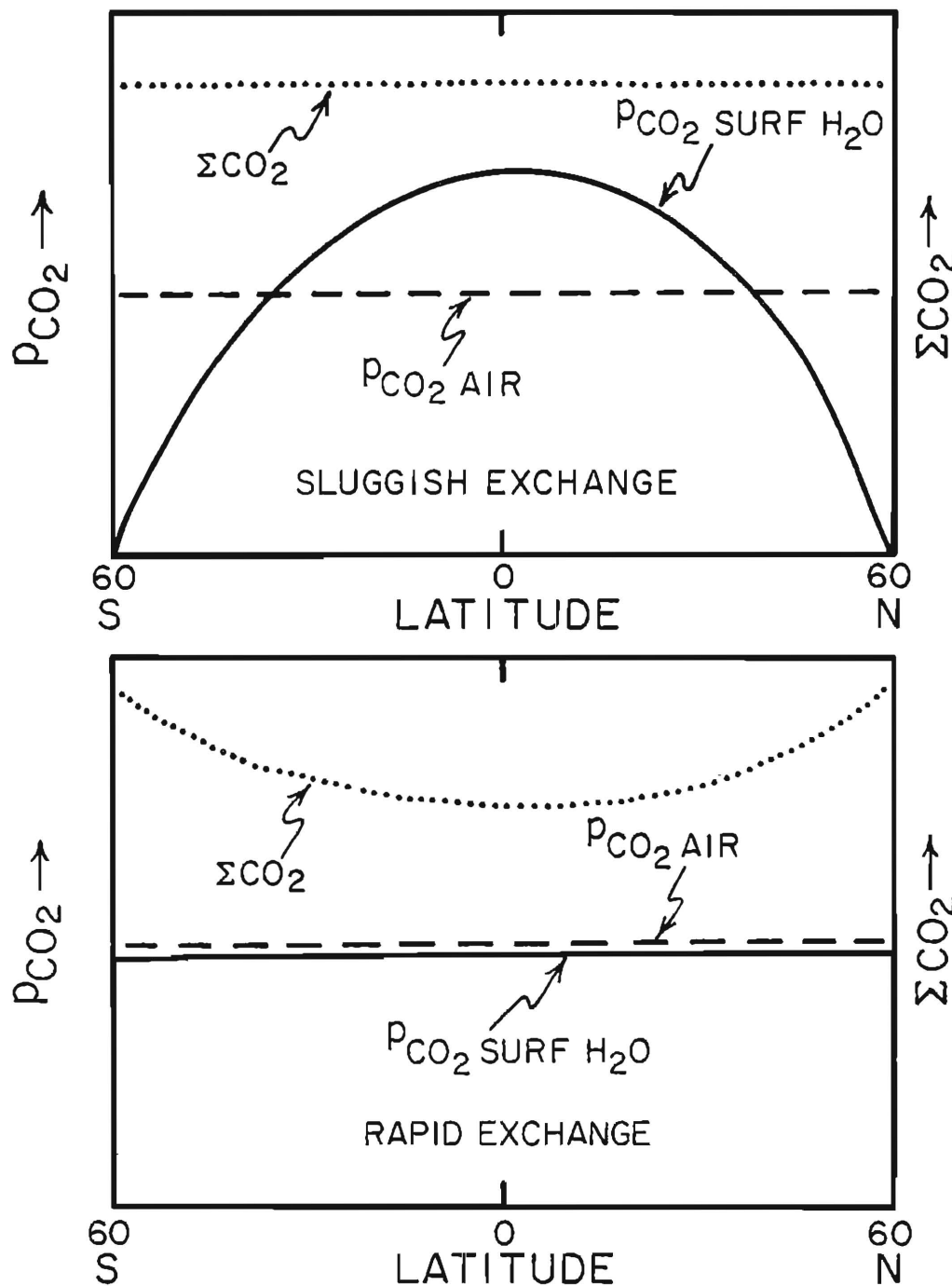
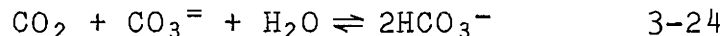


Figure 3-21. Extreme scenarios for the latitudinal variation of $p\text{CO}_2$ and ΣCO_2 in the surface ocean (assuming constant alkalinity).

processes tending to drive the CO_2 pressure in a given region of the surface ocean away from the atmospheric value. We should have a surface ocean which had a nearly uniform CO_2 partial pressure and a ΣCO_2 concentration increasing from equator to poles. The equilibration time for CO_2 is not the same as that for other gases. The reason is that in order to change the partial pressure of CO_2 in surface water, not only the CO_2 content of the water must change, but also the HCO_3^- and $\text{CO}_3^{=}$ ion contents. Since the ΣCO_2 content of surface sea water is about 150 times the CO_2 gas content, one might be tempted, then, to say that it would require 150 times longer to adjust the CO_2 partial pressure in surface water than, let's say, the O_2 partial pressure. This would also be wrong. Actually, it takes about 10 times longer to adjust the CO_2 partial pressure than that of ordinary gases.

To understand why this is the case is not easy. In fact, it involves one of the more complex aspects of marine chemistry. We will delay our consideration of the precise explanation until chapter 10 where we deal with the uptake of fossil fuel CO_2 by the ocean. At this point it will suffice to say that it is not the CO_2 or ΣCO_2 contents of sea water that set the equilibration time but rather the $\text{CO}_3^=$ ion content of the sea water. As the concentration of carbonate ion in surface water averages about one tenth the ΣCO_2 content, the multiplier is closer to 15 than to 150!

It is the $\text{CO}_3^=$ ion content which is important because the main reason CO_2 enters and leaves sea water with, lets say, changing temperature is through the reaction:



This reaction between CO_2 and $\text{CO}_3^=$ leads to much larger changes in ΣCO_2 content than does the change with temperature of the solubility of CO_2 gas.

In any case, the response time of the pCO_2 and ΣCO_2 in surface ocean water averages about one year. An example of the response of the pCO_2 and ΣCO_2 content of surface water to a sudden temperature change is shown in figure 3-22. Clearly, this time is too long to allow the ocean to keep exact pace with seasonal changes. Further, as surface waters in regions of rapid upwelling and in regions of deep water formation are not in contact with the atmosphere for a time as long as one year, these waters would not be expected to achieve equilibrium with the atmosphere.

In figure 3-23 are shown the temperature, salinity, ΣCO_2 and alkalinity along a north-south traverse in the western Pacific. As can be seen, the ΣCO_2 content of the surface waters does increase from temperate to polar regions. However, contrary to the assumptions regarding our idealized surface ocean, the alkalinity of the water increases as well. Thus it is not immediately clear how much of this increase is due to temperature and how much is associated with the higher alkalinity of polar waters (as for nitrate and silicate, the alkalinity of Antarctic surface waters is more akin to the alkalinity of deep water than to that of warm surface water). Also seen in figure 3-23 is a curious peak in ΣCO_2 content at the equator. In this case there is no matching alkalinity anomaly.

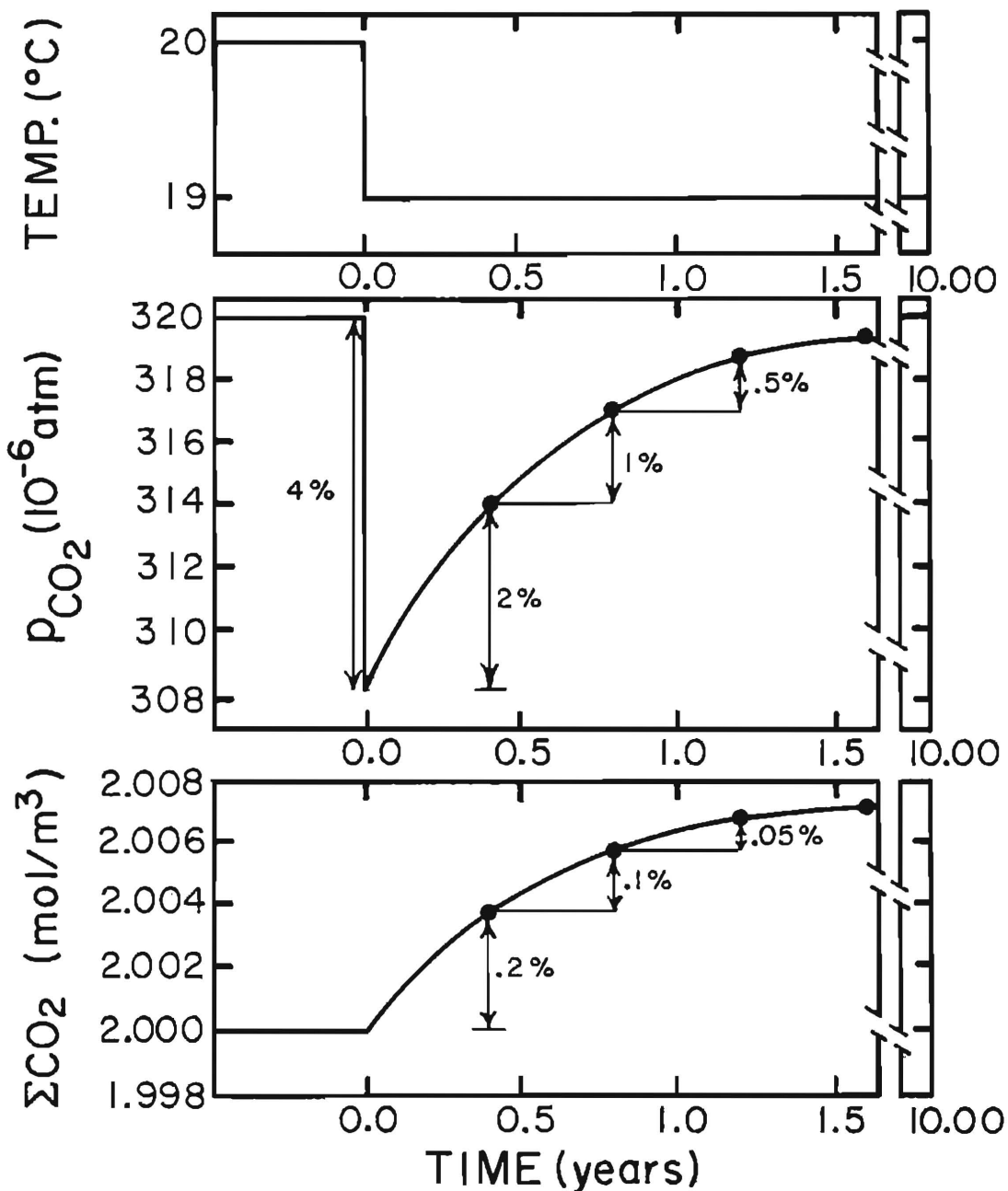


Figure 3-22. Response of a 50 meter deep thick surface mixed layer initially at equilibrium with the air to a sudden cooling from 20°C to 19°C . Its PCO_2 drops by 4 percent (12×10^{-6} atm). The invasion of atmospheric CO_2 then causes the ΣCO_2 content to rise and the PCO_2 to move back toward the atmospheric value (320×10^{-6} atm). The half-time for the reestablishment of air-water equilibrium is about 0.4 years.

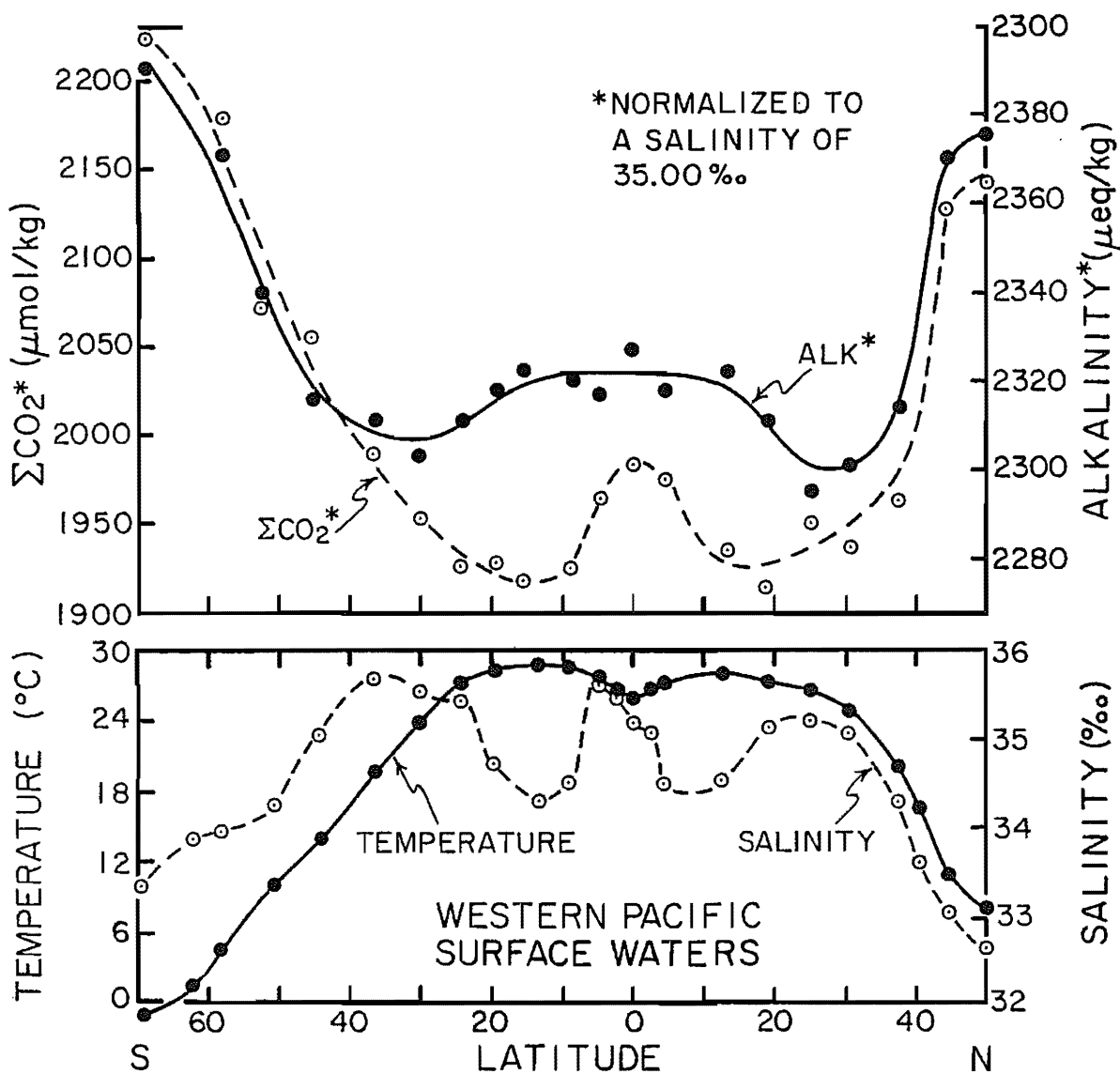


Figure 3-23. Plots of alkalinity (normalized to a salinity of 35‰), ΣCO_2 (normalized to a salinity of 35‰), temperature and salinity for surface waters in the western Pacific Ocean as a function of latitude. Strong equatorial anomalies are seen in ΣCO_2 , temperature and salinity but not in alkalinity. Based on results obtained during the GEOSECS program (406).

In figure 3-24 are shown the CO_2 partial pressures measured along the same traverse. As can be seen, there is remarkably little variation from the temperate to the polar regions. Apparently these waters have remained in their respective zones long enough to achieve more or less the ambient CO_2 partial pressure of the atmosphere. We say more or less because, even after steady state has been achieved, seasonal temperature changes will drive the CO_2 partial pressure back and forth across the atmospheric value. The startling feature of this diagram is the strong peak in CO_2 partial pressure at the equator. It nicely matches the peaks in ΣCO_2 , temperature and salinity seen in figure 3-23. Here is an example of surface waters which have not had the time to achieve equilibrium with the atmosphere. As we shall see, this feature is a product of the strong upwelling along the equator in the Pacific Ocean.

Also shown in figure 3-24 are the $\text{CO}_3^{=}$ ion content of surface water and the values of a parameter termed the Revelle factor.* As can be seen, one has roughly the inverse shape of the other. The Revelle factor is the number by which the ratio of the mixed layer thickness to the piston velocity for CO_2 gas must be multiplied in order to get the actual ΣCO_2 equilibration time. This number ranges from 14 for the coldest waters to 8 for the warmest waters in the surface ocean. Its ocean-wide average of 10 is the factor we referred to above as the difference between the equilibration times for CO_2 and other gases.

ORIGIN OF THE EQUATORIAL PACIFIC CO_2 ANOMALY

The surface waters of the equatorial Pacific profile provide an excellent example of the interaction between ocean dynamics, meteorology, the activity of organisms and gas exchange. As seen in figure 3-23 surface water in the equatorial Pacific also has a lower temperature and higher salinity than the adjacent waters as well as anomalies in CO_2 pressure and the ΣCO_2 concentration. Further, as shown in figure 2-2, sediments of very high opal content are found immediately beneath this belt. All of these features can be explained by upwelling.

The oblique convergence of the trade winds onto the equatorial zone leads physical oceanographers to predict a divergence of the surface waters along the equator. Filling the "gap" left by this divergence are waters rising from beneath the surface. These waters are colder than the air over the equatorial zone (leading to the low temperature anomaly); they carry higher nutrient constituents leading to high plant productivity (especially for diatoms) and high opal accumulation rates, and they carry water high in ΣCO_2 content leading to the anomalies in ΣCO_2 and in pCO_2 .

While the depth from which the upwelling waters are drawn is not known, waters from any depth below about one hundred meters

*Named after Roger Revelle, who while serving as the Director of the Scripps Institution of Oceanography, pointed out the importance of this parameter in the calculation of fossil fuel CO_2 uptake by the ocean.

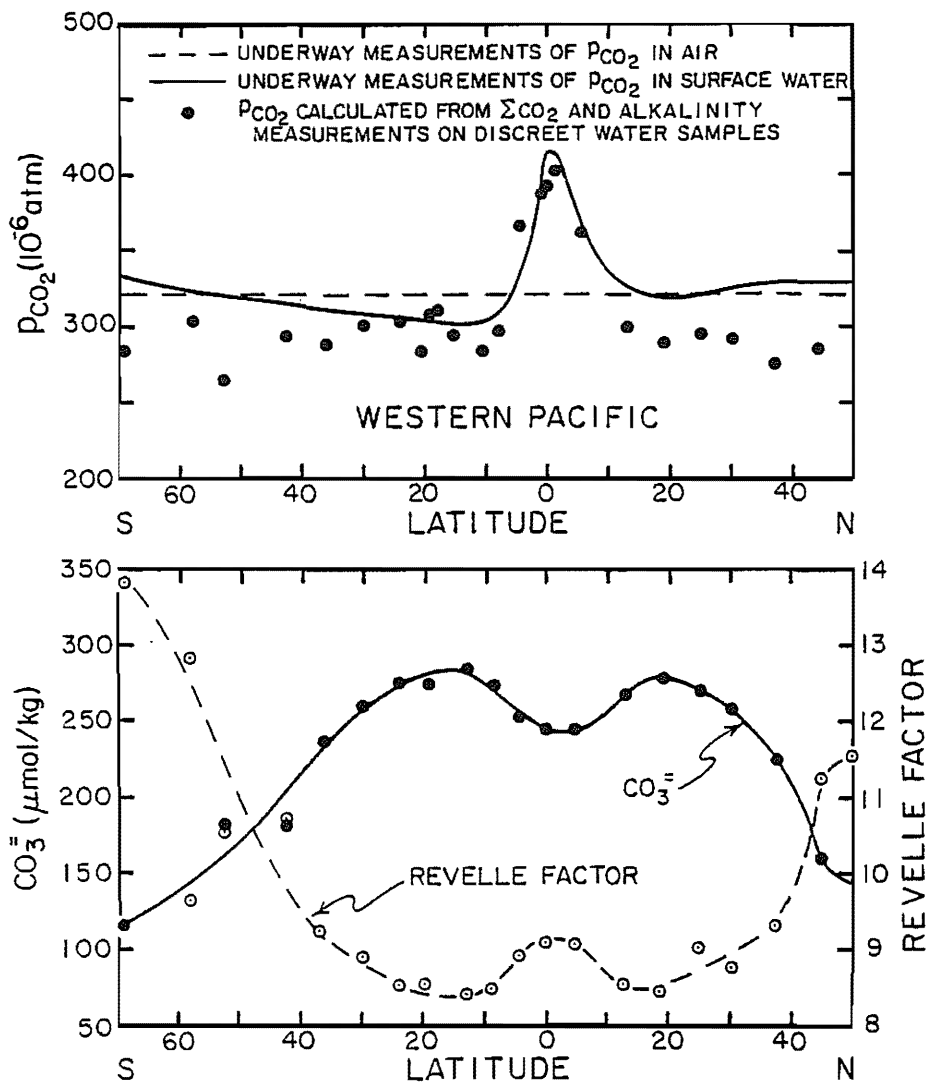


Figure 3-24. Plots of the CO_2 partial pressure, of the $\text{CO}_3^=$ ion concentration and of the Revelle factor in surface waters from the western Pacific as a function of latitude. Two measures of the surface water PCO_2 are given. The solid dots are PCO_2 values calculated from titration measurements of ΣCO_2 and alkalinity. The solid line gives the smoothed trend based on continuous measurements of the CO_2 pressure in air equilibrated on shipboard with surface sea water. The latter are more precise and accurate than the former. The Revelle factor is an exact measure of the ratio of time required for the CO_2 pressure in surface water to equilibrate with the overlying air to the time required in sea water containing no bicarbonate or carbonate ion. The Revelle factor shows an inverse correlation to the carbonate ion concentration. The Revelle factor is half again as large in the very cold Antarctic surface waters as it is in low latitude surface waters. Based on results obtained as part of the GEOSECS program (406).

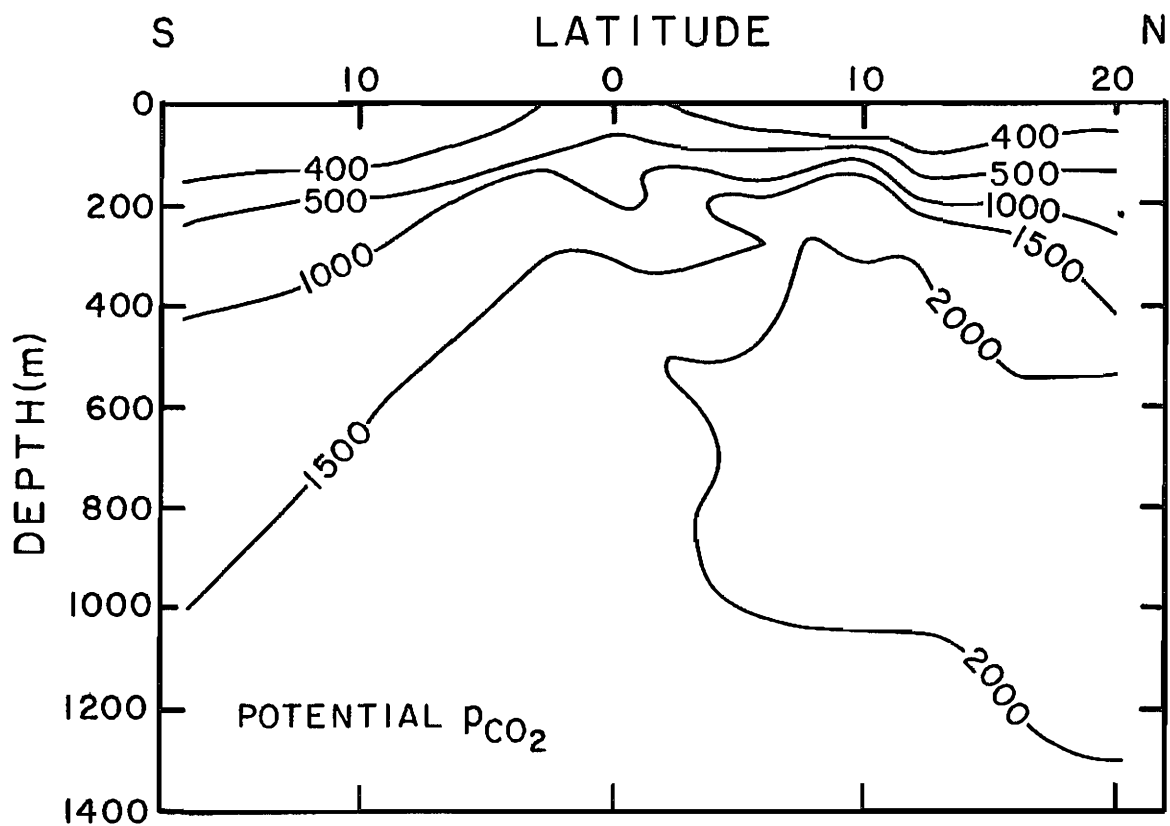


Figure 3-25. Potential CO_2 pressure as a function of depth in the equatorial Pacific. Potential CO_2 pressure is the CO_2 pressure a sample would achieve if it were isochemically depressurized (to 1 atm) and warmed (to 25°C). Based on results obtained by Dave Bos of the Scripps Institution of Oceanography as part of the Hawaii-Tahiti Shuttle Experiment (433).

could do the job. As shown in figure 3-25, all these waters have potential CO_2 partial pressures* well above those seen in the surface waters of the equatorial zone. These very high pressures are not seen at the surface because after their arrival in the mixed layer plants remove carbon to form their soft tissues and CO_2 is lost to the air. Both processes lead to a reduction in ΣCO_2 and in pCO_2 of the water. Thus part but not all of the pCO_2 and ΣCO_2 anomalies are eliminated during the residence of this water at the surface. As shown in figure 3-23, there is no equatorial anomaly in alkalinity. The plants growing in equatorial waters are mainly diatoms and the herbivores grazing on these plants do not live in calcite houses.

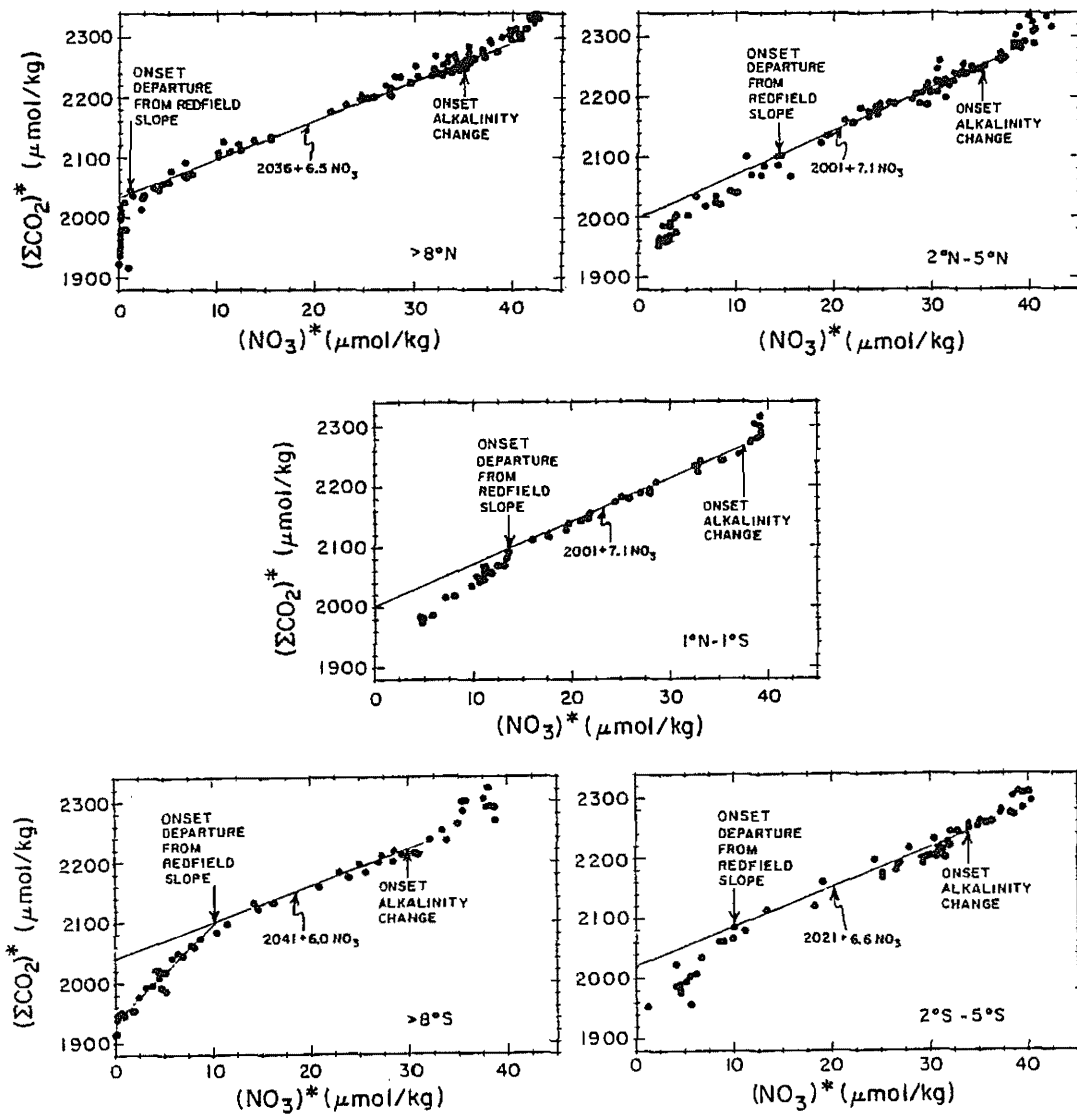
It is possible to separate the role of plant growth and of CO_2 evasion in reducing the excess carbon content of the upwelling water through plots of ΣCO_2 concentration (normalized to a salinity of 35.00‰) against nitrate concentration for samples taken at various water depths and locations in the equatorial zone. As can be seen in figure 3-26, the points for samples taken in the upper thermocline follow a trend consistent with the biochemical ratio of carbon to nitrate in marine organisms. Points for surface and near surface waters, however, deviate from this trend. They have lower ΣCO_2 contents than would be expected for their nitrate contents. This missing ΣCO_2 has presumably been lost as CO_2 gas to the overlying air.

We will pick up this thread again when we consider the problem of harnessing the information carried by ocean tracers to yield rates of thermocline ventilation (chapter 8). For now we will only point out that the upwelling process must be sufficiently rapid that the waters of the surface equatorial ocean are replaced on a time scale short enough to prevent either plants or gas evasion from completing the job of bringing the CO_2 pressure back to the atmospheric value. While we do not have a good handle on how long the plants living in equatorial surface water take to complete their task, we do know how long it would take for gas evasion to eliminate the CO_2 over pressure. This could be accomplished in about one year. Thus the upwelling process must operate at the rate of several tens of meters per year in order to maintain a CO_2 anomaly in the equatorial mixed layer!

SUMMARY

We have seen that the gases dissolved in the sea add an important dimension to marine chemistry. From measurements carried out in the laboratory their solubilities in the sea water are known and from measurements of radioactive gases in the air and sea their rate of transfer across the air-sea interface is also known. The latter is sufficiently rapid that the concentration of all gases (except CO_2) in waters descending to the deep sea can be assumed to be quite close to equilibrium with the atmosphere. The fact that this is the case allows us to put to effective use

*The CO_2 partial pressure that would be achieved if the water were brought to the surface and isochemically warmed to the ambient equatorial ocean temperature.



* NORMALIZED TO A CONSTANT SALINITY

Figure 3-26. Plots of ΣCO_2 (normalized to a constant salinity) against nitrate for samples of the surface and thermocline water in five latitude belts in the equatorial Pacific (at longitude 155°W). In each case a straight line is fit to the points with intermediate phosphate content. As in each case this line has a slope close to the Redfield ratio (~ 6.8), it is assumed that these samples have mainly been influenced by the photosynthesis-respiration cycle. For shallower waters (i.e., those with less PO_4) a deviation toward lower ΣCO_2 contents is seen. This deviation is presumably due to CO_2 loss to the atmosphere. For deeper waters (i.e., those with high phosphate content) a deviation is also seen. This deviation can be shown to be the result of calcite dissolution as its onset corresponds to the depth where the alkalinity begins to rise. Based on results obtained by Dave Bos of the Scripps Institution of Oceanography as part of the Hawaii-Tahiti Shuttle Experiment (433). The track followed during this expedition is shown on the foldout map.

the distributions of O₂, N₂O, and ³He within the sea. In later chapters we will show that the distributions of two tracer gases not yet discussed in this chapter (³⁹Ar and ⁸⁵Kr) will eventually allow a great improvement in our knowledge of the modes and rates of ventilation of the thermocline and deep sea. Finally, the sea's most interesting constituent, carbon, is partly in gaseous form. Our knowledge of the gas exchange process will help us to sort out its movements through the ocean-atmosphere system. It will also allow us to make more effective use of the distribution of the most important tracer in the sea - namely, radiocarbon.

PROBLEMS

- 3-1 A rapidly stirred tank of gas-free water at 2°C is exposed to the air. Its depth is 3 meters. After an hour, the O₂ concentration is found to be 10 percent that expected for equilibrium with the atmosphere. What is the stagnant boundary layer thickness for the water in this tank?
- 3-2 A sea water sample is quickly heated from 15°C to 25°C. If it initially had a PCO₂ equal to that in the atmosphere (3.2x10⁻⁴ atm), what would the partial pressure of CO₂ gas be once it was heated? The alkalinity of the water is 2.2 x 10⁻³ eq/kg. (Assume that no biological activity or gas exchange occurs during the heating.)
- 3-3 Mono Lake in California has a very high ECO₂ concentration (0.2 moles/liter). The lake has a mean depth of 30 meters. Its surface temperature averages 18°C. The ¹⁴C/C ratio in its dissolved carbon is uniform with depth and is 30 percent lower than that expected for equilibrium with the overlying air. If the ¹⁴C deficiency is at steady state, what must the stagnant film thickness for this lake be? The input of new carbon from the rivers supplying the lake is too small to be significant. (Hint: As in the ocean, the loss of ¹⁴C by radiodecay within the lake must be balanced by the net influx of ¹⁴C from the air.)
- 3-4 A tank held at 24°C has a mean depth of 3 meters and a stagnant film thickness of 40 microns (as measured via argon evasion experiments). If this tank of water is charged with 0.5 atm of He and 0.5 atm of Ar and then allowed to stand open in contact with the air, what percent of the Ar will have been lost when 95 percent of the He has been lost? What is the ratio of the "piston velocities" for the two gases? How would the results differ if the film replacement model rather than the stagnant film model were used? For the film replacement model the flux is given by the following equation:

$$F = \sqrt{\frac{D}{\tau}} (C_{\text{sat}} - C_{\text{water}})$$

where τ is the residence time of the film at the surface (i.e., τ replaces z as the parameter characterizing the exchange rate). The dependence on molecular diffusivity changes from the first power to the one half power.

- 3-5 Equal portions of two water samples (one at 5°C and one at 25°C), at equilibrium with the atmosphere are mixed in such a way that no gas is lost or gained. The concentration of each atmospheric gas in this mixture is then compared with that in a water sample at 15°C which has been brought to equilibrium with the air. Differences are found. Why? Would the anomaly be larger for helium or for xenon? Why?
- 3-6 Air bubbles are injected into the base of a 2 meter high column. The bubbles enter a trap and eventually dissolve into the water. The injection continues at a constant rate until steady state is achieved (i.e. the excess gas supplied from the bubbles leaves by ordinary gas evasion as fast as it is being added with the bubbles.). At this point ${}^4\text{He}$ is found to be 20% supersaturated. By how much would O_2 be supersaturated if the stagnant model applied? If the film replacement model applied. The temperature is 24°C.

SUPERPROBLEM #3

A geochemist, Carlos Chilling, sets out to experimentally check the difference in the equilibration times for ${}^{14}\text{CO}_2$, CO_2 and O_2 . To do so he builds a large column which has a cross-sectional area of one square meter and a height of 11 meters. He places one cubic meter of sea water in the bottom of the column. He then installs a fan in the air space above the water designed to agitate the air-water interface and to keep the air mixed. He also installs a stirring device to keep the water mixed. He insulates the column and installs a temperature control system which maintains the temperature at 24°C. Chilling injects a touch of mercuric chloride into the sea water to stop biologic activity. After three weeks he measures the ΣCO_2 in the water, and the PCO_2 of the water and air. He gets the following results:

$$[\Sigma\text{CO}_2] = 2,000 \times 10^{-3} \text{ moles/liter}$$

$$\text{PCO}_2^{\text{air}} = 330 \times 10^{-6} \text{ atm}$$

$$\text{PCO}_2^{\text{water}} = 330 \times 10^{-6} \text{ atm}$$

He also measures the ${}^{222}\text{Rn}$ activity of the air and the water and the ${}^{226}\text{Ra}$ activity in the water. The results are as follows:

$$A_{222\text{Rnair}} = 0.50 \text{ dpm/100 liter}$$

$$A_{222\text{Rnwater}} = 0.50 \text{ dpm/100 liter}$$

$$A_{226\text{Ra}_{\text{water}}} = 5.50 \text{ dpm/100 liter}$$

From this data he calculates the apparent stagnant film thickness. What does he get?

Now Chilling is ready for the main experiment. He replaces the air with pure nitrogen. He replaces the nitrogen in the sea water with pure oxygen. He then injects some ^{14}C tagged CO_2 gas into the sea water (mostly $^{12}\text{CO}_2$ with enough $^{14}\text{CO}_2$ atoms present to swamp out any initially present in the tank). During these operations Chilling seals off the air space so that no exchange can occur. When he has finished these injections he measures the partial pressures of O_2 and of CO_2 in the air and water. He finds the following:

$$\begin{aligned} p_{\text{O}_2}^{\text{water}} &= 1.0 \text{ atm} & p_{\text{O}_2}^{\text{air}} &= 0.0 \text{ atm} \\ p_{\text{CO}_2}^{\text{water}} &= 350 \times 10^{-6} \text{ atm} & p_{\text{CO}_2}^{\text{air}} &= 330 \times 10^{-6} \text{ atm} \end{aligned}$$

Chilling pulls the baffle separating the air and water and turns on the fan and stirrer. He then monitors the $^{14}\text{C}/\text{C}$ ratio in the air and in the sea water at frequent time intervals. He also measures the partial pressure of CO_2 in the air and in the water at the same intervals. Finally, he measures the O_2 content of the air and of the water at the same intervals. Eventually he finds that these parameters cease to change. At this point what should be the p_{CO_2} and p_{O_2} in the air and what should be the ratio of $^{14}\text{C}/\text{C}$ in the water to that just after spiking?

Now Chilling plots the p_{CO_2} in the air, the p_{O_2} in the air and the $^{14}\text{C}/\text{C}$ in the air against time. For each he finds a response such that the difference between the initial and steady state value is reduced exponentially with time (asymptotically approaching steady state). For each property he determines a half response time. What values should he find?

In the calculations use following relationship:

$$\frac{\Delta p_{\text{CO}_2}/p_{\text{CO}_2}}{\Delta \Sigma \text{CO}_2/\Sigma \text{CO}_2} = 9.0$$

The solubilities of oxygen and radon are given in tables 3-1 and 3-2. The diffusivities of ^{222}Rn , O_2 and CO_2 are given in table 3-3. Assume that the diffusivities of $^{14}\text{CO}_2$ and $^{12}\text{CO}_2$ are identical.

LAST MINUTE ADDITION (SEPTEMBER 1982)

James Ledwell of Harvard showed, as part of his Ph.D. work, that the gas exchange rates of He , CH_4 and N_2O in a wind tunnel follow the square root of diffusivity dependence as predicted by the film replacement model (721).

Chapter 4

REACTIVE METALS AND THE GREAT PARTICULATE SWEEP THE CYCLE OF METALS IN THE SEA

INTRODUCTION

In our discussion of chemical cycles within the sea we rather quickly passed by those elements which the chemist classifies as reactive metals. Some of these elements fit into the non-cycling category of chapter 1. They become firmly attached to particles and are removed to the sediment during their first pass through the sea. Others fall into the biolimiting and biointermediate categories. Our focus in this chapter will be on the marine chemistry of these constituents of sea salt.

The geochemistry of metals in the sea has only recently begun to be unraveled. The reason is that these elements are present in such low concentrations that, prior to this, little success was achieved in their measurement. Only after 1975 did reliable results begin to appear in the literature. These new results reflect a combination of care to avoid contamination during collection, storage and measurement and the use of highly sensitive analytical methods.

While prior to 1975 the sea water concentrations of these metals were not known, the concentrations in marine sediments were. These measurements showed that the red clays of the deep ocean differed from the detrital material accumulating on continental margins and in embayments of the sea. Red clays have higher concentrations of Fe, Mn, Ni, Co and Cu than do shales (indeed their red color is related to the presence of iron oxide). These same elements make up manganese nodules. Marine scientists have long puzzled over the chemical pathways leading to the enrichment of these particular elements in deep sea deposits.

To put these excesses in context, we will have to review a bit of the budget of elements in the earth's crust. Of the igneous rocks found at the surface of the earth, the granitic and basaltic varieties are the most abundant. It is reasonable to assume that they are the dominant sources for sediments. The most abundant sediment is shale; it constitutes about 80 percent of the total. A comparison of the composition of shale with that of average basalt and of average granite is shown in table 4-1. As can be seen, a mix of 50 percent granite and 50 percent basalt yields the concentrations of most elements found in shale. The elements Na, Mg and Ca are exceptions but can be readily explained. Calcium and magnesium are deficient in shale because they reside in limestone (calcium carbonate) and dolomite

Table 4-1. Comparison of the chemical composition of average igneous rock (equal parts granite and basalt) with the chemical compositions of shale and red clay. (Concentrations are in parts per million by weight.) Note the large excesses of Mn, Ni, Co, Cu and Fe in red clays.

Element	Basalt	Granite	Average Igneous Rock	Shale	Red Clay
Na	26,000	18,000	22,000	10,000	15,000
K	8,000	42,000	25,000	27,000	25,000
Rb	30	170	100	140	110
Cs	1	4	3	5	6
Mg	46,000	1,600	24,000	15,000	21,000
Ca	76,000	5,000	40,000	22,000	29,000
Sr	470	100	290	300	180
Ba	330	840	590	580	2,300
Fe	86,000	14,000	50,000	47,000	65,000
Mn	1,500	400	950	850	6,700
Ni	130	5	70	70	225
Co	50	1	25	19	74
Cu	90	10	50	45	250
Cr	170	4	90	90	90
Th	4	18	11	12	12

(calcium-magnesium carbonate) as well as in shale. If we were to add all Mg and Ca contained by dolomite and limestone to the shales, their magnesium and calcium contents would become nearly equal to the value expected from a 50-50 granite and basalt mixture. Sodium is in short supply because much of the sodium released during weathering remains dissolved in the sea. If we were to take all the sodium out of sea water and incorporate it into shale, its sodium content would be brought close to the expected value.

When we compare the composition of deep sea red clays with that of shale, the agreement is good except for barium and the elements enriched in manganese nodules (i.e., Fe, Mn, Ni, Co and Cu). It should be emphasized that this enrichment in deep sea clays relative to shale does not apply to all trace metals. Chromium and thorium are examples of metals that do not show an anomaly.

The Mn content of a mixture of equal amounts of granite and basalt would be about 950 parts per million (ppm). This is also the average value found for shales. By contrast the Mn content of deep sea sediments averages about 6700 ppm (a factor of 7 higher than expected). Ni is, on the average, a factor of 3 higher in concentration in deep sea sediment than in shale; Co is a factor of 4 higher; Cu is a factor of 5 higher. Iron shows about 40 percent enrichment in deep sea sediments over what would be expected from the granite-basalt average or from shale. Thus the same processes that caused the enrichment of Mn and Fe in nodules and in deep sea sediments appear to be at work for other metals. Our task in this chapter is to learn more about how these and other metals move through the sea.

Our information regarding the pathways followed by metals comes from three major sources. The first of these is the distribution of radioisotopes produced by radiodecay within the sea. These isotopes are all members of the decay chains of the long-lived isotopes ^{238}U , ^{235}U and ^{232}Th (see figure 4-1). The isotopes of interest are, of course, those of elements which are adsorption-prone (i.e., thorium, protactinium, lead and polonium). The second source of information is the distribution of adsorption-prone radionuclides added to the sea surface from the atmosphere. Plutonium produced during nuclear testing is one example; the lead produced by the decay of the radon released to the atmosphere from continental soils is another. The final source of information is the distribution within the sea of the metallic elements themselves.

PRODUCTS OF URANIUM AND THORIUM DECAY

The marine geochemistry of daughter products of the uranium and thorium series appears at first glance to be quite complex. As shown in table 4-2, the activities of successive daughter products of a given decay series are far from equal (as radioactive equilibrium would dictate). Rather large jumps in activity between subsequent products are seen. As shown in table 4-2, this pattern differs in detail from water type to water type! The source of these differences is as follows. The isotopes of ab-

Element	U-238 Series					Th-232 Series					U-235 Series				
Neptunium															
Uranium	U-238 4.47×10^9 yrs		U-234 2.48×10^5 yrs								U-235 7.04×10^8 yrs				
Protactinium		Pa-234 1.18 min										Pa-231 3.25×10^4 yrs			
Thorium	Th-234 24.1 days		Th-230 7.52×10^4 yrs				Th-232 1.40×10^{10} yrs		Th-228 1.91 yrs		Th-231 25.5 hrs		Th-227 16.7 days		
Actinium								Ac-228 6.13 hrs				Ac-227 21.8 yrs			
Radium			Ra-226 1.62×10^3 yrs				Ra-228 5.75 yrs		Ra-224 3.66 days				Ra-223 11.4 days		
Francium															
Radon			Rn-222 3.82 days					Rn-220 55.6 sec				Rn-219 3.96 sec			
Astatine															
Polonium		Po-218 3.05 min		Po-214 1.64×10^{-4} sec		Po-210 138 days		Po-216 0.15 sec	64 %	Po-212 3.0×10^{-7} sec		Po-215 1.78×10^{-3} sec			
Bismuth			Bi-214 19.7 min		Bi-210 5.01 days			Bi-212 60.6 min					Bi-211 2.15 min		
Lead		Pb-214 26.8 min		Pb-210 22.3 yrs		Pb-206 stable lead (isotope)		Pb-212 10.6 hrs	36%	Pb-208 stable lead (isotope)		Pb-211 36.1 min		Pb-207 stable lead (isotope)	
Thallium									Tl-208 3.05 min				Tl-207 4.77 min.		

Figure 4-1. Chart showing the decay chain of the uranium and thorium series isotopes and the half-lives of each isotope. Alpha decays are shown by the vertical arrows and beta decays by the diagonal arrows.

Table 4-2. Summary of the approximate activities of the parent and daughter isotopes for the three-decay series in various major water types of the ocean.

Isotope	Daughter Product Half-life yr	Warm Surface Water dpm/100kg	N. Atl. Bottom Water dpm/100kg	Antarctic Bottom Water dpm/100kg	N. Pac. Bottom Water dpm/100kg
^{238}U	Parent	240	240	240	240
^{234}Th	0.066	230	240	240	240
^{234}U	248,000	280	280	280	280
^{230}Th	75,200	<0.02	-	-	0.15
^{226}Ra	1620	7	13	20	34
^{222}Rn	0.010	5	>13	>20	>34
^{210}Pb	22.3	20	8	10	16
^{210}Po	0.38	10	8	10	16
^{235}U	Parent	13	13	13	13
^{231}Pa	32,500	-	-	-	0.05
^{232}Th	Parent	<0.1	<0.1	<0.1	<0.1
^{228}Ra	5.8	3	0.4	-	0.4
^{228}Th	1.9	0.4	0.3	-	0.3

Table 4-3. Soluble parent-reactive daughter pairs.

PARENT			DAUGHTER		
Isotope	Half-life yr	Decay Constant yr^{-1}	Isotope	Half-life yr	Decay Constant yr^{-1}
^{238}U	4.47×10^9	1.55×10^{-10}	^{234}Th	0.066	10.5
^{228}Ra	5.75	0.120	^{228}Th	1.91	0.363
^{234}U	2.48×10^5	2.79×10^{-6}	^{230}Th	7.52×10^4	9.22×10^{-6}
^{235}U	7.04×10^8	9.84×10^{-10}	^{231}Pa	3.25×10^4	2.13×10^{-5}
^{226}Ra	1.62×10^3	4.28×10^{-4}	^{210}Pb	22.3	3.10×10^{-2}
^{210}Pb	22.3	3.10×10^{-2}	^{210}Po	0.38	1.82

sorption-prone elements generated within the sea are rapidly removed to the sediments. Isotopes of more soluble elements are produced in turn within the sediments and leak back into the sea.

The great value of the absorption-prone daughter products to marine chemistry lies in the fact that their main input to the sea is via the in situ decay of their immediate radioactive parents. This production rate can be precisely determined by measuring the concentration of the parent in the water mass of interest. By comparing the in situ concentration of the daughter isotope with that of its parent, we not only can show whether the daughter is being removed onto particulate matter, but also at what rate this removal occurs. The parent-daughter pairs of particular interest are listed in table 4-3.

The principle behind the use of these pairs is quite simple. If significant removal of the daughter product occurs during its lifetime, then the radioactive decay rate of the daughter will be less than that of the parent. The extent of this deficiency is a measure of the removal rate.

A very simple model of this process can be constructed if it is assumed that in situ production by the decay of the parent is the only source for the daughter in the water mass of interest. In this case a "scavenging" probability equivalent to the radio-decay probability can be used to describe the removal process. A balance between production by the radiodecay of the parent, scavenging of the daughter product by particles and radiodecay of the daughter product can be written as follows:

$$\lambda_p[P] = \lambda_D[D] + f[D] \quad 4-1$$

where λ_p and λ_D are the decay constants for parent and daughter, f is the "scavenging" constant*, and $[P]$ and $[D]$ are the concentrations in dissolved form of parent and daughter. This equation can be rewritten as follows:

$$\frac{A_D}{A_P} = \frac{\lambda_D[D]}{\lambda_P[P]} = \frac{\lambda_D}{\lambda_D + f} \quad 4-2$$

where A_p and A_D are the radioactivities of parent and daughter. As would be expected if the scavenging constant is zero, the radioactivities of parent and daughter will be identical. On the other hand, if the scavenging probability is much greater than the decay probability, then the radioactivity of the daughter isotope will be much smaller than that of the parent.

Equation 4-2 can be rewritten as follows:

$$f = \frac{1 - A_D/A_p}{A_D/A_p} \lambda_D \quad 4-3$$

*Note that like the constants for radiodecay, the scavenging constants have the units of inverse time. It represents the fraction of the material scavenged from the water in a given unit of time.

or

$$\tau_{1/2} = \frac{A_D/A_p}{1-A_D/A_p} t_{1/2}$$

4-4

where $\tau_{1/2}$ and $t_{1/2}$ are, respectively, the half-lives for scavenging and for radioactive decay. As can be seen from this equation, if the activity of the daughter is one-half that of the parent, then the half-time for scavenging must be equal to the half-time for radiodecay. Of course f (and $\tau_{1/2}$) will vary from element to element.

The big picture of the results obtained from measurements of the daughter-to-parent activity ratio for major oceanic water types is shown in table 4-4. The main thing to be seen is that everywhere in the sea there are processes at work which are capable of removing reactive ions from the water column on a remarkably short time scale! The apparent* scavenging times obtained from equation 4-4 range from several decades for deep waters, to several months for open ocean surface waters, to several days for estuarine waters. This progression is clearly of interest in that it corresponds to the progression of particle concentrations in the water. If particles are responsible for the removal of the reactive substances, then the removal probability would be expected to rise with particle content.

One might ask whether we can assume the missing daughter radioactivity to be a measure of removal of the reactive ion from the water mass or whether this is merely the time for removal onto particles which remain suspended in the water mass. In our equations we designate the radioactivity of the daughter to be that in solution. Actually the measurements of the isotopes of thorium are generally made on the total samples (i.e., on dissolved plus particulate). Hence these results yield true removal times rather than just particle uptake times. For some of the lead and for some of the thorium isotope measurements care has been taken to separately estimate the particulate fraction. These results show that in the case of open ocean samples more than 90% of the activity is in dissolved form (see figure 4-2 for an example). The implication from this finding is that the residence time for particles within the water mass must be considerably smaller than the residence time for the reactive metals. Hence the scavenging times given here can be taken as removal times from the water mass.

THORIUM ISOTOPES IN THE SEA

Having viewed the big picture, let us look at some of the details. We will begin with the results on the three isotopes of thorium (^{230}Th , ^{228}Th and ^{234}Th). Due to their widely differing half-lives, each shows its greatest sensitivity in a different

*We say apparent because as we shall see, the assumption that the radiodecay of the parent is the sole source of the daughter isotope is not always valid.

Table 4-4. Typical activity ratios for daughter-parent pairs in various water types.

	Estuaries	Coastal	Surface Ocean	Deep Sea
$^{210}\text{Pb}/^{226}\text{Ra}$	-	-	>1*	0.4-1.0
$^{230}\text{Th}/^{234}\text{U}$	-	-	$<3 \times 10^{-5}$	3×10^{-4}
$^{228}\text{Th}/^{228}\text{Ra}$	0.01	0.05	0.2	0.5-1.0
$^{234}\text{Th}/^{238}\text{U}$	0.2	0.6	>0.9	~ 1
$^{231}\text{Pa}/^{235}\text{U}$	-	-	-	2×10^{-3}
$^{210}\text{Po}/^{210}\text{Pb}$	-	-	0.5	1.0

*Although ^{210}Pb is being removed from surface water by particles, it has an additional source. Radon atoms escaping to the atmosphere from continental soils decay to ^{210}Pb . These ^{210}Pb atoms are incorporated into aerosols and are brought back to the earth's surface by rain and aerosol impact. The flux of these atoms to the sea surface exceeds by about a factor of 10 the in situ production by radiodecay of ^{226}Ra in the upper 200 meters of the ocean.

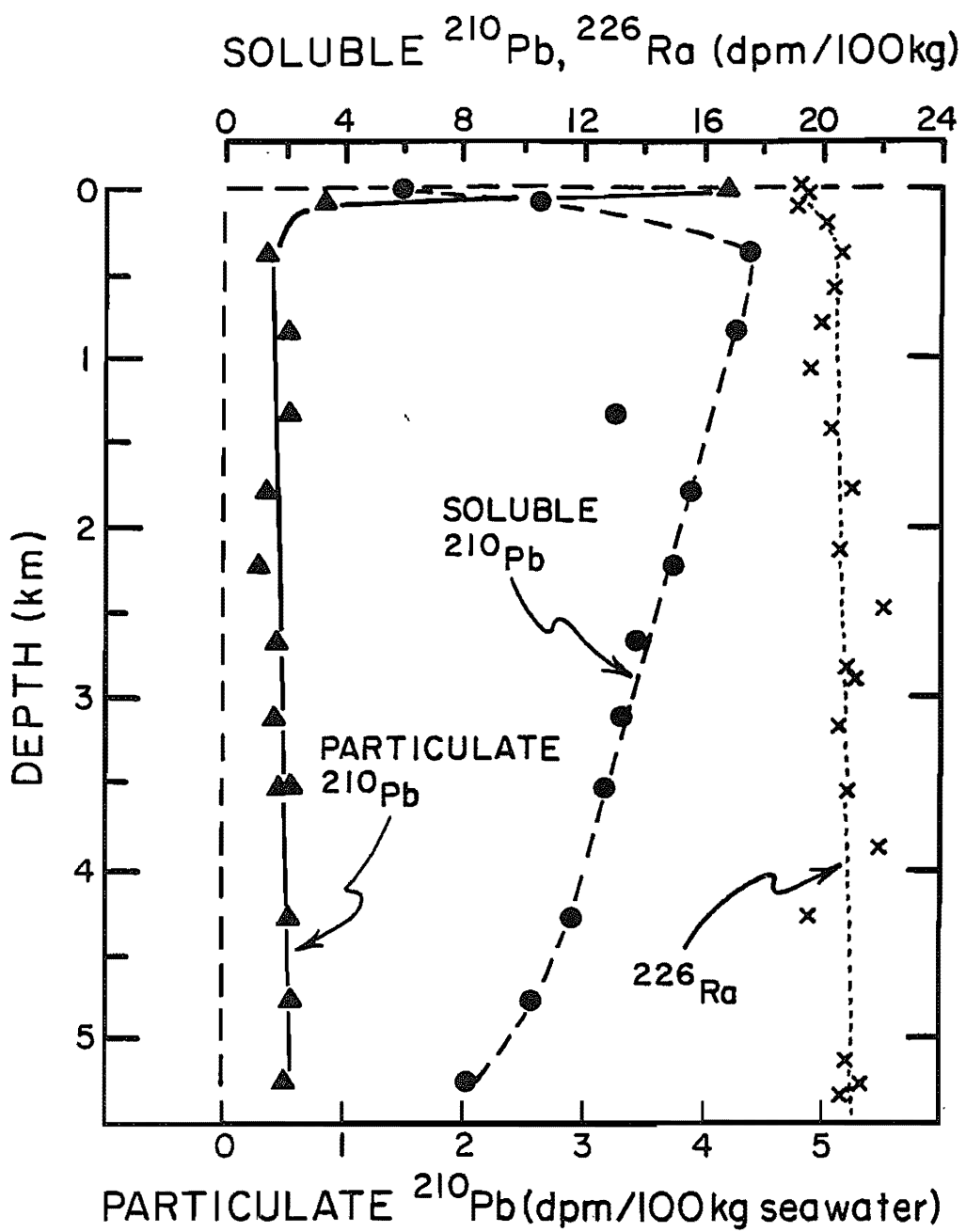


Figure 4-2. Measurements of soluble ^{210}Pb (circles) and particulate ^{210}Pb (triangles) as a function of depth in the Antarctic Ocean. The concentration of ^{226}Ra is also shown (crosses). The concentration of ^{210}Pb in particulate form averages only 0.5 dpm per 100 kg of seawater, while that of dissolved ^{210}Pb averages about 14 dpm per 100 kg of seawater. Hence only about 3% of the ^{210}Pb resides on particles and 97% is in dissolved form. These measurements were made by Somayajulu and Craig (148) at the Scripps Institution of Oceanography.

place in the ocean. ^{234}Th , with its half-life of only 24 days, is most useful in coastal and estuarine waters where the removal of thorium is exceedingly rapid. In the open ocean the scavenging times are everywhere large compared to the half-life of ^{234}Th . Hence its activity will everywhere be very close to that of its parent. ^{228}Th , with a half-life of 1.9 years, is ideally suited for open ocean surface waters where the removal times are on the order of one-half year, but too long for estuaries where the scavenging time for thorium is on the order of days.

Shown in figure 4-3 is an example of the progression of $^{228}\text{Th}/^{228}\text{Ra}$ ratios away from a coast line (130). Note the marked decrease as the coast is approached. The same data are plotted against salinity in figure 4-4 (due to the input of river water, salinity decreases from the open ocean to the coast). As can be seen, the $^{228}\text{Th}/^{228}\text{Ra}$ ratio decreases with decreasing salinity. The message is quite clear: the scavenging time is much shorter in coastal water than in open ocean surface water.

It is of interest to compare results obtained from ^{228}Th with those from ^{234}Th . As can be seen from the graph in figure 4-5, in those waters which have high enough scavenging rates to permit the deficiency of ^{234}Th to be measured, the two isotopes yield reasonably concordant results (138).

Shown in figure 4-6 is a histogram of the $^{228}\text{Th}/^{228}\text{Ra}$ activity ratios for surface ocean water. The corresponding scavenging times are also shown. The average half scavenging time is about 0.3 years and, as can be seen, the range is remarkably small. In comparing these times with the longer ones we shall find for deep waters, it must be remembered that surface waters are the habitat for all plants and most animals. In their quest for the critical nutrient, phosphorus, plants may inadvertently take up reactive metals. These metals could then be passed along to the animals and there be rejected in fecal pellets. In this connection, it is interesting to note that the apparent scavenging time of PO_4 in the surface ocean is of the same order as that of thorium.*

One of the most spectacular sets of findings in this area of the research comes from the measurements by Nozaki and his co-workers in Japan of the dissolved ^{230}Th concentration in very large sea water samples (135) and the measurements by Krishnaswami and his colleagues in India of the ^{230}Th bound onto particles filtered from the deep sea (137). Nozaki's results for a profile in the northwestern Pacific are shown in figure 4-7. The activity increases at a nearly constant rate down the water columns. The corresponding apparent half-removal times (calculated from equation 4-4) as shown along the bottom of the diagram range from less than a few years in surface water to about 50 years for bottom

* As shown in chapter 1, the removal time of PO_4 from the upper ocean (i.e., surface mixed layer plus one half of thermocline) is about five years. However, as the rates of photosynthesis exceed the rates of rain of organic matter from the mid-thermocline to the deep sea by roughly a factor of 10, the scavenging time for phosphorus by plants must be about one half year. The difference between the rate of photosynthesis and the rate of rain of organic debris is the result of nutrient recycling within the upper ocean.

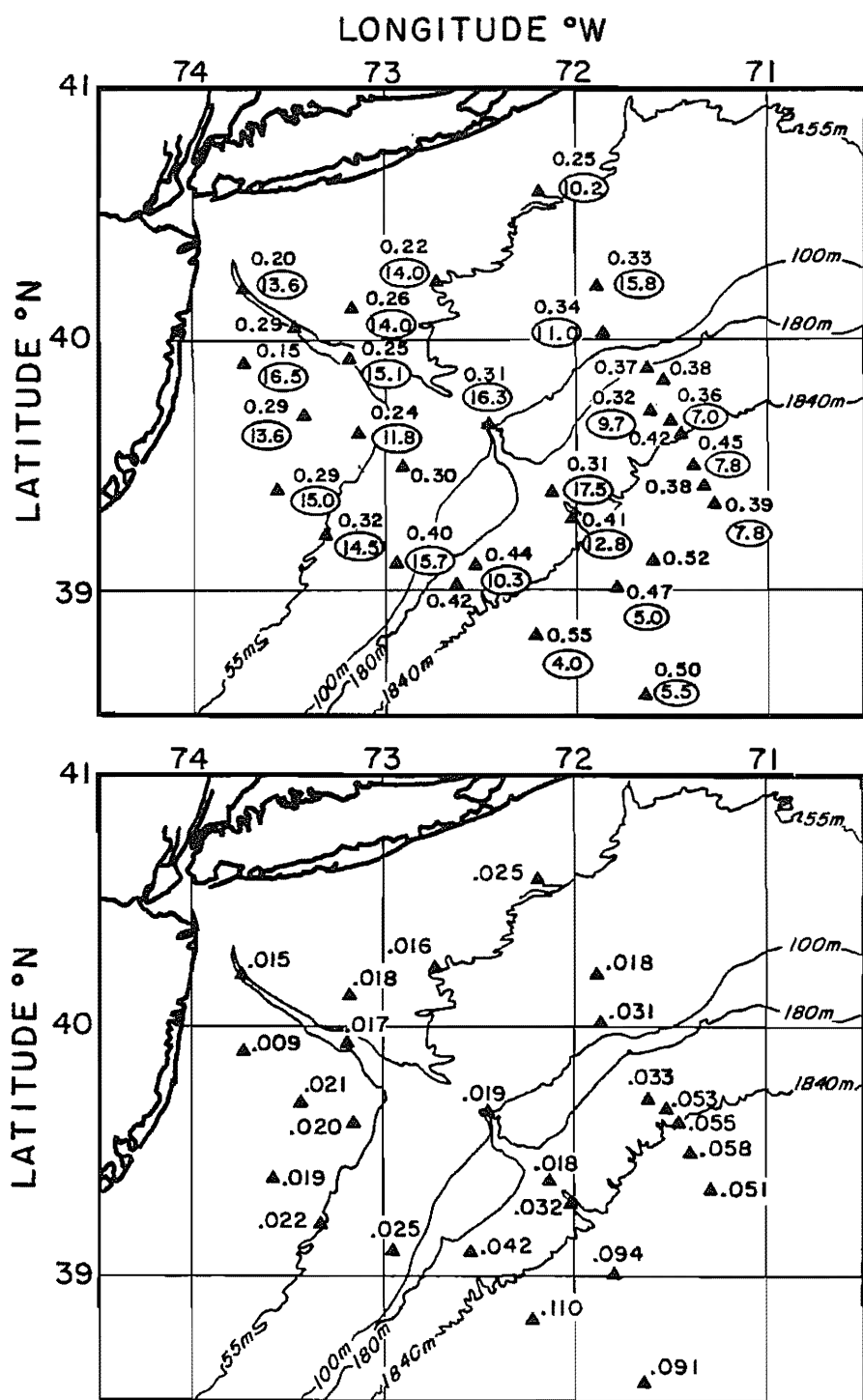


Figure 4-3. The upper map shows the distribution of ^{228}Ra concentrations (circled values) and of ^{228}Th concentrations in units of disintegrations per minute per 100 kg of water and the lower map the distribution of $^{228}\text{Th}/^{228}\text{Ra}$ activity ratios in coastal waters adjacent to New York City. These measurements were made by Feely and his colleagues at the Lamont-Doherty Geological Observatory of Columbia University (130).

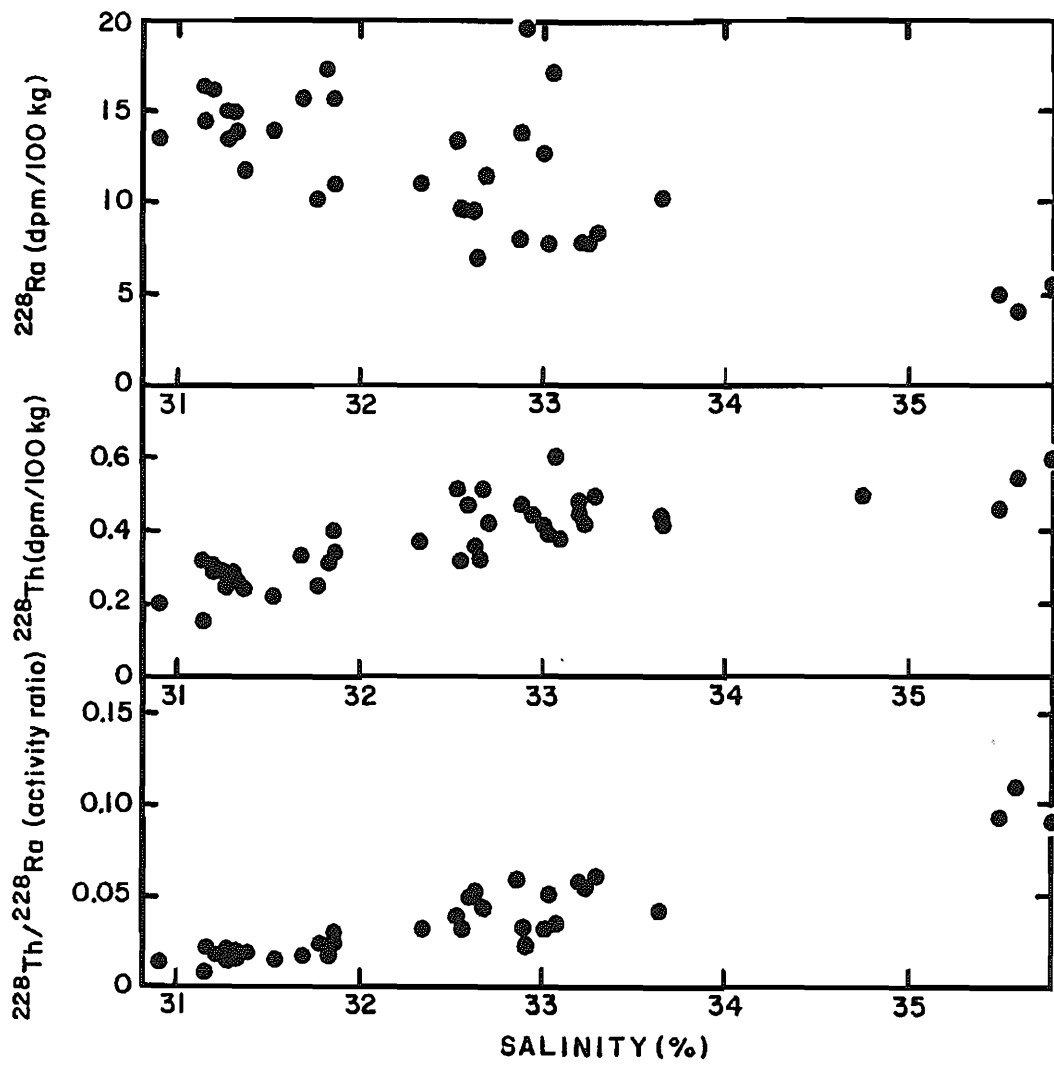


Figure 4-4. Concentrations of ^{228}Ra (upper) and of ^{228}Th (middle) plotted against salinity in coastal samples taken adjacent to New York City (see figure 4-3 for map). The activity ratio of these two isotopes is also plotted against salinity (lower). Due to the input of river water, the waters closest to the coast have the lowest salinity. Hence the increase in salinity is a measure of the effective distance from the shore. As ^{228}Ra is added to surface waters from shelf sediment, the concentration of this isotope decreases away from the shore. As plant biomass and continental detritus burdens of the water decrease away from the coast, the scavenging probability for ^{228}Th decreases. Hence the ratio of ^{228}Th to ^{228}Ra increases with increasing salinity (hence with increasing effective distance from the shore).

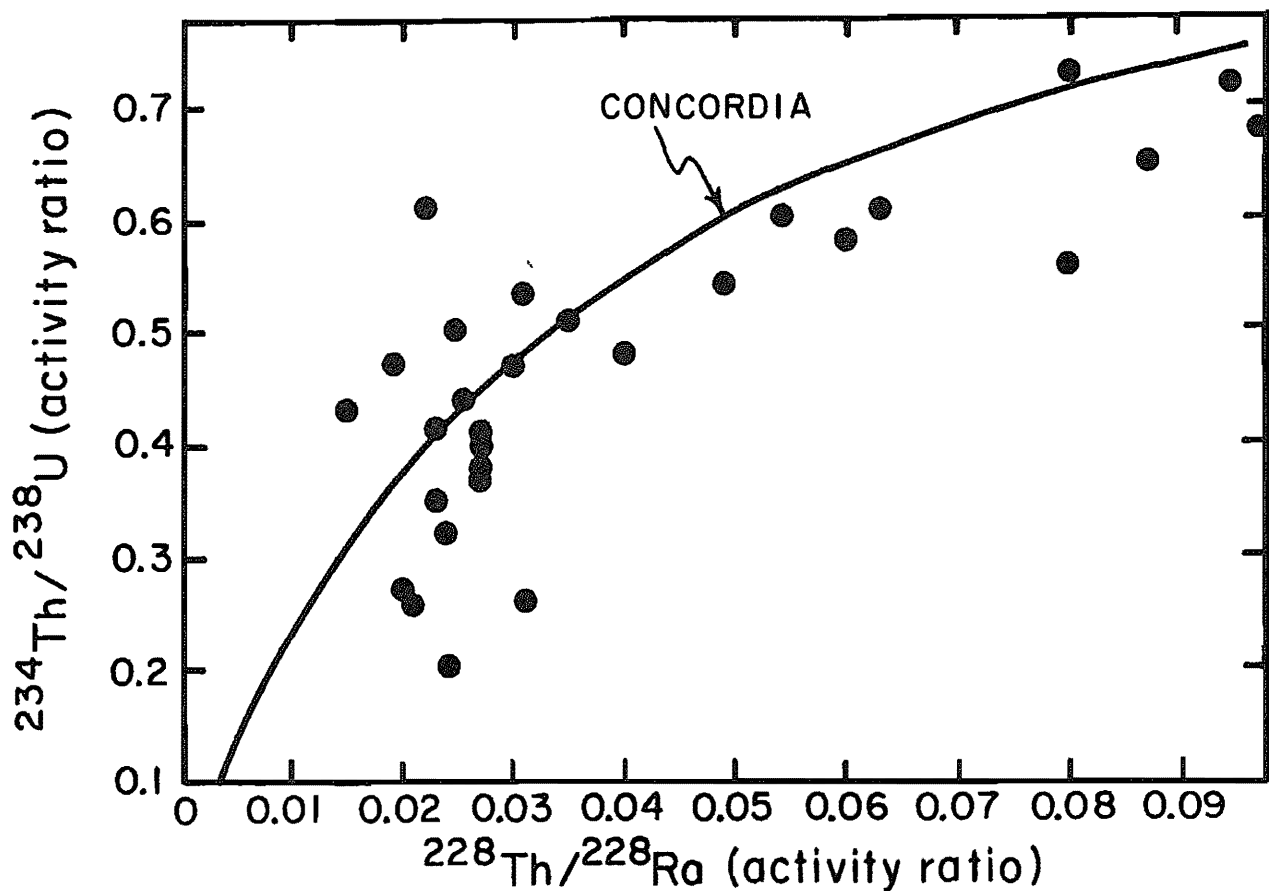


Figure 4-5. The activity ratio, $^{234}\text{Th}/^{238}\text{U}$, plotted against the activity ratio, $^{228}\text{Th}/^{228}\text{Ra}$, for coastal waters. The curve for concordance between the scavenging times calculated from these two ratios is also shown. These measurements were made by Kaufman at Yale University (138).

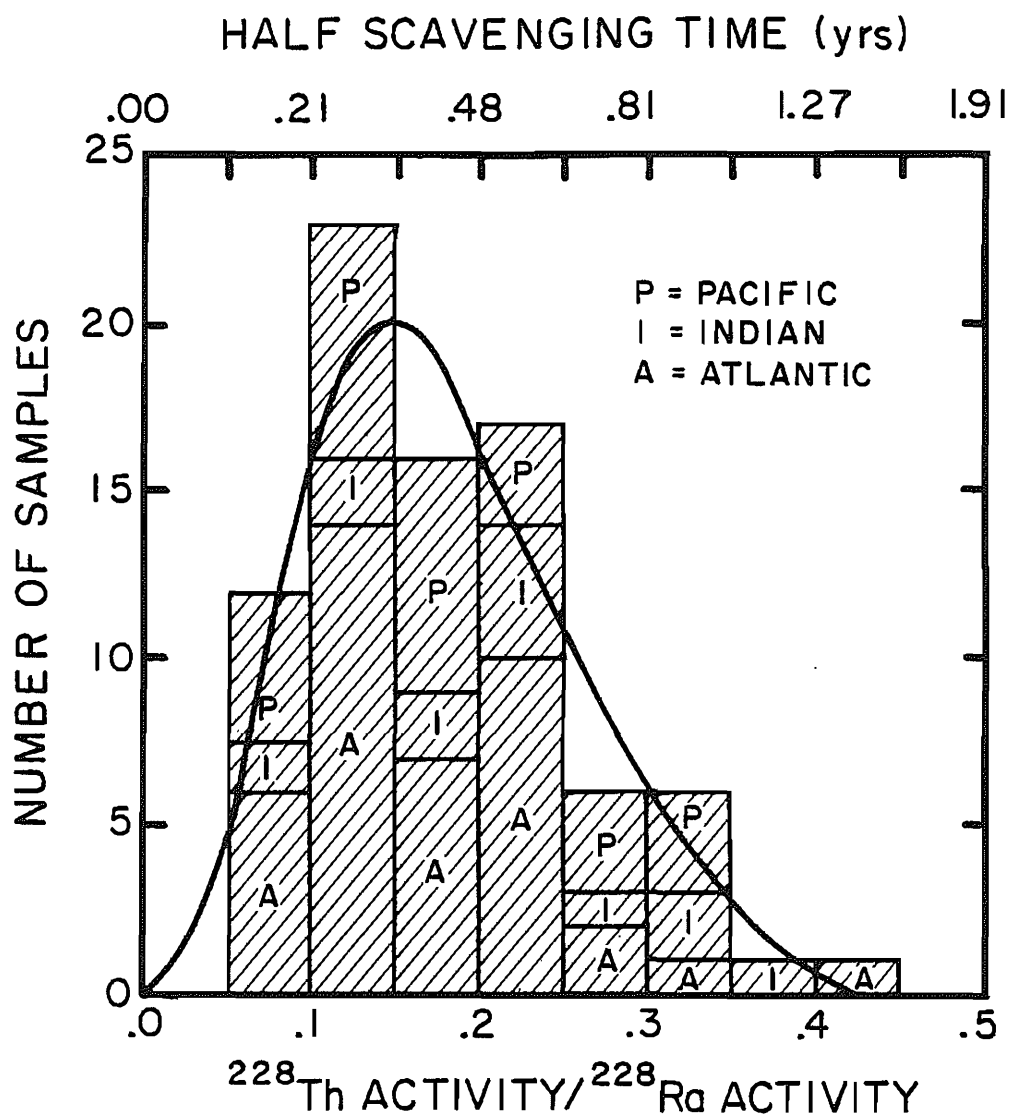


Figure 4-6. Histogram showing the $^{228}\text{Th}/^{228}\text{Ra}$ ratios for open ocean surface waters from the Atlantic, Pacific, and Indian Oceans. The corresponding half scavenging times as calculated from equation 4-4 are also given. These measurements were made at the Lamont-Doherty Geological Observatory (125).

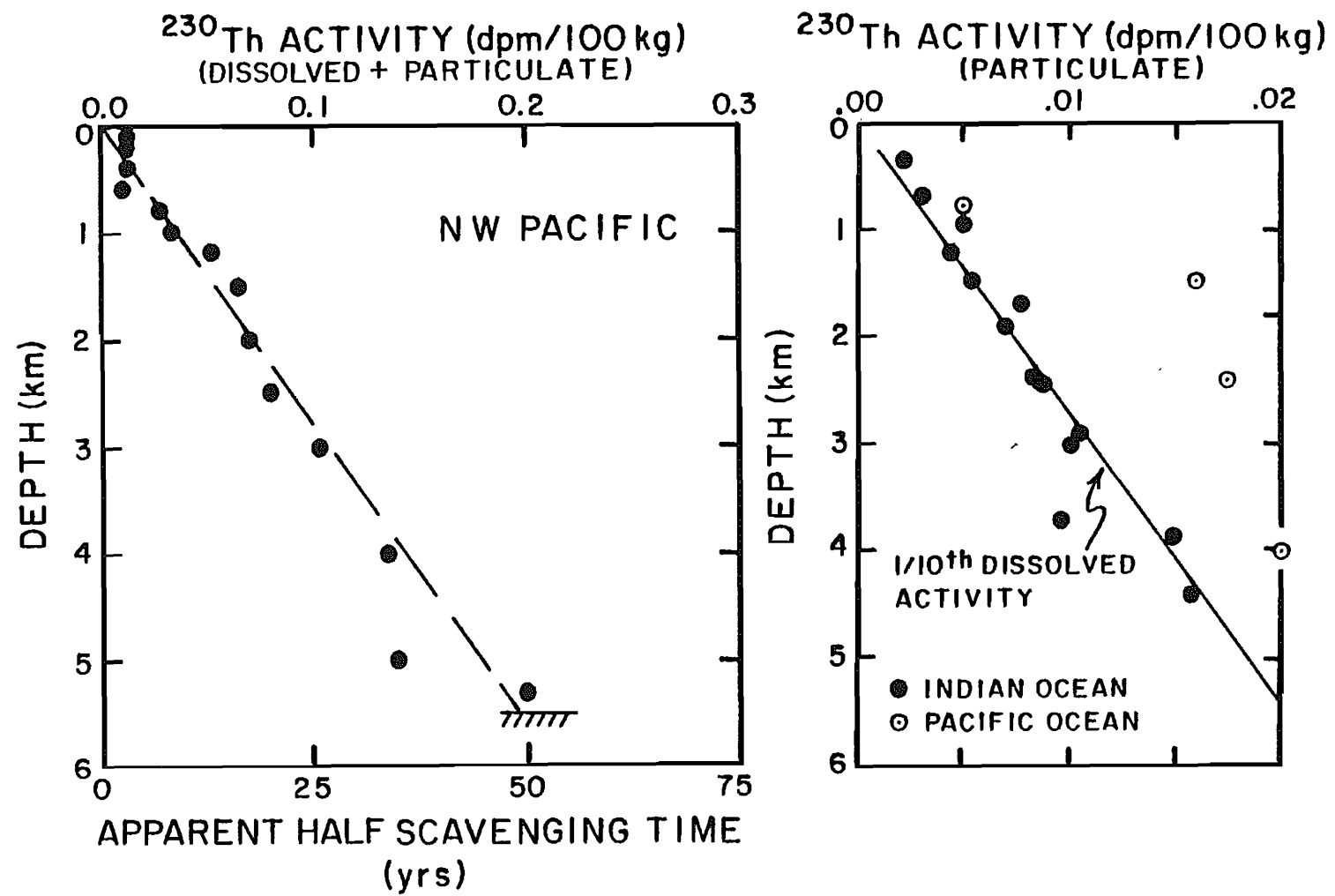


Figure 4-7. In the left-hand panel is a plot of the activity of the total ^{230}Th in sea water as a function of depth in the northwestern Pacific Ocean. For reference the activity of ^{234}U (the parent of ^{230}Th) is 280 dpm/100 kg. These measurements were made by Nozaki in Japan (135). In the right-hand panel are measurements made by Krishnaswami and his colleagues from the Applied Physics Laboratory in Amadabad, India, on particulate matter filtered by an *in situ* apparatus from waters in the Indian and North Pacific Oceans (137).

waters. Krishnaswami's results for ^{230}Th on particulate matter are also shown in this figure. As can be seen, they have a depth pattern similar to that for dissolved ^{230}Th , but per unit volume of water carry only one-tenth as much ^{230}Th . These results reveal an important aspect of metal geochemistry. The adsorption of thorium onto particulate matter must be reversible, and for the deep waters of the open Pacific Ocean, the equilibrium distribution coefficient between water and particles must be about 10.

To see why this is the case, we must first understand that, since more than 99.9% of the ^{230}Th produced in the ocean reaches the sediment, the particles falling through a given horizon in the sea must carry an amount of ^{230}Th proportional to that produced in the overlying water column. Thus the amount of ^{230}Th carried by particles must increase linearly with depth. In this regard Krishnaswami's findings confirm expectation. If reversible equilibrium is maintained between the ^{230}Th concentration on the falling particles and that in the water and if the concentration of particles remains constant with depth, then the concentration of ^{230}Th in the water must increase linearly with depth as does that on particles.

The concentration of ^{230}Th on the particles, C_p , will be determined by the requirement that the flux of ^{230}Th atoms through any horizon equals the production rate of ^{230}Th atoms in the overlying water column. Hence:

$$C_p S = Pz \quad 4-5$$

or

$$C_p = \frac{Pz}{S} \frac{\text{atoms}}{\text{g}} \quad 4-6$$

where S is the flux of particulate matter ($\text{g}/\text{cm}^2\text{yr}$), P is the production rate of ^{230}Th ($\text{atoms}/\text{cm}^3\text{yr}$), and z is the depth (cm). The concentration of ^{230}Th in the water (C_w) is given by:

$$C_w = K C_p \quad 4-7$$

where K is the distribution coefficient (i.e., the ratio of thorium in a gram of water to that on a gram of particles). Combining equations 4-6 and 4-7, we obtain:

$$C_w = \frac{K P z}{S} \frac{\text{atoms}}{\text{g}} \quad 4-8$$

At any given place in the sea the concentrations of ^{230}Th in the water will build up to that point where the particles passing through the water carry an amount of ^{230}Th equal to the production in the overlying water column. Once this concentration has been achieved, the system will be at steady state. ^{230}Th will be removed as fast as it is generated. If the average settling velocity of particles is taken to be everywhere the same, then the concentration of particles in the water will be proportional to the particle flux. In this situation the concentration of ^{230}Th in the water will be inversely proportional to the particle concentration.

Nazaki's results also suggest that recycling of ^{230}Th from the sea floor is unimportant. Were it important, one would expect the slope of the ^{230}Th activity versus depth relationship to steepen near the bottom. No such change is seen.

Based on the apparent scavenging time of several tens of years calculated from Nozaki's ^{230}Th data, it might be expected that the $^{228}\text{Th}/^{228}\text{Ra}$ activity ratio in deep water would be close to unity. Measurements of these isotopes on samples of deep water collected as part of the GEOSECS program are shown in figure 4-8. At all these stations the ^{228}Ra content decreases away from the bottom. As ^{228}Ra (half-life 5.7 years) is supplied to the sea entirely from sediments, its concentration should be highest near the sea floor. Of interest to us here is the difference between the activity of ^{228}Ra (the parent) and ^{228}Th (the daughter). As can be seen from the figure 4-8, the evidence is mixed. At some of the GEOSECS stations (28, 34, 58 and 263) the activities of these two isotopes agree within the experimental error. At others (32, 61 and 214) the ^{228}Th activity seems to be significantly lower than that of ^{228}Ra .

It can be shown that if the contribution of ^{228}Th produced from the ^{228}Ra in the upper ocean is neglected, and if the distribution of ^{228}Ra above the sea floor follows the relationship:

$$[^{228}\text{Ra}]_z = [^{228}\text{Ra}]_0 e^{-z/h} \quad 4-9$$

where z is the distance above the sea floor and h is the characteristic height above the bottom attained by ^{228}Ra atoms before undergoing radiodecay, then the ratio of ^{228}Th to ^{228}Ra will be given by the expression:

$$\frac{A^{228}\text{Th}}{A^{228}\text{Ra}} = \frac{1}{\frac{SK}{(1+Kq)\lambda h} + 1} \quad 4-10$$

S is the flux of particulate matter ($\text{g/cm}^2\text{yr}$), K is the distribution coefficient of thorium between particulate matter and water (atoms per g particulate matter/atoms per g H_2O), q is the concentration of particulate matter in the water, and λ the decay constant of ^{228}Th .

The combined work of Nozaki et al. (135) and Krishnaswami et al. (137) shows that the product Kq is about 0.1. Hence equation 4-10 can be simplified as follows:

$$\frac{A^{228}\text{Th}}{A^{228}\text{Ra}} = \frac{1}{\frac{SK}{\lambda h} + 1} \quad 4-11$$

Taking S to be $1 \times 10^{-3} \text{ g/cm}^2\text{yr}$, K to be 10^{-7} , λ to be 0.363 and h to be $7 \times 10^4 \text{ cm}$ (i.e., 700 m):

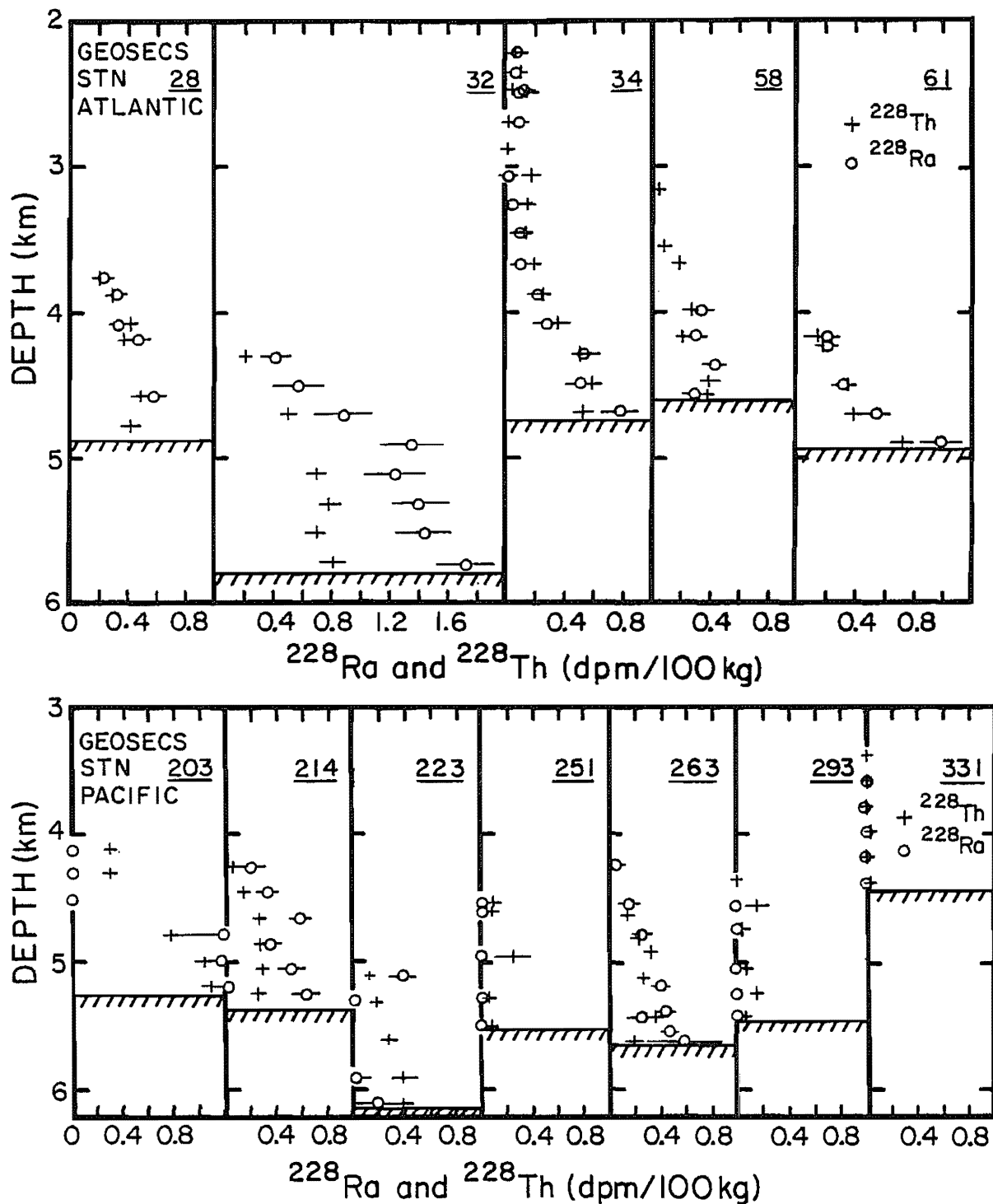


Figure 4-8. Plots of ^{228}Th activity (crosses) and of ^{228}Ra activity (circles) as a function of depth in the deep waters of the western Atlantic Ocean (upper) and in the Pacific Ocean (lower). The bottom depth is shown at each station. These measurements were made as part of the GEOSECS program by Herbert Feely and his colleagues at the Lamont-Doherty Geological Observatory.

$$\frac{A^{228}Th}{A^{228}Ra} = \frac{1}{\frac{1 \times 10^{-3}}{0.363} \times \frac{1 \times 10^7}{7 \times 10^4} + 1} = 0.72$$

The exact value will of course depend on the local particle flux (the larger the particle flux, the smaller the ratio) and on the local characteristic height attained by ^{228}Ra atom (the greater the height, the closer the ratio will be to unity). The point to be made is that deficiencies of ^{228}Th activity in bottom water are not inconsistent with the observations on ^{230}Th . Rather, in situations where daughters are carried into a water mass on particles raining down the water column, use of the scavenging times obtained using equation 4-4 can be very misleading.

Before leaving thorium, one other set of data must be mentioned. Shown in figure 4-9 are profiles of the $^{228}Th/^{228}Ra$ activity ratio in the upper thermocline of the Atlantic Ocean (132). These ratios show an increase with depth reaching values greater than unity at a few hundred meters. These results can only be explained if the ^{228}Th atoms removed from the surface water are released from their carrier particles in the upper thermocline. The most likely scenario for such release would be that the ^{228}Th atoms born in surface water are inadvertently incorporated by plants during their quest for phosphorus. The animals which eat these plants incorporate these ^{228}Th atoms into fecal pellets. The ingredients of these pellets are eventually released to the water when the organic material they contain is eaten. Once released, these ^{228}Th atoms would of course be vulnerable to uptake onto the particles present in the upper thermocline. So yet another complication enters our story. Uptake by living organisms coupled with release during respiration appears to compete with inorganic absorption at least in the upper water column.

PROTACTINIUM-231 TO THORIUM-230 ACTIVITY RATIOS

Although measurements of dissolved ^{231}Pa activity versus depth in the water column have yet to be made, we do have some information about the removal of ^{231}Pa from the sea which adds to our story. This information comes from sediments and sediment-trap material. The activity ratios of ^{231}Pa to that of ^{230}Th in sediments from well away from continental margins are lower than those expected from the ratio of the production rates of these two isotopes in sea water.* As the integrated excess ^{230}Th activity

*The ratio of ^{235}U to ^{238}U atoms is everywhere constant in the solar system. All materials including sea water have 138 ^{238}U atoms for each ^{235}U atom. Due to recoil damage, the ^{234}U atoms generated by the decay of ^{238}U in mineral can become separated from the parent ^{238}U . In the sea, for example, the activity ratio ^{234}U activity to ^{238}U activity is 1.15 (127). Because uranium atoms reside in the sea for many mixing cycles (i.e., for many times 1000 years), this ratio is everywhere the same. Hence the production ratio (in atoms) of ^{230}Th (from ^{238}U) to ^{231}Pa (from ^{235}U) is given by:

$$R_{prod} = \frac{1.15 \lambda^{238}U N^{238}U}{\lambda^{235}U N^{235}U} = \frac{1.15 \times 1.55 \times 10^{-10}}{9.85 \times 10^{-10}} \frac{138}{1} \approx 25$$

The decay rate ratio for a batch of newly produced ^{230}Th and ^{231}Pa is given by:

$$R_{decay} = \frac{\lambda^{230}Th}{\lambda^{231}Pa} R_{prod} = \frac{9.22 \times 10^{-6}}{2.13 \times 10^{-5}} 25.0 \approx 10.8$$

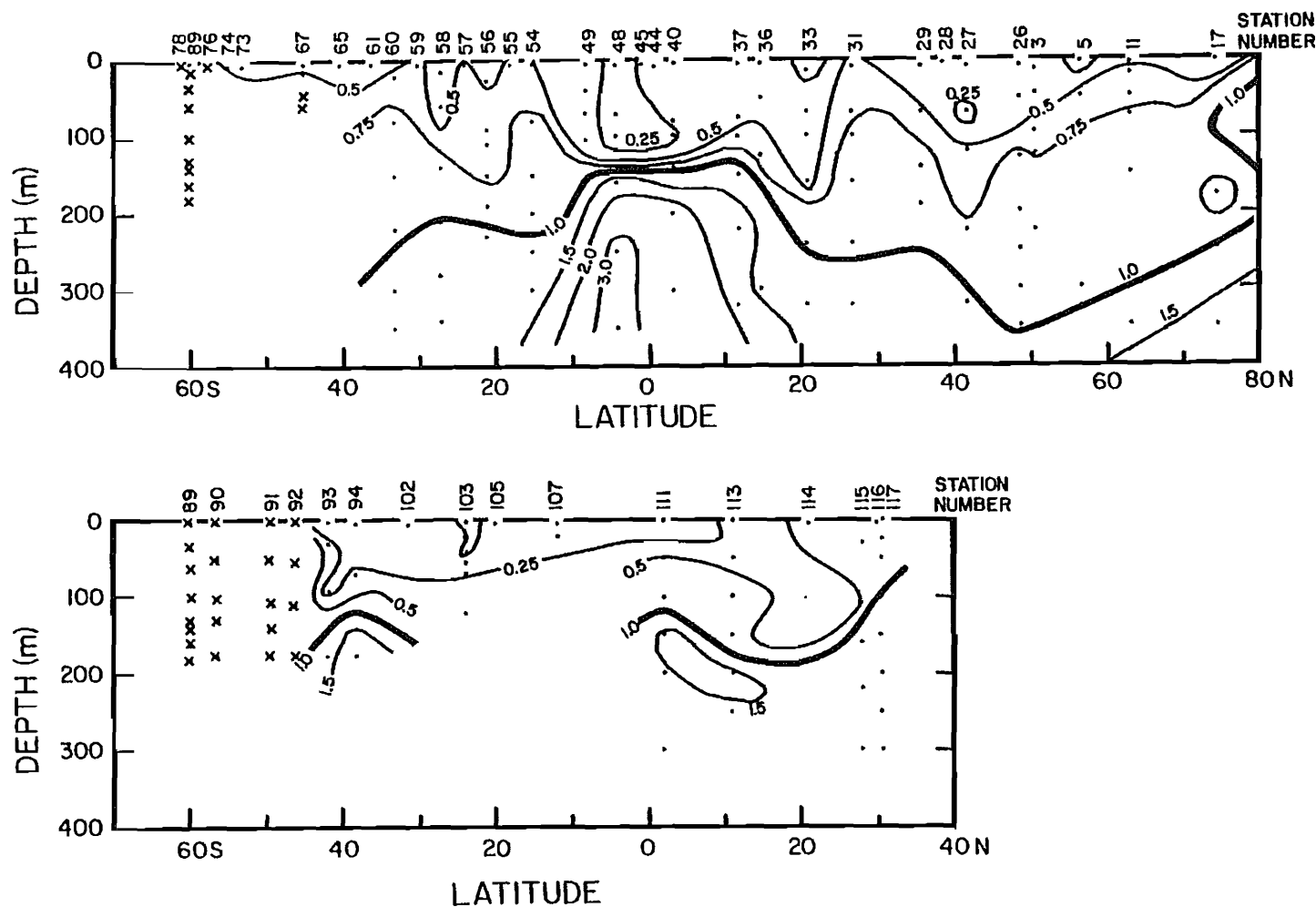


Figure 4-9. Sections in the western (upper) and eastern (lower) Atlantic of the activity ratio of ^{228}Th to ^{228}Ra in the upper 400 meters of the water column based on results from the GEOSECS program. As can be seen at every station, this activity ratio increases with water depth, reaching values greater than unity at depths ranging from about 100 meters in the equatorial zone to 200 to 300 meters in the temperate zones. These results were obtained by Feely and his colleagues at the Lamont-Doherty Geological Observatory (132).

in these sediments matches reasonably well the decay rate of ^{234}U in the overlying water column, this anomaly appears to be the result of a lower than expected rain rate of ^{231}Pa . If so, then the ^{231}Pa produced in the water column above these sites must move laterally in the ocean and undergo removal elsewhere on the sea floor. This "elsewhere" has been found recently by De Master at Yale (129) and by Mangini at Heidelberg (personal communication). Their measurements show that sediments forming beneath areas of upwelling in the Antarctic and along continental margins have much higher than expected ^{231}Pa to ^{230}Th ratios. While enough data has not been obtained to show that the excess ^{231}Pa rain in these areas compensates for the deficient rain of this isotope in the open ocean, it seems likely that this is the case.

More direct evidence for this phenomenon is available from sediment trap data. Anderson and Bacon at Woods Hole have analyzed material from Honjo's traps (134) and have shown that traps deployed in the open ocean show a deficiency of ^{231}Pa relative to ^{230}Th (see figure 4-10 for results and figure 4-11 for locations at which the traps were deployed). On the other hand, traps deployed close to Panama give just the opposite result. They accumulated an anomalously high ratio of ^{231}Pa to ^{230}Th . Care must be taken when converting sediment trap results to absolute rain rates. The efficiency of these traps varies with their dimensions and shape, with particle size, and with current velocity. No one has as yet succeeded in establishing a means to calibrate these devices. Nevertheless, if the efficiency of the traps is assumed to have been the same in all four locations, then the absolute rain rate of both ^{230}Th and ^{231}Pa must be considerable higher near Panama than for the open ocean sites.

These observations can be explained by the combination of rapid lateral mixing within the sea and particle concentration dependent scavenging rates. This phenomenon can be best understood by considering the extreme case where lateral mixing is infinitely rapid. Under such circumstances the number of ^{230}Th and ^{231}Pa atoms reaching a given place on the sea floor would be proportional to the number of particles reaching the bottom. Thus, if an area of the sea floor near a continental margin received 10 times more particles than an area of the sea floor well away from the margin, it would also receive 10 times more ^{230}Th and ^{231}Pa . This would lead to a higher than expected sediment inventory of these isotopes near the continental margin and a lower than expected inventory in the area away from the margin. If our hypothetical sea had two types of area, 10% of the high-flux type and 90% of the low-flux type, just about half of these isotopes would end up beneath each type of regime. The sediment inventory would be about half the expected value in the 90% of the sea floor receiving the low flux, and about 5 times the expected value in 10% of the sea floor area receiving the high flux.

The distributions of ^{230}Th and ^{231}Pa on the sea floor and in sediment traps can be explained by postulating a shorter water column scavenging time for ^{230}Th than for ^{231}Pa , and by postulating that the average of the ^{230}Th and ^{231}Pa scavenging times is comparable to the time required for lateral homogenization along isopycnal surfaces in a major ocean basin. In such a situation

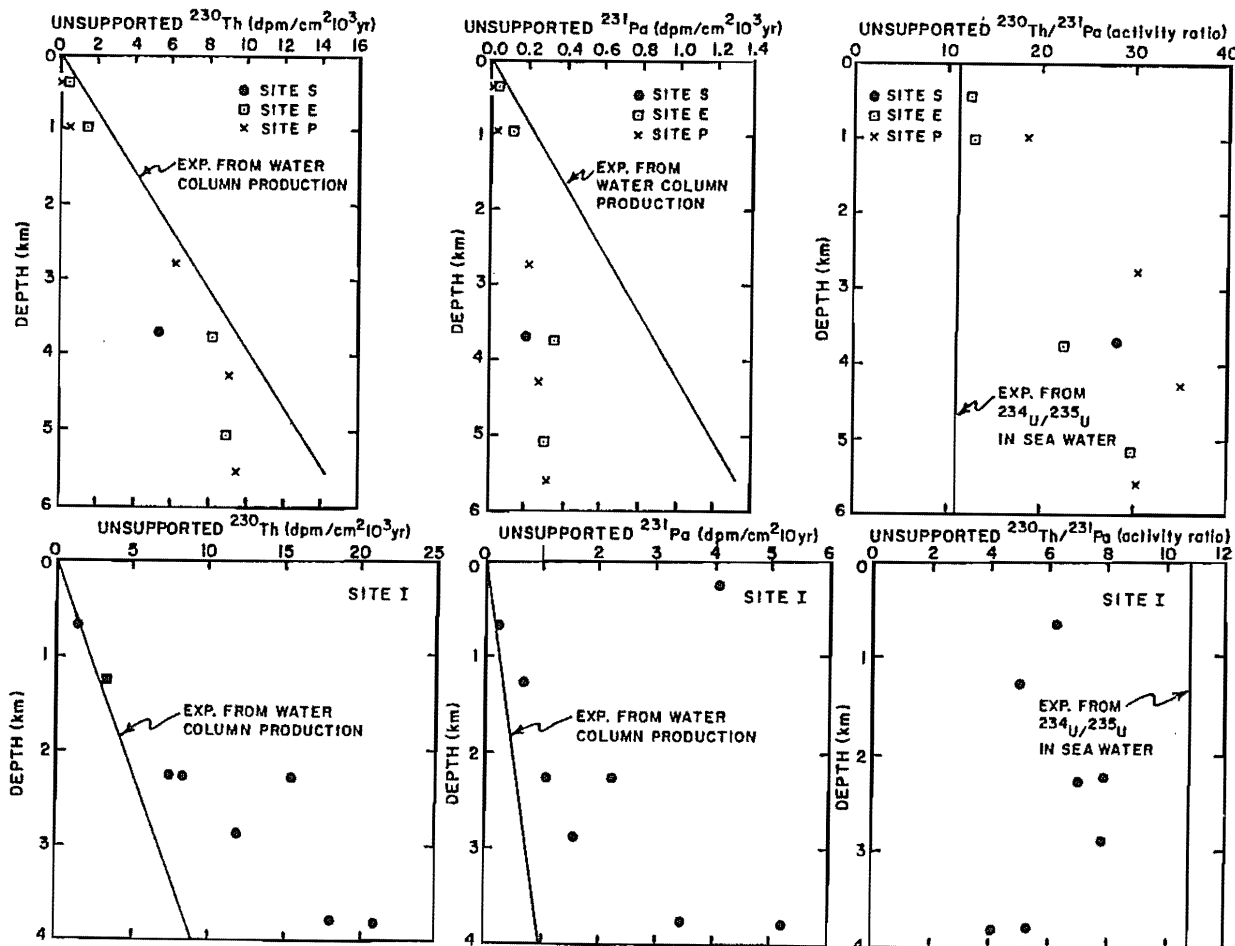


Figure 4-10. ^{230}Th and ^{231}Pa fluxes as determined from sediment trap deployments at various locations and depths in the ocean. The upper panel shows the results from three open ocean sites (for locations, see figure 4-11). The lower panel shows the results from a site close to the continental margin. The solid lines represent the results expected if the traps were collecting these isotopes at the rates they are produced in the overlying water column. These results were obtained by the geochemistry group at Woods Hole Oceanographic on samples from Honjo's sediment traps (134). By unsupported is meant the activity excess over that for the respective parent isotopes (^{234}U in the case of ^{230}Th and ^{235}U in the case of ^{231}Pa) in the trap.

Figure 4-11. Map showing the sites of sediment traps deployed by Honjo and his Woods Hole colleagues. The ^{230}Th and ^{231}Pa data concentrations in the material caught in these traps are summarized in figure 4-10.

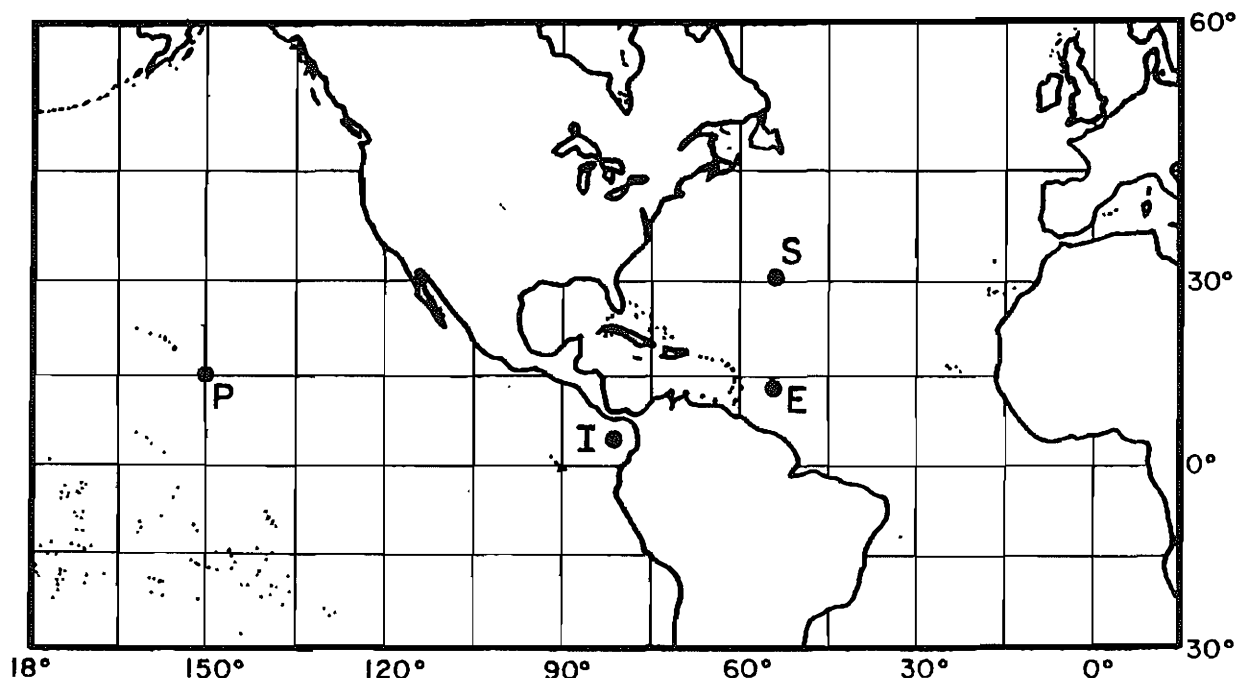


Table 4-5. Ratio of ^{230}Th to ^{231}Pa removal time as determined from their activity ratios on MnO_2 -coated nitex. Results obtained by Anderson and his colleagues at Woods Hole Oceanographic (134).

Depth km	$\frac{A^{230}\text{Th}}{A^{231}\text{Pa}}$	$\frac{\tau^{231}\text{Pa}}{\tau^{230}\text{Th}}$	Site*
5.8	3.4	3.2	P
4.2	5.3	2.1	I
4.2	5.2	2.1	I
4.2	6.1	1.8	I
4.2	5.7	1.9	I
4.2	3.9	2.8	I

*see figure 4-11.

both isotopes would show higher rain rates (and sediment inventories) in areas of high particle flux than in areas of low particle flux. The contrast, however, would be greater in the case of ^{231}Pa than in the case of ^{230}Th . This would give rise to the higher than theoretical $^{230}\text{Th}/^{231}\text{Pa}$ ratios seen in the deep sea and the lower than theoretical ratios found in areas of high particulate rain rate (i.e., along continental margins and in the Antarctic).

Evidence exists for this difference in removal times. Anderson of Woods Hole deployed manganese oxide coated passive absorbers on sediment trap moorings (134). Assuming that these absorbers have the same uptake efficiencies for dissolved ^{230}Th and ^{231}Pa , the ratio of the activities of these two isotopes on the absorber should be equal to the ratio of their activities in sea water. Were the scavenging times of these isotopes by marine particulates identical, then the activity ratio of ^{230}Th to ^{231}Pa in dissolved form should be equal to 10.8 (i.e., the decay rate ratio of newly formed ^{230}Th and ^{231}Pa). As can be seen from table 4-5, the ratios observed by Anderson on his passive ion absorbers ranged from 3.4 to 6.1. The suggestion is then that the ^{231}Pa resides 1.8 to 3.2 times longer in sea water than does ^{230}Th . This result should of course be confirmed by direct measurements on large-volume water samples.

A similar result is obtained if manganese nodules are assumed to absorb ^{231}Pa and ^{230}Th in proportion to their concentrations in sea water. During the mid-1960's Sackett showed that the $^{230}\text{Th}/^{231}\text{Pa}$ ratio in nodules averages about half that expected from the ratio of the production rates of these isotopes in the sea (220). Again the implication is that ^{231}Pa atoms reside in the water about twice as long as do ^{230}Th atoms.

Data on ^{230}Th to ^{231}Pa activity ratios in sediment traps and in core tops are summarized in figure 4-12. As can be seen, the ratio of these isotopes is inversely related to the particle content of the overlying water column. Where the particle content is low, the $^{230}\text{Th}/^{231}\text{Pa}$ ratio is high. Where the particle content is high, the ratio is low.

THE DISTRIBUTION OF LEAD-210

Let us next consider the isotope ^{210}Pb . Its distribution in the sea is complicated by the fact that it is supplied via atmospheric "fallout" as well as by the radioactive decay of the ^{226}Ra in sea water (139). The atmospheric supply is derived from radon atoms which escape to the atmosphere from soils and then decay to form ^{210}Pb . These atoms become attached to aerosols which carry them back to the land or sea surface. While the production rate of ^{210}Pb atoms within the water column can be exactly determined, the input rate of ^{210}Pb atoms from the atmosphere to the sea surface is only roughly known. A summary of ^{210}Pb fallout rates measured over land and of water column production rates in the various oceans is given in table 4-6. Assuming that the fallout rate of ^{210}Pb over the sea averages roughly the same as it does over land, then the atmosphere contributes about 20% of the amount of ^{210}Pb in the sea. While not greatly altering the situation in

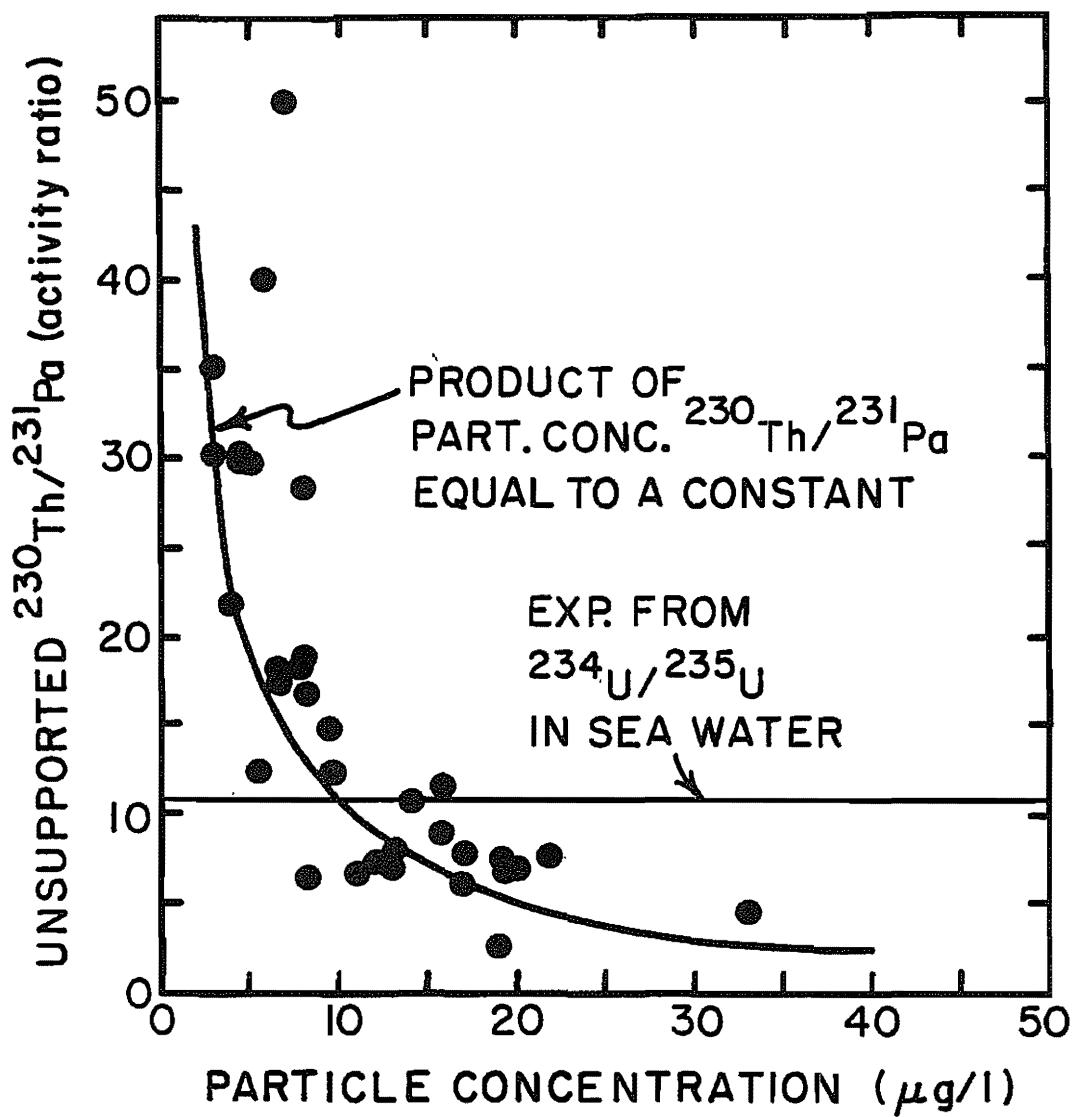


Figure 4-12. Unsupported ^{230}Th to ^{231}Pa activity ratios in sediment core tops, in sediment trap material and in particles filtered from the water as a function of the average particulate concentration in the overlying water column for a wide range of ocean sites. These data were compiled by Bob Anderson (134).

Table 4-6. Measurements of ^{210}Pb fallout rates and water column production rates.

<u>Fallout Rates</u>			
<u>Location</u>	<u>(Ref.)</u>	<u>Material</u>	<u>Fallout Rate atoms/cm²min</u>
Greenland	(140a)	Ice	3.6
Antarctica	(140a)	Ice	0.2
Mt. Olympus, WA.	(140a)	Ice	5.4
Char Lake, Canadian Arctic	(147a)	Lake Sediments	3.0
Reindeer Lake Sask., Canada	(147a)	Lake Sediments	9
E.L.A., Kenora, Can.	(147a)	Lake Sediments	17
Lake Superior	(142a)	Lake Sediments	13
Lake Michigan	(146a)	Lake Sediments	21
Lake Ontario	(147a)	Lake Sediments	19
Lake Shinhi, Japan	(147b)	Lake Sediments	25
Lake Leman, Switz.	(142a)	Lake Sediments	14
Lake Pavin, France	(142a)	Lake Sediments	41
Fayetteville, Ark.	(145a)	Rain	32
Maryland	(140)	Soil	39
Connecticut	(155)	Soil	26
Pennsylvania	(155)	Soil	33
New Mexico	(155)	Soil	65
Colorado	(153)	Soil	52
South Africa	(154)	Soil	21

Production Rates

<u>Location</u>	<u>Production[†] atoms/cm²min</u>	<u>Fallout[*] atoms/cm²min</u>	<u>Total atoms/cm²min</u>
North Atlantic (Western Basin)	54	24	78
North Atlantic (Eastern Basin)	60	24	84
South Atlantic (Western Basin)	66	12	78
South Atlantic (Eastern Basin)	72	12	84
Antarctic	78	< 5	~ 80
Central So. Pacific	90	12	102
Central No. Pacific	120	24	144

[†]For a 4000-meter water column.

^{*}The northern hemisphere values are based on the data in the first half of this table; the southern hemisphere values are based on the assumption that the fallout rate in the southern hemisphere is one-half that in the northern hemisphere.

the deep sea, the airborne component complicates the situation in the upper water column.

A typical depth profile for ^{210}Pb activity is shown in figure 4-13. In the upper water column the activity of ^{210}Pb exceeds that of ^{226}Ra (i.e., atmospheric fallout more than compensates for the ^{210}Pb removed onto particulate matter). At mid-depths the two isotopes have similar activities. In bottom waters the ^{210}Pb activity is only about half the ^{226}Ra activity (clear evidence for the removal of ^{210}Pb onto particles).

Let us start our analysis of the ^{210}Pb distribution with waters below 1500 meters where the contribution of atmospheric fallout is relatively small. As shown in figure 4-14, profiles of ^{210}Pb from various locations in the North Pacific and of the Antarctic all show the same basic trend. The activity ratio decreases toward the bottom. As shown in figure 4-15, this situation does not change dramatically in the near-bottom layer (157). As do all the waters in the lower part of the water column in the North Pacific, these near-bottom samples have a $^{210}\text{Pb}/^{226}\text{Ra}$ activity ratio close to one-half. Thus, unlike ^{230}Th , which shows an apparent half-scavenging time increasing from 20 to 50 years over the depth range 2500 to 5000 meters, ^{210}Pb shows an apparent half-scavenging time decreasing from more than 100 years at mid-depths to 15 years near the bottom.

In this regard, it would be interesting to know what scavenging time in upper waters is. Here we run into the difficulty associated with the atmospheric input. As we do not know with sufficient accuracy the delivery rate of these atoms, it is not possible to give a firm estimate. We do have a few clues, however. The map in figure 4-16 shows the distribution of ^{210}Pb in surface waters in the Pacific Ocean (151). The difference between the hemispheres reflects the higher land area in the northern hemisphere, which leads to a greater total radon release and, in turn, to a greater mean ^{210}Pb fallout rate. The important feature of this diagram is rather the drop in activity toward the ocean margins. This decrease very likely reflects the higher particle concentrations in coastal waters. Thus we have at least qualitative evidence that ^{210}Pb is being removed in significant amounts from surface water on a time scale of its half-life (i.e., 22 years).

Another clue comes through a comparison of the upper water column inventory of ^{210}Pb activity with the rate of fallout as measured over the continent. In figure 4-17 are shown the composite of a series of profiles of ^{210}Pb and ^{226}Ra for the upper 600 meters of the North Pacific Ocean. Note that the excess extends to about 600 meters. As this is the depth to which bomb-produced tritium had penetrated in the decade between its addition (~1964) and the GEOSECS survey (1974), physical mixing of the atmospherically derived ^{210}Pb could be entirely responsible for its penetration (i.e., uptake onto, followed by release from, particles need not be called upon). The integrated ^{210}Pb activity in this layer is 11 dpm/cm². Based on continental measurements, the flux of ^{210}Pb atoms onto the sea surface should lie in the range 30 ± 10 atoms/cm² minute. Adding to this the 6 atoms/cm² minute produced by the ^{226}Ra dissolved in the upper 600 meters, we

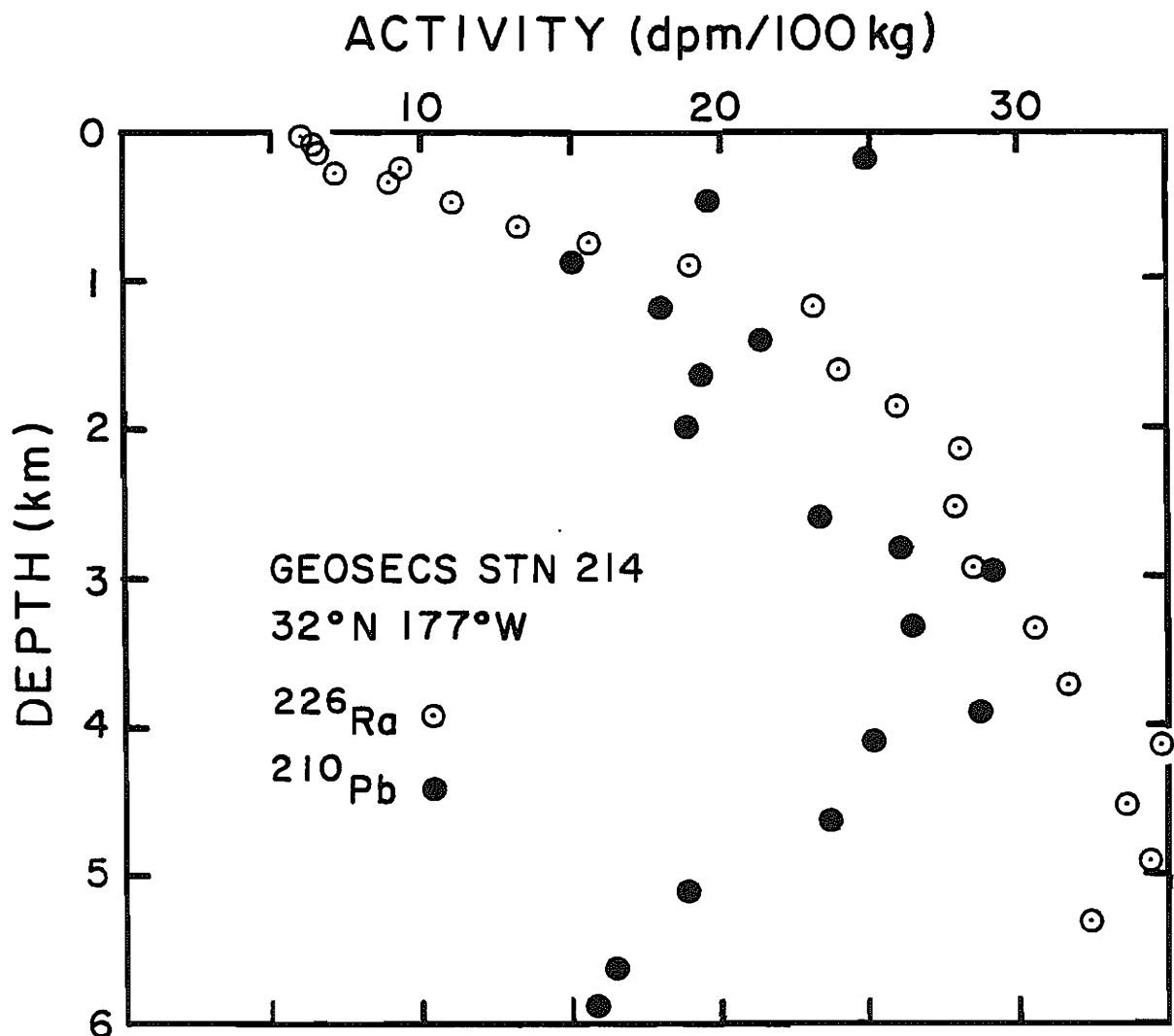


Figure 4-13. ^{226}Ra and ^{210}Pb activities versus depth at GEOSECS station 214 in the central North Pacific. The ^{226}Ra data were obtained by Chung of the Scripps Institution for Oceanography (118). The ^{210}Pb data were obtained by Turekian and his colleagues at Yale University (158).

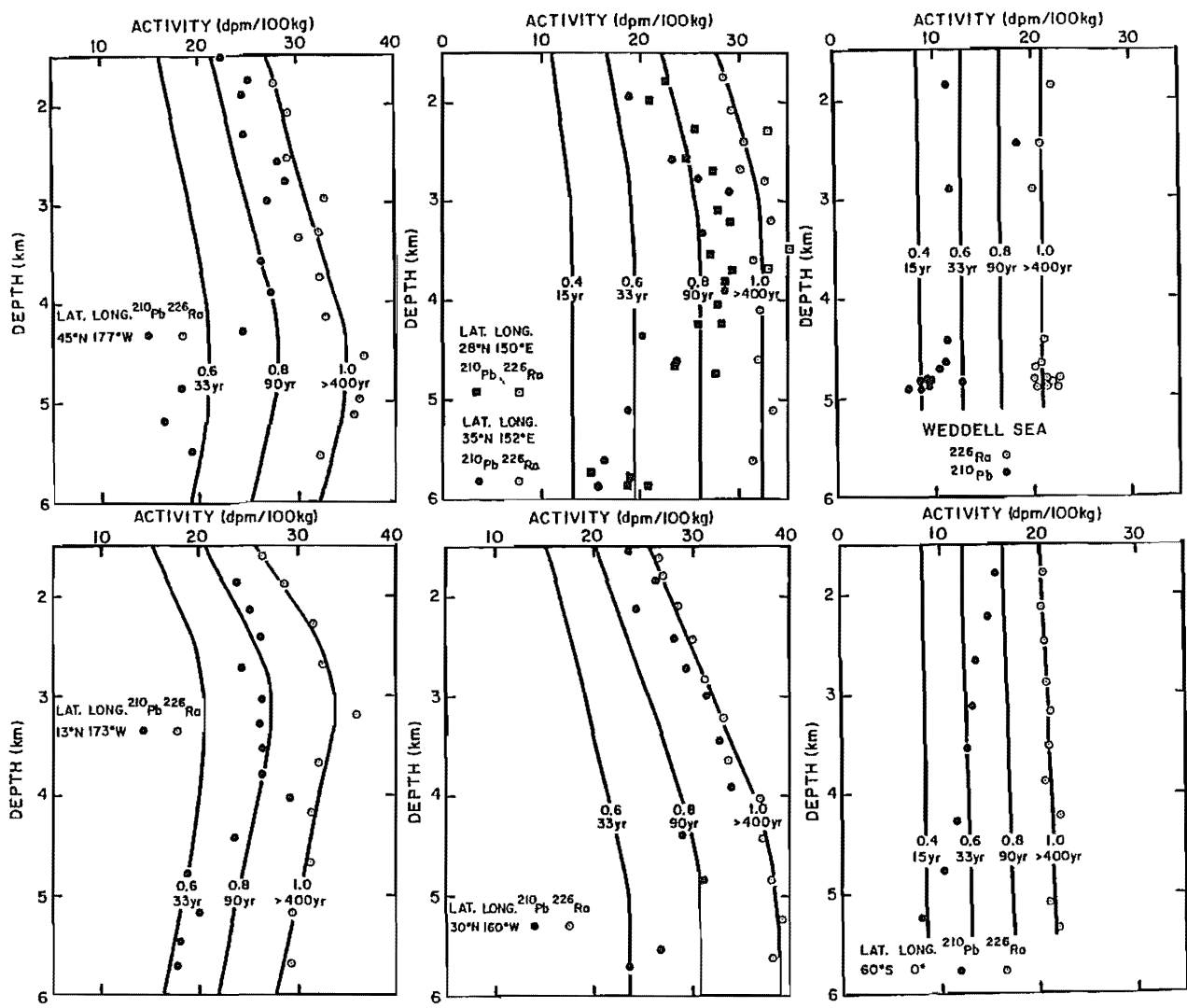


Figure 4-14. ^{226}Ra (open symbols) and ^{210}Pb (closed symbols) activities for water samples taken at various depths in the deep Pacific and Antarctic Oceans. In all cases the deficiency of ^{210}Pb is greater in bottom water than in mid-depth water. The solid curves represent various activity ratios for ^{210}Pb and ^{226}Ra . The 1.0 curve is a best fit to the ^{226}Ra data. The scavenging times (as calculated from equation 4-4) corresponding to these ratios are also given. The ^{226}Ra results are those of Chung at Scripps Institution of Oceanography (117,118,160). The ^{210}Pb results are from the Yale group (158), Hakodate Japan group (152), and the Scripps Institution for Oceanography group (160).

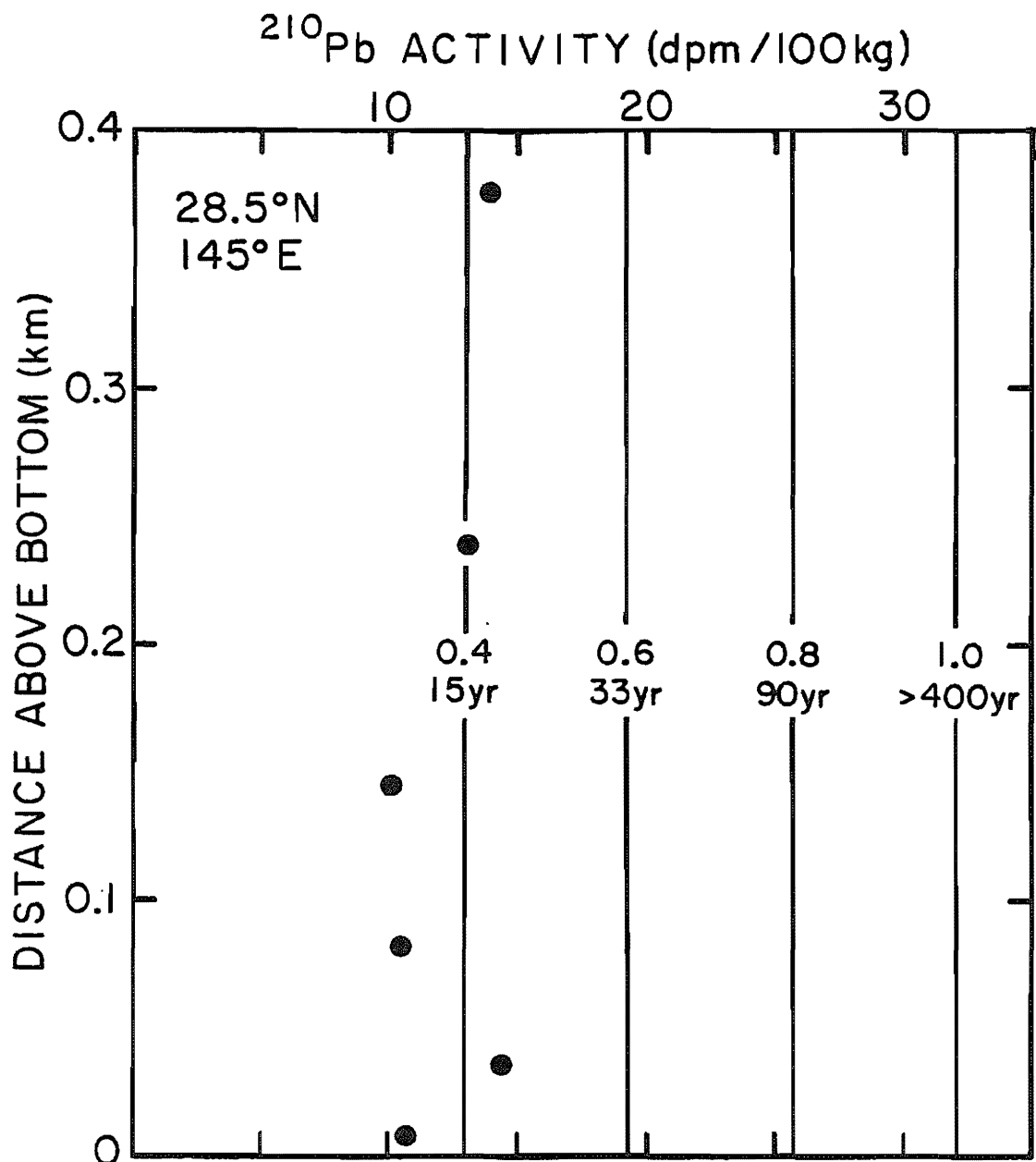


Figure 4-15. Near-bottom ^{210}Pb results for a station in the northwest Pacific. The ^{226}Ra contents were not measured but can be assumed to be the same as the values shown in figure 4-14. The lines represent various $^{210}\text{Pb}/^{226}\text{Ra}$ activity ratios. The ^{210}Pb results were obtained by the group in Hakodate, Japan (152).

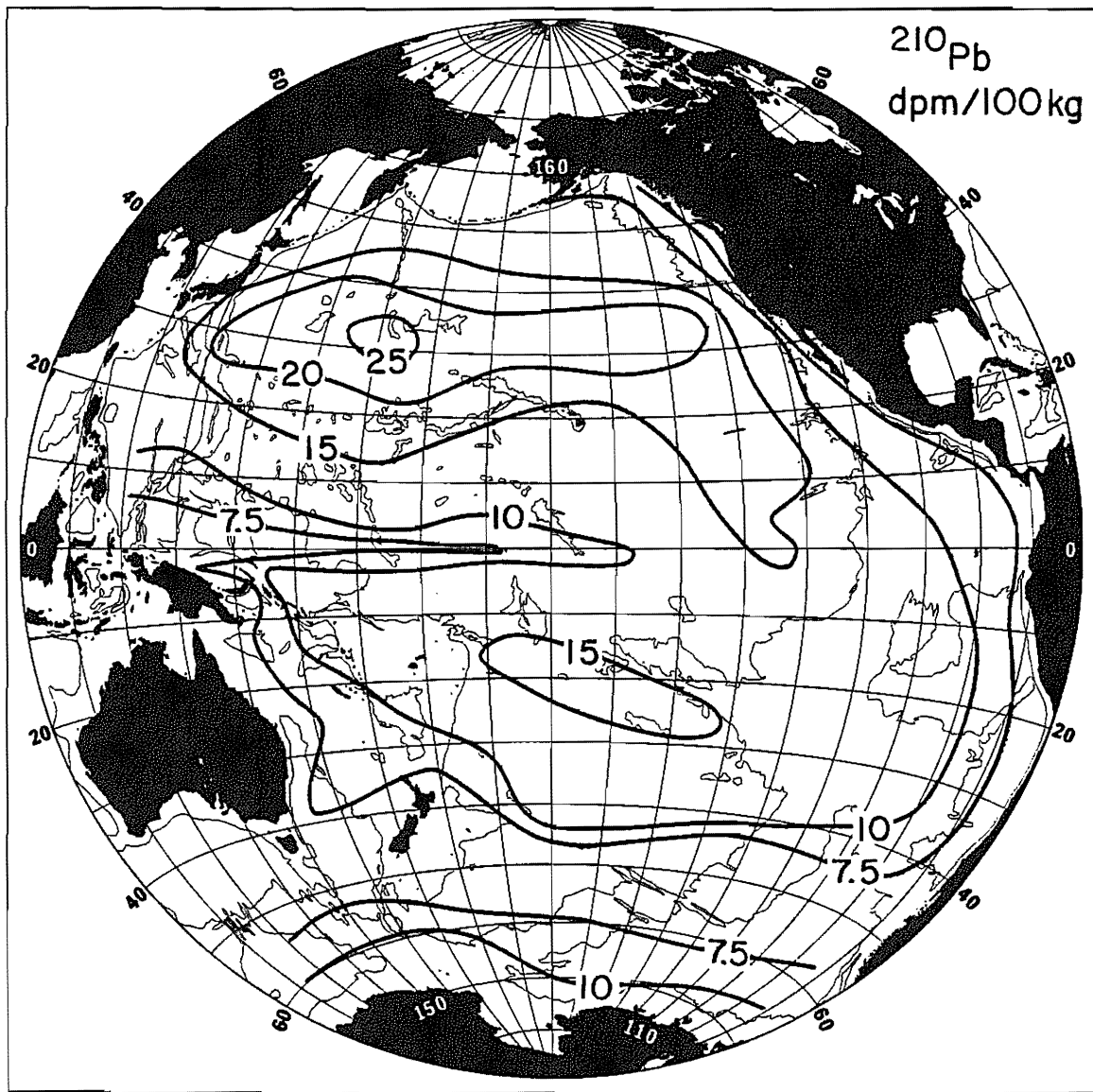


Figure 4-16. Map showing the distribution of ^{210}Pb concentrations (in $\text{dpm}/100\text{ kg}$) in the surface waters of the Pacific Ocean. The results were summarized by Nozaki, Thompson and Turekian (151).

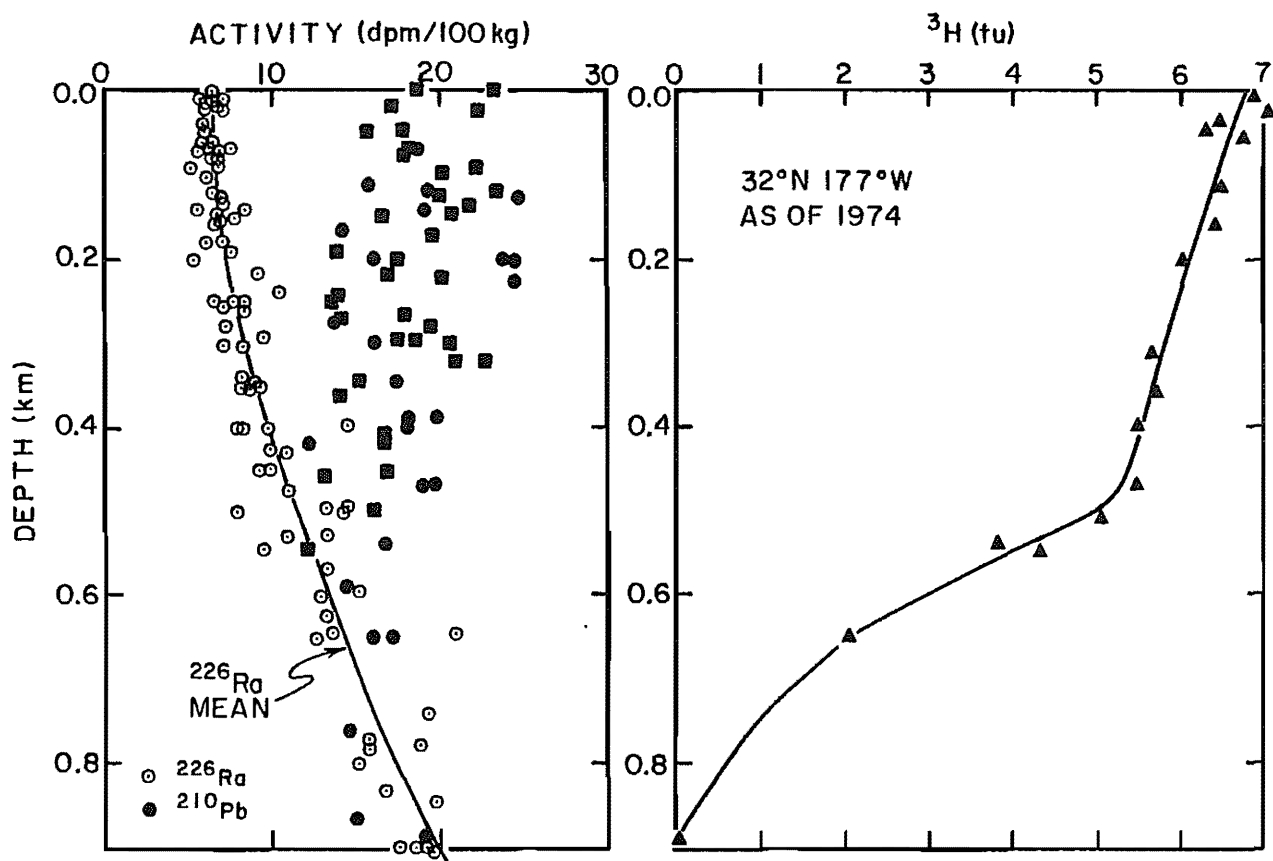


Figure 4-17. The left hand panel shows the vertical distribution of ^{226}Ra and ^{210}Pb activity in the north temperate Pacific Ocean. The solid squares represent ^{210}Pb measurement made by the Japanese and the solid circles ^{210}Pb measurements made as part of the GEOSECS program. Both sets show scatter beyond that seen in other oceanographic data sets. Whether this scatter is the result of problems with the measurements or represents large inhomogeneities in the ^{210}Pb distribution is not known. The open circles represent ^{226}Ra measurements made as part of the GEOSECS program. The right hand panel shows the distribution of tritium with depth in the center of this area as of late 1973. The tritium results were obtained by Ostlund as part of the GEOSECS program (54). The ^{226}Ra results were obtained by Chung of Scripps Institution of Oceanography (118). The ^{210}Pb results were obtained by the Yale group, solid circles, (158) and by the Hakodate Japan group, solid squares, (152).

get a total input of 36 ± 10 atoms/cm² minute. Thus, 25 ± 11 atoms/cm² minute must be lost to raining particles. If so, the average scavenging time for ^{210}Pb in the upper 600 meters of the water column is about 10 years.*

There is one last way to get an estimate of the average water column removal rate of ^{210}Pb . That is to use data from sediment traps. Shown in table 4-7 are the ratios for ^{210}Pb to ^{230}Th atoms caught in deep traps at sites E and S (155a). In both cases about two ^{210}Pb atoms are caught for every 100 ^{230}Th atoms. Based on the water column ^{234}U and ^{226}Ra distributions at these sites, it can be shown that about five ^{210}Pb atoms are produced for each 100 ^{230}Th atoms. Adding in the ^{210}Pb atoms from atmospheric fallout, the ratio rises to 6 ^{210}Pb atoms per 100 ^{230}Th atoms. We know that over 99% of the ^{230}Th atoms produced in the water column rain to the bottom. Hence these results suggest that 33% of the ^{210}Pb atoms rain to the bottom. If so, the apparent scavenging time for lead is 45 years. This result is consistent with the mean water column scavenging time obtained from the ^{210}Pb to ^{226}Ra ratio in water samples.

In the same table are given the atom collection ratios for ^{234}Th and ^{230}Th . Only about six ^{234}Th atoms are caught per 10,000 ^{230}Th atoms. As the two isotopes are produced at nearly the same rate, about 99.94% of the ^{234}Th atoms must decay in the water column! This isotope has a half-life of only 0.066 years, hence the corresponding half-scavenging time is about 100 years. As some of the ^{234}Th atoms undergo decay while riding toward the traps on particles, the removal time from a given level in the ocean would be less than 100 years. Again the result is consistent with that derived from the ^{230}Th and ^{228}Th measurements.

THE DISTRIBUTION OF POLONIUM-210

The last of the parent-daughter pairs to be discussed here is $^{210}\text{Po}-^{210}\text{Pb}$. As shown in figure 4-18, for waters beneath about 100 meters, the activities of the two isotopes are nearly equal. As the half-life of ^{210}Po is 0.38 years, this is to be expected if the scavenging time for polonium in deeper waters is similar to that for lead (i.e., several decades).

In surface waters from both the Atlantic and Pacific (see

* Most workers in this field interpret the ^{210}Pb data to yield a scavenging time for lead atoms in surface water of about one year. This is the answer obtained if all the ^{210}Pb atoms reaching the sea surface through atmospheric fallout are assumed to be removed from surface water by scavenging. This assumption need not be valid. As shown in figure 4-17, tritium (which must move with the water) is carried to a depth of many hundreds of meters on a time scale of 10 years. The mixing processes which carry ^3H atoms to these depths must, of course, also carry ^{210}Pb atoms. A more conservative interpretation of the data is to treat the entire upper water column and conclude that the average scavenging time for lead over this entire interval is 7 years. Only if the scavenging could be shown to occur mainly in the surface mixed layer would the one year scavenging time be appropriate.

Table 4-7. Measurements of uranium series nuclides in sediment trap material obtained by the Woods Hole Geochemistry Group on samples from Honjo's traps (128).

	Site E 5086 meters		Site S 3694 meters	
	$\frac{^{234}\text{Th}}{^{230}\text{Th}}$	$\frac{^{210}\text{Pb}}{^{230}\text{Th}}$	$\frac{^{234}\text{Th}}{^{230}\text{Th}}$	$\frac{^{210}\text{Pb}}{^{230}\text{Th}}$
Atom Ratio in Traps	5.5×10^{-4}	0.021	5.9×10^{-4}	0.018
Prod. Ratio in Water Column**	0.87	0.06	0.87	0.06
Relative Removal Efficiency	6.3×10^{-4}	0.35	6.8×10^{-4}	0.30
Apparent Half Scavenging Time* (Years)	105	42	97	52

*Calculated from equation 4-4.

**To the water column production rate of ^{210}Pb is added an atmospheric delivery of 15 atoms/cm²min at site E and of 25 atoms/cm²min at site S.

figures 4-18 and 4-19), the ^{210}Po activity is significantly lower than that of ^{210}Pb . About 50% of the ^{210}Po appears to have been lost to raining particles. The removal time for polonium is thus about 0.4 years (i.e., similar to that for thorium and significantly less than that for lead).

THE DISTRIBUTION OF RADIUM-226

There is one more member of the uranium series which merits discussion. It is ^{226}Ra , the 1620-year half-life daughter product of ^{230}Th . Among the constituents of the sea, radium is unique in that its input is almost entirely from sediments. Most of the ^{226}Ra present in the sea is the product of the decay of the ^{230}Th which was produced by the decay of ^{234}U dissolved in the sea and carried to the sediment on particulates. As radium is far more soluble than thorium, much of the ^{226}Ra "born" in the upper sediments becomes dissolved in the pore water and diffuses back into the overlying water column. From the average activity ratio of ^{226}Ra to ^{234}U in the sea, it can be shown that about 9 out of every 100 ^{226}Ra atoms produced from the excess ^{230}Th in sediments escapes to the overlying water column.

Because of its half-life of 1620 years, geochemists initially hoped that the distribution of ^{226}Ra might be used as is ^{14}C to determine the rate of ventilation of the deep sea (112). This hope never came to fruition. There are several aspects of the geochemistry of ^{226}Ra which conspire against its use as a time tracer. First, the fact that ^{226}Ra is added from the sea bottom reduces its effectiveness relative to ^{14}C by roughly the ratio of the volume of deep water to the volume of surface water (i.e., about 10). Second, the fact that it is fixed into particles by surface-dwelling organisms necessitates a large correction for particulate transport. Third, its release from sediments shows large geographic variations which are as yet only qualitatively understood.

Radium has no stable isotope which might be used as is ^{12}C to separate the influence of particulate transport from the influence of radioactive decay on the distribution of ^{14}C . However, as the elements Ra and Ba have nearly identical chemistries, we can consider ^{226}Ra to be an "isotope" of barium. As $^{14}\text{C/C}$ ratios are more useful time clocks than absolute ^{14}C concentrations, so also should $^{226}\text{Ra/Ba}$ ratios be more useful time clocks than absolute ^{226}Ra concentrations.

In figure 4-20 is shown a plot of ^{226}Ra versus Ba concentrations for water masses throughout the ocean. The points with the lowest ^{226}Ra and Ba contents are for warm surface waters. Those with the highest values are for bottom waters in the north-eastern Pacific. The reference line has a slope equal to the $^{226}\text{Ra/Ba}$ ratio in surface waters. Were particulate transport the only process perturbing the distributions of ^{226}Ra and Ba in the sea, then the points should all lie along this line. They do not. Most deep waters have more ^{226}Ra than expected from their barium content. These anomalies are particularly large in the case of deep and bottom waters from the eastern Pacific. Any applications of ^{226}Ra as a tracer of ocean processes must be based

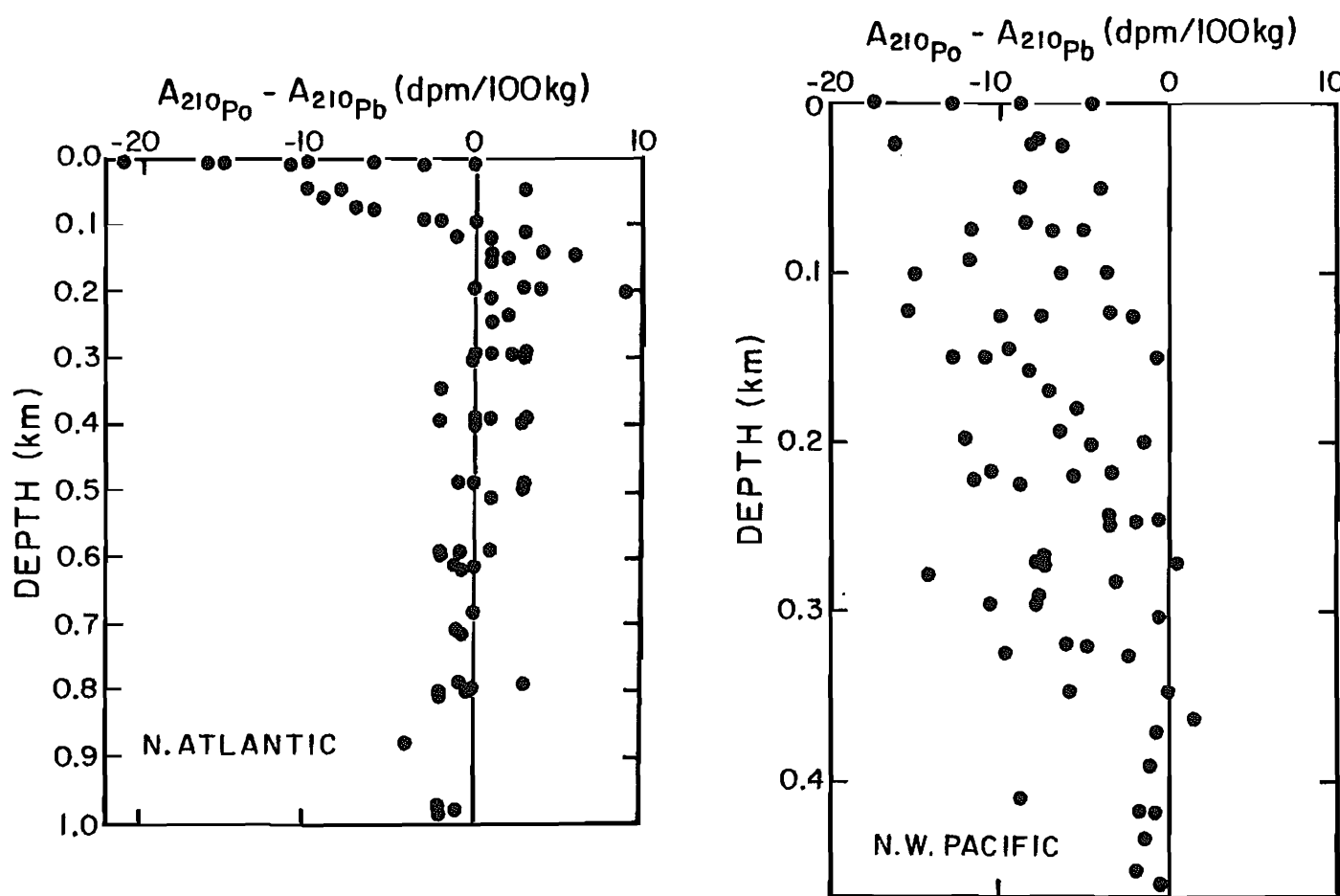


Figure 4-18. Difference between the activity of ^{210}Pb and ^{210}Po as a function of depth in the north temperate Atlantic Ocean. As can be seen surface waters show a deficiency in ^{210}Po activity relative to that of its parent ^{210}Pb . These results were obtained by Bacon and his colleagues at Woods Hole Oceanographic Institution (149).

Figure 4-19. Difference between the activities of ^{210}Pb and its daughter ^{210}Po in the upper water column of the north temperate Pacific. These results were obtained by the Yale (158) and Hakodate Japan (152) groups.

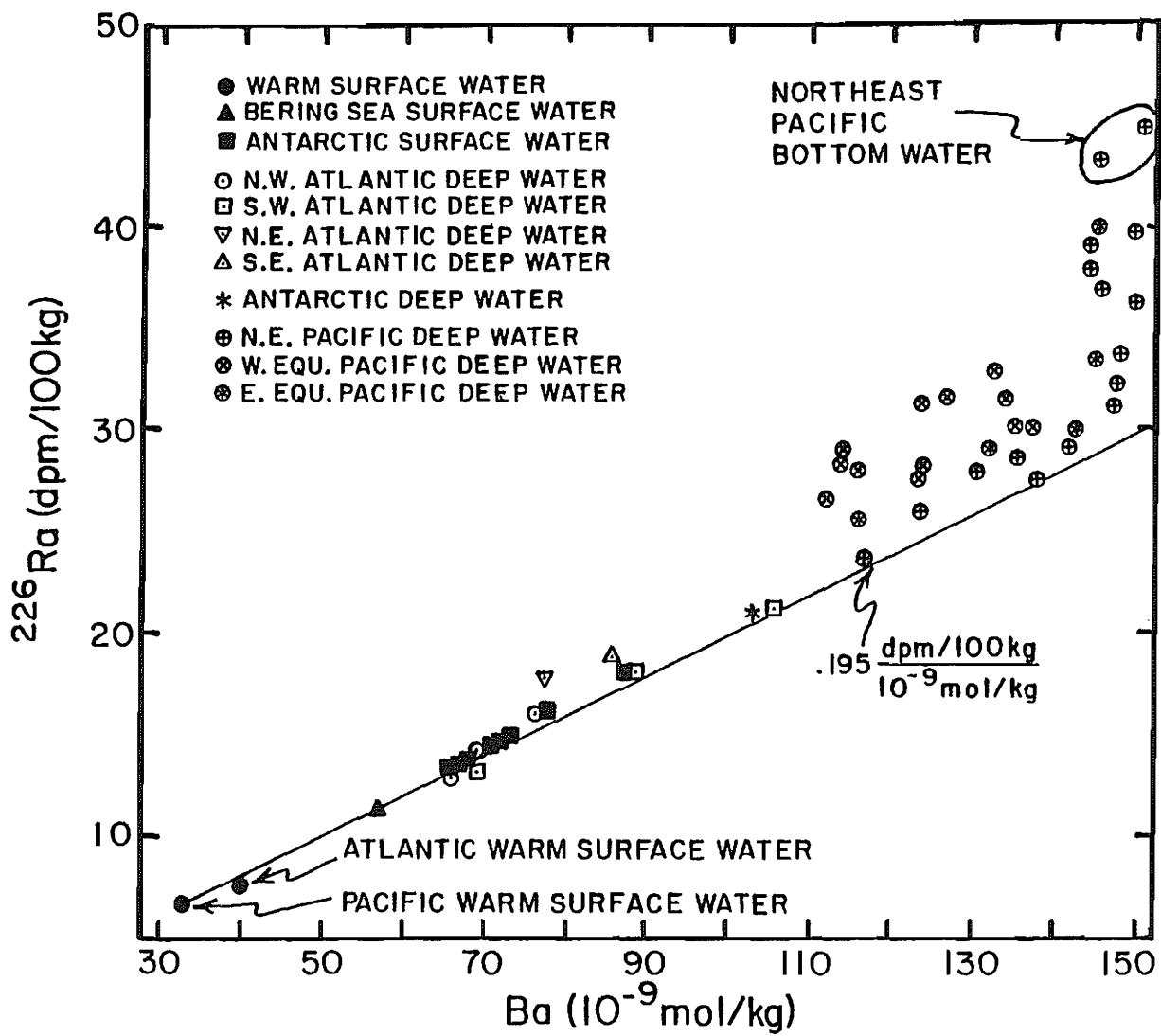


Figure 4-20. Activity of dissolved ^{226}Ra versus concentration of barium in waters from throughout the world ocean, as determined on samples collected as part of the GEOSECS program. The solid line represents the ratio of $^{226}\text{Ra}/\text{Ba}$ in surface waters (and hence in particles formed in surface waters). The barium results were obtained in the laboratories of L. Chan at LSU and of John Edmond at MIT (375). The ^{226}Ra analyses for Atlantic Ocean GEOSECS samples were carried out at the Lamont-Doherty Geological Observatory (116). Those for the Pacific Ocean GEOSECS samples were carried out partly by Chung at the Scripps Institution of Oceanography (117, 118, 160) and partly by Ku at the University of Southern California (114, 119).

on these deviations from the reference line. Were there no deviations, then the distribution of ^{226}Ra would tell us nothing beyond what we have already learned from the distribution of barium.

As we shall show in the next chapter, the radioactive decay of ^{226}Ra cannot explain the large departures from the reference line seen in figure 4-20. Rather they must be caused by a combination of sluggish interchange between various parts of the deep sea and sizable inhomogeneities in the flux of ^{226}Ra from sediments into the sea. In particular, the deep waters in the eastern Pacific must receive a disproportionately large amount of ^{226}Ra .

The flux of ^{226}Ra is not expected to be uniform over the sea floor. The flux of ^{226}Ra must depend on sedimentation rate. The higher the sedimentation rate, the lower the concentration of water column derived ^{230}Th in the sediment. The lower the ^{230}Th concentration in the sediment, the lower the concentration of ^{226}Ra in the sediment pore waters and the lower the diffusive flux of ^{226}Ra atoms into the overlying bottom water. Herein must lie part of the explanation. Due to its great breadth, the Pacific Ocean receives less continental detritus (per unit area) than does the Atlantic Ocean. Also, due to its shallower lysocline, less calcite accumulates in the Pacific Ocean than in the Atlantic Ocean. Consequently sedimentation rates in the Pacific are on the average about one-fifth those in the Atlantic.

The flux of ^{226}Ra from sediments will also depend on the fraction of the ^{226}Ra produced by ^{230}Th decay to be released to the pore water (as opposed to bound in or absorbed onto mineral grains). We have very little knowledge about the dependence of this fraction on sediment type, and hence we cannot predict the regional variability in this factor.

Fortunately, a means of directly measuring the flux of ^{226}Ra atoms from sediments exists. It involves measurements of the activities of both ^{226}Ra and ^{230}Th as a function of depth in marine sediments. Normally the upper 10 or so centimeters of sediment show a deficiency of ^{226}Ra activity. The integrated deficiency of ^{226}Ra activity is a measure of the amount of ^{226}Ra lost from the sediment. Cochran at Yale (121) and Kadko at Lamont-Doherty (120) have made such measurements. Large differences from place to place on the sea floor are found (see table 4-8). Although enough cores have not been measured to permit firm conclusions to be drawn, the cores from the eastern Pacific yield fluxes considerably higher than the global average necessary to maintain the ^{226}Ra inventory in the sea. The Atlantic cores show values lower than this mean. The next step in research in this area must be to better document these patterns of ^{226}Ra input from marine sediments. Only then will the ^{226}Ra anomalies find a meaningful application as an ocean tracer.

ANTHROPOGENIC PLUTONIUM IN THE SEA

As the result of nuclear tests, substantial amounts of the isotopes ^{239}Pu and ^{240}Pu were released to the atmosphere during the last 25 years. Like the ^{210}Pb atoms generated in the atmosphere by the decay of radon, this plutonium is carried by rainfall and by aerosol impact to the earth's surface. Thus a sizable

Table 4-8. Estimates of the ^{226}Ra flux from the sea floor based on measurements of the ^{226}Ra deficiency in deep sea sediment cores. Results obtained mainly by Cochran while at Yale University (121).

Ocean	Lat.	Long.	Sediment Type	Sed. Rate $\frac{\text{cm}}{10^3 \text{ yrs}}$	Flux atoms $\frac{\text{cm}^2}{\text{min}}$
Atl	40°N	33°W	CaCO_3 ooze	2.9	5
Atl	29°S	35°W	CaCO_3 ooze	~0.1	30
Ind	26°S	74°E	CaCO_3 ooze	0.3	60
Ind	14°S	78°E	SiO_2 ooze	0.3	80
Ind	39°S	120°E	Red clay	0.08	60
Ant	53°S	35°E	SiO_2 ooze	1.6	26
Ant	67°S	30°E	Red clay	0.3	45
Pac	9°N	151°W	SiO_2 ooze + clay	0.15	190
Pac**	12°N	137°W	SiO_2 ooze + clay	~0.1	420
Pac	11°N	139°W	SiO_2 ooze + clay	~0.1	400
Pac	15°N	126°W	SiO_2 ooze + clay	~0.1	500
World Average*					80

*Average flux of ^{226}Ra from sediments necessary to balance the decay of ^{226}Ra within the sea.

**Result by Kadko of the Lamont-Doherty Geological Observatory (120).

fraction of this plutonium now resides in the ocean. As shown in figure 4-21, a survey of the Pacific Ocean made by Vaughan Bowen and his associates at Woods Hole Oceanographic Institution as part of the GEOSECS program reveals that as of 1974 plutonium resided largely at intermediate depths (164). Like ^{228}Th , ^{239}Pu and ^{240}Pu must be removed onto particles in surface water and then at least in part released from these particles as they pass through the main thermocline. Again it seems reasonable to invoke uptake by plants followed by release from falling fecal material for this distribution.

The sediment trap results obtained in the Pacific (see figure 4-22) show that not all the plutonium-bearing particles are destroyed in the thermocline (134). The fact that more plutonium was caught in the three traps deployed in deep water than in the two deployed in the thermocline clearly demonstrates that some of the particles (fecal pellets) fall straight through to the bottom.

TOWARD A MODEL OF METAL TRANSPORT

Let us now sit back and try to generalize these findings. Our first lesson has to do with the implications of reversible absorption. This is best done by considering an aquarium filled with sea water. A pump keeps the water well mixed. Water that flows into the aquarium carries particles and tracer metals. This inflow just balances evaporation so the volume doesn't change. The particles settle to the bottom carrying an equilibrium amount of the tracer metals. Once on the bottom the tracers are assumed to remain permanently bound on the particles. The system is allowed to run until steady state is reached (i.e., the metal tracers leave at the same rate they are added). Let us see what determines the residence time of a given metal tracer in this aquarium. The residence time, τ , is given by:

$$\tau = \frac{C_a V}{C_i I} \quad 4-12$$

where C_a and C_i are respectively the concentrations of the tracer in the aquarium and in the inflow, V is the volume of the aquarium and I is the inflow rate of water.

If the amount of a given metal leaving the tank is to equal the amount entering, then:

$$C_i I = C_p S \quad 4-13$$

where C_p is the concentration of the metal on the particles and S is the flux of particles into the tank.

If equilibrium is achieved between the particles and the water, then:

$$C_p = K C_a \quad 4-14$$

where K is the distribution coefficient of the metal between water and particles.

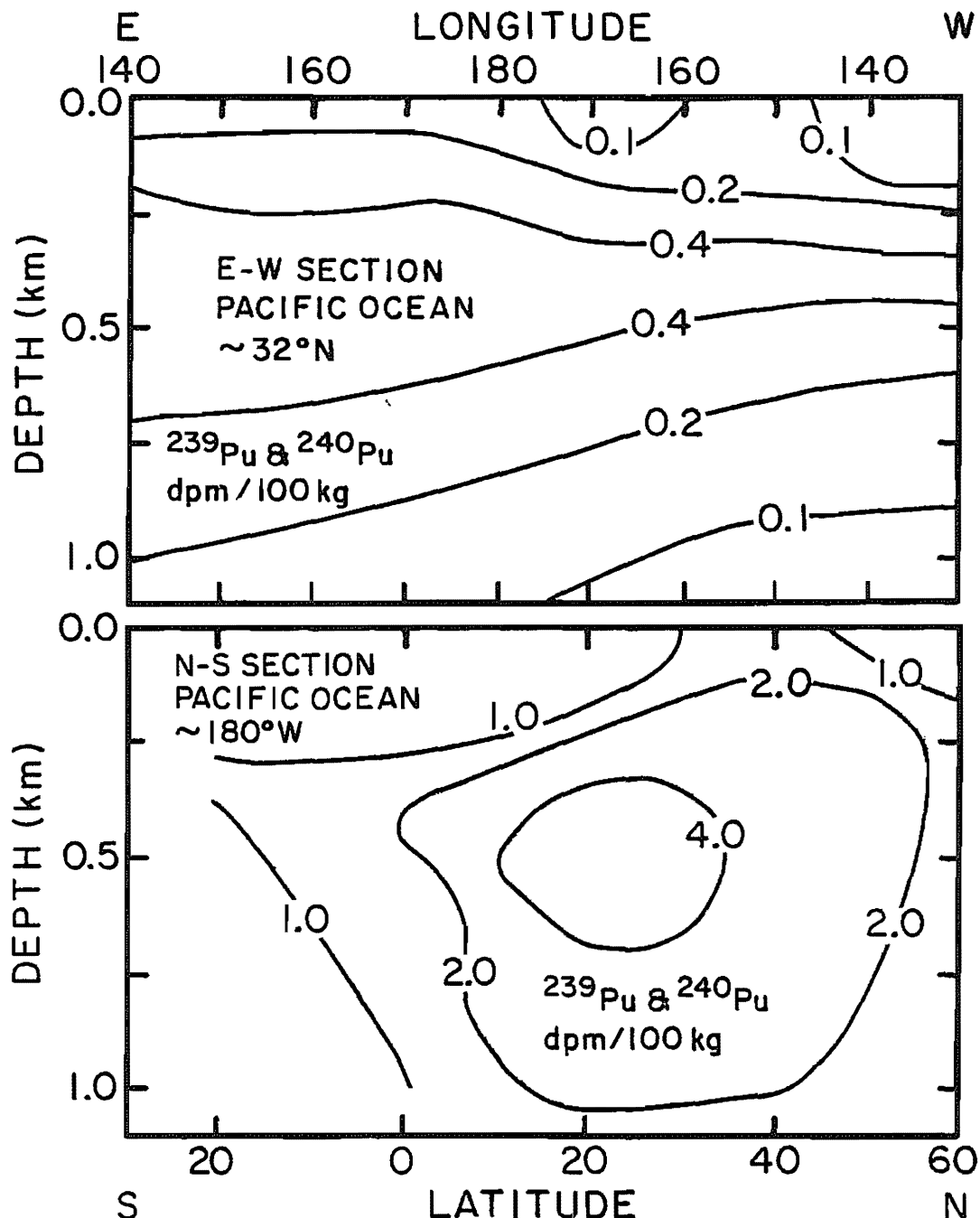


Figure 4-21. Sections of the concentration of dissolved ^{239}Pu plus ^{240}Pu across the North Pacific (upper) and along the international dateline in the North Pacific (lower). The contours are in dpm/100 kg. The concentration of ^{239}Pu and ^{240}Pu are summed because the α spectrometric technique used for the measurements does not resolve these two isotopes. These measurements were made by Bowen and his colleagues at Woods Hole Oceanographic (109).

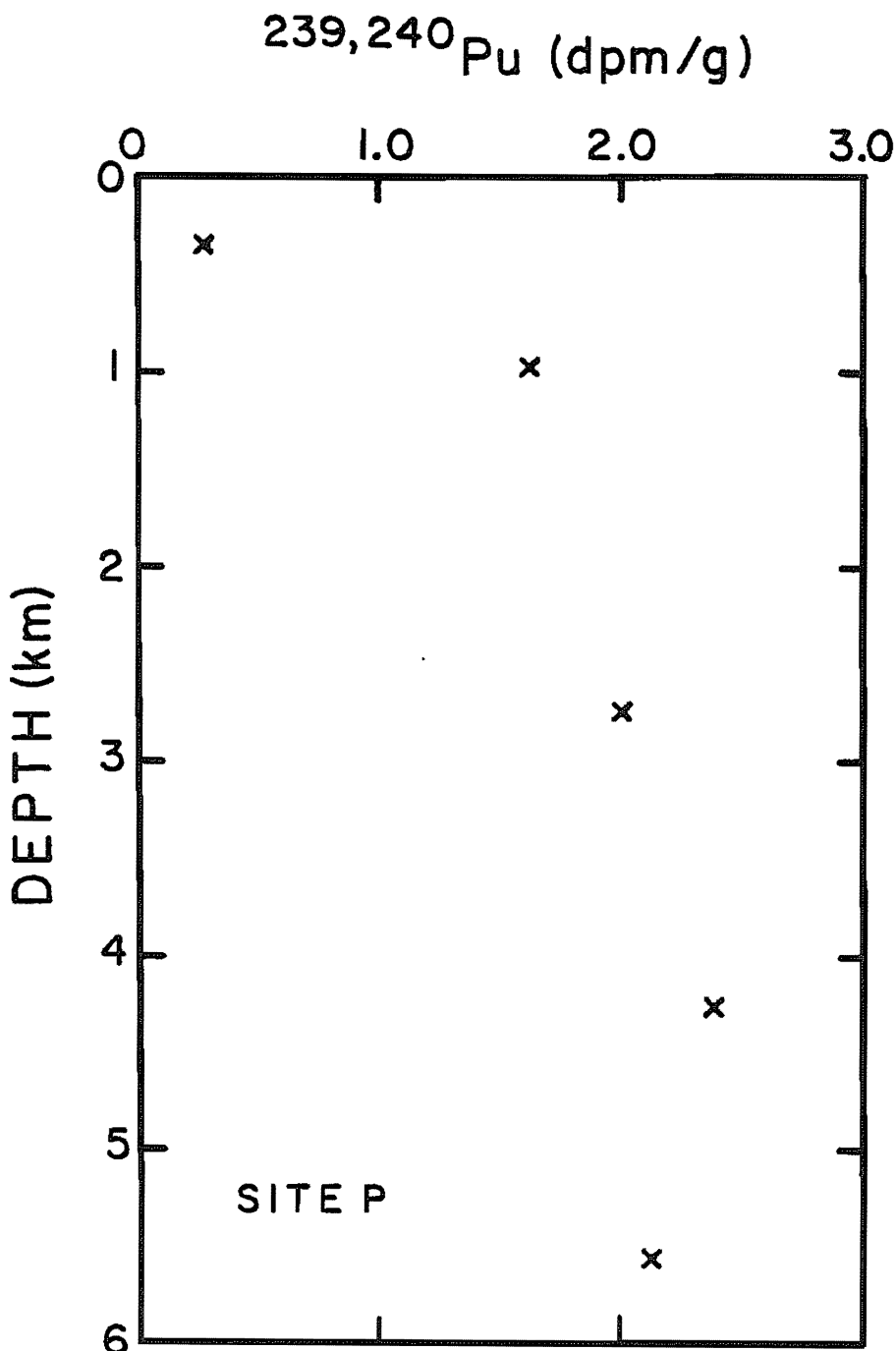


Figure 4-22. Concentrations of ^{239}Pu and ^{240}Pu on material caught in sediment traps deployed at various water depths at site P at 20°N and 150°W in the North Pacific. These measurements were made by Anderson at Woods Hole Oceanographic (134).

Combining these equations, we get:

$$\tau = \frac{V}{KS}$$

4-15

Thus the residence time is inversely proportional to the particle flux and to the distribution coefficient. The inverse dependence on the particle flux is certainly in accord with the evidence given above. The distribution coefficient dependence could explain the difference in residence time from one metal to another. We shall have more to say about the dependence of K on the chemical properties of metals.

Our second lesson is based on the observations that the flux of particles shows strong lateral gradients and that the time for mixing along isopycnal surfaces is of the same magnitude as the time for removal of the reactive metals we have been discussing. To understand the implications of these observations we will consider a model consisting of two coupled aquaria. As shown in figure 4-23, water is pumped back and forth between these aquaria. Half of the particle flux is added to the smaller (i.e., coastal) aquarium and half to the larger (i.e., open ocean) aquarium. The metals are added in proportion to the volumes of the reservoirs (i.e., 10% to the coastal and 90% to the open ocean aquarium).

The equations governing the metal concentrations in the two reservoirs are as follows. First for steady state throughput of the metals:

$$M = 0.5 S K (C_c + C_o)$$

4-16

and for steady state in the open ocean reservoir:

$$0.9M + TC_c = 0.5 SKC_o + TCO_o$$

4-17

where M is the total flux of a given metal to the aquaria, S is the total particle flux, T is the water transfer rate, K is the distribution coefficient, and C_c and C_o are the steady state concentrations of the metal in the coastal and open ocean aquarium, respectively. These equations can be solved simultaneously, yielding:

$$C_c = \frac{M}{SK} \left[2 - \frac{0.9SK + 2T}{0.5SK + 2T} \right] \quad 4-18$$

and

$$C_o = \frac{M}{SK} \left[\frac{0.9SK + 2T}{0.5SK + 2T} \right] \quad 4-19$$

If the area of the bottom of the coastal reservoir is one tenth the total area and that of the open ocean reservoir is nine tenths the total area then the ratio of the rain rate per unit area onto the floor of the coastal aquarium, R_c , to the rain rate per unit area onto the floor of the open ocean aquarium, R_o , is as

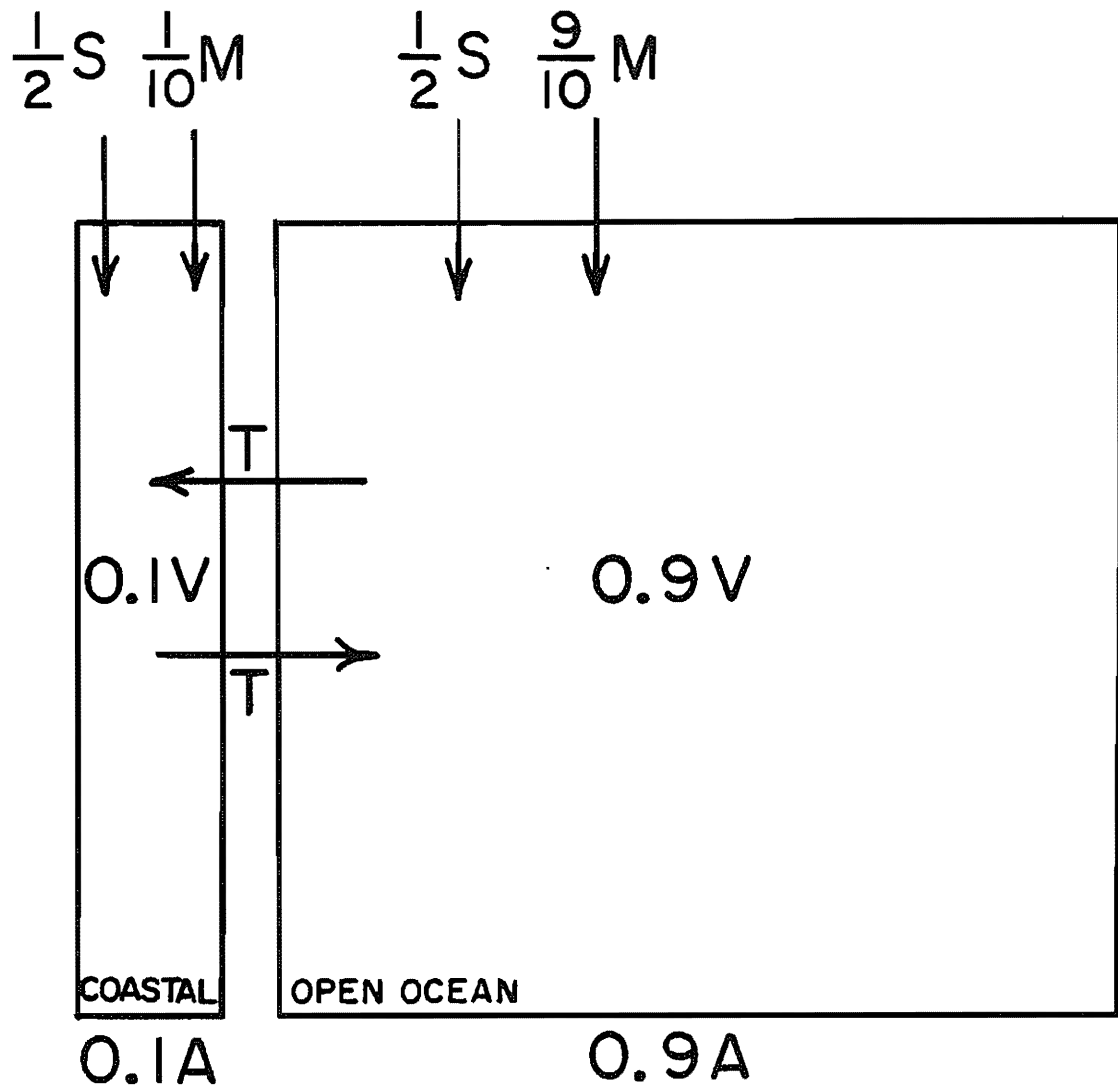


Figure 4-23. Two-box model designed to show the interaction between lateral mixing and a geographically non-uniform particle flux.

follows:

$$\frac{R_c}{R_o} = \frac{0.5 SKC_c/A_c}{0.5 SKC_o/A_o} = 9$$

$$2 - \left[\frac{\frac{0.9 + 2 \frac{T}{SK}}{0.5 + 2 \frac{T}{SK}}}{\frac{0.9 + 2 \frac{T}{SK}}{0.5 + 2 \frac{T}{SK}}} \right]$$

4-20

The rain rate ratio for various combinations of lateral mixing rate (i.e., T) and particle rain rate (i.e., S) is as follows:

T/SK	0	0.3	1	3	∞
R _c /R _o	1	4.2	6.5	8	9

Further if we compare the results for two metals which have K values differing by a factor of three, one yielding a T/SK of 0.3 and the other a T/SK of 1, the rain rate ratio of the two isotopes (i.e., R_c/R_o) would differ by a factor of 1.5. The metal with the higher K would have more similar rain rates in the two reservoirs than the one with the lower K. Thus we see in a more quantitative way how the lateral separation between ²³⁰Th and ²³¹Pa observed in the ocean might be accomplished.

Our third lesson has to do with the use of the distributions of short-lived tracers to tell us about recycling from the sea floor. The point to be made is that these distributions are misleading in this regard. To do this let us consider a large, cone-shaped tank filled with sea water. A stirring device keeps the water well mixed.

Particles are metered into the water at a constant rate. These particles settle to the bottom and become part of the sediment. They are allowed to accumulate until the plug of sediment at the apex of the cone reaches a certain mass. At this point devices are installed which mix the sediment and which remove a fixed fraction of the sediment each hour. The fraction is set so that the amount removed just matches the rain of new material. At this point a metering device is turned on which adds three isotopes of the same element to the surface of the water. Two isotopes are radioactive with differing half-lives. One is stable. The system is then allowed to run until the tracer distributions come to steady state. The operational characteristics of the system and the half-lives of the radiotracers are given in table 4-9.

Let us consider the situation where scavenging is irreversible and the removal probability of the tracers from the water column is 0.10 per hour. In this case the amount of a given isotope in the water, M_W, would be given by:

Table 4-9. Operational characteristics of the three-isotope tracer experiment described in the text.

Volume	1.00 Cubic meters
Steady State Sediment Load	1.00 grams
Sediment Addition Rate	1.00×10^{-3} grams/hr
τ Sediment	1000 hrs
$\tau_{1/2}$ Sediment	693 hrs
τ Radioisotope A	10 hrs
$\tau_{1/2}$ Radioisotope A	6.93 hrs
τ Radioisotope B	100 hrs
$\tau_{1/2}$ Radioisotope B	69.3 hrs.

Table 4-10. Summary of results from the example designed to demonstrate the insensitivity of short-lived tracers as indicators of recycling.

	Short-lived Isotope	Long-lived Isotope	Stable Isotope
In Water			
No Recycling	5.0 R	9 R	10 R
Recycling	5.2 R	16 R	110 R
In Sediment Mixed Layer			
No Recycling	5.0 R	82 R	1000 R
Recycling	4.7 R	76 R	1000 R
Total			
No Recycling	10 R	91 R	1010 R
Recycling	9.9 R	92 R	1110 R

$$M_A^W = R \frac{1}{0.10+0.10} = 5R$$

4-21

$$M_B^W = R \frac{1}{0.10+0.01} = 9R$$

4-22

$$M_C^W = R \frac{1}{0.10+0.00} = 10R$$

4-23

where R is the rate at which each metal is added to the system and A, B, C refer respectively to the short-lived, long-lived and stable isotope. The left hand number in the denominator is the scavenging probability; the right hand number is the radiodecay probability.

The steady state amount of a given isotope in the sediment M_S is given by:

$$M_A^S = 0.5R \frac{1}{0.001+0.100} = 5R$$

4-24

$$M_B^S = 0.9R \frac{1}{0.001+0.010} = 82R$$

4-25

$$M_C^S = 1.0R \frac{1}{0.001+0.000} = 1000R$$

4-26

The left hand number in the denominator is the sediment removal probability; the right hand number is the decay probability. The number preceding R is the fraction of the isotope reaching the sediment (as opposed to undergoing radiodecay while in the water).

Now let us consider how things change if recycling occurs. We will assume that one-hundredth of the sediment burden of the isotope is recycled back to the water each hour. In this case, at steady state the following mass balance equations apply. For the water:

$$R + 0.01M_S^S = (0.10 + \lambda)M_W^W \quad 4-27$$

where the terms on the left give, respectively, the amount of new material added to the water each hour and the amount recycled from the sediment each hour, and the term on the right gives the amount of the isotope removed from the water by scavenging and radiodecay each hour.

For the sediment the steady state balance is given by:

$$0.1 M_W^W = (0.001 + 0.01 + \lambda) M_S^S \quad 4-28$$

where the term on the left is the addition rate from the water, and the term on the right is the loss rate via sediment removal, recycling and radiodecay.

Simultaneous solution of these equations yields:

$$\begin{aligned}M_A^W &= 5.2R \\M_B^W &= 16R \\M_C^W &= 110R\end{aligned}$$

and

$$\begin{aligned}M_A^S &= 4.7R \\M_B^S &= 76R \\M_C^S &= 1000R\end{aligned}$$

A comparison of these results with those from the simple scavenging case (see table 4-10) reveals that for the short-lived isotope the contribution of recycling is only 4% of the total input. For the long-lived isotope the contribution of recycling constitutes about 50% of the total input. For the stable isotope the recycling constitutes 91% of the total input.

Because of the manner in which the sediment at the base of the cone was handled (i.e., it was stirred and also gradually replaced), one might ask whether this example has anything to do with the real ocean. As we shall see in the next chapter, real sediments are indeed much like our example. Burrowing organisms keep the upper 5 to 10 cm of the sediment well mixed. As new sediment is added, material gets buried beyond the reach of these burrowers. Hence, as in our cone, there is a reservoir of stirred material from which recycling may occur. The residence time of material in this bioturbated layer ranges from about 3500 years for carbonate oozes to about 20,000 years for red clays.

Any radiotracer with a half-life much smaller than the replacement time of the material in the bioturbated layer at the top of the sediment will not provide valid information regarding the recycling of its long-lived or stable counterparts. ^{210}Pb provides a good example. With a half-life of only 22 years it will act much like the short-lived tracer in our example. Its distribution in the sea has nothing to tell us about the extent to which stable lead is recycled from the sea floor. On the other hand, the distributions of ^{230}Th and ^{231}Pa , which have mean lives greater than the residence time of material in the sediment mixed layer, do carry information about recycling.

Our fourth lesson is based on the observation that the distributions of the two airborne tracers, ^{210}Pb and $^{239},^{240}\text{Pu}$, show a prominent difference. The concentration of ^{210}Pb is slightly higher at the surface than at 400 meters, while that of $^{239},^{240}\text{Pu}$ is higher at 400 meters than at the surface. What is this telling us about the difference in behavior of lead and plutonium?

To understand this, let us consider the two-reservoir system shown in figure 4-24. Radioisotopes are added to the upper reservoir at the rate M . Consistent with the findings from the distribution of bomb-produced tritium, we allow the waters in the upper reservoir to mix with those in the lower reservoir. The metals added to the upper reservoir are assumed to be in part

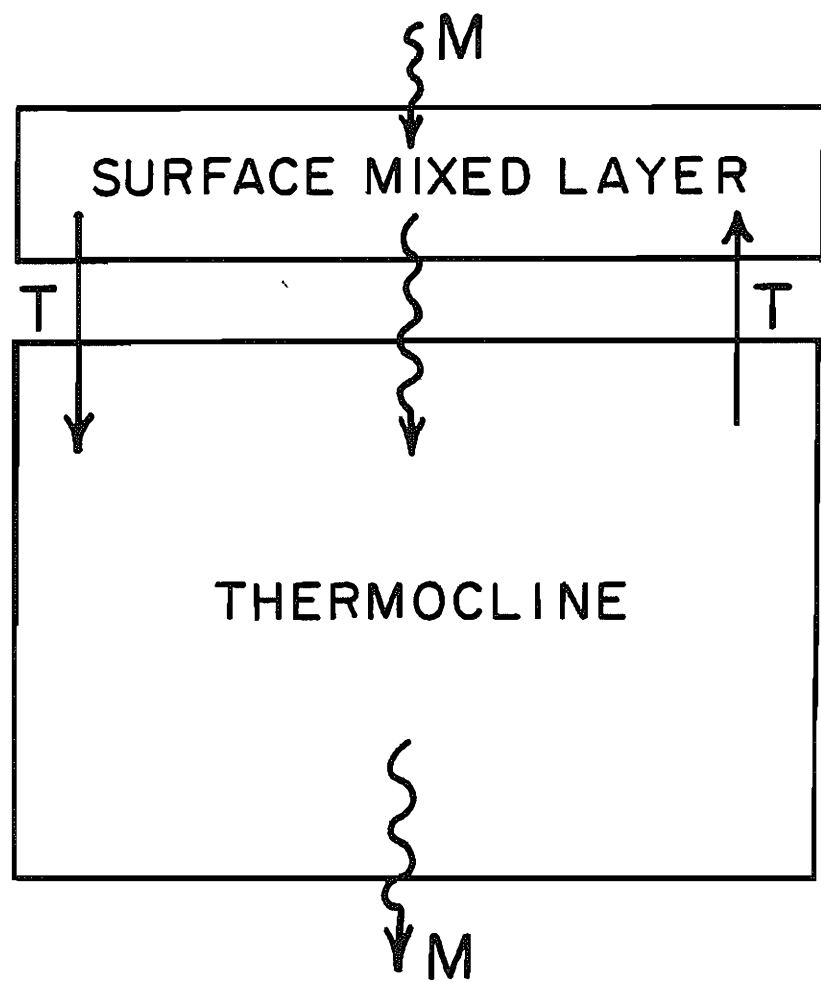


Figure 4-24. Two-box model designed to show the interaction between vertical mixing and a step-wise downward transport of metals on particulate debris.

extracted from the water by plants and transferred on particles to the lower reservoir, where the tracers are once again released to the water. In the lower reservoir they become attached to raining particles and are gradually carried to the deep sea.

Neglecting radiodecay, the mass balance of the tracer in the upper reservoir is given by:

$$M + C_L T = C_U T + C_U f_U V_U \quad 4-29$$

where M is the metal addition rate, T is the water transfer rate, f_U is the fraction of the metal incorporated in plant matter in a unit time, V_U is the volume of the mixed layer and C_U and C_L are respectively the concentrations of the metals in the upper and lower reservoirs.

The mass balance of the metal in the lower reservoir is given by:

$$C_U T + C_U f_U V_U = C_L f_L V_L + C_L T \quad 4-30$$

where f_L is the fraction of the material in the lower reservoir carried away on particulate matter per unit time, and V_L is the volume of the lower reservoir.

Based on the simultaneous solution of these two equations, the ratio of the concentration of the metal in the waters of the lower reservoir to that in the upper reservoir can be shown to be:

$$\frac{C_L}{C_U} = \frac{T + f_U V_U}{T + f_L V_L} \quad 4-31$$

Thus, if T is much larger than $f_L V_L$ and $f_U V_U$, then the concentrations in the two reservoirs will be equal. If T is small compared to $f_U V_U$ and $f_L V_L$ then the concentration ratio will depend on the ratio of these two terms. For example if $f_U V_U$ is greater than $f_L V_L$, then the concentration of the metal in the thermocline reservoir will be higher than that in the mixed layer. This is the situation for plutonium. Thus it appears that plutonium has a residence time in the oceanic mixed layer with respect to removal on particles which is much smaller than that for lead.

There is, of course, an important difference between the situations for $^{239},^{240}\text{Pu}$ and ^{210}Pb . The former was added over a short period of time about a decade before the GEOSECS survey was made. The latter has been added continuously. Thus it might be argued that the difference in the vertical distribution of these two tracers reflects their time histories rather than their particulate affinities. While this may be the case, in our estimation the distribution difference is too large to be accounted for by the time histories alone.

DISTRIBUTIONS OF STABLE METALS IN THE SEA

Let us now consider the distributions of stable trace metals in the sea. Thanks to the superb work of Bruland and his co-

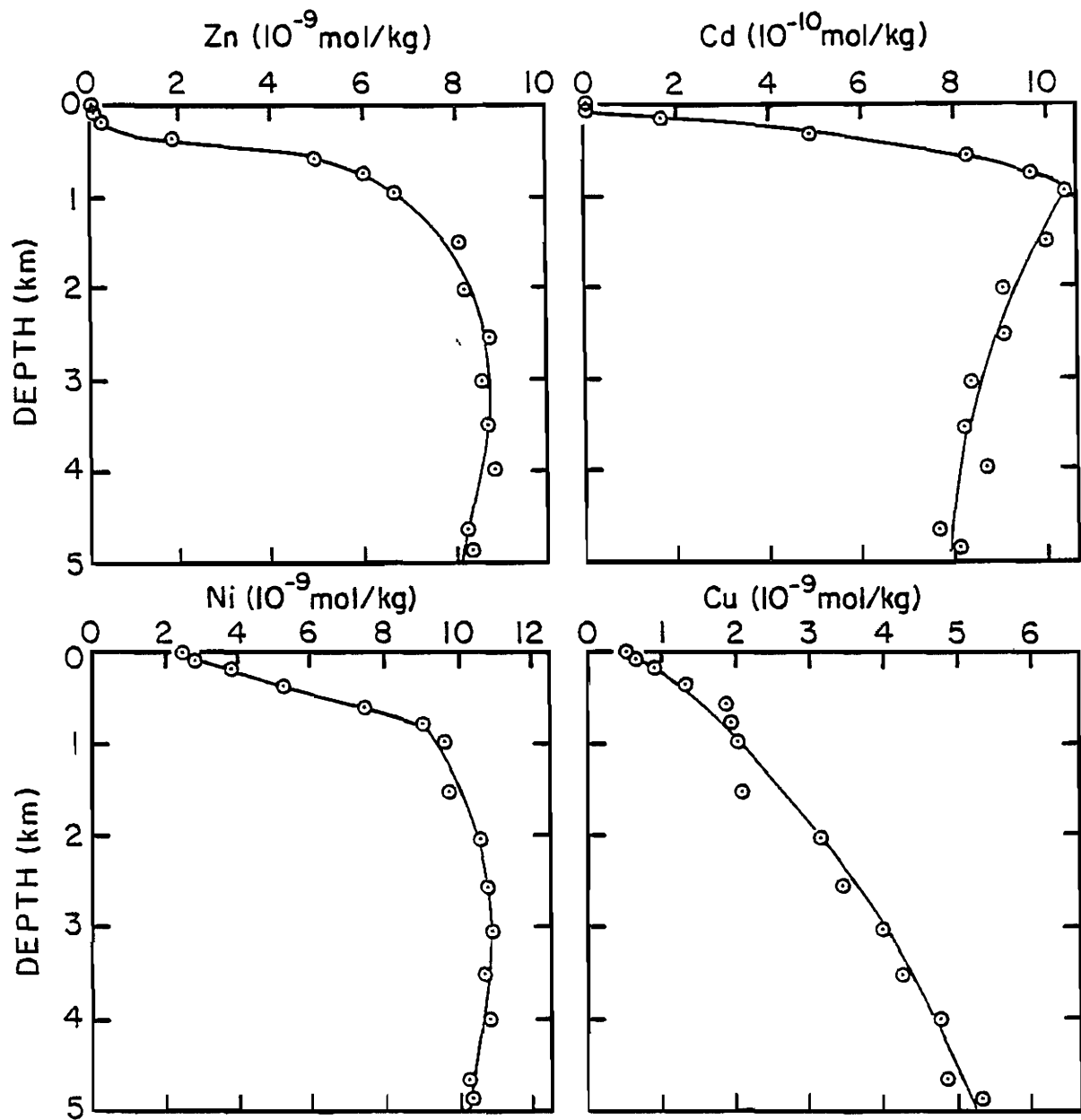


Figure 4-25. Plots of dissolved Zn, Cd, Ni and Cu as a function of depth in the central North Pacific. These results were obtained by Bruland and his coworkers at the University of California at Santa Cruz (455).

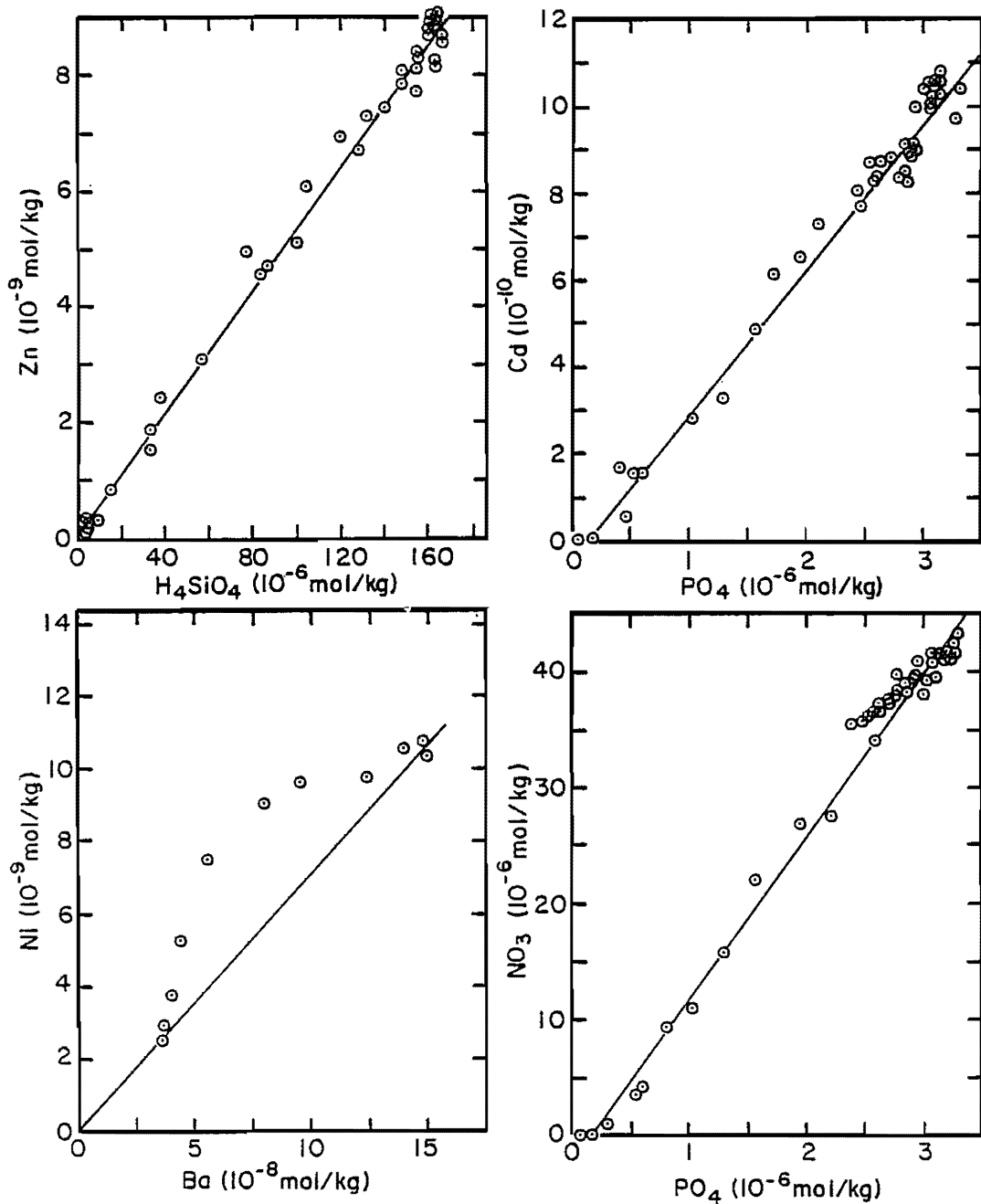


Figure 4-26. Plots of the data shown in figure 4-25 against that for nutrient elements showing similarities in their depth distribution. For the pairs $Zn-H_4\text{SiO}_4$ and $Cd-\text{PO}_4$ the covariance is almost perfect (better, for example, than even that for NO_3-PO_4 shown at the lower right). By contrast the plot for Ni versus Ba is quite nonlinear. Thus, while Ni and Ba are both biointermediate elements showing about the same removal fraction in surface waters, their release patterns from particles cannot be the same.

workers at the University of California at Santa Cruz, there are four metals for which excellent data are available (455). As shown in figure 4-25, the vertical distributions of Zn, Cd, Ni and Cu in the North Pacific Ocean are similar to those for the nutrient constituents. In fact, that for Cd has precisely the shape of that for PO₄ (see figure 4-26), and that for Zn has precisely the same shape as that for H₄SiO₄ (see figure 4-26). These resemblances require that both Cd and Zn be totally removed onto particulate matter in the surface ocean and that they have regeneration functions identical to those for PO₄ and H₄SiO₄. As shown in figure 4-26, Bruland and his coworkers demonstrated that the correlation between Cd and PO₄ is even better than that between NO₃ and PO₄. While there is no simple biological or chemical explanation for these findings, they do tell us that the formation and destruction of living matter must be very important in determining the pathways followed by these elements through the sea.

Nickel is a biointermediate element. Its concentration in warm surface is about 20% that in deep Pacific water. In this regard it is similar to barium. However, as shown in figure 4-26, the two distributions do not correlate as do those of Cd and PO₄ and of Zn and H₄SiO₄. As can be seen in figure 4-25, the shape of nickel versus depth curve is similar to that of Cd in the upper 1000 meters and that of Zn in deep water.

Copper (figure 4-25) shows a rather regular increase from surface to deep water. Its pattern is not a replica of that of any of the nutrient constituents. The copper content of surface water in the North Pacific averages about 10% that in bottom water. Hence, using the definitions given in the first chapter, Cu is also a biointermediate element. The shape of the copper profile has a characteristic not found for any nutrient. When plotted against potential temperature, the curve has a concave shape (see figure 4-27). The copper content of the water for any intermediate temperature is less than would be expected from mixing the overlying and underlying water. By contrast, the other constituents whose profiles we have examined all show a convex shape when plotted against potential temperature (i.e., the contents of these constituents is greater at any given depth than would be expected from the mixing of overlying and underlying waters). Thus there must be a net removal of copper from the interior of the deep water column and a net addition of the other components.

Patterson and Schaule of Cal Tech (436) have carried out a very difficult set of measurements on a fifth metal, lead. As shown in figure 4-28, its vertical distribution in the North Pacific is very different from that of four other elements studied by Bruland and his coworkers. Its high concentration in the upper waters must be anthropogenic in origin. It comes mainly from the anti-knock lead additive which, until a few years ago, was used in all gasolines. Stable lead is distributed with depth in a similar manner to anthropogenic tritium!

The analogy between the distributions of Cd and PO₄ and between Zn and H₄SiO₄ strongly suggest that these metals are recycled many times within the sea as are the nutrient elements. Were this not the case, then the signatures of the inputs of these

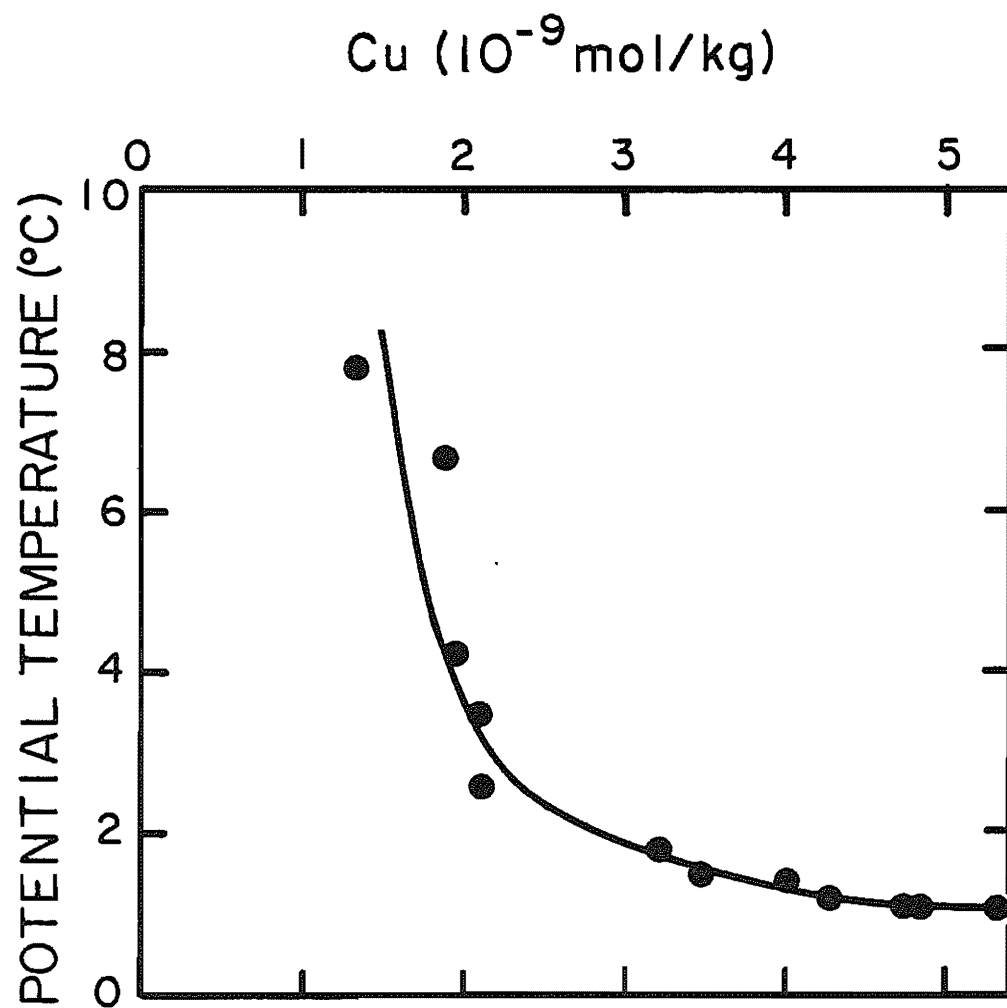


Figure 4-27. Plot of the Bruland et al. dissolved copper concentration data as a function of potential temperature in the central North Pacific. The concave shape requires that a net scavenging of copper occurs in the deep water column.

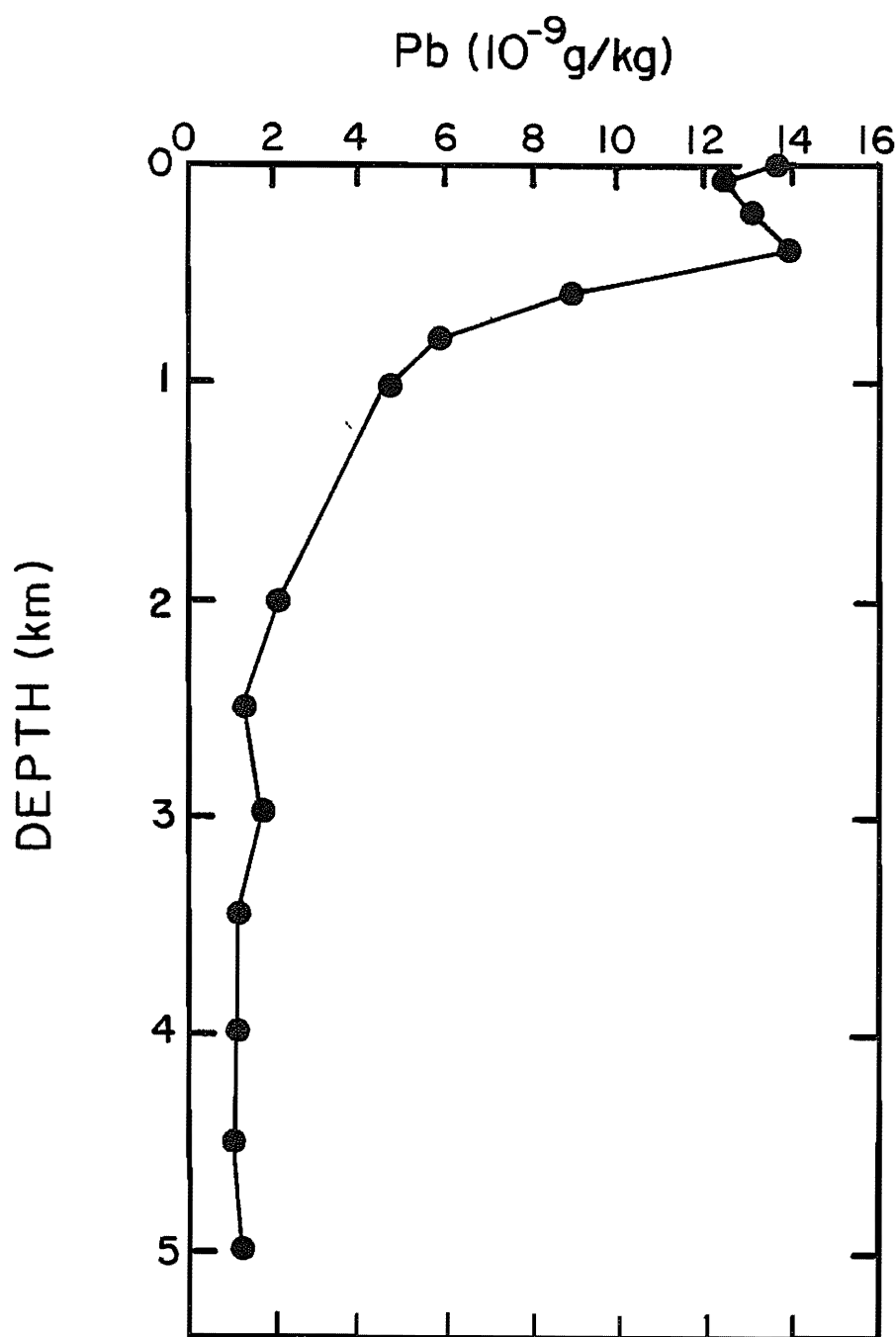


Figure 4-28. Distribution of dissolved lead with depth in the north temperate Pacific Ocean. The excess for the upper waters is thought to represent pollution (i.e., lead from gasoline). These measurements were made by Patterson and Schaule at California Institute of Technology (436).

elements to the sea would disturb the correlations. In this regard Zn and Cd appear to differ greatly from Th and Pb, which give the appearance of being removed rapidly and irreversibly from the sea. This basic difference is confirmed by the estimates of river input given in table 4-11. Although the river data (obtained by Ed Boyle and his coworkers at MIT, 632) is for the Amazon only, there is no question that Cd, Cu and Ni reside in the sea longer than the ocean's mixing time.

One last point should be made about these five metals before going on. They all show unexpectedly high concentrations in atmospheric dust and aerosols. In table 4-12 the ratio of the concentrations of these five metals to aluminum in material filtered from the air and in residues from polar ice is compared to their ratio in average crustal material. In all cases these five elements are greatly enriched. While the enrichment for lead in the air samples and in the ice sample from Antarctica is likely the result of contamination with gasoline lead, that in the pre-1900 ice sample from Greenland suggests that lead also shows a natural enrichment. Selenium shows an even stronger enrichment than do the five stable metals discussed here. While the origin of these enrichments is not known, the suspicion is that they are related to the biological affinities of these elements. The release to the air could be either from terrestrial vegetation or from froth blown off the sea surface. As can be seen from the table, not all metals show this enrichment. Some have ratios to aluminum close to the crustal average.

STABLE ISOTOPE RATIOS IN REACTIVE METALS

Isotopic separations similar to those observed for oxygen, hydrogen and carbon are not observed for the metals of interest to us in this chapter. The absence of such separations is in part due to the fact that the magnitude of these separations depends on the fractional mass difference between isotopes (i.e., on $\Delta m/m$). For the hydrogen-deuterium pair this difference is very large (i.e., $(2-1)/1$). For the $^{13}\text{C} - ^{12}\text{C}$ pair it is about 0.08 (i.e., $(13-12)/12$) and for the $^{18}\text{O} - ^{16}\text{O}$ pair it is about 0.12 (i.e., $(18-16)/16$). By contrast for metals with masses in the range 56 (iron) to 207 (lead) the fractional mass difference rarely exceeds 0.03. Further, the chemical transformation which these metals undergo in nature do not produce as large fractionations for a given mass fraction change as do some of the reactions experienced by carbon, hydrogen and oxygen. In any case, no one has found any measurable variations in isotopic composition which would prove useful in marine chemistry.

There are two exceptions, the elements lead and neodymium. Both show large natural variations in isotopic composition. These variations are, however, not the result of isotope separations. Rather they result from the fact that three of the four lead isotopes and one of the neodymium isotopes has been in part produced within the earth by the decay of long-lived radioisotopes. The isotopic compositions vary because of chemical separations between the parent and daughter isotopes within the earth. In the case of Pb the parents are isotopes of the elements U and Th. Planetary

Table 4-11. Residence time estimates for the elements dealt with in this chapter.

Element	Conc. ⁺ Rivers 10^{-9} moles/kg	Conc. ⁺⁺ Sea 10^{-9} moles/kg	River Input moles/yr	Mass In Sea moles	τ yr
Th	-	-	-	-	50*
Pb	-	-	-	-	40**
Cu	24.0	3.0	8×10^8	4×10^{12}	5000
Cd	<0.1	0.6	$<0.3 \times 10^7$	1×10^{12}	$>3 \times 10^5$
Ni	6.0	7.0	2×10^8	9×10^{12}	5×10^4

*Based on ^{230}Th data.

**Based on ^{210}Pb data. Because the half-life of ^{210}Pb is only 22-years, its distribution does not provide a measure of the importance of recycling. Hence, the τ for stable lead may be larger than 40 years. Indeed the value for stable lead in table 1-6 is 1100 years.

⁺Based on Amazon River data obtained by Boyle and his coworkers at MIT (632).

⁺⁺Based on the measurements of Bruland at the University of California Santa Cruz (455).

Table 4-12. Enrichment factors (relative to the mean crustal abundance) of various elements in material filtered from the atmosphere and in the atmospheric fallout onto the polar ice caps. In each case the concentrations have been normalized to that of aluminum* as summarized by Li (652).

Element	N. Temp. Aerosol	Greenland Ice (Pre-1900)	Antarctic Ice
Thorium	1.2	1.2	1.0
Iron	1.6	1.0	1.2
Manganese	0.5	1.0	1.2
Vanadium	1.6	1.0	1.0
Samarium	2.0	-	-
Barium	-	1.0	2.0
Nickel	25	25	-
Copper	30	16	50
Zinc	300	10	40
Cadmium	-	200	6000
Lead	1200**	20	200**
Selenium	1000	1000	500

$$\text{Enrichment factor} = \frac{([\text{Element}]/[\text{Al}])_{\text{sample}}}{([\text{Element}]/[\text{Al}])_{\text{crust}}}$$

**Anthropogenic contamination.

differentiation has led to a large enrichment of U and Th in the granitic crust and presumably to an enrichment of lead in the core. Thus lead which has spent a substantial amount of time in the earth's granitic crust, has high ratios of ^{206}Pb , ^{207}Pb and ^{208}Pb (the radiogenic isotopes) to ^{204}Pb (the non-radiogenic isotope). By contrast that lead which has recently reached the crust from the mantle has lower ratios. Planetary differentiation has enriched both samarium (the parent element of the radiogenic isotope ^{143}Nd) and neodymium in the earth's crust. However, the degree of enrichment is greater for neodymium than for samarium. Thus neodymium from the old portions of the granitic crust has a lower ^{143}Nd (radiogenic) to ^{144}Nd (non-radiogenic) ratio than neodymium recently derived from the mantle.

Measurements of lead and neodymium isotopes in seawater, in marine hydrothermal deposits, and in manganese nodules have much to offer in two areas. First, they offer a means of distinguishing the contributions of the two major natural sources of these metals, namely, continental weathering and ridge crest hydrothermal activity. Neodymium from ridge crests is derived from the mantle. Thus its isotopic composition is quite different from that for continental rocks. In the case of lead the situation is more complicated. Most of the lead dissolved in the upper sea is now anthropogenic (from the gasoline additive lead tetraethyl). This contamination has not, however, measurably altered the isotopic composition of marine sediments and nodules. Further, as most of the gasoline lead is manufactured from sedimentary lead ores with an unusual isotopic composition, it might be possible to use isotopic measurements to separate the contributions of these various sources to the lead currently dissolved in the deep sea.

The second application is to use the isotopic composition of lead and neodymium to place limits on the residence time of these elements in the sea. Because of the reactivity of these elements it is difficult to determine how much of the lead and neodymium carried by rivers will become dissolved in the sea and how much will follow the detrital material directly to the sediments. Similarly, it is difficult to determine what fraction of these elements in sediments is "detrital" and what fraction is "labile." Thus conventional estimates of residence time for these elements are not very reliable. Isotopic evidence can be used in the following way in this connection. Because of geological differences among the ocean basins, the isotopic composition of the lead and neodymium they receive will differ. For example, the Atlantic is surrounded by old continents and its ridges have slow spreading rates. By contrast the Pacific is surrounded by much younger rocks and its ridges have high spreading rates. Thus the lead and neodymium entering the Atlantic should have an isotopic composition more like those for average continental material while the lead and neodymium entering the Pacific should have an isotopic composition more like that for the mantle. Now, if in addition the residence time of these elements in the sea (i.e., the time from entry to final burial) is long compared to the interocean mixing time (i.e., ~ 500 years), then these differences should be smoothed out. On the other hand, if the residence time is short compared to interocean mixing time, substantial ocean to ocean

SEA WATER



MANGANESE NODULES HYDROTHERMAL CRUSTS METALLIFEROUS SEDS.

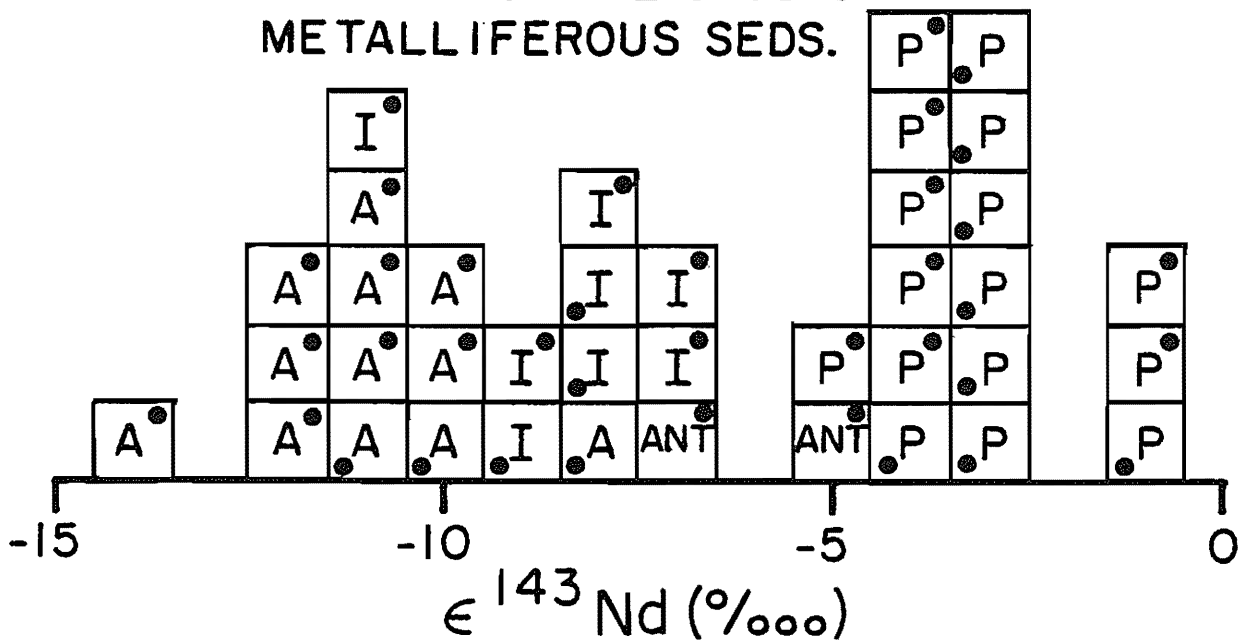


Figure 4-29. Histogram of the $\epsilon^{143}\text{Nd}/\epsilon^{144}\text{Nd}$ data (expressed as $\epsilon^{143}\text{Nd}$) following the definition given in table 4-13) for seawater and authigenic ferromanganese deposits from throughout the world ocean. The letter designations represent the ocean from which the sample was taken. The dots designate the laboratory in which the data were obtained. Those marked in the upper right are analyses made at Cal Tech (333, 336, 337) and those marked in the lower left are analyses made at the Lamont-Doherty Geological Observatory (339, 344).

Table 4-13. Geochemical abundances of neodymium and samarium and the isotopic composition of neodymium.

	Sm 10^{-6}g/g	Nd 10^{-6}g/g	$\frac{\text{Nd}}{\text{Sm}}$	$\epsilon^{143}\text{Nd}^*$ °/ooo
Average Earth	0.32	0.97	3	0
Mid-ocean Basalts	3.5	10	3	+10
Granitic Crust	4.5	27	6	-20
Atlantic Ocean	-	-	-	-11
Pacific Ocean	-	-	-	- 3

$$* \quad \epsilon^{143}\text{Nd} = \frac{\left(\frac{143\text{Nd}}{144\text{Nd}} \right)_{\text{samp}} - \left(\frac{143\text{Nd}}{144\text{Nd}} \right)_{\text{std}}}{\left(\frac{143\text{Nd}}{144\text{Nd}} \right)_{\text{std}}} \times 10^4$$

differences would be expected.

Let us first examine the isotopic data for neodymium. Measurements by the Cal Tech group (333,336,337) and by the Lamont group (339) on ferromanganese deposits and water samples are summarized in figure 4-29. These data show clear differences between the Atlantic and Pacific Oceans and hence suggest that residence time of neodymium* in the sea is smaller than the interocean mixing time. The sense of the differences is consistent with that expected from the geological argument presented above (see table 4-13).

Analogous isotopic patterns would be expected for lead. As we have seen, this element is removed from the sea on a time scale of several decades. Hence, if recycling from the sea floor is not important then the isotopic composition of the lead in manganese nodules should be similar to that of the mixture of lead reaching a given basin from its surrounding continents and from its ridge crests. As shown in figure 4-30, Patterson and Chow at Cal Tech (341,342) demonstrated this to be the case. Nodules from the Atlantic have lead richer in the radiogenic lead than nodules from the Pacific.

TRANSPORT OF IRON AND MANGANESE IN THE SEA

One of the motivations for looking into the transport of metals through the sea was to understand the growth of manganese nodules on the sea floor and the enrichment of Fe and Mn in red clays. So far we have not presented any data for either of these elements.

No data exists for iron. The reason is that iron has an extremely low concentration in seawater and that iron contamination on ships and in labs is large and difficult to control. No one has yet been able to beat this nearly insuperable combination of difficulties.

From laboratory and coastal ecosystem tracer studies there is good reason to believe that iron will act much like thorium in sea water (i.e., it will within a few decades be removed to the sediment). However, unlike thorium, iron may become reduced in the sediments and remobilized. Hence it is likely seeping into the sea from sediments rich in organic matter as well as entering from rivers and ridge crests.

The concentration of Mn has been determined in seawater. The data in hand strongly suggest that, once in the sea, manganese, like thorium and lead, is rapidly removed to the sediment. As shown in figure 4-31, the concentration of manganese is higher in surface water than in deep water and higher in surface waters near the continent margin than in open ocean surface waters (449). Hence the manganese released from coastal sediments and added to the sea from rivers never becomes thoroughly mixed within the sea. Rather, it is captured on particulate debris and taken to the sea floor.

Dramatic evidence for the rapid removal of manganese from the

*As manganese nodules contain ten times more neodymium than sediments, this Nd is likely derived from solution.

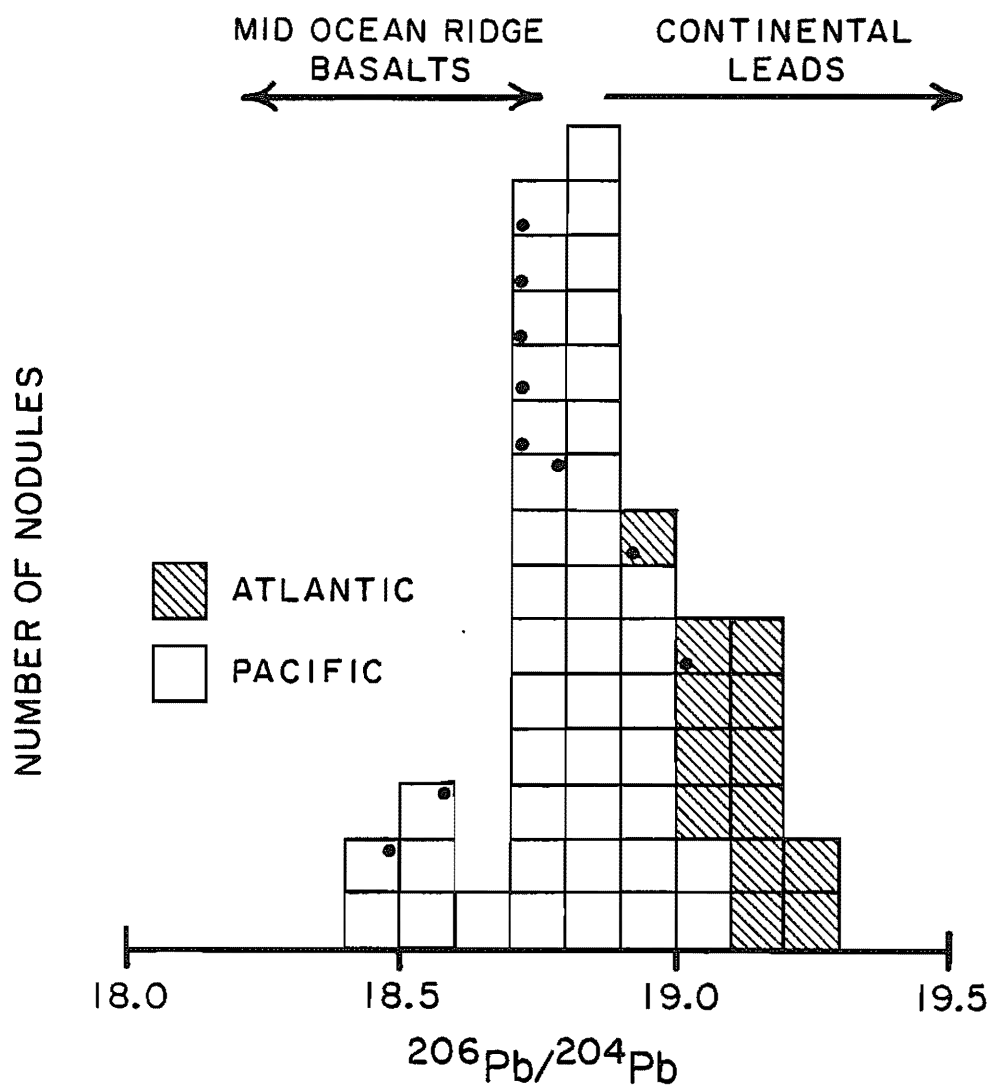


Figure 4-30. Histogram of ^{206}Pb to ^{204}Pb ratios in manganese nodules from the Atlantic and Pacific Oceans. As uranium is enriched over lead in the earth's continental crust relative to the mantle, the ratio of ^{206}Pb (produced by the decay of ^{238}U) to ^{204}Pb will be higher in continental leads than in leads recently derived from the mantle (i.e., leads in mid-ocean ridge basalts). It can be seen from this histogram that Atlantic leads have a larger continental component than do Pacific leads. Most of the analyses shown here were carried out at Cal Tech by Chow and Patterson (341,342). Those squares with a dot in the upper right hand corner represent analyses carried out by O'Nions and his colleagues at the Lamont-Doherty Geological Observatory (344) and those with a dot in the lower left hand corner analyses by Reynolds and Dasch at Oregon State University (343).

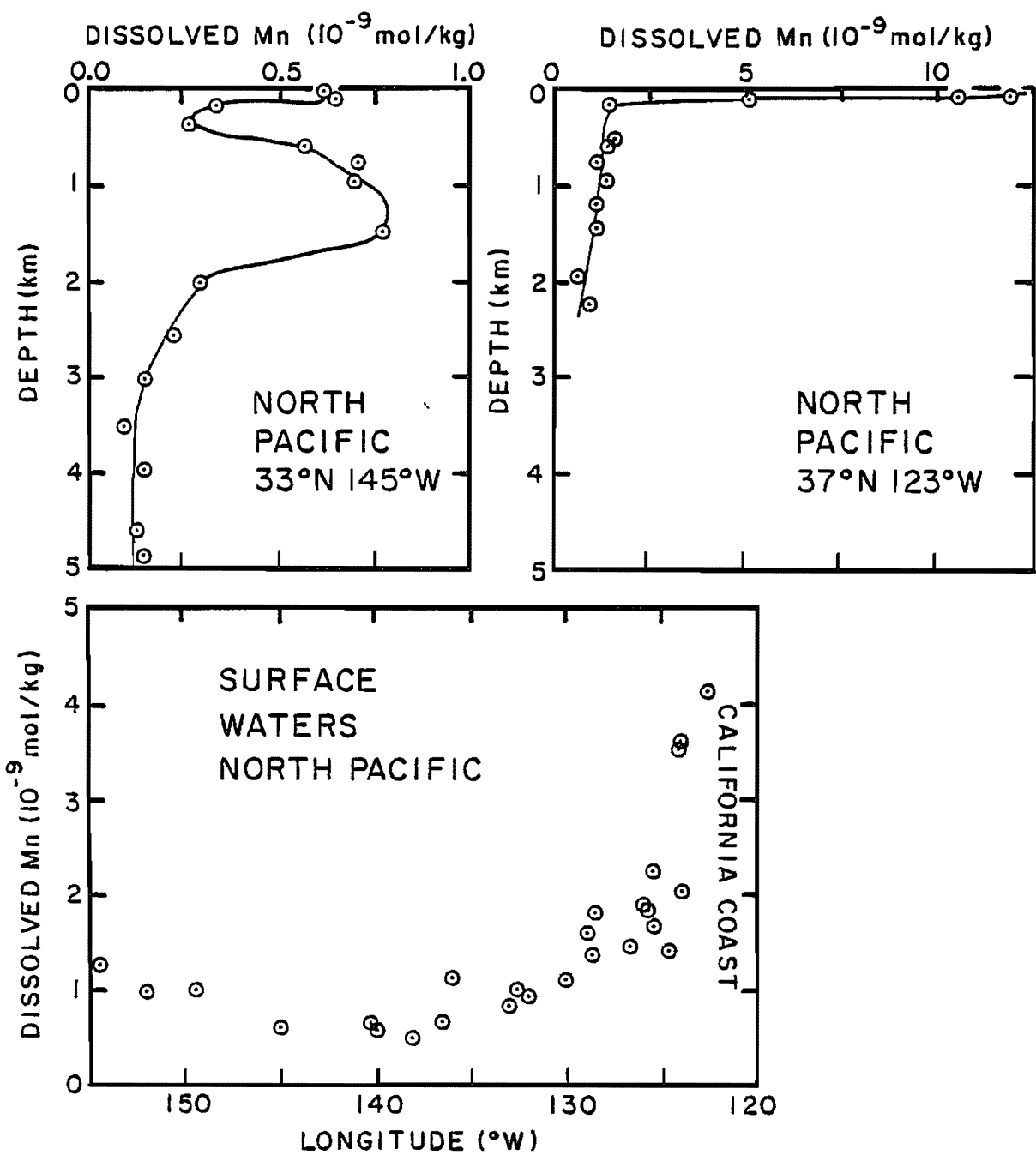


Figure 4-31. Upper panels show vertical profiles of manganese in the North Pacific Ocean. That on the left is for an open ocean station and that on the right for a coastal station. Note the ten-fold scale difference between these two diagrams. The coastal waters carry an order of magnitude more Mn! The lower panel shows the decrease in the Mn content of surface water away from the coast of California. The results are the work of Landing and Bruland of the University of California Santa Cruz (449).

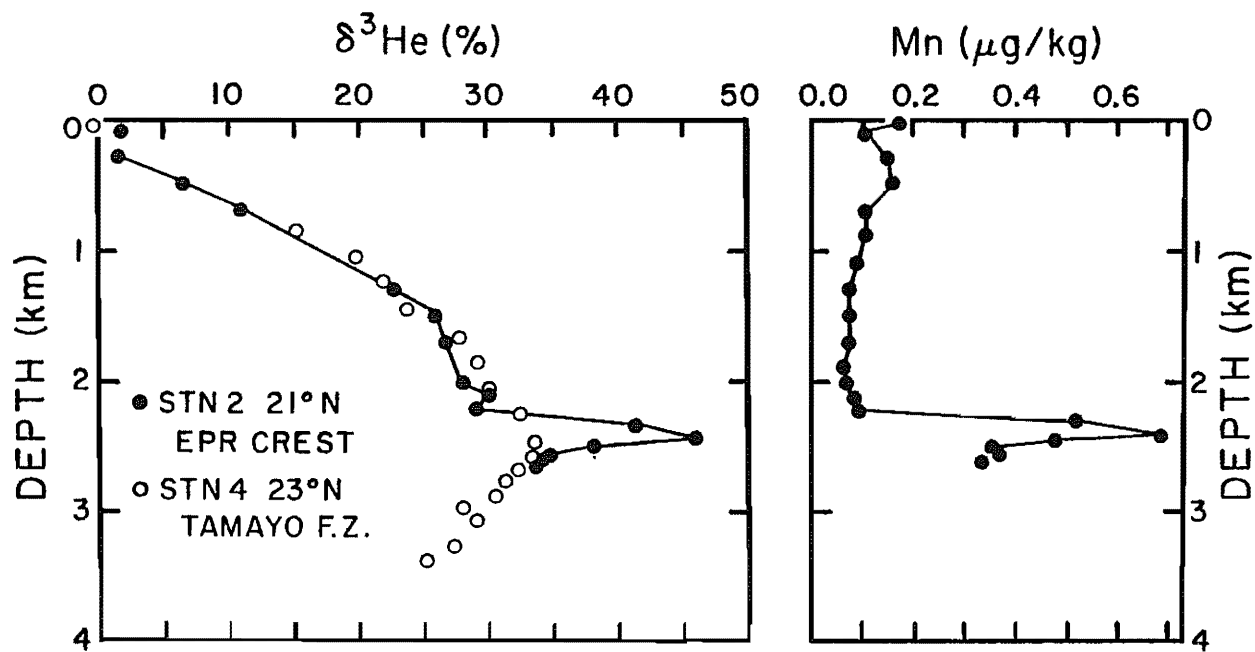


Figure 4-32. Vertical profiles of excess ${}^3\text{He}$ and of dissolved manganese for a station right over the crest of the East Pacific Rise at 21°N (solid circles). Injection of new ${}^3\text{He}$ and manganese from the rise crest can be clearly seen. ${}^3\text{He}$ results from a station at some distance from the rise crest (open circles) establish the ambient ${}^3\text{He}$ background. The samples were collected by Weiss of the Scripps Institution of Oceanography (447). The manganese measurements were made by Klinkhammer of the University of Rhode Island (446). The helium isotope measurements were made under the supervision of Lupton in the laboratory of Craig at Scripps Institution of Oceanography.

interior of the sea is shown in figure 4-32. As can be seen, samples taken above the East Pacific Rise show strong anomalies in both ^3He and manganese (446). Both substances must hence be added to the sea locally from hydrothermal vents. Unlike ^3He , which shows a broad maximum produced by the integrated imprint of hydrothermal activity all along the Rise crest, manganese shows no such feature. As shown by Weiss of Scripps, this difference can only be explained if manganese is rapidly removed from the water column (447).

LESSONS FROM CONTROLLED ECOSYSTEM STUDIES

Experiments carried out in large tanks designed to duplicate the conditions in Narragansett Bay shed light on the relative absorption tendencies of a number of the elements discussed above. These experiments, conducted by Santschi and his coworkers at the Lamont-Doherty Geological Observatory, involve measurements of the removal times of γ -ray-emitting tracers to the sediments at the bottom of these tanks (635). It was found (see table 4-14) that the elements Fe, Pb, Po, Th, Pa and Pu were all removed far more rapidly than the elements Cd, Zn, Se, Ba and Ra. Mn and Co had intermediate removal times. These results are consistent with our oceanographic findings.

DISTRIBUTION COEFFICIENTS

As we showed above, the absorption of metals onto particulate matter appears to be reversible. If so, this absorption can be characterized by distribution coefficients. Chemists working in the laboratory, using the oxides of manganese, silica, aluminum and iron as absorption media, have measured the absorption tendency for a variety of metals (684). They find a correlation between the absorption tendency and the first hydrolysis constant of the metal. The larger the hydrolysis constant, the more strongly is a metal absorbed. Iron has the highest hydrolysis constant of all the metals discussed here. That for thorium is one order of magnitude smaller. Those for other of the elements dealt with here are listed in table 4-15. As can be seen, there is some similarity between the order of these constants and the removal times of elements from the sea. Manganese, however, is so far out of order that one wonders how applicable these constants are in representing the reactivity of elements in the sea. Uptake by organisms, oxidation-reduction reactions and stabilization of metals by complexing ligands are possible causes for the lack of agreement.

SUMMARY

We have seen in this chapter that the flow of metals through the sea is complex. It involves both transport on particles and movement with the water. Because of differences in chemistry each metal has its own set of pathways. Thorium, protactinium, lead, polonium and plutonium are rapidly removed to the sediments. Manganese and iron likely have ocean geochemistries similar to

Table 4-14. Removal time groupings for the elements studied in MERL tanks by Santschi and his coworkers from the Lamont-Doherty Geological Observatory (133). These tanks are designed to duplicate the situation in Narragansett Bay. The results shown here were obtained by studying the removal to the sediments of radiotracers added to the waters in these tanks.

Group	Elements	Half Removal Time	
		Winter days	Summer days
1	Fe, Pb, Po, Th, Pa, Pu	10-20	2-3
2	Mn, Co	30-50	5-30
3	Cd, Zn, Se	60-100	10-50
4	Ba, Ra	150-600	80-150

Table 4-15. Hydrolysis constants for the elements of interest in this chapter.

Element	First Hydrolysis Constant
Fe	$\sim 10^{-3}$
Th	$\sim 10^{-4}$
Pb	$\sim 10^{-7}$
Nd	$\sim 10^{-8}$
Co	$\sim 10^{-9}$
Ni	$\sim 10^{-9}$
Zn	$\sim 10^{-9}$
Mn	$\sim 10^{-11}$

those for these highly reactive elements. By contrast, copper, zinc, cadmium and nickel remain in the sea for many mixing cycles. Except for copper, whose distribution shows definite evidence for scavenging from the deep water column, these elements appear to be involved mainly with the biological cycles of the sea. While these studies give us some clues regarding the processes responsible for the enrichment of the elements Fe, Mn, Ni, Cu, Co and Zn in manganese nodules and red clays, they fall well short of providing the answers we seek. This young science will have to be greatly expanded before these answers are forthcoming.

PROBLEMS

- 4-1 Shale contains on the average about 3×10^{-6} g U/g. Assume that soils have the same uranium content. Consider two soils, one dry in the upper 20 cm and the other water-saturated to the top. Both have porosities of 50% (i.e., they are 50% by volume pore space and 50% by volume mineral matter). The mean density of the mineral grains is 2.5 g/cm³. Assume that the activity of ²²⁶Ra in the soil is the same as that of ²³⁸U and that one-third of the radon produced in the soils is released to the pore space. Calculate the fluxes of radon atoms from the two soils (the molecular diffusivity of radon in water is 1.4×10^{-5} cm²/sec and in air 0.1 cm²/sec). Also calculate the characteristic depth of radon depletion in the water saturated soil (i.e., the depth where the depletion is 1/e as great as at the top of the soil). Compare the fluxes obtained with the fallout rates of ²¹⁰Pb atoms shown in table 4-6.
- 4-2 Sediment traps are deployed for one month at a depth of 75 meters in a saline desert lake. Material caught in these traps yields the following activity ratios for the uranium series isotopes:

$$\frac{^{234}\text{Th}}{^{230}\text{Th}} = 25^* \quad \frac{^{231}\text{Pa}}{^{230}\text{Th}} = 0.11$$

$$\frac{^{228}\text{Th}}{^{230}\text{Th}} = 3.5 \times 10^4 * \quad \frac{^{210}\text{Pb}}{^{230}\text{Th}} = 0.13$$

Analyses of the water yield the following results:

$$\begin{aligned} \text{U} &= 108 \times 10^{-6} \text{ g/liter} \\ ^{234}\text{U}/^{238}\text{U} &\text{ activity ratio of unity} \\ ^{226}\text{Ra} &= 15 \text{ dpm/liter} \\ ^{228}\text{Ra} &= 3 \text{ dpm/liter} \end{aligned}$$

Assuming that these concentrations are all at steady state, calculate the apparent residence times of Th, Pa and Pb in the lake waters. The ²¹⁰Pb fallout rate over the lake is 50 atoms/cm² minute.

- 4-3 If the mean ^{226}Ra activity in sea water were 50 dpm/100 liters, what would be the mean flux of ^{226}Ra flux from the sea floor necessary to maintain this concentration? The volume-to-area ratio for the ocean is 3800 meters. What would the "equilibrium" ^{226}Ra content of the sediment pore waters have to be to support this flux (by "equilibrium" is meant that which would be present were there no loss to the overlying sea). How deep would the zone of ^{226}Ra depletion in the pore waters extend? Assume a porosity of 50 percent and a pore water resaturation time of one day.
- 4-4 If the average sedimentation rate in the ocean is $1.5 \text{ g/cm}^2 \cdot 10^3 \text{ yrs}$, the uranium content of sea water is $3.2 \times 10^{-6} \text{ g/liter}$ and the $^{234}\text{U}/^{238}\text{U}$ activity ratio in sea water is 1.16, then what must be the concentration of water column derived ^{230}Th in the average newly formed sediment at a depth of 4000 meters? Give your answer in units of dpm/g.
- 4-5 If the excess ^{210}Pb atoms carried to the sea floor on particulate matter are homogenized throughout the upper 3 cm of the sediment, then what would be the concentration of these atoms in the core top material from the North Pacific Ocean? Assume that there is 1.0 g of solid matter per cubic centimeter of sediment.

SUPERPROBLEM #4

Intrigued by Theft's four-reservoir aquarium, Spencer Crane decides to build a similar device to study the uptake of reactive metals. He starts with a two-reservoir system with sediment at the bottom of the lower aquarium. Following Theft's lead, he puts mixers in each reservoir to keep the water homogeneous, and also a device which will keep the sediment well stirred. Pumps are installed to transfer water (and the suspended matter in this water) between the two reservoirs. He fills the reservoirs with water and then adds HgCl_2 to poison any organisms it might contain. He then installs devices to inject particulate matter into the surface waters and filtering devices similar to those used by Theft. The material recovered by the filter in the upper reservoir is regularly "back-flushed" into the lower reservoir. The material recovered by the filter in the lower reservoir is regularly scraped off and mixed into the sediment. Another gadget removes material from the well mixed sediment (so that the amount of sediment remains constant). The operating characteristics of this two-reservoir system are as follows:

Volume upper reservoir	= 1 m^3
Volume lower reservoir	= 9 m^3
Water exchange rate	= 0.1 m^3/hr
Mass sediment	= 100 g
Rate of particle injection	= 1×10^{-3} g/hr
Filtering rate in upper reservoir	= 0.3 m^3/hr

$$\text{Filtering rate in lower reservoir} = 0.3 \text{ m}^3/\text{hr}$$

To simulate the in situ production of short-lived isotopes to the sea, Crane meters isotopes into both the upper and lower reservoirs. The addition rate to the lower reservoir is nine times greater than to the upper reservoir (so that the addition rate per unit volume is the same in both reservoirs). For this purpose Crane selects a reactive metal with two radioisotopes of differing half-life (6.93 hours and 69.3 hours). The injection rate of each isotope is 2.0×10^8 atoms/m³ hr (referred to as I below).

Once everything is set up, Crane switches things on and then lets his J-machine, as he calls it, run until the distribution of the isotopes between the three reservoirs (i.e., upper water, lower water and sediment) comes to steady state. Crane then determines the concentration of each isotope in the upper and lower reservoir in particulate form. For the long-lived isotope, he finds:

$$\begin{aligned} C_{\text{upper}} &= 9.3 \text{ I} \\ C_{\text{lower}} &= 39.3 \text{ I} \end{aligned}$$

Crane assumes that the removal onto particles is reversible (i.e., the isotope achieves an equilibrium distribution between the particles and the water). He describes this distribution by the fraction, f, of the tracer on the particles (i.e., $f = \text{amt on particles}/(\text{amt on particles} + \text{amt dissolved in the water})$). He assumes that this fraction is the same in both reservoirs. Crane further assumes that a certain fraction, g, of the isotope in the sediment is released to the water each hour. From the results on the two tracers what are the values of f and g? What are the concentrations of the short-lived isotope?

A colleague named Suess Banjo, who is interested in the role organisms play in determining the chemical pathways through the sea, looks in on Crane's experiment and suggests that he repeat it with plants, animals and bacteria present in the system. Crane agrees and replaces the poisoned sea water and sediment. He adjusts the nutrient content of the water till he gets the desired plant growth rate in the upper reservoir and makes sure that the animals and bacteria in the lower reservoir consume any organic debris received during the back-flushing of the filters. He then starts a new tracer experiment. When steady state is established, he performs the same analysis as before. For the short-lived isotope, he finds the following concentrations in the particulate matter:

$$\begin{aligned} C_{\text{upper}} &= 0.0 \text{ I} \\ C_{\text{lower}} &= 3.1 \text{ I} \end{aligned}$$

Crane interprets these results to indicate that removal by plants overwhelms removal on inorganic particles for both of the isotopes in the upper reservoir. He assumes that, when the organic material formed in the upper reservoir is destroyed in the lower reservoir or in the sediment, the isotopes are released (those released

to the water dissolve and are mixed throughout the lower reservoir and those released in the sediment become attached to inorganic particles and are mixed throughout the sediment reservoir). He further assumes that all the organic material is quickly eaten. Finally, he assumes that the distribution coefficient for inorganic particles established by his first experiment remains the same and that the fraction of the isotope recycled from the sediment per unit time established in the first experiment also stays the same. What must be the fraction of the metal released by the oxidations of organic residues to the sediment as opposed to that released to the water in the lower reservoir?

LAST MINUTE ADDITION (SEPTEMBER 1982)

Wasserburg and his colleagues at Cal Tech have demonstrated that the isotopic composition of Nd in Drake Passage deep water places restrictions on the ratio of the contributions of new water from the northern Atlantic Ocean to recirculated water from the deep Indian and Pacific Oceans to the deep circumpolar flow (702). If this approach proves valid it may resolve an important question of long standing in physical oceanography (see chapter 7).

Chapter 5

HOW FAST DOES THE MILL GRIND ?

RATES OF VERTICAL MIXING AND SEDIMENT ACCUMULATION

INTRODUCTION

In chapter 1, we state that the residence time of water in the deep sea is about 1000 years. In chapter 2, we state that the rate of rain of CaCO_3 toward the deep sea floor averages about 1 $\text{g/cm}^2 \cdot 10^3 \text{ yrs}$. How were these rates established? Neither the pattern of composition of sea salt nor of the major sedimentary components tell us anything about the rate at which the system runs. As we will see in this chapter, these rates are based primarily on the measurement of trace quantities of a radioisotope of carbon which travel through the sea and into the sediments along with the nutrient constituents. Let us first see how the distribution of this isotope can be made to divulge the residence time of water in the deep sea. Then we will consider how it can be used to determine the rate at which CaCO_3 bearing the sediment accumulates.

RATE OF VERTICAL MIXING

A radioisotope of any given element has a chemistry nearly identical^{*} to that of the element's nonradioactive or "normal" isotope.* So a radioactive carbon atom moves through the ocean just as any other carbon atom. Since we have already worked out the cycle of carbon in sea water, we can use this information in connection with the application of carbon-14 (^{14}C) as a time-keeper.

Radioactive carbon is continually being produced in our atmosphere. There, cosmic rays from interstellar space encounter atoms and fragment some of them, releasing neutrons from their nuclei. Many of these neutrons find their way to nitrogen atoms

*Small separations between the isotopes of carbon occur during chemical reactions. These so-called "isotope fractionations" are on the order of a few percent. Although we will have a fair amount to say about these fractionations in the chapters to come it suffices here to say that in the case of ^{14}C they are merely a nuisance in that we are interested in differences produced by radiodecay. Fortunately, the $^{13}\text{C}/^{12}\text{C}$ ratios in the samples of carbon used for ^{14}C studies can be used to correct the $^{14}\text{C/C}$ ratios to what they would have been in the absence of any isotope separation. Theory tells us that the separation between ^{14}C and ^{12}C will be twice that between ^{13}C and ^{12}C .

(nitrogen gas makes up 80 percent of our atmosphere). Upon entering a nitrogen-14 nucleus this neutron can knock out a proton and remain behind in its place (like a cueball in pool). Now, as the nucleus of a nitrogen atom has 7 protons and the nucleus of a C atom has 6 protons, in losing one proton the nitrogen nucleus changes into a carbon nucleus. The number of nucleons (that is, the number of neutrons plus protons) in the new nucleus is still 14, the same number as in the old nucleus. The difference is that one neutron has entered the nucleus and one proton has been expelled. The ^{14}C nuclei so produced are unstable; the mixture of 8 neutrons and 6 protons is not a durable one and endeavors to change itself back into the stable 7-7 configuration of ^{14}N . To do so, the ^{14}C nucleus must hurl out an electron. In so doing it converts one of its neutrons into a proton and the nucleus again assumes the form of ^{14}N . This cycle is shown in figure 5-1.

About 100 ^{14}C atoms are being generated by cosmic rays over each square centimeter of the earth's surface each minute. Over many thousand of years, the amount of ^{14}C on the surface of the earth has become nearly constant.* ^{14}C is disappearing by its own radioactive decay at the same rate that it is being produced by cosmic rays (i.e., 100 atoms of ^{14}C undergo radioactive decay per square centimeter of earth surface each minute).

The property that makes ^{14}C a very interesting and important isotope in natural science investigations is that the average ^{14}C atom requires 8200 years to undergo the transformation back to ^{14}N ! Thus, in their lifetimes, ^{14}C atoms have a chance to mix reasonably well but not completely with the ordinary carbon in the ocean-atmosphere system. The fact that the mixing is not complete makes ^{14}C a very valuable tool in oceanography.

Before exploring the tracer potential of natural ^{14}C , let us first review the rules governing radioactive decay. The disappearance of a batch of radioactive atoms is a logarithmic process: a set fraction of the atoms undergo radioactive transformation each year. For ^{14}C , this fraction is 1 atom in 8200. This logarithmic decay pattern gives rise to the concept of half-life. If we were to start with a given number of radiocarbon atoms today and let them age for 5700 years, half of them would have become ^{14}N atoms and the other half would still be ^{14}C atoms. Half of the half of ^{14}C atoms that remained would undergo transformation in the next 5700 years, and so forth.

For an analogous situation, consider a roomful of students. Each has a coin which he flips once every second. No one can

*The concentration of a radioisotope is often expressed in radioactivity rather than mass units. Since the mass of a given radioactive species is proportional to the rate at which it undergoes radioactive decay, stating the rate of radioactive decay rate for an isotope in a given volume of water is equivalent to stating its concentration. The units of radioactivity are disintegrations per unit time: disintegrations per second (dps), disintegrations per minute (dpm), and so on. Since radioisotopes are generally measured by intercepting the radiations emitted during the disintegration events, it proves more convenient to use activity rather than mass units.

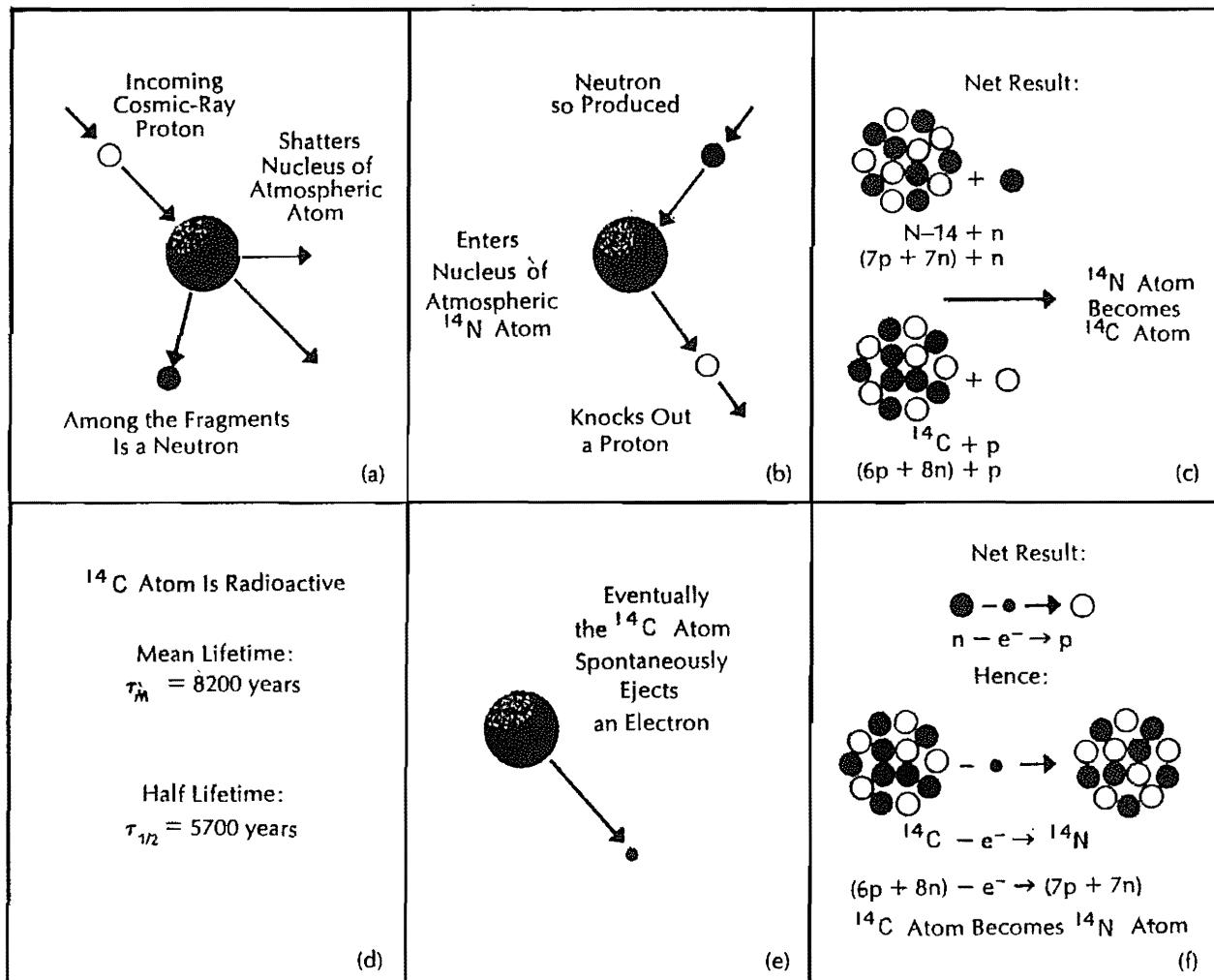


Figure 5-1. The "life cycle" of a carbon-14 atom. Created in the atmosphere by the collision of a neutron (produced by primary cosmic-ray protons) with a nitrogen atom, the average ^{14}C atom "lives" for 8200 years. Its life is terminated by the ejection of an electron which returns the atom to its original form, ^{14}N .

leave the room until he has flipped ten heads in a row. One student might be lucky enough to accomplish this feat in the first few minutes; another might not have succeeded even after several hours of steady flipping. From the laws of probability, however, we would predict exactly what the average success time would be. The fraction of students present who would leave in a given time interval would be the reciprocal of this average success time. If there were enough students in the room when the flipping began, we would observe that the number remaining would decrease in accord with the same halving pattern that holds for the radioactive decay of ^{14}C . Although we could not predict the time required for any specific individual to make a successful run of ten heads, we could predict the number of departures for a known time interval rather closely.

Since there is not enough time for complete mixing during the average lifetime of the ^{14}C atom, the more "remote" parts of the system will have less ^{14}C per unit of ordinary carbon than those parts "closer" to the birthplace of the ^{14}C atoms. Since ^{14}C is created in the atmosphere, the atmosphere has the highest ratio of ^{14}C to ordinary carbon. Since the deep North Pacific Ocean is the most remote part of the ocean, it has the least ^{14}C per unit of ordinary carbon. The $^{14}\text{C}/\text{C}$ ratios that interest us most are those for average surface and average deep water. The difference in $^{14}\text{C}/\text{C}$ ratios between the mean carbon in these two water types allows us to establish the rate of mixing across the main thermocline of the ocean.

If we want to make our estimates rigorous, we need a model that corresponds to the ocean in all its complexity. However, the first principles can be demonstrated by the simple two-box model we used in chapter 1. If we can understand how a hypothetical ocean consisting of two major water types - warm surface water and cold deep water - operates, we will have a basis for understanding the methods used to treat the vastly more complicated problem involving the real ocean. This model as applied to ^{14}C is shown in figure 5-2.

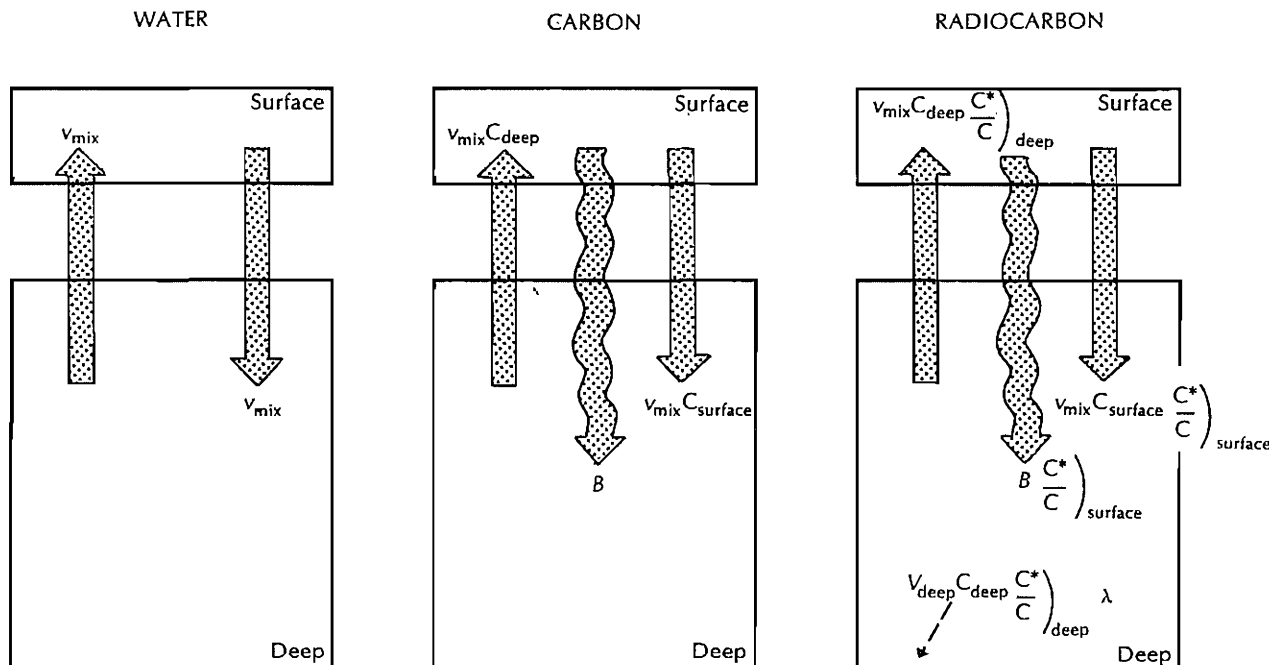
For the deep reservoir of our two-box ocean, three substances must be conserved: water, ordinary carbon, and ^{14}C . We assume that the surface and deep reservoir sizes and their carbon contents have achieved constant values. These reservoir sizes and the distribution of ordinary carbon between them in no way betrays the rate of mixing. To find the rate we need a time clock. Because ^{14}C is disappearing by radioactive decay, its distribution between the surface and deep reservoirs does depend on the rate of mixing!

Thus we will write three equations: one for water, one for ordinary carbon, and one for ^{14}C . The water conservation equation very simply states that the amount of water going up, v_{up} , must equal the amount of water coming down, v_{down} . We set both v_{up} and v_{down} equal to the parameter v_{mix} :

$$v_{\text{up}} = v_{\text{down}} = v_{\text{mix}}$$

5-1

As stated in chapter 1, v_{mix} is the rate at which water is exchanged between the two reservoirs.



$$B + v_{\text{mix}} C_{\text{surface}} = v_{\text{mix}} C_{\text{deep}}$$

$$B = v_{\text{mix}} (C_{\text{deep}} - C_{\text{surface}})$$

$$v_{\text{mix}} C_{\text{surface}} \frac{C^*}{C}_{\text{surface}} + B \frac{C^*}{C}_{\text{surface}}$$

$$= v_{\text{mix}} C_{\text{deep}} \frac{C^*}{C}_{\text{deep}} + v_{\text{deep}} C_{\text{deep}} \frac{C^*}{C}_{\text{deep}} \lambda$$

Figure 5-2. Two-box model for the cycle of water, carbon, and radiocarbon (^{14}C) between the surface and deep sea. If the system is at steady state, then the amount of each of these substances entering the deep reservoir must exactly match the amount lost. Although the fluxes of carbon and ^{14}C from rivers and to sediments should be included, they are negligible compared to the other fluxes. The straight arrows represent the fluxes of substances carried by water; the wavy arrows, substances carried by particles. The dashed arrow represents loss by radioactive decay.

Carbon is added to the deep reservoir in two ways: it comes down with the descending surface water and it falls from the surface in the form of particles destined for destruction in the deep sea. The sum of these two contributions must be exactly balanced by the amount of carbon carried away by upwelling water. We can write the balance between these fluxes in the form of the equation:

$$v_{\text{mix}} C_{\text{deep}} = v_{\text{mix}} C_{\text{surface}} + B \quad 5-2$$

where C_{deep} is the carbon content of upwelling deep water, C_{surface} is the carbon content of descending surface water, and B is the carbon added to the deep reservoir each year by the destruction of particles falling from the surface. Solving for B , we obtain:

$$B = v_{\text{mix}} (C_{\text{deep}} - C_{\text{surface}}) \quad 5-3$$

A similar equation can be written for ^{14}C . Again, we have two water fluxes. First, ^{14}C is carried up from the deep to the surface water and down from the surface to the deep water as the result of physical mixing. Second, ^{14}C enters the deep water with descending particles. But there is still another factor to consider here: one part in 8200 of all the radiocarbon in the deep ocean undergoes radioactive decay each year. We therefore need a term that will give us the radioactive decay rate.

Radiocarbon is measured in sea water samples by extracting carbon from the water and measuring that carbon's radioactivity. This yields the amount of ^{14}C contained in the dissolved carbon, or the $^{14}\text{C/C}$ ratio.* Laboratory measurements thus do not give the absolute amount of radiocarbon in the same water sample, but the ratio of radiocarbon atoms (designated C^*) to ordinary carbon atoms (C). So the amount of ^{14}C in descending surface water is equal to the volume of descending water v_{mix} times the carbon content of this descending water C_{surface} times the ratio of ^{14}C atoms to ordinary C atoms in this carbon:

$$v_{\text{mix}} C_{\text{surface}} \left(\frac{\text{C}^*}{\text{C}} \right)_{\text{surface}}$$

The amount of ^{14}C in upwelling deep water is equal to v_{mix} times the concentration of carbon in deep water C_{deep} times the ratio of ^{14}C atoms to ordinary C atoms in deep water:

$$v_{\text{mix}} C_{\text{deep}} \left(\frac{\text{C}^*}{\text{C}} \right)_{\text{deep}}$$

Particles carry ^{14}C down in almost the same proportion to other carbon that is present in surface water. So the particle flux

*In the ocean-atmosphere system, for every ^{14}C atom there are about 10^{12} ordinary carbon atoms.

will be the amount of carbon descending each year in particles B times the ratio of ^{14}C atoms to ordinary C atoms in surface water:

$$B \left(\frac{C^*}{C} \right)_{\text{surface}}$$

To calculate the radioactive decay of ^{14}C , we first find the total number of ^{14}C atoms in deep water (by taking the volume of deep water, V_{deep} , times the carbon content of deep water, C_{deep} , times the ratio of ^{14}C atoms to ordinary C atoms in deep water carbon) and multiply it by the fraction of ^{14}C atoms decaying each year, which we designate as λ . Thus:

$$\lambda V_{\text{deep}} C_{\text{deep}} \left(\frac{C^*}{C} \right)_{\text{deep}}$$

We can now write the conservation equation for ^{14}C in the deep reservoir as:

$$v_{\text{mix}} C_{\text{surface}} \left(\frac{C^*}{C} \right)_{\text{surface}} + B \left(\frac{C^*}{C} \right)_{\text{surface}} = 5-4$$

$$= v_{\text{mix}} C_{\text{deep}} \left(\frac{C^*}{C} \right)_{\text{deep}} + \lambda V_{\text{deep}} C_{\text{deep}} \left(\frac{C^*}{C} \right)_{\text{deep}}$$

The conservation equation for carbon demanded that the particle flux of carbon B be given by $v_{\text{mix}} C_{\text{deep}} - v_{\text{mix}} C_{\text{surface}}$. Thus we can eliminate B in equation 5-4 by substitution. After combining terms, the result is:

$$v_{\text{mix}} C_{\text{deep}} \left(\frac{C^*}{C} \right)_{\text{surface}} = (v_{\text{mix}} C_{\text{deep}} + \lambda V_{\text{deep}} C_{\text{deep}}) \left(\frac{C^*}{C} \right)_{\text{deep}} \quad 5-5$$

Note that each term in this equation contains the concentration of carbon in deep water C_{deep} . Therefore, this common factor can be cancelled. This is logical, since the rate of vertical mixing cannot be dependent on the amount of carbon dissolved in the sea! If we then solve the ^{14}C balance for the unknown mixing rate v_{mix} , we obtain:

$$v_{\text{mix}} = \lambda V_{\text{deep}} \left[\frac{\left(\frac{C^*}{C} \right)_{\text{deep}}}{\left(\frac{C^*}{C} \right)_{\text{surface}} - \left(\frac{C^*}{C} \right)_{\text{deep}}} \right] \quad 5-6$$

We can express the volume of the deep ocean, V_{deep} , in

terms of the product of its mean depth, h , and its surface area, A_{ocean} . Equation 5-6 then becomes:

$$v_{\text{mix}} = \lambda h A_{\text{ocean}} \left[\frac{\frac{C^*}{C} \text{) deep}}{\frac{C^*}{C} \text{) surface} - \frac{C^*}{C} \text{) deep}} \right] \quad 5-7$$

Dividing numerator and denominator by $C^*/C \text{) deep}$, we obtain:

$$v_{\text{mix}} = \frac{\lambda h A_{\text{ocean}}}{\frac{C^*/C \text{) surface}}{C^*/C \text{) deep}} - 1} \quad 5-8$$

In this equation, λ is equal to $1/8200$ years and h is 3000 meters (3.0×10^5 centimeters). Measurements of the radiocarbon content of carbon extracted from sea water reveal that, as expected, there is a deficiency of ^{14}C relative to C in deep water with respect to surface water; the ^{14}C has not completely mixed with the ordinary carbon. The $^{14}\text{C}/\text{C}$ ratio in average deep water is about 12 percent lower than it is in surface water. When we place these values in the equation 5-8 and solve, we find that the yearly volume of water exchanged between the surface and the deep ocean is equal in volume to a layer 300 centimeters thick with an area equal to that of the ocean:

$$\frac{v_{\text{mix}}}{A_{\text{ocean}}} = \frac{\frac{1}{8.2 \times 10^3} \times 3.0 \times 10^5}{1.12 - 1} = 300 \text{ cm/yr}$$

Since the mean thickness of the deep reservoir is about 3000 meters, the transfer of a layer 3 meters thick between the deep and surface ocean each year yields a mean residence time of water in the deep sea of $3000/3$, or 1000 years. A unit of water (or salt) has one chance in 1000 of returning to the warm surface reservoir each year.

IMPLICATION TO THE DISTRIBUTION OF Ra-226

In the last chapter we discussed the distribution of ^{226}Ra in the sea. The statement was made that the ratio of ^{226}Ra to Ba would not differ enough between surface and deep water to be useful as a crosscheck on the ventilation rate obtained from the ratio of ^{14}C to C. Using the same model as for ^{14}C , we can write down equations for the balance of Ba and ^{226}Ra . Since the major addition of ^{226}Ra is to the deep reservoir, we shall write these balances for the surface reservoir.

For steady state for the barium in the surface reservoir:

$$C_{\text{surface}} v_{\text{mix}} + B = C_{\text{deep}} v_{\text{mix}}$$

5-9

where C_{surface} and C_{deep} are, respectively, the barium contents of mean surface and mean deep water, B is the particle flux of barium from surface to deep water, and v_{mix} is the water transfer rate between the reservoirs.

For steady state for ^{226}Ra in the surface reservoir:

$$\begin{aligned} & \frac{^{226}\text{Ra}/\text{Ba})_s}{^{226}\text{Ra}/\text{Ba})_d} C_{\text{surface}} v_{\text{mix}} + \frac{^{226}\text{Ra}/\text{Ba})_s}{^{226}\text{Ra}/\text{Ba})_d} B + \\ & \lambda \frac{^{226}\text{Ra}/\text{Ba})_s}{^{226}\text{Ra}/\text{Ba})_d} C_{\text{surface}} V_{\text{surface}} = \frac{^{226}\text{Ra}/\text{Ba})_d}{^{226}\text{Ra}/\text{Ba})_s} C_{\text{deep}} v_{\text{mix}} + P \end{aligned} \quad 5-10$$

where $\frac{^{226}\text{Ra}/\text{Ba})_s}{^{226}\text{Ra}/\text{Ba})_d}$ and $\frac{^{226}\text{Ra}/\text{Ba})_d}{^{226}\text{Ra}/\text{Ba})_s}$ are, respectively, the concentration ratios of these species in average surface and deep water, λ is the decay constant of ^{226}Ra , V_{surface} is the volume of the surface reservoir and P is the input of ^{226}Ra from the sediments and rivers to the surface reservoir. By simultaneous solution of equations 5-9 and 5-10, B can be eliminated. Also, P may be re-presented as follows:

$$P = f \left(\lambda \frac{^{226}\text{Ra}/\text{Ba})_s}{^{226}\text{Ra}/\text{Ba})_d} C_{\text{surface}} V_{\text{surface}} + \lambda \frac{^{226}\text{Ra}/\text{Ba})_d}{^{226}\text{Ra}/\text{Ba})_s} C_{\text{deep}} V_{\text{deep}} \right) \quad 5-11$$

where f is the fraction of the new ^{226}Ra reaching through the surface reservoir. In this way we obtain:

$$\frac{^{226}\text{Ra}/\text{Ba})_s}{^{226}\text{Ra}/\text{Ba})_d} = \frac{v_{\text{mix}} + f \lambda V_{\text{deep}}}{v_{\text{mix}} + (1-f) \lambda V_{\text{surface}} \left(\frac{C_{\text{surface}}}{C_{\text{deep}}} \right)} \quad 5-12$$

We can now replace v_{mix} with the ratio of $V_{\text{deep}}/\tau_{\text{mix}}$, where τ_{mix} is the mean flushing time of the deep sea and λ with $1/\tau^{226}\text{Ra}$, where $\tau^{226}\text{Ra}$ is the mean lifetime of ^{226}Ra atoms and obtain:

$$\frac{^{226}\text{Ra}/\text{Ba})_s}{^{226}\text{Ra}/\text{Ba})_d} = \frac{1 + f \frac{\tau_{\text{mix}}}{\tau^{226}\text{Ra}}}{1 + (1-f) \frac{\tau_{\text{mix}}}{\tau^{226}\text{Ra}} \frac{V_{\text{surface}}}{V_{\text{deep}}} \frac{C_{\text{surface}}}{C_{\text{deep}}}} \quad 5-13$$

The maximum difference between the ^{226}Ra to Ba ratio of surface and deep water is obtained if $f = 0$ (i.e., all the ^{226}Ra is added to the deep reservoir). In this case:

$$\frac{^{226}\text{Ra}/\text{Ba})_s}{^{226}\text{Ra}/\text{Ba})_d} = \frac{1}{1 + \frac{\tau_{\text{mix}}}{\tau^{226}\text{Ra}} \frac{V_{\text{surface}}}{V_{\text{deep}}} \frac{C_{\text{surface}}}{C_{\text{deep}}}} \quad 5-14$$

Taking $V_{\text{surface}}/V_{\text{deep}}$ to be about 0.1, $C_{\text{surface}}/C_{\text{deep}}$ to

be 0.3 and the value of τ_{mix} to be 1000 years, we obtain:

$$\frac{{}^{226}\text{Ra/Ba})_S}{{}^{226}\text{Ra/Ba})_d} = \frac{1}{1 + \frac{1000}{2340} \times 0.1 \times 0.3} = 0.99$$

Thus, looked at in this way, the ${}^{226}\text{Ra}$ ratio difference between mean surface and mean deep water should lie within the experimental error in measurements of ${}^{226}\text{Ra/Ba}$ ratios (i.e., 3-5%).

It is not possible a priori to say what is the fraction of the ${}^{226}\text{Ra}$ entering the ocean which does so via the surface. Rivers contribute an amount of ${}^{226}\text{Ra}$ equal to several percent of that decaying in the sea. Shelf sediments constitute about 10% of the sea floor. Hence, were the flux of ${}^{226}\text{Ra}$ into the sea from sediments everywhere the same, the proportion of ${}^{226}\text{Ra}$ entering the surface sea would roughly match its proportion of the volume. If we take as an upper limit that 15% of the ${}^{226}\text{Ra}$ entering the sea does so in the surface layer, then from equation 5-13:

$$\frac{{}^{226}\text{Ra/Ba})_S}{{}^{226}\text{Ra/Ba})_d} = \frac{\frac{1000}{2340}}{1 + (1 - 0.15) \frac{1000}{2340} \times 0.1 \times 0.3} = 1.05$$

Again this is close to the limit of error on the ${}^{226}\text{Ra/Ba}$ ratio measurements.

DISTRIBUTION OF RADIOCARBON IN THE OCEAN

Before moving on to the other rates needed to understand the flow of chemical constituents through the sea it is important to point out that in averaging all the ${}^{14}\text{C}$ data for deep ocean samples for use in the two-box model we have thrown out an enormous amount of valuable information with regard to rates of mixing within the sea. Thus, we will pause here to take a look at the distribution of ${}^{14}\text{C}$ in the world ocean. Figure 5-3 shows vertical profiles of ${}^{14}\text{C/C}$ ratio* in the ocean as they looked prior

*These ratios are expressed as the per mil difference from the ${}^{14}\text{C/C}$ ratio in the atmosphere prior to the onset of the industrial revolution (i.e., about 1850) and normalized to a constant ${}^{13}\text{C}/{}^{12}\text{C}$ ratio. The equation used is as follows:

$$\Delta {}^{14}\text{C} = \delta {}^{14}\text{C} - 2(\delta {}^{13}\text{C} + 25)(1 + \frac{\delta {}^{14}\text{C}}{1000}) \quad 5-15$$

where:

$$\delta {}^{14}\text{C} = \left[\frac{{}^{14}\text{C/C}_{\text{sample}} - {}^{14}\text{C/C}_{\text{standard}}}{{}^{14}\text{C/C}_{\text{standard}}} \right] \times 1000$$

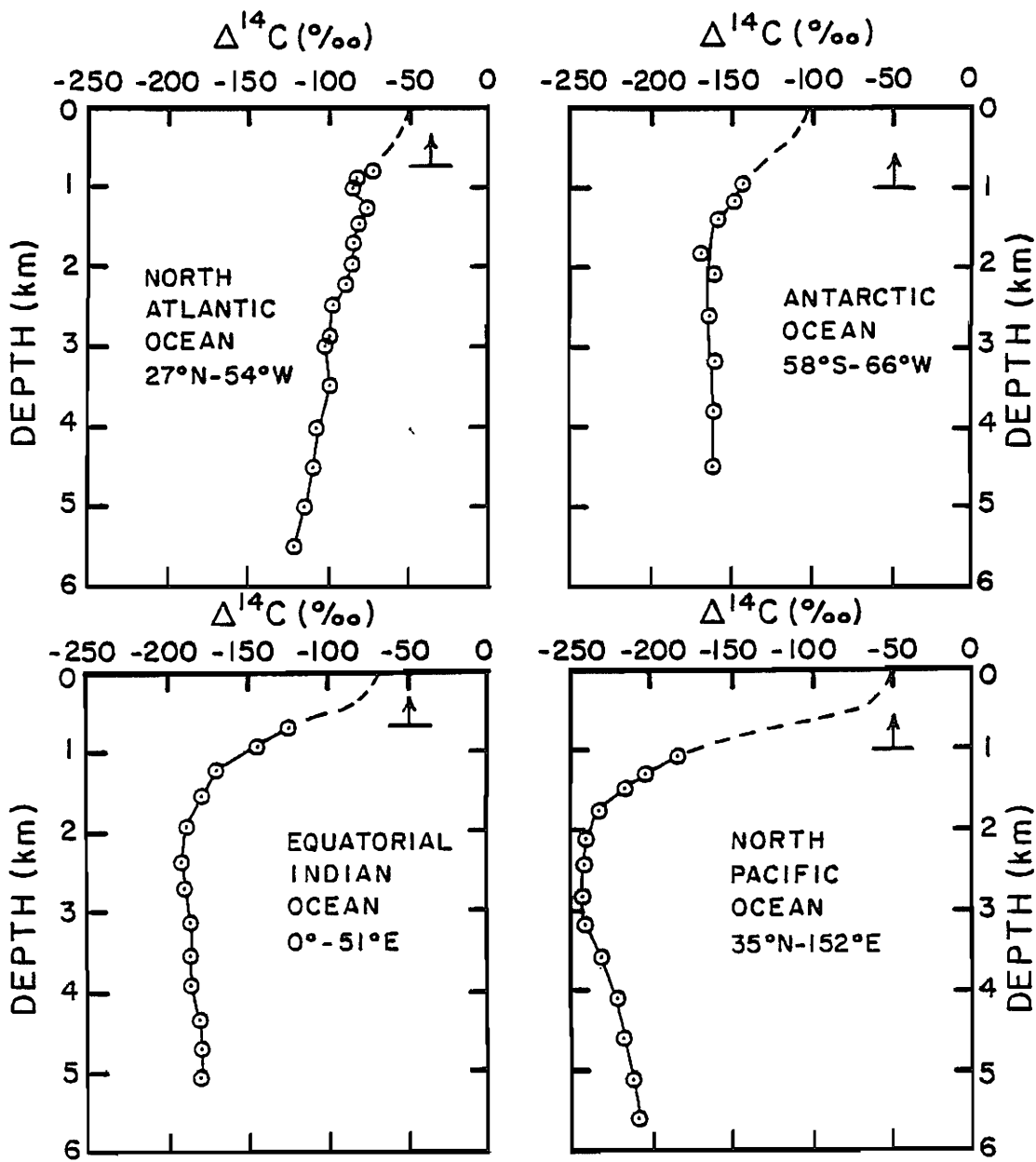


Figure 5-3. $^{14}\text{C/C}$ (expressed as $\Delta^{14}\text{C}$) versus water depth at stations in the world's three major oceans and in the Antarctic. The progressive decrease in the values for deep water from Atlantic to Antarctic to Indian to Pacific can be seen. The arrow denotes that portion of the upper water column contaminated with radiocarbon produced by nuclear tests at the times these samples were collected. This depth was determined from the tritium data for these stations. The dashed lines are the prenuclear $\Delta^{14}\text{C}$ trends for this depth zone. These results were obtained on samples collected as part of the GEOSECS program. The analyses were made by Minze Stuiver of the University of Washington and by Göte Ostlund of the University of Miami (21, 22, 23).

to the influence of the testing of thermo-nuclear bombs (i.e., prior to 1957). We make this point because a substantial amount of radiocarbon was produced during these tests. As we shall discuss in chapter 8 this "anthropogenic" radiocarbon has penetrated into the upper oceans.

The profiles in figure 5-3 show the trends expected from the distribution of oxygen and of the nutrient constituents. Surface water carbon contains more ^{14}C than deep water carbon but less than that in carbon from the preindustrial atmosphere. Carbon in deep Atlantic waters has more ^{14}C than carbon from the deep Pacific. Deep waters from Antarctic and Indian Oceans have intermediate values. The trend in radiocarbon through the deep ocean is well displayed along the 4000-meter depth horizon (see figure 5-4). As can be seen, the $^{14}\text{C/C}$ ratios are highest at the northern end of the Atlantic and lowest in the northern Pacific. Finally, the details of the natural radiocarbon distribution are shown in a series of the vertical sections drawn from north to south through the major ocean basins (see figures 5-5 to 5-9). These sections show that neither the new deep water formed at the northern end of the Atlantic nor that formed in the Weddell Sea have the same $^{14}\text{C/C}$ ratio as seen in the warm surface ocean (see figure 5-5). The waters forming in the North Atlantic had (prior to nuclear testing) a $\Delta^{14}\text{C}$ value of about $-70^{\circ}/\text{oo}$ (compared to about $-50^{\circ}/\text{oo}$ for warm surface water); those forming in the Weddell Sea had a value of $-150^{\circ}/\text{oo}$, which is only slightly higher than that for ambient circumpolar water. These differences reflect the fact that the source of deep water is mainly intermediate depth water which rises to the surface in the deep water source regions. These waters are exposed to the atmosphere only long enough to be cooled but not long enough to exchange their carbon with the atmosphere.

Another feature of interest is the penetration of the waters flowing around Antarctica into the Atlantic above and below the North Atlantic Deep Water mass. This is well shown by the tongues of low $^{14}\text{C/C}$ water (see figure 5-5).

The distribution of ^{14}C is hence quite consistent with what we have learned of the distributions of the biologically cycled constituents. The oldest waters in the ocean have the least dissolved oxygen, the most nitrate, phosphate and silicate and the lowest $^{14}\text{C/C}$ ratio. In chapter 7 we will have more to say about the time information carried by the distribution of $^{14}\text{C/C}$ ratios in the deep sea.

RATE OF CONTINENTAL RUNOFF

In chapter 1 we stated that the ratio of the rate of upwelled water to runoff water entering the warm surface ocean was 30. Now that we have established the upwelling rate, let us turn our attention to the runoff rate. In this case, no radioisotope is needed. A very direct means is used: the amount of water leaving the mouths of the world's rivers is monitored and totalled. We can estimate the approximate magnitude of the result expected from this effort from two pieces of information: the average annual rate of rainfall on the continents ($\sim 70 \text{ cm/yr}$) and the average

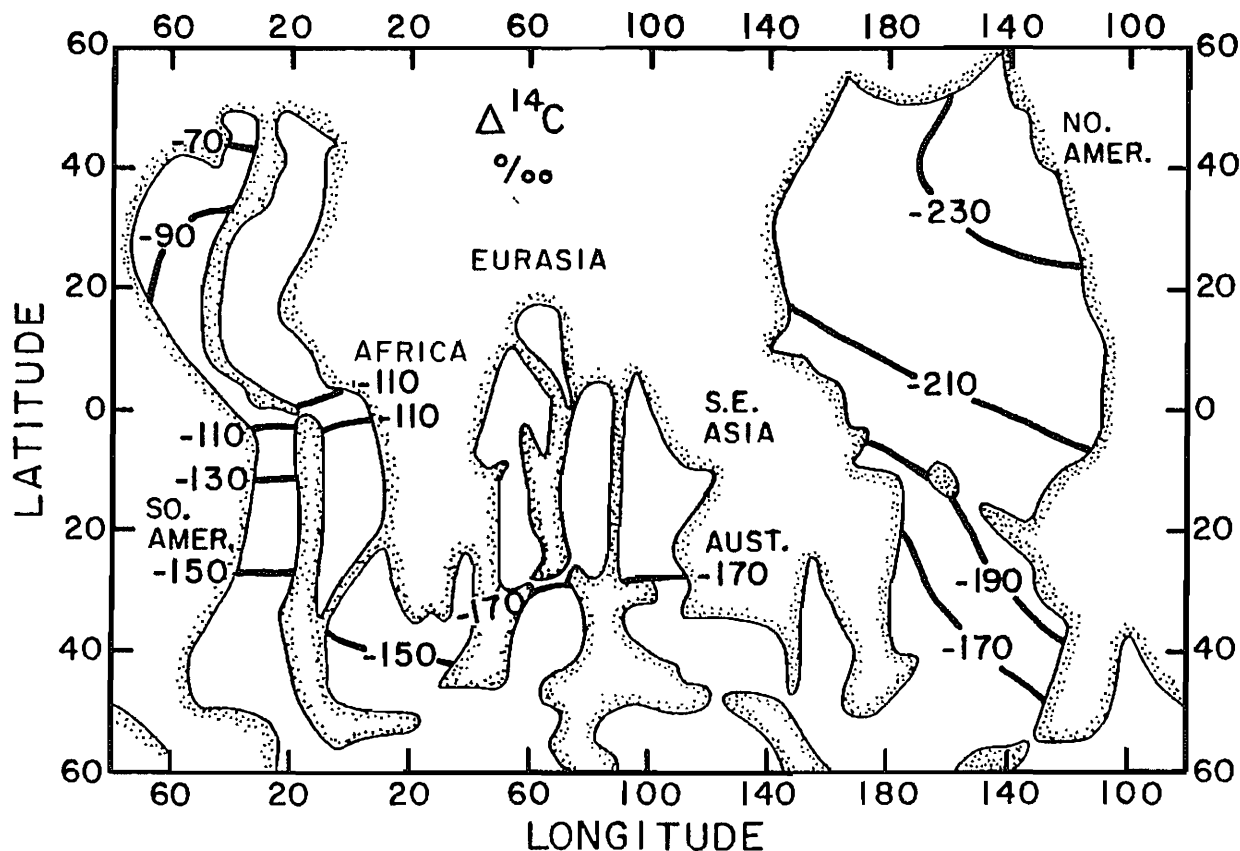


Figure 5-4. Map showing the distribution of $\Delta^{14}\text{C}/\text{C}$ ratios (expressed as $\Delta^{14}\text{C}$) at a depth of 4000 meters in the main basins of the world ocean. Based on results obtained by Stuiver and by Ostlund as part of the GEOSECS program (21,22,23).

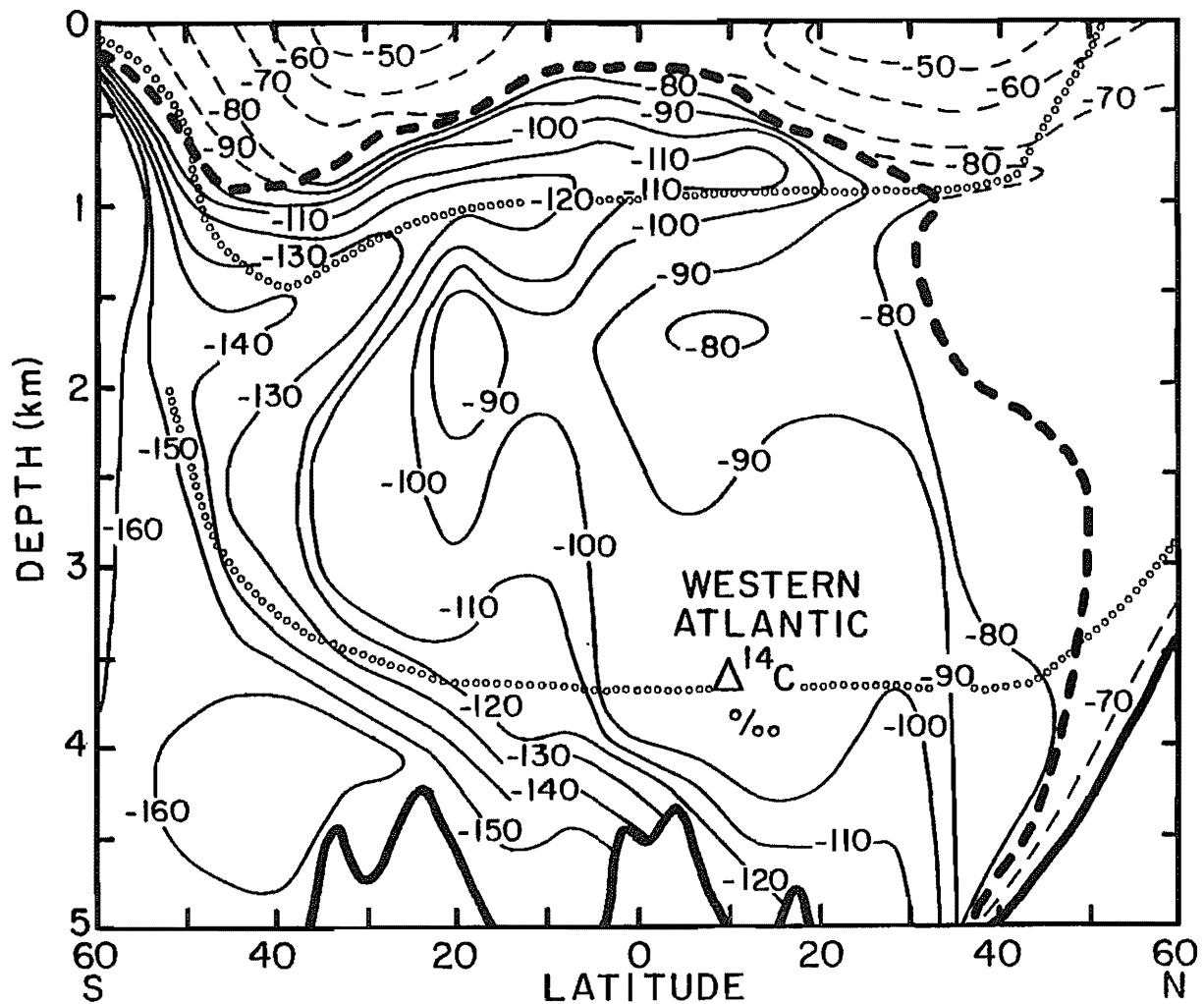


Figure 5-5. Vertical section of natural $\Delta^{14}\text{C}$ /C ratios (expressed as $\Delta^{14}\text{C}$) along the western basin of the Atlantic Ocean. The values shown are for natural radiocarbon (i.e., the distribution prior to the influx of ^{14}C produced by weapons testing). The thick dashed line designates the depth to which significant amounts of bomb ^{14}C has penetrated into the Atlantic at the time of the GEOSECS survey in 1973 (as indicated by the depth at which tritium reached about 5% its surface water value). The $\Delta^{14}\text{C}$ contours above this line are dashed because they are based on a rather limited number of analyses for samples collected prior to 1957. Also shown by dotted lines are the $\sigma_0 = 27.5\text{‰}$ (upper) and $\sigma_4 = 45.2\text{‰}$ (lower) isopycnal horizons. The results were obtained by Stuiver and by Ostlund (21). The tracks along which this and the sections which follow were drawn can be found on the foldout map.

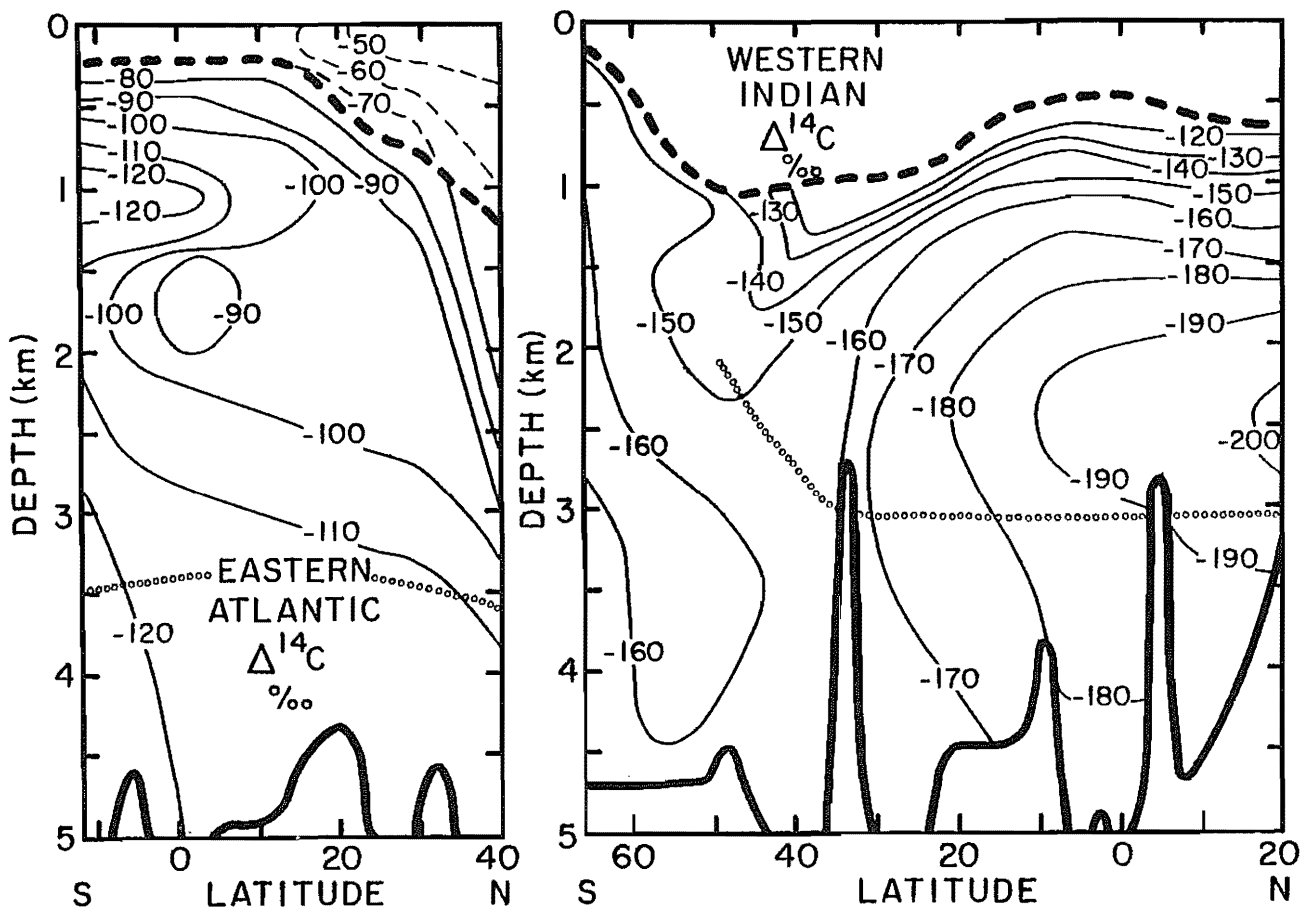


Figure 5-6. Vertical section of natural $^{14}\text{C}/\text{C}$ ratios (expressed in $\Delta^{14}\text{C}$ units) in the eastern Atlantic Ocean. As in figure 5-5 the dark dashed line marks the depth to which significant amounts of ^{14}C produced by nuclear testing had penetrated at the time of the GEOSECS survey in early 1973. Also shown by the dotted line is the $\sigma_4 = 45.2\text{‰}$ isopycnal horizon. The results were obtained by Stuiver and by Ostlund (21).

Figure 5-7. Vertical section of natural $^{14}\text{C}/\text{C}$ ratios in the western Indian Ocean. The contours terminate at the depth to which significant amounts of ^{14}C produced during nuclear testing had penetrated at the time of the GEOSECS survey in 1978. As we have almost no data on samples collected prior to 1957 no attempt has been made to reconstruct the contours of natural $^{14}\text{C}/\text{C}$ ratios in the upper part of this ocean. Also shown by the dotted line is the $\sigma_4 = 45.2\text{‰}$ isopycnal horizon. The results were obtained by Ostlund (23).

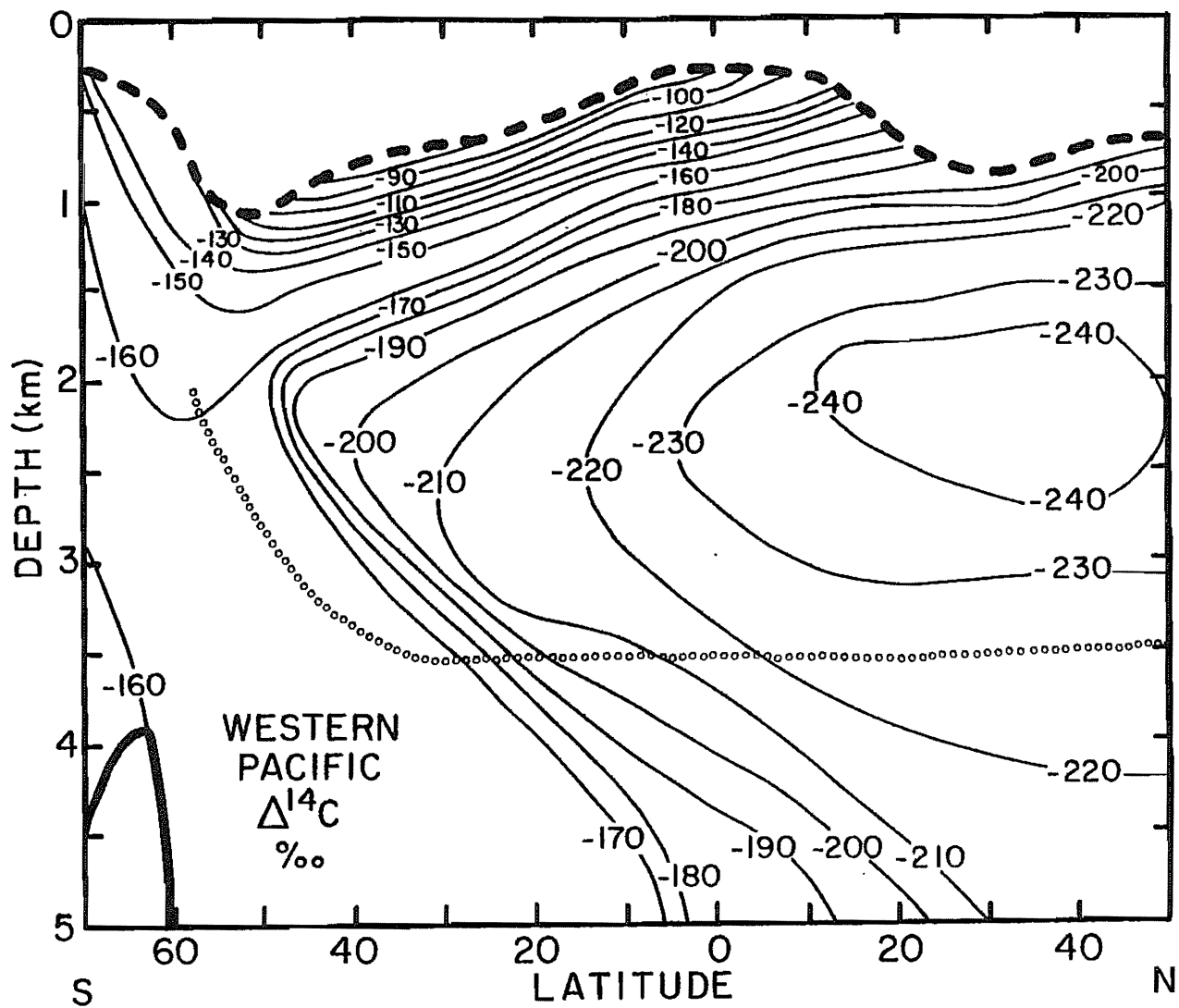


Figure 5-8. Vertical section of natural $^{14}\text{C}/\text{C}$ ratios (expressed in $\Delta^{14}\text{C}$ units) for the western Pacific Ocean from the Aleutian Arc at the north to the Antarctic continent on the south. As in the other ^{14}C sections the dark dashed line marks the depth to which significant ^{14}C produced by nuclear testing had penetrated as of 1974 when the GEOSECS Pacific survey was conducted. The limited data available for samples collected prior to 1957 suggest that the $\Delta^{14}\text{C}$ values for surface water had a pattern similar to that shown for the Atlantic in figure 5-5. Also shown by the dotted line is the $\sigma_4 = 45.2\text{‰}$ isopycnal horizon. The results were obtained by Stuiver and by Ostlund (22).

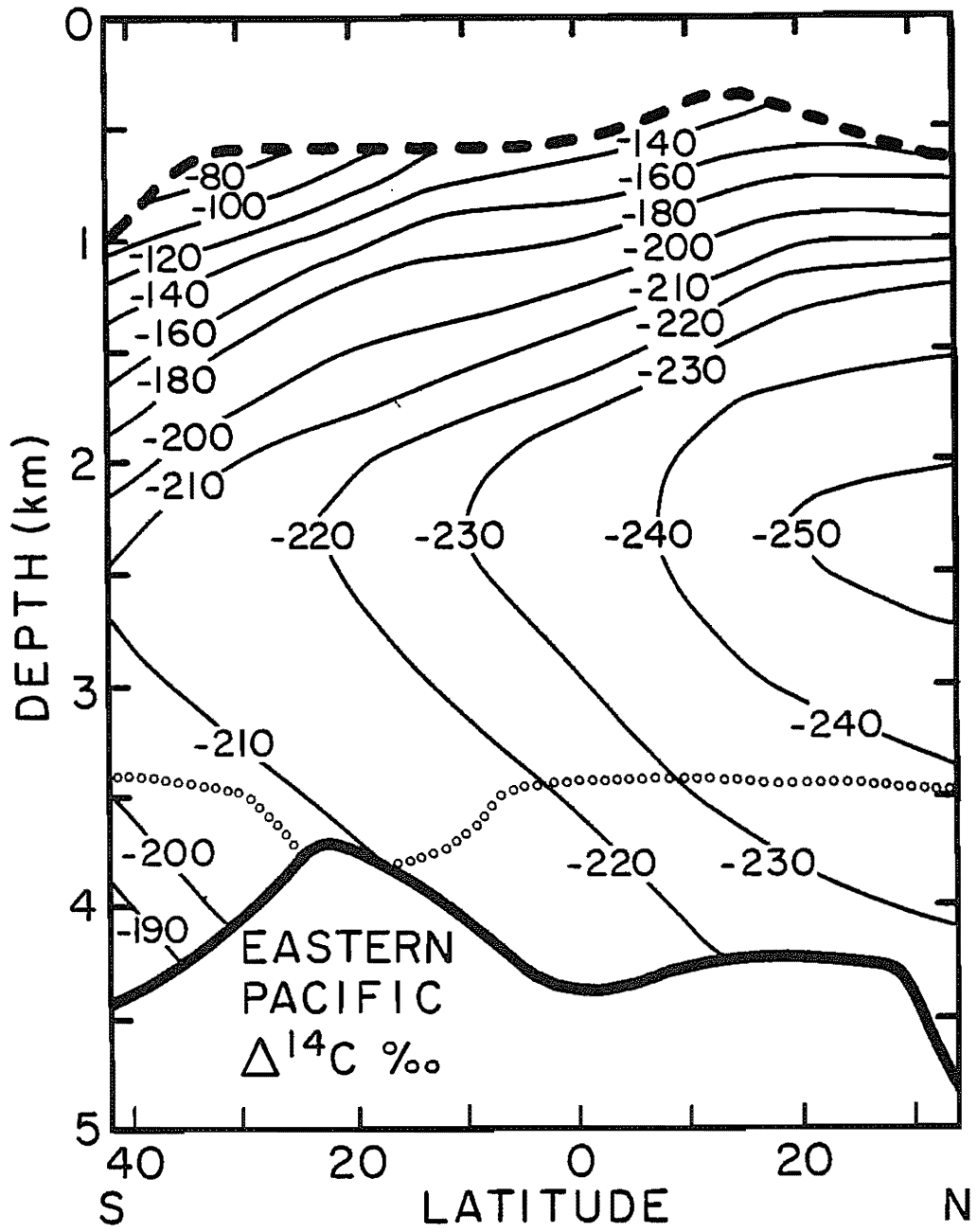


Figure 5-9. Vertical section of natural $^{14}\text{C}/\text{C}$ ratios (expressed in $\Delta^{14}\text{C}$ units) for a north-south section drawn through the eastern Pacific. Once again the dark dashed line shows the depth to which significant amounts of ^{14}C produced by nuclear testing had penetrated at the time of the GEOSECS survey in 1974. Also shown by the dotted line is the $\sigma_4 = 45.2\text{‰}$ isopycnal horizon. The results were obtained by Ostlund and by Stuiver (22).

percent of this water which survives evaporation and reaches the sea (35 percent). With this knowledge, we can calculate that in one year a layer of water 25 centimeters thick with the area of the continents will reach the sea. Since the continents occupy 30 percent of the area of the globe, if this water were spread over the sea, it would make a layer about 10 centimeters thick (see figure 5-10). This is very close to the result of 32×10^{15} liters/yr obtained from the river gauges.

Since upwelling brings an amount of water equal to an ocean-wide layer 300 centimeters thick and since rivers bring an ocean-wide layer 10 cm thick, the ratio of v_{mix} to v_{runoff} must be 30:

$$\frac{v_{mix}}{v_{runoff}} = \frac{300 \text{cm/yr } A_{\text{ocean}}}{10 \text{cm/yr } A_{\text{ocean}}} = 30$$

SEDIMENT ACCUMULATION RATES

Let us turn our attention, then, to the ways in which sedimentation rates are determined. All sedimentation rates in the ocean are based on four methods of absolute dating. One involves ^{14}C , the same isotope we used to establish the rate at which the ocean is mixing. A second method involves the uranium daughter products thorium-230 and protactinium-231, two radioactive isotopes produced by the decay of the uranium dissolved within the sea. The third method involves the decay of ^{10}Be an isotope which like ^{14}C is produced by cosmic ray interactions in the atmosphere. The fourth method involves radioactive potassium-40, which decays to a gas, argon-40. These four radioisotopic methods have all been used to date deep sea sediments and, as we will see, they give self-consistent results.

Deep sea cores contain unique stratigraphic markers which can be traced over large regions of the sea floor. Once a core containing such a marker has been dated, the level in all other deep sea cores where that stratigraphic marker is found can be assigned this age. Once the ages of several such horizons have been established, the determination of the distribution of accumulation rates for the various components of marine sediments is greatly simplified. There are three kinds of marks made in deep sea sediments that can be used for this purpose. One is magnetic. Reversals in the polarity of the earth's magnetic field are recorded in deep sea sediments. The times when these transitions occurred have been accurately determined by the potassium-argon dating of volcanic rocks whose magnetism also records the polarity of the earth's field. If we can establish which magnetic transition is which in a given core, ages can be assigned to these levels. The irregular sequence in time of these magnetic transitions (see figure 5-11) makes this assignment possible.

Another series of stratigraphic markers is based on faunal changes. For every group of organisms there are, over periods of millions of years, a few extinctions of old species, a few appearances of new species, and some unique changes in relative abundances. These changes also constitute key stratigraphic

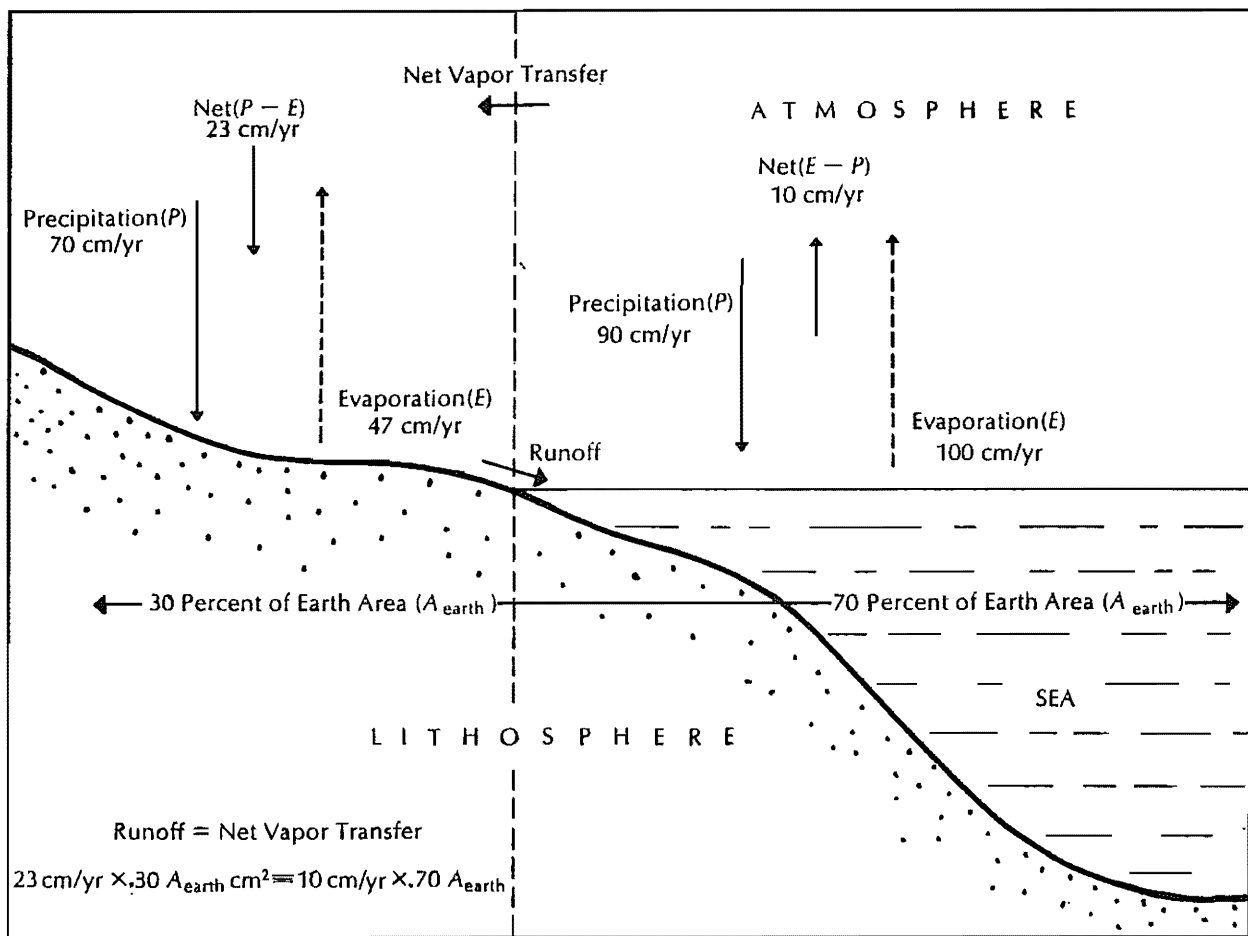


Figure 5-10. The global water cycle. About 10 percent more water evaporates from the ocean than returns as rainfall. The excess falls on the continents as rain and snow and runs from the continents into the oceans through the world's rivers.

horizons that, when dated, complement the use of magnetic reversals in assigning ages to various levels in a particular deep sea core.

The final stratigraphic marker involves climatic changes. The technique is less reliable because climatic changes are repetitive at intervals of roughly the same duration. In the main, this method is helpful for the last two climate cycles. Further back in time it is too easy to mismatch two curves and end up with the wrong age. However, as the last magnetic reversal occurred 700,000 years ago and as faunal methods are useful primarily from a few hundred thousand to a few million years ago, the climatic record is important for correlations over the last 200,000 years. Climatic changes are recorded in deep sea cores in many ways, including the CaCO_3 content changes mentioned above. $^{18}\text{O}/^{16}\text{O}$ ratio changes in the CaCO_3 from the shells of benthic foraminifera have proven to be the most reliable. The reason is that these changes are produced by the removal from (or addition to) the ocean of water isotopically depleted in ^{18}O during the formation (or destruction) of continental ice sheets. The changes in $^{18}\text{O}/^{16}\text{O}$ ratio for sea water so produced are spread uniformly through the sea. Shells formed in deep water prove superior because the deep sea is less subject to changes in temperature and river input which produce $^{18}\text{O}/^{16}\text{O}$ variations in shells formed in surface water. The ^{18}O record from benthic forams taken from a core collected on the Solomon plateau in the western equatorial Pacific is shown in figure 5-12.

RADIOCARBON DATING

Now let us examine each of the dating methods in turn, beginning with the one based on radiocarbon. We have already discussed the way in which ^{14}C is generated in the atmosphere and mixed with the carbon in the ocean. Foram shells and coccolith tests when formed in surface ocean water contain ^{14}C atoms as well as ordinary C atoms. Once formed, the shells constitute an isolated system; their ^{14}C content decreases with time in the logarithmic manner described previously: half of the ^{14}C disappears during the next 5700 years, and so on.

The fundamental assumption of radiocarbon dating is that the $^{14}\text{C/C}$ ratio at any place in the sea has always been the same as it is today. If this is so, then a shell sample from a deep sea core yielding a $^{14}\text{C/C}$ ratio half that in present-day sea water carbon must have formed 5700 years ago. If we find the level in the core where the ratio of $^{14}\text{C/C}$ is only 25 percent of that in the present surface ocean, the sample must have formed 11,400 years ago, and so on. At an age of about 40,000 years, about 1 percent of the original ^{14}C remains. Beyond this point, the exchange of carbon in the shells with their surroundings is thought to produce significant contamination and the method becomes questionable.

Although the halving method is an easy way to envision what is happening, it is only in rare cases that our sample will have aged some multiple of 5700 years. If we want to make actual age calculations, we need an equation which relates the $^{14}\text{C/C}$ ratio in time, or:

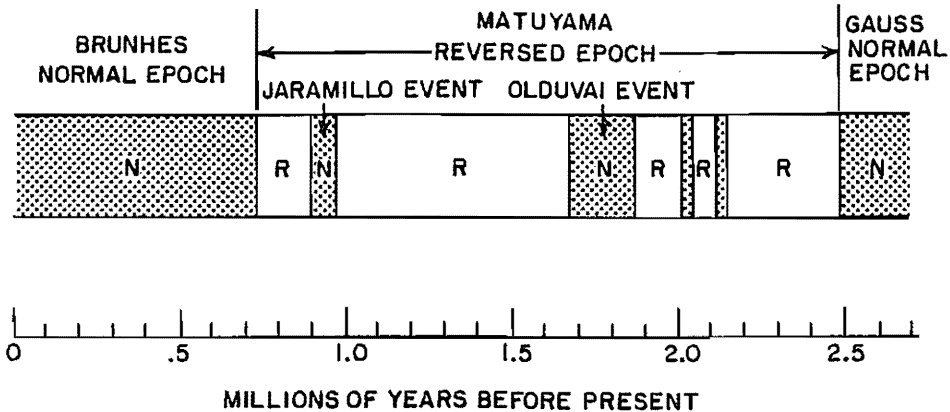


Figure 5-11. The time sequence of magnetic reversals as determined by the potassium-argon dating of volcanic rocks. The shaded areas marked N (normal) indicate times when the magnetic field had the same polarity it does today, and the open areas marked R (reversed) indicate times when it had the opposite polarity. Long intervals of time dominated by either normal or reversed polarity are called magnetic epochs and are named after scientists who made important contributions to the field of magnetism. Brief intervals of opposite polarity within these epochs are called events and are named after the localities at which they were discovered.

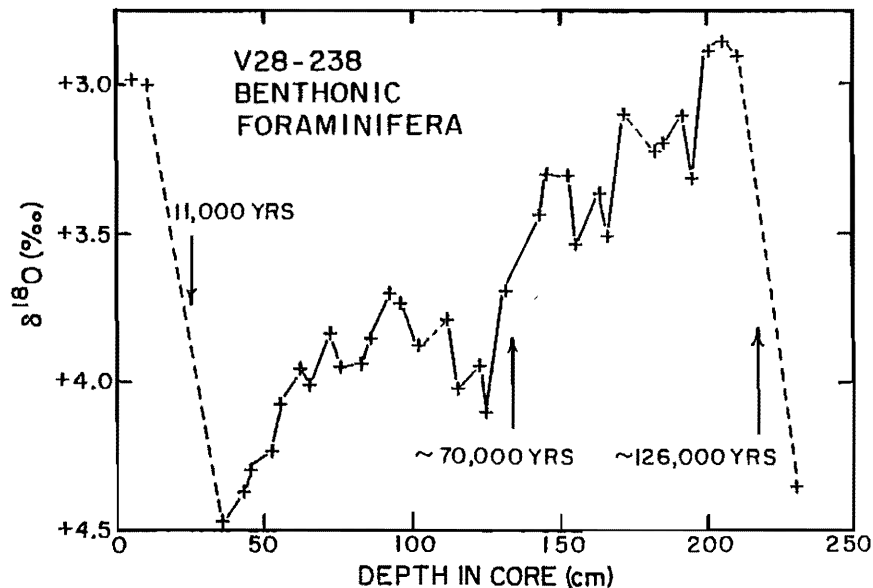


Figure 5-12. $\delta^{18}\text{O}/\delta^{16}\text{O}$ record from core V28-238 collected in the western equatorial Pacific. Just over one full climatic cycle is shown. The large $\delta^{18}\text{O}$ values are for glacial time and reflect the storage of water deficient in ^{18}O in the continental glaciers which existed at that time. Note that the cycle consists of a gradual decline toward glacial conditions followed by a sharp return to interglacial conditions. This record covers the last 130,000 years. Cycles of this type extend back over the last million years. These results were obtained by Nick Shackleton of Cambridge, England (602). The definition of the $\delta^{18}\text{O}$ notation is given on page 681.

$$\left(\frac{^{14}\text{C}}{\text{C}} \right)_{\text{today}} = \left(\frac{^{14}\text{C}}{\text{C}} \right)_{\text{formation}} \times e^{-\lambda t}$$

5-16

The equation states that the $^{14}\text{C/C}$ ratio in the shell at any given time t after formation is equal to the original $^{14}\text{C/C}$ ratio times e (the base of the natural logarithmic system) to the power $-\lambda t$, where λ is the decay constant of ^{14}C (1 part disappears every 8200 years). Solving this equation for t , we obtain:

$$t = 8200 \ln \frac{(^{14}\text{C/C})_{\text{formation}}}{(^{14}\text{C/C})_{\text{fossil CaCO}_3}} \quad 5-17$$

The age t of the sample is equal to 8200 years (the average life-time of a ^{14}C atom) times the natural logarithm (\ln) of the ratio of the $^{14}\text{C/C}$ ratio at the time of formation to the $^{14}\text{C/C}$ ratio found in the sample today. We assume that $(^{14}\text{C/C})_{\text{formation}}$ is identical to the ratio we find in present surface ocean water (and hence in living shells and coccoliths).

In figure 5-13 are shown radiocarbon ages made at series of depths in two deep sea cores. Both show a surprising feature. The age at the core top is not zero! Rather the upper 7 centimeters of material in each core show a nearly uniform radiocarbon age. Below 7 centimeters in each case the age begins to rise in a regular way with depth as would be expected. The cause of these core top anomalies is "bioturbation". Organisms living on the sea floor must "stir" the upper sediment much as worms living on the continents "stir" the soil. Only when material has been buried beyond a depth of 7 or so centimeters does it escape the stirring action of these organisms. The radiocarbon age of this bioturbated layer is given approximately by the ratio of its thickness to the sedimentation rate. While not having any appreciable influence on ages obtained beneath the mixed layer or on sedimentation rates obtained from age versus depth plots beneath the mixed layer, this process does have significance to some of the processes going on in the sea. We have already dealt with one example of the role of bioturbation (i.e., its importance to the recycling of short lived radioisotopes). We shall deal with others in the chapters to come.

URANIUM SERIES DATING

The second dating method involves the element uranium and two radioactive "daughter" isotopes produced by the decay of uranium, ^{230}Th and ^{231}Pa . We will concentrate first on ^{230}Th , the product of long-lived ^{238}U . Uranium-238 was produced in the interiors of massive stars that subsequently exploded and dispersed their products within our galaxy. It was incorporated into the solar system when it formed from a galactic dust and gas cloud about 4.5 billion years ago. Uranium-238 is unstable (that is, radioactive) and has been gradually decaying since its stellar birth. Since a uranium atom has a mean life of about 7 billion years, not enough time has elapsed for ^{238}U to disappear and much of it remains to-

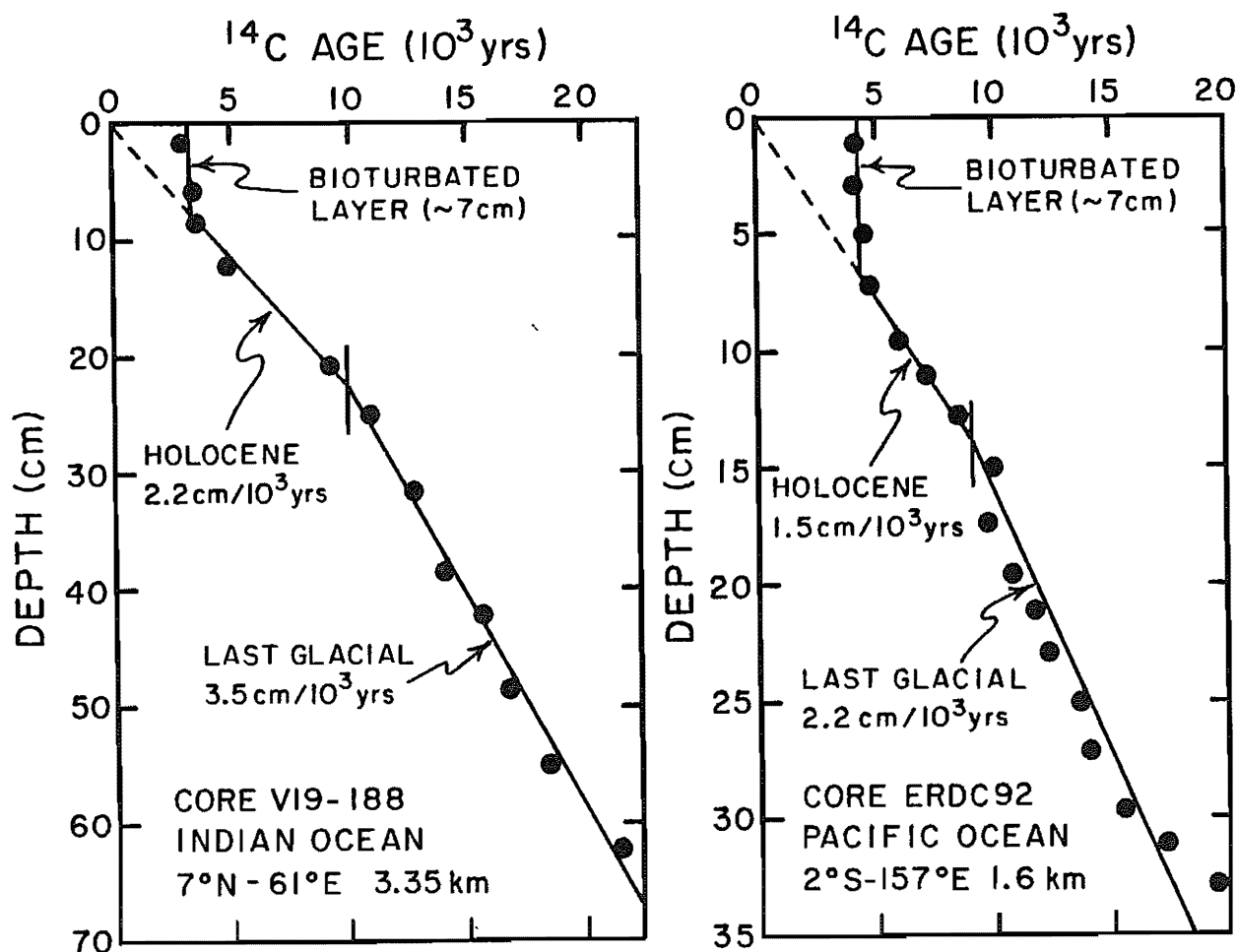


Figure 5-13. Radiocarbon ages as a function of depth in two deep sea cores. The near constancy of these ages down to a depth of about 7 cm bears witness to the action of organisms which "burrow" into the sediment. Below this zone of bioturbation the ages show the expected regular increase. The changes in the slope of the age versus depth line at the time close to the end of the last glacial period (i.e., ~10,000 years ago) reflects the influence of climate on the rate at which the various materials making up the sediment rain onto the sea floor. These results were obtained by Peng of the Lamont-Doherty Geological Observatory (197, 199).

day in our solar system. As we discussed in the last chapter, ^{238}U decays through a whole series of radioactive forms to stable lead (^{206}Pb). Many billions of years from now all the ^{238}U will have been converted into ^{206}Pb . Until then, we will have in nature a whole series of uranium decay products, produced as uranium atoms and decaying towards lead (see figure 4-1).

The transition from ^{238}U to ^{206}Pb requires the emission of 8 alpha particles, each carrying away 2 neutrons and 2 protons. It also requires an equivalent number of electron emissions. Thus, an atom must go through many stages in the transition from ^{238}U to ^{206}Pb , and the most interesting step, at least as far as dating goes, is its pause at ^{230}Th . This isotope has a half-life of 75,000 years (ideal for dating in the range of a few hundred thousand years). Fortunately for dating purposes, ^{230}Th has a much different chemical cycle in the ocean than uranium does. Uranium has a mean residence time in the ocean of about 500,000 years. Its concentration is thus relatively high with respect to its abundance in natural rock. On the other hand, as we have seen in chapter 4, thorium is extremely reactive in sea water; it is removed to the sea floor in a matter of a few decades. This separation between parent ^{238}U and daughter ^{230}Th is the basis for uranium dating. Recently formed deep sea sediments have a great excess of ^{230}Th atoms (over those supported by the decay of the parent ^{238}U). The age of the sediments can be computed from the disappearance after burial of these excess ^{230}Th atoms. However, successful dating by the ^{230}Th method is possible only under special circumstances: both the rate at which the sediment particles fall onto a given area of the sea floor and the rate at which the ^{230}Th atoms are incorporated into this falling sediment must remain constant with time. The trick is to develop criteria to show whether these assumptions are valid for any given core. If the core meets these criteria, we use the ^{230}Th content to calculate ages; if it does not, the measurements are of little value for dating. Most of the sediments deposited in the open ocean do not accumulate at a sufficiently constant rate to make reliable dating by this method possible. Fortunately some do.

In figure 5-14 is shown a plot of ^{230}Th as a function of depth in an ideal core that has a constant sedimentation rate of 2 cm/ 10^3 yrs. If we measured the ^{230}Th content of this material, we would find that at a depth of 150 centimeters (or 75,000 years in age) the amount of excess ^{230}Th had dropped by a factor of 2 from that found at the top of the core. If we then took a sample at 300 centimeters (150,000 years in age), we would find only one-fourth of the original excess ^{230}Th content. If we went down to 450 centimeters, the age of the sample would be 225,000 years (three half-lives would have passed) and only one-eighth of the initial should remain. In such a core the ^{230}Th concentration should follow an exponential curve with depth. In order to test whether points fall along such a curve, it is best to transform the coordinates of the graph in such a way that they lie along a straight line. This can be accomplished by plotting the logarithm of the concentration of excess ^{230}Th atoms against depth. If the core meets the criteria of the method then the points should fall along a straight line, as they do in figure 5-14.

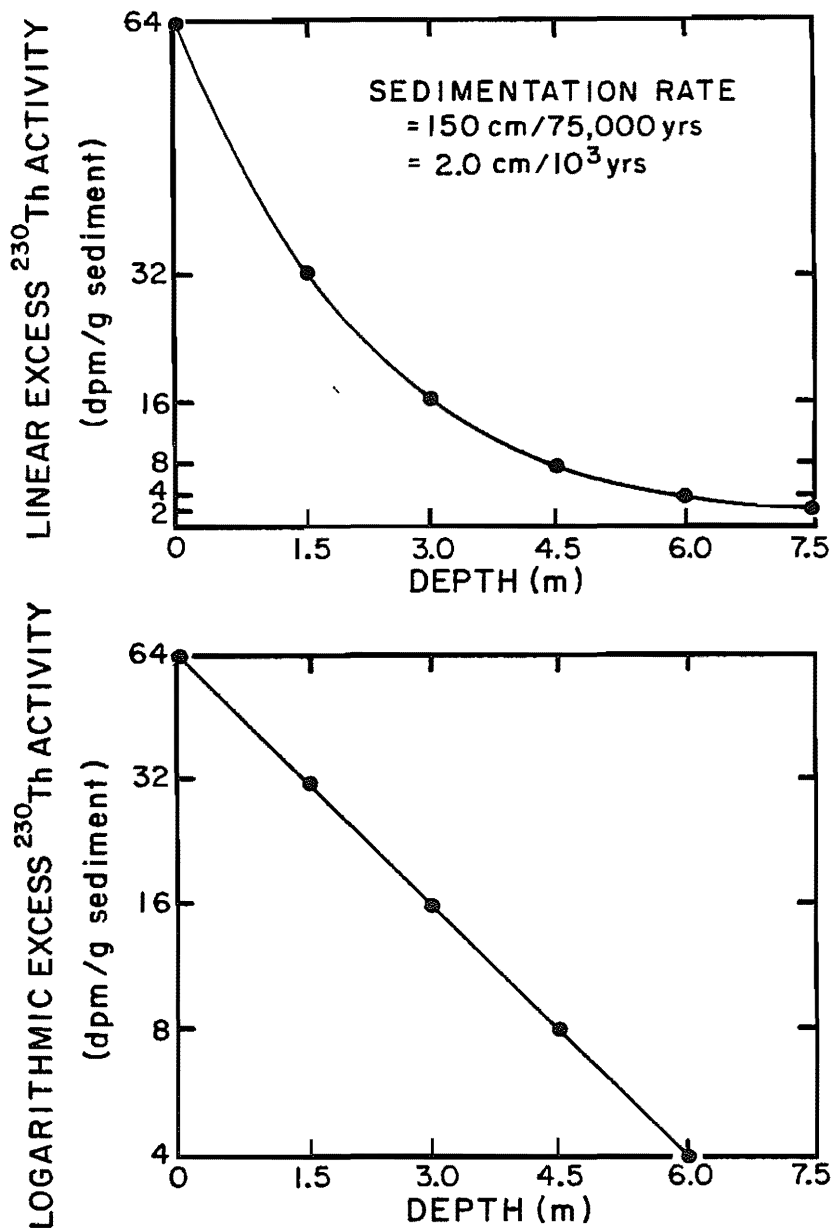


Figure 5-14. The distribution with depth of excess ^{230}Th in an ideal core with a constant sedimentation rate of $2.0 \text{ cm}/10^3 \text{ yrs}$ and a constant rate of ^{230}Th influx. In such a core, the amount of excess ^{230}Th shows a drop by a factor of 2 for each interval of 150 centimeters penetrated (i.e., the thickness of sediment is deposited in one half-life of ^{230}Th). The upper graph employs a linear scale for the ^{230}Th content; the lower graph employs a logarithmic scale.

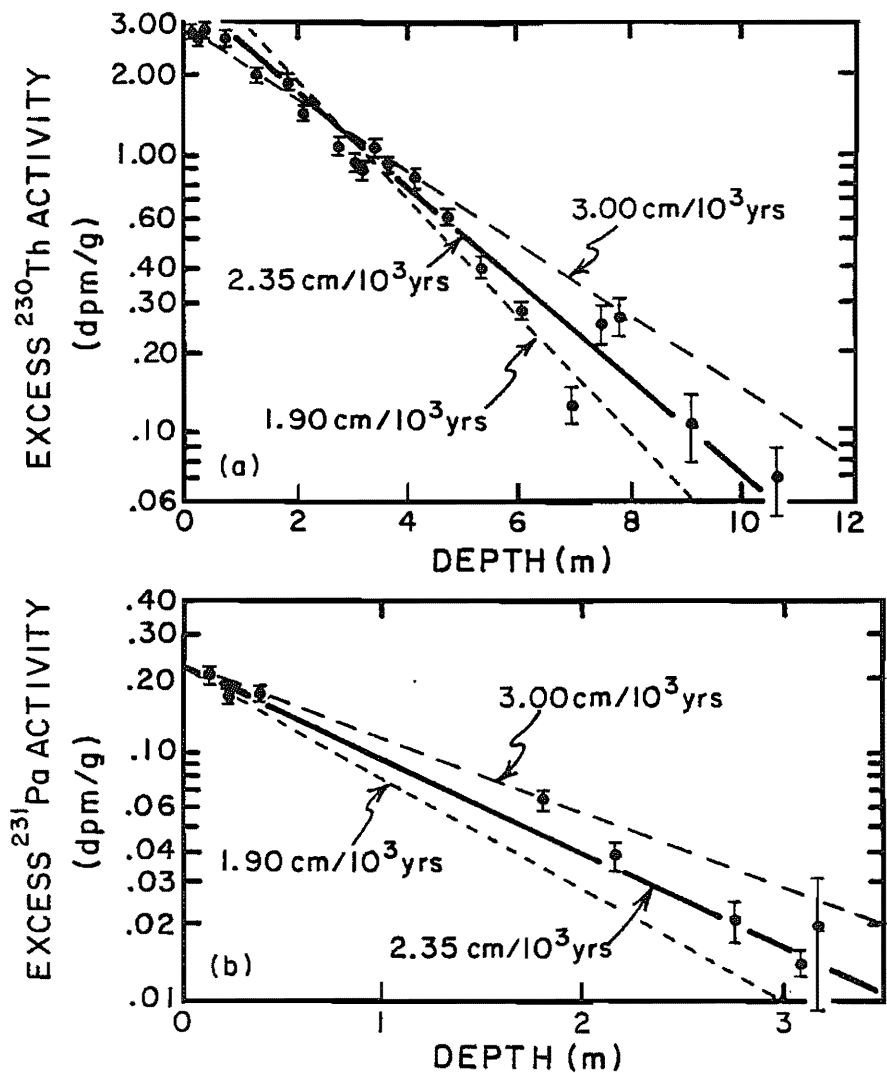


Figure 5-15. Actual ^{230}Th (a) and ^{231}Pa (b) measurements for core V12-122 raised by the Columbia University research vessel Vema in the Caribbean Sea. The failure of the points to fall along a single straight line in either graph reflects a combination of experimental uncertainty in the measurements (note error bars) and of nonideality in the core (the sedimentation rate and/or the isotope influx rate did not remain exactly constant with time). The best fit solid line (a rate of $2.35 \text{ cm}/10^3 \text{ yrs}$) and dashed lines representing sedimentation rates 25 percent greater ($3.00 \text{ cm}/10^3 \text{ yrs}$) and 25 percent smaller ($1.90 \text{ cm}/10^3 \text{ yrs}$) are shown for both isotopes. Clearly with the observed scatter, the rate (and hence the age at any given depth) cannot be determined to better than ± 10 percent. The agreement between the best fit rates for ^{230}Th and ^{231}Pa adds support to the validity of the ages derived in this way. The results were obtained by Ku, Goddard and Middel of the Lamont-Doherty Geological Observatory (611).

Figure 5-15 shows an actual set of ^{230}Th measurements on a core from the Caribbean Sea. This core proves to be close to ideal. Although there is some scatter from a single straight line, most of the points lie within twice the measurement error of this line. The best fit line corresponds to a sedimentation rate of $2.35 \text{ cm}/10^3 \text{ yrs}$. To show the sensitivity of the sedimentation rate to the choice of the best fit line, dashed lines representing sedimentation rates of $3.00 \text{ cm}/10^3 \text{ yrs}$ (25 percent higher) and $1.90 \text{ cm}/10^3 \text{ yrs}$ (25 percent lower) have been included for comparison. Even in the best cores, this method allows the average sedimentation rate to be determined with an accuracy no better than 10 percent.

The other product of uranium decay of interest for dating, ^{231}Pa , is generated by the decay of a second isotope of uranium, ^{235}U . Like ^{238}U , ^{235}U has a long half-life (0.7 billion years). Uranium-235 decays to stable ^{207}Pb , and like ^{238}U it must go through many stages to make this transition to stability. One stopping point is ^{231}Pa , an isotope with a half-life of 32,500 years. Like ^{230}Th , ^{231}Pa is very insoluble and is removed from sea water to the sediments within a century after it is produced. We can measure the concentration of the isotope ^{231}Pa at various depths in a deep sea core and plot these data on a logarithmic graph in the same manner we did with ^{230}Th . If the points yield a straight line on such a plot, then the slope of this line can be used to calculate the sedimentation rate for the particular core. Shown in figure 5-15 are plots of the ^{231}Pa measurements for the Caribbean core just discussed. Since ^{231}Pa is less abundant in core tops and since it disappears more rapidly than ^{230}Th , it can be measured with sufficient accuracy only to a depth of 3 meters (compared to a depth of 9 meters for ^{230}Th). Like ^{230}Th , the best fit line for ^{231}Pa has a slope that yields a sedimentation rate of $2.35 \text{ cm}/10^3 \text{ yrs}$! So, in this particular core, both isotopes tell us that the sediment has accumulated at roughly a constant rate. Thorium-230 allows the mean rate to be established over an interval of 400,000 years; ^{231}Pa , over an interval of 150,000 years.

These isotopes have also been used to determine the growth rate of manganese nodules. Because these objects grow so slowly a special sampling technique had to be devised. Teh-Lung Ku did this job by measuring off an area on the face of a nodule and scraping material from this area (224). By weighing these scrapings Ku could estimate the depth interval to which each successive sample corresponded. An example of the results obtained in this way is shown in figures 5-16. As can be seen all three samples taken from this nodule come from the outer millimeter. The slopes of the lines joining the measurements give growth rates of $4.0 \text{ mm}/10^6 \text{ years}$ (^{230}Th) and $4.3 \text{ mm}/10^6 \text{ years}$ (^{231}Pa).

Ku also measured the ratio of ^{234}U to ^{238}U activity in these three samples and in four others from deeper below the surface (see figure 5-17). As mentioned in chapter 4 the activity of ^{234}U in sea water is about 15% higher than that of ^{238}U . The reason for this excess is that during their creation in deep sea sediments ^{234}U atoms are knocked loose (by recoil from the departing α particle) from their positions in the clay minerals which carry

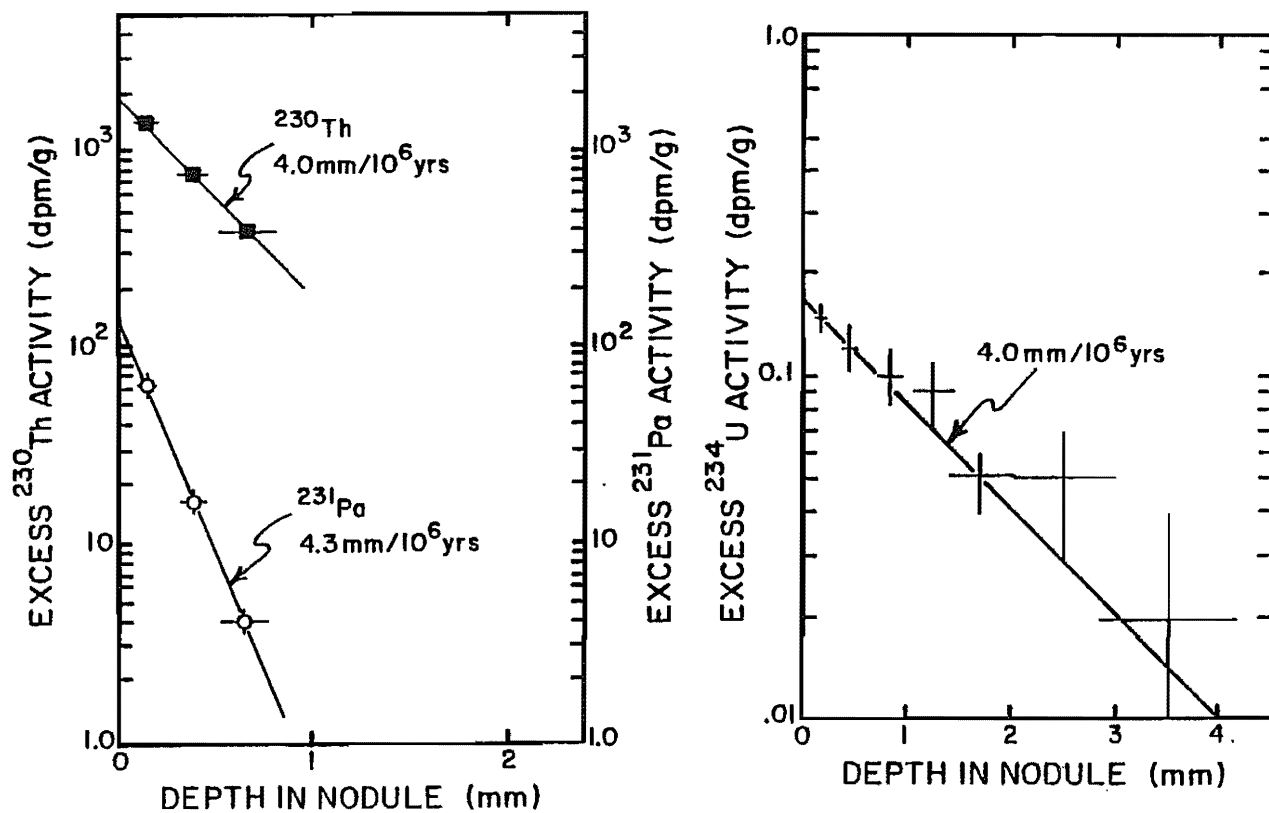


Figure 5-16. Plots of the logarithm of excess ^{230}Th and ^{231}Pa versus depth in a manganese nodule from the North Pacific Ocean. The growth rates derived from these measurements are also shown. These measurements were obtained by Ku while at Lamont-Doherty Geological Observatory (224).

Figure 5-17. Plot of the logarithm of excess ^{234}U activity in the same nodule for which ^{231}Pa and ^{230}Th diagrams are given in figure 5-16. The slope expected for the growth rate obtained using ^{230}Th is shown for reference.

the bulk of the uranium in these sediments. These loosened ^{234}U atoms have a better chance of migrating into the sea than do their more strongly bound ^{238}U brothers. Nodules incorporate their uranium from sea water, hence newly formed nodule material has 15% more ^{234}U than ^{238}U activity. Ku monitored the decrease of this excess with depth in the nodule and found that like ^{230}Th and ^{231}Pa this decrease could be approximated as exponential. Using the half-life of 250,000 for ^{234}U the slope of the excess ^{234}U trend yields an accumulation rate consistent with that for ^{230}Th and ^{231}Pa .

Many nodules have now been studied in this way. They all show growth rates on the order of 2 to 5 mm/10⁶ years.

BERYLLIUM DATING

Beryllium-10 is produced when the nuclei of atmospheric gases are smashed apart during collisions with high energy cosmic protons. As this isotope has a half-life of 1.5×10^6 years it has potential applications in the dating of ocean sediments and manganese nodules. The idea is that much of the ^{10}Be produced in the atmosphere is delivered to the sea by rainfall and aerosol impacts. Like other metals these Be atoms find their way to the sediments and manganese nodules on the sea floor. To harness ^{10}Be for dating the same two requirements must be met as for the ^{230}Th method; i.e., the accumulation rate of both ^{10}Be and of the host material must remain constant with time.

The application of the ^{10}Be method was rather limited in that its activity is very small. Larger samples had to be dissolved and the beryllium isolated. The ^{10}Be in this beryllium then had to be measured by low-level beta counting. Counting times of several days are required for each sample. An example of results obtained in this way is given in figure 5-18. As can be seen the three points when placed on a logarithm activity versus depth plot form a straight line. The slope of this line gives a growth rate of 2.4 mm/10⁶ yr. This and other ^{10}Be results on nodules are very important because they confirm the ^{230}Th and ^{231}Pa based growth rates. Because the latter were based on the outer millimeter of material many scientists were hesitant to accept them. As the ^{10}Be results shown in figure 5-18 cover a depth interval of 1.5 centimeters they are not so easily disposed of.

Recently a new means of measuring ^{10}Be has been found. Instead of measuring the beta decays of this isotope the atoms themselves are measured in a high-energy mass spectrometer. This method requires only small samples (milligrams) and the measurements can be done quickly (a few minutes). An example of results by this method is also shown in figure 5-18. Again the growth rate obtained from ^{10}Be is in agreement with that obtained from the uranium series measurements. As summarized in table 5-1 this is true for all the nodules studied to date by the ^{10}Be method.

POTASSIUM-ARGON DATING

The time scale for deep sea cores beyond 400,000 years is based on ages obtained by the potassium-argon method. Potas-

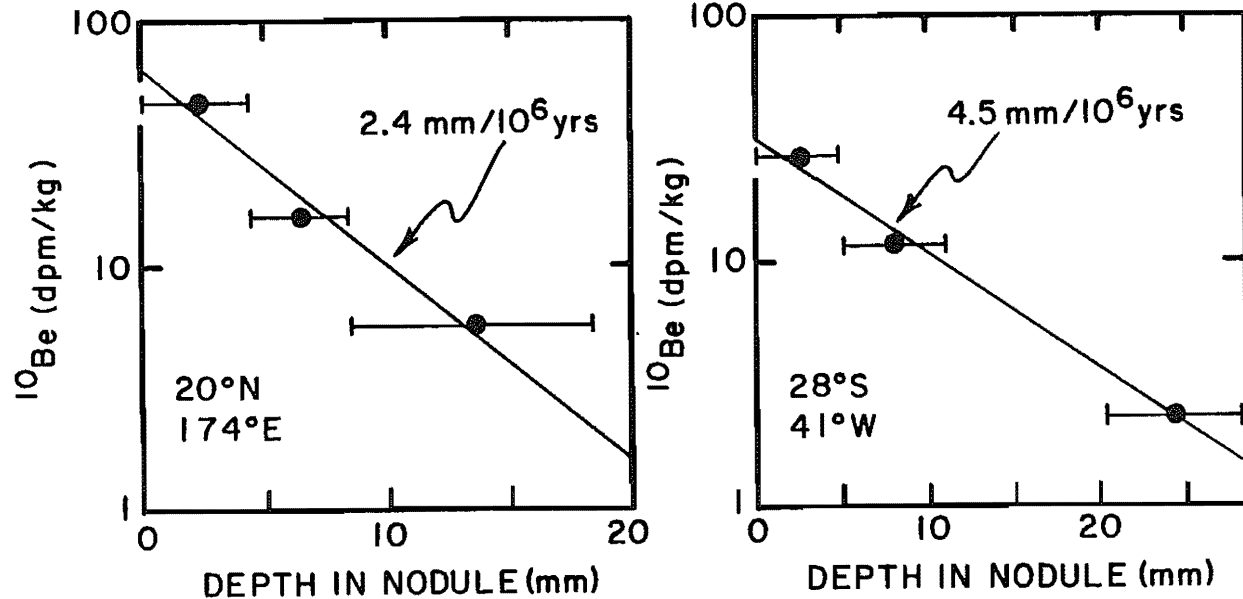


Figure 5-18. The left hand graph shows the logarithm of the ^{10}Be activity as a function of depth in a manganese nodule from the North Pacific Ocean. These measurements were made by Ku and his colleagues at the University of Southern California using the conventional β -counting technique (260). The right hand graph shows the logarithm of the number of ^{10}Be atoms as a function of depth in a manganese nodule from the South Atlantic Ocean. These measurements were made by Turekian and his colleagues at Yale University (262).

Table 5-1. Summary of manganese nodule growth rates as determined by the ^{10}Be method.

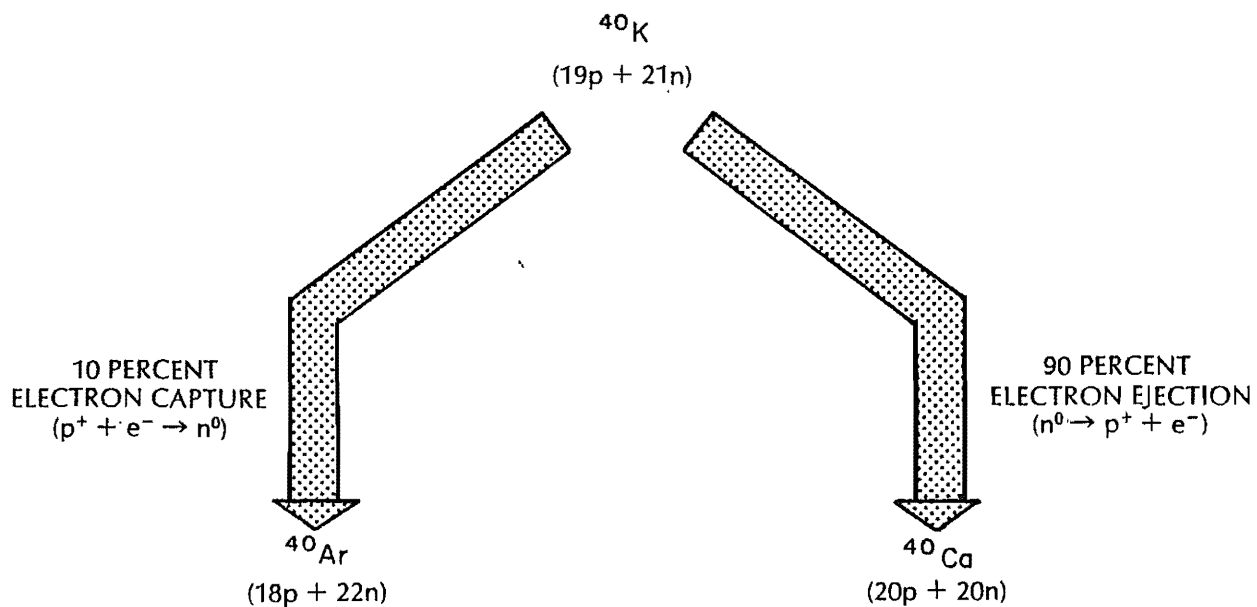
Location	^{10}Be Flux $10^4 \text{ atoms/cm}^2 \text{yr}$	Growth Rate $\text{mm}/10^6 \text{yr}$	Investigators & Institution	Ref.
40°N 170°E	3.8	1.3	Bhat et al. PRL (India)	(254)
21°N 113°W	5.0	6.3	Bhat et al. PRL (India)	(254)
19°N 162°W	1.4	3.0	Somayajulu Tata (India)	(251)
21°N 173°W	2.1	2.3	Sharma and Somayajulu PRL (India)	(263)
21°N 173°E	2.4	3.3	Sharma and Somayajulu PRL (India)	(263)
13°S 149°W	1.7	2.8	Guichard et al. Centre des Faibles Radioactivities Gif-Sur-Yvette (France)	(256)
9°N 151°W	1.4	~2	Krishnaswami et al. Yale University	(264)
15°N 125°W	2.1	~2	Krishnaswami et al. Yale University	(264)
21°N 175°E	3.7	2.4	Ku et al. U.S.C.	(260)
20°N 139°W	3.5	1.3	Ku et al. U.S.C.	(260)
28°S 41°W	2.7	4.5	Turekian et al. Yale University	(261)

sium-40 is another of the isotopes generated long ago in stars and later incorporated in our solar system. Its half-life is just over a billion years; so although it is also destined for extinction, some ^{40}K still remains in our earth. Roughly 90 out of 100 ^{40}K atoms change themselves into ^{40}Ca ; the remaining 10 change themselves into ^{40}Ar (see figure 5-19). The proportion of ^{40}K undergoing decay by each of these routes is a constant. When age determinations are made, it is the argon produced by the decay of potassium that is measured rather than the calcium. The reason for this is that when a volcanic rock forms, gases are almost totally excluded from the minerals that crystallize out of the hot liquids. Hence volcanic rocks are initially free of ^{40}Ar . With time, the ^{40}K in these rocks undergoes radioactive decay and produces argon which remains trapped in the crystal lattices of the rock. If we measure the amount of ^{40}Ar and the amount of ^{40}K in one of these rocks, it is possible to calculate the length of time that has elapsed since the rock crystallized.

To apply this method directly to deep sea sediments requires the chance presence of a layer of volcanic ash. The normal K-bearing minerals found in sediments are detrital in origin and bear the great age of the rocks from which they were eroded. Unfortunately, volcanic ashes in deep sea sediments are quite rare, so the potassium-argon method does not prove to be very profitable for the direct dating of sediments.

The most powerful application of the potassium-argon method was in the establishment of the chronology for magnetic reversals. Volcanic rocks believed to have formed in the last few million years were collected from all over the earth for this purpose. For each sample, the polarity of the magnetic field at the time that the rock crystallized was established by measuring the magnetic vector in an oriented sample of the rock. This is possible because the iron-bearing minerals in basaltic rocks were magnetized in accord with the direction of the earth's magnetic field at the time the rock cooled. If a rock cooled during an interval when the magnetic field was reversed, then its magnetic vector will point toward the south pole instead of the north pole. Roughly half the rocks collected fell in the north pole category and half fell in the south pole category. The potassium-argon age of each rock was then carefully measured. The results showed that all the rocks with ages of less than 0.7 million years were normal in polarity and that most of the rocks dating between 0.7 and 2.5 million years were reversed polarity, except for those formed in several time intervals during which the earth's magnetic field briefly returned to normal (see figure 5-11).

The same temporal sequence of magnetic polarity observed in volcanic rocks exists in deep sea cores. The orientation of iron bearing grains settling to the sea floor is in accord with the earth's field. Thus the ages obtained from the volcanic rock record can be applied to the reversals seen in deep sea cores. Of course, for a core to be dated in this way, it must penetrate at least the youngest of these magnetic reversals (i.e., that at 700,000 years). Magnetic correlation dating allows dating back to about 4,000,000 years.



$$t_{1/2} = 1.1 \times 10^9 \text{ yrs}$$

Figure 5-19. The scheme for radioactive decay of the long-lived potassium isotope, ^{40}K . One nucleus in ten transforms by capturing an electron, the other nine transform by emitting an electron. The argon isotope, ^{40}Ar , produced by the electron capture process provides a means of dating volcanic rocks.

AGREEMENT AMONG DATING METHODS

We will cite two examples of the agreement obtained when several dating methods are applied to a single core. The first core, RC11-209, was taken by the Columbia University research vessel ROBERT CONRAD in the equatorial ocean just north of the equator. One sample from a depth of 11 centimeters yielded a $^{14}\text{C}/\text{C}$ ratio 25 percent the ratio in surface water, indicating that the sample had aged for two half-lives of ^{14}C (that is, for 11,400 years). This measurement gives a sedimentation rate very close to $1.0 \text{ cm}/10^3 \text{ yrs}$. In this core, the first magnetic boundary occurs at 700 centimeters. As this reversal has been dated by the potassium-argon method to be 740,000 years in age, the average sedimentation rate was again $1.0 \text{ cm}/10^3 \text{ years}$. By measuring the variation in CaCO_3 content with depth in the core, it was possible to establish the climatic record and, particularly, the point at which the second sharp warming before present occurred. In other cores, the age of this boundary has been determined by the ^{230}Th method to be 125,000 years. The use of this time marker yielded a sedimentation rate for the core of about $1.2 \text{ cm}/10^3 \text{ yrs}$. So the three methods - direct ^{14}C dating, the magnetic correlation of an event dated by the potassium-argon method, and the climatic correlation of an event dated by the ^{230}Th method - all give roughly the same result!

The second core, V12-122, is the Caribbean core already used as an example of ^{230}Th and ^{231}Pa dating (see figure 5-15). These two methods yielded concordant rates of $2.35 \text{ cm}/10^3 \text{ yrs}$. At 9 meters depth in this core, there is a faunal change that can be correlated from core to core. This paleontologic event has been dated at 400,000 years by interpolating between the core top and the level of the first magnetic reversal (740,000 years) in 5 cores for which a magnetic stratigraphy has been established. From this age we can obtain a sedimentation rate of $2.25 \text{ cm}/10^3 \text{ yrs}$. In the same core, ^{14}C ages of 8950 years at 27 centimeters and 18,300 years at 57 centimeters were obtained. These ages suggest a sedimentation rate of $3.0 \text{ cm}/10^3 \text{ yrs}$. Thus, again rates of sedimentation based on ^{40}Ar , ^{230}Th , ^{231}Pa , and ^{14}C dating methods are reasonably consistent.

COMPARISON OF MODEL AND OBSERVED RATES OF CaCO_3 SOLUTION

We can use the two-box ocean model to predict the rate at which CaCO_3 dissolves in the deep sea. As we discussed in chapter 1, it is possible to show, from the variations in alkalinity and total dissolved carbon from water mass to water mass, that for every 4 moles of C in the form of organic molecules oxidized in the deep sea roughly 1 mole of C is dissolved in the form of CaCO_3 . The total amount of carbon returned to solution per unit area in the deep sea is given by:

$$B = v_{\text{mix}}(C_{\text{deep}} - C_{\text{surface}})$$

5-18

Hence the amount of CaCO_3 dissolving per unit area is given by:

Table 5-2. Calcite accumulation rates during interglacial times for cores taken above the lysocline (the ΔCO_3 entry in the table shows extent of supersaturation of the water at the depth the core was taken).

Core No.	Lat.	Long.	Water Depth km	ΔCO_3 $\mu\text{m}/\text{kg}$	Bulk Accum. Rate $\text{cm}/10^3 \text{yr}$	Frac. CaCO_3 %	CaCO_3^* Accum. Rate $\text{g}/\text{cm}^2 10^3 \text{yr}$	Ref.
NORTH ATLANTIC								
280	35°N	44°W	4.30	~ 2	3.5	60	1.5	(211)
1665	26°N	45°N	2.90	~25	0.84	85	0.6	(+)
1681	26°N	45°N	3.97	~10	0.77	83	0.6	(+)
V29-192K	54°N	17°W	2.37	~	3.5	65	1.7	(+)
V30-101K	44°N	32°W	3.30	~	2.2	77	1.4	(+)
V22-226	30°N	45°W	3.13	~25	1.2	95	1.1	(+)
CARIBBEAN								
A240-MI	15°N	68°W	4.18	~10	2.3	56	0.9	(213)
V12-122	17°N	74°W	2.80	~28	2.4	64	1.2	(229)
EQUATORIAL ATLANTIC								
A180-73	0°	23°W	3.75	~22	3.1	68	1.6	(196)
A180-74	0°	24°W	3.32	~31	2.3	(85)	1.8	(195)
V30-41K	0°	23°N	3.87	~20	2.0	88	1.6	(+)
SOUTH ATLANTIC								
V22-72	29°S	35°W	3.12	~40	1.3	84	1.0	(+)
EQUATORIAL PACIFIC								
ERDC	2°S	157°E	1.60	~15	1.5	86	1.2	(199)
RC20-16	6°N	86°W	1.97	~ 5	3.6	27	0.5	(+)
SOUTH PACIFIC								
V19-54	17°S	114°W	2.96	~12	1.25	60	0.5	(235)
V19-56	17°S	115°W	3.15	~ 5	1.3	78	0.9	(+)
V19-61	17°S	116°W	3.42	~ 7	0.44	90	0.4	(235)
EQUATORIAL INDIAN								
V19-188	7°N	61°E	3.36	~ 5	2.2	82	1.6	(197)
RC14-35	0°S	90°E	3.02	~ 5	2.6	85	2.0	(+)
SOUTH INDIAN								
RC9-150	31°S	115°E	2.70	~10	3.7	70	2.1	(+)
RC17-69	32°S	33°E	3.31	~ 3	3.8	48	1.1	(+)
V18-207	26°S	87°E	2.45	~12	1.0	96	1.0	(+)

*Mean for all cores in this table: $1.2 \text{ g}/\text{cm}^2 10^3 \text{yr}$

+Unpublished Lamont data.

$$B_{CaCO_3} = \frac{1}{5} v_{mix}(C_{deep} - C_{surface})$$

We have also shown that v_{mix} is equal to a layer of ocean water 300 centimeters thick per year (or $\sim 0.3 \text{ kg/cm}^2 \text{ yr}$). The concentration of dissolved carbon in deep water averages $2.25 \times 10^{-3} \text{ moles/kg}$. In warm surface water it averages $2.00 \times 10^{-3} \text{ moles/kg}$. We find, then, that $CaCO_3$ must be falling from the surface ocean into the deep ocean and dissolving at the rate of $1/5 \times 0.3 \text{ kg/cm}^2 \text{ yr} \times 0.25 \times 10^{-3} \text{ moles/kg}$, or $0.015 \times 10^{-3} \text{ moles of carbon per square centimeter of ocean surface per year}$. Accumulation rates of material in deep sea sediments are not normally expressed in these units, but rather in units of grams of $CaCO_3$ per square centimeter of sea floor per 1000 years. So we need to convert from one set of units to the other. It happens that 1 mole of $CaCO_3$ weighs almost exactly 100 grams. Thus $0.015 \times 10^{-3} \text{ moles/cm}^2 \text{ yr}$ of $CaCO_3$ is equivalent to $1.5 \text{ g/cm}^2 \text{ yr}$ of $CaCO_3$, or:

$$B_{CaCO_3} = 1.5 \frac{\text{g}}{\text{cm}^2 \cdot 10^3 \text{ yrs}}$$

Calcite accumulates on about 20% of the sea floor and dissolves from the other 80%. As summarized in table 5-2 the mean accumulation rate of calcite for cores from above the lysocline is $1.2 \text{ g/cm}^2 \text{ yr}$.* If the rain rate of calcite onto the other 80% of the sea floor is also assumed to be $1.2 \text{ g/cm}^2 \text{ yr}$ then the total rate of solution of calcite is $0.80 \times 3.6 \times 10^{18} \text{ cm}^2 \times 1.2 \text{ g/cm}^2 \text{ yr}$ or $3.4 \times 10^{15} \text{ g/year}$. The average calcite so-lution rate per unit area of sea floor becomes $0.95 \text{ g/cm}^2 \text{ yr}$.

To this rate of calcite solution we must add the contribution of aragonite. From sediment trap studies it is estimated that the rain rate of aragonite is about 20% that of calcite. As virtually all the aragonite reaching the deep sea dissolves, the solution rate of aragonite is 0.2×1.2 or $0.25 \text{ g/cm}^2 \text{ yr}$. Adding together the solution rates of aragonite ($0.25 \text{ g/cm}^2 \text{ yr}$) and calcite ($0.95 \text{ g/cm}^2 \text{ yr}$) we get a total "observed" solution rate for $CaCO_3$ of $1.2 \text{ g/cm}^2 \text{ yr}$. This compares favorably with the value of $1.5 \text{ g/cm}^2 \text{ yr}$ obtained from the two-box model. Hence, the rates of ocean mixing based on the ^{14}C within the ocean is consistent with sedimentation rates based on ^{14}C measurements on sediments!

SUMMARY

In this chapter we have considered the means by which the absolute rates of oceanic processes are established. The rate of

*This value can be compared with those of $0.9 \text{ g/cm}^2 \text{ yr}$, $0.4 \text{ g/cm}^2 \text{ yr}$ and $0.4 \text{ g/cm}^2 \text{ yr}$ obtained by Honjo from his sediment trap deployments at sites, respectively, in the equatorial Atlantic, the temperate North Atlantic and the North Pacific (see table 1-3).

river influx is estimated from river gauge records. The rate of vertical mixing is derived from the difference between the $^{14}\text{C}/\text{C}$ ratio in average surface and average deep water. The rate of CaCO_3 accumulation is obtained by absolute age determinations made using radioisotopes found in deep sea sediments. A cross-check was conducted by comparing the observed CaCO_3 solution rate with the rate predicted from the two-box model of oceanic mixing. The agreement of these two estimates shows that the estimate of the rate of oceanic mixing is consistent with the rate at which calcite is accumulating on the sea floor.

The fact that deep sea sediments have accumulated at similar rates over the last few million years (based on the potassium-argon calibrated magnetic reversal chronology), as over the past few hundred thousand years (based on the ^{230}Th and ^{231}Pa dating methods), and as over the past few tens of thousand of years (based on ^{14}C dating), suggests that the present mode of ocean operation is not atypical. The mill has been grinding at more or less the same rate for at least 1,000,000 years!

PROBLEMS

- 5-1 Planet X has an ocean with a stratification similar to ours but with a mean depth of 8000 meters. Measurements reveal that its surface water has a $^{14}\text{C}/\text{C}$ ratio twice that in its deep water. What is the average residence time of water beneath the thermocline of this ocean? Assume the mid-depth of the thermocline to be 800 meters.
- 5-2 What cosmic ray production rate ($\text{atoms}/\text{cm}^2 \text{ min}$) was needed to balance the decay of ^{14}C on the surface of the earth prior to nuclear testing? The needed data are as follows:

Reservoir	Amount of Carbon 10^{16} moles	$\frac{^{14}\text{C}/\text{C}}{^{14}\text{C}/\text{C}_{\text{atm}}}$
Atmosphere	5	-
Ocean	295	0.83
Living biosphere	5	0.97
Soils	10	0.90
Marine sediment	7	0.95

The mass of CaCO_3 in marine sediments is taken to be equal to the amount in superlysocline sediment down to one mean life of ^{14}C (i.e., $0.2 \times 3.6 \times 10^{18} \text{ cm}^2 \times 8.2 \times 10^3 \text{ yrs} \times 1.2 \text{ g CaCO}_3/\text{cm}^2 \text{ yr} \times 10^{-2} \text{ mole/g}$). The preindustrial specific activity of atmospheric CO_2 was 13.5 dpm/g C.

- 5-3 Sediment taken at a depth of 50 centimeters in a deep sea core contains foram shells with a $^{14}\text{C}/\text{C}$ ratio 12 percent that for sediment from a depth of 10 centimeters. What is the

apparent sedimentation rate?

- 5-4 The following results were obtained using uranium series measurements at various depths in a deep sea core. The units are disintegrations per minute per gram of sediment (dpm/g).

Depth cm	^{238}U dpm/g	^{234}U dpm/g	^{230}Th dpm/g
2	1.3	1.4	65.5
22	1.5	1.6	33.6
42	1.4	1.3	17.4
62	1.2	1.3	9.6
82	1.5	1.5	5.7
102	1.2	1.3	3.5
122	1.4	1.5	2.4

What is the apparent sedimentation rate? If the ^{231}Pa activity is 6.9 at 2 centimeters, what should it be at 42 centimeters?

- 5-5 The first change from a normal to a reversed magnetic field is found at 14 meters depth in a core. If the sedimentation rate has been roughly constant, over what depth range could the ^{14}C method be used to reliably date this core? Over what depth range could the ^{230}Th and ^{231}Pa methods be used to obtain average sedimentation rates?

SUPERPROBLEM #5

After learning about Theft's four-reservoir aquariums two geochemists specializing in radiocarbon measurements, Measly Stover and Cyote Eastland, decide to use the same approach to explain to their students why radiocarbon is distributed as it is in the ocean. They quickly abandon the idea of using an actual aquarium, however, because while Theft could scale all the dimensions and rates to match the oceanic proportions, the half-life of radiocarbon cannot be scaled. Thus they decide to recreate the four-reservoir model in a computer. Stover and Eastland increase Theft's volumes (see figure 1-19) by a factor of 1.3×10^{17} (i.e., the total volume becomes $\sim 1.3 \times 10^{21}$ liters) and Theft's flow rates (see figure 1-19) by a factor of 8×10^{14} (i.e. the transport of water from the surface reservoir above Atlantis to Atlantis becomes 4×10^{15} liters/day or 1.5×10^{18} liters/yr). They simulate Theft's filters and backflushers by the appropriate computer manipulations. They delete the input and output fluxes and assume that phosphorus is entirely recycled. They fix the C/P ratio in the reservoir system as a whole to be 1000/1 and assume that the particles carrying P to the deep reservoirs have C/P ratios of 100/1. They then run the model until the phosphorus and carbon distributions come to steady state. If the average PO_4 concentration (i.e., that obtained were the waters from all four reservoirs thoroughly mixed) is 2.4×10^{-6} moles/liter then what

are the PO_4 and ΣCO_2 concentrations found by Stover and Eastland for the individual reservoirs?

Stover and Eastland then adjust the alkalinity of their sea water to yield a pCO_2 of 280×10^{-6} atmospheres in the surface reservoirs. As they do not allow CaCO_3 to form and include no NO_3 in their model the alkalinity is uniform among the four reservoirs. The atmosphere over the model is also given a pCO_2 of 280×10^{-6} atmospheres. They set the interface areas of the two surface reservoirs to be 2.4×10^{14} square meters (for Indopac) and 1.2×10^{14} square meters (for Atlantis). The CO_2 exchange rate across these interfaces is set at 20 moles/ $\text{m}^2 \text{ yr}$. The amount of CO_2 in the atmosphere comes out to be one-sixtieth of that in the model ocean.

To keep things simple Stover and Eastland assume that no carbon isotope fractionation occurs across the air-sea interface and during photosynthesis (thus the $^{14}\text{C/C}$ ratio in falling particles is just the same as that in surface water). They also assume that no soils or forests exist (thus all the ^{14}C atoms are either in the atmosphere or dissolved in the sea).

Stover and Eastland then add ^{14}C atoms to their model atmosphere at the rate of 2×10^{26} atoms/yr. They let the computer run through a period of 40,000 years so that ^{14}C decay comes to steady state with ^{14}C production. During this time the distribution of ^{14}C among the 5 reservoirs comes to steady state. What values do Stover and Eastland get for the $^{14}\text{C/C}$ ratio in each of the ocean reservoirs relative to that in the atmospheric reservoir? How would these results differ if the ocean were lifeless?



WOOFER THE TRACER DOG

Chapter 6

WHAT KEEPS THE SYSTEM IN WHACK ?

CONTROL MECHANISMS OPERATING IN THE SEA

INTRODUCTION

In chapter 1 we stated that any given constituent must, on the time scale of its residence in the sea, be removed from the sea at nearly the same rate as it is added to the sea. We did not, however, consider the means by which the ocean maintains this balance. This will be the major task of this chapter.

The general principles governing the constituent balances in the sea are similar to those governing economics. Natural mechanisms are at work which tend to drive the rate of output of any constituent toward equality with the rate of input. We will refer to these mechanisms as negative feedback controls. The adjective negative refers to the fact that they work to eliminate any imbalances. The principle is simple. Let's say for some reason the rate of loss of a given constituent were to become greater than its rate of input. Then the amount of this constituent stored in the sea would begin to fall (i.e., its concentration throughout the sea would become smaller). Somehow this lower concentration would lead to a reduction in the rate of output of this constituent from the sea.

Although we will discuss the factors controlling the concentrations of the major anions and cations in the sea, our discussions in this chapter will emphasize the controls operating on the biologically important constituents of sea salt (i.e., P, Si, C, N and O₂). In these discussions we will use the two-box model of chapter 1 and in so doing will circumvent the complications stemming from variations in the concentrations of these properties among the deep ocean basins. At the end of this chapter, we will consider what geological events might have pushed the system out of whack and were such events to have occurred how they might be recorded in the sediments.

PHOSPHATE CONTROLS

We start with phosphate for two reasons. First, its control mechanisms are more easily understood than, for example, those for nitrate or for total dissolved carbon. Second, phosphate is the ultimate limiting nutrient.

A reexamination of figure 1-5 reminds us that the following processes are important to the budget of phosphate in the sea (at least within the context of our two-box ocean).

1. the rate at which phosphate is supplied to the sea by rivers;
2. the rate of transfer of water between the surface and deep sea;
3. the fraction of these residues returned to solution in the deep sea.

If any of these three parameters were for some reason to change, the balance between phosphorus input to the oceans and loss from the oceans would be disrupted. Feedback controls would become operative and would restore balance.

Let us take a hypothetical example, where one of these parameters is changed and the others are kept constant. Specifically, let us assume that the rate of transfer of water between the surface and deep sea were suddenly to double. The situation before and after this doubling is shown in figure 6-1. For simplicity we have neglected the small flux of phosphate with downwelling water and have assumed 100% utilization of this constituent in surface water. Prior to the change the system is assumed to have been in balance, the flux of phosphorus to the sediments just balancing that from rivers. As a first approximation we will assume that after the change all the fluxes within the ocean would double. Each year twice as much phosphate would reach the surface ocean, twice as much phosphorus would sink in organic residues, twice as much phosphorus would be returned to solution in the deep sea and twice as much phosphorus would become entrapped in sediments. However, the amount of phosphate entering the sea would remain the same. Hence, the ocean would lose more phosphorus each year than it gained and the phosphate content of the deep sea would begin to decrease.

As the phosphorus content of the sea fell all the fluxes within the sea would fall by corresponding amounts. As shown in the figure 6-1, when the phosphate concentration has reached 0.75 its initial value, the mismatch between input and loss will drop to half the value which existed just after the mixing rate was doubled. When the phosphate concentration of deep sea water had reached half of its initial value the mismatch would have disappeared altogether. All the phosphorus fluxes would have returned to their initial values.

How long would this readjustment take? Just after the rate increase two percent of the ocean's phosphate would be lost to sediments each 1000 years. This yields a response time of 50,000 years (and a half adjustment time of $50,000 \times \ln 2$ or about 35,000 years). Thus, the phosphate concentration would decrease to 0.75 its initial value 35,000 years after the mixing rate was doubled. The change of deep ocean phosphate ion concentration with time is shown in figure 6-2. The approach to balance would be asymptotic and would go on for many half-times before becoming imperceptible.

Similar imbalances could be generated by halving the river input rate or by doubling the fraction of organic residues preserved. Table 6-1 summarized the critical information for these other scenarios. In each case the imbalances in the phosphate budget are remedied by a negative feedback loop operating between the concentration of phosphorus in the deep sea and the productivity of plant matter. The adjustment time (in thousands of years)

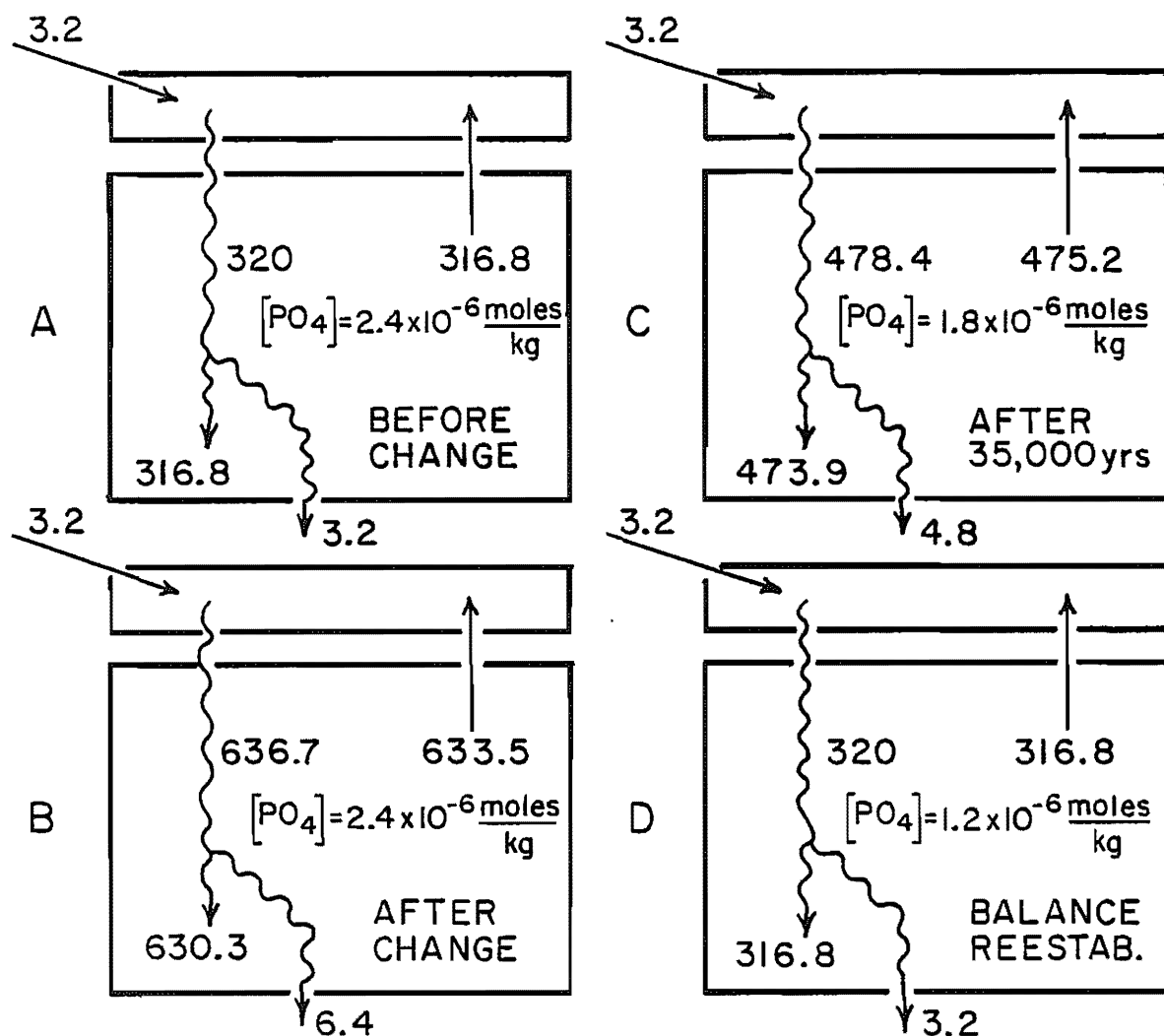


Figure 6-1. Response of the phosphate cycle to a change in rate of transfer of water between the deep and surface reservoirs. Panel A shows the steady state before the change occurred; output matches input. Panel B shows the situation immediately after the transfer rate is doubled. All the fluxes within the sea are close to twice what they were before the change; loss exceeds gain. Panel C shows the situation 35,000 years after the change. The phosphate content of the sea has been reduced to three quarters of its initial value. The excess of loss over gain has been reduced to half what it was just after the mixing rate was doubled. Panel D shows the situation several hundred thousands of years later when balance has been restored. All the fluxes are the same as they were originally. The phosphate concentration in deep water is, however, only half as large.

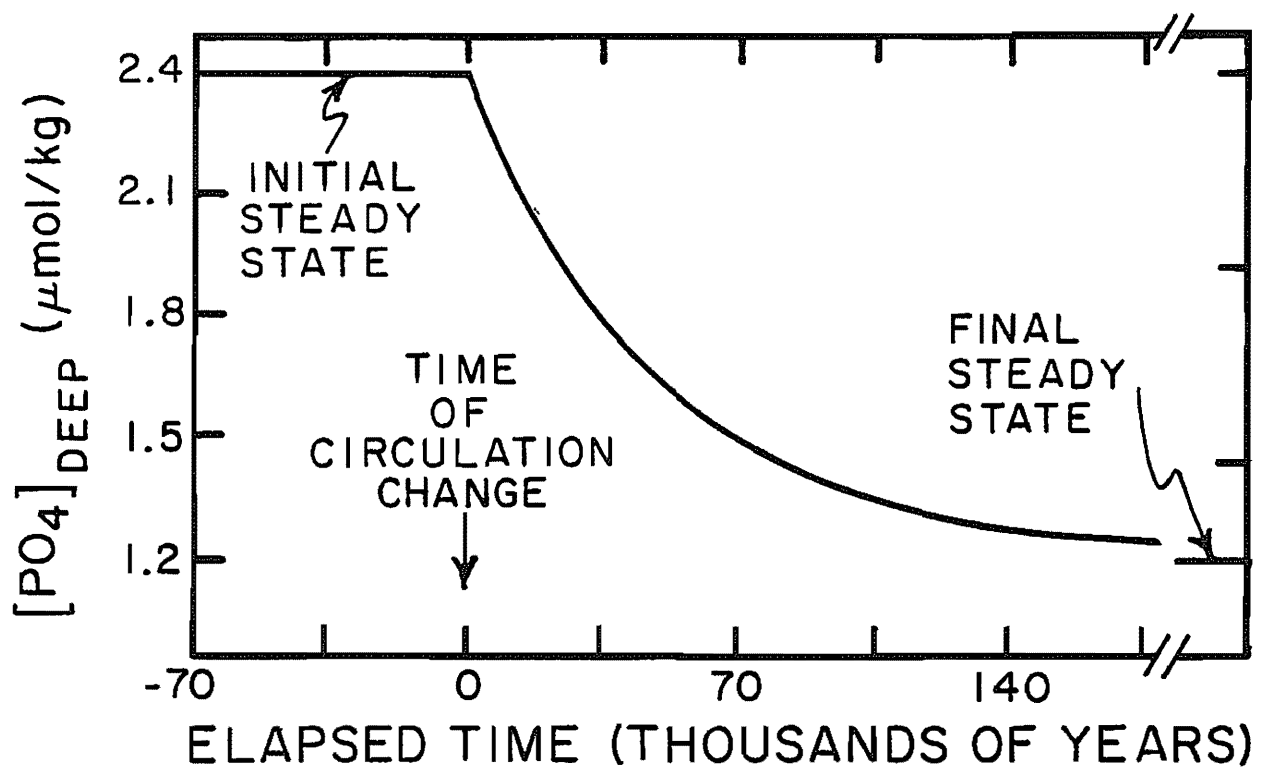


Figure 6-2. Phosphate concentration in the deep reservoir as a function of time after the change in mixing rate.

Table 6-1. Effect of changes in the operational parameters (i.e., deep sea ventilation rate, river input rate and preservation fraction for organic particulates) for the two-box model on the fluxes and contents of phosphate in the ocean. The times are in thousands of years.

QUANTITY	UNITS	INIT. VALUE	DOUBLE MIXING RATE				HALVE MIXING RATE			
			t = 0	t = 35	t = 70	t = ∞	t = 0	t = 140	t = 280	t = ∞
Mass in sea	10^{15} moles	3.2	3.2	2.4	2.0	1.6	3.2	4.8	5.6	6.4
Conc. in deep	10^{-6} moles/kg	2.4	2.4	1.8	1.5	1.2	2.4	3.6	4.2	4.8
River input	10^{10} moles/yr	3.2	3.2	3.2	3.2	3.2	3.2	3.2	3.2	3.2
Upw. Flux	10^{10} moles/yr	316.8	633.6	475.2	396.0	316.8	158.4	237.6	277.2	316.8
Part. Flux	10^{10} moles/yr	320.0	636.8	478.4	399.2	320.0	161.6	240.8	280.4	320.0
Loss to seds	10^{10} moles/yr	3.2	6.4	4.8	4.0	3.2	1.6	2.4	2.8	3.2

QUANTITY	UNITS	INIT. VALUE	HALVE INPUT RATE				DOUBLE INPUT RATE			
			t = 0	t = 70	t = 140	t = ∞	t = 0	t = 70	t = 140	t = ∞
Mass in sea	10^{15} moles	3.2	3.2	2.2	2.0	1.6	3.2	4.8	5.6	6.4
Conc. in deep	10^{-6} moles/kg	2.4	2.4	1.8	1.5	1.2	2.4	3.6	4.2	4.8
River input	10^{10} moles/yr	3.2	1.6	1.6	1.6	1.6	6.4	6.4	6.4	6.4
Upw. Flux	10^{10} moles/yr	316.8	316.8	237.6	198.0	158.4	316.8	475.2	554.4	633.6
Part. Flux	10^{10} moles/yr	320.0	318.4	239.2	199.6	160.0	323.2	481.6	560.8	640.0
Loss to seds	10^{10} moles/yr	3.2	3.2	2.4	2.0	1.6	3.2	4.8	5.6	6.4

QUANTITY	UNITS	INIT. VALUE	DOUBLE FRACTION PRES.				HALVE FRACTION PRES.			
			t = 0	t = 35	t = 70	t = ∞	t = 0	t = 140	t = 280	t = ∞
Mass in sea	10^{15} moles	3.2	3.2	2.4	2.0	1.6	3.2	4.8	5.6	6.4
Conc. in deep	10^{-6} moles/kg	2.4	2.4	1.8	1.5	1.2	2.4	3.6	4.2	4.8
River input	10^{10} moles/yr	3.2	3.2	3.2	3.2	3.2	3.2	3.2	3.2	3.2
Upw. Flux	10^{10} moles/yr	316.8	313.6	235.2	196.0	156.8	158.4	237.6	277.2	316.8
Part. Flux	10^{10} moles/yr	320.0	316.8	238.4	199.2	160.0	161.6	240.8	280.4	320.0
Loss to seds	10^{10} moles/yr	3.2	6.4	4.8	4.0	3.2	1.6	2.4	2.8	3.2

is given by the reciprocal of the fraction of the ocean phosphate lost during a period of a thousand years.

SILICATE CONTROLS

The situation for silicate is quite similar to that for phosphate. The main link between input and loss is through the productivity of plants. Within the context of our model the rate of silicate loss to sediments is proportional to the rate at which silicate reaches the surface ocean. Thus in the simplest of all worlds, were the rate of ocean mixing to double, the amount of silica raining toward the sea floor would also initially double. This would certainly increase the amount of opal buried each thousand years in the sediment. This would lead to a deficit in the silicate budget which would in turn cause the silicate content of the deep sea and in turn the flux of opal toward the sediments to fall. Eventually, the silicate budget would come back into balance.

There is one important difference between the cycles of silica and phosphorus. The fraction of opal dissolved would also change. As we have shown in chapter 2, the preservation probability of opal depends on the rain rate of opal to the sea floor. The higher the rain rate, the greater the preservation probability. This higher preservation probability would further enhance the rate of opal storage. Thus the imbalance between silicate supply and burial would be even larger than those caused by the production rate change alone.

CARBON CONTROLS

We have seen that carbon is removed from the ocean both in the form of organic residues and in the form of calcium carbonate hardparts. This fact complicates the system of controls for this constituent. If we assume for the sake of simplicity that the organic residues being stored in marine sediments carry carbon and phosphorus in their 105 to 1 biochemical proportion, then the situation can be rather easily sorted out. Under these circumstances, a fixed fraction of the carbon will be tied to the phosphorus cycle and will leave in the form of organic residues. The remainder will then be available for loss as calcite. The fraction tied to the phosphorus cycle is given by the ratio of C/P in organic residues (i.e., ~105) divided by the C/P ratio in river input. The ratio of carbon atoms to phosphorus atoms reaching the sea from rivers is about 500. Thus, about 20% (100 out of 500) of the incoming carbon atoms leave the sea as organic residues and 80% (400 out of 500) leave the sea as calcite. Our problem is to determine what keeps the accumulation rate of calcite in tune with the input of "excess" carbon (i.e., that beyond the amount needed to match phosphorus in organic residues).

The first point to be made here is that both calcium ions and carbonate ions exist in surface water in amounts far beyond that needed by marine organisms to form their CaCO_3 cages. As we saw in chapter 2, the surface ocean is highly supersaturated (i.e., about five fold) with respect to the mineral calcite. Thus, there

is no way to impose a feedback control on the amount of CaCO_3 formed per unit of phosphorus upwelled. Marine plants and animals can form as much CaCO_3 as they need. The control must rather involve the fraction of CaCO_3 preserved in marine sediments.

In today's ocean marine organisms generate about four times more calcite than is being preserved in marine sediments. About three quarters dissolves (the basis for this estimate is given in table 6-2). It is in this solution process that the control lies. This is easily seen as follows. If calcite storage in sediments were to exceed the "excess" carbon made available then both the alkalinity and ΣCO_2 content of the sea would begin to drop. The alkalinity would drop at twice the rate (in $\mu\text{eq}/\text{kg}$) as the ΣCO_2 concentration (in $\mu\text{m}/\text{kg}$). This would cause the difference between alkalinity and ΣCO_2 and hence the $\text{CO}_3^{=}$ ion concentration to decrease. A decrease in $\text{CO}_3^{=}$ ion concentration in the deep sea would expand the domain of undersaturated water and thereby reduce the fraction of calcite preserved in the sediment (see figure 6-3). Eventually this would restore the carbon balance!*

We have already shown in chapter 1 that the time constant for the replacement of carbon atoms in the ocean is about 180,000 years. The time constant for readjustment of the CaCO_3 budget is, however, much shorter than this. Rather than being equal to the total amount of carbon dissolved in the sea divided by the removal rate of carbon to sediments, the response time of the $\text{CO}_3^{=}$ ion concentration to changes in the budget of CaCO_3 is equal to the total amount of carbonate ion in the sea divided by the removal rate of calcite to marine sediments. Since only about 1/30th of the carbon in the sea is in the form of $\text{CO}_3^{=}$, the adjustment time for the CaCO_3 cycle is only 6000 years!

INTERACTIONS BETWEEN THE PHOSPHATE AND CARBON CONTROLS

With these facts we have the wherewithal to consider simultaneously the impact of a change in operation of the ocean system on both the balances of total dissolved carbon and phosphate. Let us return to our original example (i.e., what would happen if the rate of water transfer between the deep and surface reservoir of our two-box ocean were to double?). Initially this would throw both the balances for C and P out of balance. Both organic residues and calcium carbonate would accumulate at too rapid a rate. This would cause the PO_4 concentration in the sea to fall (and hence also the rate of production of organic residues and their associated CaCO_3). It would also cause the $\text{CO}_3^{=}$ ion content of the deep sea to fall (and hence also the fraction of calcite which dissolves). Because the time constant for the adjustment of the CaCO_3 budget (~6000 yrs) is more than an order of magnitude smaller than that for the adjustment of the phosphorus

*As there are 100 Ca^{++} ions in the sea for every $\text{CO}_3^{=}$ ion, on a short time scale it will be the $\text{CO}_3^{=}$ ion concentration which shifts rather than the Ca^{++} ion concentration. For times longer than a million years (i.e., longer than the residence time of calcium in the sea) both shifts in Ca^{++} and in $\text{CO}_3^{=}$ ion concentration would have to be considered.

Table 6-2. Preservation of calcite for various depth ranges in the world's major oceans. The last column gives estimates of the fraction of the global calcite production preserved in the particular zone. The sum of the entries in this column give the global preservation factor for calcite.

Depth Range km	Fraction of Calcite Preserved	Area (10^{14} m 2)				Contribution to Preservation Factor ⁺
		Atl.	Ind.	Pac.	Total	
0.0 to 0.2	~0.10*	0.14	0.03	0.10	0.27	0.01
0.2 to 2.8	~0.20*	0.22	0.11	0.21	0.54	0.03
2.8 to Lysocl. Transition Zone	~0.90	0.35	0.18	0.18	0.71	0.18
Red Clay Zone	~0.10	0.21	0.14	0.14	0.49	0.01
Total	~0.24	1.06	0.76	1.78	3.60	0.24

*These percentages are low because much of the sediment in these depth ranges contains sizable amounts of organic matter. The consumption of this organic matter by benthic animals and bacteria and worms releases CO₂ to the pore waters and hence dissolves CaCO₃.

⁺Obtained as follows:

$$\frac{\text{Area in Depth Range}}{\text{Area of Sea Floor}} \times \text{Fraction Calcite Preserved}$$

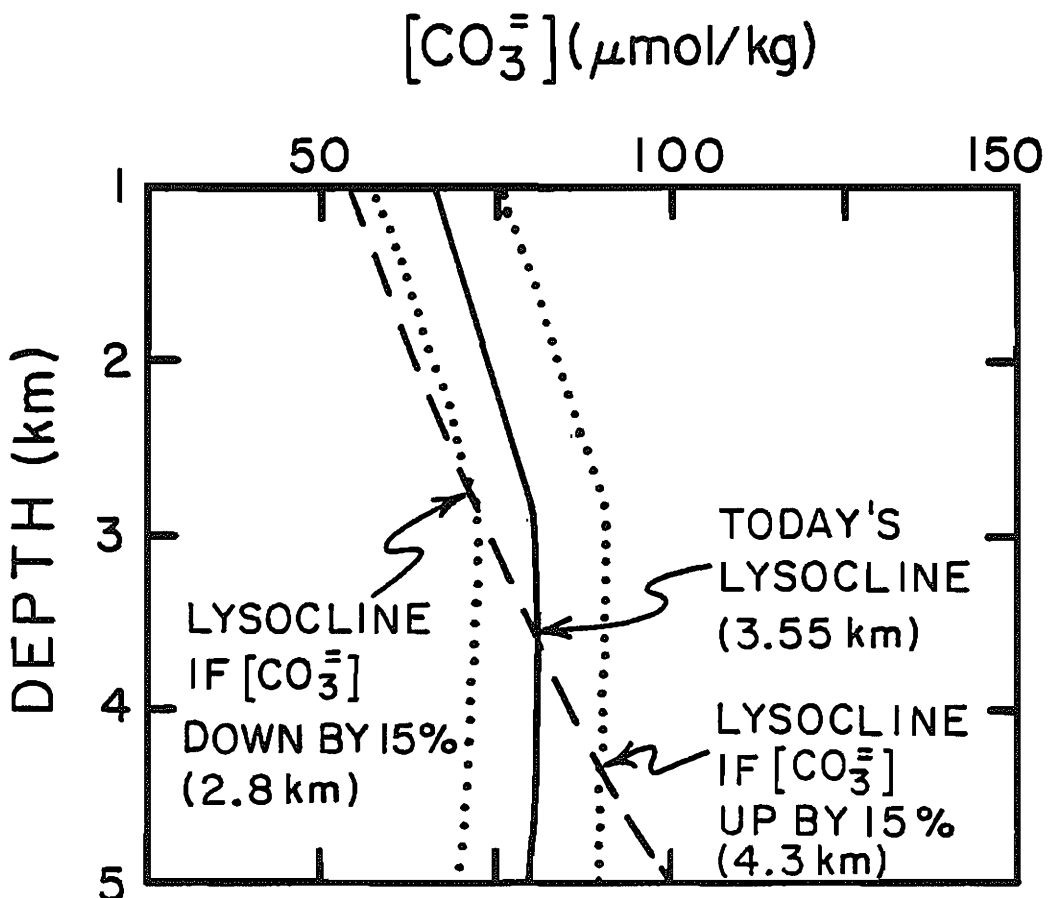


Figure 6-3. Plot of carbonate ion content (solid curve) and calcite saturation carbonate ion content (dashed curve) in the western South Atlantic. Today's lysocline is located at the depth where these two curves cross. The dotted curves show hypothetical situations where the carbonate ion content of the deep sea is raised and lowered by 15%. As can be seen the resulting changes in lysocline depth are substantial.

budget (~ 100,000 yrs) the mismatch between the rate of entry to the sea of "excess" carbon and the calcite accumulation rate would be remedied more rapidly than would the discrepancy in the phosphate budget.

NITRATE CONTROLS

We have already stated that the nitrate cycle is probably tied to the phosphate cycle through ecologic feedbacks. If the ratio of the amount of nitrate in the ocean to that of the amount of phosphate were for some reason to fall below the ideal biochemical ratio of about 15 then nitrogen-fixing organisms living in surface water would be given an ecological advantage over those organisms which cannot fix nitrogen. This would lead to a restoration of the biochemical ratio. On the other hand, if the ocean were to find itself with an excess of N over P then the non-nitrifying organisms would gain an advantage pushing the ratio back toward the ideal value.

The time constant for the adjustment of the N/P ratio in the sea is not known. The reason is that neither the rate of fixation of N_2 (to form NO_3^-) nor the rate of denitrification of NO_3 (to form N_2) is known. We saw in chapter 3 that roughly 0.1% of the NO_3 is lost to N_2O during each mixing cycle (i.e., each thousand years). Were this the only mode of nitrate destruction, then the current adjustment time of the N/P ratio would be about 1,000,000 years. However, we have already seen that substantial amounts of nitrate are being utilized for oxidation of organic matter in waters free of O_2 . We have also seen that there is evidence for NO_3 utilization (i.e., reduction to N_2) in large regions of the deep Pacific where O_2 is present in the water column. In this situation the utilization is thought to occur within fecal pellets as they fall through the water column or after they reach the sea floor. As no one has found a way to quantify the importance of these processes it is currently not possible to give a time scale for the adjustment of the nitrate balance in the sea. Our assumption will be that nitrate balance can be achieved on a shorter time scale compared to that required for phosphate. This remains however, an unproven assumption. As such it constitutes one of the key missing pieces in the marine chemistry puzzle.

DISSOLVED OXYGEN CONTROLS

So far in this discussion we have assumed the fraction of organic residues destroyed in the deep sea to be a constant. Clearly, this fraction must vary with the condition of the system. One obvious dependence would be on the oxygen content of deep sea water. Observations of the composition of sediments show that those bathed in anaerobic water have far higher organic carbon contents than sediments bathed in aerobic waters. The reason is apparently that the organisms which use NO_3 and SO_4 as oxidizing agents and the organisms capable of fermentation (i.e., breaking organic material down into CH_4 and CO_2) are all single celled and hence incapable of the complexity of biochemical manipulation employed by O_2 utilizing organisms. Thus, they less efficiently use the

available food and leave more residues. Were the oxygen content of the sea to fall the fraction of the sea floor bathed in anaerobic waters would as a consequence expand, and so also would the fraction of organic residues preserved. Thus, there is a tie between the cycles of phosphate and dissolved oxygen.

The ratio of the amount of O_2 in the atmosphere (plus ocean) to the net rate at which O_2 is being produced gives a replacement time for atmospheric oxygen of about 10 million years.* Thus, for the short times we have been discussing, the oxygen content of the atmosphere can be considered to be constant.

Do the changes in the cycles of carbon and phosphorus in themselves lead to a change in the O_2 content of deep ocean water? The answer is yes, but the situation is complicated. We can see what goes on by considering our favorite example. What would happen to the O_2 content of the deep sea if the water transfer rate between the surface and deep sea were doubled? Initially there would be no change. Although the amount of organic residues reaching the deep sea would double, so also would the amount of oxygen carried by the downwelling surface water. One fundamental of marine chemistry is that for any given pattern of ocean operation the amount of oxygen in deep sea water depends only on the ratio of the PO_4 concentration in the deep sea to the partial pressure of oxygen in the atmosphere and not on the rate at which the deep sea is ventilated.

The following hypothetical experiment will help the reader to grasp this concept. A bucket full of deep sea water is placed in the sunlight on a winter day and is allowed to remain there until plants have converted all the PO_4 (and NO_3) to organic residues and until the O_2 content of the water has achieved equilibrium with the atmosphere. All the organic matter is then removed from the water (and the sides of the bucket) and is placed in a small vial. The bucket is taken to a dark room, at which point the organic matter is returned to the water and the bucket is sealed so that there is no air space above the water. It remains this way until bacteria have consumed all the organic matter. If the water initially had the average composition of deep sea water then it contained about $2.25 \mu\text{m}/\text{kg}$ of PO_4 . Plant matter containing this amount of phosphorus would have an O_2 demand of about $300 \mu\text{m}/\text{kg}$. The amount of O_2 dissolved in the water when it was taken inside would have been about $350 \mu\text{m}/\text{kg}$. Thus during storage in the dark room the oxygen content would drop to about $50 \mu\text{m}/\text{kg}$. This outside to inside cycle could be repeated over and over again. At the end of each exposure the result would be the same. As long as the bucket was stored outside long enough for the plants to utilize the limiting nutrients and inside long enough for the bacteria to

*As this net is a very small fraction of the rate at which O_2 is produced by photosynthesis it is not estimated by subtraction of the worldwide respiration rate from the worldwide photosynthesis rate. Rather it is estimated from the rate at which organic carbon accumulates in marine and continental sediments. The small net production of O_2 by photosynthesis is largely matched by corresponding oxidation of carbon, iron and sulfur passing through the erosion-deposition sequence. Thus, it need not lead to a rise in atmospheric O_2 .

consume the organic matter then the result would be independent of the rate at which the bucket was cycled.

Now let's say that after one of the exposures to the sun and air the organic material sieved from the water were divided into two equal parts. Half is put aside and half is put back into the water in the dark room. In this case the O_2 content would drop during storage in the dark room by only 150 $\mu\text{m}/\text{kg}$ (to 200 $\mu\text{m}/\text{kg}$). Were the cycle repeated under this new condition only half as much organic matter would be produced and consumed each time (because half of the phosphorus and nitrogen would remain in the organic matter put aside in the small vial). The ratio of $[\text{PO}_4]$ (after exposure in the dark room) to $[\text{O}_2]$ (after exposure to the air) would be only half as great as before and hence the O_2 demand (in darkness) would be only half as great.

Let us consider yet one more perturbation of this hypothetical system. The half of the organic matter put aside is restored to the water to bring us back where we started. Then instead of placing the bucket outside on a cold winter day we place it outside on a warm summer day. Again, plants would grow and fully utilize the nutrients and again the water would become saturated with atmospheric O_2 . However, the O_2 content of the water would be only about 200 $\mu\text{m}/\text{kg}$. This being the case, when the bucket was taken to the dark room and sealed from the air the O_2 would be consumed before the organic debris in the water had been consumed. This would then permit organisms capable of using NO_3^- as an oxidant to take over. The water in the bucket would have become anaerobic!

These bucket experiments provide quite a good analogue to the ocean. The exposure to sun and air of course is equivalent to the time spent by water in the surface mixed layer. The separation and readdition of the organic matter is equivalent to the settling of organic fragments from the surface mixed layer to the deep sea. The organic matter and water follow different routes to the deep sea where they are recombined. The deep sea is dark and is isolated from the air as was the bucket in the dark room. We approximated a change in the PO_4 and NO_3^- contents of the sea by removing half of the organic matter from the bucket cycle. We approximated a change in the atmospheric oxygen content by changing the air temperature over the bucket. The point of all this is to demonstrate that the oxygen content of the bucket after storage in dark isolation was controlled by the ratio of phosphate to dissolved oxygen and not by the frequency at which the bucket was moved back and forth between the two environments.

Now back to our consideration of perturbations in the ocean's dissolved oxygen cycle. Immediately after the deep to surface mixing rate was changed, the O_2 content of deep sea water would remain unchanged. However the amount of O_2 in the deep sea would then begin to rise as the PO_4 content of deep sea water fell. The less PO_4 in the sea the smaller the amount of organic rich residues formed per unit of water upwelled and the smaller the demand for O_2 in the deep sea. After the sea had reestablished the balance between loss and gain of phosphorus it would have half the original PO_4 content. The average AOU (i.e., saturation minus in situ oxygen content) for the deep sea would be half its initial

value. A smaller area of ocean floor would be bathed in O_2 free water. Also O_2 would invade more deeply into fecal pellets and into marine sediments permitting scavengers to burrow more deeply into the sediment. Thus the fraction of organic residues preserved would likely be smaller. In this sense our treatment of the phosphorus cycle was oversimplified in that we failed to take into account the change in the O_2 content of deep water and hence in the fraction of organic matter preserved.

MAJOR ANION CONTROLS

What controls the makeup of anions in the sea? We have seen that chloride is the most abundant anion, that sulfate is the second most abundant, and that bicarbonate runs a very poor third. As these three anions do not find happy homes in igneous rock, when liquids and gases from the interior reach the surface and crystallize, the chlorine, sulfur, and carbon they contain are largely released either in volatile form to the atmosphere or in dissolved form to the ocean. The place of residence on the earth's surface for these three elements is either in the sea itself or in chemical precipitates formed within the sea and buried in the sediments. Inventories of the amounts of these chemical precipitates show that roughly one third of the chloride currently resides in sodium chloride ($NaCl$) deposits in sediments and that about three-quarters of the sulfur is present in sulfate and sulfide minerals in sediments. By contrast only about 0.1 percent of all of the carbon released from the earth's mantle is now dissolved in the sea (as shown in table 6-3 the remaining carbon, about 1000 times more, resides in sediments as limestone, dolomite, and organic residues).

Have the proportions of these elements contained in the ocean changed with time? At present, the ocean is far from saturated with respect to any salt capable of precipitating chloride (Cl^-) ion or significant quantities of sulfate ($SO_4^{=}$) ion. If all the sodium chloride and calcium sulfate in sediments were dumped back into the ocean they would readily dissolve. Thus one might wonder why all this salt has not dissolved in the sea. The answer lies in the observation that salinities considerably higher than the ocean average are generated in isolated arms of the ocean, like the Persian Gulf, where water is evaporated more rapidly than it is added to the basin by rain and by runoff from adjacent lands. In some of these basins, the salinity rises to the point where $CaSO_4$ and even $NaCl$ precipitate. We suspect from the geologic record that most of the very large salt deposits found buried in sedimentary sequences were formed in arid peripheral basins which did not communicate rapidly with the sea. Once such an evaporite deposit has formed, it can be preserved for hundreds of millions of years if it is buried under a layer of impermeable shale. Eventually, continental drift and the resultant crustal upheavals bring these salt deposits back to the surface where fresh water can dissolve them. The contained salt is then dissolved and sent back to the ocean.

From this discussion we can see that the fractions of these two major anions present in the ocean at any one time depend on

Table 6-3. Distribution of the volatile elements among the atmosphere, ocean, and sediment reservoirs(679a). Amounts are given in moles.

Element	Hydrogen	Carbon	Chlorine	Nitrogen	Sulfur
ATMOSPHERE					
Form	H ₂ O	CO ₂	-	N ₂	-
Amount	1 x 10 ¹⁸	5 x 10 ¹⁶	-	3 x 10 ²⁰	-
OCEAN					
Form	H ₂ O	HCO ₃ ⁻ +CO ₃ ⁼	Cl ⁻	NO ₃ ⁻	SO ₄ ⁼
Amount	8 x 10 ²²	3 x 10 ¹⁸	7 x 10 ²⁰	3 x 10 ¹⁶	4 x 10 ¹⁹
SEDIMENT					
Form	H ₂ O	CaCO ₃ +MgCa(CO ₃) ₂ +Kerogen*	NaCl	Kerogen	CaSO ₄ FeS ₂ + FeS
Amount	~8 x 10 ²¹	~3 x 10 ²¹	~4 x 10 ²⁰	~1 x 10 ²⁰	~1.5 x 10 ²⁰
TOTAL					
Amount	880 x 10 ²⁰	~30 x 10 ²⁰	~11 x 10 ²⁰	4 x 10 ²⁰	2 x 10 ²⁰

*Kerogen refers to the residues of organic matter found in sediments.

chance tectonic factors. How often is a large basin formed that has just the right geometry (and climate) to extract salt rapidly from the ocean? How often does a salt deposit thus formed come back into contact with fresh waters and dissolve? At times in the past when peripheral basins in arid areas extracted salt more rapidly than usual or when old deposits were being destroyed less rapidly than usual, the salt content of the ocean must have decreased. When the reverse was true, the salt content of the sea must have increased. The salinity of the ocean has therefore probably fluctuated over the epochs of geologic time. Such fluctuations, however, have probably been fairly small because not enough salt is stored in the sediments to effect very large salinity changes. For example, if all the NaCl and CaSO₄ now known to exist in sediments were dissolved in the sea, the salinity of the ocean would only increase by about a factor of 1.5.

The fluctuations that have occurred must have been very gradual. From the rates at which these processes are currently taking place, we estimate that a Cl⁻ ion remains in the ocean for perhaps 200 million years before being "captured" in a basin where NaCl is actively precipitating. The Cl⁻ ion may reside in the sediment so formed for another 100 million years before returning to the ocean. Thus a typical Cl atom has spent about one third of its time in the sediments as NaCl and two thirds of its time in the ocean as Cl⁻ ion. Sulfur, on the other hand, must spend a greater fraction of its time entrapped in sediments. A typical S atom remains in the ocean several tens of million years before it is fixed into gypsum (CaSO₄) or iron sulfide (FeS or FeS₂). This S atom then remains in the sediments for 100 or so million years before it is released by solution and carried back to the ocean.

Thus we see that the salinity of the ocean is determined by two factors: the ratio of the elements hydrogen*, chlorine, and sulfur in volatiles released from the earth's interior and the tectonic factors influencing the partitioning of sulfur and chlorine between the ocean and the sediments. The earth received these elements in a particular ratio from the solar nebula, and it is in roughly this ratio that they appeared at the surface. Since their arrival, the earth's geography has dictated their distribution between solid NaCl, solid CaSO₄, solid FeS or FeS₂, and dissolved sea salt.

MAJOR CATION CONTROLS

The ocean must remain electrically neutral. That means that once the anion content of the sea is fixed, the cation content is automatically determined. For each negative charge due to Cl⁻ and SO₄⁼ ions, a corresponding positive charge must exist. A great many cations could conceivably contribute to this balance. However, only four elements - sodium, potassium, calcium, and magnesium - are both sufficiently soluble in sea water and abundant in crustal material to make significant contributions. Just as SO₄⁼ and Cl⁻ contribute the major part of the negative charge,

*Virtually all the hydrogen on the earth's surface is now, and always has been, in the ocean as water.

Table 6-4. Comparison between the chemical composition of sea water and the chemical composition of average river water for the major cations in sea salt. Also given are the corresponding residence times in the sea.

Element	Mean Sea Water moles/m ³	Mean River Water moles/m ³	Ratio Sea River	Residence Time 10^6 yrs
Na	470	~0.10*	~5000	~200
K	10	0.04	~250	~10
Mg	53	0.16	~330	~13
Ca	10	0.36	~30	~1

*Corrected for sea salt.

Na^+ , K^+ , Ca^{++} , and Mg^{++} contribute the major part of the positive charge. Whereas the major anions in sea salt are found in only trace quantities in igneous rocks, the major cations are present in large quantities. Continental erosion therefore carries more K^+ , Mg^{++} , Na^+ and Ca^{++} ions to the sea than it does SO_4^- and Cl^- ions. How then does the sea manage to maintain the required electrical balance? Somehow the ocean must dispose of the cation excess which it continually receives from rivers by precipitating new minerals similar in chemical composition to those being weathered on the continents. If the amount of cations contained by the sea were to become a little too high (compared to the amounts of Cl^- and SO_4^- ions), the OH^- content of sea water would rise. This in turn would lead to a more rapid formation of the mineral phases that remove these cations. Some such self-balancing mechanism must exist to maintain equality between cations and anions within the sea. Unfortunately, we are only beginning to learn about the alumino-silicate mineral phases being formed in the sea. Until we know more, arguments such as the above must remain vague.

What controls the proportions of these four cations in sea water? Let us begin by examining their relative abundance in river water and, in turn, in the rocks undergoing erosion. In river water (see table 6-4), we find that for every mole of K there are about 2.5 moles of Na, 4 moles of Mg, and 9 moles of Ca. In the ocean, for every mole of K there are 50 of Na, 5 of Mg, and only 1 of Ca. Rivers therefore carry these ions to the ocean in much different proportions than are currently present in the sea. The reason the sea stores these cations in proportions, which differ so radically from the proportions found in river water, is that their probabilities of removal from the sea are quite different. The sea rids itself of calcium most readily. This element is a constituent of the calcite produced in great quantities by marine organisms. After Ca, potassium removal is the most rapid. Apparently (we are not yet certain) K is taken up on the detrital alumino-silicate minerals brought to the sea by wind and water. By comparison, the sea has considerable difficulty getting rid of the sodium and magnesium it receives. The only way it can do so is to let such very high contents of Na and Mg build up relative to K and Ca that the minerals which form and the volcanic rocks which are altered on the sea floor are literally flooded with sodium and magnesium.

The ratios of the four major cations in the sea thus depend upon the ratios in which these cations are being added from rivers and the difficulty the sea has in ridding itself of them. The former is fixed by the composition of continental rocks. The latter is fixed by the affinity of the minerals forming within the sea for a particular cation. For each unit of "difficulty" the ocean has in getting rid of Ca, the sea currently has 10 units of "difficulty" in getting rid of K, 13 units of "difficulty" in getting rid of Mg, and 200 units of "difficulty" in getting rid of Na.

An analogy might help here. Four teams are competing in a game of musical chairs. The players walk around a circle until the music stops and then everyone dives for a chair. As there are many more participants than there are chairs, not every player

gets a seat. The first team is comprised of professional athletes, the second of high school students, the third of housewives, and the fourth of retired office workers. Clearly, in the first round, the athletes and the students will get the greater number of seats. Now, contrary to the normal rules in such a game, those who succeed in grabbing chairs step aside and let those who failed try again. In the second round, the housewives and the retired office workers will fare considerably better against the diminished ranks of their opponents. Obviously, in our analogy, Ca and K are the athletes and the students of the ocean and Mg and Na are the housewives and retired office workers of the ocean. The sites in the lattices of forming minerals are the chairs. As the Ca and K ranks are depleted, the less reactive Mg and Na atoms find it easier to capture their share of lattice sites.

A comparison between the cation composition of the ocean and other saline water bodies in closed basins is revealing in this connection. As shown in table 6-5 despite major differences in total salt content and anion composition, these saline lakes have Na/K and Mg/Ca ratios ranging over only a factor of ten. The Na+K/Mg+Ca ratios, on the other hand, cover an enormous range, suggesting that the singly charged Na and K ions compete for a different set of mineral lattice sites than do the doubly charged Mg and Ca ions. In our analogy, it would be as if the retired office workers and the students were competing for chairs of one color and the housewives and the athletes for chairs of another color. The rivers feeding the saline lakes have chemical compositions reasonably similar to the average composition of those rivers feeding the sea. Apparently any water body that must ultimately dispense the ions it receives to its sediments (rather than through an outlet to the sea) achieves a Na/K ratio roughly 25 times and a Mg/Ca ratio roughly 25 times higher than the respective ratios in incoming river water. These ratios suggest that in competing for sites accommodating singly charged ions, Na is only about one-twentyfifth as effective as K, and that in competing for doubly charged ion sites, Mg is only one-twentyfifth as effective as Ca.

There are three major routes by which the cations Na, Mg, and K leave the sea. First, they are being precipitated within the sea or at the sediment water interface as silicate minerals. Second, they are precipitating within the sediment as authigenic minerals. Third, they react with the basalts beneath this sediment cover. Are there ways in which we can quantify these processes?

Recent studies of the hot waters issuing forth from hydrothermal vents dotted along the crest of the East Pacific Rise provide a breakthrough with regard to the study of the interaction between sea water and the hot basalt being emplaced along ridge axes. As shown in figure 6-4 chemical analyses of waters issuing forth from these vents are not the same as those for bottom water. Further, when the concentration of any given element whose concentration in hydrothermal water is anomalous with regard to that in bottom water is plotted against temperature of the water, a strong correlation is found. The hotter the water, the larger the

Table 6-5. Comparisons of the cation composition of sea water with the cation composition of various inland seas. See reference 547 for data sources.

Water Body	Na	K	Mg moles/m ³	Ca	$\frac{Na}{K}$	$\frac{Mg}{Ca}$	$\frac{Na + K}{Mg + Ca}$
Dead Sea (Israel)	1390	205	1150	350	7	3	1.1
Desmet (U.S.A.)	60	2.2	18	1.9	27	10	3.1
Bolac (Australia)	14	0.2	3.3	0.7	0	5	3.6
Caspian (USSR)	140	1.8	31	7.5	78	4	3.7
Tagar (USSR)	260	5.4	35	1.4	48	25	7.3
Timboram (Australia)	1570	10.2	175	34	154	5	7.6
Gnarport (Australia)	165	1.0	20	1.6	165	12	7.7
Ocean	470	10	53	10	47	5	7.6
Murdeduke (Australia)	165	1.0	17	0.6	165	28	9.4
Great Salt (U.S.A.)	3640	104	300	6.0	35	50	12
Corangamite (Australia)	300	2.6	25	0.9	115	27	12
Pyramid (U.S.A.)	70	2.6	4.5	0.2	27	22	15
Walker (U.S.A.)	100	2.4	4.3	0.2	42	21	23
Bitter (USSR)	820	21	31	2.2	39	14	25
Little Borax (U.S.A.)	150	19	1.0	0.2	8	5	33
Big Borax (U.S.A.)	270	7.5	1.0	0.1	36	10	250
Albert (U.S.A.)	165	4.5	0.5	0.1	37	5	280
Mono (U.S.A.)	945	29	1.5	0.1	33	15	610

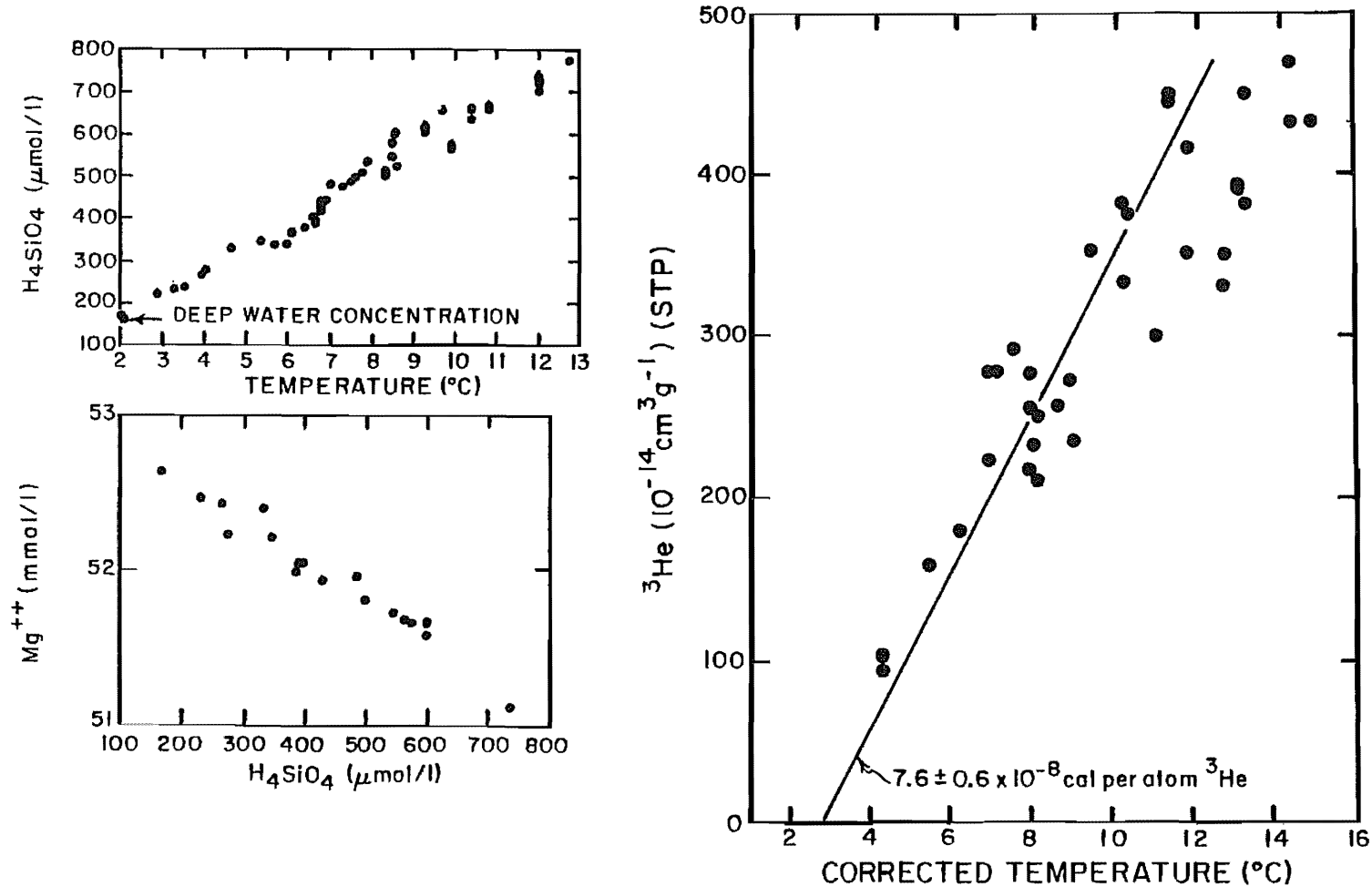


Figure 6-4. Silicate content versus temperature for waters from ridge crest hot springs (upper diagram). Magnesium content versus silicate content for these same samples (lower diagram). These measurements were made by John Edmond and his colleagues (642).

Figure 6-5. ^3He concentration versus water temperature for waters from ridge crest hot springs. These measurements were made by Bill Jenkins of the Woods Hole Oceanographic Institution (276).

anomaly. These plots suggest that the waters sampled are mixtures between local bottom water and a very hot water which has equilibrated with hot basalt. A lower limit can be placed on the temperature of this hot water from recent measurements made in the so-called "black smoker" vents (intense plumes of very hot water about a foot in diameter, which shoot many meters up into the water column precipitating CaSO_4 and black sulfide minerals along their paths). Inside the vents from which these waters emanate, temperatures as high as 300°C have been measured! From the high-temperature data on the solubility of silicate and on the basis of the temperature at which the Mg content goes to zero, John Edmond and his coworkers at MIT, who have made these measurements, estimate that the temperature of the hot endmember of this series is 330°C . Knowing this, an estimate of the chemical composition of the endmember hydrothermal water could be made by extrapolating the concentration versus temperature lines to 330°C .

In order to estimate the impact of this process on the ocean's chemical budget, the total flux of this hot water must be known. Bill Jenkins of Woods Hole came up with an ingenious method to estimate this flux. His measurements of He in samples of these hot waters reveal that they also contain large excesses of both ^3He and of ^4He . As shown in figure 6-5 when Jenkins plotted the ^3He excess against temperature he obtained a straight line. The importance of this finding was that the slope of this line corresponds to what is thought to be the ratio of global heat release through ridge crest hydrothermal activity to global ^3He release from ridge crests.*

Together John Edmond and Bill Jenkins postulated that the ratio of the chemical anomalies to either the temperature or ^3He anomaly in the sample analyzed was typical of the global ratio. If so, then they had the means to assess the overall importance of interaction of sea water on the budget of a given element in the sea. They merely multiplied the chemical anomaly to heat (or ^3He) anomaly ratio found in the vent samples by the global heat (or ^3He) release rate. The estimates obtained in this way are compared with the rate of delivery from rivers in table 6-6. As can be seen, hydrothermal circulation removes Mg and S from the sea and adds K, Ca and Si to the sea.

The second sink to be considered is the formation of authigenic minerals within marine sediments. An estimate of the importance of this sink can be obtained from the measurement of the chemical gradients in the pore waters of sediments. For any given constituent the product of the concentration gradient times the effective molecular diffusivity gives its flux through the particular horizon of the sediment column. This flux provides a measure of the net production or consumption of the constituent beneath the horizon at which the gradient measurement was made. Thus by measuring the gradients in the concentration of a given ion at

*The total heat transport is obtained by subtracting the amount of heat being carried by conduction (as measured by thermal probes in the sediment) and the theoretical total heat flow based on models for plate cooling. The total helium-3 input is based on the integrated helium-3 excess in deep water divided by the ventilation time for the deep sea.

Table 6-6. Comparison hydrothermal fluxes with those from rivers and to the sediments (all in moles/yr). These estimates were made by John Edmond and his coworkers (642).

Constituent	GAINS		LOSSES	
	River Input	Hydro. Input	Sediment Loss	Hydro. Loss
Mg ⁺⁺	5.3×10^{12}	-	?	8×10^{12}
Ca ⁺⁺	12×10^{12}	3.5×10^{12}	-	-
Ba ⁺⁺	10×10^9	2.4×10^9	?	-
Li ⁺	1.4×10^{10}	16×10^{10}	?	-
K ⁺	1.9×10^{12}	1.2×10^{12}	?	-
Rb ⁺	0.4×10^9	2.4×10^9	?	-
SO ₄ =	4×10^{12}	-	?	4×10^{12}
F ⁻	16×10^{10}	-	?	1.1×10^{10}
Si	6×10^{12}	3×10^{12}	?	-
P	$\sim 3 \times 10^{12}$	$<0.1 \times 10^{10}$	3×10^{10}	$<0.1 \times 10^{10}$
ΣCO_2	$\sim 2 \times 10^{13}$	$\sim 0.1 \times 10^{13}$	2×10^{13}	-

various depths in the sediment column it should be possible to estimate not only the its flux into or out of the sediment but also the places within the sediment column where these reactions are taking place. Considerable evidence has been obtained to show that pore waters are depleted in Mg^{++} . An example of the decrease with depth in the sediment column of the Mg content of pore fluids is shown in figure 6-6. The missing Mg appears to replace iron which is removed from oxide or silicate minerals to form iron sulfide (a secondary mineral resulting from the conversion of $SO_4^=$ ion to $S^=$ ion by anaerobic bacteria). Figure 6-7 shows the correlation between $SO_4^=$ and cation loss in pore water samples squeezed from deep sea drill hole material.

The third sink for cations from the sea is the precipitation of silicate minerals within the water column or at the sediment water interface. Success in determining the extent to which this process contributes has been very limited. The x-ray diffraction patterns for recent sediments are dominated by reflections from detrital grains from the continents. That the K bearing phases are largely detrital can be shown by the high argon ages obtained on recent sediment samples (80 to 400 million years). Had these minerals recrystallized they would have lost their ^{40}Ar . Similarly the $^{18}O/^{16}O$ ratios and $^{87}Sr/^{86}Sr$ ratios in these minerals are more akin to those in continental soils than to those expected for minerals precipitated in the sea. While these observations do not prove that silicate phases are not forming on the sea floor or in the water column they do make the search quite difficult. As nearly all of what is seen in x-ray diffraction patterns and in isotopic analysis can be explained by continental detritus there is no way to pin down the contribution of ocean "precipitates".

As our knowledge of the removal mechanisms of cations is quite primitive, beyond a few general statements we cannot say much about the controls acting to maintain these ratios. One generalization that can be made is that the difference between the total anion and total cation charge must be balanced by H^+ or OH^- ions. Were such a difference to develop the pH of the solution would change. For example, if the cation charge were to become larger than the anion charge the difference would have to be made up by OH^- ion and the solution would become basic (i.e., its pH would rise). The reactions which remove cations to the sea floor are all increased in rate with a rise in ocean OH^- ion concentration. Hence a feedback loop via the ocean's pH would always drive the ocean's cation and anion charge to equality. Any tendency towards a buildup in cation concentration (i.e., in alkalinity) would be countered by more rapid cation removal. Working in concert with the mechanism controlling the cation loss rate would be a feedback loop involving the cation gain rate. A more basic ocean would have a lower PCO_2 . Hence continental weathering rates would also be lower. While we don't know the specifics of these processes the generalization must be valid. The total cation charge in the sea must very nearly balance the total anion charge; otherwise large pH change would occur. As discussed above the anion charge is fixed largely by the formation and destruction of salt deposits.

The ratio of the cations yielding the proper total need not

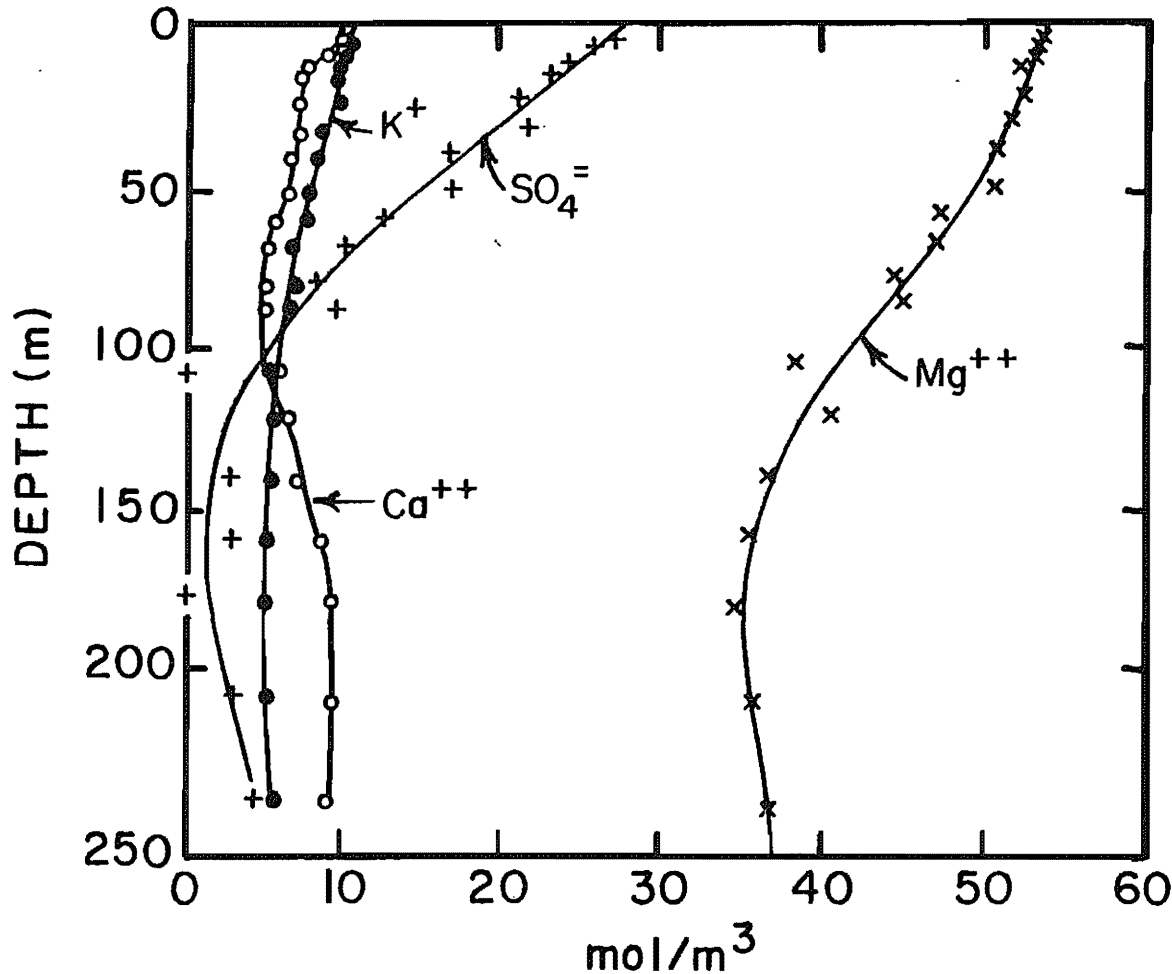


Figure 6-6. The K^+ , Mg^{++} , Ca^{++} , and $SO_4^{=}$ ion contents of pore water squeezed from various depths in a core taken at $13^\circ N$ latitude and $64^\circ W$ longitude and at a water depth of 1.2 kilometers in the Caribbean Sea as part of the National Science Foundation's Deep Sea Drilling Program. These data were obtained by Fred Sayles and Frank Manheim, Woods Hole Oceanographic Institution (529b).

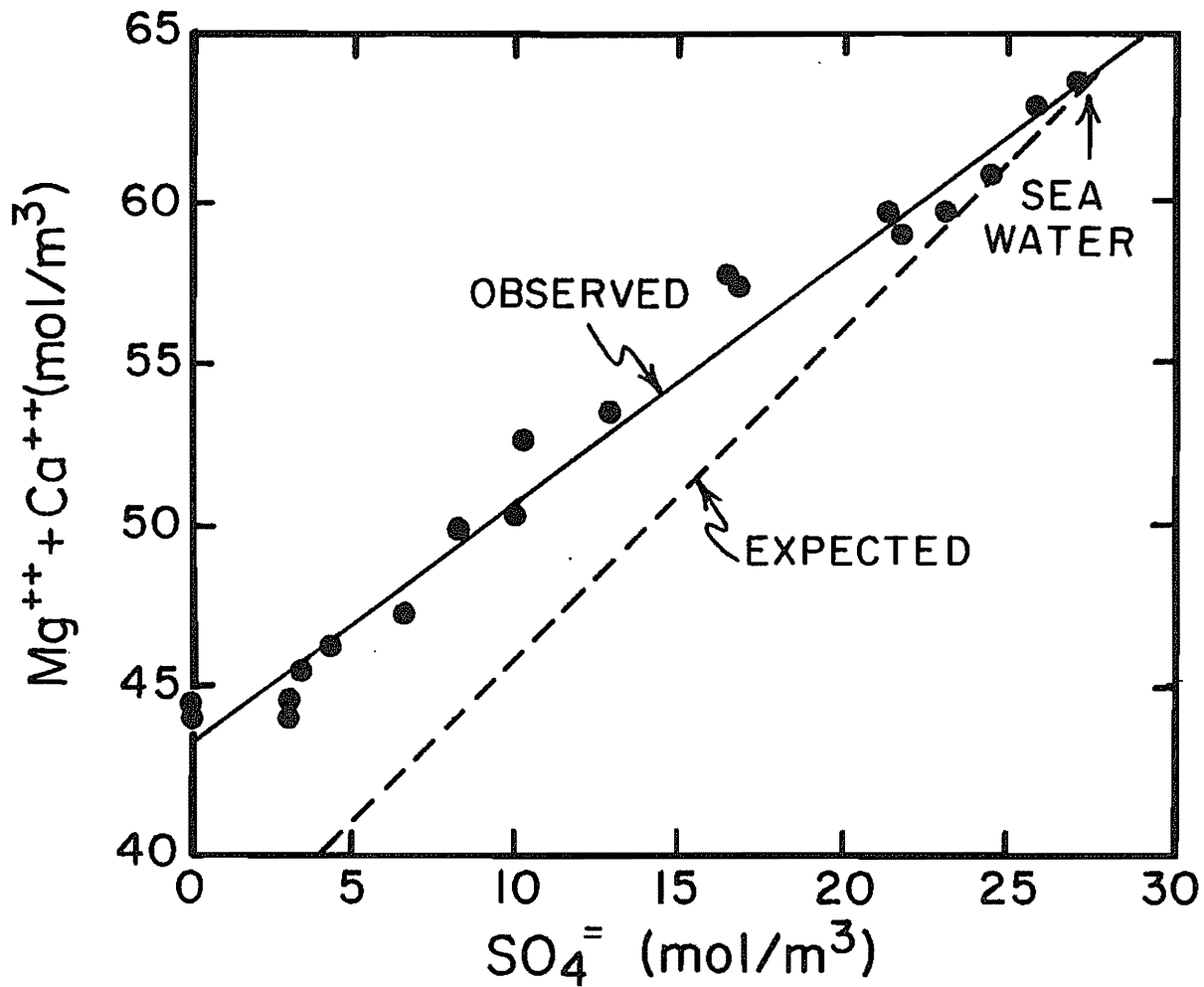


Figure 6-7. Plot of the $Mg^{++} + Ca^{++}$ versus $SO_4^=$ ion contents of pore waters squeezed from sediments for the data shown in figure 6-6 (529b). The solid line represents the average relationship derived from these measurements. The dashed line represents the relationship expected if Ca^{++} and Mg^{++} were the only ions replacing the iron removed from oxide minerals for precipitation by the reduced sulfur. The shallower slope of the observed line indicates that ions other than Ca^{++} and Mg^{++} are involved. Potassium is one candidate, but the decrease in K^+ (as shown in figure 6-6) accounts for only one-third of the slope difference. The logical candidate for the remaining difference is Na^+ . Since the Na^+ concentration is so large, the loss of the needed amount would not produce a measurable gradient in the pore water column.

of course remain constant with time. Changes in the geometry of the sea floor produced by plate motions, changes in type of organisms living in the sea through evolution and changing habitats, and changes in the oxygen content of the atmosphere will lead to relative removal probabilities for these cations.

POSSIBLE CAUSES FOR PERTURBATIONS

So far we have been speaking largely in the abstract about changes in the operational characteristics of the ocean. Have we just been playing thought games or is there a reason to consider such scenarios? To answer this question we first need to remind the reader that during the past million years our planet has undergone very large quasi-cyclic variations in climate called glaciations. The length of these cycles has been about 100,000 years (hence on the order of the residence time of C and P in the sea). It does not stretch the imagination to believe that climatic changes which built and destroyed ice sheets of continental dimension might have changed the rate of ventilation of the deep sea, the delivery rate of ions to the sea, and the ecology of the sea. If so, then these changes must have upset the balance between input and loss and caused the steady state concentrations of the various nutrient constituents to shift.

On a longer time scale the movements of the great plates which make up the earth's outermost shell have surely altered conditions in the oceans for they would have altered the geography of the ocean basins and of the continents. These changes were sufficiently slow that the cycles of the nutrient constituents should have been able to keep pace. If so, the sea must have undergone long term changes in the concentrations of these constituents. On these time scales the concentration of other constituents might also have changed. For example, the concentrations of O_2 , Ca^{++} and K^+ adjust on time scales of millions of years. Those of $SO_4=$ and Mg^{++} , Cl^- and Na^+ adjust with time scales of tens to hundreds of millions of years.

In addition to the gradual changes associated with the long term alterations of the earth's surface geometry, we know of several geological catastrophes. The greatest of these occurred 60 million years ago when during a short interval of time (<10,000 years) over half the species of organisms on the planet became extinct. Among those to go were all the hard part producing micro-organisms which inhabited the Cretaceous surface ocean (694). There is now good evidence linking these extinctions to the impact of a large asteroid or comet. Again it does not stretch one's imagination to believe that the nutrient constituent concentrations in the sea must have suffered some perturbations as the result of this major ecologic disruption.

Finally, man is now conducting his greatest geochemical experiment. CO_2 is being added to the atmosphere at a stupendous rate by the combustion of fossil fuels. By the end of the next century we will have produced an amount of CO_2 equal to several times that in the atmosphere prior to man's impacts. About one quarter of this CO_2 will at that time reside in the ocean. The

remaining three quarters will reside in the atmosphere. While the immediate concern to mankind is the climatic warming that this excess atmospheric CO₂ will cause, there will also be impacts of this CO₂ on the chemistry of the ocean, which will last for thousands and even tens of thousands of years. It behooves us to think through in advance what the consequences of this "experiment" will be.

Thus the analysis of the control systems we conducted at the beginning of the chapter were not just a thought game. These systems must have played an important role in the history of our planet and they surely will be brought into action by the perturbations man will induce on the ocean's chemistry.

RECORDERS OF PALEOOCEAN CHEMISTRY

If we are to learn about the changes in ocean chemistry that occurred in response to glacial to interglacial changes, to geologic catastrophes, and to the long term geographic changes induced by plate motions then we must develop a means of reading these changes from the record in sediments. This is no simple task. No one has yet discovered a reliable means by which the concentration of any of the ingredients of sea salt is directly recorded in marine sediments. We can understand why this is difficult by remembering that everything that enters the sea must eventually leave. Thus the composition of the average sediment formed at any given time is related far more closely to the composition of the material entering the sea at that time than to the composition of the sea salt at that time. The chemistry of sea salt continually adjusts so as to promote throughput of the material arriving from rivers. These changes need not bear any simple relationship to the changes in inputs.

By contrasting sediments deposited during the last glacial period with those deposited since the end of this period (i.e., during Holocene time) there are several means by which we can gain information about changes in the ocean's nutrient constituent concentrations.

1). Through the application of the dating methods described in chapter 5 it is possible to determine how the accumulation rate of calcite at various places on the sea floor changed between late glacial and post glacial time. If these cores are taken at sites above the lysocline then these measurements give information regarding the rate of production of calcite by organisms living in the overlying water column. Changes between glacial and interglacial time of course could be brought about by a change in ocean ecology, by a change in ventilation rate, or by a change in the supply rate of carbon to the oceans.

2). By studying calcite from cores taken in the transition layer below the lysocline it is possible to determine how the extent of calcite solution has changed with time at this particular point on the sea floor between glacial and interglacial time. An example of such a record is shown in figure 6-8. If such a study included cores from various water depths, it should be possible to determine how the lysocline changed between glacial and interglacial time and also how the thickness of the transition zone

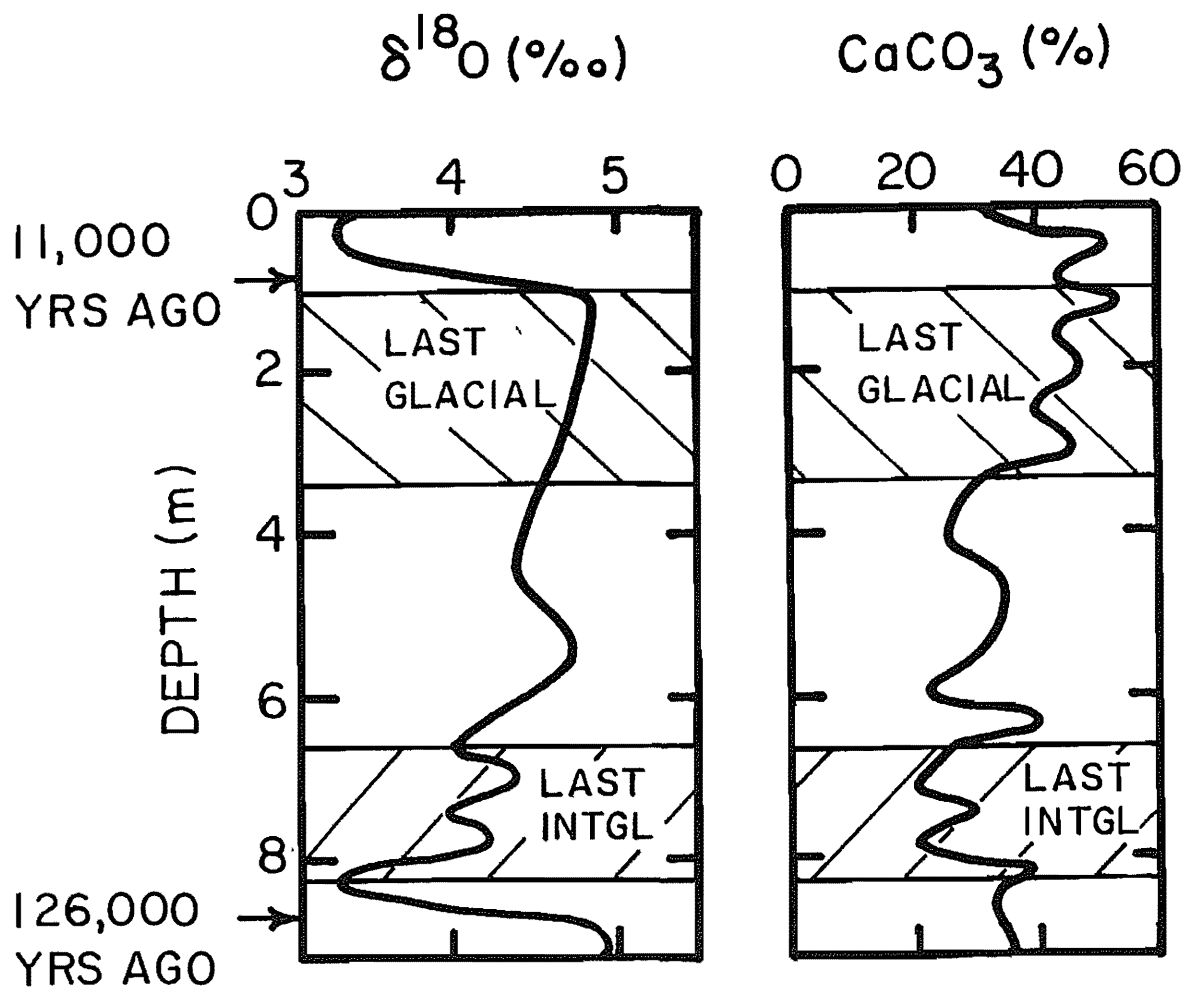


Figure 6-8. CaCO_3 and $\delta^{18}\text{O}$ records for core V19-29 (4°S , 84°W , 3.2 km) from the east equatorial Pacific. This site currently lies beneath the lysocline for calcite. The variations in CaCO_3 content with time are mainly the result of changes in the extent of calcite solution (more in warm periods less in cold). The CaCO_3 changes appear to lag the ice volume changes by about 10,000 years. The measurements were made by Nick Shackleton at Cambridge University (328).

(from no calcite solution to complete calcite solution) changed. Glacial to interglacial variations in the depth of the lysocline would signal changes in the $\text{CO}_3^{=}$ ion concentration in the deep sea. Changes in the thickness of the transition zone would signal changes in the calcite rain rate or in the gradient of $\text{CO}_3^{=}$ ion content in the water column beneath the lysocline.

3). Studies of the relationship between the distribution of the habitats of various species of benthic foraminifera on the sea floor and the distribution of dissolved oxygen in the deep sea reveal that certain species compete more favorably at sites bathed in highly oxygenated bottom water while others compete more favorably on sites bathed in poorly oxygenated bottom water. Thus reconstructions of the distribution during glacial time of species of benthic forams with affinity for high oxygen water and of species with affinity for low oxygen water should provide important information regarding changes in the oxygen content of the deep sea between glacial and interglacial time. An example of such a change is shown in figure 6-9. As we have discussed above, such changes would signal shifts in the phosphorus content of deep water.

4). Measurements on samples of Holocene age from borings in the Greenland and Antarctic ice caps made by Oeschger and his colleagues in Bern, Switzerland, suggest that the air trapped in small bubbles in the ice has a CO_2 content close to that in the pre-1850 atmosphere. By contrast, samples from glacial time have CO_2 to air ratios distinctly lower than those from post glacial time. An example of these results will be shown in chapter 9. Thus a means exists for reconstructing the CO_2 partial pressure in the atmosphere (and hence also in the surface ocean) over the last several hundred thousand years!

5). As we have seen, the $^{18}\text{O}/^{16}\text{O}$ -ratio in sea water changes between glacial and interglacial time because the water that goes into building the continental ice masses is depleted by several percent in the heavy isotope of oxygen. The changes in the $^{18}\text{O}/^{16}\text{O}$ ratio of deep sea water produced by the waxing and waning of these ice sheets are recorded by the shells of benthic foraminifera. As salt is left behind when vapor is carried from the sea surface, the ^{18}O record kept by benthic forams provides a salinity record for mean sea water. Further, as mentioned above, the ^{18}O record allows us to tie together reliably information from deep sea cores taken throughout the world ocean. An example of such a record was given in figure 5-12.

6). There is one constituent of sea salt which we have not as yet mentioned; namely $\Sigma^{13}\text{CO}_2$. ^{13}C is a stable isotope of carbon. On the average 1 atom of carbon in the earth out of 90 is of this type. As we shall now show, the distribution of $^{13}\text{C}/^{12}\text{C}$ ratios in the carbon dissolved in the ocean is closely tied to the distribution of PO_4 (and NO_3) in the sea. Foraminifera record the $^{13}\text{C}/^{12}\text{C}$ ratio of the carbon in sea water just as they do the $^{18}\text{O}/^{16}\text{O}$ ratio. By measuring the $^{13}\text{C}/^{12}\text{C}$ ratios in forams which grew at different depths and locations in the ocean at some time in the past we should be able to reconstruct the distributions of PO_4 (and NO_3) for that time! An example of such a record is shown

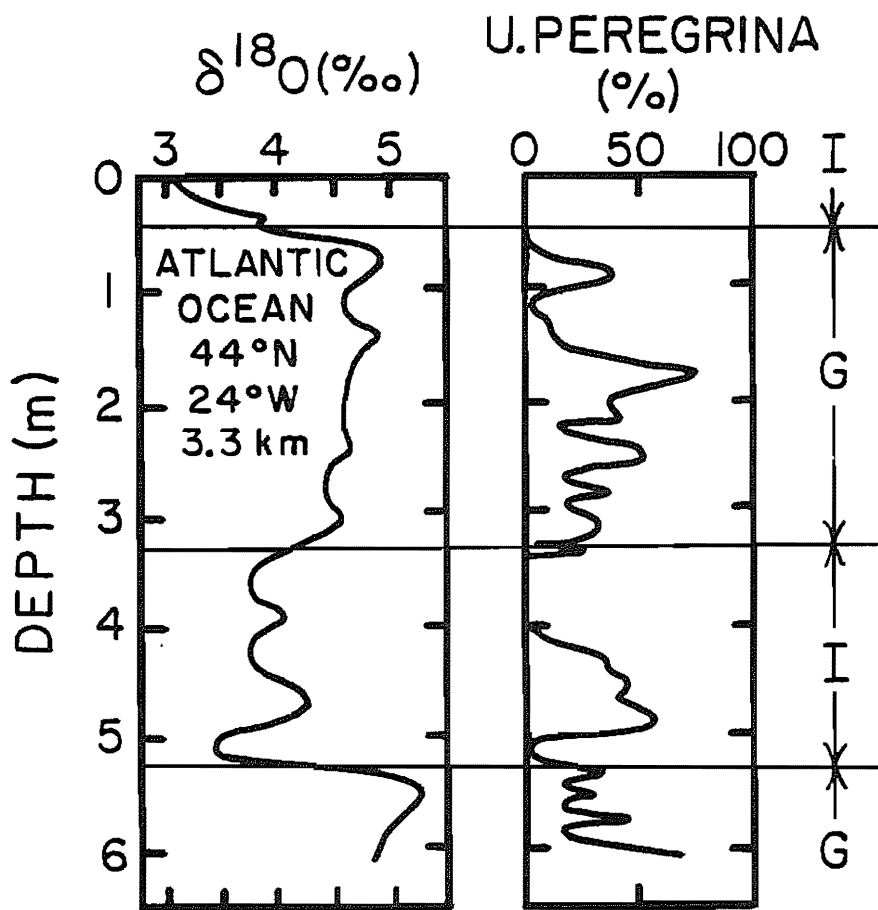


Figure 6-9. Plots of $\delta^{18}\text{O}$ versus depth for the benthic foraminifera species Uvigerina peregrina and of percent Uvigerina peregrina in the benthic foraminifera assemblage versus depth in a core from the flanks of the Mid-Atlantic Ridge at 44°N. These results show that Uvigerina peregrina is absent from this part of the sea floor during post-glacial time and during parts of the last interglacial period. This species is associated with high oxygen content waters in today's ocean. The $\delta^{18}\text{O}$ measurements were made by Nick Shackleton at Cambridge University and the benthic faunal studies were made by Streeter at the Lamont-Doherty Geological Observatory (619).

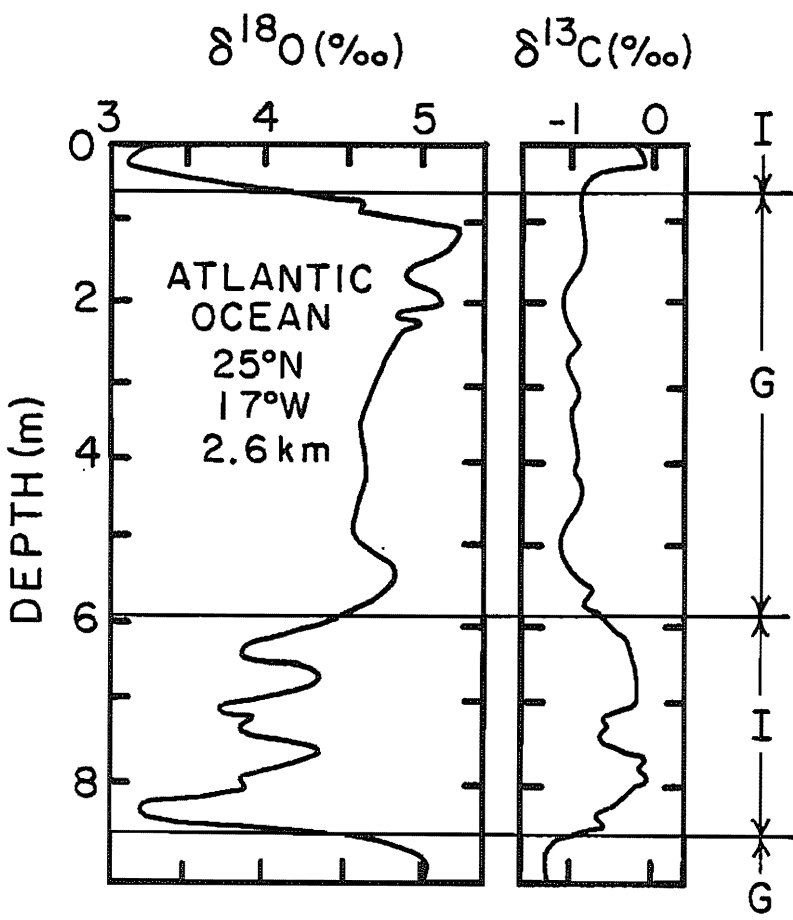


Figure 6-10. Plots of $\delta^{18}\text{O}$ and $\delta^{13}\text{C}$ for benthic foraminifera as a function of depth in a core from the eastern margin of the North Atlantic Ocean. It can be seen that the $\delta^{13}\text{C}$ values for forams which grew on the sea floor during glacial time were lower than for those which grew during interglacial time. These measurements were made by Nick Shackleton of Cambridge University (328).

in figure 6-10.

THE MARINE GEOCHEMISTRY OF CARBON-13

The ratio of ^{13}C to ^{12}C in the dissolved inorganic carbon in the sea varies from place to place for two reasons. First, when plants draw carbon from surface sea water for photosynthesis, ^{12}C is fixed with slight preference over ^{13}C yielding a $^{13}\text{C}/^{12}\text{C}$ ratio in plant matter about 20‰ lower than that in the ΣCO_2 in the water in which the plants grow. When animals consume the plants they incorporate in their tissues carbon of nearly the same isotopic composition as in the food they eat. They also respire carbon of nearly the same isotopic composition as that in their food supply. Because plant matter is formed only in the ocean mixed layer, and because some of this material is oxidized only after falling to deeper layers of the sea, the $^{13}\text{C}/^{12}\text{C}$ ratio in surface water is higher than that in deep waters (i.e., ^{12}C is preferentially transferred from surface to deep water through the photosynthesis-respiration cycle).

The second reason that the $^{13}\text{C}/^{12}\text{C}$ ratio in dissolved inorganic carbon varies from place to place within the sea is that there is a fractionation between the carbon in atmospheric CO_2 and the ΣCO_2 in surface ocean water. The $^{13}\text{C}/^{12}\text{C}$ ratio in atmospheric CO_2 is on the average about 9‰ lower than that in surface ocean ΣCO_2 . The extent of this fractionation depends on temperature. The depletion varies from 10.6‰ at 0°C to about 7.6‰ at 30°C. Thus the carbon in surface ocean waters from high latitudes should have higher $^{13}\text{C}/^{12}\text{C}$ ratios than the carbon in surface waters from low latitudes.

Before proceeding with an analyses of how these two sources of variation are imprinted on the distribution of $^{13}\text{C}/^{12}\text{C}$ ratios in the sea, we must mention the units used by geochemists doing ^{13}C studies. Like $^{14}\text{C}/^{12}\text{C}$ and $^{18}\text{O}/^{16}\text{O}$ results, $^{13}\text{C}/^{12}\text{C}$ results are given as the per mil difference from that in a reference sample. The equation is as follows:

$$\delta^{13}\text{C} = 1000 \left[\frac{(^{13}\text{C}/^{12}\text{C})_{\text{sample}} - (^{13}\text{C}/^{12}\text{C})_{\text{ref}}}{(^{13}\text{C}/^{12}\text{C})_{\text{ref}}} \right] \quad 6-1$$

The reference standard is a belemnite from the PeeDee formation in North Carolina used by Urey in his early work (see page 681). On this scale mean ocean carbon is close to zero, i.e.,

$$\delta^{13}\text{C}_{\text{moc}} = 0 \text{ ‰}$$

The difference between the $\delta^{13}\text{C}$ values for various samples is designated as follows:

$$\Delta\delta^{13}\text{C}_{\text{A-B}} = \delta^{13}\text{C}_{\text{A}} - \delta^{13}\text{C}_{\text{B}}$$

Thus the difference between the $\delta^{13}\text{C}$ of marine plant tissue and that of ΣCO_2 in the water in which the plant grew is given as:

$$\Delta \delta^{13}\text{C}_{\text{plant}-\Sigma\text{CO}_2} = -20 \text{ ‰}$$

A profile of $\delta^{13}\text{C}$ versus water depth for a station in the North Pacific is shown in figure 6-11. Also shown in this figure is a profile of phosphorus. The relationship of $\delta^{13}\text{C}$ to PO_4 in this and other parts of the ocean is summarized in the plot of $\delta^{13}\text{C}$ versus PO_4 concentration shown in figure 6-12. There is an inverse correlation between the two parameters.* The reason for this correlation is that the variations of both parameters in the sea are mainly controlled by the photosynthesis-respiration cycle. Were this the only source of perturbation then the expected slope could be approximated by the relationship:

$$\frac{\Delta \delta^{13}\text{C}}{\Delta \text{PO}_4} = \Delta \delta^{13}\text{C}_{\text{plant}-\Sigma\text{CO}_2} \frac{\text{C/P) organic tissue}}{\Sigma\text{CO}_2 \text{ mean ocean water}} \quad 6-2$$

$\Delta \delta^{13}\text{C}_{\text{plant}-\Sigma\text{CO}_2}$ averages about -20 ‰ , the C/P ratio in marine plants about 105, and the ΣCO_2 content about $2250 \mu\text{m/kg}$. Thus:

$$\frac{\Delta \delta^{13}\text{C}}{\Delta \text{PO}_4} = -20 \times \frac{105}{2250} = -0.93 \frac{\text{‰}}{\mu\text{m/kg}}$$

Thus the observed and predicted slopes agree reasonably well, suggesting that the photosynthesis-respiration cycle dominates the temperature dependent air-sea interaction.

If so, then what is the fractionation induced by air-sea exchange? The $\delta^{13}\text{C}$ values for the ΣCO_2 in surface waters are plotted against water temperature in figure 6-13. Also shown is the expected trend for equilibrium with the atmosphere. Clearly the surface ocean does not achieve local carbon isotope equilibrium with the overlying atmosphere. This is not surprising for the time required for isotopic equilibrium to be achieved is given by the following relationship:

$$\tau_{\text{carbon isotopes}} = \frac{[\Sigma\text{CO}_2]}{[\text{CO}_2]} \tau_{\text{gas}} \quad 6-3$$

To exchange the isotopes of carbon in the ΣCO_2 , the HCO_3^- and CO_3^{2-} must exchange as well as the CO_2 . The ratio of ΣCO_2 to CO_2 in surface water ranges from about 180 in warm water to about 150 in cold water. Thus the carbon isotopic replacement time is about 15 years (and the half replacement time about 10 years). Surface waters simply do not "sit still" this long for local equilibrium

*As will be discussed in chapter 10 the addition of fossil fuel and forest soil CO_2 to the atmosphere during the last 200 years has reduced the $\delta^{13}\text{C}$ value for surface ocean water by about 0.8 ‰ . Hence prior to 1850 the mean $\delta^{13}\text{C}$ for warm surface water was likely about 2.7 ‰ (as opposed to the value of 1.9 ‰ measured in the early 1970's).

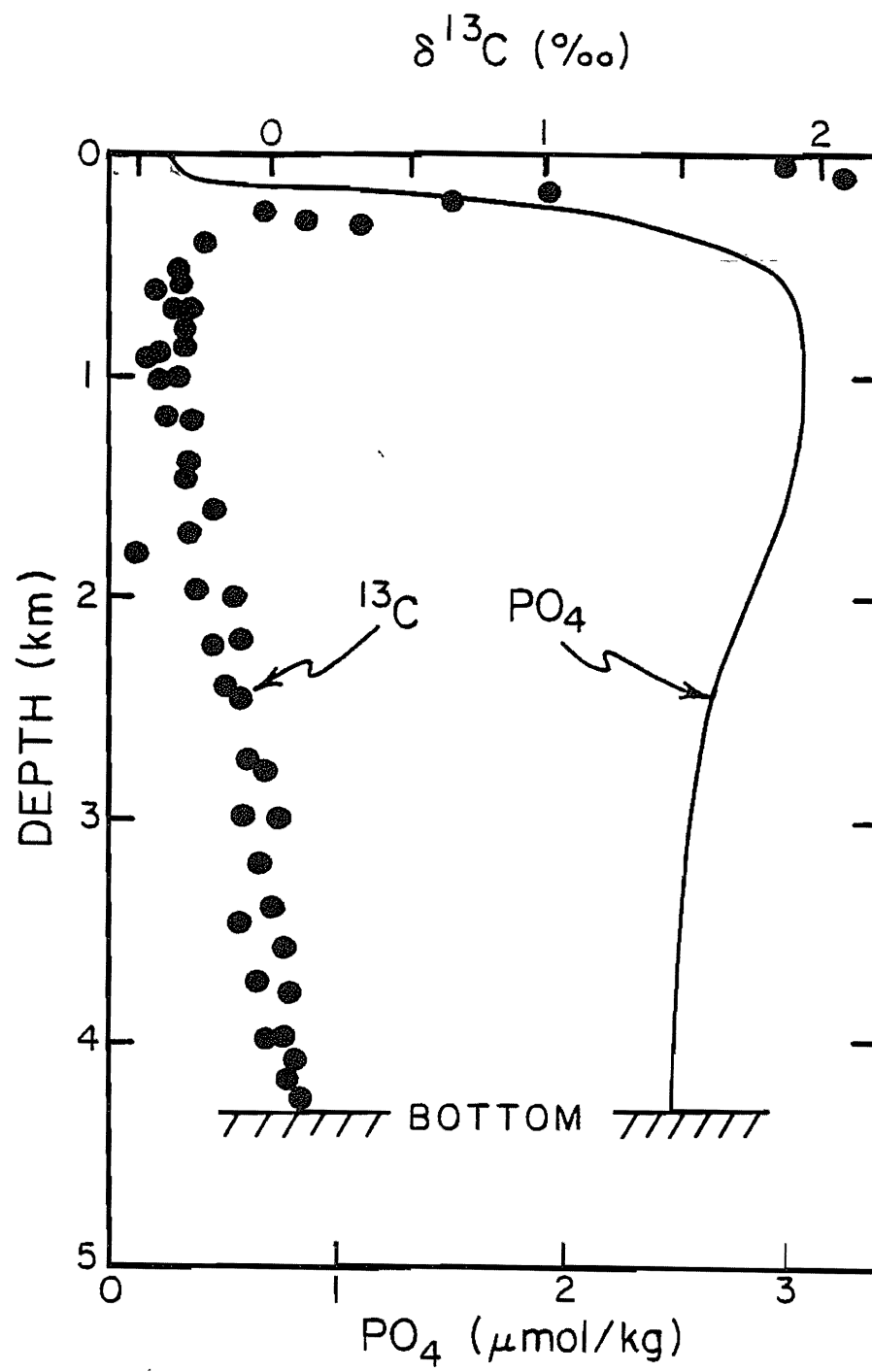


Figure 6-11. Plots of $\delta^{13}\text{C}$ and PO_4 versus depth at GEOSECS station 346 (28°N , 121°W) in the northwestern Pacific Ocean. The $\delta^{13}\text{C}$ analyses were made by Craig and Kroopnick at the Scripps Institution of Oceanography (292) and the PO_4 analyses as part of the GEOSECS program (425).

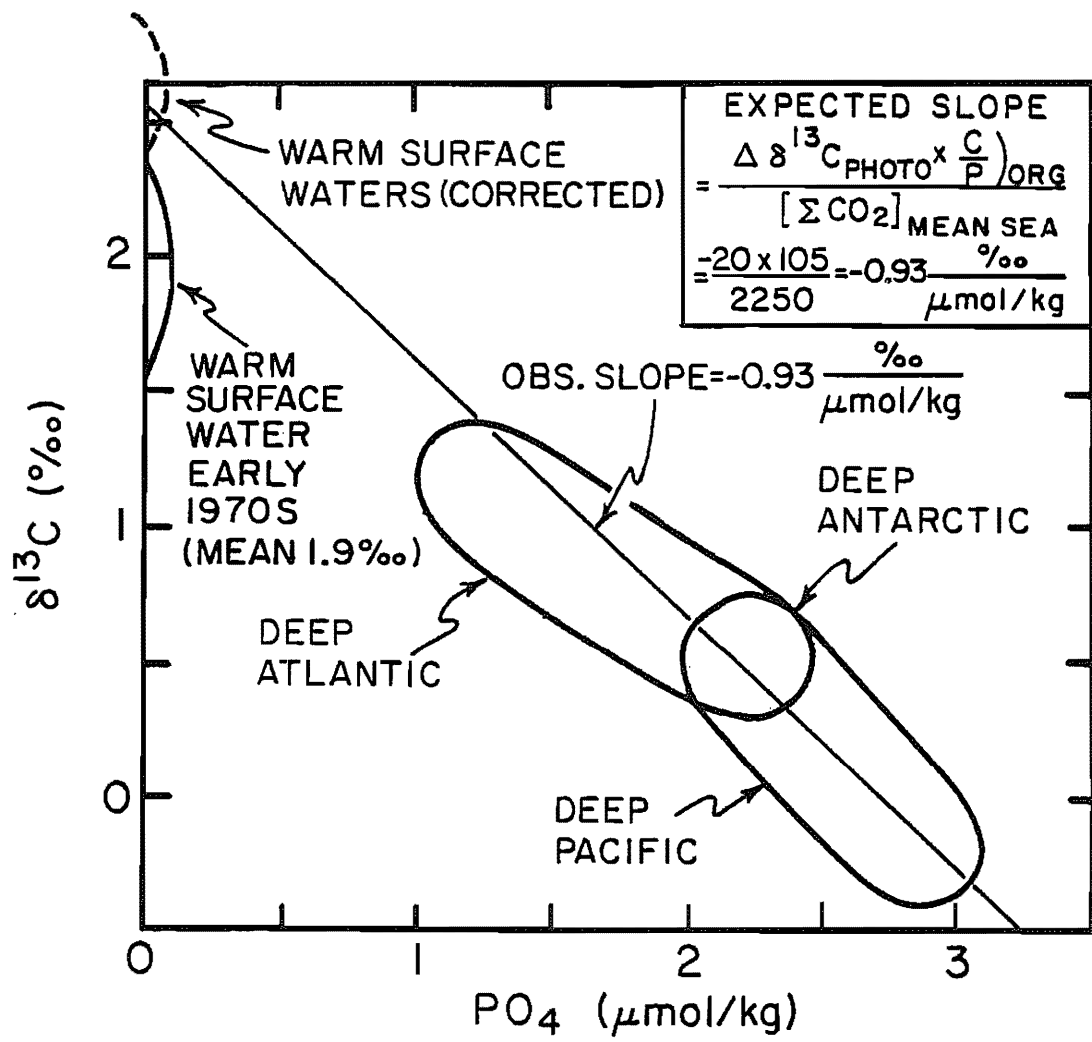


Figure 6-12. Relationship between $\delta^{13}\text{C}$ and PO_4 in the world ocean. The $\delta^{13}\text{C}$ values for warm ocean water have been corrected by 0.8‰ to remove the decrease which has taken place over the last century as the result of the invasion of CO_2 produced by the burning of fossil fuels and the decline of forest-soil reservoirs. The slope defined by these results is close to that expected from photosynthesis and respiration cycle (i.e., $-0.93\text{‰}/^\circ\text{C}$). The ^{13}C data on which this diagram is based were obtained in the laboratories of Harmon Craig at the Scripps Institution of Oceanography and of Peter Kroopnick at the University of Hawaii (292, 293, 294, 295, 296, 298, 301).

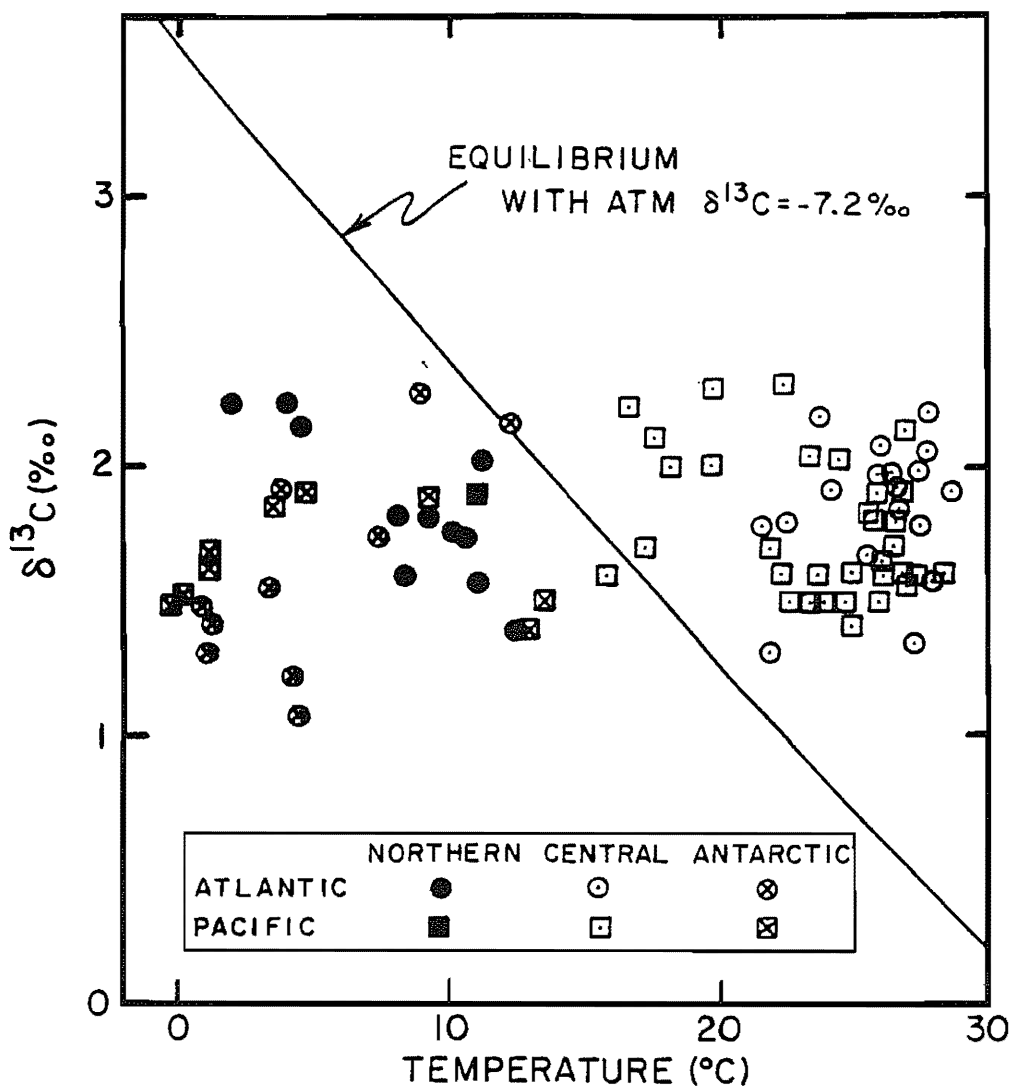


Figure 6-13. Plot of $\delta^{13}\text{C}$ measured on the ΣCO_2 extracted from surface ocean water as a function of surface water temperature. The straight line shows the $\delta^{13}\text{C}$ for equilibrium with the atmosphere at the time these samples were collected. Clearly the surface water results do not follow the trend expected if local isotope equilibrium were established with the overlying atmosphere. The ^{13}C data are from the references cited in the figure 6-12 caption. The equilibrium values are calculated from data obtained by Mook of Groningen in the Netherlands (297).

to be achieved. They are replaced by vertical or horizontal transport on the time scale of a few years. So we see that local exchange with the atmosphere does not make a strong imprint on the $^{13}\text{C}/^{12}\text{C}$ ratio distribution in the sea.

The long exchange time for carbon isotopes also influences the $^{14}\text{C}/^{12}\text{C}$ distribution in the sea. We have already seen that nowhere did surface ocean water have the atmospheric $^{14}\text{C}/^{12}\text{C}$ ratio prior to the onset of nuclear testing. The ^{14}C deficiency ranged from 4-5 percent in the temperate surface ocean to more than 10 percent in the surface waters of the Antarctic. We shall have more to say about the implications of this slow exchange in the chapters to come.

The important point to emphasize here is that in today's ocean $^{13}\text{C}/^{12}\text{C}$ ratio differences from water mass to water mass provide an excellent measure of PO_4 differences between these masses. If the temporal record of $^{13}\text{C}/^{12}\text{C}$ ratio in the shells of foraminifera which grew on the sea floor (benthic forams) and in the shells of foraminifera which lived in surface water (planktonic forams) provide a proxy record of the temporal variations in the $\delta^{13}\text{C}$ for these waters between glacial and interglacial time, we have the wherewithal to reconstruct the changes in the PO_4 content of various water masses between glacial and interglacial time. As we shall see in chapter 9 this will prove very important to reconstructions of the chemistry of the glacial ocean.

THE URANIUM CONTENT OF CORAL

Let us consider one last paleocean indicator which may give us information about changes which occurred on the time scale of 10 million years. Uranium is present in the sea in remarkably great quantities compared to its abundance in crustal rocks. It is a biounlimited element with a reactivity so low that it remains in the sea for about 700,000 years before being removed to sediments.

Measurements on saline lakes also reveal high uranium contents. In fact, the U content of the waters of these lakes is proportional to their total dissolved carbon content. Pyramid Lake in Nevada, for example, has a tenfold higher ΣCO_2 and a tenfold higher U content than sea water. Mono Lake in California has a hundredfold higher ΣCO_2 and a hundredfold higher U content. We can imply from this that if, in the past, the ocean had a different ΣCO_2 concentration it probably had a different U concentration, too. Uranium owes its remarkably low reactivity in natural waters to the fact that it forms highly stable complexes with $\text{CO}_3^{=}$ ion.

Uranium has another peculiarity. Corals incorporate uranium in their CaCO_3 in nearly the same proportion to calcium as found in sea water. Apparently, these organisms cannot distinguish between the doubly charged cations of Ca, Sr, Ba, Ra, and U, and use them indiscriminately in building their CaCO_3 reefs. Thus the U/Ca ratio in a well-preserved marine coral should be an index of the U/Ca ratio in ancient sea water. More important, since the U content of the sea apparently reflects its $\text{CO}_3^{=}$ ion content, if corals grown at some time in the past are found to have a different U/Ca ratio, then the water in which they formed probably had a

different $\text{CO}_3^{=}/\text{Ca}^{++}$ ratio than today's sea.

Figure 6-14 shows histograms of the U contents of corals for four time intervals: (a) the last 8000 years, (b) 80,000-220,000 years ago, (c) 2-5 million years ago, and (d) 5-20 million years ago. No significant differences are found back to 5 million years. The U/Ca ratios in corals from each interval in this time period are much the same as the U/Ca ratios in the living corals in today's ocean. In the 5-20 million year interval, however, the U/Ca ratio is an average of only half as great as it is in living corals. Since the corals used for this study show no conversion of aragonite to calcite and since they yield uranium-helium ages* consistent with those based on the geologic ages of the deposits in which the corals were found, the low U content of the oldest group of corals does not appear to be the result of U loss during the millions of years which have elapsed since these corals formed.

From studies of marine sediment borings we know that during this 5-20 million year time period the saturation horizon separating CaCO_3 -rich and CaCO_3 -poor sediments was at approximately the same elevation as it is today (see figure 2-31). We can conclude then that the product of the Ca^{++} and $\text{CO}_3^{=}$ ion contents was also roughly the same as it is today. If this is true, to have had a twofold lower $\text{CO}_3^{=}/\text{Ca}^{++}$ ratio, the Ca^{++} ion content must have been 1.4 times that of today and the $\text{CO}_3^{=}$ ion content must have been 0.7 times that of today. The uranium content would then have been 0.7 times that of today and the U/Ca ratio one-half that found in today's ocean.

If so then the Ca content of sea water must have decreased during the last 20 million years. If the anion content ($\text{Cl}^- + \text{SO}_4^{=}$) has remained the same, then the Ca^{++} decrease must have been accompanied by an increase in Mg^{++} , K^+ , or Na^+ .

FACTORS INFLUENCING NUTRIENT GRADIENTS IN THE DEEP SEA

We have seen that the present mode of ventilation of the deep sea (i.e., from northern Atlantic through Antarctic to the Indian and the Pacific) has a strong impact on the distribution of properties in the deep sea. The concentrations of the nutrient constituents (phosphate, nitrate, silicate, ΣCO_2 , alkalinity and barium) all increase along the path of this flow. That of dissolved oxygen and of carbonate ion decrease. The ratios of $^{14}\text{C}/^{12}\text{C}$ (because of radiodecay) and that of $^{13}\text{C}/^{12}\text{C}$ (because of respiration) also decrease. This pattern is imprinted in deep sea sediments in three ways:

- 1) The depth of the lysocline decreases along the path of the deep current.
- 2) The $^{13}\text{C}/^{12}\text{C}$ ratio in benthic forams decreases along the path of the deep current.
- 3) The abundances of those species of benthic forams adapted to low oxygen water increase along the path of the current.

By studying the change in these parameters with time in cores

*The uranium-helium method is closely analogous to the potassium-argon method we discussed in chapter 5.

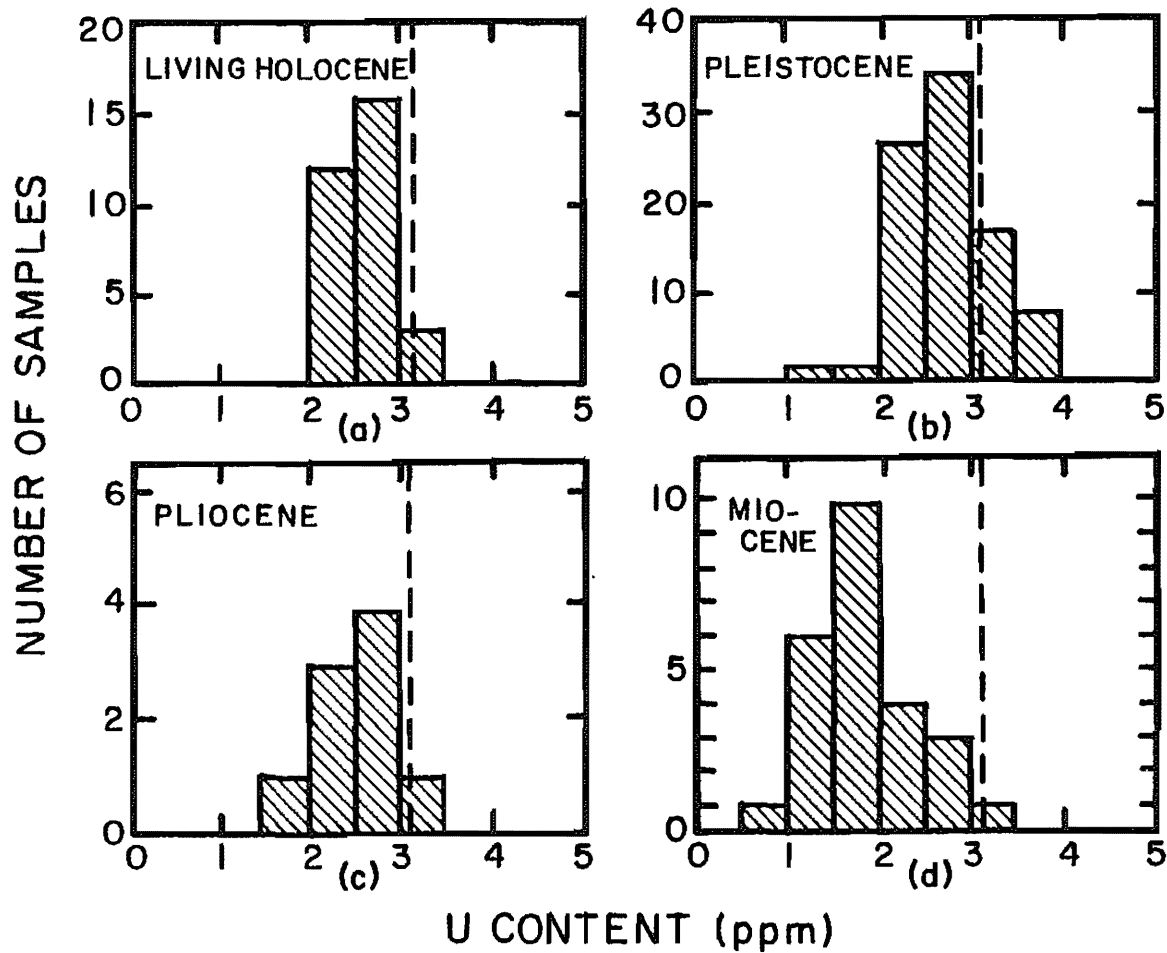


Figure 6-14. Histograms showing the uranium contents of corals in four different age groups. In each case, the U content expected if the corals formed with the same U/Ca ratio found in today's ocean is indicated by a dashed line. The data are shown in (a) for living corals and those formed during the last 8000 years (the present interglacial period); in (b) for corals which lived during the two previous periods of interglaciation (80,000-220,000 years in age); in (c) for corals from the Pliocene Epoch (2-5 million years in age); and in (d) for corals from the Miocene Epoch (5-20 million years in age). These uranium measurements were drawn from a variety of sources listed in reference (547).

taken throughout the world ocean, it should be possible to learn about changes in the sources and flow-patterns of deep water. We will have more to say about this in chapter 9.

SUMMARY

In this chapter we have seen that there is good reason to suspect that the concentrations of the various nutrient constituents in the sea as a whole, and even in one part of the sea relative to another, have changed with time. They have been drifting about in an effort to minimize the differences between loss and supply created by geologic and climatic changes. The glacial cycles of the recent past provide the ideal opportunity to search for such changes. As the length of these cycles is similar to the residence time of a number of the key constituents, chemical changes are likely to have occurred. We have complete and well dated records of deposition over the last complete glacial cycle from many places on the sea floor. Much of chapter 9 will be devoted to an attempt to piece together and interpret this record.

Man's activities will alter the course of ocean chemistry. The CO₂ produced by burning of coal, oil and natural gas is the chief culprit in this regard. In chapter 10 we will study the interplay between man's CO₂ inputs and nature's control systems.

The answer to the question, "What Keeps the System in Whack?", is negative feedback controls. If the throughput of any of the constituents of sea salt gets out of balance, its concentration will begin to change. The change in concentration will feed back by altering the rates of formation of the particulate phases which carry the constituent to the sea floor and by altering the degree of preservation of these phases on the sea floor. These feedbacks tend to eliminate the imbalances created by geologic and climatic change. It must be emphasized that we have as of now only a slight glimmering regarding the identity of the important control mechanisms. Thus we are bound to be in for surprises. The main point to be made here is that the ocean's chemistry has almost certainly changed with time and that economic logic is an important ingredient in the understanding of these changes.

PROBLEMS

6-1 Measurements on an equatorial Pacific Ocean core reveal the following accumulation rates for post glacial time:

Organics	<0.01	g/cm ² 10 ³ yr
Calcite	1.0	g/cm ² 10 ³ yr
Opal	0.2	g/cm ² 10 ³ yr
Other	0.5	g/cm ² 10 ³ yr
Total	1.7	g/cm ² 10 ³ yr

Sediment traps from the same area yield the following rain rates:

Organics	10	g/m ² yr
Calcite	10	g/m ² yr
Opal	20	g/m ² yr
Other	5	g/m ² yr
Total	45	g/m ² yr

Assuming that the rate limiting step for opal dissolution is the pore water resaturation, what must S^* _{opal} be?

In the same core measurements for late glacial time reveal the following accumulation rates:

Organics	<0.01	$\text{g/cm}^2 \text{yr}$
Calcite	1.5	$\text{g/cm}^2 \text{yr}$
Opal	0.7	$\text{g/cm}^2 \text{yr}$
Other	0.6	$\text{g/cm}^2 \text{yr}$
Total	2.8	$\text{g/cm}^2 \text{yr}$

If the silicate concentration in deep sea water during late-glacial time was the same as it is today, what must have been the rain rate of opal during glacial time?

- 6-2 Assume that the input of silicate from rivers to the two-box ocean varies with climate. Assume further that the climatic cycles are rectangular with each glacial and interglacial interval 40,000 years in duration. If the river input of silicate is twice as high during glacial times as during interglacial times, what is the temporal pattern of the silicate concentration in the deep sea reservoir? Assume that all the silica reaching the surface is utilized by plants. Assume that in interglacials 97% of the opal is recycled and that in glacials 99% is recycled. Assume that the mixing rate in the sea is twice as great during glacials than during interglacials.
- 6-3 Assume that during glacial times the mean C/P ratio in organic matter falling from the surface to the deep sea is 115 while that during interglacial time is 95. Assuming that this change occurred abruptly at the end of glacial time how would the O₂ content of deep water change over the first few thousand years of interglacial time? How would the difference between the δ¹³C for surface water and for deep water carbon change on this time scale? Would the δ¹³C change be larger for deep water or for surface water? Why? Assume that the N/P ratio in marine organic residues remains constant from glacial to interglacial time. No changes in the chemistry of rivers or sea occur nor do any changes in circulation pattern or rate.
- 6-4 If 50 million years ago the Ca content of the sea was four times today's value and if at that time the lysocline stood at today's mean depth, then according to the hypothesis presented in the text, what would have been the uranium content of corals living at that time?
- 6-5 Thick salt deposits found beneath the floor in the Mediterranean Sea have an age of 4.5 million years. They cover an area of $2 \times 10^{11} \text{ m}^2$ and have an average thickness of 1000m. They consist of about half CaSO₄ and about half NaCl. By how much would the deposition of this salt have changed the ocean's salinity? By how much would it have changed its Ca content?

SUPERPROBLEM #6

Jim Brie, a marine geologist interested in the earth's climatic record, puzzles over the influence of bioturbation and changing sedimentation rate on the character of the record contained in deep sea sediments. To study these effects he constructs a simple sediment machine which reproduces what he considers to be the major elements of the problem. His machine consists of a mixing hopper and an accumulation column. Batches of new sediment are added to the hopper, thoroughly mixed with what is already there and then batches of the same size as those added are dropped from the hopper onto the sediment column. After each batch is dropped the hopper is raised an appropriate distance before the procedure is repeated. Each batch of sediment represents 1000 years of sediment rain. Jim Brie approximates glacial to interglacial cycles by varying the rain rate of input materials. He assumes that individual glacial and interglacial periods have a duration of 40,000 years and that the transitions from one climate to the other are quite sharp.

For his first experiment he adopts the following batch sizes:

	GLACIAL	INTERGLACIAL
Clay	400 grams	200 grams
CaCO ₃	800 grams	600 grams
Benthic	2,000 shells	10,000 shells
Planktonic	10,000 shells	1,000 shells
$\delta^{18}\text{O}$ (Planktonic)	2.00/oo	0.00/oo
$\delta^{18}\text{O}$ (Benthic)	-2.00/oo	-4.00/oo
^{230}Th Atoms	10^{10}	10^{10}

Prior to the addition of each batch the hopper contains 4,000 grams of sediment.

If Jim Brie's sediment column has a cross-sectional area of 250 cm² and if the clay makes a sediment of mineral density 0.6g/cm³ and the CaCO₃ a sediment of mineral density 1.0 g/cm³, what are the depth profiles of percent CaCO₃, of the ratio of benthic to planktonic forams, of the $\delta^{18}\text{O}$ for the planktonic shells and of the $\delta^{18}\text{O}$ for the benthic shells?

Jim Brie sends the profiles he obtains in this way to a friend who has the bad habit of reading sedimentary records in a rather simplistic way. If this friend were to assume that age increases linearly with depth and were he to disregard bioturbation effects, what faulty conclusions might he come to with regard to the shape of the climatic cycle and to the phasing of the various changes?

In his calculations Jim Brie first treats ^{230}Th atoms as stable. Having obtained the ^{230}Th profile he then corrects for aging (using time elapsed since each batch left the hopper plus the time of residence in the hopper). He then plots the logarithm of the ratio of ^{230}Th atoms to sediment mass against depth in the column. Again he sends these results to his friend. What false conclusions might this friend come to with regard to the sedimentation rates for this sediment?

Chapter 7

FREIGHT TRAINS AND FICKIAN CONFUSION

THE MOVEMENT OF WATER THROUGH THE DEEP SEA

INTRODUCTION

In this chapter we will take a closer look at what our tracers have to say about the ventilation of the deep sea. We have already established a rough time scale for the renewal of these waters and have seen something of their pattern of flow through the deep sea. What we seek is a more realistic quantitative representation for this process. As we shall see this remains one of the major unsolved problems in oceanography. The material in this chapter constitutes a status report on progress toward this difficult goal.

TYPES OF MOTION

One of the problems lies in the definition of the nature of the motions of the water within the deep sea. In chapter 1 we spoke of this flow as if it were a river of water moving from the source regions toward the remote regions of the deep sea. While such a flow is the net result of the combined motions in the deep sea, were we to follow any single water molecule we would find that its path was highly tortuous and it would be found moving upstream and across stream almost as frequently as downstream. In the course of its trip through the deep sea it would log 100 to 1000 times more kilometers of movement than were it to have simply followed one of the vectors shown in figure 1-12. In an attempt to simplify the motions in the ocean, oceanographers often separate them into two categories; advection and diffusion. Advection constitutes net movement along a major current. Diffusion is the random mixing accomplished by the hosts of eddies and backwashes which are everywhere at work in the sea. A comparison might be made to flies in a freight train. As the train moves along the track, the flies move chaotically about in all directions. Mathematically, advection is described by a velocity (dimensions cm/sec) and diffusion by mixing coefficient (dimensions cm^2/sec). The latter was introduced early in the 19th century by a chemist named Fick as a way to describe mixing on a molecular scale.

In addition to the horizontal motions which carry water from one geographic locale to another there are also vertical motions. We have already discussed the gradual upwelling of the water spreading through the deep sea. It advects toward the surface. Again, this motion is not unidirectional. Superimposed on the

upwelling motion are mechanisms which stir the rising water back down the column.

Thus, the physical oceanographer is faced with the rather awesome task of describing this complex of vertical and horizontal motions. His main tools, current meters and neutrally buoyant floats allow him to study the chaotic motions which we classify here as the diffusion part of the horizontal motions. However, unless placed in very special locations on the sea floor where strong unidirectional currents flow, these devices tell us little about the advective motions which carry water from one ocean basin to another. Only in special cases can they tell anything about vertical motions. To get at the horizontal advective transports, the physical oceanographer uses a theoretical argument which relates the flow of water to the tilt of horizons of constant pressure. Only with the aid of yet to be implemented satellite topographic techniques can this so-called geostrophic technique give absolute rates of flow. The physical oceanographer has no way to directly measure vertical advection or vertical diffusion.

Because of the inability to get at the major motions of interest in connection with deep sea ventilation by physical measurements, the tracers we have been describing are looked to as the great hope for working out the roles of "freight train motion" and the roles of "Fickian confusion" in the ventilation of the deep sea. As we shall see, while the distributions of these tracers will add much to our knowledge, they will not by themselves provide the solution to the problem.

ONE DIMENSIONAL ADVECTION - DIFFUSION MODEL

An example of advection and diffusion in a vertical column will help the reader comprehend the interaction between these two types of motion. To make the example as much like the ocean as possible, we will make our column 4000 meters high. Sea water with a temperature of 2°C and a salinity of $35.0^{\circ}/\text{oo}$ is pumped into the bottom of the column so that an upwelling velocity of 4 m/yr is generated.* In other words, the volume of water pumped into the base of the column (in m^3) in a year is equal to 4 meters times the cross-sectional area of the column (in m^2). At the top of the column there is a well-mixed layer 100 meters thick (stirred with a mechanical mixing device). Interactions with the overlying atmosphere maintain this layer at a temperature of 25°C . An excess of evaporation over rainfall maintains the salinity at $36.0^{\circ}/\text{oo}$. In the absence of any mechanism for vertical stirring beneath the 100-meter-thick surface layer, the temperature and salinity would be the same as in the input water all the way to the base of the mixed layer. Here they would change abruptly to

*Because the ^{14}C -based ventilation time for the deep sea is about 1000 years, oceanographers envision an upwelling at the rate of about 4 meters per year (the mean depth of the ocean is 3800 meters).

the surface values.* Water would of course have to be pumped off the top of the column at the same rate that it was added at the bottom. This water would be cooled and reduced in salinity before it was recycled. (In the real ocean the water would flow along the surface toward the poles where it would be cooled by contact with the atmosphere and reduced in salinity through the receipt of an excess of rainfall (and continental runoff) over evaporation.

A more realistic temperature and salinity profile would be achieved if diffusive mixing within the column were included. As shown in figure 7-1, such mixing carries the warm and saline surface water downward into the upwelling plume. The characteristic penetration depth of the surface water z^* would be given by:

$$z^* = \frac{\kappa}{w} \quad 7-1$$

and the half-penetration depth, $z_{1/2}$, is equal to $0.693z^*$. Where κ is the coefficient of diffusive mixing (units m^2/yr) and w is the upwelling velocity (m/yr). We have already seen that for $\kappa = 0$ (no mixing), $z_{1/2}$ is zero (no penetration beneath the mixed layer). To produce a half-penetration depth of 400 meters would require a κ of $2300 m^2/yr$ (or $0.73 cm^2/sec$). Temperature profiles from the Pacific Ocean show a penetration of warm water to a characteristic depths up to about 1400 meters. The κ needed to produce this penetration is $5700 m^2/yr$ (or $1.8 cm^2/sec$). Temperature profiles produced in our column by various choices for these values of w and κ are shown in figure 7-1.

The distribution of radiocarbon can be used in quite another way in connection with our simple 1-D ocean. Let us assume that the $\Delta^{14}C$ for the surface mixed layer carbon is at steady state $-50^{\circ}/oo$ and that the $\Delta^{14}C$ for the water pumped into the bottom of the column is $-160^{\circ}/oo$ (in the Pacific Ocean, after which our column is patterned, the new bottom water entering from the Antarctic has this $\Delta^{14}C$ value). We will also assume for the sake of clarity that the column is abiotic (i.e., that the carbon moves only with the water rather than in part sinking down the column in particulate form). As ^{14}C undergoes radiodecay within the water column, the $^{14}C/C$ ratio will be lower in the interior of the column than at the ends! The extent and vertical distribution of this deficiency will depend on the rates of upwelling and diffusion. Examples are shown in figure 7-2. Thus, had we come upon such a column, and wished to determine its operating characteristics, we would need only to measure the depth profile of salinity (or potential temperature) and the profile of $^{14}C/C$ ratio. The former would yield the ratio of κ to w and the latter would permit the absolute value of w (and hence also of κ) to be established.

Were this 1-D model to apply to the real ocean, it would permit the utilization rate of oxygen to be determined. This can be

*To maintain the temperature in the surface layer a flow of 10^4 calories/ $cm^2 yr$ from atmosphere to sea would be necessary (i.e., to balance the cooling caused by the inflow of the cold water from below). To maintain the salinity of the surface water a net evaporation rate of about $11 cm/yr$ would be required.

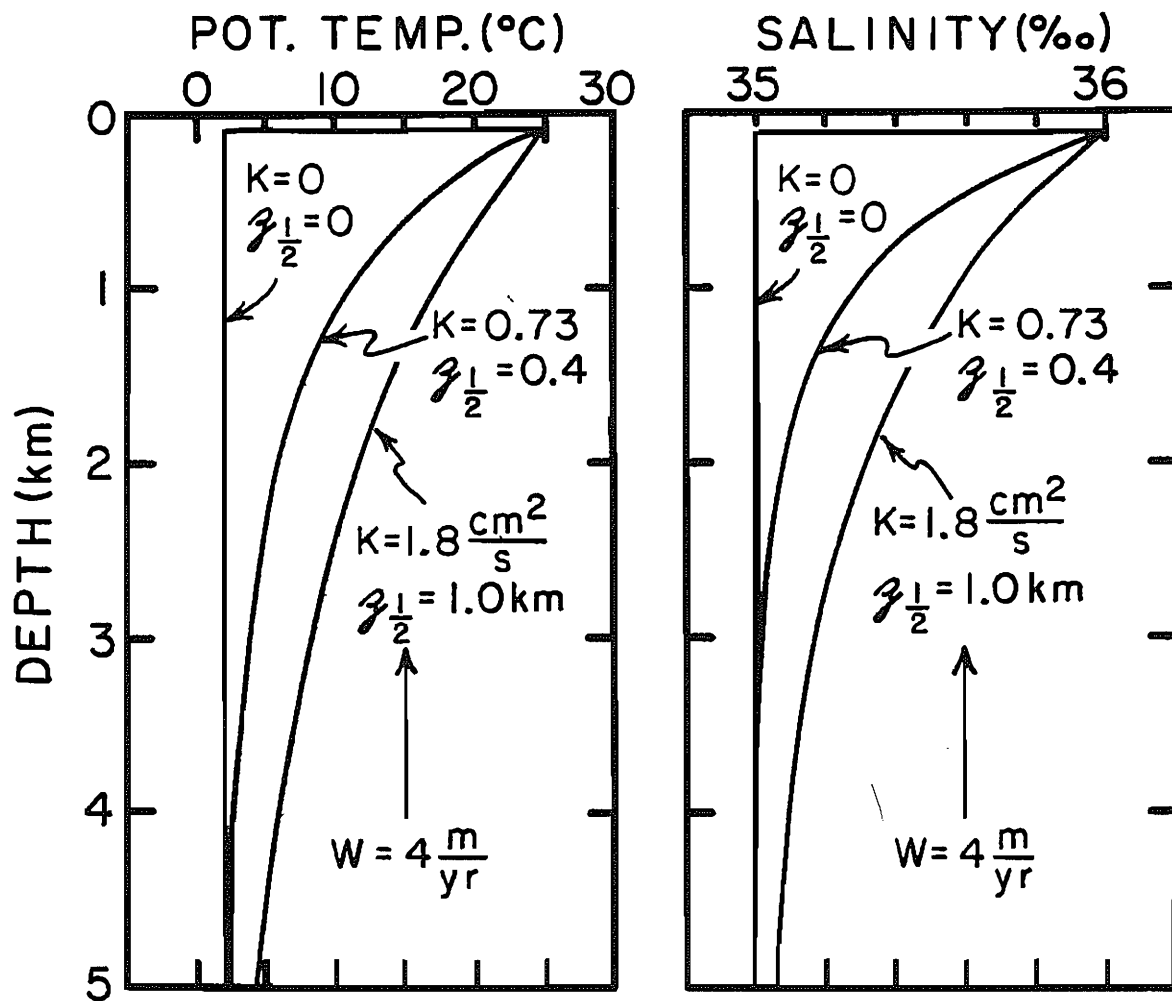


Figure 7-1. Plots of potential temperature and salinity versus depth in the hypothetical column discussed in the text. In each case the upwelling velocity is 4 meters/year. The situations for the eddy mixing coefficient equal to 0.0, 0.73 and $1.8 \text{ cm}^2/\text{sec}$ are shown. The corresponding z^* values are 0.0, 0.58 and 1.44 km and the corresponding $z_{1/2}$ values are 0.0, 0.4 and 1.0 km. As can be seen for the largest of these diffusivities, the warm and salty water penetrates all the way to the bottom of the column.

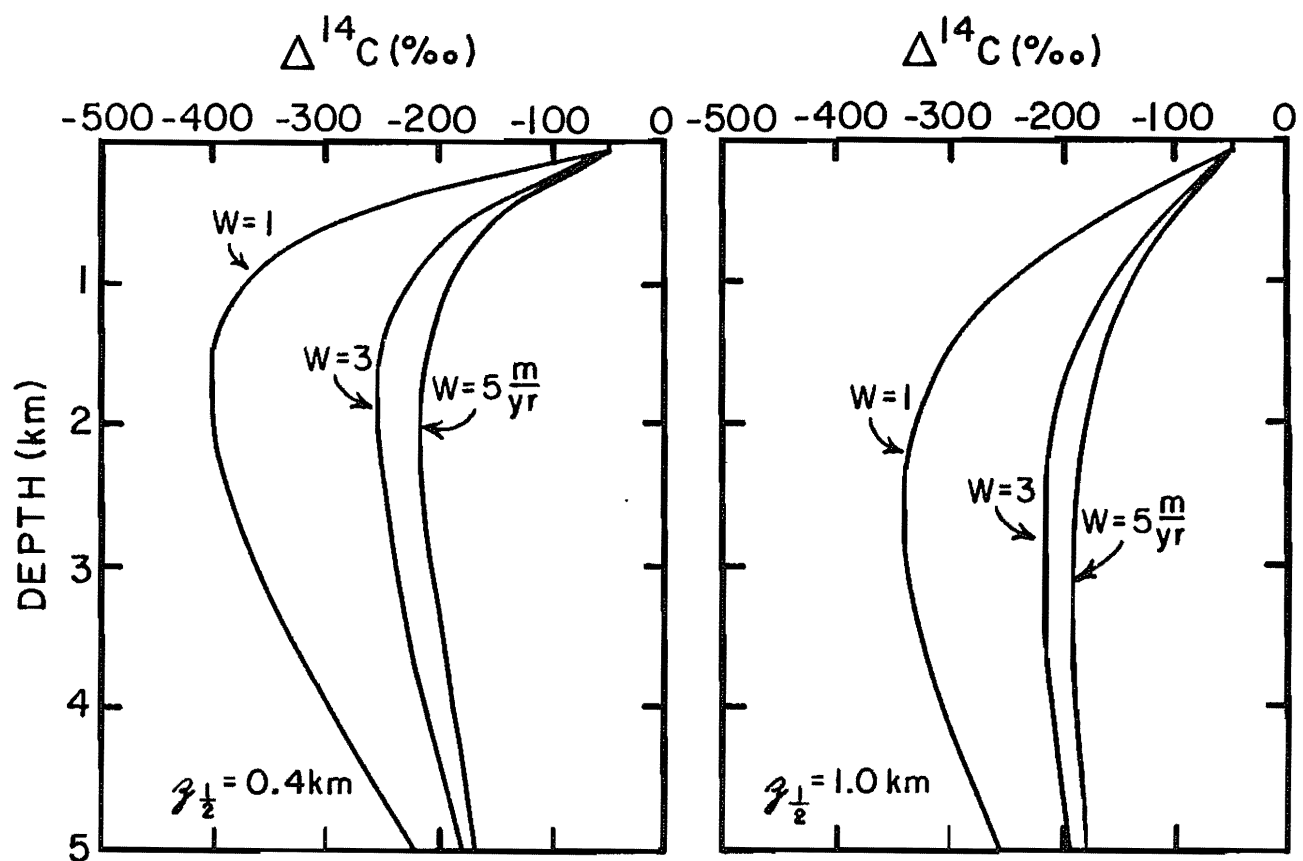


Figure 7-2. Plots of $^{14}\text{C/C}$ ratio (expressed as $\Delta^{14}\text{C}$) as a function of depth in the hypothetical column discussed in the text for various upwelling velocities. Cases for a half penetration depth of 0.4 km are given on the left and those for a half penetration depth of 1.0 km on the right. As would be expected the larger the upwelling rate the smaller the mid depth minimum in $\Delta^{14}\text{C}$. In all cases the $\Delta^{14}\text{C}$ for the water entering the bottom of the tank is taken to be $-160^{\text{o}/\text{o}}$.

seen if we allow our column to be inhabited by organisms. We will assume that the water entering the bottom of the column carries with it 235 $\mu\text{m}/\text{kg}$ of dissolved oxygen and that the water at the top of the column carries an oxygen content of 205 $\mu\text{m}/\text{kg}$. We will further assume that the rate of oxygen utilization is the same at all depths beneath the mixed layer. The profiles of oxygen for various values of $z_{1/2}$ and oxygen consumption rate are shown in figure 7-3.

Were only the ocean functioning in accord with the assumptions of the 1-D model! The distribution of tracers could be readily harnessed to yield all sorts of useful information. Unfortunately it does not. The rates of upwelling vary with location and depth (they may even go negative in some regions and depth intervals). Similarly, the rate of vertical mixing varies throughout the interior of the sea. Furthermore, as gradients in the properties of tracers are found in the horizontal as well as in the vertical, horizontal advection and diffusion will influence the vertical gradients of the properties at any given place in the sea. As we have implied from the distributions of ^{230}Th and ^{231}Pa in sediment traps, a molecule can be mixed basin-wide along its own density horizon in a time which is quite short compared to that for its transit up the water column. One more concept has to be introduced before the reasons for the inadequacy of the 1-D approach can be fully appreciated. We shall call this the concept of "outcropping isopycnals". As stated in an earlier chapter an isopycnal surface is one along which potential density remains constant. The movement of water along such a surface requires no work against gravity. Thus these are the preferred surfaces along which lateral mixing takes place. In the interior of the ocean basins these horizons are sufficiently close to horizontal that the distinction between horizontal and isopycnal mixing is not important. At high latitudes, however, these horizons rise toward the surface. Thus, instead of speaking of horizontal and vertical mixing, it is more appropriate to speak of isopycnal and diapycnal mixing (by diapycnal we mean perpendicular to isopycnal surfaces).

Equally important to the changes in the geometry of mixing which comes about when isopycnals are adopted as the preferred horizons for mixing is the fact that some isopycnal surfaces "outcrop" at the sea surface. The existence of these outcrops creates two new mechanisms for the transport of properties across isopycnal horizons. The first is that wind driven currents operating at the ocean surface will carry water across isopycnal surfaces and in so doing produce diapycnal mixing. Also seasonal cycles in temperature and salinity will move the isopycnal horizons along the ocean surface! The second is that gases can leave the ocean at the outcrop of one isopycnal horizon and reenter the ocean at the outcrop of another. Since ^{14}C has the gaseous form $^{14}\text{CO}_2$, this latter mechanism becomes important when we use the distribution of natural radiocarbon to calibrate models for the transport of other oceanic properties.

We must conclude at this point that while the two-box and the 1-D advection-diffusion models constitute important preliminary steps in understanding what goes on in the ocean, neither is adequate. Oceanographers are facing up to the difficult task of

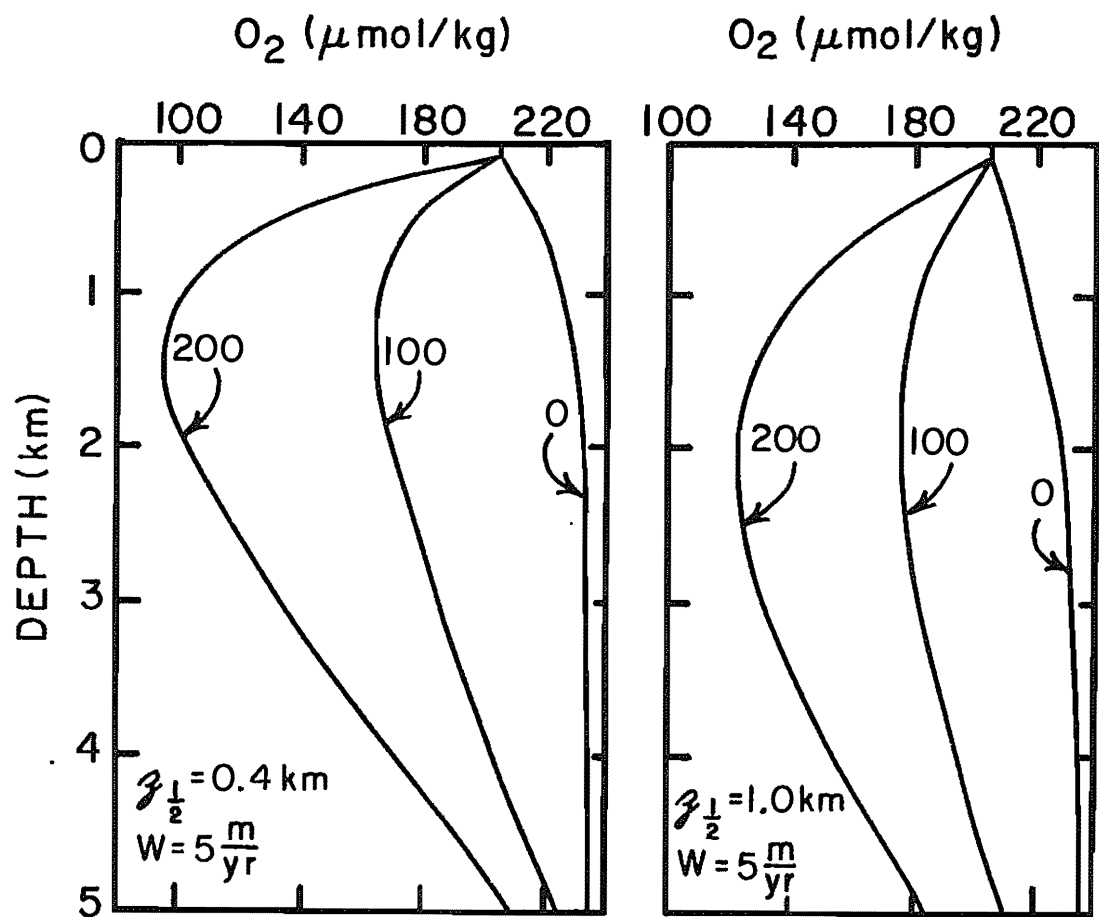


Figure 7-3. Plots of dissolved oxygen content versus depth for two sets of dynamic conditions. For both the upwelling rate is 5 m/yr. For the example on the left the half penetration depth of the surface temperature and salinity anomalies is 0.4 km. For the example on the right it is 1.0 km. In each example curves for three oxygen consumption rates are shown (i.e. for 0, 100, and 200 $\mu\text{m}/\text{10}^3 \text{ yrs}$).

creating a truly three-dimensional model. Such a model, however, is a long way off. Right now we can only examine some of its pieces.

TRACERS FOR DIAPYCNAL AND ISOPYCNAL MIXING

One of the pieces of the great 3-D ocean puzzle is the matrix of values for the coefficients of isopycnal and diapycnal mixing. As these parameters almost certainly vary from place to place and from depth to depth within the sea, their dependence on the measurable properties of the sea (i.e., density gradient, current shear ...) must be determined.

Three tracers are particularly useful in this regard. One of these is the isotope ^{222}Rn , whose application to establishing the rate of gas exchange across the air-sea interface we have already discussed. Radon gas is produced in sea floor sediments in large amounts compared to its production in sea water. Much of this radon escapes the mineral grains upon which its parent ^{226}Ra is absorbed and takes up residence in the water-filled pore space between the grains. During its mean lifetime of 5.5 days much of the radon occupying the pores of the upper centimeter or so of the sediment escapes to the overlying bottom water, producing an excess in the ^{222}Rn activity in these waters (over that maintained by the ^{226}Ra dissolved in these waters). The distribution of this excess above the sea floor carries information about the rate of vertical mixing of the sea.

The second tracer is ^{228}Ra with a mean lifetime of about 8 years. This tracer is formed from the decay of ^{232}Th . As ^{232}Th has such a low abundance in sea water, the *in situ* produced ^{228}Ra is not measurable. Like ^{222}Rn , ^{228}Ra is produced in copious amounts in deep sea sediment. Some of the ^{228}Ra generated in the sediments diffuses through the sediment pore waters into the overlying sea, and so the distribution of ^{228}Ra in the abyssal sea also has something to tell us about rates of mixing in this domain. There is one major difference between these two tracers. The half-life of ^{228}Ra (5.8 years) is 550 times that of ^{222}Rn (0.0105 years). As the distance a radio isotope can travel by diffusion before undergoing decay depends on the square root of time, ^{228}Ra can travel about 24 times further than can ^{222}Rn !

The third tracer, ^3He , is released at the crests of the mid-ocean ridges. These linear features act as would a long line of chimneys releasing smoke to the atmosphere. This ^3He is carried away from the ridge crest by the prevailing oceanic "wind". It should also be spread in the vertical by any diapycnal mixing processes at work in the deep sea. Unlike the isotopes ^{222}Rn and ^{228}Ra , the excess ^3He in the sea does not disappear from the water by radiodecay. Instead, it makes its way to the sea surface and from there escapes to the atmosphere. Rather than giving us the kind of absolute mixing rate information potentially available from the distribution of ^{228}Ra and ^{222}Rn , the distribution of ^3He has something to tell us about the relative magnitudes of isopycnal and diapycnal mixing in the deep sea.

MIXING RATES BASED ON THE RADON-222 AND RADIUM-228

As ^{222}Rn and ^{228}Ra have so many things in common it is appropriate to treat their distributions together. If we make two major assumptions we can construct a rather simple model with which to interpret their distributions. The first assumption is their distributions in the vertical are established entirely by diapycnal processes. If so then the model can be one-dimensional. The second is that on these short time scales the role of vertical advection is small compared to that of vertical diffusion. If so, the 1-D model need involve only the balance between diffusion and radiodecay. As we shall see, while the second of these assumptions rests on a firm foundation, the first is shaky.

If the excess ^{222}Rn and ^{228}Ra given off by the sediments are carried away from the sediment mainly by vertical mixing then it can be easily shown that their vertical profiles are governed by the following equation:

$$C_z = C_{oe} - \sqrt{\frac{\lambda}{\kappa}} z \quad 7-2$$

where C_z and C_{oe} are, respectively, the concentrations of the excess at some height z above the bottom and at the sediment water interface, κ is the diffusion coefficient and λ is the decay constant (i.e., $0.693/t_{1/2}$) for the isotope. This equation calls for an exponential drop off in the excess with distance above the sea floor. The distance $z_{1/2}$ over which the concentration decreases by a factor of two is related to the vertical diffusivity and decay constant by the following equation:

$$z_{1/2} = 0.693 \sqrt{\frac{\kappa}{\lambda}} \quad 7-3$$

or since we are interested in using the distribution of the excess to determine κ :

$$\kappa = \left[\frac{z_{1/2}}{0.693} \right]^2 \lambda \quad 7-4$$

Two examples of sites where the profiles of both excess ^{228}Ra and of excess ^{222}Rn have been measured are shown in figure 7-4. In each case a plot of potential temperature versus depth is also given. These plots provide some very important clues as to what determines the rate of vertical mixing in the deep sea. First of all, as expected, the ^{228}Ra excess extends at both sites much further above the bottom than the ^{222}Rn excess. Next the ^{222}Rn profiles show the expected exponential shape. This is best shown by plotting the logarithm of the excess radon content against distance off the bottom. If the equation given above is obeyed, then the points should fall along a straight line on such a plot. As shown by the inserts in figure 7-4 this is the case. Second, the shape of the ^{228}Ra profile shows a marked change at about the

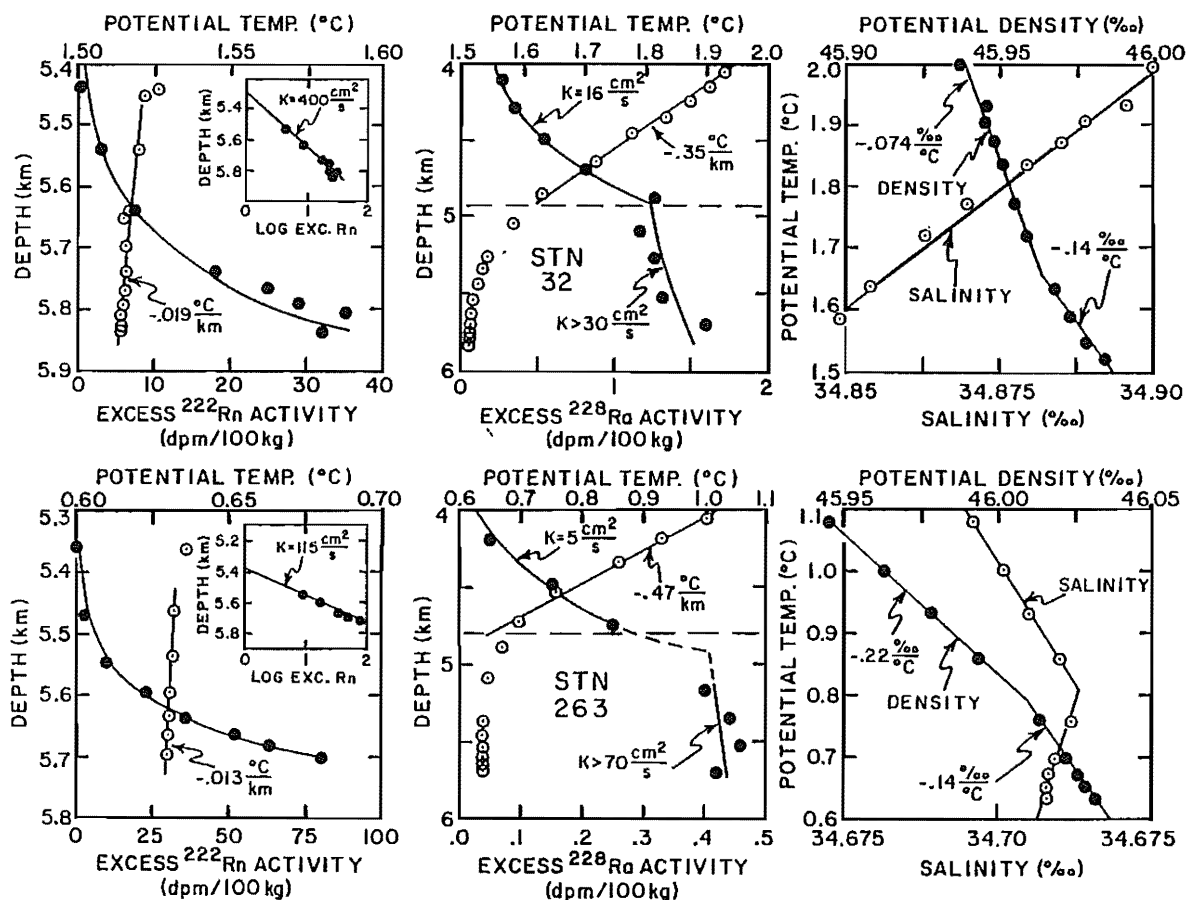


Figure 7-4. Plots of excess ^{222}Rn and ^{228}Ra activity versus depth at two GEOSECS stations (left hand and middle diagrams respectively). The upper panel shows the results for station 32 (24°N , 54°W) in the Atlantic. The lower panel shows results for station 263 (17°S , 167°W) in the Pacific. The potential temperature profiles (open circles) are shown along with the isotope profiles (solid circles). Also shown are plots of salinity (open circles) and potential density (closed circles) versus potential temperature over the depth range in which excess ^{228}Ra activity is found (right hand diagrams). The density gradient for the depth interval over which excess radon is found is calculated by multiplying the potential temperature gradient in that zone by the ratio of potential density change to potential temperature change in the zone 0.5 to 1.0 kilometers above the bottom. This gradient cannot be established in the lower half kilometer of the water column because the salt gradient is too small to be measured. The hydrographic and radon data were obtained as part of the GEOSECS program (81). The ^{228}Ra measurements at station 32 were made at the Lamont-Doherty Geological Observatory and those at station 263 at the University of South Carolina (91).

depth where the potential temperature gradient (and hence density gradient) shows a marked steepening. Below this break the density gradient is small and the ^{228}Ra content is nearly uniform. Above this break, the density gradient is almost ten times larger and the excess ^{228}Ra content shows a steep decline. Hence we employ different diffusivities in the two depth ranges. Table 7-1 summarizes the diffusivities derived from this data. As can be seen at each site there appears to be an inverse relationship between density gradient and diffusivity. This is not unreasonable. The steeper the density gradient, the greater the amount of work against gravity required to mix the water!

Near-bottom ^{222}Rn profiles have been measured at perhaps 200 localities. At many of these sites the density structure shows a pattern similar to that seen near the air-sea interface. Immediately above the sediment-water interface there is a mixed layer ranging from 30 to 200 meters in thickness. This mixed layer is capped by a benthic thermocline. In such situations the radon is usually nearly uniformly distributed throughout the benthic mixed layer and penetrates only a very short distance into the overlying benthic thermocline. Thus only upper limits can be placed on the diffusivity in the benthic thermocline and only lower limits can be placed on the diffusivity in the benthic mixed layer. Hence, such regions yield only qualitative information regarding the relationship between vertical diffusivity and density gradient.

There are, however, a number of sites which show the neat exponential gradients seen in the two examples given above. The diffusivities obtained at these sites are plotted against the corresponding density gradients in figure 7-5. As can be seen, these results fortify the conclusion drawn from the two examples. Vertical diffusivity appears to be inversely proportional to density gradient!

On this same diagram are given vertical diffusivities determined in the ocean's thermocline using the penetration of the tritium produced by nuclear testing and those determined in small lakes through artificial tritium injections. These results fall along the trend established from the ^{222}Rn and ^{228}Ra results from the deep sea. The near constancy of the product of vertical diffusivity and density gradient suggests that the energy expended against gravity in mixing less dense with more dense water has the same order of magnitude in all these situations!

While the plot in figure 7-5 provides compelling evidence that a major factor influencing the rate of vertical mixing in the ocean (and also in lakes) is the density gradient, this conclusion cannot go unchallenged. The problem lies in one of the two simplifying assumptions made in order to analyze the ^{222}Rn and ^{228}Ra data. Let us examine them. The assumption regarding the neglect of advection poses no great problem. If the rate of upward advection is anywhere near the value of about 4 m/yr obtained from the ^{14}C based ventilation time for the deep sea, then the movement on the time scale of the half-life of radon (0.01 years) is trivial (0.01 years \times 400 cm/yr is only 4 cm). In the case of ^{228}Ra where the half-life is 5.5 years again the amount of movement (i.e., about 22 meters) is small compared to the observed upward penetration of ^{228}Ra into the water column.

Table 7-1. Relationship between the density gradient ($\Delta\rho/\Delta z$) and apparent vertical diffusivity (κ) at GEOSECS station 32 in the northwestern Atlantic and at GEOSECS station 263 in the southwestern Pacific. As the near bottom density gradient is too small to measure at these stations, the density gradient is computed from the near bottom temperature gradient ($\Delta\theta/\Delta z$) and the density potential temperature relationship ($\Delta\rho/\Delta\theta$) for the deep part of the water column. The product of the mixing rate and the density gradient is a measure of the work done against gravity. The ^{222}Rn measurements were made as part of the GEOSECS program (81). The ^{228}Ra measurements were made under the direction of Herb Feely at the Lamont-Doherty Geological Observatory and of Willard Moore at the University of South Carolina (91).

Depth Range km	Tracer	$\Delta\theta/\Delta z$ $^{\circ}\text{C}/\text{km}$	$\Delta\rho/\Delta\theta$ $^{\circ}/oo/^{\circ}\text{C}$	$\Delta\rho/\Delta z$ $^{\circ}/oo/\text{km}$	κ cm^2/sec	$\kappa(\Delta\rho/\Delta z)$
Station 32						
4.1 - 5.0	^{228}Ra	-0.35	-0.074	0.026	16	0.4
5.4 - 5.9	^{222}Rn	-0.019	-0.14	0.0027	400	1.1
Station 263						
4.2 - 4.7	^{228}Ra	-0.47	-0.22	0.103	5	0.5
5.4 - 5.7	^{222}Rn	-0.013	-0.14	0.0018	115	0.2

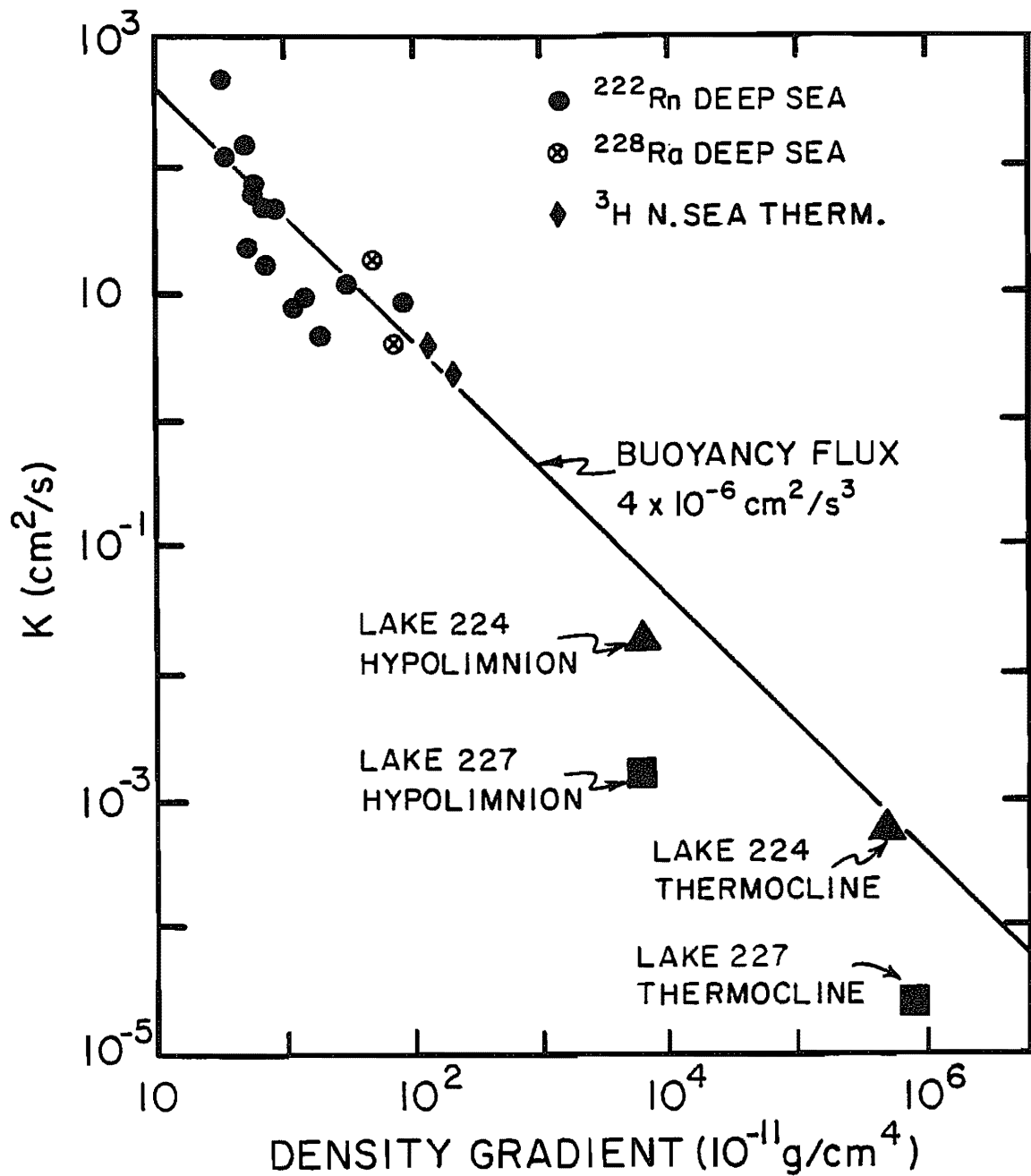


Figure 7-5. Apparent coefficient of vertical diffusivity versus density gradient based on fourteen ^{222}Rn profiles in the deep sea (91), for two ^{228}Ra profiles in the deep sea (91), and for penetration of bomb-produced tritium into two regions of the thermocline of the Norwegian Sea (62). Also given are the results from tritium injections made by Paul Quay of the Lamont-Doherty Geological Observatory in two small lakes of the Experimental Lakes Area near Kenora, Canada (67). The solid line represents a constant product of diffusivity and density gradient. This product, called buoyancy flux, is the rate at which energy is expended against gravity in accomplishing the mixing.

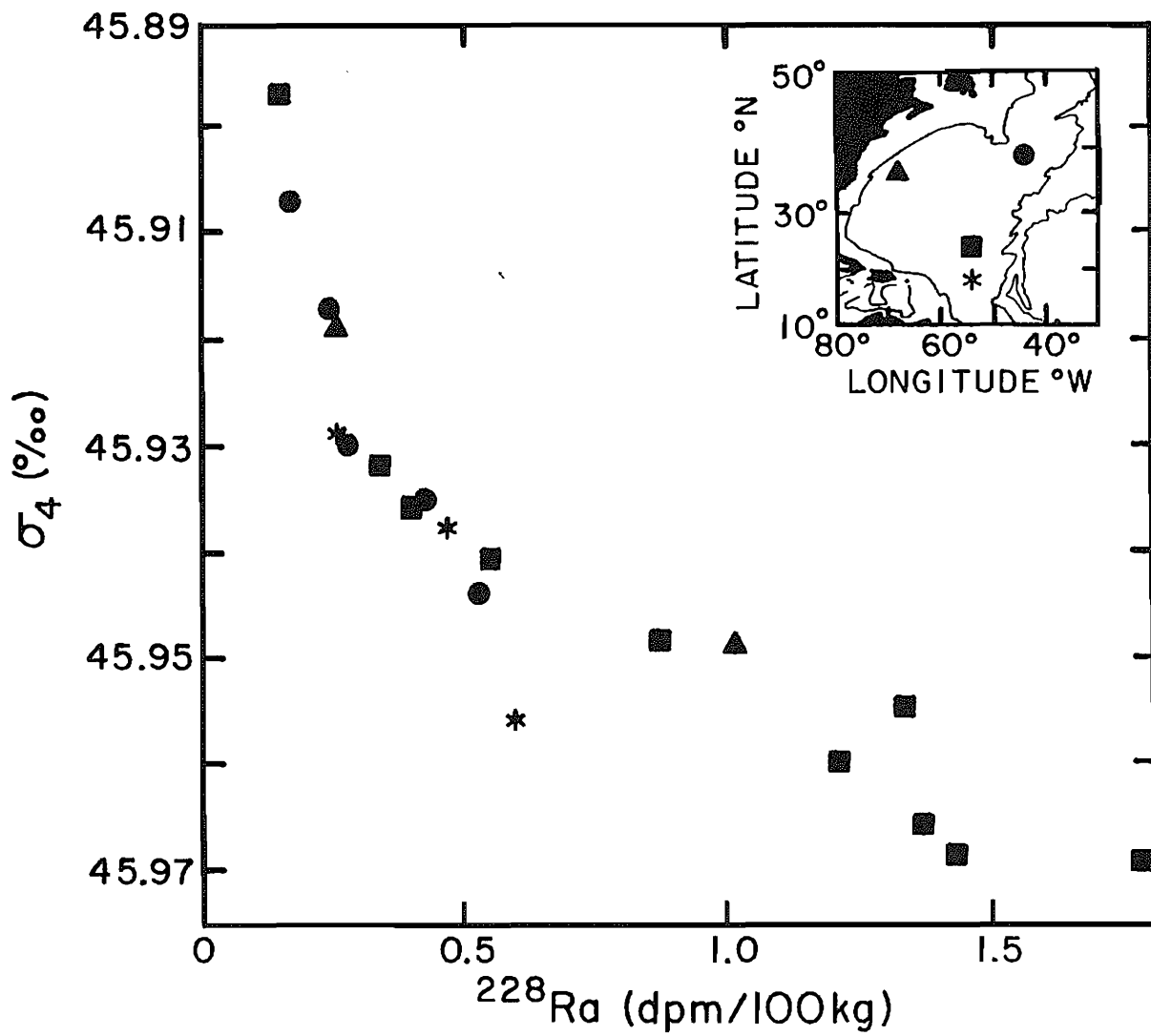


Figure 7-6. Plots of ^{228}Ra activity versus potential density (referenced to a depth of four kilometers) at several stations in the western basin of the North Atlantic (96). The station locations are shown on the inset map. The measurements were made at the Lamont-Doherty Geological Observatory on samples collected during the GEOSECS program.

The trouble stems rather from the neglect of horizontal transport. It is possible that much of the ^{222}Rn and ^{228}Ra found above the benthic mixed layer was carried along isopycnal horizons from adjacent benthic hills (or in the case of the longer lived ^{228}Ra from very distant continental margins and ridge flanks). One piece of evidence in support of this hypothesis is shown in figure 7-6. ^{228}Ra profiles from several widely separated places in the northwestern Atlantic Ocean all show roughly the same concentration on a given isopycnal surface. This is the pattern to be expected if ^{228}Ra were spread rapidly across the isopycnals in this deep sea basin.

There is also a theoretical problem with the inverse correlation between diffusivity and density gradient. If this relationship applies throughout the deep sea then there is no place for upwelling. The observed down water column decreases in the gradients of temperature and salinity would be a consequence of the changing density gradient. This proves unsatisfactory for two reasons. First, the water descending from the deep water source regions has somehow to return to the surface. Upwelling is the only way to dispose of it. Second, if diffusivity is determined by the density gradient and the density gradient by diffusivity then the ocean is in a rather precarious dynamic state. The hypothesis that the profiles of temperature, salinity, and density are produced by the diffusion down into an upwelling plume is far more acceptable from a theoretical standpoint.

One might then ask why horizontal processes generate such a neat correlation between density gradient and the apparent diffusivities calculated from the vertical profiles. No one knows the answer to this question. We have reached the forefront of research in this area.

THE DISTRIBUTION OF HELIUM-3 IN THE DEEP PACIFIC

The third tracer which offers information with regard to the diffusive processes at work in the deep sea is ^3He . As mentioned above, the distribution of this isotope has something to say about the relative importance of isopycnal and diapycnal mixing. This plume of ^3He is well documented in the Pacific Ocean. The ridge crests in the Pacific are shown in the map in figure 7-7. Hot water issuing forth from these crests are thought to be the major source of excess ^3He . An east-west section of excess ^3He across the East Pacific Rise at 15°S is shown in figure 7-8 (the position of this section is marked A-B on the map in figure 7-7). One look at this diagram leaves no question with regard to the source of the excess helium. A plume extending across the entire Pacific to the west of the Rise is seen. A north-south section (marked C-D on the map in figure 7-7), somewhat west of the crest of the East Pacific Rise, is shown in figure 7-9. A second north-south section (marked E-F on the map in figure 7-7), along the western part of the Pacific basin, is also shown in this figure. Although less distinct in the far north, the mid-depth maximum of ^3He is found throughout the Pacific. These diagrams make it remarkably clear that the ^3He released from the ridge crests is able to spread the entire width of the Pacific Ocean before it is carried to the

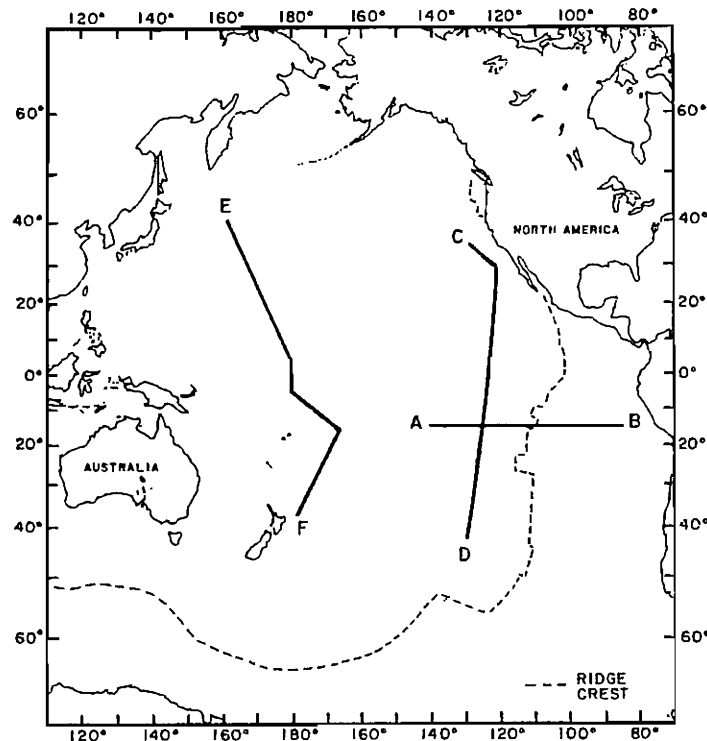


Figure 7-7. Map showing the locations of the ${}^3\text{He}$ sections shown in figures 7-8 and 7-9. Also shown are the active ridge crests.

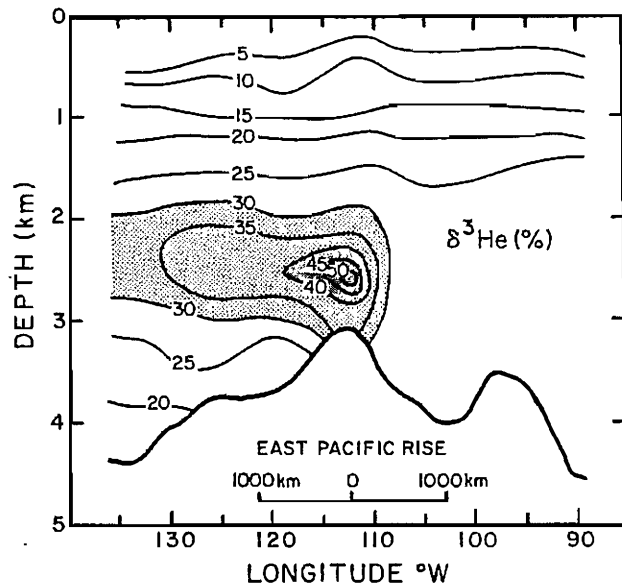


Figure 7-8. Section of excess ${}^3\text{He}$ content (expressed as $\delta {}^3\text{He}$ in percent) across the East Pacific Rise at 15° south (line A-B in figure 7-7). The westward extending plume of ${}^3\text{He}$ originating at the crest of this spreading center is quite apparent. The measurements on which this diagram is based were made by John Lupton in the Laboratory of Harmon Craig at the Scripps Institution of Oceanography (280).

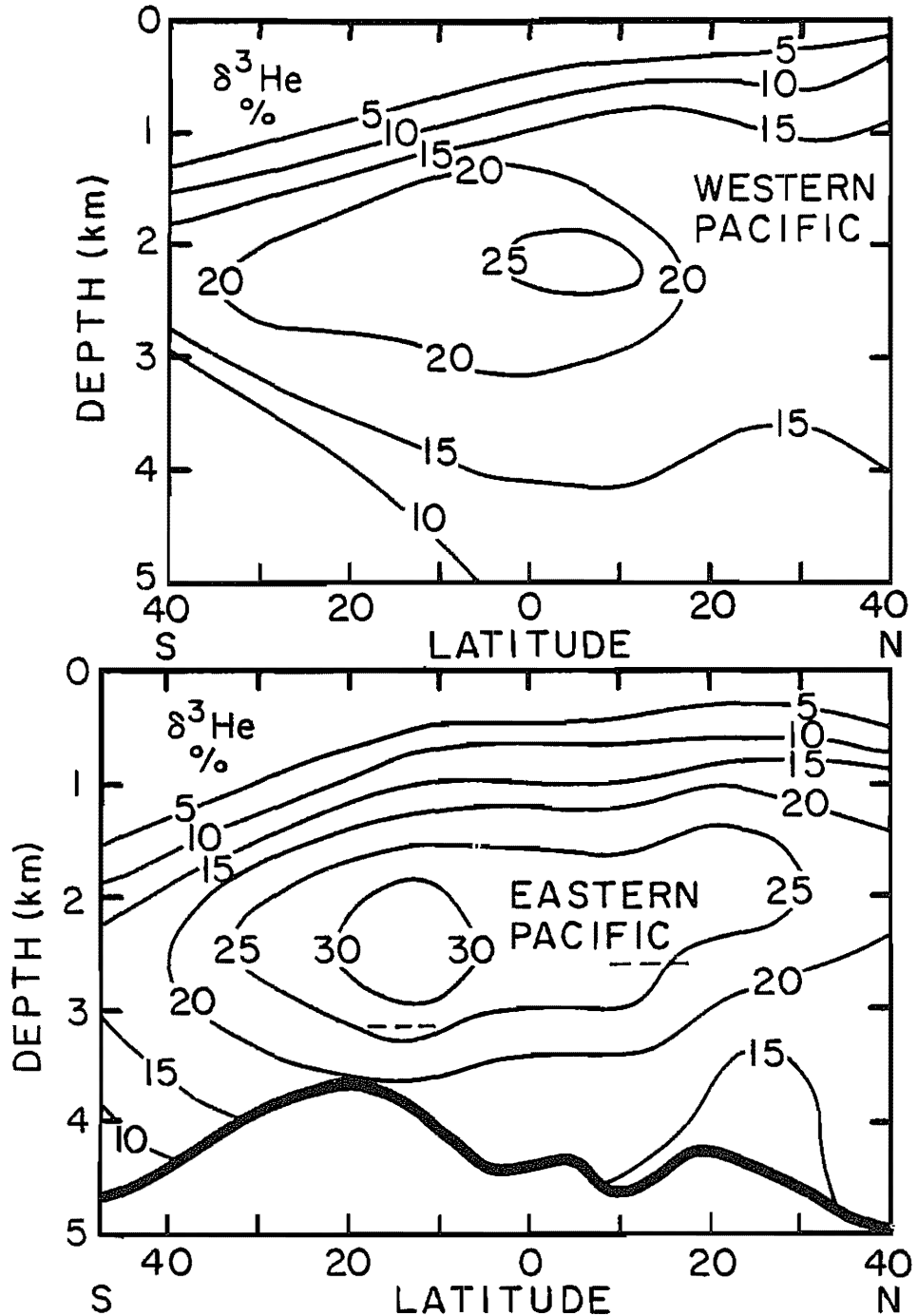


Figure 7-9. North-south sections of excess ${}^3\text{H}$ in the western (line E-F in figure 7-7) and eastern (line C-D in figure 7-7) Pacific. The ${}^3\text{He}$ maximum generated by the release of hot waters from the ridge crests is displayed prominently across the entire ocean. Only in the northwestern Pacific does it lose its identity. The dashed lines show the depth of the ridge crests at 15°S and 13°N where intense hydrothermal activity has been observed. The measurements on which these diagrams are based were made by Brian Clarke at McMaster University in Hamilton, Canada on samples collected as part of the GEOSECS program.

surface by upwelling. In fact, ^3He released from the ridge crests of the Pacific reaches the deep circumpolar Antarctic and even into the deep Atlantic Ocean!

Thus, the distribution of excess ^3He in the deep sea reinforces the suspicion that ^{228}Ra may move considerable distances (1000 kilometers or more) in the horizontal during its nine-year mean lifetime. If so, the vertical profile of ^{228}Ra , measured at any given place on the sea floor, is created by a complex interaction between horizontal and vertical motions and is strongly influenced by the topography of the basin and by the distribution of sediment type with depth in the basin. The importance of the shape of the topography can best be seen by considering how ^{228}Ra would be distributed if horizontal mixing was exceedingly rapid and vertical mixing did not occur. In this case, ^{228}Ra would be distributed uniformly across each isopycnal. The amount of ^{228}Ra at any given depth would then depend on the ratio of the volume of water between any pair of isopycnal surfaces to the area of sediment intersected by these surfaces. This ratio would in turn depend on the shape of the basin (the ratio of water volume to sediment area would always increase with distance above the sea floor but the pattern of this increase would depend on the details of the topography of the basin). The mean concentration of ^{228}Ra between a pair of isopycnal horizons would also depend on the sediment type intersected by these isopycnals. As the amount of ^{228}Ra released from the sediment would be proportional to its ^{232}Th content, sediments rich in calcite and opal (phases free of ^{232}Th) should show lower ^{228}Ra fluxes than red clays. Thus the increase in ^{228}Ra concentration expected, due to the rise in sediment area to volume ratio with depth, would be to some extent compensated by the decrease in calcite content of the sediment with depth.

SOURCES OF DEEP WATER

Deep waters are being formed in two regions of the ocean: in the northern Atlantic and along the perimeter of the Antarctic continent. In the discussion which follows we will designate the former as the northern component and the latter as the southern component to global deep water. The proportions of these two components vary from place to place in the deep sea. As the two components differ in their concentrations of the tracers of interest, part of the geographical variation in the properties of abyssal waters is the result of the differences in the proportions of the two components. If we are to make effective use of these tracers, we must develop a means of determining the relative contributions of these two water types to a given water sample. Thus, we must learn more about the conservative* properties of these two components.

The establishment of the compositions of these two water types is more difficult than one might suspect. The reason is

*A conservative property is one that does not change during residence in the deep sea (i.e., one that is not altered by respiration, solution, or radiodecay).

that the process of deep water formation is quite complicated. The cooling which triggers the descent of new water into the abyss occurs during very brief periods at winter's peak. Oceanographers find work in these regions at this time of year very difficult because of darkness, cold, ice and frequent storms. Furthermore, the actual sinking process is confined to small areas whose locations are not well known and may vary from year to year. Thus, the chances of finding and properly documenting them is difficult (like sitting in a very large bathtub with ten drains waiting to describe the action when, by surprise, one of the plugs is pulled).

Even if adequate studies could be made of these plumes of descending winter water, we still would not have our answer. As the waters descend they entrain water through which they pass. In some cases the water first reaches a temporary holding basin. From here it cascades over a barrier into the open ocean. While in the holding basin it may lose oxygen, gain nutrient constituents... As it cascades from the holding basin into the open sea more entrainment occurs. Thus, our choice of an endmember composition becomes somewhat a matter of definition. We must sample water far enough away from the source regions that the cascade entrainment has already occurred, but not so far away that mixing with the "old" waters present in the basin has introduced water from the other source.

NORTHERN COMPONENT WATER

Northern component water is a mixture of water from three distinct sources. The pathways followed by these waters are shown in figure 7-10. Two of these waters have as their ultimate source waters which sink in the northern part of the Norwegian Sea. This water is held behind the sills which connect Greenland to Iceland and Iceland to the British Isles. The bottom water behind the sills has a temperature of about -1.0°C and a salinity of about $34.91^{\circ}/\text{oo}$. Periodically, (presumably mainly during the winter when more new water is descending into the Norwegian Sea holding basin), this deep water spills out over the connecting sills and cascades into the deep Atlantic. That water spilling over the sill to the west of Iceland enters directly into the head of the western basin. This water, which is called the Denmark Straits Overflow Water (DSW), has the highest density of the three contributors to northern component water (see table 7-2). Water also spills over the sill to the east of Iceland. This water enters the eastern basin of the Atlantic. Coriolis forces (i.e., forces resulting from the rotation of the earth) cause this descending cascade to hug the margin of the Mid-Atlantic Ridge and then to flow through the Gibbs Fracture Zone (a deep gap in the Mid-Atlantic Ridge) into the western basin. Surprisingly, this water does not ventilate the abyssal eastern basin of the Atlantic but passes almost entirely into the western basin.* This second component

*The eastern basin is ventilated by western basin deep water which passes through the Ridge via another major gap called the Romanche Fracture Zone. This gap is located just south of the equator.

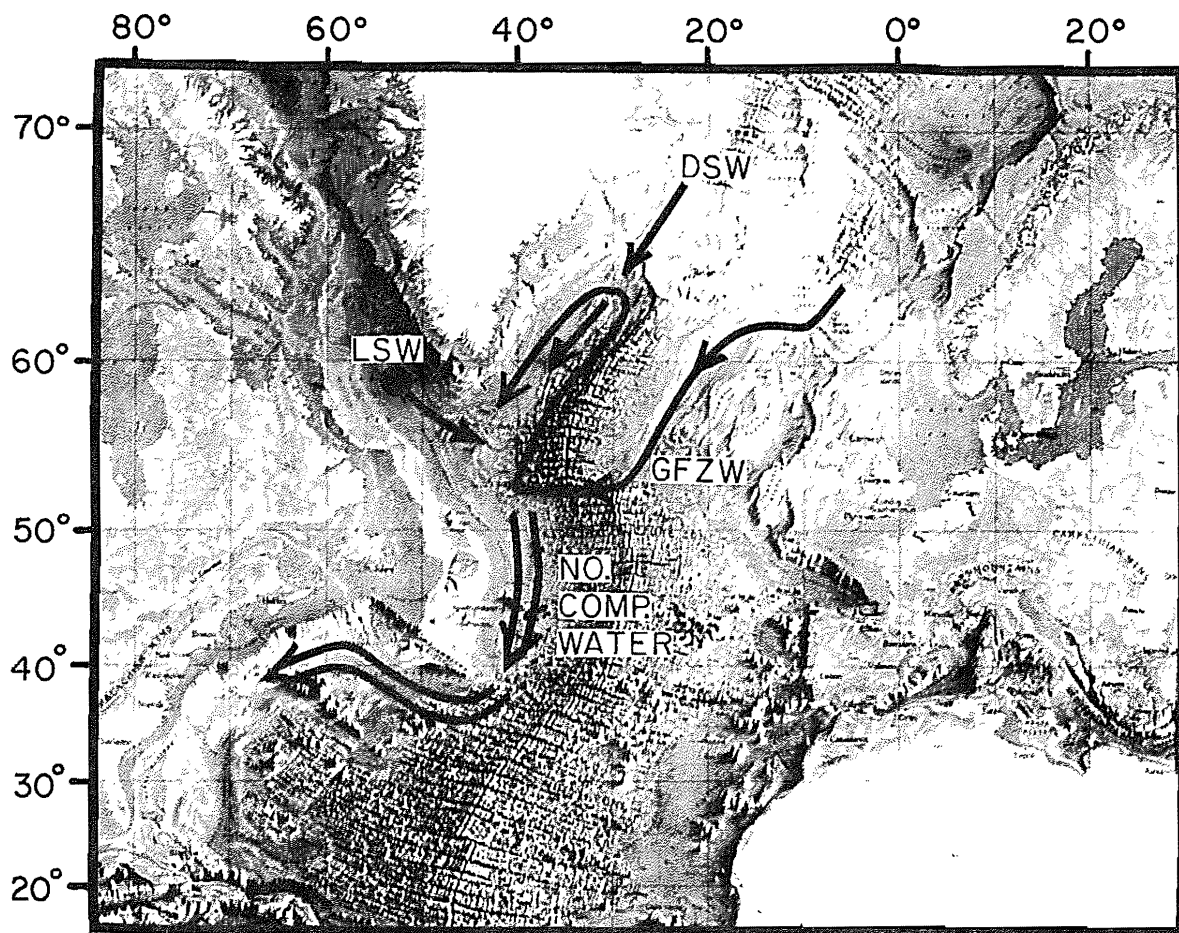


Figure 7-10. Map showing the paths followed by the deep waters formed in the northern Atlantic. Water from the surface of the Labrador Sea sinks to the bottom of the western arm of the western basin forming LSW. Water trapped behind the ridge connecting Iceland with Greenland spills over the sill into the eastern arm of the western basin forming DSW. Water trapped behind the ridge connecting Iceland and the British Isles spills over the sill and flows along the east side of the Mid-Atlantic Ridge. When it reaches the Gibbs Fracture Zone, it passes through the Ridge into the eastern arm of the western basin. Because it is less dense, GFZW overrides the DSW flowing along the bottom of this arm of the western basin. These waters mix to form northern component water which enters the main western basin along the continental margin of North America.

of northern component water is called the Gibbs Fracture Zone Water (GFZW). It has a lower potential density than DSW (see table 7-2). The third contributor to northern component water is water which sinks from the surface of the Labrador Sea during the winter. This water descends directly into an arm of the western basin rather than via a holding basin as do the other two. Its density is less than those of the other two (see table 7-2).

One might ask how we know that these are the chief and only contributors to northern component waters. Our best evidence comes from plots of θ and S for deep waters from the far northern Atlantic. As shown in figure 7-11, these waters occupy a triangular region on such a diagram. The compositions of the water at the three corners of this triangle correspond to that of water filling the Gibbs Fracture Zone, to waters flowing along the bottom south of the Denmark Straits and to deep water in the Labrador Sea. The waters within the triangle are presumably formed by mixing these three endmembers in various proportions. A point near the center of the triangle would correspond to a mixture consisting of roughly equal proportions of the three endmembers. A point half way along one of the sides of the triangle would correspond to 50 - 50 mixtures of two water types defining this edge. While it is possible that other water types with compositions lying within the triangle also contribute, this is unlikely since source regions for such waters have not been identified.

A traverse of stations down the northernmost part of the western basin (see figure 7-12) reveals that the mixing along density surfaces is quickly accomplished (rather than having waters with a variety of temperature-salinity combinations only a narrow range of temperatures are observed on any given isopycnal). Further, the density of the bottom-most water decreases to the south. This presumably is the result of vertical mixing. As this traverse is extended further south, mixing with "old" waters in the deep western basin becomes significant. This is best seen on a plot of dissolved silica versus salinity (see figure 7-13). While all three contributors to northern component water have low silicate contents, waters to the south of 50°N have progressively high silicate contents. This increase is primarily the result of the intrusion of southern component water.

To understand this argument, we must look more carefully at the distribution of silicate in the Atlantic Ocean. The silica content of the three of the contributors to northern component water are as follows: 11 $\mu\text{m}/\text{kg}$ for LSW, 11 $\mu\text{m}/\text{kg}$ for DSW and 1⁴ $\mu\text{m}/\text{kg}$ for GFZW. By contrast, the silica content of Antarctic Bottom Water (AABW) entering the abyssal western Atlantic from the south is 125 $\mu\text{m}/\text{kg}$. Because of mixing with AABW (and perhaps also because of opal solution), the deep waters in the central Atlantic contain significantly higher amounts of silicate than northern component water. Because of this, increases in silica content are a good tip-off that mixing between "new" and "old" water has occurred.

If we assume that the sole source of the excess silica is mixing with AABW, the temperatures and salinities for the northern

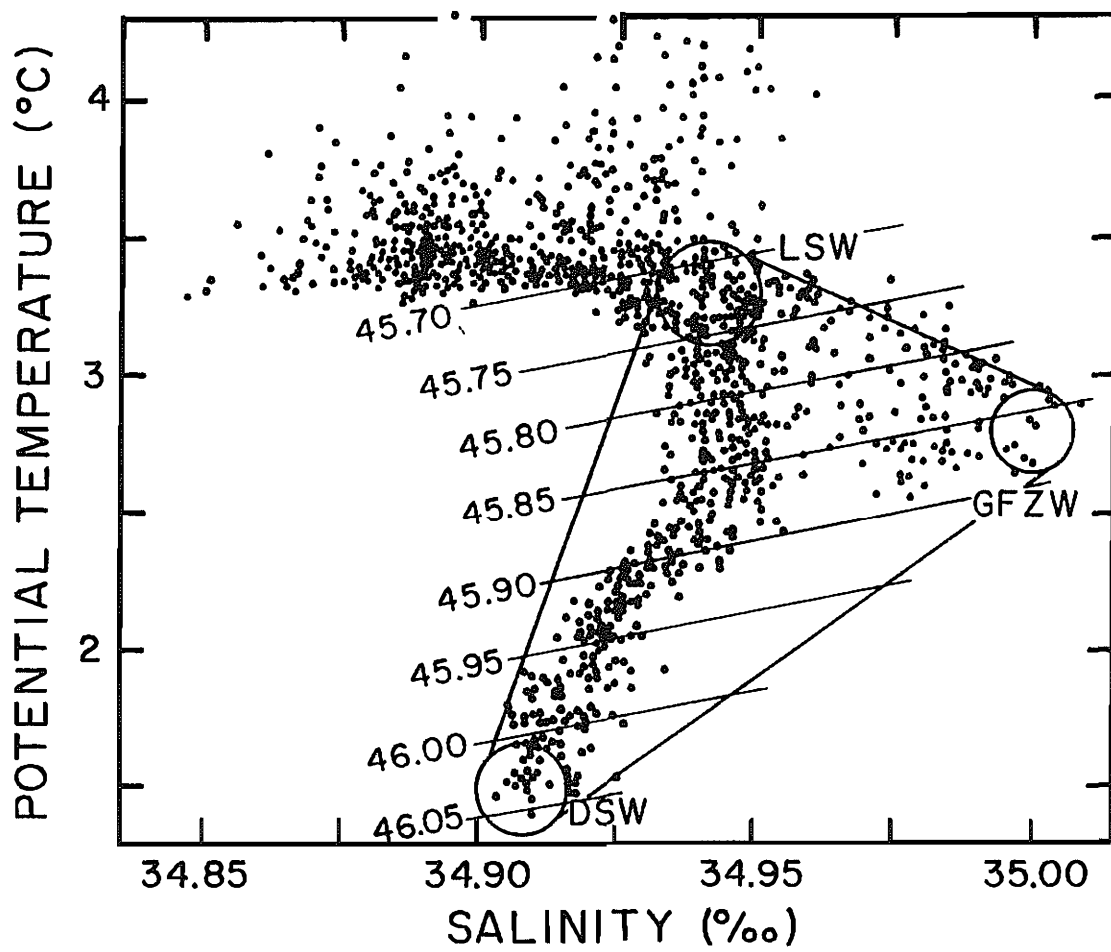


Figure 7-11. Diagram showing the potential temperature-salinity relationship for waters from the northernmost part of the western Atlantic (i.e., $> 50^{\circ}\text{N}$). Contours of potential density referenced to 4000 meters are also shown. The circle at the right designates the composition of water found in the Gibbs Fracture Zone; the upper circle designates the composition of deep water in the Labrador Sea and the lower circle waters generated by the spillover at the Denmark Straits. Points within the triangle defined by these three circles are mixtures of these three end members. Based on a compilation of the data for many expeditions in the Atlantic Ocean made by Reid and his colleagues at the Scripps Institution of Oceanography.

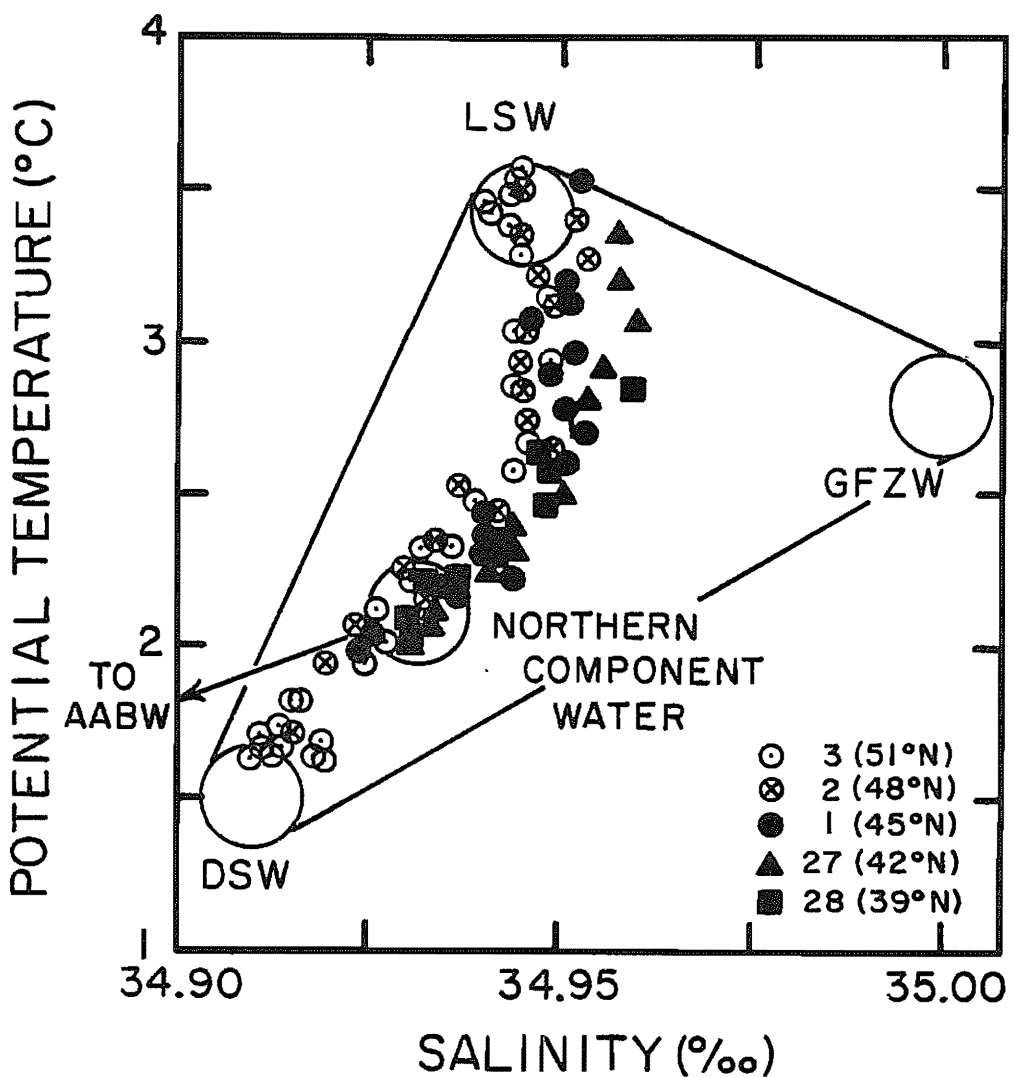


Figure 7-12. Potential temperature and salinity of the northern component waters found in the northern part of the Atlantic's western basin (i.e., 39°N to 51°N). A correction has been applied to remove the influence of the small amounts of AABW water found at these latitudes. The potential temperature of AABW is -0.1°C and its salinity is $34.67^{\circ}/\text{oo}$. This correction is based on the excess silicate concentration in the water (southern component water carries $125 \mu\text{m}/\text{kg}$ of silica and the northern component waters only $12 \mu\text{m}/\text{kg}$). The most dense northern component water reaching the main basin of the central North Atlantic has a potential temperature of about 2.1°C and a salinity of about $34.93^{\circ}/\text{oo}$. The arrow extends from the composition of this water toward the coordinates of AABW. The points shown are for GEOSECS stations (424).

Table 7-2. The compositions of the waters trapped to the north of the topographic barrier connecting Greenland with Iceland, and Iceland with the British Isles, the compositions of the three contributors to northern component water, and the composition of the most dense northern component water reaching the western basin of the North Atlantic. Based on measurements made as part of the GEOSECS program (21, 424). Recent discussion of the origins of these waters can be found in references 724, 725 and 726.

Water Type	θ °C	S ‰	σ_4^* ‰	NO_3 μm/kg	PO_4 μm/kg	SiO_2 μm/kg	AOU μm/kg	PO_4° μm/kg	$\Delta^{14}\text{C}$ ‰
E. Norwegian Sea Bottom	-1.04	34.913	46.46	16.1	1.02	14	53	0.62	-67
W. Norwegian Sea Bottom	-0.93	34.920	46.45	14.9	0.94	11	59	0.56	-
Denmark Straits Overflow	1.79	34.915	45.99	15.1	0.97	11	43	0.65	-
Gibbs Fracture Zone	2.81	35.000	45.86	16.2	1.07	14	50	0.71	-
Deep Labrador Sea	3.50	34.945	45.68	17.6	1.10	11	43	0.79	-
Densest NCW entering Western Atlantic	2.10	34.932	45.93	16.1	1.04	12	50	0.73	-67

* σ_4 is the potential density referenced to a depth of four kilometers.

component water can be computed.* In figure 7-12, the temperatures and salinities for GEOSECS stations 1, 27 and 28 have been corrected in this way for the contribution of AABW. We can see from this diagram that the highest density northern component water reaching the north central Atlantic has a potential temperature of about 2.1°C and a salinity of about 34.93‰. These corrected θ-S values fall along the trend seen at GEOSECS station 3, where little excess silicate is present (see figure 7-13).

CONSERVATIVE PROPERTIES OF NCW

If we are to trace the contribution of northern component water to bottom waters throughout the world ocean we need some tags which will distinguish it from southern component water and from water mixed down from intermediate depths into the deep sea. Salinity is the most reliable tag in that no process occurring in the deep sea can alter it significantly. Temperature is not quite so conservative a property. Geothermal heat from the interior of the planet is entering the sea floor at the rate of about 50 calories per cm² per year. In 1000 years this heat flux would raise the temperature of a water column two kilometers in height by 0.4°C! Hence, mixtures of bottom water at various places on the sea floor will be slightly warmer than expected from the end member temperatures.

The range of potential temperature (2°C) and of salinity (0.085‰) encompassed by the three contributors to northern component water is quite large. While in the discussions which follow we will assign this water the θ and S found for the densest mixture of these contributions reaching the open Atlantic (i.e., 2.1°C and 34.93‰), it must be remembered that northern component water has the range of θ and S values shown in figure 7-12.

*These temperatures and salinities are calculated from the following equations:

$$f_n = \frac{125 - [H_4SiO_4]}{125 - 12}$$

$$\theta_n = \frac{\theta + (1-f_n)0.1}{f_n}$$

$$S_n = \frac{S - (1-f_n)34.667}{f_n}$$

where f_n , θ_n and S_n are, respectively, the fraction, potential temperature and salinity of the northern component contribution to the mixture, θ , S and $[H_4SiO_4]$ are the measured potential temperature, salinity and silicate concentration in the mixture. The characteristics of AABW are $\theta = -0.1^\circ C$, $S = 34.667\text{‰}$, and $[H_4SiO_4] = 125 \mu\text{m}/\text{kg}$. The mean $[H_4SiO_4]$ content of northern component water is 12 $\mu\text{m}/\text{kg}$.

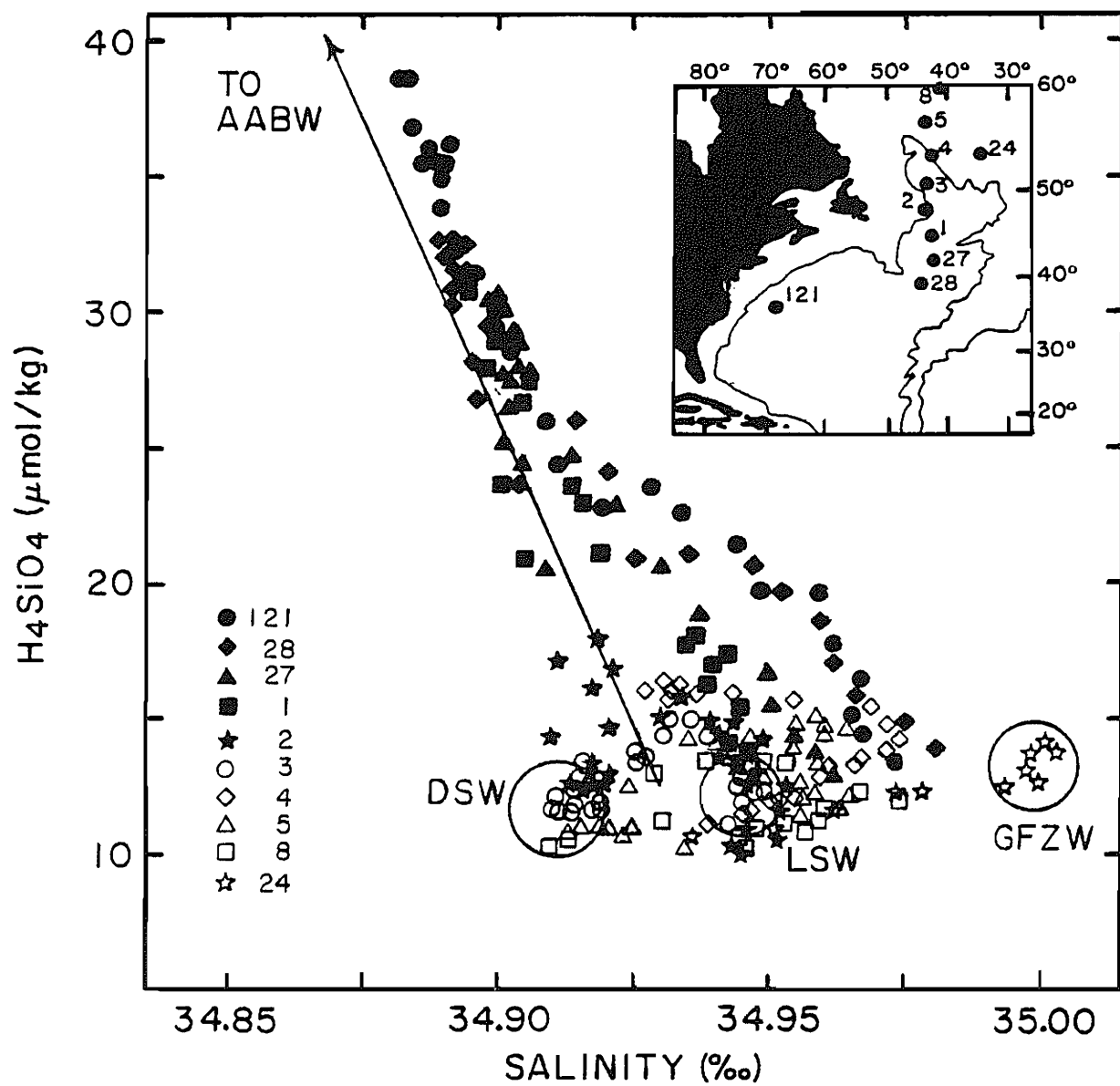


Figure 7-13. Plot of silica versus salinity for deep waters in the northern Atlantic. Waters to the north of 50°N have silicate contents less than 15 $\mu\text{m}/\text{kg}$. To the south a rapid rise in silicate content is noted. The samples with high silicate content have θ - S coordinates falling outside the triangle of northern component compositions. These deviations can all be explained through the admixture of AABW. The arrow extends from the composition of the most dense northern component water towards the composition of the bottom water entering the South Atlantic through the Vema Channel ($S=34.67\text{‰}$ and $H_4SiO_4=125 \mu\text{m}/\text{kg}$). The points shown are for GEOSECS stations (424).

Another nearly conservative property is what chemical oceanographers term preformed phosphate (i.e., the amount of phosphate carried by the water when it leaves the sea surface). This property is computed as follows:

$$[\text{PO}_4]^\circ = [\text{PO}_4]_{\text{in situ}} - \frac{\text{AOU}}{135}$$

7-5

The amount of O_2 consumed in the water (i.e., its AOU) is used to correct for the contribution of respiration to the phosphate content of the water. As we have seen, while the ratio of PO_4 generated to oxygen consumed averages 135, it does not always have this value. Hence PO_4° calculated, using a fixed ratio of 135 will not be exactly conservative. The higher the AOU value for a given water sample, the larger the uncertainty in PO_4° . As shown by the PO_4° versus depth plots in figure 7-14, this property does have considerable potential. Water formed in the northern Atlantic has a considerably lower PO_4° content than does water from the Antarctic Ocean! As shown in table 7-2 the range in PO_4° values for the three contributors to northern component water is quite small.

As we shall see later in this chapter the H/D and $^{18}\text{O}/^{16}\text{O}$ ratios in the water itself are excellent conservative tracers. However, as not enough analyses are available, only preliminary use can be made of the distribution of this property in global bottom water studies. Hence, they are not included in table 7-2.

INITIAL RADIOCARBON TO CARBON RATIO IN NCW

If we are to use the distribution of radiocarbon to estimate the ventilation time of the deep sea, we must establish the initial $^{14}\text{C}/\text{C}$ ratio for northern component water. This presents a problem because at the time of the GEOSECS survey virtually all of what we term here as new northern component water had been contaminated with ^{14}C produced during nuclear testing. Fortunately, it is possible through the simultaneous consideration of tritium measurements (the tritium present in the ocean is almost entirely from nuclear testing) and radiocarbon measurements to sort out this contamination. As shown in figure 7-15 waters from the Norwegian Sea and northern Atlantic ($>50^\circ\text{N}$) show a fairly tight correlation between their tritium and radiocarbon contents. Those waters in this region which had not as yet been contaminated with bomb-produced tritium (the prenuclear testing tritium content of waters in this region was likely on the order of a few tenths of a T.U.) have $\Delta^{14}\text{C}$ values averaging about $-67^\circ/\text{oo}$. This value is taken to be that carried by the carbon in these waters prior to the onset of nuclear testing. Although we give a $\Delta^{14}\text{C}$ value in table 7-2 only for mean northern component water, it is likely that all three contributors had nearly the same value.

FEED FOR NCW PRODUCTION

As can be seen from table 7-2, the three contributors to

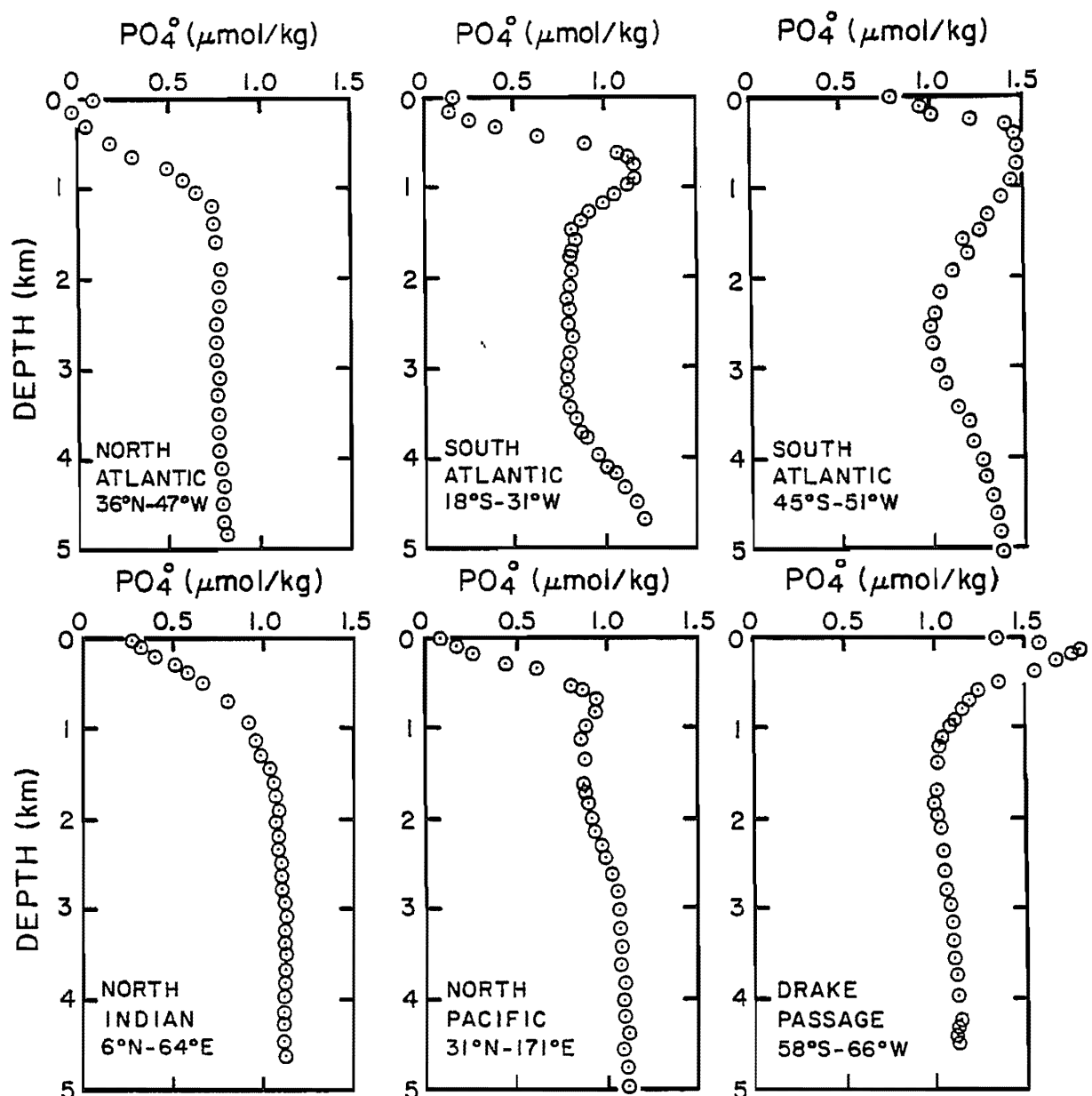


Figure 7-14. Plots of initial PO_4 content (i.e., $\text{PO}_4^{\text{measured}} - \text{AOU}/135$) versus depth for key localities throughout the world ocean. Based on data obtained as part of the GEOSECS program (424, 425, 426).

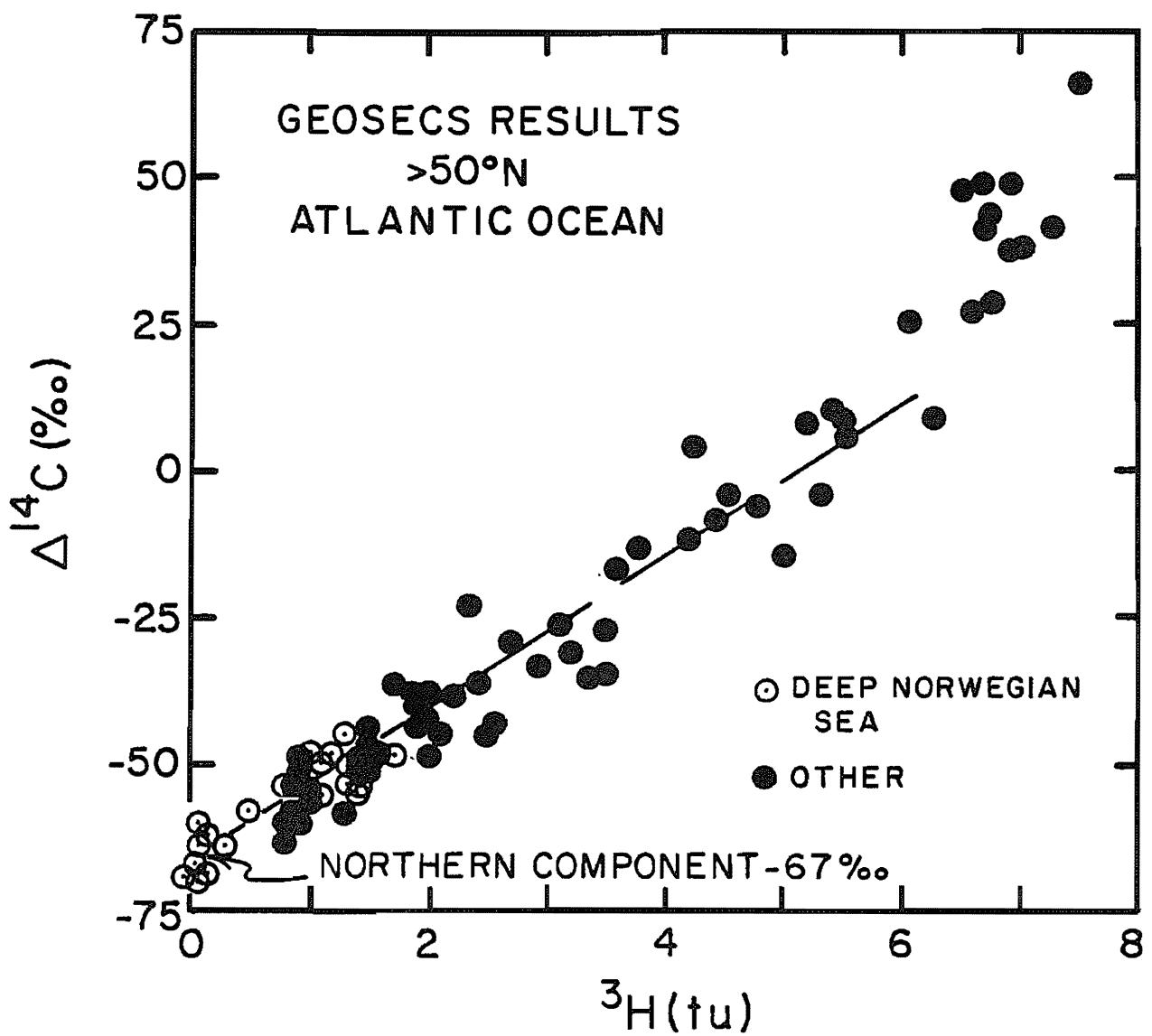


Figure 7-15. $\Delta^{14}\text{C}$ versus tritium content for waters from the northern Atlantic in 1972. The trend terminates in water with a tritium content less than 0.2 T.U. and $\Delta^{14}\text{C}$ values close to -67‰. The tritium results were obtained by Ostlund of the University of Miami as part of the GEOSECS program (51). The radiocarbon results were obtained in the laboratories of Ostlund and Stuiver (21).

northern component water have moderate nutrient constituent contents and significant oxygen depletions. Two conclusions can be drawn. First, the waters feeding deep water production in the northern Atlantic come on the average from a depth of at least 700 meters in the temperate Atlantic. Were this not true, the outgoing new deep water would be carrying more silicate, more phosphate, and more nitrate than was carried by the incoming feed water. This would require a nutrient source within the Norwegian Sea far larger than that constituted by all the world's rivers put together! As there is no possible source of these constituents within the Norwegian Sea, we can say with confidence that the concentration of these substances must be equal to or possibly slightly greater* in the waters feeding the deep water formation process than in the new deep water itself. To meet this requirement the water must come mainly from depths greater than 700 meters (see figure 7-16).

Second, the fact that this new water begins its trip through the deep sea with a sizeable AOU suggests that plant material formed in the water during its residence at the surface in the Norwegian and Labrador Seas is destroyed by respiration in the northern holding basins. As the preformed phosphate content of the exiting water averages $0.7 \mu\text{m}/\text{kg}$, while the measured phosphate content is $1.1 \mu\text{m}/\text{kg}$, about one third of the phosphate must have been utilized by plants as the feed water underwent cooling. This plant matter then falls to the holding basin where it is largely eaten by animals and bacteria.

The most likely candidate for the feed water is the silicate maximum water. As shown in figure 7-16 this water is found at about one kilometer depth. This feature is likely generated by the isopycnal transport of silicate rich water all the way from the Antarctic Ocean! In fact the reason for the existence of this maximum is likely the withdrawal of water from this density level for conversion to deep water. This withdrawal permits the northward penetration of Antarctic derived waters (at other depths in the North Atlantic, water is being exported to the south, driving back the intruding Antarctic waters).

The fact that the feed water for the source regions of northern component water is from intermediate depth rather than from the surface accounts for its rather low $\Delta^{14}\text{C}$ value, (surface water in the temperate zone had a $\Delta^{14}\text{C}$ of about $-45^{\circ}/\text{oo}$ prior to the year 1950), while new northern component water had a $\Delta^{14}\text{C}$ of about $-67^{\circ}/\text{oo}$. As shown in table 7-3, based on the few ^{14}C measurements made on water from intermediate depths made prior to the input of ^{14}C from bomb testing, and from the results of the GEOSECS expedition corrected (using tritium data) for the contribution of bomb- ^{14}C , a $\Delta^{14}\text{C}$ value of about $-89^{\circ}/\text{oo}$ is obtained for the feed water.

The difference between the $-89^{\circ}/\text{oo}$ value for the feed

*It is possible that some of the nutrient constituents carried into this region are lost to the sediments, as the result of plant growth in northern surface waters. However, as the recycling of nutrient elements in the sea is very efficient, this loss must be small.

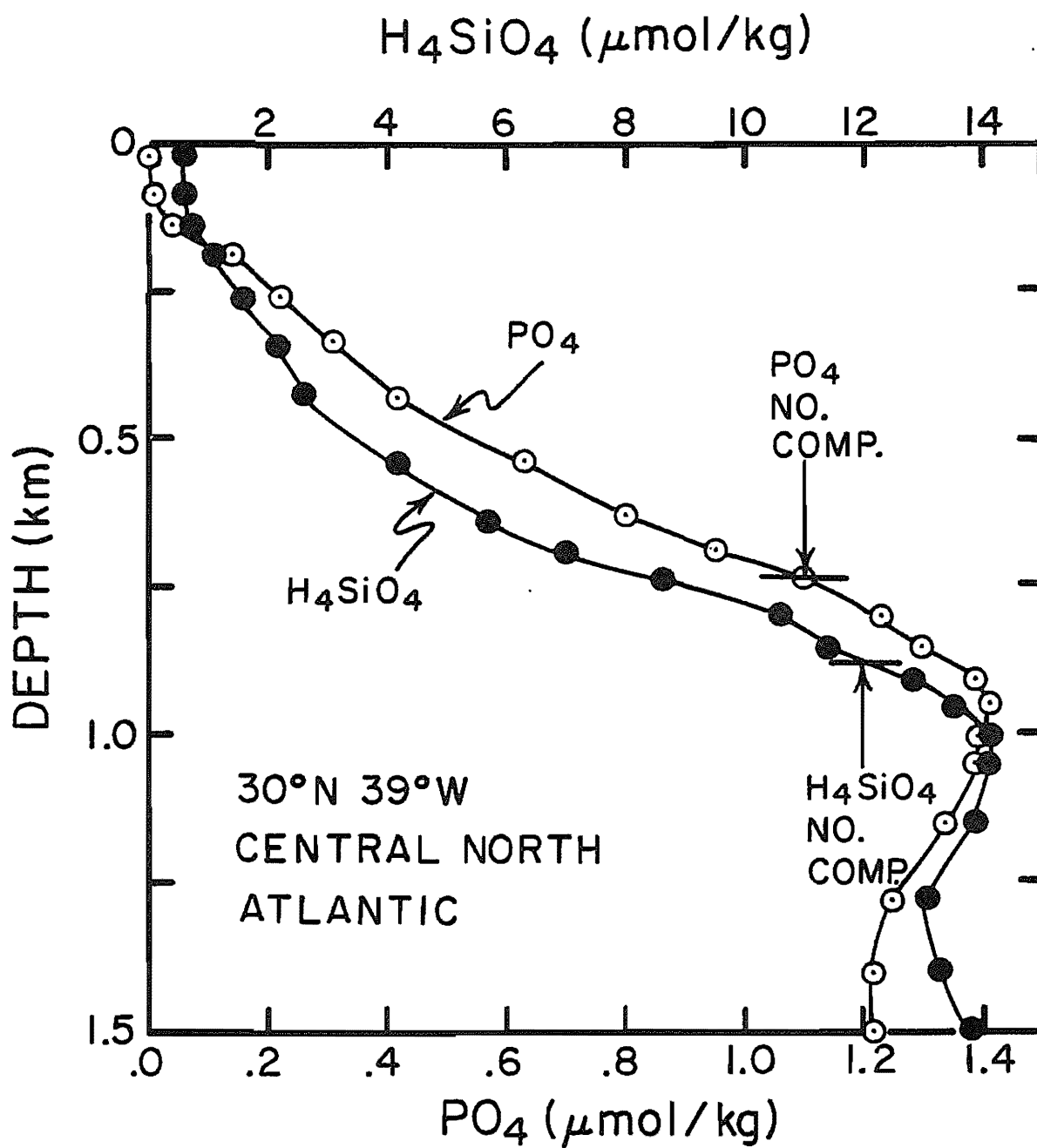


Figure 7-16. Plots of PO_4 and H_4SiO_4 content versus depth in the upper waters of the central North Atlantic. The arrows designate the concentrations of these constituents in northern component water. The horizontal line segments at the heads of these arrows designate the depths in the north temperate Atlantic at which these concentrations are found. These results were obtained as part of the GEOSECS program (424).

Table 7-3. Radiocarbon results on water samples from intermediate depths in the temperate North Atlantic. The first four samples were collected before ^{14}C from nuclear tests had measurably contaminated the ocean. The last five collected during the GEOSECS program had small amounts of tritium, necessitating a correction for bomb- ^{14}C . The measurements on the samples from the 1950's were made by Broecker of Lamont-Doherty Geological Observatory (4); those on samples from the 1970's were made by Ostlund and Stuiver as part of the GEOSECS program (21).

Collection Date	Latitude °N	Longitude °W	Depth m	^3H T.U.	$\Delta^{14}\text{C}$ ‰
10/56	24	24	1100	-	- 107
4/56	22	54	820	-	- 95
11/57	20	49	950	-	- 79
12/55	19	80	1100	-	- 91
					Mean - 93
3/73	33	57	1100	1.05	- 82*
3/73	31	39	1080	0.30	- 74*
3/73	28	26	900	0.15	- 83*
9/72	21	54	1000	0.10	- 100*
9/72	27	54	1010	0.25	- 86*
					Mean - 85

*Corrected for contribution of bomb-produced ^{14}C assuming a 20‰ change in $\Delta^{14}\text{C}$ per 1 T.U. increased in tritium.

water and the -67‰ value for new bottom water must be the result of the invasion of ^{14}C from the atmosphere into the northern waters. As we shall see below the flux of northern component water is about $13 \times 10^6 \text{ m}^3/\text{sec}$ (i.e. $\sim 4 \times 10^{14} \text{ m}^3/\text{yr}$). The volume of water contained in the formation region (i.e., north of 55°N) is about $2 \times 10^{16} \text{ m}^3$. Thus, the flushing time of water in the source region is about 50 years. During this time ^{14}C decays by about 6‰. Thus, in the absence of gas exchange the $\Delta^{14}\text{C}$ of water leaving the basin would be 6‰ lower than that for input water. Actually, we observe it to be 22‰ higher. So exchange with atmospheric CO_2 must raise the $\Delta^{14}\text{C}$ value by about 28‰. The area of the Atlantic north of 55°N is about $8 \times 10^{12} \text{ m}^2$. If we take the CO_2 exchange rate to be 20 moles/ m^2yr and the ΣCO_2 content of these waters to be 2.1 moles/ m^3 then gas exchange should reduce the $\Delta^{14}\text{C}$ difference between water and air by about 18‰. While this is not quite enough the result lies within the range permitted by the uncertainties that exist in many aspects of this argument. The calculation does make it clear that the water does not remain in the source region anywhere near long enough to achieve equilibrium with the $^{14}\text{C}/^{12}\text{C}$ ratio in the atmosphere.*

SOUTHERN COMPONENT WATER

The second major source area for bottom water in the ocean is the Weddell Sea (see figure 7-17 for location). During winter months, water which has upwelled from the deep circumpolar current to the surface in the Weddell Sea is cooled by contact with the air and made more saline by the formation of sea ice. As these processes are the most intense on the continental shelf (because of its isolation from mixing with deep water) the most dense waters are produced along the southern and western margin of the basin. Under the influence of gravity, these waters cascade over the shelf edge and into the less dense deep water. Along their traverse they entrain a mixture of winter surface water from the interior of the Weddell gyre and underlying deep circumpolar water. Diagrams showing plots of potential temperature versus salinity, dissolved oxygen versus salinity, hydrogen isotope ratio versus salinity and oxygen isotope ratio versus salinity for Weddell Sea water is shown in figure 7-18. In all cases Weddell Sea water can be seen to be a mixture of about 60% surface water and 40% entrained deep water. The surface water component consists of a mixture of shelf water and of gyre surface water.

The properties of these waters are summarized in table 7-4. The Weddell Sea bottom water has a high silica content, a rather high AOU, a high preformed phosphate content and a low $^{14}\text{C/C}$ ratio. These properties are related to two characteristics of formation process. First, the source of the water is old deep

*The mean depth of the water in the source region is $2 \times 10^{16} \text{ m}^3 / 8 \times 10^{12} \text{ m}^2$ or 2500 m. Thus, about 5250 moles of CO_2 are contained under the average square meter of sea surface. At a rate of 20 moles/ m^2yr over a period of 50 years only about one carbon atom in five is exchanged!

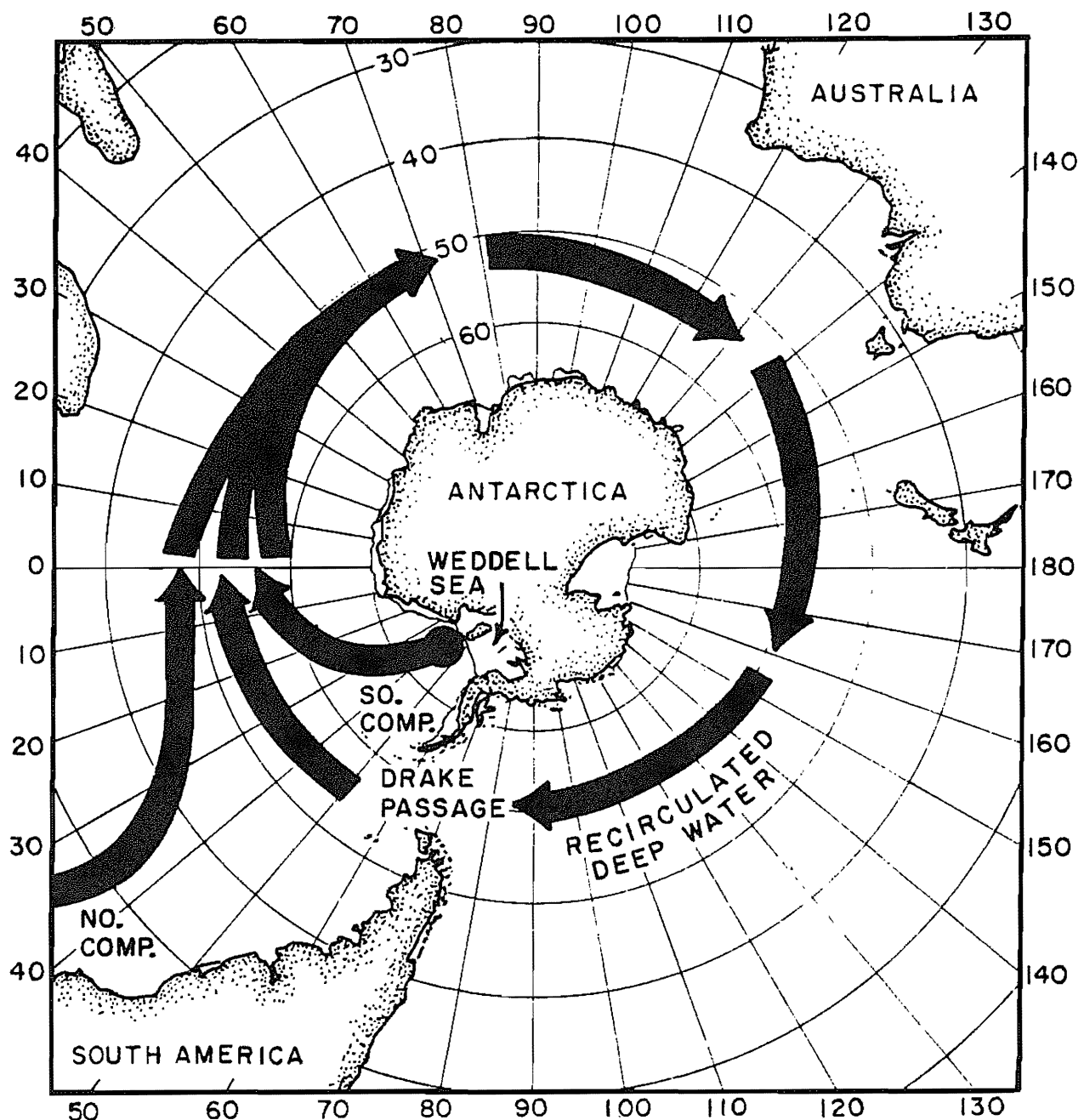


Figure 7-17. Map showing the pattern of deep water flow in the Antarctic Ocean. Northern component water joins the circumpolar flow at the south end of the Atlantic's western basin. Southern component water is formed in a large embayment in the Antarctic Continent known as the Weddell Sea.

Table 7-4 Composition of the waters contributing to the formation of Weddell Sea Bottom Water and of Weddell Sea Bottom Water itself. What we designate as southern component to deep Atlantic water is Weddell Sea Bottom Water further contaminated with ambient circum-polar water and with the products of respiration and opal solution. Based on measurements made as part of the GEOSECS program (21,424) and by Weiss and his colleagues (428).

Water Type	θ °C	S ‰	σ_4 ‰	NO_3 μm/kg	PO_4 μm/kg	SiO_2 μm/kg	AOU μm/kg	PO_4° μm/kg	$\Delta^{14}\text{C}$ ‰
Circumpolar Deep	0.62	34.708	46.030	32.1	2.20	123	137	1.16	-163
Western Shelf **	-2.0	34.7	-	27.5	2.05	70	45	1.8	
Winter Surface **	-1.8	34.4	-	27.5	2.05	70	45	1.8	-146*
Weddell Sea Bottom	-0.89	34.647	46.234	31.8	2.14	112	102	1.28	-154

*Calculated rather than observed.

**Collected beneath the summer surface water.

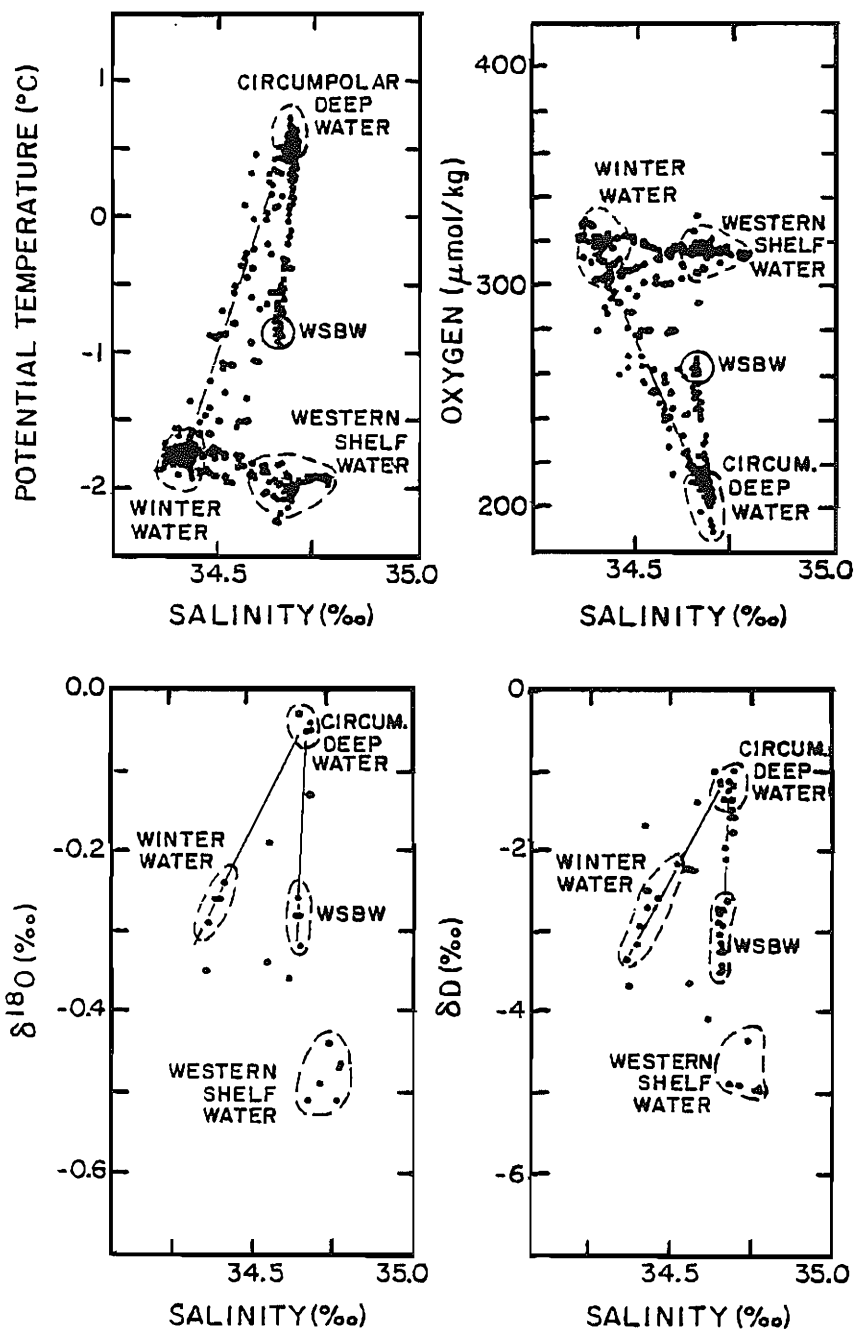


Figure 7-18. Plots of potential temperature, dissolved oxygen, $^{18}\text{O}/^{16}\text{O}$ ratio and D/H ratio against salinity for waters from the Weddell Sea. In each diagram the composition of Weddell Sea Bottom Water (WSBW) falls within the triangle defined by the compositions of winter surface water in the open Weddell Sea, western shelf water from the margin of the Weddell Sea and circumpolar deep water entering the Atlantic sector of the Antarctic Ocean through the Drake Passage. These results were obtained by Ray Weiss and Harmon Craig at Scripps Institution of Oceanography, La Jolla, California (428).

water which is being recirculated around the Antarctic. Second, the residence time of this water at the surface is so short that plants cannot fully utilize the nutrient elements and that gas exchange can make only a small dent in restoring the $\Delta^{14}\text{C}/\text{C}$ ratio to that for atmospheric CO_2 . The salinity of the water changes only a small amount (from precipitation and continental ice melting). The main thing which happens is that the water is cooled by about 1.5°C as the result of contact with the atmosphere.

The newly formed Weddell Sea water joins the circum-Antarctic deep flow and mixes upward into the older water producing the linear arrays of $\theta\text{-S}$ seen in figure 7-19, of $\theta\text{-D/H}$ seen in figure 7-20 and of $\theta\text{-PO}_4^\circ$ seen in figure 7-21. As these distributions all terminate at the composition of Weddell Sea Bottom Water (WSBW); other sources of deep water around the perimeter of the Antarctic are either too weak to make an impact on these trends or they have compositions falling along the main trend. The $\Delta^{14}\text{C}$ values for these main sequence waters are remarkably uniform (see figure 7-22). This is not unexpected in the light of the fact that little ^{14}C renewal occurs during the cooling process in the Weddell Sea.

It is this main sequence of Antarctic waters which feeds abyssal waters into each of the major oceans. In each case entry is via a barrier which partially blocks communication between the Antarctic and the ocean basins to the north. In the western Atlantic it is the Rio Grande Rise located at 31°S which blocks communication. A deep cut in this barrier, the Vema Passage (VP), permits bottom water to spill through to the north. In the western Indian Ocean the Southwest Indian Ridge, located at 32°S , partially isolates Antarctic waters from those in the western basin of this ocean. The Atlantis Passage (AP) provides a gap through which deep water can move. In the western Pacific the Samoan Ridge located at 10° S provides the impedance to mixing. The Samoan Passage (SP) provides the conduit for the deep water entering the equatorial and northern Pacific. The compositions of the waters spilling through these three passages are shown in figures 7-19, 7-20, 7-21 and 7-22. As can be seen they all lie along the main sequence of circumpolar deep water compositions.

Once beyond the passages these bottom waters begin to mix with the less dense overlying water in the major ocean basins. In the Atlantic and in the Pacific these waters have compositions which fall well off the main sequence for circumpolar waters. Thus, in these two oceans we see quite a change in the $\theta\text{-S}$ and $\text{PO}_4^\circ\text{-S}$ relationships from those observed in the Antarctic (see figures 7-23 and 7-24). For the Indian Ocean these relationships are more similar to those in the Antarctic (bearing witness to the absence of a deep water source at the north end of this ocean).

As shown in figure 7-25, the radiocarbon-salinity trends in the Pacific and Indian Oceans are quite different from those in the Atlantic. In the Indian and Pacific Oceans radioactive decay dominates, leading to an up-water-column decrease in $\Delta^{14}\text{C}$. By contrast, in the Atlantic mixing between the Vema Passage Water and the high $\Delta^{14}\text{C}$ northern component water generates an up-water-column increase in $\Delta^{14}\text{C}$.

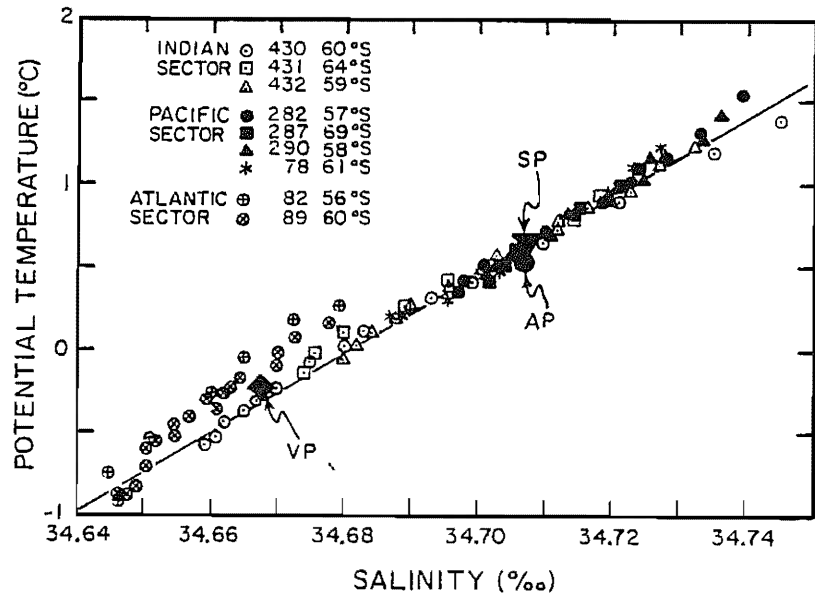


Figure 7-19. Potential temperature versus salinity for the "main sequence" of circumpolar deep waters. The coldest and least saline waters on this sequence correspond in composition to Weddell Sea Bottom Water. It is this water that we designate southern component water. Also shown are the compositions of the waters spilling northward out of the Antarctic into the western Atlantic (via the Vema Passage), the Western Indian (via the Atlantis Passage) and into the Pacific (via the Samoan Passage). The locations of these key passages are designated on the foldout map. The data shown here were obtained as part of the GEOSECS program (424, 425, 426).

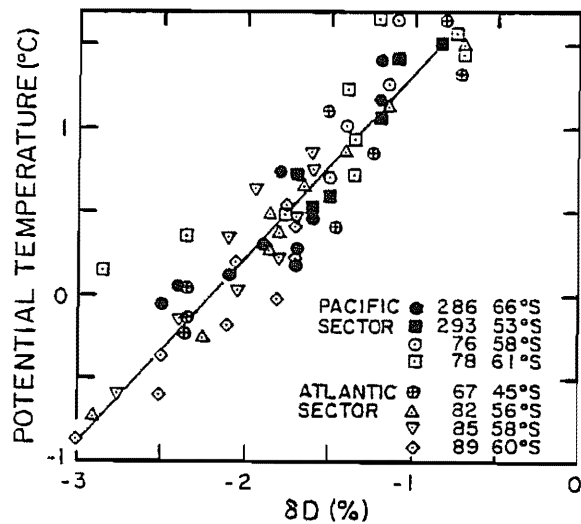


Figure 7-20. Potential temperature versus D/H ratio (given as δD) for circumpolar deep waters. The linear array terminates at the composition of Weddell Sea Bottom Water. The isotope results were obtained in the laboratory of Craig of Scripps Institution for Oceanography on samples collected as part of the GEOSECS program.

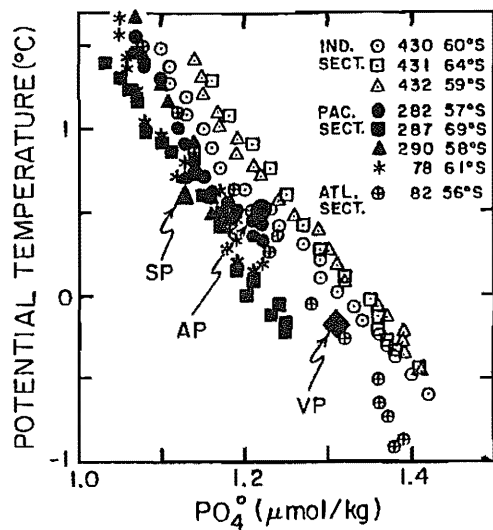


Figure 7-21. Potential temperature versus preformed phosphate content for circumpolar deep waters. The compositions of the waters flowing through the Vema Passage, the Atlantis Passage, and the Samoan Passage are also shown. The data shown were obtained as part of the GEOSECS program (424, 425, 426).

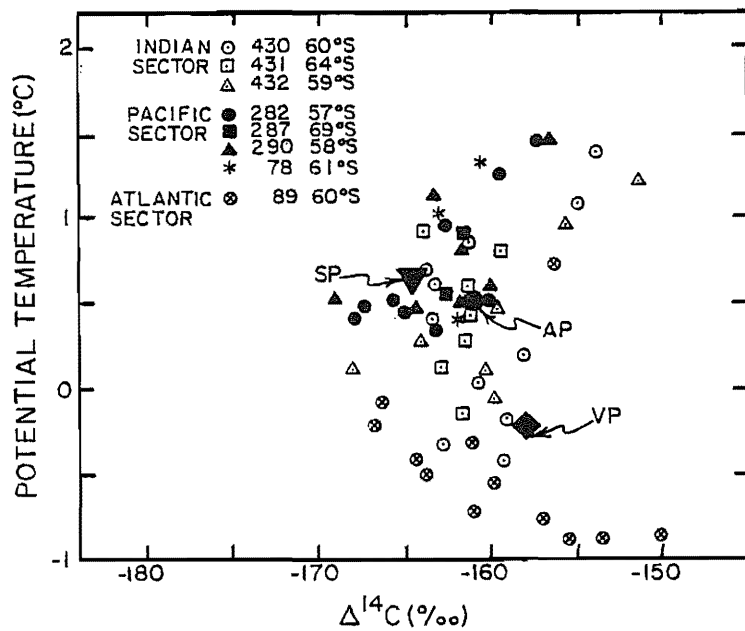


Figure 7-22. Potential temperature versus $\Delta^{14}\text{C}/\text{C}$ ratio (given as $\Delta^{14}\text{C}$) for "main sequence" waters in the circumpolar region. The compositions of waters passing through the three major passages connecting the Antarctic with the major oceans are also shown. As the error on an individual radiocarbon measurement is $\pm 4\text{‰}$, much of the scatter is experimental. The radiocarbon measurements were made in the laboratories of Ostlund of the university of Miami and Stuiver of the University of Washington (21, 22, 23).

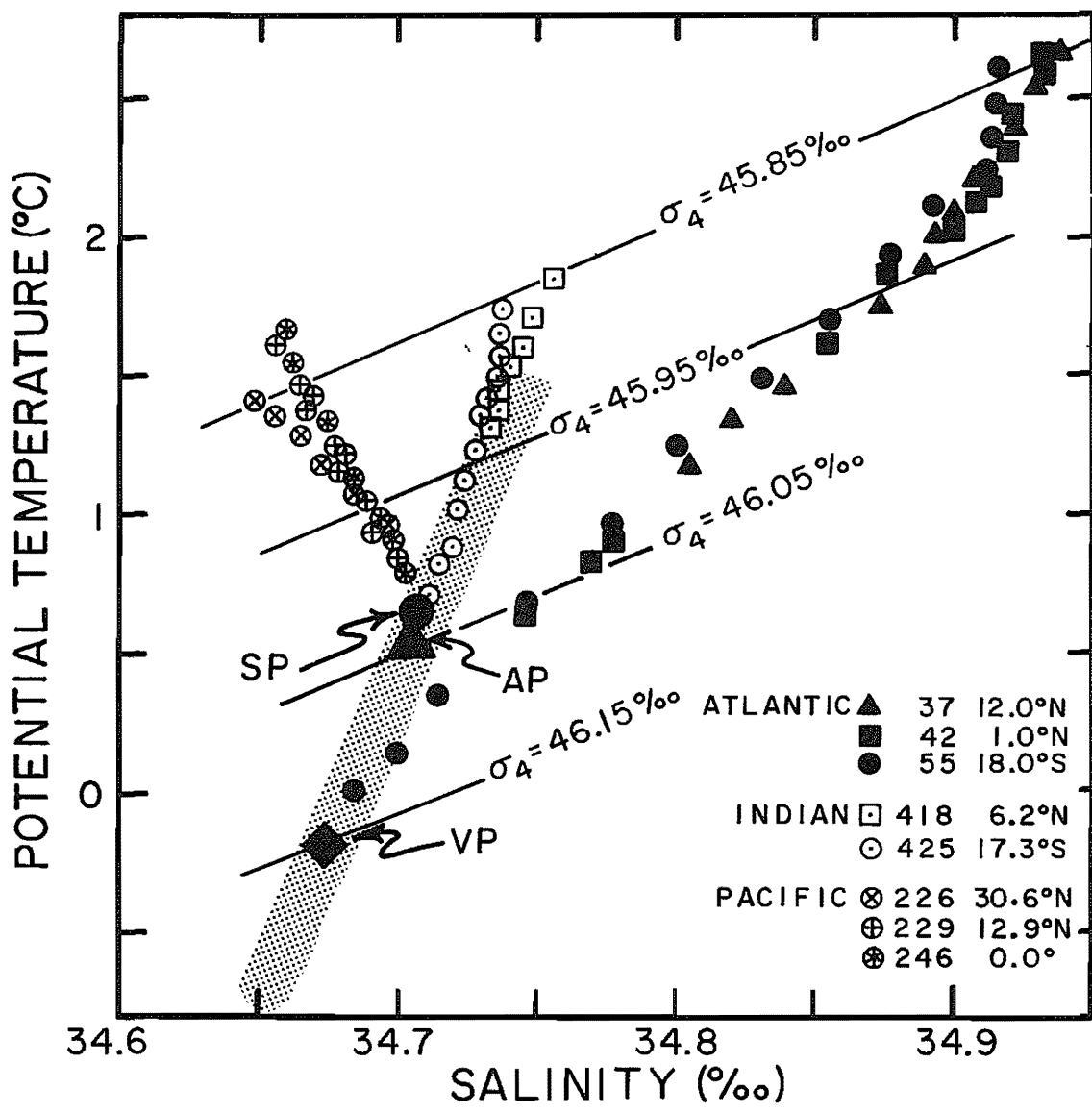


Figure 7-23. Potential temperature versus salinity diagram for the world's deep waters of potential density greater than 45.85‰ . The stippled band represents the compositions of "main sequence" water in the Antarctic. The trends along the western sides of the three major oceans are also shown. The data shown were obtained as part of the GEOSECS program (424, 425, 426).

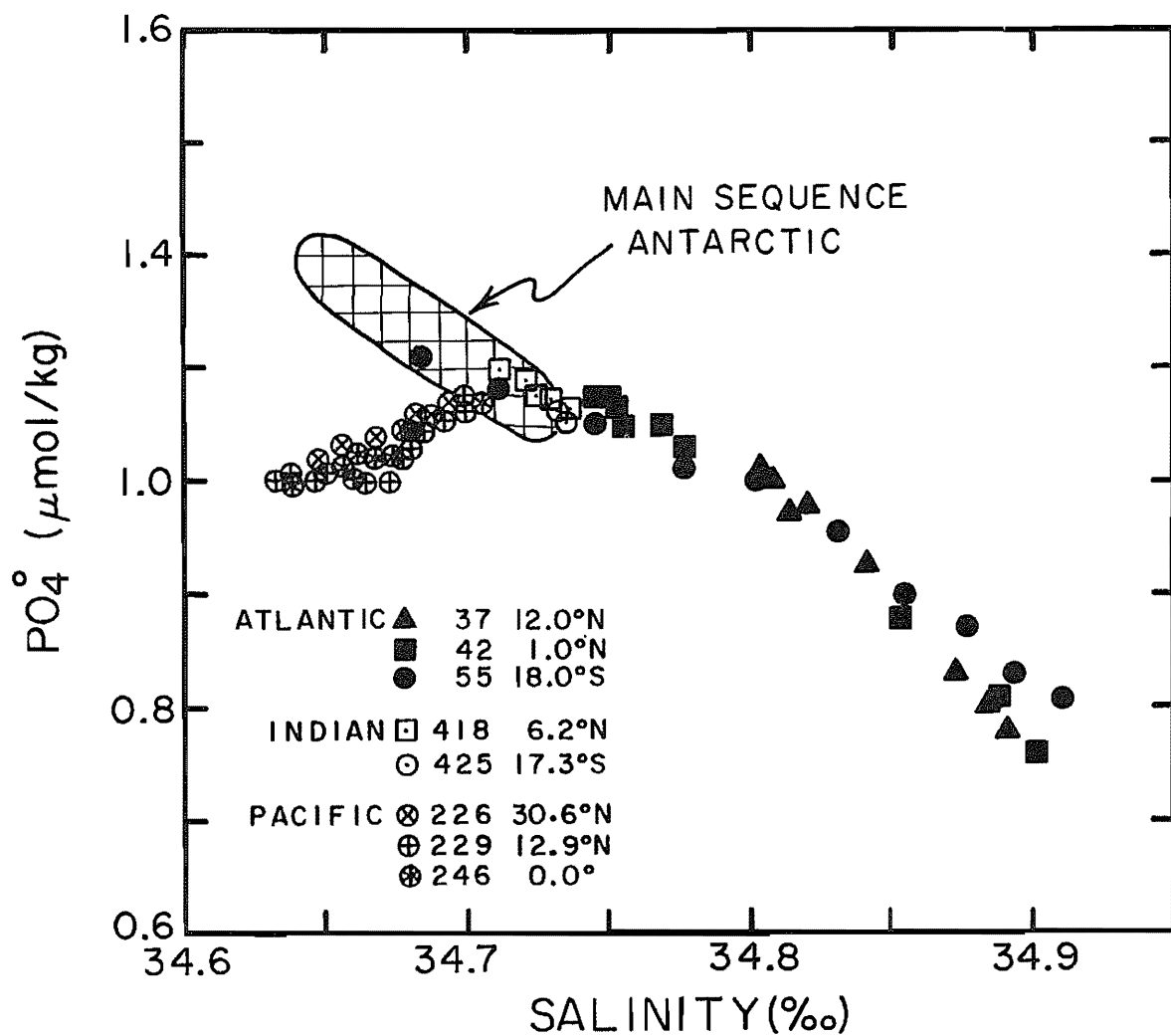


Figure 7-24. Initial phosphate concentration versus salinity for the world's deep waters of potential density greater than $45.85^{\circ}/\text{oo}$. The cross-hatched area shows the range of compositions for the Antarctic "main sequence" waters. The Antarctic, Atlantic and Indian Ocean waters fall along a line connecting the compositions of northern component ($S = 34.935$, $\text{PO}_4^{\circ} = 0.73$) and southern component water ($S = 34.66$, $\text{PO}_4^{\circ} = 1.35$). The Pacific water deviates from this trend suggesting that either a third endmember with a lower salinity and lower initial phosphate concentration is mixing with the bottom water entering the Pacific through the Samoan Passage or that the coefficient relating to AOU and PO_4 deviates from 135 in the low oxygen deep waters of the North Pacific Ocean. The data shown were obtained as part of the GEOSECS program (424, 425, 426).

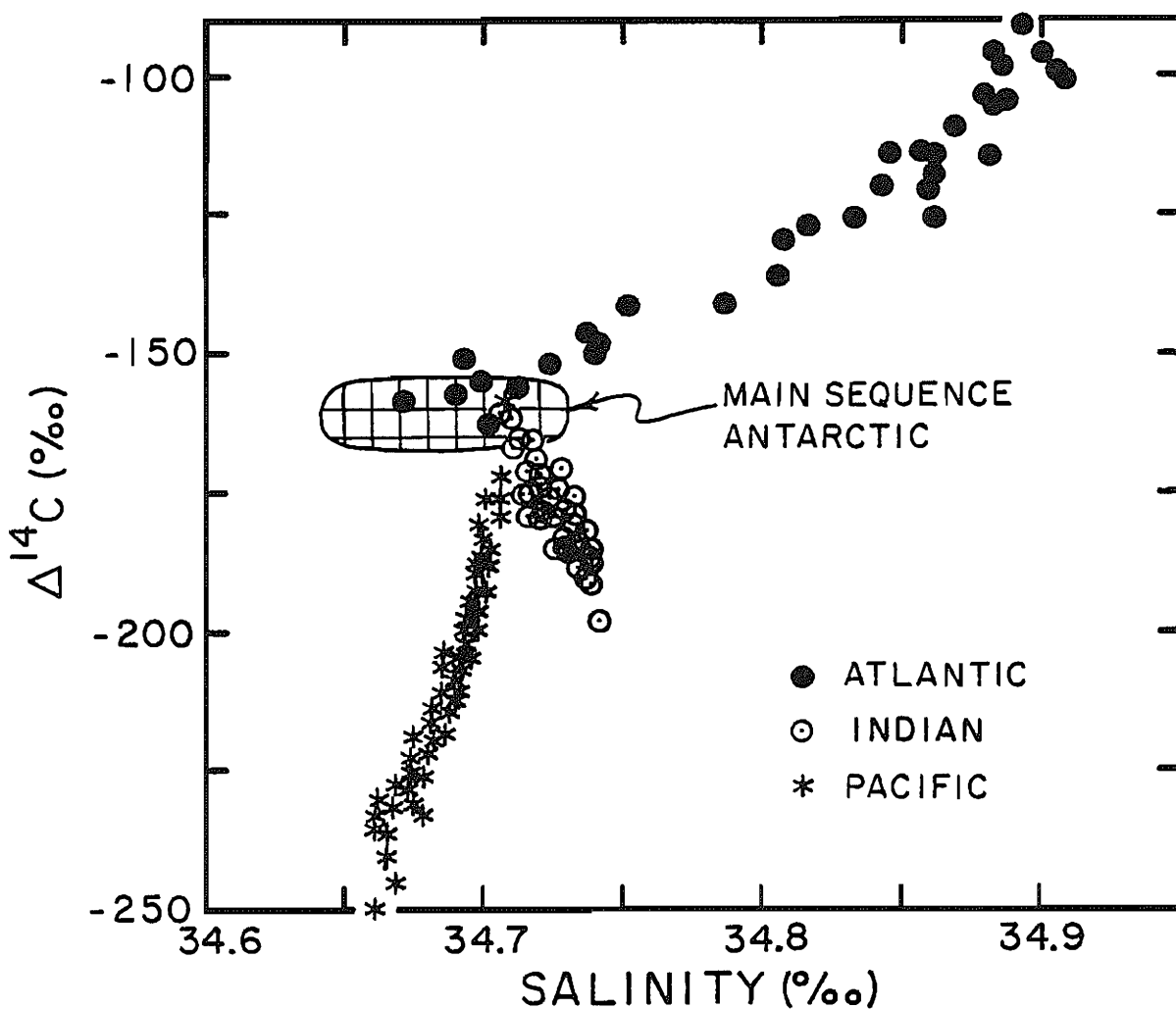


Figure 7-25. Plot of $^{14}\text{C}/\text{C}$ ratio (expressed as $\Delta^{14}\text{C}$) against salinity for the world's deep waters with densities greater than 45.85‰ . The cross-hatched area represents the main sequence of Antarctic waters. The trends in the three major oceans are generated by a combination of mixing and radioactive decay. For the Atlantic, mixing dominates. For the Indian and Pacific, the decreases below the main sequence value must be due to radio-decay. The radiocarbon measurements were made as part of the GEOSECS program in the laboratories of Ostlund of the University of Miami and Stuiver at the University of Washington (21,22,23).

As can be seen in figure 7-26, the $\Delta^{14}\text{C}$ values for these various deep water types correlate with AOU and silicate remarkably well. The lower the $\Delta^{14}\text{C}$ value, the higher the AOU and silicate concentration. This figure serves as a reminder that the consumption of oxygen and the solution of opal act as clocks recording the relative ages of various water types.

VENTILATION OF THE DEEP ATLANTIC OCEAN

The western Atlantic Ocean receives new deep water both from the north and from the south, (in this regard it differs from the other deep basins which are all fed from just one source). As even the most dense of the waters formed in the north is less dense than the water entering the western Atlantic through the Vema Channel, the southern component water underrides that coming from the north and mixes up into it. This mixing produces a linear θ -S array for waters deeper than about four kilometers. These points fall very nearly along a line joining the densest northern component water with that for the water passing through the Vema Channel (see figure 7-27). The proportions of the two contributors at any given location and depth can be obtained by scaling either one of these parameters. For example, a water with a potential temperature of 1.0°C would be roughly a 50-50 mixture of the two components.

Waters with potential temperatures warmer than about 2°C yield θ -S trends with a different slope. As shown in figure 7-27, the break between these mixing regions is quite sharp. We will refer to the slope change as the Two-Degree Discontinuity (TDD). Such a change in slope is a natural consequence of the fact that northern component waters cover a range of temperatures and salinities. This can be seen by returning to the one-dimensional column discussed earlier in this chapter. Instead of considering what happens if there is only one input at the bottom of the column, let us consider a situation where there are three separate inputs. Water with the composition of that passing through the Vema Passage is injected at the bottom of the column (i.e., at 5 km); water with the composition of the densest northern component water is injected at a depth of 4 kilometers and water with the composition of that in the deep Labrador Sea is injected at a depth of 3 kilometers. The first of these waters produces an upwelling rate of $x \text{ m/yr}$, the second produces an upwelling rate of an additional $10x \text{ m/yr}$, and the third produces an upwelling rate of an additional $10x \text{ m/yr}$. Thus, the upwelling rate beneath 4 kilometers will be $x \text{ m/yr}$, between 4 and 3 kilometers $11x \text{ m/yr}$ and above 3 kilometers $21x \text{ m/yr}$. In the absence of any vertical mixing the potential temperature of the water would be -0.15°C below 4 kilometers, 2.01°C between 4 and 3 kilometers depth and 2.77°C above 3 kilometers depth. However, if we introduce a moderate amount of mixing such that κ/w (i.e. z^*) is in all depth ranges about 300 meters, then the temperature profile will be as shown in figure 7-28. This will also produce a θ -S diagram similar to that seen for the deep waters in the deep western Atlantic.

This 1-D example helps explain the origin of the TDD. If we think of "up" as perpendicular to the isopycnal horizons, the

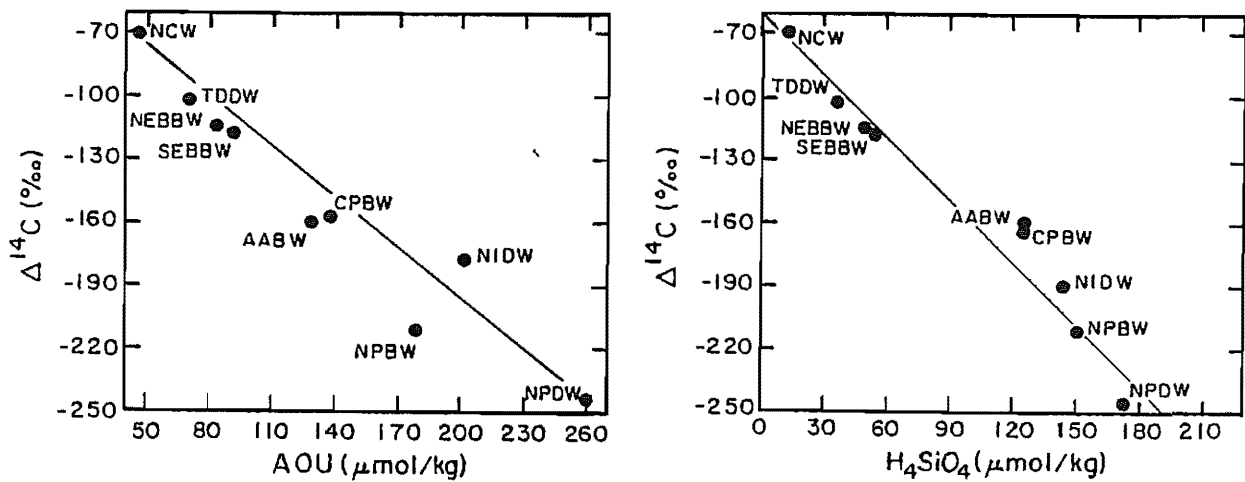


Figure 7-26. Plots of $\Delta^{14}\text{C}$ versus AOU (left hand panel) and versus dissolved silicate content (right hand panel) for various deep water types. NCW is the new water entering the western basin of the northern Atlantic. TDDW is water at a depth of about 4 kilometers in the western basin of the central Atlantic. NEBBW and SEBBW are, respectively, bottom waters from the northern and southern eastern Atlantic. AABW is the bottom water of Antarctic origin which penetrates into the western basin of the southern Atlantic. CPBW is the circumpolar deep water which passes from the Pacific sector of the Antarctic to the Atlantic sector of the Antarctic through the Drake Passage. NIDW is deep water from the northern Indian Ocean. NPBW is bottom water from the North Pacific. NPDW is water from about 2000 meters depth in the North Pacific. The slope of the $\Delta^{14}\text{C}$ -AOU trend corresponds to an O_2 consumption rate of 0.12 $\mu\text{m}/\text{kg}$ per year and that of the $\Delta^{14}\text{C}$ - H_4SiO_4 trend to an opal solution rate of 0.10 $\mu\text{m}/\text{kg}$ per year.

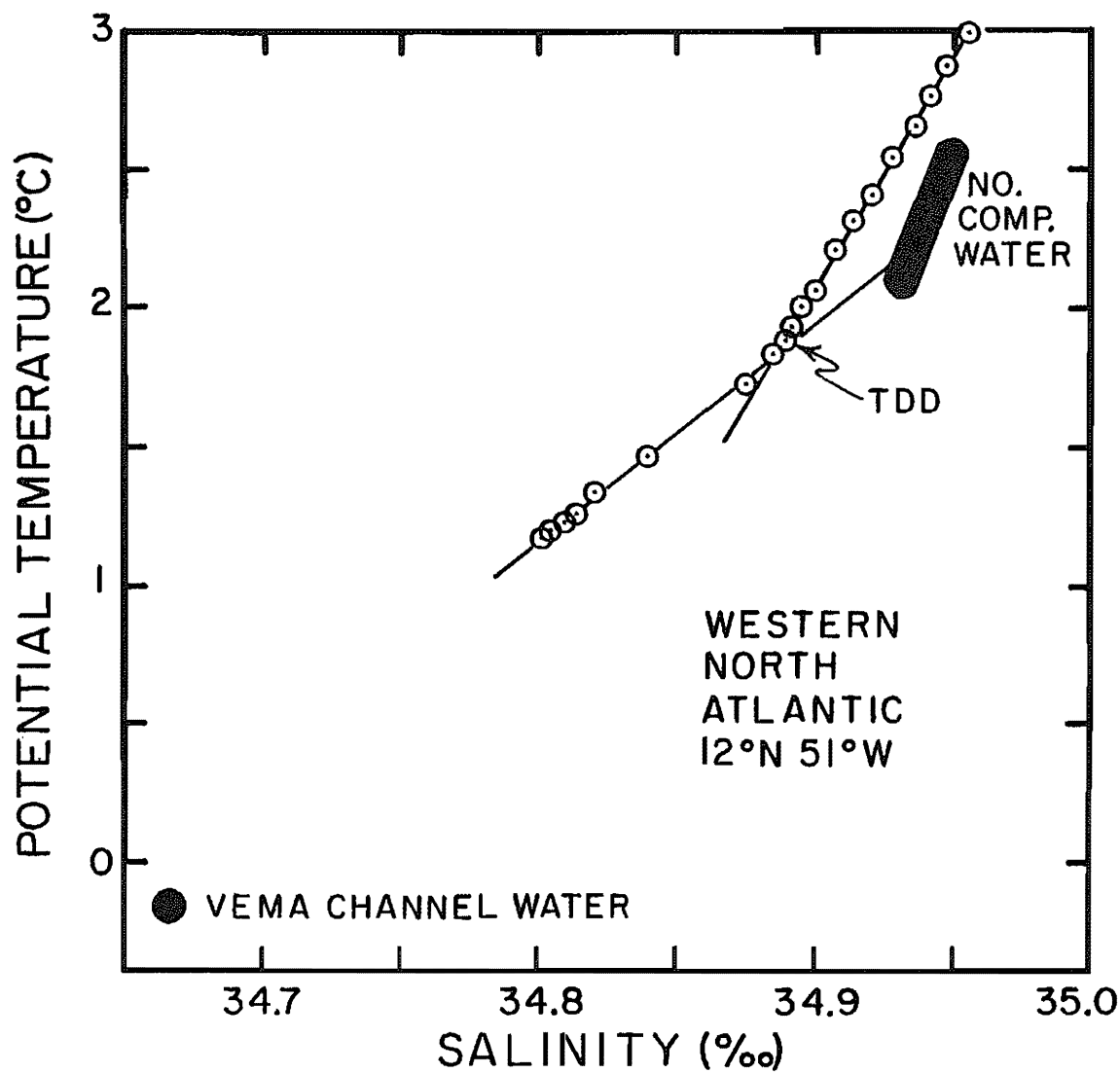


Figure 7-27. Potential temperature versus salinity diagram for deep waters at a station in the western North Atlantic 12° north of the equator. The prominent break in slope is designated as the Two-Degree Discontinuity (423). Also shown are the compositions of water entering the Atlantic through the Vema Channel and of northern component waters.

example becomes more like the actual situation in the deep Atlantic. The break in θ -S slope corresponds to the isopycnal of entry of the most dense northern component water. However, the composition of the water on this horizon does not correspond to that of the densest northern component water. Rather, it has a composition matching that of the combined flux of Vema Passage Water up through this horizon and northern component water into the system (i.e., as shown in figure 7-28 the composition lies between that of the two endmembers).

From the $\Delta^{14}\text{C}$ distribution in the waters beneath the TDD, we can get an idea as to how rapidly the deep western basin of the Atlantic is ventilated. Were this ventilation extremely rapid, then a plot of ^{14}C versus salinity should show all measurements falling on a straight line joining the composition of the end-members (i.e., $S = 34.667^{\circ}/\text{oo}$ and $\Delta^{14}\text{C} = -160^{\circ}/\text{oo}$ for Vema Channel Water and $S = 34.932^{\circ}/\text{oo}$ and $\Delta^{14}\text{C} = -67^{\circ}/\text{oo}$ for the densest northern component water). Actually, as seen in the upper panel of figure 7-29, the measured values all fall below this line, demonstrating that radiocarbon had been lost by radioactive decay during residence in the mixing zone beneath the TDD. The deviation of the $\Delta^{14}\text{C}$ from the mixing line averages about 20 per mil. The time required for this loss via radiodecay is about 180 years. However, as we are dealing with a dynamic system this deficiency is best considered within the format of the processes ventilating this zone.

While we do not understand enough about these processes to make a realistic 3-D model for the deep western Atlantic, we can use the 1-D model shown in figure 7-28 to give us some idea of the rates involved. Shown in the right panel of figure 7-29 are the $\Delta^{14}\text{C}$ versus salinity trends expected for various values of the upwelling rate produced by the input of Vema Passage Water. As can be seen the best fit is achieved with a velocity of about 4m/yr. However this fit can be obtained only if the ratio of the flux of the densest northern component water to Vema Channel Water is reduced from the value of 10 used in the figure 7-28 example to about 4. The problem with this change is that it necessitates a temperature of 2.5°C and a salinity of $34.945^{\circ}/\text{oo}$ for the densest northern component water suggesting that the density of this water is even lower than we estimated from the properties of the water entering the northern part of the western basin.

An upwelling rate of 4m/yr for the Vema Channel Water then yields an upwelling rate of 16 m/yr for the most dense northern component water. As the area of western basin of the Atlantic at a depth of 4 kilometers is about 3×10^{13} square meters the flux of most dense northern component water comes out to be 4.8×10^{14} m^3/yr or 15 Sverdrups. The composition of this water is given in table 7-5. To this must be added the production of lower density northern component water. We estimate that this contribution would raise the flux from 15 to about 20 Sverdrups.

The eastern Atlantic is fed by water originating in the western equatorial Atlantic. Water with a composition corresponding to the upper part of the sub-TDD mixing zone in the western basin spills through the Romanche Passage (located just south of the equator) and through the Vema Passage (located 10° north of

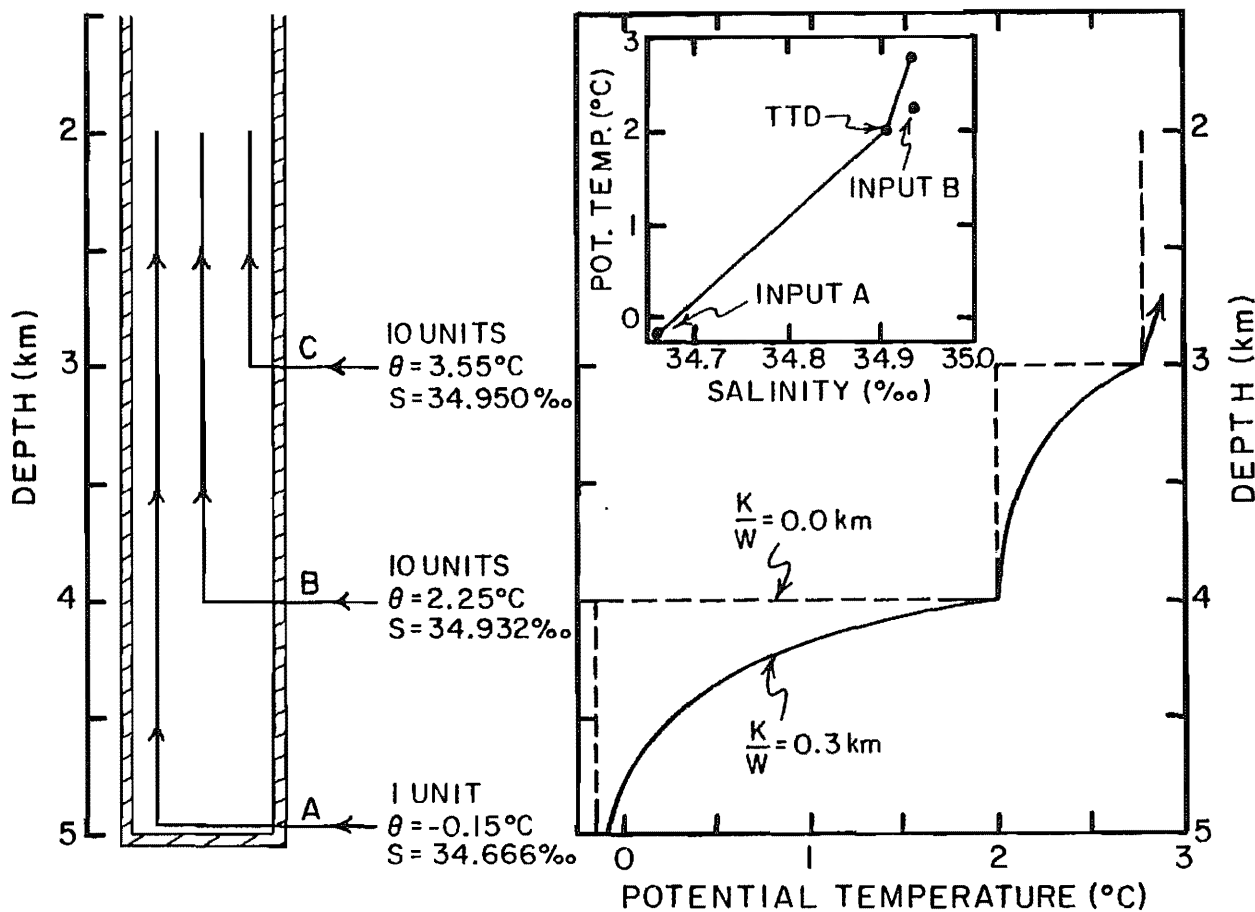


Figure 7-28. One-dimensional model designed to demonstrate the possible origin of the Two-Degree Discontinuity. Waters of differing composition are injected into a 5 kilometer high column at three different levels. This water rises and spills over the top of the column. The θ - S diagram produced in this way resembles that found throughout the deep Atlantic. The shape of the temperature profile in the column depends on the ratio κ/w . Note that the composition at the discontinuity in θ - S slope does not correspond to that of input water B! Rather it lies along the line joining the compositions of water types A and B.

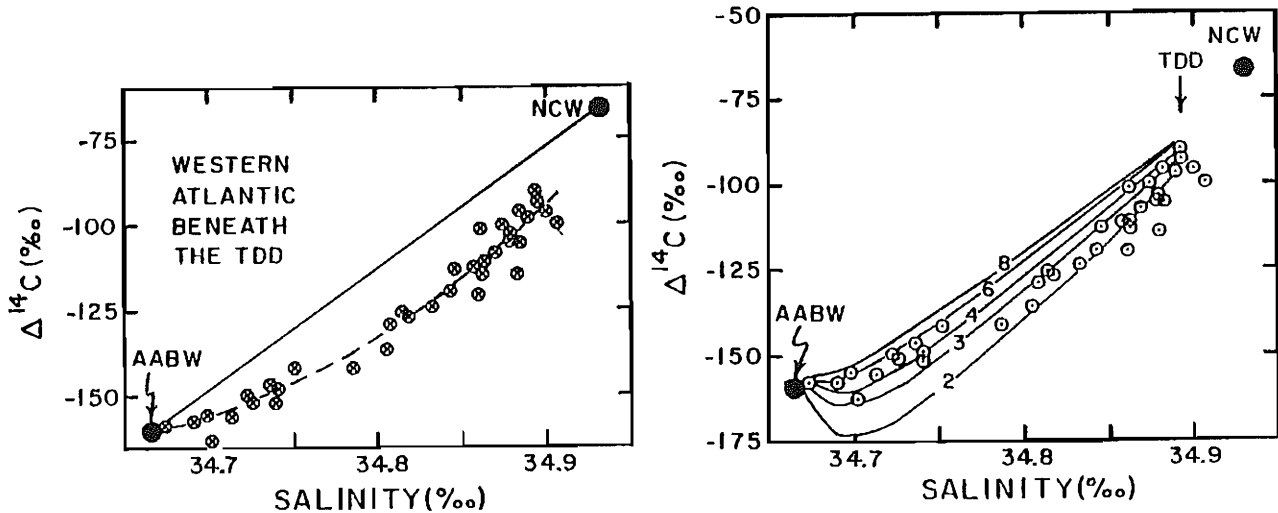


Figure 7-29. In the left hand panel is shown a plot of $^{14}\text{C}/\text{C}$ ratio (expressed as $\Delta^{14}\text{C}$) against salinity for waters below the TDD in the western Atlantic. The compositions of the water entering the southern end of this basin through the Vema Channel and of the most dense northern component water are shown by the solid circles. Were there no radiodecay, the $\Delta^{14}\text{C}$ values for the mixtures of these two water types found below the TDD should fall along the solid line. The deviation of the $\Delta^{14}\text{C}$ values below this line is thus the result of radiodecay. The radiocarbon measurements were made by Ostlund and Stuiver (21,22,23).

The right hand panel shows model calculations for the simple 1-D situation shown in figure 7-28. The individual curves are for a range of upwelling rates for AABW (given in meters/year). As can be seen a value of 4 m/yr gives the best fit. In these calculations the ratio of κ/w is set at 300 meters; the ratio of the flux of lower NADW to that of AABW is set at 4. Hence, for the best fit case the upwelling rate of lower NADW (i.e., the most dense northern component water) is 16 meters/year.

the equator) and floods the abyssal regions of the eastern basin.

VENTILATION OF THE DEEP PACIFIC AND INDIAN OCEANS

The abyssal regions of the Indian and Pacific Oceans are each fed by just one major source. This source water is in each case a mixture of northern and southern component water. The western Indian Ocean is fed by the spillover of circumpolar water through the Atlantis Passage (32°S , 50°E). The North Pacific is fed by water from the circumpolar region passing through the Samoan Passage (12°S , 179°W). Once in these basins the bottom waters show gradations in composition away from the point of entry (both along the bottom and in the vertical) as the result of cross isopycnal mixing with less dense water. The origin of this dilution water is not easily pinned down. In part, it is water that has mixed downward from intermediate depths; in part, it is water from the circumpolar region which has been transported into the basin along isopycnal surfaces. The characteristics of the water in question are summarized in table 7-5.

The reason we must be concerned with this diluting water is that it carries different $\Delta^{14}\text{C}$ values from those of the bottom water spilling in through the passages. Hence, as in the Atlantic, changes in the $\Delta^{14}\text{C}$ within the basin are in part the result of radiodecay and in part the result of mixing.

The first step in understanding this dilution is to determine to what extent the compositions of these deep waters can be accounted for by mixing of northern component and southern component water alone. We have seen that the waters of the sub-TDD mixing zone in the western basin of the Atlantic can be generated by mixing these two components. Is this also the case for the other deep waters of the world oceans? Potential temperature is a questionable tracer in this regard. The reasons are that northern component waters show a range in temperature which is significant compared to the temperature difference between the two components and that geothermal heating may significantly modify deep sea temperatures on the long time scales for the ventilation of the deep Pacific and Indian Oceans. By contrast the ranges for S and for PO_4° for northern and southern component waters are considerably smaller than the difference between mean northern and southern component water. Thus, it is of interest to explore their use in this regard.

Northern component water has a PO_4° value averaging about $0.7 \mu\text{m}/\text{kg}$. Southern component water has a PO_4° value of about $1.3 \mu\text{m}/\text{kg}$. Those for the deep and bottom waters in the ocean fall within this range (see table 7-5). Northern component water has a salinity close to 34.93. Southern component water has a salinity of 34.63. Except for the ^{14}C minimum water in the deep North Pacific the deep and bottom waters of the ocean have salinities falling within this range (see table 7-5).

Let us examine the distributions of these properties in more detail. Sections of PO_4° throughout the deep sea are shown in figure 7-30. To the extent that deep waters are mixtures only of northern and southern component waters and to the extent that the AOU correction coefficient of 135 is valid, the contours of PO_4°

Table 7-5. Composition of the bottom water supplying the deep eastern Atlantic, the western Indian and the equatorial and North Pacific oceans. Also given are the compositions of the bottom waters within the interior of these basins and of the deep waters with the lowest $^{14}\text{C}/\text{C}$ ratio within these basins. Finally, the composition of water which has completed the loop around the Antarctic continent and is about to reenter the Atlantic sector via the Drake Passage (between the tip of South America from the Palmer Peninsula of Antarctica) is given. The hydrographic and chemical measurements were made as part of the GEOSECS program (406, 424, 425, 426). The radiocarbon data were obtained in the laboratories of Minze Stuiver and Göte Ostlund (21, 22, 23).

Water Type	θ °C	S ‰	σ_4 ‰	PO_4° µm/kg	NCW %	ΣCO_2 µm/kg	Obs. $\Delta^{14}\text{C}$ ‰	$\Delta\Delta^{14}\text{C}$ ‰/‰*	$\Delta\Delta^{14}\text{C}$ ‰/‰**
Eastern Atlantic Ocean									
Input	1.69	34.858	45.96	0.90	66	2207	-113	--	-17
No. Bottom	1.94	34.886	45.94	0.86	73	2206	-115	-2	-25
No. $^{14}\text{C}/\text{C}$ min	2.20	34.909	45.91	0.86	73	2209	-119	-6	-29
So. Bottom	1.91	34.877	45.93	0.85	75	2218	-118	-5	-29
So. $^{14}\text{C}/\text{C}$ min	2.10	34.889	45.91	0.82	80	2216	-123	-10	-36
Western Indian Ocean									
Input	0.52	34.707	46.05	1.22	13	2269	-160	--	-17
Bottom (7°S)	0.84	34.716	46.00	1.17	21	2286	-171	-11	-45
$^{14}\text{C}/\text{C}$ min (6°N)	2.02	34.765	45.83	1.09	35	2334	-194	-34	-71
Equatorial and North Pacific Ocean									
Input	0.64	34.706	46.03	1.19	18	2270	-162	--	-24
Bottom (31°N)	0.97	34.694	45.96	1.13	28	2293	-205	-43	-75
$^{14}\text{C}/\text{C}$ min (32°N)	1.62	34.632	45.80	1.00	--	2370	-245	-83	--
Antarctic									
Drake Pas. Bot.	0.19	34.688	46.09	1.18	20	2264	-163	--	-27
Drake Pas. Deep	1.09	34.723	45.96	1.08	37	2264	-162	--	-25

*Difference from input water.

**Difference from endmember mixture.

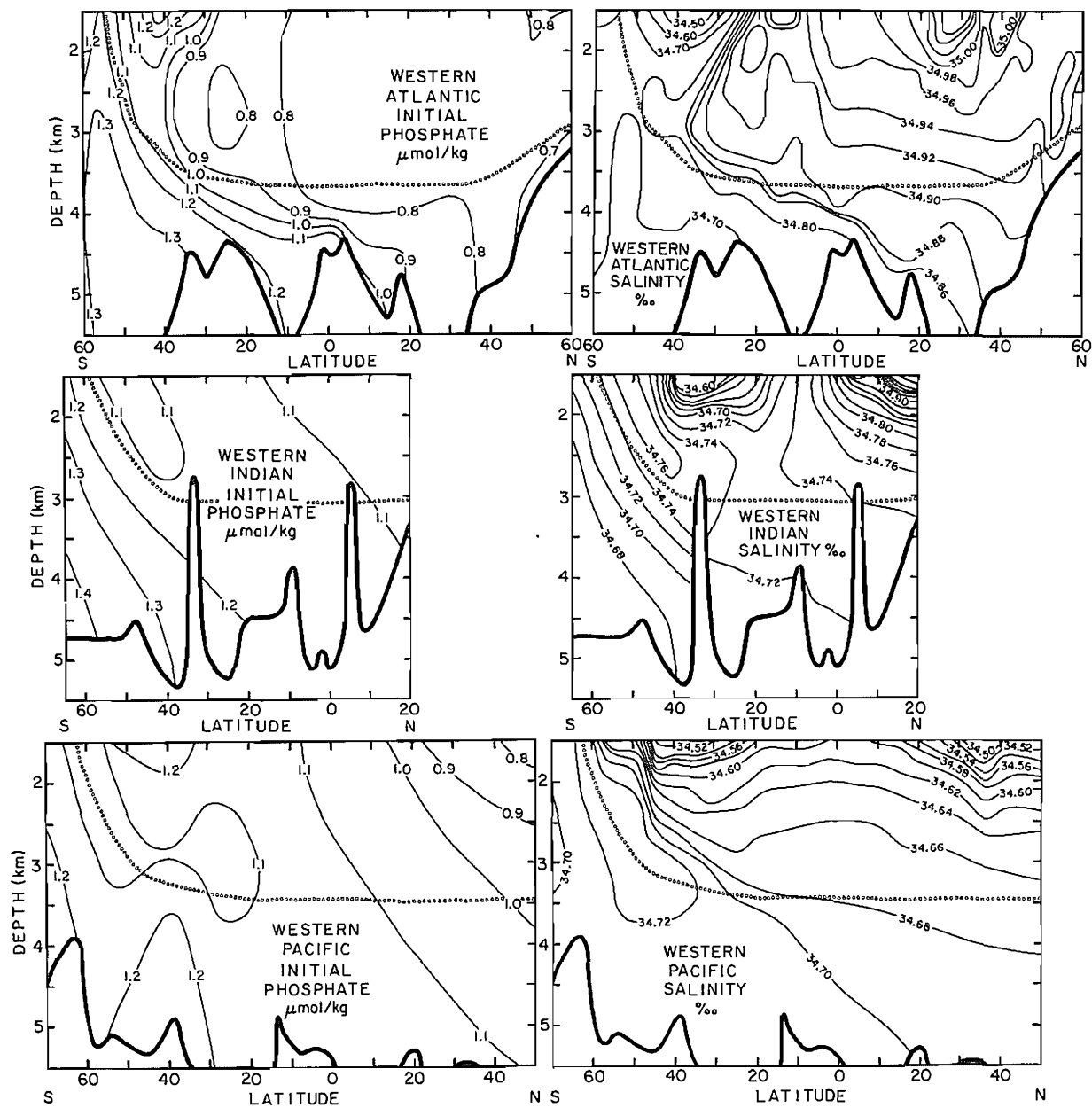


Figure 7-30. Sections of the initial phosphate concentration and of salinity in deep waters of the western Atlantic Ocean (upper panels), in deep waters in the western Indian Ocean (middle panels), and in deep waters in the western Pacific Ocean (lower panels). The measurements on which this diagram is based were made as part of the GEOSECS program (424, 425, 426). Also shown by the dotted lines is the $\sigma_4 = 45.2$ ‰ isopycnal horizon.

in these sections represent the fraction northern component water ($0.8 \mu\text{m}/\text{kg}$ would correspond to 83% northern component, 0.9 to 66%, 1.0 to 50%, 1.1 to 34%, and 1.2 to 17%). The pattern in the Atlantic (at least below 2.5 km) is consistent with what we have already learned. The bulk of the deep water in the Indian Ocean and in the equatorial and south Pacific lies in the range 1.1 to 1.2 $\mu\text{m}/\text{kg}$ (hence, appears to be $25 \pm 10\%$ northern component). In the North Pacific the PO_4° values show a decline reaching below 0.9 in the upper deep waters. This decline reflects either the input (by vertical mixing) of intermediate depth waters formed in the northern Pacific or a deviation in the C/P ratio of the organic material oxidized in the deep Pacific from the Redfield value of 135.

Corresponding sections for salinity are also shown in figure 7-30. The pattern is similar to that seen for PO_4° . The salinity grades along the path of the deep current from the high values characterizing northern component water to values closer to that for southern component water. The ambient salinity for deep and bottom waters of the Indian and Pacific Ocean again corresponds to a mixture containing $25 \pm 10\%$ northern component water. Deep water in the north Pacific is again anomalous, its salinity is very low. This water has a salinity corresponding to that of waters rich in southern component water and a PO_4° corresponding to that of waters rich in northern component. It appears that this water receives a contribution from the downward mixing of intermediate water.

Another way to look at this situation is to plot salinity against PO_4° (see figure 7-31). Most deep and bottom waters fall close to the trend expected if they were produced by mixing northern and southern component water. Deep waters from the Pacific do not. They have PO_4° -S coordinates falling well below that produced by endmember mixing.

As shown in figure 7-31 plots of potential temperature versus PO_4° for the same water types fall with one exception (i.e., Indian Ocean $^{14}\text{C}/\text{C}$ minimum water) within the composition triangle for mixtures of northern and southern component water. Surprisingly the situation for θ and PO_4° is more concordant than that for S and PO_4° (see figure 7-31). A possible reason for this is that the $\theta-\text{PO}_4^\circ$ coordinate for the third contributor to North Pacific deep water lies along the line joining the coordinates of northern and southern component water. This just demonstrates how difficult this problem is. If we are to sort it out we need highly accurate $\delta^{18}\text{O}$ (or δD) data for these waters. Like salinity these isotopic compositions are truly conservative. Unfortunately, samples collected for this purpose as part of the GEOSECS program were never analyzed.

THE GRAND CYCLE OF RADIOCARBON IN THE DEEP OCEAN

The mean $\Delta^{14}\text{C}$ value for waters at depths greater than 1.5 kilometers is about $-1750/\text{ppm}$. The mean ΣCO_2 concentration for these waters is 2.3 moles/m^3 . Their volume is about $8 \times 10^{17} \text{ m}^3$. Hence, the deep sea contains about $0.825 \times 1.20 \times 10^{-12} \times 2.3 \times 8 \times 10^{17}$ or 1.8×10^6 moles of radiocarbon. One part in 8200 or

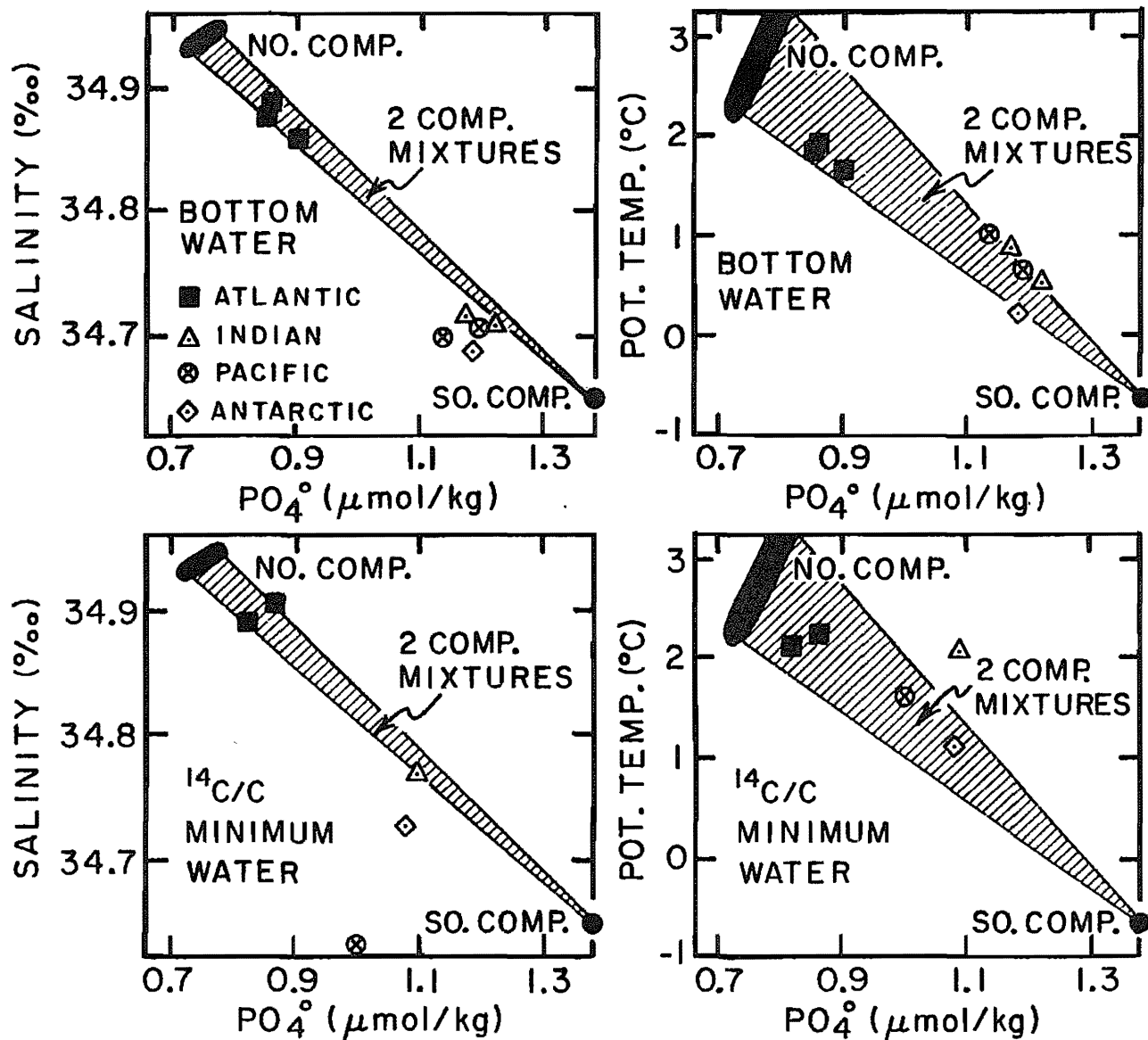


Figure 7-31. Plots of salinity and potential temperature against initial phosphate concentration for the major bottom waters (upper panel) and for the major ¹⁴C/C minimum waters (lower panel) in the world ocean. The compositions of the endmember waters are also shown.

about 222 moles of these ^{14}C atoms undergo decay each year. The $\Delta^{14}\text{C}$ value for the two major sources of ventilation of the deep sea are $-67\text{\textperthousand}$ (for northern component water) and $-154\text{\textperthousand}$ (for southern component water). The entry of this water and the rain of carbon-bearing particulates must balance the decay of radiocarbon occurring in the deep sea. Northern component water enters the deep sea at the rate of about $6 \times 10^{14} \text{ m}^3/\text{yr}$ (i.e., about 20 Sverdrups). It carries about 2.1 moles/ m^3 of ΣCO_2 ; its ^{14}C to C excess over ambient deep water is $(0.933-0.825) 1.2 \times 10^{-12}$ or 1.3×10^{-13} atoms ^{14}C per atom C. Thus, northern component water carries with it about $1.3 \times 10^{-13} \times 2.1 \times 6 \times 10^{14}$ or 164 moles of ^{14}C . Particulate debris rains to the deep sea carrying carbon with a $\Delta^{14}\text{C}$ value of about $-70\text{\textperthousand}$. The rate of fall of such debris is about 0.5 moles/ m^2yr . The area of the ocean at the 1500 meter contour is about $3 \times 10^{14} \text{ m}^2$. Thus about 1.5×10^{14} moles of carbon reach the deep sea each year in particulate form. Almost all of this carbon is returned to solution. The excess $^{14}\text{C}/\text{C}$ ratio for this carbon is $(0.930-0.825) 1.2 \times 10^{-12}$ or 1.3×10^{-13} . Thus, raining particles carry about 19 moles of ^{14}C . Combined with the 164 moles supplied by northern component water we have now explained the resupply of 183 moles out of the 222 lost to radioactive decay.

The remaining 39 moles of radiocarbon presumably accompany new southern component water. As there is no well-confined mixing chamber into which this water flows, an estimate for the flux of this water cannot be made from the ^{14}C distribution, as it was for the northern component water. One approach is to consider the relative proportions of northern and southern component water in the deep sea. Based on PO_4° data, it appears to be about 0.25 NCW and 0.75 SCW. If the mean residence time of the two components in the deep sea were similar then three times as much southern component water must reach the deep sea each year than northern component water. However, as the SCW is the most dense water in the sea and flows along the bottom of the ocean it is probably replaced on a longer time scale than NCW which overrides its more dense counterpart. We instead estimate its flux to be about the same as that of NCW (i.e., about 20 Sverdrups).

The flux of southern component water would then be $6 \times 10^{14} \text{ m}^3/\text{yr}$. The ΣCO_2 content of this water is about 2.2 moles/ m^3 . Its excess $^{14}\text{C}/\text{C}$ ratio is $(0.846-0.825) 1.2 \times 10^{-12}$ or 2.5×10^{-14} atoms ^{14}C per atom C. The flux of ^{14}C into the deep sea via this source is hence $2.5 \times 10^{-14} \times 2.2 \times 6 \times 10^{14}$ or 33 moles/yr. These calculations are summarized in table 7-6. Roughly 220 moles of ^{14}C are replaced in the deep sea each year.

These considerations suggest that the total flux of water into the deep sea is $12 \times 10^{14} \text{ m}^3/\text{yr}$ (i.e., 40 Sverdrups). The volume of the deep sea is about $8 \times 10^{17} \text{ m}^3$. Thus the characteristic flushing time is about 670 years. While this result is uncertain due to an inadequate knowledge of the rate of formation of southern component water, it is significantly less than the 1000 year figure given in chapter 3. Why the difference? Part of the reason lies in the fact that we have considered only the flushing of the sea below 1500 meters. Had we included the entire deep sea the time would have to be increased. The other reason is that in

Table 7-6. Summary of information needed to examine the budget of ^{14}C in the deep sea.

Loss

Via radioactive decay

Volume of water	$\sim 8 \times 10^{17} \text{ m}^3$
Mean ΣCO_2	2.3 moles/m ³
Mean $\Delta^{14}\text{C}$	-175‰
Mean $^{14}\text{C/C}$	1.00×10^{-12}
Amount of ^{14}C	1.8×10^6 moles
Amount ^{14}C decaying in deep sea (below 1.5km)	<u>222 moles/yr</u>

Gain

Via northern component water

Flux	$\sim 6 \times 10^{14} \text{ m}^3/\text{yr}$
ΣCO_2	2.1 moles/m ³
$\Delta^{14}\text{C}$	-67‰
$^{14}\text{C/C}_{\text{nc}} - ^{14}\text{C/C}_{\text{mean deep sea}}$	0.13×10^{-12}
Flux of ^{14}C	<u>164 moles/yr</u>

Via southern component water

Flux	$\sim 6 \times 10^{14} \text{ m}^3/\text{yr}$
ΣCO_2	2.2 moles/m ³
$\Delta^{14}\text{C}$	-154‰
$^{14}\text{C/C}_{\text{sc}} - ^{14}\text{C/C}_{\text{mean deep sea}}$	0.025×10^{-12}
Flux of ^{14}C	<u>33 moles/yr</u>

Via particulate rain

Carbon flux*	0.5 moles/m ² /yr
$\Delta^{14}\text{C}^{**}$	-70‰
$^{14}\text{C/C}_{\text{particles}} - ^{14}\text{C/C}_{\text{mean deep sea}}$	0.126×10^{-12}
Flux of ^{14}C	<u>19 moles/yr</u>

Total flux of new ^{14}C to deep sea

216 moles/yr

*The mean preformed PO_4 content of northern component water is $0.7 \mu\text{m}/\text{kg}$ and that of southern component water is $1.3 \mu\text{m}/\text{kg}$. If these two water types are fed to the deep sea in nearly the same amount then the preformed PO_4 content of new deep water averages $1.0 \mu\text{m}/\text{kg}$. The PO_4 content of deep water averages about $2.3 \mu\text{m}/\text{kg}$. Thus about $1.3 \mu\text{m}/\text{kg}$ was received by particles. If the C/P ratio for these particles is 125 then about $160 \mu\text{m}/\text{kg}$ or about 7% of the carbon was supplied by particles. The input of carbon to the deep sea is $12 \times 10^{14} \text{ m}^3/\text{yr} \times 2.15 \text{ moles C/m}^3$ or $2.6 \times 10^{15} \text{ moles/yr}$. Seven percent of this is 1.8×10^{14} moles/yr. The area of the sea at 1.5 km depth is about $3.2 \times 10^{14} \text{ m}^2$. Hence the flux is 0.56 moles/m²/yr.

**Because of the 20‰ depletion in ^{13}C relative to ^{12}C during photosynthesis there must be a 40‰ depletion in ^{14}C relative to ^{12}C . For CaCO_3 there is no depletion in ^{13}C . Hence the mean $\Delta^{14}\text{C}$ value for the raining organic matter should be -80‰ and that in the raining CaCO_3 -40‰. The composite should have a $\Delta^{14}\text{C}$ value close to -70‰.

the calculation in chapter 3 we assumed that the water ventilating the deep sea carried a $\Delta^{14}\text{C}$ of $-50\text{\textperthousand}$. As we have seen the actual values are far lower ($-67\text{\textperthousand}$ for northern component water and $-154\text{\textperthousand}$ for southern component water and hence $-125\text{\textperthousand}$ for a 1-to-2 mixture of these waters).

These ^{14}C -based rates are consistent with current meter results from key areas in the ocean where strong confined flows occur. Based on results from the northwestern Atlantic, Worthington of Woods Hole Oceanographic (701) estimates a flux of about 12 Sverdrups of new North Atlantic Deep Water (i.e., of northern component water). Nelson Hogg of Woods Hole Oceanographic placed current meters in the Vema Passage and established a flux of 4 Sverdrups of Antarctic Bottom Water (i.e., of southern component water) into the central western basin of the Atlantic (701). Current meter results from the Drake Passage reveal that deep water is being recirculated through the Antarctic at a rate of 130 Sverdrups (703,704).

BIOLOGICAL SHORT-CIRCUITING

As if we do not already have enough complications in our attempt to decipher the distribution of ^{14}C in the deep sea there are two more which must be considered. First, particles carrying ^{14}C to the deep sea short-circuit the mixing cycle. The apparent ages we get from ^{14}C reflect a composite between the age of the carbon carried by the water and the carbon carried by the particles. Second, even prior to the era of nuclear testing the $^{14}\text{C/C}$ ratio in the atmosphere varied with time. Hence, the carbon in the deep sea need not have left the surface with the $\Delta^{14}\text{C}$ values we reconstruct for the time immediately preceding the nuclear era.

In table 7-7 we give the differences between the $\Delta^{14}\text{C}$ value for deep waters within a given basin and the $\Delta^{14}\text{C}$ for the bottom water feeding these basins. We also give the ΣCO_2 contents of these waters. If we attribute the increase in ΣCO_2 to the destruction of particles within the basin, and assume that these particles originated with the $\Delta^{14}\text{C}$ for temperate and equatorial surface waters (i.e., averaging $-70\text{\textperthousand}$) we can then correct for the contribution of particles to the $^{14}\text{C/C}$ ratio. The magnitude of these corrections can be determined through a quite simple calculation. We will treat each water type shown in table 7-7 as a well-mixed reservoir fed directly by the input water. In such a situation the carbon balance is given by:

$$B + R[\Sigma \text{CO}_2]_I = R[\Sigma\text{CO}_2]_B \quad 7-6$$

where B is the flux of particulate carbon into the reservoir, R is the flux of input water into the reservoir, and $[\Sigma\text{CO}_2]_I$ and $[\Sigma\text{CO}_2]_B$ are the concentrations of dissolved inorganic carbon in the input and in the basin water, respectively. The corresponding material balance equation for radiocarbon is:

$$B \frac{^{14}\text{C/C}}{P} + R[\Sigma\text{CO}_2]_I \frac{^{14}\text{C/C}}{I} = (R+\lambda V) [\Sigma\text{CO}_2]_B \frac{^{14}\text{C/C}}{B} \quad 7-7$$

where $\frac{^{14}\text{C/C}}{I}$, $\frac{^{14}\text{C/C}}{B}$, and $\frac{^{14}\text{C/C}}{P}$ are, respectively, the

Table 7-7. Comparison of ventilation times calculated disregarding the contribution of particulates (τ) with those calculated including the contribution of particulates (τ^*).

Water Type	[ΣCO ₂] Input μm/kg	[ΣCO ₂] Basin μm/kg	$\frac{^{14}\text{C/C})_{\text{Input}}}{^{14}\text{C/C})_{\text{atm}}}$	$\frac{^{14}\text{C/C})_{\text{Basin}}}{^{14}\text{C/C})_{\text{atm}}}$	τ Basin yr	τ* Basin yr
No. East Atl. Bot.	2207	2206	0.887	0.885	18	18
No. East Atl. ¹⁴ C Min.	2207	2209	0.887	0.881	56	56
So. East Atl. Bot.	2207	2218	0.887	0.882	46	49
So. East Atl. Bot.	2207	2216	0.887	0.877	94	95
Western Ind. Bot.	2269	2286	0.840	0.829	109	115
Western Ind. ¹⁴ C Min.	2269	2334	0.840	0.806	346	371
Western Pac. Bot.	2270	2293	0.838	0.795	444	453
Western Pac. ¹⁴ C Min.	2270	2370	0.838	0.755	901	944

radiocarbon to stable carbon ratios in the input water, the basin water, and in particulate matter, and λ is the decay constant for ^{14}C . These equations can be combined to eliminate B. Also τ^*_{basin} , the basin ventilation time, can be substituted for the ratio V/R and $\tau^{14}\text{C}$, the mean life of ^{14}C , can be substituted for the $1/\lambda$. The resulting equation is:

$$\tau^*_{\text{basin}} = \frac{\left[\frac{^{14}\text{C/C})_P}{^{14}\text{C/C})_{\text{atm}}} - \frac{^{14}\text{C/C})_B}{^{14}\text{C/C})_{\text{atm}}} \right] + \left[\frac{^{14}\text{C/C})_I}{^{14}\text{C/C})_{\text{atm}}} - \frac{^{14}\text{C/C})_P}{^{14}\text{C/C})_{\text{atm}}} \right] \frac{[\Sigma\text{CO}_2]_I}{[\Sigma\text{CO}_2]_B}}{\frac{^{14}\text{C/C})_B}{^{14}\text{C/C})_{\text{atm}}}} \quad 7-8$$

This may be compared to the ventilation time, τ_{basin} , obtained if the particulate contribution is neglected (i.e., if $[\Sigma\text{CO}_2]_I = [\Sigma\text{CO}_2]_B$):

$$\tau_{\text{basin}} = \frac{\left[\frac{^{14}\text{C/C})_I}{^{14}\text{C/C})_{\text{atm}}} - \frac{^{14}\text{C/C})_B}{^{14}\text{C/C})_{\text{atm}}} \right]}{\frac{^{14}\text{C/C})_B}{^{14}\text{C/C})_{\text{atm}}}} \quad 7-9$$

The results of such comparison are shown in table 7-7. While the absolute values of the residence times are not to be taken as highly meaningful (the configuration of the ventilation model is not adequate), the ratio of one time to the other is meaningful. In other words a more realistic model will give different absolute times but not different ratios of the times. The correction for particulate rain will be on the order of 10% or less. This is the same result as was obtained for the deep ocean as a whole (19 of the 216 moles of ^{14}C entering the deep sea come with particulates). Thus, while a correction should be made, the error introduced by its neglect lies well within other uncertainties of the absolute ages.

TEMPORAL VARIATIONS IN RADIOCARBON PRODUCTION

The second complication stems from the fact that even before the onset of nuclear testing the $^{14}\text{C/C}$ ratio in the atmospheric carbon did not remain constant. This has been shown by precise $^{14}\text{C/C}$ measurements on tree rings. The record reconstructed by Minze Stuiver at the University of Washington for the last one thousand years is shown in figure 7-32. The results have been corrected for radioactive decay since growth, using the chronology obtained by counts of the growth rings. As can be seen the $^{14}\text{C/C}$ ratio in wood grown immediately before the onset of nuclear test-

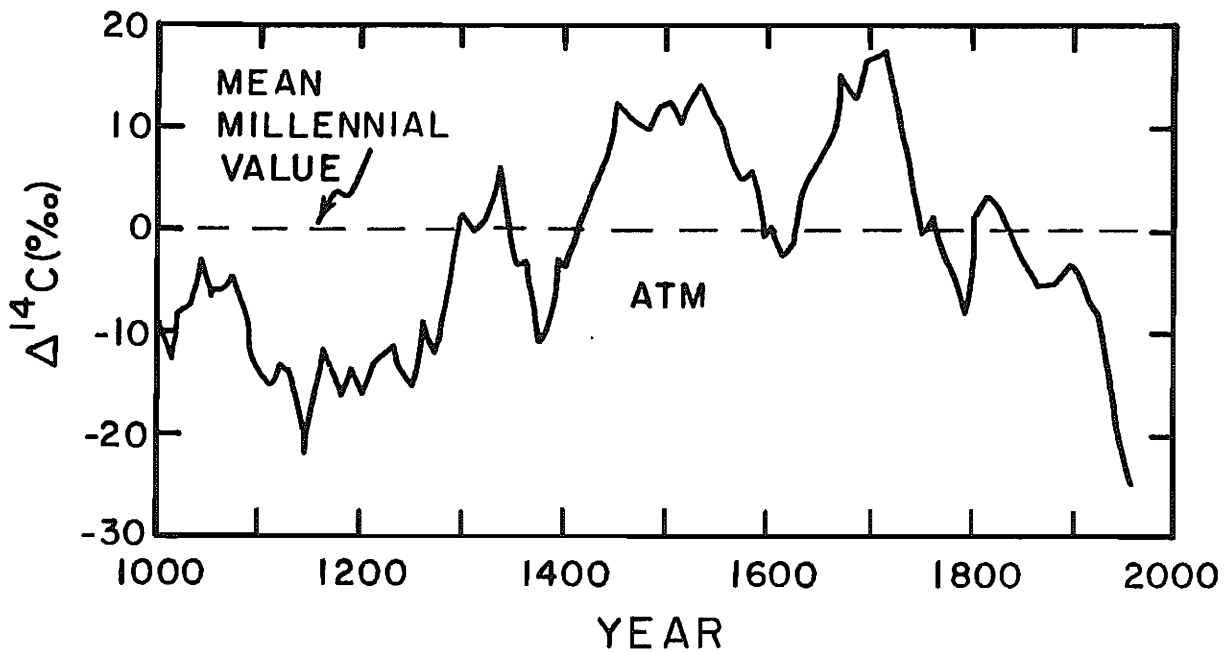


Figure 7-32. $^{14}\text{C}/\text{C}$ ratio (expressed as $\Delta^{14}\text{C}$) for atmospheric CO_2 over the last 1000 years as reconstructed from measurements made on tree rings. The fluctuations prior to 1850 are thought to be the results of changes in the activity of the sun. The decline over the last 100 years is mainly the result of the addition of ^{14}C free CO_2 to the atmosphere through the burning of fossil fuels. These measurements were made by Minze Stuiver of the University of Washington (19,26).

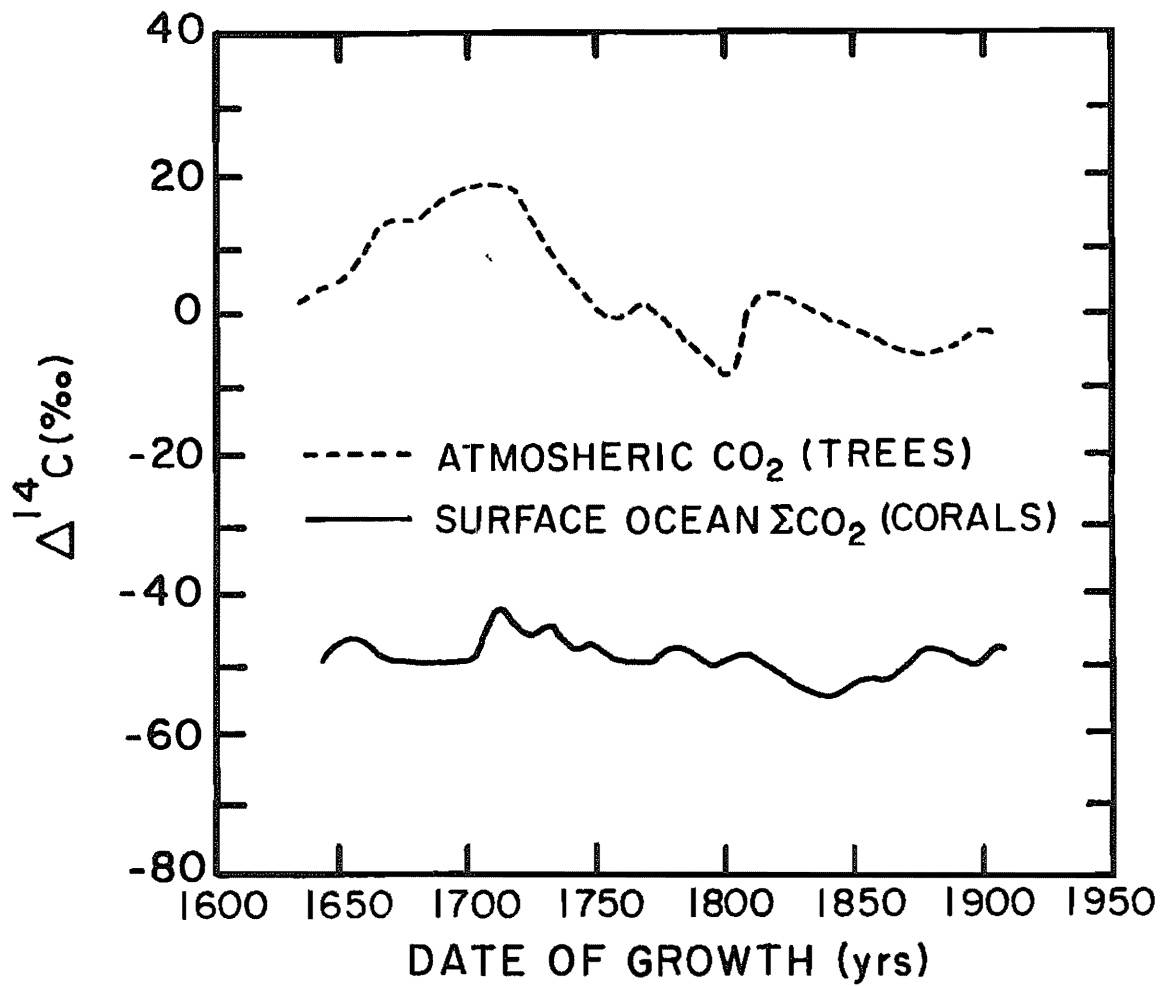


Figure 7-33. Comparison of the $\Delta^{14}\text{C}$ record for the atmosphere (based on measurements on tree rings) and the $\Delta^{14}\text{C}$ record for the surface ocean (based on measurements of coral rings) for the 1640 to 1900 AD time period. The coral measurements were made by Ellen Druffel in the laboratory of Hans Suess at the University of California at San Diego (15,16).

ing was lower than at any time during the last millennium. Three causes for these variations have been identified. First, there has been a long-term change in the strength of the earth's magnetic field. Since this field acts as a partial shield against the incoming cosmic ray protons, variations in its strength lead to variations in the rate of ^{14}C production. These variations lead to changes in ^{14}C production on the time scale of several thousand years. Second, there are shorter-term variations in conditions on the sun's surface (visible as "sun spots") which alter the sun's magnetic field. These changes also modulate the rate of ^{14}C production in the earth's atmosphere. They are responsible for the peaks in $^{14}\text{C/C}$ ratio spaced at roughly 200-year intervals. Finally, the emission of CO_2 free of ^{14}C from the burning of fossil fuels has caused the post 1850 decline in $^{14}\text{C/C}$ ratio. Because of this, the $^{14}\text{C/C}$ ratio in the atmosphere was about 22% lower during the early 1950's than it was on the average during the last millennium.

These changes must certainly have been reflected in changes in the $\Delta^{14}\text{C}$ value for the sources of bottom water. However, because of the complexity of the formation process it is not easy to gauge the relationship between the atmospheric and ocean changes. It is clear, however, that the changes in the source water $\Delta^{14}\text{C}$ values will not be as large as the changes in atmospheric $\Delta^{14}\text{C}$ values. Direct evidence is available to demonstrate that this is the case. The coral record obtained by Druffel at U.C. San Diego for the Florida Straits extends back to the year 1650. As can be seen from figure 7-33, the magnitude of the changes in the surface ocean $^{14}\text{C/C}$ ratio is much less than for the atmosphere. For example, there is no equivalent of the strong maximum in atmospheric $^{14}\text{C/C}$ ratio close to 1700 AD in the oceanic record. Between 1650 and 1900 AD the $\Delta^{14}\text{C}$ value for water in the Caribbean and Florida Straits remained constant to within $\pm 5\%$. Figure 7-34 shows the data on which the surface ocean curve is based. Since the scatter is quite large, the validity of the small wiggles seen in the mean curve is open to question. In this figure the record from 1900 to 1950 is included. Here a definite decrease paralleling that for the atmosphere is seen. Its magnitude is only about 8 per mil, which is 40 percent of that observed for the atmosphere over this period. Thus, while variations in the production rate of ^{14}C must be considered in connection with the interpretation of the ^{14}C distribution within the sea, in most cases their inclusion will produce only small changes in the results.

ARGON-39

One of the radiotracers, ^{39}Ar , mentioned in chapter 3, has yet to be discussed. As ^{39}Ar is produced by cosmic ray impacts and has a half-life of 280 years, its steady state distribution within the ocean should have much to say about the time scale of deep sea ventilation. Not only is its half-life more suitable for the task than that of ^{14}C , but unlike ^{14}C the ^{39}Ar content of new deep water should be at equilibrium with the atmosphere. Our reason for excluding this important isotope from our discussion of

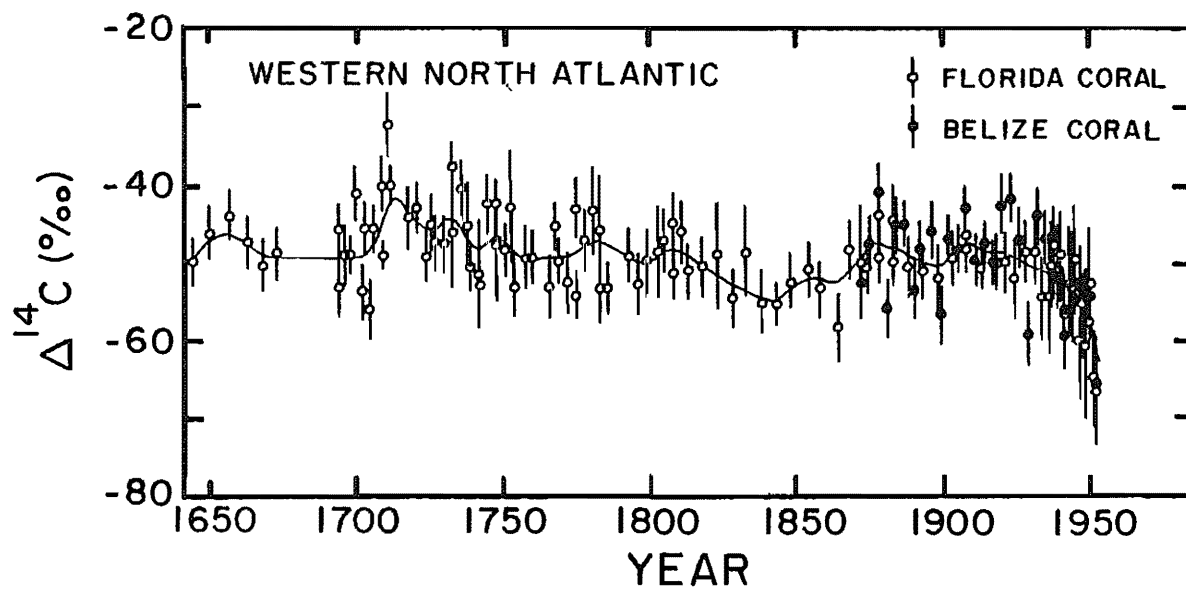


Figure 7-34. $^{14}\text{C}/\text{C}$ ratios (expressed as $\Delta^{14}\text{C}$) on growth ring dated coral samples from the Florida Straits and from the coast of Belize (Honduras) from 1650 to 1950. The post-1900 drop resulting from the input of fossil fuel CO_2 is apparent. The measurements were made by Ellen Druffel in the laboratory of Hans Suess at the University of California at San Diego (15,16).

deep sea ventilation is very simple: it has yet to be measured in the deep sea. The reason is that its abundance is so low, that even when the world's best low background counters are employed to detect its activity, about one ton of water must be processed in order to get enough ^{39}Ar to measure! Currently only the laboratory at the University of Bern in Switzerland has the capability of counting the ^{39}Ar obtained from even these very large water samples. At the time this book was being written several groups were collecting larger water samples and stripping the gas from them for delivery to Dr. Loosli in Bern. Hence, in a few years, there should be some new things to say about the time scales of deep ocean ventilation. When considered together, the distributions of ^{39}Ar and ^{14}C will put much stronger constraints on ventilation models than is possible with ^{14}C alone.

SUMMARY

The deep sea is ventilated from two small areas on the ocean surface. Northern component water is generated at the north end of the Atlantic, and southern component water is generated in the Weddell Sea on the perimeter of the Antarctic continent. Although these two water types have quite different temperatures, salinities and initial phosphate contents, their contributions to the water masses in the deep sea can be estimated in only an approximate manner. The paths by which these waters travel through the deep sea, although known in a general way, are not understood in detail. Diffusive mixing in the horizontal and in the vertical greatly blur the advective component of these motions.

The time scales for movement of these isotopes through the deep sea are largely based on the distribution of radioactive tracers. Shortlived ^{222}Rn and ^{228}Ra offer information regarding vertical and horizontal diffusive mixing within a single deep basin. ^{14}C provides the current basis for estimating the time scale for the ventilation of individual basins. However, due to the small extent of atmospheric equilibration for the carbon in the waters sinking from the surface of the Weddell Sea, the radio-carbon method does not give us a complete answer. The hope of the future is that ^{39}Ar data will allow this gap to be closed.

PROBLEMS

- 7-1 The following results were obtained for a profile of radon measurements in near-bottom waters:

<u>Distance above Bottom, meters</u>	<u>Radon Activity, dpm/100 liters</u>
200	20.3
100	19.8
50	20.7
40	21.2
30	24.1
20	36.3
10	84.0

What concentration of radon is produced by the ^{226}Ra dissolved in the water column? What is the apparent coefficient of vertical eddy diffusivity as determined from the distribution of excess (sediment-derived) radon?

- 7-2 If the coefficient for vertical (i.e., diapycnal) mixing averages $1 \text{ cm}^2/\text{sec}$ in the deep sea, then what must the coefficient for horizontal (i.e., isopycnal) mixing be in order to explain the distribution of excess ^3He in the deep Pacific Ocean?
- 7-3 How great must the coefficient of horizontal mixing be in order to be able to explain the near-uniformity of ^{228}Ra along isopycnals in the deep Atlantic?
- 7-4 What would the ratio of the $^{14}\text{C/C}$ in planktonic forams to that in benthic forams be in material formed recently in the North Pacific Ocean? Assuming that the rate of deep sea ventilation has remained constant with time what would be the ratio for material formed during the peak of Holocene time (i.e., about 6000 years ago) and for material formed during the peak of glacial time (i.e., about 18,000 years ago)? Were this method adopted to determine the ventilation rate of the ocean during glacial time, what size samples would be needed if an accuracy in the ventilation time of 200 years were desired? The conventional ^{14}C method involves the measurement of the beta particles emitted when ^{14}C atoms undergo radiodecay. Assume that these betas could be detected with 100% efficiency and that there was no background for the counter. Counts of one month would be made on each sample. A new method under development at the time this book was being written involved measuring individual ^{14}C atoms in a high-energy mass spectrometer. Assuming a detection efficiency of one atom in 10^3 in the sample used and again zero background, what sample size would be needed? Benthic forams weigh about $3 \times 10^{-5} \text{ g}$ each. The coarse fraction (>200 microns) in a deep sea core consists almost entirely of foram shells. Typically, about 3% are benthic (i.e., bottom-dwelling) and the rest are planktonic (i.e., surface-water-dwelling). How many forams would have to be viewed to find the required weight of benthics? How many benthics would have to be picked? If a person could find and isolate one benthic foram each minute, how many man hours would be required to prepare a sample?
- 7-5 Assume that deep waters form with an equilibrium amount of atmospheric gas. If so, what would you predict the ratios of the specific activity of ^{39}Ar in argon extracted from the following key water types to that in atmospheric argon to be?
Two-Degree Discontinuity Water
Southeastern Atlantic ^{14}C Minimum Water
North Pacific Bottom Water
North Pacific ^{14}C Minimum Water
Drake Passage Water

What are the major problems connected with making such estimates? Would the $^{39}\text{Ar}/\text{Ar}$ ratio in new southern component water as defined here be equal to that for the atmosphere? Why?

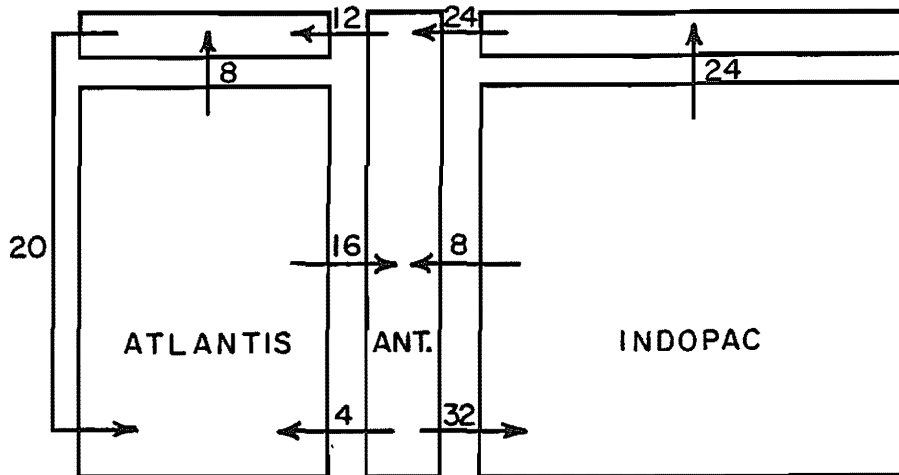
- 7-6 Were communication between the deep sea and the thermocline (plus surface ocean and atmosphere) suddenly cut, at what rate (% per hundred years), would the $^{14}\text{C/C}$ ratio in mean deep sea carbon and in atmosphere + surface ocean + thermocline carbon change? Assume that ninety percent of the carbon lies in the deep sea. Might climate-induced changes in the rate of deep sea ventilation then provide an alternate explanation for the variations in atmospheric $^{14}\text{C/C}$ ratio reconstructed from tree ring measurements?

SUPERPROBLEM #7

A geochemist named Gregg Hormone becomes interested in the relationship between the distributions of ^{14}C , ^{39}Ar and excess mantle derived ^3He in the ocean. He extends the computer aquarium of Stover and Eastland to include these two noble gases. Concerned about the role of the Antarctic Ocean, he decides to modify the number of boxes and their configuration. The box configuration and water fluxes he adopts are shown in figure 7-35.

Hormone decides, for simplicity, to neglect the biological cycles in the sea and assigns all the reservoirs a ΣCO_2 concentration of 2.2×10^{-3} moles/liter. He generates ^{14}C and ^{39}Ar atoms in the atmosphere and adds ^3He to the Indopac reservoir (but not to Atlantis). Gas exchange between the atmosphere and ocean is assumed to be limited by a stagnant film 50 microns in thickness. The areas of the interfaces are given along with the volumes of the reservoirs in figure 7-35. The area of the Antarctic outcrop is kept small in order to approximate the impedance of the thin layer of low salinity water which covers much of the Antarctic region.

Hormone then turns on the computer and allows the distributions of ^{14}C , ^{39}Ar and ^3He to come to steady state. What does he find for the $^{14}\text{C/C}$ ratio in each of the five reservoirs compared to that in the atmosphere? Compare the $^{14}\text{C/C}$ ratios with those actually observed. What is the ratio of the ^3He excess in each of the reservoirs relative to that in the Indopac reservoir? The observed ^3He excess for the Antarctic reservoir is about 0.4 that in the deep Pacific, and the ^3He excess in the Atlantic is about 0.1 that in Indopac. How do these compare with the computer model results? What does Hormone find for the $^{39}\text{Ar/Ar}$ ratio in each of the reservoirs compared to that in the atmosphere? How does the apparent radiocarbon age computed from the $^{39}\text{Ar/Ar}$ depletion in Indopac water (relative to the atmospheric argon) compare with the apparent radiocarbon age computed from the ratio of the $^{14}\text{C/C}$ depletion in Indopac water compared to warm surface water? What implications does this have to the use of ^3He to determine the rate of hydrothermal circulation in the ridge crests (see chapter 6)?



$$V_{ATLANTIS} = 2.7 \times 10^{17} \text{ m}^3$$

$$V_{ATL. SURF.} = 0.3 \times 10^{17} \text{ m}^3$$

$$V_{INDOPAC} = 8.1 \times 10^{17} \text{ m}^3$$

$$V_{INPAC. SURF.} = 0.9 \times 10^{17} \text{ m}^3$$

$$V_{ANTARCTIC} = 1.5 \times 10^{17} \text{ m}^3$$

$$A_{ATL. SURF.} = 0.9 \times 10^{14} \text{ m}^2$$

$$A_{INPAC. SURF.} = 2.7 \times 10^{14} \text{ m}^2$$

$$A_{ANTARCTIC} = 0.02 \times 10^{14} \text{ m}^2$$

Figure 7-35. Configuration, fluxes, volumes and interface areas for the reservoirs in the superproblem. The fluxes are in Sverdrups (i.e., 10^6 meter³/second).

LAST MINUTE ADDITION (SEPTEMBER 1982)

Loosli of Bern, Switzerland, has conducted several ^{39}Ar measurements on argon extracted from North Atlantic Deep Water by Smethie of Lamont-Doherty on the TTO expedition and by Roether of Heidelberg, West Germany on the METEOR expedition (both in 1981). These as yet unpublished results show a wide range of ^{39}Ar values, which are consistent with the accepted pattern of ventilation and the rough time scale provided by radiocarbon. Thus not only has Loosli demonstrated his ability to carry out reliably this very difficult measurement of the radioactivity of argon extracted from sea water, but also has proven its power as a sensitive time tracer for deep sea ventilation.

Chapter 8

THE ANTHROPOGENIC INVASION

THE MOVEMENT OF WATER THROUGH THE OCEANIC THERMOCLINE

INTRODUCTION

The activities of man result in the release of a host of substances to the environment. As might be expected, much of this material eventually reaches the sea. For our purposes we will divide these substances into two major categories. In the first category are those whose bulk is sufficient to impact the sea's chemistry. The lead released during the combustion of gasoline, the CO₂ generated by the combustion of fossil fuels, the oxides of nitrogen produced when nitrogen combines with oxygen in automobile engines, the phosphate mined for use in fertilizer and detergents and the SO₂ created during the combustion of coal and oil fall into this group. In the second category are those trace substances which can serve as tracers of oceanic processes. The ¹⁴C, ³H and ⁹⁰Sr produced during testing of nuclear devices, the freons lost from refrigerator coils and spewed forth from spray cans, and the ⁸⁵Kr produced in nuclear reactors fall in this group. In addition there are, of course, substances which have not yet been implicated with regard to possible chemical impacts and for which tracer applications have yet to be found.

In this chapter we focus our attention on the anthropogenic tracers. They constitute the most powerful tool we have for the study of the ventilation of the main oceanic thermocline. It is as if man were conducting an elaborate dye experiment to see how substances added to the ocean surface are carried to its interior. Through a knowledge of the patterns and time histories of the input of these tracers to the sea surface and a knowledge of the evolution of their distributions within the sea, much insight can be obtained with regard to the patterns and rates of circulation of waters in the ocean's upper kilometer.

INPUT FUNCTIONS

Although added to the environment over roughly the same time interval, the information obtained from individual anthropogenic tracers is not totally overlapping. Each tracer has its own special story to tell. To understand why this is the case we must look into the differences in the inputs of these tracers to the sea.

One characteristic of interest in this regard is the equilibrium partition coefficient of the tracer between air and sea

(i.e., the ratio of the amount of the tracer in the sea to the amount in the air after steady state partitioning has been achieved). We define the partition coefficient as the ratio of the amount of tracer in the sea to that in the air. For tritium and radiostrontium the partition coefficients are very large. Virtually all the tracer will be transferred from air to sea. For radiokrypton and the freons the distribution coefficients are quite small. Over 90% of these gases will remain in the atmosphere. Radiocarbon falls in between these extremes. At steady state about 1.5% of the ^{14}C will reside in the atmosphere. The differences among these three groups of tracers becomes even more pronounced when their distribution in the year 1973 (the mid-point of the GEOSECS surveys) is considered. At that time the ratio of anthropogenic ^3H in the ocean to that in the atmosphere was about 1000, for anthropogenic ^{14}C it was about 1, and for anthropogenic ^{85}Kr it was about 0.01. The fact that the wind-mixed upper layer of the sea can contain all the ^{90}Sr and ^3H reaching it from the air leads to a very rapid transfer of these isotopes from the troposphere to the sea.

These differences among the tracers affect their distributions in the sea in two major ways. First, they produce differences in the geographic pattern of entry of the tracers into the sea. Due to their very short time of residence in the atmosphere, ^3H and ^{90}Sr reach the sea surface in the same latitude belt as they were added to the troposphere. As far more nuclear testing was carried out in the northern than in the southern hemisphere, most of the tritium and radiostrontium reside in the oceans of the northern hemisphere. By contrast, ^{14}C , ^{85}Kr and the freons had spread throughout the atmosphere before entry into the sea. Hence, the inputs of ^{14}C and ^{85}Kr to the sea are nearly symmetrical about the equator.

A second way in which the contrast in partition coefficient imprints itself on the distributions of these substances in the sea is through the differences in the time histories of their inputs to the sea. The ^3H and ^{90}Sr atoms generated during nuclear tests reached the sea surface within a few weeks after their injection to the troposphere. The debris from the large tests (which generated most of the radioactivity) was carried through the troposphere into the stratosphere. Each spring stratospheric air is injected into the troposphere at latitudes of about 45° . These injections brought down the debris from the stratosphere to the troposphere in a period of a few years. The tests of very large nuclear devices were conducted by the USA, UK and USSR just prior to the signing of the test ban treaty in 1962. Most of the "fallout" from these tests reached the troposphere during 1962, 1963 and 1964. Thus at the time of the GEOSECS surveys (1972-1977), these isotopes had been in the ocean for about ten years. By contrast, at the time of these surveys, the ^{14}C produced during these same tests was still entering the sea in sizable amounts. As we shall see, this difference in input histories has particular importance to our understanding of processes taking place in the thermocline of the equatorial ocean.

As mentioned above tritium is delivered to the sea surface in two ways: THO molecules are incorporated in rain drops which fall

onto the sea and they impact the sea surface as water vapor. The contribution of rain has been assessed through measurements of the rate of rainfall and of the tritium content of rainwater during the "fallout" years. The time dependence of the tritium concentration in rain at a single station is shown in figure 8-1 and the latitude dependence of the tritium content of rain is shown in figure 8-2. This entry mechanism explains only about 20% of the ^3H present in the ocean. The remainder must have entered through the impact of water molecules onto the sea surface (a process far less easily quantified than delivery by rainfall). The geographic and time patterns of tritium input to the sea via vapor impact must be reconstructed in a less direct way. The T/H ratio in water vapor is assumed to be proportional to that in rain. As rains (but not vapors) from many places on the earth's surface were collected and analyzed for tritium during the critical years, this assumption provides an index of the delivery rate of tritium to the sea surface via vapor impact at any given place and time. The absolute delivery rate is then obtained by forcing the integrated ocean-wide vapor impact to match the amount of bomb-produced tritium found within the sea minus that accounted for by rainfall.* The results of the ^3H input reconstruction carried out by Roether and Weiss are summarized in table 8-1.

Two additional points must be made here with regard to tritium. First, the contribution of tritium produced by cosmic ray interactions is so small compared to that of tritium produced by nuclear testing that all the tritium measured during the GEOSECS surveys can be treated as anthropogenic. Second, the fact that tritium is radioactive and disappears with half-life of 12.2 years is not important to its use as an anthropogenic tracer. Its utility would be exactly the same were it stable. In fact, in the discussions which follow we will often normalize the tritium concentration for seawater samples collected in different years to the amount of tritium they would have contained had radiodecay not occurred.

What we have just said for tritium applies equally to ^{90}Sr . There is one difference: that ^{90}Sr 's reaching the continents in rain or by aerosol impact was absorbed very efficiently by soils. This has two implications. First of all, this ^{90}Sr does not move from continent to sea as does ^3H . Secondly, soils from flat grass-covered land provide excellent integrated records of the amount of ^{90}Sr fallout. Thus the latitude-dependence of ^{90}Sr fallout can be reconstructed directly from soil data. The record of ^{90}Sr delivery as function of time and of latitude are also shown in figures 8-1 and 8-2. As we see from these diagrams, the fallout patterns of tritium and ^{90}Sr are remarkably similar - so similar, in fact, that one might conclude that the information ^{90}Sr yields about the ventilation of the sea is no different from

*Actually, about 40% of the tritium added to atmosphere initially reached the continents rather than the ocean. Most of the tritium which reached the continents was subsequently transferred to the sea by either river runoff or by evaporation followed by molecular impact or rainfall on the ocean. This complicates the reconstruction of the input pattern and input history of tritium to the sea.

Figure 8-1. Plot of the mean ${}^3\text{H}$ content of rain at Valencia, Ireland from 1952 to 1974 (solid circles). Also given is the total annual northern hemisphere ${}^{90}\text{Sr}$ deposition (open circles). From this comparison it is clear that the time history of the input of these two isotopes is quite similar. The differences are related to the ratio of escaping neutrons (producing ${}^3\text{H}$) to uranium fissions (producing ${}^{90}\text{Sr}$) for the various bombs tested. This diagram was published by Dreisigacker and Roether (61).

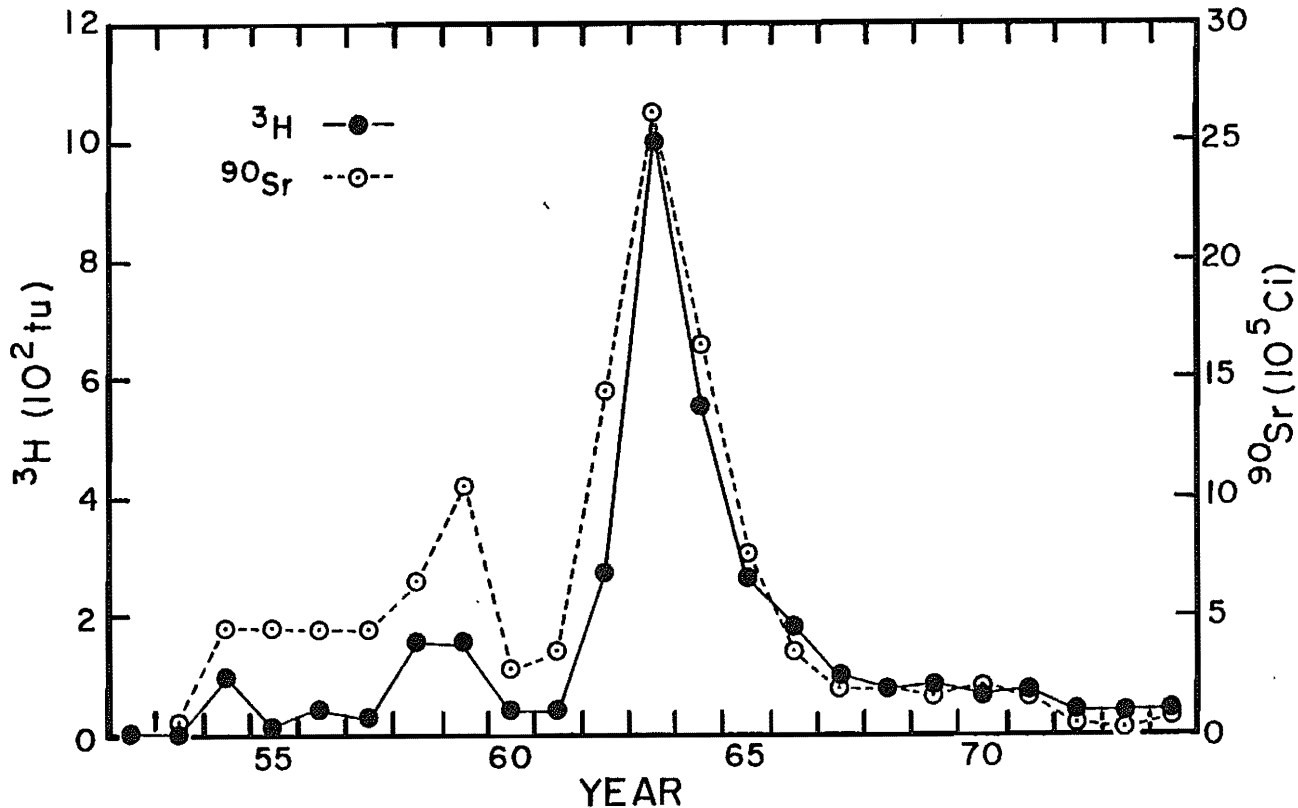


Table 8-1. Summary of the amounts of tritium added to the major oceans as of Jan. 1, 1973. The contribution of river inflow is separated from that of precipitation and vapor exchange. The units are 10^6 curies. This compilation was done by Weiss and Roether of Heidelberg, W. Germany (65).

	Northern Hemisphere			Southern Hemisphere			N + S
	Rain + Vap. exch.	Rivers	Total	Rain + Vap. exch.	Rivers	Total	Total
Atl.	520	175	695	105	10	115	810
Ind.	50	40	90	160	5	165	255
Pac.	650	60	710	230	10	240	950
A+I+P	1220	275	1495	495	25	520	2015

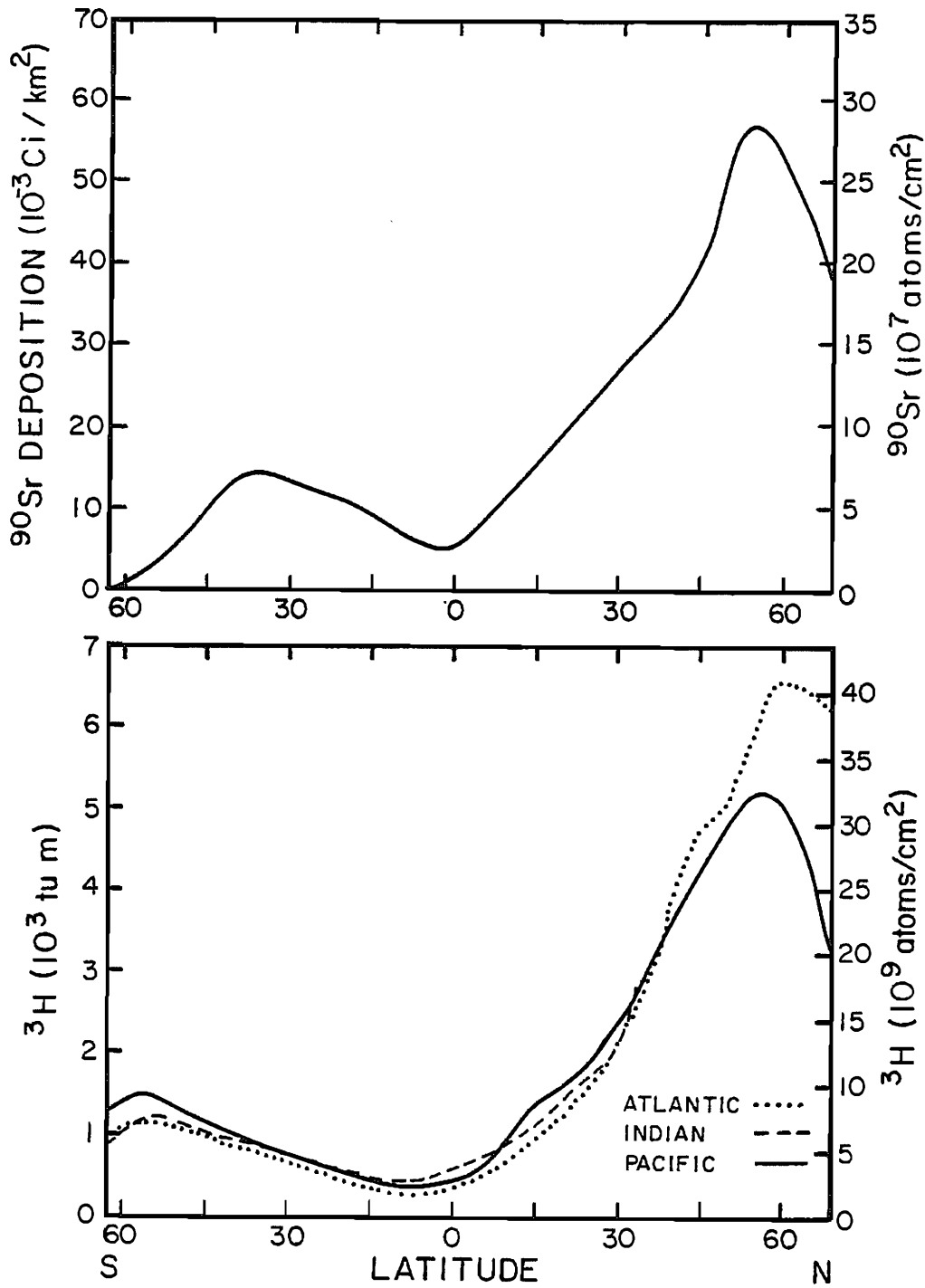


Figure 8-2. The upper panel shows the amount of ^{90}Sr accumulated on the earth's surface up to the year 1968 as a function of latitude. These estimates are based on the analyses of soils. The lower panel shows the latitude dependence of the total amount of ^3H reaching a unit area of ocean surface for the three major oceans as of 1973 as calculated by Weiss and Roether (65).

that yielded by ${}^3\text{H}$. While this is true we shall soon see, however, that there is a good reason to consider both these isotopes.

The radiocarbon produced during nuclear testing enters the ocean by molecular diffusion through the stagnant boundary layer. We get its input to the sea at any given place through a knowledge of the CO_2 exchange rate between air and sea and of the temporal records of the ${}^{14}\text{C}/\text{C}$ ratio in atmospheric CO_2 and in surface ocean ΣCO_2 . The latter is needed because some of the bomb ${}^{14}\text{C}$ atoms which enter the sea come back out again. Records for three major latitude bands are shown in figure 8-3. The atmospheric curves shown in this figure are based on measurements on CO_2 samples extracted from the air. The ocean record is based on radiocarbon measurements made on growth ring dated corals.* The $\Delta {}^{14}\text{C}$ difference between the atmosphere and surface sea curves provides a measure of the net input of ${}^{14}\text{C}$ to the sea. Part of this input is of course the steady state flux of natural ${}^{14}\text{C}$. To get the net flow of bomb-produced ${}^{14}\text{C}$, a correction must be made for the air-sea $\Delta {}^{14}\text{C}$ difference associated with this natural flux. Of course in order to calculate a flux, a CO_2 exchange rate must be assigned to the particular region of the ocean.

The concentrations of ${}^{85}\text{Kr}$ in surface ocean water should be everywhere very close to equilibrium with the partial pressure of this gas in the atmosphere (as is the case for O_2). Thus, in constructing models designed to reproduce the observed distribution of ${}^{85}\text{Kr}$ in the sea, the assumption is made that the surface ocean mixed layer is saturated with regard to this gas. The concentration of ${}^{85}\text{Kr}$ in surface water is then computed from a knowledge of the temporal history of the partial pressure of ${}^{85}\text{Kr}$ in the atmosphere (and the temperature of the water). This history (see figure 8-4) is documented by large numbers of radioactivity analyses on Kr gas separates made in air reduction plants. The situation for freon 11 and freon 12 is much the same as that for ${}^{85}\text{Kr}$. However, the history of the atmospheric partial pressures of these two compounds is not documented by measurements. Rather they are reconstructed from a knowledge of the world manufacture of these products. As freons have no place to go except the atmosphere and as their destruction rate in the atmosphere is very slow, this procedure should be valid. Curves showing the atmospheric histories reconstructed in this way are shown in figure 8-4.

HYDROLOGY OF THE MAIN THERMOCLINE

Before discussing the distributions of these anthropogenic tracers within the sea, it is necessary to set the stage by summarizing some of the pertinent information about this reservoir gained by more traditional observations. Of these, the most

*As for trees, annual growth bands can be identified in corals. This is done by cutting a several-millimeter-thick slab along the axis of corallite growth through a large coral head and then performing a medical x-ray on the slab. As the CaCO_3 precipitated by corals shows seasonal variations in density, the x-ray absorption varies producing growth bands on the film.

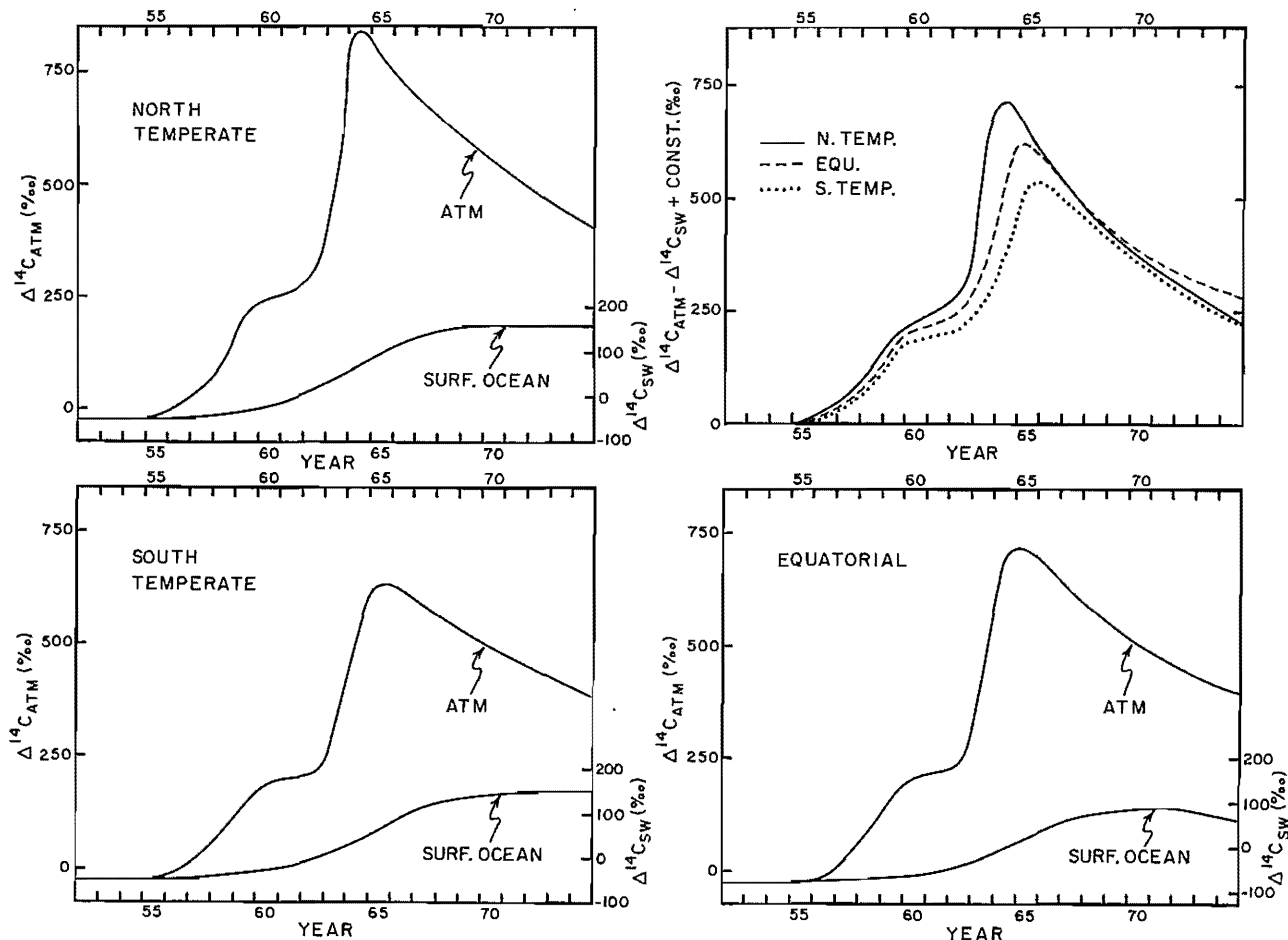


Figure 8-3. Plots of $\Delta^{14}\text{C}$ for atmospheric CO_2 and for surface water ΣCO_2 from 1952 to 1974. Separate curves are given for the north temperate zone (upper left hand panel), for the south temperate zone (lower left hand panel) and for the equatorial zone (lower right hand panel). The scale for the ocean curve has been shifted in order to eliminate the air-sea $^{14}\text{C}/\text{C}$ difference required to maintain the flux of natural radiocarbon into the sea. The differences between the three atmospheric curves stem from the finite mixing time of the atmosphere. As the tests were conducted mainly in the northern hemisphere, the north temperate atmosphere shows an earlier and stronger maximum than is seen in the other zones. In the upper right panel the difference between the atmosphere and surface ocean $\Delta^{14}\text{C}$ values are plotted against time. These curves show the extent to which the driving force for ^{14}C entry into the sea changes with time in the three zones. The zone to zone differences are quite small. The equatorial zone has an integrated driving force exactly equal to the average for the north and south temperate zones.

The radiocarbon trends for the atmosphere are based mainly on measurements made by Nydal and his coworkers in Trondheim (7,10, 24) and by Munnich and his coworkers in Heidelberg (9,25). The surface water curves are based mainly on measurements made during the GEOSECS program (21,22,23) and on the ring-dated coral measurements by Druffel (15,16,17).

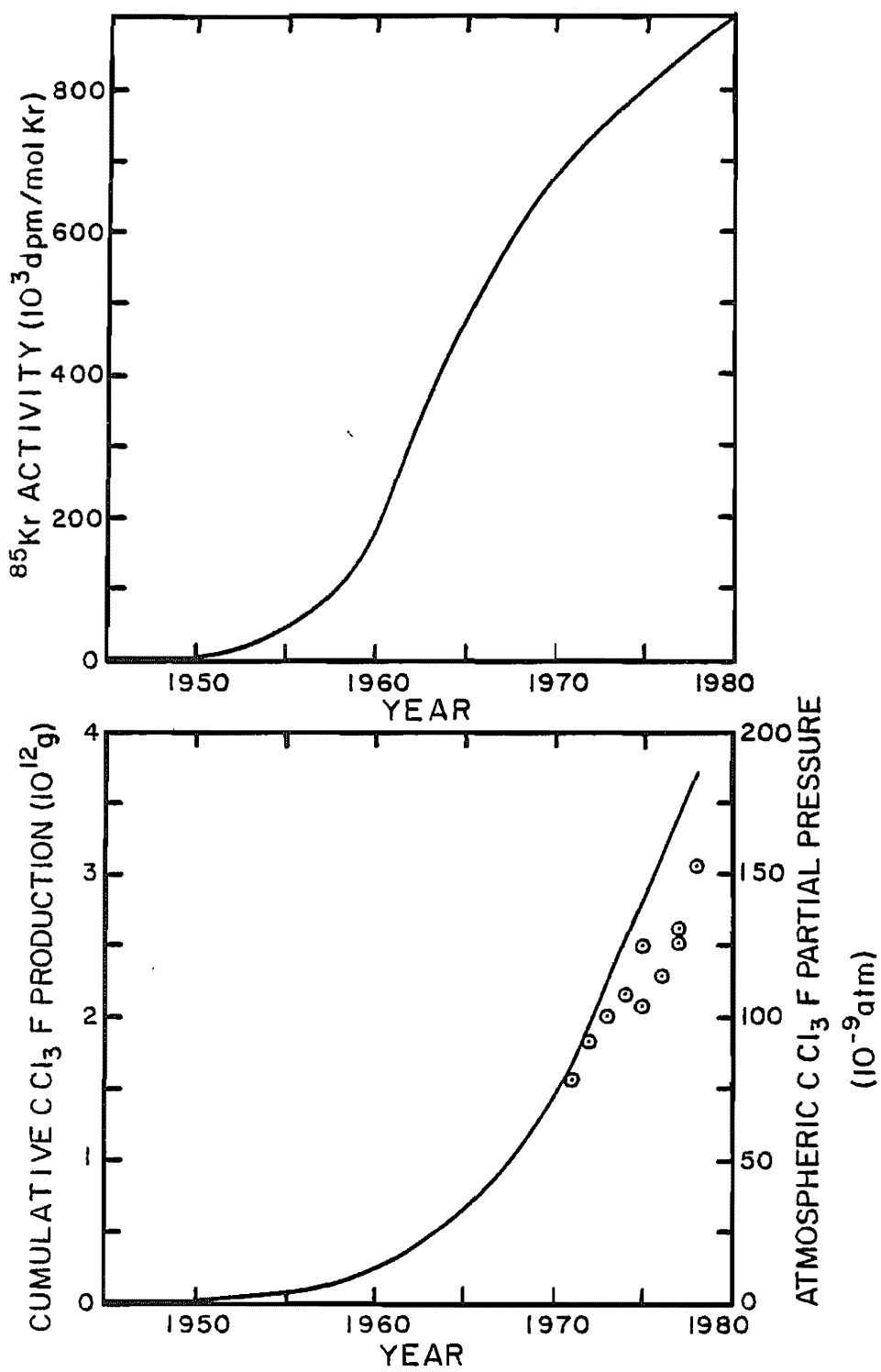


Figure 8-4. Plots of the ^{85}Kr and freon concentrations in the atmosphere as a function of time. The ^{85}Kr curve is based on direct measurements (107,110). That for CCl_3F curve is calculated from data on the manufacture of this substance.

important is depth structure of isopycnal horizons. As we shall see, this structure provides the basis for subdividing the thermocline into a number of regional units. It also provides clues to the manner in which water moves through these units.

The topography of a number of key density horizons along sections through the western sides of the three major oceans is shown in figure 8-5. The most striking feature in these sections is the upward bulge of these horizons in the equatorial zone. Another prominent feature is the rise of the isopycnal horizons toward the surface in the latitude range 40° to 50° . Had these observations been made during the peak winter months, these horizons would have reached all the way to the surface. It is these topographic features which provide the basis for our thermocline subdivision. In each ocean we designate equatorial and temperate zones. The boundary between these zones is taken to be 15° (the latitude at which the slope of the isopycnal surfaces is the greatest). The poleward boundary of the temperate zones is taken to be 45° . At this latitude the key horizons are rising most steeply.*

Another important source of information comes from θ -S diagrams. Such diagrams are shown in figure 8-6 for key stations along the above sections. To understand the point of these diagrams one aspect of the ventilation of the main thermocline must be mentioned. It is the opinion of most physical oceanographers that at least in the temperate ocean, water reaches the interior of the thermocline along isopycnal horizons (i.e., new thermocline water is generated during winter months when the isopycnal horizons reach all the way to the ocean surface). A map showing the location of these outcrops in the North Atlantic is shown in figure 8-7.

This gives rise to an interesting situation: there are two sets of outcrops for each isopycnal, one in the northern ocean and one in the southern ocean. Where then, along each isopycnal horizon, does the boundary between the two water types lie? Or is there a continuous gradation in composition along each surface?

As seen in figure 8-6, the θ -S combination producing water of a given density is quite different in the north than in the south. In the Atlantic the northern waters are more salty than the southern waters. Hence the temperature of the water on any given isopycnal surface is warmer in the north than in the south. A map of temperature along the $26.75^{\circ}/oo$ isopycnal surface in the Atlantic is shown in figure 8-8. A sharp boundary between waters of northern and southern origin is seen in the vicinity of $15^{\circ}N$. In this ocean at least the thermocline of the equatorial zone is supplied primarily by waters originating in the south!

In the Pacific the situation is the reverse of that in the Atlantic. The northern waters are considerably less salty than the southern. As in the Atlantic, the equatorial waters are more nearly akin in their θ -S characteristic to the southern than to

*The Indian Ocean does not have a full-fledged, north temperate zone. Because the Indian Ocean is bounded at $\sim 20^{\circ}N$ by the Asian continent, its isopycnals do not reach the surface even during the wintertime. This leads to the very low O_2 concentrations seen in figure 3-11.

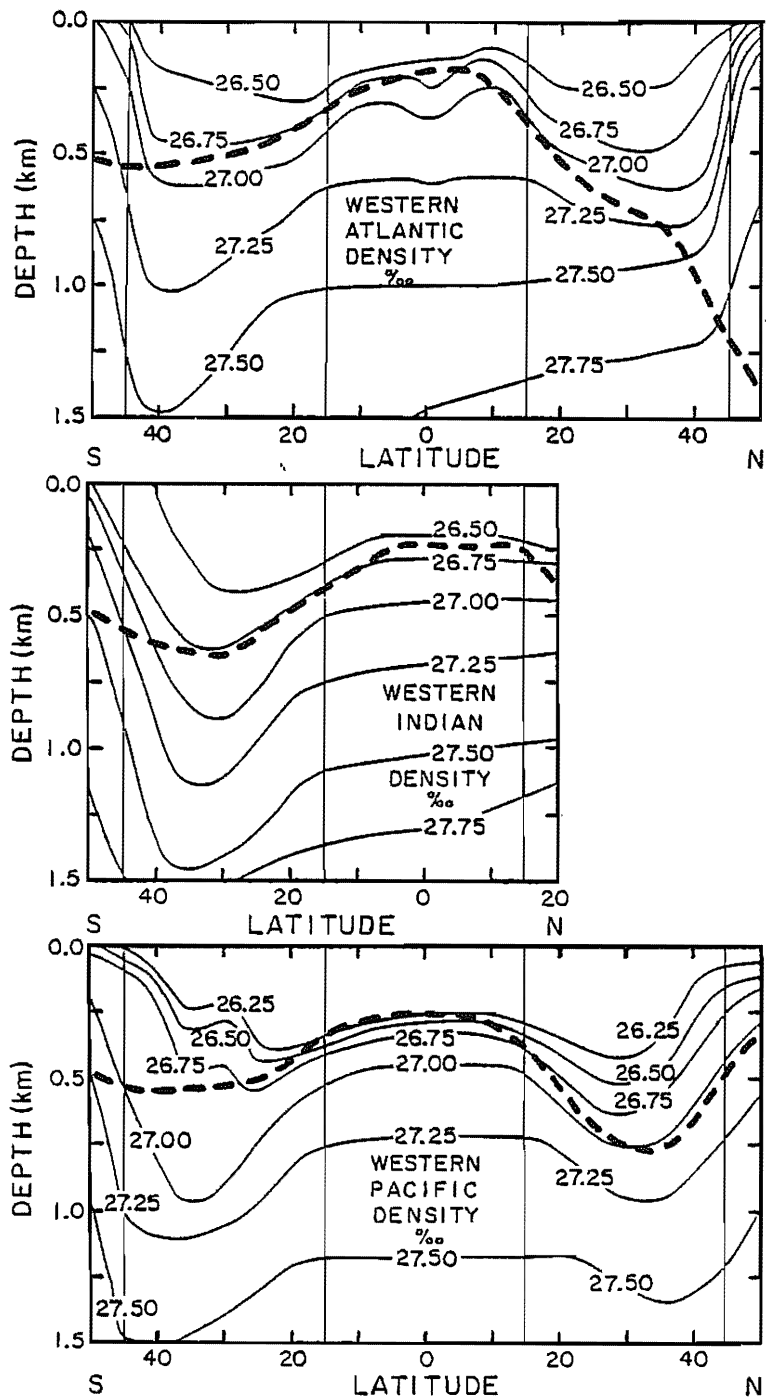


Figure 8-5. Sections along the western side of the world's three major oceans showing how the depth of various isopycnal horizons changes with latitude. The heavy dashed line shows the depth at which the tritium concentration of the water (at the time of the GESECS surveys) was one quarter that of the overlying surface water. Based on data obtained as part of the GEOSCES program (424, 425, 426).

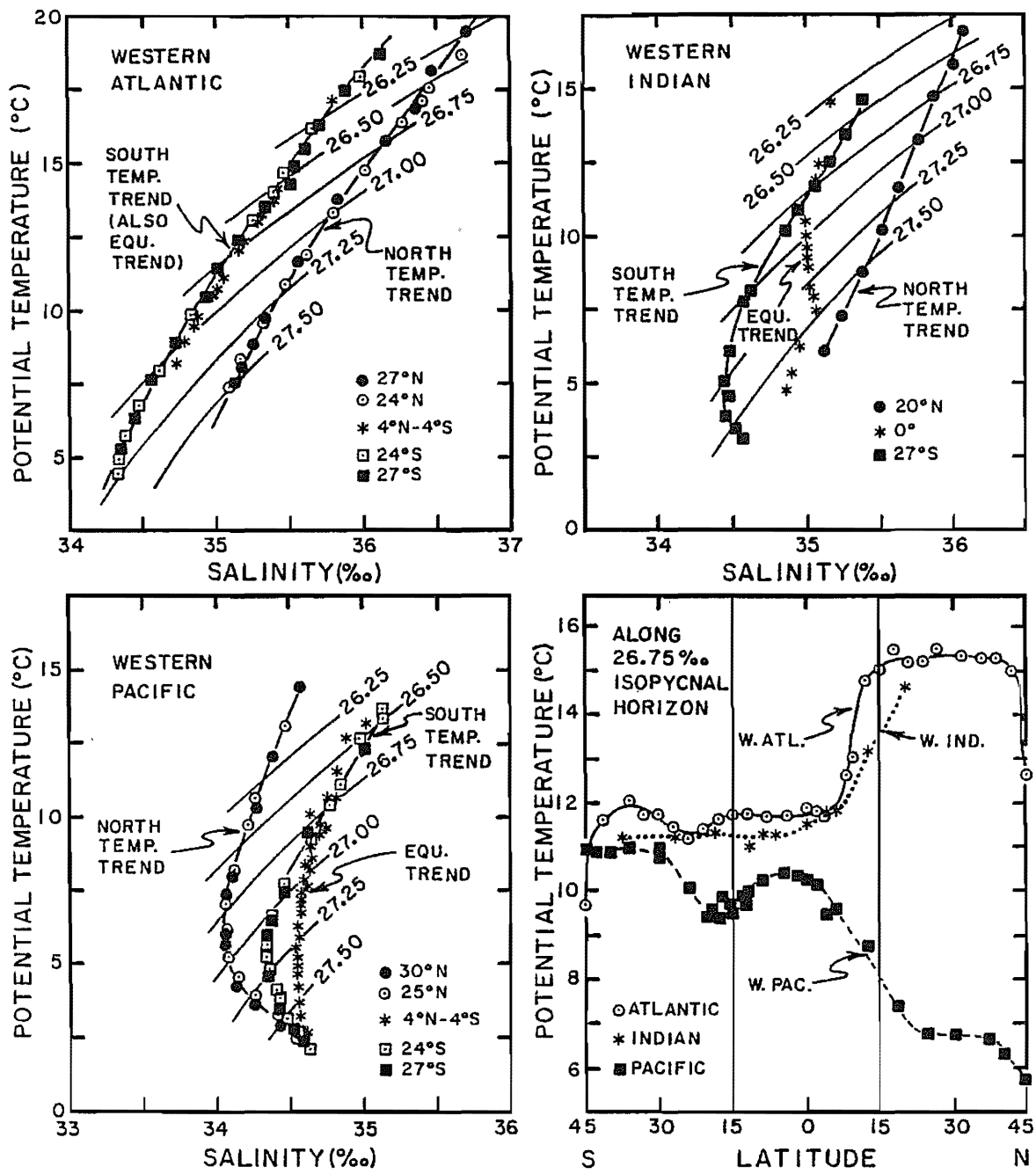


Figure 8-6. θ -S diagrams for the thermocline waters of the three major oceans. In each case the trends for north temperate, equatorial and south temperate waters are shown separately. Also shown are several key isopycnals. In the lower right hand panel the temperature of water along the $26.75^{\circ}/\text{oo}$ isopycnal horizon is shown as a function of latitude in the western part of each ocean. Based on data obtained as part of the GEOSECS program (424, 425, 426).

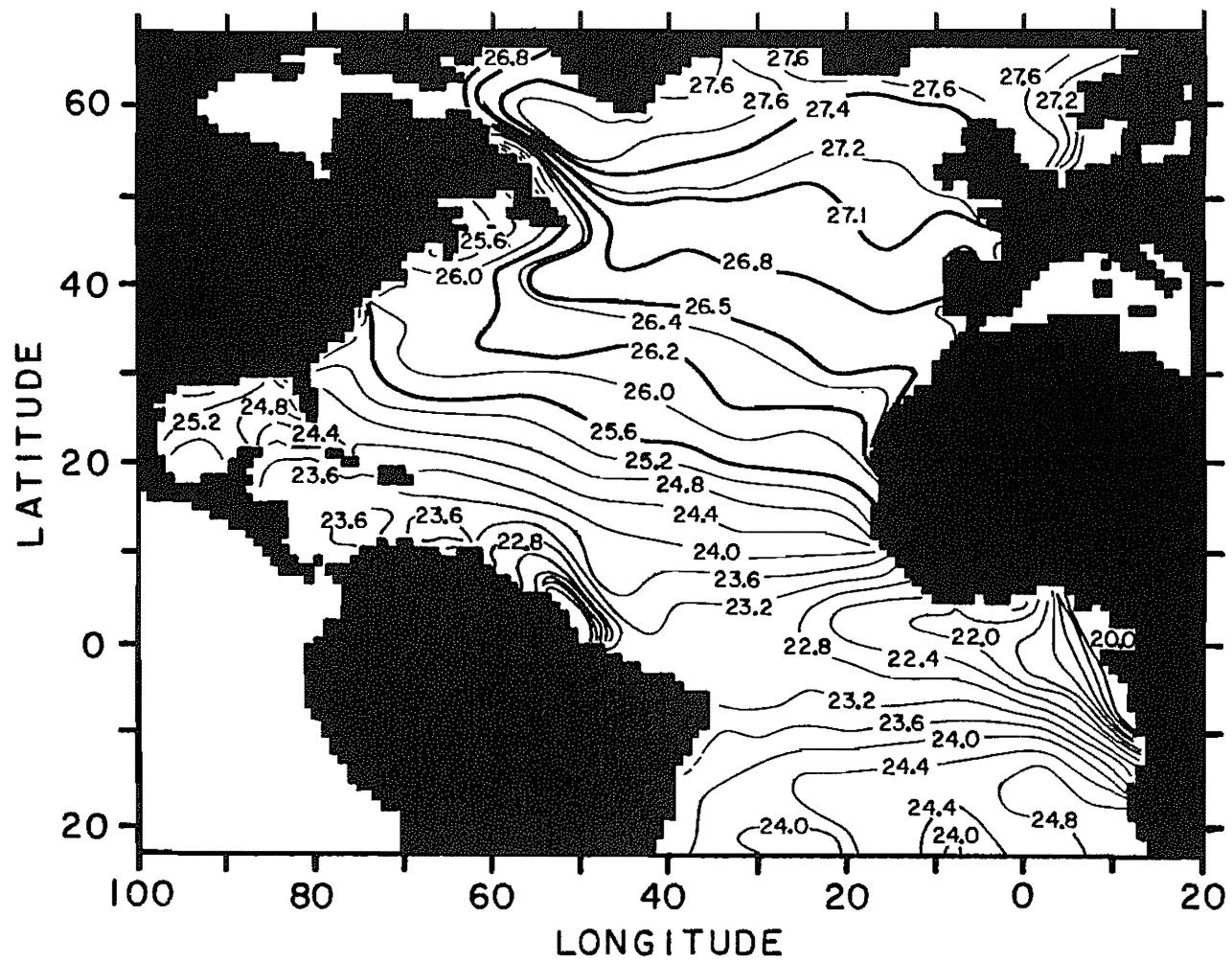


Figure 8-7. Map showing the winter outcrops of isopycnal surfaces in the North Atlantic Ocean. This map was constructed from the NOAA Geophysical Fluid Dynamics Group's oceanographic data files (689) by Jorge Sarmiento of Princeton University who kindly supplied this diagram for use in the book.

the northern water. In this connection it should be noted that in the deeper parts of the equatorial thermocline, the water on any given isopycnal has a higher salt content than either the water to the north or the south. Thus they could not have been produced by mixing of waters generated at the outcrops of the isopycnal surfaces. One explanation for this seeming dilemma is that the θ -S structure in the equatorial zone has been modified by vertical mixing (at least in density range 26.7 to 27.7‰).

The situation in the western Indian Ocean is similar to that in the Atlantic. The northern waters are saltier than the southern waters and the upper thermocline water in the equatorial zone are more akin in their θ -S relationship to the southern than to the northern waters. In the lower part of the equatorial thermocline, however, the composition moves away from the southern trend and becomes more similar to the northern trend.

The high salinity of waters in the northern Atlantic and northern Indian Oceans must have their origin in large net evaporative losses from these basins. We emphasize net because, were the evaporated water to rain back onto the basin or onto continental areas draining back into this basin, the salinity would not be enriched. There must be a loss of vapor which ends up falling as rain onto the North Pacific Ocean.* This is especially surprising in light of the fact that 60% of the world's river runoff reaches the North Atlantic! Somehow an even greater loss of water vapor from the Atlantic across Central America with the trade winds and from the Mediterranean across the Middle East to the Indian Ocean and its drainage basins must occur. If the route from the Mediterranean to the Indian is important, then a corresponding loss must occur from the northwestern Indian Ocean carrying the vapor to the North Pacific Ocean. By contrast the salinities on any given density horizon for the three south temperate regions are quite similar. This must be a consequence of interocean transport via the circumpolar current. In any case, these idiosyncrasies of the global water vapor cycle provide the oceanographer with an excellent tracer for thermocline processes!

Another set of observations having importance with regard to the thermocline is the pattern of the overlying surface currents. These currents often have roots carrying thermocline water along the same paths. Due to the rotation of the earth and the pattern of the winds, the temperate zones are characterized by strong western boundary currents which carry water poleward. These intense currents bend around to the east and carry waters across the ocean along the poleward boundary of the temperate zones. The Gulf Stream in the North Atlantic and Kuroshio in the North Pacific are currents of this type. This circulation gyre is closed by

*We exclude transport to the southern ocean because the residence time of water vapor in the atmosphere (~ 2 weeks) is small compared to the interhemisphere mixing time (~ 1 year), and because the salt deficiency in the North Pacific nearly matches the salt enrichment in the North Atlantic and North Indian Oceans. The southern oceans are similar to one another in their θ -S relationships and lie in between the North Pacific, on one hand, and the North Atlantic and North Indian, on the other.

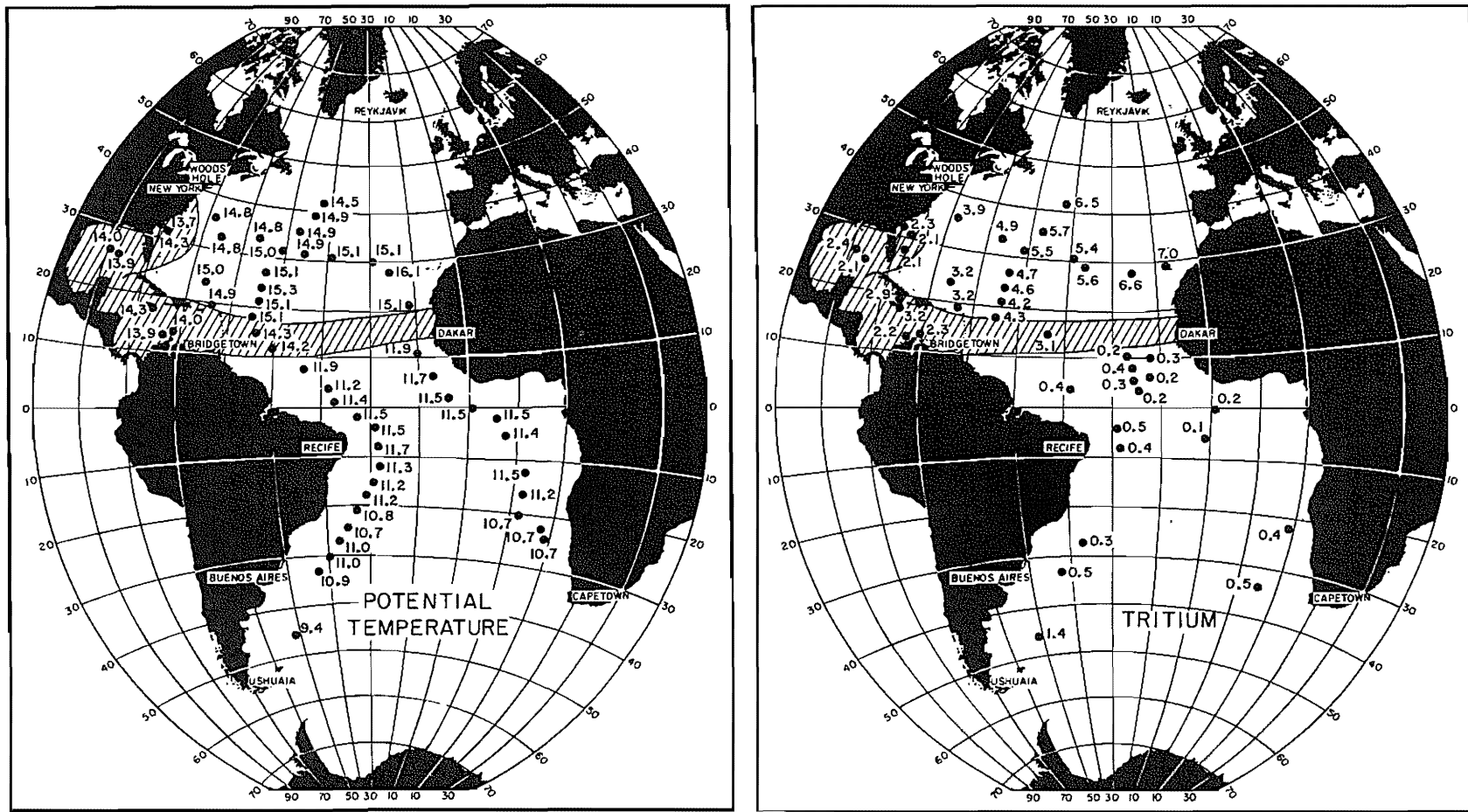


Figure 8-8. Maps showing the distributions of potential temperature and of tritium concentration along the 26.80‰ isopycnal horizon in the Atlantic Ocean. The shaded area shows the region of transition between waters with southern and northern characteristics. Based on data obtained as part of the GEOSECS program by Göte Ostlund of the University of Miami (424).

a more dispersed equatorward flow through the central and eastern parts of the zone and finally by a westward flow through the low latitude portion of the temperate zone. These same currents are known to operate at greater depths. Thus they must carry the new water entering the thermocline each winter around a similar pathway. From the sharp change in potential temperature along any given thermocline isopycnal seen at 15°N in the Atlantic, it can be inferred that this lateral stirring is confined to what we have defined as the temperate zone.

Within the equatorial zone there are strong currents running back and forth parallel to the equator. Some of these currents are strongest at the surface and some are strongest beneath the surface in the upper thermocline. While we need not be concerned with the details of these currents, we must be aware of the fact that they very effectively carry water (and our tracers) across the equatorial zone and back on the time scale of one year.

More subtle are the currents which carry water from one zone to another, and even more subtle still are those that carry water up or down (i.e., across isopycnals). One might say that they are lost in the "noise" of strong lateral currents which recirculate water within a given zone. We do, however, have some clues to the existence of these currents.

One such clue comes from the geographic pattern of potential temperatures along isopycnal horizons in the thermocline of the North Atlantic. It can be seen in figure 8-8 that the waters in the 12° to 16°N zone have temperature transitional between those for northern and southern water. Thus it must be in this zone that the two water types mix. This transition zone extends through the Caribbean, the Gulf of Mexico and the Florida Straits into the temperate Atlantic (see figure 8-8). This pattern gives the impression the water feeding the roots of the Gulf Stream consists in part of recirculated north temperate water and in part of water moving up the Atlantic from the south. As such interzonal flow must occur in order to balance the export of the deep water produced in the northern Atlantic, it is not surprising to see evidence for the intrusion of southern water in the upper ocean.

Evidence for upwelling is provided by several chemical signatures. We have already discussed the excess partial pressures of CO₂ and N₂O gas and the high nutrient constituent concentrations in surface waters of the equatorial Pacific. These anomalies can be maintained only by upwelling. The high opal content of sediments beneath this zone also provide evidence for upwelling (see figure 2-2). Another upwelling signature is provided by higher than average rates of plant activity. A section of plant productivity (as measured by the rate at which plants take up artificial ¹⁴C) across the equatorial belt in the Pacific Ocean confirms what we have already inferred from the chemical results (see figure 8-9). The high nutrient constituent content of this water supports the high plant growth rates.

The map in figure 8-10 shows a global compilation of plant growth rates. Zones of high productivity are shown by the cross-hatching. These zones are found along most continental margins and in most high latitude regions, as well as along the equator in the Pacific. The zones of high productivity in the polar regions

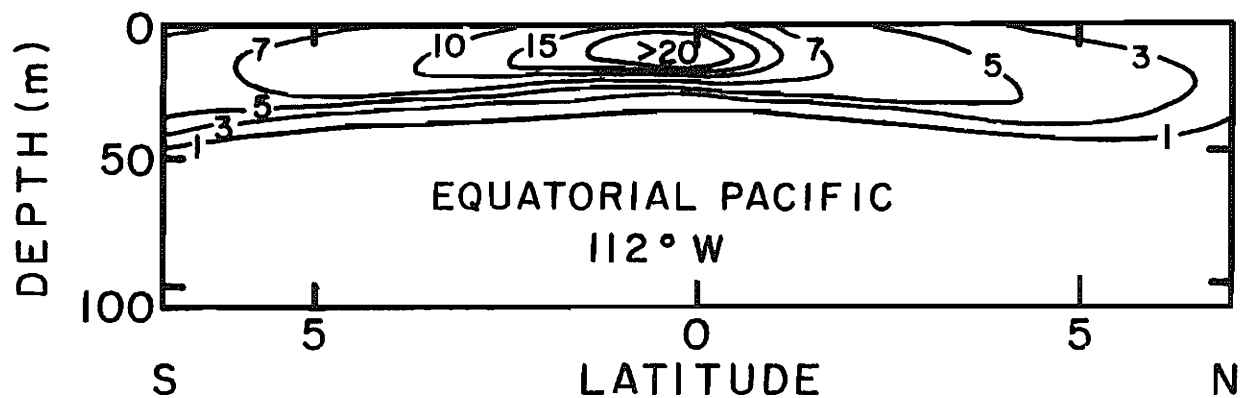


Figure 8-9. Plant productivity (in units of 10^{-3} gC/m³day) as a function of latitude and depth along a section through the equatorial Pacific Ocean. Adapted from a section in reference 687.

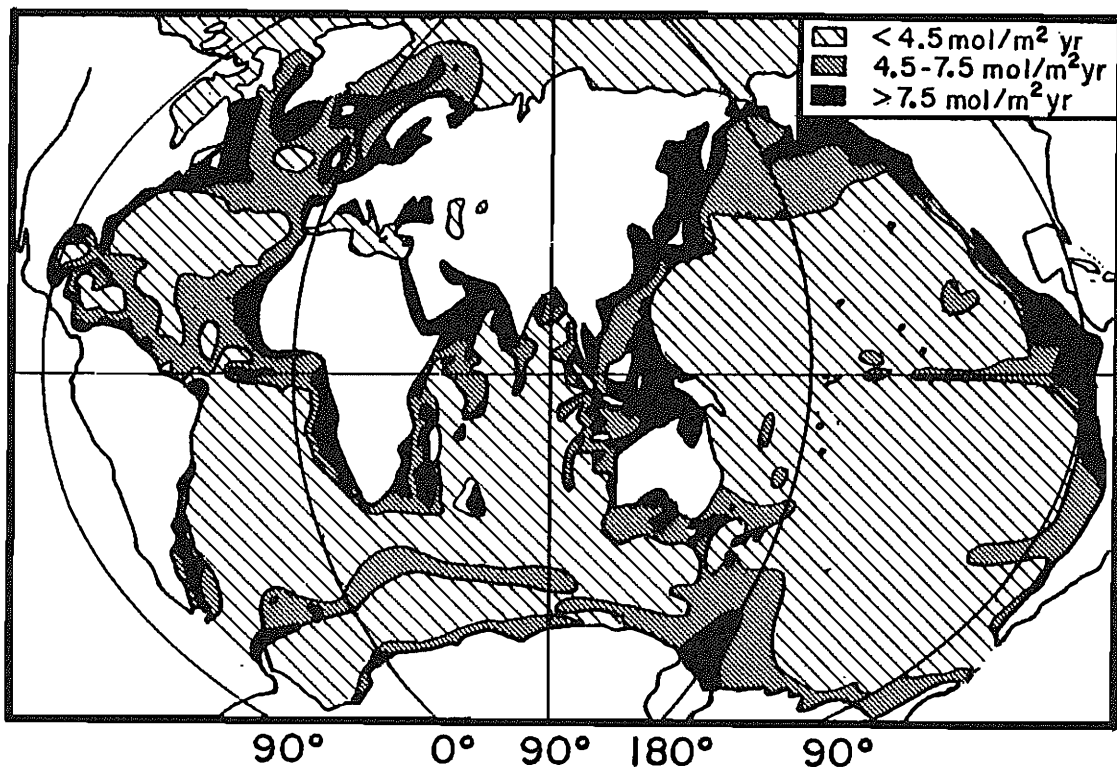


Figure 8-10. Geographic distribution of plant productivity in the ocean. Adapted from a map in reference 686.

owe their origin to the outcropping of isopycnal horizons. Nutrients are returned to the surface along these horizons of preferred mixing. The zones of high productivity in coastal areas owe their origin primarily to wind-driven upwelling, although the delivery of new nutrients from rivers and the efficient local recycling of nutrients from shallow water sediments also contribute. Our interest is of course in that part of the high productivity supported by upwelling. Physical oceanographic studies have clearly demonstrated that upwelling is the major cause for the high productivities in the eastern Atlantic, eastern Pacific and western Indian Oceans. The warm surface water capping the thermocline in these regions is periodically blown seaward drawing the underlying cold waters to the surface. This wind-driven coastal upwelling is one of the major routes by which thermocline water reaches the surface at low latitudes. Before completing the discussion of the map in figure 8-10, the reader should note that the lower limit in the high-productivity zones ($7.5 \text{ moles/m}^2 \text{ yr}$) is not even a factor of two greater than the upper limit for the low-productivity zones ($4.5 \text{ moles/m}^2 \text{ yr}$). As differences in the techniques used to measure productivity may lead to systematic errors of 15% or more, the distribution of productivity is not nearly so precise as that for chemical properties which have been measured ocean wide by a standard technique. Thus the map is best viewed as a broad brush view of the contrasts in plant productivity across the world ocean. While the major features are surely correct, the details are suspect.

TRITIUM DISTRIBUTION WITHIN THE THERMOCLINE

With this background of thermocline structure and dynamics in mind, let us have a look at where the anthropogenic tracers have gone. To date we have only global coverage for ^3H and for ^{14}C . As we shall see, the limited data on ^{90}Sr provide a valuable supplement to the more extensive ^3H data set. Surveys of the distribution of ^{85}Kr and of the freons have only recently begun. Another decade will pass before global data sets are available for these gases.

We begin this discussion with the distribution of tritium. The reason is that, as the contribution of prenuclear tritium is very small, the anthropogenic patterns are immediately apparent. Sections identical to those presented for density in figure 8-5 are presented for the distribution of tritium in figure 8-11. As transport along isopycnal horizons is thought to be very important, this figure should be compared with figure 8-5. To aid in this comparison, the dashed line showing the depth at which the tritium concentration reaches one-quarter of the value for overlying surface water is shown in both sets of diagrams.

The most dramatic aspect of these diagrams is the asymmetrical nature of the distribution of this isotope about the equator. The north temperate oceans have far more tritium at any density level than do the south temperate zones. This is of course to be expected from the input function for tritium. The integrated water inventories of tritium at the time of the GEOSECS surveys dramatically portray this asymmetry (see figure 8-12).

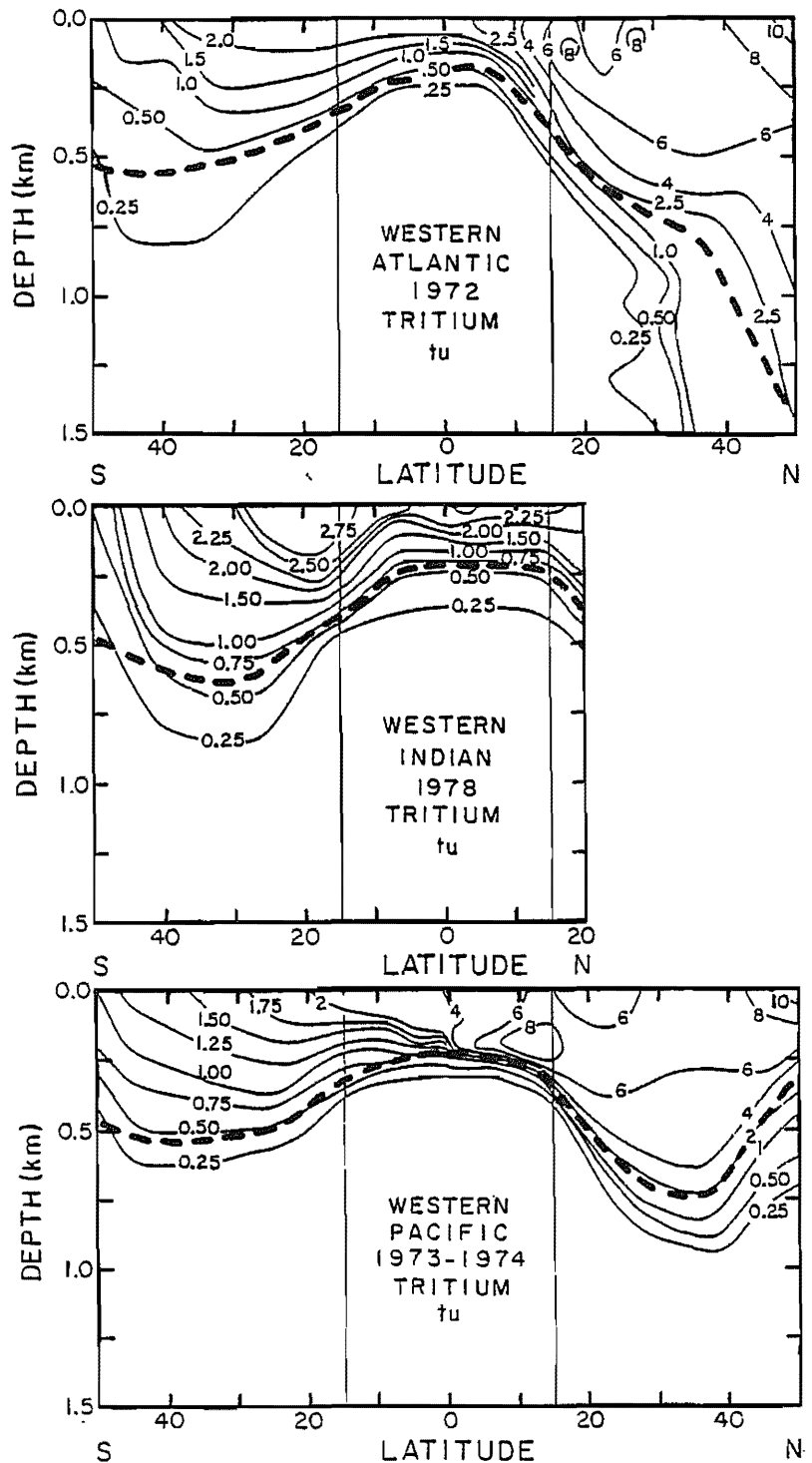


Figure 8-11. Sections showing the vertical distribution of tritium (in T.U.) along traverses in the western part of the three major oceans. The heavy dashed line denotes the depth at which the tritium concentration reaches one-quarter that in overlying surface water. These results were obtained by Göte Ostlund of the University of Miami as part of the GEOSECS program (51,52,54,56).

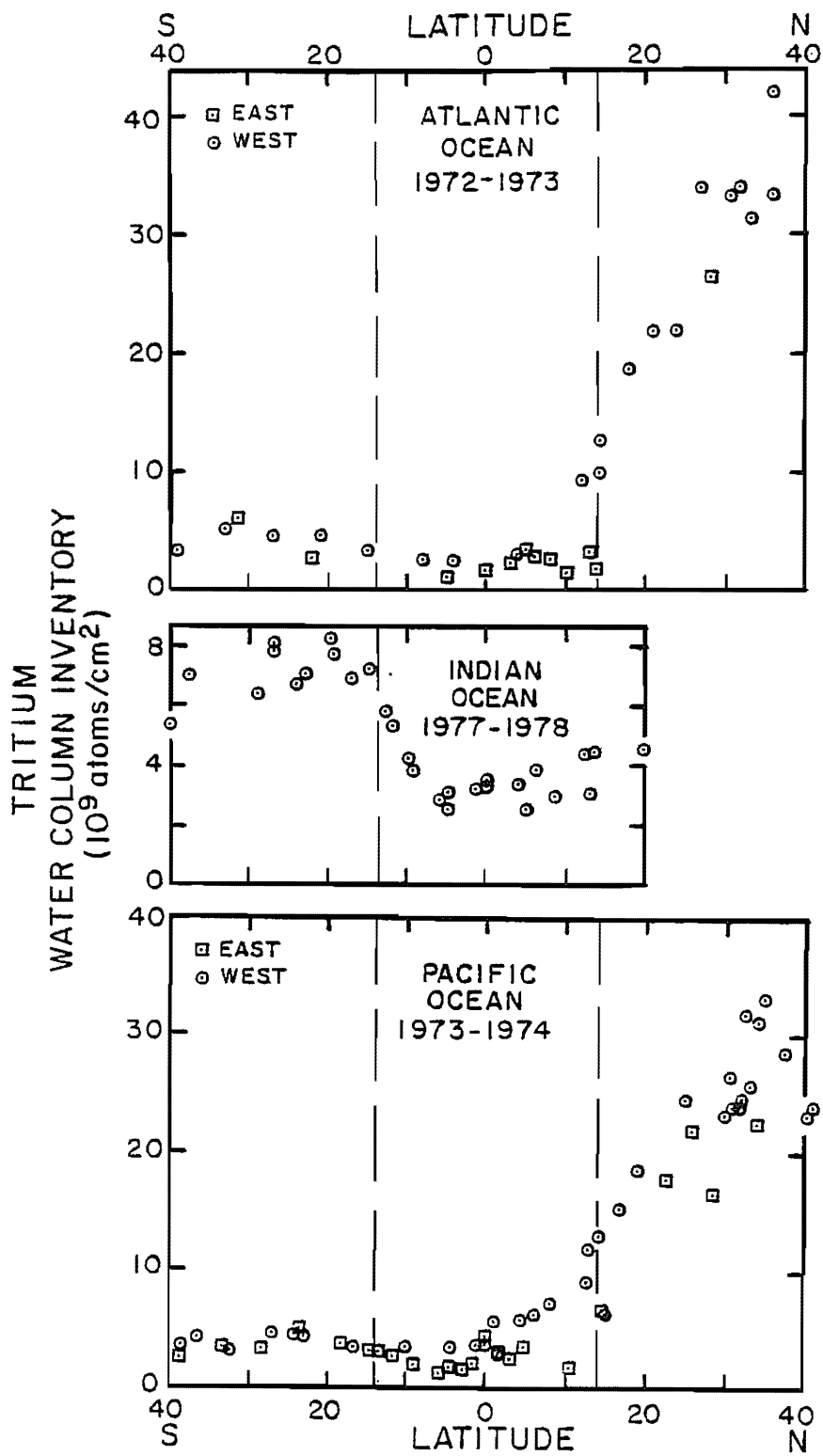


Figure 8-12. Water column inventories of tritium as a function of latitude in the three major oceans at the time of the GEOSECS surveys (51, 52, 54, 56).

A second prominent feature is the deeper penetration of tritium in the temperate zones than in the equatorial zones. As this feature is obscured by the asymmetry of the distribution, it is instructive to observe the shape of the horizon at which the tritium content reaches 25% of its value in overlying surface water.

Except for the northern Atlantic, the penetration in polar regions is not as great as in the adjacent temperate regions. In the northern Atlantic the tritium is found all the way to the bottom. This penetration is of course related to the formation of deep water in this region. The lack of penetration in the Antarctic and northern Pacific is related to the capping of these regions by low-salinity waters. Only in special places (like the Weddell Sea) is this stratification broken, permitting deep penetration of tritium.

A summary of the average penetration depth* of tritium for the central parts of each zone (i.e., away from the zone of transition separating these thermocline units) is given in table 8-2. The penetration is greatest in the north temperate zones, intermediate in the south temperate zones and smallest in the equatorial zones.

TEMPORAL TRENDS IN TRITIUM

Beyond knowing how the distribution of tritium looked at one single time, it is important to know how it evolved through time at any given place in the ocean. Two aspects are of interest, the manner in which the mean penetration depth changed and the manner in which the water column inventory changed. At the time this book was written there were only two places in the ocean where we had adequate data for this purpose.** One is in the vicinity of the island of Bermuda in the north temperate zone of the Atlantic. As shown in figure 8-13, the decay-corrected tritium concentration in the Bermuda area shows remarkably little change between 1968 and 1977. The concentration is uniform to a depth of about 400 meters. Between 400 and 800 meters there is a linear drop-off in concentration. From 800 meters to 1200 meters the values are again roughly uniform. A closer examination of these data reveals, however, that the concentrations in the upper 400 meters have declined, while those below 400 meters have increased. In terms of the water column inventory the two changes roughly balance. The small increase that is suggested by the results (see table 8-3) could in part be explained by inputs during this period. (about 6% of the total input). Thus the north temperate zone did not lose an appreciable amount of its tritium through mixing with low-tritium southern waters between 1968 and 1977.

*The average penetration depth is defined as the water column inventory (atoms/cm^2) divided by the surface water concentration (atoms/cm^3).

**Shortly after the publication of this book the results from the north and equatorial surveys from the Transit Tracers program will become available, greatly increasing our knowledge of the evolution in time of the tritium distribution.

Table 8-2. Mean penetration depth of tritium as observed during the GEOSECS surveys.*

Ocean (Year)	N. Temp. 35°N to 25°N	Equat. 10°N to 10°S	S. Temp. 25°S to 35°S
Bomb Tritium Mean Penetration Depth meters			
Atlantic (1973)	680 (5)	135 (8)	345 (3)
Indian (1978)	-	180 (12)	390 (4)
Pacific (1974)	565 (11)	195 (18)	330 (7)

*The mean penetration depth is obtained by dividing the water column inventory (atoms/m^2) by the surface concentration (atoms/m^3). The numbers in parentheses are the numbers of stations included to obtain the average. The tritium data was obtained by Ostlund of the University of Miami (51,52,54,56). The compilations summarized here were made by the authors (75).

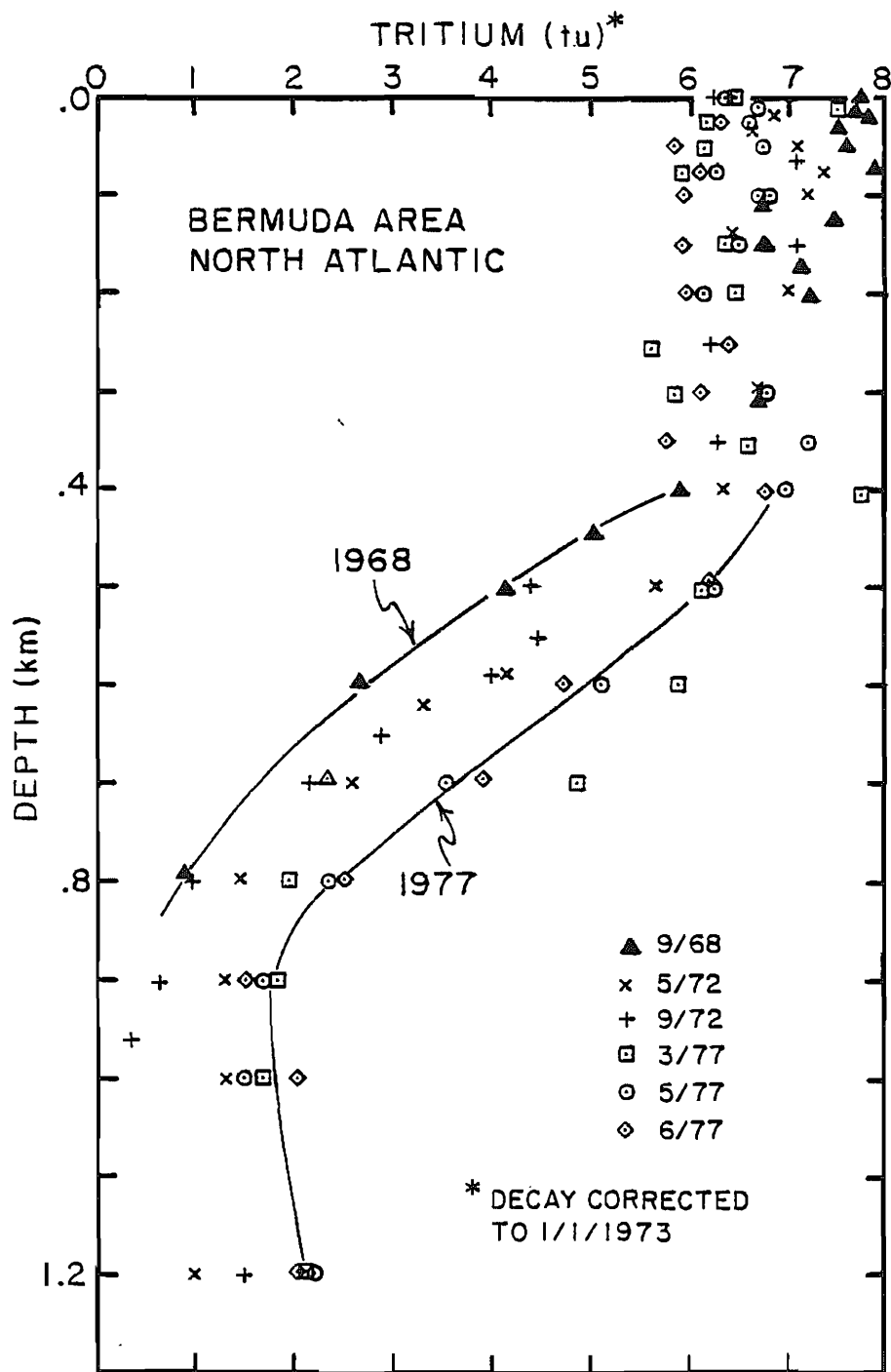


Figure 8-13. Tritium profiles in the Bermuda area in 1968, in 1972, and in 1977. The concentrations are decay corrected to the beginning of 1973. The 1968 and 1972 results were obtained by Göte Ostlund of the University of Miami (49,51) and the 1977 results by Bill Jenkins of the Woods Hole Oceanographic Institution (55).

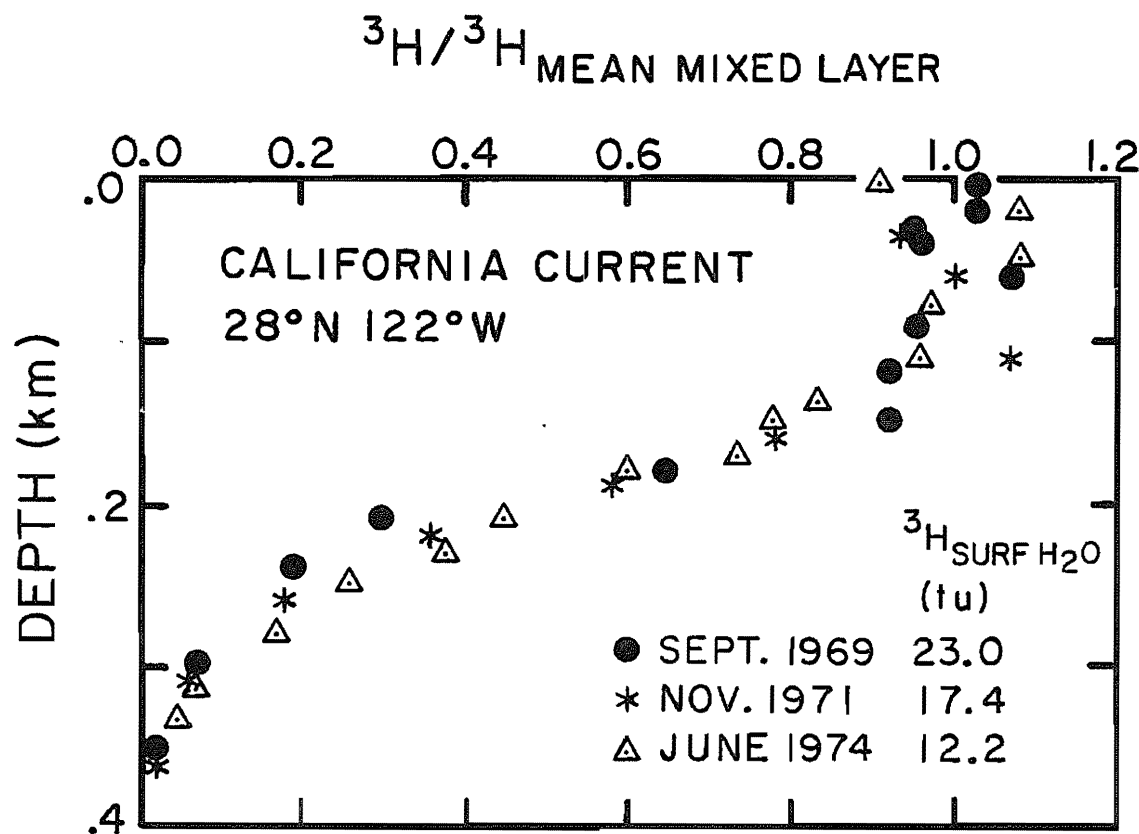


Figure 8-14. Profiles of tritium taken in 1969, 1971 and 1974 at a station in the California Current (48,54,58). The values are given as the fraction of the average value for surface mixed layer water.

The second locality is in the California Current adjacent to the Mexico-United States border. This current flows down the coast carrying low-salinity water similar to that found off the Aleutians. The situation at this locality is quite different; the decay-corrected water column inventory shows a dramatic decrease over the five-year period (1969 to 1974) and the mean penetration depth remains almost the same. The tritium profiles for this station are shown in figure 8-14. The concentrations are expressed as ratios to the mean for samples from the upper mixed layer. This mode of presentation facilitates comparison of the shapes of the depth profiles. The mean penetration depths and decay-corrected inventories are summarized in table 8-3. It appears that in this area of the ocean, tritium was being lost from all depths in about the same proportion. As part of the water carried in the south-flowing California Current may be transported into the equatorial zone, some of the missing tritium may have been lost entirely by the temperate zone. The remainder is carried around the lower part of the gyre into the western part of the temperate zone.

For some other parts of the ocean enough data from different times is available to permit rough estimates of time trends in inventory and mean penetration depth to be made. These are summarized in table 8-4.

TRITIUM AS A GUIDE TO DEEP WATER FORMATION

Before leaving the discussion of tritium, we must briefly mention its application to the study of deep-water formation. As shown in figure 8-15, tritium has penetrated all the way to the bottom of the northern Atlantic. Particularly well shown is the cascade of new Denmark Straits overflow water along the bottom down into the abyssal western basin. A program was in progress at the time this book was written to repeat the survey along this track nine years later (in 1981) to determine the extent to which this penetration has progressed.

The existence of this thin river of bottom water is very nicely shown by the profiles of temperature, salinity, light scattering, dissolved oxygen and dissolved silicate at a station located at 39°N in the western basin (see figure 8-16). Here a 25-meter-thick layer of water which is more salty and slightly warmer than the ambient bottom water is seen. The water in this layer also contains more dissolved oxygen and less silicate than the overlying water. Its higher tritium content demonstrates that it is richer in new northern component water than the overlying water.

There is evidence that this stream of deep water flows well beyond this latitude. It is thought to hug the margin of the North American continent as far south as Florida! As shown in figure 8-17, Bill Jenkins and Peter Rhines of Woods Hole have provided dramatic evidence for this continuation based on tritium data. At about 30°N this deep south-flowing stream is thought to leave the continental rise. As it does so, it loses its sediment load (torn loose from the slopes it has hugged). This sediment has built a huge abyssal delta called the Blake-Bahama Outer Rise.

Table 8-3. Time trends in the water column inventories and mean penetration depths for bomb produced tritium in various places in the Atlantic Ocean.

Stn.	Col. Date	Lat.	Long.	h m	10^9 WCI* atoms cm^{-2}	Ref.
TEMPERATE NORTH ATLANTIC						
P6808-2	Sept 1968	31.0°N	64.9°W	550	28	(49)
BRMD-72	May 1972	32.3°N	65.5°W	600	28	(49)
GEOSECS 30	Sept 1972	31.8°N	50.8°W	750	33	(51)
S74546	Nov 1974	30.5°N	67.5°W	750	34	(55)
S75625	Mar 1975	30.5°N	58.5°W	700	34	(55)
PAN001	Mar 1977	30.2°N	64.5°W	740	34	(55)
PAN002	May 1977	30.2°N	64.5°W	770	33	(55)
PAN003	June 1977	30.2°N	64.5°W	770	32	(55)
EQUATORIAL ATLANTIC						
P6706-48	Sept 1967	0.0°	4.0°W	45	1.1	(47)
P6707B-12	Nov 1967	0.0°	18.2°W	60	1.3	(47)
NAGS-8	Sept 1973	5.0°S	11.1°W	105	1.3	(51)
NAGS-3B	Sept 1973	0.2°S	10.0°W	120	1.7	(51)
CALIFORNIA CURRENT						
GEOSECS I	Sept 1969	28.0°N	121.0°W	210	29	(58)
GOGO	Nov 1971	28.0°N	121.0°W	210	24	(48)
GEOSECS 347	June 1974	28.0°N	121.0°W	210	19	(54)
EQUATORIAL PACIFIC						
STYX 3	Aug 1968	7.0°N	163.0°W	+	6.3	(50)
GEOSECS 239	Dec 1973	5.9°N	172.0°W	+	6.8	(54)
STYX 2	Aug 1968	0.0°	165.7°W	200	6.3	(50)
GEOSECS	Dec 1973	0.0°	179.0°W	200	4.0	(54)
STYX 1	Aug 1968	5.0°S	167.1°W	160	2.4	(50)
GEOSECS 251	Dec 1973	4.6°S	179.0°W	210	4.0	(54)

*The water column inventories have been decay-corrected to Jan. 1 1973.

+Profile has subsurface maximum.

Table 8-4. Summary of information regarding the time trends in the distributions of bomb-produced tritium and radiocarbon at various places in the ocean after 1967. The dashes indicate a lack of information.

	TRITIUM (Decay corrected)			RADIOCARBON		
	Concentration Surface Ocean	Mean Penetration Depth	Water Column Inventory	Concentration Surface Ocean	Mean Penetration Depth	Water Column Inventory
NORTH TEMPERATE ZONE						
Atl.	-3%/yr	+4%/yr	~Constant	~Constant	-	-
Ind.	-	-	-	-	-	-
Pac.	-7%/yr	-	~Constant	~Constant	-	-
EQUATORIAL ZONE						
Atl.	-8%/yr	Increase	Increase	~Constant	-	-
Ind.	-	-	-	-	-	-
W. Pac.	+3%/yr	Increase	Increase	~Constant	-	-
SOUTH TEMPERATE ZONE						
Atl.	-	-	-	-	-	-
Ind.	-	-	-	-	-	-
Pac.	-7%/yr	-	-	-	-	-
BOUNDARY CURRENTS						
California	-8%/yr	~Constant	-9%/yr	~Constant	-	-
Aleutian	-11%/yr	Increase	-7%/yr	-	-	-

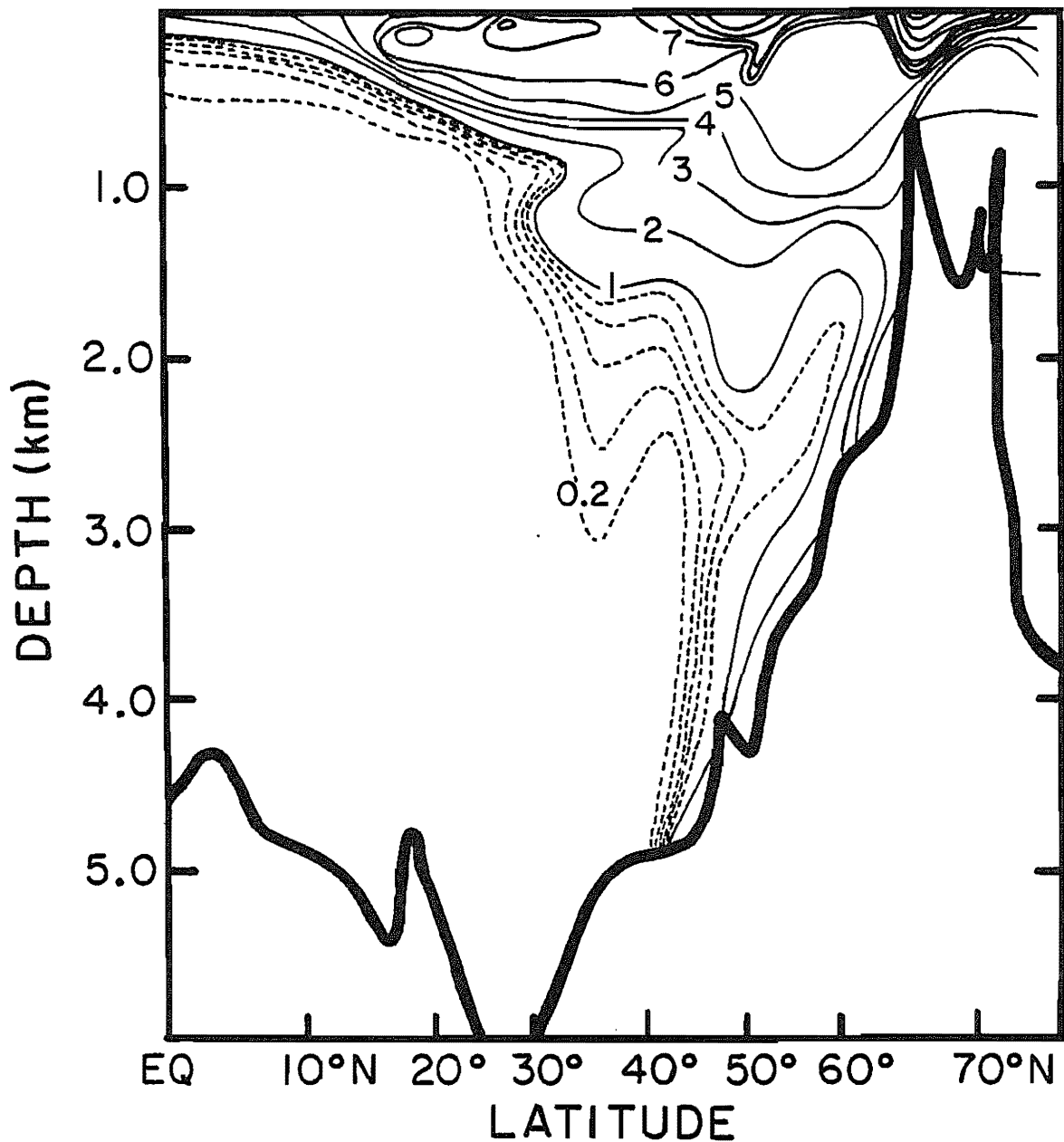


Figure 8-15. Section showing the vertical distribution of tritium in the western North Atlantic. The deep penetration north of 40°N is associated with the formation of deep water. This diagram was prepared by Göte Ostlund of the University of Miami based on his measurements on samples collected as part of the GEOSECS program (727).

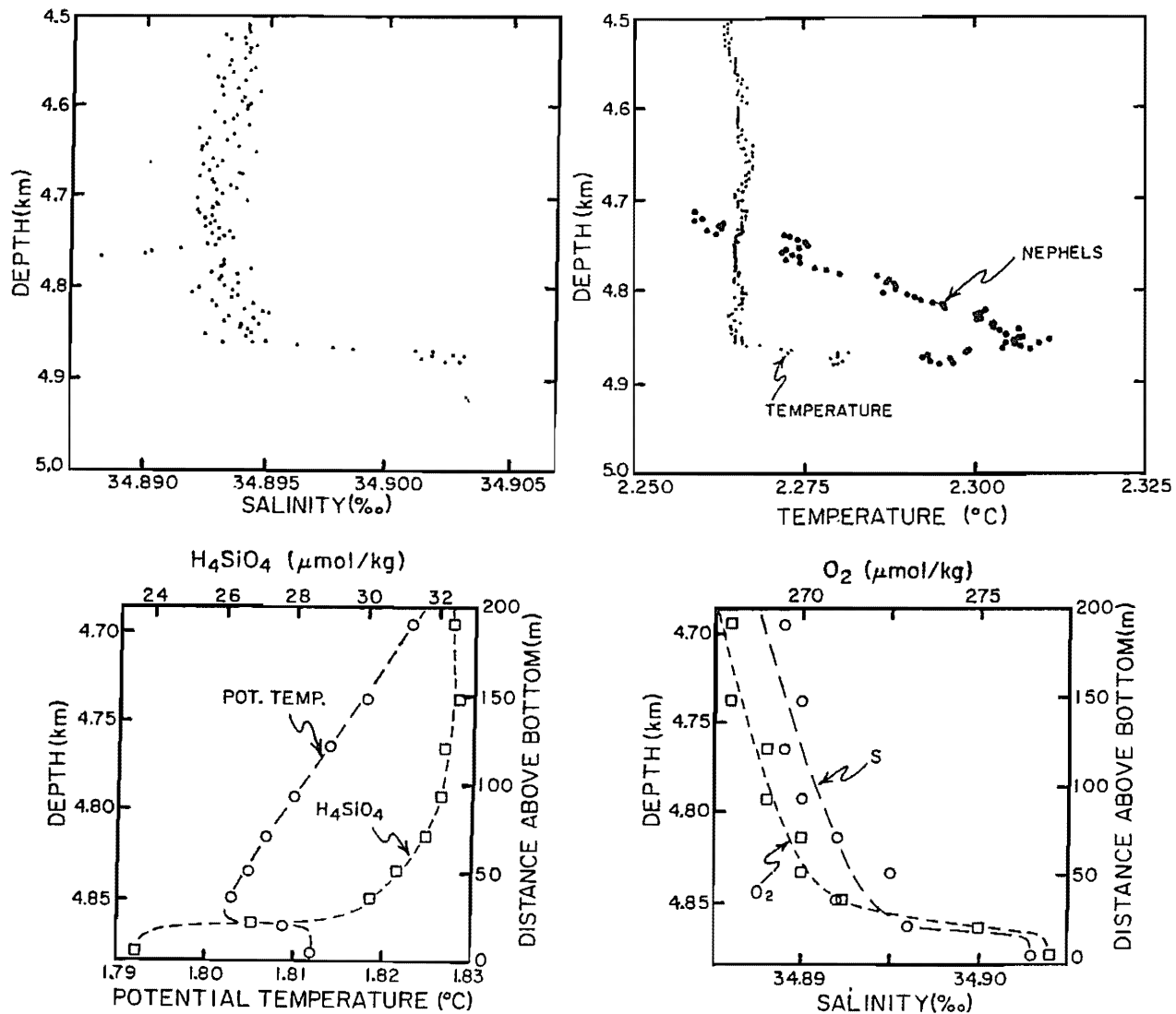


Figure 8-16. Profiles of salinity, temperature and light scattering for a station in the northern part of the Atlantic's western basin (39°N , 44°W) and obtained using *in situ* sensors (upper panels). Also shown are conventional, discrete measurements of potential temperature, silicate, dissolved oxygen and salinity (lower panels) (429). In all cases an anomaly with characteristics more like that of water entering the northern Atlantic from the Denmark Straits is seen as a several tens of meters thick bottom layer. This layer carries warmer and more saline water with higher dissolved oxygen and lower silicate than the overlying water. It also scatters less light (i.e., presumably has a lower particulate load). Its tritium concentration (not shown) is higher than that for the overlying water. These results were obtained as part of the GEOSECS program (362).

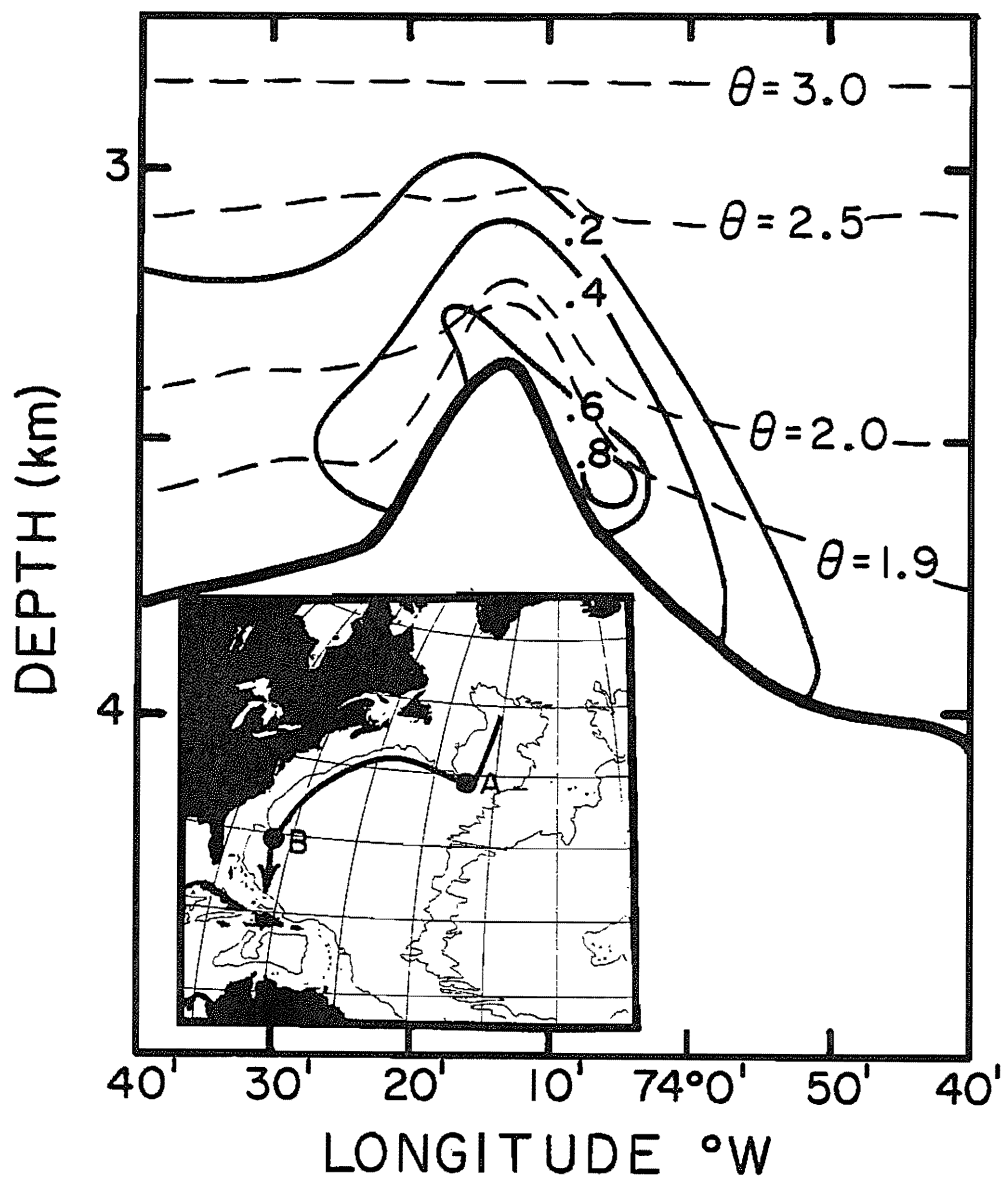


Figure 8-17. Tritium section for bottom waters flowing along the Blake-Bahama Outer Rise (location B inset map). The solid contours are for tritium (in T.U.) and the dashed contours are for potential temperature. The location of the station from which the records shown in figure 8-16 were obtained is designated in the inset by point A. The tritium measurements were carried out by Bill Jenkins of the Woods Hole Oceanographic Institution (70).

As shown in figure 8-17, a plume of tritium-bearing water flows along this feature. Although the concentrations are lower, this tritium anomaly remains identifiable 3000 miles from its source!

SUPPLEMENTARY INFORMATION FROM Sr-90

We have already pointed out that the distribution of ^{90}Sr in the sea is quite similar to that of ^3H . Because the tritium data base is more complete, and because the precision and sensitivity of ^3H measurements are superior to those of ^{90}Sr , it is the tritium data base which receives most attention. There is one aspect of the data set for ^{90}Sr , however, which is superior to that for ^3H . The time histories for the concentrations of ^{90}Sr in surface water in the latitude range about 20°N to 20°S can be reconstructed in far more detail than those for tritium. The reason is that the concentration of ^{90}Sr is recorded by corals. The $^{90}\text{Sr}/\text{Sr}$ ratio in corals must be the same as that in the water in which the corals grew.* The corals neatly average out any seasonal variability so measurements on individual annual bands remove some of the noise that would be seen if, instead, spot water samples had been analyzed. More important, as the record from spot water samples is generally inadequate due to a sparsity of coverage, it is possible to make up for this missed opportunity to collect water samples by collecting coral heads from sites of particular interest. This work had only just begun as we wrote this book, so that its full potential has yet to be realized. The four coral-based records obtained by Toggweiler at the Lamont-Doherty Geological Observatory and shown in figure 8-18 demonstrate how powerful an approach this is.

BOMB C-14 DISTRIBUTION WITHIN THE THERMOCLINE

Bomb-produced radiocarbon cannot compete with the tritium as a tracer of the details of the penetration of anthropogenic substances into the sea. The reason is that the task of separating the contributions of bomb- and cosmic-ray-produced radiocarbon cannot be done well enough. The value of bomb radiocarbon comes rather through an unexpected contrast in its water column inventory between the equatorial and temperate zones of the ocean.

In order to obtain these water column inventories, we must of course make the separation of the two types of radiocarbon. The measurements made as part of the GEOSECS program provide the profile of total (i.e., natural + bomb) ^{14}C to C ratio at many places in the ocean. The trick is to establish the prenuclear profile for these same places. As we have only fragmentary data, we cannot simply plot measurements for samples taken at various depths and draw a smooth curve through them. A less direct method must be employed. The procedure used is as follows. First the surface value is established from measurements on prenuclear water samples or on growth rings from corals. Next the GEOSECS tritium data are

*As the Sr/Ca ratio in corals is nearly the same as that in sea water, in practice it is necessary to measure only the ^{90}Sr activity per gram of coral.

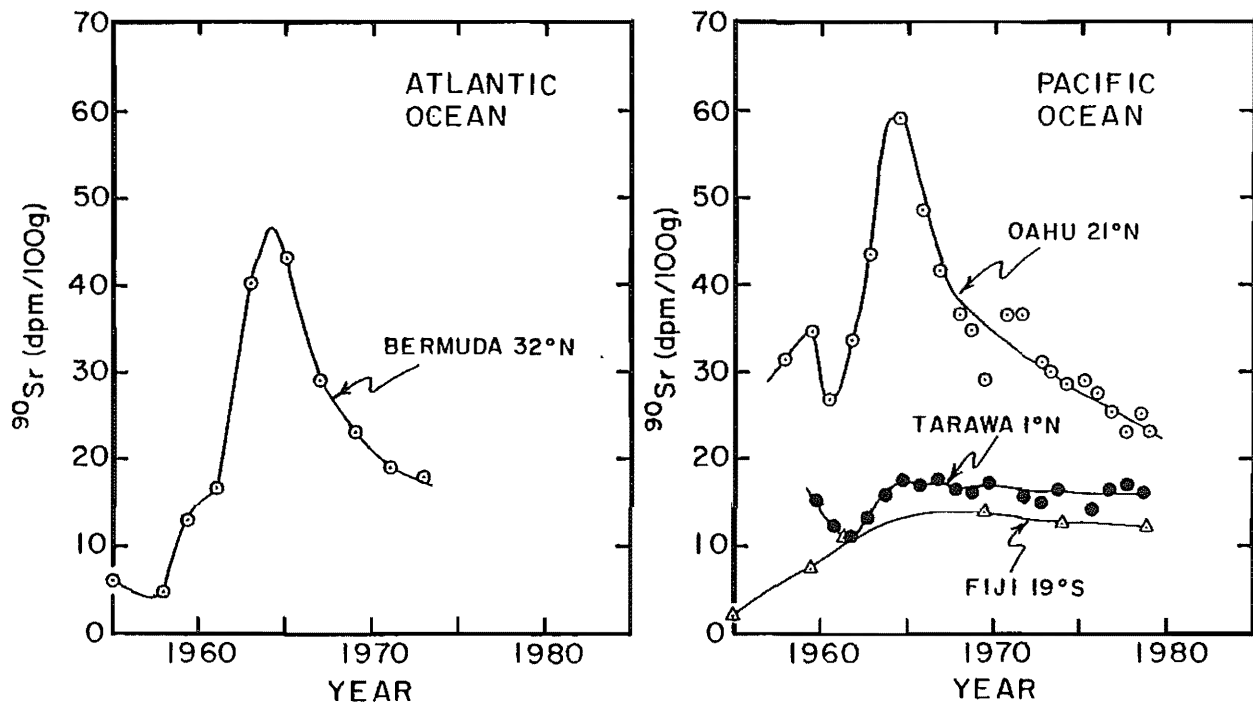


Figure 8-18. Records of ^{90}Sr concentration as a function of time in surface waters as reconstructed through measurements on growth-ring-dated corals. These results were obtained by Toggweiler of the Lamont-Doherty Geological Observatory as part of his PhD thesis research.

used to establish the depth of penetration of the anthropogenic tracers. In waters which have less than 5% the amount of tritium found in the overlying surface water, the radiocarbon is assumed to be entirely of cosmic-ray origin. Hence, the prenuclear profile must join the profile measured during the GEOSECS program at this depth. The final step is to decide on the shape for the curve joining the surface value with the profile beneath the depth of tritium penetration. As different procedures are adopted to suit the idiosyncrasies of various ocean regions, it is best to hold off on this point until we discuss each region separately. In any case, having estimated the prenuclear profile, we use the area between the total and prenuclear curves to estimate the number of excess ^{14}C atoms in the water column at each of the GEOSECS stations. To do this properly we must of course know the amount of dissolved inorganic carbon in the water. This varies slightly from region to region and from depth to depth. However, as ΣCO_2 data are available for all the GEOSECS stations, it is just a matter of arithmetic to convert the $\Delta^{14}\text{C}$ values back to $^{14}\text{C}/\text{C}$ ratios and to multiply these ratios by the appropriate ΣCO_2 values and then to sum over depth to obtain the bomb- ^{14}C inventories.

The critical step in this analysis is the establishment of prenuclear $\Delta^{14}\text{C}$ value for surface waters. Fortunately a reasonable number of water samples collected prior to 1958 were analyzed for radiocarbon. These analyses are plotted as a function of latitude for each of the oceans in figure 8-19. The GEOSECS data for surface ocean water are also shown on these diagrams. The prenuclear analyses appear to follow the pattern seen in the 1970's, i.e., the highest $\Delta^{14}\text{C}$ values are found in the temperate zone, with a small decline in the equatorial zone and a large decline at high latitudes. The similarity between the shapes of the two curves is to be expected. The processes which reduce the surface concentration of excess ^{14}C must also reduce the concentration of natural radiocarbon.

In this regard it is important to assess the validity of the early radiocarbon measurements. In the twenty years which elapsed between these early surveys and the GEOSECS survey, many improvements were made in the manner in which the large water samples needed for this work are collected, stored and stripped of their dissolved inorganic carbon, and in the procedures used to measure the radiocarbon in this CO_2 . Two methods are available for checking the reliability of the early work. One is to compare the results obtained on deep waters still free of tritium at the time of the GEOSECS surveys. Figure 8-20 shows such a comparison between the early Lamont-Doherty Geological Observatory results on deep waters in the Atlantic and results for the same geographic location and depth interpolated from the network of GEOSECS measurements. Considering the experimental error on the early results (~10‰) and the uncertainty in the result interpolated from the GEOSECS data set (~5‰) the degree of agreement is satisfactory. The other approach is to make use of new measurements on ring-dated corals and on shells from museum archives to determine the $^{14}\text{C}/\text{C}$ ratio in surface waters at specific times in the past. The work on corals looks particularly promising in this regard. At the time this book was written only three such records had been

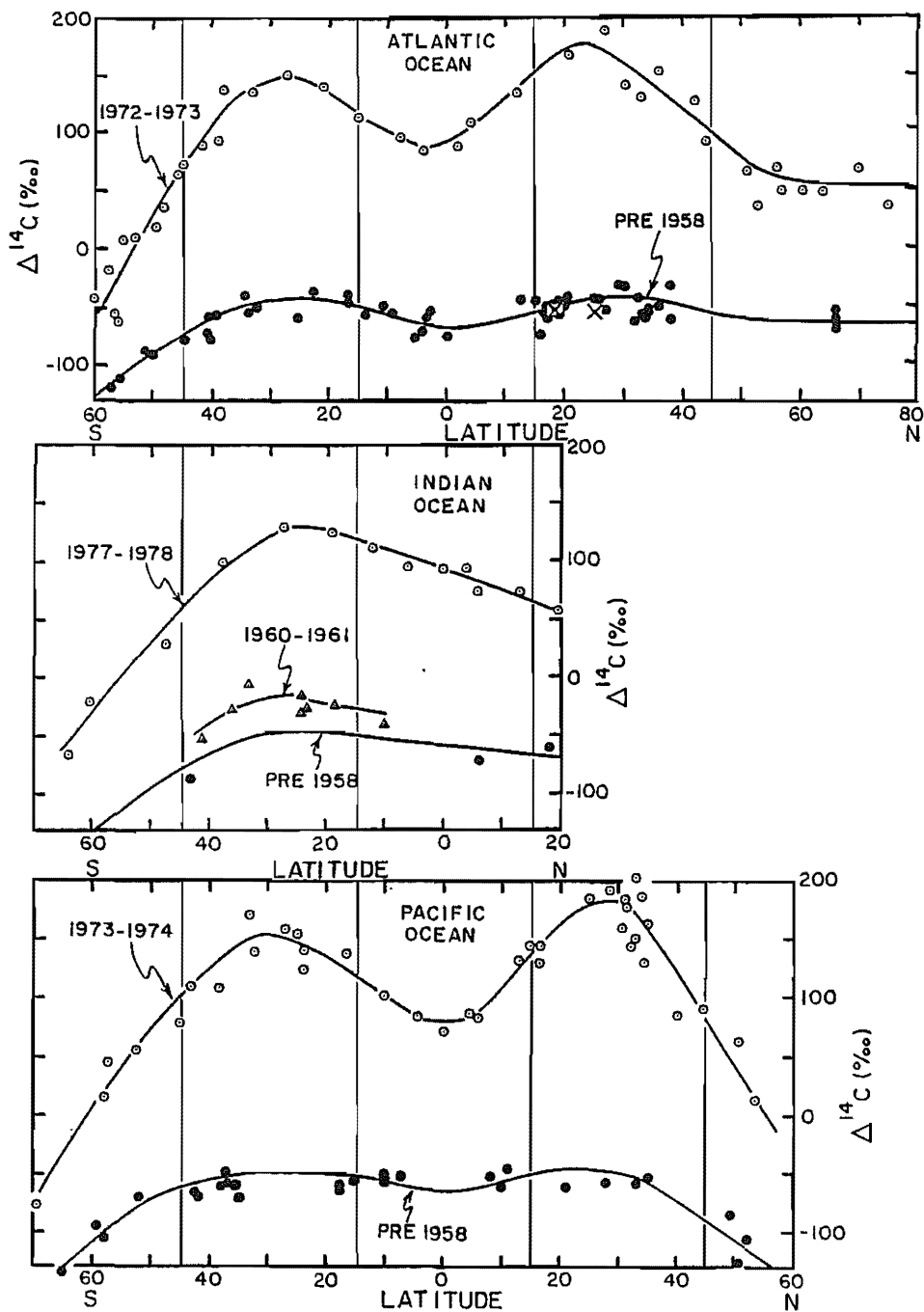


Figure 8-19. $\Delta^{14}\text{C}$ for samples of surface water as a function of latitude in the three major oceans. The solid circles are for measurements made on water samples collected prior to 1958 (i.e., before the onset of contamination with bomb- ^{14}C). These measurements are given in references 4, 5, 6 and 8. The prenuclear results obtained by the analyses of coral are shown by x's (15, 16). The open circles are the results from the GEOSECS survey (21, 22, 23). Because of the sparsity of pre-1958 data in the Indian Ocean, measurements on samples taken in 1960 and 1961 are also shown (open triangles) (13).

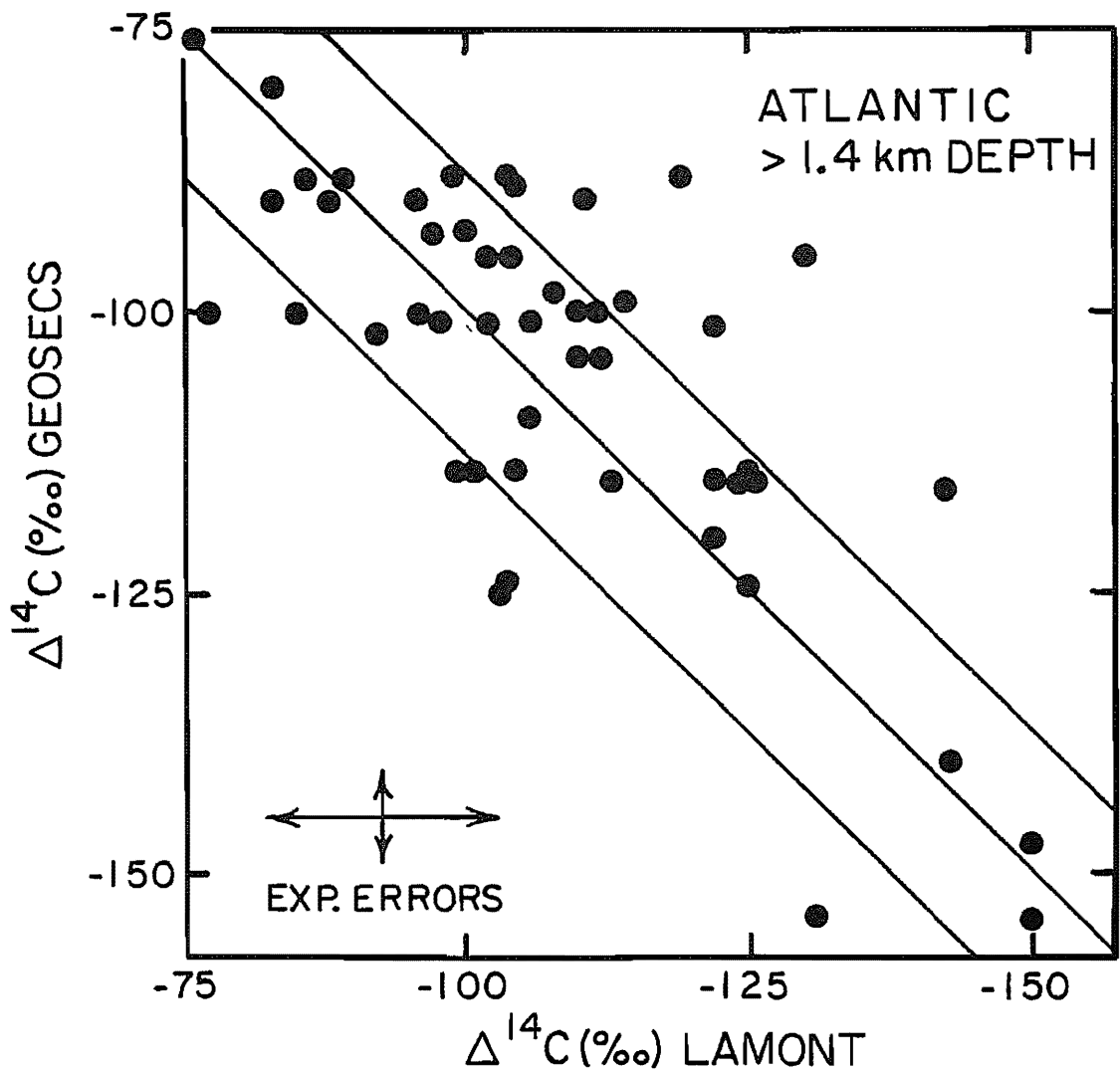


Figure 8-20. Plot of $\Delta^{14}\text{C}$ values interpolated from the GEOSECS results (21) against $\Delta^{14}\text{C}$ values measured two decades earlier on samples from greater than 1.4 km depth in the Atlantic Ocean (4). The median line is that expected if the two data sets agree. The flanking lines represent the one standard deviation error limits. The agreement between these data sets bears witness to the reliability of the early measurements.

obtained by Druffel at University of California at San Diego. They are shown in figure 8-21. For the two Atlantic corals the pre-1958 $\Delta^{14}\text{C}$ values are in excellent agreement with the early measurements on surface waters. The coral measurements also confirm that 1957 is the cutoff date for the acceptance of surface water results as free of contamination with bomb-produced ^{14}C .

So we see that our knowledge of the prenuclear $^{14}\text{C/C}$ ratios in surface ocean water rests on a reasonably firm foundation and that this foundation can be strengthened by measurements of $^{14}\text{C/C}$ ratios on growth-ring-dated corals and on shells carefully selected from museum collections.

Having established the prenuclear surface $^{14}\text{C/C}$ ratios for surface water and the depth in the water column at which the GEO-SECS results can be taken to represent prenuclear conditions, only the task of constructing a curve joining these results remains. Here we are guided by our knowledge of the vertical distribution of total radiocarbon in the upper ocean and also by some physical oceanographic horse sense.

In the equatorial zones of the oceans we have already seen that the penetration depth of tritium is much smaller than elsewhere in the oceans. As shown in figure 8-22, plots of tritium versus potential temperature generate a linear array of points. Although the scatter is greater, so also do the $\Delta^{14}\text{C}$ values. Our intuition would suggest that during pre-nuclear time the trend of $\Delta^{14}\text{C}$ through this zone should also have been linear. We can fortify our intuition by noting that if upwelling is important in the equatorial zone, then the trends of all conservative properties being mixed down into the water column against this upward flow should form straight lines when plotted against potential temperature. Thus the assumption that the trend of natural radiocarbon was linear with potential temperature (at least in the depth zone where the tritium-potential temperature relationship is now linear) is very likely valid. In any case, as can be seen in reconstruction given in figure 8-22, the inventories of excess radiocarbon do not critically depend on the exact shape adopted.

In the temperate zones the correlation between tritium and ^{14}C is not as good as it is in the equatorial zone. This being the case, we take another route. As shown in figure 8-23, the profile of total $^{14}\text{C/C}$ versus depth is remarkably linear in these areas of the ocean. This linearity extends to a depth where tritium is about 10% its surface value. Thus we fall back onto intuition which says that the profile of natural radiocarbon was probably also linear with depth (at least in the zone now contaminated with bomb tritium). Again the inventory obtained is not highly sensitive to the choice of this shape (as long as the $\Delta^{14}\text{C}$ values are required to lie between those for surface water and those for the base of the tritium-contaminated zone).

Let us now turn to the results of this enterprise. The distribution of bomb- ^{14}C water column inventories is depicted as a function of latitude for the three major oceans in figure 8-24. The striking feature is the several-fold lower inventories for stations in the equatorial zone than for those in the temperate zone. A similar pattern is seen in each of the three major oceans (only the abbreviated north temperate zone of the Indian Ocean is

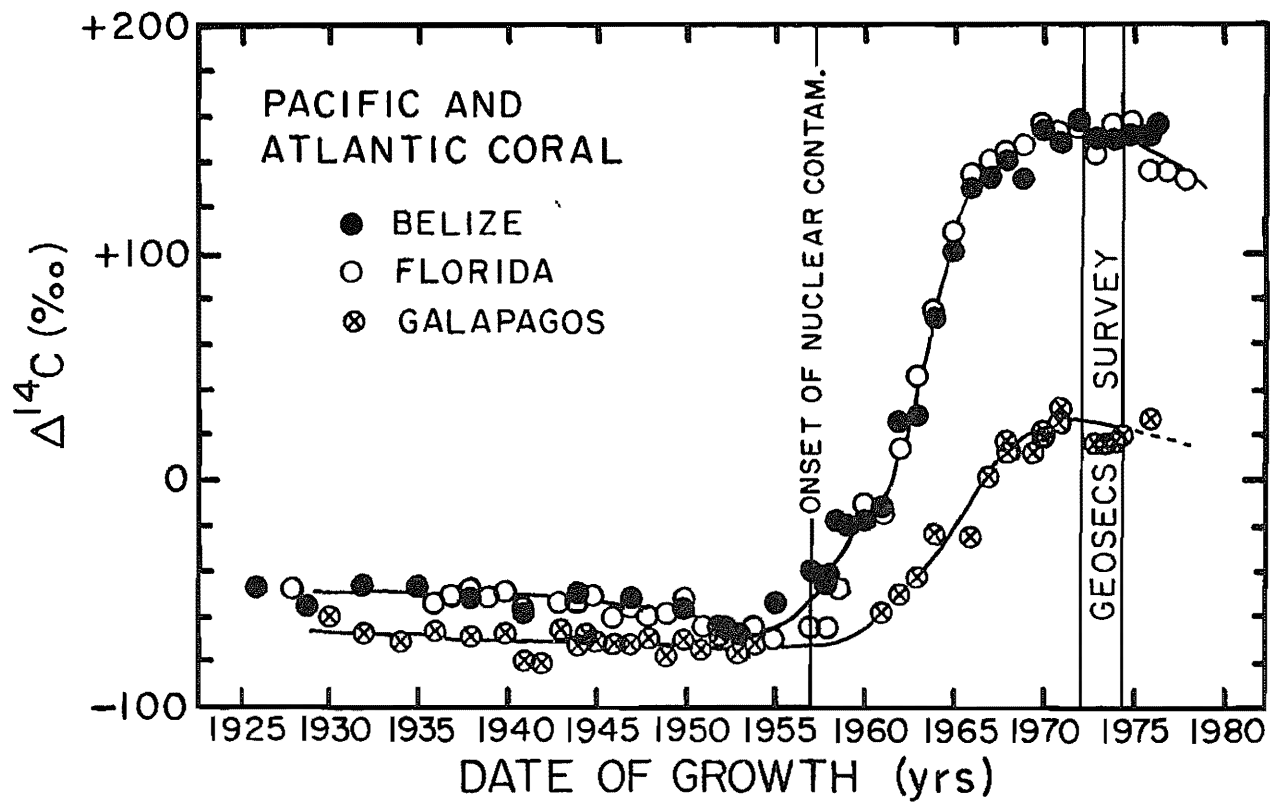


Figure 8-21. $\Delta^{14}\text{C}$ values obtained from measurements on corals. The Belize and Florida corals represent surface water of the north temperate Atlantic (15,16). The Galapagos coral comes from an area of intense upwelling in the eastern equatorial Pacific (17). The time limit for acceptance of water samples as prenuclear is shown. Also shown are the times of the Atlantic and Pacific GEOSECS surveys. These measurements were made by Druffel in the laboratory of Hans Suess at the University of California San Diego.

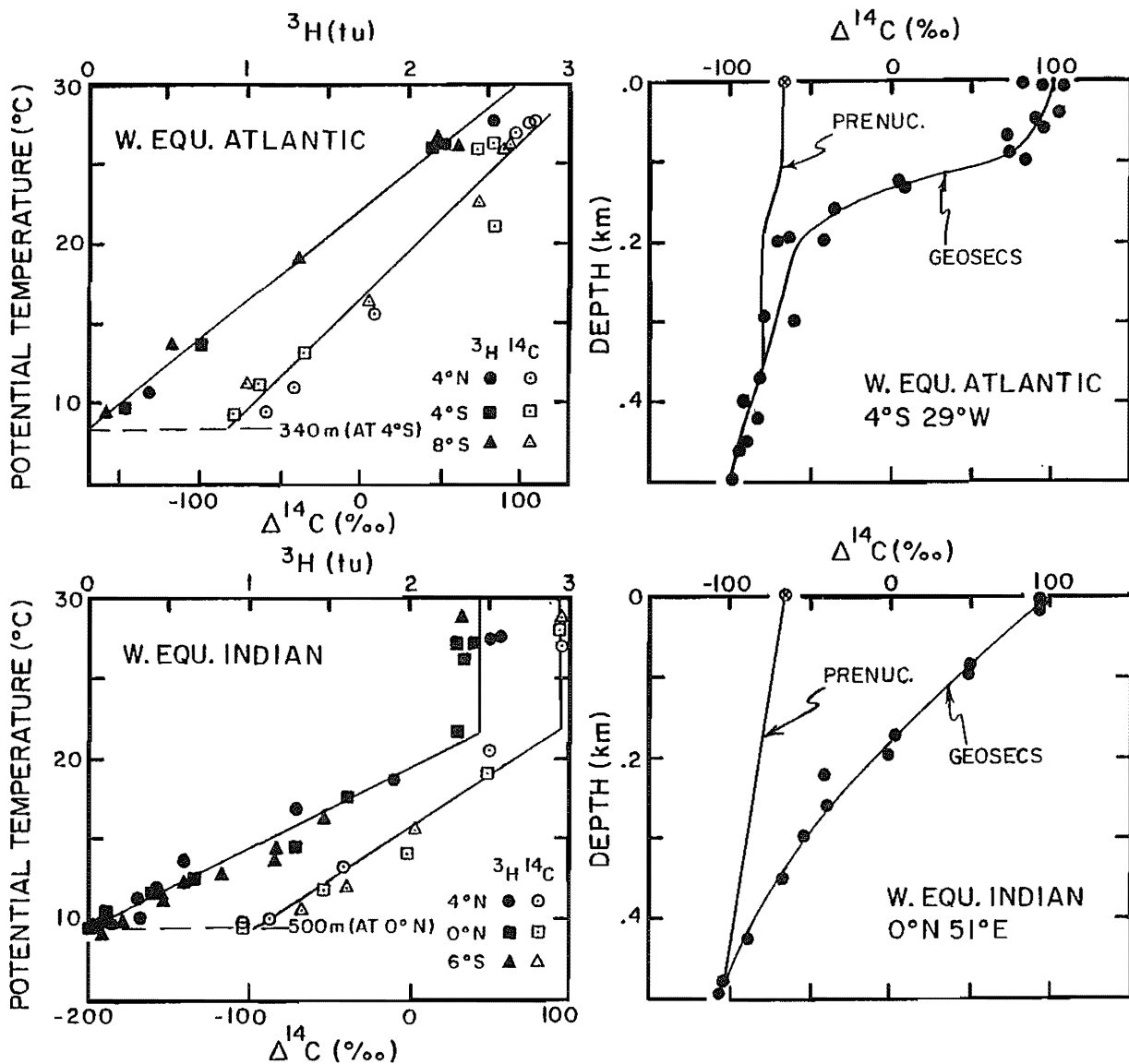


Figure 8-22. $\Delta^{14}\text{C}$ versus potential temperature and versus depth for samples taken during the GEOSECS program in the western equatorial Atlantic and in the western equatorial Indian Oceans (open symbols) (21,23). Also shown are the tritium values (solid symbols) (51,56). The linearity between both $\Delta^{14}\text{C}$ and tritium concentration with potential temperature in the main oceanic thermocline should be noted. The prenuclear $\Delta^{14}\text{C}$ profile is reconstructed assuming that the natural radiocarbon also showed a linear relationship to potential temperature. The ^{14}C analyses were made in the laboratories of Stuiver and Ostlund (21,23). The tritium analyses were carried out in the laboratory of Ostlund (51, 56).

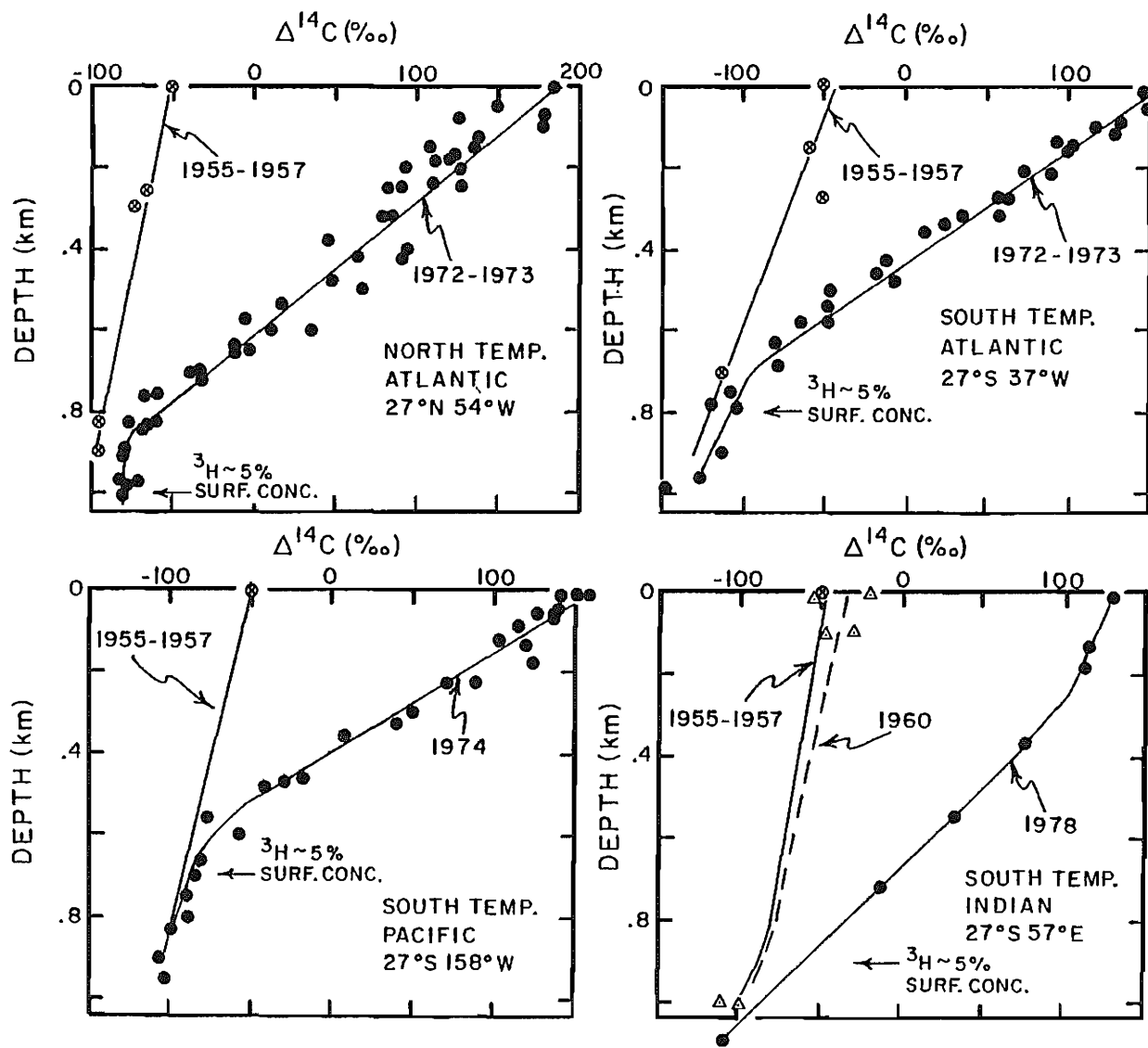


Figure 8-23. $\Delta^{14}\text{C}$ versus water depth in the temperate zones of the world ocean for prenuclear samples (open circles) and for GEOSECS samples (solid circles). The near linearity of the trend for waters containing more than 5% of the tritium concentration in surface water should be noted. In the case of the Indian Ocean where prenuclear data is sparse samples collected in 1960 are also shown (triangles). The solid lines connecting prenuclear surface water with the GEOSECS profile for samples having less than 5% the surface water tritium content represent the reconstructed prenuclear $\Delta^{14}\text{C}$ profiles. The GEOSECS $\Delta^{14}\text{C}$ measurements were made in the laboratories of Ostlund and Stuiver (21, 22, 23). The prenuclear and 1960 results are from references 4, 5, 6, 8 and 13.

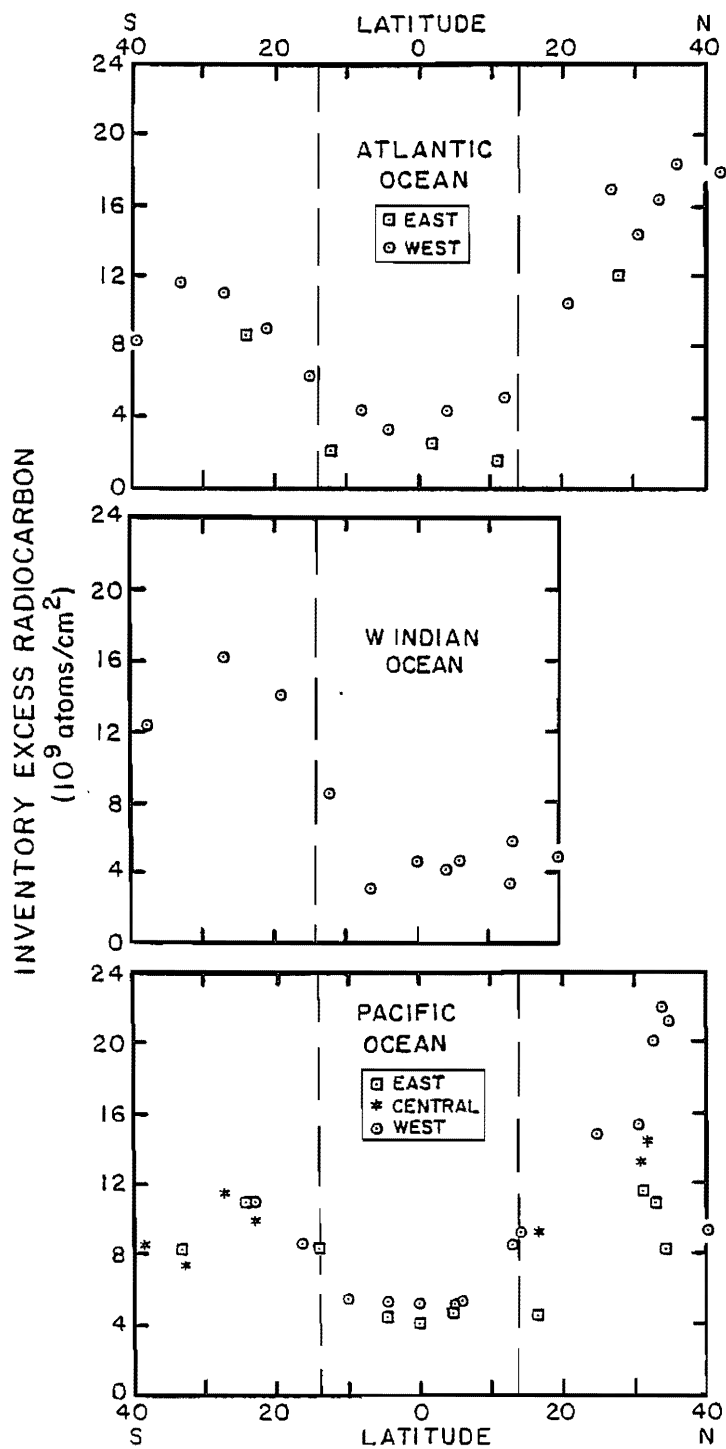


Figure 8-24. Water column inventories of bomb- ^{14}C in the temperate and equatorial regions of the three major oceans. The ^{14}C measurements were carried out in the laboratories of Ostlund and Stuiver (21,22,23). The integrations were performed by the authors (75).

anomalous in this regard).

EXPLANATIONS FOR THE LOW-EQUATORIAL BOMB C-14 INVENTORIES

The reason that this large inventory difference comes as a surprise is that the driving force for the input of bomb radiocarbon (i.e., the difference between the $^{14}\text{C}/\text{C}$ ratio in atmospheric carbon and surface ocean carbon) is very nearly the same in the equatorial ocean as in the temperate ocean. This can be seen from figure 8-3. Thus, if the impedance to gas exchange (i.e., the thickness of the stagnant film) is on the average about the same in the equatorial zone as in the temperate zone, then nearly the same amount of bomb radiocarbon must have entered the equatorial ocean as the temperate ocean.

Three explanations can be put forth to explain the difference:

1) It is the result of the combination of rapid mixing along the isopycnal surfaces and the close spacing of the isopycnal horizons in the equatorial zone. As the volume of water above any given isopycnal surface is much smaller in the equatorial zones than in the temperate zones (see figure 8-5), rapid mixing along isopycnal horizons would lead to the accumulation of more tracer in the temperate than in the equatorial zone.

2) The impedance to gas exchange is several times greater in the equatorial than in the temperate zone.

3) The upwelling of water in the equatorial zone purges this region of the bomb- ^{14}C invading from the atmosphere. The upwelling water pushes aside surface waters in the equatorial zone, driving them laterally into the adjacent temperate zones. This process would decrease the bomb- ^{14}C inventory in the equatorial zones and enhance that in the temperate zones.

Of these explanations, we will show that the first can be ruled out; the second is unlikely but remains a dark horse; and the third, while quite plausible, is not without problems.

The first explanation can be ruled out because the gradient in bomb radiocarbon along every isopycnal and every horizontal surface down to the base of the tritium-contaminated zone is toward the equatorial zone. Horizontal or isopycnal mixing would increase rather than decrease the inventory of bomb- ^{14}C in the equatorial zone. Hence the bomb radiocarbon entering the equatorial zone from the atmosphere cannot be dissipated by such mixing. This is a firm argument; the first explanation must be crossed from the list!

In chapter 3 we discussed the factors controlling the rate of gas exchange between the ocean and atmosphere and concluded that the dominant factor must be wind speed. From meteorological observations it can be shown that the average wind velocity in the equatorial zones is about 85% that in the temperate zones. Also, the average stagnant film thickness as measured by the radon method in the equatorial zone is only about 20% thicker than that measured in the temperate zone (176). Hence both theory and measurements would suggest that the gas exchange impedance in the equatorial zone is perhaps 1.2 that in the temperate zones. To explain the difference in inventories the impedance in the equa-

torial zone would have to be three to four times that in the temperate zone! While this appears quite unlikely, this explanation remains a dark horse.

Evidence for upwelling along the equator and along continental margins in the equatorial zone comes from every discipline. The geologist sees the products of upwelling (for example, the frustule of diatoms) in enhanced abundance in the sediments accumulating beneath these zones, the biologist observes enhanced rates of plant growth in these zones, the chemist observes high concentrations of PO_4 , NO_3 , H_4SiO_4 , CO_2 , ... in the surface waters of these zones, and the physical oceanographer predicts such upwelling based on the patterns of winds. Thus few would argue against upwelling. The questions in connection with the radiocarbon inventories have to do with the total flux of upwelled water (is it great enough to purge the equatorial zone of its radiocarbon on the proper time scale?) and with the origin of the upwelling water (is it recycled equatorial water or does it come from the adjacent temperate zones or from intermediate waters flowing beneath the equatorial zone?). Other disciplines have little firm evidence to offer in answer to these questions. They are difficult ones.

This being the case, we must try to get this information from the distributions of the tracers we have already mentioned (CO_2 , ^3H and ^{14}C) and perhaps supplement this with information from tracers whose potential in this regard has yet to be tested (^3He , ^{85}Kr , ...). Let us start by considering bomb radiocarbon alone. To make this calculation as straightforward as possible, we will make six simplifying assumptions. One looks for the big things first; the complicating details can be added later. First, we will assume that the upwelling water carries no bomb- ^{14}C (this assumption leads to a lower limit on the flux). Second, we will assume that at the time of the GEOSECS surveys the bomb- ^{14}C budget in the equatorial oceans had reached steady state (i.e., the input of new radiocarbon from the atmosphere nearly balanced the loss resulting from the purging action of upwelling water). This assumption is supported by the ^{14}C measurements on corals (see figure 8-21). The third assumption is that there is no input of bomb-produced ^{14}C via lateral mixing with the adjacent temperate zones. Like the first assumption, this one leads to a lower limit on the upwelling rate. The fourth assumption is that mixing along isopycnal horizons within the equatorial zone is so rapid that the exact route taken by the upwelling water has no consequence. As shown in figure 8-22, the tracers are well mixed along isothermal (and hence also isopycnal) surfaces within the equatorial zone. This assumption allows the calculation to be carried out as if upwelling were uniform throughout the zone (which it clearly is not). The fifth assumption is that the CO_2 partial pressure in surface water is the same as that in the air. The sixth assumption is that the rain of bomb radiocarbon with falling particles is negligible. While neither of the latter two assumptions is strictly correct, only second-order changes in the calculated fluxes occur when they are handled properly.

The calculation then becomes one of balancing the water and radiocarbon budgets for the upper equatorial zone. The fluxes are

Figure 8-25. Simplified model for the bomb- ^{14}C balance in the surface mixed layer of the equatorial ocean. Water upwelling into this layer is dissipated by poleward flow along the surface. While in residence at the surface, the upwelled water gains bomb ^{14}C through CO_2 exchange with the atmosphere.

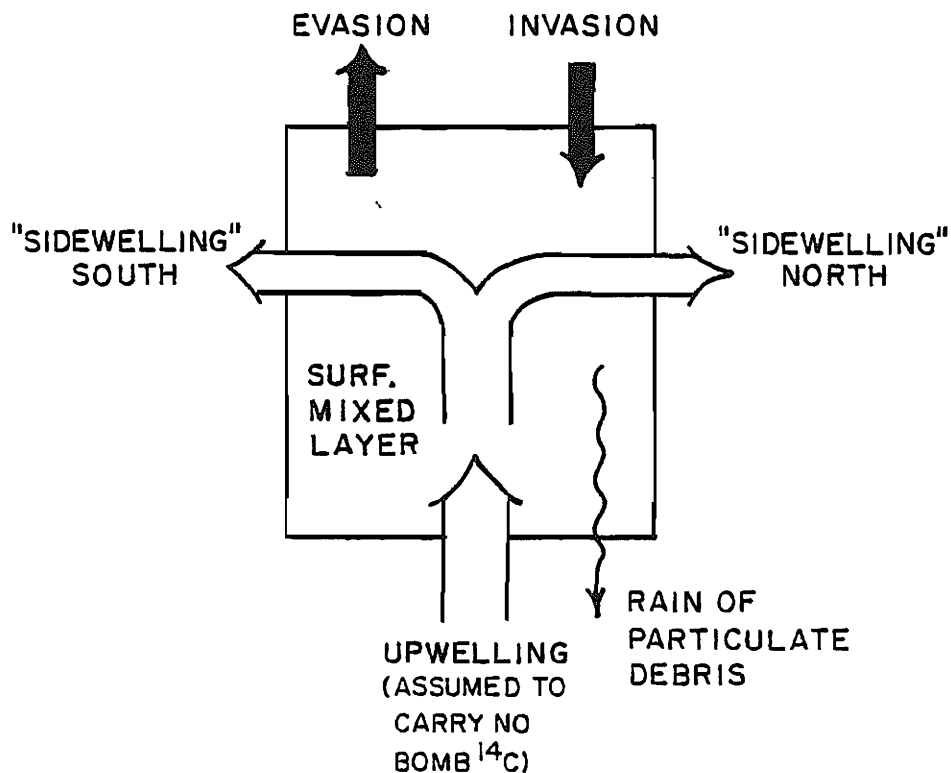


Table 8-5. Summary of the data parameters used to calculate the area averaged upwelling rate in the equatorial ocean from the distribution of bomb- ^{14}C . (The asterisk behind ^{14}C designates excess over natural).

	Date of GEOSECS Survey	GEOSECS $\Delta^{14}\text{C}$ atm °/oo		PRENUCLEAR $\Delta^{14}\text{C}$ atm °/oo		$\frac{\Delta^{14}\text{C}^*/\text{C}}{\Delta^{14}\text{C}^*/\text{C}_{\text{SW}}}$	W m/yr
Atlantic	1972	440	95	-25	-65	2.9	15
Indian	1978	330	90	-25	-65	2.3	11
Pacific	1974	390	80	-25	-65	2.9	15

shown in figure 8-25. There are just two water fluxes. Loss to the temperate zones along the surface must balance upwelling. There are three fluxes involved in bomb- ^{14}C balance; the invasion of bomb- ^{14}C bearing atmospheric CO_2 , the evasion of bomb- ^{14}C bearing surface ocean CO_2 and the loss of bomb- ^{14}C with the water exported from the equatorial zone to the temperate zone. As the upwelled water is assumed to carry no bomb- ^{14}C this source does not contribute to the ^{14}C budget.

The ^{14}C balance can then be written as follows:

$$\frac{\frac{^{14}\text{C}^*}{\text{C}}}{\text{atm}} \left. I = \frac{\frac{^{14}\text{C}^*}{\text{C}}}{\text{sw}} \right) \left[I + W[\Sigma\text{CO}_2]_{\text{sw}} \right] \quad 8-1$$

where I is the rate of CO_2 exchange (~ 16 moles/ m^2yr), $[\Sigma\text{CO}_2]_{\text{sw}}$ the concentration of inorganic carbon in the exported surface water (~ 2 moles/ m^3), $\frac{^{14}\text{C}^*/\text{C}}{\text{atm}}$ and $\frac{^{14}\text{C}^*/\text{C}}{\text{sw}}$ are respectively the bomb- $^{14}\text{C}/\text{C}$ ratio in the atmospheric CO_2 and in surface water ΣCO_2 , and W the unknown upwelling rate (in units of $\text{m}^3/\text{m}^2\text{yr}$ or m/yr) averaged over the entire area of the equatorial zone. This equation can be solved for W yielding:

$$W = \frac{I}{[\Sigma\text{CO}_2]_{\text{sw}}} \left[\frac{\frac{^{14}\text{C}^*/\text{C}}{\text{atm}}}{\frac{^{14}\text{C}^*/\text{C}}{\text{sw}}} - 1 \right] \quad 8-2$$

As can be seen from table 8-5, all three oceans yield an area averaged upwelling rate on the order of $13 \text{ m}/\text{yr}$. Since the aggregate area of the equatorial ocean (15°N to 15°S) is about $1 \times 10^{14} \text{ m}^2$ the total upwelling flux is about $1.3 \times 10^{15} \text{ m}^3/\text{yr}$ (~ 40 Sverdrups). Thus the amount is about the same as the flux of new bottom water to the deep sea.* Due to the assumption that the upwelling water contained no bomb radiocarbon and the assumption that no lateral or isopycnal mixing takes place across the 15°N and 15°S boundary zones, this flux must be considered a minimum.

IMPLICATIONS OF EQUATORIAL UPWELLING TO THE TRITIUM BUDGET

This result has an important implication to the budget of tritium in the ocean. If the water upwelling into the equatorial zone is free of bomb- ^{14}C , it must also be free of tritium. As at the time of the GEOSECS surveys the input tritium from atmosphere (and rivers) to the ocean had dropped to a very low level, upwelling should have been purging the tritium present in the equatorial zone (by pushing it along the surface into the adjacent temperate zones). The approximate time required for half the tritium to be purged is given by the following equation:

*We do not wish to imply that these two fluxes need be related in the sense that equatorial upwelling is the route by which deep water returns to the surface, but rather we use the comparison as a means of putting this very large flux into context.

$$t_{1/2} = 0.693 \text{ h/W}$$

where h is the mean penetration depth of tritium in the equatorial zone (~180 meters) and W is the rate of upwelling (at least 10 meters per year). So we get a half-time for the purging of tritium no more than 12 years. This corresponds to a purging loss of at least 8% each year. Is there evidence for such a decrease?

There are a few places in the equatorial ocean where the tritium profiles measured as part of the GEOSECS program can be compared with those measured at earlier times. The changes in inventory found in this way are summarized in table 8-3. Although scanty, and subject to rather large uncertainties these results suggest that the inventories held their own and perhaps even increased somewhat during a several-year period preceding the GEOSECS surveys.

The validity of this apparent contradiction to the upwelling model can be checked by a less direct method. No means exists by which a decrease in the mean penetration depth of tritium with time could occur once the major amount of tritium had been delivered to the sea. Hence, if the water column inventory of tritium in the equatorial zone decreased, then the surface water concentration must also have decreased. If the mean penetration depth were increasing the surface water concentration would decrease at an even higher rate than the water column inventory. In the western equatorial Pacific Ocean, where we have both extensive tritium measurements on surface water and a sequence of ^{90}Sr measurements on a coral head, the surface water shows a 3% per year increase in tritium content (see table 8-4) and almost no change in ^{90}Sr content (see figure 8-18) between 1968 and 1973. Thus we have a problem. The upwelling hypothesis, which so neatly explains the bomb- ^{14}C distribution, appears to run into a snag for tritium.

One way around this difficulty (at least for the Atlantic and Pacific) is to bring tritium into the equatorial zone from the large reservoirs of high-tritium water in the north temperate zone. This transport could be accomplished either by lateral mixing across the 15°N front or by advection of upper temperate thermocline waters into equatorial zone (as a contribution to the total upwelling flux). As the north temperate water which carries large amounts of tritium also carries bomb radiocarbon, the addition of this radiocarbon to the equatorial zone would then have to be balanced by an even greater rate of upwelling. Further, as we have shown, the θ -S relationships in the equatorial zones of the Atlantic and Pacific are more akin to those of the southern temperate zone than to those of the northern temperate zone. Thus if north temperate thermocline waters are brought in to maintain the tritium inventory then waters from the south temperate thermocline would also have to be brought in to maintain the proper θ -S relationship. The south temperate thermocline waters would also carry bomb- ^{14}C (but little tritium). Again more upwelling would be required. While it is possible to create a blend of all these waters which reproduce the distributions of bomb- ^{14}C , of tritium, of temperature and of salinity, the total rate of upwelling required goes up by at least a factor of three.

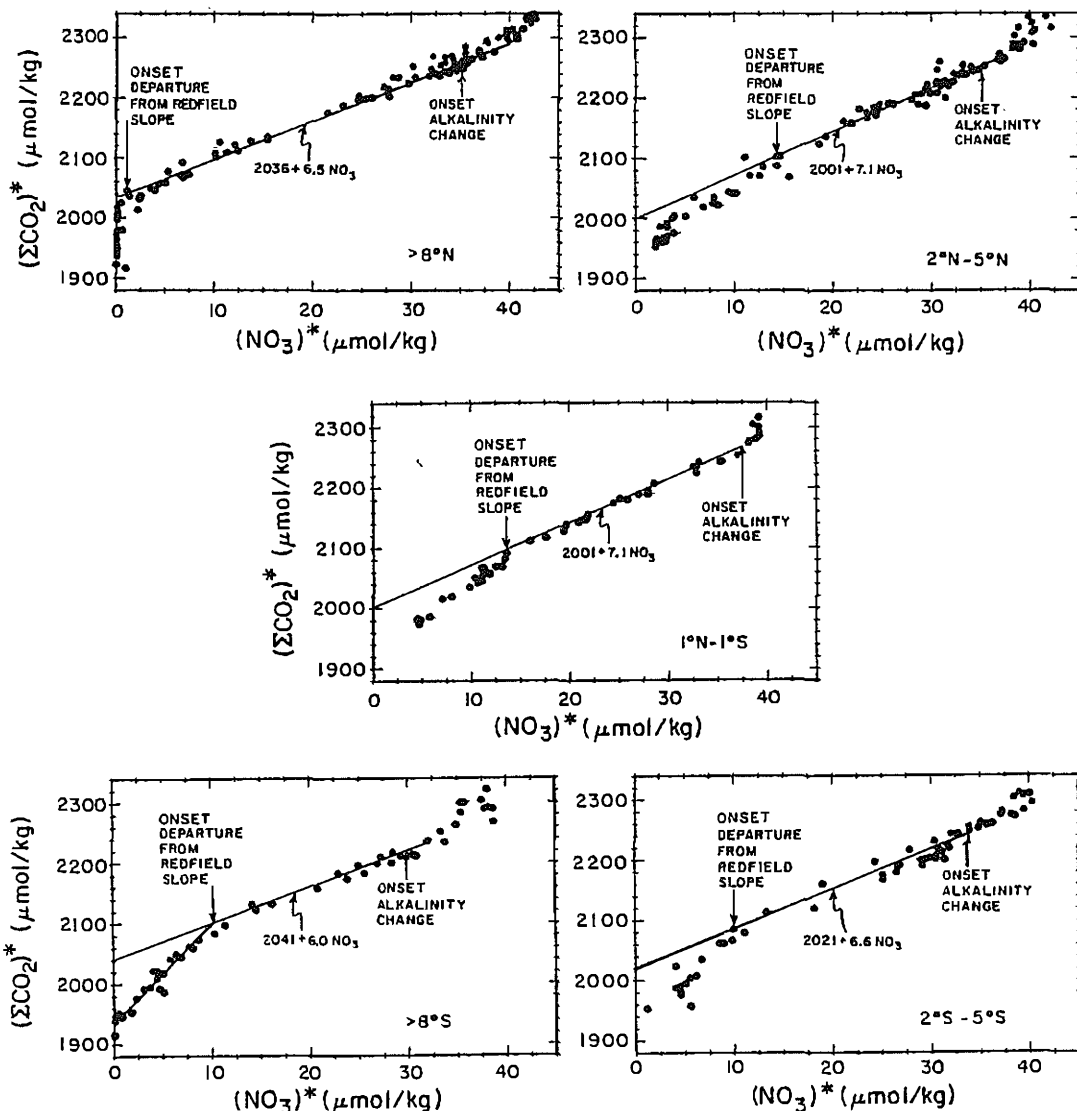
Could the total flux of upwelled water in the equatorial zones of the world ocean be as high as 120 Sverdrups? While no firm grounds for rejection can be given, many physical oceanographers would be very uneasy with such high fluxes. Thus some other new information is needed to tip the balance toward or away from acceptance of the upwelling explanation for the low equatorial zone water column inventories of bomb radiocarbon.

AN UPWELLING RATE BASED ON THE EQUATORIAL CO₂ ANOMALY

We laid the groundwork for another upwelling rate estimate by discussing the distribution of chemical properties in the surface waters of the equatorial zone in the Pacific Ocean (see chapter 3). It was shown that the concentration of virtually every property is anomalous compared to the adjacent surface waters. The temperature and salinity are low and the nutrient element concentrations and CO₂ partial pressure are high. It is the high value for the pCO₂ which permits an estimate of the upwelling rate. Were new CO₂-laden water not entering the surface layer, the CO₂ anomaly would be dissipated by loss to the atmosphere. In order to obtain a quantitative estimate of the rate of this renewal, the amount of CO₂ lost to the atmosphere by equatorial surface waters and the rate of CO₂ evasion to the atmosphere must also be known. It is the first of these that is not so easily obtained. Seemingly it would require that not only the ΣCO₂ content of upwelling water be known but also the amount of CO₂ lost to plants. As the amount of ΣCO₂ in the upwelling water depends on the depths from which these waters originate (an unknown), we are seemingly stuck. As already discussed in chapter 3, there is a clever way to circumvent the need to define the upwelling depth. This is accomplished using plots of ΣCO₂ (normalized to a constant salinity) against NO₃ for samples from the thermocline and surface. Plots of this type for three latitude zones are shown in figure 8-26. In each case the points for thermocline waters fall along a trend with a slope close to the Redfield ratio. Thus the photosynthesis-respiration cycle explains the variations seen. For samples taken from the uppermost thermocline and at the surface the points fall below this trend. The likely explanation is that the ΣCO₂ content of these waters has been altered by CO₂ loss to the atmosphere. If so, then we can take the magnitude of the deviation of the points for the surface water samples from the trend established for thermocline samples as the amount of CO₂ lost to the atmosphere. Surface water samples from the 4°N to 4°S equatorial strip showing high pCO₂ values have an average ΣCO₂ deficiency of 60 μm/kg. Each unit of upwelled water appears to have lost this amount of CO₂ to the atmosphere. The balance can be written as follows:

$$I \left[\frac{pCO_2^{surf}}{pCO_2^{air}} - 1 \right] = W\Delta\Sigma CO_2 \quad 8-3$$

where pCO₂^{surf} and pCO₂^{air} are mean CO₂ partial pressures for surface waters and air in the equatorial zone, I is the inva-



* NORMALIZED TO A CONSTANT SALINITY

Figure 8-26. Plots of ΣCO_2 (normalized to a constant salinity) against nitrate for samples of the surface and thermocline water in five latitude belts in the equatorial Pacific (at longitude 155°W). In each case a straight line is fit to the points with intermediate nitrate content. As these line have slopes close to the Redfield ratio (~ 6.8) it is assumed that these samples have mainly been influenced by the photosynthesis-respiration cycle. For shallower waters (i.e., those with lower NO_3 concentrations) a deviation from this trend is seen. This deviation is presumably due to CO_2 loss to the atmosphere. For deep waters (i.e., those with higher NO_3 concentrations) a deviation is also seen. These deviations must reflect calcite dissolution as its onset corresponds to the depth where the alkalinity begins to rise. These results were obtained as part of the Hawaii-Tahiti Shuttle program (433). This is a repeat of figure 3-26.

sion rate of CO_2 , W is the unknown upwelling rate, and ΔECO_2 is the amount of CO_2 lost by the equatorial surface waters. The equation states that in order to maintain these distributions as they are, the CO_2 being lost to the atmosphere must be replaced by the addition of upwelling water. Solving for W , we get:

$$W = \frac{I}{\Delta\text{ECO}_2} \left[\frac{\text{PCO}_2^{\text{surf}}}{\text{PCO}_2^{\text{air}}} - 1 \right] \quad 8-4$$

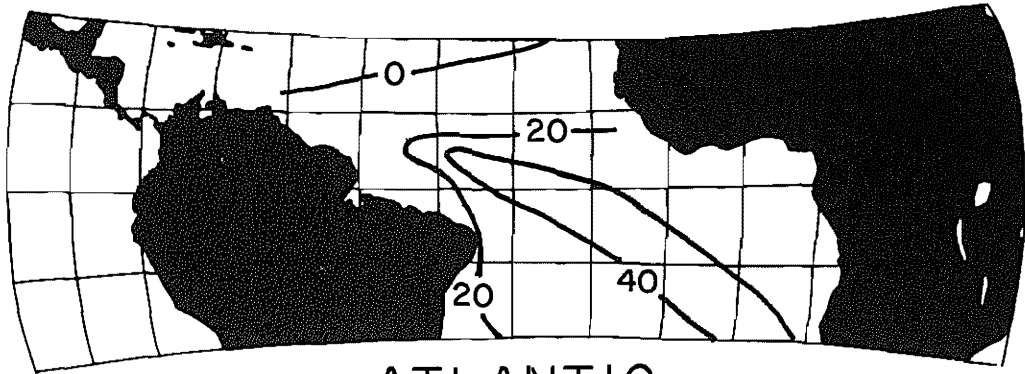
In the equatorial Pacific (4°N to 4°S) the PCO_2 in the surface water averages 410×10^{-6} atm, while that in the air is 330×10^{-6} atm. Thus the term in parentheses is about 0.25. I is about 16 moles/ m^2yr . ΔECO_2 is about 0.06 moles/ m^3 . Thus:

$$W = \frac{16 \text{ moles}/\text{m}^2\text{yr}}{0.06 \text{ moles}/\text{m}^3} \times 0.25 = 66 \text{ m/yr}$$

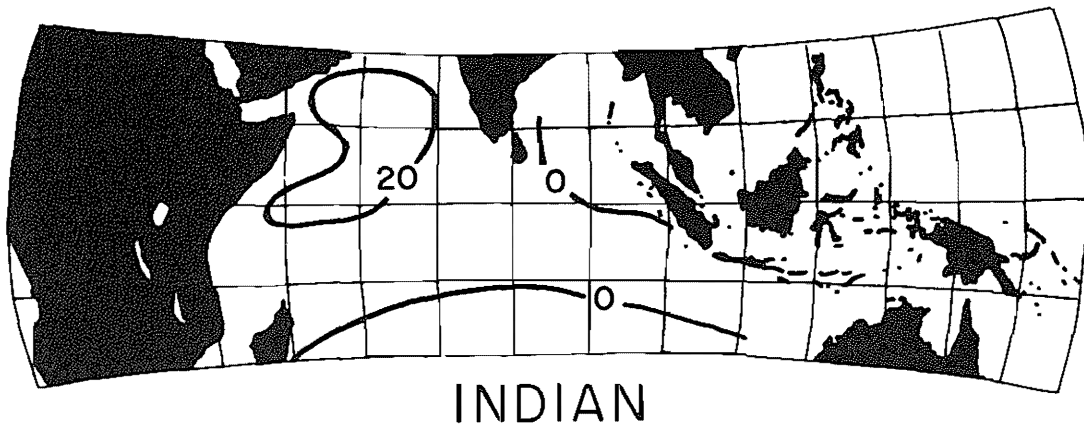
To be compared with the bomb radiocarbon-based rate which applies to a latitude belt 15°N to 15°S , this estimate must be reduced to about a factor of $4/15$ (hence from 66 to 18 m/yr). Thus both the distribution of bomb- ^{14}C and the chemical anomalies of carbon in the equatorial zone lead us roughly to the same conclusion. The area averaged upwelling rate in the equatorial zone lies in the range 16 to 40 m/yr and amounts to a global flux somewhere in the range 50 to 120 Sverdrups.

We are forced to express our results as area-averaged upwelling rates because the rapidly flowing equatorial currents are able to carry the upwelled water from one "end" of the zone to the other during their time of residence at the equatorial surface. Because ^{14}C requires a longer time to equilibrate with the atmosphere (~15 years) than the time of residence of water at the surface of the equatorial zone (~6 years) its distribution has lost any message carried by the geographic distribution of upwelling. CO_2 , on the other hand, has an equilibration time (~1 year) shorter than the residence of water at the surface (~6 years). Thus the distribution of the PCO_2 anomaly carries information regarding the point of entry of the upwelling water. It demands that the upwelling occur both along the equatorial belt and in coastal upwelling areas from which currents feed into the equatorial zone.

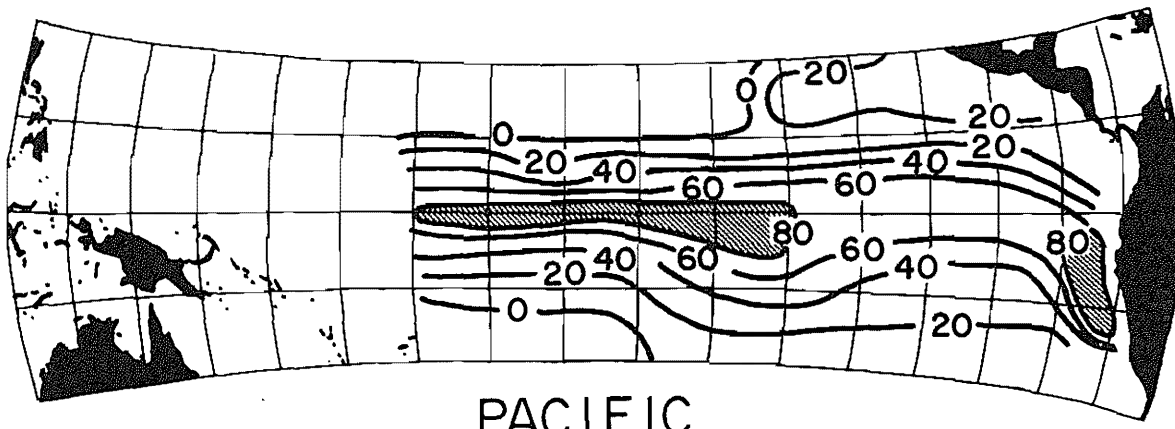
As shown in the maps for the equatorial Pacific, Atlantic and Indian Ocean (see figure 8-27), only in the Pacific has a prominent surface water CO_2 partial pressure anomaly been found along the equator. Where then does the upwelling occur in the Atlantic and Indian Oceans? Although we do not know the answer to this question our suspicion is that in all three oceans coastal upwelling makes a very important contribution to the total. As can be seen from the map for the equatorial Pacific Ocean, the region south of the equator along the South American coast appears to contribute strongly to the anomaly. The signature of this upwelled water is apparently carried far from the continental margin by the prevailing currents. A similar area of strong upwelling occurs along the coast of Africa to the south of the equator.



ATLANTIC



INDIAN



PACIFIC

Figure 8-27. Maps showing the distribution of excess CO₂ partial pressures in equatorial surface water. The contours are in units of 10^{-6} atmospheres. These maps were constructed by Taro Takahashi of the Lamont-Doherty Geological Observatory using data from many expeditions run in different years and seasons (387, 388, 393, 394, 406).

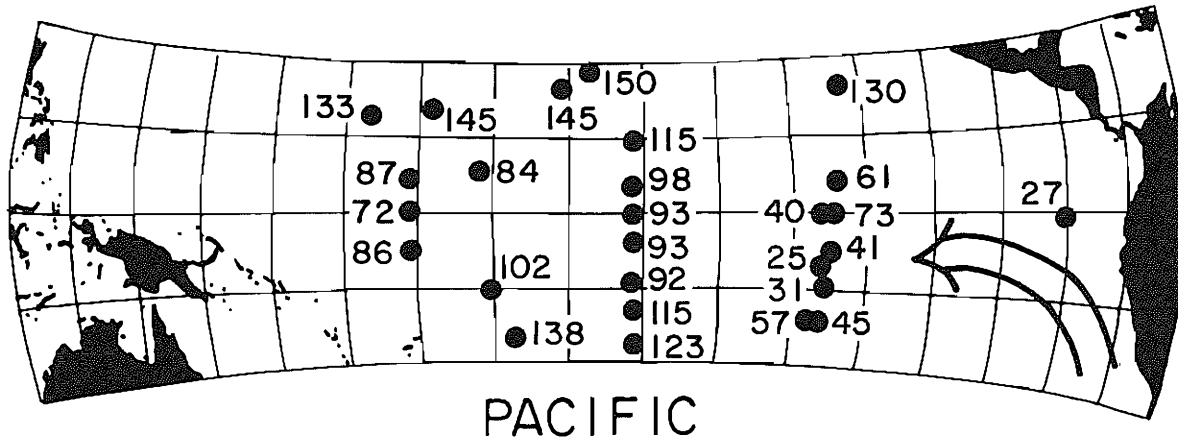
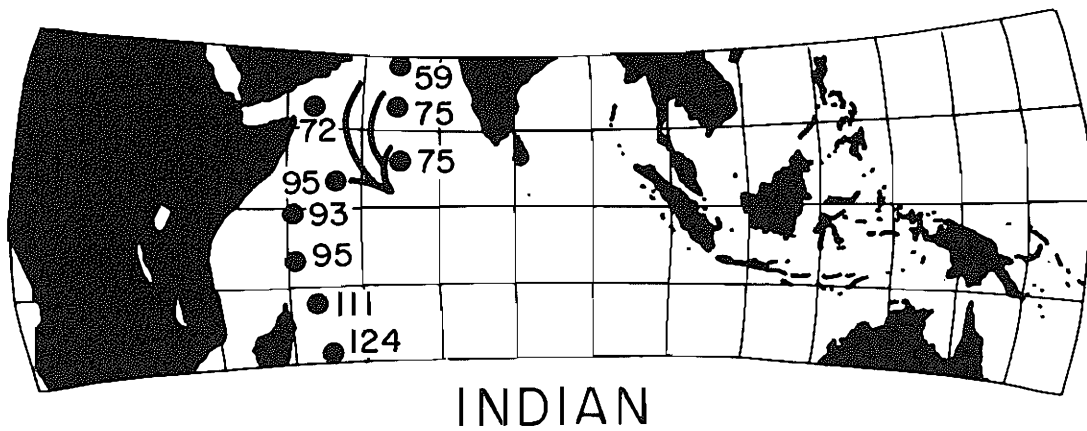
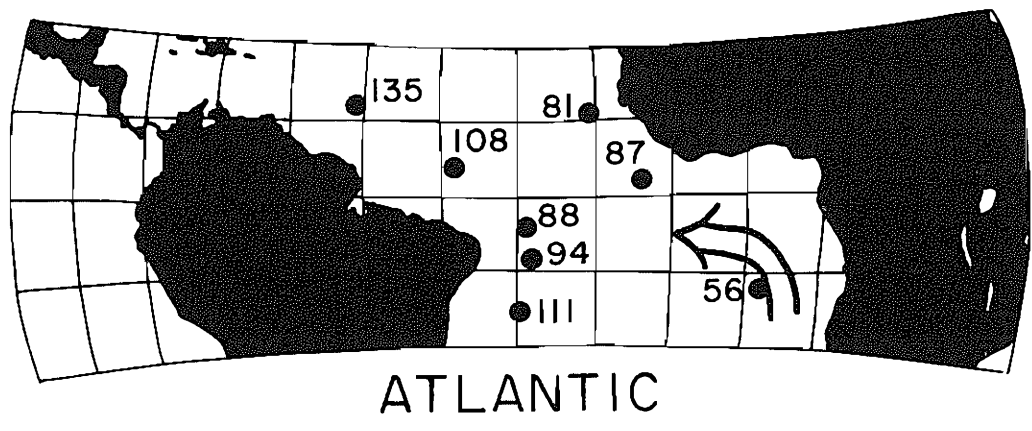


Figure 8-28. Radiocarbon measurements (expressed as $\Delta^{14}\text{C}$) on surface water samples from the equatorial zone. The arrows represent the paths followed by waters upwelled into coastal areas. The results were obtained as part of the GEOSECS program (21,22,23) and as part of the Hawaii-Tahiti Shuttle Program (Quay and Stuiver personal communication). The results obtained by Ellen Druffel on a coral from the Galapagos are also included (17).

We suspect that this area is the conduit for most of the upwelling water reaching the Atlantic equatorial zone. In the Indian Ocean strong upwelling occurs in the Gulf of Arabia. Again this may be the major conduit for upwelled water reaching the equatorial zone.

The radiocarbon content of surface waters in and near these zones of intense upwelling shows a local anomaly (exceeding that seen in the ambient surface waters of the equatorial zones). The map in figure 8-28 shows the results for surface waters collected between 1972 and 1980 in the equatorial zones of the world ocean. As shown by the results on corals (see figure 8-21), the $^{14}\text{C}/\text{C}$ ratio in surface water was quite uniform over this time interval; hence despite the differing times of collection the results on these samples should be directly comparable. It can be seen that the lowest values are found in and downstream from the areas of intense coastal upwelling (namely, off South America in the eastern Pacific, off Africa in the eastern Atlantic, and in the Gulf of Arabia in the northwestern Indian Ocean). Unfortunately, we do not as yet have systematic CO_2 partial pressure surveys for the surface waters in these areas. Also, the ^{14}C data are quite sparse.

HE-3 DISTRIBUTION IN THE MAIN OCEANIC THERMOCLINE

In the preceding sections we have provided evidence supporting a strong role for upwelling in the ventilation of the equatorial ocean. This upwelled water must flow along the surface into the adjacent temperate zones. Then where does it go? Some of it flows across the temperate zone into the polar areas and contributes to new deep water formation. Some sinks within the temperate zone. This sinking is likely via flow along isopycnal horizons from their winter outcrops. That portion of the water entering the temperate thermocline eventually passes across the 15° fronts into the equatorial zone completing the loop.

Yet another of our tracers gives us some insight into the processes responsible for the ventilation of the temperate thermocline. The ^3He generated by the decay of bomb tritium adds important information not obtainable from the tritium distribution alone.

In order to appreciate the added information provided by ^3He let us first consider the vertical distributions of tritium and bomb- ^{14}C with depth in the equatorial and temperate zones. Depth profiles for these isotopes in the equatorial and temperate zone of the North Atlantic are shown in figures 8-29 and 8-30. The simplest model to explain these distributions would be one involving upwelling in the equatorial ocean coupled with downwelling in the temperate zones. Half of the water upwelling in the equatorial zone is assumed to flow across the surface to the north and then to downwell in the north temperate zone. The other half goes to the south temperate zone. In both zones eddy diffusive mixing in the vertical is also assumed to operate. As the density gradient in the equatorial zone is much larger than that in the temperate zone, the eddy diffusivities need not be the same in the two zones. A mixed layer 100 meters thick is assumed in the equator-

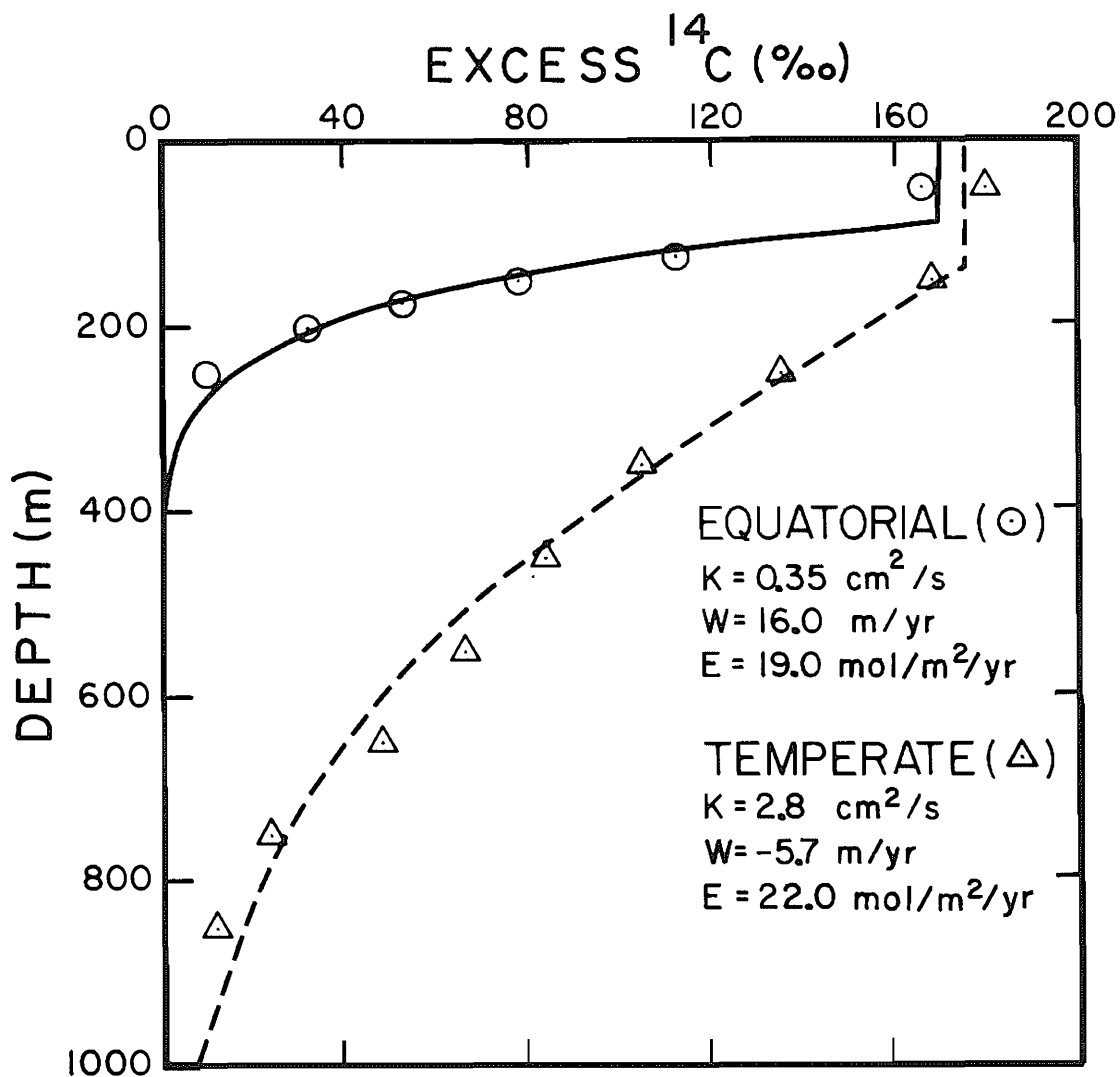


Figure 8-29. Mean profiles for $\Delta^{14}\text{C}$ in the north temperate and equatorial zones of the Atlantic as of 1973 (21) compared with the profiles (lines) yielded by the regional 1-D model described in the text. The parameters used in the model are given. Also shown are the thicknesses assumed for the surface layers in these regions.

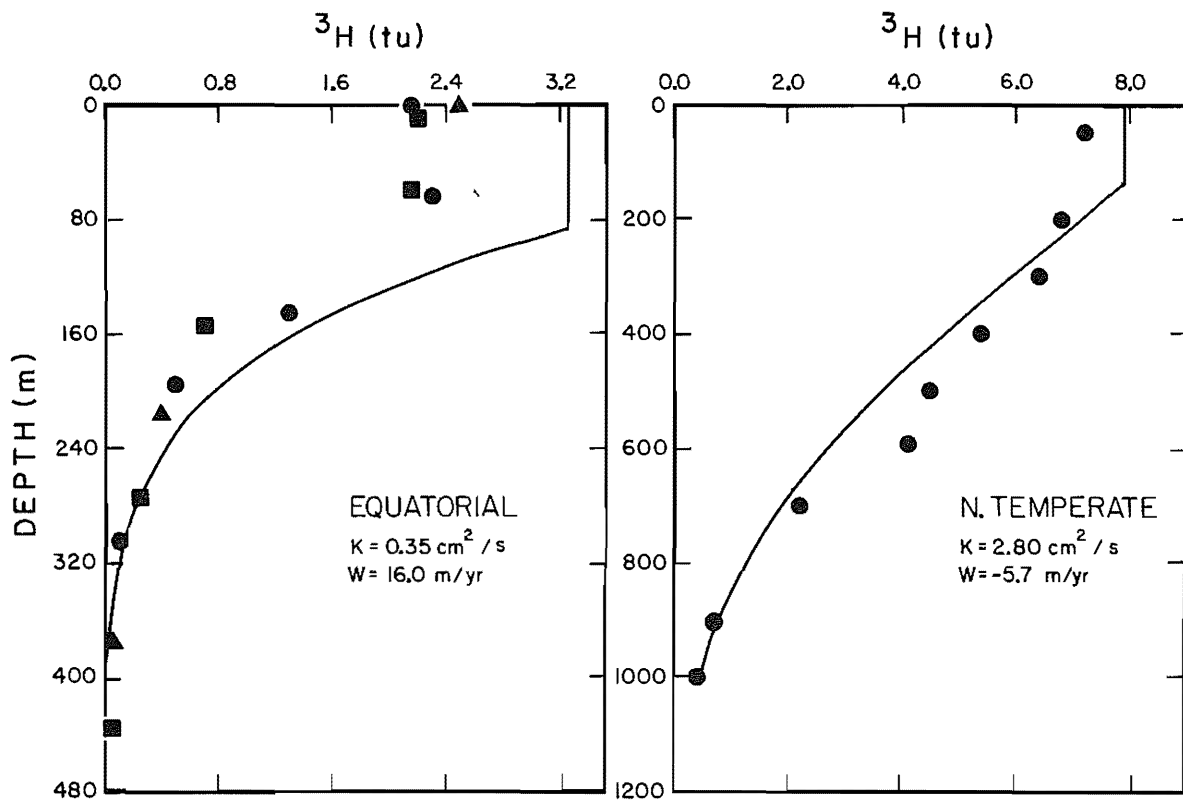


Figure 8-30. Mean profiles of tritium in the north temperate and equatorial zones of the Atlantic Ocean (52,52) compared with the profiles (lines) yielded by the regionalized 1-D model. The parameters used in the modeling are those for the best fit to the bomb- ${}^{14}\text{C}$ distribution (see figure 8-29).

ial zone and a mixed layer 150 meters thick is assumed for the temperate zone. The latter is larger because of deep winter convection which thickens the mixed layer in the temperate zone. The CO₂ invasion rate is taken to be 19 moles/m²/yr in the equatorial zone and 22 moles/m²/yr in the temperate zone (consistent with the difference in rates based on wind velocity and on radon measurements).

A numerical model is then constructed which allows these processes to be simulated. The model runs begin with the ¹⁴C at its natural steady state and with no tritium. Bomb tritium and radiocarbon are then added to the sea surface in accord with the temporal and geographic input functions described above. The upwelling rate in the equatorial zone and the vertical eddy diffusivities in both zones are then adjusted to give the best fit. The results are shown in figures 8-29 and 8-30. As can be seen, the distributions can be satisfactorily explained by this simple linked regional 1-D model. The equatorial upwelling rate obtained in this way is similar to that calculated above. The eddy diffusivity needed for the temperate zone is about 8 times higher than that needed in the equatorial zone. Both the radiocarbon and tritium distributions are fit reasonably well.*

The fact that the model fits cannot, of course, be taken as evidence that the ocean functions in accord with the model. The ability of the simplest of models to fit the primary features of these distributions rather says that these distributions carry little information about the nature of the ventilation process. Models involving ventilation along isopycnals could equally well achieve the observed distribution.

With this background in mind, let us consider the distribution of ³He. The properties of this tracer of importance to the problem of thermocline ventilation are, first, that its production is tied to the radiodecay of tritium; and second, that when thermocline water carrying excess ³He reaches the surface, its excess ³He is lost to the atmosphere. Thus, unlike the other anthropogenic tracers which are produced in the atmosphere and from there penetrate into the sea, ³He is generated within the sea and escapes to the air. In the absence of mixing within the sea the ³He/³H ratio would constitute an hourglass type keeper of time. Once isolated from the air, a water sample would accumulate the ³He produced by the decay of ³H and the ³He/³H ratio would be a simple function of time; the relationship being:

$$\frac{[{}^3\text{He}^*]}{[{}^3\text{He}^*] + [{}^3\text{H}]} = e^{-\lambda t} \quad 8-5$$

where ³He* is the concentration of excess mass three helium in the sample and ³H is the concentration of tritium in the sample. This ideal situation never exists in the ocean. All the samples we obtain are mixtures of waters which left the surface at

*The fit for tritium in the equatorial zone would be better if an input rate 25% higher than that obtained by the procedures outlined in this chapter were used.

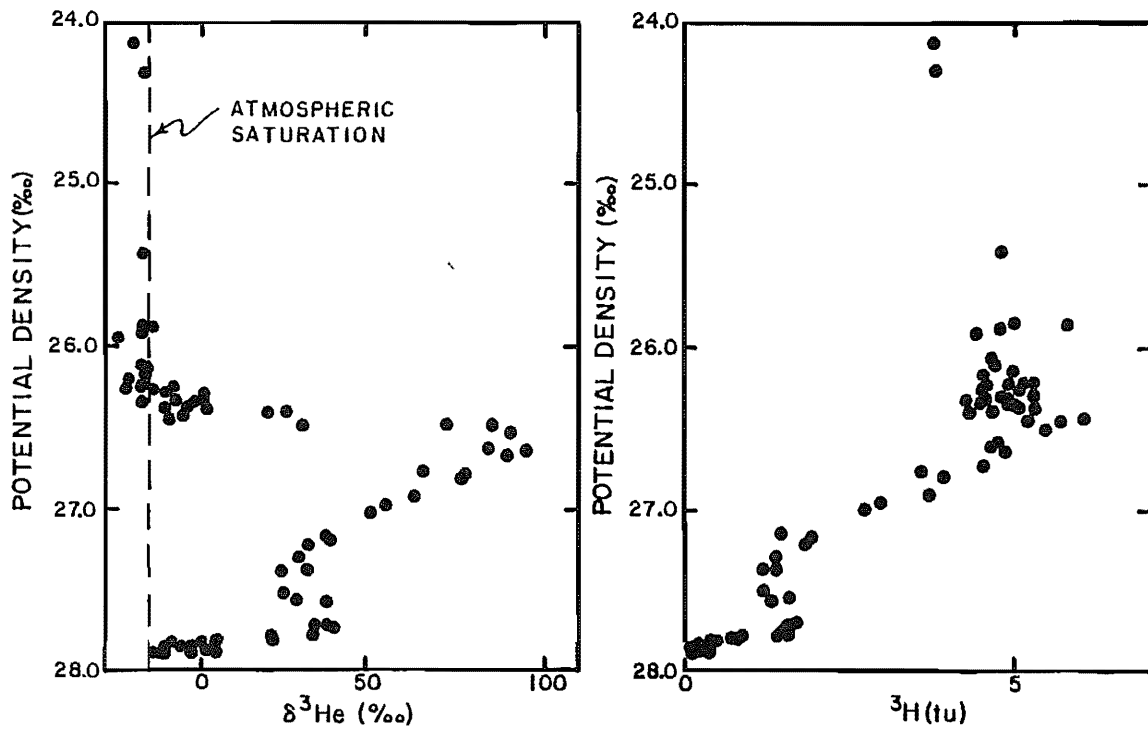


Figure 8-31. Plots of ${}^3\text{H}$ (in T.U.) and excess ${}^3\text{He}$ (in δHe units) as a function of density for samples from the upper 1000 meters of the water column in the Sargasso Sea. Density rather than depth is used to permit the overlay of results taken at different times and places. The important point these results make is that there is a sharp break in the profiles at a density of about 26.4‰. Above the density horizon the tritium is well mixed and the waters are free of excess ${}^3\text{He}$; (the difference in solubility of ${}^3\text{He}$ and ${}^4\text{He}$ leads to a $\delta{}^3\text{He}$ value of $-14\text{\textperthousand}$ for surface water at equilibrium with the air). At a density of about 26.4‰ the excess ${}^3\text{He}$ concentration shows a sharp increase. For more dense waters both the concentrations of tritium and of excess ${}^3\text{He}$ decrease with depth to a density of about 27.2‰. These measurements were made by Bill Jenkins of the Woods Hole Oceanographic Institution (279). See page 681 for definition of $\delta{}^3\text{He}$.

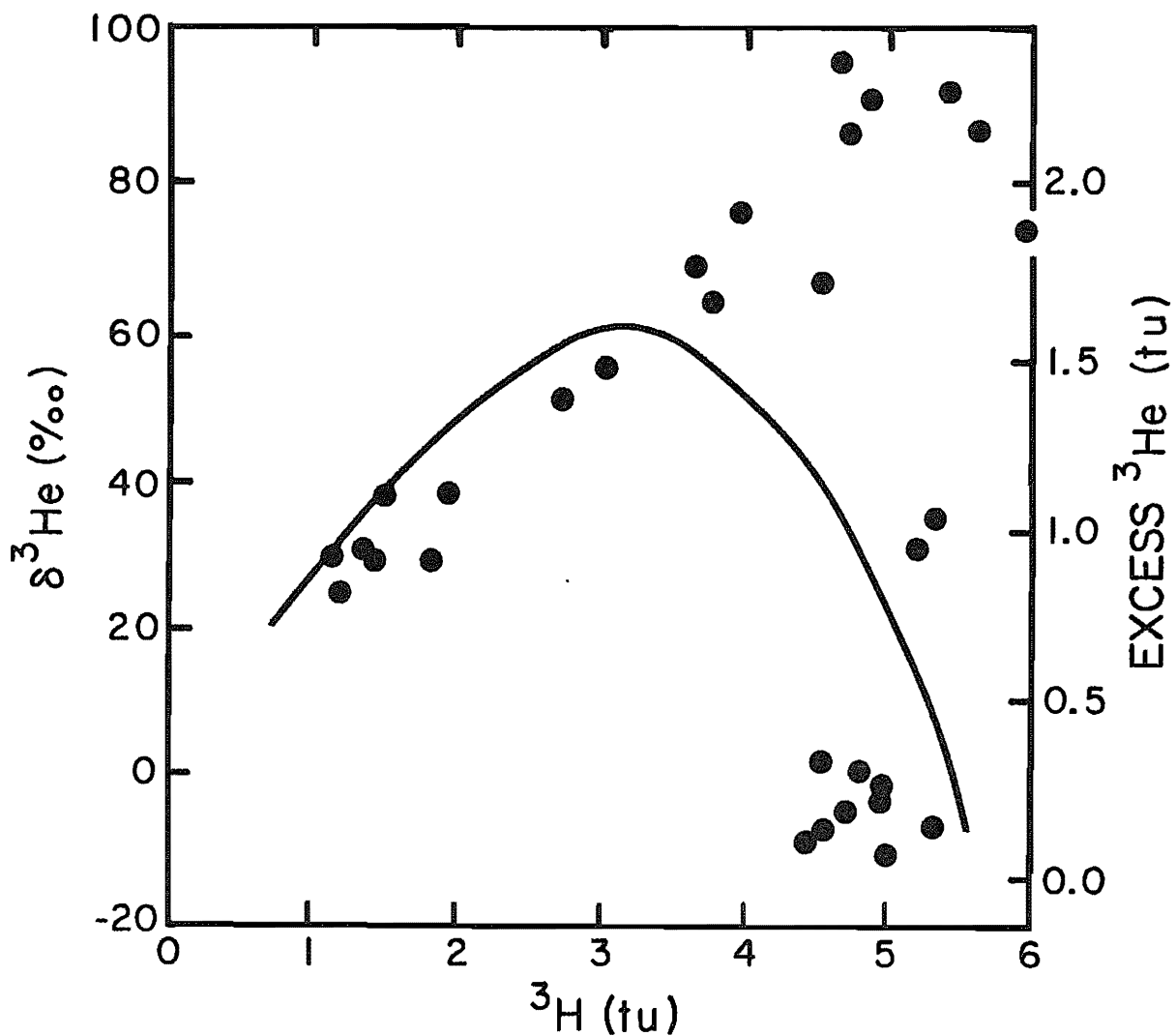


Figure 8-32. Plot of $\delta {}^3\text{He}$ versus tritium concentration for the data in figure 8-31. The curve obtained from the 1-D model of figures 8-29 and 8-30 is shown for comparison. No 1-D model can yield the distributions of both these tracers. Lateral processes must be operative.

different times carrying different tritium concentrations. Thus we can only interpret ^3He data in the context of some sort of mixing model.

Shown in figure 8-31 are profiles of ^3H versus potential density and of excess ^3He versus potential density for profiles taken in the Sargasso Sea of the North Atlantic by Jenkins of Woods Hole. Potential density rather than depth is used so that data from different stations and different times can be shown together.* As can be seen, the upper horizons (constituting approximately the 0 to 400-meter depth range) has nearly constant tritium and is nearly free of excess ^3He . This water must be returned to the surface every winter and lose the ^3He generated during the previous year. Below this layer the tritium content begins to decline and the excess ^3He rises abruptly to a maximum and then declines along with the tritium. A secondary maximum in both tritium and ^3He is seen at a potential density of about 27.5‰. Beneath this, both the tritium and excess ^3He content drop to zero.

Jenkins showed that, even if the vertical diffusivity were allowed to change with depth, no 1-D model could explain the distributions of these isotopes for densities less than 27.5‰. (Of course it goes without saying that the secondary maximum could not be generated by vertical processes alone.) Thus the ^3He data provides a compelling confirmation that ventilation along isopycnal horizons must be very important in the temperate regions!

Just to show how bad the fit would be using the 1-D model discussed above, we have compared in figure 8-32 the excess ^3He versus ^3H curve based on the measurements with that calculated by the 1-D model. This model (or any 1-D model) cannot produce the large bulge to high ^3He and tritium values shown by the data!

PURPOSEFUL TRACERS

So far we have discussed only tracers which happen to be present in the sea. While extremely valuable to the field of oceanography, these tracers appear to be incapable of yielding more than an upper limit on the rate of diapycnal mixing (i.e. those yielded by the 1-D model). As the entry of the anthropogenic tracers into the main ocean thermocline can be explained entirely by along-isopycnal penetration from surface outcrops, it is possible that little diapycnal mixing occurs within the main oceanic thermocline. Also, the distributions of anthropogenic tracer do not require any across-isopycnal advection in the temperate zones. Is it possible that tracers could be introduced into the sea by the oceanographer in such a way that the time evolution of their distributions would prove more enlightening in this regard? A tracer (some perfluorocarbon not currently present in nature) would be injected at a single point in the main thermocline. Careful attention would be given to keeping the initial patch as thin as possible and to documenting the density horizon on which it came to rest. Once in the ocean, the tracer would be allowed

*Internal waves within the thermocline can cause temporary changes of the height of a given isopycnal by several tens of meters.

to spread for several years before an attempt was made to locate or map it. A search would then be launched. If it could be found, a program of mapping would be initiated. Ideally, then, its vertical distribution would be determined as a measure of the degree of cross isopycnal mixing, the displacement of the median density horizon would be determined as a measure of the extent of upwelling or downwelling, and its lateral dimensions would be determined as a measure of along-isopycnal mixing.

One might ask whether the spread of such a tracer in the vertical could be the result of contact with the outcrop during the wanderings of the patch along its isopycnal horizon. The answer would be no. The reason is that if the tracer did reach the outcrop, it would be lost to the atmosphere! Hence, any cross isopycnal mixing observed during the experiment would reflect only mixing processes within the interior (including frictional mixing along the "sides" of the basin).

An even more elegant experiment could be carried out if two tracers were added together: one a gas and one a nonvolatile compound. The nonvolatile compound would not be lost during outcrop contacts and hence, if along-surface mixing followed by reentry into the thermocline were to occur, it would be recorded by the nonvolatile compound.

Is it feasible to do such an experiment? The answer is yes. The reason is that gas chromatographs are capable of detecting as little as 10^6 molecules of various perfluorocarbons. If, for example, 30 kilograms of a perfluorocarbon compound (molecular weight ~ 300 g/mole) were added to the sea, there would be 6×10^{25} molecules to trace. Thus even after the tracer had been spread over a volume 5000 km on a side and 100 meters thick (i.e., 2.5×10^{18} liters) there would still be 2.4×10^7 molecules per liter of water.

Perfluorocarbons are biologically inert. Hence the tracer would not be degraded by marine organisms nor would its addition pose any pollution hazard. The large amount needed for the experiment could be diffused into the ocean through silicon tubing thus avoiding the need to predissolve it in many tons of sea water. A nonvolatile compound could be made by substituting an ionic group in the structure of a perfluorocarbon. Analysis of this compound could then be done by fluorinating the sample and converting the nonvolatile back to a volatile compound.

One very serious problem could void the whole concept. It is almost certain that the initial patch would break up into a series of filaments. No one knows on what time scale these filaments would coalesce into a continuous patch. Were the patch to break up into a multitude of fragments and remain even years later after dispersal to all parts of the isopycnal horizon in this inhomogeneous state, then mapping to yield the type of information we seek would prove impossible. Once again the ocean would have foiled an attempt by man to pin down the details of its operation!

SUMMARY

The distributions within the sea of the anthropogenic tracers, bomb tritium and bomb radiocarbon, have much to tell about the ventilation of the upper ocean and about the formation

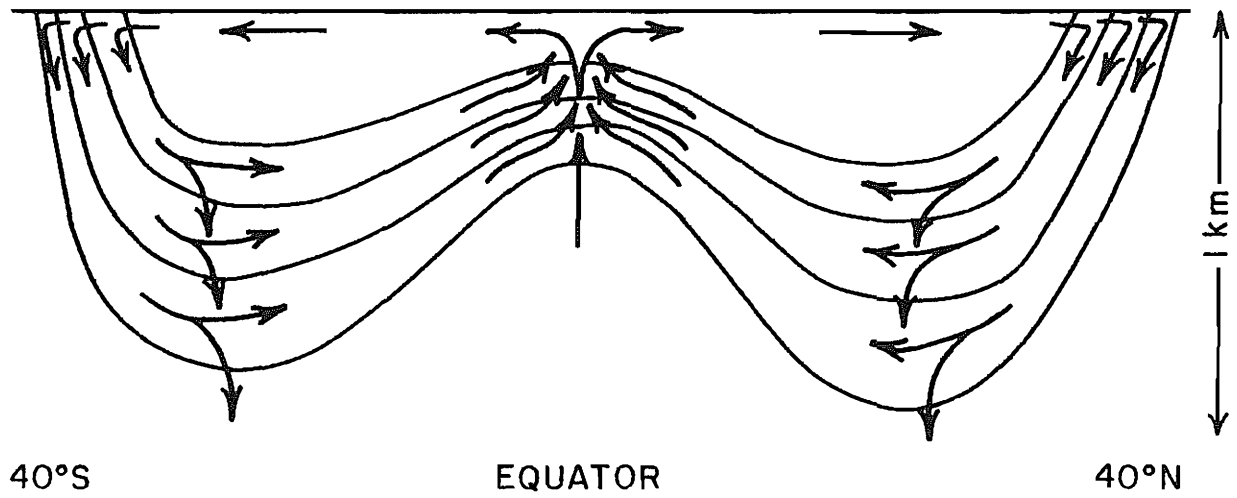


Figure 8-33. The authors' guess regarding the pathways followed by the water ventilating the main oceanic thermocline.

of deep water. The first global survey of these distributions was made as part of the GEOSECS program. While clearly showing where materials added to the sea surface go on the time scale of ten years, these results provide only hints regarding the pathways of this penetration. The hints with regard to the pathways followed by water ventilating the thermocline obtained from bomb- ^{14}C and bomb- ^3H must be tested through the use of other data. For example, the large CO_2 partial pressure anomaly in the surface waters of the equatorial Pacific can only be maintained by rates of upwelling somewhat greater than the minimum value required to explain the distribution of bomb radiocarbon. Another example is the use of ^3He to show that the distribution of tritium in the temperate thermocline cannot be the result of downward mixing across isopycnals. It must rather involve mainly movements along isopycnal surfaces. Further clues await us from the distributions of ^3He and of ^{85}Kr in the oceanic thermocline. The purposeful addition of man-made tracers within the thermocline would greatly facilitate our understanding of these phenomena.

What may emerge from these studies is the pattern of ventilation shown in figure 8-33. Water descends into the main thermocline from the outcrops of isopycnals in the temperate zones. This water leaves the thermocline by a combination of downwelling from the temperate thermocline into the underlying intermediate water and upwelling in the equatorial zone. The flux of temperate surface water upward through the equatorial thermocline is supplemented by water coming from the intermediate waters beneath the thermocline. The water reaching the surface by upwelling spreads to the north and south along the surface, returning to the temperate zones for another cycle.

PROBLEMS

- 8-1 What is the value of the apparent coefficient of vertical eddy diffusion in a water column which has an upwelling rate of 10m/yr and z^* value of 250 meters?
- 8-2 If a near-bottom water sample from the North Atlantic collected in 1976 yields an excess ^3He to ^3H ratio of 0.8, (in atoms) when did this water leave the surface? Assume that this water is free of mantle-derived helium and that it did not mix with other waters.
- 8-3 At the time of the Atlantic and Pacific GEOSECS surveys, the $\Delta^{14}\text{C}$ value for atmospheric CO_2 was close to 400‰. How many excess ^{14}C atoms were there in the atmosphere? How many were in the living biosphere? The mass of carbon in the atmosphere is 6×10^{15} moles. That in the living biosphere is also about 6×10^{15} moles. Most of that in the living biosphere is in trees. State your assumptions. The specific activity of carbon with a $\Delta^{14}\text{C}$ of 0‰ is 13.0 dpm/g.
- 8-4 The production rate of tritium by cosmic rays is about 0.2 atoms/cm²sec. If prior to bomb testing the 85% of the tritium produced reached the oceans before undergoing radiodecay, and if the mean mixing depth of this tritium was 350 meters, then what must have been the average tritium concentration in

surface ocean water (in T.U.)? One T.U. corresponds to one tritium atom per 10^{18} hydrogen atoms. The half-life of tritium is 12.4 years.

- 8-5 During the summer the mixed layer depth in the temperate ocean is about 50 meters. Winter cooling causes it to thicken to about 150 meters. During the early 1970's, when the atmosphere had a $\Delta^{14}\text{C}$ value of about 400‰ and the surface ocean a value of about 150‰, what sort of seasonal cycle would one expect in $\Delta^{14}\text{C}$? Assume a ΣCO_2 concentration of 2.0 moles/m³ and an exchange rate of 20 moles/m²yr. For simplicity, also assume that the mixed layer has the summer depth for six months and the winter depth for six months. Also assume that during the early 1970's the annual average $\Delta^{14}\text{C}$ in the surface ocean was constant (i.e., the annual amount of bomb- ^{14}C gained by CO_2 through the invasion of atmospheric CO_2 is lost to deeper water by below 150 meters vertical mixing).
- 8-6 If 100 kg of a perfluorocarbon with a molecular weight of 300 g/mole were dissolved in sea water, how many molecules would be present? If this tagged sea water were then mixed into a volume 5000 km on a side and 100 m thick, how many molecules would be present in a typical one liter sample from this volume?

SUPERPROBLEM #8

A geochemist named Lyle de Vendra becomes interested in upwelling and decides to construct a computer aquarium to study the processes occurring in a surface mixed layer perched on top of an upwelling water column. He envisions a column 1000 meters high. Water is added to the base of the column and upwells at the rate of 15 meters per year. The upper 75 meters of the column is well mixed. Beneath the mixed layer mixing occurs so as to produce an apparent eddy diffusivity of 0.5 cm²/sec. The upwelling water has a temperature of 10°C and a salinity of 34.50‰. Professor de Vendra first considers the water budget in the mixed layer. The rates of rainfall and evaporation are respectively 90 cm/yr and 75 cm/yr. What is the surface salinity? The rate of tritium rain (due to a continuous release from the world's nuclear reactors) is 10 atoms/cm² sec. What is the steady state tritium concentration in the mixed layer (in T.U.)? What is the steady state profile of tritium beneath the mixed layer? How would the steady state tritium content of the mixed layer change if the eddy diffusivity beneath the mixed layer were reduced to zero?

Professor de Vendra then turns his attention to the carbon cycle. He starts with an abiotic water column. The water entering the bottom has a ΣCO_2 concentration of 2.0 moles/m³ and a potential* CO_2 partial pressure of 600×10^{-6} atmospheres. The surface water temperature is 25°C. The CO_2 invasion rate is 20 moles/m² yr. What is the steady state pCO_2 for surface water? What is the steady state ΣCO_2 ? Assume that $d\text{pCO}_2/\text{pCO}_2 = 10$

*By potential pCO_2 is meant the CO_2 pressure achieved if the water is isochemically depressurized to one atmosphere and warmed to 25°C.

$d\text{ECO}_2/\Sigma\text{CO}_2$ and that this value is independent of PCO_2 .

Getting the hang of things Prof. de Vendra moves on to ^{14}C . He assumes that a nuclear society maintains the $\Delta^{14}\text{C}$ of the atmospheric CO_2 at +300‰. He assigns the carbon in the upwelling water a $\Delta^{14}\text{C}$ of -100‰. What would be the steady state $\Delta^{14}\text{C}$ value for the surface mixed layer? Would the answer be any different if he dropped vertical diffusivity beneath the mixed layer to zero? Compare the fraction of PCO_2 equilibrium with the atmosphere achieved by the surface water with the fraction of $^{14}\text{C/C}$ equilibrium.

Gaining momentum Prof. de Vendra decides to put biology into his model. He inserts PO_4 into the upwelling water (concentration 2×10^{-3} moles/m³) and assumes that one-tenth of the PO_4 in the mixed layer is removed each year (by sinking plant remains). What is the steady state PO_4 concentration in surface water if none of the plant remains falling into the deep water are oxidized (i.e., they fall to the bottom of the column and accumulate as sediment)?

Assuming that the C/P ratio in falling particulate debris is 100 (and that no CaCO_3 forms) Prof. de Vendra tackles the carbon cycle. What are the steady state PCO_2 and ΣCO_2 in surface water? If the falling organic debris has the same $\Delta^{14}\text{C}$ as the carbon in surface water what is the steady state $\Delta^{14}\text{C}$ for surface water?

Professor de Vendra then assumes that through its actions society raises the PO_4 content of the input water to 3×10^{-3} moles/m³. What would happen to the PCO_2 of the surface water? Assume that the PCO_2 content of the atmosphere remains at 300×10^{-6} atm.

Finally, Prof. de Vendra considers the $\delta^{13}\text{C}$ for the surface water in his column. He feeds in ΣCO_2 of $\delta^{13}\text{C} = 0$ at the base of the column. He assumes that the plants living in surface water produce organic matter with a $\delta^{13}\text{C}$ value 20‰ lower than that for the $\delta^{13}\text{C}$ in surface water. He also assumes that the CO_2 escaping from surface water has a $\delta^{13}\text{C}$ of 9‰ lower than the CO_2 in the $\delta^{13}\text{C}$ in the surface water. He assumes that the CO_2 entering the sea carries a $\delta^{13}\text{C}$ equal to that in the atmosphere over the column. What is the $\delta^{13}\text{C}$ for surface water ΣCO_2 (i.e., -7‰) in the abiotic case; in the case where the input PO_4 is 2×10^{-3} moles/m³; and in the case where the input PO_4 concentration is 3×10^{-3} moles/m³?

LAST MINUTE ADDITION (SEPTEMBER 1982)

During the last two years Richard Gammon and Joel Cline, using equipment designed at the Pacific Marine Laboratory of NOAA, have measured the distribution of freon 11 and freon 12 in the North Pacific (731, 732) and North Atlantic Oceans. Their measurements clearly indicate the enormous potential of these tracers. For example, Gammon found, during the TTO expedition in 1981, freons in the countercurrent flowing beneath the Gulf Stream along the margin of the North American continent. From the ratio of freon 11 to freon 12 he could show that the freons must have left contact with the atmosphere within the last five years. These tracers have two great advantages over the tritium-helium pair. First, they can be measured at sea. Second, they are abundant in southern as well as northern hemisphere waters.

Chapter 9

ICE SHEETS AND OCEAN PHOSPHATE

GLACIAL TO INTERGLACIAL CHANGES IN OCEAN CHEMISTRY

INTRODUCTION

Of all the changes in ocean chemistry which may have taken place during the 4.5 billion-year history of our planet, only those which occurred during the past several hundred thousand years can be documented in sufficient detail to develop a reasonably firm case history. As we saw in chapter 6, the waxing and waning of the great continental glaciers brought about changes in the sedimentary parameters sensitive to ocean chemistry. Surprisingly enough it was, however, measurements made on polar ice rather than on marine sediments that generated a major interest in this subject. Scientists working in Bern, Switzerland and in Grenoble, France developed means of measuring the CO₂ content of the air trapped in bubbles in ice and applied this method to samples from borings made in the Greenland and Antarctic ice caps. As shown in figure 9-1, measurements on air extracted from bubbles in ice formed during the peak of the last glacial period yield CO₂ partial pressures averaging about 200×10^{-6} atm, while those on bubbles from ice formed during post glacial time yield CO₂ partial pressures averaging about 290×10^{-6} atm.* This discovery had a major impact on scientific thinking because of the ability of CO₂ to absorb outgoing "earth" light and hence to influence the temperature of the earth's surface. The results of atmospheric modeling studies made in order to assess the climatic change to be expected from the excess CO₂ produced by the burning of fossil fuels suggest that a doubling of CO₂ content would warm the planetary surface by $3.0 \pm 1.5^{\circ}\text{C}$. A halving of CO₂ content would cool it by about the same amount. Hence the change in atmospheric CO₂ content between glacial and interglacial time postulated by the Swiss and French groups would significantly amplify the forces driving the glacial to interglacial climatic change.

As the low CO₂ partial pressures of glacial time and the high CO₂ partial pressures of post-glacial time persisted for thousands of years, there was in each case adequate opportunity for the

*The ice formed during glacial times can be readily distinguished from that formed during post-glacial time by its $^{18}\text{O}/^{16}\text{O}$ ratio. During glacial time the polar regions were colder leading to lower $^{18}\text{O}/^{16}\text{O}$ ratios in the snow which fell at the locations of these drilling sites (see figure 9-1).

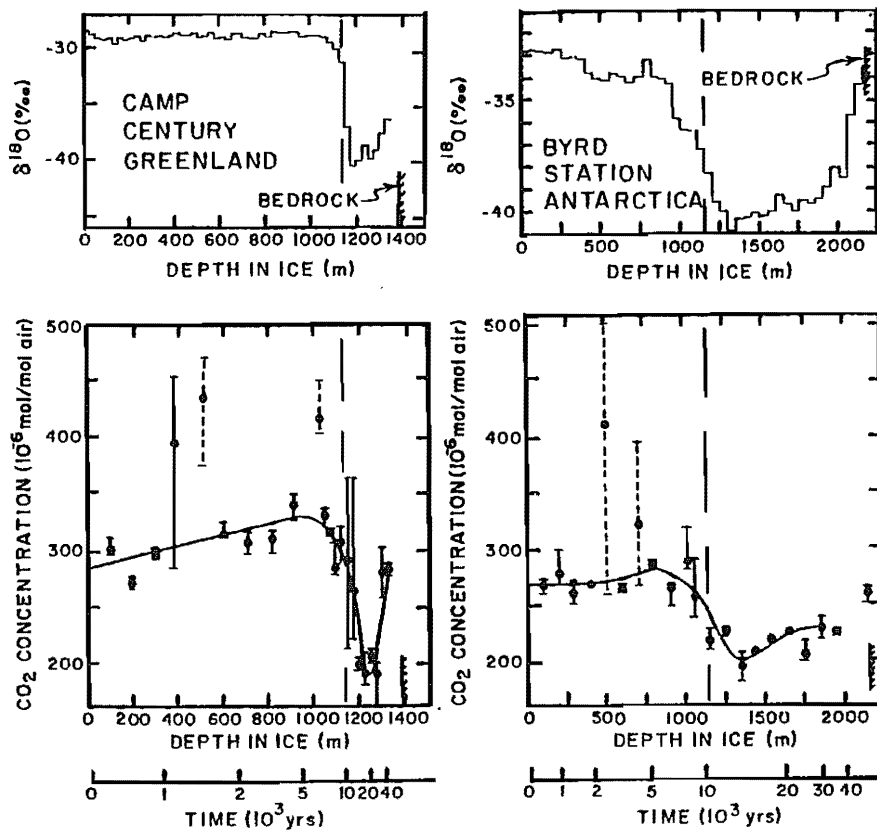


Figure 9-1. Atmospheric CO_2 concentrations as reconstructed by Neftel, et al. from measurements of the ratio of CO_2 to air trapped in bubbles in ice cores from Camp Century, Greenland (lower left), and Byrd Station, Antarctica (lower right). Also shown are $\delta^{18}\text{O}$ versus depth records in the same cores (upper panels). Approximate age scales are also given for each of these ice cores. The nonlinearity in the age versus depth relationship is the result of the foreshortening of each layer as the result of the flow of the ice. At each depth in these cores a series of samples were measured for their CO_2 to air ratio. The range of results for these samples is shown by the vertical lines. The circle is the median value. For those depths showing a large range in results the median values are quite high. It is thought that this combination of high values and high variability is the result of contamination with the kerosene-glycol mixture used during the drilling to keep the hole from collapsing. Thus the results for those depths showing low variability are the ones upon which the conclusions are based. The CO_2 measurements were carried out at the University of Bern in Switzerland by Neftel, Oeschger and their colleagues (622). The change in $^{18}\text{O}/^{16}\text{O}$ ratio with depth in these cores follows changes in air temperature at the site of accumulation of snow from which the ice in these cores was formed. The increase in this ratio at a depth of about 1100 meters in each of these cores marks the close of glacial time. The $^{18}\text{O}/^{16}\text{O}$ ratio measurements on samples from the Greenland ice core were carried out by Dansgaard and his associates in Copenhagen; those on the Antarctic core were carried out by Epstein and his colleagues at Cal Tech.

chemistries of the ocean and atmosphere to achieve equilibrium. Further, since the ocean contains about 60 times more carbon than the atmosphere, the glacial to interglacial change in atmospheric content must have been driven by changes in ocean chemistry. Something must have happened within the ocean which caused the mean CO₂ pressure in its surface waters to change!

TEMPERATURE AND SALINITY CHANGES

Two possibilities immediately come to mind. First, the surface waters of the ocean must have been colder during glacial time and second, the waters of the ocean must have been saltier.* It has been possible to reconstruct the changes in surface ocean temperature in two quite different ways. The first involves the comparison of the δ¹⁸O records for the shells of benthic foraminifera (microscopic animals that live on the sea floor) and of planktonic foraminifera (free-floating microscopic animals that live in the upper waters of the sea). As shown in figure 9-2, these records have on the average a similar full glacial to full interglacial amplitude. This similarity demands that the glacial to interglacial change in surface ocean temperature be quite small. The logic is as follows. The benthic δ¹⁸O records come from places on the sea floor with present day potential temperatures ranging down to 0.5°C. Since the freezing point of sea water is about -1.8°C, the bottom waters in the sea during glacial time could have been no more than 2.3°C colder than they are today. Since the fractionation between the oxygen in water and that in the CaCO₃ formed by shells changes by about 0.22‰ per °C, no more than 0.5‰ of the observed 1.9‰ full glacial to full interglacial change in the δ¹⁸O for benthic shells can be attributed to temperature change. This observed change must rather be largely the result of the storage of δ¹⁸O deficient water in the continental ice sheets. This ice storage effect would be uniformly distributed through the sea. The similarity between the δ¹⁸O records for planktonic and benthic forams therefore requires then that the glacial to interglacial temperature change in surface ocean water be about the same as that in the deep sea (i.e., <2.3°C).

The second method for establishing the temperature of surface waters during glacial times involves a multivariate statistical analysis of the relative abundances of the species of various types of microorganisms (i.e., of planktonic foraminifera, of radiolaria, of coccolithophorids, and of diatoms). In this analysis an equation is generated relating present-day surface ocean temperatures to the microorganism abundances in core top samples from throughout a major ocean basin. When this is done it is found that changes in surface temperature account for a major portion of the changes in the relative abundances of the various species from place to place in the basin. Also, temperatures back calculated from the equation for individual locations show a mean

*Salt is left behind during evaporation hence the growth of the great ice sheets of glacial time enriched the salt content of residual sea water.

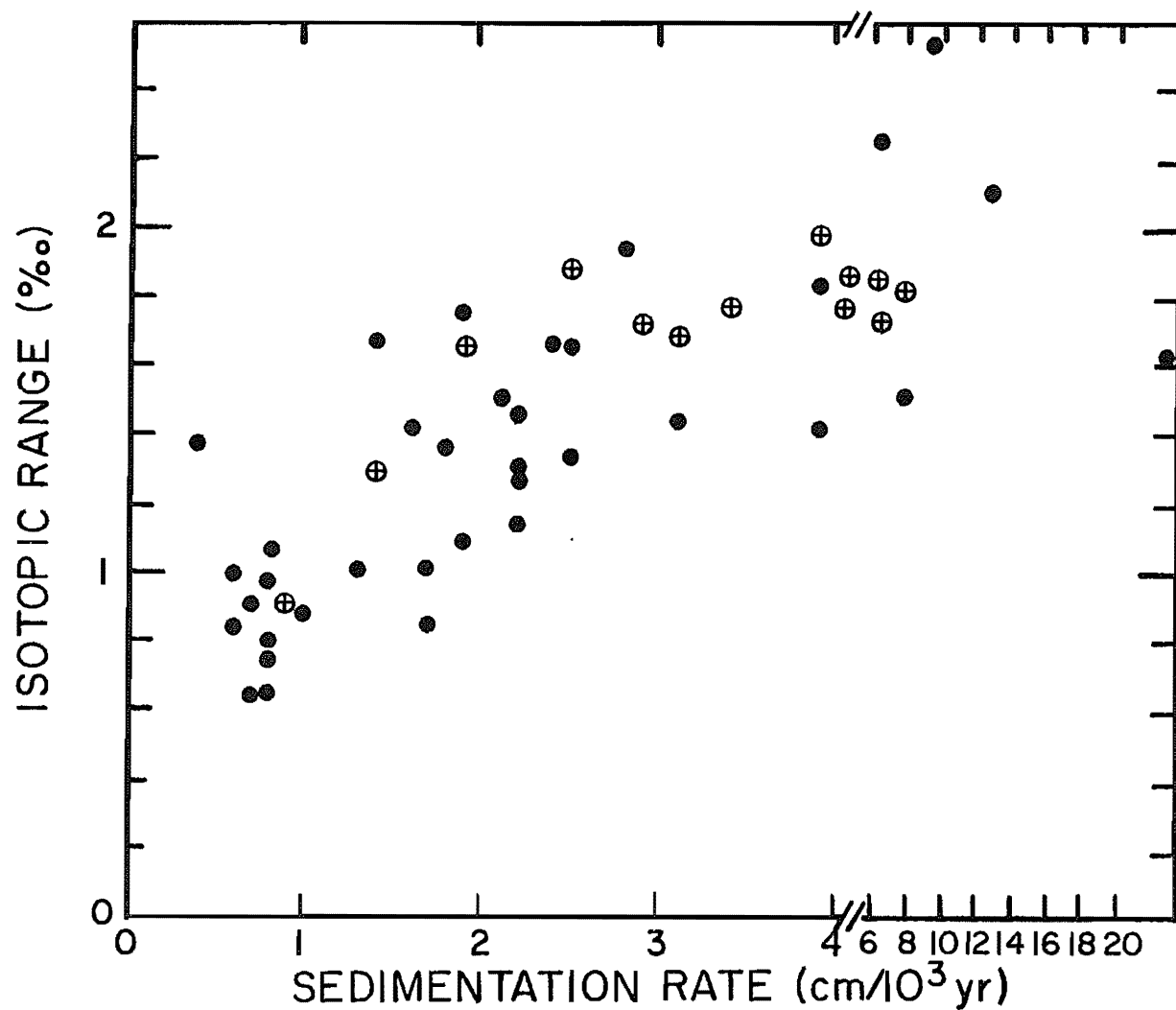


Figure 9-2. Amplitude of the glacial to interglacial change in $\delta^{18}\text{O}$ for planktonic (solid circles) and benthic (open circles) forams from deep sea cores collected throughout the world ocean as a function of sedimentation rate. The smaller values for cores with sedimentation rates less than 2 cm/10³ years are the result of a blurring of the record through bioturbation. For cores with sedimentation rates of more than 2 cm/10³ there is no significant difference between the average amplitudes for the benthic and for the planktonic records (197).

deviation from the observed surface water temperature at these locations of only about 1°C (see figure 9-3). Based on these successes, Imbrie and his coworkers concluded that their equations could be reliably applied to abundance data for samples from sediments deposited during full glacial time. After the long job of analyzing sediments from throughout the world ocean was completed these researchers found that the difference between the average surface water temperature for full glacial and full interglacial time was only about 1.5°C ! Maps showing the global distribution of these changes are shown in figure 9-4. Imbrie and his coworkers point to the agreement between temperature differences obtained at the same point on the ocean floor from different groups of organisms (for example by comparing those based on the abundances of various species of planktonic foraminifera with those based on the abundances of various species of diatoms) as evidence for the reliability of their approach. As their method yields a result which is consistent with that obtained from the $\delta^{18}\text{O}$ record, the conclusion that on the average the surface ocean was only $1.5 \pm 1.5^{\circ}\text{C}$ cooler during glacial time than it is today appears firm!

There are several methods by which the salinity of the glacial ocean can be estimated. The most direct is to estimate the volume of excess (over today's) continental ice present during glacial times. This is done from maps of the margins of the full glacial ice sheets established by geologic studies. If the ice sheets which lay within these margins are assumed to have had an equilibrium shape* then the volume of ice can be calculated. The result obtained in this way is 50 million cubic kilometers (equivalent to a sea level lowering of 150 meters). As the volume of the sea is presently about 1330 million cubic kilometers, its glacial volume must have been about 3.7% smaller and hence its glacial salinity about 3.7% higher. A similar estimate of the ice volume is obtained from the magnitude of the glacial to interglacial $\delta^{18}\text{O}$ change for benthic forams. If the deep sea is assumed to have been $1.5 \pm 1.5^{\circ}\text{C}$ colder during full glacial than during full interglacial times, then the magnitude of the $\delta^{18}\text{O}$ change attributable to ice growth is about $1.6^{\circ}/\text{oo}$. If the mean $\delta^{18}\text{O}$ for the excess glacial ice is taken to be $-35^{\circ}/\text{oo}$ then the excess ice volume must have corresponded to about 4.5% of the water in today's sea (i.e., to 60 million cubic kilometers of sea water). Three other means of estimating the volume of excess ice all involving the elevations of paleo-shorelines have been pursued. These yield excess ice volumes in the range 25 to 50 million cubic kilometers. Giving some weight to all these studies, we adopt an estimate of 45 ± 15 million cubic kilometers for the volume of water bound up in excess continental ice during full glacial time. This corresponds to a salinity change of $3.5 \pm 1.0\%$ (higher during glacial time).

Were these the only changes which took place in the ocean during glacial time then the PCO_2 of its surface water can be easily calculated. The PCO_2 rise caused by the 1.5°C warming at

*Equilibrium implies that ice is flowing toward a melting at the edges of the sheet as fast as snow is accumulating on its interior.

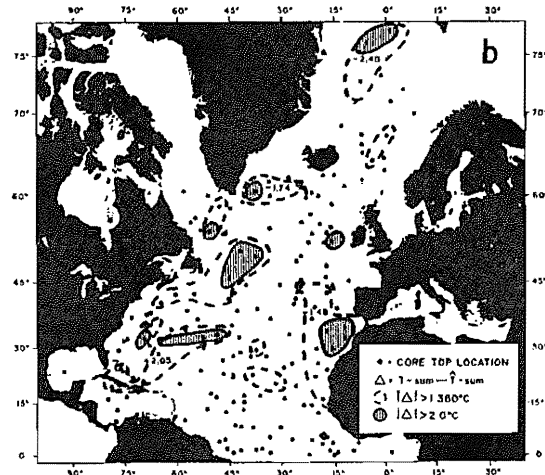
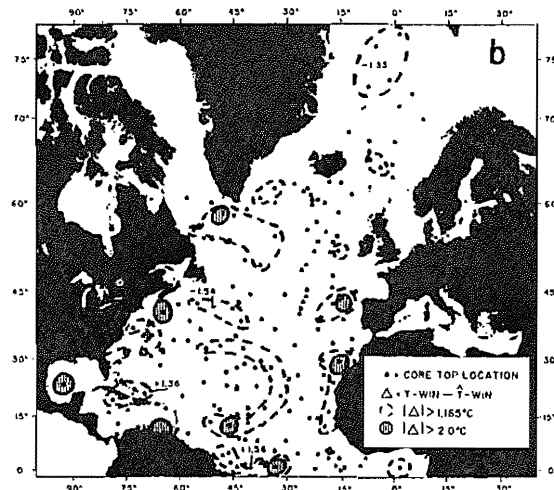
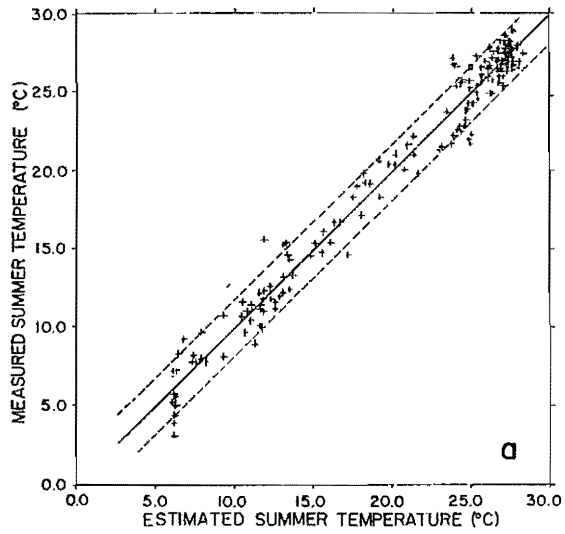
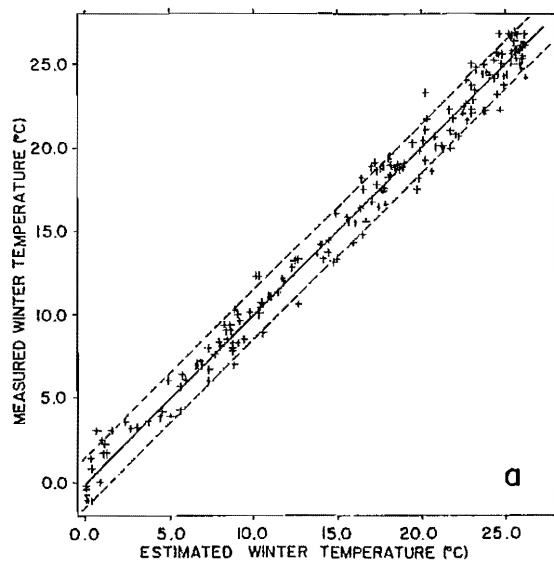


Figure 9-3. Temperatures calculated by the factor analysis method compared to measured surface ocean temperatures. The map shows the locations of the cores and the distribution of the anomalies between estimated and measured temperature. This work was carried out by John Imbrie and Nilva Kipp at Brown University (600, 603).

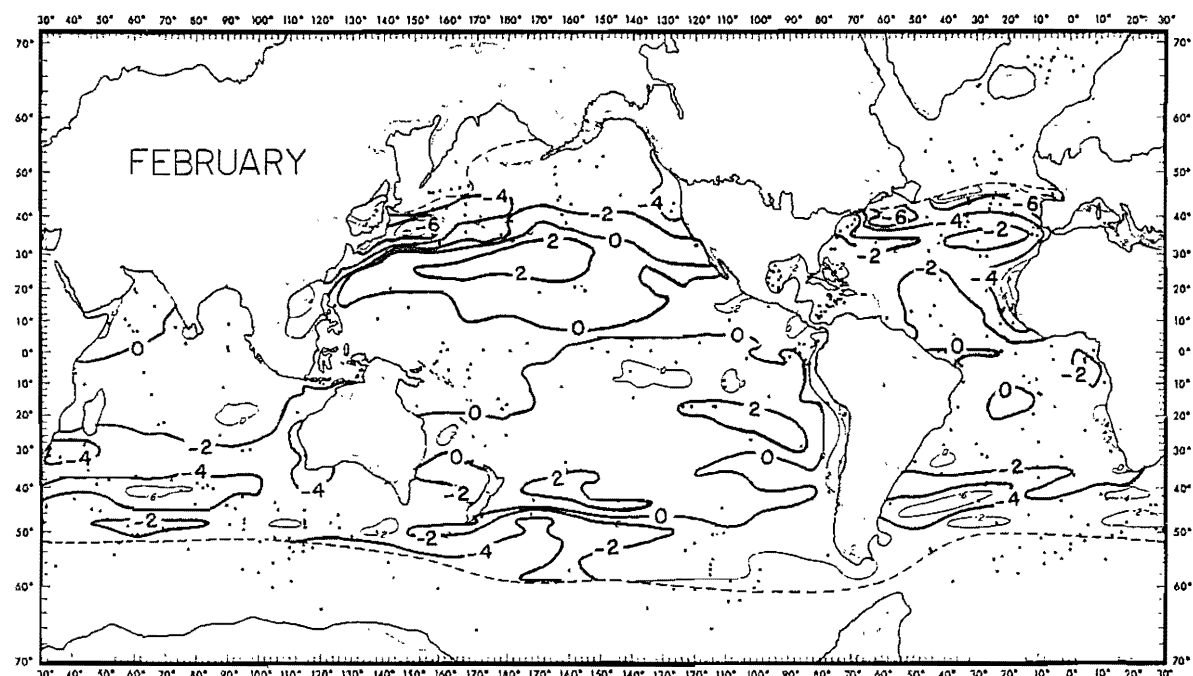
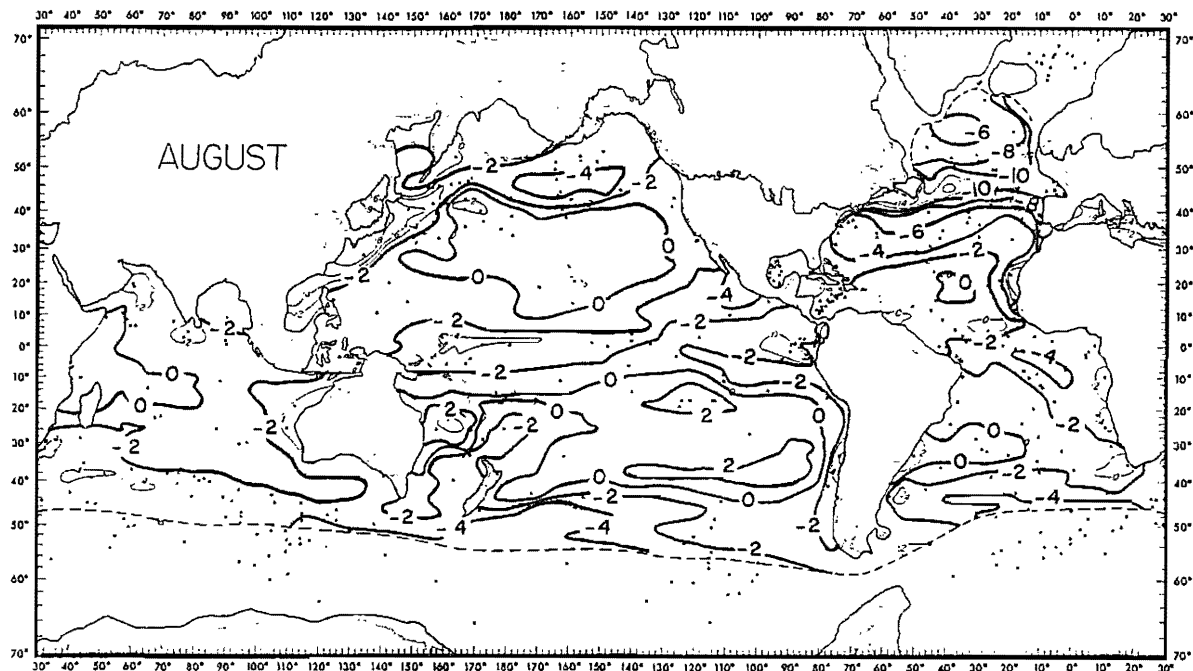


Figure 9-4. Maps showing the pattern of interglacial to glacial temperature differences for the surface ocean as reconstructed through factor analysis of the abundances of organism remains in the underlying sediment. Negative numbers indicate lower temperatures (in °C) during glacial time. This work was carried out by the CLIMAP group (610).

the close of glacial time is almost exactly balanced by the PCO_2 drop caused by the 3.5% drop on salinity! (The PCO_2 of surface ocean water rises about 20×10^{-6} atm for a 1.5°C warming and falls about 14×10^{-6} atm for a 3.5% decrease in salinity). Hence if we are to explain the ice core results, some other changes must have occurred.

FORMATION AND DESTRUCTION OF ORGANIC MATERIALS

The most obvious possibility is that the amount of ΣCO_2 in the sea was different during glacial time than it is today. Were the ΣCO_2 lower than the PCO_2 in surface water would have been lower. How might such a change have taken place? The first possibility which comes to mind is that one or more of the factors (mixing rate, river input rate, preservation probability of the organic matter generated by plants,...) controlling the steady state concentration of ΣCO_2 in the sea undergoes glacial to interglacial changes. It can be quickly shown that this is not the explanation for the CO_2 to air ratio changes seen in polar ice borings. The reason is that while the mean replacement time of carbon atoms in the sea is about 200,000 years, the ice core record (see figure 9-1) shows that the CO_2 to air ratio changed from its glacial to its interglacial value in just a few thousand years. It is impossible to envision a scheme by which changes in the parameters controlling the steady state ΣCO_2 content of sea water could produce such an abrupt change!

Instead, we must look to pulses of formation and destruction of temporary carbon reservoirs. Forests, soils, and shelf sediments come to mind. What evidence would such transfers leave? In the case of reservoirs of organic carbon, the isotopes of carbon come to mind. As we have seen, the heavy isotope, ^{13}C is discriminated against during photosynthesis. The $^{13}\text{C}/^{12}\text{C}$ ratio in plants is about 20‰ lower than in the inorganic carbon utilized by the plant. Thus just as any growth or depletion of continental ice leaves its mark on the $^{18}\text{O}/^{16}\text{O}$ ratio in sea water, any growth or depletion of reservoirs of organic carbon will leave its mark on the $^{13}\text{C}/^{12}\text{C}$ ratio in oceanic ΣCO_2 .

The production and destruction of reservoirs containing CaCO_3 would of course also change the ocean's ΣCO_2 . They would in addition change the ocean's alkalinity. They would not, however, significantly change the $^{13}\text{C}/^{12}\text{C}$ ratio in ocean-atmosphere carbon. As the fractionation between the carbon in CaCO_3 and the dissolved carbon in the sea is only about 1‰ (compared to 20‰ for organic material), the ^{13}C record speaks only to changes in the sizes of organic carbon reservoirs. We will have to look elsewhere for evidence regarding changes in the size of the sedimentary CaCO_3 reservoirs.

The best place to look for the changes generated by the formation and destruction of reservoirs of organic matter would be in the shells of benthic foraminifera. Their carbon comes from the deep sea reservoir which contains about 90% of the carbon in the ocean-atmosphere system. They live in an environment nearly free of temperature changes. They do not migrate through the water column as do planktonic foraminifera. Hence changes in their

$\delta^{13}\text{C}/\delta^{12}\text{C}$ ratio should most nearly reflect those for the average carbon in the ocean-atmosphere system.

In chapter 6 we showed that a glacial to interglacial change in the $\delta^{13}\text{C}$ of benthic forams has been found (see figure 6-10). Forams living in glacial periods were observed by Shackleton to have lower $\delta^{13}\text{C}/\delta^{12}\text{C}$ ratios than those living during interglacial periods. Table 9-1 summarizes the results available at the time this book was written. All show a lower glacial than interglacial $\delta^{13}\text{C}$ value. The average difference is 0.7‰.

When the data in figure 6-10 are examined it becomes evident that the glacial to interglacial shift for the two species analyzed are not the same (see figure 9-5). Hence a word of caution must be given regarding the acceptance of the 0.7‰ average. Benthic forams may have more surprises in store for us!

If we accept the $\delta^{13}\text{C}$ results at face value the reservoirs containing organic carbon must have been smaller during glacial time. This would lead to higher CO_2 contents of the ocean and atmosphere during glacial time! The magnitude of the difference can be estimated from the magnitude of the $\delta^{13}\text{C}$ change observed in benthic forams between glacial and interglacial time. Taking the mean $\delta^{13}\text{C}$ value for the organic carbon to be $-23 \pm 3\text{‰}$,* it turns out that $3.0 \pm 0.4\%$ of the carbon in the glacial ocean must have been converted to organic carbon at the end of glacial time. Were this the only chemical change to have occurred in the sea, the CO_2 partial pressure in the atmosphere must have fallen about 150×10^{-6} atmospheres at the end of glacial time! As the ice boring data suggests instead that it rose by 100×10^{-6} atmospheres at the close of glacial time we must probe further.

Before going on, we must mention where the excess organic material formed during early post-glacial time might be stored. Shackleton, who discovered the $\delta^{13}\text{C}$ change in benthic forams, proposed that this carbon is locked up in forests and soils. He points out that during glacial time the north temperate forests which now store about half the carbon in the living biosphere were largely non-existent. The land they now occupy was either covered by ice or by treeless tundra. He also points out that the tropical forests appear to have covered a smaller area during glacial time because of generally drier conditions in the tropics. As can be seen from the data in table 9-2, glacial to interglacial changes in forest cover alone cannot account for the transfers of carbon needed to explain the glacial to interglacial $\delta^{13}\text{C}$ change in benthic forams. Shackleton realized this and proposed that changes in the amount of organic carbon stored in soils must also have occurred. As can be seen from table 9-2, there is enough soil carbon to do the remaining job.

Another possibility is that deposition of organic rich sediment on the world's shelves occurred during the post-glacial sea level rise. During the peak of glaciation, the sea stood

*Terrestrial organic matter has a $\delta^{13}\text{C}$ value averaging -26‰ .

Marine organic matter has a $\delta^{13}\text{C}$ value averaging -20‰ . As we have no way of determining the relative contributions of the two types, we take a value half way in between and an uncertainty large enough to bridge the entire range.

Table 9-1. Summary of ^{13}C data on benthic foraminifera. These results were all obtained by Nick Shackleton of Cambridge University in England (328).

Core No.	Lat.	Long.	Depth km	$^{13}\text{C}_{\Sigma\text{CO}_2}^*$	Species	Glacial $\delta_{^{13}\text{C}}^{\text{O}}$	Holocene $\delta_{^{13}\text{C}}^{\text{O}}$	$\Delta\delta^{13}\text{C}_{\text{G-I}}$
Atlantic								
V29-179	44.0°N	24.5°W	3.3	+0.9	Uvig. per.	-1.1+	-0.2+	+0.9+
Meteor 12392	25.2°N	16.8°W	2.6	+0.9	Uvig. per. Plan. woel.	-1.0 +0.3	+0.2 +1.0	+1.2 +0.7 0.8
V22-174 RC12-267	10.1°S 38.7°S	12.8°W 25.8°E	2.6 4.1	+0.8 +0.3	Uvig. aub. Uvig. per.	0.1 -0.9	+0.5 -0.1	+0.4 +0.8
Pacific								
V19-29	3.6°S	83.9°W	3.2	-0.0	Uvig. prob.	-1.45	-0.75	+0.7
Y71-6-12MG	16.3°S	77.5°W	2.7	-0.0	Uvig. per.	-1.3	-0.8	+0.5
Antarctic								
RC11-120	43.5°S	79.9°E	3.2	+0.4	Uvig. per.	-0.9	-0.1	+0.8
					MEAN			<u>+0.7</u>

[†]Across termination II (125,000 years ago) rather than termination I (11,000 years ago).

*For the carbon dissolved in the sea water at the depth and location the core was taken.

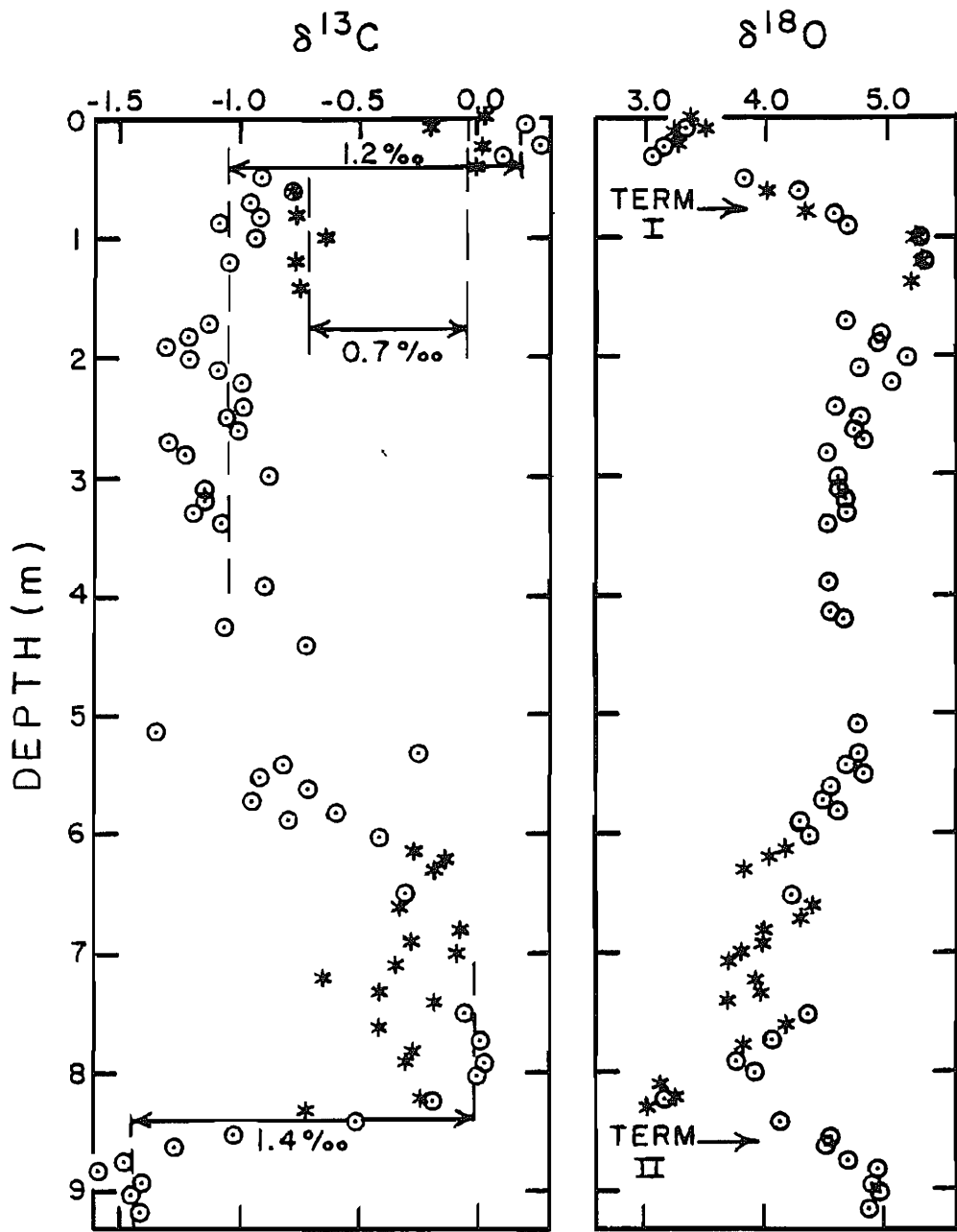


Figure 9-5. Plots of $\delta^{13}\text{C}$ and $\delta^{18}\text{O}$ versus depth in METEOR core 12392 from the eastern North Atlantic. Analysis carried out on Uvigerina peregrina are designated by circles. Those carried out on Panulina woellerstorfi are designated by stars. To make the Panulina woellerstorfi results compatible with those for Uvigerina peregrina $1.0^{\circ}/\text{oo}$ was subtracted from the Panulina woellerstorfi $\delta^{13}\text{C}$ results. The last two transitions from glacial to interglacial time are designated as termination I and II. The glacial to interglacial change for the $\delta^{13}\text{C}$ of Uvigerina peregrina is $1.2^{\circ}/\text{oo}$, that for Panulina woellerstorfi is $0.7^{\circ}/\text{oo}$. The reason for this difference is not known. These measurements were made by Shackleton at Cambridge University (328).

Table 9-2. Today's reservoir sizes and the magnitude of glacial to interglacial carbon transfers.

Reservoir	Mass Carbon 10^{16} moles
Ocean & Atm.	310
Forests	6
Soil	~20
Glacial to Interglacial Organic C Storage Change	9
Glacial to Interglacial CaCO_3 Compensation	9

about 140 meters below its present level leaving the shelves high and dry. Thus during glacials it is likely that material was eroded from the shelves. On the other hand, as the sea rose and reflooded the shelves, net deposition would be expected. This could contribute to the glacial to interglacial cycle in organic carbon storage and hence to the $\delta^{13}\text{C}$ change observed in benthic forams. Whether terrestrial organic materials (forests and soils) or marine organic material (shelf sediment) dominated the change in the glacial to interglacial inventory of organic carbon will be important to the arguments which follow. Thus we will have more to say about this matter.

CHANGES IN CaCO_3 STORAGE

What about the changes in the CaCO_3 reservoirs? The removal of 3% of the carbon in the ocean-atmosphere system at the end of glacial time to form organic material would have produced an increase in $\text{CO}_3^=$ ion concentration. In the extreme (i.e., were there no compensation due to excess CaCO_3 accumulation during the period of storage of this organic carbon) the $\text{CO}_3^=$ ion content would have risen about $15 \times 10^{-6} \mu\text{m}/\text{kg}$. As can be seen from figures 2-10, 11 and 12 such an increase would have caused almost the entire deep sea to become supersaturated with respect to calcite and would have caused the aragonite lysocline to deepen by more than one kilometer! Such a change would of course throw the ocean's CaCO_3 budget badly out of balance, leading to an excess of CaCO_3 accumulation over input from rivers of carbon destined for this fate. This excess accumulation would gradually bring down the $\text{CO}_3^=$ ion concentration and eventually restore balance between input and loss. The loss of ΣCO_2 to organic matter would in this way be "compensated" by an equivalent loss of ΣCO_2 to CaCO_3 . For each mole of carbon removed as organic material about a mole would be removed as CaCO_3 .

When the CaCO_3 compensation was completed the ocean would have lost an additional 3% of its carbon. It would also have lost about one mole of alkalinity for each mole of ΣCO_2 . As precipitation of CaCO_3 raises the CO_2 pressure in sea water, the CaCO_3 compensation would have countered much of the CO_2 pressure reduction caused by the loss of ΣCO_2 to organic carbon. Thus this compensation would undo most of the difficulty created by the observed $\delta^{13}\text{C}$ change in benthic foraminifera!

Before looking to other causes for the CO_2 pressure increase observed in ice cores at the end of glacial time, there are some aspects of this CaCO_3 compensation process which we must consider. The first is how long it would take. A rough estimate can be quickly obtained as follows. The replacement time for carbon in the sea is about 200,000 years. However, as the ratio of ΣCO_2 ion to $\text{CO}_3^=$ in deep ocean water is about 30, the response time of carbonate ion will be about 30 times smaller (hence about 7000 years).

A more easily understood way to estimate the compensation time is to consider how much excess CaCO_3 has to be precipitated and compare this with the rate of production of CaCO_3 by marine organisms. The ocean contains about 3×10^{18} moles of ΣCO_2 . As

the compensation process required the deposition of 3% of this carbon, then 9×10^{16} moles of excess CaCO_3 had to be formed. The average production rate of calcite is $1.0 \text{ g/cm}^2 10^3 \text{ yrs}$, or $100 \text{ moles/m}^2 10^3 \text{ yrs}$. Over the entire ocean this comes to 3.5×10^{16} moles per 10^3 years. If one-half of this production (i.e. about 1.8×10^{16} moles/ 10^3 yrs) went into the accumulation of excess* CaCO_3 then the time constant for the compensation would be about 5000 years. We refer to it as a time constant rather than as a time because as $\text{CO}_3^=$ ion content of the sea fell the area covered by supersaturated water would correspondingly diminish. As for all the feedback recoveries discussed in chapter 6, full recovery of the CaCO_3 balance would be approached asymptotically. The time estimates given above are the so-called e-folding times (i.e., the time required for the departure from equilibrium to be reduced by a factor of $1/e$). The half recovery time would be $\ln 2$ (or 0.693) times the e-folding time. (Hence the half time for CaCO_3 compensation would be 0.693×5000 or 3500 years). In any case, the rough estimates made here suggest that the compensation would persist well into the Holocene. Possibly it still goes on today!

EVIDENCE FOR AN EARLY POST-GLACIAL LYSOCLINE CHANGE

Can we see evidence for this compensation process in the sediments? The answer is yes. Spikes of aragonite preservation found at the appropriate level in sediments from the Caribbean Sea and from the eastern basin of the Atlantic are shown in figure 9-6. These cores were all obtained beneath the present-day lysocline for aragonite. The fact that aragonite is absent from these cores during glacial time suggests that the lysocline for aragonite resided at depths shallower than the collection depths for these cores during glacial time as well as during Holocene time. The preservation spike then denotes a period several thousands years in duration during which the aragonite lysocline was located at a greater depth. The timing of this drop is centered about the glacial to interglacial transition. In the case of the eastern Atlantic study a series of cores were taken down the continental rise over the depth interval 0.5 to 3.7 km. As shown in figure 9-7 by comparing the results on all these cores it is possible to roughly determine how far the lysocline for aragonite dropped during the preservation event. As can be seen from this figure the drop was quite large (i.e., about 2 kilometers). Hence we have a dramatic confirmation that the removal of ΣCO_2 from the ocean in the form of organic matter at the close of glacial time caused a response in the aragonite lysoclines. However, as aragonite is quite rare in sediments it cannot be the sought after storage phase for CaCO_3 .

If we are to rigorously demonstrate the CaCO_3 compensation phenomenon it must be through an evaluation of the extent of excess calcite storage. This is not so easily done. In order to

*It is an excess because this deposition would have to be over and above that to balance the input from rivers of carbon destined to become CaCO_3 .

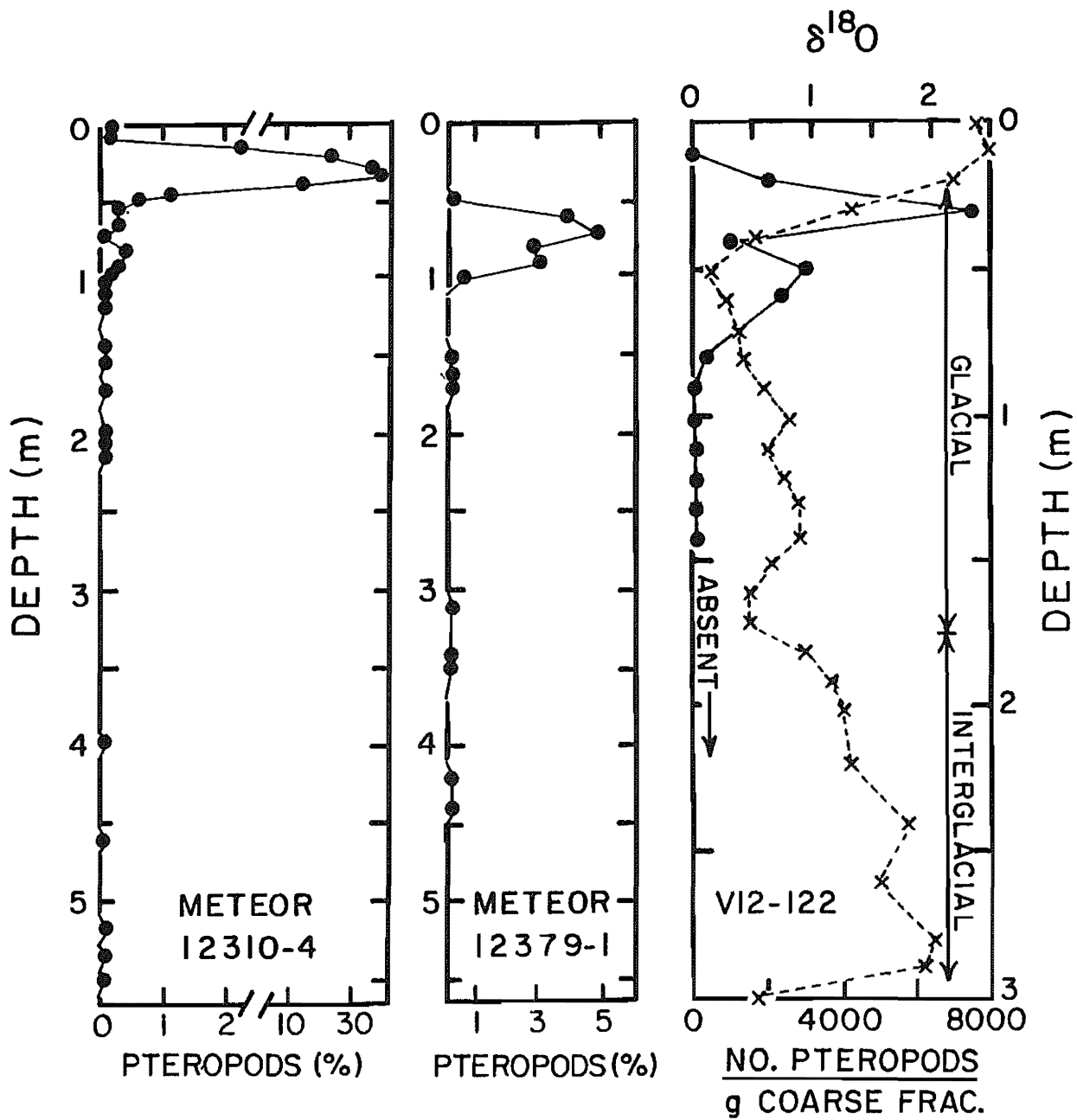


Figure 9-6. Pteropod abundance (solid circles) as a function of depth in a core from the Caribbean Sea (501) and in two cores from the continental margin off Africa (503,509). All three records show preservation peaks centered in early post-glacial time. Both sites lie below the present day aragonite lysocline. The time scale for core V12-122 is based on $^{18}\text{O}/^{16}\text{O}$ measurements (see x's). Those for the other cores are based on faunal evidence.

Figure 9-7. Changes in the lysocline depth for pteropods as reconstructed for a series of cores from off the coast of Africa. The suggestion is that the depth of this horizon increased by about 2 kilometers at the end of glacial time and then decreased by about 3 kilometers during mid-Holocene time. The entries are for depths where cores were obtained. The designations at each of these depths are for the relative abundances of pteropods in late glacial sediment, in early Holocene sediment and in late Holocene sediment. This reconstruction was carried out by Berger of the Scripps Institution for Oceanography (511).

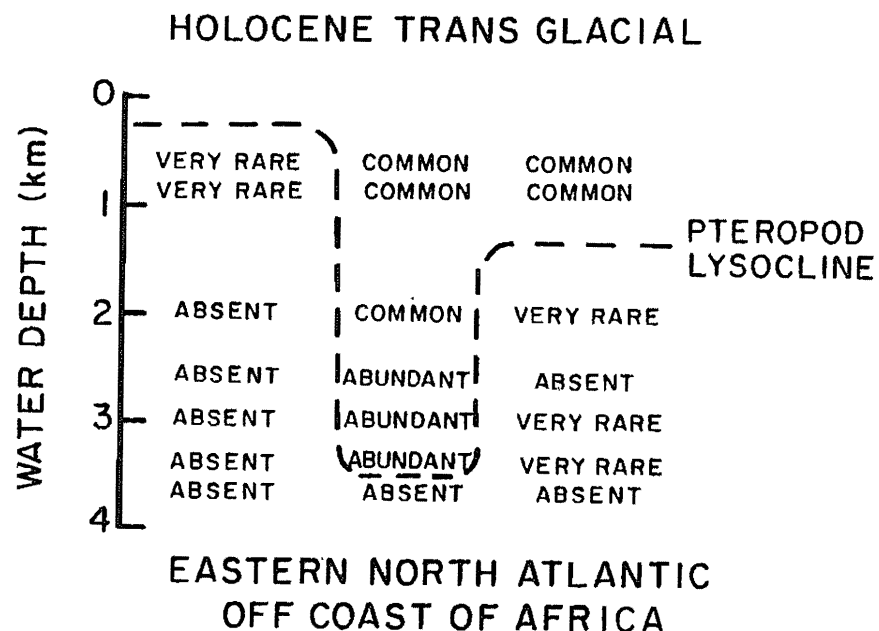


Table 9-3. Areas covered by various sedimentary domains (in units of 10^{14} m^2).

Zone	Atlantic	Indian	Pacific	Total
Above Lysocline	0.71	0.32	0.49	1.52
Trans. Zone	0.21	0.14	0.14	0.49
Red Clay Zone	0.14	0.30	1.15	1.59
Total	1.06	0.76	1.78	3.60

put this quest into context let us first consider how thick a layer of calcite we seek. A rough idea can be obtained by dividing the total amount of CaCO_3 required for compensation ($\sim 9 \times 10^{16}$ moles) by the total area of the deep sea floor ($\sim 3 \times 10^{18}$ cm^2). This yields about 3×10^{-2} moles $\text{CaCO}_3/\text{cm}^2$ or 3 grams of $\text{CaCO}_3/\text{cm}^2$. Since a cubic centimeter of calcite rich deep sea sediment contains close to one gram of mineral matter if uniformly spread over the entire deep sea floor, this CaCO_3 would produce a layer about 3 cm thick. Because the layer would not be formed everywhere the actual thickness would be somewhat larger.

For the purposes of our search let us divide the sea floor into three regions: that above the present-day lysocline for calcite, that lying in the transition zone beneath the lysocline and that beneath the transition zone. The areas of these zones are given in table 9-3. The zone above the lysocline for calcite will not show any evidence for the compensation phenomenon. The reason is that the phenomenon is one of preservation rather than of deposition. All the calcite raining above the lysocline is preserved even in the absence of such an event! Thus a temporary deepening of the lysocline will not alter the accumulation rate of calcite above the lysocline.

Next, let us turn our attention to the sediments nearly free of calcite which lie beneath the transition zone. Here we might expect to observe a calcite preservation spike similar to the aragonite preservation spike discussed above. The situation is, however, quite different because of low accumulation rates in this domain. The aragonite preservation spike is found in sediments accumulating at the rate of several centimeters per thousand years (most of the bulk in these sediments is calcite and alumino-silicates). In such sediments burrowing organisms stir only the sediment laid down in the last several thousand years. Hence, while slightly blurring the preservation spike, the bioturbation does not obliterate it. Beneath the transition zone the deposition rates are only a few tenths of a centimeter per thousand years. In this domain the entire column of Holocene sediment is being actively churned into the underlying glacial sediment!

Let us imagine what would happen if a 6 cm thick layer of calcite were deposited during Holocene time on the top of glacial red clay. Through the action of the worms living within the sediment this calcite would be thoroughly mixed with the red clay deposited during late glacial time and with the red clay deposited during Holocene time. Thus, unlike the aragonite preservation event which appears as a discrete layer within the sediment, the calcite preservation event would be largely homogenized throughout the upper eight or so centimeters of sediment. It would give every appearance that calcite accumulation had commenced at the close of glacial time and continued right up to the present. Indeed, how could these two scenarios be distinguished? In both, the fauna and flora in the sediment would be Holocene in age. Further, as continuous deposition over the Holocene represents a simpler hypothesis, its adoption would be favored by the usual "rules" of science.

There is, fortunately, one way in which the two hypotheses might be distinguished. Were the calcite to have been deposited

continuously from early Holocene time until now its average radiocarbon age would be about 5000 years (the transition between glacial and Holocene time occurred about 11,000 years ago). On the other hand, if it were deposited mainly during early Holocene time, its mean age should be considerably older (8000 to 10,000 or more years). So we should look at sediments from beneath the transition zone to see whether they have an 8 or so centimeter thick carbonate bearing layer at their top. If such a layer is found its calcite should be subjected to radiocarbon dating.

Such a study was carried out on sediments from beneath the lysocline on the west flank of the East Pacific Rise. In this area of the ocean the sediments above the lysocline are very rich in calcite (90-96%) (except at the ridge crest where they are diluted with the oxides of Fe and Mn). As shown in figure 9-8, prominent solution effects commence at a depth of about 3.95 km. Sediments from below this water depth have a layer of CaCO_3 -rich sediment on top of the underlying red clay (see figure 9-9). These layers are a few tens of centimeters thick, and yield radiocarbon ages in the range 9,000 to 17,000 years (see figure 9-9 and table 9-4). These layers are considerably thicker than the expected global average and have radiocarbon ages several thousand years older than expected. This situation is further complicated by the finding that core tops from above the lysocline have ages in the range 3,000 to 16,000 years.

When considered together with the ^{230}Th based sedimentation rate as low as $0.4 \text{ cm}/10^3 \text{ years}$ for cores from above the lysocline cores (see table 9-4) another explanation for both the high ^{14}C ages on both super - and sublysocline core tops comes to mind. If the bioturbation depth is 8 cm, then the mean ^{14}C age of the mixed layer in superlysocline cores would be about 20,000 years.

So then what is the origin of the sublysocline calcite rich core top material? The integrated mass of calcite in these layers comes out to be 10 to 25 g/cm². At a rain rate of $0.4 \text{ g}/\text{cm}^2 \cdot 10^3 \text{ yrs}$, the accumulation of this material would take 25 to 60 thousand years. Furthermore, as this sublysocline core top material appears to have been subjected to calcite solution the time for accumulation must have been even longer. Thus we are likely looking at a change in lysocline depth on the time scale of much greater than that for the Holocene. Our calcite preservation event may also be there, but its message is hidden by the complexity of the situation. Unfortunately, we cannot use the results from sediments in this area of the ocean either in support of or in opposition to an early post-glacial calcite preservation event.

The third sedimentary domain is the transition zone in which partial calcite solution occurs. In this zone the calcite preservation event should appear as both a maximum in accumulation rate and a minimum in extent of dissolution. An example of the CaCO_3 versus depth record for a core taken from such an area is shown in figure 6-8, along with an ^{18}O record for the same core. While the major feature of this record is an indication (through lower CaCO_3 contents) that dissolution was more intense during interglacials than during glacials, there is also a marked lag between the CaCO_3 and $\delta^{18}\text{O}$ changes. This lag is most easily seen

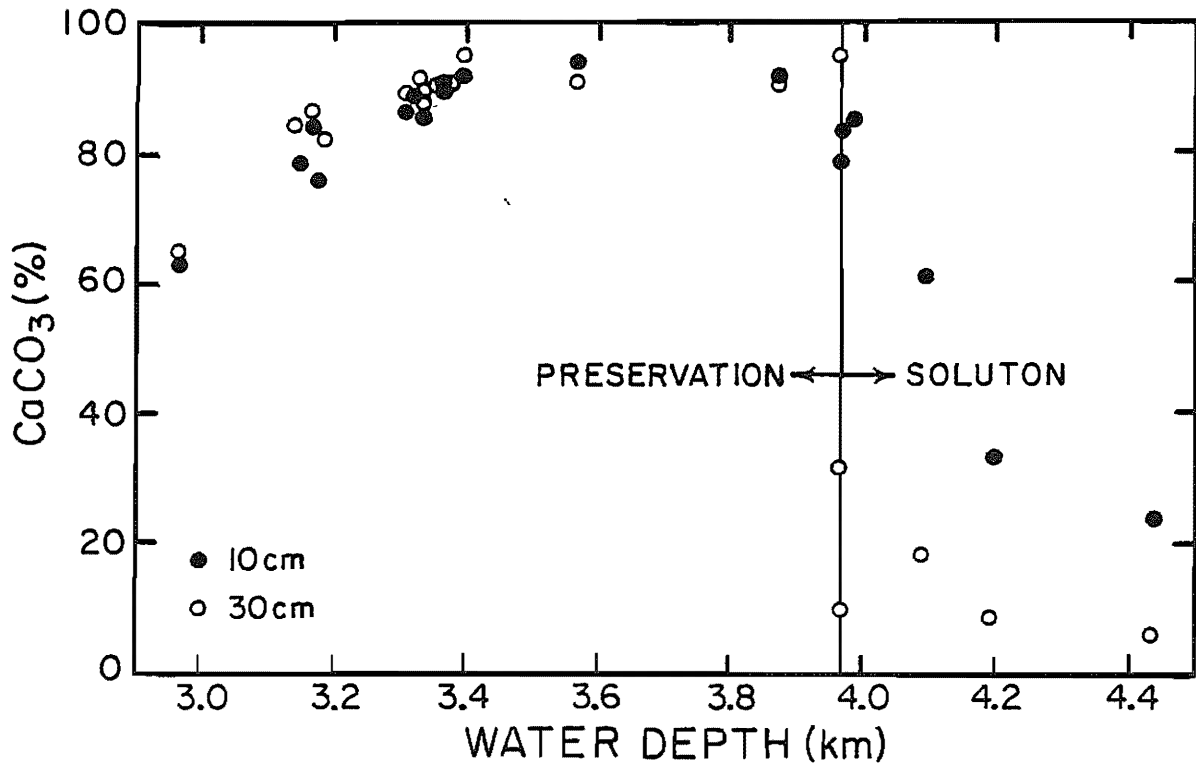


Figure 9-8. CaCO₃ content (% by weight) at depths of 10 and 30 centimeters for cores from the west flank of the East Pacific Rise plotted against the water depth at which the core was collected. For the samples taken at 30 cm a sharp transition occurs at a water depth of 3.95 km. This research was carried out at the Lamont-Doherty Geological Observatory (487).

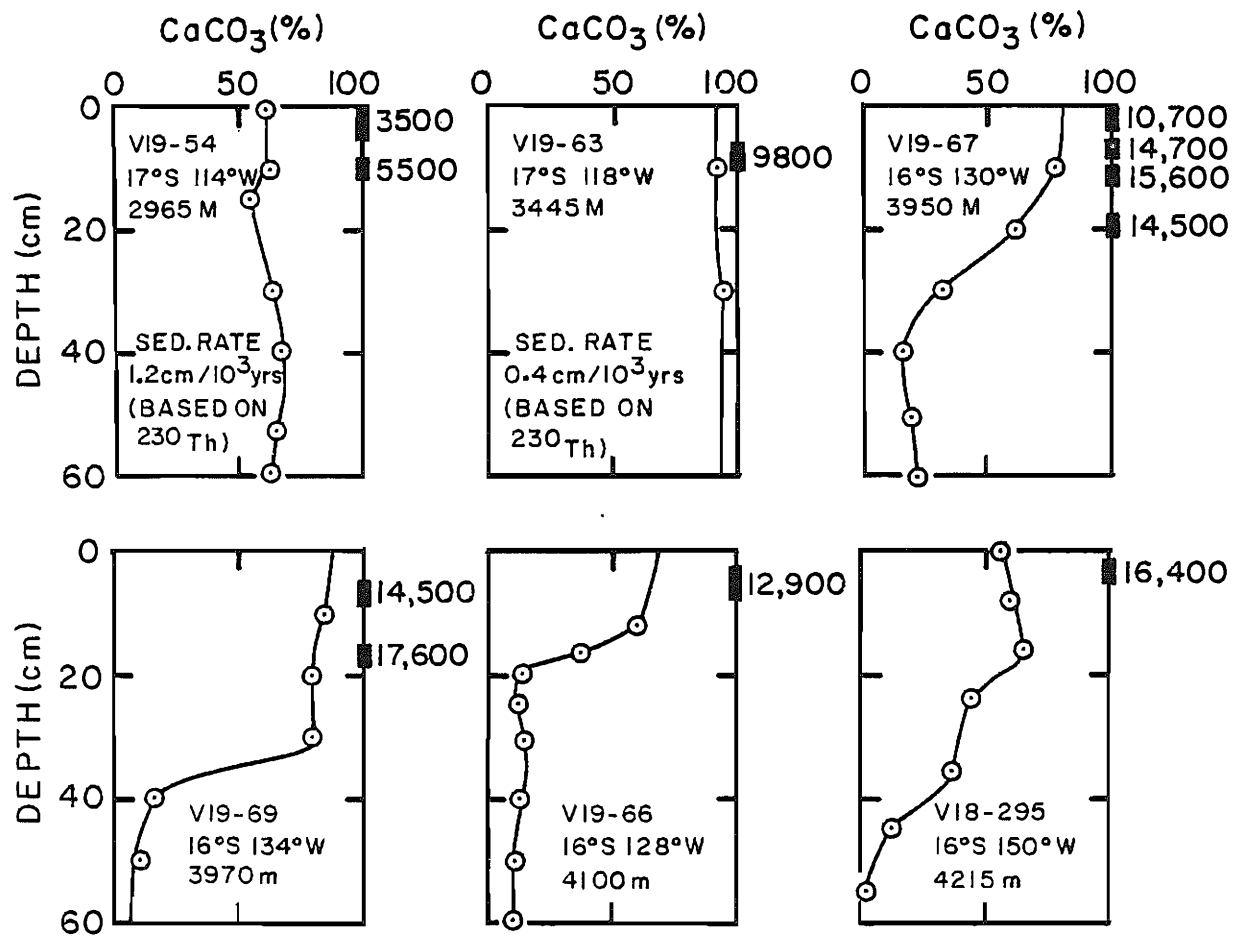


Figure 9-9. Plots of CaCO_3 (in weight %) against depth in the sediment column for cores taken on the west flank of the East Pacific Rise. Radiocarbon ages on the CaCO_3 are also given. V19-54 and V19-63 are from above the lysocline. The others are from beneath the lysocline. These measurements were made at the Lamont-Doherty Geological Observatory (487, 512).

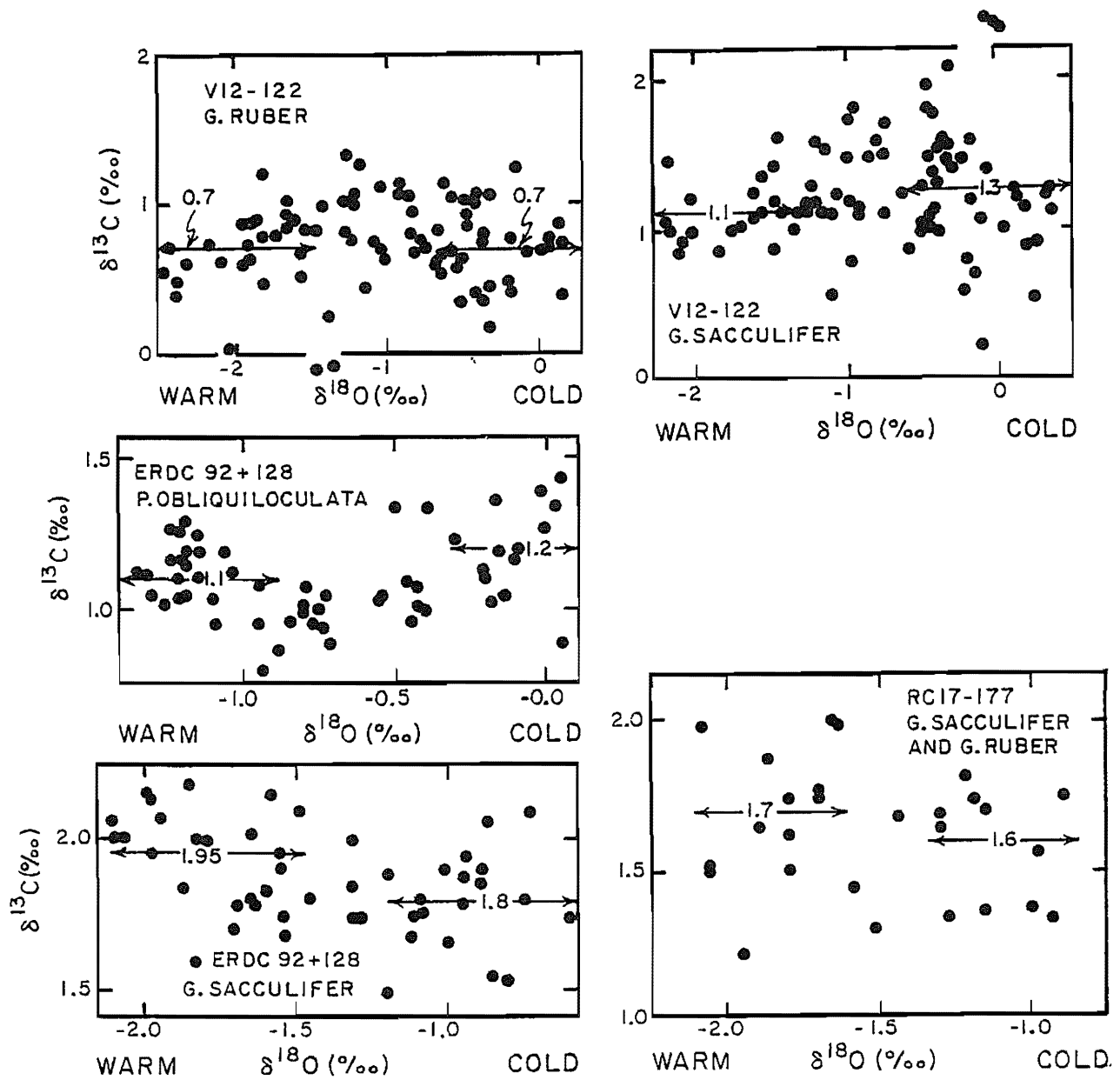


Figure 9-10. Plots of $\delta^{13}\text{C}$ versus $\delta^{18}\text{O}$ for planktonic foraminifera from Caribbean Sea core V12-122 (327) and from western equatorial Pacific core ERDC 98 (329), ERDC 128 (329) and RC 17-177 (personal communication, Shackleton). Averages for samples from glacial time (high $\delta^{18}\text{O}$) and for samples from interglacial time (low $\delta^{18}\text{O}$) are shown.

Table 9-4. Core top radiocarbon ages for sediments on the west flank of the East Pacific Rise. These measurements were made at the Lamont-Doherty Geological Observatory (487, 512).

Core No.	Lat.	Long.	Water Depth km	Depth In core cm	CaCO ₃ %	¹⁴ C Age yrs	Sed.* Rate cm/10 ³ yrs
Above Lysocline							
V19-53	17°S	114°W	3.06	2-6		3,300	-
V19-54	17°S	114°W	2.96	0-5	61**	3,500	1.2
V19-61	17°S	117°W	3.42	0-5	90	16,600	0.4
V19-63	17°S	121°W	3.45	6-10	92	9,800	0.4
Below Lysocline							
V19-66	16°S	128°W	4.10	2-8	61	12,900	-
V19-67	16°S	130°W	3.95	1-4	78	10,700	-
V19-69	16°S	134°W	3.97	2-6	83	17,700	-
RC13-74	18°S	146°W	3.96	0-5	70	12,600	-
RC13-80	19°S	127°W	4.03	0-6		14,800	-
RC13-81	19°S	124°W	3.75	0-2		14,800	-
V18-302	13°S	141°W	4.13	5-9		12,800	-
RC15-25	7°S	137°W	4.48	0-2		9,400	-
V18-295	16°S	150°W	4.22	3-8	65	16,400	-

*Based on ²³⁰Th dating.

**Dilution by Fe and Mn oxides rather than depletion by calcite solution.

for the three warm peaks of the last interglacial period and for the Holocene. In each case the CaCO_3 change occurs well after the ^{18}O change. It is possible that we see in this core the combination of two phenomena. First, the steady state lysocline level in this area of the equatorial Pacific was deeper during glacial than during interglacial times. Second, a calcite preservation event temporarily counters the change in the steady state lysocline level and in so doing generates what appears to be a delay in response. Again, while a tantalizing hint that a calcite compensation event occurred, verification and quantification await further studies. And so it stands; we have hints but no solid evidence.

CHANGES IN PHOSPHATE CONCENTRATION

As the title of this chapter implies, phosphate must have a part to play in this story. To understand why this is the case we need to understand the role of phosphate in controlling the CO_2 partial pressure in today's surface ocean. As shown in table 9-5, if deep sea water were brought to the surface and merely warmed without any biological activity (i.e., heated isochemically),* then its CO_2 partial pressure would be about three times higher* than that in the present day atmosphere. The removal of ΣCO_2 by plants draws down the CO_2 pressure in the water. The extent of this drawdown depends on the $\text{PO}_4/\Sigma\text{CO}_2$ ratio in deep water. The greater this ratio the greater the reduction in CO_2 partial pressure due to plant growth! Thus a glacial to interglacial variation in the ratio of PO_4 to ΣCO_2 in the sea would lead to a corresponding variation in the partial pressure of CO_2 in surface ocean water and in the atmosphere.

How would such a change be recorded in deep sea sediments? We saw in chapter 6 that the distributions of $\delta^{13}\text{C}$ and PO_4 were closely correlated in today's ocean (see figure 6-11). This is because the main source of $^{13}\text{C}/^{12}\text{C}$ variations from place to place within the sea is the photosynthesis-respiration cycle. The difference in the $^{13}\text{C}/^{12}\text{C}$ ratio between phosphate-free surface water (i.e., PFSW) and mean deep water (i.e., MDW) is given by the relationship:

$$\delta^{13}\text{C}_{\text{PFSW}} - \delta^{13}\text{C}_{\text{MDW}} = -\Delta^{13}\text{C}_{\text{photo}} \text{ C/P)}_{\text{org}} \frac{[\text{PO}_4]_{\text{MDW}}}{[\Sigma\text{CO}_2]_{\text{MDW}}} \quad 9-1$$

In today's ocean the photosynthetic fractionation factor, $\Delta^{13}\text{C}_{\text{photo}}$, is -20‰ ; the carbon to phosphorus ratio in

*This might be thought of as the "Strangelove" effect. Were life in the ocean to be suddenly destroyed, then the ocean's surface chemistry would change on the time scale of a few decades to that shown for isochemical warming in table 9-5. Such a disaster appears to have occurred at the end of Cretaceous time due to an impact of an asteroid or comet. Some of the effects described here should be sought in the records for that time (i.e., a CO_2 -induced warming, a shift in surface water $\delta^{13}\text{C}$ values,...).

Table 9-5. Interglacial to glacial changes in ocean chemistry.

P atm	θ $^{\circ}\text{C}$	S $^{\circ}/\text{oo}$	Alk $\mu\text{eq/kg}$	ΣCO_2 $\mu\text{m/kg}$	$\text{CO}_3^{=}$ $\mu\text{m/kg}$	PO_4 $\mu\text{m/kg}$	NO_3 $\mu\text{m/kg}$	PCO_2 10^{-6} atm
INTERGLACIAL								
400	1	34.7	2365	2250	86	2.2	33	-
	Brought to the Surface and Isochemically Heated							
	22	34.7	2365	2250	101	2.2	33	1043
	After Loss of PO_4 (and NO_3) to Plants							
	22	34.7	2398	2019	269	0.0	0	266
1	After CaCO_3 Loss							
	22	34.7	2282	1961	226	0.0	0	311
GLACIAL								
390	1	35.9	2577	2466	89	3.2	48	-
	Brought to Surface and Isochemically Heated							
	20	35.9	2577	2466	103	3.2	48	1151
	After Loss of PO_4 (and NO_3) to Plants							
	20	35.9	2625	2130	354	0.0	0	194
1	After CaCO_3 Loss							
	20	35.9	2457	2046	289	0.0	0	233

marine plants, C/P_{org} , is about 105; the mean phosphate concentration in deep water, $[PO_4]_{MDW}$, is $2.25 \mu\text{m}/\text{kg}$; and the mean dissolved inorganic carbon concentration in deep water, $[\Sigma CO_2]_{MDW}$, is $2250 \mu\text{m}/\text{kg}$. Hence:

$$\delta^{13}\text{C}_{\text{PFSW}} - \delta^{13}\text{C}_{\text{MDW}} = 20 \times 105 \times 2.25/2250 = 2.1 \text{ ‰}$$

If we assume that the fractionation during photosynthesis and the elemental composition of marine plants was the same during peak glacial time as it is today, then the difference between the $^{13}\text{C}/^{12}\text{C}$ ratio in glacial phosphate free surface water and glacial mean deep water provides a measure of the ratio of the phosphate concentration to dissolved inorganic carbon concentration in the deep water of glacial time. This $^{13}\text{C}/^{12}\text{C}$ ratio difference can be reconstructed by studies of planktonic forams and benthic forams which lived during peak glacial time.

The temperature dependence of the carbon isotope fractionation between CaCO_3 and the dissolved inorganic carbon in sea water is quite small. Also, as we have seen, the temperature changes in both surface water and deep water between glacial and interglacial times were on the average quite small. Hence the difference between the $^{13}\text{C}/^{12}\text{C}$ ratio in the growing shells and in the dissolved inorganic carbon in the water in which they grew should not have been significantly different during glacial than during interglacial time. Hence, if we see a change in the $\delta^{13}\text{C}$ value for a given species of either benthic or planktonic foram between glacial and interglacial time, there is a good chance that it reflects a change in the $\delta^{13}\text{C}$ for the dissolved inorganic carbon in that part of the ocean.

A problem to be faced in this connection is that each species of foraminifera shows a somewhat different fractionation factor. Geochemists term these differences "vital effects" (a name which hides the fact that we don't understand them). Because of these vital effects we cannot simply estimate the difference in the $\delta^{13}\text{C}$ between glacial phosphate-free surface water and glacial mean deep water directly from the difference between the $\delta^{13}\text{C}$ values for the shells of planktonic organisms grown in phosphate-free surface water and for the mean of shells of benthic organisms grown in various places in the deep sea. Rather, we estimate this difference in a less direct way from the following equation:

$$(\delta^{13}\text{C}_{\text{PFSW}} - \delta^{13}\text{C}_{\text{MDW}})_G = (\delta^{13}\text{C}_{\text{PFSW}} - \delta^{13}\text{C}_{\text{MDW}})_{\text{today}} + \quad 9-2 \\ (\delta^{13}\text{C}_G - \delta^{13}\text{C}_I)_{\text{plank}} - (\delta^{13}\text{C}_G - \delta^{13}\text{C}_I)_{\text{benthic}}$$

The term on the left hand side of this equation is the answer we seek. The first of the three terms on the right is the measured $\delta^{13}\text{C}$ difference between phosphorus-free surface water and mean deep water in today's ocean. The second term on the right is the glacial to interglacial change for a given species of planktonic foraminifera as measured in individual deep sea cores. The third term on the right is the glacial to interglacial change for a given species of benthic foraminifera as measured in individual deep sea cores. If the vital effect for a given species is assumed to remain constant from glacial to interglacial time, its

influence is eliminated by this procedure.

We have already shown that the glacial to interglacial $\delta^{13}\text{C}$ difference for benthic species collected from throughout the deep sea averages 0.7‰ (the $^{13}\text{C}/^{12}\text{C}$ ratio is lower during glacial than during interglacial time). It remains only to establish this difference for phosphate-free surface water. In figure 9-10 are shown plots of $\delta^{13}\text{C}$ against $\delta^{18}\text{O}$ for different species of planktonic foraminifera in cores from the temperate tropical ocean (hence from beneath phosphate-free surface water). Samples having high $\delta^{18}\text{O}$ values grew during times of large ice cover (glacials) and those with low $\delta^{18}\text{O}$ values grew during times of small ice cover (interglacials). It can be seen from these plots that while the scatter of individual points is large, the difference between the average $\delta^{13}\text{C}$ for the glacial and interglacial samples is quite small. These differences as summarized in table 9-6 average only 0.1‰. Hence, as do benthics, the planktonics grown during glacial time have a lower $^{13}\text{C}/^{12}\text{C}$ ratio than do those grown during interglacial time. However, in the case of planktonics, the difference is far smaller and might even be said to be not significantly different from zero.

It is because the $\delta^{13}\text{C}$ difference for planktonics is so small and the scatter of individual measurements so large that the mode of presentation in figure 9-10 was selected. While this procedure allows us to pick out a small signal in the presence of considerable noise, the question as to the cause of the noise remains. Were it just a matter of random variation this noise could be overcome by averaging large numbers of analyses as has been done here. The problem is that the factors generating the sample to sample variation might produce a bias in the glacial to interglacial difference (i.e., the difference obtained from the analysis of forams might not be the same as the difference for the carbon dissolved in the water). While no one has yet figured out why $\delta^{13}\text{C}$ analyses on planktonic forams show greater scatter than those on benthic forams, there is one clue. When different size fractions of the same species are analyzed, the smaller shells show lower $\delta^{13}\text{C}$ values than the larger shells (see figure 9-11 for an example). As these organisms add chambers to their shells as they age, the smaller shells represent organisms that died at a "young" age, and the larger shells represent organisms that died after a full life. Hence the $\delta^{13}\text{C}$ values for the calcite deposited by these species increase as they grow older. This could be either the result of a change in vital effect with maturity or a shallowing of their depth habitat with maturity (i.e., less shell material grown in the lower $\delta^{13}\text{C}$ thermocline water and more in the higher $\delta^{13}\text{C}$ mixed layer water). The latter explanation is unlikely as the ^{18}O change is in the same sense as the ^{13}C change (see figure 9-11). Were these changes produced by vertical migration the ^{13}C and ^{18}O changes should be in the opposite sense.*

*The $^{13}\text{C}/^{12}\text{C}$ ratio in ΣCO_2 decreases with depth. As the temperature dependence of the $\Sigma\text{CO}_2 - \text{CaCO}_3$ fractionation is small so also should the $^{13}\text{C}/^{12}\text{C}$ ratio in shell material grown at various depths. The $^{18}\text{O}/^{16}\text{O}$ ratio remains nearly the same with depth. However, the $\text{H}_2\text{O} - ^{18}\text{O}/^{16}\text{O}$ fractionation increases by about 0.2‰ for each degree the water cools. Hence the $^{18}\text{O}/^{16}\text{O}$ ratio should increase with the depth at which the CaCO_3 is deposited while the $^{13}\text{C}/^{12}\text{C}$ ratio should decrease.

Table 9-6. ^{13}C results on planktonic foraminifera.

Core No.	Ref. No.	Lat.	Long.	Depth km	$\delta^{13}\text{C}^{++}$ (ΣCO_2) °/oo	Species	Glacial $\delta^{13}\text{C}$ °/oo	Holocene $\delta^{13}\text{C}$ °/oo	$\Delta\delta^{13}\text{C}_{\text{G+I}}$ °/oo
Caribbean									
V12-122	(327)	17°N	74°W	2.8	~2.7	ruber.	0.7	0.7	0.0
V12-122	(327)	17°N	74°W	2.8	~2.7	sacc.	1.3	1.1	-0.2
Atlantic									
V22-174	(328)	10°S	13°W	2.6	~2.7	ruber.	1.0	1.4	+0.4
V22-174	(328)	10°S	13°W	2.6	~2.7	sacc.	1.8	2.0	+0.2
Pacific									
ERDC-92	(329)	2°S	157°E	1.6	~2.7	sacc.	1.8	1.95	+0.15
ERDC-128	(329)	0°S	161°E	3.7	~2.7	obliq.	1.2	1.1	-0.1
RC17-177	†	2°N	159°E	2.6	~2.7	sacc. + rub.	1.6	1.7	+0.1
MEAN								+0.1	

† Shackleton (personal communication)

++In 1973 the $\delta^{13}\text{C}$ for warm surface ocean water averaged 1.9°/oo. The recent influx of forest, soil and fossil fuel CO_2 has reduced the ratio by about 0.8°/oo. Thus prior to 1850 it was likely close to 2.7°/oo.

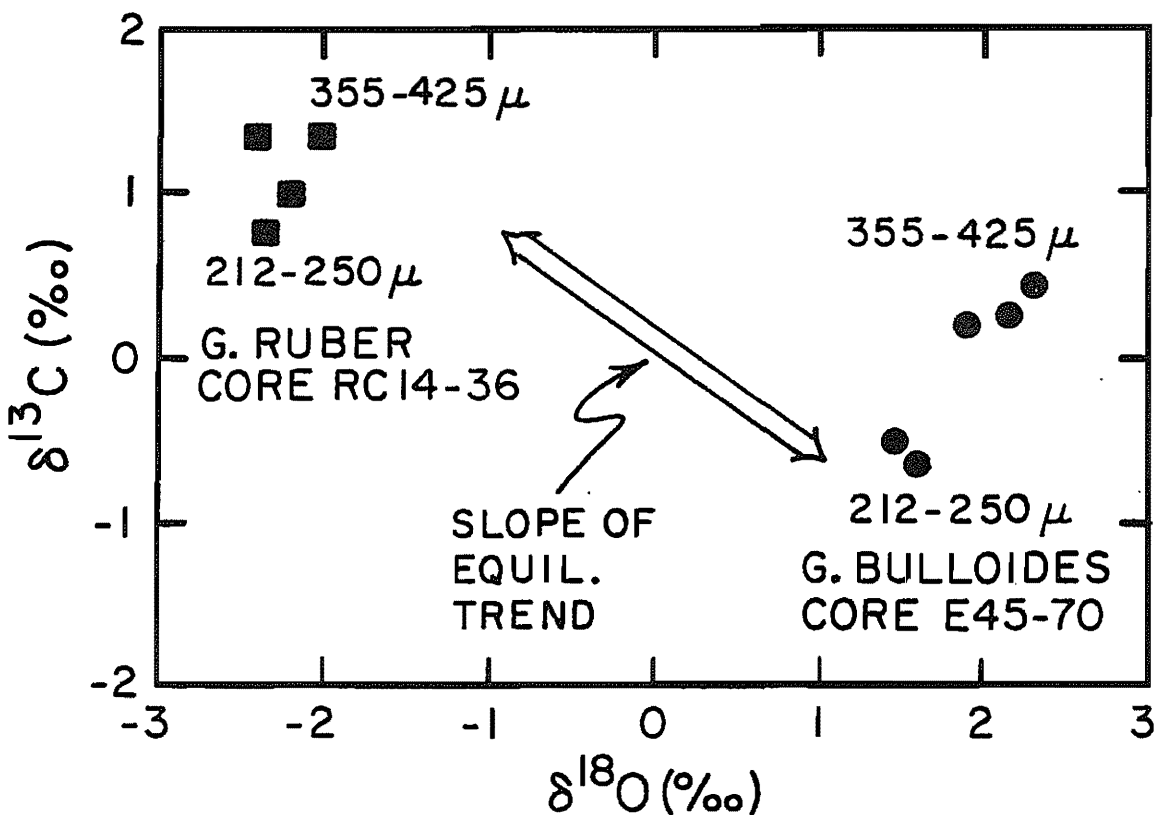


Figure 9-11. Plots of $\delta^{13}\text{C}$ versus $\delta^{18}\text{O}$ for different size fractions of the species G. ruber (upper left) and G. bulloides (lower right) from core top samples from two sites in the Indian Ocean cores. In both sets, the smaller shells have both lower $\delta^{18}\text{O}$ and lower $\delta^{13}\text{C}$ values than their larger counterparts. The trend with size does not correspond with that expected if the organisms changed their depth habitat with age. In this case the $\delta^{13}\text{C}$ should decrease with increasing $\delta^{18}\text{O}$ following the trend shown by the large arrow. The results were obtained by Matthews and his colleagues at Brown University (330).

In any case, we have no way to know how glacial planktonics differed from their interglacial brothers, either with regard to vital effect or depth habitat. Thus we must fall back on the hope that by analyzing enough different species at enough different locations on the sea floor any bias introduced in this way is averaged out.

If we accept the glacial to interglacial differences obtained for planktonic and for benthic forams as meaningful estimates of the changes in the $\delta^{13}\text{C}$ value for phosphate-free surface water and for mean deep water, then the difference in $\delta^{13}\text{C}$ between these waters in glacial times becomes:

$$(\delta^{13}\text{C}_{\text{PFSW}} - \delta^{13}\text{C}_{\text{MDW}})_G = 2.1 - 0.1 + 0.7 = 2.7^{\circ}/\text{oo}$$

These changes are shown diagrammatically in figure 9-12. If we further assume that the magnitude of the photosynthetic isotope fractionation factor and of the carbon to phosphorus ratio in marine plants during glacial time was the same as during interglacial times, then the mean phosphate content of deep ocean water during glacial time is given by:

$$[\text{PO}_4]_{\text{MDW}}^G =$$

9-3

$$\frac{(\delta^{13}\text{C}_{\text{PFSW}} - \delta^{13}\text{C}_{\text{MDW}})_G}{(\delta^{13}\text{C}_{\text{PFSW}} - \delta^{13}\text{C}_{\text{MDW}})_{\text{today}}} \times \frac{[\Sigma\text{CO}_2]_{\text{MDW}}^G}{[\Sigma\text{CO}_2]_{\text{MDW}}^{\text{today}}} \frac{[\text{PO}_4]_{\text{MDW}}^{\text{today}}}{[\text{PO}_4]_{\text{MDW}}}$$

As stated above, the mean phosphate content of today's deep sea water is 2.25 $\mu\text{m}/\text{kg}$. We have shown that the amount of dissolved inorganic carbon in the sea was about 6% higher during glacial than during interglacial time and that the amount of water in which this carbon was dissolved was about 3.5% lower than today. This yields a ratio of $[\Sigma\text{CO}_2]_G$ to $[\Sigma\text{CO}_2]^{\text{today}}$ of about 1.09. Thus:

$$[\text{PO}_4]_{\text{MDW}}^G = \frac{2.7}{2.1} \times 1.09 \times 2.25$$

or

$$[\text{PO}_4]_{\text{MDW}}^G = 3.2 \mu\text{m}/\text{kg}$$

THE COMBINED EVIDENCE FROM DEEP SEA CORES

We can now put all these results together and calculate the CO_2 partial pressure for surface water during glacial times. As shown in table 9-5, we start with the composition of average present-day deep water (line 1). We then show (line 2) that if this water were to reach the surface in a "Strangelove" ocean (i.e., one with no life), then the CO_2 pressure would be close to three times the present atmospheric value. In the real ocean

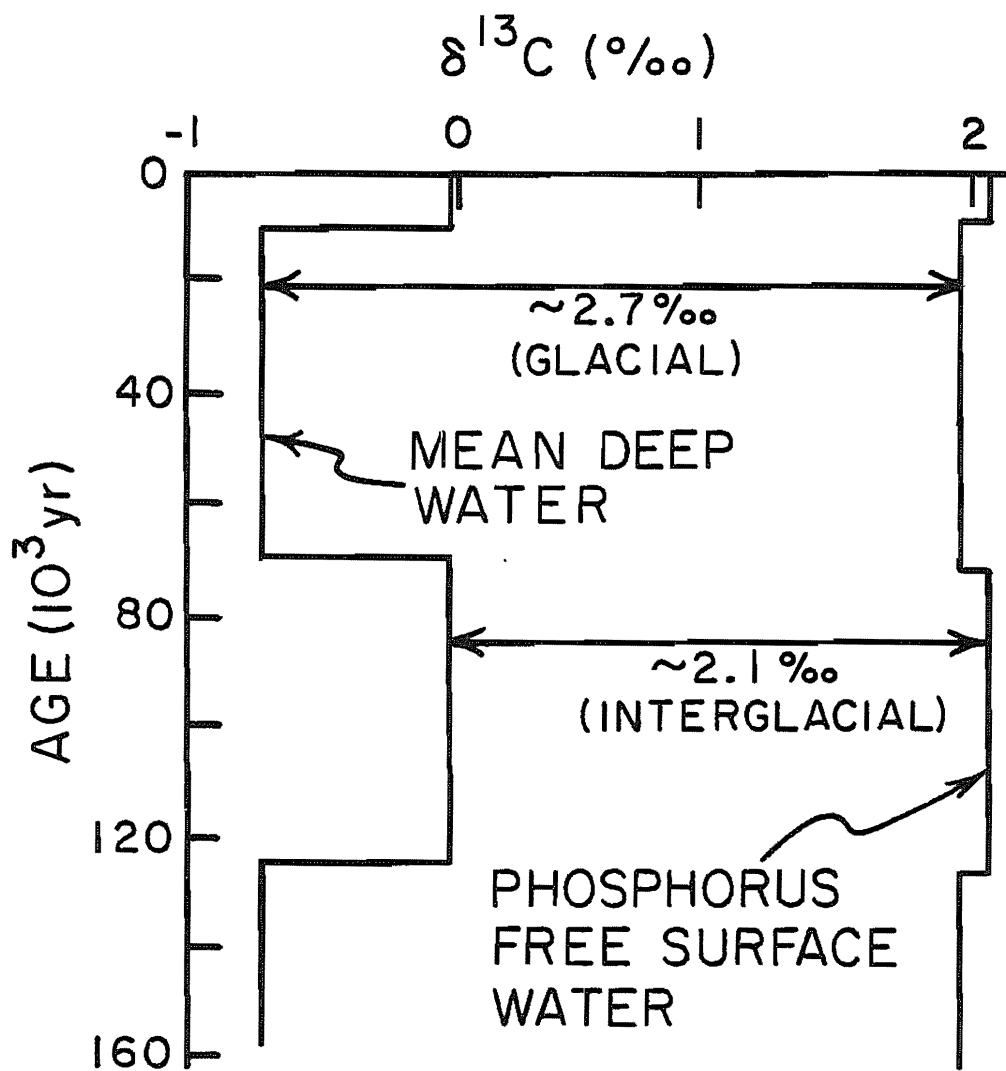


Figure 9-12. Schematic diagram of the glacial to interglacial cycle in the $\delta^{13}\text{C}$ values for the ΣCO_2 in mean deep water and for the ΣCO_2 in phosphate-free surface water.

however, the activity of plants would deplete the phosphate (and nitrate) and utilize some of the carbon to form soft tissue. The chemistry of the water after this had happened is given in line 3 of the table. The alkalinity change between lines 2 and 3 is the result of nitrate utilization. We have one step to go. Some of the plants which live in surface water form CaCO_3 cages; some of the animals which eat these plants form CaCO_3 shells. The impact of CaCO_3 formation is shown in line 4.

Here we must digress a bit to show how the ratio of CaCO_3 formation to plant tissue formation (i.e., the ratio of CaCO_3 rain to PO_4 rain) in today's ocean is obtained. We adopt a value of one mole of carbon lost to CaCO_3 for each four moles of carbon lost to organic tissue. This value is obtained from the comparison of the chemical composition of warm surface waters from various regions of the ocean with that for mean deep water. If chemical differences between surface water and mean deep water (after normalization to the same salinity) are attributed to the production of CaCO_3 and organic tissue, then the magnitudes of the removal of each phase can be calculated. The amount of CaCO_3 produced is obtained taking half of the nitrate corrected alkalinity change, i.e.,

$$\Delta C_{\text{CaCO}_3} = \frac{\Delta \text{Alk} + \Delta \text{NO}_3}{2} \quad 9-4$$

As we have mentioned before, the removal of NO_3 ion to form organic tissue raises the alkalinity of surface water, partly compensating for decrease in alkalinity resulting from CaCO_3 formation.

The amount of carbon fixed into organic tissue can be estimated in two ways. It can be obtained by subtracting the amount of CaCO_3 produced from the difference between the ΣCO_2 concentrations for deep and surface water:

$$\Delta C_{\text{Org}} = \Delta \Sigma \text{CO}_2 - \Delta C_{\text{CaCO}_3} \quad 9-5$$

It can also be estimated by multiplying the change in phosphate concentration by the C/P ratio in organic tissue (i.e., by 105). An example of such a calculation is shown in table 9-7. The ratio $\Delta C_{\text{Org}} / \Delta C_{\text{CaCO}_3}$ is then calculated by averaging the two ΔC_{Org} estimates. The results of a number of such estimates are given in table 9-8. They range from 3.5 to 7.2 and average 4.5. This result must be corrected for the fraction of each phase which accumulates in the sediment. As we have seen only about 1% of the organic tissue survives destruction hence no correction need be made. However, in the case of CaCO_3 about 15% of that produced accumulates in the sediments. Hence the ΔC_{CaCO_3} estimate must be multiplied by 1.15. This brings the ratio $\Delta C_{\text{Org}} / \Delta C_{\text{CaCO}_3}$ close to 4. We adopt this value.

While the exact choice of the ratio of $\Delta C_{\text{Org}} / \Delta C_{\text{CaCO}_3}$ is not very important, the extent to which it changes from glacial to interglacial times is. Such changes would generate a difference in the CO_2 pressure for surface water between glacial and interglacial time! The control on this ratio is ecological. It

Table 9-7. Example of the method used to calculate the ratio of organic carbon to CaCO_3 carbon produced in surface waters.

	PO_4 $\mu\text{m}/\text{kg}$	NO_3 $\mu\text{m}/\text{kg}$	ΣCO_2 $\mu\text{m}/\text{kg}$	Alk $\mu\text{eq}/\text{kg}$
Average Deep Water	2.22	32.1	2245	2354
GEOSECS Station 214 Surf H_2O *	0.04	0.1	1926	2266
Difference	2.18	32.0	319	88
$\Delta C_{\text{CaCO}_3} = \frac{88+32}{2} = 60 \mu\text{m}/\text{kg}$				
$\Delta C_{\text{Org}} = 319 - 60 = 259 \mu\text{m}/\text{kg}$ (Method #1)				
$\Delta C_{\text{Org}} = 105 \times 2.18 = 229 \mu\text{m}/\text{kg}$ (Method #2)				
$\frac{\Delta C_{\text{Org}}}{\Delta C_{\text{CaCO}_3}} = \frac{244}{60} = 4.1$				

*Normalized to salinity of average deep water.

Table 9-8. Estimates of the organic to CaCO_3 carbon fixation rate for surface waters from throughout the temperate and equatorial ocean. Based on results obtained as part of the GEOSECS program (424, 425, 426, 406).

Stn. No.	T $^{\circ}\text{C}$	ΔC_{CaCO_3} $\mu\text{m}/\text{kg}$	Method #1* ΔC_{org} $\mu\text{m}/\text{kg}$	Method #2* ΔC_{org} $\mu\text{m}/\text{kg}$	$\Delta C_{\text{org}}/\Delta C_{\text{CaCO}_3}$
ATLANTIC					
31	27	34	260	227	7.2
37	28	38	298	231	7.0
42	27	59	263	224	4.1
54	26	61	277	222	4.1
61	17	56	229	217	4.0
105	25	56	243	210	4.0
115	19	55	234	230	4.2
120	18	65	240	226	3.6
					<u>4.8</u>
INDIAN					
438	27	66	239	222	3.5
442	30	65	254	221	3.7
446	28	38	242	226	6.2
417	27	59	240	183	3.6
420	27	54	227	209	4.0
427	26	56	245	217	4.1
					<u>4.2</u>
PACIFIC					
214	28	60	259	229	4.0
201	18	37	133	190	4.4
227	27	66	232	228	3.5
244	26	48	220	174	4.1
260	29	47	291	208	5.1
269	27	49	275	225	5.1
					<u>4.4</u>

*Note that method #1 gives on the average a 40 $\mu\text{m}/\text{kg}$ higher answer than method #2. One reason for this difference is the higher preformed ΣCO_2 content of cold than warm surface water which contributes to the difference between the ΣCO_2 content of phosphate free surface water and cold deep water. Were the results from method #2 alone used then the mean would drop to about 4.0.

depends on what fraction of the plants form CaCO_3 cages and on what fraction of the animals which eat these plants form CaCO_3 shells. As we have at present no way to assess the change in ocean ecology from glacial to interglacial time, we assume that the ratio of 4 applies to both periods.

Now back to the calculations in table 9-5. The composition of glacial mean deep sea water is obtained as follows. The PO_4 content of $3.2 \mu\text{m}/\text{kg}$ obtained above is used. The NO_3 to PO_4 ratio in the sea is assumed to have remained at 15. As the process which removed PO_4 from the ocean at the end of glacial time would likely have also removed NO_3 it is unlikely that the NO_3/PO_4 would have changed. If it did change then we would have to call on the ecologic mechanism described in chapter 6 to produce the adjustment. Thus we take the glacial NO_3 concentration of deep water to be 15×3.2 or $48 \mu\text{m}/\text{kg}$.

The mass of ΣCO_2 in the ocean is taken to be 6% higher during glacial than during interglacial time and the salinity of the ocean to be 3.5% higher. Thus the ΣCO_2 concentration in deep water is taken to be 1.06×1.035 the interglacial value. There are two ways in which the alkalinity might be computed. One way would be to make the alkalinity change exactly equal to the ΣCO_2 change. While this is approximately the result expected if the compensation were complete, it is not the best estimate that can be made. A better approach is to use the difference in the global lysocline level between full glacial and full interglacial to fix the difference between the $\text{CO}_3^=$ ion concentration in average glacial and interglacial deep water. If the ΣCO_2 and $\text{CO}_3^=$ concentrations for glacial deep water are known then the alkalinity is determined.

Studies of the extent of dissolution in cores taken in the transition zone where calcite is partially dissolved reveal that waters in the equatorial Pacific and Indian Oceans were slightly less corrosive during glacial than during interglacial time (496, 501). Those in the equatorial Atlantic appear to have been slightly more corrosive (497, 507). Although the exact level of the lysocline during glacial time has yet to be established, it appears that the glacial to interglacial shifts were on the order of only a few hundred meters. In today's ocean a 1.0 to $1.5 \mu\text{m}/\text{kg}$ change in $\text{CO}_3^=$ ion will produce a 100-meter shift in lysocline depth (see chapter 2). Thus the changes in lysocline observed between glacial and interglacial time likely require no more than $5 \mu\text{m}/\text{kg}$ changes in $\text{CO}_3^=$ ion content. We estimate that during glacial time average deep water had a $3 \pm 3 \mu\text{m}/\text{kg}$ higher $\text{CO}_3^=$ ion content than during interglacial time. Based on this assumption the alkalinity in glacial deep water is obtained. As can be seen from table 9-5, the alkalinity difference between glacial and interglacial time calculated in this way comes out to be $212 \mu\text{eq}/\text{kg}$, while the ΣCO_2 difference is $216 \mu\text{m}/\text{kg}$. Thus the two approaches give almost the same answer. This completes the reconstruction of the chemical parameters for the average deep water of glacial time (line 5, table 9-5).

Were this water brought to the surface in a "Strangelove" ocean (line 6) it would have had an even higher PCO_2 than its interglacial equivalent. However, after plants complete their

Table 9-9. Sensitivity of the CO_2 partial pressure in surface water and to various properties of surface water. These calculations were carried out using the apparent dissociation constants of carbonic acid in sea water determined by Mehrbach *et al.*, at Oregon State University (400), and the CO_2 solubility of Weiss at Scripps Institution of Oceanography (403) following the procedures outlined by Broecker and Takahashi (463). In each example one parameter is changed and the others are held constant.

Temp. °C	Sal. ‰	PO_4^* $\mu\text{m}/\text{kg}$	Alk. $\mu\text{eq}/\text{kg}$	ΣCO_2 $\mu\text{m}/\text{kg}$	$\frac{\Delta\text{Org}}{\Delta\text{CaCO}_3}$	Alk- ΣCO_2 $\mu\text{m}/\text{kg}$	$\text{CO}_3^=$ $\mu\text{m}/\text{kg}$	PCO_2 10^{-6} atm
Change Temperature								
23	34.7	2.2	2276	1961	4	315	222	332
22	34.7	2.2	2276	1961	4	315	222	319
21	34.7	2.2	2276	1961	4	315	221	305
20	34.7	2.2	2276	1961	4	315	220	292
Change Salinity								
23	34.7	2.2	2276	1961	4	315	222	332
23	35.0	2.2	2296	1978	4	318	224	336
23	35.3	2.2	2315	1995	4	320	226	342
23	35.6	2.2	2335	2012	4	323	228	346
Change ΣCO_2 (hold alk. constant, i.e., no CaCO_3 compensation occurs)								
23	34.7	2.2	2276	1961	4	315	222	332
23	34.7	2.2	2276	2001	4	275	196	404
23	34.7	2.2	2276	2041	4	235	171	498
23	34.7	2.2	2276	2081	4	195	146	622
Change ΣCO_2 (hold alk-ΣCO_2 constant, i.e., CaCO_3 compensation occurs)								
23	34.7	2.2	2276	1961	4	315	222	332
23	34.7	2.2	2316	2001	4	315	224	344
23	34.7	2.2	2356	2041	4	315	225	357
23	34.7	2.2	2396	2081	4	315	227	370
Change $\Delta\text{Org}/\Delta\text{CaCO}_3$								
23	34.7	2.2	2216	1931	2.6	285	200	364
23	34.7	2.2	2246	1946	3.2	300	211	347
23	34.7	2.2	2276	1961	4.0	315	222	332
23	34.7	2.2	2306	1976	5.4	330	233	318
23	34.7	2.2	2336	1991	8.2	345	244	305
Change PO_4 in upwelled water								
23	34.7	3.0	2234	1856	4	378	262	237
23	34.7	2.6	2255	1909	4	346	242	281
23	34.7	2.2	2276	1961	4	315	222	332
23	34.7	1.8	2297	2013	4	284	203	393
23	34.7	1.4	2318	2066	4	252	183	471

*In upwelled water.

task of utilizing the PO_4 (and NO_3) the PCO_2 drops well below the value for interglacial water. The PCO_2 for the glacial surface ocean is 80×10^{-6} atmospheres below that for the interglacial surface water. The ocean sediment record does indeed generate a result which is consistent with that obtained directly from measurements on ice!

The sensitivity of the PCO_2 difference to uncertainties in the specifics of the reconstruction is given in table 9-9. While it is difficult to assign an overall uncertainty to the glacial PCO_2 reconstructed in this way, it is probably no less than $\pm 25 \times 10^{-6}$ atmospheres.

CAUSE OF THE OCEANIC PHOSPHATE CHANGE

What caused the PO_4 content of the sea to drop at the close of glacial time? The mean replacement time for PO_4 in the sea (~100,000 years) is too long to permit us to call on the steady state control mechanisms outlined in chapter 6. Rather, we must once again turn to the generation and destruction of a small phosphorus bearing reservoir. Of the small reservoirs discussed above, the terrestrial ones (soil and trees) are of no use. Phosphorus cannot be transferred through the atmosphere from sea to continent. Hence while the growth of trees and the development of organic-rich soils during early post-glacial time could bring about a change in the ΣCO_2 content of the ocean, the enlargement of these reservoirs would not lead to any change in the phosphorus content of the ocean! On the other hand, the loss of carbon to shelf sediments would be accompanied by a loss of phosphate (and nitrate). It is interesting to note in this regard that the ratio of C atoms lost to organic matter to phosphorus atoms removed from the sea at the close of glacial time needed in order to produce no change in the $\delta^{13}\text{C}$ for planktonic foraminifera is close to 105. Thus if the organic matter deposited on the shelves contained carbon and phosphorus in roughly their "Redfield" ratio, then shelf removal could explain what we observe!

So we come back to a loose end we dropped earlier in this chapter. What were the relative contributions of terrestrial reservoirs (trees and soil) and marine reservoirs (shelf sediment) to the removal of carbon from the ocean-atmosphere reservoir at the close of glacial time? Shackleton makes a good case that at least part of the loss must have been to the terrestrial reservoirs. Let us attempt a corresponding estimate of how much material might have been deposited on the shelves during early post-glacial time. We know from engineering borings that the world's estuaries received several tens of meters of sediment during early post-glacial time. This sediment rebuilt the sedimentary ramp from river to the shelf edge destroyed by erosion during the low sea stand of glacial time.

While similar deposition is likely to have occurred on many parts of the shelves eroded during glacial time, it is difficult to assess the magnitude of these deposits. We can, however, estimate roughly how large they would have to be to explain the benthic $\delta^{13}\text{C}$ shift. If we assume that the average shelf sediment contains 1% by weight organic carbon, then the mass of these

sediments would have to be $100 \times 9 \times 10^{16}$ moles $\times 12$ g C/mole or 1×10^{20} g. The area of the world's shelves is about 3×10^{17} cm². Thus if this sediment were spread uniformly over the entire shelf area it would make a deposit with 360 grams of mineral matter/cm² or a layer three to four meters thick. While such a mass is not so large that it would cause a person familiar with shelf geomorphology and sedimentation to flinch, such a person might be more comfortable with an amount 3 or so times smaller. Thus, as is the case for trees and soils, we can only show that shelf sedimentation could do the job. Hence the loose end remains. Both terrestrial and marine reservoirs must have contributed to the $\delta^{13}\text{C}$ change observed for benthics but it is not possible to state which played the more important role.

A compromise could be made by assuming both terrestrial and marine contributions to the organic carbon removal and a lower than Redfield C/P ratio in the organic material accumulating on the shelves. In the above discussions we have assumed that the organic residues falling into the deep sea and the organic residues accumulating in shelf sediments have C/P ratios of close to 105. However, these elements might be differentially released during decomposition. Indeed measurements of the organic C to P ratio in shelf sediments range all the way from 50 to 250. As these sediments are extremely heterogeneous, it is difficult to come up with a meaningful average.

AN ALTERNATE SCENARIO

The possibility of substantial deviations between the chemical composition for the particulate debris falling into the deep sea and the standard Redfield ratios opens a whole new explanation for the difference between glacial to interglacial $\delta^{13}\text{C}$ changes for benthic and planktonic shells. The $\delta^{13}\text{C}$ record could be equally well explained by a 30% glacial to interglacial decrease in the C/P ratio for the organic debris falling from surface to deep water. In chapter 3 we demonstrated that there is a difference in the C/P ratio of material oxidized from place to place in today's deep ocean (see table 3-5). Thus a 30% change from glacial to interglacial time is not beyond the realm of possibility. A 30% reduction in this ratio would cause the observed 0.6‰ reduction in $\delta^{13}\text{C}$ difference between surface and deep water ΣCO_2 . If this change were coupled with storage of organic matter in trees and soils then both the $\delta^{13}\text{C}$ history for planktonics and benthic forams could be explained. In fact, everything else about which we have spoken (the calcite compensation, the pCO₂ change,...) would be the same as for the shelf storage hypothesis. So the plot thickens! We now have not only the relative importance of terrestrial and marine organic carbon storage to worry about, but also the relative importance of phosphorus removal to shelf sediments and of a change in the C/P ratio in organic debris falling to the deep sea.

Is there any way to get a handle on the latter? Perhaps! To understand how, we must consider the sequence of events at the close of glacial time. To simplify things we will contrast the two extreme scenarios: i.e., organic carbon and phosphorus storage

in marine sediments on one hand, and terrestrial storage of organic carbon coupled with a change in the C/P ratio in falling organic debris on the other. These endmember scenarios are shown in figure 9-13. Also shown are the corresponding time histories of the $\delta^{13}\text{C}$ changes corresponding to each.

While the benthic records should be basically the same (a unidirectional rise in $\delta^{13}\text{C}$ during early post-glacial time) the planktonic records might be different in one respect. In the case of the residue composition scenario it is possible that a "spike" might have occurred in the planktonic $\delta^{13}\text{C}$ record. This spike would be produced by the lack of synchronicity between the change in ocean ecology (which would decrease the $\delta^{13}\text{C}$ for planktonics) and the growth of forests and soils (which would increase the $\delta^{13}\text{C}$ for planktonics). If, for example, the ecology change occurred before the forest and soil development, then the spike would be toward low $\delta^{13}\text{C}$ values (see figure 9-13). The duration and magnitude of the spike would depend on extent of separation in time of the ocean ecology and terrestrial storage events. In no case, however, could the magnitude exceed 0.7‰. No such spike would be possible for the shelf storage scenario because the removal of carbon and phosphorus to the shelves would take place simultaneously.

Is there any evidence for a spike in the planktonic $\delta^{13}\text{C}$ values in early post-glacial time? As was the case for the calcite preservation event a systematic search has yet to be made. As shown in figure 9-14, the results on cores run to date show no sign of such a spike. While the record for core V12-122 from the Caribbean Sea shows an anomaly during Holocene time, this anomaly is seen for sacculifer and not for ruber. Also this record is so noisy that what appears to be an anomaly may well be just another random fluctuation. The more detailed records for cores ERDC 92 and 128 from the western equatorial Pacific do not show such anomaly. In examining these records it must, however, be kept in mind that bioturbation would take a heavy toll on an event only a few thousand years in duration. Until more detailed studies have been made on cores with higher deposition rates this question must remain open.

WRAP UP OF THE CO₂ RECORD

Summarizing, then, it has been shown that at the close of glacial time about 3% of the carbon in the ocean-atmosphere system was removed as organic residues. The removal of this carbon triggered a CaCO₃ preservation event in the deep sea. Further, either the phosphorus to carbon ratio for mean ocean water decreased through phosphorus removal to shelf sediments, or the phosphorus to carbon ratio in the organic debris raining to the deep sea decreased by about 30%. This reconstruction yields a glacial to interglacial increase in the CO₂ partial pressure for surface water (and hence also the atmosphere) close to that observed in the air bubbles trapped in polar ice. It was not possible, on the basis of the information available when this book was written, to distinguish between the roles of the terrestrial reservoirs, of shelf reservoirs, and of ocean ecology in producing these changes.

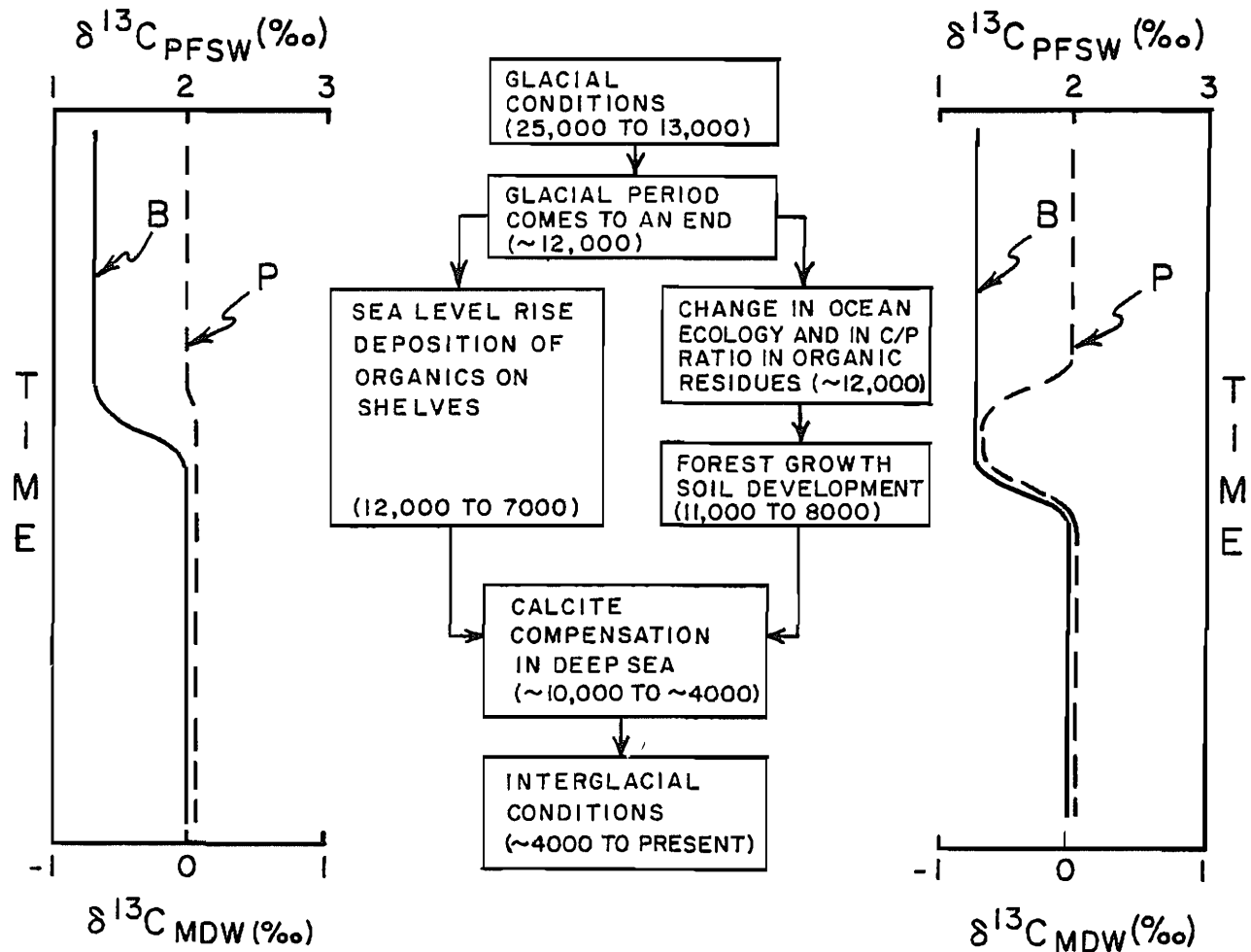


Figure 9-13. Comparison of two scenarios which could explain the $\delta^{13}\text{C}$ record for planktonic (P) and benthic (B) forams and the PCO_2 record obtained from ice cores. The records differ only in that the right hand scenario might have produced a brief spike in the $\delta^{13}\text{C}$ value for planktonic forams in early post-glacial time.

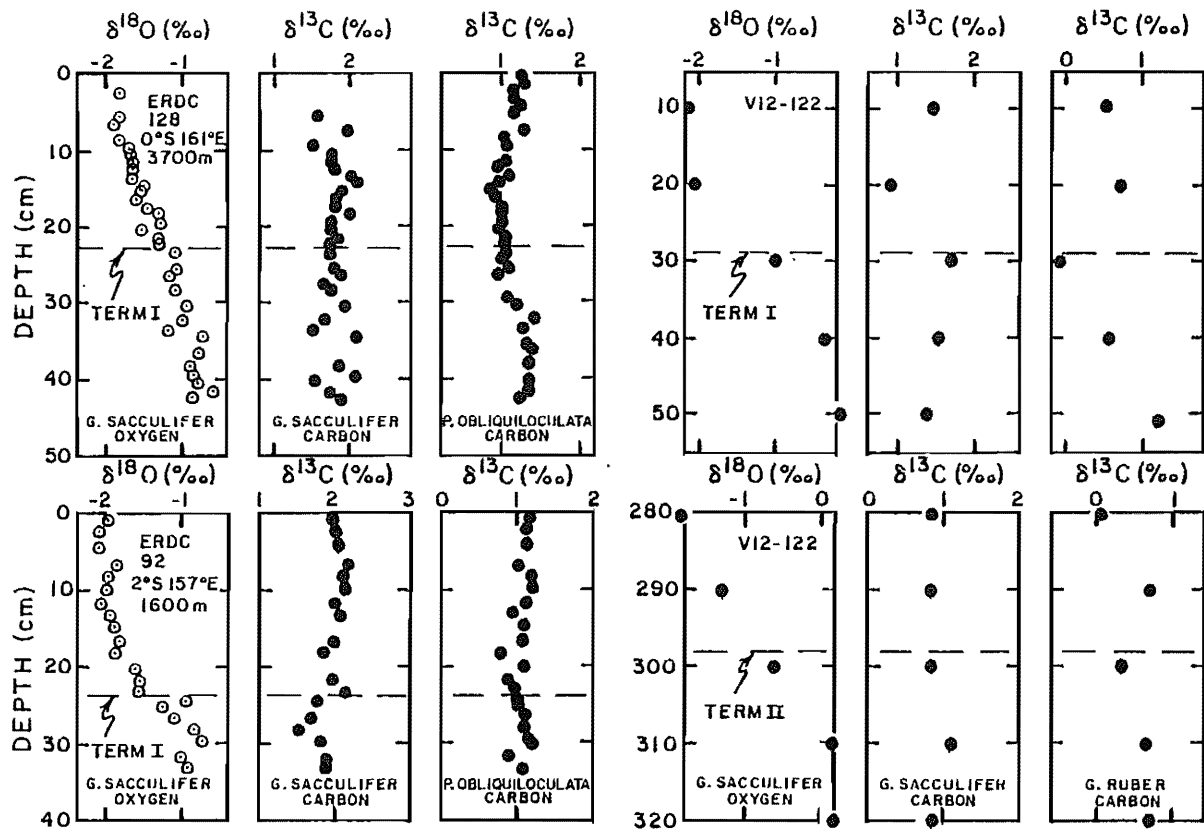


Figure 9-14. The records of $\delta^{18}\text{O}$ and $\delta^{13}\text{C}$ for planktonic forams in two equatorial Pacific cores and in one Caribbean core. There is no evidence of a $\delta^{13}\text{C}$ spike in early post-glacial time. The results on ERDC 92 and 128 were obtained by Berger and his co-workers at Scripps Institution of Oceanography (329); those on core V12-122 were obtained by Van Donk at the Lamont-Doherty Geological Observatory (327).

However, more detailed studies of the records in ice and in marine sediments should yield additional evidence needed to narrow down the range of possibility.

THE OXYGEN RECORD

If during glacial time the phosphorus to carbon ratio in either mean ocean water or in particulates falling to the deep sea were larger than today's then the dissolved oxygen content of the deep sea water would have to have been lower. The reason is as follows. As the temperature of deep water in the sea during glacial times was only $1.5 \pm 1.5^{\circ}\text{C}$ colder than today's, the solubility of oxygen in the descending glacial deep water would have been nearly the same as in today's. Further, the oxygen content of the atmosphere could not have been appreciably different than in today's.* The amount of dissolved oxygen brought to the deep sea with each unit of new deep water would also have been the same. On the other hand, the demand for oxygen in the deep sea would have been greater. If there were more phosphorus dissolved in glacial deep water, then for each unit of deep water upwelled more phosphorus would have reached the surface and more organic material would have rained to the deep sea. If, on the other hand, the particles raining to the deep sea during glacial time carried more carbon per unit of phosphorus than those falling today, the oxygen demand would also be higher. Thus, regardless of which explanation is adopted for the $\delta^{13}\text{C}$ results, a lower dissolved oxygen content for glacial deep water than for interglacial deep water is required.

While the amount of the decrease in oxygen in glacial deep waters depends on the details of how the ocean circulated during glacial time, a rough estimate can be made from the PO_4 content difference between glacial and interglacial deep water required by the shelf storage hypothesis. As listed in table 9-5 the phosphate content of mean deep water dropped by close to $1 \mu\text{m}/\text{kg}$ at the close of the glacial time. Using the ordinary Redfield ratios, this leads to a difference in the oxygen content of deep water of $135 \mu\text{m}/\text{kg}$. As the mean oxygen content of deep water is now only about $150 \mu\text{m}/\text{kg}$, such a reduction would by no means be minor.

Is there any way to read paleooxygen contents from the record in deep sea sediments? In chapter 6 we discussed one possible method. It appears that the shells of the same benthic foraminifera that record ice volume through their $^{18}\text{O}/^{16}\text{O}$ ratios

*As the mean replacement time of oxygen in the atmosphere is currently on the order of 10 million years, no significant change on the time scale of a few thousand years could have occurred. The 12×10^{16} moles of O_2 made available when the 9×10^{16} moles of carbon were stored as organic residues during early post glacial time is trivial compared to the $15,000 \times 10^{16}$ moles of O_2 already in the atmosphere. Finally, experimental evidence exists for this constancy. The O_2/N_2 ratio in the air bubbles from ice of glacial age is identical within the measurement error to that in today's atmosphere.

and the mass of stored organic material through their $^{13}\text{C}/^{12}\text{C}$ ratios may also record dissolved oxygen concentration by their species abundance. Studies of the benthic communities in deep Atlantic sediments by Streeter at the Lamont-Doherty Geological Observatory (619) show that those species whose abundance is greater where low-oxygen bottom waters bathe today's sediment, dominated in abundance over a wider area of sea floor during glacial time than during Holocene time. Correspondingly, those species found in abundance in sediments bathed today in high-oxygen waters had more restricted areas of dominance during glacial time. As similar studies have yet to be carried out in Pacific and Indian Ocean sediments even a qualitative inventory of oxygen contents of mean deep water cannot yet be attempted. All that can be said at this point is that the Atlantic results are consistent with the other chemical changes which appear to have taken place between glacial and post-glacial time.

GLACIAL TO INTERGLACIAL CHANGES IN OCEAN MIXING RATE

So far we have devoted all our efforts in this chapter to glacial to interglacial changes relating to the change in atmospheric CO_2 pressure suggested by measurements on ice cores. Other changes may have occurred which are not tied to the transfer of C and P to and from small reservoirs or to changes in the C/P ratio in raining particulate debris. Is there, for example, any evidence that the rate of oceanic mixing was different during glacial than during interglacial time? One way to get at this problem is to look for a change in the rate of accumulation of CaCO_3 above the lysocline. Other things being equal, a higher mixing rate should produce a higher calcite rain rate. As the preservation event discussed above would be felt only below the lysocline, we need not be concerned with its effects.

The results from cores on which appropriate ^{14}C dating and calcite percentages have been measured are summarized in table 9-10. In all three cores CaCO_3 accumulated faster during late glacial time than during post-glacial time. However, because the cores analyzed represent only a few spots in the equatorial and subtropical ocean it would be premature to claim that they are indicative of the entire ocean.

Although the calcite compensation spike would not confuse attempts to estimate the mean ocean mixing rate from super lysocline CaCO_3 accumulation rates, one other aspect of the scenario presented above might confuse the situation. If there were 30% more phosphorus present in the ocean during glacial time then the same rate of mixing would produce 30% more plant growth and presumably 30% more CaCO_3 . Hence, if the phosphate content explanation for the pCO_2 change is adopted then a somewhat higher glacial rain rate of CaCO_3 would be expected. Perhaps this is the explanation for the results on two of the cores in table 9-10.

GLACIAL TO INTERGLACIAL LYSOCLINE CHANGES

The lysocline of the ocean may have undergone glacial to interglacial changes independent of the preservation event we have

Table 9-10. Calcite accumulation rates for late glacial and for Holocene time as determined by radiocarbon dating of cores taken above the lysocline.

Core No.	Lat.	Long.	Depth km	Glacial	Holocene	Ratio	Ref.
				$\frac{\text{g}}{\text{cm}^2 \text{ 10}^3 \text{ yr}}$	$\frac{\text{g}}{\text{cm}^2 \text{ 10}^3 \text{ yr}}$		
V19-188	7°N	61°E	3.4	2.4	1.7	1.4	(197)
A180-74	10°S	24°W	3.3	3.7	1.6	2.3	(195)
ERDC92	2°S	157°E	1.6	2.3	1.8	1.3	(199)

discussed. For example, if the rate of ocean mixing was higher during glacial time and if this change induced a higher CaCO_3 rain rate then it should have produced a change in the steady state depth of the lysocline. As stated in chapter 6, the level of the global lysocline must vary with the rate of oceanic mixing and with the rate of carbon input from rivers. The adjustment time would be several thousands of years. Thus during the same period that the CaCO_3 preservation spike was in progress, the oceanic lysocline may also have been simultaneously adjusting to the new interglacial CaCO_3 budget.

If our understanding of the history of the lysocline is to improve we must develop a more quantitative scheme for assessing the extent the calcite in any given sediment has been dissolved. If this could be done both accumulation rates and rain rates could be obtained. Although the methods described in chapter 6 provide indices of calcite dissolution, these indices remain uncalibrated. Let us consider a method by which this might be accomplished.

The approach has to do with the radiocarbon age of the calcite in the core-top bioturbated layer. We have already mentioned that this age should be approximately equal to the thickness of the mixed layer divided by the sedimentation rate. We did not mention that this approximation holds only in the absence of calcite solution. Let us now do the job rigorously including the possibility that solution occurs. Figure 9-15 shows the fluxes involved. Radiocarbon is added to the bioturbated zone with the raining calcite. It is lost from the bioturbated zone by radio-decay, by burial, and by calcite solution. For steady state the equation relating these fluxes is as follows:

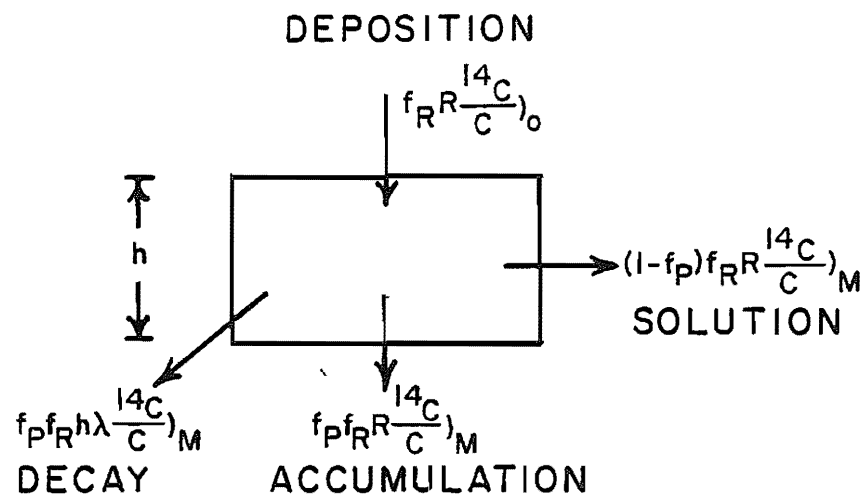
$$\begin{aligned} f_{RR} \frac{^{14}\text{C}}{\text{C}} \Big)_o &= [f_p f_R h \lambda + (1-f_p) f_{RR} + f_P f_{RR}] \frac{^{14}\text{C}}{\text{C}} \Big)_M \\ &= (f_{RR} + f_P f_R h \lambda) \frac{^{14}\text{C}}{\text{C}} \Big)_M \end{aligned} \quad 9-6$$

The symbols in this equation are defined in figure 9-15. This equation can be solved for the ratio of the ^{14}C contents of mixed layer and surface ocean carbon:

$$\frac{^{14}\text{C/C}}{^{14}\text{C/C}}_M = \frac{1}{1 + f_p h \lambda / R} \quad 9-7$$

This ratio is related to the ^{14}C age for mixed layer carbon by the following equation:

$$\frac{^{14}\text{C/C}}{^{14}\text{C/C}}_M = e^{-\lambda t} \quad 9-8$$



R = TOTAL DEPOSITION RATE

A = TOTAL ACCUMULATION RATE

f_R = FRACTION CALCITE IN RAINING MATERIAL

f_P = FRACTION CALCITE PRESERVED

f_S = FRACTION CALCITE IN SEDIMENT

h = DEPTH OF BIOTURBATION

λ = DECAY CONSTANT OF ^{14}C

$\frac{^{14}C}{C}_0$ = RATIO IN SURFACE OCEAN ΣCO_2

$\frac{^{14}C}{C}_M$ = RATIO IN MIXED LAYER CALCITE

Figure 9-15. Flux balance for radiocarbon in the bioturbated layer of a marine sediment undergoing partial calcite dissolution.

Eliminating the activity ratio by simultaneous solution of these two equations and solving for t we get:

$$t = \frac{1}{\lambda} \ln \left[1 + \frac{f_P h \lambda}{R} \right] \quad 9-9$$

Substituting the mean life of radiocarbon τ_M , for $1/\lambda$, we get:

$$t = \tau_M \ln \left[1 + \frac{f_P h}{\tau_M R} \right] \quad 9-10$$

At this point it should be noted that if f_P is unity then:

$$t = \tau_M \ln \left[1 + \frac{h}{\tau_M A} \right] \quad 9-11$$

For $h/A \ll \tau_M$ this equation can be approximated as follows:

$$t = \frac{h}{A} \quad 9-12$$

This is the approximation we used earlier for the age of CaCO_3 in the bioturbated layer in cores not subject to CaCO_3 solution.

In situations where calcite solution occurs, R , the rain rate of sediment, need not equal A , the accumulation rate of sediment. Further the rain rate is not known (the accumulation rate can be measured by ^{14}C dating beneath the bioturbated layer). Hence we must establish the relationship between R and A in terms of the fractions of f_P and f_S . This relationship is as follows:

$$A = (1 - f_R)R + f_P f_R R \quad 9-13$$

where $(1 - f_R) R$ is the accumulation rate of noncalcite and $f_P f_R R$ is the accumulation rate of calcite. Unfortunately f_R is also an unknown. It can, however, be related to f_S and f_P by the following equation:

$$f_S = \frac{f_P f_R}{f_P f_R + (1 - f_R)} \quad 9-14$$

where the numerator is the fraction calcite in the sediment and the denominator is the sum of the fraction calcite and the fraction noncalcite in the sediment. Solving for f_R we obtain:

$$f_R = \frac{f_S}{f_P + f_S - f_P f_S} \quad 9-15$$

Now by combining equations 9-10, 9-13 and 9-15 an equation relat-

Table 9-11: Estimates of the extent of solution of calcite based on the radiocarbon method for two cores from above the lysocline.

Core #1 ERDC 92 (2°S, 157°E, 1.6 km) EQUATORIAL PACIFIC OCEAN (199)

$$A = 1.2 \text{ cm}/10^3 \text{ yrs} \quad \tau_M = 8.27 \times 10^3 \text{ yrs} \quad h = 8 \text{ cm} \quad f_S = 0.86$$

$$t = 8.27 \times 10^3 \ln \left[1 + \frac{8f_P}{1.2 \times 8.27} \left(1 - \frac{0.86(1 - f_P)}{f_P + 0.86(1 - f_P)} \right) \right]$$

$f_P = 1.0$	$t = 4890 \text{ yr}$	$t_{\text{obs}} = 4300 \pm 300$
$f_P = 0.9$	$t = 4200 \text{ yr}$	i.e., $f_P = 0.92 \pm 0.05$
$f_P = 0.8$	$t = 3520 \text{ yr}$	

Core #2 V19-188 (7°N, 61°E, 3.4 km) EQUATORIAL INDIAN OCEAN (197)

$$A = 2.0 \text{ cm}/10^3 \text{ yrs} \quad \tau_M = 8.27 \times 10^3 \text{ yrs} \quad h = 9 \text{ cm} \quad f_S = 0.84$$

$$t = 8.27 \times 10^3 \ln \left[1 + \frac{9f_P}{2.0 \times 8.27} \left(1 - \frac{0.84(1 - f_P)}{f_P + 0.84(1 - f_P)} \right) \right]$$

$f_P = 1.0$	$t = 3593$	$t_{\text{obs}} = 3200 \pm 200$
$f_P = 0.9$	$t = 3060$	i.e., $f_P = 0.93 \pm 0.04$
$f_P = 0.8$	$t = 2540$	

ing to t and f_p can be written in terms of measurable parameters (h , f_S and A). The result is:

$$t = \tau_M \ln \left[1 + \frac{f_p h}{\tau_M A} \left(1 - \frac{f_S (1 - f_p)}{f_p + f_S (1 - f_p)} \right) \right] \quad 9-16$$

While this equation is not conveniently solved for f_p a graphical solution can be made (i.e., calculate t for various values of f_p and then plot one variable against the other).

To date the information needed to apply this method exists for only two cores. Both are from above the lysocline. As can be seen in table 9-11, both yield preservation factors for calcite (i.e., values of f_p) close to unity. The ^{14}C results support the assumption made throughout the book that minimal solution occurs above the lysocline. The next step is to examine cores from beneath the lysocline. The idea would be to use the f_p values obtained from ^{14}C data to calibrate dissolution indices (ratio of foraminifera fragments to whole tests, the ratio of whole planktonic to whole benthic tests,...). Once calibrated these indices could be used to quantify the change in the extent of calcite solution between glacial and interglacial time.

There is, however, a potential pitfall with this method. It lies in the implicit assumption that all the grains of calcite lose the same fraction of their calcite each year. We know that this cannot be the case. The fact that the shells of certain species of foraminifera lose their identity through solution-induced breakup into fragments faster than others suggests that the solution process is not homogeneous. The way to check the impact of this assumption would be to perform radiocarbon dating on various size fractions (i.e., fragments versus whole forams) and even on hand-picked specimens of a single species. While the latter is currently impossible because of the sample size required for ^{14}C dating (i.e., 3 to 10 g of CaCO_3), the recent invention of the high energy mass spectrometry technique* will reduce the sample size by a factor of 1000.

CHANGES IN THE DISTRIBUTION OF NUTRIENTS IN THE DEEP SEA

In our discussions of glacial to interglacial changes in ocean chemistry, we have thus far spoken only of the mean composition of deep water. We must also consider the gradient in these properties from the North Atlantic through the Antarctic into the North Pacific. Studies of the sedimentary record in the northern Atlantic suggest that the source of North Atlantic Deep Water (at least as it now exists) was cut off during much of glacial time. If so, the pattern of deep sea ventilation during glacial time must have been quite different from today's. So also would the distribution of nutrients.

How do we know that the present sources of northern component water was cut off during glacial time? One such line of evidence

*This technique measures the ^{14}C atoms themselves rather than the β^- particles they emit during radioactive decay.

comes from paleontologic data. In today's ocean the position of the Gulf Stream is clearly seen in the sediments. Because of the difference in the organisms living within and to the north of the stream, the material raining to the sea floor changes as the boundary is crossed. The same contrast can be seen in glacial sediments but the course marked out is quite different (see figure 9-16). During glacial time the stream left the margin of the Americas at roughly the same place as it does today but rather than moving to the northeast as it does now, during glacial time it went directly to the east (i.e., toward Spain rather than toward Iceland). The Gulf Stream's Pacific Ocean counterpart, the Kuroshio, has at present an eastward rather than a northeastward trend. To the north of the Kuroshio lies a zone of lower surface water salinity. Upwelling occurs in this zone. It is thought that a similar situation may have existed in the Atlantic during glacial time.

Another line of evidence comes from the oxygen isotope record for benthic foraminifera in the Norwegian Sea sediments (see figure 9-17). The deep water in the Norwegian Sea is now about 4°C colder than that in the open Atlantic. This difference is reflected in the $\delta^{18}\text{O}$ values for shells of Holocene benthic foraminifera in the two basins. For benthics deposited during glacial time, the $\delta^{18}\text{O}$ difference changes sign suggesting that the Norwegian Sea waters were slightly warmer than those in the open Atlantic! If so then the deep Norwegian Sea must have been ventilated by waters spilling in from the North Atlantic rather than through the sinking of Norwegian Sea surface waters. This evidence shows dramatically that the North Atlantic deep water source as we know it today was not functioning during glacial time.

If indeed NADW was not flowing during glacial time, it is possible that all three major ocean basins were ventilated by deep water formed in the Antarctic (as the Pacific and Indian Oceans are today). If so, then the gradient in deep water properties from the North Atlantic around to the North Pacific is not likely to have been as pronounced during glacial time as it is today.

There are three ways to assess this contrast from the sedimentary record. First, the $\delta^{13}\text{C}$ difference between the deep waters in the North Atlantic and those in the equatorial Pacific now averages about $1^{\circ}/\text{oo}$ (see figure 6-12). Benthic foram $\delta^{13}\text{C}$ data might then be expected to show a smaller Atlantic to Pacific contrast in $\delta^{13}\text{C}$ during glacial than interglacial time. Second, Atlantic deep waters now have considerably higher oxygen contents than Pacific waters. Oxygen-sensitive benthic species should show less contrast in their distributions between the Pacific and Atlantic during glacial than during interglacial time. Third, the lysocline now stands deeper in the Atlantic than in the Pacific. The levels should have been more nearly equal during glacial time.

What does the record show? No paleooxygen estimates are as yet available for the Pacific Ocean. As can be seen from table 9-1, the glacial to interglacial change in $\delta^{13}\text{C}$ for benthic forams living in the Atlantic averages slightly more than the change for benthic forams from the Pacific. While this is consistent with a glacial reduction in the interocean difference during glacial time, more cores will have to be run before the difference can be

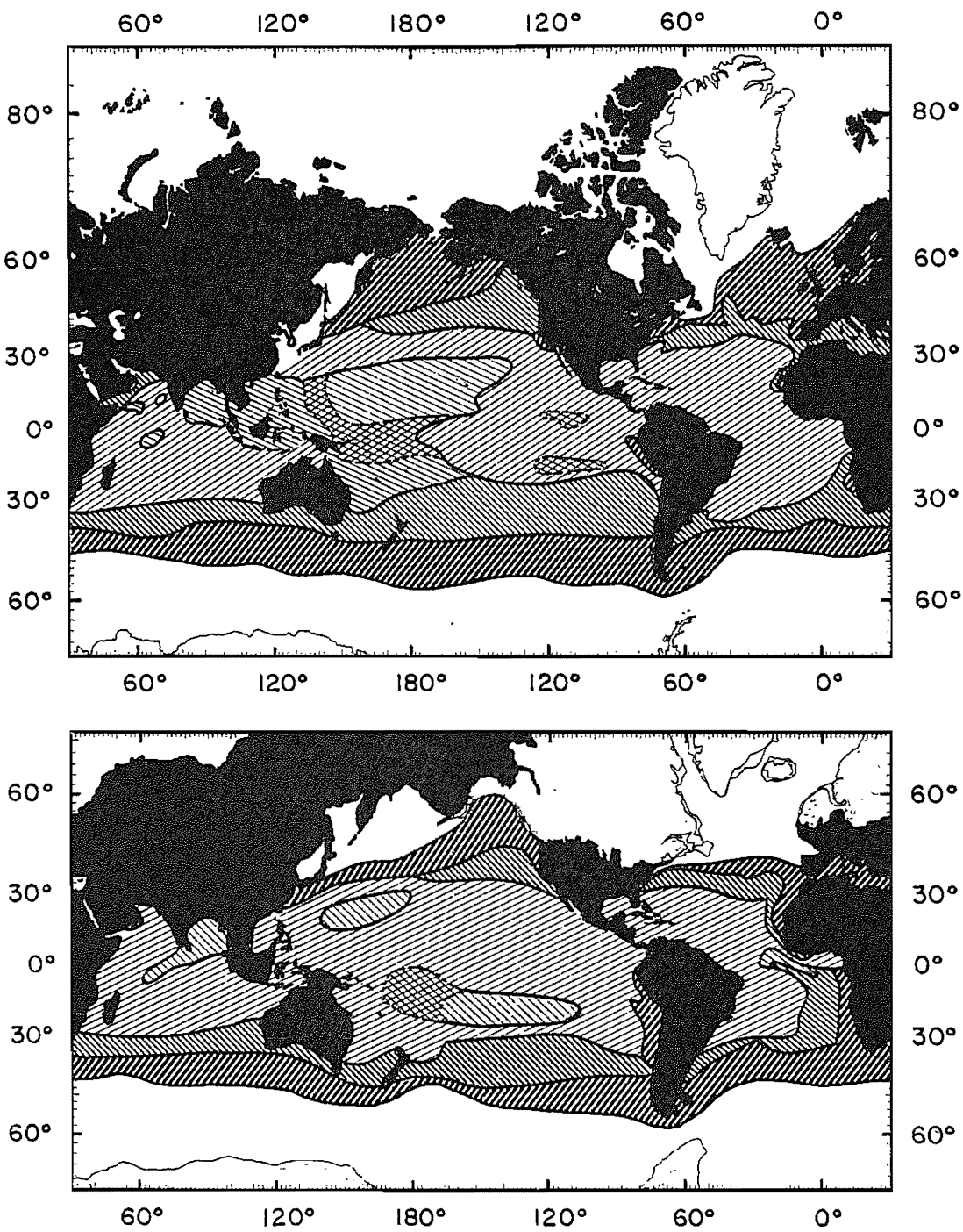


Figure 9-16. Maps showing the boundaries of various faunal assemblages found in sediment of Holocene age (above) and for the peak of the last glacial time (below). A striking difference between these maps is seen in the North Atlantic. The assemblage boundary which follows the present course of the Gulf Stream went straight across to Spain during glacial time. The white areas designate ice (glaciers on the continents and winter sea ice in the oceans). These maps were prepared by members of the CLIMAP group (609).

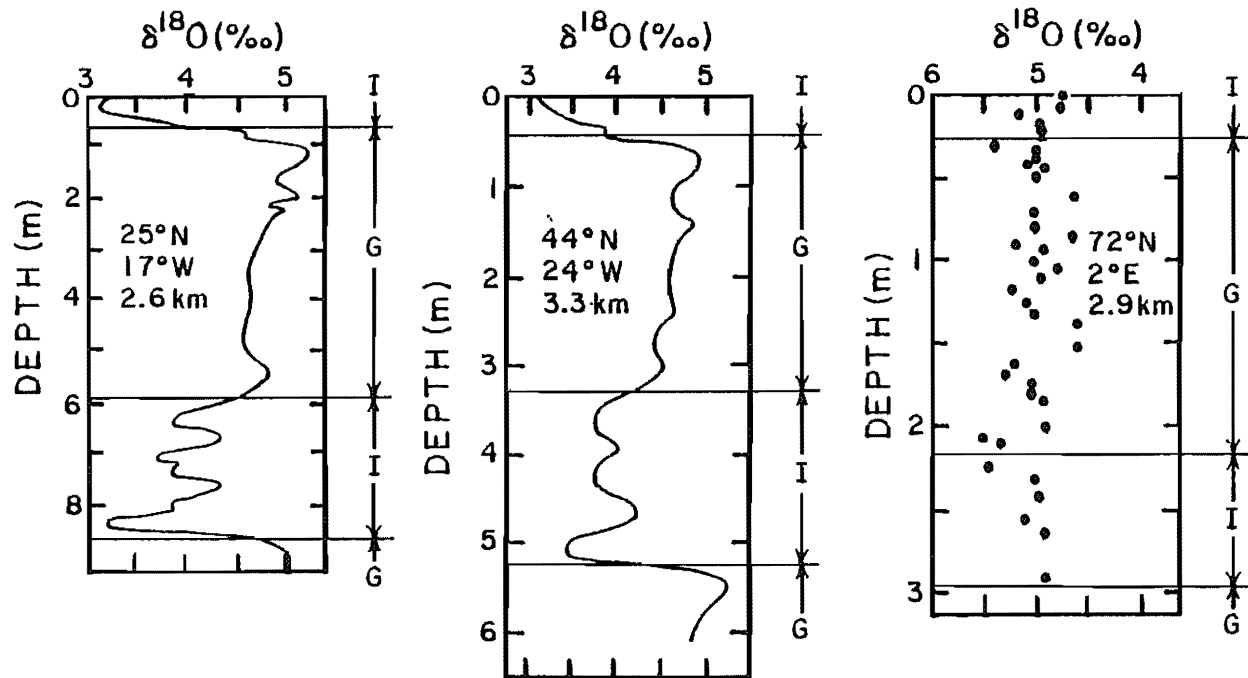


Figure 9-17. Comparison of $^{18}\text{O}/^{16}\text{O}$ records for benthic foraminifera in cores taken at 25°N, 44°N and 72°N in the Atlantic Ocean. As can be seen the northernmost of these cores fails to show any significant change in $\delta^{18}\text{O}$ value between glacial and interglacial time. The ~2‰ decrease in $\delta^{18}\text{O}$ which occurred throughout the world ocean as the result of the melting of continental ice sheets appears to have been countered in the Norwegian Sea by a major cooling (~8°C) of its deep waters at the close of glacial time. This observation by Duplessy and his coworkers in France (618) led them to conclude that the Norwegian Sea was ventilated from the Atlantic during glacial time much as the Bering Sea is currently ventilated today by waters from the deep North Pacific (618).

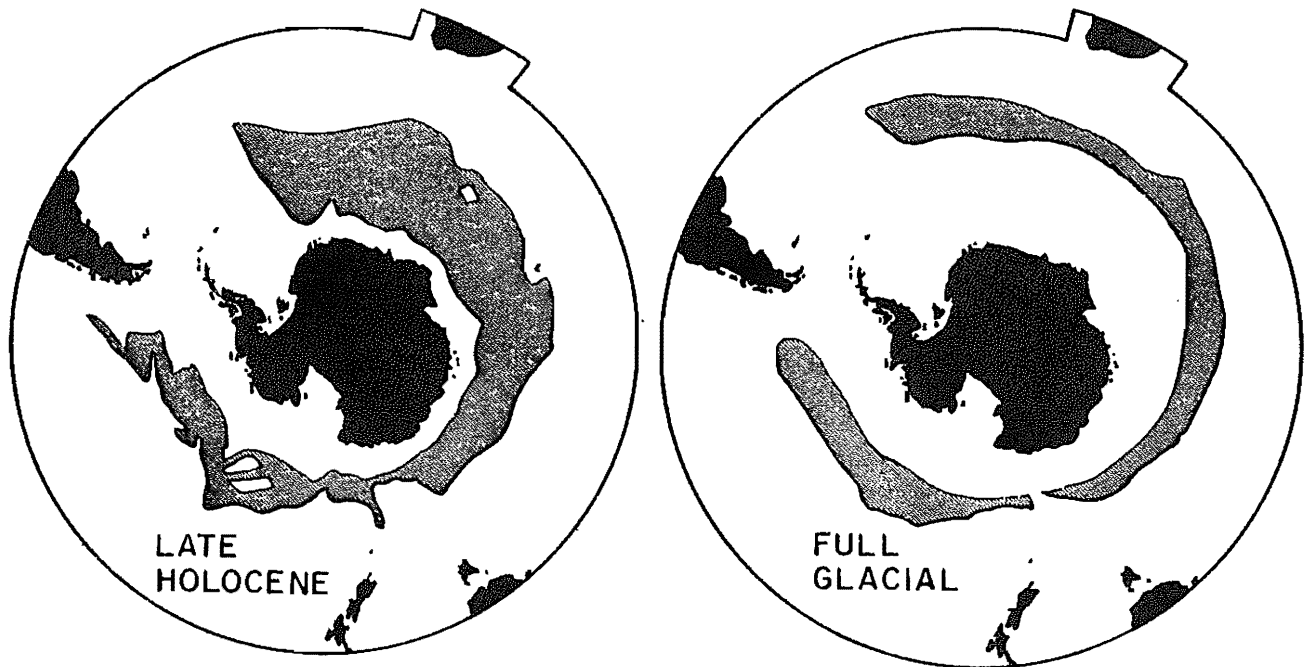


Figure 9-18. Maps showing the location of opal-rich sediment in the Antarctic Ocean during late Holocene time (left) and during full glacial time (right). These maps were prepared by Jim Hays and his coworkers at the Lamont-Doherty Geological Observatory (523).

demonstrated to be significant. Finally, we have already pointed out that the lysocline appears to have been deeper in the Pacific and Indian Oceans during glacial time and shallower in the Atlantic during glacial time. However, the magnitude of this reduction in contrast between the levels in the two oceans has yet to be established.

Another approach to the problem as to how the pattern of deep circulation changed from glacial to interglacial time is to compare the patterns of opal accumulation during these two climatic regimes. Hays and his coworkers at the Lamont-Doherty Geological Observatory have done this for the Antarctic Ocean. As can be seen in figure 9-18 the belt of opal rich sediment was located further off the Antarctic continent during glacial time than during Holocene time. A likely explanation is that the floating ice which now surrounds Antarctica was more extensive during glacial time pushing the upwelling zone further to sea.

SUMMARY

The first chink in the ocean's armor of secrecy regarding its chemical history has been found. Measurements of the CO_2 content of air trapped in ice and of the $^{13}\text{C}/^{12}\text{C}$ ratio in the CaCO_3 of foraminifera shells seem to be telling us that the partial pressure of carbon dioxide in the atmosphere was lower during glacial time and that this change is related to changes in the ocean's nutrient constituent cycles. Specifically the ratio of PO_4 to ΣCO_2 either in mean ocean water or in the particulate matter raining from the surface to the deep sea must have been higher during glacial time than today.

We also have evidence that the circulation pattern of waters in the deep sea was not the same during glacial time as it is today. The flow of deep water originating in the North Atlantic, which is responsible for large differences in the deep water nutrient element concentrations between the oceans, appears to have been cut off during glacial time. Although confirmation that the flow pattern was different based on paleo ^{13}C and paleooxygen reconstruction has yet to be obtained, the potential is certainly there.

The task of carrying these studies much further back in time will prove very difficult. The greater the time span, the more constituents which might vary. The greater the time span, the more difficult the sedimentary record is to read. But the challenge is there and marine scientists will surely make concerted attempts to find more chinks in the ocean's armor of secrecy.

PROBLEMS

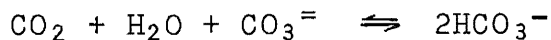
- 9-1 Assuming that the hypothesis given in the text is valid, construct a $\delta^{13}\text{C}$ versus PO_4 concentration plot for the water masses of the glacial ocean. Assume that the pattern of circulation was the same as today's.
- 9-2 If the $\text{CO}_3^=$ ion content in the deep sea during glacial time was 5 $\mu\text{m}/\text{kg}$ higher than it is now in all the water masses of

the ocean, how much deeper would the lysocline in the western equatorial Atlantic and in the eastern equatorial Pacific have been?

- 9-3 If the phosphorus-induced O_2 reduction in deep ocean oxygen content was everywhere about $125 \mu\text{m}/\text{kg}$ during glacial time what areas of the sea floor below 3 km would have been bathed in anaerobic water at that time? How would this affect the distribution of benthic forams?
- 9-4 Fossil benthonic and planktonic forams are recovered from a horizon dating 20 million years in a deep sea boring. The $\delta^{13}\text{C}$ value for the benthics is 0.0 per mil and, for the planktonics is 4.0 per mil. If the photosynthetic fractionation factor and the C/P ratio in marine organisms were the same 20 million years ago as they are now, by how much did the C/P ratio in the ancient deep sea differ from the C/P ratio in today's sea?
- 9-5 Consider a hypothetical earth with no glaciers. This earth has 30% continents and 70% oceans. It is at hydrostatic equilibrium. As glaciation occurs, 4% of the surface area is buried by ice sheets three kilometers thick. Were hydrostatic balance to be reestablished by how much would the rock surface beneath the ice be depressed? By how much would the sea level fall? Geologists living in the next ice-free period attempt to assess the extent of ice formation by studying submerged shorelines. By how much would the elevations of shorelines for continental margins differ from those flanking islands rising from the ocean floor? Assume the mean density of ice to be 0.9 and of rock 3.3 g/cm^3 .
- 9-6 A biologist builds a two reservoir aquarium. One reservoir has a volume equal to 10% of the total and is exposed to the light. The other has a volume equal to 90% of the total and is kept in darkness. The lit reservoir is also exposed to the atmosphere. Water is circulated back and forth between the reservoirs. The dark reservoir has the following chemical composition:

$$\begin{aligned} [\Sigma\text{CO}_2] &= 2030 \times 10^{-6} \text{ moles/kg} \\ [\text{HCO}_3^-] &= 1900 \times 10^{-6} \text{ moles/kg} \\ [\text{CO}_3^{2-}] &= 100 \times 10^{-6} \text{ moles/kg} \\ [\text{CO}_2] &= 30 \times 10^{-6} \text{ moles/kg} \\ [\text{Alk}] &= 2100 \times 10^{-6} \text{ moles/kg} \\ [\text{NO}_3^-] &= 30 \times 10^{-6} \text{ moles/kg} \\ [\text{PO}_4^{3-}] &= 2 \times 10^{-6} \text{ moles/kg} \end{aligned}$$

The $\delta^{13}\text{C}$ value for the ΣCO_2 in this reservoir is 0.00/oo. The surface reservoir has no measurable PO_4 and NO_3^- , the same alkalinity and a 10% lower ΣCO_2 content. Its $\delta^{13}\text{C}$ is 2.00/oo. What is the equilibrium constant for the reaction



in the dark tank? What must be the photosynthetic fractionation factor?

Calculate the concentrations of CO_2 , HCO_3^- and $\text{CO}_3^=$ in the surface reservoir (it has the same temperature and P as the dark one). Remember:

$$\begin{aligned} [\Sigma\text{CO}_2] &= [\text{CO}_3^=] + [\text{HCO}_3^-] + [\text{CO}_2] \\ [\text{Alk}] &= 2[\text{CO}_3^=] + [\text{HCO}_3^-] \end{aligned}$$

The oxygen content of the lit reservoir is 350 $\mu\text{m}/\text{kg}$. What is the oxygen content of the dark reservoir?

Now the biologist adds enough PO_4 and NO_3^- to raise the concentration of these species in the dark reservoir to 4 $\mu\text{m}/\text{kg}$ and 60 $\mu\text{m}/\text{kg}$ respectively. He observes more plant growth and that the PO_4 and NO_3^- content of surface water remains very low. What will be the new steady state CO_2 , HCO_3^- and $\text{CO}_3^=$ concentration in the lit reservoir? What will be the $\delta^{13}\text{C}$ for the ΣCO_2 in this reservoir?

SUPERPROBLEM #9

Turk Reekian, a geochemist, becomes interested in the chemical changes associated with the great extinction of marine organisms which marked the abrupt close of Cretaceous time. He adopts the computer aquarium of Stover and Eastland (see superproblem #7). He first calculates the steady state $^{13}\text{C}/^{12}\text{C}$ distribution in the ΣCO_2 of the four reservoirs. In so doing he assumes that the fractionation during photosynthesis is 20‰. He assumes that the mean ΣCO_2 content of the combined reservoir water is 2.1 moles/ m^3 and that of PO_4 is 2.1×10^{-3} moles/ m^3 . He takes the mean $\delta^{13}\text{C}$ of the computer ocean's carbon to be 0.0‰. He assumes complete recycling of carbon and of phosphorus (i.e., he allows no throughput of either element).

Reekian then abruptly cuts off the computer "life" (i.e., the phosphorus reaching the surface reservoirs is no longer converted to particulate debris). He then calculates the time trends for PO_4 , $\delta^{13}\text{C}$ and PCO_2 in the surface reservoirs. What does he find? What would be the ratio of the atmospheric CO_2 partial pressure for the new steady state to that prior to the extinction of life?

Once steady state is achieved Reekian turns on the river input. Each year they carry amounts of carbon and of phosphorus equal to one part in 10^5 of that in the computer ocean and an amount of calcium equal to one part in 10^6 of that in the computer ocean. He also arranges things so that the concentrations of Mg, K, Na, SO_4 and Cl remain unchanged. The initial ratio of Ca to C in the ocean is 5. Develop a scenario for the chemical changes which would occur over the next million years assuming that the ocean remained abiotic. In particular how would the surface water CO_2 partial pressure change? Assume that when the ocean reaches a state of 10-fold supersaturation with regard to calcite that inorganic precipitation of CaCO_3 would match the input from rivers. Reekian realizes that within a few thousands of years after the Cretaceous catastrophe, life once again flourished in the ocean

but is interested in speculating about the chemical conditions in a lifeless ocean. There are of course some intangibles in such a calculation. State what they are and how Reekian might have handled them.

LAST MINUTE ADDITIONS (SEPTEMBER 1982)

Froelich and his coworkers at Florida State have recently suggested that the Ge/Si ratio in opal may prove to be a valuable means of accessing changes in the oceanic silicate cycle during glacial time. This prediction is based on their finding that the Ge/Si ratio in the hot waters emanating from ridge crests is considerably higher than that for mean river water. If so, glacial to interglacial changes in the amount of silicate entering the sea from rivers or in the residence time of silicate in the sea would produce changes in the germanium content of sedimentary opal.

Boyle and Hester at M.I.T. have recently shown that the Cd to Ca ratio in benthic foraminifera is proportional to that in sea water (712). As we have seen in chapter 4, the Cd to PO₄ ratio in today's ocean is everywhere the same. Hence measurements of the Cd content of benthic foraminifera from various parts of the ocean for a single time horizon should provide a picture of the PO₄ distribution (and hence the circulation pattern) in the sea at that time. Boyle, working with Keigwin at Woods Hole, has shown that during glacial time the North Atlantic Ocean had about twice its present Cd/Ca ratio, strongly suggesting that production of deep water in the northern Atlantic was greatly reduced at that time (711).

Chapter 10

CAN MAN OVERRIDE THE CONTROLS ?

THE BUILDUP OF FOSSIL FUEL CO₂ IN THE ATMOSPHERE AND OCEANS

INTRODUCTION

In the last chapter we saw that the great climatic fluctuations of the last million years had an impact on ocean chemistry. The cycles of C, P, N, and O₂ all appear to have changed in tune with the advances and retreats of the ice. Man has the potential to make changes in climate and ocean chemistry larger than those which took place between glacial and interglacial time. This capability is a byproduct of our need for fuel. We are now, and will be for many decades to come, dependent on the energy derived from burning of coal, oil, and natural gas. A major byproduct of this combustion is CO₂ gas. The elevated CO₂ partial pressure in the atmosphere generated in this way will warm the earth's surface. A decrease in the amount of carbon stored in forests and in soils, as the result of man's need for agricultural land and wood, has also added CO₂ to the atmosphere. This CO₂ will gradually be taken up by the ocean, and will alter its chemical cycles. Our goal in this chapter is to use the information we have compiled in the earlier chapters of this book to develop a means for predicting the partitioning of this excess CO₂ between air and sea. Because we do not know exactly how much coal, oil, and natural gas will be burned nor at what pace we will conduct this combustion, and because we do not know what new pressures will be placed on our forests and soils, the model we develop will have to be adaptable to a wide range of CO₂ production scenarios.

CO₂ PRODUCTION IN THE PAST

The first step in our analysis is to look into how much CO₂ we have produced to date. The amounts produced by fossil fuel burning in the past can be reasonably well reconstructed from records of the amounts of coal and lignite mined and of the amounts of oil and natural gas taken from the world's "wells". From a knowledge of the mean carbon content of these fuels we can convert the tons of coal and lignite, the barrels of oil, and the cubic feet of natural gas to moles of CO₂ gas. A summary of the amounts of CO₂ produced each year from fossil fuels is shown in figure 10-1. The cumulative amount of CO₂ produced up to any given time is also shown in this figure. As of 1980 this total was about 14×10^{15} moles. For comparison the atmosphere in 1980 contained 55×10^{15} moles of CO₂.

In addition to the CO₂ produced by the burning of fossil fuels, man has added CO₂ to the atmosphere through his forestry

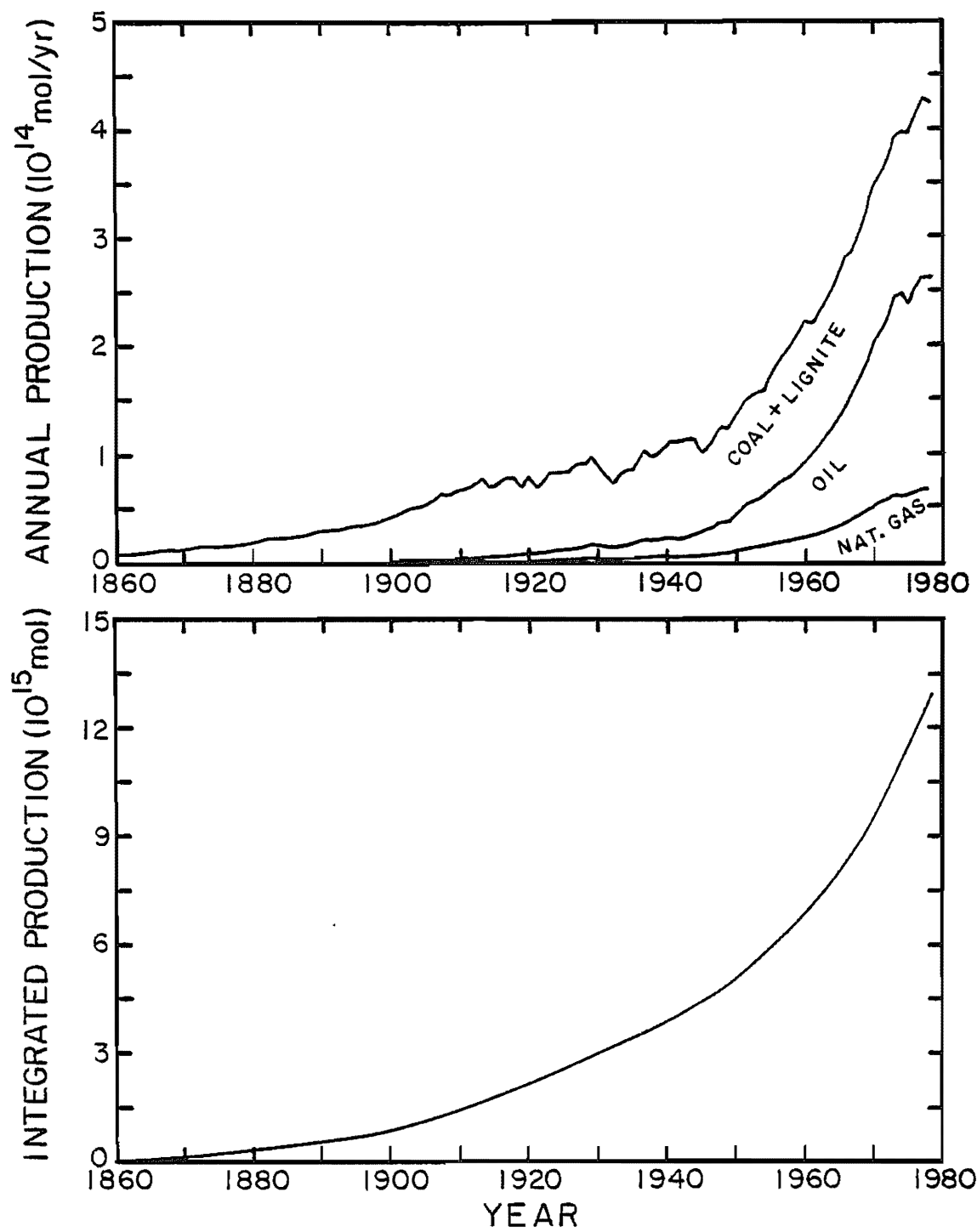


Figure 10-1. Plots of the annual production of fossil fuel CO_2 (upper) and the integrated production of fossil fuel CO_2 (lower) from 1860 to 1980. The relative contributions of coal and lignite, of oil and of natural gas are indicated in the upper panel (559, 562).

and agricultural practices. About 10% of our planet's land has been harnessed for agriculture. Some of this land was originally forested. Tilling increases the oxidation rate of the organic matter contained in soils and thereby decreases the global inventory of these compounds. We have also cut forests which are still in the early stages of regrowth. The mass of carbon present in today's living material is about equal to the amount of CO₂ in today's atmosphere. The mass of carbon in soils is 2 to 4 times that in today's atmosphere. While a decrease in the mass of living material and in the mass of carbon stored as organic compounds in soils has contributed to the rise in atmospheric CO₂ content, our records of these activities are not nearly good enough to permit the exact accounting possible for fossil fuels. Rough estimates suggest that over the last 200 years soils and forests have contributed an amount of CO₂ to the atmosphere comparable to that from fossil fuels. A scenario for these releases is shown in figure 10-2. As it is obtained by an indirect method to be discussed later in the chapter, we shall not say any more about it at this point.

Before moving on to the future, it is worth mentioning a few of the imponderables involved in any attempt to evaluate these trends in terrestrial biomass.

One of these imponderables has to do with the regrowth of previously cut forest. An idealized response function shown in figure 10-3 demonstrates the problem. First of all, when a forest is cut the biomass does not disappear immediately. The wood may be used in buildings or for making paper. The roots (which constitute up to 50% of the forest biomass) are left in the ground to decay. The small branches and bark are often left to be eaten by bacteria. Where material is burned on the site, ten or so percent of the carbon is converted to charcoal and becomes a semi-permanent constituent of the soil. Thus the biomass associated with a cut forest does not immediately disappear. Rather, like a mixture of radioactive isotopes with widely varying half-lives, its disappearance has a long history.

Soon after a forest is cut new growth begins. If uninterrupted, this growth will on the time scale of a few tens to a few hundreds of years produce a new steady state biomass. More likely the forest will be cut again when the timber company or Swidden* farmer judges it "ready". Thus many of the forests of the world are somewhere in the midst of a regrowth. Of these some are in a decay phase where the decomposition of the cut material outweighs new growth. Some are in the growth phase where the formation of

*In developing countries where commercial fertilizer is too expensive farmers often rotate their lands. The farmer cultivates a plot of land for several years and then when its soil nutrients become depleted he allows it to go "wild" and moves to a new plot. Forest growth in the wild patch renews its nutrients (presumably by drawing on nutrients from deeper in the soil, through nitrogen fixation, and via atmospheric fallout of PO₄, K, S,...). A decade or so later the farmer returns this plot to cultivation, completing the cycle of his acreage. This type of rotating land use is called Swidden farming.

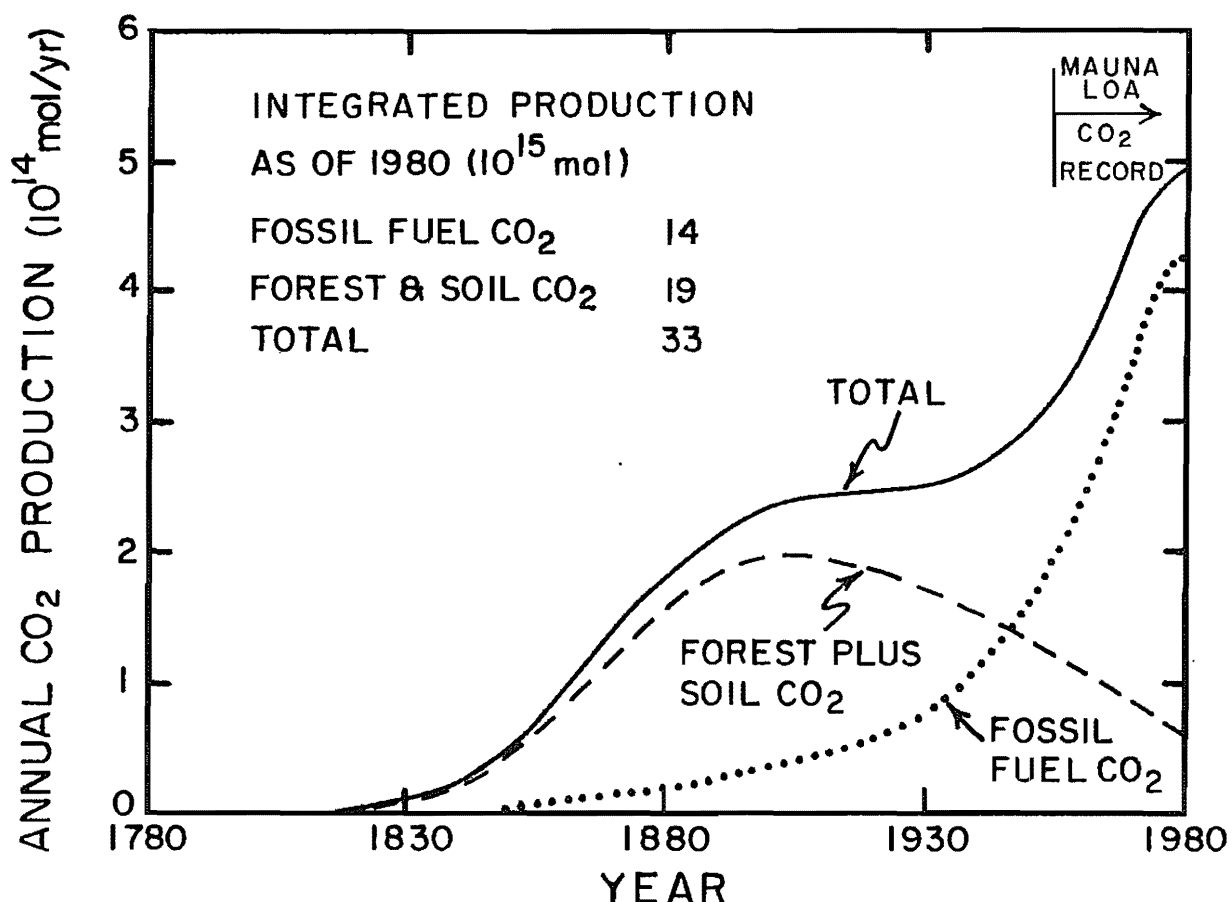


Figure 10-2. A scenario (based on the tree-ring-based atmospheric $^{13}\text{C}/^{12}\text{C}$ record) for the net release of CO_2 from the forests and soils over the last 200 years. Also shown is the documented record of fossil fuel CO_2 release. The total production from these sources is also given.

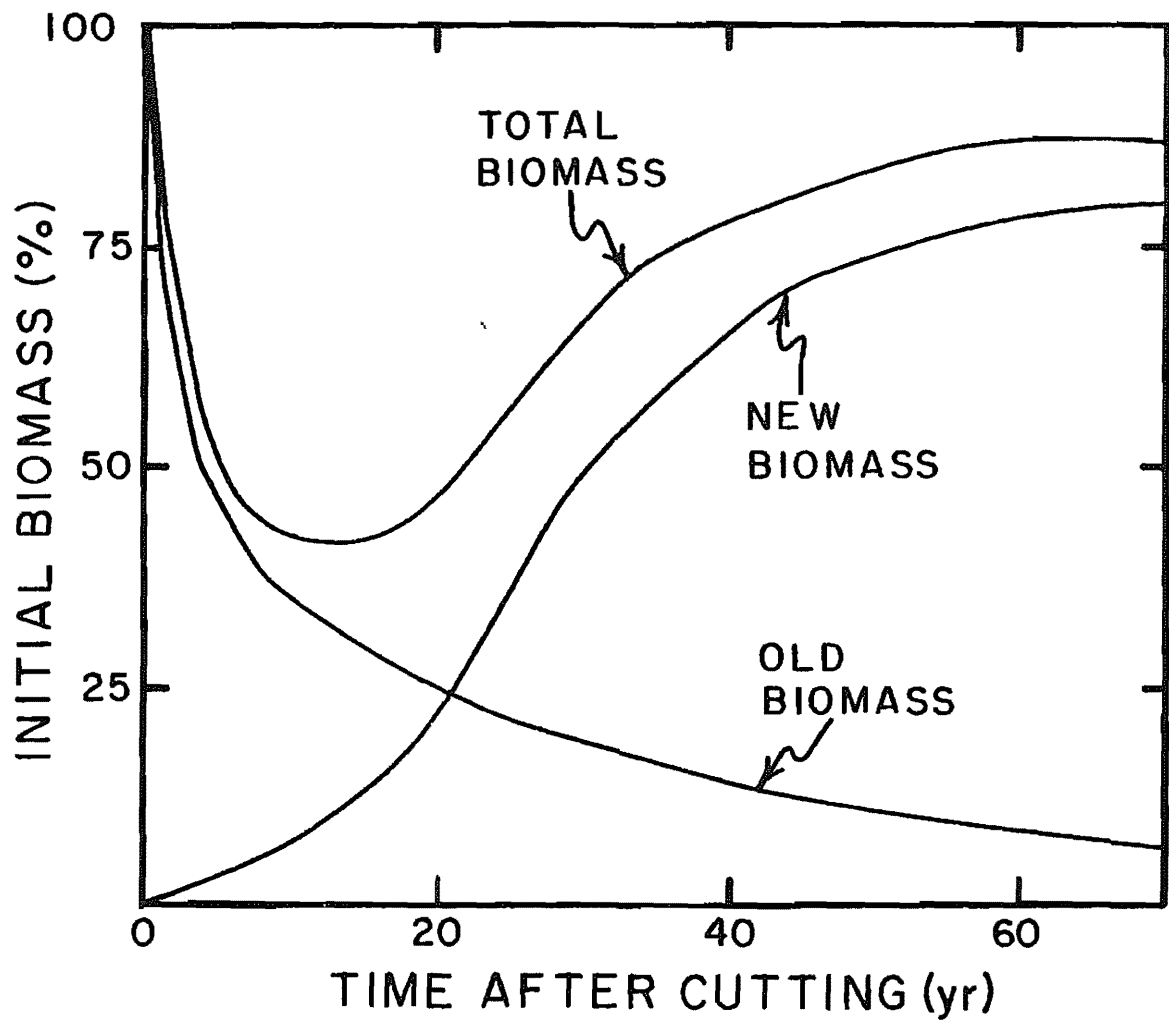


Figure 10-3. Hypothetical curves showing the change in carbon storage experienced by a forest plot after cutting. The curve labeled new biomass represents new forest growth. The curve labeled old biomass represents the composite decay curve for leaves, bark, roots, and wood (or wood products) present on the plot at the time of cutting.

new timber outweighs decomposition. The point of all this is that it is the differential rather than absolute rate of forest cutting that matters. To assess forest biomass changes from estimates of forest cutting alone would be equivalent to judging a man's financial status by looking only at his expenditures!

We have already mentioned a second imponderable. When forests burn some of the carbon goes to the inert form of charcoal. By contrast, when trees experience "natural" deaths, bacteria (and termites) do a more complete job of recycling the carbon. In the industrial countries an attempt has been made to control forest fires. These containment efforts have been rather successful. Forests in these areas are destroyed less frequently by fire than prior to man's "management." In developing countries both grass and forested areas are frequently burned. Presumably this practice has intensified along with population growth. Thus, while it is hard to tell how much charcoal production has enhanced the carbon inventory in soil, this contribution is unlikely to have been negligible (571).

A third imponderable has to do with the anthropogenic fertilization of forests. Automobile engines and fossil-fuel-powered electricity generators fix atmospheric N₂ (i.e., make oxides of nitrogen). These oxides go into the air and are eventually converted to NO₃, which is carried to the earth (and sea) by rainfall and aerosol impact. Some of the NH₄OH used to fertilize agricultural lands is released to the air as NH₃ gas. When this NH₃ encounters H₂SO₄- or HNO₃-bearing aerosols it combines as part of the aerosol and soon returns to the earth's surface. Rains also deliver appreciable PO₄ to the land surface. While the origin of this phosphate is not well understood, part of it is anthropogenic (for example, from coal burning). The CO₂ content of the air is also steadily rising. Thus, three of the limiting ingredients for terrestrial plant growth are being made available through man's activities. A wealth of experimental data shows that given more nutrients plants grow faster. Presumably the trees in our forests are, on the average, growing a bit faster as the result of this inadvertent fertilization. Presumably these higher growth rates would lead to a greater forest biomass than would exist in the absence of these fertilizations. As of 1980 the CO₂ content of the atmosphere was about 20% higher than prior to the turn of the century. It is surely safe to place this percentage as a firm upper limit on the increase in forest photosynthesis rates. The true growth enhancement is likely considerably smaller.

The list of imponderables does not end here. However, the point has been made. When considering the terrestrial biomass we are dealing with a complex and very heterogeneous system. Our information base is simply inadequate to yield the kind of answers we would like. Hence, we will have to find ways to work around the rather large uncertainties in the time history of the net CO₂ release by the terrestrial biosphere and soils.

CO₂ PRODUCTION IN THE FUTURE

So much for the past. What can we expect in the future? First, we need to know the magnitude of our reserves. They are

Table 10-1. Estimate of recoverable fossil fuel reserves. For comparison today's atmosphere contains 5.5×10^{16} moles of CO₂ and today's forests contain about 5.5×10^{16} moles of carbon. The amount of fossil fuel CO₂ produced as of 1980 was 1.4×10^{16} mole (560,561).

Fuel	Mass of Carbon 10^{16} moles
Coal and lignite	~ 30
Petroleum	1.9
Natural gas	1.2
Oil shale	1.4
Tar sands	0.6
TOTAL	~ <u>35</u>

Table 10-2. CO₂ production per unit of energy produced (560).

Fuel	10^{-6} Moles CO ₂ calorie energy	CO ₂ Production Index *
Methane	5.0	(1)
Petroleum	6.6	1.3
Coal	8.3	1.7
Oil shale	~13	2.6
Tar sand	~13	2.6
Synthetic methane	~12	2.5
Synthetic petroleum	~12	2.5

* Relative to methane.

listed in table 10-1. Together they add up to a total of six times more carbon than is now in the air! The greater part of this is coal. Thus the future CO₂ levels in the air depend very much on the extent to which we utilize these coal reserves. However, it must be kept in mind that even if we were to burn only 10% of this coal, and a major portion of the oil and gas, we would still generate an amount of CO₂ equal to that presently in the atmosphere. To provide some idea as to how fast we might run through our fossil fuel reserves, if the present rate of fossil fuel use were maintained, we would generate an amount of CO₂ equal to that in the atmosphere in about 65 years.

One has only to consider the events of the 1970's to realize how hazardous it is to make long-range energy-use forecasts. A typical forecast of late 1960 called for growth rates of from 3% to 4% per year in energy usage. Then came the Arab oil boycott. Soon after came the rapid increases in oil prices. As can be seen in figure 10-4 the growth rate dropped dramatically. Serious questions with regard to the safety of nuclear power plants and concerns with regard to the storage of the radioactive "ashes" from these plants have been raised during the last decade. Reacting to these unforeseen events energy growth predictions have been dramatically modified. The example shown in figure 10-5 is that released by Exxon at the time this book was being written. It calls for a 2% per year growth rate during the next 20 years. Even as you read this book the situation is likely to have changed again. This is why we say that any model of future CO₂ levels must accommodate itself to a wide range of scenarios.

While we have no intention of making our own prediction, a few paragraphs about the ingredients of such scenarios is in order. The amount of energy used must be related to the number of people who inhabit our planet. Currently the population of the globe rises by 2% per year. At this rate the population will double in 35 years. While this growth rate is gradually being stemmed by more effective birth control practices few believe that the population will level off before reaching 8 billion (as of 1980 it was about 4.5 billion). More pessimistic outlooks would predict growth to continue until the population is 12 to 16 billion. As the standard of living of the world's poor people is closely related to their per capita energy consumption, despite energy conservation efforts by the world's "rich", the demand for energy will certainly rise along with population. In this connection it must be remembered that 3 out of 4 people are in the "poor" category and that the growth in population is almost entirely through children born to "poor" families. Eventually it will be the energy habits of the "poor" rather than of the "rich", which will determine global energy use. This rapidly expanding demand by the people of the developing countries is reflected in Exxon's prediction of the distribution of world energy demand (see figure 10-6).

In order to make a prediction of future CO₂ production rates, we also must estimate what fraction of our energy will come from fossil fuels. During the 1970's about 90% came from this source (see figure 10-7). The prospects that this situation will change dramatically in the next several decades are indeed small.

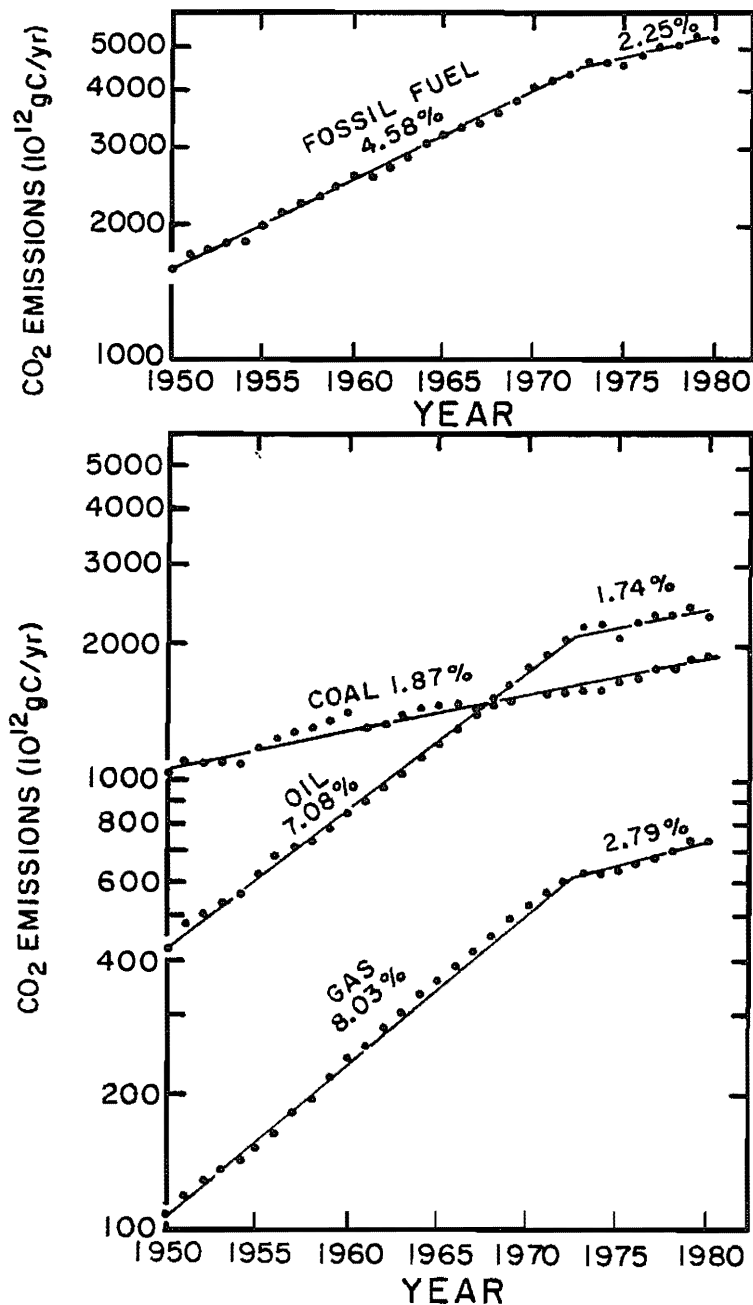


Figure 10-4. Logarithmic plot of CO₂ emissions from fossil fuel use as a function of time from 1950 to 1980 (upper panel). The slopes of the line segments on such a plot are measures of the growth rate of these emissions (shown in % per yr). Note the sharp drop in growth rate which took place in 1973. The lower panels show separate plots for coal, oil, and natural gas. Both oil and natural gas usage underwent a very sharp drop in growth rate in 1973. Coal usage did not show this change. This compilation is the work of Ralph Rotty of Oak Ridge Associated Universities (562).

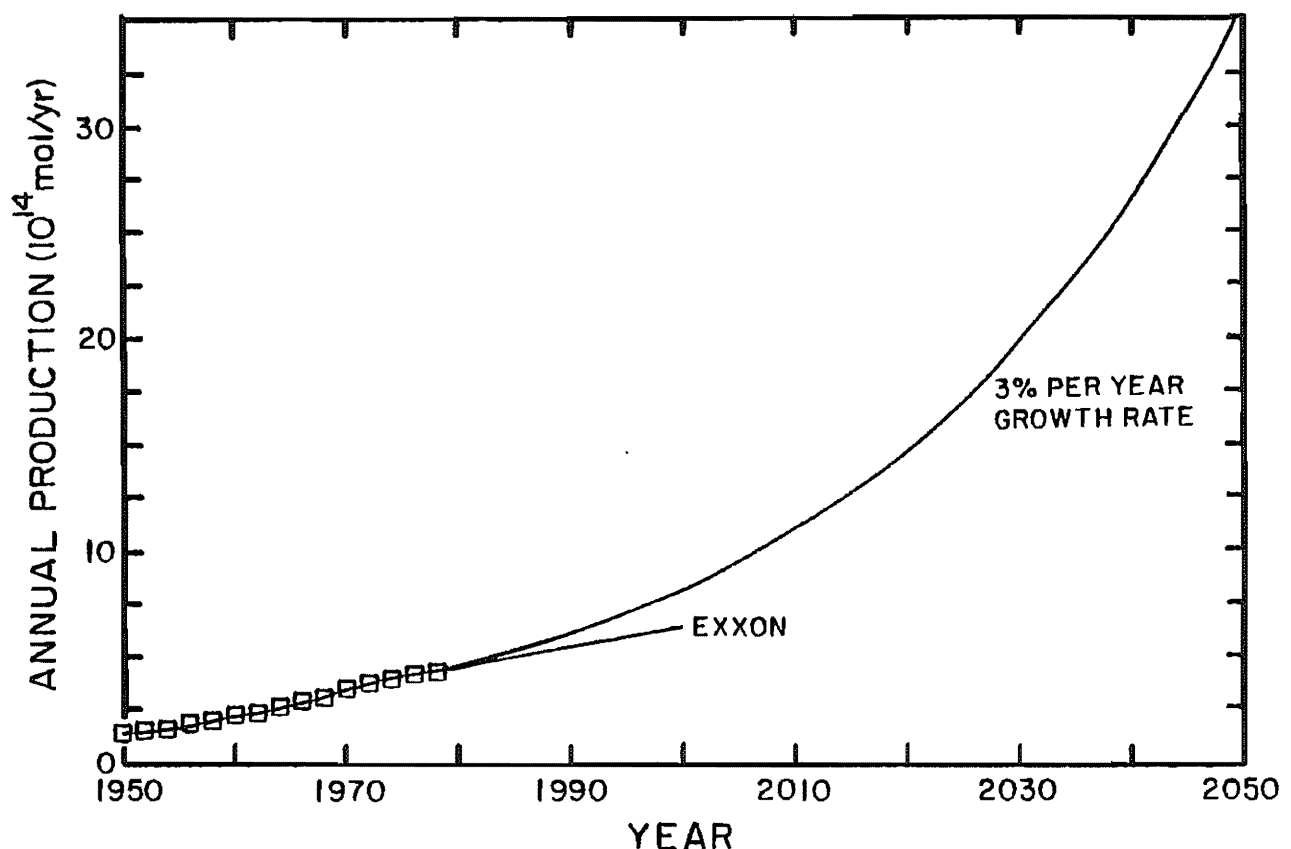


Figure 10-5. Plot showing projections of fossil fuel use. The 3% per year growth curve represents a median estimate made prior to the Arab oil boycott and the OPEC price hikes. The Exxon projection was made in 1980 (691). The squares represent historic production records.

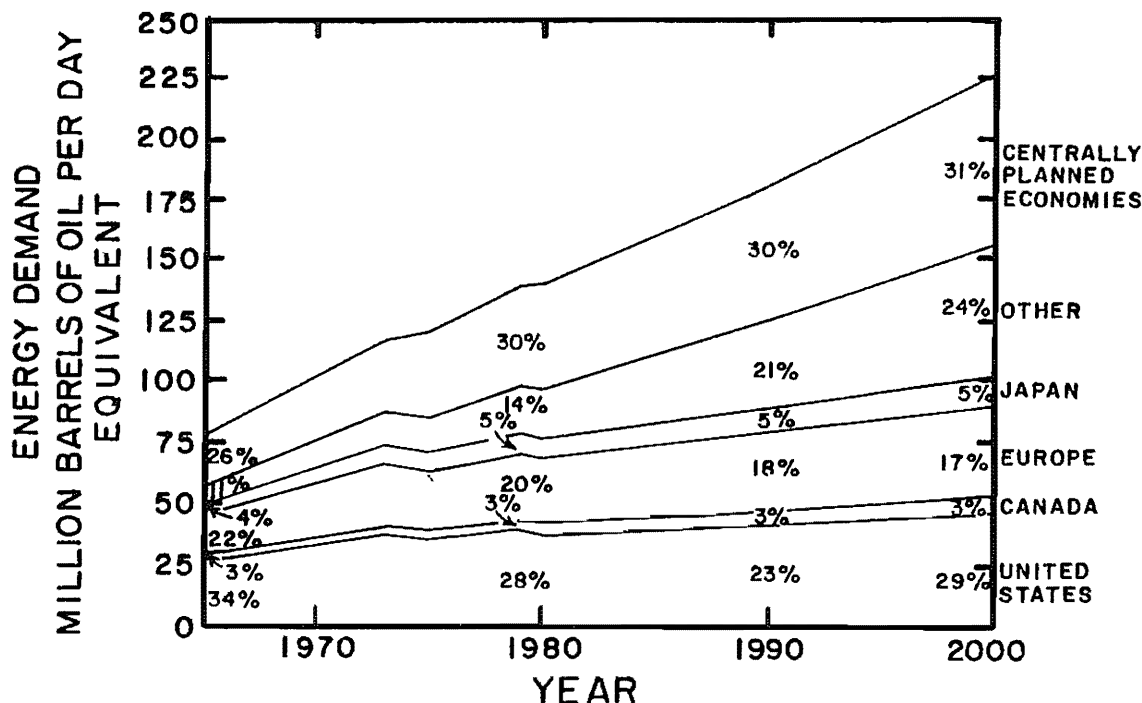


Figure 10-6. Historic (up to 1980) and projected (1980 to 2000) energy use for various countries and blocs of countries. The area designated "other" is made up mainly of the developing countries. The projections were made by Exxon Corporation © 1981 (691).

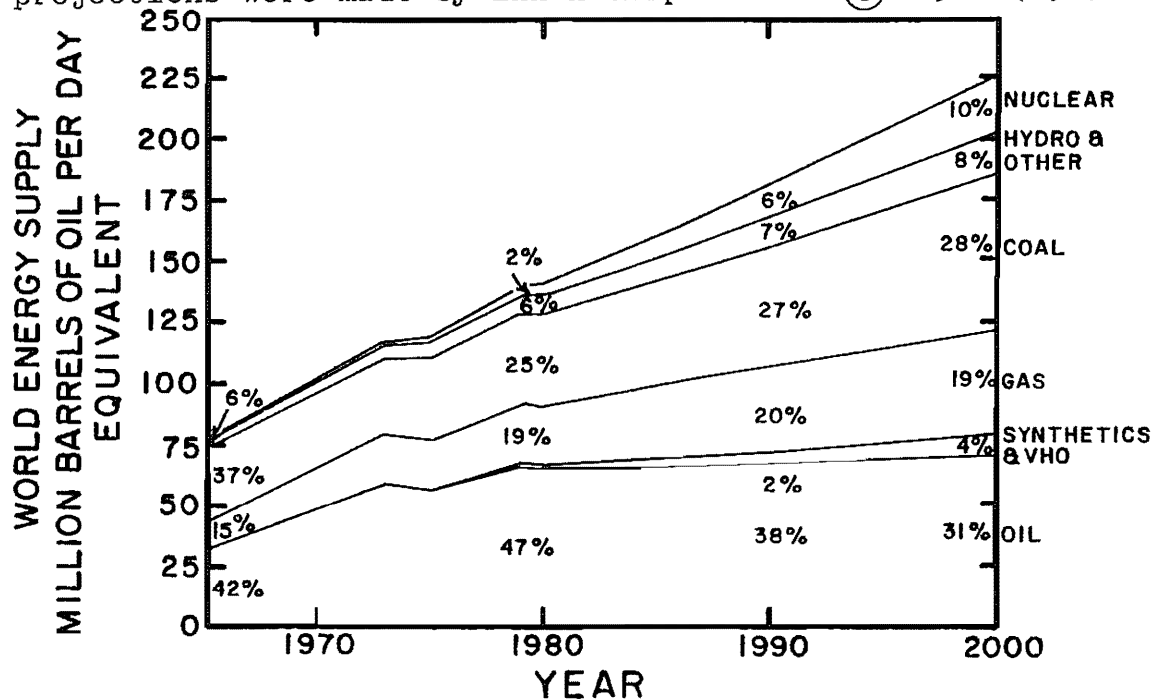


Figure 10-7. Historic (up to 1980) and projected (1980 to 2000) estimates of the energy supplied from various sources. As of 1980 fossil fuels accounted for 92% of the total. The projection made by Exxon Corporation © 1981 is that, as of the year 2000, fossil fuels will still account for 82% of the total (691).

Resistance to the large scale usage of nuclear power runs high. Despite the considerable talk of solar power, its fraction of the "pie" will remain small until a major breakthrough in technology comes which will permit electrical energy to be produced at a competitive price. In a world pushed to grow enough food and fiber it is difficult to believe that vegetation will become a major source of energy. And so it goes; the end to the dominance of fossil fuels is surely many decades away.

Another ingredient to CO₂ production estimates comes from the fact that per unit of energy delivered to the user quite different amounts of CO₂ are delivered to the atmosphere depending on the kind of fuel used (see table 10-2). Methane, which has the lowest CO₂ production to energy delivery ratio, is used as a reference. For oil the ratio of CO₂ produced to energy delivered is 1.3 times greater, for coal it is 1.7 times greater and for synthetic fuels (methane and liquid hydrocarbons manufactured from coal) and for oil derived from tar sands and shales the ratio averages 2.5. Thus we see that, as we run out of natural gas and oil and begin to use other fossil fuel sources, the amount of CO₂ produced per unit energy consumed will rise dramatically.

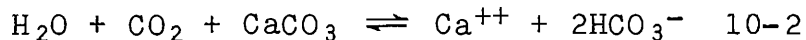
Finally, it should be mentioned that as the population increases and as fuel prices rise the temptation to even further reduce the planet's standing forest stocks will dramatically rise. Forests will be converted to farms and forests will be cut for fuel. We currently have more carbon in our forests than in our oil plus natural gas reserves.

CAPACITY OF THE SEA FOR FOSSIL FUEL CO₂ UPTAKE

The distribution of the CO₂ produced by man's activities between the air and the sea is a function of both thermodynamic (i.e., capacity) and kinetic (i.e., rate) factors. We will consider the capacity factors first. Although CO₂, like any other gas, dissolves in the sea, were simple solution the only mechanism for its uptake then the CO₂ produced by man would remain almost entirely airborne. The ocean would take up only about 3% of that added to the air. Significant amounts of CO₂ enter the ocean only because of the reactions:



and



The CO₃⁼ in reaction 10-1 is that which is dissolved in the ocean. The CaCO₃ in reaction 10-2 is that in the sediments on the sea floor. If present in great enough quantities these natural bases will eventually neutralize the man-made carbonic acid.

Is there enough base to neutralize the amount of CO₂ which would be produced if all our fossil fuel reserves were burned? The sea contains a total of about 12×10^{16} moles of CO₃⁼ ion. The upper 10 cm of marine sediments* contain about 8×10^{15}

*We take 10 cm as this is the depth to which burrowing organisms penetrate.

moles of CaCO_3 . Our combined fossil fuel reserves amount to about 35×10^{16} moles of carbon (see table 10-1). Thus viewed in this way the system could neutralize only about one-half of the carbonic acid man might ultimately produce.

As it turns out, both the estimate of the amount of base in the sea and that in the dynamically available sediment are too low. Our use of the mean amount of $\text{CO}_3^=$ ion in the sea as a measure of its capacity to take up CO_2 is misleading. Because most of the water in the ocean is deep water, this inventory is heavily biased toward the carbonate ion content of deep water. Actually, the atmosphere "sees" only the carbonate ion in surface-water, which, as shown in chapter 3, ranges from 1.3 times the mean deep water value in regions of cold surface water to as much as three times the deep water value in regions of warm surface water. Hence, the capacity of the sea to neutralize CO_2 is larger than the value of 12×10^{16} moles given above. As most of the deep water in the ocean is cold it is the $\text{CO}_3^=$ ion of cold surface water which is most important. Hence we should increase our ocean capacity estimate by about 25 percent to a value of 15×10^{16} moles. This is a more realistic estimate of the neutralization capacity of the sea itself.

Our estimate of the neutralization capacity of marine sediments is also low. We assumed that only that amount of CaCO_3 lying within 10 cm of the sediment-water interface is available for solution on a reasonable time scale (i.e., several thousand years), the reasoning being that molecular diffusion through several centimeters of sediment coupled with the low solubility of calcite would yield extremely low solution rates. Hence, we focus on the layer stirred by organisms. This mixing would continually bring new calcite close to the sediment water interface removing the necessity for a long diffusion path. This reasoning is in error in that as the calcite in the upper 10 cm of sediment is dissolved, organisms would reach down into sediment which had previously been beyond their burrowing range. Indeed calcite would continue to reach the interface as a consequence of their churning until a layer of calcite-free residue 10 cm thick had been generated! The amount of calcite kinetically available then becomes:

$$M = \frac{f_{\text{CaCO}_3}}{1 - f_{\text{CaCO}_3}} \times 10 \text{ g/cm}^2 \quad 10-3$$

where f_{CaCO_3} is the fraction of calcite in the original sediment.

In order to obtain a rough estimate of this capacity marine sediments can be divided into two categories: calcite oozes covering about 20% of the sea floor and averaging 85% calcite by mass and red clays covering about 80% of the sea floor and containing negligible calcite. The dynamically available calcite in the carbonate oozes would then be:

$$M = \frac{0.85}{0.15} \times 10 = 57 \text{ g/cm}^2 \\ = 0.57 \text{ moles/cm}^2$$

The total calculated in this way comes out to be about 40×10^{16} moles.

These revised estimates are more promising! The total neutralization capacity is half again the amount of carbon locked up in recoverable fossil fuels. The bulk of this capacity, however, resides in the sediments rather than in the water column. As we shall see, it will take man's CO₂ several thousands of years to get at this CaCO₃.

UTILIZABLE CAPACITY - SIMPLIFIED CALCULATION

While the approach we have just taken provides a ready means of getting at the ultimate buffering capacity of the ocean, it says nothing about the amount of this capacity utilizable for any given amount of CO₂ added to the atmosphere. As we are involved with a reversible chemical reaction, only a fraction of the CO₂ will be neutralized before an equilibrium distribution is achieved. Once the pressure of CO₂ in the atmosphere has fallen to the equilibrium pressure, the neutralization will proceed no further.

In the discussions which follow, we will consider separately the cases of neutralization by the carbonate ion in the sea alone and of the sea plus the calcium carbonate in its sediment because the time required for atmosphere and sea to come to equilibrium is many hundreds of years while the time for atmosphere, sea, and sediment to come to equilibrium is many thousands of years. The case for the sea alone will be considered in this section.

We will first consider the situation for an ocean with uniform chemistry and with no borate. This simplification is useful in that it allows us to understand the big picture without mathematical complexity. The equilibrium equation for reaction 10-1 is as follows:

$$K_\alpha = \frac{[\text{HCO}_3^-]^2}{[\text{CO}_3^{=}] \text{ pCO}_2} \quad 10-4$$

where K is the equilibrium constant for reaction 10-1 (see table 3-7) and α is the solubility of CO₂ in sea water (see table 3-7).

In our hypothetical borate-free ocean we can write down the following equation relating alkalinity to the concentrations of CO₃⁼ and HCO₃⁻:

$$[\text{Alk}] = [\text{HCO}_3^-] + 2[\text{CO}_3^=] \quad 10-5$$

Eliminating the [HCO₃⁻] concentration between the two equations yields:

$$K_\alpha = \frac{([\text{Alk}] - 2[\text{CO}_3^=])^2}{\text{pCO}_2 [\text{CO}_3^=]} \quad 10-6$$

This equation contains only [CO₃⁼] as an unknown.

A rough estimate of what happens when additional CO₂ is added to our simplified ocean-atmosphere system can be obtained by assuming that the numerator of this expression remains constant.

This approximation yields the following relationship:

$$p\text{CO}_2 [\text{CO}_3^{\text{=}}] = p^{\circ}\text{CO}_2 [\text{CO}_3^{\text{=}}]^{\circ} \quad 10-7$$

Thus to the first approximation for each 10% the CO₂ content of the atmosphere rises the CO₃⁼ ion content of surface water drops by 10%. CO₃⁼ ion constitutes between 7% (for cold water) and 12% (for warm water) of the ΣCO₂ in the surface ocean. As the total CO₂ content rises by the same amount as the CO₃⁼ ion content falls (see reaction 10-1) a 10% rise in pCO₂ will lead to a 0.7% rise in ΣCO₂ for cold surface water and a 1.2% rise in ΣCO₂ for warm surface water.

What we seek is the equilibrium fraction of CO₂ remaining in the atmosphere. In honor of Charles D. Keeling whose monitoring of the atmospheric CO₂ forms the foundation for all studies of the fate of fossil fuel CO₂ we sill refer to this fraction as the Keeling fraction, f_K, where:

$$f_K = \frac{M^{\ast}_{\text{atm}}}{M^{\ast}_{\text{atm}} + M^{\ast}_{\text{ocean}}} \quad 10-8$$

The amount of fossil fuel CO₂ accumulated in the air, M^{*}_{atm}, is given can be approximated by:

$$M^{\ast}_{\text{atm}} = \frac{(p\text{CO}_2 - p^{\circ}\text{CO}_2)}{p^{\circ}\text{CO}_2} M^{\circ}_{\text{atm}} \quad 10-9$$

where p[°]CO₂ is the partial pressure of CO₂ in the air prior to the industrial revolution and M[°]_{atm} is the mass of CO₂ in the preindustrial atmosphere. The amount of excess CO₂ taken up by the ocean can be approximated by:

$$M^{\ast}_{\text{ocean}} \approx ([\text{CO}_3^{\text{=}}]^{\circ} - [\text{CO}_3^{\text{=}}]) V_{\text{ocean}}$$

where [CO₃⁼][°] is the mean carbonate ion content of the surface ocean prior to the industrial revolution and V_{ocean} is the volume of the ocean. It is the drop in CO₃⁼ ion concentration in surface water that provides the measure of the amount of CO₂ taken into the sea (one mole of CO₃⁼ is utilized for each mole of CO₂ removed from the atmosphere). Thus f_K is given by the following equation:

$$f_K = \frac{\frac{(p\text{CO}_2 - p^{\circ}\text{CO}_2)}{p^{\circ}\text{CO}_2} M^{\circ}_{\text{atm}}}{\frac{(p\text{CO}_2 - p^{\circ}\text{CO}_2)}{p^{\circ}\text{CO}_2} M^{\circ}_{\text{atm}} + ([\text{CO}_3^{\text{=}}]^{\circ} - [\text{CO}_3^{\text{=}}]) V_{\text{ocean}}} \quad 10-11$$

Using the approximate relationship between $p\text{CO}_2$ and $\text{CO}_3^=$ given above, this equation becomes:

$$f_K = \frac{1}{1 + \frac{(1 - p^\circ\text{CO}_2/p\text{CO}_2) [\text{CO}_3^=]^\circ V_{\text{ocean}}}{(p\text{CO}_2/p^\circ\text{CO}_2 - 1) M^\circ \text{atm}}} \quad 10-12$$

The values of the constants in this equation are as follows:

$$\begin{aligned} V_{\text{ocean}} &= 13.3 \times 10^{20} \text{ liters} \\ [\text{CO}_3^=]^\circ &= 200 \times 10^{-6} \text{ moles/liter} \\ M^\circ \text{atm} &= 5 \times 10^{16} \text{ moles} \\ p^\circ\text{CO}_2 &= 280 \times 10^{-6} \text{ atm} \end{aligned}$$

Thus:

$$f_K = \frac{1}{1 + 5.3 \frac{(1 - 280/p\text{CO}_2)}{(p\text{CO}_2/280 - 1)}} \quad 10-13$$

It can be seen that for small increases in atmospheric CO_2 content the Keeling fraction lies close to 1/6.3 or to 0.16. On the other hand, as the CO_2 content of the atmosphere becomes very large, the Keeling fraction approaches unity (the $\text{CO}_3^=$ ion content of the ocean would eventually reach very low values and the sea would cease to take up the excess CO_2 added to the atmosphere). The relationship between the Keeling fraction and the atmospheric CO_2 partial pressure given by this simplified equation is shown in figure 10-8.

The total amount of fossil fuel CO_2 generated is related to Keeling fraction and the atmospheric CO_2 partial pressure as follows:

$$M_{\text{FF}} = \left[\frac{p\text{CO}_2 - p^\circ\text{CO}_2}{p^\circ\text{CO}_2} \right] \frac{M^\circ \text{atm}}{f_K} \quad 10-14$$

For the simplified assumption that the product of surface ocean $\text{CO}_3^=$ ion concentration and atmospheric CO_2 partial pressure remains constant the relationship between M_{FF} and $p\text{CO}_2$ is shown in figure 10-8. It can be seen from this figure that in order to raise the atmosphere's CO_2 pressure by a factor of two (i.e., to about 600×10^{-6} atm) an amount of CO_2 equal to about 4 times that in the preindustrial atmosphere would have to be released by fossil fuel CO_2 combustion.

It must be remembered that this calculation is made with the assumption that the entire ocean (but not of the sediments) is thoroughly equilibrated with the atmosphere. As we shall see over the next century or so, only a rather small fraction of the ocean will equilibrate with the air. Thus the Keeling fractions given

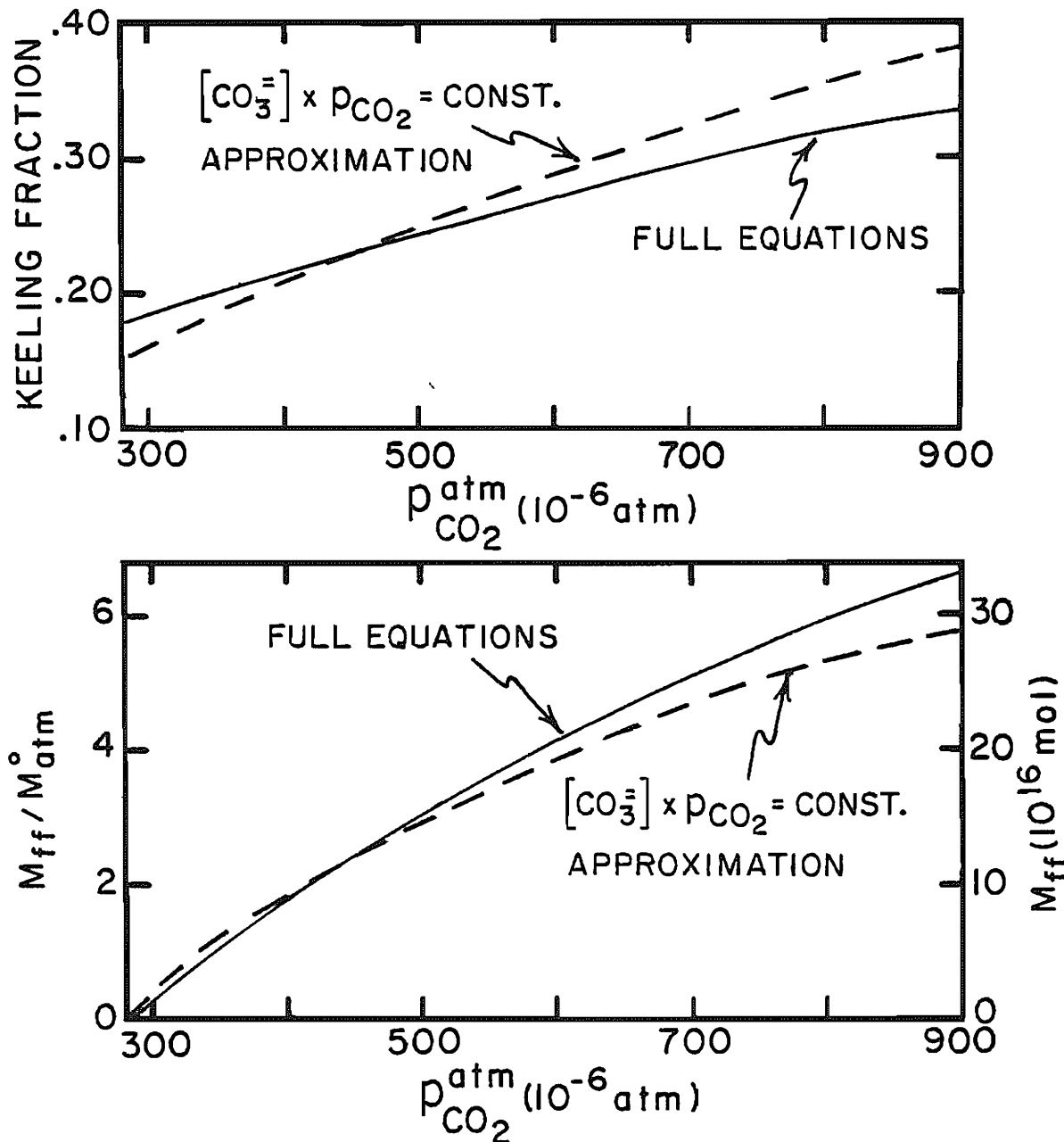


Figure 10-8. Plot of the Keeling fraction as (upper) and of the amount of fossil fuel CO_2 added to the atmosphere (lower) as a function of atmospheric p_{CO_2} , assuming that the atmosphere and entire ocean maintain equilibrium, and that no interaction with sedimentary CaCO_3 occurs. Two sets of curves are given. One is for the simplified situation where the product of $\text{CO}_3^{=}$ concentration in surface water and the p_{CO_2} partial pressure in the atmosphere is assumed to remain constant. The other is based on rigorous calculations outlined in the text.

in figure 10-8 are lower limits.

As our interest is centered on the CO₂ buildup in the coming century, it is appropriate to repeat these calculations for the case where only 10% of the ocean volume is equilibrated with the atmosphere (as we shall see, the effective equilibration volume during the next 100 years will be in the range of 10% to 20% of the ocean volume). The Keeling fraction for equilibration between the atmosphere and 10% of the sea is as follows:

$$f_K = \frac{1}{1 + 0.53 \frac{(1 - 280/p_{CO_2})}{(p_{CO_2}/280 - 1)}} \quad 10-15$$

The graphs in figure 10-9 show the relationships between f_K and pCO₂ and M_{FF} and pCO₂ obtained in this way. As can be seen from this figure, the Keeling fraction rises from 0.65 for small amounts of CO₂ production and approaches unity for large amounts of CO₂ production. In this case the amount of CO₂ production required to yield a CO₂ pressure of 600 x 10⁻⁶ atm is only about 1.5 times the amount of CO₂ in the preindustrial atmosphere.

UTILIZABLE CAPACITY - RIGOROUS CALCULATION

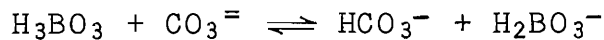
Let us now do the ocean-atmosphere problem in a more rigorous way. There are seven equations governing the steady state distribution. As before, we have the equilibrium for reaction 10-1:

$$\alpha K = \frac{[HCO_3^-]^2}{[CO_3^{=}] p_{CO_2}} \quad 10-16$$

Next we have the full alkalinity equation:

$$[Alk] = [H_2BO_3^-] + 2[CO_3^{=}] + [HCO_3^-] \quad 10-17$$

Further we have the equilibrium equation for the chemical reaction:



which is:

$$K_B = \frac{[HCO_3^-][H_2BO_3^-]}{[H_3BO_3][CO_3^{=}]} \quad 10-18$$

We also have the mass balance equation for the dissolved inorganic carbon species:

$$[\Sigma CO_2] = [HCO_3^-] + [CO_3^{=}] + \alpha p_{CO_2} \quad 10-19$$

and the mass balance equation for borate species:

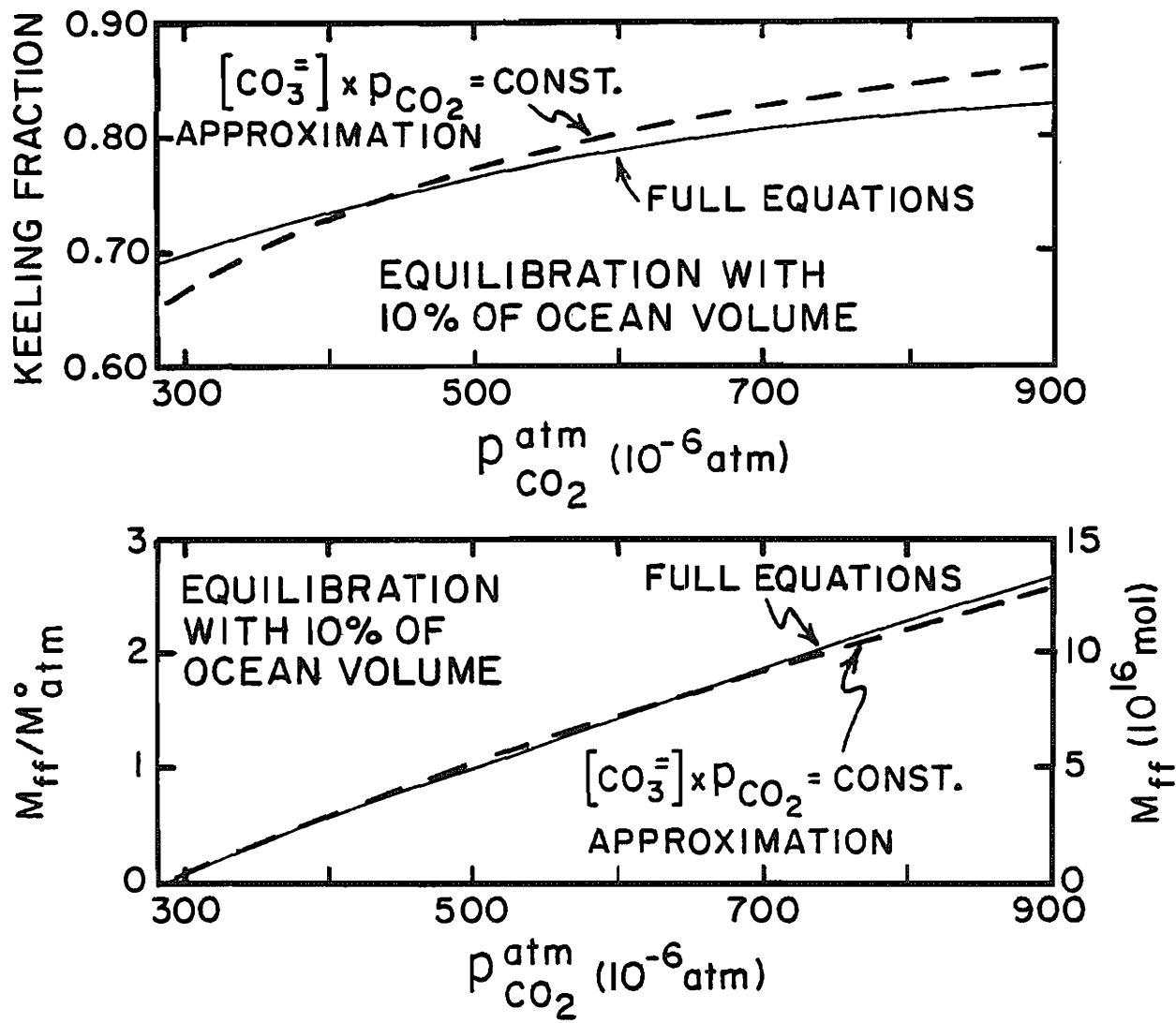


Figure 10-9. Plots of the Keeling fraction (upper) and mass of fossil fuel CO_2 added to the atmosphere (lower) versus atmospheric p_{CO_2} , assuming that only 10% of the ocean volume equilibrates with the atmosphere (and, of course, that no interaction with sedimentary CaCO_3 occurs). The dashed line is for the simplified calculation where the constancy of the product of the surface water carbonate ion concentration and the atmospheric CO_2 partial pressure in the atmosphere is assumed. The solid line is for the rigorous calculation outlined in the text.

$$[\Sigma B] = [H_2BO_3^-] + [H_3BO_3]$$

10-20

Finally we have the equation for the Keeling fraction:

$$f_K = \frac{(pCO_2/p^{\circ}CO_2 - 1) M^{\circ}atm}{(pCO_2/p^{\circ}CO_2 - 1) M^{\circ}atm + ([\Sigma CO_2]/[\Sigma CO_2]^{\circ} - 1) M^{\circ}ocean} \quad 10-21$$

and the equation starting the relationship between the mass of fossil fuel CO_2 produced and the Keeling fraction:

$$M_{FF} = \left[\frac{pCO_2}{p^{\circ}CO_2} - 1 \right] \frac{M^{\circ}atm}{f_K} \quad 10-22$$

These seven equations contain seven unknowns ($[H_2BO_3^-]$, $[H_3BO_3]$, $[\Sigma CO_2]$, $[HCO_3^-]$, $[CO_3^{=}]$, f_K and M_{FF}). The values of $[\Sigma CO_2]^{\circ}$, $p^{\circ}CO_2$, $[Alk]$, $[\Sigma B]$, α , K , K_B , $M^{\circ}atm$, and $M^{\circ}ocean$ are knowns ($[Alk]$ does not change in the absence of interactions with the ocean sediments).

Were the ocean homogeneous in its properties we could apply these equations as we did the simplified ones given above. However, as we are now trying to get the best answer possible from this approach, we must take the spatial distribution of properties in real ocean into account. Our strategy will be to divide the interior of the ocean into a number of subunits and to establish for each the properties for its source waters.

The subdivision will be made according to temperature. Boundaries are placed at intervals at $4^{\circ}C$ (i.e., at 4° , 8° , 12° , 16° , 20° and $24^{\circ}C$). The volumes of ocean water in each of these subdivisions are listed in table 10-3. We also need to establish the $CO_3^{=}$ ion content of surface waters as a function of temperature. The $CO_3^{=}$ ion concentrations for all the surface water samples taken as part of the GEOSECS program are plotted against temperature in figure 10-10. A strong correlation is found; the warmer the water, the higher its $CO_3^{=}$ concentration. The trend seen in this diagram is approximately that expected from the temperature dependence of the equilibrium constants for surface waters equilibrated with the CO_2 partial pressure of the atmosphere. This can be seen from the dashed line shown in the figure which depicts the carbonate ion content of a single water sample with an alkalinity of $2330 \mu eq/kg$ equilibrated with the atmosphere ($pCO_2 = 330 \times 10^{-6} atm$) at temperatures ranging from 0 to $30^{\circ}C$. The departures from this trend reflect the fact that alkalinity, surface water salinity and surface water pCO_2 vary from place to place.

While the carbonate ion content of a given surface water provides a good measure of its capacity to take up excess CO_2 from the atmosphere, there is another parameter which proves more precise in this regard. It is called the Revelle factor, R . It is the ratio of the fractional rise in atmospheric CO_2 content to the fractional rise in the ΣCO_2 content of a water sample at equilibrium with the atmosphere, i.e.,

Table 10-3. Subdivision of the ocean for the purpose of calculating the equilibrium response of the ocean to a doubling of atmospheric CO₂ content.

Temp. Range °C	Volume 10^{16}m^3	Fraction Total / Ocean Volume	Outerop Alk $\mu\text{eq/kg}$	Outerop ΣCO_2^+ (1850) $\mu\text{m/kg}$	Outerop $\text{CO}_3^{=+}$ (1850) $\mu\text{m/kg}$	Revelle Factor [†] (1850)	Outerop ΣCO_2^* (future) $\mu\text{m/kg}$	Outerop $\text{CO}_3^{=+}$ (future) $\mu\text{m/kg}$	Revelle Factor [*] (future)	Mass** Excess CO ₂ 10^{16} moles
>24	1.0	0.008	2330	1938	276	8.5	2097	172	11.1	0.16
20-24	0.7	0.005	2330	1975	249	9.0	2127	151	11.9	0.11
16-20	1.7	0.013	2330	2012	223	9.5	2156	132	12.9	0.25
12-16	2.7	0.020	2330	2048	197	10.2	2183	114	14.0	0.37
8-12	3.3	0.025	2330	2081	173	11.0	2208	98	15.2	0.43
4-8	14.9	0.113	2330	2112	152	11.8	2231	84	16.3	1.82
<4	107.7	0.816	2330	2139	135	12.7	2252	73	17.2	12.43
TOTAL	132.0	1.000	-	-	-	-	-	-	-	15.57

[†]For atmospheric CO₂ pressure equal to 280×10^{-6} atm.

^{*}For atmospheric CO₂ pressure equal to 600×10^{-6} atm.

^{**}Equilibrium mass of CO₂ taken up by the particular ocean subvolume for an atmospheric pCO₂ of 600×10^{-6} atm. For comparison the amount of excess CO₂ in the atmosphere for this pCO₂ is 11×10^{16} moles.

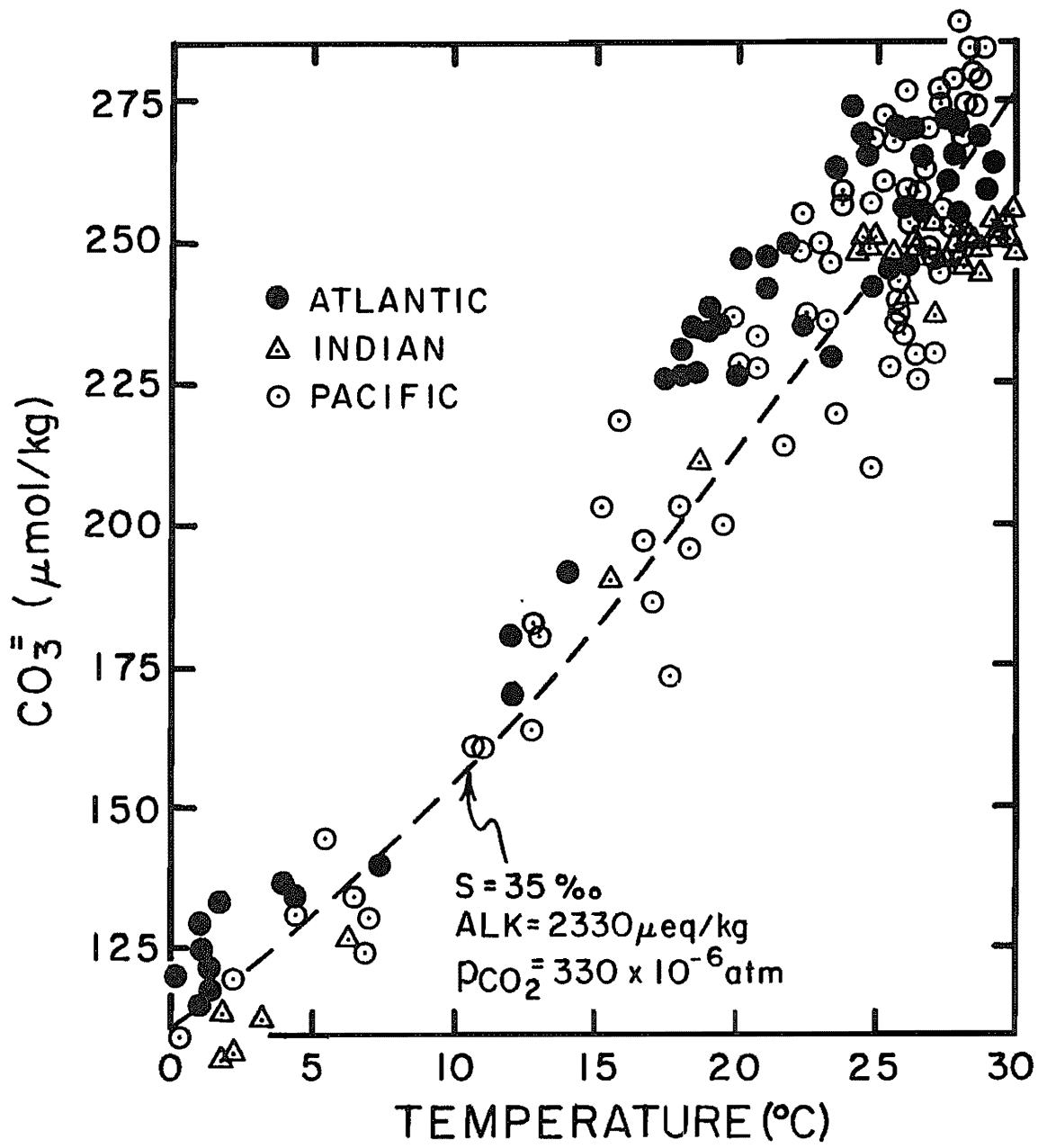


Figure 10-10. Carbonate ion concentration measured in surface waters of the ocean during the GEOSECS program as a function of surface water temperature. The dashed line represents the values expected if a single water sample were equilibrated with an atmospheric CO_2 pressure of $330 \times 10^{-6} \text{ atm}$ at different temperatures. The data points are based on measurements made during the GEOSECS program (406).

$$R = \frac{\Delta p_{CO_2}/p_{CO_2}}{\Delta \Sigma CO_2/\Sigma CO_2} \quad 10-23$$

or:

$$\frac{\Delta \Sigma CO_2}{\Sigma CO_2} = \frac{1}{R} \frac{\Delta p_{CO_2}}{p_{CO_2}} \quad 10-24$$

A rough idea regarding the relationship between the Revelle factor to the carbonate ion content can be obtained using the approximations that:

$$p_{CO_2} [CO_3^{=}] \approx p^o_{CO_2} [CO_3^{=}]^o \quad 10-25$$

and that:

$$\Delta[\Sigma CO_2] = [CO_3^{=}]^o - [CO_3^{=}] \quad 10-26$$

If equation 10-26 is divided by $[\Sigma CO_2]^o$ and if equation 10-25 is used to eliminate $[CO_3^{=}]$ from equation 10-26, we obtain:

$$\frac{\Delta[\Sigma CO_2]}{[\Sigma CO_2]^o} \approx \left[\frac{p_{CO_2} - p^o_{CO_2}}{p_{CO_2}} \right] \frac{[CO_3^{=}]^o}{[\Sigma CO_2]^o} \quad 10-27$$

Rearranging this equation and substituting Δp_{CO_2} for $p_{CO_2} - p^o_{CO_2}$ we obtain:

$$\frac{\Delta[\Sigma CO_2]}{[\Sigma CO_2]^o} \approx \frac{[CO_3^{=}]^o}{[\Sigma CO_2]^o} \frac{\Delta p_{CO_2}}{p_{CO_2}} \quad 10-28$$

Hence:

$$R \approx \frac{[\Sigma CO_2]^o}{[CO_3^{=}]^o} \quad 10-29$$

While this expression gives the approximate value of R in order to obtain its precise value, we must use the set of equations given above.

We can now check the extent to which this approximation holds. Shown in figure 10-11 are the Revelle factors for surface waters from throughout the Atlantic Ocean plotted against the ΣCO_2 to $CO_3^{=}$ concentration ratio. For warm surface waters the $\Sigma CO_2/CO_3^{=}$ approximation gives a value which is about 10% too low. For cold surface waters the approximation gives a value which is about 25% too high. It must be pointed out that just as the $[\Sigma CO_2]/[CO_3^{=}]$ ratio for any given surface water sample increases with the atmospheric CO_2 content so also does the Revelle factor. In carrying out calculations for progressively increasing atmospheric CO_2 contents, the Revelle factor must be recalculated as the $CO_3^{=}$ ion content of surface ocean water falls.

Now back to our rigorous static calculation. Having established the volumes and outcrop properties of the various subvolumes of the ocean (see table 10-3) we can apply the full set of

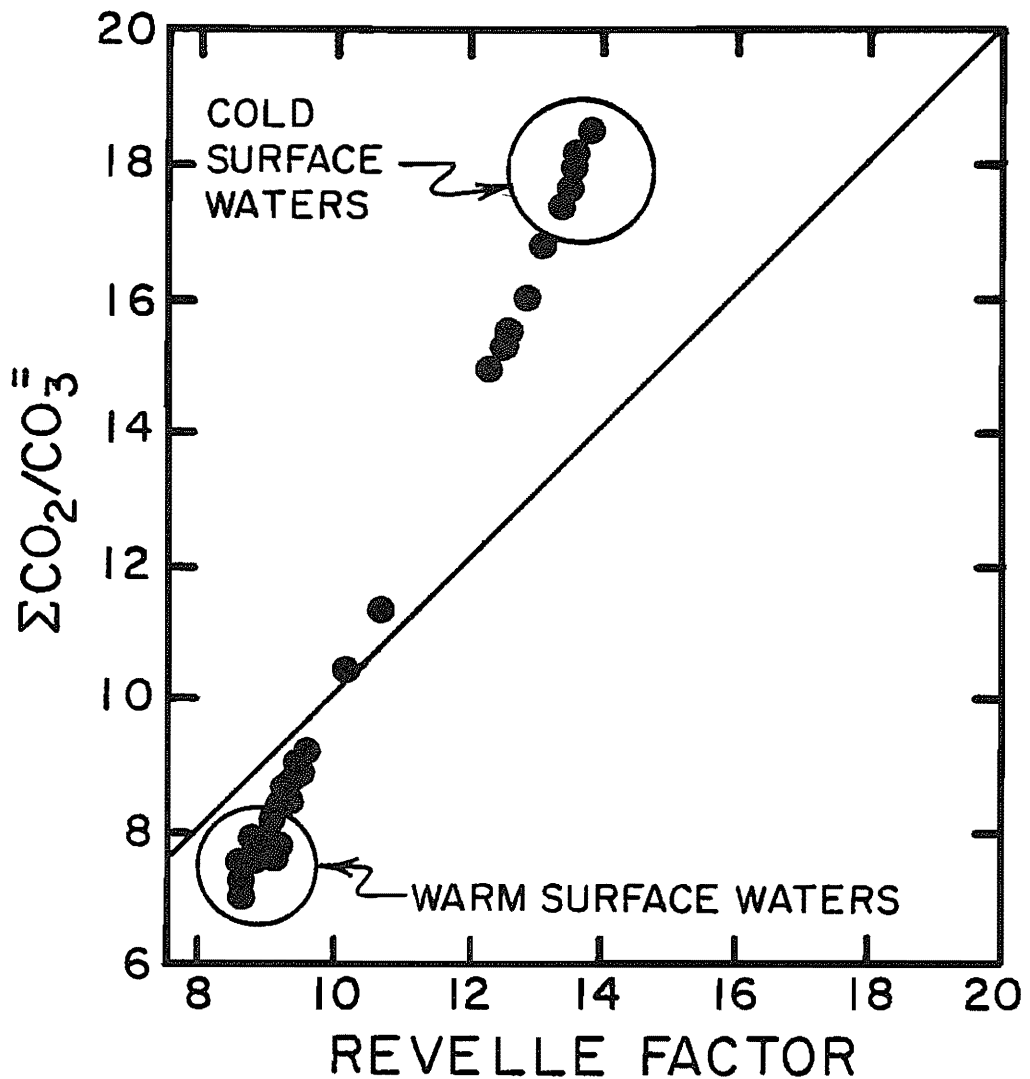


Figure 10-11. Comparison of the ratio of ΣCO_2 to $\text{CO}_3^=$ concentration for surface waters with the Revelle factor calculated for these waters. The Revelle factor is the ratio between the fractional change in the CO_2 partial pressure and the fractional change in ΣCO_2 content for the water.

equations given above to each. The results for one value of PCO_2 (600×10^{-6} atm) are listed in table 10-3. Plots for f_K vs. PCO_2 and M_{FF} vs. PCO_2 are given in figure 10-8. The results are not much different from those obtained using the simple approximation.

Similar rigorous static calculations for an equilibration with 10% of the ocean volume yields the plots of f_K vs. PCO_2 and of M_{FF} vs. PCO_2 given in figure 10-9. Again they do not differ greatly from those obtained when the simplifying assumptions were used.

KINETICS OF FOSSIL FUEL CO_2 UPTAKE BY THE SEA

While the calculations leading to the partition estimates in figure 10-9 handle the capacity factors for the sea correctly the kinetic factors are handled in a highly simplified manner. It was assumed that 10% of the ocean fully equilibrated with the atmosphere and that the remaining 90% was totally isolated. In reality the ocean would be expected to show a gradation from nearly complete equilibration for surface waters to no equilibration for the older deep waters. If we are to get a meaningful answer then a model must be developed which incorporates the kinetic resistances to equilibration (namely the finite rate of transfer of CO_2 across the air-sea interface and the finite rate of mixing between surface and interior waters).

Before doing a proper kinetic model let us consider the origin of the 10% figure used for the calculations summarized in figure 10-9. It is based on the average of penetration depths for tritium as measured at the stations in the Atlantic and Pacific Oceans occupied during the GEOSECS program (see table 10-4). As the mid-date of the addition of tritium to the ocean was 1963 and the mid-date of the Atlantic and Pacific GEOSECS surveys was 1973, this average penetration depth gives an estimate of the fraction of the ocean contaminated with tritium on a ten-year time scale. As shown in table 10-4, the result comes out to be 375 m (corresponding to 10% of the ocean's volume).

In applying the tritium-based penetration depth we must first consider the difference in the time available for the average fossil fuel CO_2 molecule to penetrate into the sea and the time the average bomb tritium atom had to penetrate into the sea (as of 1973). At first glance one might be tempted to take the ratio of the mean-age of fossil fuel CO_2 molecules (i.e., 30 years) to the mean-age tritium atoms as of the time of the GEOSECS survey (i.e., 10 years). This would be incorrect because the CO_2 age reflects the mean time after addition to the atmosphere, while the tritium age is the time since entry into the sea. The numerical model developed in the section which follows shows that the equivalent ocean residence time for fossil fuel CO_2 molecules is 0.57 their mean age. Thus the ocean residence time for fossil fuel CO_2 molecules is 17 years.

The longer a substance resides in the ocean, the greater will be its penetration depth. While we do not know exactly what the time dependence is, our observations of bomb tritium show that the volume does not grow linearly with time (i.e., after 30 years have

Table 10-4. Summary of the mean tritium penetration depths as of 1973 for various parts of the ocean. The numbers in the right hand column are the product of the mean penetration depth for a given zone times the fraction of ocean area constituted by that zone. The penetration depths for the Indian Ocean are assumed to be the same as the average for the Atlantic and Pacific. Based on tritium measurements made by Ostlund at the University of Miami as part of the GEOSECS program (21,22,23).

	Atl. m	Pac. m	Global Mean m	Frac. Ocean Area	Contribution to Global Mean Depth m
Antarctic (>45°S)	270	475	375	0.169	62
S. Temp. (45°S-15°S)	340	340	340	0.264	90
Equator (15°S-15°N)	220	225	225	0.281	63
N. Temp. (15°N-45°N)	700	490	560	0.192	107
N. Pac. (>45°N)	-	310	-	0.028	9
N. Atl. (>45°N)	1060	-	-	0.036	38
Arctic (~70°N)	-	-	~200	0.032	6
Global Mean					375

passed, tritium will not have reached three times the penetration depth observed at the time of the GEOSECS surveys). A more appropriate estimate appears to be that the penetration depth increases as the square root of time (as would be expected if it were being moved downward by eddy diffusion). If so then after 17 years the mean depth would be 1.3 times that for 10 years.

Because of the finite rate of CO₂ exchange between the surface ocean and atmosphere, even the uppermost waters of the ocean are not quite at equilibrium with the CO₂ content of the air. The numerical to be presented below suggests that at present it has only 0.86 the equilibrium amount of fossil fuel CO₂. Hence the tritium-based mean penetration depth must be multiplied by 1.30 to account for the longer time available for CO₂ penetration and by 0.86 to account for the failure of the surface waters to achieve full equilibrium with the atmosphere. The result is 420 meters or 11% of the ocean volume.

This type of analysis can be extended to the future. For any fuel use scenario we can compute the mean age of the fossil fuel CO₂ molecules present in the atmosphere ocean system at any time in the future. In figure 10-12 are given several fossil fuel scenarios and their corresponding mean CO₂ ages. If we confine our attention to the next 80 years, these graphs make it clear that we are interested mainly in those portions of the ocean which are ventilated by fossil fuel CO₂ molecules with mean ages in the range 30 and 60 years (i.e., effective ocean penetration times in the range 17 to 34 years).

Figure 10-13 shows a possible relationship between the fraction of ocean ventilated and the square root of the penetration time. A straight line joins the origin and the bomb tritium calibration point (i.e., 10% ventilated in 10 years). The range of ventilation times consistent with the distribution of natural radiocarbon in the sea is shown to straddle the extension of this line lending support to the approximation that the volume equilibrated increases as the square root of penetration time. The range for the natural calibration radiocarbon stems from the difference between the deep sea ventilation time for radiocarbon (~ 1000 years) and the ventilation time for heat and helium (~ 400 years). Following the arguments presented in chapter 3, the deep-sea ventilation time for CO₂ should lie somewhere in between those for ¹⁴C and heat. Exactly where in this range we do not know.

NUMERICAL MODEL

Rather than using the graph in figure 10-13 to calculate the fraction of the ocean equilibrated for a given mean age for the fossil fuel CO₂ molecules, we will adopt a more rigorous approach. It involves the use of the 1-D numerical model referred to by workers in the field as the "Oeschger" model (the name of the senior member of a group in Bern, Switzerland, responsible for the development of this model). The basics of this model are illustrated in figure 10-14. The model's ocean consists of 76 boxes of equal volume one above the other. Each box represents a layer in the ocean 50 meters thick. Mixing is accomplished by exchang-

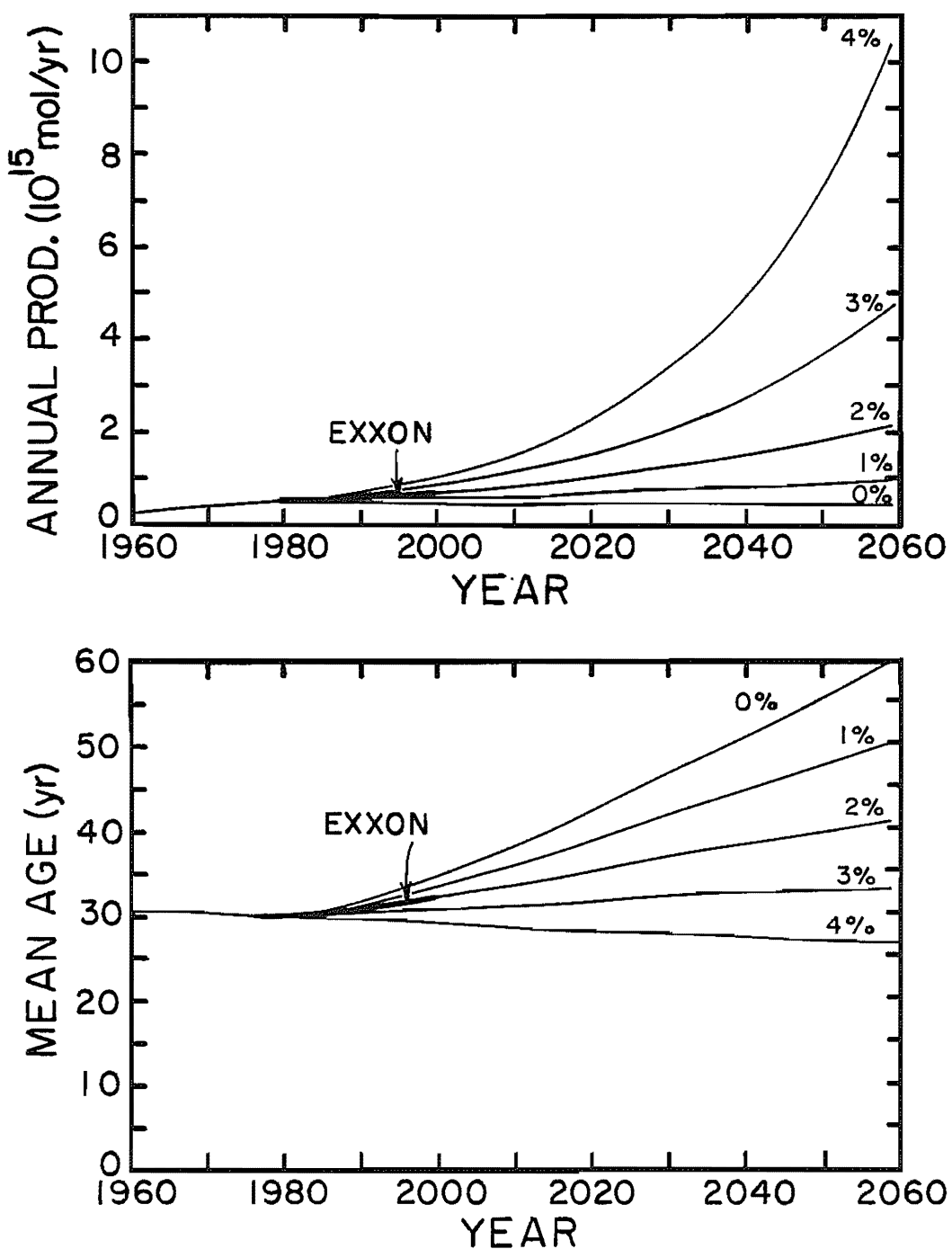


Figure 10-12. Projections of fossil fuel CO₂ production rates over the next 80 years for a variety of energy scenarios (upper panel) and the corresponding mean ages for fossil fuel CO₂ molecules so produced (lower panel).

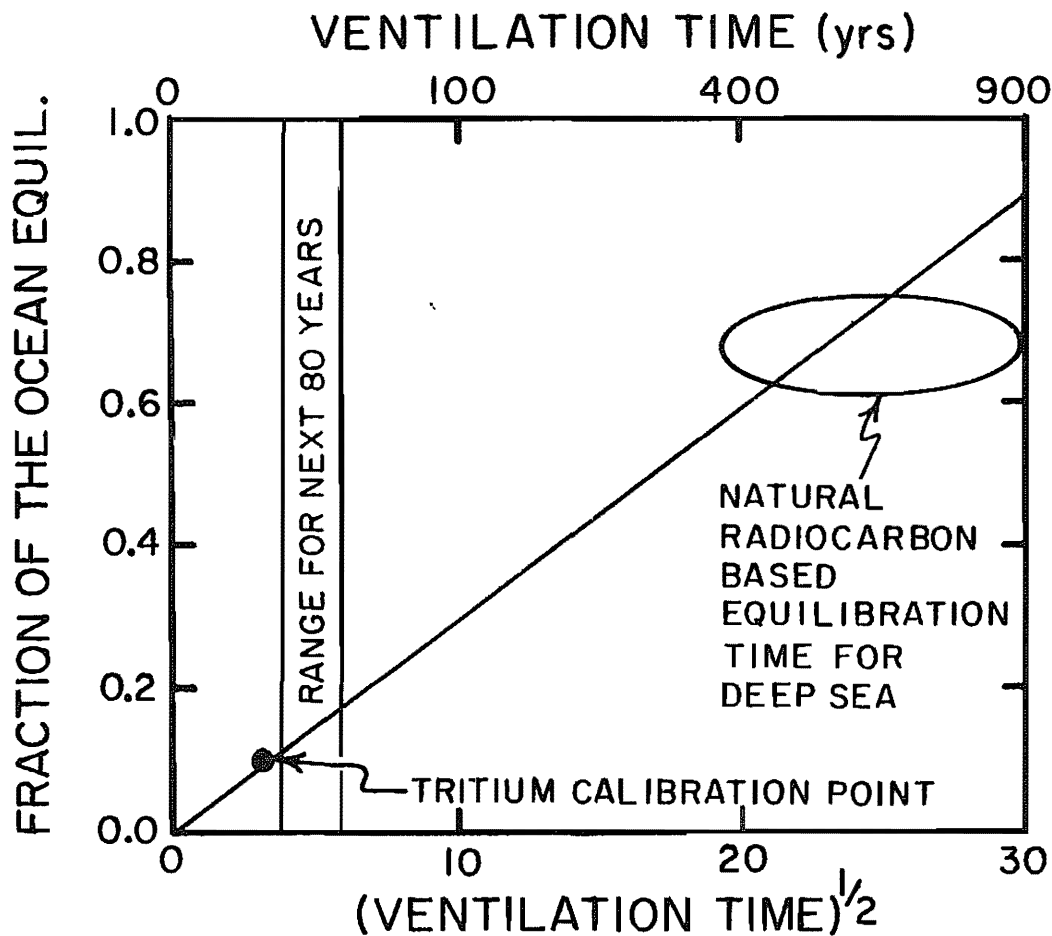


Figure 10-13. Plot of fraction of ocean volume equilibrated against ventilation time. One calibration point is based on the distribution of bomb tritium in 1973 and the other one on the steady state distribution of natural radiocarbon. The straight line is drawn assuming that the fraction of volume equilibrated with fossil fuel CO₂ increases with the square root of the mean age of the fossil fuel CO₂ molecules. The range limits are for ventilation times corresponding to mean CO₂ ages of 30 and 60 years (the conversion factor from mean CO₂ age to equivalent ocean ventilation time is 0.57).

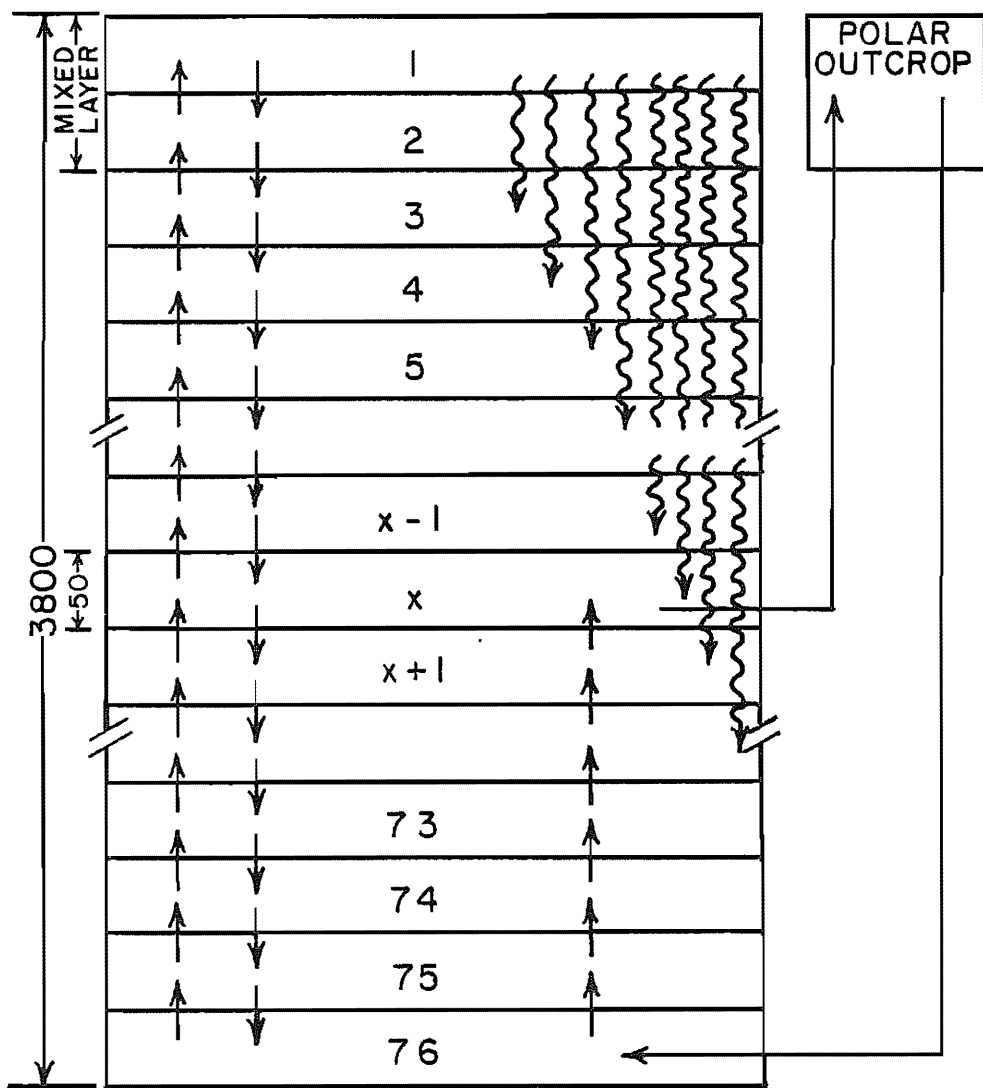


Figure 10-14. Multibox ocean model used to calculate the uptake of fossil fuel CO₂ by the ocean. The ocean is divided into 76 layers each with the same volume. Water is traded between adjacent reservoirs (equivalent to vertical eddy diffusion). Water also passes up from the bottom of the model to the level designated as the source for new deep water. From here it is transferred to the polar outcrop where it is cooled without undergoing modification in its ΣCO₂ content and carbon isotope ratios. This water is then transferred to the model's bottom box. The PO₄ reaching the uppermost reservoir is entirely utilized by plants. These plants are assumed to incorporate 105 carbon atoms for each phosphorus atom. The organic matter so produced falls toward the bottom. As it falls it is progressively oxidized returning the carbon and phosphorus to solution.

ing water between these boxes (see left hand arrows). Bottom water formation is accomplished by transferring water from one of the intermediate depth boxes (consistent with our discussions of the origin of deep water in chapter 8) to a polar surface box, where it is cooled. The assumption is made that no ΣCO_2 or $^{14}\text{C}/\text{C}$ change occurs during this cooling. This water is then added to the bottom box from whence it upwells through the series of boxes (right hand arrows) completing the cycle. Organic matter produced in the surface water settles toward the sea floor. As it falls it is progressively consumed by animals and bacteria. Thus this model includes all the basic first-order processes going on within the sea (with the exception of CaCO_3 formation and dissolution). Being a one-dimensional model, it averages the lateral inhomogeneities in the sea.*

Our task now is to calibrate the parameters in the model. They are as follows:

- 1) the CO_2 exchange rate between the atmosphere and surface ocean
- 2) the exchange rate of water between the ocean reservoirs
- 3) the flux of deep water
- 4) the depth in the ocean from which new deep water is drawn
- 5) the rate of rain of organic matter from surface water toward the deep sea
- 6) the fraction of this debris oxidized at each level in the model

*It must be pointed out that the modifications we have made in the Oeschger model are more of a cosmetic than a substantive nature. First, we use a somewhat higher vertical mixing rate in the upper part of the ocean ($1.6 \text{ cm}^2/\text{sec}$ compared to $1.25 \text{ cm}^2/\text{sec}$). We do so based on the global tritium data set, which was not available at the time Oeschger and his colleagues wrote their paper. As the uptake of fossil fuel CO_2 by the sea varies with square root of the diffusivity, this adjustment does not change things very much. Second, we include the cycle of particulate matter in the ocean. The Oeschger model has received unjust criticism for not including this mode of transport. The addition of fossil fuel CO_2 to the oceans should not significantly alter the amount of carbon transported by the ocean's particulate cycles (as we have seen, they are limited by the availability of P and N). Thus inclusion of particulate cycles does not change the amount of fossil fuel CO_2 taken up by the model ocean. The third change we have made is the inclusion of deep water production. Because we do not permit ΣCO_2 or $^{14}\text{C}/\text{C}$ changes in the polar reservoir, this change has little effect on the 30 to 60 year time scale of importance as over the next 100 years. The loop we have inserted merely provides an alternate means of stirring the deep sea, which yields more reasonable deep water profiles for $^{14}\text{C}/\text{C}$ and temperature. We decrease the vertical diffusivity from $1.6 \text{ cm}^2/\text{sec}$ to $0.5 \text{ cm}^2/\text{sec}$ below 700 meters depth to compensate for the mixing generated by the deep water loop. Thus, while our modifications of the Oeschger model yield more realistic vertical profiles, they do not substantially change the amount of fossil fuel CO_2 taken up by the ocean.

We accomplish this by forcing the model to meet the following constraints:

- 1) It must carry tritium to the proper mean depth (i.e., 375m in 10 years).
- 2) It must produce a natural $^{14}\text{C}/\text{C}$ vs. depth relationship consistent with that observed in the ocean.
- 3) It must match the input of natural radiocarbon across the air-sea interface with radiodecay within the sea.
- 4) It must produce the appropriate vertical profiles of phosphate.

The first step in this calibration is to select a set of dynamic parameters which will simultaneously fit the distributions of bomb tritium and of natural radiocarbon. We found by trial and error that the following values yield satisfactory fits to both of these data sets:

Vertical diffusivity 100 to 700 meters	1.6 $\frac{\text{cm}^2}{\text{sec}}$
Vertical diffusivity 700 to 3800 meters	0.5 $\frac{\text{cm}^2}{\text{sec}}$
Deep water upwelling rate	4.4 m/yr (50 Sverdrups)
Depth of origin of deep water	1000 meters

In order to get the preanthropogenic $\Delta^{14}\text{C}$ for surface water (i.e., $-50^{\circ}/\text{oo}$) the CO_2 invasion rate must be $17.5 \text{ moles/m}^2 \text{ yr}$ (for $\text{PCO}_2 = 280 \times 10^{-6} \text{ atm}$).

The rate of rain of organic matter from the mixed layer is obtained by multiplying the flux of phosphorus to the mixed layer (in $\text{moles/m}^2 \text{ yr}$) by 105. The mixed-layer PO_4 content is maintained at zero. The model ocean is given a total amount of phosphorus equal to that in real ocean. Then by trial and error the depth distribution of the destruction of organic residues is adjusted so as to generate a steady state PO_4 depth distribution similar to that found in the sea. It is assumed that no PO_4 is lost during the passage of water through the polar reservoir. The proper depth of distribution of PO_4 achieved using the relationship:

$$R_z = R_1 \exp \left[-\frac{z}{577} \right]$$

where R_1 is the organic residue oxidation in the first box beneath the mixed layer and z is the depth in meters. R_1 is equal to 8.5% of the total settling rate of organic residues from the surface reservoir.

As can be seen in figure 10-15, the natural radiocarbon profile gives a reasonable representation of the horizontally averaged ocean distribution for this isotope. Surface water has a

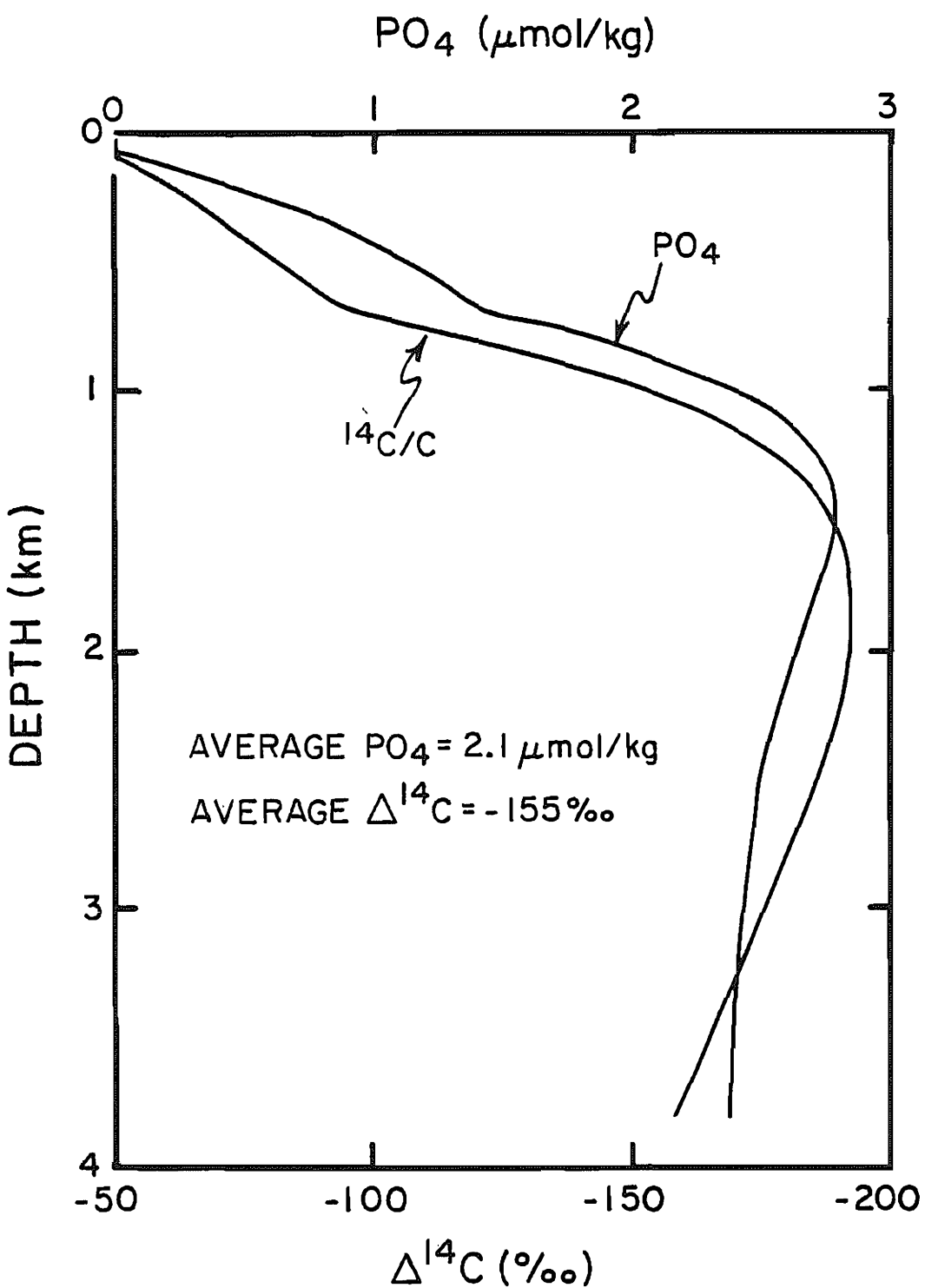


Figure 10-15. Distributions with depth of phosphate and $\Delta^{14}\text{C}$ for the modified Oeschger model described in the text. The parameters used in these calculations are given in the text. These curves are both reasonable approximations of the actual horizontally averaged vertical distributions of these properties.

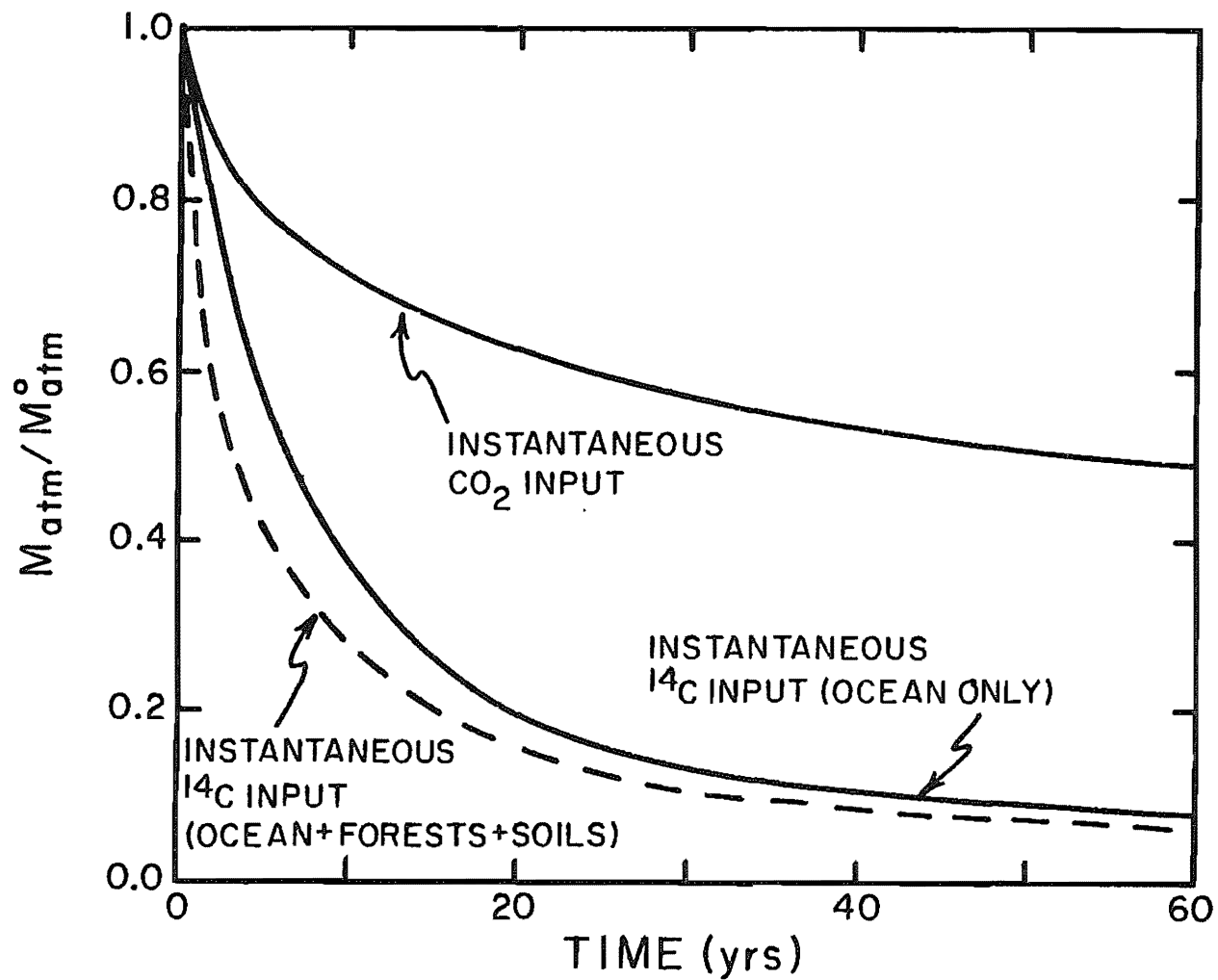


Figure 10-16. The fate of a single sudden input of CO_2 (upper solid curve) and of ^{14}C (lower solid curve) to the atmosphere, as predicted by our modified Oeschger model. The decay of these so-called "delta" functions is represented by the fraction of the amount of the original amount remaining in the air at any given time after the injection. The lower dashed curve shows the decrease in ^{14}C if dilution by the soil and forest reservoirs are included. As these reservoirs will not take up any CO_2 , the upper curve is not altered by the addition of these reservoirs in the model.

$\Delta^{14}\text{C}$ value of $-50^{\circ}/\text{oo}$. The $^{14}\text{C/C}$ value decreases across the main oceanic thermocline reaching a minimum of about $-190^{\circ}/\text{oo}$ at a depth of 2 kilometers. Below this depth it rises, reaching a value of $-160^{\circ}/\text{oo}$ at the model's bottom. The mean $\Delta^{14}\text{C}$ for the model ocean (i.e., $-155^{\circ}/\text{oo}$) is close to that for the real ocean.

The model yields a mean penetration depth for bomb-produced tritium of 374 meters as of 1973. The mean residence time for bomb tritium atoms in the ocean at this time was 9.9 years.

As shown in figure 10-15, the depth profile for PO_4 is a reasonable representation of the horizontally averaged distribution of this property in the sea. Surface water is phosphate free. The PO_4 concentration increases steadily through the thermocline, reaching a maximum of 2.8×10^{-6} moles/kg at a depth of about 1.3 km. The value then drops, reaching about 2.35×10^{-6} moles/kg at the bottom of the model ocean.

The response of this model to instantaneous injections to the atmosphere of bomb radiocarbon and of fossil fuel CO_2 is shown in figure 10-16.

CROSSCHECKS ON THE VALIDITY OF THE NUMERICAL MODEL

Fortunately in fixing the parameters of our one-dimensional ocean model we did not use all the available information. That left over can be used to check the reliability of the model. Four types of information are available for this purpose. First, we have the results of Keeling and his coworkers who have kept track of the CO_2 pressure in the atmosphere from 1958 to present. These long records are available from two places: high on an extinct volcano on the island of Hawaii and on the continent of Antarctica. The Hawaii record is shown in figure 10-17. The CO_2 partial pressure at Mauna Loa shows an increase of 21×10^{-6} atm between 1958 and 1978. It is this difference which provides one of the crosschecks on the model. The modified "Oeschger" model presented above yields an increase over this time interval of 24×10^{-6} atm. The calculation is carried out by stepping the model through time. At the start of the calculation the CO_2 distribution in the system is at steady state. This steady state is perturbed by the year by year addition of excess CO_2 to the model's atmosphere (following the historic sequence as shown in figure 10-1).

We speak of the increase in PCO_2 over this twenty-year period rather than the absolute values because of the uncertainty in the CO_2 concentration in the atmosphere prior to the industrial revolution. Unfortunately, we have no measurements of sufficient accuracy or reliability prior to 1958 to permit the atmospheric record to be extended back in time. Instead, by adjusting the pre-industrial atmospheric CO_2 content, we force the model to yield the atmospheric CO_2 content observed in 1958. This approach is not entirely adequate, because it neglects the contribution of the forest and soil CO_2 .

We can get an idea of the influence of the CO_2 from forests and soils by running the scenario shown in figure 10-2 through the model. As we have as yet not shown why this scenario is to be

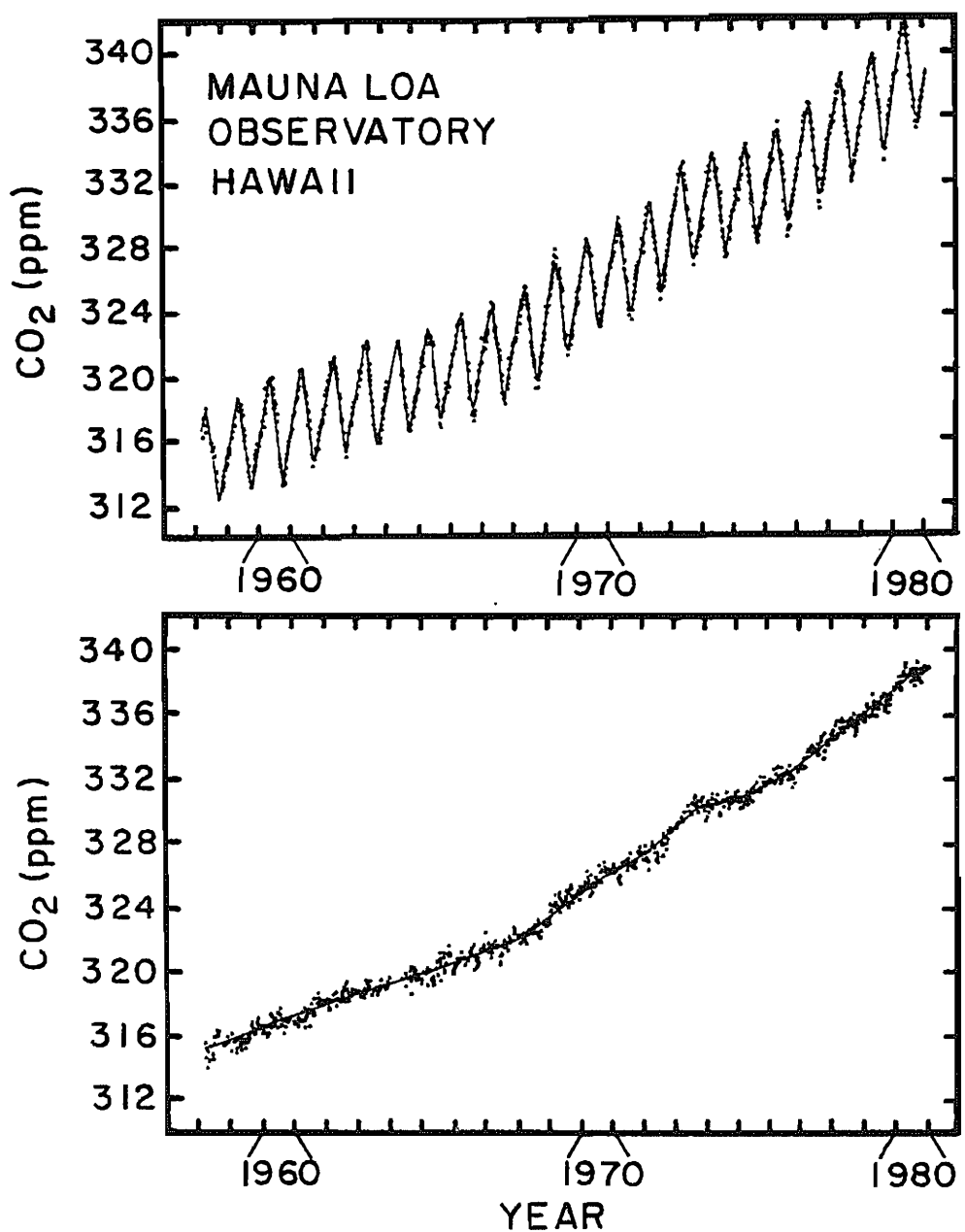


Figure 10-17. Plot of atmospheric CO₂ partial pressure (in dry air) for the period 1958 to 1980 as measured on the island of Hawaii. The upper panels show weekly means. The lower panel shows running means designed to remove the annual cycle. The strong seasonal cycle in the Hawaii record represents seasonal uptake and release of CO₂ by the terrestrial vegetation in the northern hemisphere. The station at Mauna Loa was established by Charles Keeling of Scripps Institution of Oceanography (556,558,562a).

preferred, the reader will have to bear with us until this is done in a few more pages. As can be seen in figure 10-18, the forest plus soil CO₂ input raises the atmospheric CO₂ pressure by 49 x 10⁻⁶ atmospheres as of 1980. However, because of the decline in the input of forest and soil CO₂ over the last 50 years (see figure 10-2), the change in atmospheric CO₂ content produced over the period 1958 to 1978 by the forest and soil CO₂ contribution alone is only about 2 x 10⁻⁶ atm. Hence, while the decline in forest cover and in soil organics has influenced the overall buildup of atmospheric CO₂, it has not played a major role over the 1958 to present period.

When the 2 x 10⁻⁶ atm rise in PCO₂ from forests and soils is added to the 24 x 10⁻⁶ atm rise from fossil fuels, a total of 26 x 10⁻⁶ atm is obtained. This is 20% larger than the 21 x 10⁻⁶ atm increase observed at Mauna Loa during the same interval of time. Thus our model does not take up enough CO₂ to pass this calibration test. Before discussing why this might be the case, let us consider the other crosschecks.

The second potential crosscheck comes from the ¹³C/¹²C record for atmospheric CO₂. As both fossil fuel and biomass carbon have $\delta^{13}\text{C}$ values averaging -26‰ (compared to that of about -6‰ for the preindustrial atmosphere), the addition of excess CO₂ to the atmosphere from these sources should have driven down the ¹³C/¹²C ratio in atmospheric CO₂. As is the case for the CO₂ content of the atmosphere, the magnitude of the atmospheric ¹³C change will depend on the amount of CO₂ released and on the extent to which this CO₂ has equilibrated with ocean carbon. There is, however, a difference in the CO₂ pressure response and the ¹³C/¹²C ratio response. Any atmospheric carbon isotope anomaly will eventually be diluted in accord with the ratio of ocean carbon to atmosphere carbon (i.e., about 60). As we have seen the corresponding reduction for fossil fuel CO₂ with the ocean after full equilibration will only be one-tenth as large (i.e., about 6). Further, the carbon in living biomass and in soils will also dilute the carbon isotope anomalies. On the other hand, these reservoirs will not take up a significant amount of the excess CO₂.

The living biosphere and soil reservoirs are incorporated into the model as follows. We take the mass of living biosphere carbon to be equal to that in the preindustrial atmosphere (i.e., 50 x 10¹⁵ moles) and that of soil carbon to be three times that in the preindustrial atmosphere (i.e., 150 x 10¹⁵ moles). We assume that 30% of the living biosphere consists of leaves, rootlets, and small plants which are replaced annually. The remaining living biosphere is assumed to be wood. Half is given a replacement time of 20 years and the other half a replacement time of 100 years. We assume that soil carbon is replaced on a 250-year time scale. The difference in isotope effects between the models run with and without the biospheric reservoirs is about 20% (see figure 10-16).

We can get an idea of the expected size of the ¹³C anomaly as follows. As of 1978 the amount of fossil fuel carbon released to the atmosphere was equal to 25% of the amount of CO₂ in the preindustrial atmosphere. A mixture of 100 units of carbon with

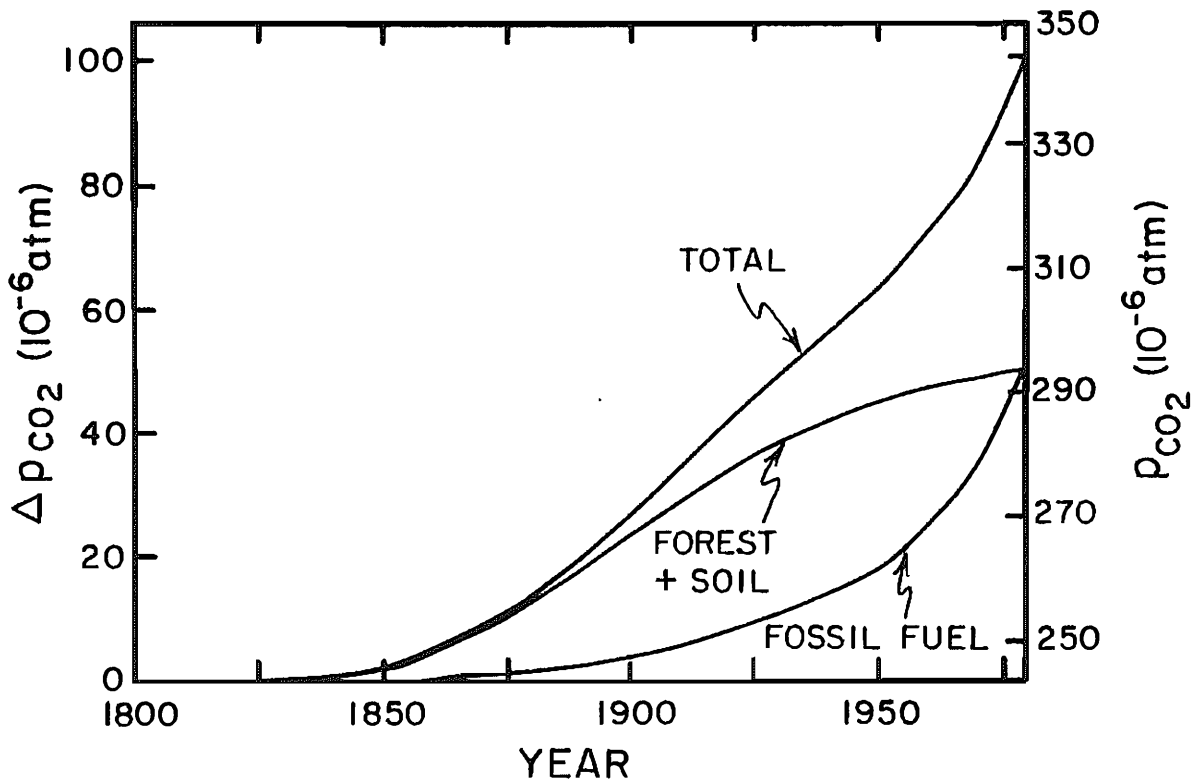


Figure 10-18. Atmospheric CO_2 partial pressure reconstruction made with the modified Oeschger ocean model described in the text. Both fossil fuel CO_2 (as estimated from historic records) and forest - soil CO_2 (as given in the scenario of figure 10-2) were input to the model. The contributions of the two CO_2 sources are shown separately. The curve for the total is constrained to go through the value of 315×10^{-6} atmospheres obtained by Keeling and his coworkers for the year 1958.

a $\delta^{13}\text{C}$ of $-6^\circ/\text{oo}$ (the preanthropogenic value for atmospheric CO_2) and 25 units with a $\delta^{13}\text{C}$ of $-26^\circ/\text{oo}$ (the value for mean fossil fuel and terrestrial biosphere CO_2) would have a $\delta^{13}\text{C}$ of $-10^\circ/\text{oo}$. Thus in the absence of any dilution with carbon from other reservoirs the atmosphere would have decreased in its $\delta^{13}\text{C}$ value by $4^\circ/\text{oo}$ from the fossil fuel CO_2 contribution alone. The model is run for ^{13}C the same way as it is for CO_2 . Fossil fuel CO_2 and forest and soil CO_2 are added to the model atmosphere in a series of time steps. Mixing of carbon between the atmosphere and ocean occurs diluting the atmospheric ^{13}C anomaly generated by these anthropogenic additions.

Our model, when run for fossil fuel CO_2 alone, predicts a $\delta^{13}\text{C}$ drop of $0.58^\circ/\text{oo}$. When the forest-soil scenario of figure 10-2 is included, this result decreases to $0.51^\circ/\text{oo}$. In this case the continuing dilution of the earlier large forest and soil input more than compensates for the current release of CO_2 from these sources. The earliest accurate $^{13}\text{C}/^{12}\text{C}$ ratios made on atmospheric CO_2 samples were carried out during the mid-1950's. Keeling, who conducted these early measurements, provided samples collected during 1978 to Mook of the Groningen Laboratory in the Netherlands for comparison analyses. They concluded from this effort that the $\delta^{13}\text{C}$ dropped by $0.55^\circ/\text{oo}$ between 1956 and 1978. As the uncertainty in the atmospheric change over the 1956 to 1976 period is probably of the order of $0.15^\circ/\text{oo}$, the agreement between observation and prediction is adequate.

It is now time to show how we obtained the forest-soil scenario in figure 10-2. It was derived from a consideration of an extended atmospheric ^{13}C record obtained by measurements on the cellulose from tree rings. The idea behind this approach is that even though there is a large fractionation between cellulose ($-26^\circ/\text{oo}$) and atmospheric CO_2 ($-6^\circ/\text{oo}$), the mean $\delta^{13}\text{C}$ in cellulose must change with changing atmospheric $\delta^{13}\text{C}$. The question is whether this message can be separated from other sources of variation.*

Freyer at the KFA in Julich, West Germany has conducted extensive research on the $^{13}\text{C}/^{12}\text{C}$ record kept in tree rings. After finding that trees growing within forests did not give the expected trend, Freyer concentrated his efforts on solitary trees. He obtained such trees from the French Atlantic coast, from the Spanish Pyrenees, from North Carolina in the U.S., from the Eifel and Black Forest in West Germany and from northern Sweden and Norway. The results on the Swedish Scots pines, which go back to 1530, suggest that the atmospheric $^{13}\text{C}/^{12}\text{C}$ ratio was quite constant

*Climatic changes will alter conditions at the leaf surface and hence change the magnitude of the isotope fractionation which occurs during photosynthesis. Canopy effects are produced by the passage through the canopy of the CO_2 produced by the decay of vegetation in the soils beneath the trees. Reincorporation of this ^{13}C depleted CO_2 would further reduce the $^{13}\text{C}/^{12}\text{C}$ ratio in the forming cellulose. Thus changes in the geometry of the canopy due to growth and death of neighboring trees and due to the growth of the tree of interest could lead to changes in the isotopic composition of the cellulose formed in the tree.

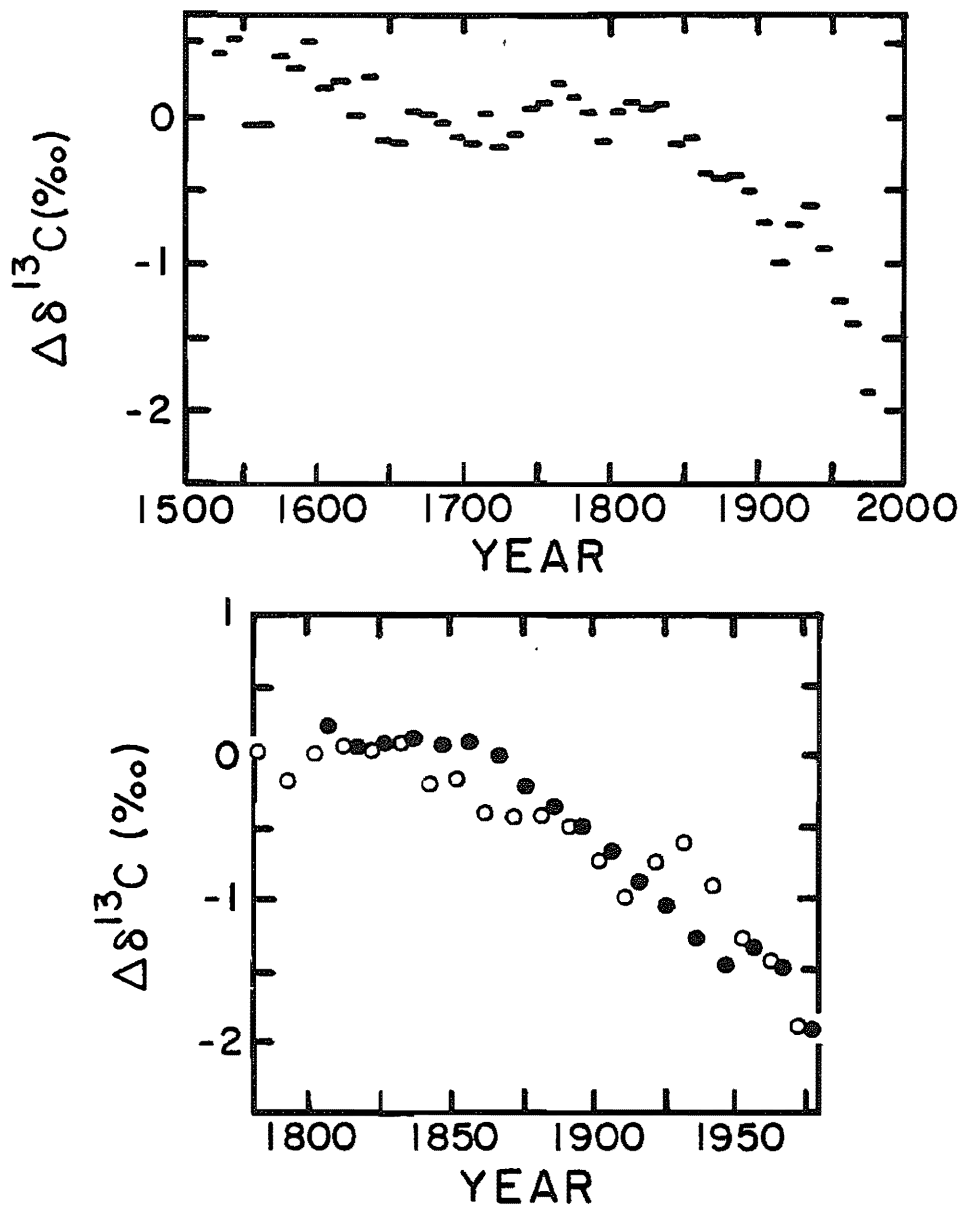


Figure 10-19. Average trend for the last 500 years in atmospheric $^{13}\text{C}/^{12}\text{C}$ ratios as estimated from measurements on solitary Scots pine trees from northern Sweden and Norway (upper panel). Comparison of the Scots pine record (open circles) with the average record established from measurements on trees from the Pyrenees, the west coast of France, North Carolina, and the Eifel and Black Forests in Germany (closed circles). These measurements were made by Freyer and his colleagues at KFA in Julich, West Germany (574).

prior to 1830 (see figure 10-19). Between 1830 and 1970, a drop of $1.8^{\circ}/\text{oo}$ occurred. Also shown in this figure is a comparison for the last 200 years of the Scots pine record with the mean trend from the other areas mentioned above. As can be seen, the agreement is quite good.

Before interpreting this record, it must be pointed out that other workers have not been so successful in finding trees that give smooth records. Stuiver of the University of Washington has studied solitary trees from sites along the west coast of the Americas and Francey of Australia has studied trees from Tasmania. Neither has found the trend obtained by Freyer. Their records show considerable variability on time scales of 100 years and less. Freyer himself was of course not able to find the expected records in Spessart oak trees from forests in Germany. Until the reasons for these differences between species of trees and growth sites is understood, the assumption that Freyer's records represent the decline in atmospheric $\delta^{13}\text{C}$ rests on shaky ground. Nevertheless, we will proceed on the assumption that Freyer's curve is a valid representation of the atmospheric record.

Shown in figure 10-20 are the model results* for the input of fossil fuel CO_2 alone, for the input of forest-soil CO_2 alone and for the sum of these two inputs. As can be seen by comparisons with Freyer's results (black circles in figure 10-20), the fossil fuel effect alone yields only half the amplitude and differs considerably in shape from the tree-ring-based atmospheric record. If the difference between the tree-ring-based curve and the fossil fuel CO_2 curve yielded by the model is ascribed to the addition of the forest and soil CO_2 in the atmosphere, then an input function for this CO_2 can be constructed which, when combined with the fossil fuel CO_2 input curve, will yield the tree-ring-based curve. This is the origin of the scenario in figure 10-2. As shown in figure 10-20, the combined forest-soil and fossil-fuel input yields a $\delta^{13}\text{C}$ record in accord with Freyer's $\delta^{13}\text{C}$ record.

A possible crosscheck on this forest + soil scenario would be to reconstruct the $\delta^{13}\text{C}$ record in the surface ocean using measurements on ring-dated corals. The trends expected from fossil fuel CO_2 alone and from the combination of fossil fuel CO_2 and forest-soil CO_2 is shown in figure 10-21. The single record available to date (i.e., that on a Bermuda coral) is shown for comparison.

When faced with our forest scenario, Mook of the Netherlands made an interesting observation. He pointed out that the $\delta^{13}\text{C}$ values for the surface ocean as of 1973 (see figure 6-12) showed the ocean as a whole to be nearly at steady state with the atmosphere. He asked if our combined forest-soil and fossil fuel scenario would disrupt this steady state (i.e., would the surface ocean and the atmosphere have been at stable carbon isotope steady state prior to 1850). As shown diagrammatically in figure 10-22, if anything, the agreement would have been better at this time.

*In these calculations we use the kinetic fractionation factor for CO_2 invading the sea of $2^{\circ}/\text{oo}$ suggested by Siegenthaler and Munnich rather than that of $14^{\circ}/\text{oo}$ observed for CO_2 uptake into strong alkali solutions.

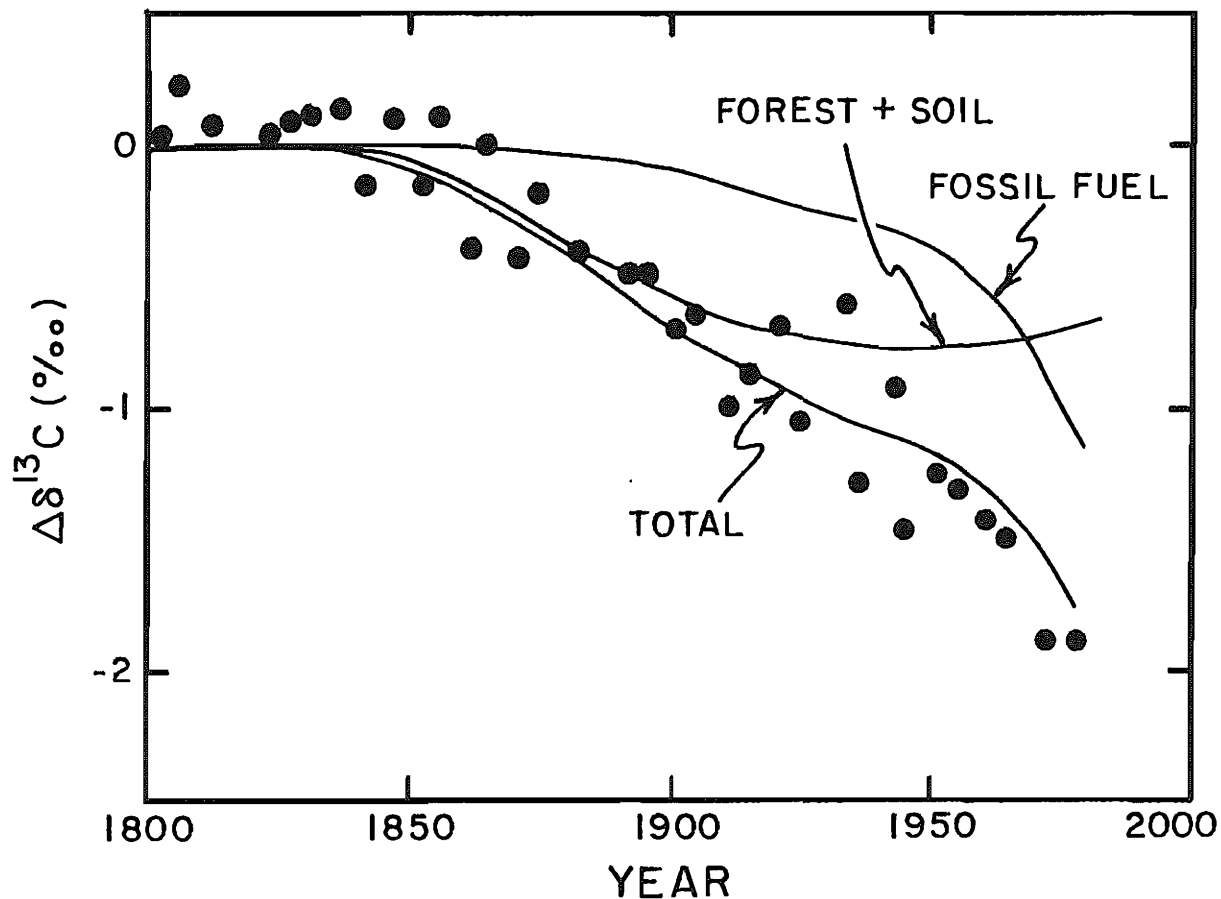


Figure 10-20. Atmospheric $\delta^{13}\text{C}$ response calculated using the modified Oeschger model described in the text. As for the CO_2 partial pressure reconstruction, both the contributions of fossil fuel CO_2 and forest-soil CO_2 are included in the calculation. The contributions of the two sources are given separately. As was the case for CO_2 partial pressure the slope over the last 20 years is not strongly influenced by forest-soil inputs. The trend established through Freyer's tree-ring measurements is shown for comparison.

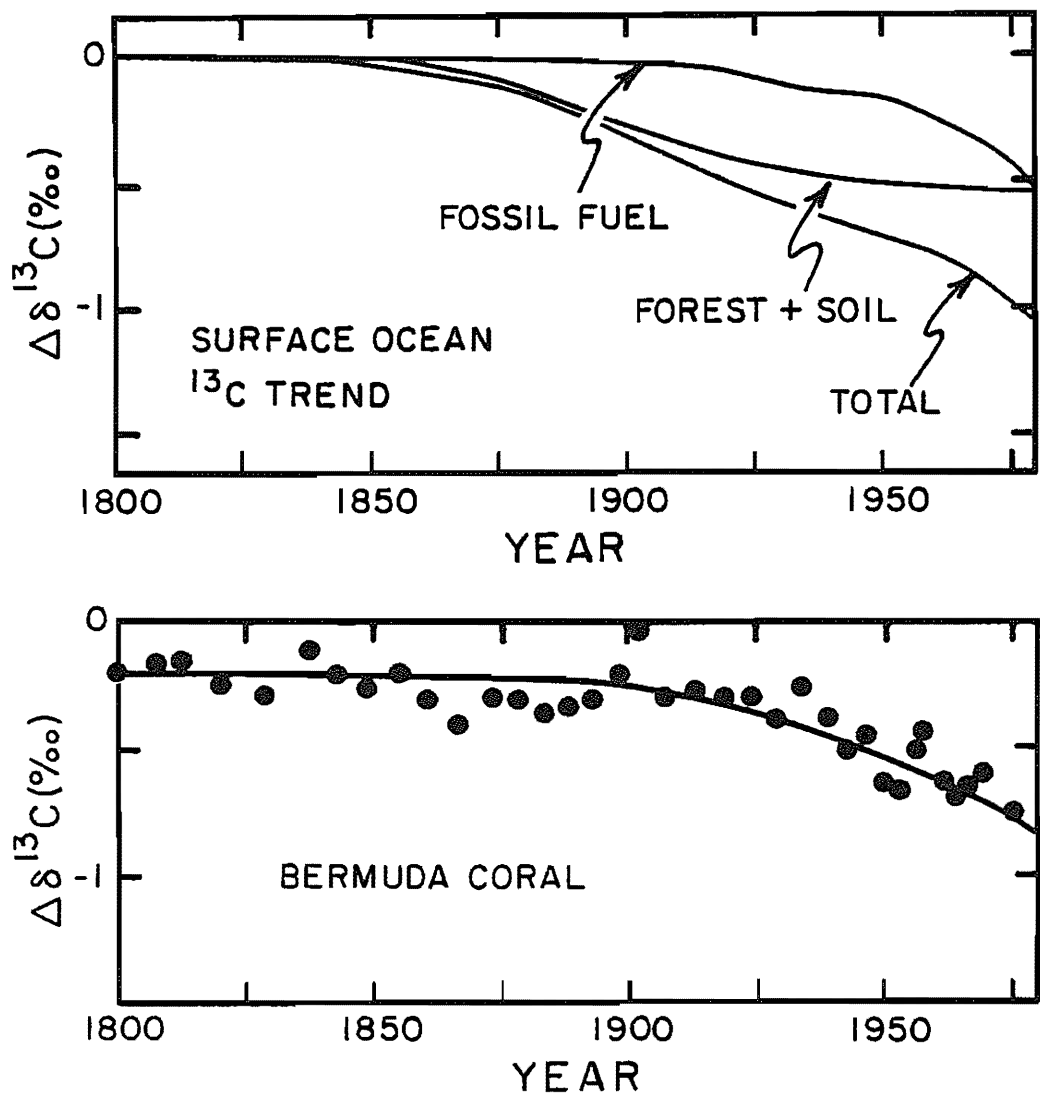


Figure 10-21. The change in the $\delta^{13}\text{C}$ for average surface ocean water as calculated using the modified Oeschger model described in the text. The contributions of fossil fuel CO_2 and forest-soil releases are shown separately. In the lower panel the results obtained by Nozaki and his associates at Yale University on a Bermuda coral (14) are shown for comparison.

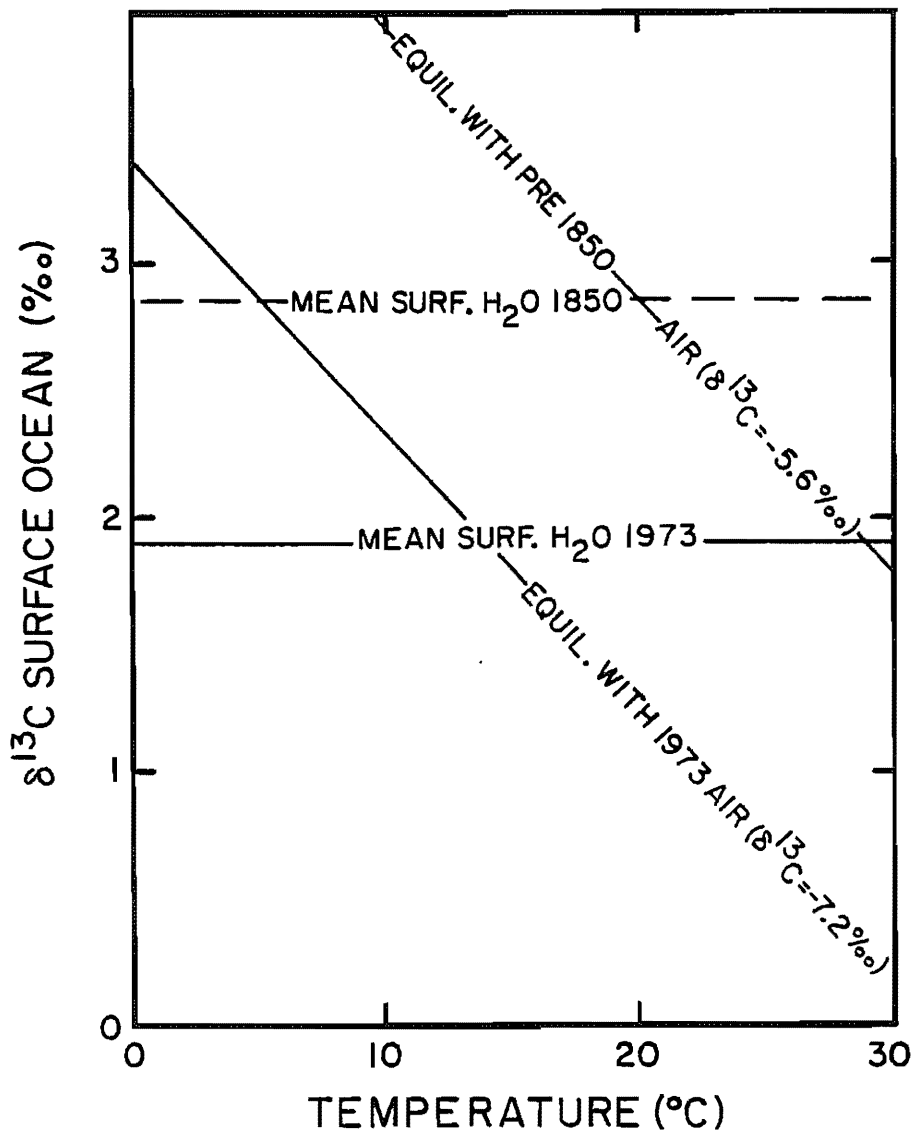


Figure 10-22. Diagrammatic representation of the relationship between the $\delta^{13}\text{C}$ for surface water carbon and temperature as measured in 1973 (see figure 6-12 for data) and the $\delta^{13}\text{C}$ which surface water carbon would have had were it at equilibrium with the 1973 atmosphere ($\delta^{13}\text{C} = -7.2\text{\textperthousand}$). Also shown are the surface water $\delta^{13}\text{C}$ averages reconstructed for the period before the impacts of man (the combined forest-soil and the fossil fuel CO₂ input yielded a drop of 0.95 \textperthousand in the model's surface ocean between 1850 and 1973). Finally, the $\delta^{13}\text{C}$ values for ocean water at equilibrium with the pre-1850 atmosphere ($\delta^{13}\text{C} = -5.6\%$) is shown. The 1.6 \textperthousand decrease in $\delta^{13}\text{C}$ for atmospheric CO₂ between 1850 and 1973 is that obtained from the model. While individual areas of the ocean were not at isotope equilibrium with the air the sea surface as a whole must have been at steady state prior to the year 1800.

Our model suggests that the $\delta^{13}\text{C}$ for average surface ocean water was $0.95^{\circ}/\text{oo}$ higher prior to 1850 than it was in 1973 and that the $\delta^{13}\text{C}$ for the atmosphere was $1.6^{\circ}/\text{oo}$ higher. Making these corrections, the crossover between the equilibrium curve comes at 20°C as opposed to 14°C in 1973. As the mean surface ocean temperature is 18°C , the pre-1850 situation is, if anything, an improvement. While this cannot be taken as support for the forest hypothesis, at least it does not lead to difficulties in this regard.

The third crosscheck comes from the decrease in the atmospheric $^{14}\text{C/C}$ ratio between 1860 and 1950. As fossil fuels carry no ^{14}C , input of CO_2 from this source lowers the atmospheric ratio. On the other hand, forest and soil carbon have $^{14}\text{C/C}$ ratios reasonably close to the atmospheric value, hence input of CO_2 from this source would have no significant effect on the atmospheric $^{14}\text{C/C}$ ratio. We must terminate this comparison in 1950, because soon thereafter the input of bomb ^{14}C to the atmosphere became significant. Were no mixing of atmospheric, ocean and biosphere carbon occurring, then a decrease in $^{14}\text{C}/^{12}\text{C}$ ratio of 10% would be expected. The atmospheric $^{14}\text{C/C}$ record is preserved in tree rings, and in this case the small changes in the fractionation factor, which bedevil the ^{13}C reconstructions, have no significant effect. The measurements of Stuiver of the University of Washington on tree rings from 1860 to 1950 are shown in figure 10-23. A 2% decline is found between 1850 and 1950. Also shown in this figure are the trends predicted by our modified Oeschger model. The agreement is excellent.

In comparing the observations with the model curves, it must be kept in mind that during the period of the $^{14}\text{C/C}$ decline, changes in the production of ^{14}C similar to those which affected the $^{14}\text{C}/^{12}\text{C}$ ratio of the atmosphere prior to 1850 (see figure 7-32) must also have been operative. Minze Stuiver, working with his associate Paul Quay, has developed a relationship between sunspot activity and ^{14}C production which accounts for much of the variability in the $^{14}\text{C}/^{12}\text{C}$ ratio for atmospheric CO_2 for preindustrial times (19). Based on the record of solar activity between 1850 and the present these investigators have reconstructed the cosmic ray production of ^{14}C over the past 100 years. They conclude these changes have led to a decline in the natural $^{14}\text{C/C}$ ratio of about $3.0^{\circ}/\text{oo}$ during the last century. They recommend that this amount be deducted from the observed change when looking for the change due to fossil fuel CO_2 . Thus the fossil fuel CO_2 induced decrease between 1850 and 1950 appears to have been about $18^{\circ}/\text{oo}$. As can be seen from figure 10-23, the model predicts a slightly larger change. However, because of the uncertainty in the correction for the variability in the cosmic ray production rate, the agreement between the observed and model curves is adequate.

The surface ocean should also show a Suess effect due to the addition of CO_2 free of ^{14}C . As shown in figure 10-24, the model predicts an $8^{\circ}/\text{oo}$ between 1850 and 1950. The reader is referred to figure 7-34 which shows the results on corals. While an effect of about the right magnitude is seen, the experimental errors on the measurements are too large to yield a meaningful test of the

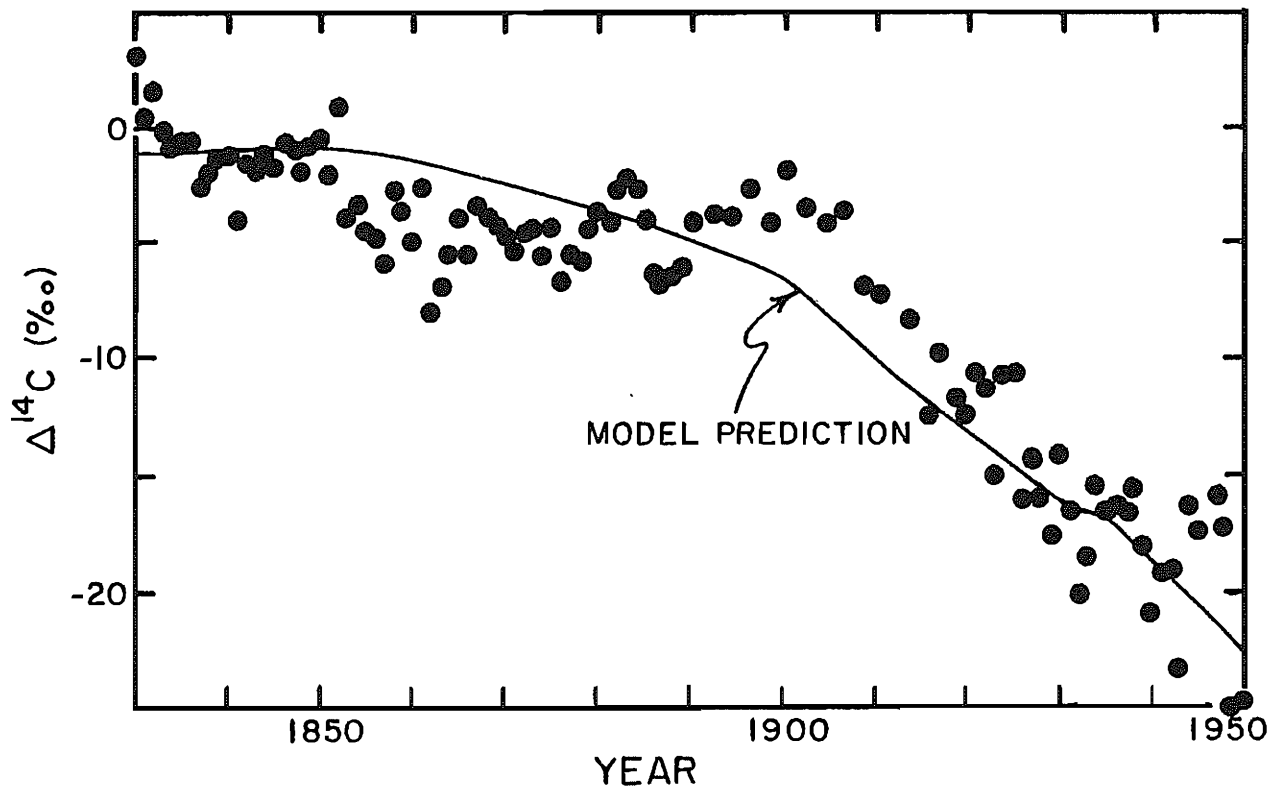


Figure 10-23. Comparison of the model derived $\Delta^{14}\text{C}$ decrease caused by the addition of ^{14}C -free fossil fuel CO_2 to the atmosphere (i.e., the Suess effect) with the measurements of Stuiver of the University of Washington on tree rings covering the period 1800 to 1950 (26).

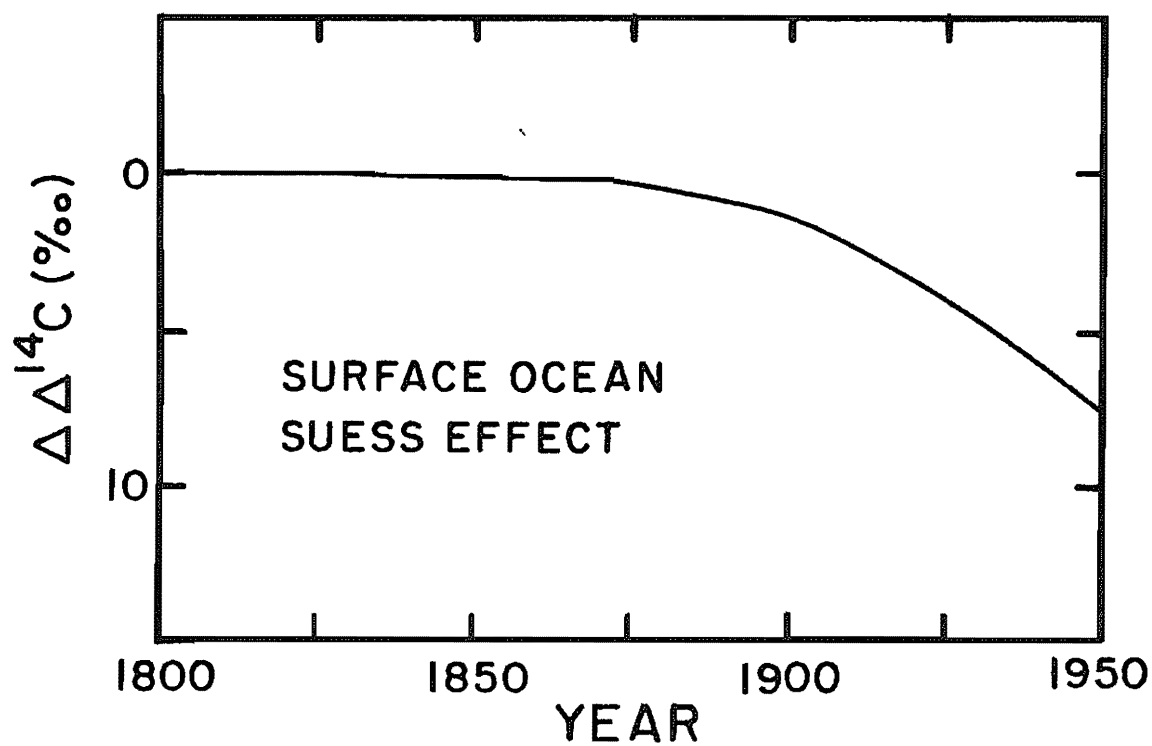


Figure 10-24. Model calculation of the $\Delta^{14}\text{C}$ reduction expected for surface ocean carbon due to the addition of ^{14}C -free fossil fuel CO_2 to the atmosphere.

model.

The fourth and last of the crosschecks comes from measurements of the distribution of the ^{14}C produced during bomb testing. In particular we are interested in comparing the distribution of the ^{14}C between the atmosphere and the sea predicted by the models with that observed at the time of the GEOSECS program. The amount of bomb- ^{14}C in the ocean at the time of the survey can be estimated from the water column inventory data discussed in chapter 8. As summarized in table 10-5, $314 \pm 35 \times 10^{26}$ atoms were in the sea as of 1973.

Our model is then run using the observed atmospheric $\Delta^{14}\text{C}$ curve from 1950 to 1973 (see figure 8-3) to predict the number of bomb ^{14}C atoms taken up by the ocean. In this case the atmospheric $^{14}\text{C/C}$ ratio measured in atmospheric CO_2 samples taken over the time interval 1955 to present is used for the calculation rather than the rate at which bomb ^{14}C atoms were added to the atmosphere. For 1973 the model gives 302×10^{26} bomb ^{14}C atoms in the ocean. The agreement between the predicted and observed values is excellent!

This same ocean uptake could be achieved with several different combinations of gas exchange and vertical mixing rate. To see if we have the right combination another check can be performed. The average excess $\Delta^{14}\text{C}$ for surface water in 1973 can be compared to the model calculated value. If, for example, our gas exchange rate were too high and our vertical mixing rate too low, we could get the right bomb ^{14}C inventory but too high a surface water excess. The $\Delta^{14}\text{C}$ increase (over natural levels) for surface water as measured during the GEOSECS program is summarized in table 10-6. The average is $160 \pm 15\%$. Our model yields a prediction of 172% in satisfactory agreement with observed value.

In summary, then our model satisfactorily predicts the carbon isotope anomalies due to fossil fuel CO_2 release and due to the invasion of bomb- ^{14}C into the ocean. On the other hand, it seems to underpredict the uptake of fossil fuel CO_2 by the oceans. This apparent disagreement between isotopic and chemical response may stem from the one-dimensional character of the model. To understand why this is the case we must turn our thoughts back to the outcropping isopycnals of chapter 8. An alternate model could be made which would permit entry to the main thermocline directly from these outcrops. This model could then be calibrated so that it gave the right distribution of natural radiocarbon, the right Suess effect and the right bomb- ^{14}C inventory and bomb- ^{14}C excess in surface water. When such a model is run for fossil fuel CO_2 uptake, it will likely yield a greater ocean uptake than would be obtained by the model used here. The reason is that the resistance to entry through the outcrops is greater for ^{14}C than for CO_2 (remember we showed in chapter 3 that the equilibration time for CO_2 was an order of magnitude shorter than that for carbon isotopes). Siegenthaler of Bern (699) has done some preliminary calculations designed to get some idea of the magnitude of this enhancement. Their results show that as much as 20% more CO_2 would be transferred into the sea. If so, the discrepancy noted above for CO_2 uptake would be largely

Table 10-5. Summary of the bomb- ^{14}C inventories for various zones of the ocean (as of 1973). Based on measurements made by Stuiver of the University of Washington and Ostlund of the University of Miami (21,22).

	Atl.	Pac.	Mean Global 10^9 atoms/cm 2	Frac. Ocean Area	Excess ^{14}C 10^{26} atoms
Antarctic ($>45^\circ\text{S}$)	~5	~9	~7	0.167	~40
S. Temp. ($45^\circ\text{S}-15^\circ\text{S}$)	9.5	9.7	9.6	0.264	92
Equator ($15^\circ\text{S}-15^\circ\text{N}$)	3.3	5.4	5.0	0.281	51
N. Temp. ($15^\circ\text{N}-45^\circ\text{N}$)	15.3	14.2	14.6	0.192	101
N. Pac. ($>45^\circ\text{N}$)		~6	—	0.028	~ 6
N. Atl. ($>45^\circ\text{N}$)	18.6	—	—	0.036	19
Arctic Ocean	—	—	~4	0.032	~ 5
					<u>314 ± 35</u>

Table 10-6. Summary of surface bomb- ^{14}C excesses for surface waters (as of 1973). Based on measurements made by Stuiver at the University of Washington and Ostlund of the University of Miami as part of the GEOSECS program (21,22).

Region	No. of Stns.	GEOSECS $\Delta^{14}\text{C}$ ‰/‰	Prenuclear $\Delta^{14}\text{C}$ ‰/‰	Excess $\Delta^{14}\text{C}$ ‰/‰
ATLANTIC				
N. Polar	8	50	-70	120
N. Temp.	8	145	-50	195
Equa.	6	85	-65	150
S. Temp.	6	126	-50	176
Antarctic	6	-	-	~100
PACIFIC				
N. Polar	4	-	-	~130
N. Temp.	15	163	-50	213
Equa.	5	61	-70	131
S. Temp.	7	141	-50	191
Antarctic	4	-	-	~115
WHOLE OCEAN				
N. Polar	(0.096)*			125
N. Temp.	(0.192)*			205
Equa.	(0.281)*			140
S. Temp.	(0.264)*			185
Antarctic	(0.169)*			110
Mean				<u>160±15</u>

*Fraction of ocean area

removed. It will be a long time, however, before we know enough about the ocean to permit reliable 2-D modeling.

PREDICTION OF FUTURE CO₂ LEVELS

Keeping in mind that our 1-D model may slightly underestimate the uptake by the sea of fossil fuel CO₂, let us use it to predict future atmospheric CO₂ pressures for a variety of scenarios. Our first effort in this regard will be to look at the next 80 years (i.e., 1980 to 2060). As shown in figure 10-12, in so doing we are not making long extrapolations from the time scales for the tracers used to calibrate and test the model. Even if on the average we produce over the next 80 years the same annual amount of fossil fuel CO₂ as we did in 1980, the mean age of the CO₂ molecules will not exceed 60 years. On this time scale they should penetrate only about twice as far into the sea as had tritium at the time of the Atlantic and Pacific GEOSECS surveys.

In making these calculations we raise the rate of CO₂ invasion into the ocean in accord with the CO₂ pressure in the atmosphere, i.e.,

$$I = 17.5 \frac{p_{CO_2}}{280 \times 10^{-6}} \text{ moles/m}^2 \text{ year}$$

We also change the Revelle factor as the CO₃⁼ ion content of the model's surface reservoirs falls.

Four cases have been considered. Man's production of CO₂ is assumed to increase at rates of 3%/yr, 2%/yr, 1%/yr, and 0%/yr. The calculation is begun in 1980. At this time the model has the characteristics achieved at the end of our combined fossil fuel forest CO₂ scenario. The results are portrayed on a plot of mean age of CO₂ versus total amount of CO₂ produced (see figure 10-25). As can be seen, the predicted pCO₂ depends mainly on the amount of CO₂ produced.

The question comes to mind why the atmospheric CO₂ content is so insensitive to the time history of the input. To see why this is the case let us compare the two points on figure 10-25. One is for the no-growth scenario in the year 2060. The other is for the 3%-growth scenario within the year 2020. For both points the CO₂ input is about 4.8×10^{16} moles. The atmospheric pCO₂ for the no-growth point is 450×10^{-6} atmospheres. For the 3%/yr growth it is 475×10^{-6} atm. The excess pCO₂ over that in 1980 (340×10^{-6}) is 110×10^{-6} atm for the 0%/yr point and 135×10^{-6} atm for the 3%/yr point. The difference in mean CO₂ age (and hence in ocean residence time) for the two cases is a factor of two. Hence the penetration depth difference should be the square root of two. As in both situations roughly twice as much CO₂ remains in the air as it enters the sea, an increase of 1.41 in the ocean uptake will lead to only an 0.80 decrease in the extent of atmospheric buildup. This agrees with the actual reduction given by the model (i.e., 110/135). Thus we see that at least within the context of our model extrapolation to the future can be done quite reliably using figure 10-25. Any scenario (exponential or otherwise) yielding a mean residence time in the range 30 to 60 years,

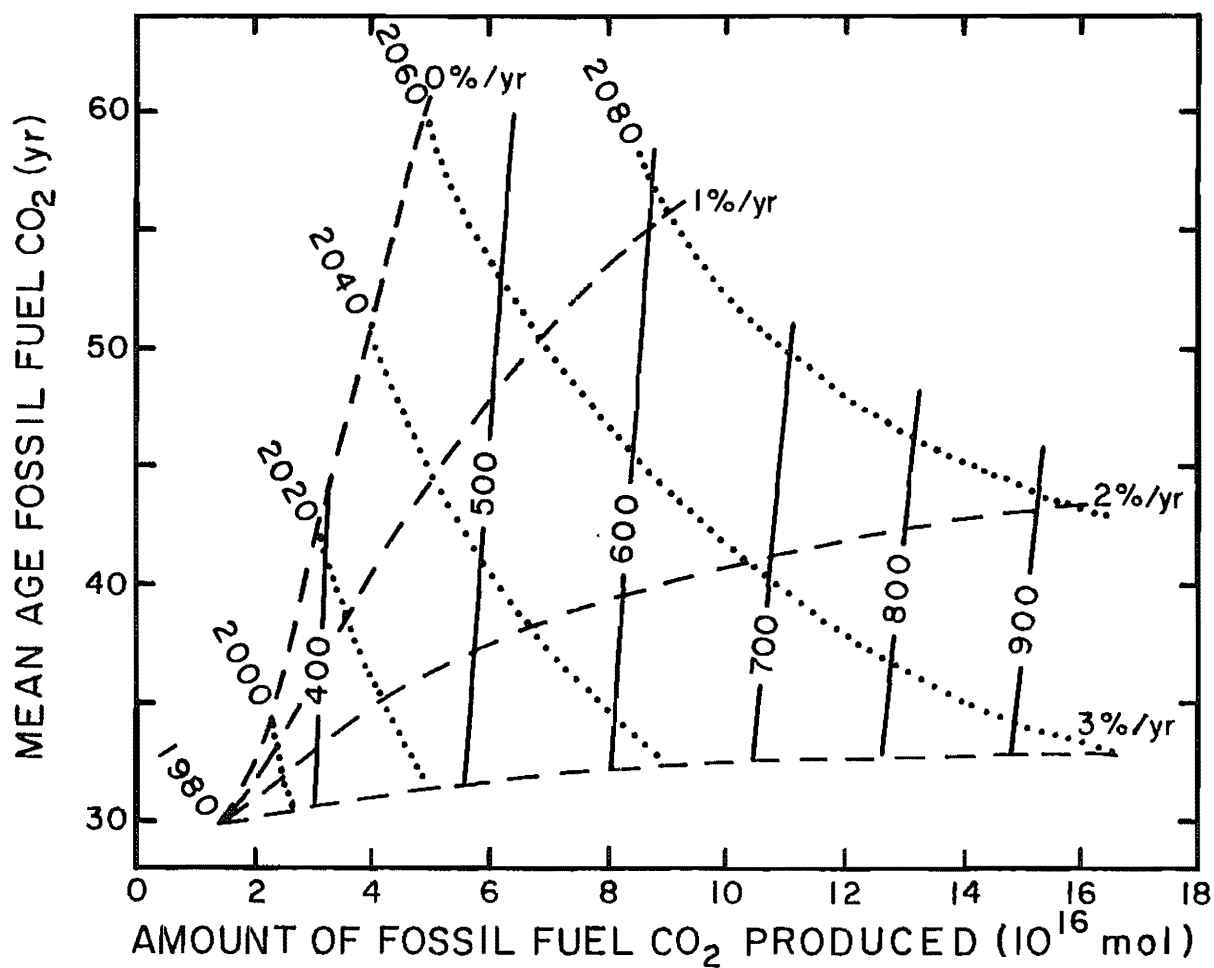


Figure 10-25. Contours of CO_2 partial pressure predicted for the future as a function of the mean age of fossil fuel CO_2 molecules and of the total amount of fossil fuel CO_2 generated. These contours were computed by inputting to the model CO_2 scenarios involving 0, 1, 2, and 3%/year growth rates for fossil fuel CO_2 emissions. The traverses for each scenario are shown by the dashed lines. Time lines (dotted) are shown. While the scenarios used to construct the diagram are based on exponential growth, these diagrams are also applicable to more complicated scenarios yielding mean age - total production combinations falling within the field of the diagram.

the $p\text{CO}_2$ read from this graph should agree within 2% of that calculated by running this particular scenario through the model.

We must hasten to add that this should not be taken to mean that the predictions given here are accurate to 2%. As mentioned above, the model itself is not entirely adequate. While matching the isotope effects, the model ocean appears to take up less CO_2 than it should. A model which satisfies the isotope constraints and fit the CO_2 rise over the period 1958 to 1978 would predict CO_2 increases in the atmosphere over the 1980 level somewhat lower than those shown in figure 10-25.

As an example of what might happen on a longer time scale we have run the fossil fuel use scenario shown in figure 10-26. In this scenario we assume that fossil fuel use will continue to rise until the latter part of the next century at which point it will reach a value of about 2.5 times its present value. After that the usage is assumed to fall returning to the present level in about the year 2220. As of the year 2300 about two thirds of the present reserves are assumed to have been consumed. While quite arbitrary in its construction this scenario is not unreasonable.

The atmospheric CO_2 pressures predicted using this scenario (see figure 10-26) continue to rise for more than a century after the peak in fossil fuel CO_2 usage and then levels off at just over 900×10^{-6} atmospheres.

Shown in table 10-7 are the carbonate ion contents of surface water and the isotopic compositions of atmospheric CO_2 for this scenario. The carbonate ion content of surface water decreases by a factor of two between 1980 and 2300. The $\delta^{13}\text{C}$ value reaches a minimum in about 2175 and then slowly rises. Finally the $\Delta^{14}\text{C}$ value drops below its prenuclear value reaching a minimum in the year 2200. After that it begins to rise.

SOLUTION OF SEA FLOOR CALCITE

A calculation similar to the simplified one we did for the atmosphere-sea equilibrium can be carried out for equilibrium between air, sea and the calcite in marine sediments. The equilibrium equation for reaction 10-2 is as follows:

$$\alpha K = \frac{[\text{Ca}^{++}] [\text{HCO}_3^-]^2}{\text{pCO}_2} \quad 10-30$$

Since the amount of Ca^{++} in the ocean is about 5 times higher than the amount of HCO_3^- , as an approximation, Ca^{++} can be assumed to remain constant. Hence:

$$\frac{[\text{HCO}_3^-]}{[\text{HCO}_3^-]^\circ} \approx \sqrt{\frac{\text{pCO}_2}{\text{p}^\circ \text{CO}_2}} \quad 10-31$$

As most of the carbon dissolved in the sea is in the form of bicarbonate ion we get:

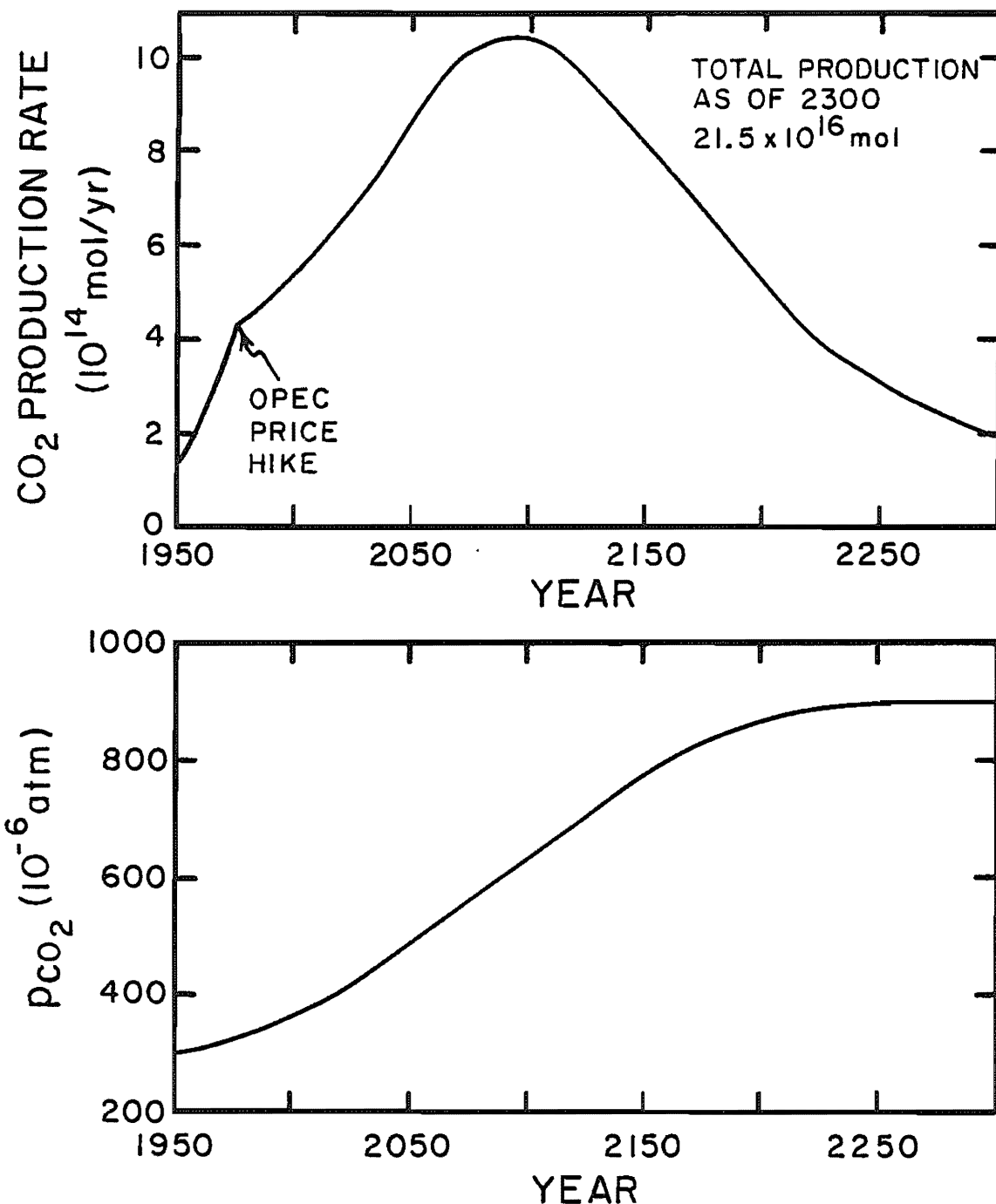


Figure 10-26. Possible fossil fuel use scenario to the year 2300 (upper panel) and the atmospheric CO₂ partial pressures calculated for this scenario using the model discussed in the text.

Table 10-7. Changes in the carbonate ion content of surface ocean water and in the $\delta^{13}\text{C}$ and $\Delta^{14}\text{C}$ values for atmospheric CO_2 associated with the fossil fuel use scenario shown in figure 10-26.

Year	Total Fossil Fuel CO_2 Production 10^{16} moles	pCO_2 Atm 10^{-6} atm	Surf Water $[\text{CO}_3^{=}]$ 10^{-6} moles kg	$\delta^{13}\text{C}$ Atm CO_2 ‰	$\Delta^{14}\text{C}$ Atm CO_2 ‰
1800	0.0	249	253	-5.6	0
1950	0.5	308	226	-6.8	-24
1980	1.4	340	212	-7.3	285
2000	2.3	369	202	-7.6	95
2050	5.7	470	172	-8.6	-36
2100	10.7	632	138	-9.6	-111
2150	15.3	778	118	-10.0	-141
2200	18.6	864	108	-10.0	-147
2250	20.5	900	104	-9.7	-143
2300	21.5	904	104	-9.5	-135

$$\frac{[\Sigma\text{CO}_2]}{[\Sigma\text{CO}_2]^\circ} \approx \frac{[\text{HCO}_3^-]}{[\text{HCO}_3^-]^\circ} \approx \sqrt{\frac{p\text{CO}_2}{p^\circ\text{CO}_2}}$$

10-32

The Keeling fraction can be written as:

$$f_K = \frac{\left[\frac{p\text{CO}_2 - p^\circ\text{CO}_2}{p^\circ\text{CO}_2} \right] M^\circ \text{atm}}{\left[\frac{p\text{CO}_2 - p^\circ\text{CO}_2}{p^\circ\text{CO}_2} \right] M^\circ \text{atm} + \left[\frac{[\Sigma\text{CO}_2] - [\Sigma\text{CO}_2]^\circ}{[\Sigma\text{CO}_2]^\circ} \right] M^\circ \text{ocean}} \quad 10-33$$

Substituting the approximate relationship between $p\text{CO}_2$ and ΣCO_2 in equation 10-32, we obtain the following relationship:

$$f_K = \frac{1}{1 + \frac{280}{5} \left[\frac{\sqrt{\frac{p\text{CO}_2}{p^\circ\text{CO}_2}} - 1}{\frac{p\text{CO}_2}{p^\circ\text{CO}_2} - 1} \right]} \quad 10-34$$

As shown in figure 10-27 the Keeling fraction calculated in this way does not vary too much with atmospheric $p\text{CO}_2$. As long as there is calcite present in the sediment to affect the equilibrium, it remains close to 0.04. The mass of fossil fuel CO_2 corresponding to any atmospheric CO_2 concentration can be calculated from equation (10-14). This relationship is also shown in figure 10-27. As can be seen, much larger CO_2 releases are required to produce a given atmospheric $p\text{CO}_2$ value if the atmosphere remains at equilibrium with the calcite in marine sediments.

While the interaction with sea floor calcite can greatly reduce the amount of fossil fuel CO_2 in the atmosphere, this interaction will take several thousand years. Let us look into the reasons for this rather long time scale.

The first point to be made is that the calcite solution process can be effective on no shorter a time scale than that for deep sea ventilation. As the calcite to be dissolved lies on the deep sea floor, the fossil fuel CO_2 laden water must reach the deep sea before this process can begin. While in the deep sea this water is not in communication with the atmosphere; hence it is only when it once again returns to the surface that an impact on the ocean's fossil fuel CO_2 uptake occurs. The amount of fossil fuel CO_2 this water picks up during its second pass against the atmosphere will depend on the extent to which its alkalinity was increased through calcite solution during its traverse through the deep sea. The more calcite it dissolves in the deep sea the more CO_2 it will be able to absorb during its contact with the atmosphere. Thus the minimum time scale on which calcite solution

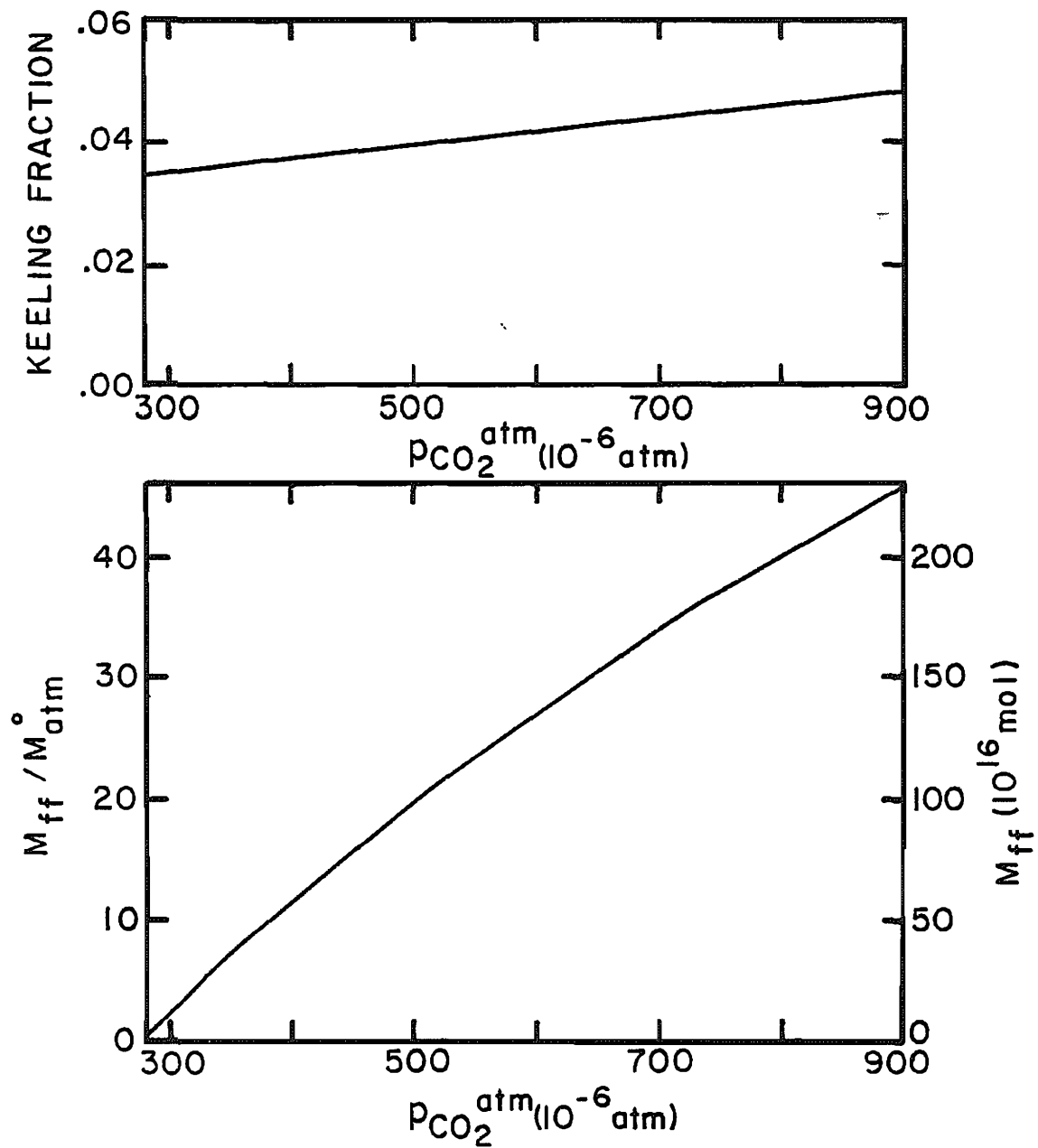


Figure 10-27. Plots of the Keeling fraction and mass of fossil fuel CO_2 added to the atmosphere versus the CO_2 partial pressure in the atmosphere, assuming that the deep waters of the ocean are maintained at saturation with regard to calcite.

could impact fossil fuel CO₂ uptake would be the time scale for deep ocean ventilation (i.e., ~ 500 years).

We say minimum because complete neutralization of the fossil fuel CO₂ contained by a parcel of deep water is not likely to be accomplished during a single pass through the deep sea. If, for example, only 10% of this neutralization occurred during each pass then ten passes would be needed! The solution time scale would then be 5000 years! Clearly then, we must get some idea of the extent of neutralization to be expected for a single pass through the deep sea. It is instructive in this regard to calculate the change in the CO₃⁼ content of bottom water necessary to produce a calcite solution rate one-tenth today's rate of fossil fuel CO₂ production rate. About 20% of the sea floor is blanketed with sediment rich in calcite (i.e., 0.7 x 10¹⁸ cm²). Today's fossil fuel CO₂ production rate is about 5 x 10¹⁴ moles/yr. Thus, if excess calcite solution is to compensate for one tenth today's rate of fossil fuel CO₂ production then calcite will have to dissolve at a rate of 7 x 10⁻⁵ moles/cm²yr (i.e., 7 x 10⁻³ g/cm²yr). This is about 7 times today's mean rain rate of calcite toward the sea floor!

In chapter 2 we showed that CO₃⁼ ion contents 10 μm/kg below the saturation value were adequate to dissolve most of the raining calcite. We can use this result to "calibrate" the rate of the solution process. The relationship between solution rate, F, and CO₃⁼ ion content can be written as follows:

$$F = a \sqrt{f} ([CO_3^=]_{sat} - [CO_3^=]) \quad 10-35$$

where f is the fraction calcite in the sediment, and a is the constant to be evaluated.

At points on the sea floor where carbonate ion content of bottom water reaches 10 μm/kg below the saturation value the calcite content of the sediment drops to about 10%. To achieve such a low calcite content requires that over 95% of the raining calcite be dissolved. The solution rate is hence comparable to the rain rate (i.e., about 1 g/cm² 10³ yrs or 1 x 10⁻⁵ moles/cm² yr). From these numbers we can get the value of the constant a:

$$a \approx \frac{1 \times 10^{-5} \text{ moles/cm}^2 \text{ yr}}{\sqrt{0.1} \quad 10 \text{ } \mu\text{m}/\text{kg}} \approx 3 \times 10^{-6} \frac{\text{moles}}{\text{cm}^2 \text{ yr}} / \frac{\mu\text{m}}{\text{kg}}$$

Now let us apply this relationship to the excess dissolution rate of calcite from sediment by fossil fuel CO₂. We can rewrite the equation 10-35 as follows:

$$[CO_3^=]_{sat} - [CO_3^=] = \frac{1}{a} \frac{F}{\sqrt{f}} \quad 10-36$$

As most of the fossil fuel CO₂ induced calcite solution will take place in sediments which currently lie above the lysocline we can take f to be about 0.85. Thus for a solution rate of 7 x 10⁻⁵ moles/cm² yr the undersaturation value becomes:

$$[\text{CO}_3^{\text{=}}]_{\text{sat}} - [\text{CO}_3^{\text{=}}] \cong \frac{1}{3 \times 10^{-6}} \times \frac{7 \times 10^{-5}}{\sqrt{0.85}} \cong 25 \text{ } \mu\text{m/kg}$$

Thus for a solution rate of 7×10^{-5} moles/cm²yr a reduction in $\text{CO}_3^{\text{=}}$ ion concentration of about 25 $\mu\text{m/kg}$ would have to occur. Because the sediments to be attacked now lie in supersaturated water, to this would have to be added the current extent of supersaturation (i.e., 0 to 20 $\mu\text{m/kg}$). This calculation tells us that sizable reduction in $\text{CO}_3^{\text{=}}$ ion content is necessary before a dissolution rate comparable to even 10% of the current rates of CO_2 production is achieved.

Next let us consider how the reduction in $\text{CO}_3^{\text{=}}$ ion content of the deep sea is related to the amount of fossil fuel CO_2 in the atmosphere. In our considerations so far we have spoken only of the changes in the $\text{CO}_3^{\text{=}}$ concentration in surface water. We now must consider the factors relating the $\text{CO}_3^{\text{=}}$ ion content of deep water to that for the appropriate source water (i.e., the modifications through respiration and CaCO_3 solution). Listed in table 10-8 are the $\text{CO}_3^{\text{=}}$ ion concentrations, alkalinites, ΣCO_2 contents and apparent dissolved oxygen utilizations of the two major deep water sources and for waters at a depth of about 3500 meters in the major ocean basins. As can be seen, although the deep waters of the ocean have been subject to significant amounts of respiration and CaCO_3 solution, the two processes nearly balance, yielding only a small reduction in the carbonate ion concentration.

To calculate the fossil fuel CO_2 induced drop in the carbonate ion content of the deep water sources, we will assume that these waters retain the same alkalinity as measured during the GEOSECS program and that they achieve equilibrium with the atmosphere prior to their descent. Plots of $\text{CO}_3^{\text{=}}$ for northern component source water against $p\text{CO}_2$ in the atmosphere are given in figure 10-28. We can obtain an upper limit on the reduction in $\text{CO}_3^{\text{=}}$ ion content for deep water by assuming that these reductions are the same as those for these source waters.*

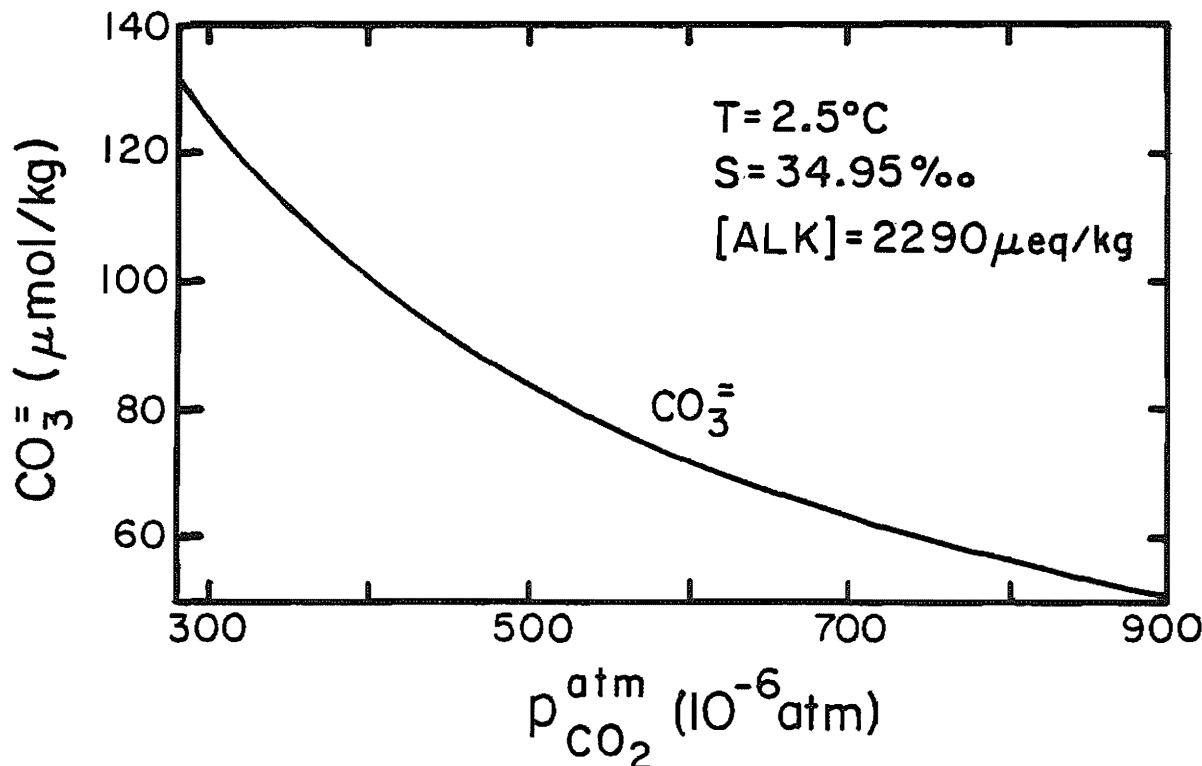
If, as we expect, the CO_2 partial pressure in the atmosphere stays below 800×10^{-6} atm, then the carbonate ion content of deep sea water should drop by no more than 60 $\mu\text{m/kg}$. Such a drop would induce an excess solution rate of calcite of only a few tens of percent of the current rate of fossil fuel CO_2 production. This being the case it is safe to say that during each pass through the deep sea only a relatively small fraction of the excess CO_2 carried by the deep water will be neutralized by calcite in the

*Fossil fuel CO_2 -induced-solution of calcite will raise the carbonate ion content of the deep waters. Failure of the source waters to achieve equilibrium with the CO_2 in the atmosphere before descent will also raise the $\text{CO}_3^{\text{=}}$ ion concentration in the source waters. Finally, as long as the CO_2 pressure in the atmosphere continues to rise, the reduction in the $\text{CO}_3^{\text{=}}$ ion content of deep water will lag behind that in the source waters. Hence our method of calculation yields a maximum lowering in the carbonate ion content for deep water.

Table 10-8. Carbonate ion concentrations for deep waters in the ocean. Based on a compilation of GEOSECS results by Takahashi and his coworkers (406).

Water Type	Alk $\mu\text{eq}/\text{kg}$	$\Sigma\text{CO}_2 \mu\text{m}/\text{kg}$	AOU $\mu\text{m}/\text{kg}$	$\text{CO}_3^{\pm} \mu\text{m}/\text{kg}$
Source waters (after descent)				
NCW	2290	2168	65	98
SCW	2360	2250	105	79
Basin waters (at 3500 meters)				
N.W. Atl.	2340	2195	65	102
S.E. Atl.	2363	2224	102	100
Equ. Ind.	2417	2315	170	81
N.W. Pac.	2420	2324	200	78

Figure 10-28. Carbonate ion content of high-latitude surface water as a function of atmospheric CO_2 partial pressure. The water is assumed to be at chemical equilibrium with the air.



sediment. Complete neutralization will require many "cycles" (hence many times 500 years). It is for this reason that we said early in the chapter that the time scale for neutralization of the fossil fuel CO_2 by calcite in the sediment will take several thousand years.

This concept can be stated in another way which may make it easier to grasp. It is likely that man will consume over the next century or two on the order of 15×10^{16} moles of fossil fuel carbon. Thus at a calcite dissolution rate of 5×10^{13} moles/year (one tenth the current CO_2 production rate) it would take 3000 years to neutralize this CO_2 .

— There is one big IF in all this. That IF has to do with the dependence of solution rate on carbonate ion concentration. We have assumed this dependence to be first order (i.e., the percentage increase in solution rate is equal to the percentage reduction in carbonate ion content of deep water). There is, however, evidence that this might not be the case. Experiments conducted in the laboratory yield a reaction rate which depends on the fourth power of $\Delta\text{CO}_3^{\text{eq}}$ (see figure 10-29). If so then the solution rate for water with a $\Delta\text{CO}_3^{\text{eq}}$ of $20 \mu\text{m}/\text{kg}$ would be 16 times (rather than 2 times) that for water with a $\Delta\text{CO}_3^{\text{eq}}$ of $10 \mu\text{m}/\text{kg}$! As the experiments which yielded this dependence were carried out on calcite particles suspended in a very rapidly stirred solution they are not necessarily a valid analogue to what happens on the sea floor. In the rapidly stirred laboratory flask the "stagnant" boundary film surrounding each grain is likely to be so thin that it does not limit the rate of solution. Rather, the rate at which ions escape from the crystal surfaces controls the rate of solution under these conditions. The question then is whether the rate at which ions escape from the crystal surfaces also controls the resaturation time for the waters in the pores of marine sediments. If it does, then the solution rate will increase with increasing $\Delta\text{CO}_3^{\text{eq}}$ much faster than we have assumed and the neutralization time will correspondingly diminish (as long as the resistance posed by the benthic boundary layer is not the limiting resistance).

Two other barriers must be considered. One is diffusion from the crystal face to the interior of the adjacent pore and the other is coatings of organic material over the calcite. The importance of the former can be assessed by comparing the time required for an ion to diffuse the "width" of a pore with the time for resaturation. As long as the transit is far less than the resaturation time diffusion from crystal face to pore interior is not the rate limiting step. The time, τ , for an ion to traverse a pore by diffusion can be approximated as follows:

$$\tau = \frac{\ell^2}{D} \quad 10-37$$

where ℓ is the pore width and D is the ion diffusivity. In calcite rich deep sea sediments the average pore width is on the order of 10 microns (1×10^{-3} cm) and the diffusivity is on the order of $4 \times 10^{-6} \text{ cm}^2/\text{sec}$. Hence the time for an ion to traverse

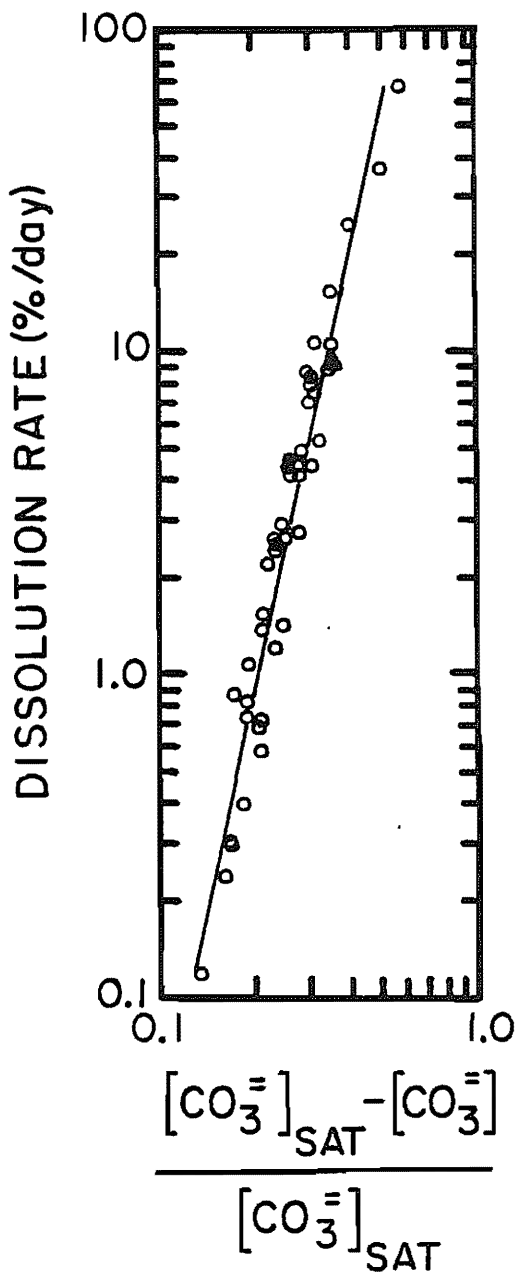


Figure 10-29. Laboratory measurements of the rate of solution of calcite grains suspended in rapidly stirred solutions maintained at various degrees of undersaturation. As can be seen, a 10-fold change in the degree of undersaturation leads to roughly a 10,000-fold change in solution rate. These results were obtained by Keir (479) while working in the laboratory of Berner at Yale University.

a pore should be on the order of one second. As the pore water resaturation time is on the order of 1 minute, this simple calculation suggests that the resaturation process is not limited by the rate of diffusion of ions from crystal face to pore interior.

The extent to which the calcite in marine sediments is coated with an organic film is not known. However, as the organic content of these sediments is very low, we might be safe in assuming that bacteria have removed the organic sheathing which surrounds the platelets of calcite in living organisms.

In chapter 2 we mentioned the possibility that the rate of calcite solution on the sea floor might be limited by the presence of a "stagnant film" just above the sediment water interface. If such a film constituted the major resistance to calcite solution, then first-order kinetics would be entirely appropriate. As stated in chapter 2, we do not yet have the information needed to evaluate the role of this resistance on the sea floor. At the time this book was being edited, the first experiment designed by Santschi and his colleagues at the Lamont-Doherty Geological Observatory to measure this resistance was completed. Flat plates of alabaster ($\text{CaSO}_4 \cdot 2\text{H}_2\text{O}$) were brought to the sea floor by the submersible ALVIN and allowed to dissolve under sea floor conditions for four days before recovery. A stagnant film thickness of 110 microns was obtained. Further studies of this type will allow the importance of this film in limiting the rate of fossil fuel induced calcite solution to be defined.

One other process which must be understood if we are ever to make quantitative predictions of the rate of excess calcite solution induced by fossil fuel CO_2 is the rate at which organisms churn the upper several centimeters of sediment. Is this process sufficiently rapid with respect to the rate of solution that the calcite content of the bioturbated layer assumed to remain uniform, or will an insoluble residue build up at the sediment water interface? Such a residue would impede the rate of solution. The distribution of the isotope ^{210}Pb has something important to tell us in this regard. As we learned in chapter 4 much of the ^{210}Pb produced by the decay of the ^{226}Ra within the sea and added to the ocean from the atmosphere reaches the sea floor before undergoing radiodecay. These excess ^{210}Pb atoms trace the bioturbation process. Measurements of the concentration of excess ^{210}Pb (over ^{226}Ra) as a function of depth in deep sea cores show that these atoms are able to penetrate to a depth averaging about 2 cm in their mean lifetime of 32 years (see figure 10-30). If the bioturbation process is assumed to follow the rules of diffusion (a likely but unproven assumption) then the effective stirring depth will vary as the square root of time. Thus mixing to an average depth of 4 cm would take 128 years and to a depth of 8 cm, 512 years. As the apparent radiocarbon ages change by only a few hundred years from the top to the base of the bioturbated zone (figure 5-13) they are consistent with this ^{210}Pb -based mixing scenario. When compared to the projected rates of fossil fuel CO_2 induced calcite solution these stirring rates prove rapid enough to maintain a nearly homogeneous calcite content in the bioturbated layer. Hence the worms living on the sea floor will do their part in promoting the transfer of fossil fuel CO_2 from air to sea!

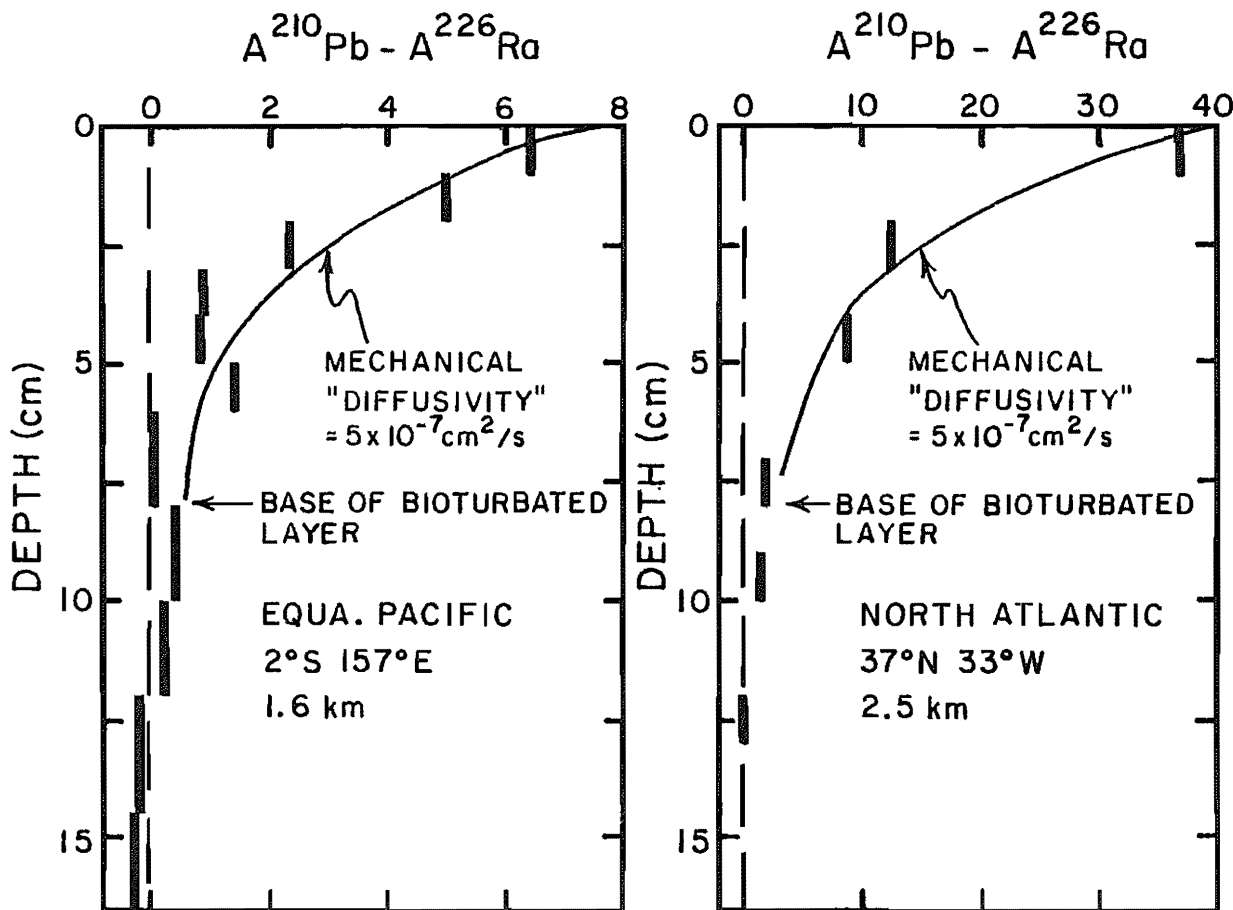


Figure 10-30. Plots of excess ^{210}Pb activity versus depth in two deep sea cores. The core on the left was taken by Berger at Scripps, and the ^{210}Pb analyses were made at Lamont-Doherty Geological Observatory (245). The core on the right was collected by divers in the submersible ALVIN during a study of the Mid-Atlantic Ridge and the ^{210}Pb analyses were made by Nozaki and Cochran at Yale (243). The solid curves are those expected if the ^{210}Pb were being moved downward by a mechanical stirring process which follows the mathematics of diffusion. The required rate is about one-tenth that for molecular diffusion of dissolved ions in sea water.

SUMMARY

Over the next 200 years man will, through his energy and land management practices, release an amount of CO₂ equal to somewhere between 2 and 5 times that present in the atmosphere in the early 1800's. Because the buildup of CO₂ in the atmosphere will modify our planet's climate there is considerable interest in the rate at which the sea will take up this man-made CO₂. The transfer of CO₂ from the atmosphere to the sea is made possible by the CO₃⁼ ion dissolved in the sea and by the CaCO₃ in the sediments lining the sea floor.

Our knowledge of the rate at which this uptake process will occur comes almost entirely from our knowledge of the distribution of tracers in the atmosphere-ocean system. These tracers tell us the rate of invasion of CO₂ into the sea, they tell us of the rate of stirring in the sea, they tell us of the rate of dissolution of CaCO₃ on the sea floor and of the rate of stirring of the upper sediment column. This knowledge allows us to calibrate models of the fossil fuel CO₂ uptake process. Fortunately, enough information is left over after the model has been constructed to allow crosschecks on the model's reliability to be made. While the model by necessity is far more simplified than one would like, the fact that it can adequately reproduce a very diverse set of tracer distributions leads us to believe that the answers it gives with regard to the uptake of man-made CO₂ by the sea are reasonably good.

The results show that the uptake by the various reservoirs are on very different time scales. The surface mixed layer equilibrates with the atmosphere in about one year. The waters of the main ocean thermocline equilibrate with the atmosphere on the time scale of several tens of years (see superproblem #10). The waters of the deep sea equilibrate with the atmosphere on time scales of many hundreds of years. The calcite in marine sediments will equilibrate with the atmosphere on the time scale of several thousands of years. Finally, the excess Ca dissolved in the sea as the result of the calcite-CO₂ reaction will be removed on the time scale of many tens of thousands of years (see superproblem #10). Hence the effects of the CO₂ added to the atmosphere by man over the next two centuries will alter the ocean's chemistry even on geologic time scales!

PROBLEMS

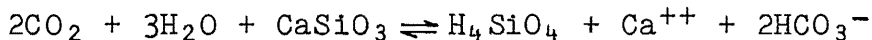
- 10-1 From the information given in this chapter estimate what the atmospheric Δ¹⁴C value would have been in 1973 were no radiocarbon to have been produced by nuclear testing.
- 10-2 If at some time in the next hundred years the CO₂ pressure of the atmosphere reaches twice its present value by roughly how much will the pH of the surface ocean have changed? Do this calculation using simplifying assumptions similar to the constant $p\text{CO}_2 \times [\text{CO}_3^=]$ approximation.
- 10-3 Assume that the annual use of fossil fuels rises at the rate of 2%/year until the year 2020 and then remains constant at the 2020 value until the year 2060. Based on the informa-

tion given in this chapter estimate the atmospheric CO₂ partial pressure in the year 2060. Also estimate the Keeling fraction at that time.

- 10-4 Assume that a decision is made by the global leaders of 2050 not to permit the CO₂ content of the atmosphere to rise any further. At this time the CO₂ partial pressure has already reached 600×10^{-6} atmospheres. The total fossil fuel CO₂ production up to that time is 8.3×10^{16} moles. The mean age of the fossil fuel CO₂ molecules at that time is 40 years. How much production would this permit during the next year if the CO₂ pressure were to be maintained at 600×10^{-6} atmospheres? How much would be permitted in 2080 if this lid on CO₂ pressure were continued?

SUPERPROBLEM #10

Dieter Netherland, a geochemist, becomes interested in the long term effects of fossil fuel CO₂ on ocean-atmosphere chemistry. He realizes that even after all the fossil fuels have been burned and the CO₂ produced in this way has been mixed throughout the ocean and come to equilibrium with the calcite in the sediments, the chemistry of the oceans and the atmosphere will not have returned to their preindustrial composition. The CO₂ content of the atmosphere and the Ca content and ΣCO₂ content of the ocean will be higher. Netherland devises a hypothetical ocean to guide his thinking in this matter. His model is shown in figure 10-31. The model's lithosphere consists of a mixture of three solid compounds, CaSiO₃, CaCO₃ and SiO₂. Calcite and opal (but not CaSiO₃) are precipitated from the waters of his model ocean. These phases along with detrital CaSiO₃ (as the mineral wollastonite) and detrital SiO₂ (as the mineral quartz) make up the sediment on his model's sea floor. The accumulation of new sediment is matched by subsidence of the floor of the ocean. The sinking sediment eventually becomes buried to a depth at which the temperature is high enough to react the CaCO₃ and SiO₂ to form CaSiO₃ and CO₂. (Any leftover opal is converted to quartz). The wollastonite and quartz make up the model's metamorphic crust. The CO₂ (released by the breakdown of calcite) and the H₂O (released by the breakdown of opal) are driven to the surface and become part of the ocean-atmosphere system. The metamorphic rock is pushed around and up to the surface of the model's continent. Here it undergoes weathering. CO₂ from the atmosphere reacts with the wollastonite to produce Ca⁺⁺, HCO₃⁻, and H₄SiO₄ ions. The weathering reaction is as follows:



The ions so formed are carried by the model rivers to the model ocean. Here they are reprecipitated as calcite and opal completing the grand geochemical cycle.

Netherland envisions a rather simple set of rules controlling the flow of material through his model ocean prior to its industrial revolution. The tectonic processes in the earth set the

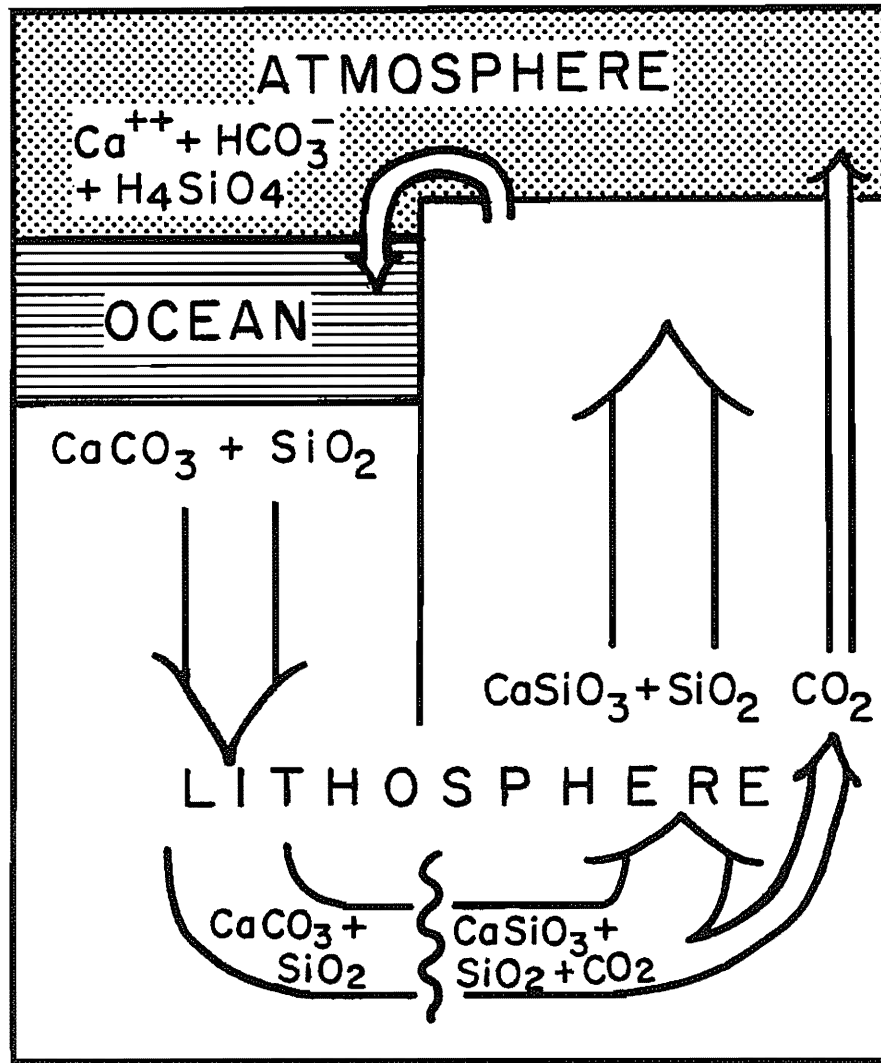


Figure 10-31. Dieter Netherland's simplified earth cycling model of the earth's geochemical cycles (see Superproblem #10).

rate at which the crust moves from sea floor to continent. In so doing it determines the rate at which CO₂ gas percolates out of the lithosphere into the ocean-atmosphere system. As this CO₂ can only be precipitated onto the sea floor (as CaCO₃) as fast as CaSiO₃ is weathered on the continents the weathering rate must at steady state match the CO₂ production rate by metamorphism. Netherland envisions that the weathering rate depends on the CO₂ partial pressure in the atmosphere - the higher the pressure the higher the weathering rate. Hence the partial pressure of CO₂ in the atmosphere prior to industrialization had achieved that level where the weathering rate matches the rate at which CO₂ is produced by metamorphism. Finally, he assumed that his model ocean remains close to saturation with respect to both opal and calcite. This fixes the chemistry of his model's ocean. The concentrations of its five ions (i.e., CO₃⁼, HCO₃⁻, CO₂, Ca⁺⁺ and H₄SiO₄) are fixed by the following restrictions:

1) charge neutrality

$$2[\text{Ca}^{++}] + [\text{HCO}_3^-] + 2[\text{CO}_3^=] = 0$$

2) weathering rate balances metamorphism rate

$$[\text{CO}_2] = \text{constant}$$

3) opal saturation

$$[\text{H}_4\text{SiO}_4] = \text{constant}$$

4) calcite saturation

$$[\text{Ca}^{++}][\text{CO}_3^=] = \text{constant}$$

5) equilibrium among the carbon species

$$\frac{[\text{HCO}_3^-]^2}{[\text{CO}_3^=][\text{CO}_2]} = \text{constant}$$

Netherland now assigns some numerical values to his steady state system:

$$V_{\text{ocean}} = 1.0 \times 10^{18} \text{ m}^3$$

$$A_{\text{ocean}} = 4.0 \times 10^{14} \text{ m}^2$$

$$h_{\text{ocean}} = V_O/A_O = 2.5 \times 10^3 \text{ m}$$

$$[\text{CO}_2] = 1 \times 10^{-2} \text{ moles/m}^3$$

$$[\text{HCO}_3^-] = 200 \times 10^{-2} \text{ moles/m}^3$$

$$[\text{CO}_3^=] = 30 \times 10^{-2} \text{ moles/m}^3$$

$$[\text{Ca}^{++}] = 130 \times 10^{-2} \text{ moles/m}^3$$

$$[\text{H}_4\text{SiO}_4] = 60 \times 10^{-2} \text{ moles/m}^3$$

$$M_{\text{atm}}^{\text{CO}_2} = 2.3 \times 10^{16} \text{ moles}$$

$$R_{\text{CO}_2} = 2.3 \times 10^{13} \text{ moles/yr}$$

These concentrations of course fix the constants for restrictions 2 through 5.

Now Netherland is ready to subject his model to an industrial revolution. To do so he injects 2.3×10^{17} moles of CO_2 into the ocean atmosphere system. He allows this CO_2 to mix through the ocean and attack the CaCO_3 in the ocean's sediments until calcite saturation is reestablished. At this point he computes the following composition for its ocean (and its atmosphere).

$$[\text{CO}_2] = 1.8 \times 10^{-2} \text{ moles/m}^3$$

$$[\text{HCO}_3^-] = 248 \times 10^{-2} \text{ moles/m}^3$$

$$[\text{CO}_3^{=}] = 26 \times 10^{-2} \text{ moles/m}^3$$

$$[\text{Ca}^{++}] = 150 \times 10^{-2} \text{ moles/m}^3$$

$$[\text{H}_4\text{SiO}_4] = 60 \times 10^{-2} \text{ moles/m}^3$$

Do these values satisfy the restrictions 1, 3, 4 and 5?

Now Netherland is ready to consider the long-term future of his model ocean. Even after equilibration with the sea and its sedimentary calcite, the excess industrial CO_2 has left Netherland's model ocean with an atmospheric CO_2 content about 1.8 times higher than its preindustrial value. This higher atmospheric CO_2 content would of course lead to a higher continental weathering rate. Netherland envisions two scenarios. First, he assumes that continental weathering rate is proportional to the atmospheric CO_2 pressure. If so, how long will it take for the atmospheric CO_2 content to drop halfway back to its preindustrial value?

Netherland is concerned with this result, however. He is aware that the decay of terrestrial plant material leads to CO_2 pressures in soils averaging about 10 times the steady state atmospheric CO_2 pressure. He decides to repeat the calculation assuming that the soil CO_2 pressure controls the weathering rate and that this pressure increases only the same increment as the atmospheric CO_2 pressure. To calculate the new soil CO_2 pressure he uses the following equation:

$$\text{soil PCO}_2 = 10 \frac{\text{P.I.A.}}{\text{PCO}_2} + \left(\frac{\text{atm}}{\text{PCO}_2} - \frac{\text{P.I.A.}}{\text{PCO}_2} \right) = 9 \frac{\text{P.I.A.}}{\text{PCO}_2} - \frac{\text{atm}}{\text{PCO}_2}$$

P.I.A.

where PCO_2 is the steady state preindustrial atmospheric CO_2 pressure. Under these circumstances how long would it take for the atmospheric CO_2 content to drop halfway to its preindustrial value?

References

INTRODUCTION

The references are arranged according to a subject outline. In each sub-category the references are placed in order of publication. For each reference a brief summary of its bearing on the mission of this book is given. The numbers (1 through 737) are used to designate specific references in the text, table and figures.

SUBJECT OUTLINE

I. PAPERS DEALING WITH RADIOTRACERS (#1 to #264)

A. PAPERS DEALING WITH RADIOTRACERS OF WATER MOTION (#1 to #111)

1. PAPERS DEALING WITH THE DISTRIBUTION OF NATURAL RADIO CARBON IN THE OCEAN-ATMOSPHERE SYSTEM (#1 to #26)
 2. PAPERS DEALING WITH MODELING OF THE DISTRIBUTION OF RADIOCARBON IN THE OCEAN-ATMOSPHERE SYSTEM (#27 to #41)
 3. PAPERS DEALING WITH THE DISTRIBUTION OF TRITIUM IN THE OCEAN (#42 to #56)
 4. PAPERS DEALING WITH THE INTERPRETATION AND MODELING OF THE ADDITION OF TRITIUM TO THE SEA AND ITS PENETRATION INTO THE BODY OF THE SEA (#57 to #70)
 5. PAPERS DEALING WITH THE JOINT INTERPRETATION OF THE DISTRIBUTIONS OF BOMB RADIOCARBON AND TRITIUM IN THE OCEAN (#71 to #75)
 6. PAPERS DEALING WITH THE DISTRIBUTION OF EXCESS ^{222}Rn IN THE DEEP SEA (#76 to #86)
 7. PAPERS DEALING WITH THE DISTRIBUTION OF ^{228}Ra IN THE SEA (#87 to #96)
 8. PAPERS DEALING WITH THE DISTRIBUTIONS OF ^{90}Sr , ^{137}Cs , ^{85}Kr and ^{39}Ar IN THE SEA (#97 to #111)
-
- B. PAPERS DEALING WITH RADIOTRACERS OF PARTICLE MOVEMENT AND THE SCAVENGING OF REACTIVE METALS (#112 to #170)
 1. PAPERS DEALING WITH THE DISTRIBUTION OF ^{226}Ra IN THE OCEAN (#112 to #121)

2. PAPERS DEALING WITH THE DISTRIBUTION OF ^{234}Th , ^{228}Th , ^{230}Th AND ^{231}Pa IN THE OCEAN (#122 to #138)
 3. PAPERS DEALING WITH THE DISTRIBUTION OF ^{210}Po AND ^{210}Pb IN THE SEA (#139 to #161)
 4. PAPERS DEALING WITH THE INPUT OF AND DISTRIBUTION OF PLUTONIUM WITHIN THE SEA (#162 to #165)
 5. PAPERS DEALING WITH THE DISTRIBUTION OF ^{14}C IN PARTICULATE DEBRIS AND ORGANISMS (#166 to #167)
 6. MODELS FOR PARTICULATE SCAVENGING IN THE OCEAN (#168 to #170)
- C. PAPERS DEALING WITH RADIO TRACERS OF GAS EXCHANGE (#171 to #194)
1. PAPERS DEALING WITH THE RADON METHOD (#171 to #177)
 2. PAPERS DEALING WITH THE $^3\text{H} - ^3\text{He}$ METHOD (#178 to #179)
 3. PAPERS DEALING WITH THE RADIOCARBON METHOD (#180 to #184)
 4. PAPERS DEALING WITH LABORATORY MEASUREMENTS OF GAS EX-
CHANGE RATES (#185 to #188)
 5. THEORETICAL TREATMENTS OF VARIOUS ASPECTS OF THE GAS
EXCHANGE PROCESS (#189 to #194)
- D. PAPERS DEALING WITH RADIOISOTOPES IN OCEAN SEDIMENTS (#195 to #264)
1. PAPERS DEALING WITH RADIOCARBON MEASUREMENTS IN DEEP
SEA SEDIMENTS (#195 to #199).
 2. PAPERS DEALING WITH ^{230}Th AND ^{231}Pa DATA IN DEEP SEA
SEDIMENTS AND MANGANESE NODULES (#200 to #239)
 3. PAPERS DEALING WITH ^{210}Pb AND OTHER BIOTURBATION
TRACERS IN DEEP SEA SEDIMENTS (#240 to #247)
 4. PAPERS DEALING WITH THE DISTRIBUTIONS OF ^{26}Al , ^{32}Si AND
 ^{10}Be IN SEDIMENTS AND MANGANESE NODULES (#248 to #264)

II. PAPERS DEALING WITH STABLE ISOTOPE TRACERS (#265 to #345)

- A. PAPERS DEALING WITH STABLE ISOTOPE TRACERS OF WATER MOTION (#265 to #284)
1. PAPERS DEALING WITH THE DISTRIBUTION OF THE $^3\text{He}/^4\text{He}$
RATIO IN THE SEA (#265 to #281)

2. PAPERS DEALING WITH THE DISTRIBUTIONS OF D/H AND OF $^{18}\text{O}/^{16}\text{O}$ RATIOS IN THE OCEAN (#282 to #284)
- B. PAPERS DEALING WITH STABLE ISOTOPE TRACERS OF BIOLOGICAL PROCESSES IN THE SEA (#285 to #317)
 1. PAPERS DEALING WITH THE $^{13}\text{C}/^{12}\text{C}$ RATIO IN DISSOLVED OCEANIC CARBON AND IN MARINE ORGANISMS (#285 to #305)
 2. PAPERS DEALING WITH THE $^{18}\text{O}/^{16}\text{O}$ RATIOS IN ATMOSPHERIC O_2 AND IN THE O_2 DISSOLVED IN THE SEA (#306 to #317)
- C. STABLE ISOTOPE TRACERS IN SEDIMENTS AND MANGANESE NODULES (#318 to #345)
 1. PAPERS DEALING WITH THE $^{18}\text{O}/^{16}\text{O}$ RATIOS IN CaCO_3 FROM DEEP SEA SEDIMENTS (#318 to #326)
 2. PAPERS DEALING WITH THE $^{13}\text{C}/^{12}\text{C}$ RECORD FOUND IN FORAMINIFERA FROM DEEP SEA SEDIMENTS (#327 to #331)
 3. PAPERS DEALING WITH $^{143}\text{Nd}/^{144}\text{Nd}$ RATIOS IN SEA WATER, MARINE SEDIMENTS AND MANGANESE NODULES (#332 to #340)
 4. PAPERS DEALING WITH LEAD ISOTOPE RATIOS IN DEEP SEA SEDIMENTS AND MANGANESE NODULES (#341 to #345)

III. PAPERS DEALING WITH CHEMICAL TRACERS (#346 to #456)

- A. PAPERS DEALING WITH CHEMICAL TRACERS OF BIOLOGICAL CYCLES (#346 to #433)
 1. PAPERS DEALING WITH THE DISTRIBUTIONS OF NO_3^- , PO_4^{3-} AND DISSOLVED OXYGEN IN THE SEA (#346 to #364)
 2. PAPERS DEALING WITH THE DISTRIBUTIONS OF H_4SiO_4 , Ge AND Ba IN THE SEA (#365 to #378)
 3. PAPERS DEALING WITH THE DISTRIBUTIONS OF ΣCO_2 , CO_3^{2-} AND ALKALINITY IN THE SEA (#379 to #409)
 4. PAPERS DEALING WITH THE DISTRIBUTION OF NITROGEN SPECIES (OTHER THAN NITRATE IN THE SEA (#410 to #421)
 5. PAPERS BASED ON THE GEOSECS DATA SET DEALING WITH THE RELATIONSHIP BETWEEN POTENTIAL TEMPERATURE, SALINITY AND THE DISTRIBUTIONS OF SEVERAL OF THE NUTRIENT CONSTITUENTS (#422 to #433)
- B. CHEMICAL TRACERS OF PARTICLE-WATER INTERACTIONS OCCURRING IN THE SEA (#434 to #456)
 1. PAPERS DEALING WITH THE DISTRIBUTION OF LEAD IN THE SEA (#434 to #436)

2. PAPERS DEALING WITH THE DISTRIBUTION OF CADMIUM IN THE SEA (#437 to #438)
3. PAPERS DEALING WITH THE DISTRIBUTION OF COPPER IN THE SEA (#439 to #441)
4. PAPERS DEALING WITH THE DISTRIBUTION OF ZINC AND NICKEL IN THE SEA #442 to #443)
5. PAPERS DEALING WITH THE DISTRIBUTION OF MANGANESE IN SEA WATER (#444 to #449)
6. PAPERS DEALING WITH THE DISTRIBUTION OF SELENIUM IN SEA WATER (#450 to #451)
7. PAPERS DEALING WITH SEVERAL METALS (#452 to #456)

IV. PAPERS DEALING WITH BIOGENIC MATERIAL (#457 to #543)

- A. PAPERS DEALING WITH BIOGENIC MATERIAL IN THE SEDIMENTS (#457 to #531)
 1. PAPERS DEALING WITH THE SOLUBILITY OF CALCITE AND ARAGONITE (#457 to #468)
 2. PAPERS DEALING WITH CaCO_3 SATUROMETRY (#469 to #472)
 3. PAPERS DEALING WITH THE RESULTS OF CALCITE AND ARAGONITE IN SITU DISSOLUTION EXPOSURES (#473 to #476)
 4. LABORATORY STUDIES OF THE DEPENDENCE OF THE RATES OF CALCITE AND ARAGONITE DISSOLUTION RATE ON THE CARBONATE ION CONTENT (HENCE pH) OF THE WATER (#477 to #479)
 5. PAPERS DEALING WITH THE DISTRIBUTIONS OF CALCITE AND ARAGONITE IN RECENT SEDIMENTS (#480 to #495)
 6. PAPERS DEALING WITH GLACIAL TO INTERGLACIAL CHANGES AND ARAGONITE DISSOLUTION (#496 to #512)
 7. MODELS OF THE DISSOLUTION OF CALCITE ON THE SEA FLOOR (#513 to #519)
 8. PAPERS DEALING WITH THE DISTRIBUTION OF OPAL IN MARINE SEDIMENTS (#520 to #523)
 9. PAPERS CONTAINING PORE WATER PROFILES OF DISSOLVED SILICATE (#524 to #529)
 10. PAPERS CONTAINING DATA REGARDING THE DISTRIBUTION OF ORGANIC MATERIAL IN SEDIMENTS (#530 to #531)
- B. PAPERS DEALING WITH BIOGENIC MATERIAL IN THE WATER COLUMN (#532 to #543)

1. PAPERS DEALING WITH SUSPENDED MATTER IN THE WATER COLUMN (#532 to #536)
2. PAPERS DEALING WITH MATERIAL CAUGHT IN SEDIMENT TRAPS (#537 to #541)
3. PAPERS DEALING WITH MODES OF TRANSPORT OF PARTICULATE MATTER THROUGH THE WATER COLUMN (#542 to #543)

V. PAPERS DEALING WITH CONTROLS ON OCEAN CHEMISTRY (#544 to #547)

- A. PAPERS CONCERNED WITH THERMODYNAMIC CONTROLS ON OCEAN CHEMISTRY (#544 to #546)
- B. PAPERS CONCERNED WITH KINETIC CONTROLS ON OCEAN CHEMISTRY (#547)

VI. PAPERS CONCERNED WITH MAN-MADE PERTURBATIONS IN THE EARTH'S CARBON CYCLE (#548 to #599)

- A. PAPERS DEALING WITH THE PRODUCTION OF FOSSIL FUEL CO₂, ITS BUILD-UP IN THE ATMOSPHERE, AND ITS DISTRIBUTION WITHIN THE ATMOSPHERE (#548 to #562)
- B. PAPERS DEALING WITH CHANGES IN THE LIVING BIOMASS AND SOIL CARBON RESERVOIRS (#563 to #574)
- C. PAPERS DEALING WITH THE UPTAKE OF ANTHROPOGENIC CO₂ BY THE SEA (#575 to #597)
- D. PAPERS DEALING WITH THE REACTION BETWEEN ANTHROPOGENIC CO₂ AND CaCO₃ IN MARINE SEDIMENTS (#598 to #599).

VII. PAPERS DEALING WITH THE GLACIAL TO INTERGLACIAL CHANGE IN VARIOUS OCEAN PROPERTIES (#600 to #624)

- A. PAPERS DEALING WITH THE RECONSTRUCTION OF SEA SURFACE TEMPERATURE (#600 to #610)
- B. PAPERS DEALING WITH THE RECONSTRUCTION OF ICE VOLUME AND HENCE OCEAN SALINITY (#611 to #617)
- C. PAPERS DEALING WITH CHEMICAL CHANGES IN THE OCEAN AND ATMOSPHERE (#618 to #624)

VIII. PAPERS DEALING WITH RATES OF INPUT, RATES OF LOSS, AND RESIDENCE TIMES OF VARIOUS CONSTITUENTS IN THE SEA (#625 to #670)

- A. PAPERS DEALING WITH RIVER INPUTS TO THE SEA (#625 to #633)
- B. PAPERS DEALING WITH THE REMOVAL RATES OF CONSTITUENTS TO DEEP SEA SEDIMENTS (#634 to #635)

- C. PAPERS DEALING WITH INTERACTIONS BETWEEN SEA WATER AND RIDGE CREST BASALTS (#636 to #643)
 - D. PAPERS DEALING WITH ATMOSPHERIC AEROSOLS AND DUST (#644 to #652)
 - E. PAPERS DEALING WITH GAS SOLUBILITY IN SEA WATER (#653 to #660)
 - F. PAPERS DEALING WITH MOLECULAR DIFFUSIVITY OF GASES IN SEA WATER (#661 to #666)
 - G. PAPERS DEALING WITH THE EVOLUTION OF OCEAN CHEMISTRY (#667 to #670)
- IX. BOOKS ON RELATED SUBJECTS (#671 to #684)
- X. ATLASES CONTAINING CHEMICAL DATA (#684a to #685g)
- XI. MISCELLANEOUS PAPERS AND LATE ENTRIES (#686 to #737)

ANNOTATED REFERENCE LIST

I. PAPERS DEALING WITH RADIOTRACERS (#1 to #264)

- A. PAPERS DEALING WITH RADIOTRACERS OF WATER MOTION (#1 to 111)
 - 1. PAPERS DEALING WITH THE DISTRIBUTION OF NATURAL RADIO-CARBON IN THE OCEAN-ATMOSPHERE SYSTEM (#1 to #26)
 1. Suess, H.E. 1955. Radiocarbon concentration in modern wood. *Science*, V122, p. 415-417.
The first measurements showing the decline in the atmospheric $^{14}\text{C}/\text{C}$ ratio due to the build up of fossil fuel CO_2 in the atmosphere and the first demonstration that the magnitude of this decline could be used as a measure of the extent of mixing between atmosphere, biosphere and ocean carbon on the time scale of several decades.
 2. Vries, H. de. 1958. Variations in concentration of radiocarbon with time and location on the earth: *Koninkl Nederlandse Akad Wetensch. Proc. sec. B.* V61, p. 1-9.
The first demonstration that the atmosphere has undergone short-term variations in $^{14}\text{C}/\text{C}$ ratio due to natural causes.
 3. Fergusson, G.J. 1958. Reduction of atmospheric radiocarbon concentration by fossil fuel carbon dioxide and the mean life of carbon dioxide content in the atmosphere. *Proc. Roy. Soc. London A*, V243, p. 561-574.
A follow up to the work of Suess involving accurate $^{14}\text{C}/\text{C}$ ratio measurements on samples from southern hemisphere trees covering the period 1890 to 1955.

4. Broecker, W.S., R. Gerard, M. Ewing, and B.C. Heezen. 1960. Natural Radiocarbon in the Atlantic Ocean. *Jour. of Geophys. Res.* V65, p. 2903-2931.
Radiocarbon measurements on samples from throughout the Atlantic Ocean collected before significant amounts of bomb testing ^{14}C had reached the oceans.
5. Bien, G.S., N.W. Rakestraw and H.E. Suess. 1960. Radiocarbon concentration in Pacific Ocean water, *Tellus* V12, p. 436-443.
Radiocarbon measurements on samples from the Pacific Ocean collected before significant amounts of bomb testing ^{14}C had reached the ocean.
6. Burling, R.W., and D.M. Garner. 1960. A section of ^{14}C activities of sea water between 9°S and 66°S in the southwest Pacific Ocean, New Zealand *J. Geol. Research* V2, p. 2903.
Radiocarbon measurements on samples from the Pacific Ocean collected before significant amounts of bomb testing ^{14}C had reached the ocean.
7. Nydal, R. 1963. Increase in radiocarbon from the most recent series of thermonuclear tests. *Nature*, V6, p.212-214.
Measurements on atmospheric CO_2 showing the increase in the $^{14}\text{C/C}$ ratio resulting from nuclear testing.
8. Broecker, W.S. 1963. $^{14}\text{C}/^{12}\text{C}$ ratios in surface ocean water. *Nat. Acad. Sci., Nat. Res. Counc. Publ.* 1075, p. 138-149.
A summary of radiocarbon measurements made on surface ocean water and shell samples collected prior to the onset of the contamination of the ocean with nuclear radiocarbon.
9. Munnich, K.O., and W. Roether. 1967. Transfer of bomb ^{14}C and tritium from the atmosphere to the ocean: Internal mixing of the ocean on the basis of tritium and ^{14}C profiles, in: *Symposium on Radioactive Dating and Methods of Low Level Counting*. International Atomic Energy Agency UN DOC SM-87/22, p. 93-103.
Measurements of bomb radiocarbon in atmospheric CO_2 over the period 1959 to 1966 and in the North Atlantic Ocean samples collected in 1966.
10. Nydal, R. 1968. Further investigation of the transfer of radiocarbon in nature, *Jour. Geophys. Res.* V73, p. 3617-3635.
This paper describes the transfer of bomb-produced radiocarbon from stratosphere to troposphere and from the atmosphere to the mixed layer of the ocean.
11. Rafter, T.A. 1968. Carbon-14 measurements in the South Pacific and Antarctic Oceans. *New Zealand Jour. Sci.*, V11, p. 551-589.
Measurements of the bomb ^{14}C in surface waters in the South Pacific over the time interval 1954 to 1968.
12. Broecker, W.S., and R. Gerard. 1969. Natural radiocarbon in the Mediterranean Sea. *Limnology and Oceanography*, V14, p. 883-888.

The distribution of radiocarbon in the Mediterranean Sea prior to nuclear testing. Estimates of the ventilation times of the deep waters in the eastern and western basins are given.

13. Linick, T.W. 1978. La Jolla Measurements of Radiocarbon in the Oceans. *Radio carbon*, V20, p. 333-359.
Radiocarbon measurements on samples from the Pacific and Indian Oceans collected after the onset of the build-up of bomb radiocarbon in the oceans.
14. Nozaki, Y., D.M. Rye, K.K. Turekian and R.E. Dodge. 1978. A 200 year record of carbon-13 and carbon-14 variations in a Bermuda coral. *Geophys. Research Letters*, V5, p. 825-828.
The first paper on the radiocarbon record in corals. For reasons which are not clear this record is not entirely representative of the surrounding ocean.
15. Druffel, E.M. and T.W. Linick. 1978. Radiocarbon in annual coral rings of Florida. *Geophys. Res. Letters*, V5, p. 913-916.
A reconstruction of the $^{14}\text{C}/\text{C}$ ratio in surface ocean water in the Florida Straits from 1800 to 1974 based on measurements in growth ring dated corals.
- 15a. Gillespie, R. and H.A. Polach. 1979. The suitability of marine shells for radiocarbon dating of Australian prehistory. *Radiocarbon Dating*, edited by R. Berger and H. Suess, University of California Press, Los Angeles, p. 404-421.
 $^{14}\text{C}/\text{C}$ ratios on shells collected before 1950 along the east coast of Australia yielding estimates of the prenuclear $^{14}\text{C}/\text{C}$ ratios in surface water carbon from the western Pacific. Also given are the results on shells collected in 1973 showing the bomb ^{14}C build-up in this area.
16. Druffel, E.M. 1980. Radiocarbon in annual coral rings of Belize and Florida. *Radio carbon*, V22, p. 363-371.
Reconstruction of the $^{14}\text{C}/\text{C}$ ratio in surface ocean water of the eastern Caribbean Sea from 1890 to 1977 based on measurements in growth ring dated corals.
17. Druffel, E.M. 1980. Radiocarbon in annual coral rings of the Pacific and Atlantic Oceans. Ph.D. thesis, Chemistry Dept., University of California, San Diego.
Radiocarbon measurements of corals from the Florida Straits, from the Gulf of Honduras and from the Galapagos Islands in the eastern equatorial Pacific.
18. Stuiver, M. 1980. ^{14}C distribution in the Atlantic Ocean. *Jour. Geophys. Res.* V85, p. 2711-2718.
Description of the distribution of bomb-produced radiocarbon in the thermocline of the Atlantic Ocean.
19. Stuiver, M. and P.D. Quay. 1980. Changes in atmospheric ^{14}C attributed to a variable sun. *Science*, V207, p. 11-19.

- Ultra-high accuracy measurements on tree ring samples of the $^{14}\text{C}/\text{C}$ record for the period 1000 to 1900 AD. The authors show that the variations are correlated with the sun spot, auroral and magnetic index records. Changes in the sun's magnetic field have modulated the flux of cosmic rays to the earth's atmosphere and hence the rate of ^{14}C production.
20. Roether, W., K.O. Munnich, B. Ribbot, and J.L. Sarmiento. 1980. A transatlantic ^{14}C -section near 40°N . "Meteor" Forsh.-Ergelenisse Reihe A, V22, p. 57-69.
Radiocarbon measurements on a track from Lisbon to Nova Scotia run by the West German research vessel "Meteor" in 1971. These measurements nicely complement those of the GEOSECS survey in the Atlantic Ocean.
21. Stuiver, M. and H.G. Ostlund. 1980. GEOSECS Atlantic Radiocarbon. Radiocarbon, V22, p. 1-24.
Radiocarbon measurements on samples collected as part of the GEOSECS survey of the Atlantic Ocean during the period July 1972 to April 1973.
22. Ostlund, H.G. and M. Stuiver. 1980. GEOSECS Pacific Radiocarbon. V22, p. 25-53.
Radiocarbon measurements on samples collected as part of the GEOSECS survey of the Pacific Ocean during the period September 1973 to June 1974.
23. Ostlund, H.G., R. Oleson, and R. Brescher. 1980. GEOSECS Indian Ocean Radiocarbon and Tritium Measurements (Miami). Tritium Laboratory Data Report #9, Rosenstiel School of Marine and Atmospheric Science, University of Miami.
Report containing the radiocarbon data obtained on samples collected during the period Jan. 1978 to Feb. 1978 in the western Indian Ocean as part of the GEOSECS program.
24. Nydal, R., K. Lovseth and F.H. Skogseth. 1980. Transfer of bomb ^{14}C to the ocean surface. Radiocarbon, V22, p. 626-635.
Measurements of the bomb ^{14}C content of atmospheric CO_2 and surface ocean water over the period 1966 to 1978 from a wide variety of localities in both hemispheres.
25. Levin, I., K.O. Munnich, and W. Weiss. 1980. The effect of anthropogenic CO_2 and ^{14}C sources in the distribution of ^{14}C in the atmosphere. Radiocarbon, V22, p. 379-391.
 ^{14}C measurements on weekly samples of atmospheric CO_2 and hydrocarbon to detect fossil fuel CO_2 dilution and nuclear power plant ^{14}C addition.
26. Stuiver, M. and P.D. Quay. 1981. Atmospheric ^{14}C changes resulting from fossil fuel CO_2 release and cosmic ray flux variability. Earth and Planet. Sci. Lett., V53, p. 349-362.
The definitive set of measurements documenting the magnitude of the Suess effect and the shape of this decline. Also an attempt is made to separate the contributions of fossil fuel CO_2 and cosmic ray variations.

2. PAPERS DEALING WITH MODELING OF THE DISTRIBUTION OF RADIOCARBON IN THE OCEAN-ATMOSPHERE SYSTEM (#27 to #41)

27. Craig, H. 1957. The natural distribution of radiocarbon and the exchange time of carbon dioxide between the atmosphere and sea. *Tellus*, V9, p. 1-17.
One of the Tellus triad of papers discussing the implications of the distribution of ^{14}C between the atmosphere and oceans. This paper lays out the principles of box modeling in a very elegant way and thus provides the foundation for the wide use of this approach to ocean modeling.
28. Suess, H.E. and R. Revelle. 1957. Carbon dioxide exchange between the atmosphere and ocean and the question of an increase of atmospheric CO_2 during the past decades. *Tellus*, V9, p. 18-27.
The second of the Tellus triad of papers discussing the implications of the distribution of ^{14}C between the atmosphere and oceans. Using a one-box ocean model these authors made the first attempt to estimate the rate of uptake of fossil fuel CO_2 by the oceans.
29. Arnold, J.R. and E.C. Anderson. 1957. The distribution of radiocarbon in nature. *Tellus*, V9, p. 28-32.
The third of the Tellus triad of papers discussing the implications of the distribution of ^{14}C between the atmosphere and oceans.
30. Bolin, B. and E. Eriksson. 1959. Changes in the carbon dioxide content of the atmosphere and sea due to fossil fuel combustion. *Rossby Memorial Volume*, Rockefeller Inst. Press, New York, p. 130-142.
The first application of the two-box ocean model to the uptake of fossil fuel CO_2 by the ocean.
31. Munk, W.H. 1966. Abyssal recipes. *Deep-Sea Res.* V13, p. 707-730.
The first attempt to calibrate a one-dimensional advection-diffusion model using radiocarbon data.
32. Keeling, C.D. and B. Bolin. 1967. The simultaneous use of chemical tracers in oceanic studies 1. *Tellus*, V19, p. 566-581. Keeling, C.D. and B. Bolin. 1968. The simultaneous use of chemical tracers in oceanic studies 2. *Tellus*, V20, p. 17-54.
A very elaborate multibox ocean model designed to include both the transport of carbon with the water and with particulate matter falling from surface water to the interior of the sea.
33. Craig, H. 1969. Abyssal Carbon and Radiocarbon in the Pacific. *Jour. of Geophys. Res.* V74, p. 5491-5506.
A more rigorous attempt to calibrate a one-dimensional

advection diffusion model using radiocarbon and carbon data. Done with the characteristic Craig style, this paper paved the way for further application of this type of model by marine geochemists.

34. Broecker, W.S. and Y.-H. Li. 1970. Interchange of water between the major oceans. *Jour. of Geophys. Res.* V75, p. 3545-3552.
A three-box model of the world ocean designed to evaluate the rate of exchange of water between the three major water types in the ocean: warm surface water, North Atlantic deep water and Pacific and Indian deep water.
35. Stuiver, M. 1976. The ^{14}C distribution in west Atlantic abyssal waters. *Earth and Planet. Sci. Lett.* V32, p. 322-330.
A discussion of the distribution of radiocarbon with latitude in the deep waters of the western Atlantic based on the GEOSECS data set.
36. Broecker, W.S., T.-H. Peng and M. Stuiver. 1978. An estimate of the upwelling rate in the equatorial Atlantic based on the distribution of bomb radiocarbon. *Jour. of Geophys. Res.* V83, p. 6179-6186.
The deficiency in the water column inventory of bomb-produced radiocarbon in the equatorial ocean is explained by the flushing action of upwelled water. In the paper a means is presented to determine the flux of upwelled water based on magnitude of this inventory anomaly.
37. Broecker, W.S. 1979. A revised estimate for the radiocarbon age of North Atlantic deep water. *Jour. of Geophys. Res.* V84, p. 3218-3226.
Much of the variation in the radiocarbon concentration in deep water carbon from the Atlantic is the result of mixing of ^{14}C -rich deep waters originating in the northern Atlantic with ^{14}C -poor deep waters originating in the southern Atlantic. In this paper an attempt is made to separate the contributions of mixing and radiodecay within the Atlantic and to use the latter to estimate the rate of ventilation of the deep Atlantic.
38. Bjorkstrom, A. 1979. A model of CO_2 interaction between atmosphere, ocean, land biota. In: *Global carbon cycle*, ed. by B. Bolin, Wiley & Sons, New York, p. 403-457.
A five-box ocean made up of the warm and cold surface ocean, the upper and lower main thermocline and the deep sea is used to describe the transport of carbon in the world ocean.
39. Broecker, W.S. and T.-H. Peng. 1980. Seasonal variability in the $^{14}\text{C}/^{12}\text{C}$ ratio for surface ocean water. *Geophys. Res. Lett.* V7, p. 1020-1022.
In the temperate zones of the oceans the surface mixed layer thickens greatly during winter months. This leads

to a seasonality in the bomb ^{14}C content of the carbon in surface water.

40. Quay, P.D. and M. Stuiver. 1980. Vertical advection-diffusion rates in the oceanic thermocline determined from ^{14}C distributions. Radiocarbon, V22, p. 607-625.
Use of the one-dimensional advection-diffusion equation to estimate the apparent rates of vertical advection and diffusion at individual GEOSECS stations in the Atlantic Ocean.
41. Rooth, C.G.H., R.A. Fine and H.G. Ostlund. 1980. Abyssal mixing and circulation in the north Pacific from radiocarbon data. Technical Report, Univ. of Miami, TR 80-2.

3. PAPERS DEALING WITH THE DISTRIBUTION OF TRITIUM IN THE OCEAN (#42 to #56)

42. Buttlar, H.V. and W.F. Libby. 1955. Natural distribution of cosmic ray produced tritium. Jour. of Inorg. Chem., V1, p. 75-95.
The discovery of natural tritium.
43. Giletti, B.J., F. Bazan, and J.L. Kulp. 1958. The geochemistry of tritium, EOS Trans. AGU, V39, p. 807-818.
Measurements of the tritium content of ocean water samples collected prior to the onset of nuclear contamination.
Because of the very low tritium content of these samples and the rather large blank correction applied, the validity of these measurements remains an open question.
44. Houtermans, J. 1965. Tritium in surface water of the North Pacific Ocean. 6th Carbon-14 and Tritium Dating Conference, CONF 650652, p. 565-572.
The distribution of bomb-produced tritium in the Pacific Ocean.
45. Dockins, K.O., A.E. Bainbridge, J.C. Houtermans and H.E. Suess. 1967. Tritium in the mixed layer of the North Pacific Ocean. In: Radiocative Dating and Methods of Low-Level Counting. International Atomic Energy Agency, Vienna, p. 129-142.
Tritium measurements on surface water samples collected at 12 stations in the north and south Pacific over the period 1959 to 1966. Also given are measurements on surface water samples collected along north-south traverses in the Pacific Ocean during the same period.
46. Munnich, K.O. and W. Roether. 1967. Transfer of bomb- ^{14}C and tritium from the atmosphere to the oceans: Internal mixing of the ocean on the basis of tritium and ^{14}C profiles. In: Radioactive Dating and Low-Level Counting. International Atomic Energy Agency, Vienna, p. 93-104.
North-south traverses in the North Atlantic of the tritium content of surface water taken during the period 1965-1966.

Also given are vertical profiles of tritium at stations along these traverses.

47. Ostlund, H.G., M.O. Rinkle and C. Rooth. 1969. Tritium in the equatorial Atlantic Current System. *J. Geophys. Res.* V74, p. 4535-4543.
Measurement of the vertical distribution of tritium at several equatorial Atlantic stations occupied in 1964.
48. Roether, W. 1974. The tritium and ^{14}C profiles at the GEOSECS I (1969) and GOGO I (1971) North Pacific station. *Earth & Planet. Sci. Lett.* V23, p. 108-115.
Tritium and ^{14}C measurements at 28.5°N , 121.6°W in 1969 and 1971.
49. Ostlund, H.G., R. Brescher and W.H. Peterson. 1974. Ocean tritium profiles 1965-1972. Tritium Laboratory Data Report #3. Rosenstiel School of Marine and Atmospheric Sciences, University of Miami.
Tritium measurements from the north and equatorial Atlantic on samples collected during the period 1965 to 1972.
50. Michel, R.L. and H.E. Suess. 1975. Bomb tritium in the Pacific Ocean. *Jour. of Geophysical Res.* V80, p. 4139-4152.
Extensive measurements of the distribution of tritium in the Pacific Ocean over the period 1959 to 1973.
51. Ostlund, H.G., H.G. Dorsey and R. Brescher. 1976. GEOSECS Atlantic Radio carbon and Tritium Results (Miami). Tritium Laboratory Data Rept. #5, Rosenstiel School of Marine and Atmospheric Science, Univ. of Miami.
All the tritium results obtained on samples from the Atlantic GEOSECS program are given in this report.
52. Ostlund, H.G., H.G. Dorsey, R. Brescher, and W.H. Peterson. 1977. Tritium Laboratory Data Report #6, Oceanic Tritium Profiles North Atlantic Gyre Sections, 1972-1973, Rosenstiel School of Marine and Atmospheric Science, Univ. of Miami.
Tritium measurements on profiles taken in 1972 and 1973 along east-west sections at 29°N and 14°N . Also included in this report are the results from eastern Atlantic stations from 14°N to 30°S occupied during the same time interval. These results compliment those by GEOSECS.
53. Roether, W. and W. Weiss. 1978. A transatlantic tritium section near 40°N . 1971. "METEOR" Forsch-Ergebn A, V20, p. 101-108.
Tritium measurement on samples collected in 1971 along a traverse across the Atlantic at 40°N . These results nicely complement those obtained on samples collected during the Atlantic GEOSECS program in 1972.
54. Ostlund, H.G., R. Brescher, R. Oleson and M.J. Ferguson. 1979.

GEOSECS Pacific radiocarbon and tritium results (Miami). Tritium Laboratory Data Report #8, Rosenstiel School of Marine and Atmospheric Science, Univ. of Miami.

All the tritium results obtained on samples from the Pacific GEOSECS program are given in this report.

55. Jenkins, W.J., W.V. Collentro and R.D. Boudreau. 1979. Woods Hole Oceanographic Institution Helium Isotope Laboratory Data Release #1, Technical Report Woods Hole Oceanographic Institution, Woods Hole, Mass.

A listing of tritium and helium 3 results from the Sargasso Sea surface waters and thermocline collected over the period 1974 to 1977.

56. Ostlund, H.G., R. Oleson and R. Brescher. 1980. GEOSECS Indian Ocean radiocarbon and tritium results. Tritium Laboratory Data Report #9, University of Miami, Miami, Florida.

All the tritium and half of the ^{14}C results obtained on samples from the Indian GEOSECS program are given in this report.

4. PAPERS DEALING WITH THE INTERPRETATION AND MODELING OF THE ADDITION OF TRITIUM TO THE SEA AND ITS PENETRATION INTO THE BODY OF THE SEA (#57 to #70)

57. Craig, H. and D. Lal. 1961. The production rate of natural tritium. Tellus, V13, p. 85.

Estimate of the rate of natural tritium production based on an integration of the cosmic ray production rates at various heights and geographical locations in the atmosphere.

58. Roether, W., K.O. Munnich, and H.G. Ostlund. 1970. Tritium profile at the North Pacific (1969) GEOSECS intercalibration station. Jour. of Geophys. Res. V75, p. 7672-7675.

An attempt is made to model the vertical distribution of tritium in the eastern North Pacific using the steady state advection-diffusion equation.

59. Rooth, C.G. and H.G. Ostlund. 1972. Penetration of tritium into the Atlantic thermocline. Deep Sea Res. V19, p. 481-492. Concluding from the data in hand that the distribution of bomb tritium in the north temperate Atlantic thermocline had reached steady state, the balance between tritium decay and diffusive mixing is used to obtain upper limits of the vertical diffusivity in the oceanic thermocline.

60. Fine, R.A. and H.G. Ostlund. 1977. Source function for tritium transport models in the Pacific, Geophys. Res. Lett. V4, p. 461-464.

Equations describing the latitude and time histories of tritium in the surface waters of the Pacific Ocean.

61. Dreisigacker, E., and W. Roether. 1978. Tritium and ^{90}Sr in

North Atlantic Surface Water. Earth & Planet. Sci. Lett. V38, p. 301-312.

Two-box model designed to explain the observed temporal evolution of surface water tritium concentrations in the North Atlantic Ocean.

62. Hoffert, M.I. and W.S. Broecker. 1978. Apparent vertical eddy diffusion rates in the pycnocline of the Norwegian Sea as determined from the vertical distribution of tritium. Geophysical Res. Lett. V5, p. 502-504.
A determination of vertical eddy diffusion rates in the Norwegian Sea based on the vertical distribution of tritium.
63. Weiss, W., W. Roether and E. Dreisigacker. 1979. Tritium in the North Atlantic Ocean: inventory, input, and transfer into the deepwater. In: The Behavior of Tritium in the Environment IAEA-SM-232/98.
The primary goal of this paper is to provide estimates of the latitude and time dependence of the delivery of bomb tritium to the surface of the North Atlantic Ocean.
64. Broecker, W.S. and H.G. Ostlund. 1979. Property distributions along the $\sigma_0=26.8$ isopycnal in the Atlantic Ocean. J. Geophys. Res. V84, p. 1145-1154.
The relationship between the distributions of tritium and of potential temperature on a surface of constant density in the thermocline of the Atlantic Ocean. The role of fronts at 15°N and 15°S is emphasized.
65. Weiss, W. and W. Roether. 1980. The rates of tritium input to the world oceans. Earth & Planet. Sci. Lett. V49, p. 434-446.
This paper extends the technique employed by these authors in reconstructing the tritium input to the North Atlantic to the other oceans.
66. Fine, R.A. and H.G. Ostlund. 1980. Exchange times in the Pacific equatorial current system. Earth & Planet. Sci. Lett. V49, p. 447-452.
Attempt to estimate the exchange time of water between the North Equatorial Counter Current and the North Equatorial Current based on the distribution of bomb tritium.
67. Quay, P.D., W.S. Broecker, R.H. Hesslein and D.W. Schindler. 1980. Vertical diffusion rates determined by tritium tracer experiments in the thermocline and hypolimnion of two lakes. Limnology and Oceanog. V25, p. 201-218.
A discussion of vertical diffusion rates in lakes as determined by measuring the distribution of purposeful tritium tracers and the evolution of the summer temperature profiles with emphasis on the relationship to density gradient.

68. Fine, R.A., J.L. Reid, H.G. Ostlund. 1981. Circulation of Tritium in the Pacific Ocean. *Jour. of Phys. Ocean.*, V11, p. 3-14.

Three-dimensional picture of the penetration of tritium in the thermocline of the Pacific Ocean.

69. Viecelli, J. A., H.W. Ellsaesser and J.E. Burt. 1981. A carbon cycle model with latitude dependence, *Climatic Change* V3, p.281-302.

A regional box-diffusion model is constructed using the distribution of bomb radiocarbon and tritium to calibrate the mixing parameters.

70. Jenkins, W.J. and P.B. Rhines. 1980. Tritium in the Deep North Atlantic. *Nature*, V286, p. 877-880.

Measurement of tritium along the Blake-Bahama Outer Ridge showing that the southward flowing deep current has carried bomb tritium to a latitude of 30°N.

5. PAPERS DEALING WITH THE JOINT INTERPRETATION OF THE DISTRIBUTIONS OF BOMB RADIOCARBON AND TRITIUM IN THE OCEAN (#71 to #75)

71. Peterson, W.H. and C.G. Rooth., 1976. Formation and exchange of deep water in the Greenland and Norwegian Seas. *Deep Sea Res.* V23, p. 273-283.

Tritium and radiocarbon data are used to calibrate a model for the ventilation of the Greenland and Norwegian Seas.

72. Broecker, W.S., T.-H. Peng and T. Takahashi. 1980. A strategy for the use of bomb-produced radiocarbon as a tracer of fossil fuel CO₂ into the deep sea source regions. *Earth & Planet. Sci. Lett.* V49, p. 463-468.

An attempt is made in this paper to explain the near linear relationship between the bomb tritium and bomb radiocarbon distributions observed for waters in the northern Atlantic Ocean.

73. Broecker, W.S. and T.-H. Peng. 1980. The distribution of bomb-produced tritium and radiocarbon at GEOSECS station 347 in the eastern North Pacific, *Earth & Planet. Sci. Lett.* V49, p. 453-462.

An attempt to extend the advection-diffusion approach of Roether et al., to both the vertical distribution of radiocarbon and tritium at a station in the eastern North Pacific. As three sets of data exist for this station (Sept. 1969, Nov. 1971 and June 1974), an attempt was made to match the time distribution as well as the vertical distributions of these transient tracers.

74. Roether, W., K.O. Munnich, and H. Schoch. 1980. On the ¹⁴C to tritium relationship in the North Atlantic Ocean. *Radio-carbon*, V22, p. 636-646.

The two-box model previously proposed to explain the temporal history of tritium in the surface waters of the North Atlantic is applied to radiocarbon in an attempt to explain the evolution of the radiocarbon to tritium ratio in surface waters.

75. Broecker, W.S., T.-H. Peng and R. Engh. 1980. Modeling the Carbon System. Radiocarbon, V22, p. 565-598.

The application of the distribution of natural and bomb-produced ^{14}C and of tritium in calibrating ocean box-diffusion models and regional ocean models.

6. PAPERS DEALING WITH THE DISTRIBUTION OF EXCESS ^{222}Rn IN THE DEEP SEA (#76 to #86)

76. Broecker, W.S. 1965. An application of natural radon to problems in ocean circulation. In: Symposium on Diffusion in Oceans and Fresh Waters, ed. by T. Ichiye, Lamont-Doherty Geological Observatory, Palisades, New York, p. 116-145.

Discussion of the potential of the radon method for measurement of the vertical mixing rate in near bottom waters.

77. Broecker, W.S., J. Cromwell and Y.-H. Li. 1968. Rates of vertical eddy diffusion near the ocean floor based on measurements of the distribution of excess ^{222}Rn . Earth & Planet. Sci. Lett. V5, p. 101 - 105.

The first paper on near bottom radon measurements and the vertical diffusivities derived therefrom. Also a discussion of the factors controlling the magnitude of the flux of radon from the sea floor.

78. Broecker, W.S. and A. Kaufman. 1970. Near-surface and near-bottom radon results for the 1969 North Pacific GEOSECS Station. Jour. Geophys. Res. V75, p. 7679-7681.

The radon profile at this station shows a distinct maximum 50 meters above the bottom demonstrating the importance of horizontal transport from adjacent "hills".

79. Chung, Y.C. and H. Craig. 1972. Excess radon and temperature profiles from the eastern Equatorial Pacific, Earth & Planet. Sci. Lett. V14, p. 55-64.

An attempt to relate the distribution of ^{222}Rn above the sea floor to the pattern of potential temperature change.

80. Sarmiento, J.L., H.W. Feely, W.S. Moore, A.E. Bainbridge and W.S. Broecker. 1976. The relationship between vertical eddy diffusion and buoyancy gradient in the deep sea. Earth & Planet. Sci. Lett. V32, p. 357-370.

Demonstration of the inverse relationship between the apparent coefficient of vertical diffusion as established from the profile of excess ^{222}Rn and the density gradient in the deep sea.

81. Bainbridge, A.E., P.E. Biscaye, W.S. Broecker, R.M. Horowitz,

- G. Mathieu, J.L. Sarmiento and D.W. Spencer. 1976. GEOSECS Atlantic bottom hydrography radon, and suspended particulate Atlas. GEOSECS Operations Group, Scripps Institution of Oceanography Internal Report.
- Complete listing of deep Atlantic radon and associated potential temperature, salinity and density data.
82. Bainbridge, A.E., P.E. Biscaye, R.M. Horowitz, G. Mathieu, J.-L. Sarmiento and D.W. Spencer. 1977. GEOSECS Pacific bottom hydrography, radon, and suspended particulate Atlas. GEOSECS Operations Group, Scripps Institution of Oceanography, Internal Report.
- Complete listing of deep Pacific radon and associated potential temperature, salinity and density data.
83. Sarmiento, J.L., W.S. Broecker and P.E. Biscaye. 1978. Excess bottom radon distribution in deep ocean passages. *J. Geophys. Res.* V83, p.5068-5076.
- Demonstration that waters passing through oceanic passages experience very high vertical mixing rates and receive large amounts of excess radon (presumable from the Mn oxide-lined floor and walls of the passage).
84. Sarmiento, J.L. and C.G.H. Rooth. 1980. A comparison of vertical and isopycnal mixing models in the deep sea based on radon-222 measurements, *Jour. Geophys. Res.* V85, p. 1515-1518.
- An attempt to show that the distribution of excess radon-222 in the deep sea might reflect horizontal as well as vertical mixing processes.
85. Sarmiento, J.L. and W.S. Broecker. 1980. Ocean floor ^{222}Rn standing crops in the Atlantic and Pacific Oceans. *Earth & Planet. Sci. Lett.* V49, p. 341-350.
- Relationship of standing crops of excess ^{222}Rn in the bottom waters of the world ocean to the rate of sedimentation and to the presence of manganese nodules.
86. Kadko, D. 1980. ^{230}Th , ^{226}Ra and ^{222}Rn in abyssal sediments. *Earth & Planet. Sci. Lett.* V49, p. 360-380.
- An attempt to quantify the relationship between the radon flux from the sea floor, the rate of sedimentation, the extent of bioturbation and the extent of ^{226}Ra loss from the sediment mixed layer.
- 7. PAPERS DEALING WITH THE DISTRIBUTION OF ^{228}Ra IN THE SEA (#87 to #96)**
87. Moore, W.S. and W.M. Sackett. 1964. Uranium and thorium series in equilibrium in seawater. *Jour. of Geophys. Res.* V69, p. 5401-5405.
- The discovery of ^{228}Th and ^{228}Ra in seawater.
88. Moore, W.S. 1969. Oceanic concentrations of ^{228}Ra . *Earth & Planet. Sci. Lett.* V6, p. 437-446.

Preliminary measurements on the distribution of ^{228}Ra in the sea.

89. Trier, R.M., W.S. Broecker and H.W. Feely. 1970. Radium-228 profile at the second GEOSECS intercalibration station, 1970, in the North Atlantic. *Earth & Planet. Sci. Lett.* V16, p. 141-145.
Profile of ^{228}Ra showing surface and bottom maxima.
90. Kaufman, A., R.M. Trier and W.S. Broecker. 1973. Distribution of ^{228}Ra in the world ocean. *Jour. of Geophys. Res.* V78, p. 8827-8848.
Data showing the contrast between the ^{228}Ra concentration in near shore and open ocean surface water samples and estimate of lateral mixing rates derived therefrom.
91. Sarmiento, J.L., H.W. Feely, W.S. Moore, A.E. Bainbridge and W.S. Broecker. 1976. The relationship between vertical eddy diffusion and buoyancy gradient in the deep sea. *Earth & Planet. Sci. Lett.* V32, p. 357-370.
Two deep water ^{228}Ra profiles, one from the North Atlantic and one from the South Atlantic which yield apparent vertical diffusivity-density gradient products similar to those obtained from ^{222}Rn profiles.
92. Knauss, K.G., T.L. Ku and W.S. Moore. 1978. Radium and thorium isotopes in the surface water of the east Pacific and coastal southern California. *Earth & Planet. Sci. Lett.* V39, p. 235-240.
Gradients of ^{228}Ra away from the continental margin and implications regarding rates of lateral mixing.
93. Li, Y.-H., H.W. Feely and P.H. Santschi. 1979. ^{228}Th - ^{228}Ra radioactive disequilibrium in the New York Bight and its implications for coastal pollution. *Earth & Planet. Sci. Lett.* V42, p. 13-16.
Gradients of ^{228}Ra away from the continental margin and implications regarding rates of lateral mixing.
94. Li, Y.-H., H.W. Feely, and J.R. Toggweiler. 1980. ^{228}Ra and ^{228}Th concentration in GEOSECS Atlantic surface waters. *Deep Sea Res.*, V27A, p. 545-555.
Distribution of ^{228}Ra in the upper 350 meters of the Atlantic Ocean.
95. Moore, W.S., H.W. Feely and Y.-H. Li. 1980. Radium isotopes in sub-arctic waters. *Earth & Planet. Sci. Lett.* V49, p. 392-340.
Distribution of ^{228}Ra in the surface waters of the Greenland, Norwegian and Labrador Seas.
96. Sarmiento, J.L., C.G. Rooth and W.S. Broecker. 1982. Radium-228 as a tracer of isopycnal mixing in the deep ocean *Jour. Geophys. Res.*

An analysis of the Ra-228 data obtained from the deep North Atlantic as part of the GEOSECS program suggests that isopycnal mixing has a more important influence on the distribution of this isotope than vertical mixing.

8. PAPERS DEALING WITH THE DISTRIBUTION OF ^{90}Sr , ^{137}Cs , ^{85}Kr AND ^{39}Ar IN THE SEA (#97 to #111)

97. Bowen, V.T. and T.T. Sugihara. 1958. Marine geochemical studies with fallout radioisotopes. In: Proc. Intern. Con. Peaceful Uses At. Energy, 2nd, Geneva, V18, p. 434.
Measurements of fallout radioisotopes in the Atlantic Ocean.
98. Bowen, V.T. and T.T. Sugihara. 1960. Strontium-90 in the 'mixed layer' of the Atlantic Ocean, Nature, V186, p. 71-72.
Measurements of ^{90}Sr in surface waters from the Atlantic Ocean.
99. Rocco, G.G. and W.S. Broecker. 1963. The vertical distribution of Cesium-137 and Strontium-90 in the oceans. J. Geophys. Res., V68, p. 4501-4512.
Measurements of the vertical distribution of ^{137}Cs and ^{90}Sr in the Caribbean Sea showing that as of 1965 these isotopes had not penetrated beneath 500 meters.
100. Broecker, W.S., E.R. Bonebakker, and G.G. Rocco. 1966. The vertical distribution of Cesium-137 and Strontium-90 in the ocean, 2. J. Geophys. Res. V71, p.1999-2003.
Measurements of ^{137}Cs and ^{90}Sr profiles in the North Atlantic and equatorial Pacific.
101. Bowen, V.T., V.E. Noskin, H.L. Volchok and T.T. Sugihara. 1969. Strontium-90: concentrations in surface waters of the Atlantic Ocean. Science V164, p.825-827.
Measurements of ^{90}Sr in samples of Atlantic surface water.
102. Volchok, H.L., V.T. Bowen, T.R. Folsom, W.S. Broecker, E.A. Schuert and G.S. Bien. 1971. Oceanic distributions of radio-nuclides from nuclear explosions. In: Radioactivity in the Marine Environment, edited by A.H. Seymour, U.S. Government Printing Office, Washington, D.C. p. 42-89.
Summary of the ^{90}Sr and ^{137}Cs data for ocean samples up to 1969.
103. Volchok, H.L. and M.T. Kleinman, 1971, 1972, 1974 and 1975. Global strontium-90 fallout and precipitation: summary of data by 10 degree bands of latitude, Q. Rep. 245, HASL, USAEC 1-2; Q. Rep. 276, HASL, USAEC 1-2; Q. Rep. HASL USAEC 1-17; Q. Rep. HALS USAEC 1-2.
Latitude and time dependence of ^{90}Sr fallout as estimated from rainfall and soil measurements.

104. Bowen, V.T. and W. Roether. 1973. Vertical distributions of strontium-90, cesium-137 and tritium near 45° north in the Atlantic. *J. Geophys. Res.* V78, p. 6277-6285.
 Measurements showing the deep penetration of the fallout isotopes in the northern Atlantic Ocean.
105. Volchok, H.L. 1974. Is there excess ^{90}Sr fallout in the oceans? *Q. Rep.* 286, HASL, USAEC 1-82.
 Addresses the question of the ratio of ^{90}Sr fallout over land to that over the ocean.
106. Schroeder, J. 1975. Krypton-85 in the ocean, *Z. Naturforsch.*, V30a, p. 962-967.
 First report of ^{85}Kr measurements in sea water.
107. Stockburger, H., H. Sartorius and A. Littkus. 1977. Messung der Krypton-85 und Xenon-133-Aktivität der atmosphärischen Luft, *Z Naturforsch*, V32a, p. 1249-1253.
 Description of the techniques to measure the ^{85}Kr and ^{133}Xe activities in the atmosphere.
108. Dreisigacker, E. and W. Roether. 1978. Tritium and ^{90}Sr in North Atlantic surface water. *Earth & Planet. Sci. Lett.* V38, p. 301-312.
 Relationship between the space and time distribution of tritium and ^{90}Sr in the North Atlantic.
109. Bowen, V.T., V.E. Noskin, H.D. Livingston and H.L. Volchok. 1980. Fallout radionuclides in the Pacific Ocean: vertical and horizontal distributions, largely from GEOSECS stations. *Earth & Planet. Sci. Lett.* V49, p. 411-434.
 Distribution of ^{137}Cs in the North Pacific as determined from samples collected during the GEOSECS program.
110. Weiss, W., A. Sittkus, H. Stockburger, H. Sartorius. (in press) Large-scale atmospheric mixing derived from meridional profiles of krypton-85. *Jour. Geophys. Res.*
 Measurements of ^{85}Kr in the atmosphere along a south to north track in the Atlantic Ocean showing a sharp change from the ambient southern hemisphere to the higher ambient northern hemisphere value close to the ITCZ.
111. Loosli, H.H. A dating method with ^{39}Ar . *Earth & Planet. Sci. Lett.* (in press);
 First report of ^{39}Ar measurements in sea water.

B. PAPERS DEALING WITH RADIOTRACERS OF PARTICLE MOVEMENT AND THE SCAVENGING OF REACTIVE METALS (#112 to #170)

1. PAPERS DEALING WITH THE DISTRIBUTION OF ^{226}Ra IN THE OCEAN (#112 to #121)
112. Koczy, F.F. 1958. Natural radium as a tracer in the ocean. *Proc. Second U.N. Int. Conf. Peaceful Uses of Atomic Energy*

V18, p. 351-357.

Paper showing how Ra-226 might be used as a tracer of water motion.

113. Broecker, W.S., Y.-H. Li and J. Cromwell. 1967. Radium-226 and radon-222 concentrations in the Atlantic and Pacific Oceans. *Science* V158, p. 1307-1310.
Measurements showing the difference in the ^{226}Ra concentration between waters in the deep Atlantic and in the deep Pacific.
114. Ku, T.L., Y.-H. Li, G.G. Mathieu and H.K. Wong. 1970. Radium in the Indian-Antarctic Ocean south of Australia. *Jour. of Geophys. Res.* V75, p. 5286-5292.
Distribution of Ra-226 in the Antarctic waters.
115. Chung, Y.-C. 1974. Radium-226 and Ra-Ba relationships in Antarctic waters. *Earth and Planetary Science Lett.* V23, p. 125-135.
Vertical distribution of ^{226}Ra at several stations in the Pacific and Antarctic Ocean.
116. Broecker, W.S., J. Goddard and J.L. Sarmiento. 1976. The distribution of ^{226}Ra in the Atlantic Ocean. *Earth & Planet. Sci. Lett.* V32, p.220-235.
Presentation of the ^{226}Ra results from the GEOSECS Atlantic program.
117. Chung, Y.-C. 1976. The deep ^{226}Ra maximum in the northeast Pacific. *Earth & Planet. Sci. Lett.* V32, p. 249-257.
Presentation of the ^{226}Ra measurements made on GEOSECS samples from the North Pacific.
118. Chung, Y.-C and H. Craig. 1980. The distribution of radium-226 and its relationship with barium and silicate in the Pacific. *Earth & Planet. Sci. Lett.* V49, p. 267-292.
Presentation of ^{226}Ra results from the GEOSECS Pacific program.
119. Ku, T.L., C.A. Hub, and P.S. Chen. 1980. Meridional distributions of ^{226}Ra in the eastern Pacific along GEOSECS cruise tracks. *Earth & Planet. Sci. Lett.* V49, p. 293-308.
Presentation of ^{226}Ra results from the GEOSECS Pacific program.
120. Kadko, D. 1980. ^{230}Th , ^{226}Ra , and ^{222}Rn in abyssal sediments. *Earth & Planet. Sci. Lett.* V49, p. 360-380.
A discussion of ^{222}Rn flux out of deep sea sediments. This flux is related to the ^{226}Ra profile in the sediment which in turn depends on the ^{230}Th rain rate and the bulk sedimentation rate.
121. Cochran, J.K. 1980. The flux of ^{226}Ra from deep sea sediments. *Earth & Planet. Sci. Lett.* V49, p. 381-382.

Estimates of the flux of ^{226}Ra from deep sea sediments based on $^{226}\text{Ra}/^{230}\text{Th}$ ratio measurements. The results show far higher fluxes for cores from the eastern Pacific than for those from the Atlantic.

2. PAPERS DEALING WITH THE DISTRIBUTION OF ^{234}Th , ^{228}Th , ^{230}Th AND ^{231}Pa IN THE OCEAN (#122 to #138)

122. Moore, W.S. and W.M. Sackett. 1964. Uranium and thorium series inequilibrium in sea water. Jour. Geophys. Res. V69, p. 5401-5405.
The demonstration of the lack of equilibrium between ^{228}Th and ^{228}Ra .
123. Kaufman, A. 1969. The ^{232}Th concentration of surface ocean water. Geochim. Cosmochim. Acta V33, p. 717-724.
Upper limit on the concentration of ^{232}Th in surface ocean water.
124. Bhat, S.G., S. Krishnaswami, D. Lal, M. Rama, and W.S. Moore. 1969. $^{234}\text{Th}/^{238}\text{U}$ ratios in the ocean. Earth and Planetary Science Lett., V5, p. 483-491.
Demonstration of the lack of equilibrium between ^{234}Th and ^{238}U in surface waters.
125. Broecker, W.S., A. Kaufman, and R.M. Trier. 1973. The residence time of thorium in surface seawater and its implications regarding the fate of reactive pollutants. Earth and Planet. Sci. Lett. V20, p. 35-44.
 ^{228}Th to ^{228}Ra measurements in surface ocean water.
126. Matsumoto, E. 1975. $^{234}\text{Th}/^{238}\text{U}$ disequilibrium in the surface layer of the ocean. Geochim. Cosmochim. Acta, V39, p. 205-212.
Measurements showing the deficiency of ^{234}Th in surface waters.
127. Ku, T.L., K.G. Knauss, and G.G. Mathieu. 1977. Uranium in open ocean: concentration and isotopic compensation. Deep Sea Res. V24, p. 1005-1007.
Summary of data demonstrating the constancy of the uranium content of sea salt and of the $^{234}\text{U}/^{238}\text{U}$ in sea water.
128. Spencer, D.W., P.G. Brewer, A.P. Fleer, S. Honjo, S. Krishnaswami and Y. Nozaki. 1978. Chemical fluxes from a sediment trap experiment in the deep Sargasso Sea. J. Mar. Res. V36, p. 493-523.
Thorium isotope concentrations in the material caught in sediment traps and their implications to trapping efficiency and particulate scavenging rates.
129. DeMaster, D.J. 1979. The marine budgets of silica and ^{32}Si . Ph.D. thesis, Yale University, New Haven, Conn.
Measurements of ^{231}Pa and ^{230}Th concentrations in sediment core tops showing that ^{231}Pa is preferentially

deposited beneath areas of upwelling.

130. Li, Y.-H., H.W. Feely and P.H. Santschi. 1979. ^{228}Th - ^{228}Ra radioactive disequilibrium in the New York Bight and its implications for coastal pollution. *Earth and Planet. Sci. Lett.*, V42, p. 13-26.
Measurements showing the decrease in ^{228}Th residence time in surface waters as the coast is approached.
131. Minagawa, M. and S. Tsunogai. 1980. Removal of ^{234}Th from a coastal sea: Funka Bay. *Earth and Planet. Sci. Lett.*, V47, p. 51-64.
Measurements demonstrating the rapid removal of thorium from coastal waters.
132. Li, Y.-H., H.W. Feely and J.R. Toggweiler. 1980. ^{228}Ra and ^{228}Th concentrations in GEOSECS Atlantic surface waters. *Deep Sea Research*, V27A, p. 545-555.
Demonstration that the ^{228}Th extracted from surface waters must be in part returned to solution in the upper thermocline.
133. Santschi, P.H., D. Adler, M. Amdurer, Y.-H. Li and J. Bell. 1980. Thorium isotopes as analogues for "particle-reactive" pollutants in coastal marine environments. *Earth and Planet. Sci. Lett.* V47, p. 327-335.
Comparison between the removal rates of thorium isotopes in Narragansett Bay and in controlled ecosystems designed to duplicate the conditions in this water body.
134. Anderson, R.F. 1981. The marine geochemistry of thorium and protactinium. Ph.D. thesis. Woods Hole Oceanographic Institution, Woods Hole, Mass.
Measurements of thorium and protactinium isotopes in materials from sediment traps, filtered particulates, and manganese adsorbers at four ocean stations.
135. Nozaki, Y., Y. Horibe and H. Tsubota. 1981. The water column distributions of thorium isotopes in the western North Pacific. *Earth and Planet. Sci. Lett.* V54, p. 203-216.
Measurements of ^{230}Th dissolved in sea water as a function of depth in the North Pacific Ocean. A first! Also a demonstration that the adsorption of thorium onto particles must be reversible.
136. Moore, W.S. 1981. The thorium isotope content of ocean water. *Earth & Planet. Sci. Lett.* V53, p. 419-426.
Measurements of the ^{230}Th content of surface and deep water showing that the residence time increases with depth reaching as much as 100 years in near bottom waters.
137. Krishnaswami, S., M.M. Sarin and B.L.K. Somayajulu. 1981. Chemical and radiochemical investigations of surface and deep

particles in the Indian Ocean. Earth & Planet. Sci. Lett., V54, p. 81-96.

Measurements of the vertical distribution of the amount of ^{230}Th on suspended particulate matter in the Indian Ocean.

138. Kaufman, A.; Y.-H. Li and K.K. Turekian. 1981. The removal rates of ^{234}Th and ^{228}Th from waters of the New York Bight. Earth & Planet. Sci. Lett., V54, p. 385-392.
Comparison of thorium removal times calculated from $^{234}\text{Th}/^{238}\text{U}$ and $^{228}\text{Th}/^{228}\text{Ra}$ ratios.

- 138a. Bacon, M.P. and R.F. Anderson. 1982. Distribution of thorium isotopes between dissolved and particulate forms in the deep sea. Jour. Geophys. Res. V87, p.2045-2056.
Demonstration that the fraction of thorium on particulates depend on the half-life of the isotope and on the concentration of the suspended matter.

3. PAPERS DEALING WITH THE DISTRIBUTION OF ^{210}Po AND ^{210}Pb IN THE SEA (#139-#161)

139. Rama, M., Koide, M. and E.D. Goldberg. 1961. Lead-210 in natural waters. Science V134, p. 98-99.
First paper showing that ^{210}Pb from atmospheric fallout is present in natural waters.
140. Fisenne, I.M. 1968. Distributions of lead-210 and radium-226 in soil. Rep. UCRL-18140 U.S. Dept. of Energy, Wash., D.C. p. 145-158.
Use of soil data to estimate the flux of ^{210}Pb atoms out of the atmosphere.
- 140a. Windom, H.L. 1969. Atmospheric dust records in permanent snowfields: Implications to marine sedimentation. Geol. Soc. Amer. Bull. V80, p.761-782.
Evaluation of the contribution of atmospherically transported solids to recent marine sediments based on the dust accumulation in the permanent snowfields.
141. Shannon, L.V., R.D. Cherry and M.J. Orren. 1970. Polonium-210 and lead-210 in the marine environment. Geochim. Cosmochim. Acta, V34, p. 98-99.
 ^{210}Pb concentrations in marine plankton.
142. Tsunogai, S. and Y. Nozaki. 1971. Lead-210 and polonium-210 in the surface water of the Pacific. Geochem. J., V5, p. 165.
Distributions of ^{210}Pb and ^{210}Po in the sea.
- 142a. Krishnaswami, S., D. Lal, J.M. Martin, M. Meybeck. 1971. Geochronology of lake sediments. Earth & Planet. Sci. Letts. V11, p. 407-414.
This paper describes partially successful attempts to measure rates of sedimentation in lakes using ^{210}Pb

technique. Other radiometric techniques including ^{55}Fe , ^{137}Cs and ^{32}Si are also described.

143. Nozaki, Y. and S. Tsunogai. 1973. Lead-210 in the North Pacific and the transport of terrestrial material through the atmosphere. *Earth & Planet. Sci. Lett.* V20, p. 88-92.
Distribution of ^{210}Pb in the North Pacific Ocean.
144. Beasly, T.M., R.J. Eagle and T.A. Jokela. 1973. Polonium-210, lead-210 and stable lead in marine organisms. U.S. Atomic Energy Commission, HASL-273, p 1.
 ^{210}Pb concentrations in marine plankton.
145. Craig, H., S. Krishnaswami and B.L.K. Somayajulu. 1973. $^{210}\text{Pb}-^{226}\text{Ra}$: radioactive disequilibrium in the deep sea. *Earth & Planet. Sci. Lett.* V17, p. 295-305.
Determination of the ^{210}Pb to ^{226}Ra activity ratio in sea water.
- 145a. Gavini, M.B., J.N. Beck, and P.K. Kuroda. 1974. Mean residence time of the long-lived radon daughters in the atmosphere. *J. Geophys. Res.* V79, p. 4447-4452.
Measurements of the activities of ^{210}Pb , ^{210}Bi and ^{210}Po in rain samples at Fayetteville, Arkansas. Mean residence time of these nuclides in the atmosphere are calculated.
146. Bruland, K.W., M. Koide and E.D. Goldberg. 1974. The comparative marine geochemistries of lead-210 and radium-226. *J. Geophys. Res.* V79, p. 3083-3086.
Measurements of ^{226}Ra and ^{210}Pb concentration in the Gulf of California and eastern North Pacific waters.
- 146a. Robbins, J.A. and D.N. Edgington. 1975. Determination of recent sedimentation rates in Lake Michigan using ^{210}Pb and ^{137}Cs . *Geochim. Cosmochim. Acta* V39, p. 285-303.
This paper describes the use of ^{210}Pb and ^{137}Cs radioactivity measurements to determine the rates of sedimentation in large lakes.
147. Krishnaswami, S., B.L.K. Somayajulu and Y.-C. Chung. 1975. $^{210}\text{Pb}/^{226}\text{Ra}$ disequilibrium in the Santa Barbara Basin. *Earth & Planet. Sci. Lett.* V27, p. 388-392.
Measurements of ^{210}Pb and ^{226}Ra in a small coastal basin.
- 147a. Kipphut, G.W. 1978. An investigation of sedimentary processes in lakes. Ph.D. thesis, Columbia Univ., Lamont-Doherty Geological Obs., Palisades, N.Y.
A discussion of the rates of sediment accumulation, rates and extents of sediment mixing, and rates of trace metal accumulation in the sediments of small lakes.
- 147b. Matsumoto, E. 1973. ^{210}Pb geochronology of sediments from Lake Shinji. *Geochem. Jour.* V9, p. 167-172.

Excess ^{210}Pb is used successfully for dating lake sediment cores.

148. Somayajulu, B.L.K. and H. Craig. 1976. Particulate and soluble ^{210}Pb activities in the deep sea. *Earth & Planet. Sci. Lett.* V32, p. 268-276.
Comparison of the amount of ^{210}Pb on particles and the amount dissolved in sea water.
149. Bacon, M.P., D.W. Spencer and P.G. Brewer. 1976. $^{210}\text{Pb}/^{226}\text{Ra}$ and $^{210}\text{Po}/^{210}\text{Pb}$ disequilibria in sea water and suspended particulate matter. *Earth & Planet. Sci. Lett.* V32, p. 277-296.
Measurements of ^{210}Po , ^{210}Pb and ^{226}Ra in seawater and in suspended particulates.
150. Thomson, J. and K.K. Turekian. 1976. ^{210}Po and ^{210}Pb distributions in ocean water from the eastern South Pacific. *Earth & Planet. Sci. Lett.* V32, p. 297-303.
The distributions of ^{210}Po and ^{210}Pb in the sea.
151. Nozaki, Y., J. Thomson and K.K. Turekian. 1976. The distributions of ^{210}Pb and ^{210}Po in the surface waters of the Pacific Ocean. *Earth & Planet. Sci. Lett.* V32, p. 304-312.
The distributions of ^{210}Po and ^{210}Pb in the sea.
152. Nozaki, Y. and S. Tsunogai. 1976. ^{226}Ra , ^{210}Pb , and ^{210}Po disequilibria in the western North Pacific. *Earth & Planet. Sci. Lett.*, V32, p. 313-321.
The distributions of ^{226}Ra , ^{210}Pb , and ^{210}Po in the sea.
153. Moore, H.E. and S.E. Poet. 1976. ^{210}Pb fluxes determined from ^{210}Pb and ^{226}Ra soil profiles. *J. Geophys. Res.* V81, p. 1056-1058.
Use of soil data to estimate the flux of ^{210}Pb atoms from the atmosphere.
154. Turekian, K.K., Y. Nozaki and L.K. Benninger. 1977. Geochemistry of atmospheric radon and radon products. *Ann. Rev. Earth & Planet. Sci.* V5, p. 227-255.
Review paper discussing the sources of atmospheric radon and the sinks for the ^{210}Pb produced by the decay of radon in the atmosphere.
155. Nozaki, Y., D.J. DeMaster, D.M. Lewes and K.K. Turekian. 1978. Atmospheric ^{210}Pb fluxes determined from soil profiles. *Jour. of Geophys. Res.* V83, p. 4047-4051.
Use of soil data to estimate the flux of ^{210}Pb atoms from the atmosphere.
- 155a. Spencer, D.W., P.G. Brewer, A. Fleer, S. Honjo, S. Krishnaswami and Y. Nozaki. 1978. Chemical fluxes from a sediment trap experiment in the deep Sargasso Sea. *Jour. Mar. Res.* V36, p. 493-523.

Measurements of the flux of ^{210}Pb atoms toward the deep sea floor.

156. Beasly, T.M., M. Heyraud, J.J.W. Higgo, R.D. Cherry and S.W. Fowler. 1978. ^{210}Po and ^{210}Pb in zooplankton fecal pellets. *Mar. Biol.* V44, p. 325-328.
 ^{210}Pb in waste products of organisms.
157. Tsunogai, S. and K. Horada. 1980. ^{226}Ra and ^{210}Pb in the western North Pacific. In: *Isotope Marine Chemistry*, ed. by E.D. Goldberg, Y. Horibe and K. Saruhashi, Uchida Rokahu Ho, Tokyo, p. 165-191.
Profiles of ^{210}Pb and ^{226}Ra in the North Pacific Ocean.
158. Nozaki, Y., K.K. Turekian and K. von Damm. 1980. ^{210}Pb in GEOSECS water profiles from the North Pacific, *Earth & Planet. Sci. Lett.* V49, p. 393-400.
The distribution of ^{210}Pb in the sea.
159. Turekian, K.K. and Y. Nozaki. 1980. ^{210}Po and ^{210}Pb in the eastern South Pacific. The role of upwelling on their distribution in the water column. In: *Isotope Marine Chemistry*, ed. by E.D. Goldberg, Y. Horibe and K. Saruhashi, Uchida Rokahu Ho, Tokyo, p. 157-164.
The distribution of ^{210}Pb in the sea.
160. Chung, Y. and M.D. Applequist. 1980. ^{226}Ra and ^{210}Pb in the Weddell Sea. *Earth & Planet. Sci. Lett.* V49, p. 401-410.
The distribution of ^{210}Pb in the Antarctic Ocean.
161. Moore, W.S., K.W. Bruland, and J. Michel. 1981. Fluxes of uranium and thorium series isotopes in the Santa Barbara Basin. *Earth & Planet. Sci. Lett.* V53, p. 391-399.
Demonstration that the ^{210}Pb flux to the sediments of the Santa Barbara Basin is about seven times the sum of the water column production and atmospheric fallout rate.
 ^{210}Pb from the adjacent surface ocean must enter the Santa Barbara basin and be removed onto particles there.
- 161a. Spencer, D.W., M.P. Bacon and P.G. Brewer. 1980. The distribution of ^{210}Pb and ^{210}Po in the North Sea. *Thalassia Jugoslavia* V16, p. 125-154.
Strong depletions in ^{210}Pb content are found in North Sea waters.

4. PAPERS DEALING WITH THE INPUT OF AND DISTRIBUTION OF PLUTONIUM WITHIN THE SEA (#162 TO #165)

162. Hardy, E.P., P.W. Krey and H.L. Volchok. 1973. Global inventory and distribution of fallout plutonium. *Nature*, V241, p. 444-445.
Estimate of the amount and latitude dependence of plutonium fallout.

163. Noskin, V.E., and K.M. Wong. 1980. Plutonium in the North Equatorial Pacific. In: Processes Determining the Input Behaviour and Fate of Radionuclides and Trace Elements in Continental Shelf Environments, U.S. Dept. of Energy, Rep. CONF-790382, p. 11-28.
Measurements of plutonium in sea water samples from the Pacific.
164. Bowen, V.T., V.E. Noskin, H.D. Livingston and H.L. Volchok. 1980. Fallout Radionuclides in the Pacific Ocean: vertical and horizontal distributions, largely from GEOSECS stations. Earth & Planet. Sci. Lett. V49, p. 411-434.
The vertical distribution of ^{239}Pu and ^{240}Po in the North Pacific. Evidence for regeneration within the thermocline.
165. Santschi, P.H. and Y.-H. Li. Removal Pathways of Th and Pu Isotopes in Coastal Marine Environments. Proceedings of the Second Symposium on Natural Radiation Environment, Bombay, India. D.O.E. Symposium Series, (in press).
The correlation between plutonium and thorium in the coastal waters off New York suggest that these two elements are removed by the same mechanism. Evidence is presented that ^{228}Th is removed by adsorption onto particles.

5. PAPERS DEALING WITH THE DISTRIBUTIONS OF ^{14}C IN PARTICULATE DEBRIS AND ORGANISMS (#166 to #167)

166. Somazajulu, B.L.K., D. Lal, and S. Kusumger. 1966. Man-made carbon-14 in deep Pacific waters: transport by biological skeletal material. Science, V166, p. 1379-1399.
Demonstration that the CaCO_3 particles falling through the deep sea are of quite recent origin based on the presence of bomb-produced radiocarbon in samples of suspended particles filtered from deep sea water.
167. Williams, P.M., J.A. McGowan and M. Stuiyer. 1970. Bomb-carbon-14 in deep sea organisms. Nature, V227, p. 375-376.
Demonstration that the food eaten by deep dwelling fish is of recent origin through the finding that the flesh of these organisms contains bomb-produced radio carbon.

6. MODELS FOR PARTICULATE SCAVENGING IN THE OCEAN (#168 to #170)

168. Craig, H. 1974. A scavenging model for trace elements in the deep sea. Earth & Planet. Sci. Lett. V23, P. 149-159.
Application of the one dimensional advection-diffusion model to trace metals. A scavenging term which assumes first order irreversible removal onto particles is added to the water transport equations. Unlike the nutrient

elements which show excesses when plotted against potential temperature, the metals copper, antimony and scandium show deficiencies suggesting that they are being scavenged from deep water faster than they are being added by particle destruction.

169. Tsunogai, S. and M. Minagawa. 1978. Settling model for the removal of insoluble chemical elements in sea water. *Geo-chem. J.*, V12, p. 47-56.
Modeling the removal mechanism of chemical elements in the ocean based on the behavior of insoluble radio-nuclides in seawater.
170. Spencer, D.W., M.P. Bacon, and P.G. Brewer. 1981. Models of the distribution of ^{210}Pb in a section across the north equatorial Atlantic Ocean. *Jour. of Mar. Res.* V39, p. 119-138.
Two-dimensional model of the removal of ^{210}Pb from the ocean involving enhanced removal near the boundaries.
This enhanced removal could either be the result of direct uptake by the sediment or the result of higher particulate content of the water near the oceans' boundaries.

C. PAPERS DEALING WITH RADIO TRACERS OF GAS EXCHANGE (#171 to #194)

1. PAPERS DEALING WITH THE RADON METHOD (#171 to #177)

171. Broecker, W.S. 1965. An application of natural radon to problems in ocean circulation. In: *Symposium on Diffusion in Oceans and Fresh Waters*. Lamont-Doherty Geological Observatory, Palisades, N.Y., p. 116-145.
First publication showing the potential of radon as a gas-exchange tracer.
172. Broecker W.S. and T.-H. Peng. 1971. The vertical distribution of radon in the BOMEX area. *Earth & Planet. Sci. Lett.* V11, p. 99-108.
The first field application of the radon method. A long time series of ^{222}Rn and ^{226}Ra measurements in the mixed layer and upper thermocline in the open Atlantic off the island of Barbados permitted the establishment of the gas exchange rate under trade-wind conditions.
173. Peng, T.-H., T. Takahashi and W.S. Broecker. 1974. Surface radon measurements in the North Pacific Ocean station Papa. *J. Geophys. Res.* V79, p. 1772-1780.
A time series of ^{222}Rn and ^{226}Ra measurements under stormy winter conditions at 50°N in the Pacific Ocean.
174. Emerson, S. 1975. Gas exchange rates in small Canadian shield lakes. *Limnol. Oceanogr.*, V20, p. 754-761.
Addition of a ^{226}Ra spike to the mixed layer of small lake to enhance the ^{222}Rn production and thereby allow estimates of the gas transfer rate to be made.

175. Bainbridge, A.E., W.S. Broecker, R.M. Horowitz, Y.-H. Li, G. Mathieu and J. Sarmiento. 1977. GEOSECS Atlantic and Pacific Surface Hydrography and Radon Atlas. GOG Publication #120, Scripps Institution of Oceanography, La Jolla, Calif. Report containing listings of the radon and associated hydrographic data for the Atlantic and Pacific GEOSECS expeditions.
176. Peng, T.-H., W.S. Broecker, G.G. Mathieu and Y.-H. Li. 1979. Radon evasion rates in the Atlantic and Pacific Oceans as determined during the GEOSECS program. *Jour. of Geophys. Res.*, V84, p. 2471-2486.
 ^{222}Rn and ^{226}Ra measurements for surface mixed layer and upper thermocline samples from the Atlantic, Pacific and Antarctic Oceans. The gas exchange velocities obtained in this way permit regional and global averages to be obtained.
177. Kromer, B. and W. Roether. 1980. Wind dependence of gas exchange determined in field experiments with the radon method. Symposium on "Capillary waves and gas exchange", Trier 1979, published by SFB94 Meeresforschung, Hamburg, p. 87-90.
Use of integrated ^{222}Rn profiles to estimate the rate of gas exchange.

2. PAPERS DEALING WITH THE $^3\text{H}/^3\text{He}$ METHOD (#178 to #179)

178. Torgersen, T., Z. Top, W.B. Clarke, W.J. Jenkins, W.S. Broecker. 1977. A new method for physical limnology; tritium/helium-3 ages; results for Lakes Erie, Huron, and Ontario. *Limnol. Oceanog.* V22, p. 181-193.
Demonstration that the helium-3 to tritium ratio in the mixed layer of fresh water lakes can be used to determine the gas exchange rate.
179. Torgerson, T., G. Mathieu, R.H. Hesslein and W.S. Broecker. 1982. Gas exchange dependency on diffusion coefficient: Direct ^{222}Rn and ^3He comparisons in a small lake. *J. Geophys. Res.* V87, p. 546-556.
The mixed layer of a small Canadian shield lake was spiked with tritium and with ^{226}Ra permitting the simultaneous measurement of the evasion fluxes of ^3He and ^{222}Rn . Under these low-wind conditions the stagnant film model appears to provide a better approximation to the gas exchange process than the film replacement model.

3. PAPERS DEALING WITH THE RADIOCARBON METHOD (#180 to #184)

180. Craig, H. 1957. The natural distribution of radiocarbon and the exchange time of carbon dioxide between the atmosphere and the sea. *Tellus*, V9, p. 1-17.
Method of determining the average CO_2 exchange rate between air and sea based on the distribution of natural radiocarbon.

181. Munnich, K.O. and W. Roether. 1967. Transfer of bomb ^{14}C and tritium from the atmosphere to the ocean. Internal mixing of the ocean on the basis of tritium and ^{14}C profiles. In: Radioactive Dating and Methods of Low Level Counting. Proceedings IAEA-ICSU Symposium, Vienna, V92, p. 93-104.
Use of the ocean inventory of bomb-produced radiocarbon to determine the CO_2 invasion rate.
182. Broecker, W.S., T.-H. Peng and R. Engh. 1980. Modeling of the carbon system. Radiocarbon, V22, p. 565-598.
Use of the inventory of bomb ^{14}C in the ocean to estimate the rate of CO_2 invasion.
183. Hesslein, R., W.S. Broecker, P.D. Quay and D.W. Schindler. 1980. Whole lake radiocarbon experiment in an oligotrophic lake at the Experimental Lakes Area Northwestern Ontario. Canadian J. Fish. Aquatic Sci. V37, p. 454-463.
A discussion of carbon cycling in lakes based on data obtained by spiking the whole lake with radiocarbon.
184. Peng, T.-H. and W.S. Broecker. 1980. Gas exchange rates for three closed-basin lakes. Limnol. and Oceanog. V25, p. 789-796.
Utilization of the bomb ^{14}C inventory in saline lakes from Great Basin of the western U.S. to determine the CO_2 invasion rates.

4. PAPERS DEALING WITH LABORATORY MEASUREMENTS OF GAS EXCHANGE RATES (#185 to #188)

185. Downing, A.L. and G.A. Truesdale. 1955. Some factors affecting the rate of solution of oxygen in water. J. Appl. Chem., V5, p. 570-581.
Demonstration of the role of wind velocity in determining the rate of gas exchange.
186. Kanwisher, J. 1963. On the exchange of gases between the atmosphere and the sea. Deep Sea Res., V10, p. 195-207.
Lab experiments showing the effect of wind velocity and waves on the exchange rate of CO_2 between air and sea water.
187. Liss, P.S. 1973. Processes of gas exchange across an air-water interface. Deep Sea Res. V20, p. 221-238.
A review of our knowledge of the factors controlling the rate of gas exchange between the atmosphere and natural waters.
188. Broecker, H.-C., J. Peterman and W. Siems. 1979. The influence of wind on CO_2 -exchange in a wind-wave tunnel, including the effects of monolayers. Jour. of Marine Res., V36, p. 595-610.
Wind tunnel measurements demonstrating the importance of capillary waves on the rate of gas exchange.

5. THEORETICAL TREATMENTS OF VARIOUS ASPECTS OF THE GAS EXCHANGE PROCESS (#189 to #194)

189. Bolin, B. 1960. On the exchange of carbon dioxide between the atmosphere and the sea. *Tellus*, V12, p. 274-281.
Discussion of the role of the reactions between CO₂ and H₂O and CO₂ and OH⁻ in the enhancement of CO₂ exchange. A classic paper in the field of CO₂ exchange.
190. Danckwerts, P.V. 1970. Gas-liquid reactions. McGraw-Hill, New York.
The definitive chemical engineering text on gas exchange theory and experiment.
191. Munnich, K.O. and D. Flothmann. 1975. Gas exchange in relation to other air/sea interaction phenomena. SCOR Workshop on "Air/Sea Interaction Phenomena" Miami.
The relationship between momentum, heat and gas transfer.
192. Emerson S. 1975. Chemically enhanced CO₂ gas exchange in a eutrophic lake: a general model. *Limnol. and Oceanog.* V20, p. 743-753.
Demonstration that under the high pH conditions generated by excess algal growth in dissolved carbon-poor lakes a significant enhancement (over that for other gases) in the rate of CO₂ invasion occurs.
193. Deacon, E.L. 1977. Gas transfer to and across an air-Water interface. *Tellus* V29, p. 363-374.
Theoretical treatment of the gas exchange process suggesting that the film replacement model should provide a better approximation than the stagnant film model.
194. Munnich, K.O., W.B. Clarke, K.H. Fisher, D. Flothmann, B. Kromer, W. Roether, U. Siegenthaler, Z. Top and W. Weiss. 1978. Gas exchange and evaporation studies in a circular wind tunnel, continuous radon-222 measurements at sea and tritium/helium-3 measurements in a lake. In: Turbulent fluxes through the sea surface, wave dynamics and prediction, edited by A. Favre and K. Hasselmann, Plenum Publishing Corporation, p. 151-166.
By measuring both the rate of heat transfer and gas transfer in a circular wind it was shown that the film replacement model yields a better approximation than the stagnant film model.

D. PAPERS DEALING WITH RADIOISOTOPES IN OCEAN SEDIMENTS (#195 to #264)

1. PAPERS DEALING WITH RADIOCARBON MEASUREMENTS IN DEEP SEA SEDIMENTS (#195 to #199)

195. Broecker, W.S., K.K. Turekian and B.C. Heezen. 1958. The

relation of deep sea sedimentation rates to variations in climate. American Jour. Sci., V256, p. 503-517.

Detailed dating of a deep sea core from the equatorial Atlantic showing a large change in the rate of deposition between glacial and interglacial time for both the clay and carbonate fractions.

196. Ericson, D.B., M. Ewing, G. Wollin, and B.C. Heezen. 1961. Atlantic deep sea sediment cores. Bull. Geol. Soc. Am., V72, p.193-285.

Radiocarbon dates for the end of the last glaciation as recorded in deep sea cores.

197. Peng, T.-H., W.S. Broecker, G. Kipphut and N. Shackleton. 1977. Benthic mixing in deep sea cores as determined by ^{14}C dating and its implications regarding climate stratigraphy and the fate of fossil fuel CO_2 . In: "The Fate of Fossil Fuel CO_2 in the Ocean", editors N. Andersen and A. Malahoff, Plenum Press, New York, p. 355-374.

One of the two independent discoveries that the CaCO_3 in the upper 7-10 cm of deep sea cores yields constant ^{14}C ages of several thousands of years and that this anomaly must be the result of bioturbation.

198. Nozaki, Y., J.K. Cochran, K.K. Turekian and G. Keller. 1977. Radiocarbon and ^{210}Pb distributions in submersible-taken deep sea cores from Project FAMOUS. Earth & Planet. Sci. Lett. V34, p. 167-173.

One of the two independent discoveries that the CaCO_3 in the upper 7-10 centimeters of deep sea cores yields constant ^{14}C ages of several thousand years and that this anomaly must be the result of bioturbation.

199. Peng, T.-H., W.S. Broecker and W.H. Berger. 1979. Rates of benthic mixing in deep-sea sediment as determined by radioactive tracers. Quaternary Res. V11, p. 141-149.

Another example of the use of radiocarbon measurements to establish the thickness of the bioturbated zone in deep sea cores.

2. PAPERS DEALING WITH THE ^{230}Th AND ^{231}Pa DATA IN DEEP SEA SEDIMENTS AND MANGANESE NODULES (#200 to #239)

200. Joly, J.J. 1908. On the radium content of deep sea sediments. Philos. Mag. V6, p. 190-197.

The earliest report of measurements of uranium series daughter products in marine sediments.

201. Piggot, C.S. 1933. Radium content of ocean bottom sediments. Am. J. Sci. V239, p. 81-91.

First measurement of ^{226}Ra in a deep sea sediment.

202. Piggot, C.S. and W.D. Urry. 1939. The radium content of an ocean bottom core. J. Wash. Acad. Sci. V29, p. 405-410.

Use of the depth distribution of ^{226}Ra in deep sea cores as a means of estimating the ^{230}Th depth distribution and hence the sedimentation rate by the ionium method.

203. Piggot, C.S., and W.D. Urry. 1941. Radioactivity relations in ocean water and bottom sediments. Am. J. Sci. V239, p. 81-91.
The geochemistry of ^{226}Ra and ^{230}Th in the sea.
204. Piggot, C.S. and W.D. Urry. 1942. Time relations in ocean sediments. Bull. Geol. Soc. Amer. V53, p. 1187-1210.
Age estimates based on the ^{226}Ra distribution in deep sea sediments.
205. Piggot, C.S. and W.D. Urry. 1942. Radioactivity of ocean sediments IV. The radium content of sediments of the Cayman Trough. Am. J. Sci. V240, p. 1-12.
 ^{226}Ra distribution in cores from the Caribbean Sea.
206. Kroll, V.S. 1953. Vertical distribution of radium in deep sea sediments. Nature, V171, p. 742.
 ^{226}Ra distribution in deep sea cores.
207. Kroll, V.S. 1954. On the age-determination in deep sea sediments by radium measurements. Deep-Sea Res. V1, p. 211-215.
Ages obtained from the ^{226}Ra distribution in deep sea cores.
208. Picciotto, E. and W. Wilgain. 1954. Thorium determination in deep sea sediments. Nature V173, p. 632-633.
First direct measurement of ^{230}Th in deep sea sediments.
209. Koczy, F.F., E. Picciotto, G. Poulart and S. Wilgain. 1957. Measures des isotopes du thorium dans l'eau de mer. Geochim. Cosmochim. Acta, V11 p. 103-129.
Direct measurements of ^{230}Th in deep-sea cores.
210. Volchok, H.L. and J.L. Kulp. 1957. The ionium method of age determination. Geochim. et Cosmochim. Acta, V11, p. 219-246.
More ^{226}Ra measurements on deep-sea cores.
211. Emiliani, C. 1958. Paleotemperature analysis of core 280 and Pleistocene correlations, J. Geol. V66, p. 264-275.
Correlations of paleotemperature record in core 280 from mid-North Atlantic with cores from equatorial Atlantic, Caribbean, and Mediterranean, and with continental temperature variations during last 300,000 years.
212. Sackett, W.M. 1960. The protactinium-231 content of ocean water and sediments. Science V132, p. 1761-1762.
First measurement of ^{231}Pa in marine sediments.
213. Rosholt, J.N., C. Emiliani, T. Geiss, F.F. Koczy and

J. Wangersky. 1961. Absolute dating of deep-sea cores by the $^{231}\text{Pa}/^{230}\text{Th}$ method. *J. Geol.* V69, p. 162-185.

First simultaneous measurements of ^{230}Th and ^{231}Pa in deep sea cores and first ages based on $^{230}\text{Th}/^{231}\text{Pa}$ ratios. These ages were used to establish what is often referred to as the Emiliani chronology for the last several major climatic cycles.

214. Goldberg, E.D. and M. Koide. 1962. Geochronological studies of deep sea sediments by the ionium/thorium method. *Geochim. Cosmochim. Acta*, V26 p. 417-450.

Sedimentation rates determined using $^{230}\text{Th}/^{232}\text{Th}$ ratios on material leached from deep sea sediments with strong acid.

215. Goldberg, E.D. and M. Koide. 1963. Rates of sediment accumulation in the Indian Ocean. In: *Earth Sci. & Meteorites*, Ed. J. Geiss, North Holland, Amsterdam, p. 90-95.

^{230}Th based sedimentation rates for cores from the Indian Ocean.

216. Thurber, D.L. 1963. Natural variations in the ratio of ^{234}U and ^{238}U ; In: "Radioactive Dating," Internat. Atomic Energy Agency, Vienna, p. 113-120.

First demonstration of the existence of a $^{234}\text{U}/^{238}\text{U}$ in sea water.

217. Sarma, T.P. 1964. Dating of marine sediments by ionium and protactinium methods. Ph.D. Thesis, Carnegie Institute of Technology.

First suggestion that bioturbation altered the profiles of uranium series isotopes in deep sea cores.

218. Goldberg, E.D., M. Koide, J.J. Griffin, M.N.A. Peterson. 1964. A geochronological and sedimentary profile across the North Atlantic Ocean. In: *Isotopic and Cosmic Chemistry*, ed. by H. Craig, S.L. Miller and G.J. Wasserberg, North-Holland, Amsterdam, p. 211-232.

^{230}Th profiles in cores showing large changes in sedimentation rate.

219. Goldberg, E.D. and J.J. Griffin. 1964. Sedimentation rates and mineralogy in the South Atlantic. *J. Geophys. Res.* V69, p. 4293-4309.

Sedimentation rates on South Atlantic cores as determined by the $^{230}\text{Th}/^{232}\text{Th}$ method.

220. Sackett, W.M. 1966. Manganese nodules: thorium-230: protactinium-231 ratios. *Science*, V154, p. 646-647.

Demonstration that the $^{231}\text{Pa}/^{230}\text{Th}$ ratio is higher in manganese nodules than in the adjacent sediment.

221. Bender, M.L., T.L. Ku and W.S. Broecker. 1966. Manganese nodules: their evolution. *Science* V151, p. 325-328.
 Arguments in favor of the very low growth rates found for manganese nodules on the basis of ^{230}Th measurements.
222. Ku, T.L. 1966. Uranium series disequilibrium in deep sea sediments. Ph.D. thesis. Columbia University, New York, N.Y.
 Detailed measurement of the $^{232}\text{Th}/^{238}\text{U}$, $^{234}\text{U}/^{238}\text{U}$, $^{230}\text{Th}/^{234}\text{U}$ and $^{226}\text{Ra}/^{230}\text{Th}$ ratios in a series of deep sea cores.
223. Somayajulu, B.L.K. and E.D. Goldberg. 1966. Thorium and uranium isotopes in sea water and sediments. *Earth & Planet. Sci. Lett.* V1, p. 102-106.
 Discussion of thorium and uranium isotopes in seawater and sediments.
224. Ku, T.L. and W.S. Broecker, 1967. Uranium, thorium, protactinium in a manganese nodule. *Earth & Planet. Sci. Lett.* V2, p. 317-320.
 Growth rates for a manganese nodule based on the distributions of ^{230}Th , ^{231}Pa and ^{234}U in thinly sliced samples.
225. Barnes, S.S. and J.R. Dymond. 1967. Rates of accumulation of ferromanganese nodules. *Nature*, V213, p. 1218-1219.
 Measurements of the $^{40}\text{Ar}/^{40}\text{K}$ for the volcanic cores found in manganese nodules and the growth rates obtained from the ^{40}Ar age.
226. Ku, T.L., W.S. Broecker and N. Opdyke. 1968. Comparison of sedimentation rates measured by paleo-magnetic and the ionium methods of age determination. *Earth & Planet. Sci. Lett.* V4, p. 1-6.
 Comparison of sedimentation rates over the last 300,000 years based on ^{230}Th measurements with those based on the depth of the last magnetic reversal (i.e., that at about 700,000 years ago).
227. Ku, T.L. and W.S. Broecker. 1969. Radiochemical studies on manganese nodules of deep-sea origin. *Deep Sea Res.* V16, p. 625-637.
 Distributions of U and Th in nodules from different depths in the sea.
228. Bender, M.L., T.L. Ku and W.S. Broecker. 1970. Accumulation rates of manganese in pelagic sediments and nodules. *Earth & Planet. Sci. Lett.* V8, p. 143-148.
 Comparison of the accumulation rates for Mn in nodules and in pelagic sediments showing that the rate for sediments is higher than that for nodules.
229. Broecker, W.S., and J. Van Donk. 1976. Insolation changes, ice volumes, and the ^{18}O record in deep sea

cores. *Reviews of Geophysics and Space Physics*, V8, p. 169-196.

Revision of the Emiliani chronology for the last several climatic cycles based on detailed ^{231}Pa and ^{230}Th measurements on deep sea sediment core V12-122 from the Caribbean Sea.

230. Bender, M.L., W.S. Broecker, V. Gornitz, V. Middel, R. Kay, S.S. Sun and P.E. Biscaye. 1971. Geochemistry of three cores from the East Pacific Rise. *Earth & Planet. Sci. Lett.* V12, p. 425-433.

Manganese accumulation rates for ridge crest sediments receiving the products of hydrothermal activity as determined by the ^{230}Th method.

231. Cherdynsen, V.V. 1971. Uranium-234. Israel Program for Scientific Translation. Jerusalem, p. 1-234.

Discovery of the separation between ^{234}U and ^{238}U in nature.

232. Somayajulu B.L.K., G.R. Heath, T.C. Moore, and D.S. Cronan. 1971. Rates of accumulation of manganese nodules and associated sediments from the equatorial Pacific. *Geochim. Cosmochim. Acta*, V35, p. 621-624.

Measurements of ^{230}Th in manganese nodules.

233. Ku, T.L., J.L. Bischoff and A. Boersma. 1972. Age studies of Mid-Atlantic Ridge sediments near 42°N and 20°N . *Deep Sea Res.* V19, p. 233-247.

Uranium series isotope measurements in deep sea cores from the flank of the mid-Atlantic ridge.

234. Thomson, J. and A. Walton. 1972. Natural radioactive decay series elements in the oceans and sediments. *Proc. R. Soc. Edinb. Ser. B.* V15, p. 167-182.

Measurements of ^{231}Pa and ^{230}Th in an equatorial Atlantic core.

235. W.S. Broecker and S. Broecker. 1974. Carbonate dissolution on the western flank of the east Pacific Rise. In: "Studies in Paleo-oceanography", edited by W.W. Hay, Society of Economic Paleontologists and Mineralogists Special Publication No. 20, pp. 44-57.

^{230}Th measurements on cores from the East Pacific Rise.

236. Ku, T.L. 1976. The uranium-series methods of age determination. *Ann. Rev. Earth & Planet. Sci.* V4, p. 347-379.

A review of the uranium series dating methods as applied to deep sea cores and manganese nodules.

237. Mangini, A. and C. Sonntag. 1977. ^{231}Pa dating of deep sea cores via ^{227}Th counting. *Earth & Planet. Sci. Lett.* V37, p. 252-256.

An alternate means of measuring ^{231}Pa in deep sea cores.

238. DeMaster, D.J. 1979. The marine budgets of silica and ^{32}Si . Ph.D. thesis, Yale University, New Haven, Conn.
 Demonstration that cores taken beneath upwelling areas have unusually high $^{231}\text{Pa}/^{230}\text{Th}$ ratios.
239. Ku, T.L. 1979. Rates of manganese accretion. In: Marine Manganese Deposits, ed. by G.P. Glasby, Elsevier, Amsterdam. p. 249-268.
 An excellent review paper on measurements of the growth rates of manganese nodules.
- 239a. Bacon, M.P. and J.N. Rosholt. 1982. Accumulation rates of ^{230}Th and ^{231}Pa and some transition metals on the Bermuda Rise. *Geochim. Cosmochim. Acta* V46, p. 651-666.
 Demonstration that a deep sea sediment accumulating at a very high rate (36 cm/10³ yrs) carries concentrations of ^{230}Th and transition metals similar to sediments accumulating at normal rates (i.e., a few centimeters per thousand years) and the implications of this finding to particulate scavenging models.
- 239b. Veeh, H.H. 1982. Concordant ^{230}Th and ^{231}Pa ages of marine phosphorites. *Earth & Planet. Sci. Lett.* V57, p. 278-284.
 Demonstration that reliable uranium series ages can be obtained on marine phosphorites.
- 3. PAPERS DEALING WITH ^{210}Pb AND OTHER BIOTURBATION TRACERS IN DEEP SEA SEDIMENTS (#240 to #247)**
240. Goldberg, E.D. and M. Koide. 1962. Geochronological studies of deep sea sediments by the thorium and ionium method. *Geochim. Cosmochim. Acta* V26, p. 417-450.
 First mention of the role of bioturbation in altering the distribution of radioisotopes in marine sediments.
241. Berger, W.H. and Heath, G.R. 1968. Vertical mixing in pelagic sediments. *Jour. Mar. Res.* V26, p. 134-143.
 A simple model for bioturbation using the distribution of volcanic ash as an example.
242. Guinasso, N.L. and D.R. Schink. 1975. Quantitative estimates of biological mixing rates in abyssal sediments. *Jour. of Geophys. Res.* V80, p. 3032-3043.
 A modification of the Berger-Heath model to incorporate a finite rate of mixing within the bioturbated layer.
243. Nozaki, Y., J.K. Cochran, K.K. Turekian and G. Keller. 1977. Radiocarbon and ^{210}Pb distribution in submersible-taken deep sea cores from Project FAMOUS. *Earth & Planet. Sci. Lett.* V34, p. 167-173.
 First demonstration that the excess ^{210}Pb in deep sea cores could be used as a measure of the rate of bioturbation.

244. Schink, D.R., and N.L. Guinasso, Jr. 1978. Redistribution of dissolved and absorbed materials in abyssal marine sediments undergoing biological stirring. Amer. Jour. Sci. V278, p. 687-702.
 Application of their bioturbation model to a series of substances.
245. Peng, T.-H. W.S. Broecker and W.H. Berger. 1979. Rates of benthic mixing in deep sea sediments as determined by radioactive tracers. Quaternary Res. V11, P. 141-149.
 Profile of excess ^{210}Pb in a deep sea core from the western equatorial Pacific Ocean.
246. Kadko, D. 1980. ^{230}Th , ^{226}Ra and ^{222}Rn in abyssal sediments. Earth & Planet. Sci. Lett. V49, p. 360-380.
 Detailed analyses of all the key uranium series isotopes (including ^{210}Pb) in the upper 25 cm of two deep sea cores showing very low deposition rates.
247. Cochran, J.K. and S. Krishnaswami. 1980. Radium, thorium, uranium and ^{210}Pb in deep-sea sediments and sediment pore waters from the North Equatorial Pacific. Amer. Jour. Sci. V280, p. 849-889.
 Measurements of ^{210}Pb in the pore waters of deep sea sediments.
- 247a. Olsen, C.R., H.J. Simpson, T.-H. Peng, R.F. Bopp and R.M. Trier. 1981. Sediment mixing and accumulation rate effects on radionuclide depth profiles in Hudson estuary sediments. J. Geophys. Res. V86, p. 11020-11028.
 Use of ^{134}Cs , ^{137}Cs and $^{239},^{240}\text{Pu}$ as tracers of sediment mixing and accumulation in estuaries.
- 4. PAPERS DEALING WITH THE DISTRIBUTIONS OF ^{26}Al , ^{32}Si , AND ^{10}Be IN SEDIMENTS AND MANGANESE (#248 to #264)**
248. Goel, P.S., D.P. Kharkar, D. Lal, N. Narsappaya, B. Peters and V. Yatirajam. 1957. The beryllium-10 concentration in deep sea sediments. Deep Sea Res. V4, p. 202-210.
 The first measurement of ^{10}Be in deep sea sediments.
249. Merrill, J.R., E.F.X. Lyden, M. Honda, and J.R. Arnold. 1960. The sedimentary geochemistry of the beryllium isotopes. Geochim. et Cosmochim. Acta, V18, p. 108-129.
 A discussion of dating marine sediments with ^{10}Be and ^{26}Al . The sedimentation rates determined from ^{10}Be measurement are all consistent with those obtained from ^{14}C dating.
250. Amin, B.S., D.P. Kharkar, and D. Lal. 1966. Cosmogenic ^{10}Be and ^{26}Al in marine sediments. Deep-Sea Res. V13, p. 805-824.
 A discussion of dating marine sediments with ^{10}Be and ^{26}Al . The sedimentation rates determined from ^{10}Be

measurement are all consistent with those obtained from ^{14}C dating.

251. Somayajulu, B.L.K. 1967. ^{10}Be in a manganese nodule. *Science* V156, p. 1219-1220.
 ^{10}Be dating of a manganese nodule as a confirmation of their low growth rates.
252. Somayajulu, B.L.K. 1969. Study of marine processes using naturally occurring radioactive nuclides. Ph.D. Thesis, Univ. of Bombay, India.
Measurements of ^{32}Si in sea water.
253. Krishnaswami, S., B.L.K. Somayajulu and W.S. Moore. 1972. Dating of manganese nodules using beryllium-10. In: "Ferromanganese deposits on the ocean floor". ed., D.R. Horn, Lamont-Doherty Geological Observatory, Palisades, N.Y. p. 117-122.
Confirmation of the mean growth rate for manganese nodules by ^{10}Be measurements.
254. Bhat, S.G., S. Krishnaswami, D. Lal, M. Rama and B.L.K. Somayajulu. 1973. Radiometric and trace element studies of ferromanganese nodules. In: Proc. Sump. Hydrogeochemistry and Biogeochemistry 1. The Clark Co. Wash., D.C., p. 443-462.
Measurement of ^{10}Be and ^{230}Th in ferromanganese nodules from the Pacific Ocean.
255. Reyss, J.L. and Y. Yokoyama. 1976. Aluminum-26 in deep sea sediments. *Science* V193, p. 1119-1121.
Measurements of ^{26}Al in an Al_2O_3 sample prepared from a Pacific sediment.
256. Guichard, F. J-L Reyss and Y. Yokoyama. 1978. Growth rate of manganese nodule measured with ^{10}Be and ^{26}Al . *Nature* V272, p. 155-156.
Confirmation of radioactive decay hypothesis (as opposed to the inward diffusion hypothesis) for radioisotopes in manganese nodule using ^{10}Be and ^{26}Al .
257. Raisbeck, G.M., F. Yiou, M. Fruneau, J.M. Soiseaux. 1978. Beryllium-10 mass spectrometry with a cyclotron. *Science* V202, p. 215-217.
Description of a technique for the measurement of ^{10}Be using cyclotron mass spectrometry.
258. Boudreau, B.P. and M.R. Scott. 1978. A model for the diffusion-controlled growth of deep sea manganese nodules. *Am. J. Science*, V278, p. 903-929.
Calculations based on hydrodynamic theory showing the magnitude of the resistance to chemical transport posed by the benthic boundary layer. Also it is shown that this resistance could well be the limiting one for manganese nodule growth.

259. Raisbeck, G.M., F. Yiou, M. Fruneau, J.M. Loiseaux, M. Lieuvin. 1979. ^{10}Be concentration and residence time in the ocean surface layer. *Earth Planet. Sci. Lett.* V43, p. 237-240.
 Measurements of ^{10}Be concentration in Pacific surface water by using the accelerator technique.
260. Ku, T.L., A. Omura and P.S. Chen. 1979. ^{10}Be and U-series isotopes in manganese nodules from the central North Pacific. *Marine Geology and Oceanography of the Pacific manganese nodule province* ed. by J.L. Bischoff and D.Z. Piper, Plenum Publishing Corp, p. 791-814.
 ^{10}Be and uranium series measurements on the same nodule permitting a direct comparison of growth rates obtained by these two methods. Diffusive redistribution of these isotopes is suggested.
261. Turekian, K.K., J.K. Cochran, S. Krishnaswami, W.A. Sanford, P.D. Parker and K.A. Bauer. 1979. The measurement of ^{10}Be in manganese nodules using a tandem Van de Graaff accelerator. *Geophys. Res. Lett.* V6, p. 417-420.
 The first ^{10}Be dating of nodules carried out using the high energy mass spectrometry method.
263. Sharma, P. and B.L.K. Somayajulu. 1980. Growth rate and composition of two ferromanganese nodules from the central North Pacific. In: *Sur la genese des nodules de manganese* (Colloque international du CNRS No. 289) p. 281-288.
 Measurements of ^{10}Be , U, ^{230}Th , ^{232}Th , ^{226}Ra , ^{210}Pb , Mn, Fe in two ferromanganese nodules from the Central North Pacific.
264. Krishnaswami, S., J.K. Cochran, K.K. Turekian and S.S. Sarin. 1980. Time scales of deep-sea ferromanganese nodule growth based on ^{10}Be and α track distributions and their relation to uranium decay series measurements in *Sur la genese des nodules de manganese* (Colloque International du CNRS No. 289) p. 251-260.
 Measurements of U/Th series nuclides, alpha track density and ^{10}Be to determine growth rates and decipher growth history in ferromanganese nodules from the northeast equatorial Pacific.
- 264a. Krishnaswami, S., A. Mangini, J.H. Thomas, P. Sharma, J.K. Cochran, K.K. Turekian and P.D. Parker. 1982. ^{10}Be and Th isotopes in manganese nodules and adjacent sediments: nodule growth histories and nuclide behavior. *Earth & Planet. Sci. Lett.* V59, p. 217-234.
 Demonstration that both Th and Be accumulate preferentially in sediment over Mn nodules.

II. PAPERS DEALING WITH STABLE ISOTOPE TRACERS (#265 to #345)

A. PAPERS DEALING WITH STABLE ISOTOPE TRACERS OF WATER MOTION (#265 to 284)

1. PAPERS DEALING WITH THE DISTRIBUTION OF THE ${}^3\text{He}/{}^4\text{He}$ RATIO IN THE SEA (#265 to #281)

265. Suess, H.E. and H. Wanke. 1965. On the possibility of a helium flux through the ocean floor. In: Progress in Oceanography, V3, Pergamon Press, Oxford, p. 347-353.
Assuming that the ${}^4\text{He}$ escape from the earth's interior matches its production by the decay in the earth's interior, a prediction of the escape rate of this gas into the deep sea is made. Assuming that as suggested by ${}^{14}\text{C}$ data the residence time of water in the deep Pacific is 700 years, an excess of 20% in the ${}^4\text{He}$ content of deep Pacific Ocean water is predicted. Measurements are reported showing that the actual excess is not more than 6%.
266. Bieri, R.H., M. Koide and E.D. Goldberg. 1964. Noble gases in sea water. Science, V146, p. 1035-1037.
An attempt to measure the excess ${}^4\text{He}$ in sea water. The values reported have subsequently been shown to be in error.
267. Bieri, R.H., M. Koide and E.D. Goldberg. 1966. The noble gas contents of Pacific seawaters. J. of Geophys. Res. V71, p. 5243-5265.
Supersaturation of noble gases including He, Ne, Ar, and Kr in seawaters is discovered. The distributions of these gases with depth and their relationship to mixing and advection are discussed.
- 267a. Bieri, R.H., M. Koide and E.D. Goldberg. 1968. Noble Gas Contents of Marine Waters. Earth & Planet. Sci. Lett. V4, p. 329-340.
Measurements of He, Ne, Ar, and Kr in the Atlantic and Pacific Oceans showing deviations from saturation.
268. Mamyrin, B.A., I.N. Tolstiklien, G.S. Anufriev, and I.L. Kamenski. 1969. Anomalous isotopic composition of helium in volcanic gases. Dokl. Akad. Nank. SSSR, V184, p. 1197.
The discovery of primordial ${}^3\text{He}$ in volcanic gases.
269. Clarke, W.B., M.A. Beg and H. Craig. 1969. Excess ${}^3\text{He}$ in the Atlantic. Earth & Planet. Sci. Lett., V6, p. 213-220.
The discovery of excess ${}^3\text{He}$ in sea water and the demonstration that this ${}^3\text{He}$ must be primordial.
270. Clarke, W.B., M.A. Beg and H. Craig. 1970. Excess helium-3 at the North Pacific GEOSECS station. Jour. of Geophys. Res.

Res. V75, p. 7676-7678.

Profile of ${}^3\text{He}/{}^4\text{He}$ ratio for a station in the eastern North Pacific. The maximum in this ratio at a depth of about 3 kilometers depth bears witness to the release of ${}^3\text{He}$ from the ridge crests.

271. Jenkins, W.J., M.A. Beg, W.B. Clarke, P.J. Wangersky, and H. Craig. 1972. Excess ${}^3\text{He}$ in the Atlantic Ocean. Earth & Planet. Sci. Lett. V16, p.122-126.
First results on excess ${}^3\text{He}$ in waters from the Atlantic Ocean.
272. Craig, H., W.B. Clarke and M.A. Beg. 1975. Excess ${}^3\text{He}$ in deep water on the East Pacific Rise. Earth and Planet. Sci. Lett. V26, p. 125-132.
Measurements of excess ${}^3\text{He}$ in the Pacific Ocean close to the ridge crest showing that the anomalies are, as expected, higher close to the source of mantle exhalations.
273. Lupton, J.E. 1976. The ${}^3\text{He}$ distribution in deep water over the Mid-Atlantic Ridge. Earth and Planet. Sci. Lett. V32, p. 371-374.
Measurements showing the absence of a ${}^3\text{He}$ anomaly over the Mid-Atlantic Ridge. Evidence for an excess in ${}^4\text{He}$ in the deep eastern Atlantic is also given.
274. Jenkins, W.J. and W.B. Clarke. 1976. The distribution of ${}^3\text{He}$ in the western Atlantic Ocean. Deep Sea Res. V23, p. 481-494.
The distribution of ${}^3\text{He}$ excesses in the western Atlantic. In the northern part of this basin these anomalies are largely from the decay of tritium. In the southern part deep water anomalies are generated by the entry from the Antarctic of water previously contaminated with primordial helium in the Pacific Ocean.
275. Jenkins, W.J. 1977. Tritium-helium dating in the Sargasso Sea: A measurement of oxygen utilization rates. Science V196, p.291-292.
Correlation of the excesses of ${}^3\text{He}$ produced by tritium decay with oxygen deficiencies in the thermocline of the temperate North Atlantic.
276. Jenkins, W.J., J.M. Edmond, and J.B. Corliss. 1978. Excess ${}^3\text{He}$ and ${}^4\text{He}$ in Galapagos submarine hydrothermal water. Nature V272, p. 156-158.
The relationship between the release of ${}^3\text{He}$ and of heat from the mid-ocean ridges. Also these measurements yield the ratio of excess ${}^3\text{He}$ to excess ${}^4\text{He}$ entering the sea from ridge crests.
277. Jenkins, W.J., W.V. Collentro and R.D. Boudreau. 1979. Woods

Hole Oceanographic Institution. Helium Isotope Laboratory
Data Release #1.

Listing of tritium and ^3He data from the Sargasso Sea.

278. Broecker, W.S. 1980. The distribution of ^3He anomalies in the deep Atlantic. *Earth and Planet. Sci. Lett.* V49, p. 513-519.
A discussion of published data in which an attempt is made to separate the contributions of excess ^3He added directly to the Atlantic from the contribution of excess ^3He carried into the Atlantic by waters from the Antarctic (previously contaminated by ridge crest emissions in the Pacific). Evidence is also given for a narrow plume of excess ^3He bearing water hugging the continental margin of North America. The origin of this plume is not known.
279. Jenkins, W.J. 1980. Tritium and ^3He in the Sargasso Sea. Sears Foundation: *J. of Marine Research*, V38, p. 533-569.
Vertical profiles of tritium and ^3He are shown to be incompatible with one-dimensional mixing models. Along-isopycnal ventilation of the temperate thermocline must be invoked if these distributions are to be explained.
280. Lupton, J.E. and H. Craig. 1981. A major helium-3 source at 15°S on the East Pacific Rise. *Science* V214, p. 13-18.
 ^3He excesses of 50% are reported over the East Pacific Rise. A plume of excess helium at 2.5 km depth is shown to extend 2000 km to the west of the rise crest.
281. Craig, H. and J.E. Lupton. 1981. Helium-3 and Mantle Volatiles in the Ocean and the Oceanic Crust. *The Sea V7: The Oceanic Lithosphere*. Edited by C. Emiliani, Wiley and Son, New York, p. 391-428.
An excellent review of research dealing with the release of rare gases by the oceanic crust and the movement of these gases through the ocean.
- 2. PAPERS DEALING WITH THE DISTRIBUTIONS OF D/H AND OF $^{18}\text{O}/^{16}\text{O}$ RATIOS IN THE OCEAN (#282 to #284)**
282. Epstein, S and T. Mayeda. 1953. Variation of ^{18}O content of waters from natural sources. *Geochim. Cosmochim. Acta* V4, p. 213-224.
First paper showing the variations in the $^{18}\text{O}/^{16}\text{O}$ ratio within the oceans.
283. Craig, H. and L.I. Gordon. 1965. Isotopic Oceanography: Deuterium and oxygen-18 variations in the ocean and the marine atmosphere. *Proc. Symp. Mar. Geochem.*, Univ. of Rhode Island, Occ. Publ. 3, p. 277-374.
A discussion of the origin of bottom waters formed in the Antarctic region based on the $^{18}\text{O}/^{16}\text{O}$ ratios in

various oceanic water types.

284. Weiss, R.F., H.G. Ostlund and H. Craig. 1979. Geochemical studies in the Weddell Sea. Deep Sea Res. V26, p. 1093-1120.
Use of $^{18}\text{O}/^{16}\text{O}$ and D/H ratios to aid in defining the source of Weddell Sea Bottom Water.

B. PAPERS DEALING WITH STABLE ISOTOPE TRACERS OF BIOLOGICAL PROCESSES IN THE SEA (#285 to #317)

1. PAPERS DEALING WITH THE $^{13}\text{C}/^{12}\text{C}$ RATIO IN DISSOLVED OCEANIC CARBON AND IN MARINE ORGANISMS (#285 to #305)

285. Craig, H. 1953. The geochemistry of the stable carbon isotopes. Geochim. Cosmochim. Acta. V3, p. 53-92.
Paper dealing the distribution of $^{13}\text{C}/^{12}\text{C}$ ratios in natural materials including marine macrophytes and algae.
286. Keeling, C.D. 1961. The concentrations and isotopic abundances of carbon dioxide in rural and marine air. Geochim. Cosmochim. Acta, V24, p. 277-298.
 CO_2 partial pressures and $^{13}\text{C}/^{12}\text{C}$ ratios for atmospheric CO_2 .
287. Sackett, W. M., W. R. Eckelmann, M. C. Bender and A. W. H. Be. 1965. Temperature dependence of carbon isotope composition in marine plankton and sediments. Science V148, p. 235-237.
 $^{13}\text{C}/^{12}\text{C}$ ratios in marine plankton from various parts of the ocean.
288. Deuser, W. G. and E. T. Degens. 1967. Carbon isotope fractionation in the system CO_2 (gas) - CO_2 (aqueous). Nature V215, p. 1033-1035.
Measurements of the carbon isotope fractionation factor between atmospheric CO_2 and surface ocean ΣCO_2 .
289. Wendt, I. 1968. Fractionation of carbon isotopes and its temperature dependence in the system CO_2 gas- CO_2 in solution and HCO_3^- - CO_2 in solution. Earth & Planet. Sci. Lett. V4, p. 64.
Measurements of the carbon isotope fractionation factor between gas phase CO_2 and dissolved CO_2 and HCO_3^- .
290. Williams, P. M. and L. I. Gordon. 1970. Carbon-13:carbon-12 ratios in dissolved and particulate organic matter in the sea. Deep Sea Res. V17, p. 19-27.
 $^{13}\text{C}/^{12}\text{C}$ ratios in particulate carbon filtered from sea water.
291. Vogel, J.C., P.M. Grootes and W.G. Mook. 1970. Isotopic fractionation between gaseous and dissolved carbon dioxide. Z. Physik V230, p. 225-238.

Measurements of the carbon isotope fractionation factor between gas phase and aqueous phase CO₂.

292. Kroopnick, P., W. G. Denser and H. Craig. 1970. Carbon-13 measurements on dissolved inorganic carbon at the North Pacific (1969) GEOSECS station. J. Geophys. Res., V75, p. 7668-7671.
 $^{13}\text{C}/^{12}\text{C}$ ratios in oceanic ΣCO_2 .
293. Craig, H. 1970. Abyssal carbon-13 in the South Pacific. J. Geophys. Res., V75, p. 691-695.
 $^{13}\text{C}/^{12}\text{C}$ ratios in oceanic ΣCO_2 .
294. Kroopnick, P., R. F. Weiss and H. Craig. 1972. Total CO₂, ^{13}C , and dissolved oxygen - ^{18}O at GEOSECS II in the North Atlantic. Earth Planet. Sci. Lett., V16, p. 103-110.
 $^{13}\text{C}/^{12}\text{C}$ ratios in oceanic ΣCO_2 .
295. Kroopnick, P. 1974. Correlations between ^{13}C and ΣCO_2 in surface waters and atmospheric CO₂. Earth Planet. Sci. Lett. V22, p. 397-403.
 $^{13}\text{C}/^{12}\text{C}$ ratios in oceanic ΣCO_2 .
296. Kroopnick, P. 1974. Modeling the dissolved O₂ - CO₂ - ^{13}C system in the eastern equatorial Pacific. Deep Sea Res. V21, p. 211-229.
 $^{13}\text{C}/^{12}\text{C}$ ratios in oceanic CO₂.
297. Mook, W.G., J.C. Bommerson and W.H. Stoverman. 1974. Carbon isotope fractionation between dissolved bicarbonate and gaseous carbon dioxide. Earth Planet. Sci. Lett. V22, p. 69-176.
Measurements of the carbon isotope fractionation factor between atmospheric CO₂ and dissolved gaseous carbon and bicarbonate ion.
298. Kroopnick, P., S.V. Margolis and C.S. Wong. 1977. $\delta^{13}\text{C}$ variations in marine carbonate as indicators of the CO₂ balance between the atmosphere and oceans. In: The Fate of Fossil Fuel CO₂ in the Oceans, N.R. Anderson and A. Malahoff, eds., Plenum Press, New York, N.Y., p.295-231.
 $^{13}\text{C}/^{12}\text{C}$ ratios in oceanic ΣCO_2 .
299. Siegenthaler, U., M. Heimann and H. Oeschger. 1978. Model responses to the atmospheric CO₂ level and $^{13}\text{C}/^{12}\text{C}$ ratio to biogenic CO₂ input. In: Williams, J. (ed.), Carbon dioxide, climate and society, Pergamon Press, New York, p. 79-87.
Calculations using the Oeschger model showing the impact of releases of soil and living biosphere CO₂ during the past century on the $\delta^{13}\text{C}$ record for atmospheric CO₂.
300. Keeling, C.D., M.G. Mook and P.P. Tans. 1979. Recent trend in the $^{13}\text{C}/^{12}\text{C}$ ratio of atmospheric carbon dioxide. Nature, V277, p. 121-123.
Update on the $^{13}\text{C}/^{12}\text{C}$ ratio in atmospheric CO₂. Taken

together with the earlier Keeling results, an estimate can be made of the rate of decline of this ratio due to the burning of fossil fuels and of changes in the living biomass and soil carbon reservoir.

301. Kroopnick, P. 1980. The distribution of ^{13}C in the Atlantic Ocean. *Earth Planet. Sci. Lett.*, V49, p. 469-484.
 $^{13}\text{C}/^{12}\text{C}$ ratios for oceanic CO_2 as obtained for the Atlantic GEOSECS Program.
302. Keeling, C.D., R.B. Bacastow and P.P. Tans. 1980. Predicted shift in the $^{13}\text{C}/^{12}\text{C}$ ratio of atmospheric carbon dioxide. *Geophys. Res. Lett.*, V7, p. 505-508.
If a carbon isotope kinetic separation factor of 0.986 for the CO_2 entering the sea is assumed, these authors show that the time history of the $\delta^{13}\text{C}$ for atmospheric CO_2 does not provide a very sensitive way to estimate the contribution of forests and soils to the anthropogenic build up of the atmospheric CO_2 concentration. However, if the 0.998 value of Seigenthaler and Munnich is used then the situation is much improved.
303. Ostlund, H.G. 1980. GEOSECS Atlantic and Pacific ^{13}C measurements on radiocarbon samples. Tritium Laboratory Data Release #80-09, Rosenstiel School of Marine and Atmospheric Sciences, University of Miami.
 $^{13}\text{C}/^{12}\text{C}$ ratios obtained on the CO_2 collected for radiocarbon analyses of the Atlantic and Pacific GEOSECS program.
304. Siegenthaler, U. and K.O. Munnich, 1981. ^{13}C fractionation during CO_2 transfer from air to sea. In: SCOPE report #16. Carbon Cycle Modeling, B. Bolin, ed., John Wiley & Sons, p.249-257.
Estimate of the kinetic fractionation during uptake of CO_2 by the ocean.
- 2. PAPERS DEALING WITH THE $^{18}\text{O}/^{16}\text{O}$ RATIOS IN ATMOSPHERIC O_2 AND IN THE O_2 DISSOLVED IN THE SEA (#306 to #317)**
306. Dole, M. 1935. The relative atomic weight of oxygen in water and air. *J. Am. Chem. Soc.*, V57, p. 2731.
The first in a long series of papers dealing with the difference in the $^{18}\text{O}/^{16}\text{O}$ ratio in atmospheric O_2 and in sea H_2O . The measurements were made by density determination in the era before precise mass spectrometry.
307. Dole, M. and G. Jenks. 1944. Isotopic composition of photosynthetic oxygen. *Science*, v. 100, p. 409.
Another in the Dole series.
308. Dole, M., R.C. Hawkins and H.A. Barker. 1947. Bacterial fractionation of oxygen isotopes. *J. Amer. Chem. Soc.* V69, p.

226-228.

Another in the Dole series.

309. Rakestraw, N.W., D.P. Rudd and M. Dole. 1951. Isotopic composition of oxygen in air dissolved in Pacific Ocean water as a function of depth. *J. Am. Chem. Soc.*, V73, p. 2976.
Another in the Dole series.
310. Dole, M., G.A. Lane, D.P. Rudd and D.A. Zankelies. 1954. Isotopic composition of atmospheric oxygen and nitrogen. *Geochim. Cosmochim. Acta*, V6, p. 65-78.
Another in the Dole series.
311. Lane, G.A. and M. Dole. 1956. Fractionation of oxygen isotopes during respiration. *Science* V123, p. 574-576.
Another in the Dole series.
312. Kroopnick, P. and H. Craig. 1971. Isotopic composition of molecular oxygen in the atmosphere and the sea. *Trans. Am. Geophys. Union* V52, p. 255.
Measurements of the isotopic composition of O₂ from sea water.
313. Kroopnick, P. and H. Craig. 1972. Atmospheric oxygen: isotopic composition and solubility fractionation. *Science*, V175, p. 54-56.
¹⁸O/¹⁶O fractionation between gaseous and dissolved O₂.
314. Kroopnick, P., R.F. Weiss and H. Craig. 1972. Total CO₂, ¹³C, and dissolved oxygen-18 at GEOSECS II in the North Atlantic. *Earth Planet. Sci. Lett.* V16, p. 103-110.
An ¹⁸O/¹⁶O profile for the O₂ dissolved in the sea at a station in the eastern North Pacific.
315. Kroopnick, P. 1975. Respiration, photosynthesis, and oxygen isotope fractionation in oceanic surface water. *Limnol. Oceanogr.* V20, p. 988-992.
¹⁸O/¹⁶O measurements on O₂ dissolved in the sea.
316. Kroopnick, P. and H. Craig. 1976. Oxygen isotope fractionation in dissolved oxygen in the deep sea. *Earth Planet. Sci. Lett.* V32, p. 375-378.
¹⁸O/¹⁶O measurements on O₂ dissolved in seawater.
317. Kroopnick, P. 1980. Isotopic fractionations during oxygen consumption and carbonate dissolution within the North Atlantic deep water. *Earth Planet. Sci. Lett.* V49, p. 485-498.
¹⁸O/¹⁶O measurements on dissolved O₂ samples collected during the Atlantic GEOSECS expedition.

C. STABLE ISOTOPE TRACERS IN SEDIMENTS AND MANGANESE NODULES
#318 to #345)

1. PAPERS DEALING WITH THE $^{18}\text{O}/^{16}\text{O}$ RATIOS IN CaCO_3 FROM DEEP SEDIMENT (#318 to #326)

318. Emiliani, C. 1955. Pleistocene temperatures. *J. Geol.* V63, p. 538-578.
The first paper dealing with the $^{18}\text{O}/^{16}\text{O}$ method as applied to deep sea cores. The depiction of climatic cycles from the down core records is a classic piece of science which had a great impact on the field of paleoclimatology.
319. Broecker, W.S. and J. Van Donk. 1970. Insolation changes, ice volumes and the ^{18}O record in deep-sea cores. *Rev. Geophys. Space Phys.* V8, p. 169-196.
A demonstration of the relationship between the $^{18}\text{O}/^{16}\text{O}$ record in deep-sea cores and the sea level record as represented by the flight of uplifted coral reefs on the island of Barbados.
320. Shackleton, N.J. and N.D. Opdyke. 1973. Oxygen isotope and paleomagnetic stratigraphy of Equatorial Pacific core V28-238: oxygen isotope temperatures and ice volumes on a 10^5 -year and 10^6 -year scale. *Quat. Res.*, v. 3, p. 39-55.
The first long and detailed record of the $^{18}\text{O}/^{16}\text{O}$ ratio in both planktonic and benthic forams.
321. Shackleton, N.J. 1974. Attainment of isotopic equilibrium between ocean water and benthonic foraminifera genus *Uvigerina*: isotopic changes in the ocean during the last glacial. *Colloques Internationaux du Centre National de la Recherche Scientifique*, V219, p. 203-210.
The record of $^{18}\text{O}/^{16}\text{O}$, as preserved in benthic forams. As the temperature of the deep sea cannot have changed much between glacial and interglacial time, this record provides an estimate of the $^{18}\text{O}/^{16}\text{O}$ ratio changes in the sea as a whole caused by the growth and retreat of continental ice sheets.
322. Shackleton, N.J. and N.D. Opdyke. 1976. Oxygen isotope and paleomagnetic stratigraphy of Equatorial Pacific core V28-239, late Pliocene to latest Pleistocene. In: *Investigation of Late Quaternary Paleoceanography and Paleoclimatology*, ed. R. M. Cline and J. D. Hays, *Geol. Soc. Amer. Mem.* V145, p. 449-464.
An even longer detailed record of the $^{18}\text{O}/^{16}\text{O}$ variations in planktonic and benthic forams.
323. Hays, J.D., J. Imbrie, N.J. Shackleton. 1976. Variations in the earth's orbit: pacemaker of the ice ages. *Science*, V194, p. 1121-1132.
Demonstration that the $^{18}\text{O}/^{16}\text{O}$ records in deep sea cores have periodicities of about 20,000, 40,000 and 100,000 years. As two of these (the 20,000 and 40,000) match those in the earth's insolation record, this work pro-

- vides strong support for the influence of changes in the earth's orbital characteristics on climate.
324. Shackleton, N.J. 1977. The oxygen isotope record of the late Pleistocene: Phil. Trans. Roy. Soc. Lond. B, V280, p. 169-182.
 A review of the $^{18}\text{O}/^{16}\text{O}$ record from deep-sea cores.
325. Duplessy, J.-C. 1978. Isotope studies. In: Climatic Change, ed. John Gribbin, Cambridge Press, p. 46-47.
 A review article on the geochemistry of ^{18}O in the ocean and atmosphere.
326. Broecker, W.S. 1978. The cause of glacial to interglacial climatic change. In: "Evolution of Planetary Atmosphere and Climatology of the Earth", Centre National d'Etudes Spatiales (France), p. 165-177.
 An apparent inconsistency between the amplitude of ice volume changes as recorded by $^{18}\text{O}/^{16}\text{O}$ in benthic forams and by raised coral reefs.
- 2. PAPERS DEALING WITH THE $^{13}\text{C}/^{12}\text{C}$ RECORD FOUND IN FORAMINIFERA FROM DEEP SEA SEDIMENTS (#327 to #331)**
327. Van Donk, J. 1970. The Oxygen Isotope Record in Deep Sea Sediments. Ph.D. Thesis. Columbia University, New York City.
 The first published detailed down core records of $^{13}\text{C}/^{12}\text{C}$ ratio in planktonic foraminifera.
328. Shackleton, N.J. 1977. Tropical rainforest history and the equatorial Pacific carbonate dissolution cycles. In: The Fate of Fossil Fuel CO₂ in the Oceans, eds. N.R. Anderson and A. Malahoff, Plenum Press, New York, p. 401-428.
 A demonstration that the $^{13}\text{C}/^{12}\text{C}$ ratio in the dissolved inorganic carbon from abyssal waters in the ocean underwent glacial to interglacial changes and the implication of these changes to the earth's carbon budget. A classic paper!
329. Berger, W.H. and J.S. Killingsley. 1977. Glacial-Holocene transition in deep-sea carbonates: selective dissolution and the stable isotope signal. Science, v. 197, p. 563-566.
 Demonstration that the $^{13}\text{C}/^{12}\text{C}$ ratio in planktonic organisms underwent almost no change from glacial to interglacial time.
330. Belanger, P.E., W.B. Curry and R.K. Matthews. 1981. Core-top evaluation of benthic foraminiferal isotopic ratios for paleo-oceanographic interpretations. Palaeogeog. Paleo-climat. Palaeoecol., V33, p. 205-220.
 The ^{13}C and ^{18}O variations in benthic foraminifera are used as sensors of bottom water conditions.
331. Broecker, W.S. 1981. Glacial to interglacial changes in ocean and atmosphere chemistry. In: Climatic Variations and

Variability: Facts and Theories, A. Berger, editor, D. Reidel Publishing Co., 109-120.

An explanation for the difference between the $^{13}\text{C}/^{12}\text{C}$ record for planktonic and benthic foraminifera between glacial and interglacial time.

- 331a. Curry, W.B. and R.K. Matthews. 1981. Equilibrium ^{18}O fractionation in small size fraction planktic foraminifera: Evidence from recent Indian Ocean sediments, *Marine Micropaleontology*, V6, p. 327-337.

Measurements of both $\delta^{18}\text{O}$ and $\delta^{13}\text{C}$ in different size fractions of a single species of foraminifera showing that the size dependence of the $^{13}\text{C}/^{12}\text{C}$ ratio is not simply an artifact of changing depth habitat with maturity.

3. PAPERS DEALING WITH $^{143}\text{Nd}/^{144}\text{Nd}$ RATIOS IN SEA WATER, MARINE SEDIMENTS AND MANGANESE NODULES (#332 to #340)

332. O'Nions, R.K., S.R. Carter, R.S. Cohen, N.M. Evensen and P.J. Hamilton. 1978. Pb, Nd and Sr isotopes in oceanic ferromanganese deposits and ocean floor basalts. *Nature*, V273, p. 435-438

Measurements of $^{143}\text{Nd}/^{144}\text{Nd}$ ratios in manganese nodules and in metalliferous sediments.

333. McCulloch, M.T. and G.J. Wasserburg. 1978. Sm-Nd and Rb-Sr chronology of continental crust formation. *Science*, V200, p. 1003-1011.

Measurements of $^{143}\text{Nd}/^{144}\text{Nd}$ ratios in red clay.

334. Cohen, R.S., N.M. Evensen, P.J. Hamilton and R.K. O'Nions. 1980. U-Pb, Sm, Nd, and Rb-Sr systematics of mid-ocean ridge basalt glasses. *Nature*, V283, p. 149-153.

Measurements of Pb, Nd, and Sr isotopes in basalt glasses from mid-ocean ridges.

335. O'Nions, R.K., N.M. Evensen and P.J. Hamilton. 1979. Geochemical modeling of mantle differentiation and crustal growth. *J. Geophys. Res.*, V84, p. 6091-6101.

A discussion of two-reservoir model with time-dependent transport coefficient between the reservoirs to model the abundances of K, Ar, Rb, Sr, Sm, Nd, U, Th, and Pb and the isotopic compositions of Ar, Sr, Mn, and Pb in the earth's mantle and continental crust.

336. Piepgras, D.J., G.J. Wasserburg, E.J. Dasch. 1979. The isotopic composition of Nd in different ocean masses. *Earth Planet. Sci. Lett.*, V45, p. 223-236.

Measurements of $^{143}\text{Nd}/^{144}\text{Nd}$ in manganese nodules, metalliferous sediments, red clays, hydrothermal crusts and sea water.

337. Piepgras, D.J. and G. J. Wasserburg. 1980. Neodymium isotopic

variations in seawater. *Earth Planet. Sci. Lett.* V50, p. 128-138.

Measurements of $^{143}\text{Nd}/^{144}\text{Nd}$ ratios in seawater samples from the Atlantic and Pacific Oceans.

338. Allegre, C.J. and Othman, B. 1980. Nd-Sr isotopic relationship in granitoid rocks and continental crust development: A chemical approach to orogenesis. *Nature*, V286, p. 335-342.
A discussion of a mixing model to explain the generation of granites from the mantle and the recycling of continental material based on Nd-Sr isotopic compositions.
339. Goldstein, S.L. and R.K. O'Nions. 1981. Nd- and Sr-isotopic relationships in pelagic clays and ferromanganese nodules. *Nature*, V292, p. 324-327.
Measurements of $^{143}\text{Nd}/^{144}\text{Nd}$ ratios in marine sediments and manganese nodules.
340. Taylor, S.R. and S.M. McLennan. 1981. The composition and evaluation of the continental crust: rare earth element evidence from sedimentary rocks. *Phil Trans. Roy. Soc. Lond. A*, V301, p. 381-399.
A discussion of the composition and evolution of the continental crust using rare earth element patterns from sedimentary rocks.

4. PAPERS DEALING WITH LEAD ISOTOPE RATIOS IN DEEP SEA SEDIMENTS AND MANGANESE NODULES (#341 to #345)

341. Chow, T.J. and C.C. Patterson. 1959. Lead Isotopes in manganese nodules. *Geochimica et Cosmochimica Acta*, V17, p. 21-31.
A discussion of isotopic composition of lead in manganese nodules of the Atlantic and Pacific Oceans.
342. Chow, T. and C.C. Patterson. 1962. The occurrence and significance of lead isotopes in pelagic sediments. *Geochim. Cosmochim. Acta*, V26, p. 263-308.
Lead isotope measurements in deep sea sediments and manganese nodules.
343. Reynolds, P.H. and E.J. Dasch. 1971. Lead isotopes in marine manganese nodules and the ore-lead growth curve. *J. Geophys. Res.*, v. 76, p. 5124-5129.
Lead-isotope composition in marine manganese nodules.
344. O'Nions, R. K., S.R. Carter, R.S. Cohen, N.M. Evensen and P.J. Hamilton. 1978. Pb, Nd and Sr isotopes in oceanic ferromanganese deposits and ocean floor basalts. *Nature*, V273, p. 435-438.
Measurements of Pb-, Nd- and Sr-isotope compositions of oceanic ferromanganese deposits.

345. Dasch, E.J. 1981. Lead isotopic composition of metalliferous sediments from the Nazca plate. Geol. Soc. Am. Memoir 154, p. 199-210.

Lead isotope measurements in hydrothermal deposits compared to those in manganese nodules and basalts.

III. PAPERS DEALING WITH CHEMICAL TRACERS (#346 to #456)

A. PAPERS DEALING WITH CHEMICAL TRACERS OF BIOLOGICAL CYCLES (#346-#433).

1. PAPERS DEALING WITH THE DISTRIBUTION OF NO₃, PO₄, AND DISSOLVED OXYGEN IN THE SEA (#346 to #364)

346. Redfield, A.C. 1934. On the proportions of organic derivatives in sea water and their relation to the composition of plankton. James Johnson Memorial Vol., Liverpool, p. 176-192.

The relationship between the composition of marine plants and animals and the variations in the NO₃, PO₄, ΣCO₂ and O₂ content of sea water.

347. Redfield, A.C. 1942. The processes determining the concentrations of oxygen, phosphate and other organic derivatives within the depths of the Atlantic Ocean. Papers Phys. Oceanogr. Meteorol., V9, p. 1-22.

Again the relationship between the chemical gains and losses during respiration and the chemical changes in deep water.

348. Rakestraw, N.W. 1947. Oxygen consumption in sea water over long periods. J. Mar. Res. V6, p. 259-263.

Discussion of the rate and extent of oxygen comusmption in sea water under a variety of conditions.

349. Richards, F.A. and A.C. Redfield. 1954. A correlation between the oxygen content of sea water and the organic content of marine sediments. Deep Sea Res., V1, p. 279-281.

The lower the oxygen content of sea water the higher the organic carbon content of underlying sediments.

350. Riley, C.A. 1954. Oxygen, phosphate and nitrate in the Atlantic Ocean. Bull. Bingham Oceanogr. Coll. 13-14, p. 1-126.

A model for the distribution of respiration products in the deep Atlantic.

351. Richards, F.A. 1957. Oxygen in the ocean. Memoirs Geolog. Soc. Amer., v. 67, p. 185-238.

Distribution of dissolved oxygen in the oceans.

352. Redfield, A.C. 1960. The distribution of phosphorous in the deep oceans of the world. Proc.-Verbaux Assoc. Oceanogr. Phys. Union Geol. Geophys. Intern., v. 7, p. 189-193.

Distribution of PO₄ in the deep waters of the world ocean.

353. Wyrtki, K. 1962. The oxygen minima in relation to ocean circulation. Deep Sea Res., V9, p. 11-23.
Application of a one-dimensional advection-diffusion model to the vertical distribution of dissolved oxygen in the ocean.
354. Redfield, A.C., B.H. Ketchum and F.A. Richards. 1963. The influence of organisms on the composition of sea water. In: The Sea, V2, edited by M.N. Hill, Interscience, New York, p. 26-77.
Review article on the relationship between the changes in the chemical composition of sea water and the composition of marine organisms.
355. Carpenter, J.H. 1965. The Chesapeake Bay Institute technique for the Winkler dissolved oxygen method. Limnology and Oceanography V10, p.141-143.
Description of the universally used method for the measurement of dissolved oxygen in sea water.
356. Gordon, A.L. 1966. Potential temperature, oxygen and circulation of bottom water in the Southern Ocean. Deep Sea Res. V13, p. 1125-1138.
The relationship between the distribution of dissolved oxygen and the hydrography of the Antarctic Ocean.
357. Menzel, D.W. and H.H. Ryther. 1968. Organic carbon and the oxygen minimum in the South Atlantic Ocean. Deep Sea Res. V15, p. 327-337.
A discussion of the relationship between the rain rate of organic matter and the rate of ventilation in the generation of oxygen minimum layers.
358. Weiss, R.F. 1970. The solubility of nitrogen, oxygen and argon in water and seawater. Deep-Sea Res. V17, p. 721-735
The relationship between gas solubility and temperature and the salinity.
359. Wyrtki, K. 1971. Oceanographic Atlas of the International Indian Ocean Expedition. National Science Foundation, Wash. D.C.
Sections of the hydrographic and nutrient constituents in the Indian Ocean.
360. Spencer, D.W. 1972. GEOSECS II, the North Atlantic station: hydrographic features of oxygen and nutrients. Earth & Planet. Sci. Lett. V16, p. 91-102.
Relationship between the nutrient constituent profiles and the profiles of potential temperature and salinity at a station in western North Atlantic.

361. Broecker, W.S. 1974. "NO" a conservative water-mass tracer. *Earth & Planet. Sci. Lett.* V23, p. 100-107.
Demonstration that by adding the concentration of dissolved oxygen to nine times the nitrate concentration a quasi-conservative property is obtained. As this property has a far different value for deep waters formed in the Antarctic Ocean than for those formed in the northern Atlantic it provides a useful adjunct to the conventional θ -S method of distinguishing water types.
- 361a. Alvarez-Borrego, S., D. Guthrie, C.H. Culberson and P.K. Park. 1975. Test of Redfield's model for oxygen-nutrient relationships using regression analysis. *Limnol. & Oceanog.* V20, p. 795-805.
Derivation of Redfield ratios from regression analyses of concentration data for dissolved constituents in the sea.
- 361b. Froelich, P.N., M.L. Bender, N.A. Luedtke, G.R. Heath and T. DeVries. 1982. The marine phosphorus cycle, *Am. J. Sci.*, V282, p. 474-511.
Discussion of sources and sinks of phosphorus in the ocean. The input and output flux and the mean residence time for phosphorus in the ocean are given.
362. Bainbridge, A.E. 1975. GEOSECS Atlantic Ocean: final hydrographic data report. GEOSECS Operations Group/National Science Foundation, Wash. D.C.
Listing of the potential temperature, salinity, density, and nutrient constituent concentrations for samples obtained during the Atlantic Ocean GEOSECS expedition.
363. Bainbridge, A.E. 1976. GEOSECS Pacific Ocean: final hydrographic data report. GEOSECS Operations Group/National Science Foundation, Wash. D.C.
Listing of the potential temperature, salinity, density, and nutrient constituent concentrations for samples obtained during the Pacific Ocean GEOSECS expedition.
364. Bainbridge, A.E. 1978. GEOSECS Indian Ocean: final hydrographic data report. GEOSECS Operations Group/National Science Foundation, Wash. D.C.
Listing of the potential temperature, salinity, density, and nutrient constituent concentrations for samples obtained during the Indian Ocean GEOSECS expedition.
- 364a. Williams, R.T. 1981. Hawaii-Tahiti Shuttle Experiment; Hydrographic Data Reports, V1, 2 and 3. Scripps Institution of Oceanography (reference nos. 81-5, 6 and 7) Univ. of California, San Diego.
Nutrient constituent and oxygen for bimonthly traverses from 20°S to 20°N in the central Pacific from Feb. 1979 to Feb. 1980.

2. PAPERS DEALING WITH THE DISTRIBUTIONS OF H_4SiO_4 , Ge AND Ba IN THE SEA (#365 to #378)

365. Wolgemuth, K. and W.S. Broecker. 1970. Barium in sea water. *Earth and Planet. Sci. Lett.* V8, p. 372-378.
First demonstration of the close parallel between the distributions of barium and ^{226}Ra in the sea.
366. Wolgemuth, K. 1970. Barium analyses from the first GEOSECS test cruise. *J. Geophys. Res.* V75, p. 7686-7687.
A profile of barium in the eastern North Pacific.
367. Bernat, M., T. Church, C.J. Allegre. 1972. Barium and Strontium concentrations in Pacific and Mediterranean sea water profiles by direct isotope dilution mass spectrometry, *Earth & Planet. Sci. Lett.* V16, p.75-80.
A novel procedure for rapid barium analysis.
368. Bender, M., T. Snead, L.-H. Chan, M.P. Bacon and J. M. Edmond. 1972. Barium intercalibration at GEOSECS I and III. *Earth & Planet. Sci. Lett.* V16, p. 81-83.
Intercomparisons of barium analyses made in different laboratories.
369. Bacon, M.P. and J.M. Edmond. 1972. Barium at GEOSECS III in the southwest Pacific, *Earth and Planet. Sci. Lett.* V16, p. 66-74.
A profile of barium in the southwestern Pacific.
370. Li, Y.-H., T.L. Ku, G.G. Mathieu and K. Wolgemuth. 1973. Barium in the Antarctic Ocean and implications regarding the marine geochemistry of Ba and ^{226}Ra . *Earth and Planet. Sci. Lett.* V19, p. 352-358.
The relationship between the distributions of barium and ^{226}Ra in the Antarctic Ocean.
371. Mann, C.R., A.R. Coote and D.M. Gardner. 1973. The meridional distribution of silicate in the western Atlantic Ocean. *Deep Sea Res.* V20, p. 791-802.
Demonstration that the distribution of high dissolved silicate water closely parallels that of the low temperature and low salinity Antarctic Bottom Water.
372. Cormack, E.C. 1973. Silicate and potential temperature in the deep and bottom waters of the western Weddell Sea. *Deep Sea Res.* V20, p. 927-932.
A discussion of potential temperature-silicate correlations as a means of distinguishing the water masses of the Weddell Sea.
373. Chung, Y.-C. 1974. Radium-226 and Ra-Ba relationships in Antarctic and Pacific Waters. *Earth & Planet. Sci. Lett.* V23, p. 125-135.
Relationship between the distributions of barium and

^{226}Ra in the Antarctic Ocean.

374. Chan, L.H., J.M. Edmond, R.F. Stallard, W.S. Broecker, Y.-C. Chung, R.F. Weiss and T.L. Ku. 1976. Radium and barium at GEOSECS stations in the Atlantic and Pacific. *Earth & Planet. Sci. Lett.* V32, p. 258-267.
Comparison of the distributions of radium and barium in the sea.
375. Chan, L.H., D. Drummond, J.M. Edmond and B. Grant. 1977. On the barium data from the Atlantic GEOSECS Expedition. *Deep Sea Res.* V24, p. 613-649.
Presentation and discussion of the distribution of barium in the Atlantic Ocean based on measurements made on samples collected as part of the Atlantic GEOSECS expedition.
376. Edmond, J.M., S.S. Jacobs, A.L. Gordon, A.W. Mantyla and R.F. Weiss. 1979. Water column anomalies in dissolved silica over opaline pelagic sediments and the origin of the deep silica maximum. *Jour. of Geophys. Res.* V84, p. 7809-7826.
Distribution of silicate throughout the world ocean.
377. Chung, Y. 1980. Radium-barium-silica correlations and a two dimensional radium model for the world ocean. *Earth & Planet. Sci. Lett.* V49, p. 319-328.
Correlation between the distributions of barium and silicate in the oceans.
378. Froelich, P.N. and M.O. Andreae. 1981. The marine geochemistry of germanium: ekasilicon. *Science* V213, p. 205-207.
A discussion of marine geochemistry of germanium. The geochemical behavior of dissolved germanium in rivers, estuaries and the oceans is similar to that of silicon.
- 3. PAPERS DEALING WITH THE DISTRIBUTIONS OF ΣCO_2 , $\text{CO}_3^=$, CO_2 AND ALKALINITY IN THE SEA (#379 to #409)**
379. Buch, K., H.W. Harvey and S. Grifenberg. 1932. Über der Kohlen - sourcesystem in Meerwasser, Rapp. Proc. Verb. C.P.I.E.M. V79, p.1-70.
Discussion of the CO_2 , HCO_3^- , $\text{CO}_3^=$ equilibria in sea water.
380. Buch, K. 1933. Der Borsauregehalt der Meerwassers and seine Bedeutung bei der Berechnung des Kohlensauresystems in Meerwasser, Conseil Perm. Intern. l'Explor. Mer. Rapp. Proc-Verb. V85, p. 71-75.
The importance of boric acid to the CO_2 , HCO_3^- , $\text{CO}_3^=$ equilibria in sea water.
381. Buch, K. 1933. On boric acid in sea and its influence on the carbonic acid equilibrium. Conseil Perm. Intern. l'Explor. Mer. Rapp. Proc-Verb. V85, p. 71-75.

The first paper showing the importance of taking into account borate when considering the relationship between the concentrations of CO_2 , HCO_3^- , $\text{CO}_3^{=}$ and alkalinity in sea water.

382. Wattenberg, H. 1933. Über die Titrationsalkalinität und den Kalziumkarbon algehalt des Meerwassers, Duetche Atlantische Exped., Meteor 1925-1927, V8, p. 122-231.
Measurements of alkalinity and ΣCO_2 in waters from the South Atlantic.
383. Buch, K. 1938. New determination of the second dissociation constant of carbonic acid in seawater. Conseil Perm. Acta Acad. Aboenis Math. Pys. V11, p. 18.
An early but surprisingly accurate measurement of the second dissociation constant of carbonic acid (i.e., K'_{2}) in seawater.
384. Buch, K. 1939. Beobachtungen über das Kohlenosaure gleichgewicht und über den Lohlensauraustansch zwischen atmosphere und Meer in nord atlantischen Ozean, Acta Acad. Aboenis Math Phys. V11, p.5-16.
Measurements of pH, alkalinity, ΣCO_2 , pCO_2 and dissolved oxygen on surface waters in the North Atlantic over the period June through September 1935.
385. Buch, K. 1951. Das Kohlensaure Gleichgewichtssystem in Meerwasser. Hansforskning Inst. Skr. No. 151, p. 18.
 CO_2 , HCO_3^- , $\text{CO}_3^{=}$ equilibria in sea water.
386. Lyman, J. 1956. Buffer mechanism of sea water, Ph.D. thesis, University of California, Los Angeles, p. 1-196.
Measurements of the first and second dissociation constants of carbonic acid in sea water and of the dissociation constant of boric acid in sea water.
387. Takahashi, T. 1961. Carbon dioxide in the atmosphere and in Atlantic Ocean water. J. Geophys. Res. V66, p. 477-494.
Traverses of CO_2 partial pressure in the atmosphere and in the surface ocean along a north-south traverse in the Atlantic Ocean carried out as part of the International Geophysical Year Program in 1958.
388. Keeling, C.D., N.W. Rakestraw and L.S. Waterman. 1965. Carbon dioxide in surface waters of the Pacific Ocean 1, measurements of the distribution. J. Geophys. Res. V70, p. 6087-6097.
Summary of CO_2 partial pressure measurements in the surface waters of the Pacific Ocean made during and after the International Geophysical Year Program.
389. Keeling, C.D. 1965. Carbon dioxide in surface waters of the Pacific Ocean 2, calculation of the exchange with the atmosphere. J. Geophys. Res. V76, p. 6099-6102.

Based on the concentration of CO₂ in the atmosphere and ocean water, an exchange rate across sea-air interface is estimated to be 18 mol/cm² yr in the Pacific Ocean.

390. Disteche, A. and S. Disteche. 1967. The effect of pressure on the dissociation of carbonic acid from measurements with buffered glass electrode cells. J. Electrochem. Soc. V114, p. 330-340.
First direct measurements (using high pressure pH electrodes) of the dissociation constants for sea water at conditions approximating those in deep water.
391. Culberson, C., D.R. Kester, and R.M. Pytkowicz. 1967. High pressure dissociation of carbonic and boric acids in sea water. Science V157, p.59-61.
Another study of the pressure effects on the dissociation constants of carbonic acid in seawater.
392. Culberson, C.H. and R.M. Pytkowicz. 1968. Effect of pressure on carbonic acid, boric acid and the pH in seawater. Limnol. and Oceanog. V13, p. 403-417.
A study of the pressure effects on the carbonate chemistry of sea water.
393. Keeling, C.D. and L.S. Waterman. 1968. Carbon dioxide in surface ocean waters 3. Measurements on Lusiad Expedition 1962-1963, J. Geophys. Res. V73, p. 4529-4541.
Further measurements of the CO₂ partial pressure in surface ocean waters.
394. Keeling, C.D. 1968. Carbon dioxide in surface ocean waters 4. Global distribution. J. Geophys. Res. V73, p. 4543-4553.
A global synthesis of CO₂ partial pressure distribution in the surface ocean.
395. Edmond, J.M. 1970. High precision determination of titration alkalinity and total carbon dioxide content of sea water by potentiometric titration. Deep Sea Res. V17, P. 737-750.
The development of a closed titration cell designed to allow high precision analyses of the alkalinity and total dissolved inorganic carbon content of sea water samples.
396. Takahashi, T., R.F. Weiss, C.H. Culberson, J.M. Edmond, D.E. Hammond, C.S. Wong, Y-H Li and A.E. Bainbridge. 1970. A carbonate chemistry profile at the 1969 GEOSECS intercalibration station in the eastern Pacific Ocean. Jour. of Geophys. Res. V75, p. 7648-7666.
Intercomparison of the results of pH, titration ΣCO₂ and alkalinity, gas chromatograph ΣCO₂ and CO₂ partial pressure measurements on samples collected at the GEOSECS intercalibration station in the eastern North Pacific.

397. Craig, H. and R.F. Weiss. 1970. The GEOSECS 1969 Intercalibration Station: Introduction and hydrographic features, and total CO_2 - O_2 relationships. *J. Geophys. Res.* V75, p. 7641 - 7647.
Profile of ΣCO_2 and O_2 at the GEOSECS intercalibration station in the eastern North Pacific.
398. Brewer, P.G., G.T. Wong, M.D. Bacon, and D. Spencer. 1975. An oceanic calcium problem? *Earth and Planet. Sci. Lett.* V26, p. 81-87.
Demonstration that the uptake of nitrate by plants in surface water leads to an increase in the alkalinity of surface water and that the release of nitrate during respiration leads to a decrease in the alkalinity of deep water.
399. Millero, F.J. and R.A. Berner. 1972. Effect of pressure on carbonate equilibria in seawater. *Geochim. et Cosmochim. Acta.* V36, p. 92-98.
A calculation based on partial molar volumes of the pressure dependence of the solubility of calcite in seawater.
400. Merbach, C., C.H. Culberson, J.E. Hawley and R.M. Pytkowicz. 1973. Measurement of the apparent dissociation constants of carbonic acid in sea water at atmospheric pressure, *Limnol. and Oceanog.* V18, p. 897-907.
Redetermination of the dissociation constants of carbonic acid. These constants are currently accepted by most workers.
401. Haussin, I. 1973. A new set of acidity constants for carbonic acid and boric acid in sea water. *Deep Sea Res.* V20, p. 461-478.
Yet another determination of the dissociation constants for carbonic acid in sea water.
402. Gieskes, J. 1974. The alkalinity - total carbon dioxide system in sea water, *The Sea* V5 ed. by E.D. Goldberg, J. Wiley and Sons, New York, N.Y., p. 123-156.
A review article on measurements of ΣCO_2 and alkalinity in sea water.
403. Weiss, R.F. 1974. Carbon dioxide in water and seawater: The solubility of a non-ideal gas. *Marine Chem.* V2, p. 203-215.
Measurements of the solubility of CO_2 in seawater.
404. Takahashi, T., P. Kaiteris, W.S. Broecker and A.E. Bainbridge. 1976. An evaluation of the apparent dissociation constants of carbonic acid in sea water. *Earth and Planet. Sci. Lett.* V32, p. 458-467.
Use of redundant measurements of CO_2 , ΣCO_2 and alkalinity made as part of the GEOSECS program to evaluate the reliability of various sets of equilibrium constants.

405. Fiadero, M. 1980. The alkalinity of the deep Pacific. *Earth & Planet Sci. Lett.* V49, p. 499-505.
 An analysis of the GEOSECS alkalinity measurements in the deep Pacific Ocean.
406. Takahashi, T., W.S. Broecker, A.E. Bainbridge and R.F. Weiss. 1980. Carbonate Chemistry of the Atlantic, Pacific and Indian Oceans: The results of the GEOSECS expeditions 1972-1978. Technical Report No. 1, CU-1-80, Lamont-Doherty Geological Observatory, Palisades, N.Y., p. 211.
 A listing of the CO_2 , ΣCO_2 and alkalinity measurements made during the Atlantic, Pacific, and Indian Ocean GEOSECS expeditions: Also given are calculated *in situ* CO_3^{2-} , HCO_3^- and CO_2 concentrations and the extent of supersaturation of the water with respect to calcite and aragonite.
407. Bradshaw, A.L. and Brewer, P.G. 1980. The titration of sea water with strong acid: An evaluation of the GEOSECS total carbon dioxide-alkalinity potentiometric titration procedure. In: "Workshop in Oceanic CO_2 Standardization, La Jolla, Calif. Nov. 30-Dec. 1, 1979" ed. by H.G. Ostlund and D. Dryssen, U.S. Dept. of Energy, CO_2 Effects Research and Assessment Program, Washington, D.C.
 An evaluation of the procedures used to analyze the GEOSECS titration data and suggestions for the improvement of these procedures.
408. Takahashi, T., W.S. Broecker, S.R. Werner and A.E. Bainbridge. 1980. Carbonate chemistry of the surface waters of the world oceans. In: "Isotope Marine Chemistry", Chap. 15, ed. by E.D. Goldberg, Y. Horibe and K. Sarubashi, Uchida Rokakuho Pub. Co., Tokyo, Japan.
 Distribution of carbonate ion concentrations, alkalinity, and ΣCO_2 in the surface waters of the world ocean as determined by the GEOSECS program.
409. Takahashi, T., W.S. Broecker and A.E. Bainbridge. 1981. The alkalinity and total carbon dioxide concentration in the world oceans. In: "Carbon Cycle Modeling", ed. by B. Bolin, SCOPE 16, p. 271-286.
 Average alkalinity and ΣCO_2 profiles for various regions of the ocean.
- 409a. Broecker, W.S., T. Takahashi, P. Quay, D. Bos, D. Chipman and M. Stuiver, in press. Carbon dioxide and radiocarbon budgets for the equatorial Pacific Ocean and the equatorial upwelling rate. *J. Geophys. Res.*
 An estimate of the rate of upwelling in the equatorial Pacific based on measurements of pCO_2 , ΣCO_2 and nutrient constituents.
4. PAPERS DEALING WITH THE DISTRIBUTION OF NITROGEN SPECIES (OTHER THAN NITRATE IN THE SEA) (#410 to #421)

410. Delwiche, C.C. 1956. Denitrification. In: Inorganic nitrogen metabolism. ed. by W. D. McElroy and B. Glass, Johns Hopkins Press, Baltimore, Md. p. 233-256.
A general discussion of the mechanism of denitrification.
411. Craig, H. and L. I. Gordon. 1963. Nitrous oxide in the ocean and marine atmosphere. *Geochimica et Cosmochim. Acta*, V27, p. 949-955.
First precise measurements of nitrous oxide in the atmosphere and surface ocean.
412. Goering, J.J. 1968. Denitrification in the oxygen minimum layer of the eastern tropical Pacific Ocean. *Deep Sea Res.* V15, p. 151-164.
Evidence for the utilization of nitrate in thermocline waters free of O₂.
413. Delwiche, C.C. 1970. The nitrogen cycle. *Scientific American*, V223, p. 136-147.
A review of the nitrogen cycle in nature.
414. Wada, E. and A. Hattori. 1971. Nitrite distribution and nitrate reduction in deep sea waters. *Deep Sea Res.* V19, p. 123-132.
Measurements of nitrite concentrations in Sagami and Suruga Bays, and in the central Pacific. A discussion of nitrate reduction in deep seawater is also given.
415. Cline, J.D. and F.A. Richards. 1972. Oxygen deficient conditions and nitrate reduction in the eastern tropical North Pacific Ocean. *Limnology and Oceanog.* V7, p. 885-900.
A study of nitrate utilization in the O₂ free water of the thermocline in the eastern North Pacific.
416. Cline, J.D. 1973. Denitrification and isotopic fractionation in two contrasting marine environments; the eastern tropical North Pacific and the Cariaco Trench. Ph.D. thesis, University of California, Los Angeles, 270 pp.
Nitrogen isotope fractionation accompanying the utilization of nitrate in O₂ free waters.
417. Pierotti, D. and R.A. Rasmussen. 1976. Combustion as a source of nitrous oxide in the atmosphere. *Geophys. Res. Lett.* V3, p. 265-267.
Anthropogenic production of nitrous oxide.
418. Weiss, R.F. and H. Craig. 1976. Production of atmospheric nitrous oxide by combustion. *Geophys. Res. Lett.* V3, p. 751-753.
Anthropogenic production of nitrous oxide.
419. Yoshinari, T. 1976. Nitrous oxide in the sea. *Marine Chemistry* V4, P. 189-202.

The distribution of nitrous oxide with depth in the North Atlantic Ocean and its anti-correlation with dissolved oxygen.

420. Cohen, Y. and L. I. Gordon. 1978. Nitrous oxide in the oxygen minimum of the eastern tropical North Pacific: evidence for its consumption during denitrification and possible mechanisms for its production. Deep Sea Res. V-25, p. 509-524.

The consumption of nitrous oxide under O₂ free conditions.

421. Cohen, Y. and L.I. Gordon. 1979. Nitrous oxide production in the ocean. Jour. of Geophys. Res. V84, p. 347-353.

The production of nitrous oxide during respiration.

5. PAPERS BASED ON THE GEOSECS DATA SET DEALING WITH THE RELATIONSHIP BETWEEN POTENTIAL TEMPERATURE, SALINITY AND THE DISTRIBUTIONS OF SEVERAL OF THE NUTRIENT CONSTITUENTS (#422 to #433)

422. Craig, H., Y. Chung and M. Fiadero. 1972. A benthic front in the South Pacific. Earth & Planet. Sci. Lett. V16, p. 50.

The use of hydrographic and nutrient element data to define a major deep water front in the South Pacific Ocean.

423. Broecker, W.S., T. Takahashi and Y.H. Li. 1976. Hydrography of the central Atlantic-I: The two-degree discontinuity. Deep Sea Res. V23, p. 1083-1104.

The use of hydrographic and nutrient constituent data to define a major discontinuity present throughout the deep Atlantic Ocean.

424. Bainbridge, A.E. 1976. GEOSECS Atlantic Final Hydrographic Data Report. GEOSECS Operations Group, Scripps Institution of Oceanography, La Jolla, California.

Listings of potential temperature, salinity, silicate, nitrate, phosphate and dissolved oxygen data for the GEOSECS Atlantic Ocean Expedition.

425. Bainbridge, A.E. 1976. GEOSECS Pacific Final Hydrographic Data Report. GEOSECS Operations Group, Scripps Institution of Oceanography, La Jolla, California.

Listings of potential temperature, salinity, density, silicate, nitrate, phosphate and dissolved oxygen data for the GEOSECS Pacific Ocean Expedition.

426. Bainbridge, A.E. 1978. Hydrographic Report for GEOSECS Indian Ocean Expedition, Scripps Institution of Oceanography, La Jolla, California.

Listings of potential temperature, salinity, silicate, nitrate, phosphate and dissolved oxygen data for the GEOSECS Indian Ocean Expedition.

427. Broecker, W.S., T. Takahashi and M. Stuiver. 1980. Hydrography of the central Atlantic-II: Waters beneath the two-degree discontinuity. Deep-Sea Res. V27A, p. 397-419.
 The relationship between nutrient constituent concentrations and salinity for waters beneath the Two-Degree Discontinuity in the western basin of the deep Atlantic.
428. Weiss, R.F., H.G. Ostlund and H. Craig. 1979. Geochemical Studies of the Weddell Sea. Deep Sea Res. V26, p. 1093-1120.
 The use of potential temperature, salinity, isotopic ratios, and nutrient constituent relationships to define the contributions of various water types to the formation of Weddell Sea bottom water.
429. Broecker, W.S. and A. Bainbridge. 1978. An Abyssal shear zone. J. of Geophys. Res. V83, p. 1963-1966.
 Evidence for a thin layer of young deep water moving along the bottom into the western basin of the North Atlantic.
430. Broecker, W.S. and T. Takahashi. 1980. Hydrography of the central Atlantic-III: The North Atlantic deep-water complex. Deep Sea Res. V27A, p. 591-613.
 Nutrient constituent relationships within the North Atlantic Deep Water complex of the Atlantic Ocean.
431. Broecker, W.S., J.R. Toggweiler and T. Takahashi. 1980. The Bay of Bengal - a major nutrient source for the deep Indian Ocean. Earth and Planet. Sci. Lett. V49 p. 506-512.
 Demonstration that the rain of organic matter in the Bay of Bengal constitutes a major sink for dissolved oxygen and source for nutrient constituents in the deep waters of the western Indian Ocean.
432. Broecker, W.S. and T. Takahashi. 1981. Hydrography of the central Atlantic-IV: Intermediate waters of Antarctic origin. Deep Sea Res. V28, p. 177-193.
 Demonstration that O₂ minimum waters from the Antarctic Ocean penetrate along isopycnal horizons far into the Atlantic Ocean carrying with them a strong nutrient constituent signature.
433. Williams R.T. 1981. Hawaii-Tahiti Shuttle Experiment Hydrographic Reports Vol.I, II and III., Scripps Institution of Oceanography, PACODF Publ.#209, 210, 211 La Jolla, Calif.
 Listings of potential temperature, salinity, density, silicate, nitrate, phosphate, dissolved oxygen, ΣCO₂ and alkalinity data taken over the period February 1979 to February 1980 along traverses from Hawaii to Tahiti.

B. CHEMICAL TRACERS OF PARTICLE-WATER INTERACTIONS OCCURRING IN THE SEA (#434 to #456)

1. PAPERS DEALING WITH THE DISTRIBUTION OF LEAD IN THE SEA (#434 to #436)

434. Tatsumoto, M. and C.C. Patterson. 1963. The concentrations of common lead in sea water. In: Earth Science and Meteorites, ed. by J. Geiss and E.D. Goldberg, North-Holland, Amsterdam, p. 74-89.
First reliable measurements of lead in sea water.
435. Patterson, C. 1974. Lead in seawater. Science, V183, p. 553. Discussion of the importance of the contribution of lead from gasoline to the lead content of surface water.
436. Schaule, B.K. and C.C. Patterson. 1981. Lead concentrations in the northeast Pacific: evidence for global anthropogenic perturbations. Earth & Planet. Sci. Lett. V54, p. 97-116. Vertical profiles of dissolved lead in the Pacific Ocean and estimates of the relative contributions of natural and anthropogenic lead.

2. PAPERS DEALING WITH THE DISTRIBUTION OF CADMIUM IN THE SEA (#437 to #438)

437. Boyle, E., F. Sclater and J.M. Edmond. 1976. On the marine geochemistry of cadmium. Nature V263, p. 42-44.
First reliable measurements of cadmium in sea water. Profiles showing a depletion in surface water.
438. Bruland, K.W., G.A. Knauer and J.H. Martin. 1978. Cadmium in northeast Pacific waters. Limnology and Oceanog. V23, p. 618-625.
Highly precise measurements of cadmium in waters from the North Pacific demonstrating the near perfect correlation between the distribution of this metal and that of PO₄ in the sea.

3. PAPERS DEALING WITH THE DISTRIBUTION OF COPPER IN THE SEA (#439 to #441)

439. Boyle, E. and J.M. Edmond. 1975. Copper in surface waters south of New Zealand. Nature, V253, p. 107-109.
Demonstration that the concentration of copper in surface water increases toward the Antarctic as does that for the nutrient constituents.
440. Boyle, E., F.R. Sclater, and J.M. Edmond. 1977. The distribution of dissolved copper in the Pacific. Earth & Planet. Sci. Lett. V37, p. 38-54.
Vertical profiles of copper in the Pacific Ocean showing a continuous increase from surface to sea floor.
441. Moore, R.M. 1978. The distribution of dissolved copper in the eastern Atlantic Ocean. Earth & Planet. Sci. Lett. V41, p. 461-468.

A discussion of dissolved copper concentrations at five stations in the eastern Atlantic between 20° and 24°N.

4. PAPERS DEALING WITH THE DISTRIBUTION OF ZINC AND NICKEL IN THE SEA (#442 to #443)

442. Sclater, F.R., E. Boyle and J.M. Edmond. 1976. On the marine geochemistry of nickel. *Earth & Planet. Sci. Lett.* V31, p. 119-128.

First reliable vertical profiles of nickel in the sea. The concentration decreases up the water column but does not go to zero in surface water.

443. Bruland, K.W., G.A. Knauer and J.H. Martin. 1978. Zinc in northeast Pacific water. *Nature*, V271, p. 741-743.

Vertical profile of zinc in the northeast Pacific Ocean and demonstration of its excellent correlation with that of silica.

5. PAPERS DEALING WITH THE DISTRIBUTION OF MANGANESE IN SEA WATER (#444 to #449)

444. Bender, M.L., T.L. Ku and W.S. Broecker. 1970. Accumulation rates of manganese in pelagic sediments and nodules. *Earth & Planet. Sci. Lett.* V8, p. 143-148.

A comparison of the rate of accumulation in Mn nodules with that in sediments.

445. Bender, M.L., G.P. Klinkhammer and D.W. Spencer. 1977. Manganese in sea water and the marine manganese balance. *Deep Sea Res.* V24, p. 799-812.

First reliable measurements of the concentration of manganese in sea water.

446. Klinkhammer, G.P., M. Bender and R.F. Weiss. 1977. Hydrothermal manganese in the Galapagos Rift. *Nature*, V269, p. 319-320.

Demonstration that manganese accompanies the excess ${}^3\text{He}$ in the hot waters issuing forth from the ridge crests in sufficient quantities to serve as a tracer for these waters.

447. Weiss, R.F. 1977. Hydrothermal manganese in the deep sea: scavenging residence time and Mn/ ${}^3\text{He}$ relationships. *Earth & Planet. Sci. Lett.* V37, p. 257-262.

Based on the contrast between the Mn/ ${}^3\text{He}$ ratio in ridge crest hydrothermal waters and in ambient ${}^3\text{He}$ contaminated deep water it is shown that the residence time of Mn in deep water can be no more than a few decades.

448. Klinkhammer, G.P. and M.L. Bender. 1980. The distribution of manganese in the Pacific Ocean. *Earth and Planet. Sci. Lett.* V46, p. 361-384.

Profiles of manganese in the Pacific Ocean.

449. Landing, W.M. and K. W. Bruland. 1980. Manganese in the North Pacific. *Earth and Planet. Sci. Lett.* V49, p. 45-56.

Demonstration that the concentration of manganese in surface waters decreases away from the coasts in keeping with the short residence time of this element in sea water.

6. PAPERS DEALING WITH THE DISTRIBUTION OF SELENIUM IN SEA WATER (#450 to #451)

450. Measures, C.I. and J.D. Burton. 1980. The vertical distribution and oxidation states of dissolved selenium in the north-east Atlantic Ocean and their relationship to biological processes. *Earth & Planet. Sci. Lett.* V46, p. 385-396.

Profiles of selenium in the Atlantic Ocean. Also a demonstration that the two oxidation states of selenium are not at thermodynamic equilibrium with one another. Rather they act more like the pair N_2-NO_3 in the sea (i.e., slowly interacting.)

451. Measures, C.I., R.E. McDuff and J.M. Edmond. 1980. Selenium redox chemistry at GEOSECS I re-occupation. *Earth & Planet. Sci. Lett.* V49, p. 102-108.

Further results on the vertical distribution of selenium and its oxidation states.

7. PAPERS DEALING WITH SEVERAL METALS (#452 to #456)

452. Martin, J.H. and G.A. Knauer. 1973. The elemental composition of plankton. *Geochim. Cosmochim. Acta*, V37, p. 1639-1653.

The elemental composition of phytoplankton samples collected in Monterey Bay, Calif., is reported in this paper.

453. Knauer, G.A. and J.H. Martin. 1973. Seasonal variations of cadmium, copper, manganese, lead and zinc in water and phytoplankton in Monterey Bay, California. *Limnol. Oceanog.* V18, p. 597-604.

Concentrations of a number of metals in waters and plants in a near-shore environment.

454. Bender, M.L. and C. Gagner. 1976. Dissolved copper, nickel and cadmium in the Sargasso Sea. *J. Marine Res.* V34, p. 327-339.

Discussion of dissolved Cu, Ni, and Cd in surface and deep waters of the Sargasso Sea.

455. Bruland, K.W. 1980. Oceanographic distributions of cadmium, zinc, nickel and copper in the North Pacific. *Earth & Planet. Sci. Lett.* V47, p. 176-198.

Contrast of the profiles of four metals in the North Pacific Ocean.

456. Bruland, K.W. In press. Trace elements in the sea. In: Chemical Oceanography, V8, ed. by J.P. Riley and G. Skirrow, Academic Press, London.

Review paper on trace metal distributions in sea water.

- 456a. Balistrieri, L., P.G. Brewer and J.W. Murray. 1981. Scavenging residence times of trace metals and surface chemistry of sinking particles in the deep ocean. Deep Sea Res. V28A, p. 101-121.

Comparison of field measurements with predictions based on adsorption properties of metals as measured in the laboratory.

IV. PAPERS DEALING WITH BIOGENIC MATERIAL (#457 to #543)

A. PAPERS DEALING WITH BIOGENIC MATERIAL IN THE SEDIMENTS (#457 to #531)

1. PAPERS DEALING WITH THE SOLUBILITY OF CALCITE AND ARAGONITE (#457 to #468)

457. McIntyre, W.G. 1965. The temperature variation of the solubility product of calcium carbonate in seawater. Fisheries Res. Bd. of Canada, Manuscript Report Series V200, pl-153.

The first "modern" measurement of the solubilities of calcite and aragonite in sea water.

- 457a. Pytkowicz, R.M., and G.A. Fowler. 1967. Solubility of foraminifera in seawater at high pressure. Geochem. J. V1, p. 169-182.

Discussion of the effect of pressure on carbonate ion pairs, on the relative solubilities of calcite and aragonite, and on rates of solution of these phases.

458. Hawley, J.E. and R.M. Pytkowicz. 1969. Solubility of calcium carbonate in seawater at high pressure and 2°C. Geochim. Cosmochim. Acta. V33, p. 1557-1561.

The first measurement of the solubility of calcium carbonate in sea water at pressures corresponding to those in deep water.

- 458a. Millero, F.J., and R.A. Berner. 1972. Effect of pressure on carbonate equilibria in seawater. Geochim. Cosmochim. Acta. V36, p. 92-98.

A discussion of the effect of pressure on carbonate equilibria in seawater based on the partial molar volumes.

- 458b. Duedall, I.W. 1972. The partial molal volumes of calcium carbonate in sea water. Geochim. Cosmochim. Acta., V36, p. 729-734.

Experimental determination of the partial molal volume K_2CO_3 and Na_2CO_3 for sea water and for 0.725M NaCl solution.

459. Ingle, S.E., C.H. Culberson, J. Hawley and R.M. Pytkowicz. 1973. The solubility of calcite in sea water at atmospheric pressure and 35‰ salinity, *Marine Chemistry* V1, p. 295-307.
The first precise measurement of the solubility of calcite in sea water. These results have stood the test of time.
460. Ingle, S.E. 1975. The solubility of calcite in the oceans. *Mar. Chem.* V3, p. 301-319.
The apparent solubility product of calcite in sea water was measured as a function of temperature, salinity, and pressure using potentiometric satrometry techniques.
461. Berner, R.A. 1976. The solubility of calcite and aragonite in sea water at atmospheric pressure and 34.5‰ salinity. *Am. J. Sci.* V276, p.713-730.
Measurements of the solubility of calcite and aragonite. The calcite value is considerably higher than that of Ingle.
462. Broecker, W.S. and T. Takahashi. 1977. The solubility of calcite in sea water. In: *Thermodynamics in Geology*, ed. by D.G. Fraser, D. Reidel Pub. Co., p. 365-379.
A review of our knowledge of the solubility of calcite and aragonite in sea water.
463. Broecker, W.S. and T. Takahashi. 1978. The relationship between lysocline depth and in situ carbonate ion concentration. *Deep Sea Res.* V25, p. 65-95.
An attempt to determine the solubility of calcite and aragonite in the deep sea using satrometer measurements and lysocline depth observations.
464. Sayles, F.L. 1980. The solubility of CaCO_3 in seawater at 2°C based upon in situ samples pore water composition. *Marine Chemistry*, V9, p. 223-235.
Estimates of the apparent solubility products of sedimentary calcite and aragonite in seawater based upon measurements on water collected in situ from the pores of deep sea sediments. A particularly nice piece of research.
465. Morse, J.W., A. Mucci and F.J. Millero. 1980. The solubility of calcite and aragonite in seawater at 35‰ salinity at 25°C and atmospheric pressure. *Geochim. Cosmochim. Acta*, V44, p. 85-94.
Careful long term equilibrations of calcite and aragonite with seawater yielding solubility estimates consistent with those of Ingle.
466. Plath, D.C., K.S. Johnson and R.M. Pytkowicz. 1980. The solubility of calcite-probably containing magnesium-in sea

water. Marine Chem. V10, p. 9-29.

More precise measurements of the solubility of calcite at atmospheric pressure as a function of temperature and salinity.

467. Plath, D.C. and R.M. Pytkowicz. 1980. The solubility of aragonite in seawater at 25.0°C and 32.62‰ salinity. Marine Chem. V10, p. 3-7.
A measurement of the solubility of aragonite which agrees with the Berner value. It yields an aragonite to marine calcite solubility ratio of 2.05 opposed to that of 1.48 predicted by thermodynamic consideration. The suggestion is made that marine calcite has a lower solubility than the pure calcite.
468. Plummer, L.N. and E.T. Sundquist. 1982. Total individual ion activity coefficients of calcium and carbonate in seawater at 25°C and 35‰ salinity, and implications to the agreement between apparent and thermodynamic constants of calcite and aragonite. Geochim. et Cosmochim Acta V46, p. 247-258.
An attempt to reconcile the solubilities for calcite and aragonite in sea water with those in fresh water.

2. PAPERS DEALING WITH CaCO_3 SATUROMETRY (#469 to #472)

469. Weyl, P.K. 1961. The carbonate saturometer. J. of Geology, V69, p. 32-43.
The theory behind carbonate saturometry.
470. Weyl, P.K. 1965. The solution behavior of carbonate materials in seawater. Proceedings of International Conference on Tropical Oceanography, Miami Beach, Florida, p. 178-228.
Demonstration using the carbonate saturometer that the formation coatings of impure calcite (containing Mg) during calcite precipitation and perhaps even during dissolution makes difficult the achievement of thermodynamic equilibrium.
471. Ben-Yaakov, S. and I.R. Kaplan. 1971. Deep sea *in situ* calcium carbonate saturometry. J. of Geophys. Res. V76, p. 772-731.
The development of an automated saturometer which can operate at great depth in the sea.
472. Ben-Yaakov, S. E. Ruth and I.R. Kaplan. 1974. Carbonate compensation depth: relation to carbonate solubility in ocean waters. Science, V184, p. 982-894.
The application of *in situ* saturometry to determine the relationship between the lysocline depth and calcite saturation depth.

3. PAPERS DEALING WITH THE RESULTS OF CALCITE AND ARAGONITE IN SITU DISSOLUTION EXPOSURES (#473 to #476)

473. Peterson, M.N.A. 1966. Calcite: rates of dissolution in a vertical profile in the central Pacific. *Science*, V154, p. 1542-1544.
The first demonstration that the long-term exposure of calcite crystals to sea water on deep sea moorings offered valuable information regarding the depth dependence of dissolution rates and the depth of the horizon of calcite saturation.
474. Milliman, J.D. 1975. Dissolution of aragonite, Mg-calcite and calcite in the North Atlantic Ocean. *Geology*, V3, p 461-462.
A repeat of the Peterson experiment in the Atlantic using aragonite and high Mg calcite as well as calcite.
475. Honjo, S. and J. Erez. 1978. Dissolution rates of calcium carbonate in the deep ocean: an in situ experiment in the North Atlantic. *Earth and Planet. Sci. Lett.* V40, p. 226-234.
An improvement in the Peterson technique involving pumping of water across mineral grains. In so doing the influence of changing water turbulence with depth is eliminated.
476. Thunell, R.C., S. Honjo and R. Keir. 1980. Calcite dissolution: an in situ study in the Panama Basin. *EOS (Trans. Amer. Geophys. Union)* V61, p. 275.
Comparison of the calcite dissolution rates measured using the Honjo procedure with the percent calcite in sediments taken at various water depths in the same area.
- 4. LABORATORY STUDIES OF THE DEPENDENCE OF THE RATES OF CALCITE AND ARAGONITE DISSOLUTION RATE ON THE CARBONATE ION CONTENT (HENCE pH) OF THE WATER (#477 to #479)**
477. Morse, J.W. and R.A. Berner. 1972. Dissolution kinetics of calcium carbonate in seawater II. A kinetic origin for the lysocline. *Amer. J. Science*, V272, p. 840-851.
Measurements of the rate of dissolution of calcite dispersed in rapidly stirred water at a variety of pH's (and hence $\text{CO}_3^{=}$ ion concentrations). A nonlinear dependence is observed. Implications to calcite dissolution in sediments are given.
478. Ku, T.-L. and T. Oba. 1978. A method for quantitative evaluation of carbonate dissolution in deep-sea sediments and its application to paleoceanographic reconstruction. *Quaternary Res.* V10, p. 112-129.
An attempt to calibrate dissolution indices (i.e., the fragmentation of solution sensitive species) through laboratory studies employing tracer foraminifera.

479. Keir, R.S. 1980. The dissolution kinetics of biogenic calcium carbonates in seawater. *Geochim. et Cosmochim. Acta.*, V44, p. 241-252.
Demonstration by laboratory experiments that the rate of dissolution of calcite goes with the fourth power of CO_3^{2-} ion concentration for rapidly stirred suspended particles.
- 5. PAPERS DEALING WITH THE DISTRIBUTIONS OF CALCITE AND ARAGONITE IN RECENT SEDIMENTS (#480 to #495)**
480. Chen, C. 1964. Pteropod ooze from Bermuda Pedestal. *Science* V144, p.60-62.
Occurrence of aragonite in sediments shallower than 3 kilometers in the North Atlantic Ocean.
481. Berger, W.H. 1967. Foraminiferal ooze: solution at depths. *Science* V156, p. 383-385.
Demonstration that the shells of some species of non-spinose foraminifera are more resistant to dissolution than those of spinose species.
482. Berger, W.H. 1968. Planktonic foraminifera: selective solution and paleoclimatic implications. *Deep-Sea Res.* V15, p. 31-43.
Application of the selective preservation of the shells of various species of foraminifera to the distribution of calcite dissolution in sediments from the floor of the Pacific Ocean.
483. Berger, W.H. 1970. Planktonic foraminifera: selective solution and the lysocline. *Marine Geology* V8, p. 111-138.
Geographic distribution of dissolution patterns in the deep Pacific.
484. Parker, F.L. and W.H. Berger. 1971. Faunal and solution patterns of planktonic foraminifera in surface sediments of the South Pacific. *Deep Sea Res.* V18, p. 73-107.
The influence of partial dissolution on the distribution of foraminifera shells in the recent sediments of the South Pacific.
485. Valencia, M.J. 1973. Calcium carbonate and gross size analysis of surface sediments, western equatorial Pacific. *Pacific Science* V27, p. 290-303.
Depth dependence of the calcite content of recent sediments in the western equatorial Pacific.
486. Savin, S.M. and R.G. Douglas. 1973. Stable isotope and magnesium geochemistry of recent planktonic foraminifera from the South Pacific. *Geol. Soc. Amer. Bull.* V84, p. 2327-2342.
The influence of magnesium content on the susceptibility of foraminifera shells to dissolution.

487. Broecker, W.S. and S. Broecker. 1974. Carbonate dissolution on the western flank of the East Pacific Rise. In: Studies in paleooceanography, Society of Economic Paleontologists and Mineralogists, Special Publication #20, ed. by W.W. Hay, p. 44-57.
Demonstration that the boundary between sediments experiencing large-scale calcite dissolution and minimal calcite dissolution is quite sharp on the west flank of the East Pacific Rise and that this horizon was deeper during glacial time.
488. Melquen, M. and J. Thiede. 1974. Facies distribution and dissolution depths of surface sediment components from the Vema Channel and the Rio Grande Rise (southwest Atlantic Ocean). *Marine Geology* V17, p. 341-353.
Demonstration of a sharp boundary between sediments rich and poor in calcite in the western basin of the South Atlantic and that this boundary lies in the region of transition from North Atlantic Deep Water and Antarctic Bottom Water.
489. Biscaye, P.E., V. Kolla and K.K. Turekian. 1976. Distribution of calcium carbonate in surface sediments of the Atlantic Ocean. *Jour. of Geophys. Res.* V81, p. 2595-2603.
Contains a map showing the percent CaCO_3 in recent Atlantic Ocean sediments.
490. Kolla, V., A.W.H. Be and P.E. Biscaye. 1976. Calcium carbonate distribution in the surface sediments of the Indian Ocean. *Jour. of Geophys. Res.* V81, p. 2605-2616.
Contains a map showing the percent CaCO_3 in recent Indian Ocean sediments.
491. Berger, W.H., C.G. Adelseck, Jr. and L.A. Mayer. 1976. Distribution of carbonate in surface sediments of the Pacific Ocean. *Jour. Geophys. Res.* V81, p. 2617-2627.
Contains a map showing the percent CaCO_3 in recent Pacific Ocean sediments.
492. Berner, R.A., E.K. Berner and R.S. Keer. 1976. Aragonite dissolution on Bermuda pedestal: its depth and geochemical significance. *Earth and Planet. Sci. Lett.* V30, p. 169.
The depth dependence of the aragonite content of sediments on the Bermuda pedestal.
493. Berner, R.A. 1977. Sedimentation and dissolution of pteropods in the ocean. In: *The Fate of Fossil Fuel CO₂ in the Oceans*, ed. by N.R. Andersen and A. Malahoff, Plenum Press, New York, p. 243-260.
An estimate of the relative rain rates of calcite and aragonite in the world ocean.
494. Berger, W.H. 1978. Deep-sea carbonate: pteropod distribution and the aragonite compensation depth. *Deep Sea Res.* V25, p. 447-452.

Estimates of the aragonite compensation depth in various parts of the ocean.

495. Berner, R.A. and S. Honjo. 1981. Pelagic sedimentation of aragonite: its geochemical significance. *Science* V211, p. 940-942.
A revised estimate of the ratio of aragonite to calcite rain rate in the world ocean.

6. PAPERS DEALING WITH GLACIAL TO INTERGLACIAL CHANGES AND ARAGONITE DISSOLUTION (#496 to #512)

496. Arrhenius, G. 1952. Sediment cores from the East Pacific. *Swedish Deep Sea Expedition (1947-1948) Reports* V5, pl-227.
Analysis of CaCO_3 content, foram fragment to whole foram ratios and planktonic to benthic foram ratios with depth in a series of equatorial Pacific cores.
497. Ruddiman, W.F. and B.C. Heezen. 1967. Differential solution of planktonic foraminifera. *Deep Sea Res.* V14, p. 801-808.
Down core studies in the equatorial Atlantic Ocean showing the change in preservation of solution sensitive foraminifera with climate.
498. Chen, C. 1968. Pleistocene pteropods in pelagic sediments. *Nature*, V219, p. 1145-1147.
Measurements showing a preservation peak in the abundance of pteropods in early post glacial time.
499. Hays, J.D., T. Saito, N.D. Opdyke and L.H. Burckle. 1969. Pliocene Pleistocene sediments of the equatorial Pacific: their paleomagnetic, biostratigraphic, and climatic record. *Geol. Soc. Amer. Bull.* V8, p. 1481-1514.
Calcium carbonate cycles in long equatorial Pacific cores.
500. Hays, W.W. 1970. Calcium carbonate compensation. *Deep Sea Drilling Project Initial Reports* V4, p. 672.
Evidence for long term changes in the depth of the calcium carbonate compensation horizon.
501. Broecker, W.S. 1971. Calcite accumulation rates and glacial to inter-glacial changes in oceanic mixing. In: *The Late Cenozoic Glacial Ages*, Ed. by K.K. Turekian, Yale Univ. Press New Haven, Conn. p. 239-265.
A discussion of the factors influencing of the calcium carbonate budget in the ocean and an examination of the record of budgetary changes kept in deep sea cores.
502. Hays, J.D., A. Perruzza. 1972. The significance of calcium carbonate oscillations in eastern equatorial Atlantic deep sea sediments for the end of the Holocene warm interval. *Quaternary Res.* V2, p. 355-3622.
Demonstration that the changing dilution of calcium carbonate with wind-borne dust from Africa is the cause

of the calcium carbonate cycles in cores from the east flank of the mid-Atlantic Ridge.

503. Diester-Haass L., H.-J. Schrader and J. Thiede. 1973. Sedimentological and paleoclimatological investigations of two pelagic ooze cores off Cape Barbas, North-West Africa. Meteor Forsch Ergeben C., V7, p. 19-66.
Evidence for an aragonite preservation spike at the close of the last glacial period in cores along the African continental margin.
504. Thompson, P.R. and T. Saito. 1974. Pacific Pleistocene sediments: planktonic foraminifera dissolution cycles and geo-chronology. Geology V2, p. 333-335.
Discussion of dissolution cycles in the Pacific Ocean sediments based on the ratios of solution-susceptible to solution-resistant planktonic foraminifera.
505. Damuth, J.E. 1975. Quaternary climate change as revealed by calcium carbonate fluctuations in western equatorial Atlantic sediments. Deep Sea Res. V22, p. 725-743.
Discussion of quaternary climate changes based on fluctuation of total CaCO_3 content in deep sea cores.
506. Luz, B. and N.J. Shackleton. 1975. CaCO_3 solution in the tropical east Pacific during the last 130,000 years. In: Dissolution of Deep-Sea carbonates, Special Publication #13, Cushman Foundation for Foraminiferal Research, p. 142-150.
The relationship between changes in the extent of calcite dissolution and changes in the $^{18}\text{O}/^{16}\text{O}$ ratio for benthic foraminifera (i.e. with changes in ice volume).
507. Gardner, J.V. 1975. Late Pleistocene carbonate dissolution cycles in the eastern equatorial Atlantic. In: Dissolution of Deep Sea carbonates, Ed. by W. V. Sliter, A.W.H. Be, and W.H. Berger. Cushman Foundation for Foraminiferal Res. Special Publication #13, p. 129-141.
Evidence for glacial to interglacial changes in the extent of dissolution of the calcite accumulating in the eastern equatorial Atlantic.
508. Van Andel, T.H. 1975. Mesozoic-Cenozoic calcite compensation depth and the global distribution of calcareous sediments. Earth & Planet. Sci. Lett. V26, p. 187-194.
A reconstruction of the CaCO_3 compensation depth in the three major oceans for the last 60 million years.
509. Hartmann, M., P.J. Muller, E. Suess and C.H. van der Weijden. 1976. Chemistry of Late Quaternary sediments and their interstitial waters from the N.W. African continental margin. Meteor Forsch. Ergebnisse C. No. 24, p. 1-67.
Discussion of temporal changes in the lithology of continental margin sediments from the eastern North Atlantic Ocean.

510. Thunell, R.C. 1976. Calcium carbonate dissolution in Late Quaternary deep sea sediments, western Gulf of Mexico. *Quaternary Res.* V6, p. 281-297.
Discussion of the degree of CaCO_3 dissolution based on foraminiferal test fragmentation, benthonic foram abundance, CaCO_3 content, and various relationships between solution-resistant and solution-susceptible species in deep sea cores.
511. Berger, W.H. 1977. Deep-sea carbonate and the deglaciation preservation spike in pteropods and foraminifera. *Nature*, V269, p. 301-303.
Evidence that the lysocline for aragonite in the eastern Atlantic deepened by over 1 kilometer for a period of several thousands of years corresponding to the transition between late-glacial and post-glacial time.
512. Sundquist, E., D.K. Richardson, W.S. Broecker and T-H. Peng. 1977. Sediment mixing and carbonate dissolution in the south-east Pacific Ocean. In: *The Fate of Fossil Fuel CO_2 in the Oceans*. Ed. by N.R. Andersen and A. Malahoff, Plenum Press, New York p. 429-454.
An attempt to reconstruct the events which created the core top CaCO_3 -rich layer just beneath the present day lysocline on the west flank of the East Pacific Rise.
- 7. MODELS OF THE DISSOLUTION OF CALCITE ON THE SEA FLOOR (#513 to #519)**
513. Li, Y.H., T. Takahashi and W.S. Broecker. 1969. Degree of saturation of CaCO_3 in the oceans. *Jour. of Geophys. Res.* V74, p. 5507-5525.
Estimates of the degree of CaCO_3 saturation in the Pacific and Atlantic Oceans based on measurements of the partial pressure of CO_2 gas and the total content of dissolved inorganic carbon content of sea water samples.
514. Heath, G.R. and C.H. Culberson. 1970. Calcite: degree of saturation, rate of dissolution, and the compensation depth in the deep oceans. *Geological Soc. of Amer. Bull.* V81, p. 3157-3160.
Discussion of the hydrographic features that control the distribution of calcite in deep-sea sediments.
515. Edmond, J.M. 1974. On the dissolution of carbonate and silicate in the deep ocean. *Deep Sea Res.* V21, p. 455-480.
Discussion of the possible role of water turbulence in the dissolution of mineral phases on the sea floor.
516. Schink, D.R. and N.L. Guinasso, Jr. 1977. Modelling the influences of bioturbation and other processes on calcium carbonate dissolution at the sea floor. In: *The Fate of Fossil Fuel CO_2 in the Oceans*, ed. by N.R. Andersen and A. Malahoff,

Plenum Press, New York, p. 375-400.

A model of the interaction between the rain rate of calcite, the rain rate of other phases, the dissolution rate of pure calcite, and the rate of bioturbation.

517. Takahashi, T. and W.S. Broecker. 1977. Mechanisms for calcite dissolution on the sea floor. In: The Fate of Fossil Fuel CO₂ in the Oceans, ed. by N.R. Andersen and A. Malahoff, Plenum Press, New York, p. 455-478.

A discussion of the interaction between the potential dissolution rate of calcite, the rain rate of calcite and the rain rate of other phases for three different assumptions regarding the rate limiting step for dissolution. Also a means of distinguishing among these possible models is discussed.

518. Morse, J.W. 1978. Dissolution kinetics of calcium carbonate in sea water: VI The near-equilibrium dissolution of calcium carbonate rich sediments. Amer. Jour. Sci. V278, p. 344-353.

Discussion of CaCO₃ dissolution kinetics in CaCO₃-rich deep sea sediment.

519. Emerson, S. and M. Bender. 1981. Carbon fluxes at the sediment-water interface of the deep-sea: calcium carbonate preservation. J. Marine Res. V39, p. 139-162.

A discussion of the role of bioturbated organic material to the dissolution of calcite.

- 519a. Crowley, T.J., in press. Calcite dissolution patterns in the central North Atlantic during the last 150,000 years. Mar. Geology.

Evidence for increases in the intensity of calcite dissolution in the deep Atlantic during the peak glacial episodes 70,000 and 20,000 years ago. A clear demonstration that the Atlantic and Pacific are out of phase in this regard.

8. PAPERS DEALING WITH THE DISTRIBUTION OF OPAL IN MARINE SEDIMENTS (#520 to #523)

520. Lisitzin, A.P. 1960. Bottom sediments of the eastern Antarctic and the southern Indian Ocean. Deep Sea Res. V7, p.89-99.

Data on the opal content of sediments in the southern Indian Ocean and adjacent Antarctic.

521. Hurd, D.C. 1973. Interaction of biogenic opal, sediment and sea water in central equatorial Pacific. Geochim. Cosmochim. Acta V37, p. 2257-2282.

Discussion of the dissolution of biogenic opal in deep sea sediments.

522. Hurd, D.C. and F. Theyer. 1975. Changes in the Physical and Chemical Properties of Biogenic Silica from the Central Equatorial Pacific I, Solubility, Specific Surface Area, and Solution Rate Constants of Acid-Cleaned Samples. Analytical

Methods in Oceanography, ed. by T.R.P. Gibbs, Advance in Chemistry Series, V147, p. 211-239.

Factors influencing the solubility of opal.

- 522a. Nelson, D.M. and L.I. Gordon. 1982. Production and pelagic dissolution of biogenic silica in the Southern Ocean. *Geo-chimica and Cosmochimica Acta* V46, p. 491-501.
Budget of dissolved silicate in waters of the Antarctic.
523. Cooke, D.W. and J.D. Hays. 1982. Estimates of Antarctic Ocean seasonal sea ice cover during glacial intervals. In: *Antarctic Geoscience* U. of Wisconsin Press, p. 1017-1025.
Glacial to interglacial changes in the distribution of opal rich sediments in the Antarctic Ocean.

9. PAPERS CONTAINING PORE WATER PROFILES OF DISSOLVED SILICA (#524 to #529)

524. Siever, R., K.C. Beck and R.A. Berner. 1965. Composition of interstitial waters of modern sediments. *Jour. of Geol.* V73, p. 39-73.
Measurements of Ca, Mg, Na, K, Cl, SiO₂ and pH in interstitial water squeezed from samples of modern marine sediments.
525. Fanning, K.A. and M.E.Q. Pilson. 1971. Interstitial silica and pH in marine sediments: some effects of sampling procedures. *Science*, V173, p. 1228-1231.
Discussion of temperature effects on the measurements of interstitial silica and pH in marine sediments.
526. Fanning, K.A. and M.E.Q. Pilson. 1974. The diffusion of dissolved silica out of deep-sea sediments. *J. Geophys. Res.* V79, p. 1293-1297.
Measurements of fluxes of dissolved silica from marine sediments.
527. Heath, G.R. 1974. Dissolved silica and deep sea sediments. In: *Studies in Paleoceanography* V20, ed. by W.W. Hay, Soc. of Econ. Paleontol. and Mineral. Tulsa, Okla. p. 77-93.
A general discussion of dissolved silica in sea water and the silica content of deep-sea sediments.
528. Schink, D.R., N.L. Guinasso and K.A. Fanning. 1975. Processes affecting the concentration of silica at the sediment-water interface of the Atlantic Ocean. *J. Geophys. Res.* V80, p. 3013-3031.
Modeling pore water silica profiles.
529. Loder, T.C., W.B. Lyons, S. Murray and H.D. McGuiness. 1978. Silicate in anoxic pore waters and oxidation effect during sampling. *Nature*, V273, p. 373-374.
Discussion of oxidation effects during sampling on the silica concentration in anoxic pore water.

- 529a.Jahnke, R., S. Emerson, V. Grundmanis, D. Heggie and D. Graham (in press). Pore water of the Central Pacific Ocean: Nutrient Results. *Earth & Planet. Sci. Lett.*
Discussion of the results of the analysis of pore water for nutrients, ΣCO_2 , alkalinity, Mn^{++} , Ca^{++} and dissolved oxygen.

- 529b.Sayles, F.L., F.T. Manheim and L.S. Waterman. 1973. Interstitial water studies on small core samples. Leg 15. Initial Reports of the Deep Sea Drilling Project, V20, p. 783-804.
Listing and discussion of major constituents of pore fluids at site 148, Leg 15 of DSDP in the Caribbean Sea.

10. PAPERS CONTAINING DATA REGARDING THE DISTRIBUTION OF ORGANIC MATERIAL IN SEDIMENTS (#530 to #531)

530. Bordovsky, O.K. 1965. Accumulation of organic matter in bottom sediments. *Marine Geology*, V3, p. 33-82.
Discussion of the accumulation of organic matter in the sediments based on information derived from the Bering Sea.
531. Heath, G.R., T.C. Moore, Jr. and J.P. Dauphin. 1977. Organic carbon in deep-sea sediments. In: *The Fate of Fossil Fuel CO₂ in the Oceans*, ed. by N.R. Andersen and A. Malahoff. Plenum Press, New York, p. 605-625.
Relationship between the organic content of sediments and their rate of deposition.

B. PAPERS DEALING WITH BIOGENIC MATERIAL IN THE WATER COLUMN (#532 to #543)

1. PAPERS DEALING WITH SUSPENDED MATTER IN THE WATER COLUMN (#532 to #536)

532. Brewer, P.G., D.W. Spencer, P.E. Biscaye, A. Hanley, P.L. Sachs, C.L. Smith, S. Kadar and J. Fredricks. 1976. The distribution of particulate matter in the Atlantic Ocean. *Earth & Planet. Sci. Lett.* V32, p. 393-402.
Estimates of the total particle load based on the filtration of 10-liter water samples obtained in Niskin bottles as part of the GEOSECS Atlantic expedition.
533. Krishnaswami, S. and M.M. Sarin. 1976. Atlantic surface particulates: composition, settling rates and dissolution in the sea. *Earth and Planet. Sci. Lett.* V32, p. 430-441.
Analyses of very large filters through which large amounts of water passed during traverses from station to station along the Atlantic GEOSECS tracks.
534. Biscaye, P.E. and S.L. Eittreim. 1977. Suspended particulate loads and transports in the nepheloid layer of the abyssal Atlantic Ocean. *Mar. Geol.* V23, p. 155-172.

Using nephelometer calibrations obtained by filtering water samples from Niskin bottles, the large collection of Lamont-Doherty Geological Observatory nephelometer records was analyzed to yield distributions of suspended particle loads in the Atlantic Ocean.

535. Bishop, J.K.B., J.M. Edmond, D.R. Ketten, M.P. Bacon, and W.B. Silker. 1977. The chemistry, biology and vertical flux of particulate matter from the upper 400 m of the equatorial Atlantic Ocean. Deep Sea Res. V24, p. 511-548.

The analysis of samples of suspended particulate matter obtained using an in situ pumping system coupled to a large-diameter filtering system.

536. Dehairs, F., R. Chesselet and J. Jedwab. 1980. Discrete suspended particles of barite and the barium cycle in the open ocean. Earth & Planet. Sci. Lett., V49, p. 528-550.

Discovery of discrete barite crystals in the material obtained by filtering water from Niskin bottles during the GEOSECS program.

2. PAPERS DEALING WITH MATERIAL CAUGHT IN SEDIMENT TRAPS (#537 to #541)

537. Soutar, A., S.A. Kling, A. Crill, E. Duffrin and K.W. Bruland. 1977. Monitoring the marine environment through sedimentation. Nature, V266, p. 136-139.

One of the first papers showing the power of the sediment trap method for studies of marine chemistry and mineralogy.

538. Honjo, S. 1978. Sedimentation of material in the Sargasso Sea at a 5367m deep station. J. Mar. Res. V36, p. 469-492.

The results from the first major open ocean sediment trap deployment.

539. Brewer, P.G., Y. Nozaki, D.W. Spencer and A.P. Fleer. 1980. Sediment trap experiments in the deep North Atlantic: isotopic and elemental abundances. J. Marine Res. V38, p. 703-728.

Estimates of the rain rates of clay, CaCO_3 , opal and organic matter based on sediment traps deployed in the north temperate and equatorial Atlantic Ocean.

540. Honjo, S. 1980. Material fluxes and modes of sedimentation in the mesopelagic and bathypelagic zones. Jour. Mar. Res. V38, p. 53-97.

Further results from sediment trap deployments.

541. Honjo, S. S.J. Manganini, J.J. Cole. 1982. Sedimentation of biogenic matter in the deep ocean. Deep Sea Res., V29, p. 609-625.

Chemical composition of the organic material caught in sediment traps.

3. PAPERS DEALING WITH MODES OF TRANSPORT OF PARTICULATE MATTER THROUGH THE WATER COLUMN (#542 to #543)

542. Honjo, S., and M.R. Roman. 1978. Marine copepod fecal pellets: production, preservation and sedimentation. *J. Mar. Res.* V36, p. 45-57.
Studies of fecal pellets from laboratory cultures of common marine copepods.
543. Honjo, S. 1980. Material fluxes and modes of sedimentation in the mesopelagic and bathypelagic zones. *J. Mar. Res.* V38, p. 53-97.
Discussion of material fluxes and modes of sedimentation based on samples collected during sediment trapping experiments at deep ocean stations.

V. PAPERS DEALING WITH CONTROLS ON OCEAN CHEMISTRY (#544 to #547)

A. PAPERS CONCERNED WITH THERMODYNAMIC CONTROLS ON OCEAN CHEMISTRY (#544 to #546)

544. Holland, H.D. 1965. The history of ocean water and its effect on the chemistry of the atmosphere. *Proceedings of National Academy of Sciences*, V53, p. 1173-1182.
A general discussion of the factors controlling the chemistry of ocean water.
545. Sillen, L.G. 1966. Regulation of O₂, N₂ and CO₂ in the atmosphere: Thoughts of a laboratory chemist. *Tellus* V18, p. 198-206.
Chemical equilibria between constituents in the atmosphere and solid phases in the soils, sediments, and rocks as determinants of the O₂, N₂ and CO₂ pressures in the atmosphere.
546. Sillen, L.G. 1967. The ocean as a chemical system. *Science* V156, p. 1189-1197.
Suggestion that the ionic composition of sea water is controlled by chemical equilibria with minerals present in ocean sediments.

B. PAPER CONCERNED WITH KINETIC CONTROLS ON OCEAN CHEMISTRY (#547)

547. Broecker, W.S. 1971. A kinetic model for the chemical composition of sea water. *Quaternary Res.* V1, p. 188-207.
Arguments that the concentrations of many of the constituents in the sea (and in the atmosphere) are controlled by negative feedback loops that tend to drive the loss rate of a constituent toward balance with its rate of gain.

VI. PAPERS CONCERNED WITH MAN-MADE PERTURBATIONS IN THE EARTH'S CARBON CYCLE (#548 to #599)

A. PAPERS DEALING WITH THE PRODUCTION OF FOSSIL FUEL CO₂, ITS BUILD-UP IN THE ATMOSPHERE, AND ITS DISTRIBUTION WITHIN THE ATMOSPHERE (#548 to #562)

548. Callendar, G.S. 1938. The artificial production of carbon dioxide and its influence on temperature. Q.J. Roy. Meteorol. Soc. V64, p.223-240.
One of the early suggestions that the build-up of CO₂ from the burning of coal and oil would eventually lead to a warming of the planet.
549. Callendar, G.S. 1958. On the amount of carbon dioxide in the atmosphere. Tellus, V10, p.243-248.
Discussion of pre-industrial CO₂ concentration in the atmosphere.
550. Bray, J.R. 1959. An analyses of the possible recent change in atmospheric carbon dioxide concentration. Tellus V11, p. 220-230.
Discussion of changes in atmospheric CO₂ concentration during the recent past.
551. Keeling, C.D. 1960. The concentration and isotopic abundances of CO₂ in the atmosphere. Tellus, V12, p. 200-203.
Precise measurements of the CO₂ partial pressure in the atmosphere and of the ¹³C/¹²C ratio in this CO₂.
552. Bolin, B. and C.D. Keeling. 1963. Large scale atmospheric mixing as deduced from seasonal and meridional variations of carbon dioxide. J. Geophys. Res. V68, p. 3899-3920.
Interhemispheric mixing rates deduced from the distribution of excess CO₂ in the atmosphere (the fossil fuel CO₂ is largely produced in the northern hemisphere).
553. Bolin, B. and W. Bischof. 1970. Variations of the carbon dioxide content of the atmosphere in the northern hemisphere. Tellus, V22, p. 431-442.
Measurements of atmospheric CO₂ partial pressures.
554. Bischof, W. 1971. Carbon dioxide concentration in the upper troposphere and lower stratosphere II. Tellus, V23, p. 558-561.
Measurements of atmospheric CO₂ partial pressures.
555. Keeling, C.D. 1973. Industrial production of carbon dioxide from fossil fuel and limestone. Tellus V25, p. 174-198.
A gathering together of records of the amounts of coal, oil and natural gas burned each year and of the CO₂ derived therefrom. Also an assessment of the CO₂ released during the production of cement from limestone.
556. Keeling, C.D., R.B. Bacastow, A.E. Bainbridge, C.A. Ekdahl, Jr., P.R. Gunther, L.S. Waterman and J.F.S. Chin. 1976.

Atmospheric carbon dioxide variations at Mauna Loa Observatory, Hawaii. Tellus, V28, p. 538-551.

Presentations of the results of more than a decade of monitoring of the atmospheric CO₂ partial pressure in the northern hemisphere.

557. Keeling, C.D., J.A. Adams, Jr., C.A. Ekdahl, Jr., and P.R. Gunther. 1976. Atmospheric carbon dioxide variations at the South Pole. Tellus, V28, p. 552-564.
Presentation of the results of more than a decade of atmospheric CO₂ partial pressure monitoring in the southern hemisphere.
558. Machta, L., K. Hanson, and C.D. Keeling. 1977. Atmospheric carbon dioxide and some interpretations. In: The Fate of Fossil Fuel CO₂ in the Oceans, ed. by N.R. Andersen and A. Malahoff. Plenum Press, New York, p. 131-144.
Suggestion that the secular increase in atmospheric CO₂ is modulated by changes in sea surface temperature in the El Nino region off South America.
559. Rotty, R.M. 1977. Global carbon dioxide production from fossil fuels and cement A.D. 1950 - A.D. 2000, In: The Fate of Fossil Fuel CO₂ in the oceans. ed. by N.R. Andersen and A. Malahoff. Plenum Press, New York, p. 167-181.
An update of Keeling CO₂ production compilation to the year 1974 and some scenarios for the period 1974 to 2000.
560. Rotty, R.M. 1978. Atmospheric carbon dioxide: Possible consequences of future fossil fuel use. Resources and Energy (North-Holland Publishing Co.), Vol. 1, p. 231-249.
An estimate of the energy and CO₂ generated per unit weight of various fossil fuels burned.
561. Rotty, R.M. and G. Marland. 1980. Constraints on fossil fuel use. In: "Interactions of Energy and Climate," W. Bach, J. Pankrath, and J. Williams (eds.), D. Reidel Publishing Co., p. 191-212.
An estimate of the recoverable fossil fuel carbon reserves on earth is given.
562. Rotty, R.M. 1981. Distribution and changes in industrial carbon dioxide production. Abstracts, World Climate Program Conference on Analysis and Interpretation of Atmospheric CO₂ Data, Bern, Switzerland, p. 123-133.
A reduction in the estimates of industrial carbon dioxide production is given according to the revisions of the energy content of various coals by the United Nations.

B. PAPERS DEALING WITH CHANGES IN THE LIVING BIOMASS AND SOIL CARBON RESERVOIRS (#563 to #574)

563. Whittaker, R.H. and G.E. Likens. 1973. Carbon in the biota. In: Carbon and the Biosphere, ed. by G.M. Woodwell and E.V. Pecon, U.S. Atomic Energy Comm., p. 281-302.
Discussion of the net primary productivity of the world's biosphere and the size of the world's biomass.
564. Hall, C.A.S., A. Ekdaahl, and D.E. Wartenberg. 1975. A fifteen-year record of biotic metabolism in the Northern Hemisphere. *Nature*, V255, p. 136-138.
Analysis of the magnitude of the seasonal changes in the Mauna Loa record to ascertain whether any evidence can be found for a secular change in the productivity of the temperate northern hemisphere biomass.
Conclusion - none to be seen.
565. Whittaker, R. H. and G.E. Likens. 1975. The biosphere and man. In: Primary Production of the Biosphere, ed. by H. Lieth and R.H. Whittaker, Springer-Verlag, Heidelberg, p. 305-328.
Estimates of the net photosynthesis rate for various vegetation types and of the standing biomass of each type. Combined with areal coverage data these data yield an estimate of the total terrestrial primary production and for the total standing terrestrial biomass.
566. Lemon, E. 1977. The land's response to more carbon dioxide. In: The Fate of Fossil Fuel CO₂ in the Oceans, ed. by N.R. Andersen and A. Malahoff, Plenum Press, New York p. 97-130.
Discussion of the possible effects of higher atmospheric CO₂ contents on the rate of photosynthesis, crop yields, and the standing terrestrial biomass magnitude.
567. Schlesinger, W. H. 1977. Carbon balance in terrestrial detritus. *Annu. Rev. Ecol. Syst.* V8, p. 51-81.
Discussion of the factors influencing the amounts of carbon stored in soils.
568. Bolin, B. 1977. Changes of land biota and their importance for the carbon cycle. *Science*, V196, p. 613-615.
An attempt to assess the magnitude of the change in living biomass caused by current forestry practices in both developed and developing countries.
569. Stuiver, M. 1978. Atmospheric carbon dioxide and carbon reservoir changes. *Science* V199, p. 253-258.
Discussion based on tree ring ¹³C data of the reduction in terrestrial carbon reservoirs since 1850 and its effect on the atmospheric carbon dioxide concentration.
570. Woodwell, G.M., R.H. Whittaker, W.A. Reiners, G.E. Likens, C.C. Delwiche, and D.B. Botkin. 1978. The biota and the world carbon budget. *Science*, V199, p. 141-146.
An estimate of the magnitude of the CO₂ production

through biomass changes related to man's activities.

571. Seiler, W. and P.J. Crutzen. 1980. Estimates of gross and net fluxes of carbon between the biosphere and the atmosphere from biomass burning. *Climatic Change* V2, p. 207-247.
An estimate of the contribution of biomass change to the build-up of CO₂ in the air. The role of charcoal production by forest fires is emphasized.
572. Schlesinger, W. 1982. The world carbon pool in soil organic matter: A source of atmospheric CO₂? In: *The Role of Terrestrial Vegetation in the Global Carbon Cycle: Measurements by remote sensing.* ed. by G.M. Woodwell, John Wiley & Sons, New York.
An assessment of the changes in the soil carbon reservoir and the resulting contribution to the changing atmospheric CO₂ content.
573. Miller, P.C. 1981. Carbon balance in northern ecosystems and the potential effect of carbon dioxide induced climatic change. *Carbon Dioxide Effects Research and Assessment Program, U.S. Department of Energy*, p. 1-109.
An assessment of the likely changes to be expected in the northern ecosystems.
574. Freyer, H.D., and N. Belacy. 1981. ¹³C/¹²C record in northern hemispheric trees during the past half millennium - anthropogenic impact and climate superpositions. *Abstracts World Climate Program Conference on Analysis and Interpretation of Atmospheric CO₂ Data*, Bern, Switzerland, p. 209-215.
Measurements of ¹³C/¹²C in free standing trees and discussions of contributions of fossil fuel input into atmosphere and of climatic changes to the observed changes.

C. PAPERS DEALING WITH THE UPTAKE OF ANTHROPOGENIC CO₂ BY THE SEA (#575 to #597)

575. Revelle, R. and H.E. Suess. 1957. Carbon dioxide exchange between atmosphere and ocean and the question of an increase of atmospheric CO₂ during past decades. *Tellus*, V9, p. 18-27.
First paper dealing with the uptake of fossil fuel CO₂ by the sea. A one-box ocean model is employed.
576. Bolin, B. and E. Eriksson. 1959. Changes in the carbon dioxide content of the atmosphere and sea due to fossil fuel combustion. In: *The Atmosphere and the Sea in Motion*, Rossby Memorial Volume, ed. by B. Bolin, Rockefeller Inst., New York, p. 130-142.
Use of the two box ocean model to estimate the amount of fossil fuel CO₂ taken up by the sea.
577. Eriksson, E. 1963. Possible fluctuations in atmospheric CO₂ due to changes in the properties of the sea. *J. Geophys. Res.*

V68, p. 3871-3876.

Discussion of the possible effect of variations in sea water properties on the atmospheric CO₂ concentration.

578. Broecker, W.S., Y.-H. Li and T.-H. Peng, 1971. Carbon dioxide - man's unseen artifact. In: Impingement of Man in the Oceans, ed. by D.W. Hood, Wiley - Interscience, New York, p. 287-324.
A consideration of the reliability of two-box models in estimating the amount of CO₂ taken up by the ocean.
579. Machta, L. 1972. The role of the oceans and the biosphere in the CO₂ cycle. In: The Changing Chemistry of the Oceans. Nobel Symposium 20, ed. by D. Dryssen and D. Jagner, Almquist and Wiksell, Stockholm, p. 121-145.
The possible causes of seasonal variations in atmospheric CO₂ concentration is discussed. The conclusion is that they are mainly caused by the seasonal variation of biospheric uptake and release of CO₂ to the atmosphere. The role of ocean is considered to be less important in this regard.
580. Machta, L. 1973. Prediction of CO₂ in the atmosphere. In: Carbon and the Biosphere, ed. by G.M. Woodwell and L.V. Pecon. U.S. Atomic Energy Comm., Washington, D.C., p. 51-85.
Model predictions of future and past carbon dioxide concentration in the atmosphere.
581. Ekdahl, C.A. and C.D. Keeling. 1973. Atmospheric carbon dioxide and radiocarbon in the natural carbon cycle: I. Quantitative deduction from records at Mauna Loa Observatory and at the South Pole. In: Carbon and the biosphere, ed. by G.M. Woodwell and E.V. Pecon. U.S. Atomic Energy Comm., p. 51-85.
Discussion of airborne fraction of anthropogenic carbon dioxide. Geochemical models are used to interpret this atmospheric CO₂ data.
582. Bacastow, R.B. and C.D. Keeling. 1973. Atmospheric carbon dioxide radiocarbon in the natural carbon cycle: II. Changes from A.D. 1700 to 2070 as deduced from a geochemical model. In: Carbon and the Biosphere, ed. by G.M. Woodwell and L.V. Pecon, U.S. Atomic Energy Comm., Washington, D.C., p. 86-135.
Prediction of future changes in atmospheric CO₂ concentration using a nonlinear geochemical model of the interaction of atmospheric CO₂ with the oceans and land biota.
583. Keeling, C.D. 1973. The carbon dioxide cycle: reservoir models to depict the exchange of atmospheric carbon dioxide with the oceans and land plants. In: Chemistry of the Lower Atmosphere, ed. by S.I. Rasool, p. 251-329.
A general discussion of reservoir models for the CO₂ cycle.

584. Oeschger, H., U. Siegenthaler, U. Schotterer and A. Gugelmann. 1975. A box diffusion model to study the carbon dioxide exchange in nature. *Tellus*, V27, p. 168-192.
 The first paper on the one-dimensional diffusional model. As this model constitutes a considerable improvement over the two-box ocean model for problems involving transients it has been widely adopted for estimations of the uptake of fossil fuel CO₂ by the sea.
585. Bacastow, R.B. 1976. Modulation of atmospheric carbon dioxide by the southern oscillation. *Nature*, V261, p. 116-118.
 Demonstration that the secular increase in the CO₂ content of the atmosphere is modulated by some phenomena associated with the two-year periodicity southern oscillation.
586. Bacastow, R.B. 1977. Influence of the southern oscillation on atmospheric carbon dioxide. In: *The Fate of Fossil Fuel CO₂ in the Oceans*, ed. by N.R. Andersen and A. Malahoff, Plenum Press, New York, p. 33-43.
 More on the correlation between anomalies in the shape of the secular increase in atmospheric CO₂ content and the southern oscillation.
587. Newell, R.E. and B.C. Weare. 1977. A relation between atmospheric carbon dioxide and Pacific sea surface temperature. *Geophys. Res. Lett.* V4, p. 1-2.
 Demonstration that the secular increase in atmospheric CO₂ content is modulated by some process associated with changes in the Pacific Ocean sea surface temperature.
588. Keeling, C.D. and R.B. Bacastow. 1977. Impact of industrial gases on climate. In: *Energy and Climate*. National Academy of Sciences, Washington, D.C., p. 72-95.
 A review of predictions of future atmospheric CO₂ content rises associated with the burning of fossil fuels.
589. Zimen, K.E., P.Offermann and G. Hartmann. 1977. Source functions of CO₂ and future CO₂ burden in the atmosphere. *Z. Naturforsch.*, V32a, p. 1544-1554.
 Discussion of various source functions for CO₂ and prediction of future CO₂ concentration.
590. Bolin, B. 1977. Modeling the oceans and ocean sediments and their response to fossil fuel carbon dioxide emissions. In: *The Fate of Fossil Fuel CO₂ in the Oceans*. N.R. Andersen and A. Malahoff, (Eds.), Plenum Press, New York, p. 81-95.
 Toward a more detailed ocean model for the uptake of fossil fuel CO₂.
591. Siegenthaler, U. and H. Oeschger. 1978. Predicting future atmospheric carbon dioxide levels. *Science*, V199, p. 388-395.
 Use of the one-dimensional diffusion model to predict

future atmospheric CO₂ contents for various energy scenarios. Also the problem is inverted to show what energy scenario would be required to yield a given atmospheric CO₂ content trend.

592. Bacastow, R.B. 1979. Dip in the atmospheric CO₂ level during the mid-1960's. *J. Geophys. Res.* V84, p. 3108-3114.
Demonstration that the dip in the rise of atmospheric CO₂ during the mid-1960's can be explained by a cooling of the ocean surface during this period. The one-dimensional diffusion model is used to quantify this explanation.
593. Bacastow, R.B. and C.D. Keeling. 1978. Models to predict future atmospheric CO₂ concentrations, In: *Workshop on the Global Carbon Dioxide from Fossil Fuels*, W.P. Elliott, & L. Machta (Eds.), U.S. Dept. of Energy, CONF-770385, Washington, D.C. p. 72-90.
Prediction of future CO₂ concentrations.
594. Broecker, W.S., T. Takahashi, H.J. Simpson and T.-H. Peng. 1979. Fate of fossil fuel carbon dioxide and the global carbon budget. *Science*, V206, p. 409-418.
A review of our knowledge of ocean uptake of fossil fuel CO₂. The conclusion is that no more than 50% of the CO₂ produced to date can have taken up residence in the ocean and therefore that the forests and soil reservoirs have not been changing significantly over the last 20 years.
595. Broecker, W.S., T.-H. Peng and R. Engh. 1980. Modeling the carbon system. *Radiocarbon*, V22, p. 565-598.
Use of a regional one-dimensional advection-diffusion model calibrated using the distributions of bomb radiocarbon and tritium to estimate the uptake of fossil fuel CO₂ by the oceans.
596. Killough, G. G. and W.R. Emanuel. 1981. A comparison of several ocean models of carbon turnover in the ocean with respect to their distributions of transit time and age, and responses to atmospheric CO₂ and ¹⁴C. *Tellus*, V33, p. 274-290.
Five ocean models are compared with respect to carbon transit-time distribution, age distribution, and integrated responses to histories of fossil CO₂ and bomb ¹⁴C injection.
597. Bolin, B. 1981. *Carbon Cycle Modeling*, J. Wiley, N.Y. (SCOPE 16).
A summary of contributions to the SCOPE workshop on global carbon cycle modelling. For model calibration, a list of various carbon and carbon isotope data is given.

D. PAPERS DEALING WITH THE REACTION BETWEEN ANTHROPOGENIC CO₂
AND THE CaCO₃ IN MARINE SEDIMENTS (#598 to #599)

598. Broecker, W.S. and T. Takahashi. 1977. Neutralization of fossil fuel CO₂ by marine calcium carbonate. In: The Fate of Fossil Fuel CO₂ in the Oceans, N.R. Anderson and A. Malahoff, (Eds.), Plenum Press, New York, p. 213-241.
An attempt to estimate the amount of CaCO₃ available for dissolution by fossil fuel CO₂ and the pattern and rate of the attack of this CaCO₃ by man-made CO₂.
599. Peng, T.-H. and W.S. Broecker. 1978. Effect of sediment mixing on the rate of calcite dissolution by fossil fuel CO₂. Geophys. Res. Lett. V5, p. 349-352.
Calculations showing that the rate of bioturbation in deep sea sediments should be sufficiently rapid to prevent the build-up of an insoluble residue at the top of the bioturbated layer during the course of the attack of deep sea sediment CaCO₃ by fossil fuel CO₂.

VII. PAPERS DEALING WITH THE GLACIAL TO INTERGLACIAL CHANGE IN VARIOUS OCEAN PROPERTIES (#600 to #624)

A. PAPERS DEALING WITH THE RECONSTRUCTION OF SEA SURFACE TEMPERATURE (#600 to #610)

600. Imbrie, J. and N.G. Kipp. 1971. A new micropaleontological method for paleoclimatology: application to a Late Pleistocene Caribbean core. In: The Late Cenozoic Glacial Ages, K.K. Turekian, (Ed.), Yale University, New Haven, p. 71-181.
The first application of multivariant statistical analysis to the problem of obtaining the temperature signal from the data on the relative abundance of various species of planktonic foraminifera in marine sediments. A classic!
601. Hecht, A.D. 1973. A model for determining Pleistocene paleotemperatures from planktonic foraminiferal assemblages. Micropaleontology, V19, p. 69-77.
An alternate statistical model for deriving temperature data from the relative abundance data for planktonic foraminifera species in deep sea core material.
602. Shackleton, N.J. and N.D. Opdyke. 1973. Oxygen isotope and paleomagnetic stratigraphy of equatorial Pacific core V28-238: oxygen isotope temperatures and ice volumes on a 10⁵-year time scale. Quat. Res., V3, p. 39-55.
The first detailed benthic oxygen isotope record from a deep sea core.
603. Kipp, N.G. 1976. New transfer function for estimating past sea surface conditions from sea-bed distribution of planktonic foraminiferal assemblages in the north Atlantic. Geol. Soc. Amer. Memoir, V145, p. 3-41.

Expansion of the data base on which the multivariate analysis transfer function is based.

604. CLIMAP. 1976. The surface of the ice-age earth. *Science*, V191, p. 1131-1137.
The first global map of sea-surface temperatures obtained using the Imbrie multivariate analysis procedure. The big surprise is the small magnitude ($\sim 2.5^\circ\text{C}$) of the average difference from present conditions.
605. Moore, T.C., Jr., L.H. Burckle, K. Geitzenauer, B. Luz, A. Molina-Cruz, J.H. Robertson, H. Sachs, C. Sancetta, J. Thiede, P. Thompson and C. Wenham. 1980. The reconstruction of sea surface temperatures in the Pacific Ocean of 18,000 B.P. *Marine Micro.*, V5, p. 215-247.
Documentation of the reconstruction of sea-surface temperatures by the multivariate analysis procedure in the Pacific Ocean.
606. Hutson, W.H. and W.L. Press. 1980. A paleoecological transfer function, FI-2, for Indian Ocean planktonic foraminifera. *J. Paleontol.*, V54(2), p. 381-399.
A multivariate analysis transfer function for the calculation of sea-surface temperatures in the Indian Ocean.
607. Moore, T.C., Jr., L.H. Burckle, K. Geitzenauer, B. Luz, A. Molina-Cruz, J.H. Robertson, H. Sachs, C. Sancetta, J. Thiede, P. Thompson and C. Wenham. 1980. The reconstruction of sea surface temperatures in the Pacific Ocean of 18,000 B.P. *Marine Micro.*, V5, p. 215-247.
More on sea-surface temperature reconstructions by multivariate analyses.
608. Prell, W.L., W.H. Hutson, D.F. Williams, A.W.H. Be, K. Geitzenauer, and B. Molfino. 1980. Surface circulation of the Indian Ocean during the last glacial maximum, approximately 18,000 yr B.P. *Quat. Res.*, V14, p. 309-336.
More on surface temperature reconstruction by the multivariate analysis procedure.
609. Moore, T.C., Jr., W.H. Hutson, N.G. Kipp, J.D. Hays, W.L. Prell, P. Thompson and G. Boden. 1981. The biological record of the ice-age ocean. *Paleogeography, Paleoceanography, Palaeoecology*, V35, p. 357-370.
Distribution of faunal provinces (polar, subpolar, transitional, subtropical and eastern and western tropical) in the world ocean at present and during the peak of the last ice age.
610. CLIMAP Project Members, A. McIntyre, Leader LGM Project. 1981. Seasonal reconstructions of the earth's surface at the last glacial maximum. *Geol. Soc. Amer.*, Map and Chart Series, No. 36.

Final synthesis of the effort to reconstruct of glacial sea-surface temperature. New global temperature maps are presented. The average temperature difference between full glacial time and today turns out to be only 1.5°C!

B. PAPERS DEALING WITH THE RECONSTRUCTION OF ICE VOLUME AND HENCE OCEAN SALINITY (#611 to #617)

611. Broecker, W.S. and J. van Donk. 1970. Insolation changes, ice volumes and the ^{18}O record in deep-sea cores. Rev. Geophys. Space Phys., V8, p. 169-198.
Discussion of the relationship between the timing of climatic changes and the changes in the seasonal distribution of insolation caused by periodicities in the earth's orbital parameters.
612. Bloom, A.L., W.S. Broecker, J.M.A. Chappell, R.K. Matthews and K.J. Mesolella. 1974. Quaternary sea level fluctuations on a tectonic coast: new $^{230}\text{Th}/^{234}\text{U}$ data from the Heron Peninsula, New Guinea. Quat. Res., V4, p. 185.
Estimates of the position of sea level at five times in the past ($\sim 102,000$, $\sim 82,000$, $\sim 62,000$, $\sim 40,000$ and $\sim 28,000$ years ago) based on ^{230}Th dating of an uplifted coral reef sequence on New Guinea.
613. Shackleton, N. 1977. The oxygen isotope stratigraphic record of the Late Pleistocene. Phil. Trans. R. Soc. Lond. B, V280, p. 169-182.
Estimation of the ice volume change from the magnitude of the $^{18}\text{O}/^{16}\text{O}$ change in benthic foraminifera. The sea level lowering at the last glacial maximum obtained in this way is greater than 150 meters.
614. Fairbanks, R.G. and R.K. Matthews. 1978. The marine oxygen isotope record in Pleistocene coral, Barbados, West Indies. Quat. Res., V10, p. 181-196.
An attempt to estimate the magnitude of sea-level lowering from information obtained from borings into the coral reef sequence on the island of Barbados. The amount of sea-level lowering during full glacial time obtained in this way is at least 100 meters.
615. Peltier, W.R. and J.J. Andrews. 1976. Glacio-Isostatic adjustment I: The forward problem. Geophys. J.R. Astr. Soc. V46, p.605-646.
An attempt to explain the details of the global response of sea level to the melting of the ice sheets of the last glacial period using a global response model. One conclusion from this effort is that the lowering of sea level in full glacial times must have been about 75 meters.
616. Broecker, W.S. 1978. The cause of glacial to interglacial

climatic change. In: "Evolution of Planetary Atmosphere and Climatology of the Earth". Centre National d'Etudes Spatiales (France), p. 165-177.

Demonstration that the relationship between sea level and the $^{18}\text{O}/^{16}\text{O}$ record in benthic forams calibrated by taking the sea levels and $^{18}\text{O}/^{16}\text{O}$ ratios for the six times for which sea levels were established from the New Guinea record leads to a sea level estimate of only -65 meters for the last glacial maximum.

617. Denton, G.H. and T.J. Hughes. 1980. The last great ice sheet. J. Wiley and Sons, Inc., New York.

A synthesis of the information on the position of the ice margins during the peak of the last glacial period and a flow model which yields an estimate of the volume of the ice sheets lying within these boundaries. These volumes yield a sea level lowering of about 160 meters at peak glacial time.

C. PAPERS DEALING WITH CHEMICAL CHANGES IN THE OCEAN AND ATMOSPHERE (#618 to #624)

618. Duplessy, J.C., L. Chenguard, F. Vila. 1975. Weyl's theory of glaciation supported by isotopic study of Norwegian core K11. Science, V188, p. 1208-1209.

^{18}O data for cores from the Norwegian Sea showing that during the last glacial period this basin received its bottom water from the open Atlantic (today it supplies bottom water to the north Atlantic).

619. Streeter, S.S. and N.J. Shackleton. 1979. Paleocirculation of the deep North Atlantic: A 150,000-year record of benthic foraminifera and ^{18}O . Science, V203, p. 168-171.

A method for determining the sense of the glacial to interglacial change in the dissolved oxygen content of deep sea water based on relative abundances of key benthic forams. Also, the demonstration using this method that the O_2 content of deep Atlantic water was lower during glacial time than it is today.

620. Berner, W., B. Stauffer and H. Oeschger. 1979. Past atmospheric composition and climate, gas parameters measured on ice cores. Nature, V275, p. 53-55.

Reconstruction of atmospheric CO_2 content from the CO_2 to air ratio in air bubbles trapped in glacial ice. Results from Greenland and Antarctica suggest that the CO_2 pressure was about 30% lower during glacial time than during Holocene time.

621. Delmas, R.J., J-M. Ascencio and M. Legrand. 1980. Polar ice evidence that atmospheric CO_2 29,000 yr BP was 50% of the present. Nature, V284, p. 155-157.

A separate study of the CO_2 to air ratio in glacial ice leading to the same conclusion. The CO_2 content of the atmosphere was lower during glacial time.

622. Neftel, A., H. Oeschger, J. Swander, B. Stauffer and R. Zumbrunn. 1982. Ice core sample measurements give atmospheric CO₂ content during the past 40,000 years. *Nature* V295, p. 220-223.
Measurements of CO₂ to air ratio made by crushing one cubic centimeter ice samples in a vacuum. The CO₂ released is detected by a very sensitive laser technique. Records for both Antarctica and Greenland are given. Again 30% lower glacial values are found.
623. Broecker, W.S. 1981. Glacial to interglacial changes in ocean and atmosphere chemistry. In: *Climatic variations and variability: Facts and Theories*, A. Berger, editor, D. Reidel Publishing Co., p. 109-120.
A demonstration that the atmospheric CO₂ partial pressure changes recorded in polar glaciers were very likely caused by changes in the ratio of PO₄ to ΣCO₂ in the ocean.
624. Berner, W., H. Oeschger and B. Stauffer. 1980. Information on the CO₂ cycle from ice core studies. *Radiocarbon* V22, p.227-235.
Measurements of CO₂ content in ice cores from Camp Century (Greenland) and Byrd Station (Antarctica).
- 624a.Broecker, W.S. 1982. Glacial to interglacial changes in ocean chemistry. *Progress in Oceanography*, V11, 151-197.
Data from marine sediments supporting the lower CO₂ contents found for glacial time from ice core studies. Also models showing that this change was due to variations in either the PO₄/ΣCO₂ ratio in deep sea water or to variations in the P/C ratio in organic residues.

VII. PAPERS DEALING WITH RATES OF INPUT, RATES OF LOSS, AND RESIDENCE TIMES OF VARIOUS CONSTITUENTS IN THE SEA (#625 to #670)

A. PAPERS DEALING WITH RIVER INPUTS TO THE SEA (#625 to #633)

625. Clarke, F.W. 1924. *The Data of Geochemistry*. 5th edition. U.S. Geological Survey Bulletin, V770, p. 1-841.
Contains a compilation of chemical analyses on rivers.
626. Livingstone, D.A. 1963. Chemical composition of rivers and lakes. In: *The Data of Geochemistry*, 6th ed., M. Fleischer, (Ed.), U.S. Geological Survey Professional Paper 440, p. 1-64.
Compilation of representative chemical data for the lake and river waters of the world.
627. MacKenzie, F.T. and R.M. Garrels. 1966. Chemical mass balance between rivers and oceans. *Am. J. Sci.*, V264, p. 507-525.

Discussion of removal processes for the excess dissolved constituents in the ocean required in order to maintain the constancy of the chemical composition of ocean water.

628. Turekian, K. K. 1969. The oceans, streams and atmosphere. In: Handbook of Geochemistry VI, K.H. Wedepohl, (Ed.), Springer-Verlag, Heidelberg, p. 297-323.
Residence time estimates for many of the constituents of sea salt.
629. Garrels, R.M. and F.T. Mackenzie. 1971. Evolution of Sedimentary Rocks, W.W. Norton, New York.
A treatment of the current rates of chemical and mechanical erosion, the sediment formed by these products and the preservation of sediments formed in previous geologic epochs.
630. Holland, H.D. 1978. The Chemistry of the Atmosphere and Oceans, Wiley-Interscience, New York.
This book describes the processes which control the composition of the atmosphere and oceans, and explores the functional relationships that determine the transfer rates of the elements between the atmosphere, the biosphere, the oceans, the crust and mantle.
631. Martin, J.-M. and M. Meybeck. 1979. Elemental mass-balance of material carried by major world rivers. Mar. Chem., V7, p. 173-206.
A discussion and listing of the estimates of average river particulate and dissolved matter composition.
632. Boyle, E.A., S.S. Huested, B. Grant and J.M. Edmond, (in press). The chemical mass balance of the Amazon plume II: copper, nickel and cadmium. J. Geophys. Res., V86, p. 8048-8066.
Estimates of the average Cu, Ni, and Cd concentrations in Amazon River water.
- 632a. DeMaster, D.J. 1981. The supply and accumulation of silica in the marine environment. Geochim. et Cosmochim. Acta, V45, p. 1715-1732.
An account of the inputs and losses of silica to the sea concluding that 6×10^{14} gm SiO₂/yr enter and leave the sea. This corresponds to a residence time of about 20,000 years.
633. Martin, J.-M. and M. Whitfield, (in press). The significance of the river input of chemical elements to the ocean. Proceedings of NATO Advanced Research Institute on "Trace metals in sea water", ed. by C.S. Wong, E.A. Boyle, K.W. Bruland, J.D. Buron and E.D. Goldberg, Plenum Press, New York.
A discussion of the chemical composition of dissolved and particulate matter carried by rivers and of the quantity and composition of material discharged to the ocean system.

B. PAPERS DEALING WITH THE REMOVAL RATES OF CONSTITUENTS TO DEEP SEA SEDIMENTS (#634 to #635)

634. Froelich, P.N., M.L. Bender, N.A. Luedtke, G.R. Heath, T. DeVries. 1982. The marine phosphorus cycle. Amer. J. Sci. V282, p. 474-511.
A review of the residence time of phosphorus in the sea based on river data and a new estimate based on the rate of accumulation of phosphorus in marine sediments.
635. Santschi, P.H., D. Adler and M. Amdurer. (in press). The fate of particles and particle-reactive trace metals in coastal waters: radioisotope studies in microcosms. Proceedings of the NATO Advanced Research Institute on Trace Metals in Sea Water. C.S. Wong, E.A. Boyle and K.W. Bruland, J.D. Burton and E.D. Goldberg (Eds.), Plenum Press, N.Y.
A discussion of the transport of suspended particles and particle-reactive trace metals from coastal waters to sediments. The study was carried out in large controlled ecosystem tanks (MERL) designed to simulate Narragansett Bay. Radio-tracer techniques were employed.

C. PAPERS DEALING WITH INTERACTIONS BETWEEN SEA WATER AND RIDGE CREST BASALTS (#636 to #643)

636. Bostrom, K. and M.N.A. Peterson. 1966. Precipitates from hydrothermal exhalations on the East Pacific Rise. Econ. Geol., V61, p. 1258 - 1265.
First demonstration of the role of ridge crest hydrothermal activity in the generation of metaliferous sediments.
637. Bischoff, J.L. and F.W. Dickson. 1975. Seawater-basalt interactions at 200°C and 500 bars: implications for origin of sea-floor heavy-metal deposits and regulation of sea water Chemistry. Earth & Planet. Sci. Lett. V25, p. 385-387.
Laboratory measurements showing the kind of chemical reactions to be expected if sea water were circulated through basalt at high temperatures.
638. Wolery, T.J. and H. Sleep. 1976. Hydrothermal circulation and geochemical flux at mid-ocean ridges. J. Geol. V84, p. 249-276.
An estimate of the total amount of water recirculated through the ridge crests.
639. Bischoff, J.L. and W.E. Seyfried. 1978. Hydrothermal chemistry of sea water from 25°C to 350°C. Amer. Jour. Sci. V278, p. 838-860.
Further laboratory studies of the interaction between hot sea water and basalt.
640. Mottl, M.J. and H.D. Holland. 1978. Chemical exchange during

hydrothermal alteration of basalt by sea water I. Experimental results for major and minor components of sea water. *Geochim. Cosmochim. Acta*, V42, p. 1103-1115.

Independent study of the interaction of hot sea water with basalt.

641. Edmond, J.M., J.B. Corliss and L.I. Gordon. 1979. Ridge crest-hydrothermal metamorphism at the Galapagos spreading center and reverse weathering. In: Ewing Symposium, ed. by M. Talwani, V2, p. 383.
Discussion of chemical measurements made on hot waters coming from ridge crest hydrothermal vents.
642. Edmond, J.M., C. Measures, R.E. McDuff, L.H. Chan, R. Collier, B. Grant, L.I. Gordon and J.B. Corliss. 1979. Ridge Crest hydrothermal activity and the balances of the major and minor elements in the ocean: the Galapagos data. *Earth & Planet. Sci. Lett.* V46, p. 1-18.
Estimates of the contribution of sea water-basalt interactions at ridge crests to the oceanic budgets of various elements.
643. Mottl, M.J. and H.D. Holland. 1979. Chemical exchange during hydrothermal alteration of basalt by seawater II. Experimental results for Fe, Mn and sulphur species. *Geochim. Cosmochim. Acta*, V43, p. 869-884.
Further laboratory measurements with regard to sea water-basalt chemical interactions.

D. PAPERS DEALING WITH THE CHEMISTRY OF ATMOSPHERIC AEROSOLS AND DUST (#644 to #652)

644. Herron, M.M., C.C. Langway, H.V. Weiss and J.H. Cragin. 1977. Atmospheric trace metals and sulfate in the Greenland ice sheet. *Geochim. Cosmochim. Acta*, V41, p. 915-920.
Measurements of Zn, pb, Cd, V and sulfates in the Greenland Ice sheet.
645. Weiss, H.V., M.M. Herron and C.C. Langway. 1978. Natural enrichment of elements in snow. *Nature*, V274, p. 352-353.
Demonstrates the enrichment of certain elements in snow and discussion of the possible causes for this enrichment.
646. Buat-Menard, P. 1979. Influence de la retombee atmospherique sur la chimie des metals en trace dans la matiere en suspension de l'Atlantic nord. Ph.D. thesis, University of Paris, 434pp.
Measurements of the concentration of trace metals in particulate matter from the marine atmosphere and in the deep ocean waters.
647. Buat-Menard, D. and R. Chesselet. 1979. Variable influence of the atmospheric flux on the trace metal chemistry of

oceanic suspended matter. Earth Planet. Sci. Lett., V42, p. 399-411.

Measurements of the concentration of trace metals in particulate matter from the marine atmosphere and in the deep ocean waters.

648. Boutron, C. 1979. Trace element content of Greenland snows along an eastwest transect. Geochim. Cosmochim. Acta, V43, p. 1253-1258.

Measurements of trace element content in Greenland snows showing that certain elements are carried through the atmosphere in anomalous amounts.

649. Boutron, C. and C. Lorius. 1979. Trace metals in Antarctic snows since 1914. Nature, V277. p. 551-554.

Discussion of the concentration of various trace metals in east Antarctic snow.

650. Delmas R. and C. Boutron. 1980. Are the past variations of the stratospheric sulfur burden recorded in central Antarctic snow and ice layers? J. Geophys. Res., V85, p. 5645-5649.

Discussion of sulfate variations in central Antarctic snow and ice layers. Global sulfur pollution does not seem to be recorded in these samples.

651. Boutron, C. 1980. Respective influence of global pollution and volcanic eruptions on the past variations of the trace metals content of Antarctic snows since 1880's. J. Geophys. Res., V95, p. 7426-7432.

Measurements of a time sequence for trace metal concentrations in snow samples from central east Antarctica from 1890 to present.

652. Li, Y.-H. 1981. Geochemical cycle of elements and human perturbation. Geochim. et Cosmochim. Acta. V45, p. 2037-2084.

A discussion of the pollution inputs of various elements and their geochemical cycle in the ocean.

E. PAPERS DEALING WITH GAS SOLUBILITY IN SEA WATER (#653 to #660)

653. Weiss, R.F. 1970. The solubility of nitrogen, oxygen and argon in water and seawater. Deep Sea Res., V17, p. 721-735.

Equations are given for calculating the solubility of N₂, O₂, and Ar in sea water as a function of temperature and salinity.

654. Weiss, R.F. 1971. The effect of salinity on the solubility of argon in seawater. Deep Sea Res. V18, pp. 225-230.

Special attention is given to the salt effect on the solubility of Ar.

655. Weiss, R.F. 1971. Solubility of Helium and Neon in water and seawater. *J. Chemical & Engineering Data*, V16, No. 2, p. 235-241.
Equations are given to calculate the solubility of He and Ne in sea water as a function of temperature and salinity.
656. Weiss, R.F. 1974. Carbon dioxide in water and sea water: The solubility of a non-ideal gas. *Marine Chem.*, V2, p. 203-215.
An equation is given to calculate CO₂ solubility in sea water as a function of temperature and salinity.
657. Kester, Dana, R. 1975. Dissolved gases other than CO₂. In: *Chemical Oceanography*, V1, edited by J.P. Riley and G. Skirrow Academic Press, pp. 497-557.
A summary of solubility of gases in sea water, mostly based on R.F. Weiss equations.
658. Weiss, R.F. and T.K. Kyser. 1978. Solubility of krypton in water and seawater. *J. Chem. Engineering Data*, V23, p. 69-72.
An equation is given to calculate the solubility of Kr in sea water as a function of temperature and salinity.
659. Weiss, R.F. and B.A. Price. 1980. Nitrous oxide solubility in water and sea water. *Marine Chemistry*, V8, p. 347-359.
An equation is given for calculating the solubility of N₂O in sea water as a function of temperature and salinity.
660. CRC Handbook of Chemistry and Physics, edited by R.C. Weast, CRC press, 1980.
Solubility of Xe and Rn in pure water is given.

F. PAPERS DEALING WITH MOLECULAR DIFFUSIVITY OF GASES IN SEA WATER (#661 to #666)

661. Rona, E. 1917. Diffusionsgrosse und Atomdurchmesser der Radiumemanation. *Zeitschrift fur physikalische chemie, stochiometrie und verwandtschaftslehre*, V92, p. 213-218.
The first measurement of radon molecular diffusivity in water at 18°C.
662. Himmelblau, D.M. 1964. Diffusion of dissolved gases in liquids. *Chem. Review*, V64, p. 527-550.
A review paper on the diffusivities of gases in water.
The equation for the dependence of diffusion coefficients on temperature is given.
663. Thomas, W.J. and M.J. Adams. 1965. Measurement of the diffusion coefficients of carbon dioxide and nitrous oxide in water and aqueous solutions of glycerol. *Trans. Faraday Soc.*, V61, p. 668-673.
Measurements of the diffusivity of CO₂ and N₂O in water.

- 663a. Wise, D.L. and G. Houghton. 1968. Diffusion coefficients of neon, krypton, xenon, carbon monoxide and nitric oxide in water at 10-60°C. *Chem. Engr. Sci.*, V23, p. 1211-1216.
Measurements of the diffusion coefficients of Ne, Kr, Xe, CO and NO in water.
664. Boerboom, A.J.H. and G. Kleyn. 1969. Diffusion coefficients of noble gases in water, *J. Chemical Physics*, V50, pp. 1086-1087.
Diffusion coefficients of all noble gases (except radon) in water are measured using the same technique. The absolute values fall on the low side of previously published data. However, the ratio of diffusivities between gases should be O.K.
665. Hayduk, W. and H. Laudie. 1974. Prediction of diffusion coefficients for nonelectrolytes in dilute aqueous solutions, *AICHE Journal*, V20, pp. 611-615.
A summary of available diffusion coefficients of gases in water.
666. Muller, W. 1978. Die diffusions-, loslichkeit- und permeabilitats- koeffizienten von radon-222 in Handelsüblichen Kundststoffen, Master thesis, Institut fur Umweltphysik, Heidelberg.
A series of experiments designed to measure the diffusion coefficients of radon in various mediums.

G. PAPERS DEALING WITH THE EVOLUTION OF OCEAN CHEMISTRY (#667 to #670)

667. Conway, E.J. 1942. Mean geochemical data in relation to oceanic evolution. *Proc. Roy. Irish Acad.* V B48, p. 119-159.
Discussion of the factors controlling the chemical composition of river waters and the influence of sea salt aerosols on same.
668. Conway, E.J. 1943. The chemical evolution of the ocean. *Proc. Roy. Irish Acad.* V B48, p. 161-212.
An analysis of the manner in which the chemical composition of sea water might have evolved. A thought-filled treatment done with considerable style.
669. Rubey, W.W. 1951. Geologic history of sea water. *Bull. Geol. Soc. Amer.*, V62, p. 1111-1147.
A classic paper on the history of the outgassing of the volatiles, H_2O , HCl , H_2SO_4 and CO_2 from the earth.
670. Li, Y.-H. 1972. Geochemical mass balance among lithosphere, hydrosphere and atmosphere. *Amer. J. Sci.* V272, p. 119.
Modeling the geochemical mass balance for the constituents of the lithosphere, hydrosphere, and atmosphere, using constraints from ^{18}O , ^{13}C and ^{34}S isotope data.

VIII. BOOKS ON RELATED SUBJECTS (#671 to #684)

671. Sverdrup, H.U., M.W. Johnson and R.H. Fleming. 1942. The Oceans, their physics, chemistry and biology. Prentice-Hall, Englewood Cliffs, N.J.
The classic treatise on the physics, chemistry and biology of the oceans. An excellent compilation of the data and ideas in this field up to World War II.
672. Libby, W.F. 1955. Radiocarbon dating, second edition, University of Chicago Press.
A book giving the principles of radiocarbon dating written by the inventor of this method. As it was written only five years after the discovery of ^{14}C in nature, it treats only the method and the very early work in this field.
673. Mero, J.L. 1964. The mineral resources in the sea. American Elsevier, New York.
A compilation of information regarding the distribution, textures and chemistry of manganese nodules.
674. Danckwerts, P.V. 1970. Gas-Liquid Reactions. McGraw-Hill, New York.
The ins and outs of the gas exchange process from the viewpoint of a chemical engineer.
675. Riley, J.P. and R. Chester. 1971. Introduction to Marine Chemistry. Academic Press, New York.
The nuts and bolts of sea water chemistry.
676. Garrels, R.M. and F.T. Mackenzie. 1971. Evolution of sedimentary rocks. W.W. Norton, New York.
A treatment of the current rates of chemical and mechanical erosion, the sediments formed by these products and the preservation of sediments formed in previous geologic epochs.
677. Goldberg, E.D. (editor) 1974. The Sea V5; John Wiley and Sons, New York.
A series of papers dealing with thermodynamics, gas exchange, sediments, life, the impact of man and the origins of the sea.
678. Broecker, W.S. 1974. Chemical Oceanography, Harcourt Brace Jovanovich, New York, 214 pp.
The predecessor to this book.
679. Riley, J.P. and G. Skirrow. 1975. Chemical Oceanography, V1, 2,3 & 4. Riley, J.P. and R. Chester. 1976., V5 & 6. 1978. V7. Academic Press, London.
A series of articles on subjects in chemical oceanography authored by experts.
- 679a. Walker, J.C.G. 1977. Evolution of the Atmosphere. MacMillan

Inc., New York.

Book discussing the evolution and present chemistry of the atmosphere.

680. Holland, H.D. 1978. The Chemistry of the Atmosphere and Oceans. Wiley-Interscience, New York.
A systematic treatment of material balances involved in setting the chemical composition of sea water and the atmosphere.
681. Imbrie J. and K.P. Imbrie. 1979. Ice Ages, Enslow Publishers, Short Hills, New Jersey.
An excellent introduction to glacial cycles and their causes.
682. Berner, A. 1980. Early diagenesis: a theoretical approach, Princeton University Press, Princeton, N.J.
A treatment of the chemical reactions and bioturbation in the upper part of the sediment column.
683. Schopf T.J.M. 1980. Paleoceanography. Harvard University Press, 341pp.
A somewhat disjointed summary of evidence regarding long-term changes in the operation of the ocean-atmosphere system.
- 683a. Pearman, G.I. 1980. Carbon dioxide and climate: Australian research. Australian Academy of Science, Canberra.
A summary of the carbon dioxide problem. Especially useful are the papers on CO₂ growth enhancement and on the factors influencing the ¹³C/¹²C ratio in plants.
684. Stumm, W. and J.J. Morgan. 1981. Aquatic Chemistry (second edition). Wiley-Interscience, New York.
A superb treatment of the physical chemistry of aqueous systems.

IX. ATLASES CONTAINING CHEMICAL DATA (#684a to #685g)

- 684a. Wyrtki, K. 1971. Oceanographic Atlas of the International Indian Ocean Expedition. National Science Foundation, Washington, D.C.
Sections of hydrographic and nutrient constituents in the Indian Ocean.
685. Bainbridge, A.E. 1980. GEOSECS Atlantic Expedition, Volume 2, Sections and Profiles, National Science Foundation, Washington, D.C.
Sections of potential temperature, salinity, density, dissolved oxygen, silicate, phosphate, nitrate, alkalinity, and ΣCO₂ along the Atlantic Ocean tracks of the GEOSECS program. Also shown are property-property plots for individual stations and scatter plots for the entire Atlantic Ocean.

685a.Bainbridge, A.E. 1981. GEOSECS Atlantic Expedition Volume 1 Hydrographic data 1972-1973, National Science Foundation, Washington, D.C..

Listing of potential temperature, salinity, density, dissolved oxygen, nutrient, total dissolved inorganic carbon, alkalinity, dissolved nitrogen, dissolved argon and radon data. Also given are CO_2 , HCO_3^- , $\text{CO}_3^=$, and carbonate mineral saturation values calculated from the ΣCO_2 and alkalinity data.

685b.Broecker, W.S., D.W. Spencer, and H. Craig (in press). GEOSECS Pacific Expedition: Hydrographic Data, U.S. Government Printing Office, Washington, D.C., Vol. 3.

Listing of potential temperature, salinity, density, dissolved oxygen, nutrient, total dissolved inorganic carbon, alkalinity, dissolved nitrogen, dissolved argon and radon data. Also given are CO_2 , HCO_3^- , $\text{CO}_3^=$ and carbonate mineral saturation values calculated from the ΣCO_2 and alkalinity data.

685c.Craig, H., W.S. Broecker and D.W. Spencer. 1982. GEOSECS Pacific Expedition: Sections and Profiles, U.S. Government Printing Office, Washington, D.C., Vol. 4.

Sections of potential temperature salinity, density, dissolved oxygen, silicate, phosphate, nitrate, alkalinity and ΣCO_2 along the Pacific Ocean tracks of the GEOSECS program. Also shown are property-property plots for individual stations and scatter plots for the entire Pacific Ocean.

685d.Spencer, D.W., W.S. Broecker, H. Craig and R.F. Weiss, (in prep.). GEOSECS Indian Ocean Expedition: Hydrographic Data, U.S. Government Printing Office, Washington, D.C., Vol. 5.

Listing of potential temperature, salinity, density, total dissolved inorganic carbon, alkalinity, and radon data. Also given are CO_2 , HCO_3^- , $\text{CO}_3^=$ and carbonate mineral saturation values calculated from the ΣCO_2 and alkalinity data.

685e.Weiss, R.F., W.S. Broecker, H. Craig and D.W. Spencer, (in press). GEOSECS Indian Ocean Expedition: Sections and Profiles, U.S. Government Printing Office, Wash., D.C., Vol. 6.

Sections of potential temperature salinity, density, dissolved oxygen, silicate, phosphate, nitrate, alkalinity and ΣCO_2 along the Indian Ocean tracks of the GEOSECS program. Also shown are property-property plots for individual stations and scatter plots for the entire Indian Ocean.

685f.GEOSECS Atlantic, Pacific and Indian Oceans Expeditions CTD Data, (in prep.). U.S. Government Printing Office, Washington, D.C., Vol. 7.

Listing of the CTD data taken during GEOSECS program.

685g. GEOSECS Atlantic, Pacific and Indian Oceans Expeditions
Shorebased Data, (in prep.). U.S. Government Printing
Office, Washington, D.C., Vol. 8.
Listing of the GEOSECS ^{14}C , ^3H , ^{226}Ra , $^{13}\text{C}/^{12}\text{C}$,
 $^{18}\text{O}/^{16}\text{O}$, D/H and barium results.

X. MISCELLANEOUS PAPERS AND LATE ENTRIES (#686 to #737)

686. Koblentz-Mishke, O.J., V.V. Volkovinsky and J.G. Kabanova. 1970. Plankton primary production of the world ocean. In: Scientific Exploration of the South Pacific, ed. W.S. Wooster, National Academy of Sciences, Washington, D.C., p. 183-193.
Compilation of primary plant production data for the world ocean.
687. Love, C.M. 1974. Eastropac Atlas V3, U.S. Government Printing Office, Washington, D.C.
Data showing the vertical and longitudinal distribution of plant productivity in the equatorial Pacific Ocean.
688. Dueser, W.G. 1975. Reducing Environments. Chemical Oceanography, ed. by J.P. Riley and G. Skirrow 2nd edition, V3, Academic Press, London.
A general discussion of the development of anoxic conditions in restricted basins and in parts of the open ocean. Estimates of the time scales of water renewal and of the extent of decompositon of organic matter in anoxic environments are also given.
689. Levitus, S. and A.H. Oort. 1977. Global analysis of oceanographic data. Bull. Am. Meteor. Soc. V58, p. 1270-1284.
A summary of the distribution of temperature and salinity data for the world ocean.
690. Drever, J.I. 1977. Sea Water, Cycles of the Major Elements. Benchmark Papers in Geology V45, Dowden, Hutchinson and Ross, Inc.
A set of reprints of "classic" papers discussing the mechanisms controlling the chemical composition of sea water.
691. World Energy Outlook, Exxon Background Series, Dec. 1980.
Projections of energy use, of the sources of this energy and of the geographic distribution of this use.
692. Goldman, J.C. 1980. Physiological processes, nutrient availability and the concept of relative growth rate in marine phytoplankton ecology. Primary Production in the Sea, ed. by P.G. Falkowske, Plenum Publishing Corp. p. 179-193.
A discussion of the variability in the C:N:P ratios in plankton induced by changes in growth rate and nutrient availability.

693. Mankinen, E.A. and Dalrymple, G.B. 1979. Revised Geomagnetic polarity time scale for the interval 0-5 m.y. B.P. Jour. Geophys. Research V84, p. 615-626.
 Update of the time scale for magnetic reversal over the past five million years.
694. Emiliani, C., E.B. Kraus, and E.M. Shoemaker. 1981. Sudden death at the end of the Mesozoic. Earth & Planet. Sci. Lett. V55, p. 317-334.
 A recap of which organisms were killed by the great asteroid impact which marks the end of Cretaceous time and a thermal theory for these extinctions.
695. Hahne, A., A. Volz, D.H. Ekhalt, H. Cosatto, W. Roether, W. Weiss and B. Kromer. 1978. Pageoph., V116, p. 575-582.
 Profile of chlorofluoromethanes in the Norwegian Sea are compared with those of tritium.
- 695a. Druffel, E.M. 1981. Radiocarbon in annual coral ring from the eastern tropical Pacific Ocean. Geophys. Res. Lett. V8, p. 59-62.
 Record of the $^{14}\text{C}/^{12}\text{C}$ in surface waters adjacent to the Galapagos Islands an area of intense upwelling, based on measurements on ring-dated corals.
696. Santschi, P.H., P. Bower, U.P. Nyffeler, A. Azevedo and W.S. Broecker (in press). Measurements of the resistance to chemical transport posed by the deep sea benthic boundary layer and their significance to benthic fluxes. Limnology & Oceanography.
 The use of dissolution from alabaster plates to estimate the thickness of the boundary "stagnant film" on the sea floor and in benthic chambers.
- 696a. Druffel, E.M., 1982. Banded Corals: Changes in Oceanic Carbon-14 Levels During the Little Ice Age. Science, V218, p.13-19.
 A record of the $^{14}\text{C}/^{12}\text{C}$ ratio in the surface ocean extending back to the 17th century based on measurements on ring-dated corals.
697. Kusakabe, M., T.L. Ku, J. Vogel, J.R. Sounthor, D.E. Nelson and G. Richards, in press. Beryllium-10 profiles in seawater. Nature.
 Measurements of the ^{10}Be concentration in sea water by the accelerator technique.
698. Ku, T.L., M. Kusakabe, D.E. Nelson, J.R. Sounthor, R.G. Korteling, J. Vogel and I. Nowikow, in press. Constancy of oceanic deposition of ^{10}Be as recorded in manganese crusts. Nature.

Measurements of the $^{10}\text{Be}/^{9}\text{Be}$ ratio as a function of depth in manganese crusts with long growth histories.

699. Siegenthaler, U., in press. Uptake of excess CO_2 by an outcrop-diffusion model of the ocean. *J. Geophys. Res.*
A one and a half dimension model of the ocean designed to assess the enhancement of fossil fuel CO_2 uptake by the ocean through descent along outcropping isopycnal horizons.
700. Hogg, N.G., P. Biscaye, W. Gardner and W.J. Schmitz, Jr. 1982. On the transport and modification of Antarctic Bottom Water in the Vema Channel. *J. Mar. Res.* V40, p. 231-263.
Current-meter based measurements of the flux of southern component water into the Atlantic Ocean.
701. Worthington, L.V. 1976. On the North Atlantic Circulation. The Johns Hopkins University Press, Baltimore.
Summary of evidence for the ventilation and circulation rates at various depths in the North Atlantic Ocean.
702. Piepgras, D.J. and G.J. Wasserburg. 1982. Isotopic Composition of Neodymium in Waters from the Drake Passage. *Science*, V217, p. 207-214.
Data showing the distribution of Sm, Nd and $^{143}\text{Nd}/^{144}\text{Nd}$ ratio in the world ocean. Particular attention is given to the significance of the isotope results water from the Drake Passage as they provide a means of estimating the relative contributions of water of Atlantic and Pacific origin to the deep circumpolar current in the Antarctic Ocean.
703. Bryden, H.L. and R.D. Pillsbury. 1977. Variability of Deep Flow in the Drake Passage from Year-Long Current Measurements. *Jour. Phys. Oceanography*, V7, p. 803-810.
Estimate of the flux of water through the Drake Passage based on current-meter observations.
704. Nowlin, W.D., T. Whitworth, III and R.D. Pillsbury. 1977. Structure and Transport of the Antarctic Circumpolar Current at Drake Passage from Short-Term Measurements. *Jour. of Phys. Oceanography*, V7, p. 788-802.
Estimate of the flux of water through the Drake Passage based on current-meter observations.
705. Turner, J.V. 1982. Kinetic fractionation of carbon-13 during calcium carbonate precipitation. *Geochimica et Cosmochim. Acta.*, V46, p. 1183-1191.
Estimate of the equilibrium and kinetic fractionation factors (at 25°C) for carbon isotopes during the formation of calcite and of aragonite from HCO_3^- ion in aqueous solution.

706. Emerson, S. and M. Bender. 1981. Carbon fluxes at the sediment-water interface of the deep sea: calcium carbonate preservation. *Jour. of Marine Res.* V39, p. 139-162.
Demonstration that the bioturbation of organic residues into the upper sediment column coupled with oxidation of this buried debris is an important contributor to the dissolution of calcite in marine sediments. The inclusion of this process alters the relationship between the lysocline and saturation horizon depths.
707. Anderson, R.F., M.P. Bacon and P.G. Brewer, in press.
Removal of ^{230}Th and ^{231}Pa at ocean margins. *Earth & Planet. Sci. Lett.*
Evidence for the preferential removal of ^{231}Pa (relative to ^{230}Th) in areas of high particle rain rate.
708. Anderson, R.F., M.P. Bacon and P.G. Brewer, in press.
Removal of ^{230}Th and ^{231}Pa from the open ocean. *Earth & Planet. Sci. Lett.*
Evidence for the preferential removal of ^{230}Th (relative to ^{231}Pa) in areas of low particulate rain rate.
709. Boyle, E.A., S.S. Huested and S.P. Jones. 1981. On the distribution of copper, nickel, and cadmium in surface waters of the North Atlantic and North Pacific Oceans. *Jour. of Geophys. Res.*, V86, p. 8048-8066.
Distribution of copper, cadmium and nickel in the surface waters of open ocean, coastal and upwelling areas.
710. Boyle, E.A. 1981. Cadmium, zinc, copper and barium in foraminifera tests. *Earth & Planet. Sci. Lett.*, V53, p. 11-35.
The first demonstration that the concentrations of Zn and Cd in the shells of planktonic foraminifera might be used to determine glacial to interglacial changes in the concentrations of these metals in the sea.
711. Boyle, E.A. and L.D. Keigwin. 1982. Deep circulation of the North Atlantic over the last 150,000 years; geochemical evidence. *Science*. V217.
Records for both the $^{13}\text{C}/^{12}\text{C}$ and Cd/Ca variations in North Atlantic Deep Water (NADW) through the course of a complete glacial cycle based on the analyses of benthic forams. Evidence is presented that the contribution of NADW relative to southern water types diminished during the glacial maxima ~70,000 and ~20,000 years ago.
712. Hester, K. and E. Boyle. 1982. Water chemistry control of the cadmium content of some recent benthic foraminifera. *Nature*, V298, p. 260-262.

Analyses of recent benthic foraminifera from various places on the sea floor showing a linearity between the Cd/Ca of the shells and the phosphate content of the local bottom water.

713. Graham, D.W., B.H. Corliss, M.L. Bender, L.D. Keigwin, Jr. 1981. Carbon and oxygen isotopic disequilibria of recent deep sea benthic foraminifera. *Marine Micropaleontology*, V6, p. 483-497.
Demonstration that no temporal changes have occurred in the species to species $\delta^{18}\text{O}$ and $\delta^{13}\text{C}$ differences for four key benthic organisms. Also the relationship between AOU and $\delta^{13}\text{C}$ for the species P. wuellerstorfi is shown to be close to that expected for respiration.
714. Bender, M.L., R.B. Lorens and D.F. Williams. 1975. Sodium magnesium and strontium in the tests of planktonic foraminifera. *Marine Micropaleontology*, V21, p. 448-459.
An attempt to reconstruct the temporal variations in the Na/Ca, Mg/Ca and Sr/Ca ratio, in sea water based on the analysis of planktonic foraminifera.
715. Graham, D.W., M.L. Bender, D.F. Williams, L.D. Keigwin, Jr. 1982. Strontium-calcium ratios in Cenozoic planktonic foraminifera. *Geochim. Cosmochim. Acta* V46, p. 1281-1292.
Evidence for small (i.e., $\pm 15\%$) changes in the Sr/Ca ratio in sea water over the last 60 million years based on the analysis of planktonic foraminifera.
716. Roether, W. and B. Kromer. 1978. Field determination of air-sea gas exchange by continuous measurement of radon-222. *Pageoph*, V116, p. 476-485.
Description of system for radon profiling through the oceanic mixed layer.
717. Fairbanks, R.G. 1982. The origin of continental shelf and slope water in the New York Bight and Gulf of Maine: evidence from $\text{H}_2^{18}\text{O}/\text{H}_2^{16}\text{O}$ ratio measurements. *Jour. Geophys. Res.* V87, p. 5796-5808.
The clear demonstration of the utility $\delta^{18}\text{O}$ -salinity diagrams in differentiating different sources of the low salinity waters found in coastal regions.
718. Streeter, S.S., P.E. Belanger, T.B. Kellogg and J.C. Duplessy. 1982. Late Pleistocene paleo-oceanography of the Norwegian-Greenland Sea: benthic foraminifera evidence. *Quaternary Research*, V-18, p. 72-90.
Evidence in support of the idea that the Norwegian Sea was not a source for bottom water during most of glacial time.

719. Sharma, P. and B.L.K. Somayajulu. 1982. ^{10}Be dating of large manganese nodules from world oceans. *Earth & Planet. Sci. Lett.* V59, p. 235-244.
Growth rates of Mn nodules based on $^{10}\text{Be}/^{9}\text{Be}$ ratios confirm that the long term growth rate of these objects is generally in the range 1 to 4 mm/ 10^6 years.
720. Erez, J., K. Takahashi and S. Honjo. In-situ dissolution experiment of Radiolaria in the central North Pacific Ocean. *Earth & Planet. Sci. Lett.* V59, p. 245-254.
Demonstration that temperature is the main factor controlling the rate of opal dissolution in the sea. The results suggest that opal must dissolve at a rate 100 times faster in warm surface water (25°C) than in cold deep water (1.5°C).
721. Ledwell, J.R., 1982. Gas exchange across the air-water interface. Ph.D. thesis, Harvard University, Cambridge, Mass.
Demonstration through wind tunnel experiments that the gas exchange depends on the square root of the molecular diffusivity.
722. Measures, C.I. and J. Edmond. 1982. Be in the water column of the central east Pacific. *Nature*, V197, p. 51-53.
First measurements of the profile of Be in the sea.
723. Settle, D.M., C.C. Patterson, K.K. Turekian and J.K. Cochran. 1982. Lead precipitation fluxes at tropical oceanic sites determined from ^{210}Pb measurements. *Jour. Geophys. Res.* V87, p. 1239-1245.
Estimates of the fluxes of ^{210}Pb and stable lead to the ocean from measurements on rain water samples collected at Enewetak, Samoa and the Florida Keys.
724. Carmack, E. and K. Aagaard. 1973. On the deep water of the Greenland Sea. *Deep Sea Res.* V20, p. 687-714.
Suggestion that subsurface of waters from two advective regimes (via a double-diffusive process) leads to the formation of Greenland Sea deep water.
725. Swift, J.H., K. Aagaard and S-A Malmberg. 1980. The contribution of the Denmark Strait overflow to the deep North Atlantic. *Deep Sea Res.* V27A, p. 29-42.
Demonstration that the water spilling through the Denmark Straits forms at least in part at the surface north of Iceland.
726. Lazier, J.R.N. 1973. The renewal of Labrador Sea Water. *Deep Sea Res.* V20, p. 341-353.
Demonstration that deep water formation in the Labrador Sea may occur only during winters of extreme severity.

727. Ostlund H.G. and R.A. Fine. 1979. Oceanic distribution and transport of tritium. In: Behavior of Tritium in the Environment. International Atomic Energy Agency Publication IAEA-SM-232/67, p. 303-314.
Paper discussing the distribution of tritium in the Atlantic and Pacific Oceans.
728. Enting, I.G. and G.I. Pearman. 1982. Description of a One-Dimensional Global Carbon Cycle Model. Division of Atmospheric Physics. Technical Paper #42, CSIRO, Melbourne, Australia.
In this model the ocean is broken up into two parts (polar and equatorial). Deep water is produced by transporting surface water from the polar unit to the bottom of the polar unit. Part of this water upwells in the polar unit and part passes to the equatorial unit where it upwells. It includes the rain and destruction of carbon bearing particulates within the sea. The model is calibrated and tested using all the available natural and bomb-produced isotope distributions.
729. Hammer, P.M., J.M. Hayes, W.J. Jenkins and R.B. Gagosian. In press. Exploratory analyses of trichlorofluoromethane (F-11) in North Atlantic water columns.
Profiles of freon-11 in the Gulf of Maine, on the Scotian shelf and in the Sargasso Sea.
730. Cline, J.D., R.H. Gammon and D. Wisegarver. In press. Meridional distribution of dissolved freon-11 in the eastern North Pacific Ocean.
Comparison of the distributions of the freons with those of salinity and tritium in the thermocline of the northeastern Pacific Ocean.
731. Gammon, R.H., J.D. Cline, D. Wisegarver. 1982. Chlorofluor-metanes in the northeast Pacific Ocean: measured vertical distributions and application as transient tracers of upper ocean mixing. Jour. Geophys. Res., (in press).
One-dimensional models for the vertical distributions of freon-11 and freon-12.
732. Broecker, W.S. and E.A. Olsen. 1961. Lamont radiocarbon measurements VIII. Radiocarbon, V3, p. 176-204.
Discussion of the Δ scale for the presentation of radiocarbon results.
733. Urey, H.C. 1947. The thermodynamic properties of isotopic substances. J. Am. Chem. Soc., p. 562-581.
Early work of ^{13}C and ^{18}O isotopes from the Cretaceous belemnite.
734. Craig, H. 1957. Isotopic standards for carbon and correction factors for mass-spectrometric analysis of carbon dioxide.

Geochim. et Cosmochim. Acta., V12, p. 133-149.

Standardization of ^{13}C and ^{18}O isotope ratios from the Cretaceous belemnite. Secondary NBS reference CaCO_3 standard is also described.

735. Craig, H. 1961. Standard for reporting concentrations of deuterium and oxygen 18 in natural waters. Science, V133, p. 1833-1834.
Introduction of SMOW for reference standard of oxygen and hydrogen isotopes in seawater. Conversion of units between PDB and SMOW is also given.
736. Friedman, I. and J. O'Neil. 1977. Compilation of stable isotope fractionation factors of geochemical interest. U.S. Geol. Survey, Professional Paper 440-KK, U.S. Government Printing Office, Washington, D.C.
Conversion of stable isotope ratios units between PDB standard and SMOW standard.
737. Goldberg, E.D. 1974. The Sea, Vol. 5, Marine Chemistry. Interscience publishers, Wiley and Sons, New York, 895 pp.
A series of articles on subjects in chemical oceanography authored by experts.

FREQUENTLY USED CONSTANTS

Avagadro's Number (molecules/mole)	6.02×10^{23}
Ideal Gas Law Constant (cal/deg K)	1.99
Seconds per year	3.14×10^7
Minutes per year	5.2×10^5
Area of the Earth (cm^2)	5.1×10^{18}
Mass of the Atmosphere (grams)	5.1×10^{21}
Area of the Oceans (cm^2)	3.6×10^{18}
Volume of the Oceans (liters)	1.37×10^{21}
Mean Depth of Oceans (meters)	3.8×10^3
Continental Runoff Rate (liters/year)	3.6×10^{16}
Ocean Volume/Runoff Rate (years)	38,000
Mean Oceanic CO_2 Piston Velocity (m/day)	2.8
Mean Oceanic CO_2 Exchange Rate (moles/ m^2 year) (at $p\text{CO}_2 = 300 \times 10^{-6}$ atm)	18
$^{14}\text{C}/\text{C}$ (for $\Delta^{14}\text{C} = 0 \text{ ‰}$)	1.18×10^{-12}
Specific Activity (dpm/gC)	13.6
Halflife ^{14}C (years)	5730
$^3\text{H}/\text{H}$ (for T.U. = 1)	1.0×10^{-18}
Specific Activity (dpm/liter H_2O)	7.1
Halflife ^3H (years)	12.4

DEFINITIONS OF ISOTOPE NOTATIONS*

$$\delta^3\text{He} = \left[\frac{{}^3\text{He}/{}^4\text{He})_{\text{sample}} - {}^3\text{He}/{}^4\text{He})_{\text{atm}}}{{}^3\text{He}/{}^4\text{He})_{\text{atm}}} \right] 100$$

$$\epsilon^{143}\text{Nd} = \left[\frac{{}^{143}\text{Nd}/{}^{144}\text{Nd})_{\text{sample}} - {}^{143}\text{Nd}/{}^{144}\text{Nd})_{\text{standard}}}{{}^{143}\text{Nd}/{}^{144}\text{Nd})_{\text{standard}}} \right] 10,000$$

$$\delta D = \left[\frac{D/H)_{\text{sample}} - D/H)_{\text{standard}}}{D/H)_{\text{standard}}} \right] 1000$$

$$\delta^{18}\text{O} = \left[\frac{{}^{18}\text{O}/{}^{16}\text{O})_{\text{sample}} - {}^{18}\text{O}/{}^{16}\text{O})_{\text{standard}}}{{}^{18}\text{O}/{}^{16}\text{O})_{\text{standard}}} \right] 1000$$

$$\delta^{13}\text{C} = \left[\frac{{}^{13}\text{C}/{}^{12}\text{C})_{\text{sample}} - {}^{13}\text{C}/{}^{12}\text{C})_{\text{standard}}}{{}^{13}\text{C}/{}^{12}\text{C})_{\text{standard}}} \right] 1000$$

$$\delta^{14}\text{C} = \left[\frac{{}^{14}\text{C/C})_{\text{sample}} - {}^{14}\text{C/C})_{\text{standard}}}{{}^{14}\text{C/C})_{\text{standard}}} \right] 1000$$

$$\Delta^{14}\text{C} = \delta^{14}\text{C} - 2 (\delta^{13}\text{C} + 25) \left(1 + \frac{\delta^{14}\text{C}}{1000} \right)$$

*For ${}^{13}\text{C}$ and ${}^{18}\text{O}$ the standards are isotope ratios for the carbon and oxygen from the Cretaceous belemnite used as a standard by Harold Urey in his early work (733). As this material has been depleted, a secondary National Bureau of Standards reference CaCO_3 standard is used in most laboratories (734). It should be noted that for measurements on sea water the standard used for oxygen (and for hydrogen) is SMOW (standard mean ocean water). Because the CO_2 prepared for mass spectrometry from CaCO_3 does not have the same oxygen isotope ratio as the $\text{CO}_3^=$ in the mineral (because of interaction with the oxygen in the phosphoric acid used to release the CO_2) the PDB and SMOW scales are quite different (735). Care should be taken in converting from one set of values to the other (736).

For helium the standard is helium from the atmosphere. For neodymium the standard is the ${}^{143}\text{Nd}/{}^{144}\text{Nd}$ ratios for average earth material (337). Finally, for radiocarbon, the standard is 0.95 times the ${}^{14}\text{C/C}$ ratio in the National Bureau of Standard's oxalic acid reference standard (732).

ABBREVIATIONS

Accumulation rate	A
Advection rate	w
Alkalinity	Alk
Antarctic Bottom Water	AABW
Apparent Oxygen Utilization	AOU
Area	A
Atmosphere	atm
Calcite compensation depth	CCD
Centimeter	cm
Curie	Ci
Decay constant	λ
Denmark Straits Overflow Water	DSW
Depth	z
Disintegration per minute	dpm
Eddy diffusivity	D
Equivalent	eq, equiv
Flux	F
Gibbs Fracture Zone Water	GFZW
Gram	g, gm
Kilogram	kg
Kilometer	km
Labrador Sea Water	LSW
Liter	l
Meter	m
Microequivalent	μ eq
Micromole	μ mol, μ m
Micron	μ
Milliliter (cubic centimeter)	ml (cc)
Millivolt	mV
Minute	min
Mole	mol, m
Molecular diffusivity	κ
North Atlantic Deep Water	NADW
Percent	%
Per mil	$^{\circ}/_{\text{o}}$
Potential density	σ
Potential temperature	θ
Rain rate of particulate debris	R
Residence time	τ
Revelle factor	R
Salinity	S
Second	s, sec
Solution rate	S
Standard Temperature and Pressure	STP
Surface water	SW
Thickness of stagnant film	z
Tritium Unit	TU, tu
Two-Degree Discontinuity	TDD
Upwelling velocity	w, W
Volume	V
Weddell Sea Bottom Water	WSBW

Index

Advection, 317
Alkalinity, definition, 67
Anions, control mechanism, 287
Antarctic bottom water (AABW), 337
Anthropogenic tracers, 383
AOU:
 definition, 131
 distribution, 131
Aragonite, solubilities, 63-64
Argon-39, deep sea ventilation, 377
Authigenic mineral, 45
 formation of, 295

Barium:
 geographic pattern, 30
 mean lifetime, 21
 removal, 11
Benthic boundary layer, 88
Biogenic sediments:
 calcite, 47
 opal, 47
Biointermediate constituents, 6,8,22
Biolimiting constituents, 6
Bioturbation, sediment, 257,562
Biounlimited constituents, 6,8
Boundary stagnant film:
 sea-air interface, model, 113
 sediment-water interface, 86-88
Bubble entrainment, 127,130
Buoyancy flux, 329

Cadmium, distribution in the sea, 216,218,222
Calcite:
 biogenic, 47
 changes, glacial-interglacial, 456
 compensation depth, 100
 degree of saturation, 61
 distribution in marine sediment, 58
 pore water resaturation time, 84
 solubilities, 63
 solution, bioturbation model, 487

solution, controlling factors, 84
solution rates, 269
storage, compensation time, 456-457

Carbon:
control mechanism, 280
fixation, ratio organic to CaCO_3 , 476
reservoir sizes, 455

Carbon-13:
fractionation, 306
glacial-interglacial, 451-454, 473
marine geochemistry of, 306
phosphate changes, 466
planktonic forams, 470
tree ring, 538
units, 306

Carbon-14 (see Radiocarbon)

Carbon dioxide:
anomalies, equatorial Pacific, 158
anthropogenic production, 500, 501
atmospheric time history, 535
concentration in surface water, 149-150
equilibration times, 155
excess, equatorial surface water, 430
fossil fuel (see fossil fuel CO_2)
future levels, prediction, 550
ice cores, 445
potential partial pressure, 161, 443
release, forest & soil, 502-503
solubilities in sea water, 111, 112, 151, 152

Carbonate chemistry, 69

Carbonate ion, variation, 62

Carbonate saturation:
horizon, 71
spacial variation, 71

Carbonic acid:
1st apparent dissociation constants, 151, 152
2nd apparent dissociation constants, 151, 152

Calcium:
distribution, 11
mean lifetime, 21

Cations, control mechanism, 289

Characteristic penetration depth, 319

Chemical composition:
hydrothermal vents, 292, 294
river and sea, 26-27, 290
saline lake, 293

Circulation pattern, deep water, 32, 33

Conservative property, 334

Continental runoff, rate of, 247

Copper, distribution in the sea, 216, 218, 222

Dating:
beryllium, 264
magnetic reversals, 267

potassium-argon, 264
radiocarbon, 255
uranium-helium, 312
uranium series, 257
Deep water, sources, 334
Denmark Straits Overflow Water (DSW), 335
Density gradient, 327-331
Detrital material, 45
Detritus accumulation rate, 45
Diapycnal mixing, 322,324
Diffusion, deep water, 317,319
Distribution coefficient, 230

e-folding time, 457
Element budget, earth's crust, 166,167
Element concentrations, river and ocean, 26-27, 290
Element, hydrolysis constants, 231
Element, removal times, 231

Film replacement model, 118
Flushing time, deep sea, 370
Foram, solution index, 98
Fossil fuel, reserves, 506
Fossil fuel CO₂:
 atmospheric levels, prediction, 550
 calcite solution, 552
 oceanic uptake, capacity, 511
 oceanic uptake, kinetics, 524
 oceanic uptake, numerical model, 526,529
 production, 500, 501

Gas exchange rate, 113
Gas flux, 116
Gases:
 diffusivities in sea water, 119
 equilibrium concentration in surface water, 114
 solubilities in sea water, 112, 113
 volume partition coefficient, 112, 113
Gibbs Fracture Zone Water (GFZW), 337

Helium:
 excess, 147
 hydrothermal vents, 295
Helium-3:
 anomalies, 149
 distribution, deep Pacific, 331
 distribution, thermocline, 432
Hydrothermal vents, 292,294

Igneous rocks, chemical composition, 167
Inorganic carbon, total dissolved, 67
Input rates, river to sea, 25
Iron, transport in the sea, 226

Isopycnal mixing, 322,324
Isopycnal surface, 322,391,392
Isotope fractionation, carbon, 236
Isotope ratios in reactive metals, 221

Keeling fraction, 514

Labrador Sea Water (LSW), 337

Lead:

distribution in the sea, 218-222
isotope ratios, 223,226,227

Lead-210:

depth profile, 174
distribution, 189
excess, sediment, 562-563
fallout rates, 191
production rates, 191
scavenging time, 189,199

Lysocline:

definition, 75
glacial-interglacial, 485
transition zone, 89

Manganese, transport in the sea, 226

Manganese nodules, 98

Metal transport, model, 205

Mixing rates, deep sea, 325

Model:

advection-diffusion, sea water, 318
biolimiting constituents, 15
stagnant film, 113

Mole, definition, 17

Molecular diffusion coefficients, 116,119

Neodymium, isotope ratios, 223-226

Nickel, distribution in the sea, 216,218,222

Nitrate:

control mechanism, 284
consumption (denitrification), 142
distribution of, surface water, 47
geographic pattern, 31

Nitrous oxide cycle, 139

Northern Component Water (NCW):

definition, 335
conservative properties of, 340, 341
feed for, 345
radiocarbon in, 343

Nutrient gradients in the deep sea, 312

Ocean chemistry, glacial-interglacial, 467

Oeschger model, 526

Opal:

biogenic, 47
diffusion coefficient, pore water, 55

distribution of, 47
rain rate, 56
resaturation time, pore water, 55
solution rate, 49,56
Organic carbon in sediments, 47
Organic matter, chemical composition of, 8
Oxygen:
concentration, surface water, 127
consumption, respiration, 134
control mechanism, 284
deficiencies, deep water, 131
deficiencies, surface water, 131
excess, photosynthesis, 127
geographic pattern, 31
glacial deep water, 484
Oxygen-18:
in forams, 446-447
Outcropping isopycnals, 322
Paleolysocline, 98
Paleoocean:
chemistry, recorder of, 301
indicator, 301,311
Particulate matter, composition of, 13
Partition coefficient, 384
Phosphate:
changes, causes of, 479
changes, glacial-interglacial, 466
control mechanism, 275
Phosphorus:
input rate, 25
mean lifetime, 20,21
residence time in mixed layer, 20
scavenging time, 175
Piston velocity, 121
Plant productivity, 130
Plutonium, distribution, 203
Polonium-210, distribution, 198
Potential temperature, 3,111
Potential CO₂ partial pressure, 161,443
Preformed values, 131
Protactinium-231:
 $^{231}\text{Pa}/^{230}\text{Th}$ ratio, 184,189
rain rate, 186,187
Radiocarbon:
¹⁴C/C ratio definition, 245
cycle, deep sea, 368
decline, fossil fuel, 544
distribution in the sea, 245
production, temporal variation, 374
production rates, 236-238
production, sun-spot, 544
Radiocarbon, bomb-produced:
distribution, thermocline, 412

distribution, surface water, 415
time history, air, 389
time history, surface sea, 389

Radium:
marine geochemistry, 13
 ^{226}Ra , distribution, 200-203
 ^{226}Ra , flux from sediments, 204
 $^{226}\text{Ra}/\text{Ba}$ ratio, model distribution, 245
 ^{228}Ra , deep sea, 326

Radon-222, deep sea, 326

Red clay:
definition, 45
chemical composition, 167

Redfield ratio, 9

Removal model, radionuclides, 171

Residence time, definition, 25

Revelle factor, 158,519

Salinity:
controlling factors, 289
changes, glacial-interglacial, 448

Saturometer, 80,83

Scavenging constant, 171

Scavenging times, 172

Sea salt composition, 2

Sediment mixing, 562

Sediment recycling, model, 212

Sedimentation rates, methods, 253

Selenium, distribution of, 22

Shale, chemical composition, 167

Silica: (see also Opal)
atom ratio, mean sea water, 11
control mechanism, 280
distribution, surface water, 47
geographic pattern, 30
N-S vertical sections, 36-38

Solubilities of gases, 111,112

Southern component water (SCW), 349,359

Stagnant film:
model, sea-air interface, 113
sediment-water interface, 562
thickness, radiocarbon method, 118
thickness, radon method, 122

Steady state, definition, 17

Strangelove ocean, 466, 472

Strontium, 13

Strontium-90:
corals, 412,413
delivery mechanism, 385
deposition rate, 386

Suess effect, 544

Sverdrups, 382

Temperatures, glacial-interglacial, 446

Termination I, II, 454

Thermocline:

- definition of, 15
- hydrology of, 388

Thorium:

- activities, 170
- isotopes in the sea, 172-184
- scavenging times, 175
- $^{228}\text{Th}/^{228}\text{Ra}$ ratio, 175-179

Thorium-230:

- distribution coefficient, deep Pacific, 181
- profile in sea water, 180
- rain rate, 186,187

Trace metal, distribution, 215

Tracers, diapycnal and isopycnal mixing, 324

Tracers, purposeful, 438

Tritium:

- delivery mechanism, 384, 385
- delivery rates, 386
- distribution, thermocline, 399
- penetration depth of, 402,403
- temporal trends, 402
- vertical distribution, 409

Two-box model, 15,240

Two-degree discontinuity (TDD), 359

Upwelling:

- distributiton of, 158,319
- bomb ^{14}C , 422
- carbon dioxide anomaly, 427
- evidence for, 397
- rates of, 425,429

Uranium content:

- of coral, 311
- of saline lakes, 311

Uranium series, activities, 170

Ventilation of deep sea:

- source areas, 312,317
- deep Atlantic, 359
- deep Indian, 365
- deep Pacific, 365

Vertical mixing, rate of, 236-243

Vital effect, 468

Volatile elements, distribution of, 288

Weddell Sea Bottom Water (WSBW), 353

Zinc, distribution in the sea, 216,218